

THE JOURNAL OF PHYSICAL CHEMISTRY

Volume 71, Number 11 October 1967

- Product Isomerization in the Photolysis of Carbon Suboxide-Olefin Mixtures . . . **Clive Willis and Kyle D. Bayes** 3367
- The Adsorption of Methanol Vapor on Silver Iodide **Harry W. Edwards and M. L. Corrin** 3373
- Photoinjection from Rhodium into Hydrocarbon Liquids under Visible Excitation
. **Alfred Prock, Mihran Djibelian, and Susan Sullivan** 3378
- Thermodynamic Characterization of the Potentiometric Titration of Polyelectrolytes, with Special Reference to
Precipitating Systems **Isaac Michaeli** 3384
- The Effect of Rare Gases and Aromatic Admixtures on the Self-Induced Isotopic Exchange of Tritium with Toluene
. **Hans J. Ache** 3388
- Black Lipid Membranes in Aqueous Media: Interfacial Free Energy Measurements and
Effect of Surfactants on Film Formation and Stability **H. T. Tien** 3395
- Hydration and Association Equilibria in Molten Salt Solutions Containing Water. II. A Quasi-Lattice Model
. **Jerry Braunstein** 3402
- Localized Adsorption on Graphite Surfaces **Conway Pierce and Bland Ewing** 3408
- Ionic Association. IV. Viscosity Effect on the Ultrasonic Relaxation of Zinc Sulfate in
Water-Glycol Mixtures at 25.0° **Fabio Fittipaldi and Sergio Petrucci** 3414
- Fluorine Magnetic Resonance Spectra of Methylfluorosilanes **Stephen G. Frankiss** 3418
- Pyrolysis Kinetics of Ethyl Nitrate **Thomas J. Houser and Betty M. H. Lee** 3422
- Self-Association and Hydration of Benzoic Acid in Benzene
. **Roger Van Duynes, S. A. Taylor, S. D. Christian, and H. E. Affsprung** 3427
- The Thermal Decomposition of Solid *trans*-Diazidotetraamminecobalt(III) Azide **Taylor B. Joyner** 3431
- The Interactions of Methyl and Difluoromethyl Radicals and the Elimination of HF from "Hot" 1,1-Difluoroethane
. **J. T. Bryant and G. O. Pritchard** 3439
- Skeletal Isomerization of Olefins by Radiation **C. D. Wagner** 3445
- Autocatalysis and Deuterium Isotope Effects in the Reaction of Formic Acid and Nitrogen Dioxide
. **Donald Barton and Peter E. Yankwich** 3455
- Carbon-13 Kinetic Isotope Effect in the Structural Isomerization of Cyclopropane:
Temperature and Pressure Dependence **L. B. Sims and Peter E. Yankwich** 3459
- Microwave Measurements of Nonequilibrium Air Plasmas behind Shock Waves Containing Electrophilic Gases
. **A. P. Modica** 3463
- Ion Pairs and Solvent-Solute Interaction. I. Conductance of Lithium Chlorate in Water-Dioxane Mixtures at 25°
. **Filippo Accascina, Alessandro D'Aprano, and Roberto Triolo** 3469
- Ion Pairs and Solvent-Solute Interaction. II. Conductance of Lithium Chlorate in Methanol-Dioxane and
in Acetonitrile-Dioxane **Alessandro D'Aprano and Roberto Triolo** 3474
- Pressure-Volume-Temperature Relations in the System Methane-Tetrafluoromethane. I. Gas Densities and
the Principle of Corresponding States. **D. R. Douslin, R. H. Harrison, and R. T. Moore** 3477
- The Halide Ion Activity of Dyes and Organic Salts in Aqueous Solution **J. F. Padday** 3488
- The Adsorption and Oxidation of Hydrocarbons on Noble Metal Electrodes. IV.
n-Hexane on Smooth Platinum at 130° **S. B. Brummer and M. J. Turner** 3494
- Quantitative Studies of Ultrasonic Vibration Potentials in Polyelectrolyte Solutions **R. Zana and E. Yeager** 3502

Electrochemical Reduction of Aromatic Nitro Compounds in the Presence of Proton Donors Steven H. Cadle, Paul R. Tice, and James Q. Chambers	3517
An Examination of the Zwanzig Theory of Dielectric Friction Gordon Atkinson and Yoshihiro Mori	3523
Temperature Effects on Nature and Reactions of Metastable Species in γ -Irradiated 3-Methylpentane-Carbon Tetrachloride Glasses at 20 and 77°K R. F. C. Claridge, R. M. Iyer, and J. E. Willard	3527
The Crystal Structures of Bismuth Halide Complex Salts. I. 2-Picolinium Tetrabromobismuthate(III) and Tetraiodobismuthate(III) B. Ken Robertson, W. Gant McPherson, and Edward A. Meyers	3531
Liquid-Liquid Phase Separation in Alkali Metal-Ammonia Solutions. III. Sodium with Added Sodium Bromide and Azide Patricia White Doumaux and Andrew Patterson, Jr.	3535
Liquid-Liquid Phase Separation in Alkali Metal-Ammonia Solutions. IV. Sodium and Potassium Patricia White Doumaux and Andrew Patterson, Jr.	3540
The "Sieve Effect" in Chlorella Suspensions M. Das, E. Rabinowitch, L. Szalay, and G. Papageorgiou	3543
Coordination Disproportionation Equilibria in Solution. I. Aluminum Chloride in Acetonitrile W. Libuś and D. Puchalska	3549
Pressure Effects on Glass Transition in Polymers. II. A Study of the Factors Affecting dT_g/dP Values Umberto Bianchi, Antonio Turturro, and Giampiero Basile	3555
An Electron Paramagnetic Resonance Study of Aliphatic Ether Free Radicals Takeshi Shiga, Alain Boukhors, and Pierre Douzou	3559
The Solubility of Silver Chloride and the Concentrations of Silver-Containing Species in Ethanol-Water Mixtures K. P. Anderson, E. A. Butler, D. R. Anderson, and E. M. Woolley	3566
Electrolytic Conductance in Plasticized Polystyrene James R. Price and Walter Dannhauser	3570
Szillard-Chalmers Chemistry of $C_6H_4-R^{127}-I^{129}_2$ Solutions H. M. Chang and J. E. Willard	3576
Reaction of Dilute Aqueous CH_3I with Iodine Activated by Nuclear Processes D. D. Wilkey, J. F. Brensike, and J. E. Willard	3580
Aqueous Systems at High Temperature. XX. The Dissociation Constant and Thermodynamic Functions for Magnesium Sulfate to 200° William L. Marshall	3584
Application of Irreversible Thermodynamics to Electrolyte Solutions. III. Equations for Isothermal Vector Transport Processes in n -Component Systems. Donald G. Miller	3588
Carbon-13 Nuclear Magnetic Resonance Studies of 4-Substituted Pyridines H. L. Retcofsky and R. A. Friedel	3592
Molecular Complexes of Aromatic Nitrile N-Oxides with Iodine, β -Naphthol, and Phenol Tanekazu Kubota, Masumi Yamakawa, Mamoru Takasuka, Kouji Iwatani, Hideko Akazawa, and Itaru Tanaka	3597
The Transient Potentials Produced by the Creation of Annihilation of the Diffuse Double Layer in Dilute Solutions Fred C. Anson	3605
Solubilization of a Water-Insoluble Dye. II Hans Schott	3611
Clathrates of Tetra(4-methylpyridine)nickel(II) Thiocyanate. II. Competition for Sites in the Host Lattice Sr. M. Juana Minton and Norman O. Smith	3618
Thermodynamics of Aqueous Mixtures of Electrolytes and Nonelectrolytes. III. Transfer of Acetic Acid from Water to Nine 1 <i>m</i> Alkali Halides and Nitrates at 25° J. H. Stern, J. P. Sandstrom, and A. Hermann	3623
Equilibrium Pressures of Hydrogen Dissolved in α -Zirconium Franco Ricca and Tiziano A. Giorgi	3627
Thermodynamic Properties of Hydrogen and Deuterium in α -Zirconium Franco Ricca	3632
Controlled Potential Studies on the Kolbe Reaction and the Role of Coadsorbed Surface Oxides. I. Platinum in Trifluoroacetate Solutions B. E. Conway and A. K. Vijh	3637
Controlled Potential Studies on the Kolbe Reaction and the Role of Coadsorbed Surface Oxides. II. The Reaction at Gold A. K. Vijh and B. E. Conway	3655
Standard Potentials of the Silver-Silver Chloride Electrode in Ethylene Glycol and Its Aqueous Mixtures at Different Temperatures and Related Thermodynamic Quantities. Utpal Sen, Kiron Kumar Kundu, and Mihir Nath Das	3665
Relationship between Chemical Reactivity and the Hyperfine Structure of Polycyclic Hydrocarbons Charles P. Poole, Jr., and O. F. Griffith, III	3672

NOTES

Exact Geometrical Parameters for Pendular Ring Fluid	James C. Melrose and George C. Wallick	3676
Proton Magnetic Resonance Studies on Some Metal Complexes of Methyliminodiacetic Acid and Hydroxyethyliminodiacetic Acid	G. H. Nancollas and A. C. Park	3678
Liquid-Phase Radiolysis of 2,3,4- and 2,2,4-Trimethylpentanes. Interpretation of Carbon-Carbon Bond Rupture Reactions from the Effects of Additives	T. Kudo	3681
A Nuclear Quadrupole Resonance Study of Several Tribromide Ions	Gary L. Breneman and Roger D. Willett	3684
Mass Spectrometric-Knudsen Cell Study of the Gaseous Oxides of Platinum	J. H. Norman, H. Gene Staley, and Wayne E. Bell	3686
Ethane Diffusion in Ion-Exchanged Synthetic Zeolites of Type A Containing Water	W. Rudloff and W. W. Brandt	3689
The Electron Spin Resonance Spectrum of Chloranilic Acid Trianion Radical	M. Broze and Z. Luz	3690
Self-Consistent Field Correlations of Polarographic Oxidation Potentials	Gerald Jay Gleicher and Mary Kay Gleicher	3693
Anomalous Reductive Dimerizations of Alkylpyridinium Ions	William T. Bowie and Martin Feldman	3696
Chlorine Nuclear Quadrupole Resonance in the Symmetrical Hydrogen Dichloride Ion	J. C. Evans and G. Y-S. Lo	3697
"Virtual" Coupling in the Nuclear Magnetic Resonance Spectra of Substituted Cycloheptatrienes	K. W. Egger and W. R. Moser	3699
The Activation Energy of Hydrated Electron Reactions	M. Anbar and Edwin J. Hart	3700
An Analysis of the Excess Charge Effect in Alternant Conjugated Hydrocarbon Radical-Ions.	James R. Bolton	3702
The Calculation of Photostationary States in Systems $A \rightleftharpoons B$ When Only A Is Known	Ernst Fischer	3704
Breakthrough of Poisoning Multivalent Ions across a Permselective Membrane during Electrodialysis	F. de Kőrös and E. Zeigerson	3706

COMMUNICATIONS TO THE EDITOR

Reply to the Comments of the Paper "Gibbs Equation for the Adsorption of Organic Ions in Presence and Absence of Neutral Salts"	D. K. Chattoraj	3709
Self-Diffusion in Simple Liquids. The Linear Trajectory Approximation	A. F. Collings and C. J. Pings	3710
Living Anionic Polymerization under an Electric Field	Ichiro Sakurada, Norio Ise, Hideo Hirohara, and Tetsuo Makino	3711
Radiation Chemical Studies with Heavy Ion Radiations	Robert H. Schuler	3712
Specificity of the Photochemical and Thermal Aquation of Thiocyanatopentaamminechromium(III) Ion	Robert D. Lindholm, Edoardo Zinato, and Arthur W. Adamson	3713
Energy Transfer in Thermal Methyl Isocyanide Isomerization. Collision Cross Sections of <i>n</i> -Alkanes	B. S. Rabinovitch, Y. N. Lin, Siu C. Chan, and K. W. Watkins	3715

AUTHOR INDEX

- Accascina, F., 3469
 Ache, H. J., 3388
 Adamson, A. W., 3713
 Affsprung, H. E., 3427
 Akazawa, H., 3597
 Anbar, M., 3700
 Anderson, D. R., 3566
 Anderson, K. P., 3566
 Anson, F. C., 3605
 Atkinson, G., 3523

 Barton, D., 3455
 Basile, G., 3555
 Bayes, K. D., 3367
 Bell, W. E., 3686
 Bianchi, U., 3555
 Bolton, J. R., 3702
 Boukhors, A., 3559
 Bowie, W. T., 3696
 Brandt, W. W., 3689
 Braunstein, J., 3402
 Breneman, G. L., 3684
 Brensike, J. F., 3580
 Broze, M., 3690
 Brummer, S. B., 3494
 Bryant, J. T., 3439
 Butler, E. A., 3566

 Cadle, S. H., 3517
 Chambers, J. Q., 3517
 Chan, S. C., 3715
 Chang, H. M., 3576
 Chattoraj, D. K., 3709
 Christian, S. D., 3427
 Claridge, R. F. C., 3527

 Collings, A. F., 3710
 Conway, B. E., 3637, 3655
 Corrin, M. L., 3373

 Dannhauser, W., 3570
 D'Aprano, A., 3469, 3474
 Das, M., 3543
 Das, M. N., 3665
 de Körösy, F., 3706
 Djibelian, M., 3378
 Doumaux, P. W., 3535, 3540
 Doustin, D. R., 3477
 Douzou, P., 3559

 Edwards, H. W., 3373
 Egger, K. W., 3699
 Evans, J. C., 3697
 Ewing, B., 3408

 Feldman, M., 3696
 Fischer, E., 3704
 Fittipaldi, F., 3414
 Frankiss, S. G., 3418
 Friedel, R. A., 3592

 Giorgi, T. A., 3627
 Gleicher, G. J., 3693
 Gleicher, M. K., 3693
 Griffith, O. F., III, 3672
 Harrison, R. H., 3477

 Hart, E. J., 3700
 Hermann, A., 3623
 Hirohara, H., 3711
 Houser, T. J., 3422

 Ise, N., 3711
 Iwatani, K., 3597
 Iyer, R. M., 3527

 Joyner, T. B., 3431

 Kubota, T., 3597
 Kudo, T., 3681
 Kundu, K. K., 3665

 Lee, B. M. H., 3422
 Libuś, W., 3549
 Lin, Y. N., 3715
 Lindholm, R. D., 3713
 Lo, G. Y.-S., 3697
 Luz, Z., 3690

 Makino, T., 3711
 Marshall, W. L., 3584
 McPherson, W. G., 3531
 Melrose, J. C., 3676
 Meyers, E. A., 3531
 Michaeli, I., 3384
 Miller, D. G., 3588
 Minton, M. J., 3618
 Modica, A. P., 3463
 Moore, R. T., 3477
 Mori, Y., 3523
 Moser, W. R., 3699

 Nancollas, G. H., 3678
 Norman, J. H., 3686

 Padday, J. F., 3488
 Papageorgiou, G., 3543
 Park, A. C., 3678
 Patterson, A., Jr., 3535, 3540
 Petrucci, S., 3414
 Pierce, C., 3408
 Pings, C. J., 3710
 Poole, C. P., Jr., 3672
 Price, J. R., 3570
 Pritchard, G. O., 3439
 Prock, A., 3378
 Puchalska, D., 3549

 Rabinovitch, B. S., 3715
 Rabinowitch, E., 3543
 Retcofsky, H. L., 3592
 Ricca, F., 3627, 3632
 Robertson, B. K., 3531
 Rudloff, W., 3689

 Sakurada, I., 3711
 Sandstrom, J. P., 3623
 Schott, H., 3611
 Schuler, R. H., 3712
 Sen, U., 3665
 Shiga, T., 3559
 Sims, L. B., 3459
 Smith, N. O., 3618
 Staley, H. G., 3686

 Stern, J. H., 3623
 Sullivan, S., 3378
 Szalay, L., 3543

 Takasuka, M., 3597
 Tanaka, I., 3597
 Taylor, S. A., 3427
 Tice, P. R., 3517
 Tien, H. T., 3395
 Triolo, R., 3469, 3474
 Turner, M. J., 3494
 Turturro, A., 3555

 Van Duyne, R., 3427
 Vijn, A. K., 3637, 3655

 Wagner, C. D., 3445
 Wallick, G. C., 3676
 Watkins, K. W., 3715
 Wilkey, D. D., 3580
 Willard, J. E., 3527, 3576, 3580
 Willett, R. D., 3684
 Willis, C., 3367
 Woolley, E. M., 3566

 Yamakawa, M., 3597
 Yankwich, P. E., 3455, 3459
 Yeager, E., 3502

 Zana, R., 3502
 Zeigerson, E., 3706
 Zinato, E., 3713

THE JOURNAL OF PHYSICAL CHEMISTRY

Registered in U. S. Patent Office © Copyright, 1967, by the American Chemical Society

VOLUME 71, NUMBER 11 OCTOBER 16, 1967

Product Isomerization in the Photolysis of Carbon Suboxide-Olefin Mixtures

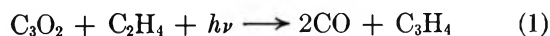
by Clive Willis¹ and Kyle D. Bayes

Contribution No. 2066 from the Department of Chemistry, University of California, Los Angeles, California 90024 (Received May 1, 1967)

The products formed by the photochemical reaction of carbon suboxide and olefins at 3000 Å have been studied at different pressures and with added gases. The allene isomer always dominates the hydrocarbon products. The percentage of acetylene isomers depends on the pressure (see Figures 1, 2, and 4) and on the original olefin (Table I). The effects of added gases (Figure 3) suggest that triplet-triplet energy transfer is involved in the stabilization of the products. This interpretation offers an alternative explanation to the *cis-trans* isomerization observed in *cis*-2-butene-carbon suboxide photolyses.

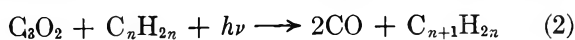
Introduction

The photochemical reaction between carbon suboxide and ethylene forms carbon monoxide, propadiene, and propyne.²



The reactive intermediate is thought to be a C_2O molecule which is in its triplet ground state when the photolysis is carried out at wavelengths of 2900 Å or longer.^{3,4}

Such a carbon insertion appears to be a general reaction for all of the olefins studied so far.^{4,5} However, as the pressure is increased, some intermediate in the reaction is stabilized by collision, resulting in a product more



complex than $\text{C}_{n+1}\text{H}_{2n}$. This pressure-quenching effect becomes more important as the complexity of the olefin increases.⁴ For 2,3-dimethyl-2-butene, where the pressure must be very low in order to observe 2,4-dimethyl-2,3-pentadiene, the more complex product ap-

peared⁴ to be a dimer, $(\text{C}_6\text{H}_{12} \cdot \text{C}_2\text{O})_2$. This observation suggests that the pressure-quenching step represents a stabilization of the olefin- C_2O adduct.

The major $\text{C}_{n+1}\text{H}_{2n}$ product observed is always the corresponding allene: the isomeric acetylenes never represent more than 25% of the hydrocarbon product.⁴ Pressure also affects the ratio of propadiene to propyne.² The dependence on total pressure is not that expected for the simple isomerization of a single hot molecule. The following paper presents the experimental behavior of the isomers under varying conditions and discusses the mechanisms which could result in this behavior.

(1) Research Chemistry Branch, Atomic Energy of Canada Limited, Chalk River, Ontario, Canada.

(2) K. D. Bayes, *J. Am. Chem. Soc.*, **84**, 4077 (1962).

(3) K. D. Bayes, *ibid.*, **85**, 1730 (1963).

(4) C. Willis and K. D. Bayes, *ibid.*, **88**, 3203 (1966).

(5) R. T. K. Baker, J. A. Kerr, and A. F. Trotman-Dickenson, *J. Chem. Soc., Sect. A*, 975 (1966).

Experimental Section

The experimental technique has been described previously.⁴ Photolyses were made at 3000 ± 15 A. Carbon suboxide decomposition was 10% or less. The hydrocarbon products were analyzed by gas chromatography using a hydrogen flame ionization detector. Products were identified by their retention times and by their mass spectra. Chromatogram areas were used as a measure of product yields: no corrections were made for the different sensitivities of isomers. Duplicate analyses were made for most runs. Reproducibility in the isomer ratio was frequently poor, owing primarily to the difficulty of measuring the small areas of the acetylene products. When the duplicate analyses agreed within $\pm 5\%$ of the mean, only the average values are shown in the figures. Larger deviations are indicated by error bars.

The olefins were Phillips Research grade, except for 2,3-dimethyl-2-butene, which was from Columbia Chemical Co. The hydrocarbons were degassed under high vacuum and used without further purification. Other gases were taken directly from commercial containers.

The $C_3O_2-C_2H_4$ reaction was tested for chemiluminescence. A photomultiplier tube (RCA 7102), which was sensitive from 3000 to 10,000 A, observed the cell at 90° to the photolyzing beam. No light emission could be observed above the background of scattered light. By comparing the light scattered from a low pressure of I_2 vapor under comparable conditions and knowing the absorption coefficients of I_2 and C_3O_2 , it was estimated that less than one molecule of excited C_3O_2 in 10^4 resulted in light emission in the detectable range of wavelengths. Since the quantum yield of decomposition is on the order of one,⁶ this negative result means that the carbon insertion reaction is not accompanied by light emission.

Results

The ratio of product isomers is found to depend on pressure, as can be seen in Figures 1 and 2 for the reactions with ethylene, propylene, and *cis*- and *trans*-2-butene. The maximum production of the acetylene isomer occurs at the lowest pressure. Measurements were not made to very low pressures, owing to the difficulties of measuring the small product yields accurately. Early measurements on propylene at pressures as low as 2 torr showed no significant departure from the line shown in Figure 1. Therefore, the approximately linear dependence on pressures has been used to extrapolate the isomer ratio to zero pressure. The resulting isomer percentages are summarized in

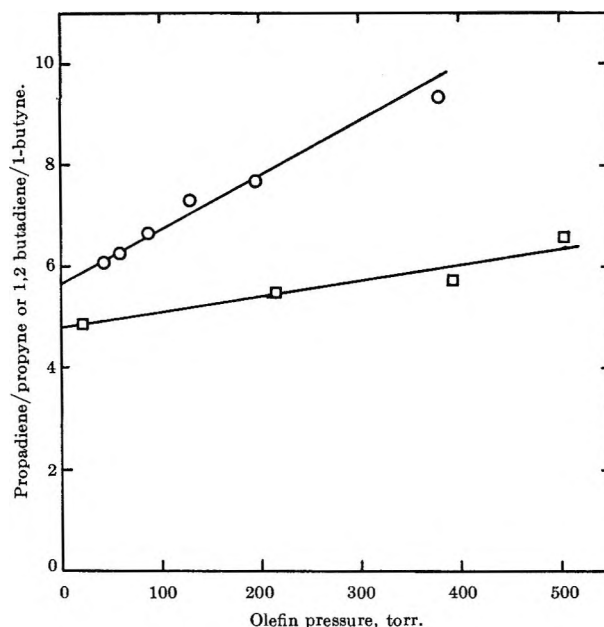


Figure 1. The ratio of isomers formed during the photolysis of C_3O_2 -olefin mixtures as a function of the olefin pressure. The runs with ethylene (\square) were carried out at 3000 ± 15 A and $25 \pm 5^\circ$, using 3 torr of C_3O_2 . The propylene runs (\circ) were made at 2900 ± 90 A and $21 \pm 2^\circ$, using approximately 15 torr of C_3O_2 .

Table I. For 2,3-dimethyl-2-butene, runs at 1 and 4 torr showed only the one hydrocarbon product.

Two generalizations concerning Table I are possible. First, the allene isomer always dominates the acetylene isomer, as well as other isomers. Second, this dominance increases as the parent olefin becomes more complex. These trends have been noted previously,⁶ although the pressure dependence was not recognized.

The effect on the isomer ratio of adding various gases to the $C_2O-C_2H_4$ reaction is shown in Figure 3. The added gases can be classified into two groups. Most of the molecules (N_2 , CO_2 , Kr, Ar, isobutane) have only a small effect on the isomer ratio for additions up to 1 atm. The magnitude of the change is similar to the effect of varying the ethylene pressure alone, which is indicated by the solid line in Figure 3. In contrast, propylene and *cis*-2-butene fall into a different class, being approximately 10 times more effective in altering the isomer ratio. Because of the direct competition between the two olefins for the C_2O , the amount of C_3H_4 product decreased rapidly as propylene or *cis*-2-butene was added. Consequently, the reproducibility of the propadiene/propyne ratios was poor. The large

(6) R. B. Cundall, A. S. Davies, and T. F. Palmer, *J. Phys. Chem.*, **70**, 2503 (1966).

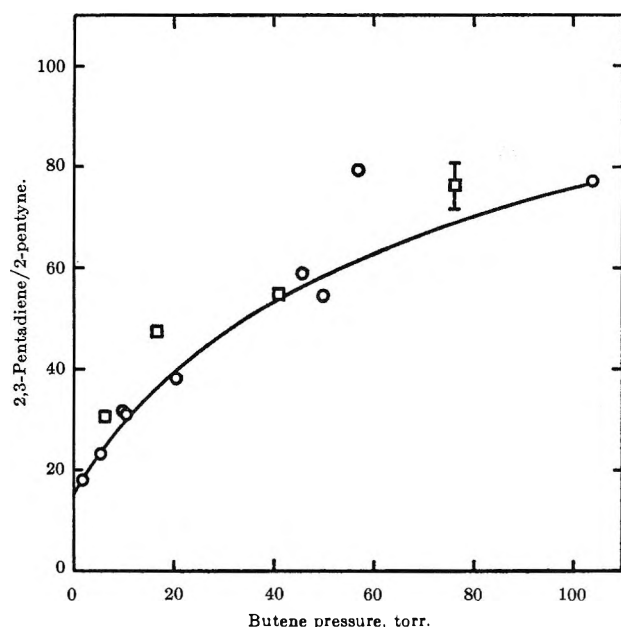


Figure 2. The ratio of isomers formed during the photolysis of C_3O_2 -olefin mixtures as a function of the olefin pressure. The *cis*-2-butene runs (O) used 2 torr of C_3O_2 at the lowest butene pressures and 5-10 torr at higher pressures. The *trans*-2-butene runs (□) used 5 torr of C_3O_2 . Both experiments were done using 3000 ± 15 Å light at $25 \pm 5^\circ$. The solid line is fitted to the *cis*-2-butene results.

Table I: The Products Formed by the Photochemical Reaction of Carbon Suboxide with Various Olefins^a

Olefin	Product	Percentage
Ethylene	Propadiene	83
	Propyne	17
Propylene	1,2-Butadiene	84
	1-Butyne	15
	1,3-Butadiene	~1
<i>cis</i> - or <i>trans</i> -2-Butene	2,3-Pentadiene	94
	2-Pentyne	6
2,3-Dimethyl-2-butene	2,4-Dimethyl-2,3-pentadiene	100

^a The percentages have been extrapolated to zero pressure. Isomers not listed either were not observed or were present in such small amounts (<1%) that identification was uncertain.

difference in the effect of these two classes of compounds will be discussed later.

A few measurements were made with propylene- C_3O_2 mixtures to investigate the ratio of isomers in the limit of high pressures. The results are plotted in Figure 4 on a reciprocal pressure plot, so that the extrapolation to infinite pressure can be made. In order to join the points measured in pure propylene with those

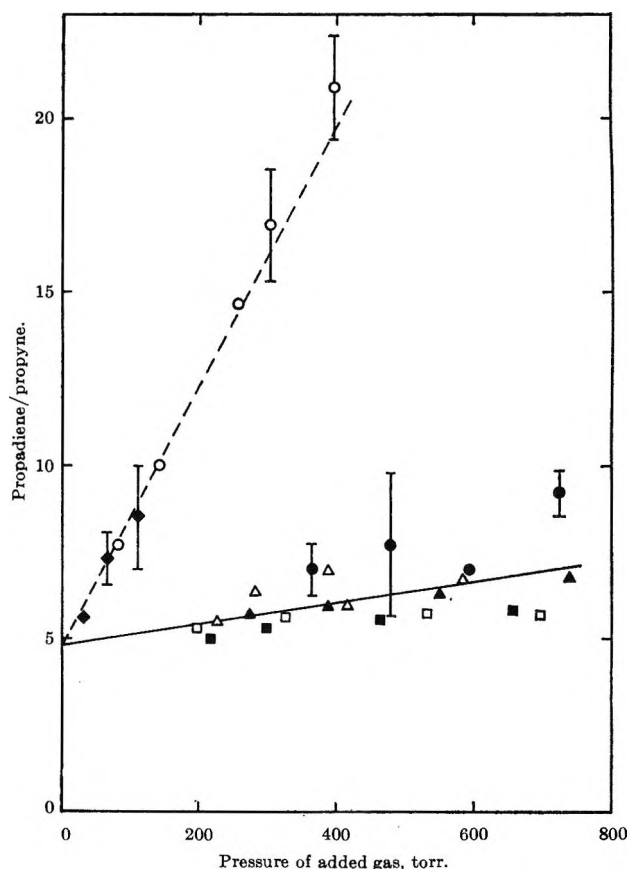


Figure 3. The effect on the propadiene/propyne ratio as other gases are added. All runs were made with 2.7-4.6 torr of C_3O_2 and 17-22 torr of ethylene. Added gases: □, argon; ■, krypton; Δ, nitrogen; ▲, carbon dioxide; ●, isobutane; ○, *cis*-2-butene; ◆, propylene. Runs with added He and H_2 showed little pressure effect. The lower solid line is taken from the ethylene runs of Figure 1.

pressurized with CO_2 , the effectiveness of CO_2 has been taken as half that of propylene. When this is done, the two sets of data fall on a smooth line which can be extrapolated to a finite intercept at infinite pressure. This result suggests that the straight line shown in Figure 1 for propylene bends over at higher pressure. A similar effect in *cis*-2-butene can be observed in Figure 2.

Discussion

The dominance of the allene isomers requires an explanation since the acetylenes are more stable thermodynamically. The heat of formation of propyne is 1.6 kcal/mole less than that of propadiene.⁷ The experimental equilibrium constant predicts that propyne will

(7) F. D. Rossini, *et al.*, "Selected Values of Physical and Thermodynamic Properties of Hydrocarbons and Related Compounds," Carnegie Press, Pittsburgh, Pa., 1953.

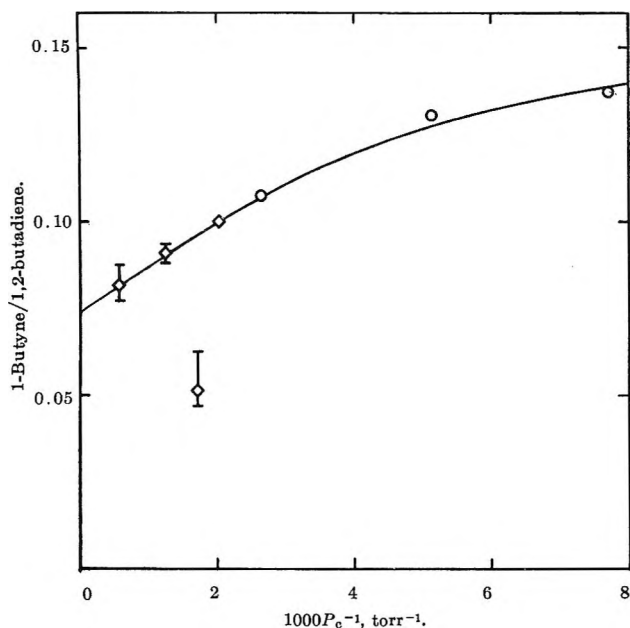


Figure 4: The effect of high pressures on the ratio 1-butyne/1,2-butadiene: open circles, propylene runs shown in Figure 1; diamond symbols, runs with 85 ± 3 torr of propylene with CO_2 added. The corrected pressure, P_c , is taken as the pressure of propylene plus half the pressure of CO_2 . All runs used approximately 15 torr of C_3O_2 .

exceed propadiene at all temperatures.⁸ Since the opposite is observed, some effect other than thermal equilibrium must be involved.

Consideration of the amount of energy contained in the newly formed allene molecules suggests another explanation. Using a heat of formation of $\text{C}_2\text{O}(X^3\Sigma)$ of 93 ± 5 kcal/mole,⁹ then the over-all reaction



would be 86 ± 5 kcal/mole exothermic. Although some of this energy may be removed by the leaving CO molecule, the majority of the energy should remain with C_3H_4 . This is certainly sufficient energy to excite C_3H_4 to its lowest excited electronic state.

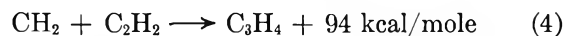
The energy of the lowest triplet state of propadiene is not known experimentally. However, the triplet state of ethylene is at 82 kcal/mole,¹⁰ and it is likely that propadiene, which involves bonding similar to that of ethylene but with a larger carbon framework, would have a triplet energy lower than 82 kcal/mole. A recent calculation placed the lowest triplet state of propadiene at 67 kcal/mole above the ground state.¹¹ More significantly, the calculation concluded that the lowest triplet state would have a planar configuration, in contrast to the ground state which has the two CH_2 groups in perpendicular planes. A planar configura-

tion for the product of reaction 3 is ideal, since the C_2O is donating a carbon atom to a planar olefin.

Spin conservation also favors the initial formation of a triplet-state C_3H_4 in reaction 3. The first triplet state of CO is at much too high an energy to be excited. Therefore the triplet nature of the C_2O molecule should be preserved, at least initially, in the C_3H_4 product. Thus arguments based on the geometry of the newly formed molecule and on spin conservation favor the initial formation of a triplet-state $\text{C}_{n+1}\text{H}_{2n}$ molecule, and estimates of the energies involved are in accord with such a reaction.

If the newly formed product is in a triplet state, then the dominance of the allene isomers becomes understandable. Although not known experimentally, the triplet states of allenes are probably lower in energy than the triplet states of the corresponding acetylene isomers. The first excited singlet state of propadiene is lower in energy than that of propyne,¹² and a similar relation is expected for the lowest triplet states. Then applying a density of states argument to the equilibration between the two isomers in their triplet states, the propadiene will be favored, in agreement with the observed products.

Two other studies support the triplet-state hypothesis given above. By coincidence, the reaction of CH_2 with C_2H_2 forms a C_3H_4 molecule with an energy content comparable to that formed in reaction 3¹³



In addition, if CH_2 is in its triplet ground state, a triplet state of C_3H_4 should be formed initially. It is most relevant then that when reaction 4 takes place in a low-temperature matrix, where collisions of CH_2 with the lattice atoms should assure that the CH_2 is in its ground triplet state, only propadiene is observed.¹⁴

Callear and Cvetanović¹⁵ studied the mercury-sensitized isomerization of *cis*-1,2-dideuterioethylene and

(8) J. F. Cordes and H. Grunzler, *Chem. Ber.*, **92**, 1055 (1959).

(9) This value is derived from the apparent exothermicity of 206 ± 5 kcal/mole for the reaction $\text{C}_2\text{O} + \text{O} \rightarrow 2\text{CO}$: K. H. Becker and K. D. Bayes, *J. Chem. Phys.*, **45**, 396 (1966). For a discussion of possible values see ref 4.

(10) D. F. Evans, *J. Chem. Soc.*, 1735 (1960).

(11) W. T. Borden, *J. Chem. Phys.*, **45**, 2512 (1966).

(12) G. Herzberg, "Molecular Spectra and Molecule Structure, III. Electronic Spectra and Electronic Structure of Polyatomic Molecules," D. Van Nostrand Co., Inc., Princeton, N. J., 1966, p 640.

(13) The ΔH_f° of $\text{CH}_2(X^3\Sigma)$ has been taken as 86 kcal/mole as recommended by H. M. Frey, *Progr. Reaction Kinetics*, **2**, 131 (1964).

(14) M. E. Jacox and D. E. Milligan, *J. Am. Chem. Soc.*, **85**, 278 (1963).

(15) A. B. Callear and R. J. Cvetanović, *J. Chem. Phys.*, **24**, 873 (1956).

found, in addition to the expected *trans*-1,2-dideuterio isomer, comparable amounts of the 1,1-dideuterio-ethylene. Formation of the 1,1 isomer from the 1,2 requires migration of the hydrogen atoms along the double bond. Just this type of migration is needed to convert propadiene into propyne. Demonstration of such migration for triplet-state ethylene supports the hypothesis of a triplet state for the newly formed C_3H_4 in the carbon suboxide-ethylene photolysis.

The proposed triplet state for the initially formed allene finds support in the effects of added gases on the propadiene/propyne ratio. Cundall and co-workers¹⁶ studied the *cis-trans* isomerization of olefins by triplet-state sensitizers and concluded that triplet-triplet energy transfer occurred on nearly every collision when the collision partner had a triplet-state energy level comparable to or below that of the sensitizer. However, when the triplet state of the collision partner was above that of the sensitizer, energy transfer was much slower. A similar mechanism should operate for the deactivation of triplet-state propadiene. Molecules with low-lying triplet states should accept electronic energy from triplet propadiene on nearly every collision, thereby preventing isomerization. Gases having triplet states higher than propadiene should be poor stabilizers. The two types of behavior seen in Figure 3 fit into such a classification (*cf.* Figure 5 of ref 16). If correct, this interpretation requires that the triplet state of propadiene be lower than the triplet state of ethylene (<82 kcal/mole), but above or comparable to that of propylene and *cis*-2-butene (~70 kcal/mole).

If *cis*-2-butene is being excited to its triplet state by energy transfer from propadiene, then some *trans*-2-butene should be formed when the butene triplet is finally deactivated. Some *cis-trans* isomerization was observed in these experiments, but quantitative measurements were not made. Recently, Cundall, *et al.*,⁶ observed *cis-trans* isomerization during the photoreaction of carbon suboxide with *cis*-2-butene at 3100 Å. They concluded that the *cis-trans* isomerization probably was being caused by a triplet state of C_3O_2 which did not undergo decomposition. The above hypothesis offers a simpler explanation, namely, that the newly formed C_5H_8 product (as well as the $C_4H_8 \cdot C_2O$ adduct) is in a triplet state and can transfer its energy to a *cis*-2-butene molecule which can then isomerize. This interpretation explains both the strong influence of *cis*-2-butene on the propadiene/propyne ratio (Figure 3) and the formation of *trans*-2-butene without the new postulate of a nondecomposing triplet state of C_3O_2 .

Since the ratio of isomers depends on pressure, the over-all reaction must involve at least two steps which differ in their pressure dependence. Triple collisions

should not be important because these effects are observed at low pressures (*e.g.*, at less than 10 torr for the butenes). Therefore, a reasonable mechanism will contain only first- and second-order steps. The nature of the first-order step determines the mechanism of isomerization.

The addition reaction generates molecules with a considerable excess of internal energy. If the unimolecular step involves the emission of radiation by these energetic molecules, in competition with collisional stabilization, the observed pressure dependence could be explained. However, a search failed to show any significant chemiluminescence in the range 3000-10,000 Å (see Experimental Section). Emission further in the infrared region should be too slow to compete with vibrational relaxation. Therefore, light emission cannot be the pressure-independent step.

Isomerization or intersystem crossing of excited $C_{n+1}H_{2n}$ and decomposition of the C_2O -olefin adduct provide alternative unimolecular steps. Mechanisms can be constructed around any of these possibilities to give an equation of the general form

$$\frac{\text{isomer 1}}{\text{isomer 2}} = \frac{A + BM}{1 + CM} \quad (5)$$

where A , B , and C represent collections of rate constants, and M is the total pressure. This equation gives different ratios of isomers in the limits of high and low pressures and has an approximately linear dependence on M at low pressures, which is the behavior observed above.

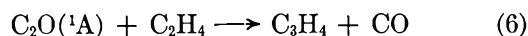
For example, if isomerization of excited $C_{n+1}H_{2n}$ is the unimolecular step, then a mechanism could consist of the initial formation of an intermediate I_1 , which could be stabilized to form both isomers, as well as undergo a reversible isomerization to I_2 , which when stabilized gives a different ratio of isomers. Thus, I_1 might be the triplet state of propadiene and I_2 could be the triplet state of propyne.

Decomposition of a C_2O -olefin adduct is an attractive unimolecular step, since it is known that pressure affects the over-all hydrocarbon yield.⁴ For example, if the addition of C_2O to the olefin forms two adducts, I and I' , which differ in their behavior (perhaps owing to slightly different geometries or energies), then both adducts will contribute to the isomer formation at low pressures, while the adduct which is less susceptible to pressure quenching will have the greater influence on the isomer ratio at high pressures. Again a dependence on pressure in the form of eq 5 may be derived. This

(16) R. B. Cundall, F. J. Fletcher, and D. G. Milne, *Trans. Faraday Soc.*, **60**, 1146 (1964).

possibility is supported by noting that the pressures necessary to cause a 50% decrease in hydrocarbon yield (20 torr for *cis*-2-butene and 250 torr for propylene; see Figure 3 of ref 4) result in an isomer ratio approximately halfway between the high- and low-pressure limits (see Figures 1 and 2).

One argument against the participation of a triplet-state product is that similar behavior is observed at shorter wavelengths. It has been proposed that the different reactivity observed at 2500 Å, as compared to photolysis at $\lambda > 2900$ Å, is the result of the formation of C_2O in a singlet state at the shorter wavelengths.³ The spin conservation rule then requires that the reaction



form only singlet-state products. However, the same products are observed from the C_3O_2 -olefin photolysis at 2500 Å as at 3000 Å. Although the intercepts and slopes are different in the short-wavelength photolysis, the behavior is similar to that shown in Figures 1 and 2. The similar behavior for the two systems implies that a similar mechanism is operating. If a triplet-state

intermediate is involved at the long-wavelength photolysis, as supported above, then the initially formed singlet intermediate, which will have more energy than the corresponding intermediate formed from $C_2O(X^3\Sigma)$, may undergo intersystem crossing, perhaps with the aid of the CO group. This hypothesis would explain both the similar isomerization behavior (but not necessarily identical behavior since different energies are involved) and the observation of *cis-trans* isomerization at 2500-Å photolysis.⁶

In summary, the products formed by the addition of $C_2O(X^3\Sigma)$ to olefins are expected to be in triplet states. There is strong experimental evidence in support of this: the dominance of the thermodynamically less stable allenes over the acetylenes, the selective effects observed in Figure 3, and the observation of *cis-trans* isomerization. It is not possible at the present time to select a specific mechanism for the variation of isomer ratio with experimental conditions.

Acknowledgments. We wish to thank the National Science Foundation for financial support through Grant GP-2489.

The Adsorption of Methanol Vapor on Silver Iodide¹

by Harry W. Edwards² and M. L. Corrin

Department of Chemistry, The University of Arizona, Tucson, Arizona (Received October 24, 1966)

The adsorption of methanol vapor on silver iodide was measured at 9.77, 19.79, and 30.02° over the pressure range 0.24–108 mm. The silver iodide was prepared by the reaction of silver and iodine *in vacuo* with subsequent liquid ammonia treatment. The adsorption isotherms do not fit into the Brunauer classification. The shape of the isotherms indicates the absence of three-dimensional clustering in the adsorbed phase. The dependence of the isosteric heats of adsorption upon surface coverage reveals the dual nature of the silver iodide surface. The surface is heteroenergetic with approximately 12% of the surface consisting of higher energy sites located patchwise over the surface. Selection of methanol vapor as the adsorbate eliminated three-dimensional clustering in the adsorbed phase due to hydrogen bonding, and thus characterization of the silver iodide surface was straightforward.

Introduction

Interest in silver iodide as a nucleant for supercooled water vapor stems from the report by Vonnegut³ that finely divided silver iodide in the form of a smoke produces ice crystals from supercooled water vapor at temperatures below -4° . Although silver iodide was originally selected on the basis of its similarity to ice in crystal structure, it is now generally recognized⁴ that the surface properties of the solid may play a major role in the mechanism of heterogeneous nucleation of supercooled water vapor.

Attempts to characterize the silver iodide surface in terms of its interaction with water vapor are in disagreement both as to the nature and to the extent of the silver iodide surface.^{5–11} In two cases,^{5,11} where the adsorption of water vapor was measured on silver iodide prepared by aqueous precipitation, the presence of surface contaminants was reported. In fact, there is strong evidence that silver iodide prepared by aqueous precipitation is always contaminated to some extent with counterions present during precipitation.¹² This result casts considerable doubt on the validity of measurements of water adsorption made on silver iodide samples prepared by aqueous precipitation; it is clear that the discrepancies may be due to the presence of varying amounts of surface contaminants.

In an earlier paper,¹³ we reported the preparation of silver iodide free of hygroscopic impurities and its

interaction with water vapor. Silver iodide was prepared in finely divided form by the reaction *in vacuo* between metallic silver and iodine and subsequent treatment with liquid ammonia. Comparison of the water vapor adsorption isotherm for this material at 30° with that of silver iodide prepared by aqueous precipitation reveals a gross difference in the behavior of the two preparations. The amount of water adsorbed per unit

(1) This paper is based, in part, on the dissertation of H. W. Edwards submitted to the faculty of the Department of Chemistry in partial fulfillment of the requirements for the degree of Doctor of Philosophy in the Graduate College of The University of Arizona, 1966.

(2) Department of Mechanical Engineering, Colorado State University, Fort Collins, Colo. 80521.

(3) B. Vonnegut, *J. Appl. Phys.*, **18**, 593 (1947).

(4) N. H. Fletcher, *Z. Angew. Math. Phys.*, **14**, 487 (1963).

(5) L. V. Coulter and G. A. Candela, *Z. Elektrochem.*, **56**, 449 (1952).

(6) S. J. Birstein, *J. Meteorol.*, **12**, 324 (1955).

(7) F. E. Karasz, W. M. Champion, and G. D. Halsey, Jr., *J. Phys. Chem.*, **60**, 376 (1956).

(8) N. M. Moskvitin, M. M. Dubinin, and A. I. Sakharov, *Izv. Akad. Nauk SSSR, Otd. Khim. Nauk*, **122**, 840 (1958); *Bull. Acad. Sci. USSR, Div. Chem. Sci.*, **23**, 2080 (1959).

(9) A. C. Zettlemoyer, N. Tcheurekdjian, and J. J. Chessick, *Nature*, **192**, 653 (1961).

(10) P. G. Hall and F. C. Tompkins, *Trans. Faraday Soc.*, **58**, 1734 (1962).

(11) N. Tcheurekdjian, A. C. Zettlemoyer, and J. J. Chessick, *J. Phys. Chem.*, **68**, 773 (1964).

(12) M. L. Corrin and N. S. Storm, *ibid.*, **67**, 1509 (1963).

(13) M. L. Corrin, H. W. Edwards, and John A. Nelson, *J. Atmospheric Sci.*, **21**, 565 (1964).

surface area at relative pressures exceeding 0.5 is considerably greater for the silver iodide prepared by aqueous precipitation. This result shows that the interaction between the silver iodide surface and water vapor is highly sensitive to small amounts of surface impurities.

The measurements reported in this paper were carried out to characterize further the silver iodide surface resulting from the direct reaction preparation. Interpretation of water vapor adsorption on silver iodide in terms of the silver iodide surface is complicated by three-dimensional clustering of adsorbate molecules in the adsorbed phase.^{10,11} The stacking effect for water is attributed to intermolecular hydrogen bonding in the adsorbed phase. In this investigation methanol vapor was selected as the adsorbate to simplify interpretation of the thermodynamic data. The simplification results in effect from the substitution of a methyl group (methyl hydrogens are essentially inactive with respect to hydrogen bonding) for a hydrogen atom in the water molecule.

The orientation of a polar molecule in an adsorbed phase has been examined in detail by Harkins for a large number of systems.¹⁴ The principle governing the orientation of polar molecules at an interface is that molecules are arranged to provide the least abrupt energetic transition between phases. For the adsorption of a gas on a solid, this principle rules out as thermodynamically unfavorable the formation of a surface of higher free energy than the bare surface. A similar argument was used by Langmuir to determine the orientation of molecules at an interface by attributing a local surface free energy to each portion of the molecule.¹⁵

The orientation of adsorbed methanol on a solid surface is dependent upon the nature of the solid surface. On the hydrophobic graphitized carbon black surface, Avgul', *et al.*, reported a planar orientation for adsorbed methanol.¹⁶ In the case of a polar ionic crystal, however, the adsorbed methanol molecule is oriented perpendicularly to the surface with the hydroxyl function adjacent to the surface.¹⁷ In neither of the two cases cited, which represent relative extremes of adsorbent surface structure and energy, was three-dimensional adsorbate cluster formation observed. It is important to note that perpendicular orientation of the methanol molecule with the methyl group adjacent to the surface does not occur even for the graphitized carbon black since the surface resulting from such an arrangement would be of higher free energy than the bare surface. Stacking of methanol molecules at less than monolayer coverages is similarly ruled out as an energetically unfavorable configuration. Variations

in the thickness of the adsorbed phase, however, could be expected after completion of the first monolayer.¹⁸

The choice of methanol vapor as the adsorbate thus provides a means for characterizing the silver iodide surface in terms of its interaction with the hydrophilic hydroxyl group in the absence of three-dimensional clustering effects which have been reported for the adsorption of water vapor on silver iodide. The simplicity of methanol adsorption at less than monolayer coverages apparently results from the fact that methanol is capable of forming only one intermolecular hydrogen bond per molecule.

Experimental Section

Two separate volumetric systems were constructed to obtain the methanol adsorption isotherm data. The low-pressure system employing a McLeod gauge was used for pressure measurements below 5 mm. The difference in height between the columns of mercury in the gauge was measured with a Gaertner telemicroscope fitted with a bifilar eyepiece. A precision-divided stainless steel scale was rigidly mounted directly behind the arms of the McLeod gauge; the smallest division on the scale was 1 mm. The bifilar eyepiece provided approximately 100 divisions between two adjacent 1-mm divisions inscribed on the scale. Using this arrangement, heights could be estimated to the nearest 0.002 mm.

Pressure measurements above 5 mm were made with the high-pressure system which employed a wide-bore mercury manometer as the primary pressure-measuring device. The wide-bore manometer was joined to the adsorption system through a capillary null manometer¹⁹ so that the volume of the adsorption system could be adjusted to the same value for all high pressure measurements. The difference in height between the columns of mercury in the wide-bore manometer was measured with a cathetometer which could be read to 0.01 mm.

In both systems mercury float valves and mercury cutoffs were employed. Prior to adsorption measurements, the systems were thoroughly outgassed for a period of at least 1 week until the system pressure de-

(14) W. D. Harkins, "The Physical Chemistry of Surface Films," Reinhold Publishing Corp., New York, N. Y., 1952.

(15) I. Langmuir, "Colloid Symposium Monograph," The Chemical Catalog Co., Inc., New York, N. Y., 1925, p 48.

(16) N. N. Avgul', G. I. Berezin, and A. V. Kiselev, *Izv. Akad. Nauk SSSR, Otd. Khim. Nauk*, 205 (1961).

(17) V. E. Vasserberg, A. A. Balandin, and M. P. Maksimova, *Zh. Fiz. Khim.*, 35, 858 (1961).

(18) W. D. Harkins, "The Physical Chemistry of Surface Films," Reinhold Publishing Corp., New York, N. Y., 1952, p 245.

(19) W. D. Harkins and G. Jura, *J. Am. Chem. Soc.*, 66, 1366 (1944).

creased to 2×10^{-7} mm. Since it has been reported that silver iodide sinters appreciably at 50° ,¹² heating could not be employed to accelerate the rate of out-gassing.

Adsorption measurements were carried out at 9.77, 19.79, and 30.02° . Three Philadelphia differential thermometers were used for temperature measurements, one for each of the three isotherm temperatures. Each of the thermometers was calibrated against a platinum resistance thermometer certified by the National Bureau of Standards. The uncertainty in reading the differential thermometers was 0.005° . The temperature of the adsorbent cell was regulated with a water bath equipped with a heating unit and a refrigeration unit. The control unit for the bath was fitted with a thermistor temperature transducer which was found sufficient for temperature control of $\pm 0.01^\circ$.

The silver iodide was prepared by the direct reaction of silver and iodine *in vacuo* with subsequent liquid ammonia treatment by the method reported earlier.¹³ The specific surface area of the silver iodide was determined by application of the BET relation to krypton adsorption isotherm data at 76.7°K . At the time of the low-pressure measurements the surface area was found by this method to be $1.14 \text{ m}^2/\text{g}$. After 3.5 months, at the time of the high-pressure measurements, the BET surface area of the silver iodide was found to have decreased to $0.84 \text{ m}^2/\text{g}$. The silver iodide was stored in a low-actinic Pyrex flask which was kept in a blackened vacuum desiccator. After each opening, the desiccator was promptly evacuated through a trap cooled to liquid nitrogen temperature.

The methanol was obtained as Mallinckrodt anhydrous methanol (acetone free) which the manufacturer specified to be greater than 99.5% CH_3OH and less than 0.05% H_2O . This material was refluxed over magnesium turnings in a closed system fitted with a mercury blow-off tube for hydrogen venting. The middle fraction of the distillate was thoroughly degassed and retained as the methanol source.

A volumetric method was used to obtain both the low- and high-pressure adsorption data. In the low-pressure system the McLeod gauge was used both as a doser and to measure the equilibrium pressure in the adsorption system. The temperature variation method was employed in both systems so that a single sample of silver iodide could be used to obtain the adsorption data at all three isotherm temperatures. After admission of a dose of methanol to the adsorption system, a period of at least 6 hr was allowed for the pressure in the system to attain a constant value.

The 6-hr period was adequate for attainment of equilibrium since in every case the pressure became

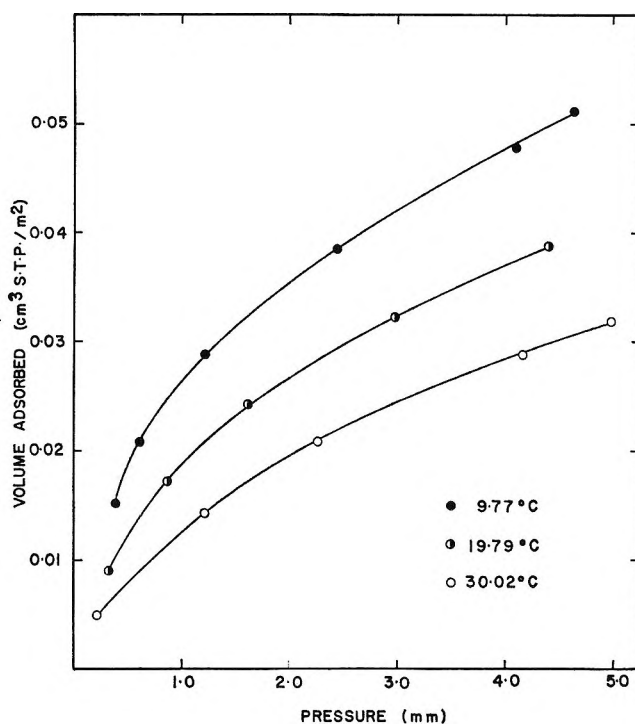


Figure 1. Low-pressure methanol adsorption isotherms.

invariant with time within a few minutes after admission of each dose of methanol vapor.

The low-pressure adsorption data were corrected for the amount of methanol taken up by the adsorption apparatus. Low-pressure blank isotherms were measured for determination of this correction. The correction was found to be negligible with respect to the high-pressure adsorption.

The points plotted in Figures 1 and 2 represent the experimental adsorption points; desorption points fell on the adsorption curves within the precision of the experiment.

Results and Discussion

The amount of methanol adsorbed as a function of pressure and temperature is shown in Figures 1 and 2. Although the adsorption at low pressures shown in Figure 1 is typical of physical adsorption at low coverages, the adsorption at higher pressures shown in Figure 2 does not fit into any of the five general categories described by Brunauer.²⁰ Type II adsorption, characterized by an initially decreasing and then increasing isotherm slope, corresponds to multilayer adsorption or three-dimensional stacking of adsorbate molecules. The concavity of the methanol adsorption

(20) S. Brunauer, "The Adsorption of Gases and Vapors," Vol. I, Princeton University Press, Princeton, N. J., 1945.

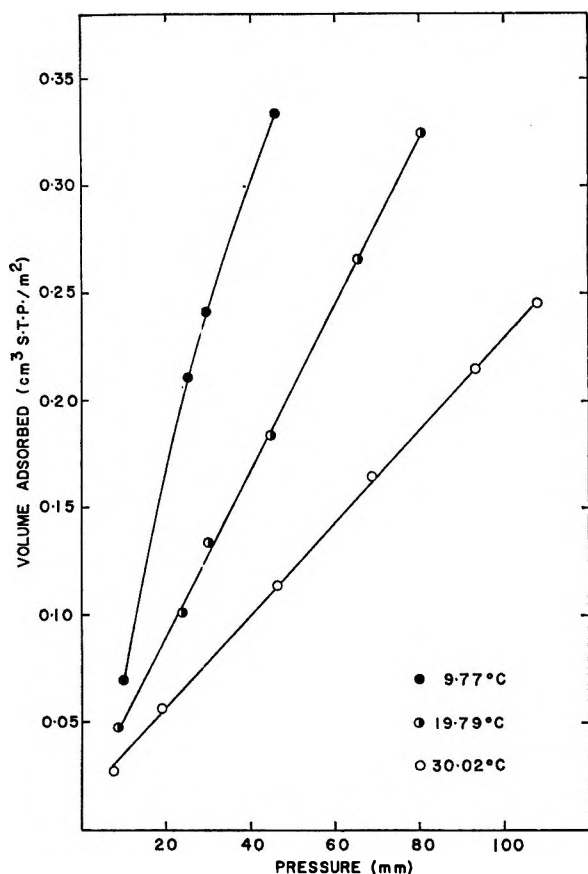


Figure 2. High-pressure methanol adsorption isotherms.

isotherms toward the pressure axis, *i.e.*, $(\partial^2 v / \partial p^2)_T < 0$, persists at higher coverages indicating that the adsorption is not type II. Multilayer formation and three-dimensional stacking of adsorbate molecules evidently do not occur in the range of pressures measured. From an energetic point of view, this behavior indicates that adsorption of methanol vapor upon the partially covered silver iodide surface does not favorably alter the free energy lowering of the system for additional methanol adsorption. This result is in sharp contrast with the usual case of type II adsorption.

The adsorption data shown in Figures 1 and 2 are based on the specific surface areas of the silver iodide at the time of adsorption measurements, 1.14 m²/g for the low-pressure measurements and 0.84 m²/g for the high-pressure measurements. Since the low- and high-pressure isotherms do not join, *e.g.*, the high-pressure points falling below the extrapolated low-pressure isotherms, a concomitant change in surface properties occurred with the decrease in surface area. Although the decrease in surface area of silver iodide with time has been reported previously,^{11,12} the observations were

made for silver iodide samples resulting from solution preparation which were contaminated to some extent by coprecipitated ionic compounds. Tcheurekdjian, *et al.*,¹¹ reported a 56-fold decrease in surface area for a silver iodide sample with no change in the number of polar sites. However, the work reported herein indicates that the higher energy sites on the silver iodide surface resulting from the direct reaction preparation are unstable with respect to time. The decrease in the number of higher energy sites is shown by the adsorption data. The fact that the amount adsorbed per unit area for the high-pressure data falls below the extrapolated low-pressure isotherms indicates a decrease in the number of high energy sites which are responsible for adsorption at low coverages.

Isosteric heats of adsorption were calculated in the usual manner by application of a form of the Clausius-Clapeyron relation to the adsorption isotherm data.²¹ The heat of adsorption is shown as a function of amount adsorbed in Figures 3 and 4. The estimated standard deviation for the low-pressure heats is 0.07 kcal/mole

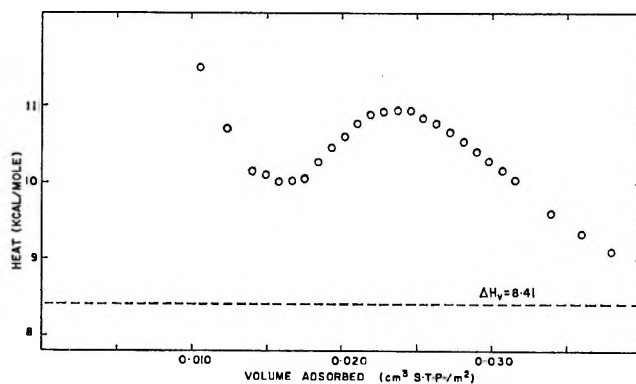


Figure 3. Isosteric heats of adsorption; low-pressure data.

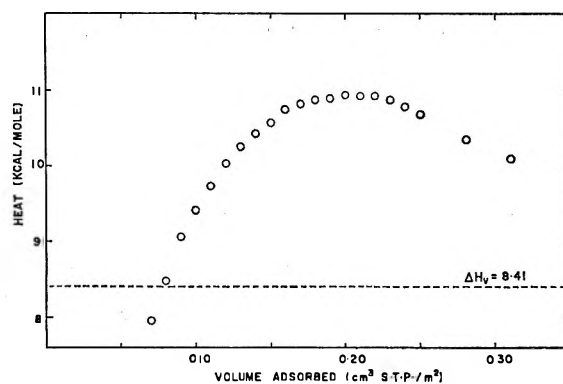


Figure 4. Isosteric heats of adsorption; high-pressure data.

(21) D. M. Young and A. D. Crowell, "Physical Adsorption of Gases," Butterworth and Co. Ltd., London, 1962.

and that for the high-pressure heats is 0.1 kcal/mole. The minimum in the low-pressure heat of adsorption curve occurs at 0.016 cm³/g and presumably results from the interplay of two opposing effects. As the higher energy sites are filled on a heterogeneous surface, the heat of adsorption decreases with increasing coverage. However, if the higher energy sites are located adjacent to one another on the surface, the cooperative effect in the adsorbed phase makes a positive contribution to the heat of adsorption. Thus the minimum in the isosteric heat of adsorption at this coverage results from the influence of the two opposing effects and constitutes strong evidence for a heteroenergetic silver iodide surface.

A maximum is observed in the low-pressure heat curve at 0.024 cm³/g. The maximum may also be interpreted in terms of the result of an interplay between two opposing effects. Although the contribution due to lateral interaction tends to increase the heat of adsorption, the number of lateral interactions decreases as the higher energy sites become completely occupied. The maximum in the low-pressure heat curve corresponds to an area per adsorbate molecule of 155 Å²; it is thus highly unlikely that monolayer formation has occurred over the entire surface. Evidently, pseudo-monolayer formation has occurred over the higher energy sites.

The higher pressure heat of adsorption curve given in Figure 4 shows a maximum at a coverage of approximately 0.20 cm³/g which corresponds to an area per adsorbate molecule of 19 Å². This value is in good agreement with the value of 17 Å² for the area of projection of an isolated methanol molecule calculated by Avgul', *et al.*,¹⁶ from van der Waals' dimensions. This result suggests that the methanol monolayer on silver iodide is less tightly packed than that for graphitized carbon black. Evidently, monolayer formation over the entire surface has occurred at 0.20 cm³/g. The

heat of adsorption then diminishes in the usual manner, presumably approaching the heat of liquefaction as the amount adsorbed increases.

A quantitative interpretation of physical adsorption on a heterogeneous surface in terms of molecular parameters requires evaluation of integral thermodynamic functions for the adsorption process. The spreading pressure was not calculated since the data were considered insufficient to permit meaningful extrapolation of the low-pressure isotherms to zero coverage. However, since the isosteric heat of adsorption is particularly sensitive to changes in the degree of lateral interaction in the adsorbed phase, it is concluded that the silver iodide surface has been fairly well characterized by this study. Selection of methanol vapor as the adsorbate eliminated three-dimensional clustering in the adsorbed phase due to hydrogen bonding. Interpretation of the thermodynamic data was therefore straightforward.

Perhaps the most significant conclusion that may be drawn from the work herein reported is that the silver iodide surface free of hygroscopic contaminants resulting from solution preparation is highly heteroenergetic, with about 12% of the surface consisting of the higher energy sites. It is also shown that the higher energy sites are not randomly distributed over the surface but occur patch-wise on the surface, as evidenced by the shape of the low pressure isosteric heat of adsorption curve. This work indicates that the hydrophilic sites resulting from the direct reaction preparation of silver iodide are very different from those resulting from contamination.

Acknowledgments. This research was supported by the Atmospheric Sciences Program, National Science Foundation, NSF Grant GP-5173. The award of a General Electric Foundation Fellowship in Chemistry to H. W. E. is gratefully acknowledged.

Photoinjection from Rhodium into Hydrocarbon Liquids under Visible Excitation

by Alfred Prock, Mihran Djibelian, and Susan Sullivan

Department of Chemistry, Boston University, Boston, Massachusetts 02215 (Received November 11, 1966)

Photoinjection from a rhodium electrode into hydrocarbon liquids and solutions of aromatic molecules has been observed to occur under sufficiently intense visible radiation. Benzene, cyclohexane, and benzene solutions of naphthalene, phenanthrene, anthracene, and pyrene were studied. The photoinjection wavelength threshold varied from that of the ultraviolet (for cyclohexane) to the deep red region (solutions of aromatic molecules). These differences are related to the electron affinities of the dissolved species and to the solvation energies of the radical anions produced.

This paper reports observations of apparent photoinjection which occurs from a rhodium electrode into hydrocarbon media under the stimulation of visible light. The liquids studied were cyclohexane, benzene, and benzene solutions of naphthalene, phenanthrene, anthracene, and pyrene; the light was from a short-arc xenon lamp with suitable combinations of liquid and interference filters. The effect is unusual in that light of low energy, 1.88 eV, is capable of producing photocurrents in the case of benzene solutions of the fused-ring aromatic compounds.

Photoinjection is the name given to the photoelectric effect when liquid rather than vacuum fills the space between electrodes.¹ Lack of photocurrent saturation, along with some small dependence of threshold wavelength on applied voltage, and other phenomena distinguish the photoinjection case from the photoelectric effect. Photoinjection has been studied using an aluminum cathode immersed in the liquid aliphatics, *n*-hexane and *n*-decane, under ultraviolet illumination¹⁻³ where it is found that the yield of photocurrent under given conditions is 2-3 orders of magnitude smaller than with vacuum present, but it is still 3 orders of magnitude larger than the dark current in the case of *n*-hexane. The photothreshold of aluminum, 4.1 eV, was found to remain nearly the same when immersed in *n*-hexane under low applied fields. Changes in threshold wavelength have been observed, on the other hand, as reported in a recent review by Adamczewski,⁴ where results are discussed for various elec-

trodes immersed in liquids and gases and some estimates of work function changes are given. More recently, response of metal surfaces in gases at high pressure has been reported,⁵ and the effect of chemisorbed gases⁶ in changing work function appeared to depend on the electron affinity of the adsorbed molecule.

In the present work the apparent lowering of the work function of rhodium is regarded to arise from the electron affinity of the dissolved species as well as from solvation energy of the ion formed. The analysis used here is similar to the first few steps in Matsen's analysis of reduction potentials for these fused-ring aromatics in a dioxane-water mixture.⁷ Along with some more recent estimates of electron affinity, these photoinjection results provide estimates of the solvation energies of these molecules in benzene solution.

Experimental Section

Apparatus. Light was supplied by an Osram 450-w xenon lamp with reflector and quartz condensers. The desired band was isolated using combinations of

- (1) M. J. Morant, *Nature*, **187**, 48 (1960).
- (2) D. W. Swan, *ibid.*, **190**, 904 (1961).
- (3) J. Terlecki and O. Gzowski, *Acta Phys. Austriaca*, **15**, 337 (1962).
- (4) J. Adamczewski, *Brit. J. Appl. Phys.*, **16**, 759 (1965).
- (5) D. H. Howling, *J. Appl. Phys.*, **37**, 1844 (1966).
- (6) R. Kh. Burshtein and N. A. Shurmovskaya, *Russ. Chem. Rev.*, **34**, 746 (1965).
- (7) F. A. Matsen, *J. Chem. Phys.*, **24**, 602 (1956).

Table I: Filter Combinations Used to Select Wavelength Regions

Region	Filters	Half band width, $m\mu$
Blue, 440 $m\mu$	2 cm circulating water + B and L { 90-5-440 45-2-540	40
Green, 540 $m\mu$	+ 1.5 cm saturated NaNO_2 + $\text{CuCl}_2, \text{CaCl}_2^a$	60
Orange, 600 $m\mu$	+ infrared filter CS-69 Corning + 1.5 cm saturated + B and L { 90-5-600 45-1-520	60
Red, 660 $m\mu$	+ $\text{K}_2\text{Cr}_2\text{O}_7$ + B and L { 90-5-660 45-1-520	65
Red, 745 $m\mu$	+ Schott Type AL	23

^a J. G. Calvert and J. N. Pitts, "Photochemistry," John Wiley and Sons, Inc., New York, N. Y., 1966, p 739.

liquid and interference filters so as to obtain sufficiently intense light. Table I lists the combinations for each band; the order of filters is the same as that in which they appear in the beam. The Bausch and Lomb (B and L) filters are normal incidence and dichroic interference filters, and the Schott filter is a normal incidence interference filter. These combinations were found to be very efficient in removing ultraviolet and undesired visible stray radiation and in reducing the infrared content to the point where heat effects were negligible. Adequate reduction of heat is seen experimentally in the lack of drift of the photocurrent; removal of ultraviolet is seen to be complete in that insertion of an extra saturated NaNO_2 filter in the beam causes only the small decrease in effect consistent with the visible transmission of the filter. For intensity variation experiments, neutral density filters of transmission 6.2, 24.4, and 51.7% (Industrial Optics, Bloomfield, N. J.) supplied with calibration curves were used. The light was focused on the cell and intensity was measured by substituting a CdS photoresistor for the cell; resistance was measured to within 1.5% error.

Dark currents and photocurrents were measured using a Cary Model 31 vibrating-reed electrometer with a shunt; the signal was recorded by a Leeds and Northrup Azar recorder. Noise level was 6×10^{-15} amp in favorable cases. Voltage was supplied by a Zener diode regulated supply; the usual applied potential was 112 v.

The cell is shown in Figure 1. The quartz stannous oxide coated electrode at the bottom presses against the ground and polished Pyrex base to make the seal. The surfaces fit well enough so that liquid leakage is no

problem. The rhodium-plated electrode passes through precision-bore tubing and is adjusted by the top micrometer arrangement. Stopcocks are glass "NO-LUB" type, and glass ball joints are used as connectors. A small pressure of oxygen-free nitrogen throughout the system prevents the entrance of significant amounts of oxygen or moisture. The cell can be heated prior to distillation up to 110° using a heat gun while nitrogen passes through it. Use of this kind of cell where liquid touches no gasket material was found necessary to eliminate the very large scatter of response noted when Viton and even Teflon gaskets came into contact with the solutions. The cell was supported on a spring-mounted plate to reduce microphonics and was enclosed by an aluminum shield, except for a hole at the base where shield and cell met for the light to enter. Nitrogen was allowed to flow into the shield throughout the duration of the experiment with the given solution.

Chemicals. Benzene and cyclohexane starting materials were fluorometry grade, Matheson Coleman and Bell. These were percolated through silica and alumina gel of chromatography grade, refluxed, and distilled over lithium aluminum hydride in a stream of nitrogen which was first passed over hot copper. As measured in the photocell at 23° (spacing 0.036 cm, constant 9.2 cm, applied voltage 112 v), apparent dark specific conductance was $1.5\text{--}2.5 \times 10^{-16}$ ohm⁻¹ cm⁻¹ for benzene⁸ and less than 2×10^{-17} for cyclohexane. Naphthalene, phenanthrene, and anthracene were obtained as zone refined, 99.99% purity, from James Hinton Co., Valparaiso, Fla. These were further chro-

(8) E. O. Forster, *J. Chem. Phys.*, **37**, 1021 (1962).

matographed on a silica gel column using spectroquality pentane as the eluent, by the method of Sangster and Ervine.⁹ This was a nontrivial step since it produced a lowering of dark conductivity by as much as a factor of 5 in the case of anthracene, and it removed a rectification effect of a factor of about 3 in the case of anthracene. This latter effect means larger conductivity for rhodium as the negative electrode. It is an effect which we had noticed before in connection with less extensively purified materials. Pyrene was prepared by the chromatography method mentioned before, zone refined, and rechromatographed to give a totally white product. This is the minimum extent of treatment which was found to remove rectification effects and to produce low dark currents in solution which were comparable with those of the first three aromatics. For all solutions studied the apparent dark conductivities were below $2 \times 10^{-15} \text{ ohm}^{-1} \text{ cm}^{-1}$ at 23° .

Results and Discussion

The photoelectric threshold for the rhodium electrode was determined in a nitrogen atmosphere using a short-arc mercury lamp, Osram HBO 200 W/2, and liquid filters with known cutoff points. The quartz condenser, a front-surface aluminum mirror, and a quartz container for liquids were the only components in the beam. A voltage of 112 v was applied between electrodes with rhodium negative; electrode spacing was 0.036 cm. The leakage current remained constant to within 6×10^{-15} amp down to the cutoff point of 1 cm of CCl_4 (Baker Spectrophotometric Quality, $265 \text{ m}\mu$) but rose "instantly" with a photocurrent of 5.3×10^{-12} amp when the filter liquid was CHCl_3 (Baker Spectrophotometric Quality, $245\text{-m}\mu$ cutoff). The effects were reproducible and are the result of several trials. A tenfold reduction in applied voltage produced

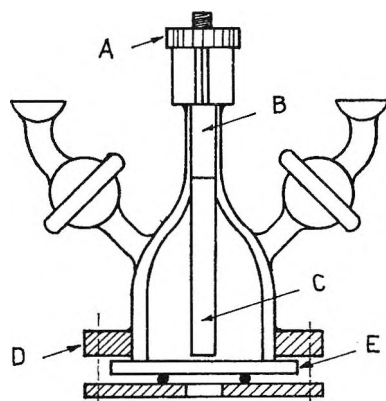


Figure 1. Photoconductivity cell: A, micrometer; B, Teflon seal; C, rhodium-plated rod; D, aluminum ring; E, quartz flat with stannous oxide coating.

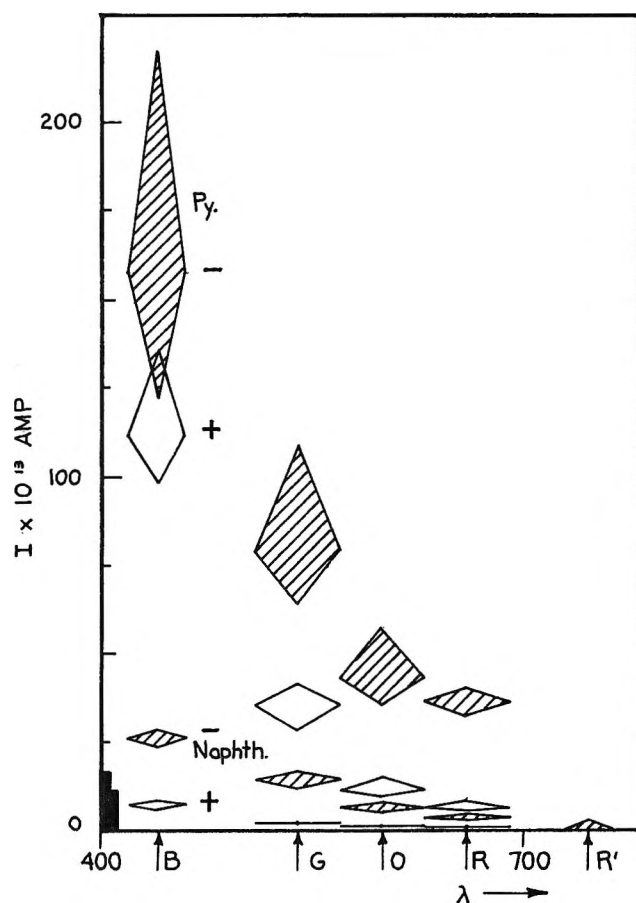


Figure 2. Photoresponse of pyrene (0.285 M) and of naphthalene (0.36 M) in benzene. Polarity of rhodium electrode is indicated at left. Vertical bars at lower left show dark currents of pyrene and naphthalene, respectively.

no detectable change in threshold wavelength and reduced photocurrent by a factor of 2.5. Reversal of polarity reduced the photocurrent by a factor of 10^2 . The apparent work function was thereby determined to lie between 4.7 and 5.1 eV, in reasonable agreement with the literature values¹⁰ for rhodium, between 4.6 and 4.9 eV for thermionic and photoelectric work functions.

With cyclohexane as the medium and the rhodium electrode negative no photocurrent was detected down to an incident wavelength of $315 \text{ m}\mu$, the lower limit for the optical system used. However, with benzene as the medium a photocurrent was observed at $440 \text{ m}\mu$ which was about as large again as the dark current and easily measurable. That heating was not responsible for the effect was seen by the virtual absence of response when the rhodium was made positive; stray

(9) R. C. Sangster and J. W. Ervine, Jr., *J. Chem. Phys.* **24**, 670 (1956).

(10) "Handbook of Chemistry and Physics," 45th ed, Chemical Rubber Publishing Co., Cleveland, Ohio, 1964-1965.

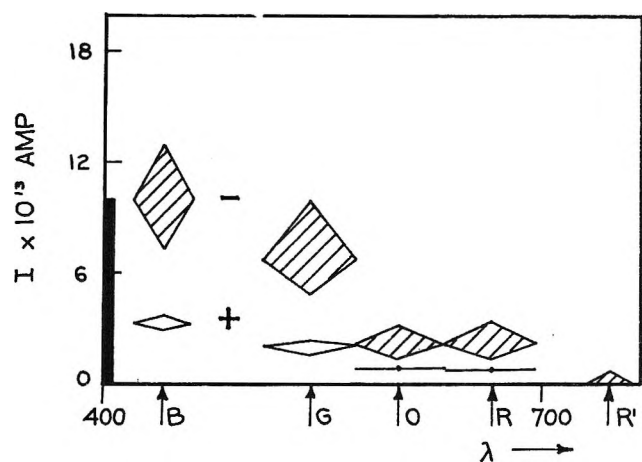


Figure 3. Photoresponse of phenanthrene (0.053 *M*) in benzene.

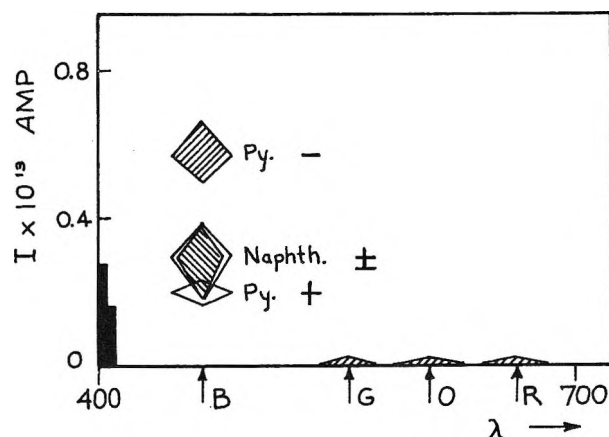


Figure 6. Photoresponse of pyrene (0.074 *M*) and of naphthalene (0.071 *M*) in cyclohexane.

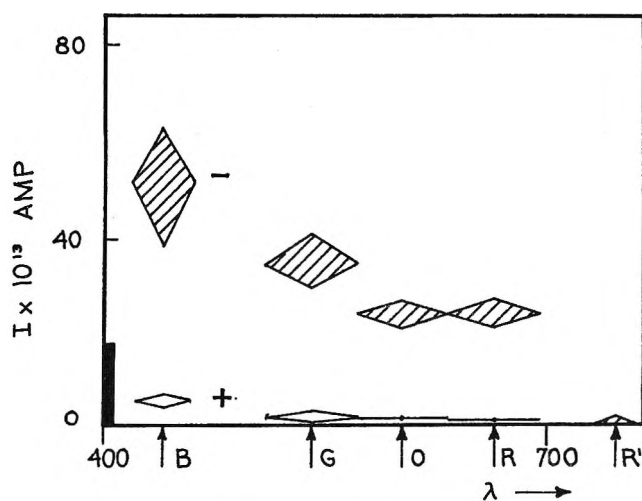


Figure 4. Photoresponse of anthracene (0.050 *M*) in benzene.

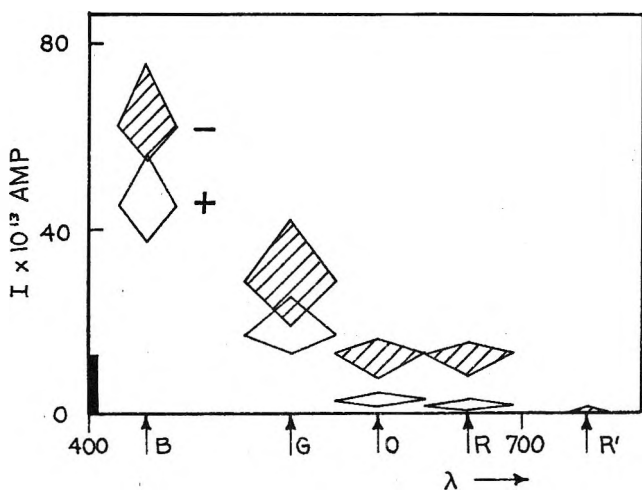


Figure 5. Photoresponse of pyrene (0.089 *M*) in benzene.

ultraviolet radiation was ruled out also by showing that insertion of an extra ultraviolet filter which transmits less than 1% below 440 $m\mu$ reduced the effect by only about 20%. There was no photocurrent evident for green light illumination.

The photoresponse of the benzene solutions of fused-ring aromatics is shown in Figures 2-5. (Figure 6 shows results for a cyclohexane solution.) The polarity shown on each graph is for the rhodium electrode. The vertical height of a mark indicates the scatter of data taken over a few days for each solution to observe whether there were any steady drifts in dark current or photocurrent; no such drifts were noticed. The vertical bar, or bars, at the lower left of each graph shows the average dark current under 112 v applied with a cell constant of 9.2 cm. As mentioned earlier, no significant dependence of dark current on electrode polarity was observed. The points have been normalized for an incident flux of 10^{17} photons $\text{sec}^{-1} \text{cm}^{-2}$, which is the actual measured flux for the 440- $m\mu$ region, where it has been assumed that photoresponse varies linearly with light intensity for all regions. This linearity is borne out for pyrene in the blue and green regions as shown in Figure 7. The photocurrents for all bands are seen to be larger with the rhodium as the negative electrode; for anthracene and naphthalene, the asymmetry of response is large in all regions, for pyrene it is largest in the long-wavelength region. Because the photocurrent shows this kind of polarity dependence but the dark current does not, the photocurrent is attributed to photoinjection, at least in the long-wavelength region near the threshold. In the case of pyrene the relatively large photocurrent seen in the blue and green regions with rhodium positive cannot be overlooked. A step in the mechanism which produces it may be excitation to the triplet state which lies 48.7

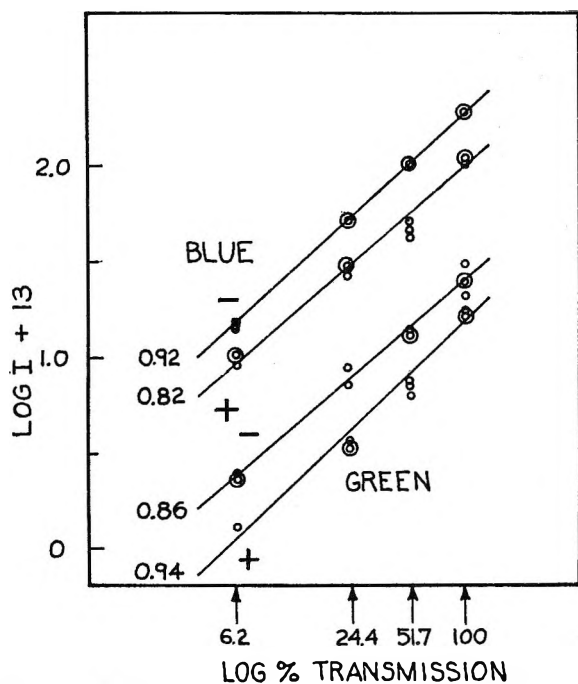


Figure 7. Plot of log of photocurrent vs. log of incident light intensity for pyrene (0.285 M) in benzene, for the blue- and green-wavelength regions, and for rhodium positive and negative.

kcal/mole (584 $m\mu$) above the ground state.¹¹ The question is under study and will be reported on in the future.

The role played by the solvent is a major one. Figure 6 shows the results for naphthalene and pyrene dissolved in cyclohexane. Photocurrents are 2 orders of magnitude smaller than those for benzene solutions and no effects are produced for light of longer wavelength than that of the blue region.

The large photocurrents produced with pyrene solutions under blue and green light excitation with rhodium positive appear to be intrinsic to pyrene and not due to impurities. Evidence for this comes from studies of light intensity dependence of photocurrent for this system and others. Results for pyrene are shown in Figure 7. The abscissa refers to the transmission of neutral density filters placed in the path of the beam. The intensity dependence is seen to be not far removed from a linear one for the conditions of the experiment. In contrast, Figure 8 shows the response under the same experimental conditions of a benzene solution of a pyrene sample kindly supplied to us by the National Bureau of Standards. This was chemically purified to a purity between 99 and 99.9% and then chromatographed on receipt by the method mentioned previously. Photocurrent is an order of magnitude larger for this material and depends more nearly on the square root of

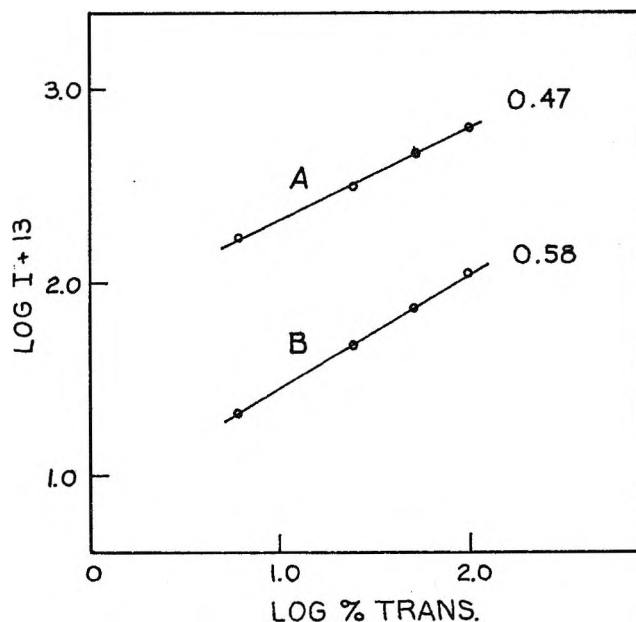


Figure 8. Plot of log of photocurrent vs. log of incident light intensity for a sample of chemically purified pyrene (0.142 M) in benzene. Rhodium polarity is positive: A, blue light; B, green light.

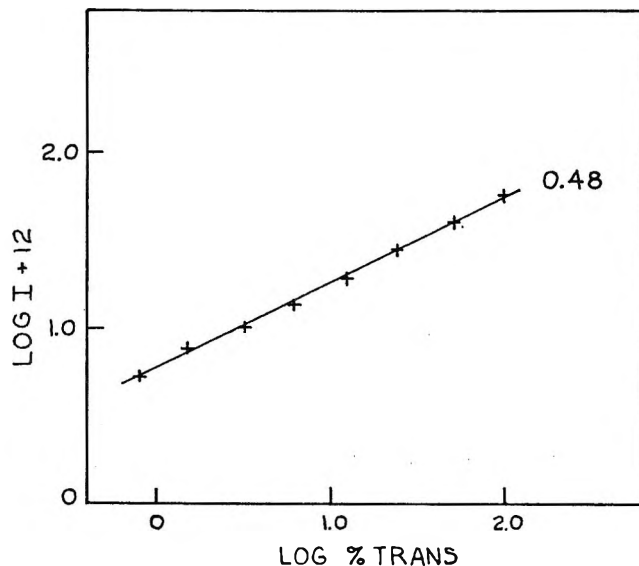


Figure 9. Plot of log of photocurrent vs. log of incident light intensity for pyranthrene ($2.5 \times 10^{-4} M$). Rhodium polarity is positive; the incident light is blue.

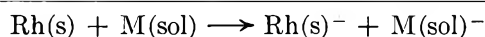
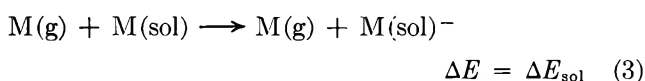
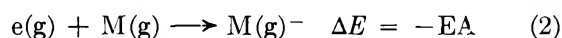
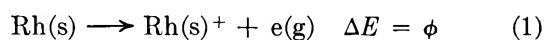
light intensity. The square root dependence is also seen, Figure 9, in the response of a benzene solution of pyranthrene, a fused-ring aromatic containing eight rings, in a strongly absorbing region of its spectrum.¹²

(11) W. G. Herkstroeter, A. A. Lamola, and G. S. Hammond, *J. Am. Chem. Soc.*, **86**, 4537 (1964).

(12) E. J. Clar, "Aromatische Kohlenwasserstoff Polycyclische Systeme," 2nd ed, Springer-Verlag, Berlin, 1952, p 380.

Finally, the square root dependence is observed in the intensity dependence of the pyrene prepared in this laboratory when it absorbs light in the near-ultraviolet region (345–400 m μ), which overlaps its region of strong singlet-singlet absorption. A sufficiently serviceable filter was made for this region using a series of cobalt blue glasses with ultraviolet filter, Corning CS 052, in addition to the circulating water and infrared filters mentioned before. It is clear that what is observed in the visible region arises from a different mechanism than that active in the ultraviolet region and that there is evidence that it is not due to a strongly absorbing impurity.

The large photocurrents which are measured when the rhodium electrode is negative appear to be explainable on the basis of a lowering of the work function of rhodium by the following scheme (compare Matsen⁷)



$$\Delta E = \phi - EA + \Delta E_{\text{sol}} = h\nu$$

where ϕ , EA, ΔE_{sol} , and M are work function in vacuum, molecule electron affinity, molecular solvation energy, and the molecule being considered, respectively. $h\nu$ represents the energy requirement of the reaction; it is the photoinjection threshold observed in the present experiments. ΔE_{sol} is the unknown in this equation, the work function is taken as 4.7 eV, and recent values for electron affinity are assumed. Table II presents the results. In the first column, the last four electron affinities are experimentally determined by the electron-capture method; the benzene value is a theoretical SCF value. The second column brackets the threshold photoemission wavelengths. The third column brackets the values determined for the solvation energies of the ions in benzene, and the last column lists solvation energies determined from polarographic experiments with 75% dioxane-water solutions along with electron affinities from the first column. The solvation energies obtained for benzene solution ($D = 2.28$) are seen to be comparable with those for dioxane-water solutions ($D = 25$); that is, they do not differ by the ratio of $1 - (1/D)$ correction factors,^{13,14} which is 1.7 for this

Table II

	EA, eV	λ , m μ	$-\Delta E_{\text{sol}}$ (benzene), eV	$-\Delta E_{\text{sol}}$, eV
Benzene	-1.40 ^a	440-540	3.3-3.8	3.58 ^{a,d}
Naphthalene	0.15 ^b	660-745	2.6-2.8	2.44 ^{b,c}
Phenanthrene	0.31 ^b	660-745	2.5-2.7	2.32 ^{b,c}
Anthracene	0.56 ^b	660-745	2.2-2.4	2.56 ^{b,c}
Pyrene	0.59 ^b	660-745	2.2-2.4	2.37 ^{b,c}

^a D. R. Scott and R. S. Becker, *J. Phys. Chem.*, **66**, 2713 (1962). ^b R. S. Becker and E. Chen, *J. Chem. Phys.*, **45**, 2403 (1966). ^c F. A. Matsen, *ibid.*, **24**, 602 (1956). ^d R. M. Hedges and F. A. Matsen, *ibid.*, **28**, 950 (1958).

case, that would be expected to apply to the model of a charged structure in a homogenous dielectric fluid. Since the present experiment deals directly with benzene solutions, the authors regard this near agreement as just more evidence that the $1 - (1/D)$ factor, with D the macroscopic dielectric constant, is not strictly applicable to solvation of ions; a considerable solvent structure may exist around the ion even in benzene solution. This is supported by the evidence of behavior of cyclohexane solutions where for naphthalene, for example, there is no clear indication of photoinjection even at 440 m μ . The solvation energy of the negative naphthalene ion in cyclohexane would then be at least 0.9 eV lower than in benzene; this is also unaccountable merely on the basis of the ratio of $1 - (1/D)$ terms between these solvents, namely, 1.1.

In conclusion, ionic solvation energy is mainly responsible for work function lowering of rhodium in benzene solutions of the fused-ring aromatic compounds reported on here. Using the known electron affinity for a given species, one should be able to determine ionic solvation energy by this simple method.

Acknowledgment. The authors express their appreciation to the National Science Foundation for support of this research under Grant GP 3526. The authors also wish to express their thanks to Dr. David H. Freeman, Chief of Separations and Purifications Section, National Bureau of Standards, for kindly supplying the sample of chemically purified pyrene.

(13) N. S. Hush and J. Blackledge, *J. Chem. Phys.*, **23**, 514 (1955).

(14) L. E. Lyons, *Nature*, **166**, 193 (1950).

Thermodynamic Characterization of the Potentiometric Titration of Polyelectrolytes, with Special Reference to Precipitating Systems

by Isaac Michaeli

Weizmann Institute of Science, Rehovoth, Israel (Received January 9, 1967)

Thermodynamic relationships are derived which characterize the potentiometric titration behavior of weak polyelectrolytes. Changes in the activities and degrees of binding of the interacting small-ion components are correlated with changes in concentration and chemical potential of the polymeric component. The special cases considered include extrapolation to zero polymer concentration and inclusion of a virial coefficient. Experimental procedures are discussed to evaluate the effect of ionization and of added salt on the standard potential of the polyelectrolyte and on the related virial terms. A two-phase equilibrium is considered between the titrated solution and a polymer precipitate with a fixed chemical potential of the polyelectrolyte species. It is shown that the conventional "solubility product" law does not apply to polyelectrolyte systems even when extrapolation is made to "ideal" conditions. A differential expression is derived which constitutes a generalized "solubility product" relationship applicable to chemical reactions as well as to nonstoichiometric interactions of the polyelectrolyte with salt components.

A number of weak polyelectrolytes have been observed to precipitate from aqueous solutions when their degree of ionization is sufficiently decreased following the addition of a neutralizing agent.^{1,2} The potentiometric titration behavior of such systems (of a weak polyacid, for example) differs markedly from that of nonprecipitating polyelectrolytes. The two-phase system has, as a rule, a rather high buffering capacity; in some cases, the chemical potential of the neutralizing species remains practically constant over a wide range of the neutralization reaction. Only when the neutralization of the polymer in the two-phase system is near completion can there be found a pronounced decrease in the buffering capacity, and a typical end point can subsequently be observed.

The quantitative characterization of the above behavior has been described by Linderstrøm-Lang and Nielsen^{3,4} and subsequently by Shatky and Michaeli² (see also Snell and Nielsen⁵). The previous derivations of the equations involved were based on the (implicit) assumption that the entropy of mixing of the polyelectrolyte molecules is given by an ideal mixing term. Moreover, in the previously derived equations, the effect of added electrolyte on the titration curve is not in-

cluded, so that these equations may apply to titrations at constant ionic strength only.

The purpose of the present paper is to characterize the potentiometric titration in terms of thermodynamic relationships of general validity which are free of the restrictions imposed by a given model. Molecular parameters are only subsequently introduced into the general relationships on the basis of model considerations. (Clearly, an extrapolation to "ideal" conditions is equivalent to an introduction of an "ideal" model.) The general thermodynamic relationships thus derived are suitable to describe the relationships that exist in titrations of precipitating polyelectrolytes.

An obvious difference between a regular titration of a polyelectrolyte system without phase separation and a titration of a solution which loses material owing to precipitation of another (concentrated) phase is in the decrease of a degree of freedom. Thus, unless

- (1) A. Grönwall, *Compt. Rend. Trav. Lab. Carlsberg*, **24**, 185 (1942).
- (2) A. Shatky and I. Michaeli, *J. Phys. Chem.*, **70**, 3777 (1966).
- (3) K. Linderstrøm-Lang, *Arch. Biochem.*, **11**, 191 (1946).
- (4) K. Linderstrøm-Lang and S. O. Nielsen in "Electrophoresis," M. Bier, Ed., Academic Press Inc., New York, N. Y., 1959.
- (5) F. M. Snell and E. B. Nielsen, *J. Phys. Chem.*, **65**, 2015 (1961).

special adjustment is made of small electrolyte concentrations, the polymer concentration is not an independent parameter that can be kept constant, and it varies very markedly during the course of the titration. The following treatment will therefore be mainly concerned with the relationships that exist between the degree of ionization of the polyelectrolyte, the chemical potentials of the neutralizing species and of other components, and the changes in concentration of the polymer and small ion species. An important special case will be considered where the precipitating polyelectrolyte phase is of constant composition and conformation and thus maintains a constant chemical potential of the polyelectrolyte. It should be stated at the outset that the relationship between the chemical potential of the neutralizing species (or pH) and the degree of ionization α is specific for each polyelectrolyte system and cannot be derived from general thermodynamic considerations. Accordingly, this relationship is not given by the equations of Linderström-Lang, and of Shatky and Michaeli. The relationships considered in both the present and the previous treatments are those between the potentiometric titration parameters (*e.g.*, pH and α) and the concentrations and chemical potentials of the other components involved.

To fix our ideas, let us consider an aqueous solution at constant temperature and pressure, containing n_m moles (in monomer units) of a weak polyacid (introduced in its H^+ form), n_b moles of NaOH, n_s moles of NaCl, and n_w moles of water. At constant n_w the system has three degrees of freedom, and μ_m the chemical potential of the polyelectrolyte component is completely defined for any given values of polyelectrolyte concentration c_m , chemical potential of the base μ_b , and chemical potential of the salt component μ_s . We have

$$d\mu_m = \left(\frac{\partial \mu_m}{\partial c_m} \right)_{\mu_s, \mu_b} dc_m + \left(\frac{\partial \mu_m}{\partial \mu_s} \right)_{c_m, \mu_b} d\mu_s + \left(\frac{\partial \mu_m}{\partial \mu_b} \right)_{c_m, \mu_s} d\mu_b \quad (1)$$

We define c_m as moles of polymer, in monomer units, per unit volume of water: $c_m = n_m/n_w \bar{v}_w$ (\bar{v}_w being the partial volume of water, taken as constant). According to this definition, conditions of constant c_m at constant n_w are equivalent to constant n_m . Considering now the complete differential of the function $\chi = G - n_s \mu_s - n_b \mu_b$, where G is the Gibbs free energy, we have

$$d\chi = \mu_m dn_m + \mu_w dn_w - n_s d\mu_s - n_b d\mu_b$$

and the following cross relations hold, at constant n_w (and temperature and pressure)

$$\left(\frac{\partial \mu_m}{\partial \mu_s} \right)_{c_m, \mu_b} = - \left(\frac{\partial n_s}{\partial n_m} \right)_{\mu_s, \mu_b} \equiv -\Gamma_s \quad (2)$$

$$\left(\frac{\partial \mu_m}{\partial \mu_b} \right)_{c_m, \mu_s} = - \left(\frac{\partial n_b}{\partial n_m} \right)_{\mu_s, \mu_b} \equiv -\Gamma_b \quad (3)$$

Introduction of eq 2 and 3 into eq 1 gives

$$d\mu_m = -\Gamma_s d\mu_s - \Gamma_b d\mu_b + \left(\frac{\partial \mu_m}{\partial c_m} \right)_{\mu_s, \mu_b} dc_m \quad (4)$$

We may express μ_s and μ_b by the corresponding chemical potentials of the cations and anions involved: $d\mu_s = d\mu_{Na} + d\mu_{Cl}$; $d\mu_b = d\mu_{Na} + d\mu_{OH}$. Also, we have $n_{Na} = n_s + n_b$ and $n_{Cl} = n_s$. Introducing these relationships into eq 4 we obtain

$$d\mu_m = -\Gamma_{Na} d\mu_{Na} - \Gamma_{Cl} d\mu_{Cl} - \Gamma_b d\mu_{OH} \left(\frac{\partial \mu_m}{\partial c_m} \right)_{\mu_s, \mu_b} dc_m \quad (5)$$

The values of Γ_s and Γ_b are experimentally available quantities. If the polyelectrolyte concentrations are not unduly high and the ratio n_m/n_s is also low, then Γ_s and Γ_b are independent of polymer concentration (but they are functions of μ_s and μ_b). If the number of free OH^- ions may be neglected in comparison with n_b , the total number of moles of NaOH added to the polyacid solution, we have in the linear range

$$\Gamma_b = \left(\frac{\partial n_b}{\partial n_m} \right)_{\mu_s, \mu_b} = \frac{n_b}{n_m} = \alpha \quad (6)$$

where α is the degree of ionization of the polyacid.

For a regular titration performed at constant n_m and n_w , the last term on the right-hand side of eq 5 is evidently zero. If eq 6 may be applied and, in addition, $d\mu_{Na} = d\mu_{Cl} = 0$, eq 5 reduces to

$$d\mu_m = -2.3RT\alpha dpH \quad (7)$$

where

$$dpH = (0.43/RT)d\mu_{OH}$$

The special case represented by eq 7 is of particular importance since the changes in the molar free energy of the polyelectrolyte component can be evaluated by straightforward integration of the α -pH titration curves. This relationship has been previously derived in a number of ways and applied in titration studies of conformational transitions⁶⁻⁸ and of polyelectrolyte interactions⁹ in a single phase.

(6) B. H. Zimm and S. A. Rice, *Mol. Phys.*, **3**, 39 (1960).

(7) J. C. Leyte and M. Mandel, *J. Polymer Sci.*, **A2**, 1879 (1964).

(8) I. Michaeli, International Symposium on Macromolecular Chemistry, Prague, 1965; *Polymer Symp.*, in press.

The values obtained by the integration of the right-hand side of eq 7 have been previously assumed to represent $\Delta\mu^\circ$ —the difference in the standard molal free energies of the un-ionized polyelectrolyte component at the given α and at $\alpha = 0$. This interpretation is valid when the α -pH relationship is independent of polymer concentration, as can be seen from the following considerations. The values of $\Delta\mu_m$ are in general dependent on the (constant) polymer concentration c_m at which the titration is performed. However, at sufficiently low c_m , $\Delta\mu_m$ is independent of c_m . In this case, it represents $\Delta\mu_m^\circ$, which by definition is the concentration-independent term. For such conditions of low c_m , eq 7 may be identified with a well-known relationship in statistical thermodynamics, $RT d \ln Q / d\mu_{H^+} = -Z\bar{\alpha}$, where Q is the grand partition function of the polyacid molecule, Z is the degree of polymerization, and $\bar{\alpha}$ is the mean degree of ionization.⁹ Thus $RT \ln Q^{1/2}$ may be identified with $-\mu_m^\circ$, and clearly, $\bar{\alpha}$, the mean α , is the thermodynamic α appearing in eq 7. The limitations of eq 7 (and of the corresponding statistical thermodynamic treatment) are evident from the assumptions and approximations involved in its derivation from eq 5. The most difficult limitation in the above derivation is the condition that both μ_{Na} and μ_{Cl} are maintained constant. This can be achieved at excess concentration of NaCl only. In general, however, μ_{Na} and μ_{Cl} cannot be adjusted independently so as to maintain both values unchanged. Clearly, at constant c_m , and at any α , changes in μ_{Na} and μ_{Cl} can be brought about by changes in n_s and the corresponding μ_s . The variation of this single degree of freedom makes it possible to adjust, say, μ_{Na} to a constant value. At the same time, however, μ_{Cl} is also set to a certain value and cannot be adjusted independently to its previous value (evidently $d\mu_s = 0$ does not imply $d\mu_{Na} = d\mu_{Cl} = 0$). Thus a rigorous thermodynamic evaluation of $\Delta\mu_m$ is obtained only according to eq 4; however, if eq 6 may be applied, we have, at constant c_m and μ_s

$$\Delta\mu_m = -\int \alpha d\mu_b \quad (8)$$

where μ_b may be measured with a pair of reversible electrodes (e.g., to Na^+ and to OH^- ions, respectively).

On the basis of general considerations,¹⁰⁻¹² μ_m may be expanded in a power series in polymer concentration, following the logarithmic term, at constant μ_s and μ_b

$$\mu_m = \mu_m^\circ + RT(1/Z) \ln c_m + 2Bc_m + \dots \quad (9)$$

where the coefficient of the linear term is written as $2B$ so that B may correspond to the well-known second virial coefficient for the osmotic pressure. (It should

be noted that since $\mu_m = \mu_m^- + \alpha\mu_{H^+}$, where μ_m^- is the chemical potential of the polyion, we obtain $d\mu_m = d\mu_m^-$ for variations at constant μ_b and μ_s , with $d\alpha = 0$.) Evidently μ_m° and B are functions of both μ_s and μ_b . According to eq 2 and 9 we can write

$$\left(\frac{\partial\mu_m}{\partial\mu_s}\right)_{\mu_b, c_m} = -\Gamma_s = \left(\frac{\partial\mu_m^\circ}{\partial\mu_s}\right)_{\mu_b, c_m} + 2c_m \left(\frac{\partial B}{\partial\mu_s}\right)_{\mu_b, c_m} + \dots \quad (10)$$

Similarly, according to eq 3 and 9, we have

$$-\Gamma_b = \left(\frac{\partial\mu_m^\circ}{\partial\mu_b}\right)_{\mu_s, c_m} + 2c_m \left(\frac{\partial B}{\partial\mu_b}\right)_{\mu_s, c_m} + \dots \quad (11)$$

Thus when the approximation to a second virial coefficient is valid, a plot of $-\Gamma_s$ vs. c_m (for given μ_b and μ_s) will give a straight line whose slope and intercept provide information on the effect of salt on B and μ_m° , respectively. The straight line for Γ_b vs. c_m will provide similar information concerning the effect of pH on B and μ_m° .

Equations 7, 8, 10, and 11 relate to (single phase) titrations at constant c_m and ionic strength. Let us now consider the case of a titration accompanied with the formation of a precipitate of constant composition and polymer conformation. In this case the solution is in equilibrium with a concentrated polymer phase at constant μ_m . According to eq 4 we therefore have

$$\left(\frac{\partial\mu_m}{\partial c_m}\right)_{\mu_s, \mu_b} = \Gamma_s \frac{d\mu_s}{dc_m} + \Gamma_b \frac{d\mu_b}{dc_m} \quad (12)$$

and according to eq 5

$$\left(\frac{\partial\mu_m}{\partial c_m}\right)_{\mu_s, \mu_b} = \Gamma_{Na} \frac{d\mu_{Na}}{dc_m} + \Gamma_{Cl} \frac{d\mu_{Cl}}{dc_m} + \Gamma_{OH} \frac{d\mu_{OH}}{dc_m} \quad (13)$$

Equations 12 and 13 provide, in principle, a way of evaluating the concentration dependence of μ_m (at constant μ_s and μ_b). The Linderström-Lang equation is a special case of eq 13, valid for systems where $d\mu_{Na} = d\mu_{Cl} = 0$, and where μ_m is represented by the ideal logarithmic term, $d\mu_m = (1/Z)RT d \ln c_m$. We obtain, after obvious transformations

$$\frac{1}{\nu} = \frac{1}{\alpha Z} = \frac{dpH}{d(\log c_m)} \quad (14)$$

where Z is the degree of polymerization of the polyacid,

(9) A. Litan, *J. Phys. Chem.*, **70**, 3107 (1966).

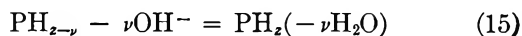
(10) L. Onsager, *Ann. N. Y. Acad. Sci.*, **51**, 627 (1949).

(11) T. L. Hill, "Ion Transport Across Membranes," Academic Press Inc., New York, N. Y., 1954, p 198.

(12) E. F. Casassa and H. Eisenberg, *Advan. Protein Chem.*, **19**, 287 (1964).

and ν is the number of ionized groups on each polymer molecule ($\nu/Z = n_b/n_m = \alpha$). Equation 14 has all of the limitations previously discussed in connection with eq 7. In addition, the degree of polymerization Z has been taken here as constant. The precipitation of the polyelectrolyte may, however, involve fractionation effects, and Z may, in general, not be regarded as a constant. An extension of the "ideal" model to include the fractionation phenomenon has been considered by Shatky and Michaeli.² However, when the parameters used in eq 12–14 are those of the single-phase system at its precipitation point, the mean value of Z is maintained constant.

Equation 14 may be recognized as a "solubility product" relationship in differential form. It relates to the neutralization reaction of the polymeric anion P with the hydrogen ions to give an un-ionized polymer precipitate $\text{PH}_{2-\nu} + \nu\text{H}^+ = \text{PH}_2$. This reaction may be written as a subtraction of base from the ionized polymer



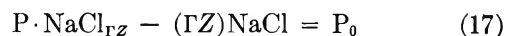
A naive application of the "solubility product" law for the above reaction might anticipate a relationship: $c_p a_b^{-\nu} = K$, where c_p is the concentration of polymer molecules ($c_p = c_m/Z$), a_b is the activity of the base, and K is a constant. (Changes in the activity of water are neglected.) Since $d \ln c_p = d \ln c_m$, we would expect according to the above that $d \log c_m = Z d(\alpha\text{pH})$ (α is *not* constant). The latter relationship does not hold, however, and the correct form of the "ideal" solubility product is given by eq 14.

The neutralization reaction of the polymeric anion with consequent precipitation of P_0 also involves the loss of interaction of the polyanion with the salt component (NaCl). In contrast to the neutralization reaction with the base, the interaction with the salt is not a chemical reaction and does not obey any simple stoichiometric relationship. Obviously, the thermodynamic treatment does not distinguish between the type of interaction involved, and we can therefore derive a "solubility product" expression related to the interaction between the polymer and salt components. The derivation is completely analogous to that of eq 14. We thus obtain

$$\frac{1}{\Gamma_s Z} = \frac{d \log a_s}{d \log c_m} \quad (16)$$

Clearly, $\log a_s$ in eq 16 replaces pH in eq 14, and Γ_s replaces α . It may be noted that previous derivations of the "solubility product" relationship considered only stoichiometric chemical equilibria like the neutralization reaction represented by eq 15. Equation

16, however, relates to the nonstoichiometric interaction between the polymer and salt components, which may be symbolically represented by



where P_0 represents the salt-free polymer precipitate. The term ΓZ in eq 16 and 17 may be regarded as the surplus NaCl bound to each polymer (compare with the analogous classical definition of surface adsorption according to Gibbs). Evidently eq 17 does not completely represent the formation of P_0 from P, since it does not include the reaction with H^+ ions, but eq 15 should be regarded similarly as "incomplete" since it does not represent the interaction with NaCl. Thus, each of the above equations (15 and 17) represents only one of the interaction processes involved in the precipitation of the polymer, and for each process there exists a "solubility product" relationship given by eq 14 and 16, respectively. It can therefore be summarized that when species i brings about precipitation of polymer species P, we have

$$\left(\frac{\partial \ln c_p}{\partial \ln a_i} \right)_{\mu_j} = Z \Gamma_i \quad (18)$$

Equation 18 may be regarded as a generalized "solubility product" relationship in differential form. It is valid both for stoichiometric (chemical) reactions and for nonstoichiometric interactions that lead to precipitation and is evidently also correct when P is not a polymeric species.

Equations 12 and 13 are convenient generalizations of eq 18 and make it possible to correlate the concentration-dependence parameter $(\partial \mu_m / \partial c_m)_{\mu_s, \mu_b}$ with readily available experimental parameters, at finite values of c_m and varying activities of the small ions in solution.

It may be of interest to consider conditions where the logarithmic term is not sufficient to describe changes in μ_m at constant μ_s and μ_b and where these changes are given by the virial expansion in eq 9. In this case we have, according to eq 9 and 12

$$\frac{RT}{Z} + 2Bc_m = \Gamma_s \left(\frac{\partial \mu_s}{\partial \ln c_m} \right)_{\mu_m} + \Gamma_b \left(\frac{\partial \mu_b}{\partial \ln c_m} \right)_{\mu_m} \quad (19)$$

Equation 19 may then be simplified for relationships at constant μ_s and μ_b , or for constant μ_{Na} and μ_{Cl} . For the last case we obtain an extension of eq 14

$$\frac{1}{Z} + \frac{2Bc_m}{RT} = \frac{\alpha \text{dpH}}{d \log c_m} \quad (20)$$

In the case of polyacids with sufficiently high degrees

of polymerization, the value of $1/Z$ is too small to be experimentally detected according to eq 14. However, the value of $\alpha dpH/d \ln c_m$ may be found significantly

different from zero, at higher polymer concentrations. According to eq 20 this is due to deviations from "ideal" behavior characterized by the virial coefficient $2B$.

The Effect of Rare Gases and Aromatic Admixtures on the Self-Induced Isotopic Exchange of Tritium with Toluene

by Hans J. Ache

Department of Chemistry, Virginia Polytechnic Institute, Blacksburg, Virginia 24061
(Received January 19, 1967)

The rate of the self-induced isotopic exchange of tritium with toluene vapor is found to be a function of the tritium concentration. Two reaction paths which lead to the labeling of toluene are discussed: (1) the β decay-induced mechanism involving $(\text{He}^3\text{T})^+$ and (2) the radiation-induced labeling in which ionized or excited toluene species and radicals react with T_2 . The effect of rare gas additives and admixtures such as benzene and *m*-xylene on each of the two reaction mechanisms is studied separately. No effect on the decay-induced labeling could be observed with helium and argon present, whereas the radiation-induced mechanism is inhibited by these bases, probably due to the fact that β -radiation energy initially absorbed by the rare gas cannot be effectively transferred to the toluene to form reactive species which eventually react with T_2 to give tritium-toluene. In gaseous benzene-toluene mixtures, the labeling of one component is not affected by the presence of the other. It occurs strictly proportional to the electron fractions of the two compounds.

Introduction

The results of the tritium gas exposure labeling of organic compounds, originally described by Wilzbach,¹ have been widely discussed in various papers, but very few systematic studies have been made about the reaction mechanisms involved.²

Wolfgang and Pratt³ and Gant and Yang⁴⁻⁷ investigated the isotopic exchange between tritium and simple hydrocarbons in the gas phase, Wexler⁸ studied the exchange mechanism in the gaseous tritium-methane system by using mass spectroscopic methods, and Garnett,^{9,10} *et al.*, did isotopic distribution studies with anthranilic acid labeled by the Wilzbach method.

Ache and Herr^{11,12} could show in the case of toluene

that the gas exposure technique does not lead to a random distribution of tritium in the toluene molecule. Depending on the reaction conditions, such as reaction

- (1) K. E. Wilzbach, *J. Am. Chem. Soc.*, **79**, 1013 (1967).
- (2) E. A. Evans, "Tritium and Its Compounds," D. Van Nostrand Co., Princeton, N. J., 1966.
- (3) R. Wolfgang and T. H. Pratt, *J. Am. Chem. Soc.*, **83**, 10 (1961).
- (4) P. L. Gant and K. Yang, *J. Chem. Phys.*, **30**, 1108 (1959).
- (5) P. L. Gant and K. Yang, *ibid.*, **31**, 1589 (1959).
- (6) P. L. Gant and K. Yang, *ibid.*, **32**, 1757 (1960).
- (7) P. L. Gant and K. Yang, *J. Phys. Chem.*, **66**, 1619 (1962).
- (8) S. Wexler, *J. Am. Chem. Soc.*, **85**, 272 (1963).
- (9) J. L. Garnett, S. W. Law, and A. R. Till, *Australian J. Chem.*, **18**, 297 (1965).
- (10) B. R. Crawford and J. L. Garnett, *ibid.*, **18**, 1951 (1965).

time, amount of tritium used, as well as on the application of external energy in forms of ultraviolet light, γ irradiation, and electric discharge, the intramolecular distribution of tritium could be varied over a relatively wide range. Especially the tritium substitution in the side chain was found to be very sensitive to variations in the method and small amounts of oxygen completely eliminated the tritium attack at the methyl group.¹³

The currently accepted view on the self-induced isotopic exchange of tritium with organic molecules is that there are two modes of labeling: (1) the β decay-induced mechanism involving $(\text{He}^3\text{T})^+$ formed by the radioactive transformation of T_2 and (2) a radiation-induced mechanism which is initiated by the excitation and ionization of the parent molecule and the T_2 by the β released in the nuclear decay (internal self-radiation).

Several experimental variables provide criteria to differentiate between the contributions made by these two mechanisms. Application of external energy increases the fraction of tritium tagged molecules labeled by (2), the radiation-induced mechanism, whereas dilution of T_2 with HT diminishes (1), since the decay of HT yields $(\text{He}^3\text{H})^+$ but not $(\text{He}^3\text{T})^+$.⁷ In most cases the fraction of labeled molecules following (1) could be evaluated by using NO^7 or O_2 .¹³ It could be shown that in the toluene- T_2 system at tritium concentrations of 50 mcuries or less the overwhelming part of the parent molecules is labeled *via* (1) and that at higher tritium concentrations (>500 mcuries) (1) becomes less important and more than 95% are labeled *via* (2).¹³ The same authors studied also the influence of the reaction type on the intramolecular T distribution in toluene.¹¹⁻¹³

Some possible mechanisms from the effect of added rare gases are discussed in detail by several authors. Mottlau¹⁴ observed yield enhancement by the addition of argon in studies of Wilzbach labeling of cyclohexane, whereas on the other hand, Cacace, *et al.*,¹⁵ in the liquid toluene-tritium system and Yang and Gevantman¹⁶ in the gaseous water-tritium system noted a definite drop in the yields of the labeled parent molecules. Although plausible suggestions have been made in each case as to the effect of the noble gases, a clearer hypothesis remains to be put forth. A serious drawback in most of the previous experiments with rare gases present was that the exchange labeling took place in heterogeneous systems (liquid-gas) and that in no case was a complete or controlled absorption of the β -radiation energy guaranteed.

In the following, the effect of a number of rare gases and other admixtures such as benzene or xylene on the various mechanisms involved in the gas ex-

posure labeling of gaseous toluene was studied, and possible mechanisms are discussed.

Experimental Section

Materials. Benzene, toluene, and *m*-xylene were of Phillips research grade. Gas chromatographic analysis did not show any impurities (detection limit <0.005%). They were carefully degassed by high-vacuum distillation and sealed in glass ampoules.

Oxygen, hydrogen, and the rare gases (Airco research grade) did not contain more than 4 ppm impurities and were used without further purification.

Tritium gas was obtained in form of T_2 from Oak Ridge or the Radiochemical Centre, Amersham, and did not contain more than 1% impurities.

Reaction Vessels and Irradiation Techniques. The experimental details have been previously described by Ache and Herr.¹³ The irradiations were done in 10,000-ml glass vessels which were thoroughly baked out at 400° and 10^{-6} mm and sealed off. Ampoules containing appropriate amounts of tritium and toluene (benzene or *m*-xylene) were attached to them. By breaking the seals of the ampoules the reaction was started.

In most of the experiments the toluene vapor pressure was about 20 mm and the tritium pressure was less than 0.1 mm. The size of the reaction vessels assured a practically complete absorption of the tritium β energy within the gas mixture.

Activity Measurements. After appropriate time intervals, small aliquots of the hydrocarbon were frozen into small glass ampoules which were previously attached to the reaction vessel and sealed off.

The weight of the labeled hydrocarbon was determined. After dilution with a known amount of the inactive hydrocarbon, the sample was purified by preparative gas chromatography. A small aliquot was checked for radioactive impurities on an analytical radio gas chromatograph. In order to determine the tritium substitution in the sidechain, the pentabromotoluene was prepared. The total substitution in the aromatic nucleus could be obtained by preparing benzoic acid. Finally, the *ortho*, *para*, *meta* distribution

(11) H. J. Ache, W. Herr, and A. Thiemann, "Chemical Effects of Nuclear Transformations," Vol. II, IAEA, Vienna, 1961, p 111; *Z. Anal. Chem.*, **181**, 551 (1961).

(12) H. J. Ache, W. Herr, and A. Thiemann, "Tritium in the Physical and Biological Sciences," Vol. II, IAEA, Vienna, 1962, p 21.

(13) H. J. Ache and W. Herr, *Z. Naturforsch.*, **17a**, 631 (1962).

(14) A. Y. Mottlau, *J. Phys. Chem.*, **64**, 931 (1960).

(15) F. Cacace, R. Cipollini, G. DiMarco, G. Gimacomello, and A. Guarino, *Gazz. Chim. Ital.*, **93**, 1105 (1963).

(16) J. H. Yang and L. H. Gevantman, *J. Phys. Chem.*, **68**, 3115 (1964).

was calculated from the activity found in derivatives such as dinitrotoluene and nitrobenzoic acid.^{11,12}

It was made sure that under the experimental conditions used no isotopic exchange occurred. The tritium activities of the purified toluene (benzene) and its derivatives were measured in a liquid scintillation counter (Packard, Model Tri-Carb).

Results and Discussion

The effects of rare gas additives and other admixtures such as benzene and *m*-xylene on the aromatic tritium labeling in toluene were studied under experimental conditions, which assured that the T exchange occurs solely or to an overwhelming extent either *via* the decay-induced mechanism or the radiation-induced mechanism. These experimental conditions were determined following the criteria mentioned in the Introduction and along the lines previously described by Ache and Herr.¹³

In the tritium-toluene gaseous system, the number of tritium atoms incorporated into the toluene per tritium β decay (= *L* value) was found to be a function of the mass of T₂ used, increasing from *L* = 0.71 at 50 mcuries to *L* = 5.5 at 500 mcuries of tritium (Figure 1).

An *L* value greater than 1 clearly indicates that besides the possible substitution *via* the (He³T)⁺, which is formed by the β decay of one T in the T₂ molecule and has a lifetime long enough to collide and eventually to react with a toluene molecule, other reaction paths probably initiated by β radiolysis lead to the incorporation of tritium into the hydrocarbon.

By using small amounts of oxygen (~1 mm) as scavenger it could be shown (Figure 1) that the *L* value remains constant over the whole range from 50 to 500 mcuries of tritium. This strongly suggests that most of the radiation-induced processes forming tritium-labeled toluene are inhibited in the presence of oxygen.

Various amounts of oxygen (0.6 to 6 mm of oxygen) were added to the system, but no significant change in the yields of tritiated toluene could be observed within this range, indicating that the presence of 0.6 mm of oxygen in the system is sufficient to suppress all radiation-induced reactions.

In Figure 2, the number of tritium atoms incorporated into the toluene (at a tritium gas concentration of 50 mcuries) is plotted as a function of reaction time. The tritium substitution of the aromatic nucleus is strictly proportional to the elapsed time. The initial rate of the side-chain substitution appears to be of the same magnitude, but it drops significantly with increasing time.

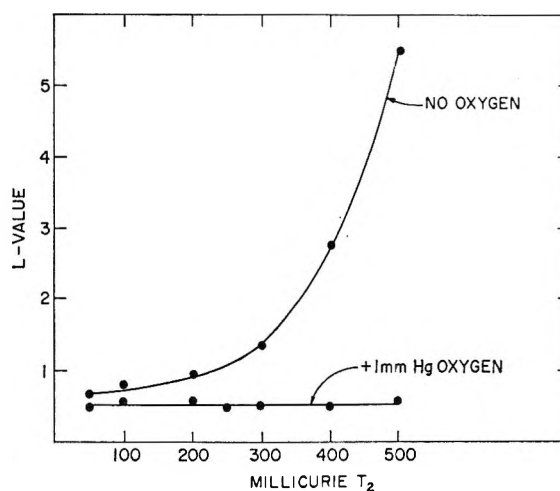


Figure 1. *L* values vs. tritium amount present in the system tritium-toluene. *L* value: number of tritium atoms incorporated into toluene per tritium- β decay.

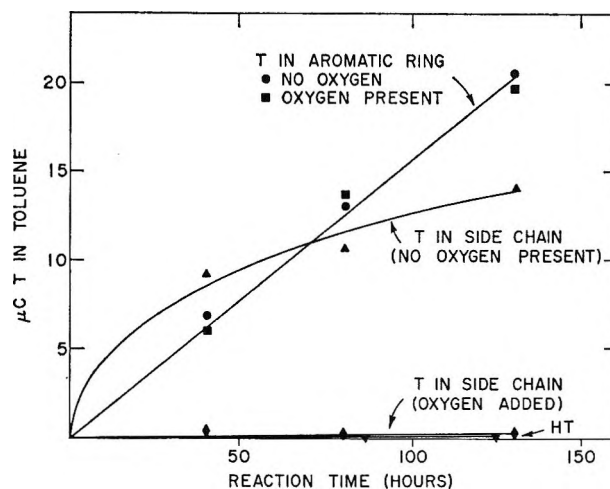


Figure 2. T incorporated into the aromatic ring of the toluene molecule (in microcuries) vs. reaction time (system containing 50 mcuries of T₂).

An addition of small amounts of oxygen (1 mm) eliminates completely the species leading to side chain substituted toluene, whereas the substitution at the aromatic ring remains practically unaffected.

The observed drop in the side-chain substitution with exposure time (in experiments in which there is no oxygen present at the start of the reaction) might have been caused by small amounts of oxygen introduced from the glass surface during the relatively long reaction period. Although the glass vessels were thoroughly baked out, traces of oxygen might have remained on the surface or might have diffused to the surface.

In a second series of experiments, 50 mcuries of tritium was added in the form of HT. (The latter was obtained by mixing an excess of H₂ with T₂ and applying a tesla discharge to the system for a very short time period.) Tritium incorporation into the aromatic ring was completely eliminated.

From these results, Ache and Herr¹³ concluded that two reaction mechanisms are effective here, one probably induced by β radiolysis and scavenged by oxygen which substitutes preferably on the side chain, the other one *via* (He³T)⁺ which is responsible for the substitution in the aromatic ring and which cannot be inhibited by oxygen. It is noteworthy that (He³T)⁺ does not seem to substitute benzylic hydrogen.

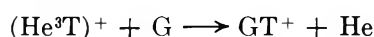
In Figure 3 the number of tritium-labeled toluene molecules obtained in tritium-toluene systems containing 500 mcuries of tritium gas is plotted *vs.* reaction time. Here again a strict proportionality of incorporated tritium atoms with the elapsed time can be observed. The side-chain substitution rate is similar to that in the 50-mcurie experiment; there is a marked decrease with increasing reaction time.

In contrast to the results of the 50-mcurie experiments, an oxygen addition affects substitution in the side chain as well as in the aromatic ring, indicating that the labeling here occurs mostly (>90%) *via* species produced by β radiolysis. The tritium distribution in the aromatic ring varies very little with the amount of tritium gas used, and is not affected by additives such as oxygen or rare gases. (Typical distribution: *ortho*, 59.0%; *para*, 13.6%; and *meta*, 27.4%.)

Effect of Rare Gases. (a) *Decay-Induced Labeling.* From the results discussed above, it could be concluded that at tritium concentrations of 50 mcuries and keeping all other experimental parameters constant (toluene ~20 mm, reaction volume 10,000 ml), the T labeling in the aromatic ring of the toluene proceeds to approximately 95% *via* (He³T)⁺.

In Figure 4, the tritium incorporation in the aromatic ring is plotted *vs.* exposure time for gaseous tritium-toluene systems with and without rare gases present. No change in the exchange rate could be observed in the presence of 70 mm of helium or argon.

These results are consistent with the findings of Wolfgang and Pratt³ in the tritium-methane system and indicate that (He³T)⁺ reacts probably in the first few collisions with the substrate, since if it did not, it would be scavenged by the rare gas in exoergic reactions of the type



(b) *Radiation-Induced Labeling.* A second series of experiments was done using 500 mcuries of T₂.

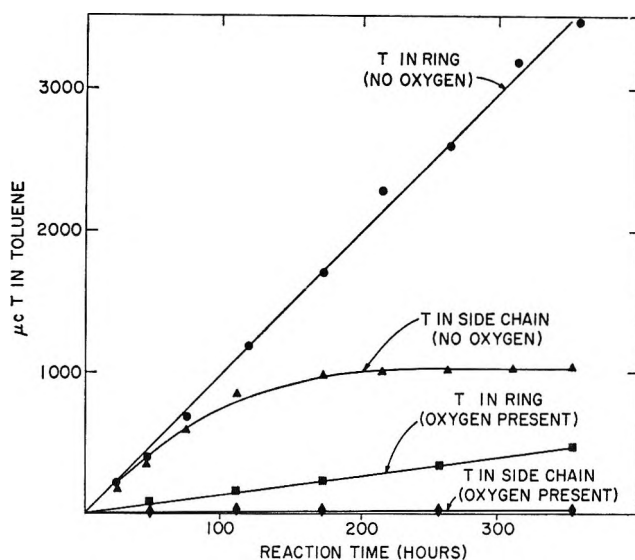


Figure 3. T incorporated into toluene (μ curies) *vs.* reaction time (system containing 500 mcuries of T₂).

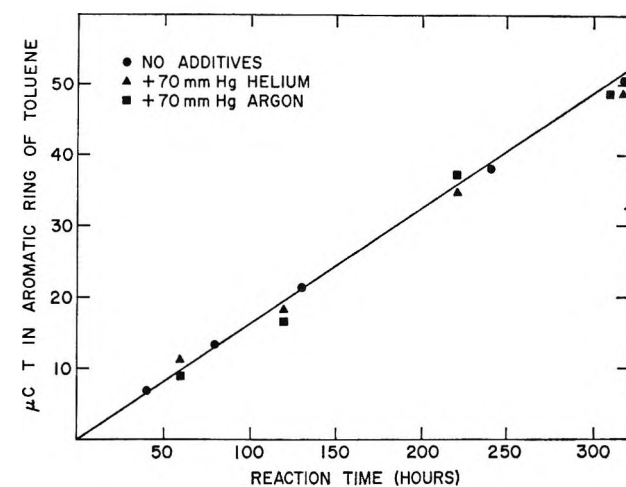


Figure 4. T incorporated into the aromatic ring of the toluene molecule *vs.* reaction time (system containing 50 mcuries of T₂) (with and without rare gases present).

In contrast to the observations made with smaller amounts of T₂ (~50 mcuries), here the addition of rare gases such as helium and argon results in a significant drop in the yield of T-labeled toluene. In Figure 5, the amount of T incorporated is plotted *vs.* reaction time using as further parameters the rare gas concentrations.

By assuming that the tritium β energy is initially dissipated between toluene and the rare gas in the ratio of their electron fractions,¹⁷ the results in Figure 5

(17) J. W. Otvos and D. P. Stevenson, *J. Am. Chem. Soc.*, **78**, 546 (1956), measured ionization cross sections for energetic β 's from C¹⁴, Sr⁹⁰, and Y⁹⁰ and found them proportional to their electron densities.

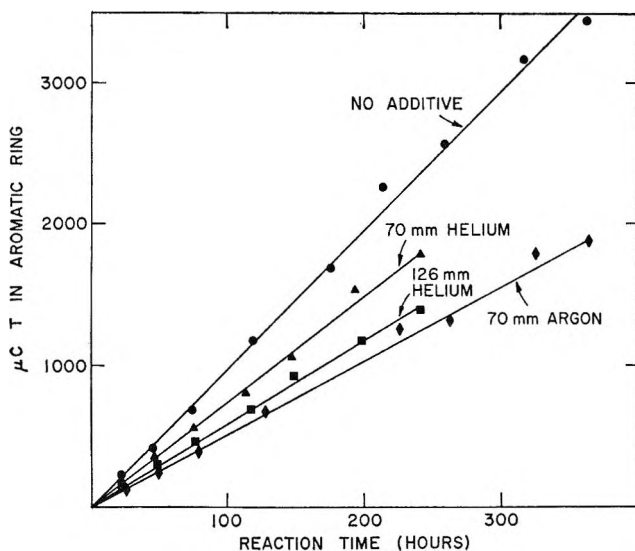


Figure 5. T incorporated into the aromatic ring vs. reaction time (with and without rare gas additives) (system containing 500 mcuries of T_2).

show that the decrease in the yields of tritiated toluene is somewhat less than that expected from those ratios. This would indicate that only a fraction of the energy initially absorbed by the rare gas is transferred to the toluene, producing reactive species which participate in the toluene-labeling process. Argon seems to be more effective in transferring energy to the toluene (30% of the absorbed energy transferred) than helium (20% transferred).

These results lead to the conclusion that the decay-induced tritium labeling *via* (He^3T^+) proceeds in an extremely fast reaction so that a charge transfer or proton transfer cannot become effective.

In radiation-induced mechanisms, on the other hand, it seems to depend on the individual system under observation whether the addition of rare gas promotes a substitution of the substrate molecule or not.

In the toluene system, the exchange is inhibited, meaning that only a fraction of radiation energy originally absorbed by the rare gas can be transferred to the substrate to become effective forming reactive species, which eventually react with T_2 to give a T-labeled parent molecule. A second possibility, the inhibition of the T exchange by ionization energy or excitation energy transfer from $C_7H_7^+$ or $C_7H_8^+$ to the rare gas, seems to be very unlikely because of the considerably higher ionization and excitation potentials of the rare gases compared with those of toluene.¹⁸

Effect of Admixtures of Benzene and m-Xylene on the Radiation-Induced Labeling of Toluene. The influence of admixtures of benzene and *m*-xylene on the radiation-

induced tritium labeling of the aromatic positions in the toluene was studied in the presence of 500 mcuries of T_2 . These experimental conditions assured that more than 90–95% of the exchange occurs *via* radiation-produced species.

The participation of ionic intermediates in the T-exchange labeling has been postulated by several authors^{3,19} in various systems. The ionic species obtained in the irradiation of toluene have ionization potentials lower than any one of the rare gases;¹⁸ thus the presence of these gases should not affect the reactions of these ions by charge transfer. On the other hand, irradiations of liquid benzene–toluene mixtures with 1.5-Mev electrons, as reported by Manion and Burton,²⁰ have brought up evidence for a transfer of ionization energy from benzene, with an ionization potential of 9.2 eV, to toluene, whose ionization potential is with 8.8 eV somewhat smaller. It now seemed interesting to study whether such a charge transfer takes place during the tritium labeling. This should be indicated by the change in the relative yields of T-labeled benzene and toluene when both compounds are present in the reaction mixture.

A series of experiments was performed in which gaseous mixtures containing benzene and toluene in various concentrations were exposed to tritium gas. After certain time intervals, both compounds were analyzed for their tritium content in aromatic positions. Typical results for the benzene–toluene system are plotted in Figure 6. They show a strict proportionality between tritium incorporation and exposure time for both compounds.

G values (= tritium activity incorporated in aromatic ring per 100 eV of energy absorbed) were calculated on the basis that the initial β -radiation energy absorption takes place according to the electron fractions of the two compounds present in the mixture.¹⁷ In Figure 7, the *G* values for benzene and toluene were plotted as a function of their electron fractions. The resulting straight line strongly suggests that the tritium labeling of the aromatic positions proceeds strictly proportional to the initial β -radiation energy absorption of each compound and that there is no evidence for energy transfer from benzene to toluene. Similar observations have been made in the toluene–*m*-xylene system. Here again the labeling of the aromatic positions in one compound is not affected by the presence of the other compound.

(18) F. H. Field and J. L. Franklin, "Electron Impact Phenomena," Academic Press, New York, N. Y., 1957.

(19) S. Wexler and N. Jesse, *J. Am. Chem. Soc.*, **84**, 3625 (1962).

(20) J. P. Manion and M. Burton, *J. Phys. Chem.*, **56**, 560 (1952).

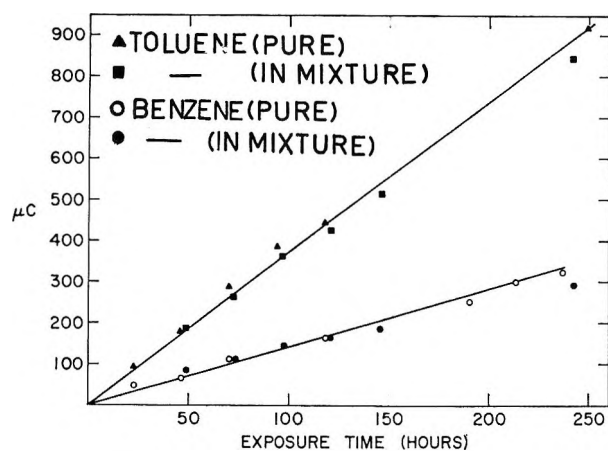


Figure 6. T incorporated into the aromatic ring. Energy absorbed by the components in the mixture has been calculated on the basis of their electron fractions.

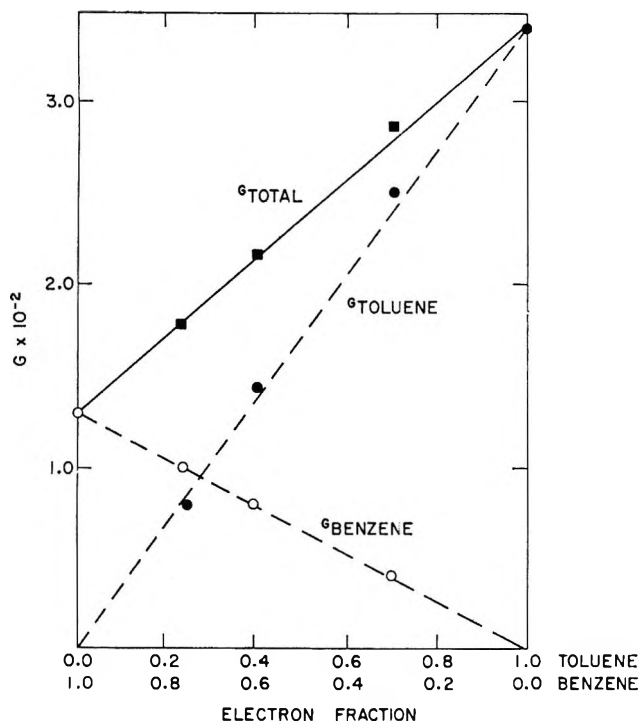


Figure 7. G values (number of tritium atoms incorporated into hydrocarbon per 100 ev of energy absorbed) of benzene and toluene in benzene-toluene mixtures vs. electron fractions of the components.

Unfortunately, the charge transfer between benzene or phenyl ions and toluene has not yet been investigated in gaseous systems and if such a transfer occurs its cross section might be small compared with the reaction rate for a possible reaction between the benzene or phenyl ion and the tritium molecule leading to a tritium-substituted benzene. Thus it would not

be justified to exclude the participation of ionic species on the above evidence alone.

The observed results now allow a direct comparison of the relative reactivity of the three compounds benzene, toluene, and *m*-xylene toward radiation-induced tritium exchange in the aromatic positions. The following sequence could be observed: benzene: toluene:*m*-xylene = 1:3.3:9. (These ratios are obtained from the G values observed in the binary mixtures: benzene-toluene and toluene-*m*-xylene.)

The differences in the observed reactivities will be mainly due to two factors: (1) differences in the reaction rates with which the intermediates produced by β radiation in the benzene, toluene, or xylene system react with T_2 , and (2) variations in the number of reactive intermediates (phenyl, tolyl, or xylyl radicals or ions) produced per unit of β -radiation energy absorbed.

Radical Reactions. Evidence for the relative radical yields per 100 ev of energy absorbed in the benzene and toluene system can be obtained from measurements done by MacLachlan and McCarthy,²¹ who observed in the liquid phase initial radical yields of $G_{\text{benzene}} = 0.3$ and $G_{\text{toluene}} = 0.5$. However, they do not differentiate between benzyl and tolyl radicals. These results would not explain the observed differences in the reactivities.

However, in gaseous systems one would expect to see a more pronounced effect, since in the gas phase (at atmospheric pressure) an energy dissipation from the initially formed excited molecule to neighbor molecules is less likely; thus the presence of alkyl substituents attached to the aromatic ring should show an increased stabilization. By better accommodating the extra amount of energy dissipated by the β particle in the molecule, alkyl groups would avoid a complete destruction of the molecule to small fragments, which of course cannot react with T_2 to form the labeled parent product.

Gäumann, *et al.*,²²⁻²⁴ irradiated liquid benzene-toluene mixtures with various types of radiation. Some of the major products isolated are the isomeric bitolyl compounds. According to the authors,^{22,24} bitolyl is mainly formed by the reaction of tolyl radicals with toluene. The ratio in which the isomers are observed depends on the LET of the applied radiation.²³ For high LET's, the isomer yields approach a ratio ex-

(21) A. MacLachlan and R. L. McCarthy, *J. Am. Chem. Soc.*, **84**, 2519 (1962).

(22) J. Hoigne and T. Gäumann, *Helv. Chim. Acta*, **47**, 590 (1964).

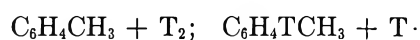
(23) J. Hoigne, W. G. Burns, W. R. Marsh, and T. Gäumann, *ibid.*, **47**, 247 (1964).

(24) J. Hoigne and T. Gäumann, *ibid.*, **46**, 365 (1963).

pected from random radical production and combination. At low LET's, the formation of *o,o'*-bitolyl is considerably smaller. The authors take the view that in the radiolysis of toluene the various tolyl radicals are formed randomly. The decrease in *o,o'*-bitolyl is supposedly due to the fact that *o*-tolyl radicals more easily abstract hydrogen from the methyl group of a second toluene to form benzyl radicals than *m*- or *p*-tolyl.

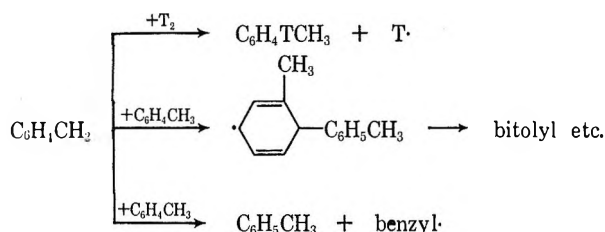
In the tritium-toluene system, undoubtedly benzyl and tolyl radicals as well as ions are formed by β -radiolysis.

Benzyl radicals are relatively stable and the abstraction of hydrogen from H_2 is endothermic by 26.5 kcal/mole.^{25,26} This does not exclude the possible reaction of "hot" benzyl radicals with T_2 , but those will not contribute to the labeling of the aromatic position in the toluene. Tolyl radicals, on the other hand, are highly reactive and abstraction of T from T_2 is only slightly endothermic, thus presenting a possible mode for T labeling.²⁷

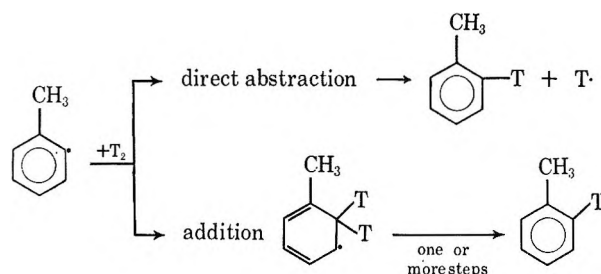


$$(\Delta H = 2 \text{ kcal/mole})$$

From Gäumann's^{22,24} observations, one might expect competition reactions between tolyl radicals on one side and tritium and toluene on the other hand according to



In analogy to the more pronounced hydrogen abstraction by *o*-tolyl from toluene, a similar preference in the reaction of *o*-tolyl with T_2 might explain the observed tritium distribution in the aromatic ring (for toluene: 59.0% *ortho*, 13.6% *para*, and 27.4% *meta*). With the exception of the *ortho* position, the T labeling is statistical, a fact which has been observed in a number of aromatic systems in addition to toluene.¹⁵ At the present time, no evidence can be presented as to the detailed mechanism, whether the T abstraction is a one-step reaction or whether it includes the formation of an intermediate, which might have the cyclohexadienyl structure as suggested by MacLachlan and McCarthy²¹ for the addition of aromatic radicals to aromatic molecules



The fact that the aromatic T labeling can be suppressed by oxygen and iodine vapor can be counted as evidence for participation of radical species in the aromatic T labeling of toluene.

Ionic Reactions. Although no evidence for the participation of ionic species in the aromatic labeling process has been derived, they cannot be excluded on the basis of the results described above.

Meyerson and Rylander^{28,29} found that when isolated molecules of toluene in the gas phase are ionized by energetic electrons, the principal fragment ion is the cyclic tropylium ion, $C_7H_7^+$, in which all carbon as well as hydrogen atoms are equivalent. Field and Franklin³⁰ observed appearance potentials for ions derived by the loss of a single methyl from alkyl benzenes and calculated from these data the energy of tolyl ions to be about 55 kcal lower than that of the phenyl ion. This extra amount of stabilization for the tolyl ion is supposedly due to the formation of the tropylium ion. It would also explain the increase of reactivity toward T labeling in the order benzene < toluene < xylene.

The fact that oxygen with an ionization potential of 13.6 eV¹⁸ suppresses the aromatic labeling cannot be explained with a simple charge transfer, but oxygen might be able to react with the cyclic tropylium ion in another unknown way, thus allowing no clear-cut decision between radical and ionic species.

It appears that in systems where the abstraction of a tritium atom from a tritium molecule by organic radicals is thermodynamically unfavorable, the fraction of substrate molecules labeled *via* ionic species becomes more important. In the aromatic labeling

(25) C. D. Hodgeman, "Handbook of Chemistry and Physics," Chemical Rubber Publishing Co., Cleveland, Ohio, 1959, p 1870 ff.

(26) A. F. Trotman-Dickenson, "Gas Kinetics," Butterworth and Co. Ltd., London, 1955, p 15 ff.

(27) Calculated on the basis of the bond energies involved. In lack of information about the aromatic C-H bond in toluene, this was considered to be equal to the C-H bond energies in benzene with 102 kcal/mole.

(28) S. Meyerson and P. N. Rylander, *J. Am. Chem. Soc.*, **79**, 842 (1957).

(29) S. Meyerson and P. N. Rylander, *J. Chem. Phys.*, **27**, 901 (1957).

(30) J. L. Franklin and F. H. Field, *J. Am. Chem. Soc.*, **75**, 2819 (1953).

where highly reactive phenyl and tolyl radicals as well as ions are formed, it seems that both species are participating in the labeling process.

The presented experimental results are certainly consistent with both types of mechanisms leading to T labeling in the aromatic ring.

Black Lipid Membranes in Aqueous Media: Interfacial Free Energy Measurements and Effect of Surfactants on Film Formation and Stability

by H. T. Tien

Department of Biophysics, Michigan State University, East Lansing, Michigan (Received January 26, 1967)

The interfacial free energy of black lipid membranes (BLM) separating two aqueous solutions has been measured quantitatively at 25°. These ultrathin membranes less than 100 Å in thickness are formed from cholesterol dissolved in *n*-dodecane and stabilized by various surface-active compounds. For membranes generated from cholesterol-dodecane-dodecyl acid phosphate, cholesterol-dodecane-dioctadecyl phosphite, and cholesterol-dodecane-hexadecyltrimethylammonium bromide systems, the interfacial free energies are, respectively, 1.1 ± 0.1 , 3.9 ± 0.5 , and 0.15 ± 0.05 ergs cm⁻². The ability to produce some of these membranes in aqueous solution is found to depend on both the interfacial tension and the critical micelle concentration of the surfactant used. The mechanism and kinetics of thinning are briefly discussed in connection with membrane formation and stability. The method developed for interfacial free energy measurements, which should be useful in the study of colloid and interfacial chemistry, is described.

Introduction

The probable structure of association colloids in aqueous solution has been considered by many investigators.¹⁻³ The two best known forms, designated as the spherical and the lamellar micelle, have been inferred from a variety of experimental evidence. In either one of these micellar forms, the limiting structure is frequently idealized as composed of a bimolecular leaflet of amphipathic molecules. The direct demonstration of the existence of such a structure as black (also variously called bimolecular or bilayer) lipid membranes has been reported by Rudin and his associates. From the consideration of interference phenomena of the reflected light and interpretation of electron micrographs, Mueller, *et al.*, have estimated the thickness of these membranes to be in the range of 60-90 Å.^{4,5}

These black lipid membranes possess many properties very similar to the bimolecular layer which is generally accepted to be the basic structural component of cellular membranes.⁶ Subsequent studies on this new

(1) J. W. McBain, *Advan. Colloid Sci.*, **1**, 118 (1942).

(2) G. S. Hartley, "Aqueous Solutions of Paraffin-chain Salts," Hermann, Paris, 1936.

(3) W. D. Harkins, "The Physical Chemistry of Surface Films," Reinhold Publishing Corp., New York, N. Y., 1952, Chapter 4.

(4) P. Mueller, D. O. Rudin, H. T. Tien, and W. C. Wescott, *Nature*, **194**, 979 (1962).

(5) P. Mueller, D. O. Rudin, H. T. Tien, and W. C. Wescott in "Recent Progress in Surface Science," Vol. I, J. F. Danielli, K. G. A. Pankhurst, and A. C. Riddiford, Ed., Academic Press, Inc., New York, N. Y., 1964, Chapter 11.

(6) A. P. Fishman, Ed., "Symposium on the Plasma Membrane," American Heart Association, Inc., New York, N. Y., 1962.

structure by others^{7,8} have established more quantitatively that the thickness of these black lipid membranes (or films) is about equal to two lengths of the lipid molecules used in their formation. Apart from the inherent interest of these black lipid membranes as a prototype for the plasma membrane of living cells, this new type of interfacial phenomena is itself of significance.⁹ For instance, this experimental structure may be adapted to the study of the stability of lyophobic colloids, of intermolecular forces, and a host of interfacial adsorption phenomena of biological and technological importance.

Owing to the fragility of the membrane and the attendant experimental difficulties, measurements of properties of these ultrathin lipid films have been mainly restricted to thickness, permeability, and current voltages. These studies have usually been made on membranes formed from solutions containing phospholipids. This paper presents interfacial tension measurements on thin lipid membranes of thickness ranging 40–100 Å by means of a new technique. These black lipid membranes (or BLM) are generated from recrystallized cholesterol and stabilized by a surface-active compound present either in the organic or aqueous phase. The experimental method developed in the course of this work is reported.¹⁰

Experimental Section

Materials. Cholesterol of high purity obtained from several commercial sources was recrystallized twice from absolute ethanol before use. This precaution was taken since it had been found that "aged" cholesterol alone was capable of producing black films.¹¹ Hexadecyltrimethylammonium bromide (HDTAB) was purchased from Eastman Kodak Co. Samples of dodecyl acid phosphate (DAP) and dioctadecyl phosphite (DODP) were provided by Hooker Chemical Corp. DODP as supplied was pale yellowish in color. It was recrystallized three times from cyclohexane. The white solids melted at 61.5–62.0°. All other chemicals and solvents were reagent grade and used without further purification. Redistilled water from an all-glass still was used throughout.

Apparatus. The interfacial free energy (γ_i) of black lipid membranes was determined in the apparatus illustrated in Figure 1. The main parts of the setup consisted of a cell for membrane formation, two ballast chambers, a device for generating hydrostatic pressure such as an infusion-withdrawal pump, a pressure transducer of high sensitivity (Model 270, Sanborn Co.), and a strip chart recorder. The outer chamber of the cell was made of glass, and its front portion was flattened to facilitate the observation of the membrane. The inner

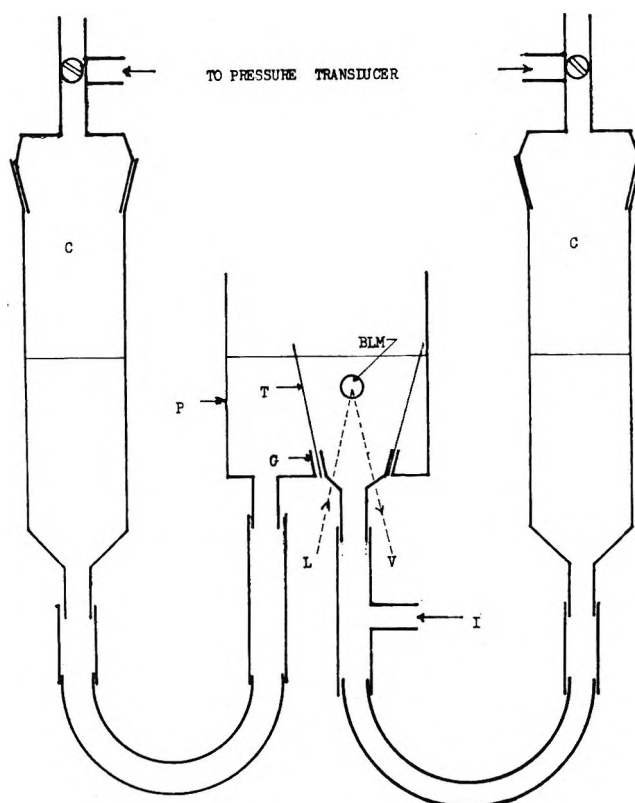


Figure 1. Schematic diagram of apparatus for measuring interfacial tension of black lipid membrane (BLM): C, ballast chambers; T, Teflon sleeve; L, light source; V, viewing tube; and I, infusion-withdrawal pump; P, Pyrex glass chamber; G, ground joints.

chamber was made from a Teflon sleeve which was held in place by tapered ground-glass joints. A small hole (1.57-mm diameter) was punched in the Teflon sleeve. This was done in a simple device made of two pieces of steel plate which were welded together with a small clearance between them to accommodate the Teflon sleeve. A smooth hole was drilled through the plates and a carefully machined rod of hardened steel was

(7) Using electrical methods: T. Hanai, D. A. Haydon, and J. Taylor, *Kolloid-Z.*, **195**, 41 (1964); C. D'Agostino and L. Smith in "Biophysics and Cybernetic Systems," M. Maxfield, A. Callahan, and L. S. Fogel, Ed., Spartan Books, Inc., Washington, D. C., 1965, pp 11–23; T. E. Andreoli, J. A. Bangham, and D. C. Tosteson, *J. Gen. Physiol.*, **50**, 1729 (1967).

(8) Using optical methods: C. Huang and T. E. Thompson, *J. Mol. Biol.*, **13**, 183 (1965); **16**, 576 (1966); A. V. Babakov, L. N. Ermishkin, and E. A. Liberman, *Nature*, **210**, 953 (1966); H. T. Tien, *J. Theoret. Biol.*, **16**, 97 (1967).

(9) H. T. Tien and E. A. Dawidowicz, *J. Colloid Interface Sci.*, **22**, 438 (1966).

(10) Experimental details were presented at the 153rd National Meeting of the American Chemical Society, Division of Colloid and Surface Chemistry, Miami, Fla., April 1967.

(11) H. T. Tien, S. Carbone, and E. A. Dawidowicz, *Nature*, **212**, 718 (1966).

fitted. The hole in the Teflon sleeve was punched simply by ramming the rod through the holes in the plates while the Teflon sleeve was placed in the clearance. The temperature of the cell was controlled by flowing water (from a thermostatic bath) through a glass coil (not shown) surrounding the inner chamber. The temperature could be maintained to within $\pm 0.1^\circ$. For lipid solution and pure solvent which were incapable of forming stable films, a modified arrangement was used. Instead of using a Teflon sleeve for film support, Teflon tubing of 2.15-mm diameter was immersed vertically in the aqueous solution while the other end was connected to one side of the transducer inlet *via* the ballast chamber. The aqueous solution outside the Teflon tubing served as the other compartment (see Figure 1).

Procedure. Since the apparatus devised is novel and has not been previously described, it was felt necessary to establish its capability for the measurement of interfacial tension, for both accuracy and reproducibility. This was first tested by measuring γ_i of pure liquids whose values have been established by classical methods. It was carried out as follows. A small quantity (about 0.005 ml) of a pure organic liquid was introduced at the end of the Teflon tubing which had been filled with and immersed in water. In so doing, two identical oil-water interfaces were created. With the pressure transducer balanced at an appropriate sensitivity, the infusion-withdrawal was then started to produce a hydrostatic head across the water-oil-water interfaces. The maximum pressure was noted with the aid of a recorder. Interfacial tension of several pure organic liquids was determined with this apparatus.¹⁰ For example, an interfacial tension value of 51.7 ± 0.8 was obtained for *n*-dodecane *vs.* water at 25.0° as compared with 51 dynes/cm reported in the literature. For determining γ_i of the black lipid membrane, the cell was first filled with an aqueous solution. After allowing sufficient time for the cell to attain equilibrium, the film was formed on the hole in the Teflon sleeve either by using the brush technique⁵ or by spreading the hole with a lipid solution through a polyethylene capillary. The pump was usually started after the membrane had become completely black (except for the Plateau-Gibbs border). The maximum pressure across the membrane was recorded as mentioned earlier. The membrane was observed with a wide-field (40 \times) microscope in reflected light. The microscope was fitted with an accurate reticle for measuring the diameter of the bulged-out membrane.

Results and Discussion

Composition of Lipid Solutions. In the hope that a

physical parameter could be found relating the formation and the stability of the black lipid membranes, the effects of surface-active compounds on membrane formation were explored. It was known from earlier observation¹¹ that freshly crystallized cholesterol would not produce a stable black film. It was decided, therefore, to adopt cholesterol dissolved in *n*-dodecane as a standard for the present study. In regard to surface-active agents, the choice had to be made in view of the fact that a vast number of such compounds are available. Therefore, only three were chosen. These were DODP [$(C_{18}H_{37}O)_2PHO$] and DAP (equimolar of mono- and diester of dodecanol and orthophosphoric acid). These compounds are classified as oil-soluble surfactants. Also chosen was HDTAB [$C_{16}H_{33}N(CH_3)_3Br$] which belongs to the water-soluble class. The choice of these surfactants was partially based on the fact that the first black lipid membrane observed was made from a solution containing phospholipids.^{4,5} As typified by lecithin, both the phosphate and quaternary ammonium groups were present. Further, the decision was made so that these surfactants represented three of the four major types. Thus, DAP is negatively charged when ionized in solution (anionic surfactant), HDTAB bears a positive charge when ionized (cationic surfactant), and DODP represents the so-called non-ionic surfactants. Initially, a wide range of concentration parameters for organic and aqueous phases was examined. After considerable tests, mainly by trial and error, stable black lipid films could be formed from cholesterol in dodecane, which required the presence of a surface-active agent in either the organic or aqueous solution. In Table I the compositions of lipid solutions and the aqueous phase used for producing stable black films are given. It should be emphasized that

Table I: Compositions of Lipid and Aqueous Solutions Used for Producing Black Lipid Membranes (BLM) at 25°

Solution	Compound	Concn, moles/l. of dodecane	Aqueous phase used
A	Cholesterol	0.0206	Water or 10^{-4} to 10^{-1} N NaCl
	DODP ^a	0.00273	
B	Cholesterol	0.0241	10^{-2} to 10^{-1} N NaCl
	DAP ^a	0.0100	
C	Cholesterol	0.0259	Water or 10^{-4} to 10^{-1} N NaCl containing 2.24×10^{-4} M HDTAB ^a

^a DODP, dioctadecyl phosphite; DAP, dodecyl acid phosphate; HDTAB, hexadecyltrimethylammonium bromide.

Table II: Interfacial Free Energy of the Black Lipid Membranes (BLM) at 25°

Film generated from	Aqueous phase	γ_i , ergs/cm ²	Remarks
Cholesterol-DODP ^a -dodecane	H ₂ O	5.7 ± 0.8	Stable black film
Cholesterol-DODP ^a -dodecane	0.1 N NaCl	3.9 ± 0.5	Stable black film
Cholesterol-dodecane	H ₂ O-HDTAB ^a	0.65 ± 0.08	Stable black film
Cholesterol-dodecane	0.1 N NaCl-HDTAB ^a	0.15 ± 0.05	Relatively unstable
Cholesterol-DAP ^a -dodecane	0.1 N NaCl	1.1 ± 0.1	Surface precipitation and some colors seen before going black

^a See footnote of Table I.

although only a few surfactants have been tried, numerous other surface-active agents including proteins and polymeric materials could be used. Without much doubt, some of these materials should also give similar results in producing stable black lipid films.

Experimental Technique and Interfacial Free Energy Calculation

Among the available methods for interfacial tension measurements, none is easily adaptable to the study of thin lipid membranes (thicknesses ranging from 50 Å to 1 μ). The so-called interfacial films which have been extensively investigated in the past¹² referred mainly to films existing at the bulk oil-water interface. The γ_i of these films were deduced from measurements of surface pressure using either the Wilhelmy hanging plate or Langmuir's method. The lipid films used in the present study differ from interfacial films in that these films possess a symmetric structure. The limiting structure of such a film together with the successive stages of bulging under hydrostatic pressure are illustrated in Figure 2.

The technique developed for γ_i measurement of these liquid films deserves a brief comment because it has general applicability for colloid and interfacial chemistry. Unlike both the Wilhelmy and Langmuir methods, the present technique measures interfacial free energy directly. It is evident from the description of the apparatus and procedure that the present method is based upon the fundamental equation of capillarity.¹³ In common with the well-known maximum bubble pressure method, it can be shown that the pressure is at a maximum when the lipid bubble attains a hemispherical shape with the base equal to the diameter of the opening used. The results given in Table II were calculated using the expression

$$P = \frac{8\gamma_i}{d} \quad (1)$$

where P is the pressure difference across the membrane

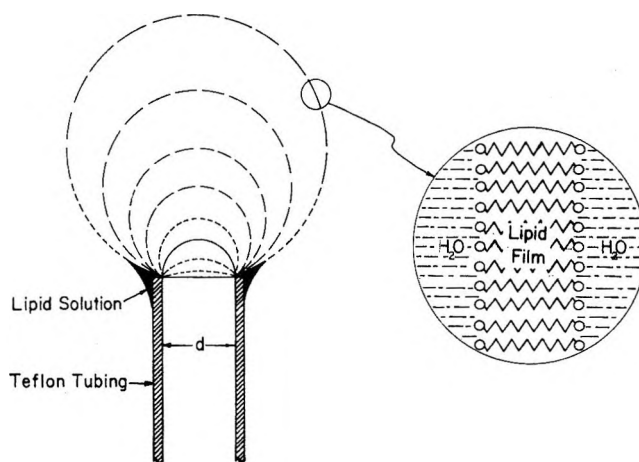


Figure 2. The bulging out of a lipid film under hydrostatic pressure. The enlarging drawing on the right illustrating the probable structure of BLM.

interposed between two aqueous phases, d is the diameter of lipid bubble, and γ_i is the interfacial free energy of the immiscible layer. In using eq 1, the local pressure differences have been neglected since the observed shapes of the lipid bubble were essentially spherical (or hemispherical when using a Teflon sleeve support). The variation of pressure difference as a function of lipid bubble diameter is shown in Figure 3.

Intuitively, it seems that a low γ_i will promote the formation of BLM and stability toward the effect of pressure difference across the membrane. In bulging the BLM under a hydrostatic pressure difference, the total interfacial free energy change is given by the equation

$$\Delta F_i = \gamma \Delta A + (A + \Delta A) \Delta \gamma \quad (2)$$

(12) See, for example, J. T. Davies and E. K. Rideal, "Interfacial Phenomena," Academic Press Inc., New York, N. Y., 1961, Chapter 5.

(13) For a recent discussion, see A. W. Adamson, "Physical Chemistry of Surfaces," Interscience Publishers, Inc., New York, N. Y., 1964, Chapter 1.

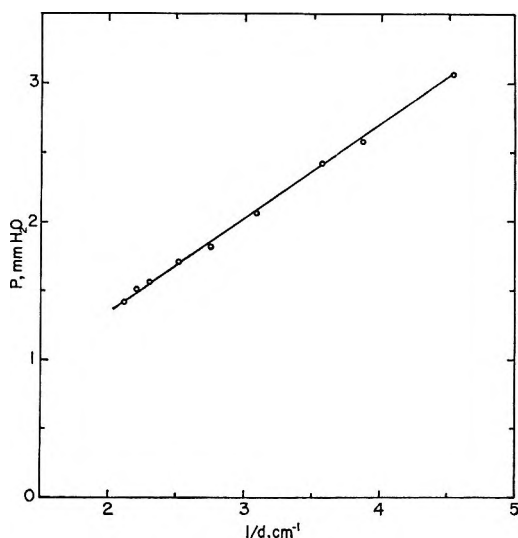


Figure 3. The observed pressure difference as a function of the reciprocal lipid bubble diameter separating two aqueous phases. A saturated cholesterol solution in *n*-dodecane at 25° was used. γ_i of the film is 9.6 ergs cm^{-2} as calculated from the slope.

where A is the area of BLM and ΔA is the increased amount as a result of bulging. The second term of eq 2 has been defined by Gibbs and is known as "the modulus of interfacial elasticity."¹⁴ According to Gibbs' derivation, the elasticity term is equal to

$$E = 2A \frac{d\gamma}{dA} \quad (3)$$

In dealing with BLM, it can be shown that the relative contribution of the Gibbs elasticity term will be less when ΔA becomes very large. Thus, when $A \simeq \Delta A$, eq 2 becomes

$$\Delta F_i = (\gamma_i + 2\Delta\gamma_i)A \quad (4)$$

The data presented in Table II were obtained by slow infusion of solution on one side of the membrane. As observed under the microscope, the membrane appeared "black" during the bulging process. Thus, viewed from the structural point of view, the γ_i of the membrane should remain unchanged whether the membrane is in a planar or curved configuration. From these considerations, it is concluded that the Gibbs effect is negligible. The measured quantities given in Table II are essentially the true γ_i of the BLM.

The Plateau-Gibbs Border and the Stretching of the Black Membrane. For lipid solutions under the conditions specified (Table I), the rate of formation starting from the thick layer to the "black" state was quite rapid and usually took place within 1 min. For certain black films, the so-called Plateau-Gibbs border which sup-

ported the black region was visible. It seems that besides supporting the films, the Plateau border serves as a reservoir for the black film. This fact is easily demonstrated by stretching an apparent black film suddenly. At this point, one again observes the interference colors which are followed by the appearance of the black film. Upon releasing the hydrostatic pressure, the film remains black. This sequence of events may be interpreted as follows. On stretching a black lipid film (*i.e.*, interfacial free energy of the film is increased), the reaction is for the lipid molecules located at the border to rush in so that the interfacial tension can be reduced. Depending upon the rate of stretching and the interfacial tension of the film, a thicker film may be generated as a result and is followed by normal thinning.⁹ When a lipid film is immersed in an aqueous solution containing surfactant, the stretching of the film would cause the migration of surfactant molecules to the interfaces according to the Gibbs adsorption equation. If the rate of change is small, no interference colors may be observable. Therefore, it seems that for planar black lipid films at least, the presence of the Plateau border is essential for the maintenance of the structural integrity and for the stability of the membrane.

Thinning and BLM Stability. The formation characteristics of BLM have been described previously in some detail.⁹ However, the relationship between thinning and BLM stability has been only briefly noted in passing. Mueller, *et al.*, stated that BLM were most prone to rupture during the transition to the black state.⁵ They also observed that once the entire area was black, the membrane was remarkably stable. These earlier observations are fully confirmed in the present study. Why a lipid film should break most easily during the increase of the black area is a question that cannot be answered quantitatively until we have a better understanding of the hydrodynamics of thin liquid films. Nonetheless, a qualitative explanation may be attempted. As is generally known, if the lipid solution used consists of only pure solvent (*i.e.*, dodecane in the present case), no stable film will result. In this case it is assumed that, if the lipid layer were made too thin by mechanical or other means, a critical thickness would soon be reached at which the van der Waals forces between the molecules situated at two interfaces would increase rapidly with decreasing film thickness. This unhindered thinning would result in a sudden rupture. To explain the stability of a thin liquid film in air, Gibbs suggested many years ago that at a "critical" thickness a "gelatinous" phase transition

(14) J. W. Gibbs, "The Scientific Papers," Vol. I, Dover Publications, New York, N. Y., 1961, p 302.

was believed to take place.¹⁴ As several groups of investigators have already shown,^{7,8} the thickness of black lipid membranes is about the length of the two lipid molecules used. It seems therefore that Gibbs' idea is even more applicable to black lipid membranes. That is, upon thinning to a "critical" thickness, the interaction due to rapidly increasing attractive van der Waals forces between the two lipid monolayers is retarded and, in the case of a stable black lipid membrane, is balanced by some repulsive forces such as the electrical double layers situated as the opposite membrane-solution interfaces. For a first approximation, the theory advanced by Verwey and Overbeek for the stability of colloids may be used.¹⁵ In principle at least, one would predict that in order to have a stable BLM, the total potential energy of the system when calculated as a function of the film thickness between two planes of lipid monolayers should exhibit a potential minimum. Theoretical calculations along these lines are now in progress.

The question still to be answered is, "why does the film rupture during transition to the black state?" Clearly this is a kinetic problem in contrast to the stability of BLM discussed above. In conjunction with soap (or foam) films, deVries has considered at length the reasons for the rupture of these films.¹⁶ High-speed cinematographic studies showed that the rupture of soap films is always preceded by a very rapid growth of "black spots." For black lipid films it has been suggested⁹ that principal thinning mechanisms are similar to those responsible for soap films (*i.e.*, Plateau border suction, gravitation flow, and diffusion). In addition, chance contacts of the two faces of the membrane resulting from local variations of interfacial tension, temperature, and other factors may initiate the formation of "black spots." Therefore, accelerated growth of the black area will follow a "zipper-like" action under the influence of van der Waals attractive forces. This zipper-like action will tend to increase the black spot rapidly in all radial directions. As was observed in soap films by deVries, the rapidly advancing boundary between the black area and the thicker adjacent region will be the seat of high concentration stress and turbulent flow. It is therefore highly likely that the rupture will occur somewhere along this boundary. Thus the high probability of the rupture of lipid films during their transition to the black state may be explained by using the suggestion of deVries for soap films.¹⁶

Interfacial Free Energy and Film Stability. It is interesting to note that these BLM possess interfacial free energy values usually less than 6 dynes cm^{-1} . (γ_i values for black lipid membranes formed from lecithin, oxidized cholesterol, and glyceryl distearate have

been also measured. Preliminary results show that γ_i for these membranes are less than 2 dynes cm^{-1} .) The meaning of these results, when viewed in the light of the widely accepted model of the plasma membrane of living cells,¹⁷ is of some significance. Briefly, the plasma membrane model proposed by Danielli and Davson consisted of a bimolecular lipid leaflet sandwiched between two adsorbed protein monolayers. The essential feature of the model was similar to the bimolecular leaflet theory of Gorter and Grendel, which was deduced from force-area measurements at the air-water interface.¹⁸ The model of Danielli-Davson was based on the supposition that if the ideas of Gorter and Grendel were correct, the expected γ_i would be of the order of 10–20 dynes cm^{-1} . Since the measured γ_i 's by various investigators¹⁷ were of the order of 0.1 dyne cm^{-1} , it was concluded that the adsorbed protein layers were essential. It should be pointed out that the above conclusion was reached largely on the basis of measurements carried out at the bulk oil-water interface. The present results indicate that the interfacial tension of bimolecular membranes (BLM) can have an intrinsic low γ_i value, the presence of adsorbed protein layers being unnecessary.

Surfactant Concentration and Film Stability. In order to establish whether there is any physical parameter governing black film formation and its stability, γ_i 's were measured as a function of surfactant concentration with and without the presence of cholesterol. Experimental results for the dodecane-HDTAB-water and cholesterol-dodecane-HDTAB-water systems are shown in Figure 4. In both cases, γ_i was found to decrease linearly as a function of $\log [\text{HDTAB}]$. However, stable black films were formed only when cholesterol was present. Although not consistently observed, the stable black film was most easily produced when the HDTAB concentration was $9 \times 10^{-6} M$ or higher. At a concentration higher than $4.5 \times 10^{-4} M$ (indicated by arrow in Figure 4), however, no films were obtainable. It is interesting to note that the extrapolated values are of the same order as the critical micelle concentration. This would seem to imply, for the water-soluble surfactants at least, that stable black film can be obtained only when the surfactant is present below the critical micelle concentration (cmc). This is in

(15) E. J. W. Verwey and J. Th. G. Overbeek, "Theory of the Stability of Lyophobic Colloids," Amsterdam, 1948.

(16) A. J. deVries, *Recueil*, **77**, 81, 441 (1958).

(17) H. Davson and J. F. Danielli, "The Permeability of Natural Membranes," Cambridge University Press, London, 1952.

(18) H. Davson in "Symposium on the Plasma Membrane," A. P. Fishman, Ed., New York Heart Association, Inc., New York, N. Y., 1962, pp 1022–1037.

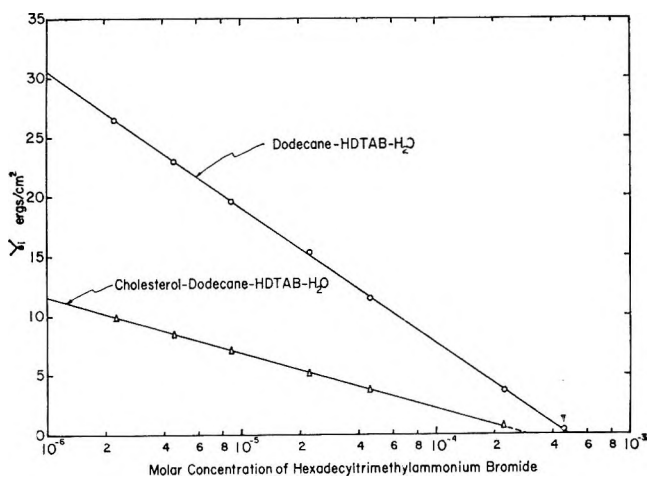


Figure 4. Interfacial free energies as a function of HDTAB concentration in the aqueous phase.

agreement with the generally known fact that the surface tension of the solution does not change appreciably when the cmc has been exceeded. From Figure 4, this cmc value corresponds to a negative γ_i , which means no interfacial tension exists between the film and the aqueous solution. This condition should produce complete miscibility of the two phases as was in fact observed in the present work. On the other hand, the film stability cannot be due to the lowering of interfacial tension alone, since stable black films were not obtained in the absence of cholesterol. The fact that cholesterol was necessary for the formation of stable black films indicates that the packing of molecules in the film would be of importance. In this connection, the idea put forth by Schulman and Cockbain¹⁹ concerning the stability of films at the bulk oil-water interface is of interest. These authors suggested that if complex formation could take place at the oil-water interface, greater mechanical strength and resistance to rupture could be attained by the film. It was said that compactness of packing of molecules through molecular interaction at the interface greatly enhanced the stability of emulsions. The stability of black lipid films under discussion requires the presence of two "emulsifying agents," a fact which has long been recognized in the field of emulsions²⁰ and seems to suggest that some sort of complex formation was involved. The resulting molecular structure of the film possessed a greater stability than the structure formed from single compounds alone.

It is perhaps worth noting that the total solute concentrations (cholesterol plus surfactant) used were generally of the order of 25 mmoles. This being so in a

sense is not entirely surprising, since these films have been shown to be about bimolecular in thickness.⁹ The concentration of the film is between 10^{-9} and 10^{-10} mole cm^{-2} . At these concentration levels, the formation and stability of the film would be greatly influenced by the presence of "trace impurities," as has been shown previously with BLM generated from oxidized cholesterol.¹¹ In addition, the presence of "trace impurities" could also affect the other properties. For instance, Castillo, *et al.*,²¹ have used these black lipid films as transducers for the detection of antigen-antibody and enzyme-substrate reactions. They have found that small amounts of oxidation products associated with cholesterol prevent the electrical impedance changes of the lipid films. This interesting observation may be explained in terms of "trace impurities" which apparently play a crucial role with regard both to film structural stability and function.

Summary

Black lipid films (BLM) less than 100 Å in thickness were generated from a system composed of purified cholesterol in *n*-dodecane together with a surface-active agent present either in the organic or aqueous solution. Quantitative measurements of the interfacial free energy of these ultrathin films were carried out by a new technique which provides a method of general utility for colloid and interfacial chemistry. For the systems investigated, both the formation and the stability of certain black films were shown to be related to the interfacial tension and the critical micelle concentration of the surfactant used. Although this work has established that three compounds can be used for the formation of stable black lipid films, any of several surfactants could have been used with similar success. This demonstrates that black lipid film can be generated from numerous compounds, and its formation is not limited to the use of classical phospholipids. The results indicate that black lipid membranes can have rather low interfacial tension value, the presence of adsorbed protein layers being unnecessary.

Acknowledgment. Grateful acknowledgment is made to the National Institutes of Health for financial support of this work (GM-14971).

(19) J. H. Schulman and E. G. Cockbain, *Trans. Faraday Soc.*, **36**, 651 (1940).

(20) P. Becher, "Emulsions: Theory and Practice," Reinhold Publishing Corp., New York, N. Y., 1965, Chapter 4.

(21) J. del Castillo, A. Rodriguez, C. A. Romero, and V. Sanchez, *Science*, **153**, 185 (1966).

Hydration and Association Equilibria in Molten Salt Solutions

Containing Water. II. A Quasi-Lattice Model¹

by Jerry Braunstein²

Department of Chemistry, University of Maine, Orono, Maine (Received January 27, 1967)

A statistical model of hydration and association equilibria of dilute solute ions in very concentrated aqueous electrolyte solutions is presented. The model assumes competition between ligand anions and water molecules for bonding to a solute cation. To test the equations of the model, values of the parameters of the model are calculated from experimental values of association constants of Cd^{2+} with Br^- in the molten salt solvent $\text{LiNO}_3\text{-KNO}_3$ and in the solvent $\text{LiNO}_3\text{-KNO}_3\text{-}0.1$ mole of H_2O /mole of nitrate at 168° . The parameters are used to calculate the association constants of CdBr^+ at 119° in the solvents $\text{LiNO}_3\text{-KNO}_3\text{-}R_{\text{H}_2\text{O}}$ as a function of the water content and are compared with the experimental association constants at 119° with $R_{\text{H}_2\text{O}} = 0.26, 0.51, 0.76, 1.00,$ and 1.26 moles of H_2O /mole of nitrate.

Introduction

It has been recognized for some time that an understanding of the properties of concentrated aqueous electrolyte solutions requires information at the molten salt end of the concentration scale as well as in dilute aqueous electrolyte solutions.³ A number of workers have investigated the effects of water on the properties of molten salts or the properties of water dissolved in molten salts. The electrical conductance,⁴ the solubility of water,^{5,6} and the cryoscopic behavior of water⁷ have been reported, as well as the vapor pressures of some moderately concentrated aqueous solutions of lithium nitrate and of ammonium nitrate.⁸ These studies have not, however, led to quantitative relations between the properties of molten salts and their concentrated aqueous solutions.

Recently, we have shown that a quasi-lattice model of molten reciprocal salt solutions⁹ is useful also in representing activity coefficients of solutes present at low concentrations in concentrated aqueous electrolyte solutions.¹⁰ In the solvent consisting of 2 moles of water/mole of ammonium nitrate, the isothermal concentration dependence of the activity coefficients of the solutes cadmium nitrate and ammonium chloride was consistent with a quasi-lattice model of molten salts if the water was considered bound to the cations.¹¹ Angell has more recently proposed that fused hydrated

salts such as calcium nitrate tetrahydrate might be treated as molten salts with large polarizable cations, *i.e.*, with the water bound to the cations.¹² The assumption that the water is firmly bound to the cations is unlikely to apply to systems with two or more high-field cations competing for the water and insufficient water to form complete hydration shells about all the

(1) This work was supported by the U. S. Atomic Energy Commission. Report No. NYO 2873-19. Presented as Paper No. 20 of the Division of Physical Chemistry at the 152nd National Meeting of the American Chemical Society, New York, N. Y., Sept 11-16, 1966.

(2) Address correspondence to the author at the Reactor Chemistry Division, Oak Ridge National Laboratory, Oak Ridge, Tenn.

(3) M. J. Rice and C. A. Kraus, *Proc. Natl. Acad. Sci. U. S.*, **39**, 802 (1953); C. A. Kraus, *J. Chem. Educ.*, **35**, 324 (1958).

(4) A. N. Campbell, E. M. Kartzmark, and D. F. Williams, *Can. J. Chem.*, **40**, 890 (1962).

(5) F. R. Duke and A. S. Doan, *Iowa State Coll. J. Sci.*, **32**, 451 (1958).

(6) T. E. Geckle, M.S. Thesis, Pennsylvania State University, 1964; U. S. Atomic Energy Commission Report TID 21511.

(7) A. G. Keenan, *J. Phys. Chem.*, **61**, 780 (1957).

(8) A. N. Campbell, J. B. Fishman, G. Rutherford, T. P. Schaeffer, and L. Ross, *Can. J. Chem.*, **34**, 151 (1956).

(9) M. Blander and J. Braunstein, *Ann. N. Y. Acad. Sci.*, **79**, 838 (1960); M. Blander, *J. Phys. Chem.*, **63**, 1262 (1959).

(10) J. M. C. Hess, Ph.D. Dissertation, University of Maine, 1961; University Microfilms, Inc., Ann Arbor, Mich., 61-5210.

(11) J. M. C. Hess, J. Braunstein, and H. Braunstein, *J. Inorg. Nucl. Chem.*, **26**, 811 (1964).

(12) C. A. Angell, *J. Electrochem. Soc.*, **112**, 1224 (1965).

cations or to systems with ligands which may displace water from the coordination spheres of the cations. We have found, for example, that the simple molten salt quasi-lattice model could not account for the variation with temperature and water content of the activity coefficients of cadmium nitrate and ammonium chloride in mixtures of ammonium nitrate and water.¹⁰ In the present work, a model is proposed which takes into account the change of the degree of hydration of the cations as well as the variation of the degree of association with anionic ligands.

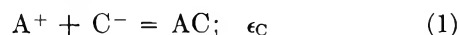
Dilute solutions of cadmium ion in anhydrous molten alkali nitrates or in very concentrated aqueous electrolyte solutions follow Henry's law in the absence of halide, as do solutions of halide ions in the absence of cadmium ion.^{10,11,13-15} Deviations from Henry's law in solutions containing cadmium ion and halide ion may be interpreted in terms of the formation of associated species.^{16,17} A quasi-lattice model of molten salt⁹ solutions has been shown to give the temperature dependence of association constants of solutes in a number of anhydrous molten alkali nitrate solvents.^{14,18} In this paper, we present a quasi-lattice model of hydration and association in very concentrated aqueous electrolyte solutions. Water molecules and halide ions are considered ligands competing for bonding to a cadmium ion, *i.e.*, competing to displace nitrate ions from the coordination sphere of a cadmium ion. A quasi-lattice calculation provides a convenient formulation of the competing association equilibria in the system and should not be construed as implying a rigid lattice structure for the solution.⁹ The model contains two energy parameters: a cadmium-halide "bond energy," ϵ_C , and a cadmium-water "bond energy," ϵ_H . The former, ϵ_C , is the specific Helmholtz free energy of formation which appears in the quasi-lattice model of anhydrous molten salt solutions.⁹ Assuming a coordination number, Z , for the cations, simple equations are derived for the variation of the association constant in aqueous melts with temperature and with water content. Values of the model parameters are calculated from measurements in anhydrous molten salt solution and in one aqueous melt. These parameters are then used to calculate the association constants in solvents of different water content and at different temperatures. The model is applied to association constants which have been reported for CdBr^+ in anhydrous equimolar lithium nitrate-potassium nitrate and in aqueous melts containing up to 56 mole % of water.¹⁹ Since, however, the model is essentially a description of mixed ligand association, it should be applicable also to the effects of dissolved polar gases other than water, or

of other anionic ligands, on association constants in solution.

A Quasi-Lattice Model of Hydration and Association

We consider a molten salt solvent BD, composed of the ions B^+ and D^- , in which may be dissolved the solute components AD, BC, and H, consisting of the ions A^+ , D^- , B^+ , and C^- and the neutral molecules H. The "lattice" is assumed to consist of two interpenetrating "sublattices." The cations, A^+ and B^+ , occupy sites on the "cation sublattice," while the anions, C^- and D^- , and water molecules, H, occupy sites on the "anion sublattice." Each site on the "cation sublattice" is surrounded by Z sites on the "anion sublattice" occupied by C^- , D^- , or H. Since the H (like all species on the "anion sublattice") are nearest neighbors of cations but only next-nearest neighbors of anions, this is equivalent to assuming that cations, but not anions, are hydrated. In order to maintain electro-neutrality, either the number of cation sites and anion sites must differ or some of the cation sites must be unoccupied. The exchange of a neutral ligand and an anionic ligand must also involve rearrangements of the ligands in the outer coordination shells of the central ions. In the first approximation, only changes in the occupancy of the first coordination shell are considered. The justification for this heuristic procedure is the success of the quasi-lattice model of molten salts, derived originally for mixtures of univalent ions, for mixtures of ions of different charge types.^{17,18}

The association reaction in the anhydrous molten salt represents the replacement of a solvent anion D^- from one of the Z anion sites adjacent to a cation A^+ (on a cation sublattice) by a ligand C^- .⁹ With water (H) present as a solute, the association reaction (eq 1)



may take place by means of the displacement by C^- of either D^- or H from one of the Z anion sites adjacent to an A^+ (as in the relationships of eq 2)

(13) J. F. Tate and M. M. Jones, *J. Inorg. Nucl. Chem.*, **24**, 1010 (1962).

(14) H. Braunstein, J. Braunstein, and D. Inman, *J. Phys. Chem.*, **70**, 2726 (1966).

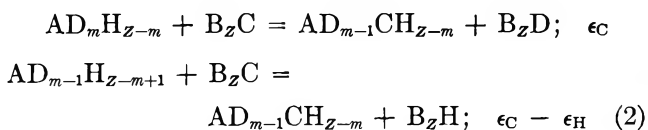
(15) J. Braunstein, A. R. Alvarez-Funes, and H. Braunstein, *ibid.*, **70**, 2734 (1966).

(16) J. Braunstein, M. Blander, and R. M. Lindgren, *J. Am. Chem. Soc.*, **84**, 1529 (1962).

(17) J. Braunstein and R. M. Lindgren, *ibid.*, **84**, 1534 (1962).

(18) J. Braunstein and A. S. Minano, *Inorg. Chem.*, **5**, 942 (1966); D. G. Hill, J. Braunstein, and M. Blander, *J. Phys. Chem.*, **64**, 1038 (1960); A. Alvarez-Funes, J. Braunstein, and M. Blander, *J. Am. Chem. Soc.*, **84**, 1538 (1962).

(19) P. C. Lammers and J. Braunstein, *J. Phys. Chem.*, **71**, 2626 (1967).



where $0 < m \leq Z$. The values of ϵ_C or ϵ_H would in general differ with different values of m . In the first approximation, for dilute solutions in which m is Z or $Z - 1$, ϵ_C and ϵ_H will be considered independent of m . Thus ϵ_C is a bond energy or extracoulombic interaction energy for an AC pair relative to an AD pair and ϵ_H is an interaction energy for an AH pair relative to an AD pair.

We consider a system dilute in AD, BC, and H in order to neglect overlapping of pairs and extend the asymmetric approximation of the quasi-lattice model derived by Blander for one ligand⁹ to include two different kinds of ligands. The total number of anion sites adjacent to an A^+ is Zn_{AD} , where Z is the coordination number and n_{AD} is the number of A^+ cations. We designate by x the fraction of these sites occupied by a ligand C and by y the fraction of these sites occupied by H. Hence $(1 - x - y)$ is the fraction of anion sites adjacent to an A^+ cation and occupied by a solvent anion D. There remain $[n_{BD} + n_H + n_{AD} + n_{BC} - Zn_{AD}]$ anion sites which are *not* adjacent to an A^+ , but only to B^+ . These anion sites will be occupied by $(n_{BC} - xZn_{AD})$ anions C^- , $(n_H - yZn_{AD})$ ligands H, and $[n_{BD} + n_{AD} - (1 - x - y)Zn_{AD}]$ solvent anions D^- . The n_i are the numbers of moles of the components multiplied by Avogadro's number.

The energy of the lattice, relative to a configuration in which no ligands C or H are adjacent to A (infinite dilution of C and H), is

$$E = xZn_{AD}\epsilon_C + yZn_{AD}\epsilon_H \quad (3)$$

Since eq 3 neglects the change of the interaction energies with addition of successive ligands, as well as the presence of next-nearest neighbor A-A pairs, it represents the limiting case of dilute solutions of BC, AD, and H in BD.

If the cations are restricted to a sublattice of cations while the anions and H occupy sites on the "anion" sublattice, the combinatorial factor for the entire lattice is

$$\Omega = \Omega_+ \Omega_- \quad (4)$$

If the cations A^+ and B^+ are considered randomly mixed on the cation sublattice

$$\Omega_+ = \frac{(n_{AD} + n_{BC} + n_{BD})!}{n_{AD}!(n_{BC} + n_{BD})!} \quad (5)$$

The combinatorial factor for the anion sublattice is

$$\Omega_- = \left(\frac{(Zn_{AD})!}{(xZn_{AD})!(yZn_{AD})!((1-x-y)Zn_{AD})!} \right) \times$$

$$\left(\frac{(n_H + n_{BC} + n_{BD} + n_{AD} - Zn_{AD})!}{(n_{BC} - xZn_{AD})!(n_H - yZn_{AD})! \times (n_{AD} + n_{BD} - (1-x-y)Zn_{AD})!} \right) \quad (6)$$

The first factor on the right-hand side of eq 6 gives the number of distributions of C, H, and D among sites adjacent to A, while the second term gives the number of distributions among sites adjacent only to B. To obtain the most probable distribution of the "ligands" C and H between sites adjacent to A and sites not adjacent to A, the logarithm of the combinatorial factor Ω is maximized subject to the constraint of eq 3 on the energy of the "lattice."²⁰ Application of Stirling's approximation leads to the distributions of C and H

$$\frac{x}{1-x-y} = \frac{n_{BC} - xZn_{AD}}{n_{AD} + n_{BD} - (1-x-y)Zn_{AD}} e^{-\epsilon_C/kT}$$

$$\frac{y}{1-x-y} = \frac{n_H - yZn_{AD}}{n_{AD} + n_{BD} - (1-x-y)Zn_{AD}} e^{-\epsilon_H/kT} \quad (7)$$

Equations for the Chemical Potential and for the Association Constants

From the Helmholtz free energy, $A = E - TS$, with $S = k \ln \Omega_{\text{most probable}}$, and using eq 3-7, the chemical potential of the component BC may be obtained

$$\frac{\mu_{BC}}{NkT} = \frac{1}{kT} \frac{\partial A}{\partial n_{BC}} = \ln \frac{1 + R_{BC}}{1 + R_{AD} + R_{BC}} +$$

$$\ln \frac{R_{BC} - xZR_{AD}}{1 + R_{AD} + R_{BC} + R_H - ZR_{AD}} \quad (8)$$

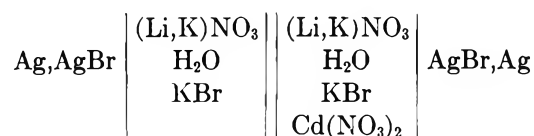
where the R are mole ratios of the solute components, moles of solute component per mole of solvent BD. Writing μ_{BC}^* for the chemical potential of BC in the absence of AD ($R_{AD} = 0$)

$$\frac{\mu_{BC} - \mu_{BC}^*}{NkT} =$$

$$\ln \left[\left(\frac{R_{BC} - xZR_{AD}}{1 + R_{AD} + R_{BC} + R_H - ZR_{AD}} \right) \times \left(\frac{1 + R_{BC}}{1 + R_{AD} + R_{BC}} \right) \left(\frac{1 + R_{BC} + R_H}{R_{BC}} \right) \right] \quad (9)$$

The difference $[\mu_{BC} - \mu_{BC}^*]$ is the quantity which is determined experimentally in the measurements of the emf of cells^{11,19} such as

(20) T. L. Hill, "Introduction to Statistical Thermodynamics," Addison-Wesley Publishing Co., Reading, Mass., 1960.



In applying the model, cadmium ion is represented by A, bromide by C, water by H, and (Li,K)NO₃ by BD. In such cells, it has been observed that in the absence of A (e.g., cadmium ion), the cell follows the Nernst equation in the concentration of BC (e.g., halide) at a fixed concentration of water. Inspection of eq 8 shows that μ_{BC}^* , the chemical potential of BC when $R_{\text{AD}} = 0$, is a linear function of the logarithm of R_{BC} when $R_{\text{BC}} \ll R_{\text{H}}$, i.e., at the concentrations studied. Thus the equation has the correct limiting form.

In a mixture at any fixed water content R_{H} , the thermodynamic association constant for the formation of AC is ^{11,16,17,19}

$$K_1 = \lim_{\substack{R_{\text{AD}} \rightarrow 0 \\ R_{\text{BC}} \rightarrow 0}} \left(\frac{\partial(\mu_{\text{BC}}^* - \mu_{\text{BC}})/NkT}{\partial R_{\text{AD}}} \right)_{R_{\text{BC}}, R_{\text{H}}} \quad (10)$$

(The values of K_1 calculated at different water contents from eq 10 will differ in general since the ligand C may displace either a solvent anion D or a ligand H.) Differentiation of eq 9 gives the corresponding equation obtained from the model

$$\lim_{\substack{R_{\text{AD}} \rightarrow 0 \\ R_{\text{BC}} \rightarrow 0}} \left(\frac{\partial(\mu_{\text{BC}}^* - \mu_{\text{BC}})/NkT}{\partial R_{\text{AD}}} \right)_{R_{\text{BC}}, R_{\text{H}}} = 1 + \frac{Z - 1}{1 + R_{\text{H}}} - \frac{Z\alpha}{1 + \beta R_{\text{H}}} \quad (11)$$

where $\alpha = e^{-\epsilon_{\text{C}}/kT}$ and $\beta = e^{-\epsilon_{\text{H}}/kT}$. Combining eq 10 and 11

$$\frac{1}{\alpha} + \frac{\beta}{\alpha} R_{\text{H}} = \frac{Z}{K_1 + 1 + \frac{Z - 1}{1 + R_{\text{H}}}} \cong \frac{Z}{K_1} \quad (12)$$

(The neglected term $1 + [(Z - 1)/(1 + R_{\text{H}})]$ in eq 12 is generally of the order of 0.2–0.5% of K_1 , but may easily be included if necessary.) Equation 12 predicts a linear dependence of the reciprocal of the association constant on the mole ratio of water at constant temperature and may be applied to the data reported previously.¹⁹ The terms α and β are temperature dependent.

Application of the Equations

Equation 12 gives the dependence of the association constants on water concentration and on temperature in terms of the parameters Z , ϵ_{H} , and ϵ_{C} (or Z , α , and β). If a reasonable value of Z is assumed, say $Z =$

6, ϵ_{C} may be determined from measurements of the association constant in the anhydrous molten salt solvent at a single temperature.^{16–18} A value of ϵ_{H} may then be determined from the association constant at a single water content. Using the parameters ϵ_{H} and ϵ_{C} obtained from measurements in the anhydrous salt and in one aqueous mixture at a single temperature, the dependence of K_1 on temperature and on water concentration may be calculated. Measured values of the association constant of CdBr⁺ in equimolar LiNO₃–KNO₃–0.10 mole of H₂O/mole of NO₃ at 168° and in anhydrous salt are used below to calculate the association constants at 119° over a range of water contents.

The association constant for CdBr⁺ in LiNO₃–KNO₃–0.1 mole of H₂O/mole of NO₃ at 168° is $K_{168,0.1} = 5800$ (moles of solvent/mole).¹⁹ The association constant for CdBr⁺ in anhydrous LiNO₃–KNO₃ has been measured at 240 and at 171°.²¹ The observed constancy²¹ of $\epsilon_{\text{C}} = \Delta A_{\text{CdBr}}$ at these temperatures makes it reasonable to calculate K at 168° in the anhydrous solvent ($K_{168,0} = 8200$) from the equation of the quasi-lattice model of molten salts, $K = Z(e^{-\epsilon_{\text{C}}/kT} - 1)$.^{9–11,19} Substitution of the values of $K_{168,0}$ and $K_{168,0.1}$ corresponding to $R_{\text{H}} = 0$ and $R_{\text{H}} = 0.1$ in eq 12 allows one to solve for the value of β at 168° and hence ϵ_{H} . The values of α and β at 119° were then calculated from ϵ_{C} and ϵ_{H} , giving the dashed line of Figure 1. The points are the values of Z/K_1 corresponding to the experimentally determined association constants.¹⁹ In Figures 2 and 3 the calculation is repeated with $Z = 4$ and $Z = 5$. Figure 3 shows also the effect of the experimental uncertainty in the measurement of $K_{168,0.1}$ on the calculation. The three dashed lines were calculated with the best value and the estimated upper and lower limits of $K_{168,0.1}$.

The fact that the equation, with parameters calculated from data in the anhydrous molten salt and in the mixture containing 10 mole % water at 168°, predicts the results of the experimental measurements at 119° and up to 50 mole % water must be at least in part fortuitous. The equations were derived for solutions dilute in all solutes including H; only the configurational entropy of the lattice was considered and the orientational disorder of the water dipoles has not been included. In spite of these approximations, the model describes the gross features of the competing equilibria and the simple form of the limiting equation (eq 12) obtained from the model is not readily apparent from an ordinary mass action treatment of the association equilibria.

(21) J. Braunstein and A. S. Minano, *Inorg. Chem.*, **3**, 218 (1964).

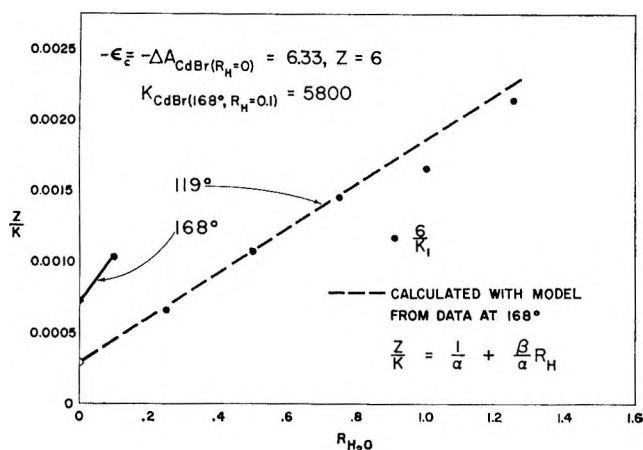


Figure 1. Z/K_1 vs. mole ratio of water with $Z = 6$. The points are the experimental values obtained by graphical analysis of the data. The dashed line at 119° is calculated with the model from the data at 168° .

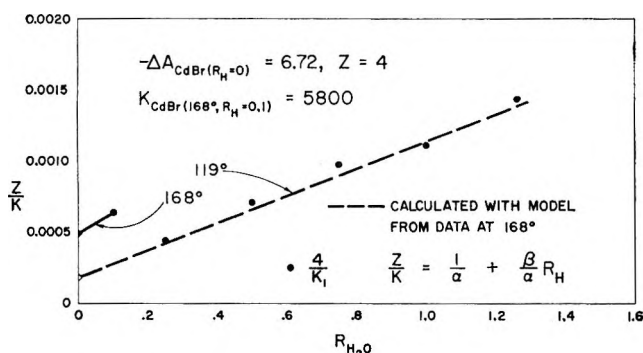


Figure 2. Z/K_1 vs. mole ratio of water with $Z = 4$: ●, experimental, obtained by graphical analysis; ---, calculated from the model.

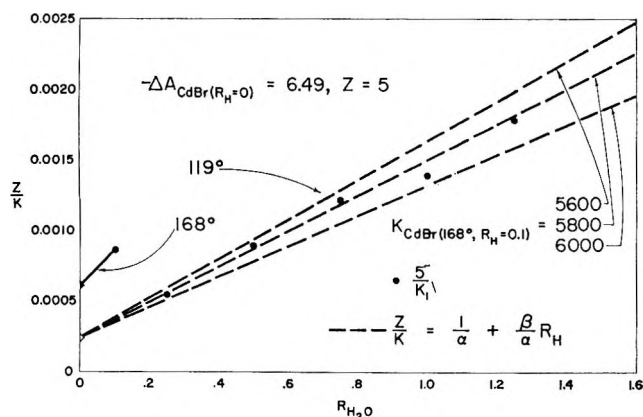


Figure 3. Z/K_1 vs. mole ratio with $Z = 5$: ●, experimental, obtained by graphical analysis; ---, calculated from the model using the best value and the upper and lower limits of K_{CdBr} (168° , $R_{H_2O} = 0.1$).

The values of the parameters with $Z = 6$ were $\epsilon_C = -6.33$ kcal/mole for association in the molten salt and $\epsilon_H = -1.33$ kcal/mole for the stability of Cd- H_2O pairs relative to Cd- NO_3 pairs in $(Li, K)NO_3$.

Association Equilibria

The parameters of the quasi-lattice model may be related to the conventional equilibrium constants of a classical mass action treatment of the association and hydration equilibria. Equations have been derived recently for the evaluation of thermodynamic association constants of mixed ligand species.²² If the solutes AD, BC, and H in the solvent BD can form associated species such as AC, AH, AHC, A_2C , etc., a material balance on the component BC may be written

$$R_{BC} = R_C + R_{AC} + R_{ACH} + 2R_{AC_2} + \dots$$

The terms on the right-hand side are mole ratios of the "free" or "unassociated" C and of the various "associated species" containing C. The phrase "formation of species such as AC, AHC, etc.," refers to the replacement of solvent anions D from the coordination sphere of a cation A by C, H, etc., so that the "species" indicated above represent shorthand notations for configurations on the quasi-lattice such as ACD_{Z-1} , $AHCD_{Z-2}$, etc., rather than the formation of immobile new entities. Introducing the formal association constants for the species, assuming that the species follow Henry's law

$$\begin{aligned} \frac{R_{AC}}{R_A R_C} &= K_{AC} \\ \frac{R_{AC_2}}{R_A R_{C_2}} &= K_{AC_2} \\ \frac{R_{ACH}}{R_A R_C R_H} &= K_{ACH} \\ \frac{R_{AH}}{R_A R_H} &= K_{AH} \end{aligned} \quad (13)$$

and identifying the stoichiometric activity coefficient γ_{BC} with the fraction of "free" C, we may write

$$1/\gamma_{BC} = \frac{R_{BC}}{R_C} = 1 + K_{AC}R_A + K_{ACH}R_A R_H' + 2K_{AC_2}R_A R_C + \dots \quad (14)$$

$R_{H'}$ is the mole ratio of "free" H, to distinguish it from R_H , the stoichiometric mole ratio of H. Similar material balances for AD and H may be written and com-

(22) J. Braunstein and R. M. Lindgren, *Electrochim. Acta*, 12, 299 (1967).

bined with eq 14 to obtain a series for $1/\gamma_{BC}$ in the stoichiometric mole ratios of the solute components. The over-all association constant for the formation of AC from AD_z , $AD_{z-1}H$, etc., is

$$K_1 = \lim_{\substack{R_{AD} \rightarrow 0 \\ R_{BC} \rightarrow 0}} \left(\frac{\partial 1/\gamma_{BC}}{\partial R_{AD}} \right)_{R_{BC}, R_H} \quad (15)$$

$$= K_{AC} + (K_{ACH} - K_{AC}K_{AH})R_H + \dots$$

(higher powers in R_H)

The experimental values of K_1 are not linear in R_H and the higher powers of R_H may not be neglected except at the lowest concentrations. To compare eq 15 with 12 of the quasi-lattice model, the reciprocal of K_1 , as given by eq 15, may be expanded to find the limit and the limiting slope. The limiting value of $1/K_1$ as R_H approaches zero is $1/K_{AC}$. The limiting slope is

$$\lim_{R_H \rightarrow 0} \left(\frac{\partial 1/K_1}{\partial R_H} \right) = \frac{K_{AH}}{K_{AC}} \left(1 - \frac{K_{ACH}}{K_{AC}K_{AH}} \right) \quad (16)$$

The statistical value of the ratio of association con-

stants $K_{ACH}/K_{AC}K_{AH}$ is $[Z(Z-1)]/ZZ = (Z-1)/Z$. If this statistical ratio is incorporated into eq 16, the limiting form of eq 15 becomes

$$\frac{Z}{K_1} = \frac{Z}{K_{AC}} + \frac{K_{AH}}{K_{AC}}R_H + \dots \quad (17)$$

but $K_{AC} = Z(e^{-\epsilon_C/kT} - 1) = Z(\alpha - 1)$ and $K_{AH} = Z(\beta - 1)$.¹⁸ If α and β are much greater than 1, the limiting forms (eq 17 and 12) become identical. The statistical value for the ratio $K_{ACH}/K_{AC}K_{AH}$ is implicit in eq 12 since ϵ_C , the energy of a ligand C on a site adjacent to A, was considered independent of the occupancy of the $(Z-1)$ other sites adjacent to A.

The quasi-lattice method and the classical mass action method are equivalent if carried to the same approximation. The quasi-lattice method, by focusing attention on the physical assumptions underlying the equations, is suggestive of more general physical relations.²³

(23) M. Blander, "Molten Salt Chemistry," John Wiley and Sons, Inc., New York, N. Y., 1964, pp 212-217.

Localized Adsorption on Graphite Surfaces

by Conway Pierce and Bland Ewing

Department of Chemistry, University of California, Riverside, California (Received February 6, 1967)

Low-pressure isotherms on graphite are reported for benzene, toluene, thiophene, cyclohexane, and *n*-hexane using an improved volumetric adsorption system based on a diaphragm gauge sensitive to 0.0001 torr. Benzene isotherms below the freezing point show no lateral interactions at any coverage, have a heat of adsorption equal to the heat of vaporization during filling of the first layer, are concave to the *p* axis at low coverage, and show no change in V_m with temperature. To explain these properties, it is postulated that there is strong localization at lattice sites due to similarity of the aromatic nucleus hexagon to lattice hexagons of graphite. Toluene also gives a concave isotherm in keeping with this localization, but all others have normal convex isotherms. The localized model provides the basis for an absolute surface area measurement.

When physical adsorption occurs on a nonuniform surface, the isotherm has the Langmuir-BET shape, concave to the *p* axis at low coverage, but when the surface is uniform, the isotherm is normally convex to the *p* axis in this region. Many studies have shown that this convex shape is due to lateral interactions between adsorbate molecules which cause an increase in the heat of adsorption as the surface population increases. These lateral interaction contributions do not show up for adsorption on a nonuniform surface for two reasons: (1) the heat decreases initially with coverage due to progressive filling of the hot sites; and (2) localization by preferential filling of these sites tends to hold ad-atoms apart so that they do not interact. Measurements of Beebe, *et al.*,¹ for heats of adsorption on a nonuniform surface carbon black and a uniform surface graphite prepared from the same black were among the first to demonstrate the difference.

The only isotherms yet reported that have the Langmuir concave shape for adsorption on uniform surfaces are those for benzene on graphite²⁻⁵ and on boron nitride,⁴ whose surface is quite similar to that of the basal plane of graphite. This unique shape suggests that when benzene molecules are adsorbed on graphite (or boron nitride), there is a localization at lattice sites, somewhat like localization at hot sites on a heterogeneous surface. This hypothesis has been tested by further studies of the adsorption of benzene and related molecules on a uniform surface graphite.

Experimental Section

A system using mercury cutoffs (in place of greased stopcocks) and McLeod gauges for pressure measurements was first used to measure isotherms of benzene, cyclohexane, and toluene. The isotherms obtained had high precision down to very low pressures, but when they were used to compute isosteric heats of adsorption it was found that the measurements at the lower pressures were not accurate; the computed heat curves in this region had anomalous peaks. This led to a re-examination of the experimental procedures and the discovery that McLeod gauge measurements at low pressures are subject to an error due to streaming of mercury vapor. As vapor flows from the gauge at room temperature to a region of lower temperature, it pumps gas from the gauge, thereby causing the measured pressure to be too low. Recent studies of this error have been made by Meinke and Reich⁶ and by Carr.⁷ The

(1) R. A. Beebe, J. Biscoe, W. R. Smith, and C. B. Wendell, *J. Am. Chem. Soc.*, **69**, 95 (1947).

(2) B. W. Davis and C. Pierce, *J. Phys. Chem.*, **70**, 1051 (1966).

(3) A. A. Isirikyan and A. V. Kiselev, *ibid.*, **65**, 6016 (1961); *Russ. J. Phys. Chem.*, **38**, 821 (1964).

(4) R. A. Pierotti and R. E. Smallwood, *J. Colloid Interface Sci.*, **22**, 469 (1966).

(5) S. Ross and J. P. Olivier, "On Physical Adsorption," Interscience Publishers, Inc., New York, N. Y., 1964.

(6) C. Meinke and G. Reich, *Vacuum*, **13**, 579 (1963).

(7) P. H. Carr, *ibid.*, **14**, 37 (1964).

magnitude of the error depends upon (1) the absolute pressure of vapor, (2) its molecular weight, (3) the conductance of the system, and (4) the temperature at the McLeod gauge. The effect was confirmed by measurements with cyclohexane vapor at an apparent pressure of 3.40μ . When the mercury reservoir was warmed a few degrees, the pressure dropped to 2.91μ , and when cooled it rose to 4.11μ , a variation that shows drastically the unreliability of the McLeod gauge. Many published isotherms based on such gauges must therefore be interpreted with caution.

After recognition of the limitation of McLeod gauges, the system was redesigned to replace these gauges by a recently developed diaphragm gauge.⁸ Tests of this gauge by Utterback and Griffith⁹ show that it gives reliable measurements down to very low pressures and that the response is independent of the molecular weight of the vapor. Pressures are measured electronically by a change of capacitance as the diaphragm is deflected by gas pressure. Since no mercury is required in the gauge, the cutoffs of the preceding design could be replaced by metal bellows valves¹⁰ using Viton O-ring seals, thereby eliminating all mercury vapor from the system.

The system now used consists of two portions, a manifold (M) for introduction of vapor and measurement of doses and a sample tube region (S) for measurement of equilibrium pressures. Two separate gauges are employed, one at M with a range of 0–30 torr and one at S with a range of 0–3 torr. The latter has a sensitivity of 0.0001 torr. In operation a dose of vapor is admitted to M and its pressure measured. The valve to S is then opened and the vapor condensed by liquid nitrogen into a U tube leading to the sample. If the pressure reading at this time is measurable, the system is pumped to remove any air present. The valve to S is then closed, the liquid nitrogen removed from the U trap, and the pressure change followed by the 3-torr gauge until it becomes constant. Equilibrium times vary from several hours at very low pressures to about 20 min at higher pressures.

The manifold is calibrated for each adsorbate by condensing several measured doses into a charcoal-filled tube in a liquid nitrogen bath and weighing the tube. A relative calibration of the volumes in M and S is made by helium at each sample temperature to use in computing the weight of unadsorbed vapor in the dead space of S. Since the system is designed for use at pressures below 3–4 torr only, no attempt is made to minimize the dead space. The room temperature volumes of M and S are each about 150 ml. The sample tube is made from 15-mm tubing, which eliminates the need for thermal transpiration corrections.

Dusting of powder into the line is prevented by a porous glass frit directly above the sample region.

Constant temperature of the sample tube is maintained by a well-stirred bath of petroleum ether, cooled by aspirating liquid nitrogen through a copper coil in the bath, as described by Graham.¹¹ The sensing element is a differential vapor pressure thermometer filled to 1 atm of pressure with an appropriate vapor for the temperature range in use. This system gives accurate control at temperatures ranging from 20 to -50° (or lower) and can be reset quickly for any desired temperature. A small bulb, packed with steel balls to facilitate heat transfer, is immersed in the bath and filled with pure adsorbate prior to each isotherm. This bulb is connected to M by a valve, so that the 30-torr gauge is used for reading p_0 at frequent intervals. For adsorbates where accurate vapor pressure data at the operating temperatures are available, the p_0 readings are used to compute the isotherm temperature. Otherwise, the bath temperature is read by a mercury or pentane thermometer.

The adsorbent is a 6.30-g sample of the graphitized carbon black, Sterling MT (3100°) used in previous studies.² The nitrogen area, if σ is taken as $16.2 \text{ \AA}^2/\text{molecule}$ at V_m , is $7.65 \text{ m}^2/\text{g}$. As previously shown,¹² however, there are reasons to question the use of 16.2 \AA^2 for N_2 when adsorbed on graphite. The MTg area

Table I: Adsorbates and Isotherm Temperatures

Adsorbate	Temp, °C	p_0 , torr
Benzene	0	24.3
Benzene	-10.5	11.0
Benzene	-20.6	4.70
Toluene	0	6.84
Toluene	-11.3	3.12
Thiophene	-20	5.7
<i>n</i> -Hexane	-38.3	3.80
Cyclohexane ^a	-45.3	1.00
Cyclohexane ^a	-28.5	4.00

^a The cyclohexane isotherms were measured by McLeod gauges only. Since their shape showed that lateral interactions are strong, they were not repeated with the new system. The more accurate one (at -28°) is plotted in Figure 2. The gauge error probably affects it in the region below $0.5V_m$ only.

(8) MKS Instruments, Inc., Burlington, Mass.

(9) N. G. Utterback and T. Griffith, Jr., *Rev. Sci. Instr.*, **37**, 866 (1966).

(10) Granville-Phillips Co., Boulder, Colo.

(11) D. Graham, *J. Phys. Chem.*, **66**, 1815 (1962).

(12) C. Pierce and B. Ewing, *ibid.*, **68**, 2562 (1964).

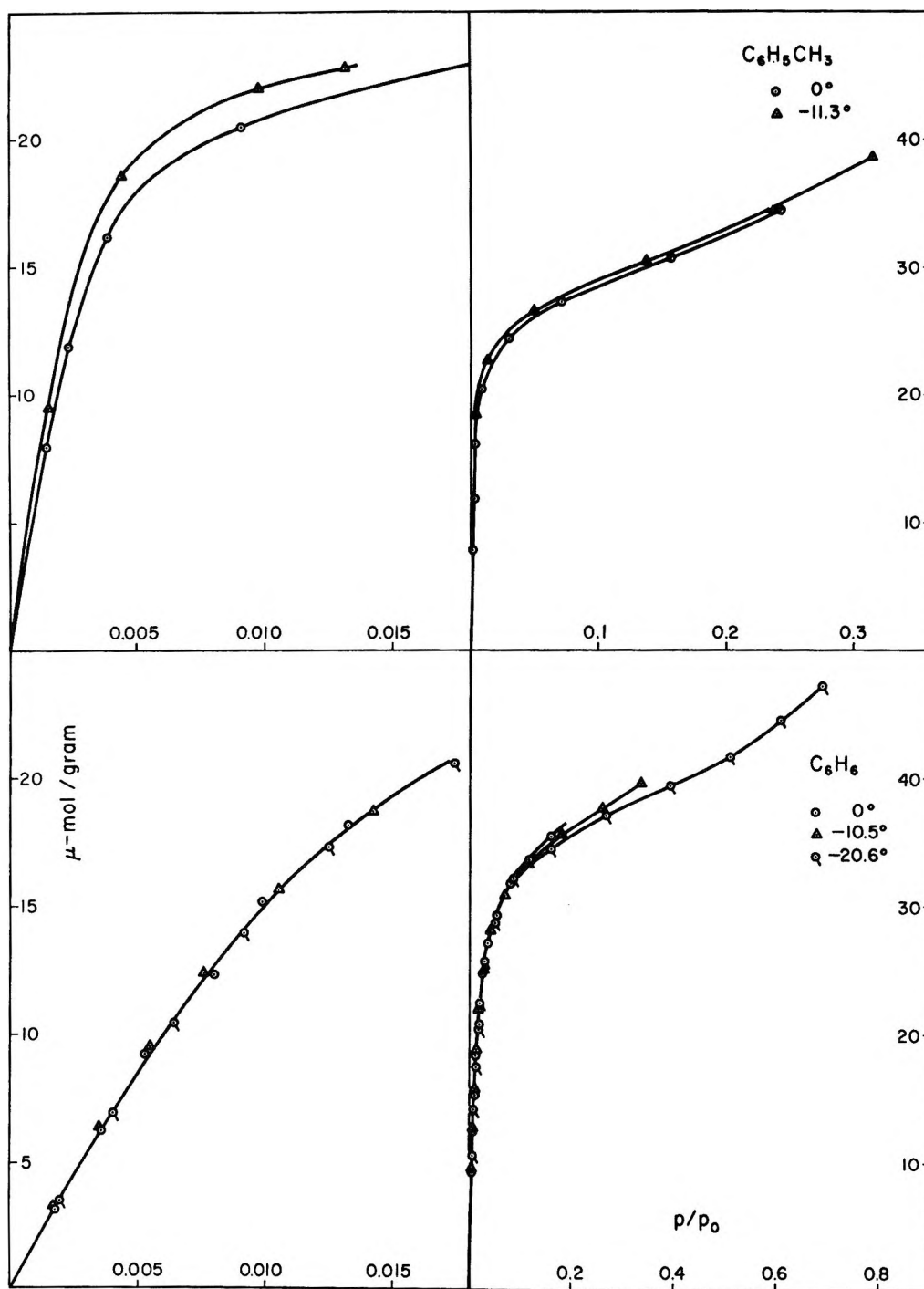


Figure 1. Isotherms for benzene (lower) and toluene (upper).

by other vapors was given as $9.1 \pm 0.4 \text{ m}^2/\text{g}$. A list of adsorbates, isotherm temperatures, and p_0 values is given in Table I.

Results and Discussion

The isotherms, Figures 1 and 2, show that toluene adsorption is like that of benzene in that the isotherm

is initially concave to the p axis. Isotherms for all the other adsorbates have the normal convex shape in the low-pressure region, and as shown by Avgul, *et al.*,¹³ pyridine does also. Thus it appears that a concave

(13) N. N. Avgul, A. V. Kiselev, and I. A. Lygina, *Bull. Acad. Sci. USSR, Div. Chem. Sci.*, 26 (1962).

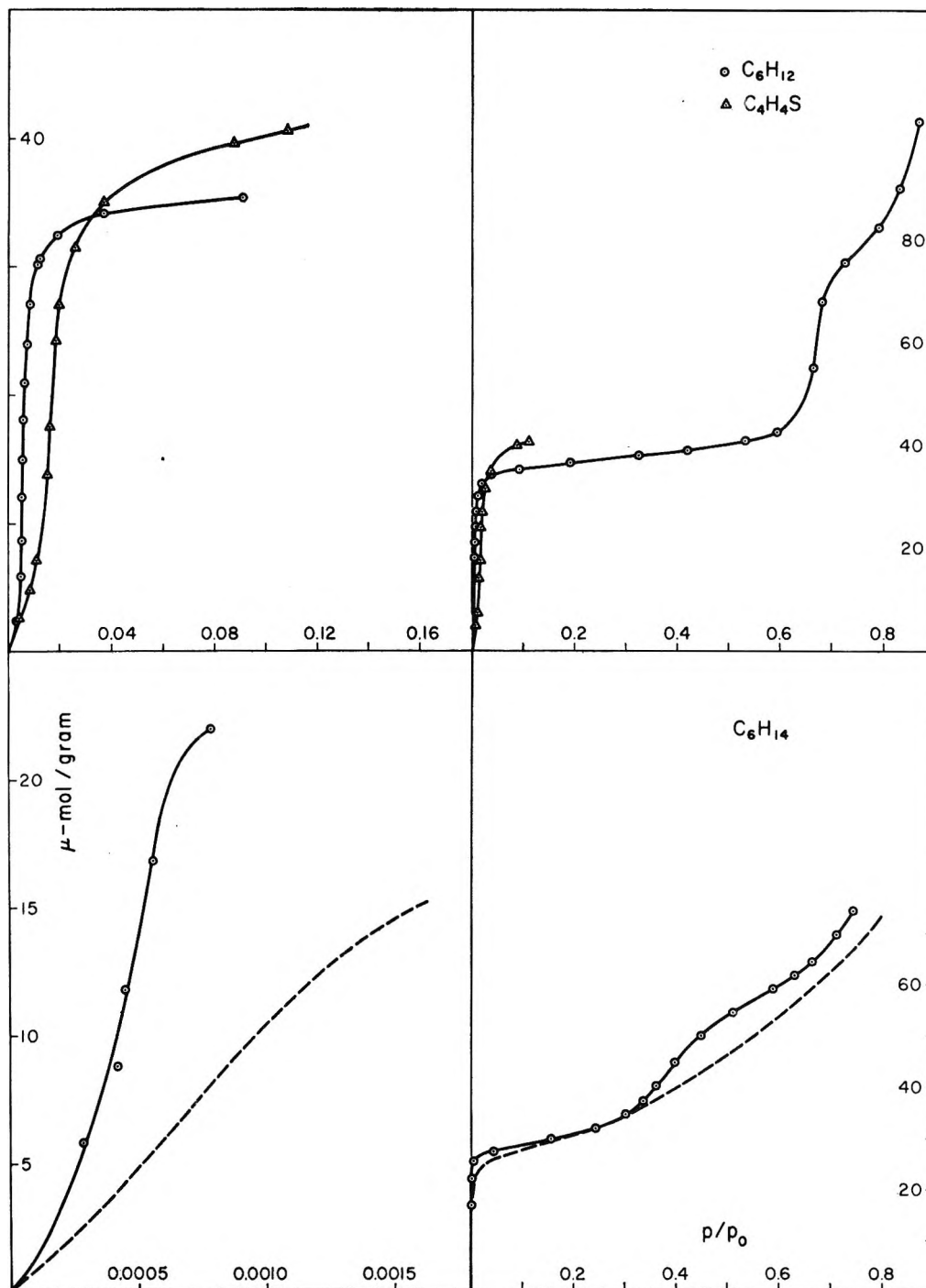


Figure 2. Isotherms for *n*-hexane (lower) and thiophene and cyclohexane (upper). Dashed curve, isotherm of Isirikyan and Kiselev at 20°.

isotherm for a uniform graphite surface is uniquely associated with presence of the benzene ring. Unusual features of benzene adsorption on graphite include the following.

1. When plotted *vs.* relative pressure, it is found that isotherms measured at temperatures below the melting

point of benzene are not temperature dependent for adsorption in the first layer. As shown in Figure 1, the isotherms at 0, -10, and -20° all fall on the same curve, which indicates that the heat of adsorption for first layer molecules is identical with the heat of vaporization. In all other systems yet investigated for

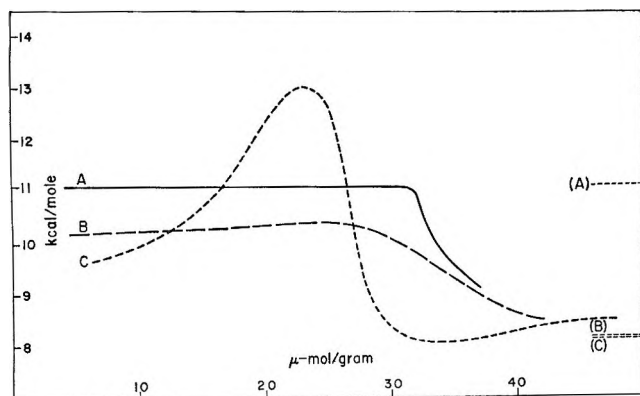


Figure 3. Differential heats of adsorption: A, isosteric heat for benzene at -15° ; B, calorimetric heats for benzene at 20° from ref 3; C, isosteric heats for *n*-hexane. Heats of vaporization shown by dashed lines at right.

a uniform surface adsorbent, a decrease in temperature is attended by increased adsorption.

Isosteric heats for benzene, computed from the isotherms at -10 and -20° , are plotted in Figure 3A along with calorimetric heats at 20° of Isirikyan and Kiselev³ in Figure 3B. The two curves have essentially the same shape, but the heat of adsorption in the first layer is some 0.9 kcal/mole higher at temperatures below the melting point than at 20° .

Neither of the heat curves for benzene shows the normal rise with increased surface coverage expected from lateral interaction between first-layer molecules. The isosteric heat for *n*-hexane in Figure 3C, computed from the isotherms at -38 and 20° , has a lateral interaction heat contribution of some 3 kcal/mole. Benzene, on the contrary, has little or no lateral interaction. Our heat curve shows no increase with coverage and that at 20° shows an increase on only 0.18 kcal/mole, from 10.20 to 10.38 kcal.

2. The previously reported effect of temperature on benzene adsorption beyond the first layer is confirmed. Past V_m , the isotherms of Figure 1 show decreased adsorption as the temperature is lowered. This abnormal behavior was attributed to an imperfect crystal effect due to orientation of first-layer molecules on the surface in a position unfavorable for further deposition of a second layer. When the temperature is increased, thermal agitation appears to permit the first-layer molecules to assume a more normal crystalline pattern, thereby favoring increased second-layer adsorption.

It appears likely that this resistance to multilayer adsorption at temperatures below the melting point is not unique for benzene but may be expected for other adsorbates. We find, for example, that when CCl_4 is adsorbed on graphite at temperatures below the

melting point, the anticipated stepwise isotherm occurs, but when the temperature is decreased, the midpoint of the second-layer step shifts from a relative pressure of about 0.75 at -26° to about 0.825 at -42° . It appears that even with the spherical CCl_4 molecules the surface forces can cause some first-layer distortion from a normal crystal pattern. Effects of this kind do not appear to occur when adsorption is at temperatures above the melting point and the adsorbed film is liquidlike.

When a decrease in temperature leads to decreased adsorption, there is, of course, a negative net heat of adsorption. As shown in Figure 3A, the heat of adsorption for benzene drops far below the heat of vaporization immediately past V_m . When the adsorbed film is liquidlike, the more normal pattern is that of Figure 3C, with a rapid fall in the heat past V_m but usually with a positive net heat as the second layer fills.

3. The monolayer volume of benzene appears to be temperature independent over a wide range, regardless of whether the isotherm is measured at temperatures above or below the freezing point. Pierotti⁴ also noted this for a temperature range from 0 to 50° . Our isotherms at 0, -10 , and -20° do not yield reliable BET plots; the best straight lines that can be drawn intercept the y axis at a point below the origin. Consequently, it is necessary to use point B estimates, but these agree well with the BET V_m of 32 $\mu\text{mole/g}$ reported by Isirikyan and Kiselev³ for adsorption on the same graphite, MT (3100°). This is the coverage at which our isotherms at three temperatures start to diverge. We know of no other adsorption system which shows such a constancy of V_m . Nitrogen on graphite¹² shows only a small change in V_m with T , but it has not been investigated on such a wide temperature range as the benzene adsorption.

These unique properties of benzene adsorption on graphite appear to support our hypothesis that benzene molecules are localized at preferred lattice positions. The structure of graphite itself suggests such an arrangement. X-Ray studies have shown that the unit hexagons of a given layer are not stacked directly over those of the next lower layer, but rather displaced in a staggered pattern, so that there is an a-b-a-b arrangement in successive layers. This indicates that long-range forces between layers, even at a separation of 3.4 Å, determine the positions of minimum energy in each layer. Since the 6-C hexagon of the benzene ring, with C-C distances of 1.39 Å, is approximately the same size as the lattice hexagon with C-C distances of 1.42 Å, each benzene ring held to the lattice may be expected to be in the same position with respect to the substrate as a unit hexagon of graphite would assume

if deposited at the surface. If so, each benzene molecule occupies nine unit hexagons, six unshared and six shared equally with a neighboring molecule.

Such a localization of benzene molecules at lattice positions would account for the unique properties of its adsorption. (1) Since each molecule is held at a lattice position, the effective cross section is determined by the lattice rather than the cross section of the molecule itself. Consequently, V_m does not change with temperature. (2) The lack of lateral interactions is due to the forces which hold each molecule within a potential well at the lattice site. If the potential well forces exceed those of lateral interaction, the molecules will not pull together as the layer fills. (3) The fact that the heat of adsorption below the melting point is the same as the heat of sublimation indicates that molecules are held at lattice sites in the same way as molecules at the surface of a benzene crystal.

As noted above, the only two molecules yet investigated whose isotherm on graphite are concave to the p axis at low coverage are benzene and toluene, the only two which possess a six-carbon ring that might fit the lattice rings so as to give localized adsorption. Even pyridine, whose six-membered ring is almost the same size as the benzene ring, does not adsorb in the same way. Rather, as shown by Avgul, Kiselev, and Lygina,¹³ both the isotherm and the heat curve indicate that there are strong lateral interactions for pyridine that are not present for benzene. Incidentally, Avgul *et al.*, suggested that the adsorption of both benzene and pyridine is "predominantly localized at ordinary temperatures," due to the correspondence of their six-membered rings to those of the graphite lattice. We feel that this is wrong with respect to pyridine because its strong lateral interactions and convex isotherm suggest a high degree of mobility for adsorbed molecules. We concur in the interpretation for benzene.

The proposed model for localization of benzene makes possible an absolute measurement of the surface area based on known lattice dimensions rather than any

assumptions regarding the cross section of the adsorbed molecule. Since each localized benzene molecule occupies nine unit hexagons, the effective cross section is $9 \times 5.24 = 47.2 \text{ \AA}^2$. If we assume that V_m is 32 $\mu\text{moles/g}$, which is the BET value at 20° (also the point at which the heat curve shows a sudden drop), and that the surface is completely uniform with all sites filled at V_m , the product of the number of first-layer molecules by the cross section of 47.2 \AA^2 gives an area of 9.1 m^2/g for MTg. This is in good agreement with our previous estimate of $9.1 \pm 0.4 \text{ m}^2/\text{g}$, based on areas by several vapors after establishing their cross sections relative to nitrogen by isotherms on a nonuniform carbon black.¹² The conventional nitrogen area is 7.65 m^2/g . We feel that altogether the evidence in favor of the higher value, 9.1 m^2 , is strong, but it is not yet conclusive. Values of the experimental cross sections of the adsorbates used in this study are therefore summarized in Table II on both standards.

Table II: Monolayer Volumes and Cross Section Areas

Absorbate	Temp, °C	V_m , $\mu\text{moles}/$ g	σ (9.1 m^2/g)	σ (7.65 m^2/g)
Nitrogen	-195	78	19.4	(16.2)
Benzene	-20 to 20	32	(47.2)	39
Toluene	-11	25	60	51
<i>n</i> -Hexane	-38	27	56	47
<i>n</i> -Hexane	20	25	60	51
Cyclohexane	-28	34	44	37
Thiophene	-20	38	40	33

Acknowledgment. This work was supported in part by a grant from the Petroleum Research Fund administered by the American Chemical Society and in part by a grant from the Intramural Research Funds of the University of California. Grateful acknowledgment is made to the donors of these funds.

Ionic Association. IV. Viscosity Effect on the Ultrasonic Relaxation of Zinc Sulfate in Water-Glycol Mixtures at 25.0°^{1a}

by Fabio Fittipaldi^{1b} and Sergio Petrucci

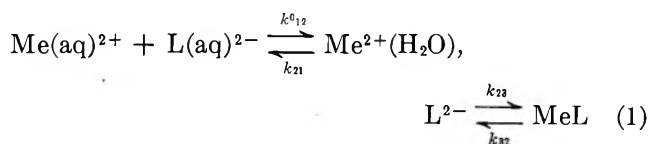
Polytechnic Institute of Brooklyn, Brooklyn, New York 11201 (Received February 7, 1967)

Measurements of ultrasonic absorption in solutions of 0.1 M ZnSO₄ in water-glycol at 25.0° in the frequency range 10–170 Mcps are presented. The observed relaxation frequencies vary from 80 Mcps in H₂O to 20 Mcps in 77 wt % glycol ($X_{\text{glycol}} = 0.5$). The relaxation times are interpreted as being due to association of ZnSO₄ with a superimposition of two steps: (1) a diffusion-controlled approach between the solvated ions and (2) a substitution of water in the first coordination sphere of the cation by the ligand. The calculated relaxation frequencies agree fairly well with the experimental ones by using a value of the substitution rate constant equal to $k_{23} = 3 \times 10^7 \text{ sec}^{-1}$ in all of the solvent mixtures investigated. It is proposed that the rate-determining step for the process is the substitution of water from the inner coordination sphere of the metal ion even in glycol-rich mixtures.

Introduction

The problem of ionic association and complexation has been studied by relaxation methods in aqueous solution by Eigen and co-workers in Göttingen;² by Hammes^{3a} and Kustin^{3b} mainly by T jump; and by Yeager⁴ and Atkinson⁵ by ultrasonics. The general view is that for 2:2 electrolytes the complexation mechanism is a multistep process involving first a diffusion-controlled approach of the two solvated ions and then the substitution of the water in the first coordination sphere of the cation during the complexation reaction.

The simplest scheme of reaction can be written as^{2,3a}



where Me(aq)^{2+} and L(aq)^{2-} are the free metal and ligand ions, $\text{Me}^{2+}(\text{H}_2\text{O})$, L^{2-} is a solvated ion pair, and MeL is the complex.

The first step is interpreted^{2,3a} as a diffusion-controlled reaction. The k_{12} can be calculated from the von Smoluchowsky⁶ and Debye⁷ relations as

$$k_{12}^0 = k_D = \frac{8NkT}{3000\eta} \left(\frac{-\beta}{e^{-\beta} - 1} \right) \quad (2)$$

where N is the Avogadro number, k is the Boltzmann constant, η is the solvent viscosity, and β is the Bjerrum parameter⁸

$$\beta = \frac{|Z_+Z_-|e_0^2}{r_D D k T} \quad (3)$$

Z_+Z_- are the ionic valencies, e_0 is the electronic charge, r_D is the distance of approach due to the diffusion process [to form $\text{Me}^{2+}(\text{H}_2\text{O})$, L^{2-}], D is the solvent dielectric constant, and T is the absolute temperature.

The second step represents the substitution of one of the coordinated waters in the inner coordination sphere

(1) (a) Grateful acknowledgment is made to the NSF through the Science Development Program of the Polytechnic Institute of Brooklyn; (b) on leave of absence from the Department of Physics of the University of Naples, G.N.S.M. of C.N.R., Naples, Italy.

(2) M. Eigen and L. De Maeyer in "Techniques of Organic Chemistry," Vol. VIII, A. Weissberger, Ed., 1963, part II, pp 895–1055.

(3) (a) G. G. Hammes and J. I. Steinfeld, *J. Am. Chem. Soc.*, **84**, 4639 (1962); (b) A. Kopawak, K. Kustin, R. F. Pasternak, and S. Petrucci, *ibid.*, **89**, 3126 (1967).

(4) J. Stuehr and E. Yeager in "Physical Acoustic," Vol. II, W. P. Mason, Ed., Academic Press Inc., New York, N. Y., 1965, part A.

(5) S. K. Kor and G. Atkinson, *J. Phys. Chem.*, **69**, 128 (1965); S. Petrucci and G. Atkinson, *ibid.*, **70**, 2550, 3122 (1966).

(6) M. von Smoluchowsky, *Z. Physik. Chem.*, **92**, 129 (1917).

(7) P. Debye, *Trans. Electrochem. Soc.*, **82**, 265 (1942).

(8) N. Bjerrum, *Kgl. Danske Videnskab. Selskab*, **7**, No. 9 (1926).

of the metal by the ligand. The generally accepted rate-determining factor is expulsion of the first water molecule from the inner coordination shell of the metal ion.^{2,3a}

Recently ultrasonic absorption of MgSO_4 in water-glycol was investigated.⁹ The purpose of the above work was to check the applicability of eq 2 to the first step of eq 1. A satisfactory description of k_{12}^0 by eq 2 could be reached. However the substitution rate k_{23} for Mg^{2+} is so much slower than k_{12}^0 (10^5 sec^{-1} compared to $10^{10} \text{ M}^{-1} \text{ sec}^{-1}$) that the pulse ultrasonics technique could only be used to study the first (and shortest) relaxation time of MgSO_4 solutions. ZnSO_4 , on the other hand, shows only one relaxation in water¹⁰ in the range of the pulse ultrasonic method.⁹

It was therefore possible to study both effects (steps 1 and 2) by a single method.

Experimental Part

The apparatus, methods, and procedures have been described elsewhere.^{9,11} The salt $\text{ZnSO}_4 \cdot 7\text{H}_2\text{O}$ (Baker reagent) was used without further purification. Analyses of the solutions (performed by the cation-exchange technique and acid titration with Tham¹² and methyl red as an indicator) gave $\pm 0.1\%$ reproducibility with the weighed amounts.

Results

Table I contains the values of α (nepers cm^{-1}) and $(\alpha/f^2)10^{17}$ ($\text{cm}^{-1} \text{ sec}^2$) at the frequencies (Mcps) investigated. The symbol X_{glycol} represents the mole fraction of glycol in the solvent mixtures.

Calculations

The relaxation frequency f_r has been calculated from the function¹³

$$\frac{\alpha}{f^2} = \frac{A}{1 + (f/f_r)^2} + B \quad (4)$$

where¹³

$$A = \frac{2\mu_{\text{max}}}{uf_r} \quad (5)$$

The parameter μ , the sound absorption per wavelength, is defined as

$$\mu = (\alpha - \alpha_0) \frac{u}{f} \text{ and } \mu_{\text{max}} = (\alpha_{f_r} - \alpha_0) \frac{u}{f_r} \quad (6)$$

where α is the absorption coefficient of sound (nepers cm^{-1}) at the frequency f , α_0 is the corresponding solvent value, u is the sound velocity (cm/sec) (approximated by the velocity of sound in the solvent and assumed independent of frequency), f_r is the relaxation frequency,

Table I: Absorption Coefficients α and Ratios (α/f^2) for 0.1 M ZnSO_4 in Water-Glycol Mixtures at 25.0°

f , Mcps	α , nepers cm^{-1}	$(\alpha/f^2)10^{17}$, $\text{cm}^{-1} \text{ sec}^2$
$X = 0.00$		
15	0.137	60.9
25	0.331	53.0
35	0.691	56.4
45	1.13	55.7
50	1.28	51.4
55	1.68	55.5
55	1.55	51.4
65	2.07	48.9
65	2.00	47.4
75	2.47	43.8
85	3.14	43.5
90	3.37	41.6
95	3.29	36.3
105	4.41	40.0
110	4.17	34.5
130	6.45	38.2
150	7.02	31.2
170	8.10	28.0
$X = 0.10$		
10	0.132	124
50	2.065	81.6
90	4.605	55.6
110	5.79	47.0
130	8.22	46.6
150	9.67	42.0
$X = 0.30$		
15	0.336	148
25	0.767	123
35	1.15	94.0
50	1.86	74.3
70	3.75	76.6
90	4.46	55.1
110	7.10	58.5
$X = 0.50$		
15	0.365	162
25	0.711	114
35	1.32	108
55	2.49	82.3
85	5.76	79.7
95	6.65	73.7
105	7.97	72.3

(9) S. Petrucci, *J. Phys. Chem.*, **71**, 1174 (1967).

(10) K. Tamm and G. Kurtze, *Acustica*, **3**, 33 (1953); **4**, 380 (1954).

(11) S. Petrucci and M. Battistini, *J. Phys. Chem.*, **71**, 1181 (1967).

(12) L. Meites in "Handbook of Analytical Chemistry," McGraw-Hill Book Co., Inc., New York, N. Y., 1963, p 334.

(13) J. Lamb in "Dispersion and Absorption of Sound by Molecular Processes," D. Sette, Ed., Academic Press Inc., New York, N. Y., 1963.

α_r is the absorption coefficient at the relaxation frequency f_r , B is the high-frequency value of (α/f^2) or the solvent value (α_0/f^2) (if no structural effects on the solvent absorption happen because of the presence of the ions¹⁰).

A fitting procedure to eq 4 of the experimental (α/f^2) and corresponding frequencies f has been applied. The precision of the present data does not allow the analysis by eq 6 or by the Mikhailov technique as done previously.⁹

In Figure 1 the values of (α/f^2) are reported as the quantity $[1 + (f/f_r)^2]^{-1}$. The solid lines in Figure 1 represent the best fit to the data. The results for A , B , and f_r are reported in Table II for all the systems investigated.

Discussion

It is assumed that ZnSO_4 follows the reaction path of scheme I. According to Eigen,¹⁴ the observed relaxation time τ $[= (2\pi f_r)^{-1}]$ is related to the rate constants and concentrations by the relation

$$\tau^{-1} = 1/2[S \pm \sqrt{S^2 - 4P}] \quad (7)$$

$$S = k_{12}\theta(c) + k_{21} + k_{23} + k_{32}$$

$$P = k_{12}\theta(c)(k_{23} + k_{32}) + k_{21}k_{32}$$

where

$$\theta(c) = \sigma c \gamma_{\pm}^2 \left(2 + \frac{\partial \ln \gamma_{\pm}^2}{\partial \ln \sigma} \right) \quad (8)$$

In order to calculate $\theta(c)$, estimates of σ , the degree of ionization, and γ_{\pm} , the mean ionic coefficient, have to be made. As in the previous case⁹ the Bjerrum function³ for the association constant has been retained

$$K_A = \frac{4\pi N r_D^3}{1000} \beta^3 Q(\beta) = \frac{1 - \sigma}{\sigma^2 \gamma_{\pm}^2 c} \quad (9)$$

with

$$Q(\beta) = \int_2^{\beta} e^{\psi} \psi^{-4} d\psi \quad (10)$$

where

$$2 = \frac{|Z_+ Z_-| e_0^2}{q D k T} \quad \psi = \frac{|Z_+ Z_-| e_0^2}{r D k T} \quad (11)$$

r is the distance between the ions and r_D is the diffusion distance as already stated.

The value $r_D = 5 \times 10^{-8}$ cm has been assumed for the above calculations. q is the Bjerrum critical distance.⁸

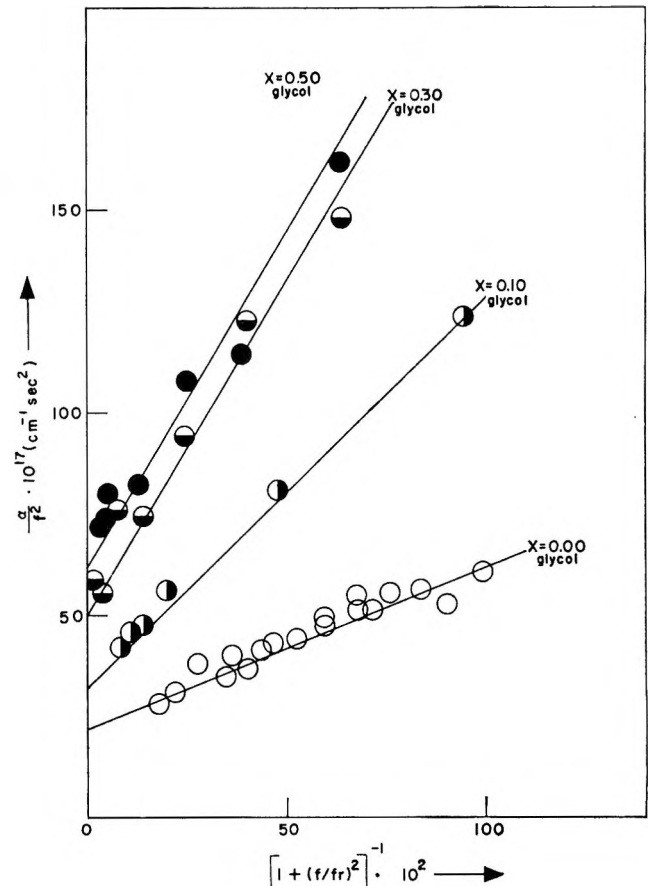


Figure 1. Graph of $(\alpha/f^2)10^{17}$ ($\text{cm}^{-1} \text{sec}^2$) vs. $[1 + (f/f_r)^2]^{-1}$ for 0.1 M ZnSO_4 in water and in water-glycol mixtures at 25°.

Table II: Values of f_r , A , and B for the Function $(\alpha/f^2) = \{A/[1 + (f/f_r)^2]\} + B$

X_{glycol}	f_r , Mcps	$10^{17}A$, $\text{cm}^{-1} \text{sec}^2$	$10^{17}B$, $\text{cm}^{-1} \text{sec}^2$
0.00	80	40	22
0.10	45	96	32
0.30	25	165	50
0.50	20	165	62

Equation 9 combined with the well-known Debye-Hückel function for the activity coefficient (and its derivative with respect to σ)⁹

$$-\log \gamma_{\pm} = \frac{S_I \sqrt{c\sigma}}{1 + A_I r_D \sqrt{c\sigma}} \quad (12)$$

gives the desired values of γ_{\pm} and σ and therefore of $\theta(c)$.

Equation 2 gives k_{12} (assuming $r_D = 5 \times 10^{-8}$ cm). The ratio is then taken

(14) M. Eigen, W. Kruse, G. Maass, and L. DeMaeyer, *Progr. Reaction Kinetics*, 2, 287 (1964).

$$\frac{k_{12}^0}{k_{21}} = K_{12}^{-1} = K_A \text{ (Bjerrum)} \quad (13)$$

Therefore $k_{21} = k_{12}^0/K_A$ (Bjerrum).

Finally, the best values to fit the results by eq 7 have been found to be $k_{23} = 3 \times 10^7 \text{ sec}^{-1}$ (in good agreement with previous results¹⁵) and $k_{32} = 10^8 \text{ sec}^{-1}$, giving $K_{23} = k_{32}/k_{23} = 3.3$. Table III contains the results for $\theta(c)$, k_{12}^0 , k_{21} , and the calculated relaxation frequencies f_r (calcd) according to eq 7. The experimental relaxation frequencies f_r (exptl) are also reported.

Table III: Calculated and Experimental Values of the Relaxation Frequency

X_{glycol}	$10^2\theta(c)$	$10^{-10}k_{12}^0$	$10^{-8}k_{21}$	f_r (calcd)	f_r (exptl)	K_{Σ}^{-1}	$K(\Lambda)$
0.00	0.60	4.24	2.53	84	80	218	200
0.10	0.40	2.42	0.89	35	45	354	355
0.30	0.18	1.65	0.19	23	25	1128	1100
0.50	0.086	0.76	0.056	23	20	1764	3160

From Table III it can be seen that the accord with the theory² is fair given the experimental error (± 5 Mcps) in the relaxation frequencies. Table III contains also

the thermodynamic association constants for the over-all process²

$$K_{\Sigma}^{-1} = \frac{1 + K_{23}}{K_{23}} K_{12}^{-1} \quad (14)$$

These data are compared in Table III with the constants $K(\Lambda)$ calculated from conductance data on the same systems.¹⁶ The agreement is excellent except for the last mixture at $X_{\text{glycol}} = 0.50$.

Conclusion

The above calculations show the effect of viscosity (changing by a factor of 8)⁹ and dielectric constant (changing by a factor of 1.5)⁹ on the relaxation frequency.

It is noteworthy that the value of $k_{23} = 3 \times 10^7$ and $k_{32} = 1 \times 10^8 \text{ cm}^{-1}$ satisfy the entire range of glycol composition.

It seems hard to avoid the conclusion that the removal of the first water around Zn^{2+} determines the rate of the over-all process even in glycol-rich mixtures.

(15) M. Eigen and R. G. Wilkins in "Mechanism of Inorganic Reactions," R. F. Gould, Ed., American Chemical Society, Washington, D. C., 1965.

(16) J. C. James, *J. Chem. Soc.*, 153 (1951).

Fluorine Magnetic Resonance Spectra of Methylfluorosilanes

by Stephen G. Frankiss

William Ramsay and Ralph Forster Laboratories, University College, London, W.C.1, England

Accepted and Transmitted by The Faraday Society (February 8, 1967)

The fluorine chemical shifts, (^{29}Si - ^{28}Si) isotope shifts, and (H,F) and (Si,F) coupling constants in six methylfluorosilanes are reported. The vicinal (H,F) coupling constants in CH_3SiFX_2 increase linearly with the vicinal (H,F) coupling constants in CH_3CFXY . Both sets of coupling constants are closely dependent on the electronegativities of the substituent groups. The geminal (H,F) coupling constants in SiHFX_2 show a general increase with the geminal (H,F) coupling constants in CHFXY , and they also increase with increasing substituent electronegativity. The directly bound (Si,F) coupling constants in methylfluorosilanes lie in the narrow range 280 ± 15 cps. The reduced directly bound (Si,F) coupling constants in a series of SiF_3X compounds become less negative with increasing electronegativity of X. The fluorine chemical shifts in methylfluorosilanes lie in a narrower region (ca. 100 ppm) than the fluorine chemical shifts in fluoroalkanes (ca. 200 ppm).

The fluorine magnetic resonance spectra of methylfluorosilanes that are reported here form part of a study of the nmr spectra of derivatives of silane. The fluorine spectra of only a few fluorosilanes have been previously reported,¹⁻¹⁰ and so it seemed worthwhile to report the spectra of a series of methylfluorosilanes, particularly as they have several similarities with the spectra of analogous fluoroalkanes.

Experimental Section

Di- and trimethylfluorosilane were prepared by previously reported methods.^{11,12} The reaction between lead fluoride and dimethyldiodosilane gave a 10% yield (based on the amount of iodide taken) of dimethyldifluorosilane. Methyltrifluorosilane and methyldifluorosilane were prepared by the fluorination of methyldiiodosilane with lead fluoride and antimony trifluoride, respectively. The yields (based on the amount of iodide taken) were 93 and 50%, respectively. A small quantity of 1,1'-dimethyl-1,1'-difluorodisiloxane was obtained (in 15% yield) as a by-product in the preparation of methyldifluorosilane.

The compounds were purified by low-temperature bulb-to-bulb distillation, their purity being checked by measurements of vapor pressure and vapor density. They were studied as solutions in trichlorofluoromethane, which was also used as an internal standard.

For each compound at least two solutions of known concentration (ca. 10 and 90% by liquid volume) were studied, but only a limited amount of 1,1'-dimethyl-1,1'-difluorodisiloxane was available, and so only two solutions of concentration (ca. 10 and 30%) of this compound were studied.

The samples were held in 5-mm o.d. Pyrex tubing, and the spectra were recorded using a Varian Associates

- (1) H. S. Gutowsky and C. J. Hoffman, *J. Chem. Phys.*, **19**, 1259 (1951).
- (2) E. Schnell and E. G. Rochow, *J. Am. Chem. Soc.*, **78**, 4178 (1956); *J. Inorg. Nucl. Chem.*, **6**, 303 (1958).
- (3) E. L. Muetterties and W. D. Phillips, *J. Am. Chem. Soc.*, **81**, 1084 (1959).
- (4) G. V. D. Tiers, *J. Inorg. Nucl. Chem.*, **16**, 363 (1961).
- (5) E. A. V. Ebsworth and J. J. Turner, *J. Chem. Phys.*, **36**, 2628 (1962).
- (6) E. A. V. Ebsworth and S. G. Frankiss, *Trans. Faraday Soc.*, **59**, 1518 (1963).
- (7) E. A. V. Ebsworth and J. J. Turner, *J. Phys. Chem.*, **67**, 805 (1963).
- (8) S. S. Danyluk, *J. Am. Chem. Soc.*, **86**, 4504 (1964).
- (9) P. L. Timms, R. A. Kent, T. C. Ehlert, and J. L. Margrave, *ibid.*, **87**, 2824 (1965).
- (10) R. B. Johannesen, T. C. Farrar, F. E. Brinckman, and T. D. Coyle, *J. Chem. Phys.*, **44**, 962 (1966).
- (11) H. J. Emeléus and M. Onyszczuk, *J. Chem. Soc.*, 604 (1958).
- (12) H. S. Booth and J. F. Suttle, *J. Am. Chem. Soc.*, **68**, 2658 (1946).

Table I: Fluorine Chemical Shifts, (^{29}Si - ^{28}Si) Isotope Shifts, and (H,F) and (Si,F) Coupling Constants in Some Methylfluorosilanes

Molecule	ϕ	$ J_{\text{SiF}} $, cps	$ J_{\text{vic}}^{\text{HF}} $, cps	$J_{\text{gem}}^{\text{HF}}$, cps	$\Delta\phi(^{29}\text{Si}-^{28}\text{Si})$
CH_3SiF_3	135 ± 1	267.9 ± 0.6	4.17 ± 0.10		0.009 ± 0.007
$(\text{CH}_3)_2\text{SiF}_2$	132 ± 1	291 ± 3	6.13 ± 0.06		0.010 ± 0.015
CH_3SiHF_2	138 ± 2	293.4 ± 0.6	6.63 ± 0.11	67.5 ± 0.2	0.007 ± 0.008
$(\text{CH}_3)_3\text{SiHF}$	159 ± 1	274 ± 2	7.15 ± 0.08		0.005 ± 0.040
$(\text{CH}_3)_2\text{SiHF}$	173 ± 3	278 ± 3	7.63 ± 0.05	52.1 ± 0.3	<i>a</i>
$(\text{CH}_3\text{SiHF})_2\text{O}$	138 ± 1	<i>a</i>	6.61 ± 0.15	68.2 ± 0.4	<i>a</i>

^a Not measured.

V4300B spectrometer operating at 40 Mc/sec with sample spinning, flux stabilization and a K-3519 field homogeneity control system. Measurements were made using side bands generated by a Muirhead Wigan D695A decade oscillator.

Results

The spectra were analyzed by a first-order treatment, and the results are given in Table I. Each measurement is the average of at least ten separate determinations, the error quoted being the calculated mean error. The directly bound (Si,F) coupling constants and the (^{29}Si - ^{28}Si) isotope shifts were measured only in the 90% solutions. The (H,F) coupling constants and fluorine chemical shifts were measured in all solutions. They showed a marginally significant concentration dependence, and so values of these parameters given in Table I are taken from measurements on the dilute (*ca.* 10%) solutions.

Discussion

Vicinal (H,F) Coupling Constants. For the limited data in Table II we find $|J_{\text{vic}}^{\text{HF}}|(\text{CH}_3\text{SiFXY})$ increases linearly with increasing $|J_{\text{vic}}^{\text{HF}}|(\text{CH}_3\text{CFXY})$, and the plot passes through the origin. This suggests that there are similar contributions to the vicinal (H,F) coupling constants in these two series of compounds; it would therefore be interesting to see if this relationship holds for other methylfluorosilanes and fluoroalkanes.

The vicinal (H,F) coupling constants in CH_3SiFXY vary approximately linearly with the sum of the Huggins electronegativities¹³ of the atoms in X and Y which are bound to the silicon atom (Figure 1). Similar relationships have been reported for the vicinal (H,F) coupling constants in fluoroalkanes¹⁴ and for the vicinal (H,H) coupling constants in substituted methylsilanes⁶ and alkanes.¹⁵⁻¹⁷

The vicinal (H,F) coupling constants in CH_3SiFXY are, to a good approximation, an additive property of

Table II: Vicinal (H,F) Coupling Constants in Methylfluorosilanes and Some Related Fluoroalkanes

Molecule	$ J_{\text{vic}}^{\text{HF}} $, (CH_3SiFXY), cps	$ J_{\text{vic}}^{\text{HF}} $, (CH_3CFXY), cps
CH_3MF_3	4.2	12.7^{19}
$(\text{CH}_3)_2\text{MF}_2$	6.1	<i>a</i>
CH_3MHF_2	6.6	20.7^{19}
$(\text{CH}_3\text{MHF})_2\text{O}$	6.6	<i>a</i>
$(\text{CH}_3)_3\text{MF}$	7.1	<i>a</i>
$(\text{CH}_3)_2\text{MHF}$	7.6	<i>a</i>
$\text{CH}_3\text{MH}_2\text{F}$	8.3^6	25.7^{19}

^a Not known.

methyl substituents, but deviations from additivity are observed for successive fluorine substitution (Table II). A similar effect is observed for the vicinal (H,H) coupling constants in CH_3SiHXY .^{6,18}

Geminal (H,F) Coupling Constants. The geminal (H,F) coupling constant in SiHFXY (where X, Y = H, F, CH_3) increases with $|J_{\text{gem}}^{\text{HF}}|(\text{CHFXY})$ in analogous compounds (Table III). Since values of $J_{\text{gem}}^{\text{HF}}(\text{CHFXY})$ in these compounds¹⁹ are almost certainly positive,²⁰ this regular increase strongly suggests that the values of $J_{\text{gem}}^{\text{HF}}(\text{SiHFXY})$ are also positive. $|J_{\text{gem}}^{\text{HF}}|(\text{SiHFXY})$ generally increases with $(E_X + E_Y)$, where E_X and E_Y are the Huggins electronegativities

(13) M. L. Huggins, *J. Am. Chem. Soc.*, **75**, 4123 (1953).(14) R. J. Abraham and L. Cavalli, *Mol. Phys.*, **9**, 67 (1965).(15) R. E. Glick and A. A. Bothner-By, *J. Chem. Phys.*, **25**, 362 (1956).(16) C. N. Banwell and N. Sheppard, *Discussions Faraday Soc.*, **34**, 115 (1962).(17) R. J. Abraham and K. G. R. Pachler, *Mol. Phys.*, **7**, 165 (1963).

(18) S. G. Frankiss, Ph.D. Thesis, Cambridge University, 1963.

(19) D. D. Elleman, L. C. Brown, and D. Williams, *J. Mol. Spectry.*, **7**, 307 (1961).(20) D. F. Evans, S. L. Manatt, and D. D. Elleman, *J. Am. Chem. Soc.*, **85**, 238 (1963).

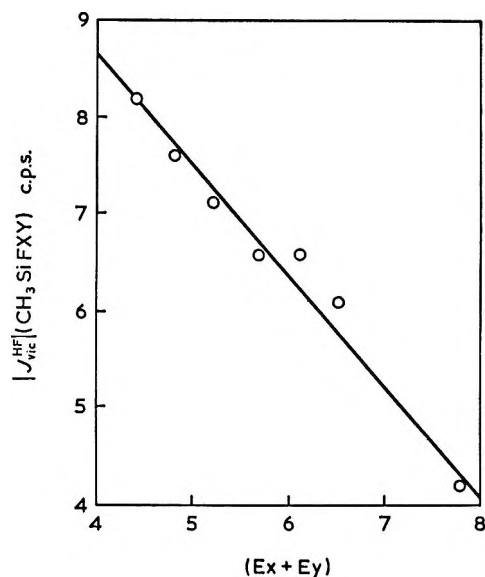


Figure 1. Plot of $|J_{vic}^{HF}|(\text{CH}_3\text{SiFXY})$ vs. $(E_X + E_Y)$, where E_X and E_Y are the Huggins electronegativities¹³ of the atoms in X and Y, respectively, which are bound to Si.

ties¹³ of X and Y. A similar relationship has been reported for $|J_{gem}^{HF}|(\text{CHF}_2\text{X})$.²¹ In spite of these regularities, neither $|J_{gem}^{HF}|(\text{SiHFXY})$ nor $|J_{gem}^{HF}|(\text{CHFXY})$ ²² is an additive property of CH_3 or F substituents.

Table III: Geminal (H,F) Coupling Constants in Fluorosilanes and Some Analogous Fluoroalkanes, and Directly Bound (Si,H) Coupling Constants in Fluorosilanes

Molecule	$ J_{gem}^{HF} $ (SiHFXY), cps	$ J_{gem}^{HF} $ (CHFXY), cps	$ J_{SiH} $ (SiHFXY), cps
MH ₃ F	45.8 ⁵	46.4 ²²	229.0 ⁶
CH ₃ MH ₂ F	48.8 ⁶	47.5 ¹⁹	222.3 ⁶
(CH ₃) ₂ MHF	52.1	<i>a</i>	215.8 ¹⁸
MH ₂ F ₂	60.5 ⁵	50.2 ²²	282 ⁵
CH ₃ MHF ₂	67.5	57.1 ¹⁹	273.1 ¹⁸
(CH ₃ MHF) ₂ O	68.2	<i>a</i>	261.1 ¹⁸
MHF ₃	96.3 ⁵	79.7 ²²	381.7 ⁵

⁶ Not known.

It is interesting to note (Table III) that $|J_{gem}^{HF}|(\text{SiHFXY})$ increases linearly with $|J_{SiH}|(\text{SiHFXY})$ for the simple fluorosilanes (though not for the methyl-fluorosilanes) since a similar relationship has been reported between the geminal (H,H) and directly bound (Si,H) coupling constants in SiH_2XY .⁵ These relationships appear to be consistent with the directly bound (Si,H) and the geminal coupling constants in

$\text{SiHF}<$ and $\text{SiH}_2<$ being dependent on the s character of the silicon hybrid orbitals.⁵

Directly Bound (Si,F) Coupling Constants. The directly bound (Si,F) coupling constants in fluorosilanes do not appear to be additive properties of the substituents. Marked deviations from additivity are observed for fluorine substitution since progressive substitution of H for F at Si in SiF_4 and CH_3SiF_3 increases and then decreases $|J_{SiF}|$. Substitution of CH_3 for H at Si in SiHFXY decreases $|J_{SiF}|$ by 1–7 cps (Table IV).

Table IV: Directly Bound (Si,F) Coupling Constants in Fluorosilanes

Molecule	$ J_{SiF} $, cps	Molecule	$ J_{SiF} $, cps
SiF ₃ SiF ₃	322 ¹⁰	SiHF ₃	275 ⁵
SiH ₂ F ₂	298 ⁵	(CH ₃) ₃ SiF	274
CH ₃ SiHF ₂	293	CH ₃ SiF ₃	268
(CH ₃) ₂ SiF ₂	291	SiF ₄	170 ²³
SiH ₃ F	281 ⁵	(SiF ₃) ₂ O	168 ¹⁰
CH ₃ SiH ₂ F	280 ⁶	(NH ₄) ₂ SiF ₆	108 ⁴
(CH ₃) ₂ SiHF	278		

The directly bound (Si,F) coupling constants in SiFXYZ , SiF_2XY , and SiF_3X (where X, Y, Z = H, CH₃) lie in the narrow range 268–298 cps, but the more symmetrical and heavily fluorinated species SiF_4 (170 cps²³) and SiF_6^{2-} (108 cps⁴) have much smaller coupling constants. For the limited number of SiF_3X compounds that have been studied (Table IV) it appears that $|J_{SiF}|$ is much smaller when X is a strongly electronegative group (*e.g.*, F or OSiF_3) than when X is a more electropositive group (*e.g.*, CH₃, H, or SiF_3). The values of the reduced (Si,F) coupling constants²⁴ K_{SiF} in these molecules, however, are almost certainly negative.⁸ Thus K_{SiF} in SiF_3X probably becomes less negative with increasing electronegativity of X, which may be related, in part, to decreasing Si–F bond ionicity along this series.

Fluorine Chemical Shifts. No simple correlations are observed between $\phi(\text{SiFXYZ})$ and $|J_{SiF}|(\text{SiFXYZ})$ like the reported increase of $\phi(\text{CFXYZ})$ with decreasing $|J_{CF}|(\text{CFXYZ})$.²⁵ There is, however, a general in-

(21) B. H. Arison, T. Y. Shen, and N. R. Trenner, *J. Chem. Soc.*, 3828 (1962).

(22) S. G. Frankiss, *J. Phys. Chem.*, **67**, 752 (1963).

(23) T. D. Coyle, R. B. Johannesen, F. E. Brinckman, and T. C. Farrar, *ibid.*, **70**, 1682 (1966).

(24) J. A. Pople and D. P. Santry, *Mol. Phys.*, **8**, 1 (1964); $K_{SiF} = (2\pi/h\gamma_{Si}\gamma_F)J_{SiF}$, where γ_{Si} and γ_F are the magnetogyric ratios of Si and F, respectively.

(25) N. Muller and D. T. Carr, *J. Phys. Chem.*, **67**, 112 (1963).

Table V: Fluorine Chemical Shifts in Fluorosilanes and Methylfluorosilanes

Molecule	ϕ	Molecule	ϕ	Molecule	ϕ	Molecule	ϕ
SiF ₄	163 ^{2,7}						
SiHF ₃	109 ⁷	CH ₃ SiF ₃	135				
SiH ₂ F ₂	151 ⁷	CH ₃ SiHF ₂	138	(CH ₃) ₂ SiF ₂	132		
SiH ₃ F	217 ⁷	CH ₃ SiH ₂ F	192 ⁸	(CH ₃) ₂ SiHF	173	(CH ₃) ₃ SiF	159

crease in $\phi(\text{SiFXYZ})$ with increasing $\phi(\text{CFXYZ})$ in analogous molecules,¹⁸ though SiF₄ and CF₄ form a significant exception. The range of fluorine chemical shifts in simple fluorosilanes and methylfluorosilanes (Table V) is about 100 ppm, which is significantly smaller than the range of fluorine chemical shifts in analogous fluoroalkanes (about 200 ppm).^{22,25} A similar effect has been noted for the proton chemical shifts in substituted silanes which are about half as sensitive to change of substituents as are the proton chemical shifts in analogous substituted alkanes.^{6,18}

The fluorine chemical shifts in methylfluorosilanes and simple fluorosilanes cannot be described by additive substituent parameters. Substitution of CH₃ or F for H at Si in SiFHXY, however, generally results in a low-field shift, though substitution in SiHF₃ is against

this trend (Table V). This effect is consistent with the fluorine shielding being determined by local paramagnetic contributions, which are negative and increase in magnitude when a neighboring group is replaced by one having more relatively low-lying states than the group it replaces.^{7,26}

Acknowledgment. The author is grateful to Dr. E. A. V. Ebsworth for his interest in this work. He is indebted to I.C.I. for the award of a research fellowship (University College) and to the D.S.I.R. for a maintenance grant (Cambridge University), during the tenure of which part of this work was done.

(26) E. Pitcher, A. D. Buckingham, and F. G. A. Stone, *J. Chem. Phys.*, **36**, 124 (1962).

Pyrolysis Kinetics of Ethyl Nitrate

by Thomas J. Houser and Betty M. H. Lee¹

Department of Chemistry, Western Michigan University, Kalamazoo, Michigan (Received February 27, 1967)

The pyrolysis rate and mechanism of ethyl nitrate have been studied in the temperature range of 242–260°. The reaction kinetics were found to be one-half order with respect to the reactant; a major portion of the organic product was a polyether, probably formed from formaldehyde. The activation energy and frequency factor were determined to be 46.8 kcal/mole and $10^{13.2}$ (mmole/l.)^{1/2} sec⁻¹, respectively. These data are consistent with a radical chain mechanism in which termination occurs through the interaction of two of the monomolecularly decomposing chain-carrying species, which is the ethoxide radical in the proposed mechanism.

Interest in the pyrolysis kinetics and mechanisms of ethyl nitrate was revived because of the ability of this compound to detonate when subjected to mechanical shock. There is evidence that the presence of gas or vapor bubbles is helpful, and in some cases necessary, in promoting detonation. In addition, the presence of oxygen in the gas bubbles greatly increases the sensitivity of compounds such as ethyl nitrate, nitroglycerine, etc.² Thus it is reasonable to conclude that detonation is initiated in the gas phase and involves the pyrolysis rates and mechanisms of the particular compound being detonated. Although mechanisms for shock-induced detonations have been discussed,^{3,4} the role of reactant pyrolysis in the process has not been clarified.

The pyrolysis rate and mechanism of ethyl nitrate has been extensively studied at temperatures up to about 200° using static systems, principally manometric techniques.^{5–9} In addition, a few higher temperature kinetic studies have been made, generally with the ethyl nitrate flame.^{10–12} Considering the very short time for detonation, the pyrolysis mechanisms of interest are those for reactions at higher temperatures. It is apparent, from the radical chain nature of explosive reactions, that the low-temperature pyrolysis mechanism, postulated to have the rate-controlling step a unimolecular type of decomposition, is considerably different from that controlling the detonation process for ethyl nitrate. In addition, the observation that oxygen inhibits the pyrolysis,⁸ contrary to its effect on detonation of ethyl nitrate, is further evidence for this

difference. Therefore, the current higher temperature study was initiated using a flow system with a stirred-flow reactor in order to obtain differential rate data¹³ under relatively well-controlled conditions.

Experimental Section

Apparatus and Procedure. The experiments were carried out in a conventional flow system utilizing a stirred-flow reactor, the design of which had been tested for stirring efficiency.¹⁴ The reactor was an 80-ml

(1) This research is in partial fulfillment of requirements for a Master's degree.

(2) F. P. Bowden, M. F. R. Mulcahy, R. G. Vines, and A. Yoffe, *Proc. Roy. Soc. (London)*, **A188**, 291 (1947).

(3) A. Maček, *Chem. Rev.*, **62**, 41 (1962).

(4) T. A. Erikson and E. L. Grove, ARF 3197-15, "Fundamentals of Liquid Propellant Sensitivity," 1962. The authors have proposed that the vaporization rate is the limiting step; however, in drop weight testing the pressures necessary to validate their mechanisms are not attained without reaction occurring first.

(5) G. K. Adams and C. E. H. Bawn, *Trans. Faraday Soc.*, **45**, 494 (1949).

(6) L. Phillips, *Nature*, **165**, 564 (1950).

(7) J. B. Levy, *J. Am. Chem. Soc.*, **76**, 3254 (1954).

(8) J. B. Levy, *ibid.*, **76**, 3790 (1954).

(9) F. H. Pollard, H. S. B. Marshall, and A. E. Pedler, *Trans. Faraday Soc.*, **52**, 59 (1956).

(10) H. Theile, *Angew. Chem.*, **A60**, 65 (1948).

(11) G. D. Adams and J. Scrivener, *Symp. Combust., 5th, Pittsburgh, 1954*, 656 (1955).

(12) J. A. Hicks, *Symp. Combust., 8th, Pasadena, Calif., 1960*, 487 (1962).

(13) A. A. Frost and R. G. Pearson, "Kinetics and Mechanism," 2nd ed, John Wiley and Sons, Inc., New York, N. Y., 1961, p 265.

cylindrically shaped Pyrex bulb with the reactant entrance tube extending about halfway down the center, terminating in five small holes pointing in all directions to act as jets to promote stirring. The flow stream exited through a tube concentric with the entrance tube. Helium, used as the carrier gas, was purified by passing through a bed of activated charcoal at liquid nitrogen temperatures. The flow rates were controlled by the customary pressure regulator and needle valve and measured by a capillary flowmeter.

After the flowmeter, the carrier gas was heated in order to vaporize the reactant being injected into the gas stream. The injection unit consisted of a motor-driven, 2-ml tuberculin syringe, Sage syringe pump, and a hypodermic needle silver soldered into a metal ball joint which connected the needle and syringe to the glass flow system. By adjusting the relative reactant injection rate and helium flow rate, it was possible to control the residence time and initial concentration of reactant. However, care had to be taken not to overheat the vaporizing reactant at the higher injection rates in order to prevent premature decomposition. Beyond the injection section it was not necessary to heat the gas stream for the reactant concentrations used.

The ethyl nitrate was passed into the reactor which was heated by an electric furnace. The temperature of the furnace was regulated to $\pm 1^\circ$ by a Versatronik controller, Model R7161H (Honeywell). Following the reactor the gas stream passed through the trapping section, which consisted of three liquid nitrogen cooled "U" traps, the last two of which were packed with glass beads to increase the cold surface area. After an experiment the volatile products and unreacted ethyl nitrate in the traps were distilled under vacuum at room temperature into a vial which contained a weighed amount of *t*-butylbenzene to be used as an internal standard for quantitative chromatographic analysis.

Chemicals. Ethyl nitrate, Eastman White Label grade, was used without further purification. However, the reactant was checked for impurities by mass spectrographic analysis (Atlas) and found to be better than 99% pure.

Analytical Techniques. For the analyses of unreacted ethyl nitrate, diethylene glycol succinate was used as the liquid phase on a Chromasorb column in an F & M Model 720 gas chromatograph. A calibration curve of known ethyl nitrate-*t*-butylbenzene weight ratios *vs.* peak area ratios was constructed. The internal standard was selected because of its relatively long retention time; thus its elution did not overlap those of the reactant and volatile products. It was apparent from the calibration data that although the inlet and

column were heated, there was no significant amount of decomposition of the reactant in the chromatograph. The mass spectra of volatile products from two experiments were obtained using an LKB-9000 instrument. Infrared (mineral oil mull) and nmr spectra of the polymer were determined with Beckman IR-8 and Varian A60 instruments, respectively.

Results

Products. The presence of NO and NO₂ was apparent from the colors observed in the traps: the characteristic brown for NO₂ and blue for condensed N₂O₃. The mass spectra of the volatile products were run on samples from pyrolyses at about 260° under reaction conditions that would produce about 60% decomposition. The relative sizes of the key peaks (from the point of product identification) of a typical mass spectrum are shown in Table I. Although without detailed calibration data of peak heights under fixed

Table I: Relative Intensities of Key Ions from Mass Spectrometer Analysis of Products

<i>m/e</i>	Relative intensity, % of base peak	Probable ion
15	17.9	CH ₃
16	1.3	O, CH ₄
18	5.3	H ₂ O
27	13.2	C ₂ H ₃
28	10.3	CO, C ₂ H ₄
29	44.2	C ₂ H ₅ , CHO
30	100	NO
31	9.4	CH ₂ OH
32	1.5	CH ₃ OH
42	2.9	C ₂ H ₂ O
43	12.3	C ₂ H ₃ O
44	10.0	CO ₂ , C ₂ H ₄ O
45	6.5	C ₂ H ₃ O
46	29.4	NO ₂ , C ₂ H ₃ OH
60	18.8	CH ₂ ONO
61	8.7	CH ₃ NO ₂
76	6.3	CH ₂ NO ₂

conditions *vs.* partial pressures it is not possible to determine exact product concentrations, based on the larger peaks, the presence or absence of significant amounts of certain species has been established with reasonable certainty. The 61 peak was attributed to the parent ion of nitromethane; none of the other possible constituents have a large 61 peak. In view of the possible reaction fragments in the mixture, the 60, 45, and 43

(14) J. M. Sullivan and T. J. Houser, *Chem. Ind. (London)*, 1057 (1965).

peaks are probably due to ethyl nitrite. It is possible to form methyl ethyl ether, isopropyl alcohol, and acetic acid from the reaction intermediates, but their formation would be less likely than that of ethyl nitrite and the 60 peak appears to be too large compared to the 45 and 43 peaks to have come from these compounds. The 32 peak indicates a significant amount of methanol present, although apparently there is more nitromethane formed. The relative sizes of the 31, 43, 44, and 45 peaks can be accounted for fairly well by the presence of ethyl nitrate, ethyl nitrite, and methanol. This does not exclude the possibility of acetaldehyde or ethanol being in the products; however, if large amounts of these were present, then it is believed that some of these ions should have been more abundant. Finally, the small 16 peak indicates that a relatively insignificant amount of methane is present since many of the products and ethyl nitrate can produce a monatomic oxygen ion when fragmented.¹⁵

A large fraction of the organic product was a polymeric solid, the quantitative determination of which is not possible since it coated the walls of the flow system and traps. The polymer was soluble in concentrated sodium hydroxide solution and cold concentrated sulfuric acid; common solvents such as alcohols, water, acetone, ether, chloroform, dimethyl sulfoxide, etc., appeared to have little effect on it. The infrared spectrum revealed moderately strong absorptions at about 1217, 1090, and 930 cm^{-1} ; the latter two were fairly broad peaks. The solubility and infrared data appear to be consistent with a polyether structure produced from the interaction of aldehydes and radicals. The lack of characteristic absorptions in the spectrum indicated the absence of NO_2 , ONO_2 , NO , ONO , $\text{C}=\text{C}$, and $\text{C}=\text{O}$ groups in the polymer. The nmr spectrum of the polymer dissolved in concentrated sulfuric acid gave three singlets at 333, 388, and 420 cps upfield from the sulfuric acid resonance. The lack of multiplet resonances indicates no hydrogens on adjacent atoms. Thus it is concluded that the polymer was probably formed from formaldehyde. On heating, the polymer appeared to soften at about 135° and sublimed with some decomposition up to about 145°. Only a small bit of brown residue was left at temperatures above 145°.

Kinetics. The kinetic data are shown in Table II. With a stirred-flow reactor, an explicit value for the rate is determined according to eq 1¹³

$$\text{rate} = (c_0 - c)/t = f(c) \quad (1)$$

where c_0 = initial concentration of ethyl nitrate and c = concentration of ethyl nitrate at contact time t . Thus, it is possible to plot values of the rate against various

functions of the concentration to obtain the best rate expression. A plot of log rate *vs.* log c was best represented by a straight line with a slope of about 0.5. The best values for the rate constants were obtained from the slopes of plots of rate *vs.* ethyl nitrate concentration to the one-half power. Table III sum-

Table II: Kinetic Data—Pyrolysis of Ethyl Nitrate

Initial concn of ethyl nitrate, mmole/l.	Contact time, sec	Decompn. ^a %	Rate ^a × 10 ² , mmoles/l. sec	[Ethyl nitrate] ^{1/2} , (mmole/l.) ^{1/2}
242°				
0.115	2.0	13.5	7.8	0.316
	3.7	26 ± 1.5	8.1	0.291
0.230	3.2	13.4 ± 0.4	9.6	0.448
	5.7	21.6	8.8	0.416
0.460	8.2	29 ± 1	8.3	0.406
	8.3	29 ± 1	16.1	0.574
	11.0	30 ± 0.5	12.5	0.570
250°				
0.115	1.3	15.2 ± 0.3	13.4	0.312
	2.0	19.8 ± 0.3	11.4	0.302
	3.2	34 ± 1.0	12.2	0.272
	3.6	38.0 ± 0.5	12.1	0.267
0.230	3.2	22 ± 2	15.8	0.422
	5.6	34.5 ± 2.5	14.2	0.386
	8.2	41.5 ± 1.5	11.5	0.365
0.460	5.6	22.5 ± 0.5	18.5	0.596
	8.2	41 ± 1	23.0	0.520
	10.8	49 ± 3	20.9	0.488
260°				
0.115	2.0	45 ± 1.5	26.0	0.250
0.230	3.1	53.5 ± 3	39.6	0.324
0.460	5.6	60 ± 1	49.3	0.430

^a The data shown represent the average when more than one experiment was conducted at the same conditions. The reproducibility of the individual points is indicated by the ± values which are the maximum deviations from the average.

marizes the values of these slopes obtained by a least-squares treatment of the data. A least-squares treatment of an Arrhenius plot of these rate constants yields

$$k = 10^{18.2} \exp(-46,800/RT) \text{ (mmole/l.)}^{1/2} \text{ sec}^{-1} \quad (2)$$

The activation energy and frequency factor are sig-

(15) Most of the reference spectra were obtained from "Index of Mass Spectral Data," ASTM. Publication No. 356, Philadelphia, Pa. The ethyl nitrate spectrum was from API, Project 44, No. 766. The ethyl nitrite spectrum was from American Oil Co., Research Department, Hammond, Ind.

Table III: Kinetic Results—Pyrolysis of Ethyl Nitrate

Temp. °K	$k \times 10^3$, (mmoles/l.) ^{1/2} sec ⁻¹	-Log t
515	2.5 ± 0.3	1.606
523	3.8 ± 0.5	1.420
533	11.4 ± 1.3	0.945

nificantly higher than those reported for the lower temperature studies. However, the value for the activation energy does agree with that reported for the pyrolysis carried out in a PbO-coated Pyrex reactor.¹⁶ This will be discussed further in the next section.

In the treatment of the data, a fit to an equation of the type $\text{rate} = k(\text{C}_2\text{H}_5\text{ONO}_2)[1/(1 + bx)]$, where x is the concentration of reactant decomposed and b is another constant, was found to be unsuitable. This form of rate equation would arise from a first-order reaction, inhibited by products, and is similar to that suggested by Levy.⁸

Discussion and Conclusions

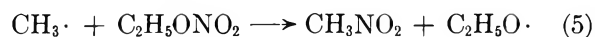
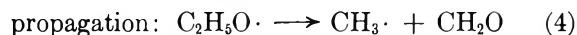
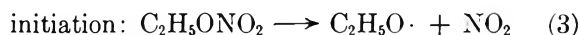
It is apparent from the results of this study that a pronounced shift in the pyrolysis mechanism of ethyl nitrate is taking place as higher temperatures are reached; it is possible that in the 240–260° range more than one mechanism may be operating.¹⁷ The principal organic products formed at the higher temperature are apparently due to fragmentation of the ethoxide radical, compared to ethyl nitrite formed in the reaction at lower temperatures. The rate is about one-half order with respect to concentration of reactant rather than the first-order rate previously reported. In comparing the present results with those obtained previously, it is worthwhile to note the criticism raised by Levy⁷ concerning the questionable validity of manometric data for systems as complex as ethyl nitrate, which yield a large number of intermediates and products that participate in several reactions simultaneously during pyrolysis.

It was found by Gray and Yoffe¹⁸ that the explosion limits of nitrate-type compounds were increased by coating the reactor walls with KCl and KI, indicating a radical chain type process for explosions. Therefore, as temperatures are increased, to produce more rapid reactions it would be predicted that a simple nonchain mechanism would shift to a radical-chain process and the mechanism with a higher activation energy would become more important.

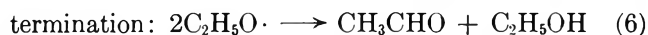
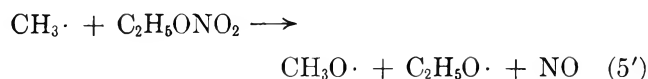
The observed activation energy of 47 kcal is about the same as those reported for the liquid-phase pyroly-

ses of compounds like erythritol tetranitrate, nitroglycerine, etc.¹⁹ These compounds produce large radicals after the initial step in the decomposition, which can relatively easily undergo further decompositions to produce chain-propagating species. The similarity in activation energies suggests that the mechanism may be similar also, resulting in a radical-chain mechanism for the pyrolysis of ethyl nitrate at about 250°.

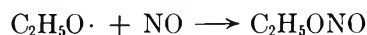
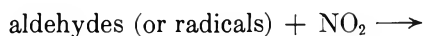
Based on the above kinetic considerations and product analysis data, the mechanism given by eq 3–6 is proposed²⁰



or



In addition there are three general steps which lead to product formation but do not enter into the kinetic scheme



A steady-state treatment of steps 3–6 yields the rate expression

$$-d(\text{C}_2\text{H}_5\text{ONO}_2)/dt = k_4(k_3/k_6)^{1/2}(\text{C}_2\text{H}_5\text{ONO}_2)^{1/2} \quad (7)$$

Although this mechanism is consistent with the current data, it is not necessarily that which would be applicable under flame and detonation conditions at higher temperatures. In support of the above mechanism are the data of Pollard, *et al.*, obtained in a cursory study of the pyrolysis of ethyl nitrate in a flow system

(16) W. R. Ellis, B. M. Smythe, and E. D. Treharne, *Symp. Combust., 5th, Pittsburgh, 1954*, 641 (1955).

(17) An attempt to obtain kinetic data at 219° using a manometric system produced data with some curvature in a $\log(P_\infty - P_t)$ vs. time plot. This may have been due to a change in mechanism as suggested by Ellis, *et al.*,¹⁶ or to the possibility that the reaction was occurring too rapidly for a static technique.

(18) P. Gray and A. D. Yoffe, *J. Chem. Soc.*, 3180 (1950).

(19) L. Phillips, *Nature*, **160**, 753 (1947).

(20) The steps leading to the formation of polymer should not be included in the kinetic scheme since polymerization took place after the reaction mixture was cooled, *i.e.*, in the line leading from the reactor and in the traps. The same is probably true for the formation of ethyl nitrite at these temperatures.

at 300°, which indicated that the formation of methyl radicals (CH_3NO_2 and CH_4 were found) and formaldehyde had become an important step in the mechanism.⁹ A second mechanism can be proposed in which the methyl radical abstracts a hydrogen atom from ethyl nitrate to form methane, but this is apparently a minor contributor to the over-all reaction.

It is appropriate to note that the results of Hicks,¹² obtained from a low-pressure flame study of ethyl nitrate, produced an activation energy and order of reaction significantly different from those reported in this paper. It is believed that these differences are mainly due to the inherent difficulty of interpreting flame speed data in terms of chemical kinetic contributions. In addition, the differences in the extent of the reaction and the amount of oxidation (*e.g.*, ethyl nitrate and NO_2 are completely consumed in the flame reaction) and that pyrolysis and oxidation do not occur in the same location in the flame (thus pyrolysis does not occur at the flame temperature) may also contribute to the lack of agreement of the results. Therefore, a detailed treatment of the flame results is not believed to be warranted in this discussion.

One final consideration is that concerned with the results of the study of the rates of decomposition on copper and PbO surfaces at about 200°.¹⁶ The rate of pyrolysis was significantly increased on the copper surface, accompanied by a drop in activation energy of about a factor of 2, typical of surface catalysis. On the other hand, the rate in a PbO -coated Pyrex reactor was significantly less than that obtained in an uncoated Pyrex reactor, accompanied by an increase of about 6 kcal in the activation energy. Although PbO coatings may be good destroyers of radicals, if the reaction in the uncoated vessel were truly homogeneous, why should there be any effect on the rate, unless a lower energy path is provided? It appears that the lower temperature mechanism may not be as simple as previously proposed and it can be concluded that there are still many questions to be answered with regard to alkyl nitrate pyrolysis.

Acknowledgment. We wish to express appreciation for the mass spectrometer analyses made by Dr. P. Bowman, Dr. M. Grostic, and Mr. R. Wnuk of the analytical sections of The Upjohn Co.

Self-Association and Hydration of Benzoic Acid in Benzene

by Roger Van Duyne, S. A. Taylor, S. D. Christian, and H. E. Affsprung

Department of Chemistry, The University of Oklahoma, Norman, Oklahoma 73069 (Received February 27, 1967)

Measurements at 25° are reported of the partition of benzoic acid between water and benzene and the solubility of water in solutions of benzoic acid in benzene at various water activities. The data indicate that the benzoic acid is highly self-associated and hydrated in the organic solvent. It is proposed that the important associated species are the acid dimer, the monomer monohydrate, the monomer dihydrate, and the dimer monohydrate. The distribution constant of the acid monomer and the formation constants for the associated species were evaluated together with their standard errors by a weighted nonlinear least-squares analysis of the data.

Introduction

Previous reports from this laboratory have described methods for determining self-association and hydration constants of polar solutes in organic solvents from partition and water solubility data.¹⁻⁵ It has been demonstrated that partition data alone, in the absence of water solubility measurements, cannot be used to calculate self-association constants of polar solutes in organic solvents.

A recent article appearing in this journal presented partition data for the system benzoic acid-benzene-water, from which dimerization constants of the acid were calculated assuming that water does not interact with the acid in the organic phase.⁶ The calculated dimerization constants are very much smaller than those obtained by Allen, Watkinson, and Webb⁷ from a careful study of the infrared spectra of anhydrous solutions of benzoic acid in benzene.

We report here a study of the hydration of benzoic acid in benzene at 25°, from which we have inferred equilibrium constants for formation of 1:1, 1:2, and 2:1 complexes between the acid and water. The results clearly indicate the important role played by small concentrations of water in the partition equilibria of carboxylic acids.

Experimental Section

Reagent grade benzoic acid (Baker and Adamson) was used without further purification. Benzene was purified by distillation through a 30-plate Oldershaw column. The temperature for all measurements was controlled at 25.0 ± 0.1°.

The benzoic acid was partitioned between water and benzene by techniques similar to those previously reported.² The equilibration of water with benzoic acid-benzene solutions at reduced water activities was achieved as described earlier.³

All benzoic acid concentrations were determined by titration with standard base. End points were detected with the aid of a Beckman Zeromatic pH meter. Measurements of water solubilities were made using a Beckman KF-3 Aquameter. The Karl Fischer reagent used in the titrations for water was standardized with solutions of pure benzene saturated with water. The solubility of water in benzene at 25° was taken to be 0.0349 *M*.⁵

Results and Discussion

Partition data for the system benzoic acid-benzene-water at 25° are presented in Figure 1, in which the distribution ratio, f_A^0/C_A^W , is plotted against C_A^W . Table I contains a compilation of the symbols used.

(1) S. D. Christian, H. E. Affsprung, and J. R. Johnson, *J. Chem. Soc.*, 1896 (1963).

(2) S. D. Christian, H. E. Affsprung, and S. A. Taylor, *J. Phys. Chem.*, **67**, 187 (1963).

(3) S. D. Christian, H. E. Affsprung, J. R. Johnson, and J. D. Worley, *J. Chem. Educ.*, **40**, 419 (1963).

(4) T. F. Lin, S. D. Christian, and H. E. Affsprung, *J. Phys. Chem.*, **69**, 2980 (1965).

(5) J. R. Johnson, S. D. Christian, and H. E. Affsprung, *J. Chem. Soc.*, 77 (1966).

(6) A. K. M. S. Huq and S. A. K. Lodhi, *J. Phys. Chem.*, **70**, 1354 (1966).

(7) G. Allen, J. G. Watkinson, and K. H. Webb, *Spectrochim. Acta*, **22**, 807 (1966).

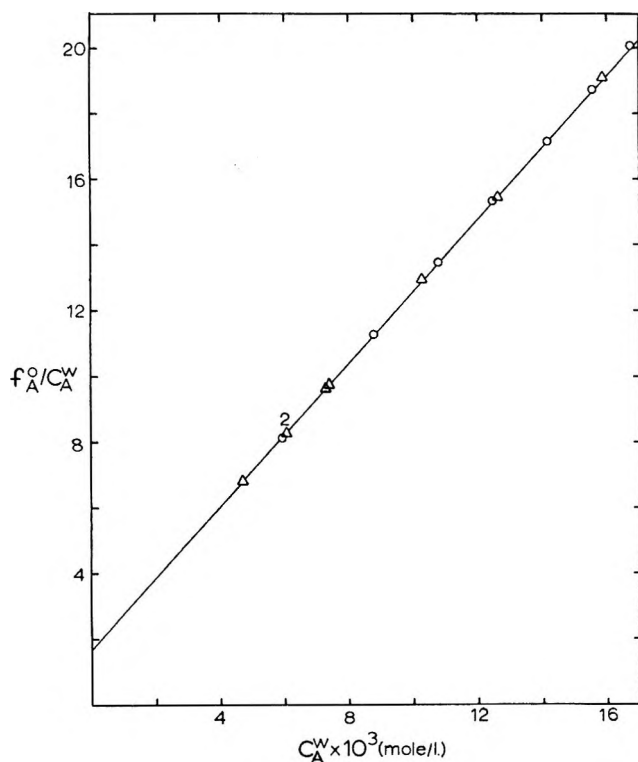


Figure 1. Partition data: O, results of this study; Δ , taken from ref 8.

Table I: Definitions of Symbols

A	Acid monomer
W	Water monomer
A ₂	Acid dimer
AW	Monomer monohydrate
AW ₂	Monomer dihydrate
A ₂ W	Dimer monohydrate
K _D	Distribution constant for the acid monomer
K ₁₁	Formation constant for monomer monohydrate
K ₁₂	Formation constant for monomer dihydrate
K ₂₀	Acid dimerization constant
K ₂₁	Formation constant for dimer monohydrate
f _A ⁰	Formal concentration of the acid in benzene
f _W ⁰	Formal concentration of water in benzene
C _A ^W	Concentration of the acid monomer in the aqueous phase
C _A	Concentration of the acid monomer in the benzene phase
C _W	Concentration of the water monomer in the benzene phase
C _W ⁰	Value of C _W at unit water activity
a _w	Water activity
Δf _W ⁰	Increase in f _W ⁰ due to hydrated acid species
S	Error function defined by eq 5
W _A	Factor weighting uncertainty in partition ratio
W _W	Factor weighting uncertainty in water solubilities
S _A	Root-mean-square deviation in partition ratio
S _W	Root-mean-square deviation in water solubility values

f_A^0 represents the formal concentration of the acid in benzene and C_A^W is the acid monomer concentration in the aqueous phase, calculated from the formal concentration of the acid and the acid ionization constant, assuming the ionic activities conform to the extended Debye-Hückel equation.⁸ Water solubility data are given in Figure 2, presented as the formal concentrations of water and acid in benzene, f_W^0 vs. f_A^0 , corresponding to several fixed values of the water activity, a_w .

Several choices of plausible hydrate species were proposed including monomer monohydrate, monomer dihydrate, and dimer monohydrate, singly and in combination in attempting to fit the partition and water solubility data by weighted, nonlinear least-squares analysis. A preliminary analysis of data following the method which has been previously described in detail² showed that hydrates of both dimer and monomer must

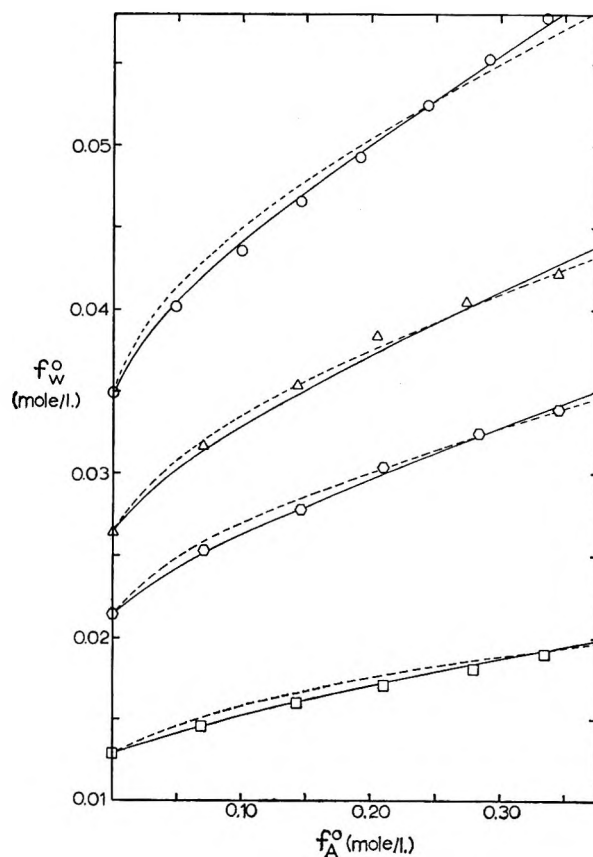


Figure 2. Water solubility data: O, $a_w = 1.0$; Δ , $a_w = 0.790$; \circ , $a_w = 0.658$; \square , $a_w = 0.400$. Dashed lines were calculated from method A; solid lines from method B.

(8) S. A. Taylor, Ph.D. Dissertation, The University of Oklahoma, 1965.

be assumed in order to obtain a satisfactory correlation of the results. When a smaller set of hydrates was assumed, the calculated curves deviated significantly from the experimental points. For these reasons the species AW , AW_2 , and A_2W were selected as being a minimum set of chemically reasonable hydrates, consistent with all of the solubility and partition results. Here, unlike the case where diphenylmethane was the solvent,⁹ the addition of a monomer monohydrate was required before the minimum uncertainties in the parameters were reached.

Assuming the presence of these three hydrates, the acid dimer (A_2), and the acid and water monomers (A and W), each of which obeys Henry's law, the data should be related by

$$f_A^0/C_A^W = K_D(1 + K_{11}C_W + K_{12}C_W^2) + 2K_{20}^2(K_{20} + K_{21}C_W)C_A^W \quad (1)$$

$$\Delta f_W^0 = K_{11}C_A C_W + 2K_{12}C_A C_W^2 + K_{21}C_A^2 C_W \quad (2)$$

$$f_A^0 = C_A + K_{11}C_A C_W + K_{12}C_A C_W^2 + 2K_{20}C_A^2 + 2K_{21}C_A^2 C_W \quad (3)$$

$$C_W = a_W C_W^f \quad (4)$$

where C_A and C_W are monomer concentrations of A and W in benzene, respectively, K_D is the distribution constant for the acid monomer; K_{20} , K_{11} , K_{12} , and K_{21} are equilibrium constants for formation of the complexes A_2 , AW , AW_2 , and A_2W from the monomers. Δf_W^0 is the increase in the formal concentration of water at a given a_W owing to the presence of the acid, and $C_W^0 = 0.0349 M$ is the concentration of the water monomer in benzene at unit water activity at 25.0°.⁵

Two methods have been utilized in analyzing the data. In method A, it is assumed that $K_{20} = 589$ l./mole (obtained by extrapolating results of Allen, Watkinson, and Webb⁷ to 25°) is accurately known. Then, values of K_D , K_{11} , K_{21} , and K_{12} are determined by nonlinear least-squares analysis in the following way. The expression

$$S^2 = W_A \Sigma \left[\left(\frac{f_A^0}{C_A^W} \right)_{\text{exptl}} - \left(\frac{f_A^0}{C_A^W} \right)_{\text{calcd.}} \right]^2 + W_W \Sigma [\Delta f_W^0_{\text{exptl}} - \Delta f_W^0_{\text{calcd.}}]^2 \quad (5)$$

is minimized with respect to all four parameters by means of a numerical optimum seeking method.¹⁰ The calculated f_A^0/C_A^W values are obtained from eq 1 by substituting K_{20} , trial values of K_{21} , K_{12} , K_{11} , and K_D , known values of C_W calculated from eq 4, and measured values of C_A^W . Calculated values of Δf_W^0 are obtained by first solving eq 3 for C_A , using K_{20} and the trial values of the constants, and then substituting the cal-

culated values of C_A and C_W and the set of equilibrium constants into eq 2. The weight factors in eq 5, W_A and W_W , are estimated from observed uncertainties in partition ratio and water solubility measurements. The set of values of K_D , K_{11} , K_{12} , and K_{21} leading to an absolute minimum in S^2 is the least-squares set of parameters for method A. Errors in the four parameters are calculated by the method of Sillén.¹¹

Method B differs from method A only in that K_{20} is treated as an additional parameter to be obtained from the present data, rather than assumed to be known from the literature.

Table II: Least-Squares Parameters for Partition and Water Solubility Data

	Method A	Method B
K_{20} , l./mole	589 ^a	298 ± 25
K_{11} , l./mole	12.4 ± 1.5	0.7 ± 2.0
K_{12} , l. ² /mole ²	248 ± 30	222 ± 18
K_{21} , l. ² /mole ²	582 ± 81	602 ± 32
K_D	0.950 ± 0.002	1.31 ± 0.05
S_W , mole/l.	0.00071	0.00043
S_A	0.0357	0.0298

^a Taken from ref 7.

Table II summarizes results obtained by the two methods for analyzing the data. Values of the equilibrium constants, standard errors in the constants, and the individual root-mean-square deviations in the distribution ratio (S_A) and in the water solubility values (S_W) are included in the table. It is apparent that method B, in which K_{20} is treated as an adjustable parameter, gives a statistically superior fit of the results. However, it should be observed that method B involves the determination of five adjustable parameters and that only slight systematic errors in the water solubility or partition ratio values would be required to increase the values S_A and S_W from their minima to the values obtained by method A. To illustrate, we have included calculated curves in Figure 2 corresponding to the parameters obtained using both method A and method B. In Figure 1 the line is calculated from the results of method B and is practically the same as the line calculated from method A (method A: slope = 1100, intercept = 1.65; method B: slope = 1095,

(9) G. O. Wood, D. D. Mueller, S. D. Christian, and H. E. Affsprung, *J. Phys. Chem.*, **70**, 2691 (1966).

(10) D. J. Wilde, "Optimum Seeking Methods," Prentice-Hall, Inc., Englewood Cliffs, N. J., 1964.

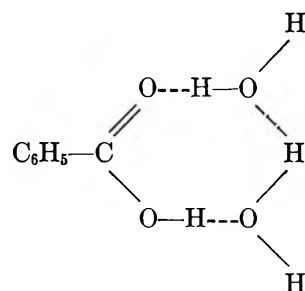
(11) L. G. Sillén, *Acta Chem. Scand.*, **18**, 1085 (1964).

intercept = 1.70). It is apparent that both methods are capable of fitting all of the data to within expected analytical uncertainties. We incline toward the belief that method A is the better fitting method, since it appears unlikely to us that the spectral results given by Allen, Watkinson, and Webb conceal systematic errors large enough to account for a 50% error in K_{20} .

It is interesting to compare the magnitudes of the hydration constants obtained using methods A and B. The largest variation occurs in K_{11} , which contributes significantly to the fit of data in method A but is not an important parameter in method B. Calculated values of the other two hydration constants, K_{12} and K_{21} , are approximately the same in both methods. It is reasonable that the 1:1 hydrate formation constant should fall in the range 2–15 l./mole, considering known values of hydration constants of other polar solutes in nonpolar solvents.^{12,13}

The equilibrium constant for the reaction $A_2 + W = A_2W$ can be shown to be equivalent to K_{21}/K_{20} , which equals 1.0 by method A and 2.0 by method B. Either of these values is smaller than might be predicted for the hydration constant of the cyclic acid dimer, A_2 . However, the hydroxyl hydrogen of the acid monomer is expected to be capable of forming a strong hydrogen bond and this could explain the relatively large value of K_{11} calculated by method A. In the dimer, the hydroxyl hydrogen is presumably not available for hydration.

We believe that the large values obtained for K_{12} lend further support to our previous assumption that the 1:2 complex is a cyclic species (see the structure above). We proposed this species to explain vapor pressure data for the system water–benzoic acid–diphenylmethane at 25° and obtained the value $K_{12} = 483 \pm 21$ l.²/mole.⁹ A similar stoichiometry has been found and



proposed for a trifluoroacetic acid hydrate in the vapor phase.¹⁴ This value for K_{12} is somewhat greater than the values obtained using either of methods A or B, which might be expected, since benzene is a more reactive solvent than diphenylmethane.

The results presented here indicate that hydrated acid species are present in relatively large concentrations in solutions of benzoic acid in benzene at various water activities. By considering the present results along with the spectral data of Allen, Watkinson, and Webb,⁷ it is possible to infer both the stoichiometries and reasonable values of equilibrium constants for the hydration reactions which occur in benzene. However, it is not possible to infer association constants from partition data alone. Dilute solutions of carboxylic acids in moist organic solvents are far more complicated than has been realized by most previous users of the partition method.

Acknowledgment. This research was supported by the National Institutes of Health.

(12) D. D. Mueller, Ph.D. Dissertation, The University of Oklahoma, 1966.

(13) M. D. Gregory, S. D. Christian, and H. E. Affsprung, *J. Phys. Chem.*, **71**, 2283 (1967).

(14) S. D. Christian, H. E. Affsprung, and C. Ling, *J. Chem. Soc.*, 2378 (1965).

The Thermal Decomposition of Solid *trans*-Diazidotetraamminecobalt(III) Azide

by Taylor B. Joyner

Chemistry Division, Michelson Laboratories, U. S. Naval Ordnance Test Station,
China Lake, California 93555 (Received March 2, 1967)

Solid *trans*-diazidotetraamminecobalt(III) azide can decompose to either CoN, a cobalt(II) complex, or under limited conditions triazidotriamminecobalt(III). The first two reactions have been studied in detail and found to resemble their counterparts in the decomposition of azidopentaamminecobalt(III) azide. The CoN reaction shows a well-defined induction period followed by a relatively fast decomposition. Kinetic parameters derived from the induction period and the final reaction are in good agreement with each other and the azidopentaamine results. The quantitative resemblance appears to extend to the more complex cobalt(II) system. The two crystal forms of *trans*-diazidotetraamminecobalt(III) azide are similar in their decomposition kinetics.

Introduction

As part of a systematic study¹ of the thermal decompositions of solid cobalt(III) ammine azides, the reactions of *trans*-diazidotetraamminecobalt(III) azide have been investigated. Preliminary studies of the hexaamminecobalt(III) azide² revealed a quite complex system of competing reactions capable of producing either a nitride or a cobalt(II) complex. Detailed kinetic studies of azidopentaamminecobalt(III) azide³ showed the same two systems with the cobalt nitride reaction proving of particular interest inasmuch as topography seems to play a major and rather intricate part in the decomposition. Extension of the kinetic studies to *trans*-diazidotetraamminecobalt(III) azide probes the importance of a second azide in the cobalt(III) coordination sphere and the effects of crystal structure variation as shown by the two crystal forms of the compound.⁴

Experimental Section

Preparation. Preparation was by previously described methods.^{4,5} Two independent preparations (designated A and B) were used as sources for samples of varying particle size and crystal structure. These are described below. The numeral indicates the crystal form of the particular sample. The structures previously designated as "form I" and "form II"⁴ are here labeled with Arabic numerals to avoid possible confusion with valence states.

"Crystals 1" were recrystallized from water.⁵ They

were thin, lath-like plates, ranging in size from $0.3 \times 0.05 \times 0.01$ to *ca.* $0.02 \times 0.01 \times 0.001$ mm. Despite the variation, screening was avoided after noting that even gentle sifting damaged the edges and corners of the crystals. It seemed preferable to accept the size distribution and preserve the crystals in as perfect a state as possible.

"Small crystals 1" resulted from plunging a 40°, aqueous solution of crystals 1 into a -80° bath and stirring vigorously. Filtration at *ca.* 2° resulted in a glistening, bronze precipitate composed of light brown needles *ca.* 0.01-0.05 mm in length.

"Ground crystals 1" were obtained by carefully grinding small batches (*ca.* 2 mg) of crystals 1 in an agate mortar. This is hazardous. Explosions should be expected and precautions taken (notably small batch size) to avoid injury. Nonrotated X-ray powder patterns and microscopic observation of the brown powder indicated particle sizes of *ca.* 0.1-10 μ . It may be mentioned that efforts to obtain a uniform powder of crystal form 1 by means of the annoyingly unpredictable⁴ fast precipitation with ethanol-ether failed.

"Powder 2" resulted from the rapid addition of 300

(1) T. B. Joyner and F. H. Verhoek, *J. Am. Chem. Soc.*, **83**, 1069 (1961).

(2) T. B. Joyner and F. H. Verhoek, *Inorg. Chem.*, **2**, 334 (1963).

(3) T. B. Joyner, *J. Phys. Chem.*, **69**, 1723 (1965).

(4) T. B. Joyner, *Inorg. Chem.*, **4**, 918 (1965).

(5) M. Linhard, M. Weigel, and H. Flygare, *Z. Anorg. Allgem. Chem.*, **263**, 233 (1950).

ml of a 1:3 ethanol-ether solution to 0.1 g of crystals (1) dissolved in 10 ml of water. Particle sizes were in the range of 0.1–1 μ .

The derivatives of preparation A provided the principal kinetic data. Preparation B was used in brief exploratory studies. The identities of all samples were checked with powder patterns. Storage was in an opaque vacuum desiccator over P_2O_5 .

Procedure. The vacuum line and procedure have been described.¹ The usual run used a 10-mg sample in a stainless steel cup. Product accumulation gave pressure increases of *ca.* 120 torr (eq 1) and 50 torr (eq 2). The usual series of runs was completed within 2 weeks of sample preparation. The longest study took 6 weeks. Check runs indicated no kinetic changes due to aging.

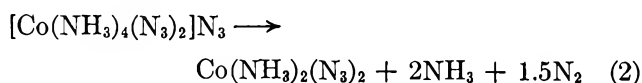
As before,³ "normal" runs were made with the system initially evacuated and the solid exposed to only its own products. "Ammonia" runs began with an initial pressure of ammonia. In the exploratory studies "trapped" runs were made as before with a liquid nitrogen trap located *ca.* 60 mm from the hot reaction vessel. Some alterations became desirable after recognition of the ability of minute quantities of ammonia to prolong the induction period. In later experiments the pressure during the induction period was maintained below 1 torr by frequent venting through the trap to the pumps. With the onset of the fast reaction—easily recognized by the suddenly increasing pressure—the trap was isolated by two stopcocks and the run was completed as a "normal" run with the products accumulating. Thus from a single run it was possible to obtain data on the length of the induction period in the nearly total absence of product gases and on the rate of the final reaction uncomplicated by the presence of a cold trap. A check run with the trap present throughout permitted an approximate comparison of the duration of the fast reactions although slow diffusion of ammonia to the trap prevented quantitatively useful kinetic measurements.

Results

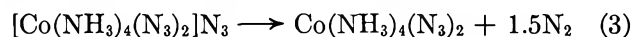
In general, *trans*-diazidotetraamminecobalt(III) azide resembles azidopentaamminecobalt(III) azide in showing either a decomposition with a well-defined induction period and a final reaction to CoN



or a reaction system yielding cobalt(II) compounds which may be represented by



Above 130° eq 2 is reasonably well adhered to and the solid product easily identifiable. Below 130° the situation is complicated by the existence of a series of labile cobalt(II) ammine azides⁶ and an obvious alteration in kinetic behavior and stoichiometry. Although the solid residues are poorly defined, a green material previously observed as a product of hexaamminecobalt(III) azide decompositions and tentatively formulated as diazidotetraamminecobalt(II) has been detected and ideally would call for the stoichiometry



Finally, under apparently restricted conditions a substitution reaction can occur



Larger crystals are prone to reaction 1 and powders to the cobalt(II) system. Ammonia also favors the cobalt(II) reactions.

The CoN Reaction. Equation 1 has been observed with crystals 1 under both trapped and normal conditions. Figure 1 gives illustrative curves with n/n_0 , the moles of gas evolved per mole of original compound, plotted against time. The length of the induction period, τ , shows good reproducibility in trapped runs (Table I, Figure 1, curves A, C, D, and F). In normal runs with ammonia accumulating above the solid it is greatly prolonged (curves B, E, and G) and quite irreproducible. In curves A, C, and F the solid symbols represent the observed gas pressure with the trap in the system. The abrupt pressure rise is apparent. The open symbols show the total gas evolution. This is composed of the gas observed after the trap was closed off plus the gas in the trap. The noncondensable gas lost by venting during the early part of the induction period is negligible. In one run (curve D), the trap was left on throughout the reaction. The similarity in the lengths of the final reactions in curves C and D is apparent.

The time needed to reach a total (untrapped) gas evolution of $n/n_0 = 1.0$ is taken as τ . In general, the pressure rise is so abrupt that there is no serious difficulty in defining the end of the induction period. At low temperatures an appreciable acceleratory period to maximum rate does raise some question as to what should be taken as the onset of fast reaction. In these cases, however, the time is so long that the relatively minor uncertainty in the end point has no significant effect on the kinetic treatments dependent on τ .

Normal runs have longer induction periods and sharper pressure rises. The 140° run exploded (Figure

(6) T. B. Joyner and F. H. Verhoek, *Inorg. Chem.*, **1**, 557 (1962).

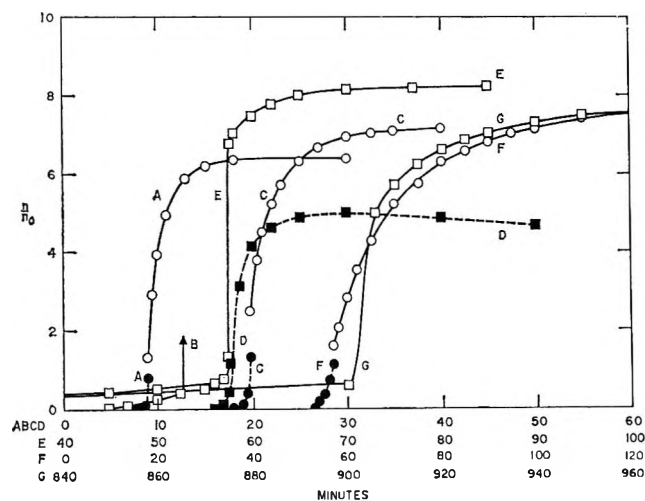


Figure 1. Crystals 1 runs under trapped and normal conditions. Trapped (with venting) during the induction period and normal during the final reaction: A, 140°; C, 130°; F, 110°. Normal runs: B, 140°; E, 130°; G, 110°. Trapped (with venting) during the induction period and trapped during the final reaction: D, 130°. The closed symbols represent the observed gas evolution with the trap on; the open symbols, the total gas evolution. The discontinuity in runs A, C, and F is caused by the change from trapped and normal conditions and the correction for the gas contained in the trap.

ray powder patterns. In many experiments a faint additional pattern established the presence of metallic cobalt (face-centered cubic phase) as well. Careful observations of the solid during first contact with air revealed a pyrophoric reaction probably due to either finely divided cobalt or amorphous CoN.⁷ Powder patterns gave no evidence of its product. Generally it appeared as only a limited sparking involving a minor amount of the solid. Nevertheless, it seemed advisable to sample the original residue under vacuum. This was accomplished by running the decomposition directly in an X-ray capillary sealed to the system with Apiezon W wax and protected from the agitated oil bath with an oil-filled guard tube. After reaction, the capillary was sealed off and X-rayed. Runs at 110 and 140° showed only CoN.

The reaction occurring during the induction period is of considerable interest. In trapped runs decomposition is too small to permit direct identification of a solid product although there is kinetic evidence (Discussion) of the CoN reaction. Conversely, in normal runs there is significant decomposition prior to the fast reaction (curves B, E, and G) but apparently to the cobalt(II) system (see below).

The Cobalt(II) Reaction. The reduction to cobalt(II) is far more difficult. It is reasonably clean only under a limited set of conditions—notably uniform, small-

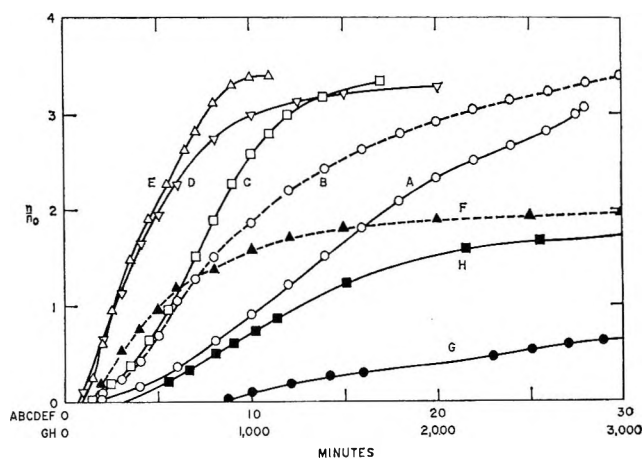


Figure 2. Ammonia runs; 140° runs: A, crystals 1, 50.6 mm of NH₃; B, crystals 1, 101.0 mm of NH₃; C, small crystals 1, 50.0 mm of NH₃; D, ground crystals 1, 50.0 mm of NH₃; E, powder 2, 50.0 mm of NH₃. 130° run: F, powder 2, preparation B, 103.8 mm of NH₃. 110° runs: G, crystals 1, 50.8 mm of NH₃; H, small crystals 1, 50.0 mm of NH₃. The samples are derivatives of preparation A with the exception of run F.

particle samples at 130–150° with added ammonia. Otherwise the behavior is complex and not well understood, the solid residues are poorly characterized mixtures labile to ammonia loss and absorption, and the investigations are severely hampered by explosions. Ammonia runs provide the clearest behavior.

A. Ammonia Runs. Figure 2 presents illustrative curves. Table II shows the alteration in gas evolution and the shapes of the reaction curves with temperature. The approximate adherence to eq 2 at high temperatures and the decline in gas evolution below 130° are apparent. Crystals I have slower reactions than the smaller particle samples but are otherwise similar in gas evolution and temperature dependence. Small crystals 1 were prone to sigmoidal curves; ground crystals 1 and powder 2, to deceleratory curves. The two crystal forms showed no notable difference in decomposition behavior.

Powder patterns identify the grayish brown product of the 140 and 150° runs as diazidodiamminocobalt(II). The low-temperature residues are mixtures giving generally weak and diffuse patterns. The green compound presumed to be diazidotetraamminocobalt(II) has been recognized with a good identification provided by a mixture (from a powder 2 run at 110° and 50 torr of ammonia) showing diffuse diazidodiamminocobalt(II) lines and a sharp pattern for the green compound.

B. Normal Runs. Normal runs gave rather irregu-

(7) O. Schmitz-Dumont, H. Broja, and H. F. Piepenbrink, *Z. Anorg. Chem.*, **253**, 118 (1947).

Table II: Variation of the Cobalt(II) Reaction Stoichiometry (n_t/n_0) and Curve Shape with Temperature

Temp., °C	n_t/n_0 curve ^a					
	Small crystals 1 50 torr of NH ₃		Crystals 1 50 torr of NH ₃		Crystals 1 100 torr of NH ₃	
150	...	E	3.60	S	3.60	S
140	3.33	S	2.90	S	3.25	D
130	2.64	S	...	E	1.71	D
120	2.15	S	...	E	1.01	D ^b
110	1.75	D	1.65	D		
Ground crystals 1 50 torr of NH ₃		Powder 2 50 torr of NH ₃		Powder 2 ^c 100 torr of NH ₃		
150	3.50	S	3.50	S	...	E
140	3.25	D	3.39	D	2.3	D
130	3.20	D	3.37	D	1.9	D
120	3.00	D	3.10	D	1.8	D
110			2.20	D		

^a E indicates an explosion, S an essentially sigmoidal curve, and D a generally deceleratory curve. ^b A second run exploded at $n/n_0 = 0.60$. ^c Derivative of preparation B. The substitution reaction (eq 4) is observed in these runs.

lar curves (Figure 3) ending in explosions or, in the case of crystals 1, the CoN reaction (Figure 1, curves B, E, and G). Direct identification of the solid product of the slow decomposition is generally impossible since small amounts accumulate prior to explosion. (Also, decompositions under low ammonia pressures yield products with poor powder patterns.⁶) A powder pattern did identify diazidotetraamminecobalt(II) as the product of the crystals 1 run at 100° which was exceptional in reaching $n/n_0 = 1.33$ after a period of 21 days. Ammonia reabsorption studies on an interrupted, crystals 1 run at 110° also established the presence of cobalt(II) but indicated a major amount of diazidodiamminecobalt(II). The run was halted at $n/n_0 = 0.89$, the solid immediately isolated, and the ammonia evolution estimated ($n_{\text{NH}_3}/n_0 = 0.53$). The solid was then exposed to 72.0 torr of ammonia and the gas absorbed in 4 days was measured ($n_{\text{NH}_3}/n_0 = 0.80$). The reabsorption of more ammonia than was evolved suggested a decomposition, at least in part, to diazidodiamminecobalt(II) and subsequent formation of hexaamminecobalt(II) azide.^{1,6}

The Substitution Reaction. Equation 4 has been observed in only one limited set of conditions. In the exploratory study with preparation B the powder 2 sample showed conventional normal runs (Figure 3, curves C and F) but anomalous 100-torr ammonia runs (Figure 2, curve F). At 150° an abnormally fast reaction evolved 1.81 moles of gas and exploded at 90 sec. Rapid reactions without explosions occurred at lower

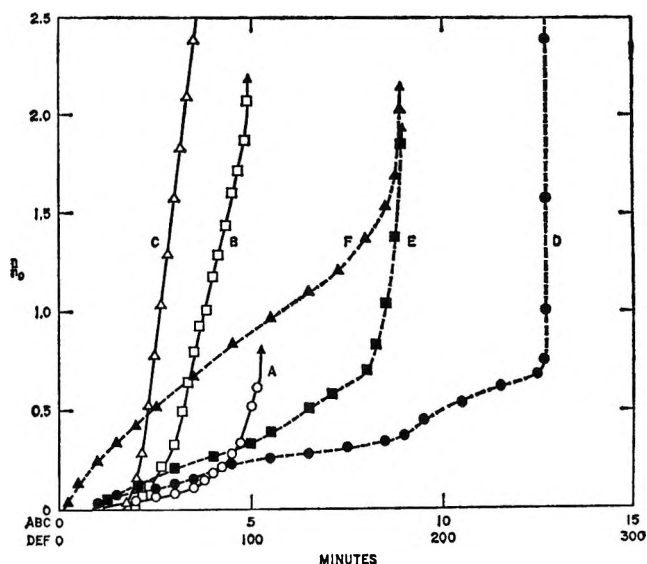


Figure 3. Normal runs; 150° runs: A, crystals 1; B, small crystals 1, C, powder 2, preparation B. 120° runs: D, crystals 1; E, small crystals 1; F, powder 2, preparation B. The samples are derivatives of preparation A with the exception of runs C and F.

temperatures (Table I). Powder patterns of the residues were rather belatedly recognized as being composed of the diazidodiamminecobalt(II) and triazidotriamminecobalt(III)⁸ patterns. Unfortunately, this precise set of experiments has not been repeated. Later studies with preparation A which might have been thought to be comparable, namely, powder 2 and crystals 1 with 50 and 100 torr of ammonia, respectively, gave no evidence of the cobalt(III) compound.

Discussion

Analysis. Treatment of the data follows the pattern of the azidopentaamminecobalt(III) azide study³ with quantitatively similar results for the CoN reaction (eq 1). The obviously complex cobalt(II) system (eq 2 and 3) shows qualitative similarities to the azidopentaammine reactions in the temperature dependency, ammonia, and particle-size effects, and the general explosive characteristics. Rate data from a number of samples indicate reasonable quantitative similarity as well. Conversely, the substitution reaction (eq 4) was not previously observed.

The CoN Reaction. Both the induction period and the fast reaction of the trapped crystals 1 runs provide useful data. The largely deceleratory (better than 70%) fast reaction is well treated by the unimolecular decay law⁹ in eq 5.

(8) T. B. Joyner, D. S. Stewart, and L. A. Burkardt, *Anal. Chem.*, **30**, 194 (1958).

$$-\ln(1 - \alpha) = k_u t + c_u \quad (5)$$

where α is the fraction decomposed, t is time, and k_u and c_u are constants. Figure 4, curve A illustrates the treatment; Table I reports the rate constants. These give a good Arrhenius plot and an apparent activation energy of 23.1 kcal/mole (Table III). This is close to the 19.8 kcal/mole of the azidopentaammine reaction.³ The length of the induction period may also be treated as a measure of reaction rate³ and plotted against $1/T$ to give an apparent activation energy, 20.2 kcal/mole, in close agreement with that of the observable, final reaction. This similarity was also found in the azidopentaammine study.

Table III: Apparent Activation Energies (E_a) and Preexponentials (A)

Sample	Conditions	Treatment	E_a , kcal/mole	Log A (sec ⁻¹)
The CoN Reaction				
Crystals 1	Trapped ^a	τ	20.2	7.94
	Normal ^a	Eq 5	23.1	10.12
Crystal 1 ^b	Trapped	τ	20.9	8.30
The Cobalt(II) Reaction				
Powder 2	50 torr of NH ₃	Eq 6	53.5	24.60
		Eq 7	53.4	25.30
		Eq 5	52.3	25.30
Powder 2 ^b	Normal	Eq 6	55.6	26.45
Small crystals 1	50 torr of NH ₃	Eq 6	54.0	25.81
		Eq 8	53.8	25.64
		Eq 9	55.0	26.97
	Normal	Eq 6	53.3	24.95
Ground crystals 1	50 torr of NH ₃	Eq 6	55.6	26.79
		Eq 7	58.0	27.68
		Eq 5	59.5	29.08
Crystals 1	100 torr of NH ₃	Eq 6	55.4	26.41
		Eq 7	50.5	23.49
	50 torr of NH ₃	Eq 6	57.6	27.32
		Eq 7	61.8	29.38
	Normal	Eq 6	49.4	22.43

^a Trapped during induction period (τ); normal during final reaction (eq 5). ^b Derivatives of preparation B.

Of the normal crystals 1 runs only the 110° run (Figure 1, curve G) has a CoN reaction measurable over a sufficient range of α to permit satisfactory treatment by eq 5. This constant (Table I) agrees well with the trapped run results. Constants for the 120 and 130° runs would represent only *ca.* 15% reaction following the anomalous bursts and could not reasonably be compared with the other data. Although the explanation of the bursts is uncertain, it seems likely that their origin lies in the accumulation of significant

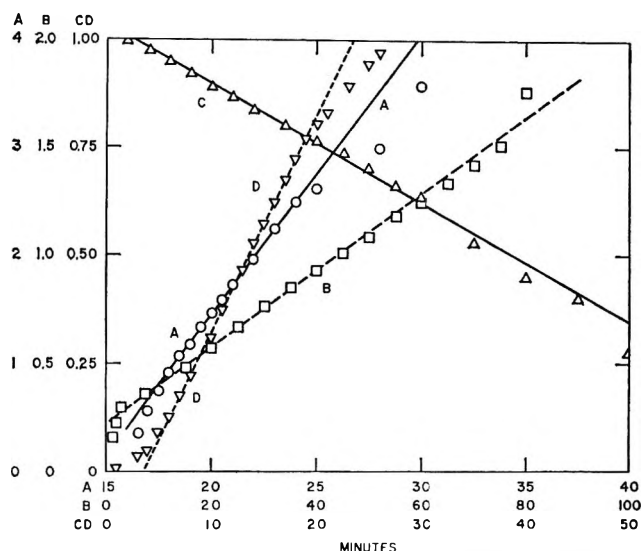


Figure 4. Illustrative kinetic treatments. The ordinate plots the functions of α as written in the equations and given below. Curve A: crystals 1, trapped (with venting) during the induction period, normal during the fast reaction, 130°, treated by eq 5, $-\ln(1 - \alpha)$. Curve B: small crystals 1, 51.0 mm of NH₃, 129.8°, treated by eq 8, $[-\ln(1 - \alpha)]^{1/2}$. Curve C: powder 2, 51.0 mm of NH₃, 130°, treated by eq 7, $(1 - \alpha)^{1/2}$. Curve D: crystals 1, 50.6 mm of NH₃, 140°, treated by eq 6, α .

amounts of the cobalt(II) compounds during the prolonged induction period. Rapid decomposition of this very sensitive material may both heat and shatter the unreacted solid and so result in an unusually fast final reaction.

The Cobalt(II) Reaction. Ammonia Runs. Analysis of the cobalt(II) system is difficult since a really well-defined reaction, eq 2, is present over only a narrow temperature range. Between 130 and 150° ammonia runs are easily treated by the usual rate equations.⁹ Below 130° the curtailment in gas evolution and tendency to explode before establishing an end point make the calculation of α difficult. (Both effects were previously observed.³) Where a final stoichiometry is indicated, it is possible to obtain rate constants valid for that particular run but not certainly comparable to other temperatures. Comparison would be appropriate if the same reaction were rate controlling throughout the temperature range with subsequent rapid equilibration of the ammonia-cobalt(II) azide system responsible for the changing stoichiometry. (Such equilibria exist at room temperature⁶ and ammonia loss, at least, is fast above 100°.¹) Although Arrhenius plots based on this as-

(9) P. W. M. Jacobs and F. C. Tompkins in W. E. Garner, "Chemistry of the Solid State," Butterworth and Co. Ltd., London, 1955, Chapter 7.

sumption are, in fact, linear over a considerable temperature range, the reactions below 130° should still be regarded with caution.

There is considerable variation in the reaction curves—an expected consequence of differing particle sizes and shapes—and no single treatment is ideal for all samples. There is, however, a consistent ability to fit better than 30% of the decomposition by a straight line centered about $n/n_0 = 1.5 \pm 1.0$. Thus the linear equation

$$\alpha = k_1 t + c_1 \quad (6)$$

permits a comparison of the early reaction rates ($\alpha < 0.5$) and so is reported for all samples.

Additionally, crystals 1 obey the linear equation for 50–80% of the reaction followed by a deceleration reasonably well described by the shrinking-cube equation

$$(1 - \alpha)^{1/3} = 1 - kt_{sc} \quad (7)$$

Linear rates are of some interest and have been discussed by Jach^{10,11} in terms of reaction at dislocations with particular reference to very slow decompositions. For these faster reactions a plausible explanation is afforded by a shrinking-volume decomposition of flat objects (which these crystals are, though the decomposing entities may very well be smaller blocklets) with the majority of the reaction accounted for by regression of the two large faces. The final deceleration probably results from the larger and thicker crystals taking more time for decomposition and, perhaps, more nearly approximating shrinking-cube geometry.

The reactions of the smaller particle samples can be described by eq 5, eq 7, or, in the case of sigmoidal curves, by the Avrami-Erofeev (eq 8) or Prout-Tompkins (eq 9) treatments⁹

$$[-\ln(1 - \alpha)]^{1/3} = k_{AE}t + c_{AE} \quad (8)$$

$$\ln[\alpha/(1 - \alpha)] = k_{PT}t + c_{PT} \quad (9)$$

Frequently there is some difficulty in selecting the best treatment for the entire temperature range; hence, where two possibilities exist, both are reported (Tables I and III). In general the agreement is good.

The presence of the substitution reaction (eq 4) makes the powder 2 ammonia runs (preparation B) obvious special cases. Equation 6 fits $\alpha < 0.5$ and rate constants are reported (excepting the very fast 150° run where temperature equilibrium is unlikely) but are of no use in indicating activation energies. At present it can only be said that under limited conditions a reaction producing sizable amounts of triazidotriamminecobalt(III) has been observed.

The results of least-squares treatment of Arrhenius plots are reported in Table III. The most satisfactory conformity to the rate laws was provided by the samples with the most uniform particle size, small crystals 1 and powder 2. Both give good Arrhenius plots and apparent activation energies and preexponentials in agreement with each other. It is worth specific mention that these samples represent both crystal forms of *trans*-diazidotetraamminecobalt(III) azide. The remaining data provide satisfactory confirmation. The most notable deviation, crystals 1, preparation B, depends on only three points and would appear reasonable if the 150° run were ignored. The faster 150° runs are always suspect owing to possible self-heating; therefore, 150° constants falling well above a line defined by three or more points were ignored in the least-squares treatment. Otherwise all data were used even though probably reasonable neglect of a single point would have brought several of the higher activation energies into closer agreement with powder 2 and small crystals 1. The values $E_a = 54 \pm 3$ kcal/mole and $\log A = 25.5 \pm 2.0$ provide limits including the majority of the data.

Normal Runs. The rather irregular curves (Figure 3) can be fairly well approximated by eq 6. Although explosions prevent a direct measurement of the stoichiometry, the ammonia absorption studies indicate production of the diammine (eq 2) down to 110°. It may also be formed during the early stages of the 100° run when ammonia pressure was low (and the percentage decomposition most comparable to other runs) even though diazidotetraamminecobalt(II) was ultimately detected. While the situation is not entirely clear, a reasonable treatment assumed eq 2 was followed throughout with the rate constant for the 100° reaction determined for the early stages of the run. The results (Table III) are in reasonable agreement with the ammonia runs.

Conclusions

An over-all consideration of the data must stress the very marked resemblance to the azidopentaamminecobalt(III) azide reactions. The CoN reactions in particular are evidently identical in topography and chemistry. The similarity of the apparent activation energies yielded by the trapped-run τ 's and the observable final decomposition suggests the presence of the CoN reaction during the induction period. The previously proposed model³ (a surface-initiated microscopic reaction growing toward an internal mosaic

(10) J. Jach, *Nature*, **196**, 827 (1962).

(11) J. Jach, "Reactivity of Solids," G. M. Schwab, Ed., Elsevier Publishing Co., New York, N. Y., 1965, p 422.

plane with subsequent rapid spreading along the intermosaic structure carving the crystal into decomposing blocklets) remains a plausible explanation for the induction period and the final reaction.

Although the cobalt(II) reactions are more complex, both compounds show eq 2 above 130°. The low-temperature decompositions are less well defined; however, the similarity in analysis permits, at the least, a direct comparison of the two compounds. By these treatments the apparent activation energies for normal and ammonia runs are similar although the *ca.* 54 kcal/mole of the *trans*-diazidotetraammine is somewhat higher than the 46 kcal/mole (ammonia runs) and 49 kcal/mole (normal runs) of the azidopentaammine. The closeness of the figures and the qualitative similarities in the reactions suggest that both compounds follow similar mechanisms in producing cobalt(II).

It therefore seems clear that substitution of a second azide into the cobalt(III) coordination sphere has little or no effect on the decomposition mechanisms. Moreover, in the case of *trans*-diazidotetraamminecobalt(III) azide, the essential identity of the small crystals 1 and powder 2 data indicates that a change in crystal structure does not alter the basic chemistry of the decomposition. Although this was an expected result, its confirmation is of some interest. Finally, it should be noted that a previously undetected substitution reaction (eq 4) has been observed under apparently quite restricted conditions. At present the data are too limited to attempt treatment. Investigations of *cis*-diazidotetraamminecobalt(III) azide and hexaamminecobalt(III) azide are in progress. Detailed consideration of the mechanisms will be reserved until they are reported.

The Interactions of Methyl and Difluoromethyl Radicals and the Elimination of HF from "Hot" 1,1-Difluoroethane¹

by J. T. Bryant and G. O. Pritchard

Department of Chemistry, University of California, Santa Barbara, California 93106
(Received March 6, 1967)

The rate of collisional stabilization *vs.* HF elimination for the "hot" molecule $\text{CF}_2\text{HCH}_3^*$, produced in the cophotolysis of *sym*-tetrafluoroacetone and acetone, is examined as a function of the pressure and the temperature. RRK theory is shown to give a quantitative description of the decomposition of the "hot" molecule, and the critical energy for the elimination is found to be about 53 kcal mole⁻¹. This is discussed in terms of an α -fluorination effect. Activation energies for the reactions $\text{CF}_2\text{H} + \text{CH}_3\text{COCH}_3 \rightarrow \text{CF}_2\text{H}_2 + \text{CH}_2\text{COCH}_3$ and $\text{CH}_3 + \text{CF}_2\text{HCOCF}_2\text{H} \rightarrow \text{CH}_4 + \text{CF}_2\text{COCF}_2\text{H}$ are also determined and found to be 9.0 and 4.3 kcal mole⁻¹, respectively. An attempt is made to establish whether the disproportionation $\text{CH}_3 + \text{CF}_2\text{H} \rightarrow \text{CH}_4 + \text{CF}_2$ occurs, but it is inconclusive.

Introduction

We² have recently summarized some of the factors governing the rate of HF elimination from vibrationally excited fluoroethanes, formed by radical combination. This investigation constitutes experiments performed with the "hot" molecule $\text{CF}_2\text{HCH}_3^*$ as α -halogenation should promote dehydrohalogenation relative to β -halogenation, and our results may be compared with our previous data^{2,3} on the "hot" molecules $\text{CFH}_2\text{CFH}_2^*$ and $\text{CFH}_2\text{CH}_3^*$.

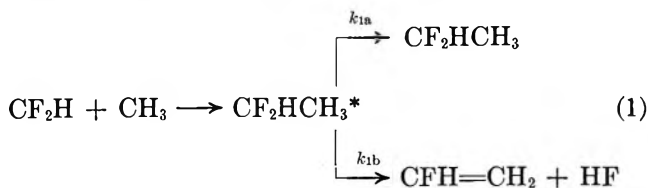
Experimental Section and Results

$\text{CF}_2\text{HCH}_3^*$ was formed by the cophotolysis of acetone and 1,1,3,3-tetrafluoroacetone (TFA). We have recently discussed⁴ the photochemistry of the latter compound. The apparatus and procedure have been described.^{3,4} Analysis was performed by low-temperature fractionation and vpc.^{2,4} The results of some experiments conducted over the temperature range 299–560°K are given in Table I. Excess acetone was used in all the experiments as its extinction coefficient is only approximately 25% of that for TFA at 3130 Å. In one series of experiments, the TFA was admitted to the reaction chamber first and the acetone pressure was found by difference from the total pressure. In a second series of experiments, a 2:1 mixture of the two compounds was made up and portions of the mixture were

expanded into the reaction cell. At the completion of these experiments, it was found that there was an apparent 10–15% excess of the mixture left over, indicating nonideality of the acetone–TFA mixtures, particularly at high pressures. The concentrations of reactants given in Table I are therefore only approximate.

Discussion

HF Elimination Data. For the formation of the "hot" fluoroethane and the competition between collisional stabilization and HF elimination, we may write reaction sequence 1



where M represents a third body, in this case acetone

(1) This work was supported by a grant from the National Science Foundation.

(2) G. O. Pritchard and R. L. Thommarson, *J. Phys. Chem.*, **71**, 1674 (1967).

(3) G. O. Pritchard, M. Venugopalan, and T. F. Graham, *ibid.*, **68**, 1786 (1964).

(4) G. O. Pritchard and J. T. Bryant, *ibid.*, **70**, 1441 (1966).

Table I: Products of Photolysis

Temp, °K	Concn of reactants, moles cc ⁻¹ × 10 ²		Rate of formation of products, moles cc ⁻¹ sec ⁻¹ × 10 ¹²							Mb ^a
	Acetone	TFA	CO	CH ₄	C ₂ H ₄	C ₂ FH ₄	CF ₂ H ₂	C ₂ F ₂ H ₄	C ₂ F ₄ H ₂	
					Series 1					
299	31.8	10.7	226	1.63	1.18	6.96	27.7	6.68	38.0	0.31
370	33.9	8.66	183	18.1	1.44	15.2	18.6	12.0	27.2	0.42
398	23.4	4.59	159	36.6	7.01	32.7	13.6	13.3	45.6	0.81
446	20.6	7.11	251	79.0	6.60	27.9	25.7	21.0	55.5	0.67
468	36.7	7.12	306	162	12.8	30.7	39.6	21.3	26.7	0.64
490	20.1	5.70	232	87.9	8.64	24.5	33.2	9.47	58.3	0.72
500	30.8	3.85	204	121	12.5	22.2	35.2	8.97	15.9	0.68
514	24.4	6.25	281	111	10.2	23.2	59.2	11.4	34.0	0.60
526	18.3	3.72	166	87.6	4.18	11.3	29.9	2.68	12.8	0.55
536	20.1	3.59	205	126	6.33	10.9	28.4	3.73	8.94	0.53
560	16.3	3.61	192	118	4.51	11.4	55.6	3.31	17.3	0.65
					Series 2					
419	3.83	1.99	30.9	4.54	1.69	9.12	2.15	0.26	16.8	1.08 ^b
419	7.78	4.02	62.2	9.35	2.88	15.0	5.12	1.71	28.3	0.93 ^b
416	22.4	11.5	141	22.1	3.09	20.3	15.0	9.34	62.9	0.85
418	14.6	7.49	110	22.5	0.89	11.9	14.2	3.39	71.9	1.06
461	10.1	5.01	83.3	19.3	0.01	8.78	12.0	1.77	52.2	1.01
461	4.73	2.37	42.1	9.45	1.15	7.29	4.17	0.36	18.6	0.85
460	13.3	6.63	109	14.1	1.24	12.1	16.1	2.68	54.5	0.83
461	2.73	1.37	26.0	4.95	0.82	5.88	2.39	0.27	12.6	0.94 ^b
460	7.25	3.63	67.4	13.1	1.38	11.2	7.03	0.46	33.8	0.89
462	16.0	8.02	129	35.5	1.06	11.3	23.6	3.70	70.3	0.95

^a Mb = mass balance = $[1/2\text{CH}_4 + 1/2(\text{CF}_2\text{H}_2 - 0.19\text{C}_2\text{F}_4\text{H}_2) + \text{C}_2\text{H}_6 + 1.19\text{C}_2\text{F}_4\text{H}_2 + \text{C}_2\text{FH}_3 + \text{C}_2\text{F}_2\text{H}_4]/\text{CO}$. The higher ketone pressures used in series 1 promoted H-atom abstraction reactions which leads to lower values of Mb. ^b The term $1/2(\text{CF}_2\text{H}_2 - 0.19\text{C}_2\text{F}_4\text{H}_2)$ is negative; therefore it has been omitted from Mb.

or TFA, necessary for collisional stabilization. As the efficiencies of the two third bodies will not be the same, we have

$$R_{\text{C}_2\text{F}_2\text{H}_4}/R_{\text{C}_2\text{FH}_3} = (k_{1a}[\text{TFA}] + k_{1a}'[\text{Ac}])/k_{1b} \quad (2)$$

where Ac represents acetone and k_{1a} and k_{1a}' will have different values. An equation of this form was originally tested by Giles and Whittle⁵ for the "hot" molecule CF_3CH_3^* formed in the cophotolysis of $(\text{CF}_3)_2\text{CO}$ and $(\text{CH}_3)_2\text{CO}$ and they found that the relative quenching efficiency of acetone was about 0.5 of that for hexafluoroacetone in the system at 150°. We will assume that TFA and acetone show about the same relative efficiency in quenching $\text{CF}_2\text{HCH}_3^*$ over the temperature range of these experiments. Since deactivation is by collision, we can replace k_{1a} by QZ , where $Q \leq 1$, and represents the probability of complete deactivation on collision. We have, from eq 2

$$R_{\text{C}_2\text{F}_2\text{H}_4}/R_{\text{C}_2\text{FH}_3} = (QZ[\text{TFA}] + Q'Z'[\text{Ac}])/k_{1b} \quad (3)$$

Making allowance for the small difference in collision rates between $\text{C}_2\text{F}_2\text{H}_4^*$ and the two quenching molecules and taking $Q' = 1/2Q$, eq 3 becomes

$$R_{\text{C}_2\text{F}_2\text{H}_4}/R_{\text{C}_2\text{FH}_3} = \{QZ([\text{TFA}] + (1.2/2)[\text{Ac}])\}/k_{1b} \quad (4)$$

$$= (k_{1a}/k_{1b})(P_{\text{TFA}} + 0.6P_{\text{Ac}}) \quad (5)$$

when P represents pressure in millimeters and k_{1a} is expressed in collisions per second per millimeter. Equation 5 is tested at two temperatures, 418 and 461°K, in Figure 1. The uncertainty in the $R_{\text{C}_2\text{F}_2\text{H}_4}/R_{\text{C}_2\text{FH}_3}$ ratios is larger at low total pressures (see Table I). The data can be represented by a straight line which does not quite pass through the origin. No distinction has been made between the two temperatures, owing to the very small temperature dependence for k_{1a}/k_{1b} (in mm^{-1}) vs. T (°K) as seen in Figure 2. A point derived from the slope of the line in Figure 1 is given in Figure 2 at an average temperature of 440°K. The line in Figure 1 could well be adjusted to pass through the origin by using a slightly smaller fraction of P_{Ac} than 0.6. However, alternatively, the plot may show some curvature at low pressures as we have indicated. Curvature was obtained in similar plots for the quenching of C_2FH_5^*

(5) R. D. Giles and E. Whittle, *Trans. Faraday Soc.*, **61**, 1425 (1965).

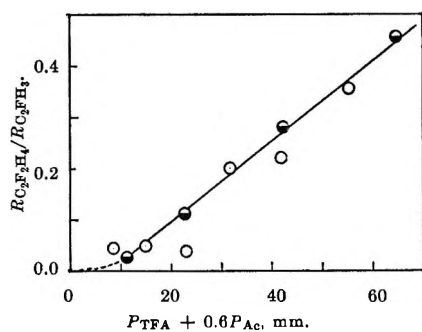


Figure 1. Pressure dependence of the stabilization/elimination rate ratios for $\text{CF}_2\text{HCH}_3^*$: \bullet , 418°K; \circ , 461°K.

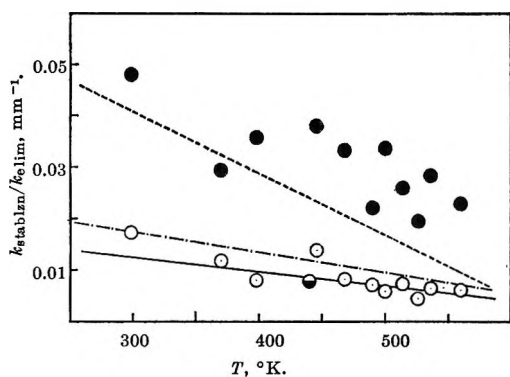


Figure 2. Temperature dependence of $k_{\text{stablim}}/k_{\text{elim}}$ for $\text{CF}_2\text{HCH}_3^*$: \circ , $R_{\text{C}_2\text{F}_2\text{H}_4}/[R_{\text{C}_2\text{FH}_3}(P_{\text{TFA}} + 0.6P_{\text{Ac}})]$; \bullet , point obtained from slope in Figure 1; \bullet , $R_{\text{C}_2\text{F}_2\text{H}_4}/[R_{\text{C}_2\text{FH}_3}P_{\text{TFA}}]$; ---, $R_{\text{CFH}_2\text{CFH}_2}/[R_{\text{C}_2\text{FH}_3}P_{\text{DFA}}]$, $(\text{CFH}_2)_2\text{CO}$ quenching molecule;³ - · - ·, $R_{\text{CFH}_2\text{CFH}_2}/[R_{\text{C}_2\text{FH}_3}P_{\text{MFA}}]$, $\text{CFH}_2\text{COCH}_3$ quenching molecule.²

and $\text{C}_2\text{F}_2\text{H}_4^*$ by $\text{CFH}_2\text{COCH}_3$.² Our choice of $0.6P_{\text{Ac}}$ in eq 5 is therefore somewhat arbitrary, but it should be a fairly good approximation.

Benson and Haugen⁶ have given a detailed discussion of the temperature dependence for the stabilization-elimination ratio for the "hot" molecule $\text{CFH}_2\text{CFH}_2^*$, produced by $(\text{CFH}_2)_2\text{CO}$ photolysis,³ in terms of the RRK theory of unimolecular reactions; this treatment has been used by us in treating the hot molecules C_2F_5^* and $\text{CFH}_2\text{CFH}_2^*$ formed in $\text{CFH}_2\text{COCH}_3$ photolysis.² A plot of $k_{1a}/k_{1b} = R_{\text{C}_2\text{F}_2\text{H}_4}/[R_{\text{C}_2\text{FH}_3}(P_{\text{TFA}} + 0.6P_{\text{Ac}})]$ is given in Figure 2, as a function of temperature, together with data on $\text{CFH}_2\text{CFH}_2^*$ obtained in the presence of the two different quenching molecules, $(\text{CFH}_2)_2\text{CO}$ and $\text{CFH}_2\text{COCH}_3$.⁷ Assuming that our evaluation of the quenching efficiency of the TFA + acetone mixture is reasonable, and to a first approximation roughly equal to the quenching efficiency of $(\text{CFH}_2)_2\text{CO}$, it would appear that HF elimination from $\text{CF}_2\text{HCH}_3^*$ is intrinsically more favorable than from $\text{CFH}_2\text{CFH}_2^*$. That this is so is borne out by the

data on $R_{\text{C}_2\text{F}_2\text{H}_4}/R_{\text{C}_2\text{FH}_3}P_{\text{TFA}}$ which are also given in Figure 2. This neglects the quenching effect of the acetone completely and yet the data are scattered near to the $(\text{CFH}_2)_2\text{CO}-\text{CFH}_2\text{CFH}_2^*$ plot, when $(\text{CF}_2\text{H})_2\text{CO}$ is presumably a better quencher than $(\text{CFH}_2)_2\text{CO}$. Our interpretation presupposes that the energy donor efficiencies of the two excited fluoroethanes in question are much the same.

Applying the RRK theory of unimolecular decomposition to the "hot" molecule formed in reaction 1, we have^{2,6}

$$\frac{k_{1a}}{k_{1b}} = \frac{1}{(P_{\text{TFA}} + 0.6P_{\text{Ac}})} \frac{R_{\text{C}_2\text{F}_2\text{H}_4}}{R_{\text{C}_2\text{FH}_3}} = \frac{QZ}{A} \left(\frac{E}{E - E^*} \right)^{n-1} \quad (6)$$

where E is the internal energy content of the molecule, E^* represents the critical energy necessary for decomposition, n is the number of effective oscillators, and A is the frequency factor for the unimolecular elimination. The temperature dependence of k_{1a}/k_{1b} is assumed to be due to the temperature dependence of E , and the temperature dependencies of Q and Z are neglected.^{2,6} $E(T)$ is given in Table II, where ΔC_v^{vib} is defined as the difference in vibrational specific heat of the two radicals and the hot molecule and

$$E = E_0 + \Delta C_v^{\text{vib}}(T - 298)$$

where E_0 is the energy change on combination, taken⁸ to be 85.4 kcal mole⁻¹. The experimental and theoretical values of k_{1a}/k_{1b} , as given by eq 6, are compared in Figure 3, using logarithmic plots, which simplifies the curve fitting.⁶ We have chosen a value of $n = 11$, for values of E^* over the range 53–62 kcal mole⁻¹. The choice of the parameters to obtain a fit is somewhat arbitrary (for several examples, see ref 2 and 6), but from the curve fitting on $\text{CFH}_2\text{CFH}_2^*$ it was found that $n = 11$ –12 and $E^* = 59$ –62 kcal mole⁻¹ gave the best description of the "hot" molecule.^{2,6} The present data indicate that E^* for $\text{CF}_2\text{HCH}_3^*$ is lower than for $\text{CFH}_2\text{CFH}_2^*$. Taking $n = 12$ for $\text{CF}_2\text{HCH}_3^*$ gives a similar result. The curve fitting is performed by varying $\log(QZ/A)$, which shifts the curves vertically.

(6) S. W. Benson and G. Haugen, *J. Phys. Chem.*, **69**, 3898 (1965).

(7) Although these dependencies are depicted as linear, they are not necessarily so over a more extended temperature range.

(8) This is the value adopted by Benson and Haugen in their original analysis⁶ and they assumed that the C–C bond energy in ethane was invariant when fluorine atoms were substituted for hydrogen atoms. This is probably not true and most recent evidence tends to indicate that fluorination increases the C–C bond strength, as it appears that $D(\text{CF}_3-\text{CF}_3) > 90$ kcal mole⁻¹; see C. A. Goy, A. Lord, and H. O. Pritchard, *J. Phys. Chem.*, **71**, 1086 (1967). A higher value of E_0 will necessitate a larger critical energy. The present value of E_0 is based upon the lower limit of $D(\text{CH}_3-\text{CH}_3) = 88 \pm 2$ kcal mole⁻¹ [J. A. Kerr, *Chem. Rev.*, **66**, 465 (1966)] - ΔnRT at 298°K.

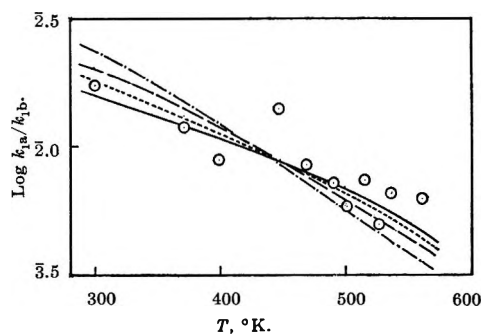


Figure 3. Comparison of the theoretical and observed temperature dependence of k_{i_a}/k_{i_b} for $n = 11$: O, experimental points; —, $E^* = 53$ kcal mole $^{-1}$, $\log(QZ/A) = -6.00$; ----, $E^* = 56$ kcal mole $^{-1}$, $\log(QZ/A) = -6.38$; - · - ·, $E^* = 59$ kcal mole $^{-1}$, $\log(QZ/A) = -6.79$; · · · ·, $E^* = 62$ kcal mole $^{-1}$, $\log(QZ/A) = -7.26$.

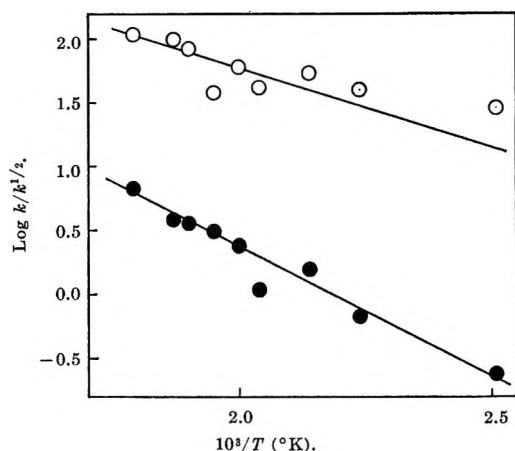


Figure 4. Arrhenius plots for H-atom abstractions: O, $\log k_9/k_{12}^{1/2}$ in mole $^{-1/2}$ cc sec $^{-1/2}$ ($\text{CH}_3 + \text{TFA} \rightarrow \text{CH}_4$); ●, $\log k_7/k_{11}^{1/2}$ in mole $^{-1/2}$ cc sec $^{-1/2}$ ($\text{CF}_2\text{H} + \text{Ac} \rightarrow \text{CF}_2\text{H}_2$).

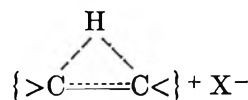
Taking values^{2,6} of $Z = 10^{7.07}$ mm $^{-1}$ sec $^{-1}$ and $A = 10^{13.5}$ sec $^{-1}$ in conjunction with the values of $\log(QZ/A)$ given in Figure 3, we obtain values of $Q = 0.15, 0.44, 1.1,$ and 2.7 ; the latter result is not meaningful. However if a value of $A = 10^{13.0}$ sec $^{-1}$ is adopted, Q becomes 0.85 for this result. We² have previously pointed out that strong collisional deactivation plays an important part in these systems and values of Q in the range 0.1–1.0 are certainly to be expected.^{2,6} Within the allowable margin of variation for these parameters, there is reasonable agreement between the theoretical model and the experimental systems.

Unimolecular dehydrohalogenations in the pyrolyses of haloethanes have recently been discussed in detail by Maccoll.⁹ To interpret the effect of substitution at or near the reaction center, he represents the transition state as having an essentially carbonium ion character

Table II: Internal Energy of $\text{CF}_2\text{HCH}_3^*$

Temp, °K	Thermal energy, ^a $\Delta C_v^{\text{vib}}(T - 298)$, kcal mole $^{-1}$	E , kcal mole $^{-1}$
298	0	85.4
370	1.5	86.9
398	2.2	87.6
446	3.5	88.9
468	4.2	89.6
490	5.0	90.4
500	5.3	90.7
514	5.8	91.2
526	6.2	91.6
536	6.5	91.9
560	7.3	92.7

^a The change in the internal energy with temperature was calculated from $\Delta C_v^{\text{vib}}(T - 298) = 3R(T - 298) + [C_v^{\text{vib}}, \text{CH}_3(T) + C_v^{\text{vib}}, \text{CF}_2\text{H}(T)]T - [C_v^{\text{vib}}, \text{CH}_3(298) + C_v^{\text{vib}}, \text{CF}_2\text{H}(298)]298$. Vibrational contribution to the heat capacities of CH_3 and CF_2H were estimated from the heat capacities of CH_4 and CF_2H_2 , respectively.⁶

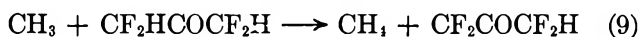
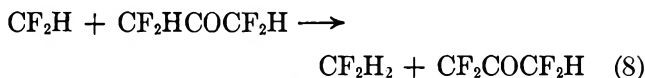
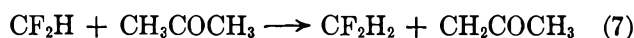


where the positive charge is distributed between the α -carbon atoms and the β -hydrogen atoms.¹⁰ In the α positions, a second halogen atom can resonance stabilize the carbonium ion, but in the β position only the inductive effect is operative.⁹ The rate of HX elimination will therefore diminish along the series $\text{CH}_3\text{CX}_3 > \text{CH}_3\text{CHX}_2 > \text{CH}_3\text{CH}_2\text{X} > \text{CH}_2\text{XCH}_2\text{X}$. The experimental data on CH_3CCl_3 , CH_3CHCl_2 and $\text{CH}_3\text{CH}_2\text{Cl}$, and CH_3CHBr_2 and $\text{CH}_3\text{CH}_2\text{Br}$ are in accord with this prediction.⁹ The activation energy for HCl elimination given⁹ for CH_3CHCl_2 (49.5 kcal mole $^{-1}$) is actually lower than for CH_3CCl_3 (54.0 kcal mole), but the A factor for the reaction is also low. The activation energy for $\text{C}_2\text{H}_5\text{Cl}$ lies in the range 56.9–60.8 kcal mole $^{-1}$. We see that the HF elimination data from "hot" fluoroethanes follow a similar trend, $\text{CH}_3\text{-CHF}_2 > \text{CH}_3\text{CH}_2\text{F} \geq \text{CH}_2\text{FCH}_2\text{F}$, with values of E^* of about 53 (this work), 59,² and 59–62^{2,6} kcal mole $^{-1}$, respectively.

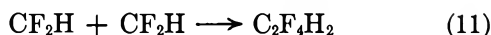
H-Atom Abstraction Data. H-atom abstraction from the ketones (eq 7–10 and Figure 4) will occur as

(9) A. Maccoll, *Advan. Phys. Org. Chem.*, **3**, 91 (1965).

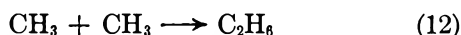
(10) A referee has pointed out that the transition state is definitely polar, although the question as to whether the structure has the character of a carbonium ion or a four-center semion pair (S. W. Benson and G. R. Haugen, *J. Am. Chem. Soc.*, **87**, 4036 (1965)) is still uncertain.



The rate constants may be evaluated in the usual way, relative to the radical recombination reactions



and



A correction must be incorporated for the disproportionation reaction



It is known that $k_{13}/k_{11} = 0.19$,⁴ independent of temperature. $\text{CF}_2=\text{CFH}$ was not identified as a product,⁴ indicating that the elimination of HF from $\text{C}_2\text{F}_4\text{H}_2^*$ (the intermediate in reaction 11) does not occur at the pressures used in these experiments. At lower pressures the elimination is found to occur readily.¹¹ No direct evidence (see next section) was found for the possible disproportionation reaction



The Arrhenius plots for the rate constant ratios $k_7/k_{11}^{1/2}$ and $k_9/k_{12}^{1/2}$ are shown in Figure 4 for the data in series 1 in Table I. They were evaluated from the expressions

$$k_7/k_{11}^{1/2} = \left(\frac{R_{\text{CF}_2\text{H}_2} - 0.19R_{\text{C}_2\text{F}_4\text{H}_2}}{R_{\text{C}_2\text{F}_4\text{H}_2}^{1/2}} - \frac{k_8[\text{TFA}]}{k_{11}^{1/2}} \right) \frac{1}{[\text{Ac}]}$$

and

$$k_9/k_{12}^{1/2} = \left(\frac{R_{\text{CH}_4}}{R_{\text{C}_2\text{H}_6}^{1/2}} - \frac{k_{10}[\text{Ac}]}{k_{12}^{1/2}} \right) \frac{1}{[\text{TFA}]}$$

both in mole^{-1/2} cc^{1/2} sec^{-1/2}. The ratio $k_8/k_{11}^{1/2}$ was obtained from our previous work⁴ and $k_{10}/k_{12}^{1/2}$ is well established.¹² Least-squares treatment of the data given in Figure 4 yields $k_7/k_{11}^{1/2} = 1.8 \times 10^4 e^{-9000/RT}$ and $k_9/k_{12}^{1/2} = 4.4 \times 10^3 e^{-4300/RT}$ mole^{-1/2} cc sec^{-1/2}, omitting the low-temperature point.¹³ Since the completion of this work, we have discovered a small impurity in our TFA, which appears to be unsymmetrical TFA, $\text{CF}_3\text{COCFH}_2$.¹⁴ This introduces uncertainty of an unknown magnitude into the above Arrhenius expression for $k_7/k_{11}^{1/2}$ and $k_9/k_{12}^{1/2}$. A value for $E_7 = 9$ kcal mole⁻¹ fits the general picture for this type of abstraction reaction,^{2,3} but some more recent experi-

ments¹⁵ on the H-atom abstraction reactions of CF_2H radicals suggest that it may be 1–2 kcal low. We have also found¹⁵ that our previously reported value⁴ of E_8 is much too low owing to the *unsym*-TFA impurity. However, it should be noted that our previous determination⁴ of $k_8/k_{11}^{1/2}$ was made with the same sample of TFA that we used in this work. Although the value of $E_9 = 4.3$ kcal mole⁻¹ seems low, it should be noted that we obtained² an activation energy of 4.6 kcal mole⁻¹ for the reaction $\text{CH}_3 + \text{CH}_2\text{FCOCH}_3 \rightarrow \text{CH}_4 + \text{CHF-COCH}_3$ or $\text{CH}_2\text{FCOCH}_2$. The preexponential ratios for both these reactions are also low, which would imply that the activation energies should be raised, if compensation between the Arrhenius parameters is occurring.

Cross-Combination and Disproportionation Reactions. The cross-combination ratio may be obtained from the expression $\Psi = (R_{\text{C}_2\text{F}_4\text{H}_2} + R_{\text{C}_2\text{F}_2\text{H}_4})/R_{\text{C}_2\text{H}_6}^{1/2}R_{\text{C}_2\text{F}_4\text{H}_2}^{1/2} (1.19)^{1/2}$, which accounts for the radical-radical interactions specified in reactions 1, 11, 12, and 13. For the runs reported in Table I, the average value of Ψ is 1.8. (Values are a little scattered, with no significant temperature dependence, varying from 1.4 to 2.6. A high value of 4.0 at 370°K has been omitted.) Collision theory predicts a value of $\Psi \sim 2$, depending on the values assigned to the collision diameters, if every collisional event leads to product formation.

If the possible disproportionation between CH_3 and CF_2H occurs to an appreciable extent (reaction 14), it should be taken into account in the evaluation of Ψ and $k_9/k_{12}^{1/2}$. Since reaction 13 is well established,^{4,16} there appears to be no *a priori* reason why reaction 14 should not occur. From the preceding reaction scheme we may show

(11) G. O. Pritchard and J. T. Bryant, submitted for publication.

(12) A. F. Trotman-Dickenson, "Gas Kinetics," Butterworth and Co., Ltd., London, 1955, p 201.

(13) The two runs below 100° were not included in either plot owing to the participation of the CH_3CO radical; note the mass balance ratios.

(14) (a) The evidence for this is based on mass spectral analysis. *unsym*-TFA is appreciably more volatile than *sym*-TFA, bp 44 and 58°, respectively (E. T. McBee, O. R. Pierce, H. W. Kilbourne, and E. R. Wilson, *J. Am. Chem. Soc.*, **75**, 3152 (1953)), and analysis of a cut taken from the ketone before it had warmed up to room temperature led to an appreciable enrichment in the ion peaks at m/e 33 (CFH_2^+), 61 (CFH_2CO^+), and 69 (CF_3^+). Our published mass spectrum⁴ of *sym*-TFA represents a relatively pure sample; the small ion peaks reported at m/e 61 and 69 should be omitted. The relatively large transference peak at m/e 33 is real and of the correct magnitude; (b) small amounts of $\text{CF}_2=\text{CH}_2$ (< one-half the C_2H_6 yield) were found in some experiments, which could be formed by the decomposition of CF_3CH_3^* .

(15) M. J. Perona and G. O. Pritchard, unpublished results.

(16) M. G. Bellas, O. P. Strausz, and H. E. Gunning, *Can. J. Chem.*, **43**, 1022 (1965).

$$\frac{R_{\text{CH}_4}}{R_{\text{C}_2\text{F}_2\text{H}_4} + R_{\text{C}_2\text{H}_4\text{F}}} = \left(\frac{k_9 k_{11}^{1/2} [\text{TFA}]}{k_1} + \frac{k_{10} k_{11}^{1/2} [\text{Ac}]}{k_1} \right) \frac{1}{R_{\text{C}_2\text{F}_4\text{H}_2}^{1/2}} + \frac{k_{14}}{k_1}$$

If the [TFA]/[Ac] ratio is held constant (second series in Table I) at a given temperature, a plot of the left-hand side of the above expression *vs.* $[\text{Ac}]/R_{\text{C}_2\text{F}_4\text{H}_2}^{1/2}$ should be linear, with an intercept of k_{14}/k_1 . Neglecting one high point in the 418°K series, such plots gave values of the two intercepts of 0.36 (418°K) and -0.32 (461°K), based on least-squares lines, yielding an average value of $k_{14}/k_1 \simeq 0$. Our evidence is inconclusive as to whether reaction 14 is important or not and further experimentation with the system did not

seem to be justified, since a similar plot for the expression

$$\frac{R_{\text{CF}_2\text{H}_2}}{R_{\text{C}_2\text{F}_4\text{H}_2}} = \left(\frac{k_7 [\text{Ac}]}{k_{11}^{1/2}} + \frac{k_8 [\text{TFA}]}{k_{11}^{1/2}} \right) \frac{1}{R_{\text{C}_2\text{F}_4\text{H}_2}^{1/2}} + \frac{k_{13}}{k_{11}}$$

for the same series of runs leads to anomalous values of $k_{13}/k_{11} \simeq 0.075$, assuming the plots to be linear, when the correct value for the ratio is ~ 0.19 .^{4,16-17} However, the plots showed distinct curvature which is probably due, at least in part, to the nonideality of the TFA-acetone mixtures.

Acknowledgment. We thank Dr. R. L. Thommarson for helpful assistance and discussion.

(17) Our previous determination⁴ of k_{13}/k_{11} is not invalidated by the impurity, if the *unsym*-TFA/*sym*-TFA ratio was constant.

Skeletal Isomerization of Olefins by Radiation

by C. D. Wagner

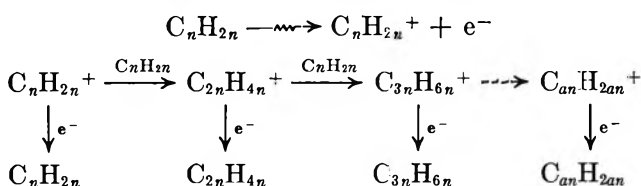
Shell Development Company, Emeryville, California (Received March 7, 1967)

Skeletal rearrangements in hydrocarbon radiolysis have been observed only rarely with cyclic hydrocarbons and not at all with acyclic hydrocarbons. A study of branched monoolefins now discloses that skeletal isomerization does occur. Structures formed include alkylcyclopropanes and olefins with the same degree of branching or less branching. The effect is particularly striking with 3,3-dimethyl-1-butene; 1,1,2-trimethylcyclopropane is the principal product, with $G = 0.23$ at -196° . The dimer, formed in ion-molecule condensation, is mainly skeletally isomerized. The codimer from 3,3-dimethylbutene and ethylene includes 1,1,2-trimethylcyclopentane and other structures that appear to be formed by reaction of ethylene with one of the *gem*-dimethyl groups. The reactions are believed to be reactions of the olefin ion, before geminate recombination. Effects of additives are complex, but in general, the slight enhancement or inhibition effects appear to be due to charge transfer.

Introduction

Radiolysis of straight-chain α -olefins leads to formation of low-molecular weight polymers. The reaction is characterized by the following facts.¹⁻⁶ (1) It is little affected by change in temperature. (2) It is little affected by a change from liquid to solid phase. (3) The product polymers are mostly monoolefinic. (4) The new carbon-carbon bond in the dimer is formed between originally double-bonded carbons of the two molecules, generally between terminal carbons but sometimes between the end carbon of one molecule and the second carbon of another.^{1,2} (5) The initiating species has the formula C_nH_{2n} .⁴ (6) Propagation is not simply head-to-tail, but appears to be much less ordered.⁴ (7) Skeletal isomerization is not significant.⁴

A mechanism proposed^{1,4} to fit these facts is



Since this mechanism was first proposed, mass spectrometric studies have verified that such a condensation actually occurs in dilute gas phase.⁷ Meisels⁸ has studied the radiolysis of gaseous ethylene and concluded that $C_4H_8^+$ and $C_6H_{12}^+$ ions are intermediates with ap-

preciable lifetimes. Recent studies of conductivities of irradiated hexane⁹ indicate that only about 3% of the electrons escape the field of the parent ion in saturated hydrocarbons ($G = 0.1$). However, studies by Williams on cyclohexane¹⁰ indicate that the geminate recombination process of the nonfree electrons and ions may require up to 10^{-7} sec, an interval many times longer than that required for ion-molecule reactions of high cross section in condensed phase.¹¹

Further studies have now been made to determine the generality of the ion-molecule condensation reaction of olefins. Branched olefins have been used. In these studies, substantial amounts of skeletal isomerization

(1) P. C. Chang, N. C. Yang, and C. D. Wagner, *J. Am. Chem. Soc.*, **81**, 2060 (1959).

(2) C. D. Wagner, *Tetrahedron*, **14**, 164 (1961).

(3) E. Collinson, F. S. Dainton, and D. C. Walker, *Trans. Faraday Soc.*, **57**, 1732 (1961).

(4) C. D. Wagner, *J. Phys. Chem.*, **66**, 1158 (1962).

(5) P. C. Kaufman, *ibid.*, **67**, 1158 (1962).

(6) Y. Tabata, H. Shibano, H. Sobue, and K. Hara, *J. Polymer Sci.*, **A1**, 1049 (1963).

(7) F. H. Field, J. L. Franklin, and F. W. Lampe, *J. Am. Chem. Soc.*, **79**, 2419 (1957).

(8) G. G. Meisels, *J. Chem. Phys.*, **42**, 2328, 3237 (1965); G. G. Meisels and T. J. Sworski, *J. Phys. Chem.*, **69**, 2867 (1965).

(9) G. R. Freeman, *J. Chem. Phys.*, **38**, 1022 (1963); **39**, 988 (1963).

(10) T. F. Williams, *J. Am. Chem. Soc.*, **86**, 3954 (1964).

(11) D. P. Stevenson, *J. Phys. Chem.*, **61**, 1453 (1957).

have been observed for the first time. Effects of additives on the skeletal isomerization have been studied.

Experimental Section

Materials. Highly purified hydrocarbons (>99%) were used. Sources of the compounds and their analysis by glpc are given below: 1-pentene, Phillips Research grade, contains 0.02% isopentane and <0.04% of any other material; 2-methyl-1-butene, American Petroleum Institute No. 284, contains 0.02% of an unknown compound, bp about 38°, and 0.02% of 1-pentene; 2-methyl-2-butene, API No. 286, contains <0.001% of any impurity; 3-methyl-1-butene, Phillips Research grade, <0.08% impurities; 1-hexene, Phillips Research grade, contains <0.01% of an unknown compound, bp ca. 65°; 3-methyl-1-pentene, API 531, said to contain <0.3% impurities; glpc shows <0.01 wt % of all foreign compounds; *cis*-3-methyl-2-pentene, API 535, contains 0.008% 3-methyl-1-pentene, 0.046% 2-ethyl-1-butene, <0.04% *trans*-3-methyl-2-pentene; *trans*-3-methyl-2-pentene, API 534, contains 0.006% 3-methyl-1-pentene, 0.0024% 1-hexene, 0.0036% 2-ethyl-1-butene, and 0.047% *cis*-3-methyl-2-pentene; 2-ethyl-1-butene, API 538, contains 0.03% 1-hexene, 0.30% *trans*-3-methyl-2-pentene, 0.0004% 3-methyl-1-pentene, and 0.01% of an unknown hydrocarbon; 3,3-dimethyl-1-butene, API 287x, contains <0.09% impurity; sulfur hexafluoride, Matheson Co., Inc.; ammonia, Matheson Co., Inc.; carbon tetrachloride, Spectroscopic grade, Mallinckrodt; benzene, Mallinckrodt Dual Reagent, thiophene-free; naphthalene, Baker and Adamson, Reagent grade; 1,3-pentadiene, laboratory sample; 3,3-dimethylbutyne, K and K Chemical Co.; cyclohexene, Phillips Research grade, purified by preparative gas chromatography; cyclohexane, Phillips Pure grade; *n*-heptane, Phillips Pure grade; chlorobenzene, Matheson Coleman and Bell, No. 2739, bp 130–132°; bromobenzene, Matheson Coleman and Bell, No. 2740, bp 154–156°; nitrobenzene, J. T. Baker Co.; benzonitrile, Matheson Coleman and Bell, No. 120S, BX400, bp 188–190°; benzoquinone, Eastman Kodak Co., No. P2496, mp 112–114°; methylene chloride, Dow Chemical Co.; acetonitrile, Matheson Coleman and Bell, Spectroquality reagent, treated with silica gel; methanol, J. T. Baker Chemical Co., Reagent grade; tetranitromethane, Columbia Organic Chemicals, Inc.; diethyl ketone, Matheson Coleman and Bell, No. P6253; triethylamine, redistilled, dried over molecular sieve; dimethyl ether, Matheson Co.; ethyl iodide, Eastman Kodak Co., No. 119, analyzed by glpc to be >99.9%; benzophenone, Eastman Kodak Co., No. 346; "Galvinoxyl," Coppinger's

radical (prepared according to G. M. Coppinger, *J. Am. Chem. Soc.*, **79**, 501 (1957)).

Irradiation Procedure. Quantities of 0.4–0.8 g were sealed *in vacuo* in 10-mm o.d. Pyrex tubes, fitted with a break-seal. Irradiation was at –196° by 3-Mev bremsstrahlung from the Van de Graaff generator. Dose rate was 100 Mrads/hr, measured by ceric dosimetry in the same geometrical arrangement. Doses of 50–100 Mrads were used.

Studies of the effects of additives on isomerization of 3,3-dimethylbutene were performed on 10-mmole samples, measured volumetrically in the gas phase in a vacuum system before condensing in a 10-mm diameter × 20-cm ampoule and sealing. Additives of low volatility were weighed into the ampoule before adding the olefin. Samples were irradiated to a dose of 20 Mrads, generally by Co⁶⁰ γ radiation at 0.6 Mrad/hr, sometimes with Van de Graaff bremsstrahlung, where indicated. These irradiations were ordinarily conducted at 30°.

Analysis. Hydrogen and methane were removed by a Toepler pump at –196° and analyzed by mass spectrometry. Liquid products were analyzed by high-resolution gas chromatography, utilizing (1) a silicone-coated glass capillary column, 0.3-mm. i.d. × 90 m long,¹² and (2) a 3-mm i.d. × 6 m long packed column with Ucon stationary phase. Both employed hydrogen flame detection. The capillary column was used mainly for identification, since all C₅ and C₆ saturates and monoolefins are resolved on this column. The packed column was used for quantitative estimates. Standard calibration solutions were used where necessary.

Carbon skeletons were verified by glpc analysis of hydrogenated material. Hydrogenation was accomplished by passing 100 μl of the sample as vapor in hydrogen over 1.5 mg of platinum dispersed on quartz chips. Alkylcyclopropanes were found in all radiolyses of branched olefins. They were characterized by emergence with the saturates upon passage through a 4-mm i.d. × 6-m packed column containing 11% silver ion.¹³ They were resistant to hydrogenation at 30°, but were hydrogenated at 200°. Cyclopropanes from the 3-methylpentenes were not individually identified because of a lack of reference compounds. Samples of the dimethylcyclopropanes were at hand and were used to confirm their presence in the radiolysis products of the methylbutenes. 1,1,2-Trimethylcyclopropane was synthesized by carbene addition to 2-methyl-2-butene.

(12) A. G. Polgar, J. J. Holst, and S. Groennings, *Anal. Chem.*, **34**, 1226 (1962).

(13) B. W. Bradford, D. Harvey, and D. E. Chalkley, *J. Inst. Petrol.*, **41**, 80 (1955).

Table I: *G* Values for Products of Radiolysis of C₅ and C₆ Olefins at 77°K

	1-Pentene	3-Methyl-1-butene	2-Methyl-1-butene	2-Methyl-2-butene	1-Hexene	3-Methyl-1-pentene	2-Ethyl-1-butene	<i>trans</i> -3-Methyl-2-pentene	<i>cis</i> -3-Methyl-2-pentene	3,3-Dimethyl-1-butene
H ₂	ND ^c	0.58	0.62	1.07	ND	0.32	ND	ND	ND	0.34
Fragments										
C ₁		0.07	0.03	0.09		0.02				0.13
C ₂		0.25	0.1	0.00		ND	0.09	0.13	0.10	0.06
C ₃		0.28	0.06	0.00						
C ₄						0.26	0.03	0.04	0.04	0.46
Alkane ^g	0.50	0.45	0.29	0.44	0.55	0.40	0.38	0.23	0.22	0.24
Alkyne ^g	0.16	0.17	0.08	0.16	0.20
Diolefin ^g	0.37 ^z	0.12 ^d	0.18 ^d	0.19 ^d	0.13 ^e	0.16 ^f		0.23 ^f	0.14 ^f	...
Adjacent olefin ^g	0.56	0.23	0.66	0.78	0.18	0.18	0.9	0.19	0.15	...
<i>cis</i> or <i>trans</i> isomer	1.3	1.2	...
Isomerized olefins										
Straight chain ^h		0.07	0.03	0.04		0.11	0.11	0.05	0.05	
2-Methylpentane										0.12 ⁱ
2,3-Dimethylbutane										0.09 ^j
Alkylcyclopropanes										
1,1-diMeCP		0.1	0.01	0.05						
<i>trans</i> -1,2-diMeCP		0.05	0.07	0.09						
<i>cis</i> -MeEtCP ^k						0.05	0.02	0.05	0.07	
<i>cis,trans</i> -1,2,3-triMeCP ^k						0.05	0.09	0.03	0.02	
1,1-MeEtCP ^k						0.01		0.02	0.05	
1,1,2-triMeCP										0.23
Dimer	1.20	1.20	1.14	1.82	1.7 ^b	1.65	2.8	2.2	1.7	0.67

^a ND = not determined. ^b Data for 25°, ref 1. ^c *trans*-1,3-Pentadiene, 0.13; *cis*-1,3-pentadiene, 0.08; 1,4-pentadiene, 0.16. ^d Isoprene. ^e Mainly *trans*-1,3-hexadiene. ^f Believed to be 3-methyl-1,4-pentadiene, 3-methyl-1,3-pentadiene, and 2-ethyl-1,3-butadiene, on basis of delayed retention on Ucon and from relation of boiling point to retention time on the silicone capillary column. ^g Hydrocarbons with same skeleton as feed. Alkyne with triple bond in same position as original double bond. Adjacent olefins include all olefins with double bond in position adjacent to that in the feed (presence of other unisomerized olefins always <0.02). ^h *n*C₆ was a mixture of *cis*- and *trans*-2-hexene. ⁱ *n*C₅ was a mixture of *cis*- and *trans*-2-pentene. ^j Includes 2-methyl-2-pentene, 0.055; 4-methyl-1-pentene, 0.04; 4-methyl-1,3-pentadiene, 0.01. ^k Includes 2,3-dimethyl-1-butene, 0.04; 2,3-dimethyl-2-butene, 0.03; 2,3-dimethyl-1,3-butadiene, 0.01. ^l These three cyclopropanes identified as cyclopropanes by their chemical and glpc behavior, and tentatively identified as these compounds by the retention time *vs.* boiling point relation.

It was used as a reference material to identify it among the products of radiolysis of 3,3-dimethyl-1-butene.

Analysis of 3,3-dimethylbutene isomerization in the presence of additives was accomplished by the 3-mm × 6-m Ucon column, after first removing additives of low volatility by distillation.

Results

Dimer Structure. Products of the radiolysis of the three methylbutenes were hydrogenated and analyzed by gas chromatography. Retention times were identical with those of the eight peaks representing isodecanes from isopentane radiolysis (ten peaks theoretically expected). No unexpected peaks were found. The distributions of C₁₀ products from the three methylbutenes were different, as expected.

It was expected that the highly branched 3,3-dimethyl-1-butene should give at most only three C₁₂ skeletons, and perhaps, if the ion-molecule condensation

is highly specific, only one structure might be formed.¹⁴ However, analysis of a sample treated like the methylbutene products showed the presence of more than five dimer skeletons. The ion fragmentation pattern in the mass spectrometric analysis of trapped samples showed that there were prominent ethyl and propyl branches, as well as methyl and *t*-butyl. It appeared that the 3,3-dimethyl-1-butene ion isomerized before condensation occurred, or the dimer ion isomerized before neutralization by the electron. This led to a careful examination of the monomeric products from all of the C₅ and C₆ branched olefins.

Monomeric Products. Data are shown in Table I. Minor fragmentation products are omitted. The following general conclusions can be drawn.

Prominent products from all alkenes irradiated at

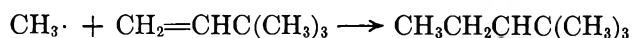
(14) In work with 1-pentene, to be published, it is shown that virtually all of the ionic dimer is straight-chain.

77°K include: (1) the *cis-trans* isomer, where possible ($G = 1.2$); (2) the alkane, by saturation of the double bond ($G = 0.2$ to 0.5); (3) the "adjacent" olefin, formed by migration of the double bond to the neighboring position ($G = 0.2$ to 0.9); and (4) alkynes or diolefins formed by ejection of two hydrogens ($G = 0.2$ to 0.6). None of these products is formed by skeletal isomerization, if we define skeletal isomerization as the intramolecular breaking of a carbon-carbon bond and formation of a new bond between two carbons not previously bonded.

Those were the only product categories formed from straight-chain olefins. However, monomethyl-branched C_5 and C_6 olefins gave not only these typical products, but also significant yields of skeletal isomers ($G = 0.11$ to 0.22). Prominent isomerized products were straight-chain olefins ($G = 0.03$ to 0.11), and dialkylcyclopropanes ($G = 0.08$ to 0.15). Furthermore, the more highly branched 3,3-dimethyl-1-butene gave many isomeric products, including 1,1,2-trimethylcyclopropane ($G = 0.23$), olefins of the 2-methylpentane skeleton ($G = 0.12$), and olefins of the 2,3-dimethylbutane skeleton ($G = 0.09$).

The radiolysis of 3,3-dimethylbutene was examined in more detail, and results are shown in Table II. Many of the olefins of isomeric skeletal structure are identified.

From the relatively complete data obtained at 0 and -196° , it would appear that there is little effect of temperature and phase upon the radiolysis of 3,3-dimethylbutene. Data on the C_6 product yields obtained at 0° (liquid phase) and -196° (crystalline solid) are in general agreement except for 2-methyl-2-pentene, which was greatly enhanced at 0° . In addition, certain C_7 products are obtained at 0° , where the addition of



methyl radicals can contribute (the reaction requires an activation energy of several kcal/mole). However, a third experiment performed at -78° (liquid phase) showed that in fact there is a substantial temperature effect. While the G value for 2-methyl-2-pentene was intermediate, that for trimethylcyclopropane was only 0.08 and that for dimethylbutyne was 0.10. Thus it is clear that the higher G values at -196° for trimethylcyclopropane and for dimethylbutyne are in some way a result of the crystalline state.

Data obtained with Co^{60} γ radiation at 30° at a dose rate of 0.6 Mrad/hr agreed well with the data in Table II for 0° and 100 Mrads/hr. Thus there is no significant dose rate effect.

Products of 3,3-Dimethylbutene plus Ethylene. Formation of complex dimer products from 3,3-dimethyl-

Table II: Radiolysis of 3,3-Dimethylbutene and of Dimethylbutene plus Ethylene (50 Mrads in 30 min)

	G values			
	Temp, $^\circ C$			+ $C_2H_4^a$
	0°	-78°	-196°	at -196°
Hydrogen	0.37		0.34	
Methane	0.14		0.13	
Ethylene + ethane	0.10		0.06	
Isobutane	0.11		0.35	0.13
Isobutylene	0.24		0.11	0.07
Isoprene	0.03		0.04	0.02
C_6 products				
Dimethylbutane	0.24		0.24	0.25
Dimethylbutyne	0.18	0.10	0.20	0.16
1,1,2-Trimethylcyclopropane	0.23	0.08	0.23	0.18
4-Methyl-1-pentene	0.04		0.04	0.02
2-Methyl-2-pentene	0.18	0.14	0.06	0.05
2,3-Dimethyl-1-butene	0.04		0.04	0.05
2,3-Dimethyl-2-butene	0.03		0.03	
C_7 products				
2,2-Dimethylpentane	0.20	0.09	0.00	0.00
<i>t</i> -4,4-Dimethyl-2-pentene	0.11	0.02	0.00	
Unknown C_6 and C_7 compounds	0.13		0.17	
C_8 products				
2,2-Dimethylhexane				0.004
2,2,3-Trimethylpentane				0.009
3,3-Dimethylhexane				0.014
2,2-Dimethylhexene ^b				0.038
3,4,4-Trimethyl-1-pentene				0.023
3,3-Dimethylhexene ^b				0.030
2,3-Dimethylhexene ^b				0.10
1,1,2-Trimethylcyclopentane				0.09
C_{12} compounds	1.29		0.67	

^a 1:1 mole ratio. ^b Location of double bond not determined.

butene made it desirable to explore the reaction in a simpler system. An equimolar mixture of 3,3-dimethylbutene and ethylene was irradiated at -196° and the product was analyzed. The data are shown in Table II. The typical monomeric products from 3,3-dimethylbutene are evident. In addition, there is (not tabulated) the expected *n*-butane and 1-butene from ethylene (G values 0.03 and 0.12). The codimer fraction is particularly interesting. Yields of saturates were determined by separation on a glpc column with silver ion, followed by re-injection of a pentane solution of the trapped products onto the Ucon column. (Yields relative to the trimethylcyclopropane were thus obtained.) Small amounts of 2,2-dimethylhexane, 2,2,3-trimethylpentane, and 3,3-dimethylhexane and a large

yield of 1,1,2-trimethylcyclopentane were thus determined. The identity of the latter was established by comparison of retention times on the silicone capillary with those of an authentic sample. Furthermore, the retention times both at 25 and 50° were consistent (Figure 1) and the retention time of the peak attributed to the trimethylcyclopentane remained the same following hydrogenation.

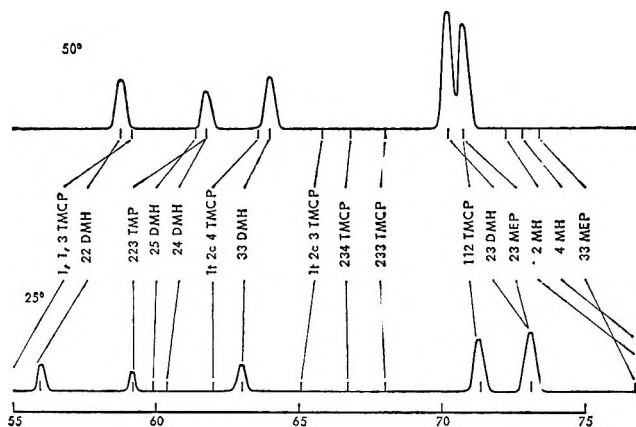


Figure 1. Gas chromatograms of hydrogenated codimer from dimethylbutene-ethylene. Silicone on glass capillary, 25 and 50°. Positions of known compounds indicated. All other C_8 alkanes, alkylcyclopentanes, and alkylcyclohexanes are outside this range. Note: M = Me, E = Et, T = tri, D = di, P = pentane, H = hexane, Hp = heptane; C = cyclo.

The other major C_8 products were four in number and were all monoolefins. Three of them, from their retention times on the capillary column, have boiling points in the range 91–108°. Hydrogenation converts them to 2,2-dimethylhexane, 2,2,3-trimethylpentane, and 3,3-dimethylhexane. No authentic samples of the ten olefins of these skeletal structures in the correct boiling range were available, and no conclusion can be drawn except one: the only candidate of proper volatility with the 2,2,3-trimethylpentane structure is 3,4,4-trimethyl-1-pentene. The fourth olefin present, which was in far larger yield, had the 2,3-dimethylhexane structure. It could be any of five of the 2,3-dimethylhexenes.

Effects of Additives upon 3,3-Dimethylbutene Isomerization. The effects of many types of compounds in admixture up to 0.5 mole fraction were studied in the hope that a correlation with additive properties could be found that would throw light on the isomerization mechanism. Most experiments were performed in the liquid phase at 30°, with a 20-Mrad dose acquired in 30 hr with Co^{60} γ radiation. A few experiments were per-

formed with the Van de Graaff bremsstrahlung to the same dose at -196° . Yields were determined for 1,1,2-trimethylcyclopropane, dimethylbutyne, 2-methyl-2-pentene, and the two C_7 products: 2,2-dimethylpentane and 4,4-dimethyl-2-pentene. Data are given in Table III.

Probably the most remarkable aspect of the data is the insensitivity of the isomerization to the presence of other compounds. This is particularly true of the isomerization to trimethylcyclopropane. Additives present at less than 0.1 mole fraction have very little effect upon the G value. The inclusion of such free radical scavengers as nitrobenzene, benzoquinone, ethyl iodide, 1,3-pentadiene, tetranitromethane, and even galvinoxyl had little effect at low concentrations. The yield of 2-methyl-2-pentene seemed more sensitive to the presence of additives. The formation of C_7 products was completely inhibited by low concentrations of free radical scavengers, as expected.

Attempts were made to observe effects of additives on the radiolysis at 77°K (in solid phase). Carbon tetrachloride at 0.2 mole fraction and n -heptane and cyclohexane each at 0.5 mole fraction had no significant effect. However, triethylamine at 0.2 mole fraction did inhibit the isomerization to trimethylcyclopropane very effectively, reducing the G value to *ca.* 0.02.

Discussion

Radiolysis of saturated open-chain hydrocarbons leads to products whose skeletal structure can be predicted as arising from the scission of carbon-carbon bonds or from the combination of fragments derived from carbon-carbon or carbon-hydrogen scission. Isomerization of skeletal structure has only been observed in cyclic hydrocarbons, such as cyclohexane, where the molecule can easily be visualized as held intact during bond rearrangement. Even then, the yield is small (G of methylcyclopentane = 0.15).

With straight-chain olefins, also, no significant skeletal isomerization has been observed. The ion-molecule condensation-polymerization of 1-hexene,¹ 1-butene,⁵ 2-butene,⁵ propylene,² and ethylene⁴ lead exclusively to dimeric (and presumably polymeric) structures that require no intramolecular carbon-carbon bond scission and re-formation. Again, with cyclic olefins, there are some special cases. In these instances of cationic polymerization by radiation,^{15,16} rearrangement occurs during propagation (as in the following scheme).

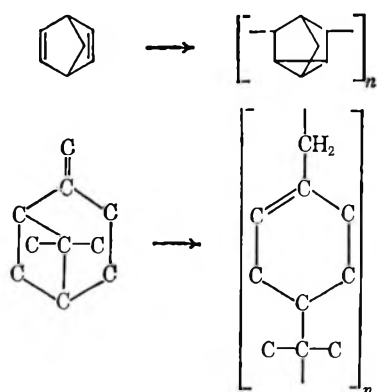
(15) R. H. Wiley, W. H. Rivera, T. H. Crawford, and N. F. Bray, *J. Polymer Sci.*, **61**, S38 (1962).

(16) T. H. Bates and T. F. Williams, *Nature*, **187**, 665 (1960).

Table III: Effect of Additives on Radiolysis of 3,3-Dimethylbutene (20 Mrads in 30 hr, 30° unless Otherwise Noted)

Additive	Additive mole fraction	Product G values				
		1,1,2-Trimethylcyclopropane	Dimethylbutyne	2-Methyl-2-pentene	2,2-Dimethylpentane	4,4-Dimethyl-2-pentene
None	...	0.23	0.18	0.18	0.20	0.11
<i>n</i> -Heptane	0.01	0.25	0.19	0.24	0.23	0.13
	0.04	0.28	0.22	0.24	0.25	0.14
	0.2	0.44	0.33	0.28	0.37	0.18
Cyclohexane	0.2	0.34	0.22	Obsd ^a	Obsd ^a	0.08
	0.5	0.51	0.23	Obsd	Obsd	0.09
1-Pentene	0.2	0.30	0.20	0.22	0.28	0.07
3,3-Dimethylbutyne	0.2	0.28	...	0.18	0.20	0.11
	0.012	0.35	0.22	0.18	0.07	0.04
Nitrobenzene	0.02	0.18	0.13	0.09	0.04	0.00
	0.06	0.21	0.11	0.08	0.02	0.00
	0.22	0.42	0.18	0.00	0.00	0.00
	0.53	0.55	0.16	0.00	0.00	0.00
	0.016	0.25	0.17	0.13	0.16	0.11
Benzonitrile	0.05	0.20	0.09	0.08	0.09	0.03
	0.11	0.24	0.10	0.10	0.11	0.03
	0.24	0.40	0.16	0.14	0.16	0.03
	0.52	0.60	0.18	0.16	0.18	0.03
Benzoquinone	0.01	0.30	0.18	0.12	0.03	0.01
	0.044	0.31	0.16	0.14	0.03	0.01
Carbon tetrachloride	0.01	0.29	0.20	0.14	0.16	0.02
	0.04	0.35	0.22	0.12	0.07	0.00
	0.20	0.46	0.16	0.07	0.02	0.00
Ethyl iodide	0.02	0.29	0.23	0.15	0.12	0.02
	0.2	0.30	0.24	0.16	0.03	0.00
Dimethyl ether	0.2	0.29	0.20	0.21	0.30	0.17
Diethyl ketone	0.02	0.18	0.18	0.16	0.40	0.09
	0.2	0.32	0.16	0.12	0.48	0.02

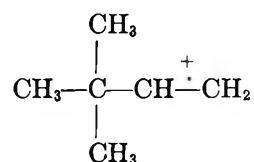
^a Obsd = peak obscured by other reaction products.



In earlier studies, there was mention of minor amounts of cyclic dimer formed from 1-hexene¹ and cyclic trimer from ethylene.⁴ With branched olefins used in the present study, cyclic monomer is formed, and in the system neohexene-ethylene, the interesting cyclic codimer, trimethylcyclopentane, is formed. In addition, we now have the additional facts of the extensive

open-chain isomerization of 3,3-dimethylbutene, both to form other C₆ olefins and also to give heavily isomerized dimer.

In view of the fact that dimerization (polymerization) of 3,3-dimethylbutene is accompanied by isomerization, and in view of the demonstrated ionic nature of the condensation reaction, one is tempted to conclude that isomerization occurs during the life of the ion. The invariance of the yield of trimethylcyclopentane with temperature, dose rate, and the presence of free radical scavengers makes it evident that thermal free radicals are not involved, and that the isomerizing state must be either ionic or excited or both. Ionic isomerization is attractive, for the electron-deficient molecule



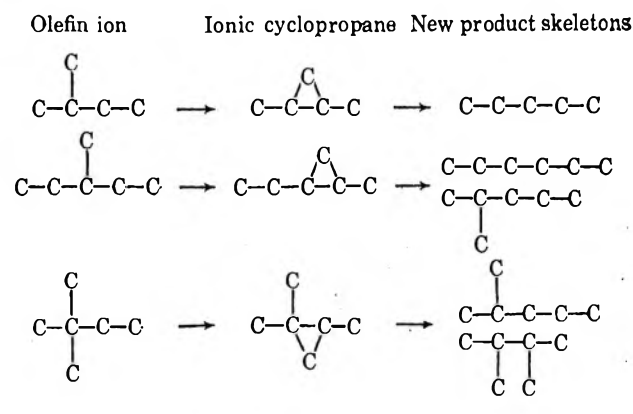
Additive	Additive mole fraction	Product <i>G</i> values				
		1,1,2-Trimethyl-cyclopropane	Dimethyl-butyne	2-Methyl-2-pentene	2,2-Dimethyl-pentane	4,4-Dimethyl-2-pentene
Acetonitrile	0.02	0.24	0.18	0.18	0.24	0.12
	0.2	0.31	0.19	0.18	0.40	0.11
	0.5	0.38	0.19	0.22	0.80	0.13
1,3-Pentadiene	0.02	0.18	0.18	0.14	0.03	0.00
	0.17	0.12	0.16	0.13	0.00	0.00
Cyclohexene	0.1	0.14	0.15	Obsd	Obsd	Obsd
	0.5	0.05	0.07			
Triethylamine	0.2	0.10	0.04	0.04	0.04	0.00
	0.025	0.25	0.18	0.13	0.31	0.07
Chlorobenzene	0.19	0.18	0.14	0.08	0.22	0.00
	0.51	0.10	0.15	0.04	0.14	0.00
Bromobenzene	0.20	0.18	0.08		0.05	
	0.52	0.06	0.06		0.04	
Benzene	0.02	0.20	0.14	0.17	0.18	0.11
	0.17	0.19	0.13	0.14	0.20	0.04
Naphthalene	0.04	0.20	0.13	0.09	0.09	0.04
	0.17	0.16	0.12	0.11	0.08	0.02
Sulfur hexafluoride	0.05	0.19	0.13	0.13	0.12	0.09
Ammonia	0.05	0.20	0.18	0.18	0.20	0.11
Methanol	0.02	0.24	0.21	0.18	0.22	0.13
	0.2	0.17	0.25	0.15	0.26	0.15
Galvinoxyl	0.012	0.25	0.13	0.11	0.00	0.00
Methylene chloride	0.1	0.20	0.18	Obsd	0.34	Obsd
	0.5	0.22	0.13	Obsd	0.17	Obsd
Benzophenone	0.1	0.22	0.13	0.13	0.16	0.06
	0.01	0.18	0.18	0.09	0.03	0.01
Tetranitromethane	0.04	0.13	0.12	0.04	0.00	0.00
	0.12	0.15	0.14	0.02	0.00	0.00
	0.2	0.23	Obsd	0.00	0.00	0.00

with the electron deficiency shared by the originally double-bonded carbons has a structural similarity to the neopentyl carbonium ion, which is known to isomerize readily in solvated systems.¹⁷

If the isomerizing entity is the electron-deficient molecule, the isomerization must occur during the lifetime of the ion or upon recombination with the electron. In any case, the *G* value is far too large to consider that the reaction involves only free ions (*G* = 0.1), so that if isomerization occurs during the lifetime of the short-lived geminate ion it must occur within 10⁻¹⁰ to 10⁻⁹ sec.

The fact that cyclopropanes are prevalent among the products suggests that ring formation is involved in an intermediate or transition state. The restricted distribution of open-chain isomerized products is consistent with this view. If we assume that a branch moves toward the electron-deficient double bond to form a three-membered ring, and that the ring can split in all possible ways to give the final open-chain skeleton,

Table IV



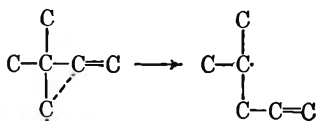
we have the possibilities shown in Table IV. All of these product skeletons were observed except the 2-

(17) F. C. Whitmore, *J. Am. Chem. Soc.*, **54**, 3274 (1932).

methylpentane from the 3-methylpentenes. No other acyclic product skeletons were observed.

The possible role of a three-membered ring in the reaction of an electron-deficient olefin molecule is not inconsistent with many proposals in solvated carbonium ion chemistry. Skell and Starer¹⁸ found that some cyclopropane is formed from *n*-propyl carbonium ion. Some years ago, Stevenson, Wagner, Beeck, and Otvos¹⁹ found it necessary to propose a nonclassical carbonium ion with a three-membered ring in order to explain isomerization and hydrogen exchange behavior of the trimethylbutyl carbonium ion. Roberts, Lee, and Saunders²⁰ proposed such an ion in norbornene chemistry. Rylander and Meyerson²¹ have shown the necessity to postulate protonated and cationated cyclopropane rings in hydrocarbon ions in the gas phase to explain spectral fragmentation results.

The possibility of rearrangement of an excited free radical species cannot be ignored, however. Slaugh, Mullineaux and Raley²² found that radicals formed by action of iodine upon olefins at 450° underwent isomerization by a mechanism best described as a 1,2-vinyl migration. Similar effects were observed by Pines and Goetschel²³ with hydrocarbons over chromia-alumina. By such a mechanism, the same product skeletons should be found as were found here from the three types of starting materials, with the exception of cyclopropanes and of 2,3-dimethylbutenes from the 3,3-dimethylbutene. By such a mechanism, branching is reduced.

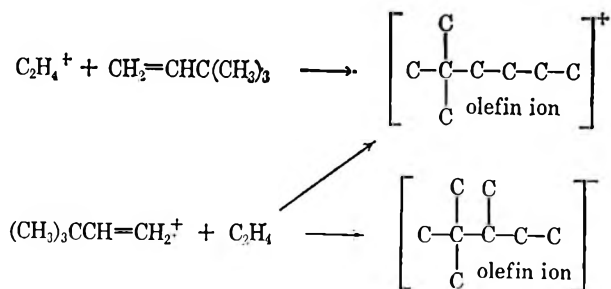


However, such a postulate does not explain the isomerization of the dimer skeleton.

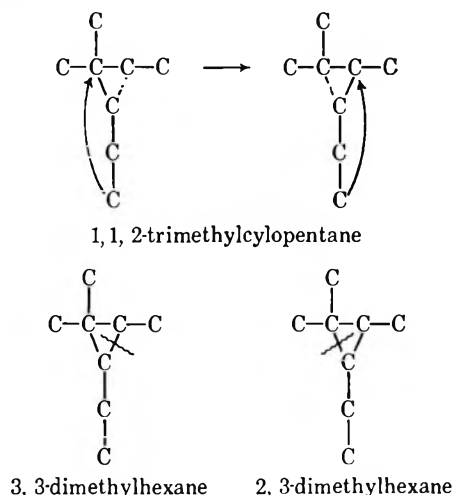
If isomerization does involve the ion, the presence of isomerized monomer demonstrates that the ion can exist long enough to isomerize without condensing with a neighboring molecule. The bimolecular reaction rate is therefore not so fast as had been previously hypothesized. In fact, evidence has recently been obtained for a rate constant for the condensation reaction of $C_2H_4^+$ with C_2H_4 of 10^9 l. mole⁻¹ sec⁻¹.²⁴

The condensation of 3,3-dimethylbutene with ethylene deserves closer attention. On the basis of the earlier work,¹ the skeletal structures expected are those of 2,2-dimethylhexane and 2,2,3-trimethylpentane (see the scheme at the top of the next column) and these structures were found, but they were minor ones.

The specificity of the isomerized C_3 products is



interesting. If we draw a structure that can be conceived as a condensation of ethylene with the trimethylcyclopropane ion, the origin of the unusual structures can be rationalized.



The hydrogen atom and electronic adjustments necessary are not shown because the locations of the olefinic double bonds are not known. Whether such a mechanism as pictured is actually valid is not at all possible to determine. It is clear, however, that the true mechanism must permit active participation by one of the *gem*-dimethyl groups.

It was hoped that the radiolysis of 3,3-dimethylbutene in the presence of additives might present a consistent picture that would provide a firmer basis for establishing the mechanism. The most clear conclusion is that the best radical scavengers (galvinoxyl, benzoquinone,

(18) P. S. Skell and I. Starer, *J. Am. Chem. Soc.*, **84**, 3962 (1962).

(19) D. P. Stevenson, C. D. Wagner, O. Beeck, and J. W. Otvos, *ibid.*, **74**, 3269 (1952).

(20) J. D. Roberts, C. C. Lee, and W. H. Saunders, Jr., *ibid.*, **76**, 4501 (1954).

(21) P. N. Rylander and S. Meyerson, *ibid.*, **78**, 5799 (1956).

(22) L. H. Slaugh, R. D. Mullineaux, and J. H. Raley, *ibid.*, **85**, 3180 (1963).

(23) H. Pines and C. T. Goetschel, *J. Org. Chem.*, **30**, 3530 (1965).

(24) P. Kebarle, R. M. Haynes, and S. Searles, *Advances in Chemistry Series*, No. 58, American Chemical Society, Washington, D. C., 1966, p 210.

tetranitromethane, and nitrobenzene) do not inhibit formation of trimethylcyclopropane even in concentrations up to 2 *M*. It is clear that thermal free radicals are not involved.

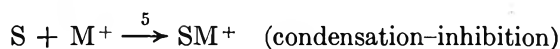
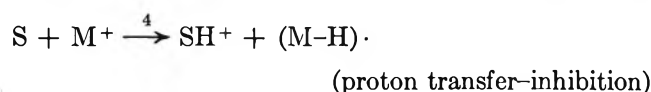
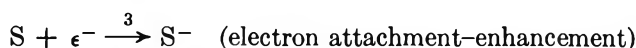
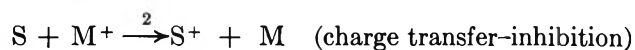
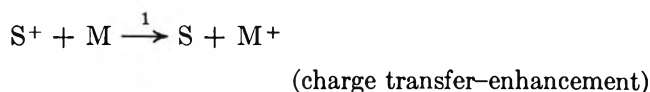
The role of other additives is more difficult to assess. The isomerization to trimethylcyclopropane is really

Table V: Properties of Additives That Affect Yield of Trimethylcyclopropane

	Ionization potential (gas phase), ev ^a	Reaction rate with e ⁻ H ₂ O, l. mole ⁻¹ sec ⁻¹ × 10 ⁻³ ^b	Proton affinity (gas phase), ev
3,3-Dimethylbutene	9.50 ^k		
Enhancing additives			
<i>n</i> -Heptane	10.08	Very low	
Cyclohexane	9.88	Very low	
1-Pentene	9.50	<0.01	
3,3-Dimethylbutyne	10.1		
Dimethyl ether	10.0	<0.01 ⁱ	
Diethyl ketone	9.32	ca. 6	ca. 8.0 ^e
Acetonitrile	12.22		
Carbon tetrachloride	11.47	31	
Nitrobenzene	9.92	30	
Benzonitrile	9.70	16	
Ethyl iodide	9.33	>0.5 ^h	>7.0 ^d
Benzoquinone	9.68 ^e	1.2	
Inhibiting additives			
Cyclohexene	8.94	<0.01 ⁱ	ca. 7.3 ^e
1,3-Pentadiene	ca. 9.0	0.24	
Naphthalene	8.12	5	6.8 ^e
Chlorobenzene	9.07	0.5	
Bromobenzene	8.98	4.3	
Triethylamine	7.50		>9.2
Methanol	10.85	<0.01	7.7-8.0 ^d
Benzene	9.24	<0.01	7.3 ^e
Other			
Tetranitromethane	>10	46	
Ammonia	10.15	Very low	9.2
Methylene chloride	11.35	0.32-20 ^g	
Sulfur hexafluoride		Very high ^f	

^a Unless otherwise noted, from review by K. Watanabe, T. Nakayama, and J. Mottl, *J. Quant. Spectry. Radiative Transfer*, **2**, 369 (1962). ^b From compilation by M. Anbar and P. Neta, *Intern. J. Appl. Radiation Isotopes*, **16**, 227 (1965). ^c A. Terenin and F. Vilesov, *Advan. Photochem.*, **2**, 385 (1964). ^d F. W. Lampe, J. L. Franklin, and F. H. Field, *Progr. Reaction Kinetics*, **1**, 97 (1961). ^e D. P. Stevenson, private communication: determinations by appearance potential of protonated fragment ions from larger molecules. Value quoted for diethyl ketone is that determined for acetone. Value quoted for cyclohexene is that determined for *cis*-2-butene. ^f B. H. Mahan and C. E. Young, *J. Chem. Phys.*, **44**, 2192 (1966). ^g Expected to lie between the values for *n*-butyl chloride and chloroform. ^h Expected to be considerably larger than the value, 0.3, for *n*-butyl chloride. ⁱ Value for diethyl ether. ^j Value for ethylene. ^k Assumed consistent with 1-pentene and 3-methyl-1-butene.

not very sensitive to the presence of additives. In mole fractions up to 0.2, some can approximately double the yield while others can cut the yield in half. In order to aid in assessing the role, the additives are listed in Table V, grouped according to whether they enhance the isomerization or inhibit it. If the reaction is one of the ion, it is conceivable that enhancement or inhibition can result from the following reactions where S represents additive and M represents dimethylbutene.



Examination of Table V shows that there appears to be no correlation of behavior with electron affinity, as measured by the rate of reaction with solvated electrons. It may be that the reaction of isomerization is so fast that increasing the time of geminate recombination has no influence on the probability of reaction.

Proton transfer, reaction 4, has no correlation. Bases like dimethyl ether and diethyl ketone should inhibit, but they enhance instead. Triethylamine and methanol do inhibit, but ammonia has a minor effect.

Condensation, reaction 5, may be the reason for inhibition by cyclohexene, 1,3-pentadiene, naphthalene, and benzene, but if so, 1-pentene and 3,3-dimethylbutyne should not enhance the yield.

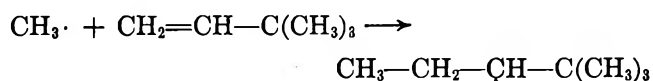
The only correlation that seems to be reasonably consistent is that of the ionization potential. All of the enhancers except diethyl ketone and ethyl iodide have higher ionization potentials than that of 3,3-dimethylbutene. All of the inhibitors have lower ionization potentials except methanol.

If charge transfer is the principal effect (and it must be with such additives as *n*-heptane and cyclohexane), the fact that the yield may be as much as doubled or halved by the addition of 0.2 mole fraction of additive means that the energy levels required for isomerization of the ion must be specific, so that the yield of the particular excited ion can be rather strongly affected.

An effort was made to determine whether the effect is noticeable at low temperatures and in the solid phase. *n*-Heptane and cyclohexane at 0.5 mole fraction and chlorobenzene, triethylamine, and carbon tetrachloride

at 0.2 mole fraction were used at 77°K. No effect was noted except with triethylamine, where almost complete inhibition was achieved.

Examination of the effects of additives on the other major products discloses that the correlations are different. The yields of 3,3-dimethylbutyne and 2-methyl-2-pentene in particular are affected by the additives in ways that afford no consistent picture. The two other major products at room temperature, 2,2-dimethylpentane and *trans*-4,4-dimethyl-2-pentene, are almost completely inhibited by all of the free radical scavengers, even at mole fractions as low as 0.01–0.02 (0.1–0.2 *M*). The compounds are undoubtedly formed by the disproportionation of radicals derived from the addition of methyl radicals to 3,3-dimethylbutene.



The rate constant for addition of a methyl radical to a terminal olefin at room temperature appears to be in the range of 10^3 to 10^4 l. mole⁻¹ sec⁻¹.²⁵ Since the concentration of 3,3-dimethylbutene is about 10 *M*, a radical scavenger at 0.1 *M* must react with methyl radicals with a rate constant of $>10^6$ to compete effectively. Benzoquinone, galvinoxyl, and some of the other radical scavengers do react with rate constants exceeding this value.

Several reagents actually enhance the formation of

both of the C₇ compounds. These are *n*-heptane, dimethyl ether, diethyl ketone, and acetonitrile. The mechanism of enhancement of what must be methyl radical production is not understood.

Conclusion

Radiolysis of branched olefins gives skeletally isomerized products of specific structure. The isomerization is especially marked with 3,3-dimethyl-1-butene. The skeletal structures formed, including substituted cyclopropanes, point to the role of a three-membered ring in the isomerization. The codimers from ethylene and 3,3-dimethylbutene also demonstrate that reaction occurs with one of the carbons of the methyl groups. The body of evidence, though not conclusive, favors a cationated cyclopropane ring intermediate.

Acknowledgment. Gratitude is expressed to Drs. M. A. Muhs, A. G. Polgar, and R. E. Thorpe for assistance with carbene insertion, silicone capillary glpc technique, and mass spectrometric data interpretations, respectively. Discussions of the work with Drs. D. O. Geymer, L. H. Gale, F. D. Mango, and C. T. Goetschel were also very helpful.

(25) The rate constant for abstraction by methyl appears to be ca. 10^3 l. mole⁻¹ sec⁻¹ in simple α -olefins (A. F. Trotman-Dickenson, *Quart. Rev.* (London), 8, 198 (1953)). The ratio of rate constants for addition to abstraction is about a factor of 3 (R. P. Buckley and M. Szwarc, *Proc. Roy. Soc.* (London), A240, 396 (1957)). The rate constant for addition must therefore be in the range of several thousand.

Autocatalysis and Deuterium Isotope Effects in the Reaction of Formic Acid and Nitrogen Dioxide

by Donald Barton¹ and Peter E. Yankwich

Noyes Laboratory of Chemistry, University of Illinois, Urbana, Illinois 61801 (Received March 13, 1967)

The rates of oxidation by nitrogen dioxide of the hydrogen isotopic formic acids (FA), HCOOH (hh), HCOOD (hd), DCOOH (dh), and DCOOD (dd) have been measured in the centimeter range of partial pressures, at 191.3° in a Vycor vessel, with and without added nitric oxide. The rate law observed is of the form $-d(\text{FA})/dt = k_1(\text{FA})(\text{NO}_2) + B(\text{NO})^{2/3}$, where B is an incompletely known function of (FA) and (NO_2) . The finding that there is a small positive intercept on the rate axis when initial rate is plotted vs. initial pressure of nitrogen dioxide suggests the possibility of a small deviation from the indicated simplicity of the nonautocatalytic term. Pollard and Holbrook reported an autocatalytic term of the form $k'(\text{FA})(\text{NO}_2)(\text{NO})$, but less than first-order dependence on nitric oxide can be seen in plots of some of their results. In experiments with added nitric oxide, a short induction period was observed. Isotope effects on k_1 are hh/hd = 1.39, hh/dh = 1.48, and hh/dd = 1.99; on B early in the reaction (all experiments at fixed initial pressures of FA and NO_2) they are hh/hd = 1.62, hh/dh = 1.51, and hh/dd = 2.25. The isotope effects are consistent with involvement of both formic acid hydrogens in rate-determining reactions.

Introduction

Pollard and Holbrook² studied the reaction between formic acid (FA) and nitrogen dioxide in packed and unpacked Pyrex vessels. They found simple stoichiometry, the products being nitric oxide, carbon dioxide, and water. It was observed that the rate depended upon the partial pressure of nitric oxide and was affected by the surface of the vessel. Their kinetics results were fitted to a rate law of the form given in eq 1; rate-controlling bimolecular association was pro-

$$-d(\text{FA})/dt = k_1(\text{FA})(\text{NO}_2) + k'(\text{FA})(\text{NO}_2)(\text{NO}) \quad (1)$$

posed for the noncatalyzed reaction, and hydrogen abstraction from FA by N_2O_3 for the catalyzed reaction.

Because the role of hydrogen abstraction reactions in the kinetics of the oxidation of organic compounds by nitrogen dioxide is but imperfectly understood, we undertook to study such processes in at least partial isolation during the oxidation of FA by nitrogen dioxide through the use of the various hydrogen isotopic formic

acids: HCOOH (hh), HCOOD (hd), DCOOH (dh), and DCOOD (dd). The comparative kinetic isotope effects results are reported here, as well as additional findings on the form of the autocatalytic term in the rate law.

Experimental Section

Reagents. The ordinary formic acid (hh) used was Baker and Adamson CP grade; formic acid- d , formic- d acid, and formic acid- d_2 were obtained from Merck Sharp and Dohme of Canada, Ltd. Samples of each acid were purified using techniques described in the literature;^{2,3} analyses by combustion showed the final samples to be pure to about ± 0.5 mole %, based on carbon dioxide, and all such were stored at -78° until aliquoted for kinetics runs. Nitrogen dioxide was purified as in a similar study⁴ and nitric oxide by the technique described by Nightingale, *et al.*⁵

(1) Visiting assistant professor, 1960-1962; Department of Chemistry, Memorial University of Newfoundland, St. John's, Newfoundland.

(2) F. H. Pollard and K. A. Holbrook, *Trans. Faraday Soc.*, **53**, 468 (1957).

(3) A. S. Coolidge, *J. Am. Chem. Soc.*, **50**, 2166 (1928).

Apparatus and Procedure. The apparatus and kinetic and analytical procedures were essentially as described by Barton.⁴ The cylindrical reaction vessel was fabricated from Vycor glass; its volume was 203 cm³ and the surface to volume ratio was 1.2 cm⁻¹. The vessel was connected to a quartz spiral gauge used as a null indicator; the pressure was measured to ± 0.02 cm on an associated mercury manometer. The reactor was enclosed in a heated steel jacket and its temperature regulated at 191.3° by means of a thermistor and electronic relay; temperature uniformity and control were both $\pm 0.1^\circ$.

Results

Generally, our experiments confirmed the simple stoichiometry observed by Pollard and Holbrook (though no loss of carbon was found in this study), as well as the principal feature of the plots of pressure *vs.* time—a section which, within the precision of the pressure measurement (± 0.02 cm), appears to be linear, *i.e.*, a region of *constant rate*. The kinetics runs carried out after a few of exploratory character were of three types, ΔP referring to the portion of the constant rate region employed in the evaluation of the rate constants, and the pressures being initial values: type A, $P_{FA} = 3$ cm, $P_{NO_2} =$ various, $0 \leq \Delta P \leq 1$ cm; type B, $P_{FA} = 6$ cm, $P_{NO_2} = 3$ cm, $0 \leq \Delta P \leq 0.5$ cm; type C, $P_{FA} = 3$ cm, $P_{NO_2} = 4$ cm, $P_{NO} =$ various, $0.1 \leq \Delta P \leq 0.8$ cm. The kinetics results are displayed in Table I; the values of $\Delta P/\Delta t$ listed were obtained from least-squares treatment of all data pairs in the appropriate pressure range indicated above.

The data for runs of types A and B are in excellent agreement with the observations of Pollard and Holbrook as to both the magnitude and form of the non-autocatalytic term in the rate law, $k_1(FA)(NO_2)$. It was observed in experiments of type B, however, that the initially constant rate increased slowly with time and passed through a maximum near 50% reaction.⁶ Also, except for dd, there is a small positive intercept on the rate axis when initial rate is plotted *vs.* initial pressure of nitrogen dioxide. The latter finding suggests a small deviation from simplicity in the nonautocatalytic term. The isotopic $(k_1)_{ij}$, equal to $(\Delta P/\Delta t)/(P_{FA}P_{NO_2})$ evaluated with initial pressures and the rate in the constant-rate region, are shown in Table II, as are certain of their ratios.

Preliminary experiments with added nitric oxide indicated that the kinetic order of the autocatalytic term with respect to nitric oxide was definitely less than unity, in contrast to the observations of Pollard and Holbrook.⁷ Further, the period of constant rate is short in experiments with added nitric oxide and we ob-

Table I: Rate Results, Constant-Rate Region

Run no.	Istp FA	Init press., cm			Run type	$\Delta P/\Delta t$, cm/min $\times 10^2$
		FA	NO ₂	NO		
9	hh	3.02	4.05	0	A	3.75
13	hh	3.04	11.52	0	A	10.05
19	hh	3.04	7.21	0	A	6.12
20	hh	3.04	1.89	0	A	1.98
24	hh	6.16	3.00	0	B	5.51
25	hh	6.19	3.03	0	B	5.72
26	hh	6.10	3.03	0	B	5.72
37	hh	3.02	4.09	10.99	C	17.81
38	hh	3.01	4.08	5.48	C	13.28
39	hh	3.04	4.03	9.03	C	17.68
40	hh	3.05	4.04	2.95	C	10.47
41	hh	3.04	4.07	0.95	C	6.50
42	hh	3.05	4.02	7.00	C	15.00
43	hh	3.03	3.99	0	A	3.60
10	hd	3.02	4.07	0	A	2.85
12	hd	3.03	11.05	0	A	8.01
21	hd	3.07	7.06	0	A	4.69
49	hd	3.04	4.04	11.81	C	12.92
50	hd	3.03	4.04	4.98	C	8.20
51	hd	3.03	4.08	1.86	C	5.68
58	hd	6.07	3.03	0	B	3.71
61	hd	3.03	4.05	12.67	C	12.70
62	hd	3.02	4.07	0	A	2.60
63	hd	3.03	10.63	0	A	6.77
11	dh	3.01	4.04	0	A	2.57
15	dh	3.00	13.44	0	A	7.55
16	dh	3.03	3.97	0	A	2.50
17	dh	3.01	7.26	0	A	4.05
18	dh	3.06	1.93	0	A	1.45
52	dh	3.04	4.08	9.72	C	11.94
53	dh	3.02	4.05	0	A	2.44
54	dh	3.02	4.02	5.00	C	8.47
55	dh	3.03	4.04	8.67	C	11.39
56	dh	3.02	4.08	1.86	C	6.03
57	dh	6.11	3.07	0	B	3.71
8	dd	3.04	4.04	0	A	1.92
14	dd	3.02	11.34	0	A	5.34
22	dd	3.03	1.99	0	A	0.97
23	dd	6.10	3.07	0	B	2.77
27	dd	6.12	3.07	0	B	2.76
30	dd	3.03	4.07	0	A	1.79
44	dd	3.04	4.06	6.40	C	6.48
45	dd	3.06	4.08	9.10	C	8.06
46	dd	3.03	4.03	1.00	C	2.95
47	dd	3.03	4.07	10.49	C	8.27
48	dd	3.03	4.02	3.82	C	5.30

(4) D. Barton, *J. Phys. Chem.*, **65**, 1831 (1961).

(5) R. E. Nightingale, A. R. Downie, D. L. Rotenberg, B. L. Crawford, Jr., and R. A. Ogg, Jr., *ibid.*, **58**, 1047 (1954).

(6) A suggestion of similar behavior may be seen in the plot for Pollard and Holbrook's run no. 17; see Figure in ref 2.

(7) Conceivably, this discrepancy could arise in the fact that our experiments were carried out at 196°, while the main part of the work of Pollard and Holbrook was done at 220°, or it might be due to the

Table II: Isotope Effects on k_1 and B^a

ij	$10^3(k_1)_{ij}$, cm ⁻¹ min ⁻¹	$(k_1)_{hh}/(k_1)_{ij}$	$10^3 B_{ij}$, ^b cm ^{1/3} min ⁻¹	B_{hh}/B_{ij}
hh	3.03 ± 0.13	...	3.15	...
hd	2.19 ± 0.11	1.39 ± 0.09	1.95	1.62
dh	2.05 ± 0.14	1.48 ± 0.12	2.09	1.51
dd	1.52 ± 0.06	1.99 ± 0.12	1.40	2.25

^a See eq 3. ^b The B_{ij} are for type C experiments at $\Delta P = 0.1$ cm.

served consistently in such runs a short induction period which has not been reported previously. (This induction period was too short to be characterized well with our manual pressure measuring technique.) Therefore, a series of runs was studied in which the initial formic acid and nitrogen dioxide pressures were fixed at convenient values, while the initial pressure of nitric oxide was varied.

It is reasonable to assume that the simple stoichiometry obtains at all t ; then, all instantaneous partial pressures are related simply to the initial pressures and ΔP . In the runs with added nitric oxide, and at a particular value for ΔP , the pressures of formic acid and nitrogen dioxide are identical for each member of the series, but that of nitric oxide is equal to the initial value plus ΔP . Rates were measured at selected values of ΔP and were assumed to conform to the general rate law

$$-d(\text{FA})/dt = k_1(\text{FA})(\text{NO}_2) + X \quad (2)$$

where X is the autocatalytic contribution to the observed rate. Plots of $\log(X)$ vs. $\log(P_{\text{NO}})$ were made for several values of ΔP ; they are linear, with slope 0.66. The slope equivalent of the scatter in the results is approximately ± 0.04 , except possibly near $P = 1$ cm, and there is no drift of the mean slope with ΔP . Thus, to a good approximation

$$X = B(\text{NO})^{2/3} \quad (3)$$

Values of the isotopic B_{ij} are listed in Table II, along with certain of their ratios. The correspondence of eq 3 for X with the experimental results over a wide range of nitric oxide pressures is shown well in Figure 1, where the curves are calculated for $\Delta P = 0.1$ cm; the fit is equally good for other ΔP values.

Discussion

Autocatalysis. Were the difference between our results and those of Pollard and Holbrook confined to the order with respect to nitric oxide in the autocatalytic term of the rate law, B would be of the form

$$B = k''(\text{FA})(\text{NO}_2) \quad (4)$$

which decreases throughout the course of the reaction. However, B is a more complicated function of the composition of the reaction mixture than is suggested by eq 4. The plots of the several components of the rate in run 38 which are shown in Figure 2 are typical. Either the order of X with respect to nitric oxide is different from $2/3$ at low pressures of nitric oxide, or B is not just a function of (FA) and (NO_2) , or both;⁸ our results are insufficient for determination of the analytic form of B .

Hydrogen Isotope Effects. The isotopic ratios of $(k_1)_{ij}$ and B_{ij} in Table II span the range 1.39–2.25; such isotope effects are small in comparison with those expected to be normal and *primary*, but somewhat larger than expected for a normal secondary effect.⁹

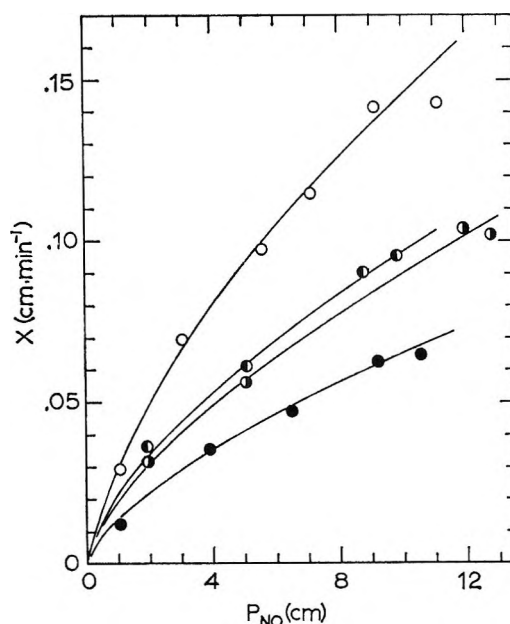


Figure 1. Comparison of X_{calcd} and X_{obsd} as functions of P_{NO} for each isotopic FA; calculations are for $\Delta P = 0.1$ cm. Initial pressures of FA and NO_2 are 3.03 and 4.05 cm, respectively; the following symbols represent the isotopic formic acids: O, HCOOH ; ◐, HCOOD ; ●, DCOOH ; and ●, DCOOD .

20% difference between reaction vessel surface to volume ratios in the two studies. However, examination of their Figure 3 (a plot of initial rate vs. initial pressure of nitric oxide) shows that in every case a curve through the data points bows upward with respect to the line drawn through them, a clear indication of an apparent kinetic order with respect to nitric oxide of less than unity.

(8) Other experiments (part of a different study and not reported here) show that B is not symmetrical in nitrogen dioxide and formic acid pressures; reversal of the initial values of the two causes a pronounced change in the shape of the P - t curve. Also, the plot of $\log(X)$ vs. $\log(P_{\text{NO}})$ suggest that there may be significant deviation from two-thirds order at low pressures of nitric oxide.

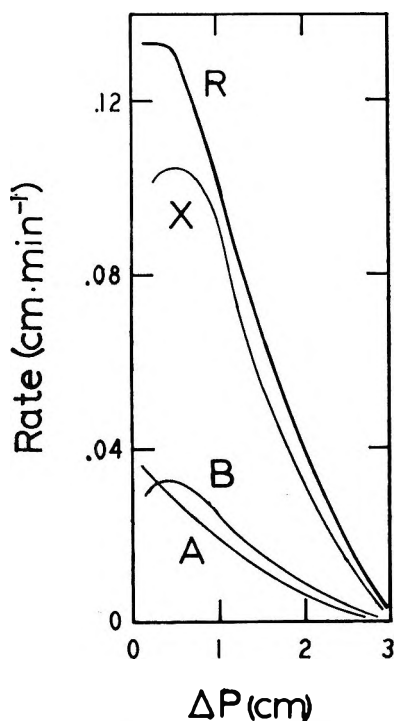


Figure 2. Variation with ΔP of the quantities R , total rate; A , noncatalytic contribution to observed rate; X , autocatalytic contribution to observed rate; and B , $= X/(\text{NO})^{2/3}$; run no. 38, type C.

Barton⁴ has shown how a modest isotope effect can be multiplied in a complicated oxidation superficially similar to that studied here. It is easy to show that such reasonable mechanistic features as dynamic opposition of chain initiation and termination steps in the oxidation of formic acid by nitrogen dioxide can yield a small apparent isotope effect when all of the isotope

effects associated with the individual elementary reactions are of normal magnitude. This reaction has a strong heterogeneous component; however, if strong adsorption of formic acid on the vessel surface resulted in preferential attack at one hydrogen (attack on C-H is favored energetically, and the adsorption would likely be strongest through O-H...O hydrogen bonding), $(k_1)_{\text{hd}}$ and $(k_1)_{\text{dh}}$ would not be expected to be so similar. The similarity of the hd and dh isotope effects indicates that changes at both O-H and C-H are important to the mechanism of the reaction; however, we have no explanation for the fact that $(k_1)_{\text{hd}} > (k_1)_{\text{dh}}$ while $B_{\text{hd}} < B_{\text{dh}}$.

Detail of the NO Catalysis. While our results do not exclude N_2O_3 as the catalytic agent, they do exclude a mechanism as simple as that proposed by Pollard and Holbrook. No doubt, NO radical addition reactions and hydrogen abstraction by nitric oxide should be among additional steps in the mechanism. It is of interest that catalysis by nitric oxide occurs also in the nitrogen dioxide oxidation of acetic acid;¹⁰ there may be a relation between the observation of catalysis and the presence in a reagent of a carboxyl or carboxyl-related function. Further study of the reaction between nitrogen dioxide and formic acid should contribute to understanding of the role of nitric oxide in such oxidations.

Acknowledgment. This research was supported by the U. S. Atomic Energy Commission, COO-1142-73.

(9) L. Melander, "Isotope Effects on Reaction Rates," Ronald Press Co., New York, N. Y., 1960, Chapters 4 and 5.

(10) D. Barton and R. N. Pandey, in preparation.

Carbon-13 Kinetic Isotope Effect in the Structural Isomerization of Cyclopropane: Temperature and Pressure Dependence¹

by L. B. Sims² and Peter E. Yankwich

Noyes Laboratory of Chemistry, University of Illinois, Urbana, Illinois 61801 (Received April 7, 1967)

The C¹³ kinetic isotope effect in the structural isomerization of cyclopropane to propylene was measured in the pressure range 1–760 mm at temperatures between 450 and 519°. The apparatus and procedure were proven by determinations of the first-order rate constant over the same ranges of experimental variables. Qualitatively, the C¹³ isotope effect exhibits the same behavior as that due to deuterium labeling: at high pressures it is relatively pressure independent, but below about 100 mm it decreases approximately linearly with log *p*. At 1 atm, $k_{C^{13}H_6}/k_{C^{12}C^{13}H_6} = (0.995 \pm 0.001) \exp[(19.1 \pm 2.0)/RT]$. The C¹³ effect is about 0.8% at 1 atm, falls to about 0.3% at 1 mm, and is surprisingly large for isotopy at only one carbon in the ring. The results indicate that the reaction coordinate involves considerable ring relaxation.

Introduction

The gas-phase structural isomerization of cyclopropane to propylene is one of the most widely studied unimolecular reactions,³ and the detailed mechanism has long been the subject of controversy in the literature. Most often, discussion has revolved around two mechanisms proposed originally by Chambers and Kistiakowsky:⁴ (1) *hydrogen transfer*, with little or no ring relaxation in the activated complex, and (2) *ring opening* to form a trimethylene biradical-like complex with little or no hydrogen bridging. The importance of hydrogen transfer in the reaction coordinate is suggested by more recent observations of a large deuterium isotope effect at high pressures.^{5,6} In addition to the structural isomerization, Rabinovitch, *et al.*,⁷ observed a geometrical *cis-trans* isomerization of *sym*-1,2-cyclopropane-*d*₂ with high-pressure Arrhenius parameters nearly identical with those observed for the structural isomerization,⁸ suggesting similar mechanisms for the two processes. The most likely mechanism for the structural isomerization involves ring relaxation with hindered rotation of the end CH₂ groups in the activated complex.⁷

Using the RRKM formulation of the theory of unimolecular reactions,^{9,10} Rabinovitch and his co-workers have shown that a complex involving both a relaxed ring structure and hydrogen bridging is able to account

adequately for the kinetics,¹¹ for the pressure and temperature dependences of the deuterium isotope effect,¹² and for the inversion of the deuterium isotope effect at low pressures,¹³ as well as being consistent with the observed geometrical isomerization.⁷

The strongest evidence for ring relaxation in the reaction coordinate comes from the results on the

(1) Taken in part from the Ph.D. Thesis of L. B. Sims.

(2) To whom correspondence should be addressed at Department of Chemistry, University of Arkansas, Fayetteville, Ark. 72701.

(3) See A. F. Trotman-Dickenson, "Gas Kinetics," Butterworth and Co. Ltd., London, 1955, for a review and for early literature citations.

(4) T. S. Chambers and G. B. Kistiakowsky, *J. Am. Chem. Soc.* **56**, 399 (1934).

(5) A. T. Blades, *Can. J. Chem.*, **39**, 1401 (1961).

(6) See also R. E. Weston, Jr., *J. Chem. Phys.*, **26**, 975 (1957).

(7) B. S. Rabinovitch, E. W. Schlag, and K. B. Wiberg, *ibid.*, **28**, 504 (1958).

(8) E. W. Schlag and B. S. Rabinovitch, *J. Am. Chem. Soc.*, **82**, 5996 (1960).

(9) R. A. Marcus and O. K. Rice, *J. Phys. Colloid Chem.*, **55**, 894 (1951).

(10) R. A. Marcus, *J. Chem. Phys.*, **20**, 359 (1952).

(11) D. W. Setser, Ph.D. Thesis, University of Washington, Seattle, Wash., 1961.

(12) B. S. Rabinovitch, D. W. Setser, and F. W. Schneider, *Can. J. Chem.*, **39**, 2609 (1961).

(13) B. S. Rabinovitch, P. W. Gilderson, and A. T. Blades, *J. Am. Chem. Soc.*, **86**, 2994 (1964).

geometrical *cis-trans* isomerization and, though seemingly irrefutable, is somewhat indirect. Examination of the related carbon isotope effect should provide a more direct route for obtaining such information. The RRKM calculated kinetic quantities¹¹ are found to be relatively insensitive to details of the activated complex structure and vibrational frequency pattern. The various hydrogen and carbon kinetic isotope effects depend upon the isotope shifts in the normal molecule and activated complex vibration frequencies. The nonskeletal vibrations are very sensitive to deuterium substitution and virtually unaffected by carbon isotopy; the deuterium isotope effect thus provides information about hydrogen transfer and bridging. The skeletal or ring mode vibrations are not very sensitive to hydrogen isotopy but are strongly affected by substitution of C¹³ for C¹²; the C¹³ isotope effect should permit one to obtain detailed information on these complex frequencies, particularly if the experimental conditions cover suitable ranges of temperature and pressure.

Heretofore, the only results available for the C¹³ isotope effect have been those of Weston,⁶ who found

$$k_{C^{13}H_6}/k_{C^{12}C^{13}H_6} = 1.0072 \pm 0.0006 \quad (1)$$

at 492° and 1 atm pressure. Such a datum does not suffice to demonstrate conclusively the importance of ring relaxation or to make possible comparisons with theory. The object of the investigation reported here was to provide a temperature-pressure map of the C¹³ kinetic isotope effect adequate to support such analysis.

Experimental Section

Materials. Cyclopropane (Matheson Co., 95%) was purified by repeated distillation *in vacuo* between traps at -78 and -196° until no impurities were detectable by gas chromatography and the mass spectrum agreed well with that reported in the literature.¹⁴ Propylene (Phillips Petroleum Co., Research grade) was purified similarly.

Apparatus and Procedure. A conventional high-vacuum apparatus was used for gas handling and for introduction of cyclopropane into a 1400-cc Vycor reaction vessel heated by a furnace assembly similar to that described by Chesick.¹⁵ The temperature was regulated by means of a gas thermometer controller like that described by Larson¹⁶ and measured using Pt-Pt-10% Rh thermocouples placed at several positions on the surface of the reaction vessel and in wells extending into it. The temperature was homogeneous over the reactor to within ±0.05° in all runs and its drift was less than 1° in the longest experiment. The reaction temperatures cited are believed accurate to 0.2°.

For reactions at pressures above 1 cm, cyclopropane was introduced into the preheated reactor from a storage bulb on the vacuum line and the pressure measured with a mercury manometer; for lower reaction pressures, cyclopropane was expanded into the reaction vessel from a small calibrated section of the inlet line and the pressure calculated from a predetermined expansion factor¹⁷ or, in some cases, measured with a McLeod gauge.

The degree of reaction in individual runs lay between 10 and 50%; the reaction was quenched by opening the reactor to a trap at -196°. Propylene and unreacted cyclopropane were separated by gas chromatography, using a 3-m column of dodecyl phthalate on 30/50 ASTM firebrick, and the fraction of reaction (*f*) was determined to ±1% from the ratio of the integrated peak areas. Unreacted cyclopropane (Δ) and propylene (P) were each oxidized at 600° over copper oxide wire and the resulting carbon dioxide was purified by vacuum sublimation.

Isotope Analyses. All samples of carbon dioxide were equilibrated for 24 hr with standard water¹⁸ to eliminate possible effects of oxygen isotope fractionation arising in the oxidations. The *m/e* ^{45/44} ratios were measured with a Consolidated-Nier Isotope-Ratio mass spectrometer modified by replacement of the original dc amplifiers with a master-slave pair of vibrating-reed electrometers (Applied Physics Corp.). The isotope ratios *R*_Δ and *R*_P, from measurements on carbon dioxide obtained from combustion of unreacted cyclopropane and propylene, respectively, were corrected as required for the effects of incomplete oxidation; in addition, the corrections described in previous publications from this laboratory¹⁹⁻²¹ were applied. The imprecision of individual *R* values was ±0.003%.

Results

The apparatus and procedures were proven by determinations of the first-order rate constant *k*_s for the structural isomerization at each of the experimental temperatures (450.3, 474.0, 493.9, and 513.8°) and over

(14) American Petroleum Institute, Research Project No. 44, "Catalog of Mass Spectral Data," spectra no. 115, 172, and 181.

(15) J. P. Chesick, *J. Am. Chem. Soc.*, **82**, 3277 (1960).

(16) J. G. Larson, Ph.D. Thesis, University of Illinois, Urbana, Ill., 1962.

(17) Details of the apparatus and procedure can be found in the Ph.D. Thesis of L. B. Sims, University of Illinois, Urbana, Ill., 1967.

(18) Procedure described in Ph.D. Thesis of W. G. Koch, University of Illinois, Urbana, Ill., 1963.

(19) P. E. Yankwich and R. L. Belford, *J. Am. Chem. Soc.*, **75**, 4178 (1953).

(20) P. E. Yankwich and R. L. Belford, *ibid.*, **76**, 3067 (1954).

(21) P. E. Yankwich and J. L. Copeland, *ibid.*, **79**, 2081 (1957).

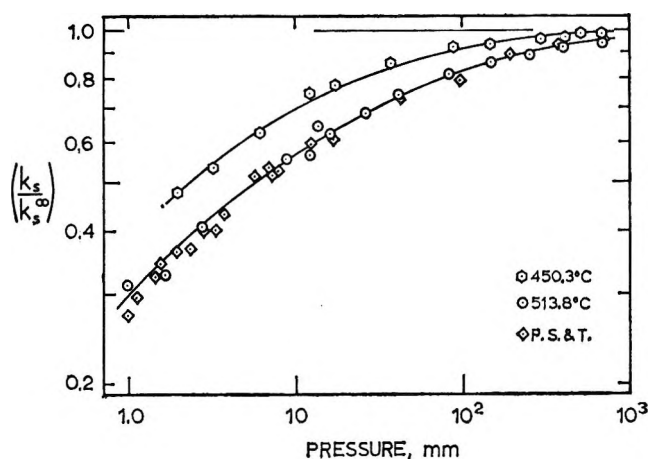


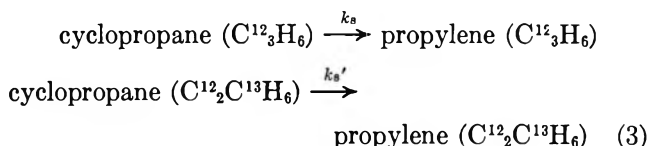
Figure 1. Effects of temperature and pressure on the first-order rate constant k_s for structural isomerization of cyclopropane. Tilted squares are data of Pritchard, Sowden, and Trotman-Dickenson,²⁶ corrected by Johnston and White²⁷ and replotted.

the same range of pressures (approximately 1–760 mm) employed in the isotope fractionation runs. High-pressure limit values of k_s were obtained by extrapolation to $p^{-1/2} = 0$ of plots of k_s^{-1} vs. $p^{-1/2}$.²² At high pressures

$$\log(k_s^\infty) = (15.39 \pm 0.01) - \frac{(65679 \pm 308)}{2.303RT} \quad (2)$$

The falloff curve, $\log(k_s/k_s^\infty)$ vs. $\log p$, shifted²³ +0.40 log p unit between 450.3 and 513.8°. The effects of temperature and pressure on k_s/k_s^∞ are shown in Figure 1; to avoid crowding, only the data for the extremal temperatures were plotted.

The isotopic rate constant ratio k_s/k_s' , whose elements are defined as



is obtained for each experiment from the isotopic ratios $(\text{C}^{12}_2\text{C}^{13}\text{H}_6)/(\text{C}^{12}_3\text{H}_6)$ for propylene and unreacted cyclopropane and the fraction of reaction f . The isotopic ratio $R_i = (\text{C}^{13}\text{O}^{16}_2/\text{C}^{12}\text{O}^{16}_2)$ obtained from measurements on carbon dioxide derived from combustion of one of the hydrocarbons is related to the hydrocarbon isotopic ratio by

$$\frac{(\text{C}^{12}_2\text{C}^{13}\text{H}_6)}{(\text{C}^{12}_3\text{H}_6)} = \frac{3R_i}{1 - 2R_i} \quad (4)$$

Combination of two expressions like eq 4 with eq IV of Tong and Yankwich²⁴ yields

$$\frac{k_s}{k_s'} = \frac{\ln \left[\frac{1}{1-f} + \left(\frac{f}{1-f} \right) \frac{3(R_\Delta - R_P)}{(1+R_P)(1-2R_\Delta)} \right]}{\ln \left[\frac{1}{1-f} + \left(\frac{f}{1-f} \right) \frac{(R_\Delta - R_P)}{R_\Delta(1+R_P)} \right]} \quad (5)$$

Equation 5 is much less sensitive to errors in f than related expressions employing $(R_\Delta)_{t=0}$ among the input data; a 1% error in f generates less than 0.1% error in k_s/k_s' . Values of k_s/k_s' as functions of temperature and pressure are shown in Figure 2. Extrapolation

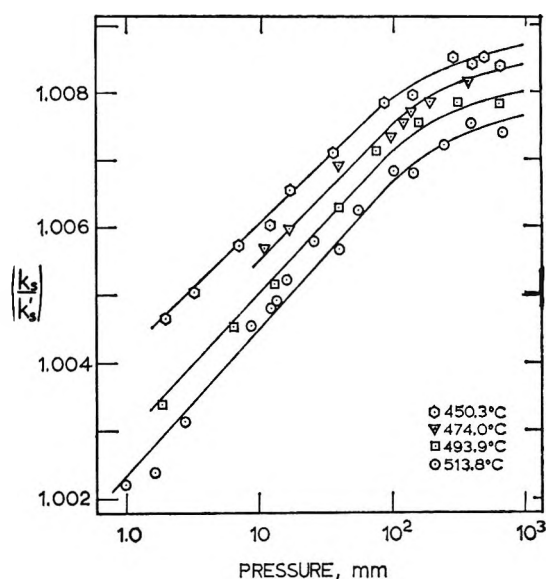


Figure 2. Effects of temperature and pressure on the C^{13} isotopic rate constant ratio k_s/k_s' .

to high pressures is less satisfactory for the isotopic rate constant ratio than for the rate constant k_s itself; the apparent high-pressure limit values, obtained by extrapolation to $p^{-1/2} = 0$ of plots of k_s/k_s' vs. $p^{-1/2}$, are 1.0080 (513.8°) and 1.0090 (450.3°). The results for pressures near 1 atm are represented adequately by

$$k_s/k_s' = (0.995 \pm 0.001) \exp[(19.1 \pm 2.0)/RT] \quad (6)$$

Discussion

The high-pressure rate constant obtained in these experiments, eq 2, agrees well with earlier results reported by Schlag and Rabinovitch⁸

$$\log(k_s^\infty) = 15.26 - (65,900/2.303RT) \quad (7)$$

(22) B. S. Rabinovitch and K. W. Michel, *J. Am. Chem. Soc.*, **81**, 5065 (1959).

(23) N. B. Slater, *Proc. Roy. Soc. (London)*, **A218**, 224 (1954).

(24) J. Tong and P. E. Yankwich, *J. Phys. Chem.*, **61**, 540 (1957).

and by Falconer, Hunter, and Trotman-Dickenson²⁵

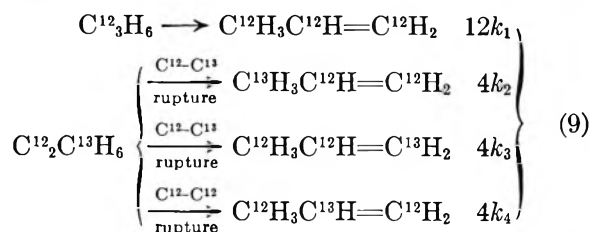
$$\log(k_s^\infty) = 15.45 - (65,600/2.303RT) \quad (8)$$

For comparison of our falloff curves to earlier work, the data of Pritchard, Sowden, and Trotman-Dickenson²⁶ (P. S. & T.), corrected to 500° by Johnston and White,²⁷ are replotted in Figure 1; since the shape of the falloff curve is relatively insensitive to temperature, the agreement is excellent.

Comparison of our results with those of Blades⁵ shows that the C¹³ isotope effect exhibits qualitatively the same behavior as the deuterium isotope effect: at high pressures the isotope effects are relatively pressure independent, but below about 100 mm they decrease (within experimental error) approximately linearly with $\log p$. Preliminary RRKM calculations for 500° indicate, however, that the C¹³ isotope effect may invert near 0.1 mm, whereas the deuterium isotope effect inverts at somewhat lower pressures.^{12,13} (Experiments to extend measurements of the C¹³ isotope effects to lower pressures are in progress.)

The C¹³ isotope effect, though small, nevertheless can be determined precisely as a function of pressure and temperature, and the magnitudes of those dependences suggest that the reaction coordinate is more complex than proposed originally;⁴ in addition to hydrogen bridging, the reaction coordinate includes considerable ring relaxation. If one reduces the C¹³ isotope effect to 25° using eq 6, a value for k_s/k_s' at 1 atm of 1.025–1.030 results; this is surprisingly large for isotopy at only one of the carbons in cyclopropane.

The statistical effect of isotopy at but one of the three positions in the cyclopropane ring complicates any interpretation of the C¹³ isotope effect and must be taken correctly into account in any theoretical calculations and comparisons. It is worthwhile to attempt a statistical correction by the method introduced by Weston.⁶ Consider the possible reactions of the isotopic cyclopropanes with skeletons C¹²₃ and C¹²₂C¹³



Then

$$\frac{k_s}{k_s'} = \frac{3k_1}{k_2 + k_3 + k_4} \quad (10)$$

If it is assumed that C¹²–C¹² bond rupture is equally probable in these two isotopic cyclopropanes

$$k_4 = k_1 = k^{12} \quad (11)$$

and if it is further assumed that the C¹³ isotope effect arises principally in C–C bond rupture, as compared with hydrogen transfer, then

$$k_2 = k_3 = k^{13} \quad (12)$$

These assumptions lead to the expression for the statistically corrected isotopic rate constant ratio in the isomerization of cyclopropane

$$\frac{k^{12}}{k^{13}} = \frac{2(k_s/k_s')}{3 - (k_s/k_s')} \quad (13)$$

Recalculation yields the following for 1 atm

$$\begin{aligned} k^{12}/k^{13} &= 0.995 \exp[(27 \pm 2)/RT] \\ &= 1.012 \text{ at } 513.8^\circ \\ &= 1.014 \text{ at } 450.3^\circ \\ &= 1.041 \text{ at } 25.0^\circ \end{aligned} \quad (14)$$

These are large C¹³ isotope effects, consistent with a transition state involving considerable ring relaxation.

Detailed comparison of the C¹³ isotope effect with theory is much more difficult than in the cases of the kinetics results or the deuterium isotope effect, because much smaller computation errors (*e.g.*, in the calculation of the RRKM rate integral) can be tolerated. Our analysis is not yet complete, but preliminary results indicate that a model for the activated complex such as that proposed by Rabinovitch and his co-workers^{11,12} does account qualitatively for the shape of the isotope effect falloff curves (Figure 2). However, certain changes in the vibrational frequency pattern of the complex are necessary to account for the *magnitude* of the C¹³ isotope effect, particularly at high pressures. Specifically, changes in the ring deformation frequencies (which are strongly affected by carbon isotope substitution) are suggested. At the same time, both the isomerization rate constant k_s and the deuterium isotope effect calculated are very insensitive to these frequencies of the complex, hence the C¹³ isotope effect can provide important new information on the vibrational frequency pattern of the activated complex. A full account of the theoretical investigation will be published subsequently.

(25) W. E. Falconer, T. F. Hunter, and A. F. Trotman-Dickenson, *J. Chem. Soc.*, 609 (1961).

(26) H. O. Pritchard, R. G. Sowden, and A. F. Trotman-Dickenson, *Proc. Roy. Soc. (London)*, **A217**, 563 (1953).

(27) H. S. Johnston and J. R. White, *J. Chem. Phys.*, **22**, 1969 (1954).

Acknowledgments. We are indebted to Dr. Donald Barton (Memorial University of Newfoundland) for invaluable assistance in the early stages of this work and to Professor R. A. Marcus for helpful discussions.

Fellowship support of L. B. S. by the National Science Foundation and Sun Oil Co. is gratefully acknowledged. This research was supported by the U. S. Atomic Energy Commission, COO-1142-74.

Microwave Measurements of Nonequilibrium Air Plasmas behind Shock Waves Containing Electrophilic Gases

by A. P. Modica

Avco Corporation, Space Systems Division, Wilmington, Massachusetts (Received March 13, 1967)

The kinetic behavior of electrons in underdense air plasmas seeded with sulfur hexafluoride (SF_6), trichlorofluoromethane (CFCl_3), and dichlorodifluoromethane (CF_2Cl_2) was studied with 3.14-cm microwaves (X-band) behind reflected shock waves. According to electron-attachment cross sections, electron attachment in plasmas with SF_6 should be 6.2 times faster than with CFCl_3 and 10.5 times faster than with CF_2Cl_2 . In the temperature range of the study, 3400–4200°K, measured electron relaxation rates instead are found to be similar for the three electrophilic gases. Analyses of the thermal decomposition rates of these halomolecules indicate that the lifetimes are extremely short compared to the air ionization reactions for electron quenching to be effective. At high temperatures, a common mechanism for electron removal is explained in terms of attachment by the halogen atom products. Experimental nonequilibrium electron density profiles are compared to those calculated from chemical rate constants. The agreement between the laboratory results and theory is demonstrated.

1. Introduction

The property of fluids to attach electrons in a plasma has immediate applications in aerospace engineering, for example, in atmosphere research of the ionosphere and communications with space craft during reentry. Experimental studies of electron attachment have been accomplished usually by mass spectrometer,¹ ionization chamber,² and microwave³ techniques. Attachment cross sections have been determined by these methods for a number of electrophilic gases at room temperature. However, the performance of such gases to attach electrons at high temperatures is little understood and may be markedly reduced by thermal de-

composition and instability of the molecular ion complex.

In the present investigation, three highly electrophilic gases, sulfur hexafluoride (SF_6), Freon 11 (CFCl_3), and Freon 12 (CF_2Cl_2) were chosen to study their effect on electron formation in high-temperature air plasmas generated by shock waves. These gases were considered for study on the basis of their relatively high electron-attachment cross sections, chemical inertness,

(1) R. E. Fox, *Phys. Rev.*, **109**, 2008 (1958).

(2) J. D. Craggs and B. A. Tozer, *Proc. Roy. Soc. (London)*, **A254**, 229 (1960).

(3) M. A. Biondi, *Phys. Rev.*, **109**, 2005 (1958).

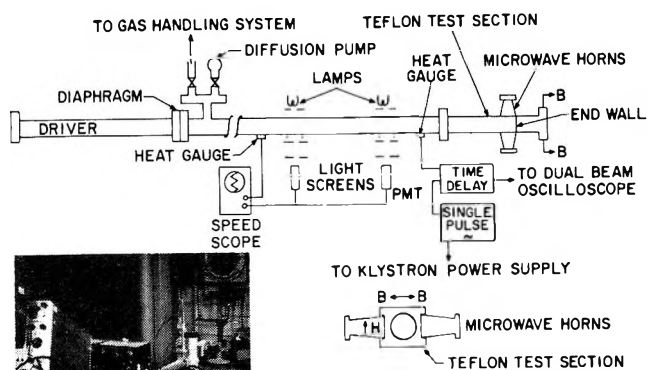


Figure 1. Experimental arrangement of shock-tube microwave apparatus.

and ease of handling. Experiments were conducted in a shock tube coupled to a Teflon microwave cell. Reflected shock waves were used to process the plasma in the microwave cell, and X-band radiation was used to follow the electron concentration in time.

2. Experimental Apparatus and Procedure

The shock tube employed was assembled from stainless steel tubing, having an interior cross section 3.8 cm in diameter. The driver chamber was 103 cm in length separated by a diaphragm from a driven section 334 cm long. The end region of the shock tube consisted of a Teflon test section 30.5 cm in length of 1.52-cm wall thickness matched precisely to the inside dimensions of the metal portion of the driven section. Microwave-horn emplacements were machined into the Teflon section to allow radiation and detection of the probing field along the shock tube axis near the end wall. A pair of identical pyramidal horns were situated across the test section with the edge of the H-plane coincident with the end wall (Figure 1). In this configuration, the time and location of the ionization buildup was accurately known with respect to the probing field.

The microwave circuitry⁴ used in the present experiments was erected from standard X-band components (Figure 2). The transmitted signal was measured by a crystal detector attached to the receiving horn, and the reflected amplitude was measured by a detector on a directional coupler. In the present setup, use was made of the transmitted amplitude to monitor the increase in ionization density following the passage of

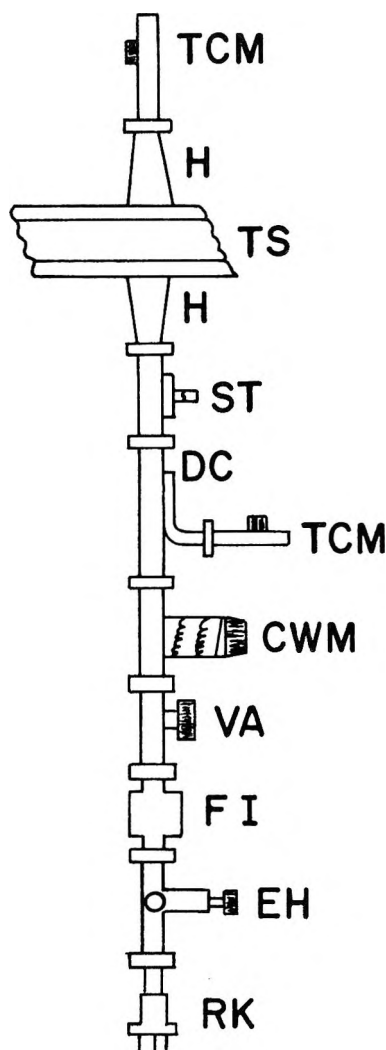


Figure 2. Diagram of microwave circuitry: RK, reflex klystron; EH, E, and H, plane tuner; FI, ferrite isolator; VA, variable attenuator; CWM, cavity wave meter; TCM, tunable crystal mount; DC, directional coupler; ST, stub tuner; H, horn; TS, Teflon section (dielectric).

the shock wave through the test gas. The reflected amplitude was used to note the time at which the electron density exceeded the critical frequency of the plasma.

During the course of the ionization buildup, the electron density passes through a range in which the microwave beam becomes logarithmically attenuated. For electron densities of main interest (10^9 – 10^{12} electrons cm^{-3}), X-band microwaves at 3.14 cm were used. The transmitted and reflected power amplitudes were recorded as a function of time on a dual-beam Tektronix oscilloscope. A single-pulse generator was used

(4) R. G. Jahn, *Phys. Fluids*, 5, 678 (1963).

to bias the accelerating voltage on the klystron to give the amplitude of the incident microwave beam immediately before shock arrival. The ionization region behind a reflected shock wave is typified by the oscillogram records shown in Figure 3.

Gas mixtures containing separately SF₆, CFCl₃, CF₂Cl₂ with air, and excess argon in mole ratios of 1:5:99 and 2:5:98 were shock heated for analysis. The conditions of temperature and electron density at equilibrium behind the reflected shock wave (Figure 4) were obtained from the incident shock velocity and state of the undisturbed gas ahead of the shock wave, using an IBM 360 systems code which couples the Rankine-Hugoniot equations with a thermochemical equilibrium program.⁵ An excess of argon buffer was used with the test gases in order to minimize changes in temperature behind the reflected shock wave due to chemical relaxation.

The incident shock velocity was measured by light screens situated along the driven section upstream of the Teflon test section. The outputs of the light screens were fed to a speed scope and displayed on a time-mark folded sweep (Tektronix 535A) driven by a Radionic (Model TWN-2A) triangular wave and marker timing generator. A platinum-film heat gauge upstream from the first light screen was used to trigger the speed scope. A similar gauge adjacent to the Teflon microwave cell was used to actuate a DuMont time delay generator which synchronized the sweep of the dual-beam Tektronix scope with the arrival of the shock wave near the microwave test cell. Shock-wave attenuation along the tube was observed to be about 0.5%/10-cm length. The shock velocity was extrapolated to the end wall with an accuracy of better than 99%, introducing

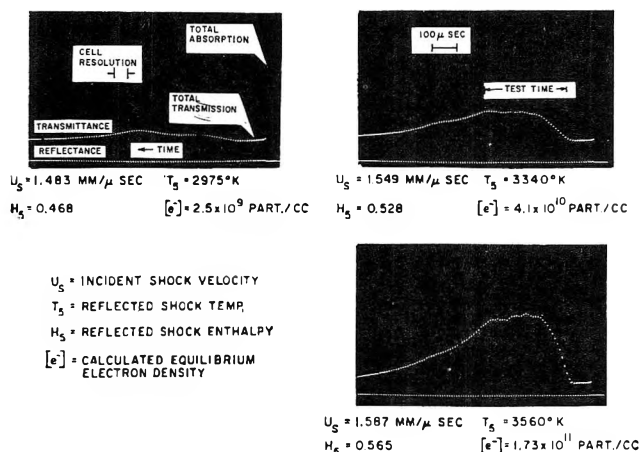


Figure 3. Oscillogram records of microwave transmission through ionization region behind reflected shock waves. Data obtained from 2:5:98 sulfur hexafluoride-air-argon tests.

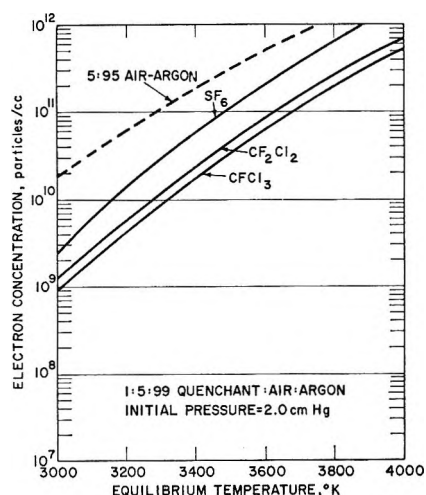


Figure 4. Calculated equilibrium electron densities behind reflected shock waves.

an uncertainty of less than 100°K in the calculated temperature for the reflected shock.

The test gases were heated in shock waves driven with pressurized helium. Mylar diaphragms of 3–6-mil thickness were used to obtain reflected shock temperatures between 3000 and 4500°K. The low-pressure section was provided with a 5.08-cm oil diffusion pump and was pumped down to <0.001 torr. The combined leak rate of the gas-handling system and shock tube was ~ 0.0005 torr/min. The impurity level of the Teflon test section on the electron concentration in the test gas plasma was established by shock heating the argon buffer to temperatures and pressures similar to those obtained for the test sample. The results indicated about a 5% contribution by the shock-tube impurities to the microwave absorption observed in the test gas experiments.

3. Microwave Calibration

The theory of microwave absorption by free electrons is derivable from the usual Maxwell equations which give for a plane wave incident normally on a uniform plane slab of ionized gas the expression⁶

$$A = \ln(I_0/I) = \epsilon L[e^-] \quad (1)$$

where A is the absorbance, I_0 and I are the incident and transmitted amplitudes, $[e^-]$ is the number of free electrons per cm³, L is the path length in centimeters, and ϵ is a complicated function of the electron concentra-

(5) R. D. Gillespie and J. Warga, "A Program for Computing Thermochemical Equilibrium Behind a Moving Shock Wave," Avco Report RAD TM-63-65 (1963); J. Warga, *J. Soc. Ind. Appl. Math.*, **11**, 594 (1963).

(6) H. S. Johnston and W. Kornegay, *Trans. Faraday Soc.*, **57**, 1563 (1961).

tion, the angular frequency of the microwaves, the dielectric constant, electrical conductivity, and electron atom collision frequency. For values of the electron density below the critical frequency of the plasma, the absorption coefficient is independent of electron density and the absorbance A is linear in both electron concentration and path length, regardless of the spatial distribution of the electrons. In the present experiments, because of the complicated geometry between the rectangular microwave beam interacting with the shock-tube plasma column, a simple calibration scheme was adopted to determine empirically an effective absorption cross section $\sigma_e(\epsilon L)$ for the free electrons in the shock tube. The microwave absorption signal at chemical equilibrium was correlated to equilibrium electron density calculated from the shock tube computer program. A log-log plot of the absorbance A with electron concentration (Figure 5) indicated, within a 15% deviation, a linear dependence as expected from theory. In the microwave calibration procedure, use was made of the data from the 2:5:98 sulfur hexafluoride-air-argon experiments. In order to check further the calibration, the empirical electron absorption cross section σ_e was applied in an independent experiment to reduce oscillogram records of shock-heated 5:100 air-argon gas samples. A comparison of the experimental nonequilibrium electron profiles and those calculated from the kinetics of air⁷ for the gas mixture is shown in Figure 6. Since the temperature in the reaction mixture behind the shock wave was not isothermal, the calculated electron profile was obtained by assuming that the temperature of the system relaxed exponentially from the frozen shock temperature at the front to the equilibrium temperature. The time dependence of the temperature decay was determined from the experimental electron density records.⁸ The correlation between experiment and theory indicated that in reducing the data with the empirical electron cross section, the correct magnitude of electrons was being given. An advantage of the internal microwave calibration was that errors caused by shock tube impurities are essentially cancelled in the data reduction.

4. Nonequilibrium Electron Density Measurements

Mixtures of air containing separately SF_6 , CF_2Cl_2 , and CFCI_3 in excess argon were shock heated to temperatures from 3400 to 4200°K behind reflected shock waves. For each of the mixtures, the rate of change of electron density was evaluated at a time during chemical relaxation corresponding to an electron density equal to approximately $1/e$ of its equilibrium

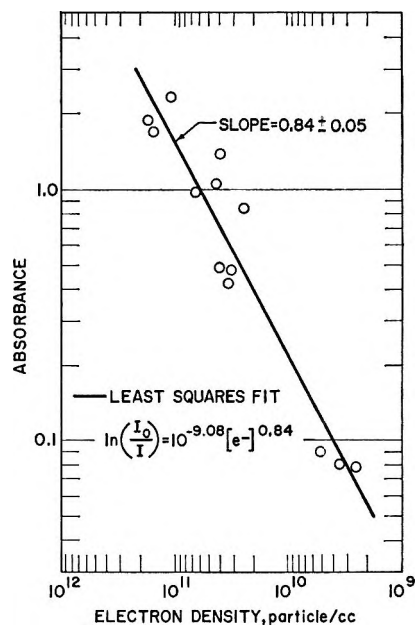


Figure 5. Log-log plot of microwave absorbance with calculated electron concentration.

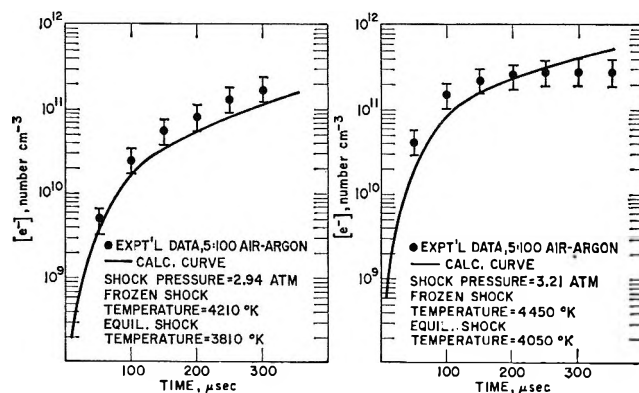


Figure 6. Comparison between experimental nonequilibrium electron profiles in shock-heated air and values calculated from kinetics of air.

value. The electron relaxation rates of the various reaction mixtures, defined by

$$k_{e1} = \left(\frac{\Delta e^-}{\Delta t} \right)_{1/e} \quad (2)$$

are compared in Figure 7. The experimental data show that the electron formation rate is nearly the same in the

(7) K. L. Wray, *Hypersonic Flow Res.*, 7, 181 (1962).

(8) The calculated electron density profiles were obtained from an IBM computer program developed by P. Lewis and J. D. Teare of the Avco-Everett Research Laboratories. It will be known later in the study that the temperature dependence of electron formation is connected with the O_2 dissociation rate. This means that the assumption of the exponentially decaying temperature should be a reasonable one since the O_2 dissociation is itself an exponential function of time.

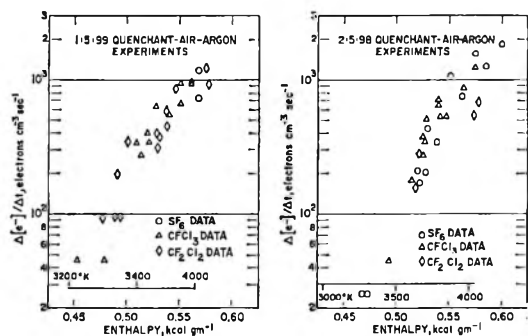


Figure 7. Electron relaxation rates in quenchant-air plasmas.

presence of the three electron-attaching gases. Consideration of the electron attachment cross sections for SF_6 , CFCl_3 , and CF_2Cl_2 (Table I) would indicate that electron formation in these mixtures would be approximately in the ratio 1:6.2:10.5, respectively. The fact that this behavior is not observed suggests that the electron-attachment mechanism in the mixtures is common to the three electrophilic gases and involves species of nearly the same electron-attachment cross sections. Calculations based on measured rate constants for the thermal decomposition of SF_6 , CFCl_3 , and CF_2Cl_2 show that under the present experimental

Table I: Attachment Cross Sections^a

Molecule	Cross section, cm^2
SF_6	5.7×10^{-18}
CFCl_3^b	9.2×10^{-17}
CF_2Cl_2	5.4×10^{-17}

^a N. S. Buchel'nikova, *Zh. Eksperim. Teor. Fiz.*, **35**, 1119 (1958). ^b Estimated as the average cross section of CCl_4 and CF_2Cl_2 .

conditions these molecules would decompose in times short compared to the electron formation from air ionization reactions (Figure 8). An analysis of the temperature dependence of the 1:5:99 sulfur hexafluoride-air-argon data shows an activation energy of 134 ± 5 kcal/mole which is in agreement with the rate-determining step for air ionization, namely the O_2 dissociation reaction. From thermochemical equilibrium calculations of the sulfur hexafluoride-air mixture, for example, the most important electron-attachment species are F, S, O, and N in the temperature range of study (Figure 9). The relatively large abundance of F^- at equilibrium suggests fluorine attachment to be

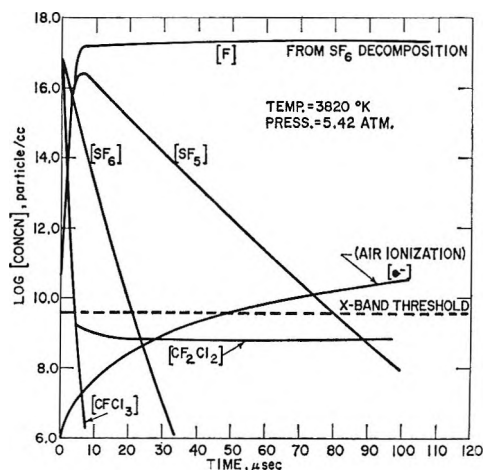


Figure 8. Thermal decomposition rates of electrophilic molecules compared to electron formation rate from air ionization reactions.

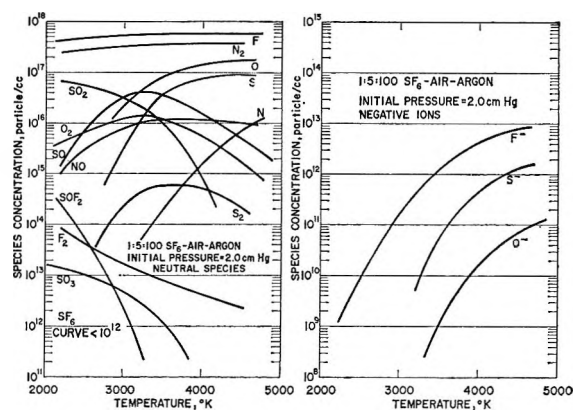


Figure 9. Important neutral and ionic species in shock-heated sulfur hexafluoride-air mixtures from thermochemical equilibrium calculations.

the dominant electron-attachment mechanism. The good agreement between experimentally measured electron density profiles in the 1:5:99 sulfur hexafluoride-air-argon mixtures and those calculated from the reactions in Table II supports this mechanism and may explain the similar performance of the three electrophilic gases at high temperatures (Figure 10).

5. Error Analysis

Earlier in the text it was pointed out that shock-tube impurities could have contributed as much as 5% to the absorbance and thereby to $[e^-]$. According to the electron reaction mechanisms shown in Table II, the over-all kinetics are linearly dependent on $[e^-]$ and therefore would be uncertain by about 5%, well within the experimental error in the calibration constant (a factor of ≈ 2 variation). For a transparent plasma,

Table II

Reaction no.	Reaction		
Air Ionization Reactions ^a			
1	O ₂ + M	= O + O + M	$RC^b = 6.00E - 06T^{**}(-1.00) \exp(-59,400/T)$
1R	O + O + M	= O ₂ + M	$RC = 8.30E - 33T^{**}(-0.50) \exp(0/T)$
2	N ₂ + M	= N + N + M	$RC = 3.20E - 07T^{**}(-0.50) \exp(-131,000/T)$
2R	N + N + M	= N ₂ + M	$RC = 3.00E - 32T^{**}(-0.50) \exp(0/T)$
3	O + N ₂	= N + NO	$RC = 1.10E - 10T^{**}(0.00) \exp(-37,500/T)$
3R	N + NO	= N ₂ + O	$RC = 2.50E - 10T^{**}(0.00) \exp(0/T)$
4	O + NO	= N + O ₂	$RC = 5.30E - 15T^{**}(1.00) \exp(-19,700/T)$
4R	N + O ₂	= O + NO	$RC = 1.60E - 12T^{**}(0.50) \exp(-3600/T)$
5	NO + M	= N + O + M	$RC = 6.60E - 04T^{**}(-1.50) \exp(-75,600/T)$
5R	N + O + M	= NO + M	$RC = 2.80E - 28T^{**}(-1.50) \exp(0/T)$
6	NO + M	= NO + E + M	$RC = 2.00E - 08T^{**}(-1.00) \exp(-107,900/T)$
6R	NO + E + M	= NO + E + M	$RC = 1.70E - 23T^{**}(-2.50) \exp(0/T)$
7	N + O	= NO + E	$RC = 1.50E - 14T^{**}(0.50) \exp(-32,400/T)$
7R	NO + E	= N + O	$RC = 3.00E - 05T^{**}(-1.00) \exp(0/T)$
Sulfur Hexafluoride Decomposition Reactions			
8	SF ₆ + M	= SF ₅ + F + M	$RC^c = 2.50E - 13T^{**}(0.50) \exp(-19,700/T)$
9	SF ₅ + M	= SF ₄ + F + M	$RC = 2.50E - 13T^{**}(0.50) \exp(-25,000/T)$
10	SF ₄ + M	= SF ₃ + F + M	$RC = 2.50E - 13T^{**}(0.50) \exp(-25,000/T)$
11	SF ₃ + M	= SF ₂ + F + M	$RC = 2.50E - 13T^{**}(0.50) \exp(-25,000/T)$
12	SF ₂ + M	= SF + F + M	$RC = 2.50E - 13T^{**}(0.50) \exp(-25,000/T)$
13	SF + M	= S + F + M	$RC = 2.50E - 13T^{**}(0.50) \exp(-25,000/T)$
Electron Attachment Reaction			
14	F + E + M	= F + E + M	$RC^d = 4.38E - 28T^{**}(-1.00) \exp(5390/T)$
14R	F + M	= F + E + M	$RC = 1.50E - 05T^{**}(-1.00) \exp(-40,700/T)$

^a See ref 7. ^b $RC = aE - 05T^{**}(n) \exp(-E/T) \equiv (a \times 10^{-5})T^n e^{-E/T}$; units in particle cm³ sec. ^c A. Modica, submitted for publication. ^d Estimated from classical collision rate theory and JANAF equilibrium constant.

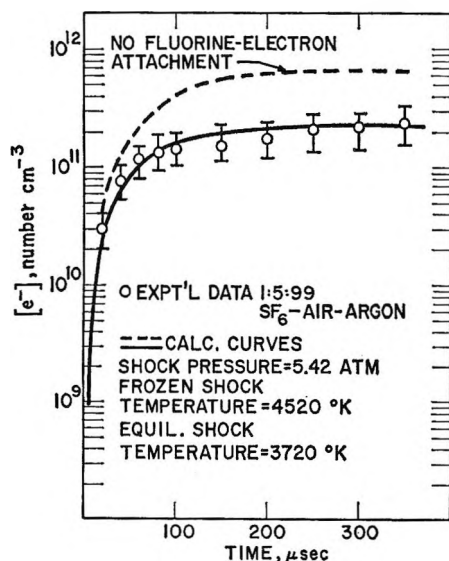


Figure 10. Experimental and theoretical nonequilibrium electron densities in a high-temperature sulfur hexafluoride-air-argon reaction mixture.

the absorption cross section (ϵL) is proportional to the electron collision frequency (ν_e) or to the square root of

the electronic temperature ($T_e^{1/2}$). The calibration constant σ_e was determined on the basis of test results obtained in the temperature range from 3000 to 3600°K. Hence, in neglecting the temperature dependence of σ_e , the uncertainty introduced amounted to at most 10% in the calibration constant. The present experiments are incapable of demonstrating that the electron and atom temperatures are equal. However, calculations show that by correcting the calibration constant to the average test gas temperature (average of frozen and equilibrium shock temperature), e.g., 4120 ± 400°K, Figure 10, the uncertainty in reducing the electron density with the calibration constant would be less than ±5%. The most serious error caused by temperature appears in the reaction kinetics. Because of the 100°K uncertainty in the calculated, reflected-shock temperature, arising from shock-velocity attenuation and extrapolation, computer results show that the calculated electron densities vary by almost ±40%. Such a situation could account for most of the scatter in the experimental data. Another source of error, boundary layer temperature gradients, does not appear to be important for the test-time intervals in the present

study. The steadiness of the microwave signals during chemical equilibrium tends to support this conclusion.

6. Discussion

In the present experiments, three electrophilic gases of widely different electron-attachment cross sections were introduced in an air plasma above 3000°K. Measurements of the electron density rates in the test mixtures were found to be nearly the same, suggesting a common electron-attachment mechanism. At first sight, analyses of the dissociation rates of these electrophilic gases, for the test conditions selected, indicate electron attachment to take place primarily between the halogen atom end products. In view of the time resolution ($\approx 50 \mu\text{sec}$) and the sensitivity threshold of the X-band instrumentation, the present work cannot directly assess the effects of the quenchant molecules and their daughter products (e.g., SF_6 , SF_4 ,

CF_2 , CCl_2 , etc.) during the early stages of electron buildup, when these species are still present in appreciable fractions. Because such electron-suppressing species are expected to be important in rapid-ionization systems as with alkali or hydrocarbon chemiionization, experimental cross-section studies involving the parent and intermediate electrophilic species are currently being designed.

Acknowledgment. The author is pleased to acknowledge the U. S. Air Force Ballistic Systems Division (BSYDR) under Contract AFO4(694)-913, RVTO Project, part of ABRES Program, in the support of the present research. Appreciation is also expressed to P. Lewis and Dr. J. D. Teare of the Avco-Everett Laboratories for the use of their nonequilibrium kinetics, computer program, and for their discussions on this work.

Ion Pairs and Solvent-Solute Interaction. I. Conductance of Lithium Chlorate in Water-Dioxane Mixtures at 25°

by Filippo Accascina, Alessandro D'Aprano, and Roberto Triolo

Institute of Physical Chemistry, University of Palermo, Palermo, Italy (Received March 22, 1967)

The conductance of lithium chlorate ($0.003 > c > 0.0005$) was measured at 25° in dioxane-water mixtures ($78.5 \geq D \geq 9.00$). Association to ion pairs can be calculated from a contact distance $d = 6.8$, using $K_A = (4\pi N a^3 / 3000) \exp(\epsilon^2 / a D k T)$. The similarity to sodium and potassium chlorates, which also show comparable association in this range of dielectric constant, and the marked contrast to lithium perchlorate, which is not associated at all over the same range, suggests a much greater solvation of the perchlorate ion than of the chlorate. Six water molecules, hydrogen bonded at the edges of the perchlorate tetrahedron, provide a structure large enough to make electrostatic pairing negligible.

A theoretical interpretation of the properties of electrolytic solutions in terms of molecular parameters is still in process of development. Considerable success has been obtained by using a very much oversimplified model, the sphere in continuum, in which ions are

represented as rigid charged spheres in a continuous medium which is described electrostatically by the macroscopic dielectric constant and hydrodynamically by the macroscopic viscosity. With this model, the only interaction which may be considered is that be-

tween ions; a continuum, by definition, is without structure and the model therefore excludes ion-solvent interactions. The latter include several distinct types, as well as their combinations. The most extreme interaction is the formation of complex ions, which, of course, includes hydrates. Even if stoichiometric compounds are not formed, there will always be an electrostatic interaction between the fields of solvent dipoles and ions. In the case of hydrogen-bonded solvents, the resulting solvent structure can in some cases be reinforced by the presence of ions and in other cases will be destroyed. It should be emphasized that all of these short-range interactions depend on the structure of the solvent and are specifically dependent on shape, size, and charge distribution of the solvent molecules, as well as on the corresponding properties of the ions. It is clear that a continuum model neglects all of these important details and necessarily throws their effect into the ion-size parameter. So, for example, it has been found that the same electrolyte in isodielectric solvents of different chemical composition gives different values for the contact distance.¹

In a general way, it has been found that the larger the ions are, the better will the simple theory account for the experimental results.²⁻⁶ An example of this kind is tetrabutylammonium tetraphenylboride, Bu₄NBPh₄, in which both anion and cation contain many more atoms than the molecules of ordinary solvents and where the volume of the ions is approximately at least an order of magnitude greater than the volume of a solvent molecule. In the case of electrolytes with small ions, such as the alkali halides in mixtures containing water, specific ion-solvent interactions have been observed.⁷⁻¹¹ This is, of course, about what one would expect: as the ions becomes larger, the solvent approaches more and more the continuum of the ideal model from the point of view of the ion. A most striking example of specific effects was found recently in our laboratory by Accascina and Schiavo, who measured the conductance of lithium perchlorate in dioxane-water mixtures covering the range from water to a mixture with dielectric constant equal to 10.¹² The experimental results for this system have shown that the electrolyte is not associated even at low dielectric constant ($D = 10$). At this value, lithium chloride in the same solvent has an association constant of several thousand.¹¹ Clearly, the simultaneous presence of lithium ion and of perchlorate ion in dioxane-water mixtures involves some special effects. We therefore started a systematic investigation of a number of related systems in order to determine whether they might show similar behavior or whether the lack of association was peculiar to the lithium perchlorate-water-dioxane

system. In order to study the influence of the anion structure on the association process, we changed the nature of the anion: instead of perchlorate, the chlorate of lithium was studied in dioxane-water mixtures. Judging from the limiting conductances,^{13,14} which are $\lambda_0(\text{ClO}_4^-) = 67.3$ and $\lambda_0(\text{ClO}_3^-) = 64.0$ in water, the two ions have approximately the same volume. The charge distribution is, however, significantly different although the geometrical structures are quite similar. We would, therefore, expect a different behavior of the two anions with respect to ion pair formation and to solvent interaction. In this paper, we present a discussion of the conductance of lithium chlorate in dioxane-water mixtures covering the range $78.54 \geq D \geq 9.00$ in dielectric constant. The data conform to the electrostatic theory of conductance¹⁵ with some deviations that call for a more detailed theory based on a model which will take into account the structures of the solvent, at least near the ions.

Experimental Section

The methods of purification of water¹⁶ and dioxane¹⁷ were those used previously. Lithium chlorate was prepared by mixing exactly stoichiometric amounts of 1 *M* solutions of barium chlorate (Fluka product) and lithium sulfate (C. Roth product) at 85°. The filtrate contained neither sulfate nor barium ions, a check on the preparation. The solution (a solvent for cellulose) was filtered through asbestos, then gradually concentrated to about 90%, after which most of the salt was precipitated by chilling. The precipitate was then dried by heating under vacuum over phosphorus

- (1) A. D'Aprano and R. M. Fuoss, *J. Phys. Chem.*, **67**, 1871 (1963).
- (2) R. M. Fuoss, J. B. Berkowitz, E. Hirsch, and S. Petrucci, *Proc. Natl. Acad. Sci. U. S. A.*, **44**, 27 (1958).
- (3) F. Accascina, S. Petrucci, and R. M. Fuoss, *J. Am. Chem. Soc.*, **81**, 1301 (1959).
- (4) R. M. Fuoss and H. Hirsch, *ibid.*, **82**, 1013 (1960).
- (5) D. S. Berns and R. M. Fuoss, *ibid.*, **82**, 5585 (1960).
- (6) R. W. Kunze and R. M. Fuoss, *J. Phys. Chem.*, **67**, 385 (1963).
- (7) J. E. Lind and R. M. Fuoss, *ibid.*, **65**, 999 (1961).
- (8) R. W. Kunze and R. M. Fuoss, *ibid.*, **67**, 911 (1963).
- (9) R. W. Kunze and R. M. Fuoss, *ibid.*, **67**, 914 (1963).
- (10) J. C. Justice and R. M. Fuoss, *ibid.*, **67**, 1707 (1963).
- (11) T. L. Fabry and R. M. Fuoss, *ibid.*, **68**, 971 (1964).
- (12) F. Accascina and S. Schiavo. "Chemical Physics of Ionic Solutions," B. L. Conway and R. G. Barradas, Ed., John Wiley and Sons, Inc., New York, N. Y., 1966, p 515.
- (13) J. H. Jones, *J. Am. Chem. Soc.*, **67**, 855 (1945).
- (14) F. Accascina and A. D'Aprano, *Ric. Sci.*, **35** (IIA), 6, 1495 (1965).
- (15) R. M. Fuoss and F. Accascina, "Electrolytic Conductance," Interscience Publishers, Inc., New York, N. Y., 1959.
- (16) A. D'Aprano, *Ric. Sci.*, **34**, (IIA) 7, 433 (1964).
- (17) F. Accascina and A. D'Aprano, *Gazz. Chim. Ital.*, **95**, 1420 (1965).

pentoxide for 4 weeks at 75°, by which time constant weight was reached.

Electrical equipment and cell have already been described.¹⁸ The conductance cell with constant 0.33534 ± 0.00004 was calibrated with potassium chloride solutions by the method of Lind, Zwolenick, and Fuoss.¹⁹ Conductance runs were made by the concentration method.¹⁷ Because lithium chlorate is extremely hygroscopic, the samples of salt were weighed as follows. The salt was kept in a desiccator over phosphorus pentoxide, from which samples were transferred into small weighing bottles in a drybox. The capped weighing bottles were placed in a desiccator and then weighed on the microbalance in a dry atmosphere until constant weight was reached. The drybox used was a closed box filled with dry nitrogen under slight pressure; open beakers of phosphorus pentoxide were kept in the box to adsorb water.

In order to test the reproducibility of the method, two runs were made in water. The agreement was practically perfect (Figure 1), giving limiting conductances equal to 102.46 for both runs. Using $\lambda_0(\text{Li}^+) = 38.68$ from the limiting conductance of lithium chloride in water^{20,21} and Longworth's value²² $n_0^+ = 0.3363$ for the lithium ion in lithium chloride, we find $\lambda_0(\text{ClO}_3^-) = 63.78$, which is about 0.3% less than the value 64.01 obtained previously from data¹⁴ on sodium and potassium chlorates. Considering the experimental difficulties involved in the preparation of the pure dried salt and in its manipulation, the discrepancy is not large.

The properties at 25° of the water-dioxane mixtures used in the conductance work are summarized in Table I, where w is the weight per cent of dioxane in the mixtures and the other symbols have their usual meanings. Conductances are given in Table II, where the different systems are identified by their dielectric constants.

Table I: Properties of Solvents

w	D	ρ	100η	$10^4\kappa_0$
0.00	78.54	0.99707	0.8903	2.87
25.02	55.50	1.01784	1.395	2.76
44.98	40.25	1.03084	1.825	1.96
59.94	27.35	1.03606	1.991	0.24
69.94	19.10	1.03678	1.925	0.063
79.95	11.99	1.03534	1.721	0.011
84.96	9.00	1.03310	1.595	0.004

Discussion

Inspection of the data of Table II shows that the equivalent conductance decreases steadily and more rapidly with increasing concentration as the dielectric

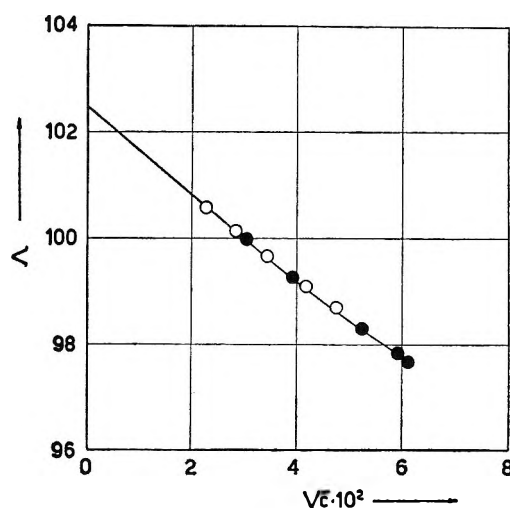


Figure 1. Conductance of lithium chlorate in water.

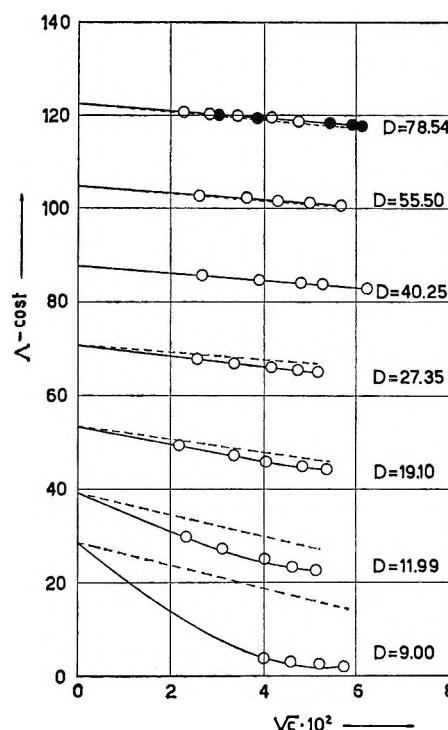


Figure 2. Conductance of lithium chlorate in water-dioxane mixtures.

(18) F. Accascina, A. D'Aprano, and R. M. Fuoss, *J. Am. Chem. Soc.*, **81**, 1058 (1959).

(19) J. E. Lind, J. J. Zwolenick, and R. M. Fuoss, *ibid.*, **81**, 1557 (1959).

(20) D. A. McInnes, T. Shedlovsky, and L. G. Longworth, *ibid.*, **54**, 2758 (1932).

(21) R. E. Jervis, J. P. Butler, D. R. Muir, and A. R. Gordon, *ibid.*, **75**, 2855 (1953).

(22) L. G. Longworth, *ibid.*, **54**, 2741 (1932).

constant decreases. Such behavior, shown graphically in Figure 2 (where Λ is plotted against $c^{1/2}$ and the dotted line is the limit tangent) shows, at least qualitatively, that in agreement with the "sphere in continuum" model the association of the ions of lithium chlorate to pairs increases with decreasing dielectric constant of the solvent.

Table II: Conductance of LiClO_3 in Dioxane-Water Mixtures at 25°

No. 1, $D = 78.54$		No. 2, $D = 78.54$	
5.156	100.58	9.312	99.98
8.153	100.13	15.402	99.26
11.814	99.68	27.476	98.30
17.484	99.08	35.184	97.83
22.618	98.67	37.479	97.67
No. 3, $D = 55.50$		No. 4, $D = 40.25$	
6.916	66.73	7.214	49.609
11.881	66.14	15.498	48.646
18.554	65.57	22.658	48.012
25.506	65.09	27.688	47.642
32.024	64.69	38.824	46.970
No. 5, $D = 27.35$		No. 6, $D = 19.10$	
6.536	41.790	4.746	37.222
11.367	40.869	11.216	35.007
17.211	40.026	17.144	33.645
22.492	39.431	23.427	32.580
26.732	39.036	28.533	31.886
No. 7, $D = 11.99$		No. 8, $D = 9.00$	
5.380	25.722	16.176	9.689
9.931	22.882	20.794	9.009
15.591	20.743	27.277	8.319
21.158	19.352	32.848	7.885
26.319	18.482		

In order to obtain association constants for lithium chlorate in the different systems, we have used different methods, depending on the magnitude of association.¹⁵ In systems with dielectric constants between 30 and 12, the constants Λ_0 , J , and K_A of the Fuoss equation²³

$$\Lambda = \Lambda_0 - S(c\gamma)^{1/2} + Ec\gamma \log c\gamma + Jc\gamma - K_A c\gamma^2 \Lambda \quad (1)$$

were evaluated by the IBM 1620 computer, using the program for associated electrolytes.²⁴ In the system with $D = 9$, where the association constant becomes of order of 1000, the program computation fails to converge and therefore we used the method of Fuoss and Kraus²⁵ which neglects the $c \log c$ and the linear term of eq 1. The conductance equation in such a case becomes that shown in eq 2 above

$$\Lambda = \gamma[\Lambda_0 - S(c\gamma)^{1/2}] \quad (2)$$

which, as suggested by Graham, Kell, and Gordon,²⁶ can be linearized in the form

$$\Lambda/F = \Lambda_0 - [c\Lambda^2 f^2 K_A / \Lambda_0 F^2] \quad (3)$$

where $F(z)$ with

$$z = (S/\Lambda_0^{1/2})(c\Lambda)^{1/2} \quad (4)$$

is a function which has been tabulated by Fuoss.²⁷ A plot of Λ/F vs. $c\Lambda^2 f^2 / F^2$ gives Λ_0 as the intercept at zero concentration and K_A / Λ_0 as the slope. In the systems with high dielectric constant ($D = 78, 55, 40$), K_A is negligibly small; therefore we used the IBM program for unassociated electrolytes²⁴ in order to obtain the constant of the Fuoss-Onsager equation²⁸

$$\Lambda = \Lambda_0 - Sc^{1/2} + Ec \log c + Jc \quad (5)$$

The values of derived constants are summarized in Table III where the various systems are identified by the numbers given in Table II. We first note that lithium chlorate is highly associated in dioxane-water mixtures at low dielectric constant and to about the same extent as lithium chloride.¹¹ We recall that no association was found by Accascina and Schiavo¹² for lithium perchlorate in the same mixtures. Figure 3 is a plot of the logarithms of association constant against reciprocal of dielectric constant. A slight curvature may be present, but the points may be approximated by a straight line. Calculation of contact distance from the slope of the line gives $a_K = 6.8 \text{ \AA}$, comparable with the value 6.4 \AA found by Fabry and Fuoss¹¹ for lithium chloride in water-dioxane mixtures. These values of a_K are considerably higher than the sum of the lattice radii, a result which suggests that the solvent enters into the structure of the ion pairs.^{1,29,30} This, in other words, means relinquishing the continuum model (by definition without structure) and considering a more detailed model in order to evaluate specific solvent-solute interactions.

Frank and Wen³¹ postulated that the solvent around an ion can be divided into three regions of different

(23) R. M. Fuoss, *J. Am. Chem. Soc.*, **80**, 3163 (1958).

(24) R. L. Kay, *ibid.*, **82**, 2099 (1960).

(25) R. M. Fuoss and C. A. Kraus, *ibid.*, **55**, 476 (1933).

(26) J. R. Graham, G. S. Kell, and A. R. Gordon, *ibid.*, **79**, 2352 (1957).

(27) R. M. Fuoss, *ibid.*, **57**, 488 (1935).

(28) R. M. Fuoss and L. Onsager, *J. Phys. Chem.*, **61**, 668 (1957).

(29) S. Winstein and G. C. Robinson, *J. Am. Chem. Soc.*, **80**, 169 (1958).

(30) E. Grunwald, *Anal. Chem.*, **26**, 1696 (1954).

(31) H. S. Frank and W. Wen, *Discussions Faraday Soc.*, **24**, 133 (1959).

Table III: Derived Constants

No.	$\Delta\epsilon$	J	K_A
1	102.461 ± 0.001	175	...
2	102.460 ± 0.001	178	...
3	68.632 ± 0.003	241	...
4	51.697 ± 0.001	357	...
5	44.70 ± 0.01	1,390	16 ± 4
6	41.22 ± 0.02	3,098	34 ± 2
7	35.02 ± 0.05	11,171	420 ± 20
8	34.00 ± 0.05	...	8,800

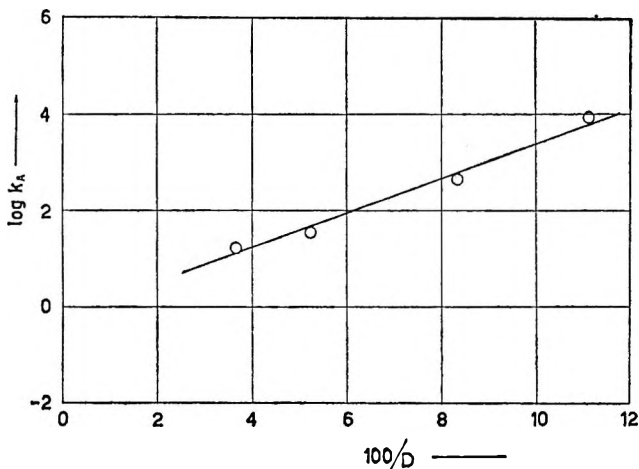


Figure 3. Association constants of lithium chlorate in dioxane-water mixtures.

structure. The region nearest the ions is one of dielectric saturation, because the ionic field is of the order of hundreds of megavolts/cm. The third region is the solvent at relatively large distances from the ion, where the solvent can be completely described by its macroscopic properties. The second region is a rather vaguely defined region of transition between completely oriented or hydrogen-bonded molecules and completely free solvent molecules. Gurney had previously introduced the convenient term of cosphere to refer to the solvent in the first two regions. This model is unfortunately too complicated to permit detailed calculations, but the approximations can be made that the cosphere for the lithium ions is due to ion-dipole forces^{32,33} and the cosphere for anions due to hydrogen-bonded solvent molecules.³⁴ We assume that the energies of interaction are high enough to hold the solvent molecules, even in the ion pairs. This hypothesis is consistent with the large value of contact distance found for lithium chlorate and also suggests an explanation of the way the specific solvent-solute interactions can affect the association process. We

have previously^{17,35} found that potassium and sodium chlorates show normal electrostatic association in dioxane-water mixtures in this range of dielectric constant. At a dielectric constant of 15, the association constants are about 600, 200, and 160 for potassium, sodium, and lithium chlorates, respectively. Such behavior confirms the hypothesis of cation solvation in the ion pair because we would expect solvation to increase in the sequence of decreasing atomic number and consequently association to decrease in the same sequence. If we now consider the anion solvation of ClO_3^- and ClO_4^- from the point of view of anion structure, the lack of association found for LiClO_4 in dioxane-water mixtures seems justified. The perchlorate ion³⁶ is a regular tetrahedron with the oxygen atoms at the corners and the chlorine at the center with the negative charge symmetrically distributed. Forslind³⁷ has pointed out that this arrangement of oxygen atoms is compatible in shape and size with the tetrahedron of the water lattice. It therefore seems reasonable to suggest that six water molecules could hydrogen bond to the perchlorate ion, giving a large, approximately spherical ion of low charge density, which would lead to much smaller association constants than the bare ion. Furthermore, this solvation would be preferential, in the sense that the six-hydration would persist in the dioxane-water mixtures, because the hydrogen bond between water and perchlorate oxygens is much stronger than a purely electrostatic ion-dipole bond between perchlorate and dioxane. The chlorate ion, on the other hand, is a symmetrical pyramid with a net unit charge and also a dipole; the dimensions and charge distribution are such that a chlorate ion should hydrate much less than a perchlorate ion. (The latter has four faces with three oxygens each; the former has only one such face.) Given these differences in structure of the solvated ions and assuming retention of water in the perchlorate ion pair, the lack of association of the perchlorate and the normal association of the chlorate can be rationalized.

Acknowledgment. Grateful acknowledgment is made for partial support of this work by a grant from the Consiglio Nazionale delle Ricerche.

(32) A. D'Aprano and R. M. Fuoss, *J. Phys. Chem.*, **67**, 1722 (1963).(33) A. D'Aprano and R. M. Fuoss, *ibid.*, **67**, 1704 (1963).(34) A. D'Aprano and R. Triolo, *Ric. Sci.*, **34** (IIA) 7, 443 (1964).(35) F. Accascina and A. D'Aprano, *Atti Accad. Sci. Lettere Arti Palermo*, **25**, 107 (1965).(36) F. S. Lee and G. B. Carpenter, *J. Phys. Chem.*, **63**, 279 (1959).(37) E. Forslind, *Proc. Intern. Congr. Rheol. 2nd, Oxford, 1953*, 151 (1954); J. L. Kavanau, "Water and Solute-Water Interactions," Holden-Day, Inc., San Francisco, Calif., 1964, p 54.

Ion Pairs and Solvent-Solute Interaction. II. Conductance of Lithium Chlorate in Methanol-Dioxane and in Acetonitrile-Dioxane

by Alessandro D'Aprano and Roberto Triolo

Institute of Physical Chemistry, University of Palermo, Palermo, Italy (Received April 10, 1967)

The conductance of lithium chlorate over the approximate concentration range $5 < 10^4 c < 25$ has been measured in methanol-dioxane ($32.7 \geq D \geq 10.5$) and acetonitrile-dioxane mixtures ($36.0 \geq D \geq 17.0$). For mixtures with the same dielectric constant, the association constant K_A is over an order of magnitude greater in the acetonitrile mixtures. The slope of the $\log K_A - D^{-1}$ plot is less in the methanol mixtures. Both of these effects suggest that solvent-separated ion pairs are formed in the hydrogen bonding systems, while only electrostatic ion-dipole effects appear in the acetonitrile systems.

Recent conductometric work^{1,2} has shown that the sphere-in-continuum model cannot describe the behavior of lithium perchlorate and chlorate in dioxane-water mixture on account of intense interaction between solute ions and solvent molecules. If, however, short-range interaction between ions and nearest-neighbor solvent molecules is assumed and the solvent is treated as a continuum beyond this zone, a model results which is consistent with the observations on these systems. The mechanism of interaction was postulated to be different for anion and cation: hydrogen bonding for the former and electrostatic ion-dipole attraction for the latter. From the contact distance found, it was also necessary to assume that the ion pairs are solvent-separated in the case of the chlorate. This hypothesis was tested further³ by studying lithium perchlorate in methanol-dioxane and in acetonitrile-dioxane, in order to have the salt in quite different hydrogen bonding environments. The purpose of this paper is to present the results of a study of lithium chlorate in the same solvent mixtures, in order to complete the comparisons.

Experimental Section

Lithium chlorate was purified and handled as before.² Solvents were purified by methods described in the literature.⁴⁻⁶ The electrical equipment,⁷ conductance cell, and method² have all been described previously. Solvent properties are summarized in Tables I and II, where w is weight per cent of dioxane and the other

Table I: Properties of Methanol-Dioxane Mixtures at 25°

No.	w	ρ	D	$10^2\eta$	$10^3\kappa$
1	0	0.7867	32.66	0.552	0.24
2	40.15	0.8725	19.05	0.584	1.18
3	50.93	0.8980	15.40	0.615	0.60
4	60.07	0.9202	12.32	0.651	0.02
5	65.71	0.9345	10.50	0.681	0.02

symbols are, respectively, density, dielectric constant, viscosity (centipoise) and solvent conductance.

Equivalent conductances at 25° are given in Table III, where the solvent systems are identified by the code numbers of Tables I and II.

Discussion

The data for systems 1, 2, 3, 4, and 6 were analyzed on the IBM 1620 computer, using Kay's program⁸

(1) F. Accascina and S. Schiavo, "Chemical Physics of Ionic Solutions," B. L. Conway and R. G. Barradas, Ed., John Wiley and Sons, Inc., New York, N. Y., 1966, p 515.

(2) F. Accascina, A. D'Aprano, and R. Triolo, *J. Phys. Chem.*, **71**, 3469 (1967).

(3) F. Accascina, G. Pistoia, and S. Schiavo, *Ric. Sci.*, **7**, 560 (1966).

(4) Acetonitrile: D. S. Berns and R. M. Fuoss, *J. Am. Chem. Soc.*, **83**, 1321 (1961).

(5) Methanol: H. Hartley and H. Raikes, *J. Chem. Soc.*, **127**, 524 (1925).

(6) Dioxane: J. E. Lind, Jr., and R. M. Fuoss, *J. Phys. Chem.*, **65**, 999 (1961).

(7) F. Accascina, A. D'Aprano, and R. M. Fuoss, *J. Am. Chem. Soc.*, **81**, 1058 (1959).

Table II: Properties of Acetonitrile-Dioxane Mixtures at 25°

No.	w	ρ	D	$10^3\eta$	$10^3\kappa$
6	0	0.7773	36.01	0.345	0.34
7	30.31	0.8409	26.85	0.416	0.41
8	39.68	0.8622	23.80	0.449	0.21
9	49.49	0.8874	20.45	0.496	0.09
10	59.92	0.9136	17.03	0.558	0.07

Table III: Conductance of Lithium Chlorate in Methanol-Dioxane and in Acetonitrile-Dioxane

$10^3\kappa$	Λ	$10^3\kappa$	Λ
1		6	
4.469	95.81	5.343	139.78
9.695	93.42	13.328	120.01
13.622	92.10	20.876	108.24
18.438	90.77	26.440	101.90
22.483	89.77	31.742	96.83
2		7	
4.451	85.06	3.964	98.57
8.819	80.75	11.035	74.86
13.617	77.49	16.975	65.07
19.384	74.48	20.821	60.71
24.083	72.56	24.674	57.19
3		8	
3.460	74.87	3.054	82.79
7.857	68.10	6.713	65.70
12.071	63.98	9.965	57.56
16.742	60.71	13.657	51.48
20.387	58.64	17.158	47.33
4		9	
4.677	56.25	4.651	56.88
7.999	50.15	8.504	46.09
12.245	45.35	13.266	39.05
15.816	42.59	16.815	35.64
18.186	41.14	22.437	31.82
5		10	
5.384	36.52	6.089	21.880
10.502	29.83	10.944	17.102
14.418	27.04	14.894	14.866
17.317	25.54	19.853	13.098
19.673	24.55	25.570	11.720

for associated electrolytes, in order to obtain the constants for the conductance equation⁹

$$\Lambda = \Lambda_0 - Sc^{1/2}\gamma^{1/2} + Ec\gamma \log c\gamma + Jc\gamma - K_{AC}\gamma^2\Lambda \quad (1)$$

For systems 5, 7, 8, 9, and 10, the association constants were so large ($K_A > 1000$) that the E and J terms became negligible compared to the association term;

these data were therefore analyzed by the simpler Fuoss-Kraus equation¹⁰

$$\Lambda = \gamma(\Lambda_0 - Sc^{1/2}\gamma^{1/2}) \quad (2)$$

The results are summarized in Table IV.

Table IV: Derived Constants

No.	Λ_0	J	K_A
Methanol-Dioxane			
1	100.97 ± 0.09	1410 ± 134	5 ± 3
2	95.20 ± 0.2	7222 ± 273	46 ± 9
3	87.93 ± 0.3	13134 ± 467	219 ± 22
4	83.68 ± 0.06	24948 ± 65	1344 ± 5
5	78.40	...	6625
Acetonitrile-Dioxane			
6	170.00 ± 0.3	1078 ± 150	401 ± 60
7	145.20	...	1760
8	135.15	...	3520
9	125.20	...	6300
10	112.00	...	39300

We note that association is much more pronounced in the aprotic acetonitrile-dioxane mixtures than in the methanol-dioxane systems. In water-dioxane mixtures,² association was negligible at dielectric constants above about 30. These results parallel the behavior of the perchlorate in the same solvents³ and demonstrate strikingly the significant part played by hydrogen bonding in the solvation process, which in turn determines the extent of association by controlling the size of the ionic entities (central ion plus solvating molecules). As shown in Figure 1, the logarithm of the association constant is linear in reciprocal dielectric constant for both solvent systems. From the slope of the lines, contact distances are found to be $\hat{a}_K = 5.04$ for methanol-dioxane as solvent and $\hat{a}_K = 3.70$ for the acetonitrile-dioxane mixtures. The value is, as expected, larger in the hydrogen bonding solvent, and furthermore, is in a consistent sequence with the value of 6.8 found in water-dioxane systems where of course the solvating molecule is H₂O instead of HOCH₃. The sequence of slopes of $\log K_A - D^{-1}$ plots clearly shows that solvating molecules remain in the ion pairs in those cases where hydrogen bonds form the solvate cluster.

For comparison, the values for lithium perchlorate³ in the same solvents are also shown in Figure 1. Both

(8) R. L. Kay, *J. Am. Chem. Soc.*, **82**, 2099 (1960).

(9) R. M. Fuoss, *ibid.*, **80**, 3163 (1958).

(10) R. M. Fuoss and C. A. Kraus, *ibid.*, **55**, 476 (1933).

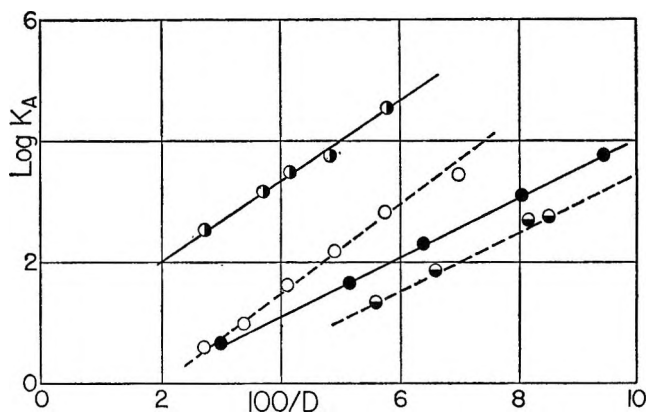


Figure 1. Dependence of association constant on dielectric constant. \circ , LiClO_3 in acetonitrile-dioxane; \circ , LiClO_4 in acetonitrile-dioxane; \bullet , LiClO_3 in methanol-dioxane; \bullet , LiClO_4 in methanol-dioxane.

salts in both solvent systems give linear plots, but the acetonitrile plots lie above those for the methanol systems, and the separation between chlorate and perchlorate is greater in the former. These differences show that each salt is associated to a higher extent in acetonitrile systems which are isodielectric with methanol systems, and that different contact distances are required for a given electrolyte in different solvents. These differences show that the simple model of charged spheres in a continuum is inadequate to describe the systems of Figure 1; other effects must be included in the equation for the association constant in addition to electrostatic attraction. First, the energy of solvent molecules with respect to two free ions and to the pair which they can make is different; a factor of the form $\exp(-E_s/kT)$ calculated by Gilkerson¹¹ must be included. Second, the arrangement of solvent molecules will in general be different around free ions and around pairs, so an entropy term $\exp(\Delta S/k)$ is needed. Finally, solvent-separated pairs will require different distance parameters to give different slopes on the $\log K_A-1/D$ plots. Summarizing, a more general expres-

sion than the one based only on charge-charge interaction and excluded volume would have the form

$$\ln K_A = \ln(4\pi N a^3/3000) + \frac{\epsilon^2/aDkT - E_s/kT + \Delta S/k}{k} \quad (3)$$

This equation is consistent with the results shown in Figure 1, if appropriate *ad hoc* assumptions are made. The dipolar structure of the chlorate ion should cause stronger attraction between it and acetonitrile, with the N atom of the solvent molecule adjacent to the (relatively positive) chlorine atom of the ion; in the pair, the lithium ion should be located on the face made up by the three oxygen atoms, and its presence would enhance the attraction for the nitrile molecule; that is, we propose a solvated, but not a solvent-separated pair, for the chlorate. Such an interaction would not be expected for the symmetrical perchlorate ion. Consequently, E_s would be larger for the chlorate, and the chlorate curve should lie above the perchlorate curve in the acetonitrile systems. In the methanol systems, if we assume solvent-separated pairs for both salts, the plots in Figure 1 would be less steep than for the acetonitrile systems, as observed. To account for the vertical displacement of the two sets of curves, we recall that methanol is a hydrogen-bonding molecule; therefore, there is more order in a methanol-dioxane system than in an acetonitrile-dioxane system. When a pair forms in the methanol system, its weaker field (compared to that of the free ions which formed it) would permit greater reorientation in methanol than in acetonitrile; that is, the entropy change would be more negative for the former. The $\exp(\Delta S/k)$ term in (3) would then lower the methanol curves with respect to those for acetonitrile.

Acknowledgment. Acknowledgment is gratefully made to the Consiglio Nazionale delle Ricerche for partial support of this research.

(11) W. R. Gilkerson, *J. Chem. Phys.*, **25**, 1199 (1956).

Pressure-Volume-Temperature Relations in the System

Methane-Tetrafluoromethane. I. Gas Densities and the

Principle of Corresponding States¹

by D. R. Douslin, R. H. Harrison, and R. T. Moore

Contribution No. 153 from the Thermodynamics Laboratory of the Bartlesville Petroleum Research Center, Bureau of Mines, U. S. Department of the Interior, Bartlesville, Oklahoma 74003 (Received March 23, 1967)

The methane-tetrafluoromethane system was examined for conformity with the principle of corresponding states in terms of the Boyle reference point, the critical reference point, and mixing rules as applied to the reference temperatures and volumes. Experimental values of gas density are given for pure methane, pure tetrafluoromethane, and three mixtures (0.25, 0.50, and 0.75 mole fraction of methane) over a temperature range from 0 to 350°, a pressure range from about 16 to 400 atm, and a density range from 0.75 to 12.5 mole l.⁻¹. Values are derived for the second, third, and fourth virial coefficients of the mixtures, B_M , C_M , and D_M , respectively, and for the cross-term virial coefficients, B_{12} , C_{112} , C_{122} , D_{1112} , D_{1122} , and D_{1222} . Based on the experimental results for B_{12} , the geometrical-mean mixing rule was found to be unsatisfactory for a corresponding states correlation. However, in terms of the Boyle temperature, T_B , and Boyle volume, $V_B = (TdB/dT)_{T=T_B}$, the experimental reduced second virial data for the methane-tetrafluoromethane system were found to follow the corresponding states function with high accuracy.

Introduction

Gas density measurements were undertaken on the methane-tetrafluoromethane system to provide sufficient information, internally consistent over a broad range of temperature, pressure, density, and mole fraction, for a definitive test of the laws of mixing in terms of the principle of corresponding states, the intermolecular potential energy, or the derived thermodynamic properties. The work was carried out as a part of a continuing project of the U. S. Bureau of Mines on the PVT relations of hydrocarbons, fluorocarbons, and mixtures of hydrocarbons and fluorocarbons. Methane and tetrafluoromethane were chosen because they have positions as first members of their respective homologous aliphatic series and because they are structurally similar, nonpolar, quasi-spherical molecules that are most likely to respond to theoretical treatments developed for central force fields. Thus, they are likely to help bridge the gap in intermolecular potential theory between simple and

complex particles. In addition, the upper temperatures to which these materials are thermally stable are high enough for the repulsive forces to become significant in the second virial coefficient.

Values for the second, third, and fourth virial coefficients, B_M , C_M , and D_M , were derived from unsmoothed gas density data on three mixtures. These results were combined with virial coefficients for pure methane and pure tetrafluoromethane, reported previously,²⁻⁴ to obtain cross-term virial coefficients for

(1) The work upon which this research is based was conducted in part under an Interservice Support Agreement between the Air Force Office of Scientific Research, Office of Aerospace Research, U. S. Air Force, Project No. 9713, Task No. 9713-02, and the Bureau of Mines, U. S. Department of the Interior.

(2) D. R. Douslin, R. H. Harrison, R. T. Moore, and J. P. McCullough, *J. Chem. Eng. Data*, **9**, 358 (1964).

(3) D. R. Douslin, R. H. Harrison, R. T. Moore, and J. P. McCullough, *J. Chem. Phys.*, **35**, 1357 (1961).

(4) D. R. Douslin, "Progress in International Research on Thermodynamics and Transport Properties," The American Society of Mechanical Engineers, United Engineering Center, New York, N. Y., 1962, pp 135-146.

unlike molecule interactions.⁵ In the second and third papers of this series, the mixture phenomena will be examined in terms of the mixed parameters of various potential functions and in terms of the thermodynamic functions, enthalpy, entropy, and Gibbs free energy of the compressed gas mixtures. In the present paper, examination of the cross-term coefficients will be limited to the principle of corresponding states and to mixing rules applied to corresponding states parameters.

Most of the work reported in the literature on hydrocarbon-perfluorocarbon interactions has concerned phenomena in the liquid phase. A very limited effort has been directed toward a study of interaction effects observed in mixtures of hydrocarbon plus perfluorocarbon gases. In a definitive study, Hamann, Lambert, and Thomas⁶ reported that they were unable to correlate second virial coefficients for the methane-sulfur hexafluoride system by means of Guggenheim and McGlashan's⁷ extension of the principle of corresponding states. Garner and McCoubrey⁸ studied two binary hydrocarbon-perfluorocarbon systems: *n*-pentane-perfluoro-*n*-pentane and *n*-pentane-perfluoro-*n*-hexane. They showed that correlations of the second virial coefficients, based on mixing laws for the Lennard-Jones [12, 6] potential parameters, were quite inadequate to explain the experimental results.

Experimental Section

Gas densities for three mixtures, 0.749787, 0.500050, and 0.250066 mole fraction of CH₄, were determined with the apparatus and by the method used previously on the pure components.^{2,3,9,10} These mixtures, hereafter referred to in text and tables by the nominal designations 0.75, 0.50, and 0.25 mole fraction of CH₄, were prepared from highly purified methane (99.994 mole %) and tetrafluoromethane (99.985 mole %) contained in the weighing bombs shown as part of the mixing manifold (see Figure 1). The gases were condensed from the weighing bombs with liquid hydrogen refrigerant into the highly evacuated sample liner of the compressibility cell, and the filled liner was sealed off at the Pyrex capillary. The uncondensed sample remaining in the small void space of the capillary below the valve was negligible in terms of total sample or mole fraction. Thus, the final weight of sample in the cell liner was checked directly against the corresponding loss of sample from the weighing bombs. All weighings were made with an accuracy estimated at 0.1 mg. Since the total sample used was about 0.1 mole, the calculated mole fractions given above were estimated to be accurate to about 0.00003, 0.00006, and 0.00009 mole fraction, respectively. However, the mole fraction values used were retained at six decimal figures to

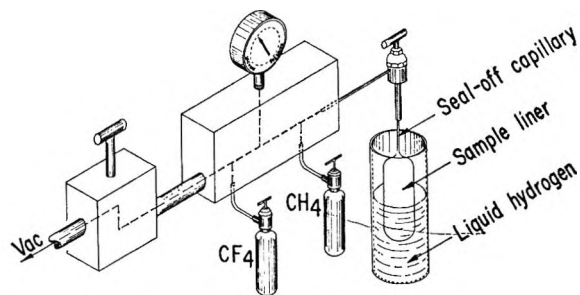


Figure 1. Sample mixing manifold.

provide the maximum possible precision in evaluating the virial coefficients and the effects of mixing. Calculations of moles of sample and mole fractions were based on the following atomic weights: H, 1.0080; C, 12.011; F, 19.000. Adjustments were made in the molal calculations for 0.005 mole % nitrogen in the methane and 0.0034 mole % oxygen plus 0.012 mole % nitrogen in the tetrafluoromethane. In previous work on pure tetrafluoromethane the impurities in the sample were estimated to be 0.04 mole % maximum. Analysis of the present sample, which was somewhat purer, was obtained by a gas-liquid partition chromatographic method known to give more accurate results than those previously obtained from the mass spectrometer. Pressures were measured on a dead-weight gauge that was calibrated against the vapor pressure of carbon dioxide at 0°, taken to be 26,144.7 mm, the value determined by Bridgeman.¹¹ A more recent determination by Greig and Dadson¹² gave a value approximately 0.025% lower, which appears to be more accurate. Possible small errors in pressure scale can be classed with a number of other small systematic errors that might be introduced through the gas constant, atomic weights, variation in the normal isotopic ratio C¹²/C¹³, or weight of sample. Adjustments for these errors, as a group, were made by the method discussed in ref 2.

(5) To preserve internal consistency and possible cancellation of systematic errors in the evaluation of mixture effects, measurements from other laboratories were not included in the present correlations. Comparisons of *PVT* data for pure methane and pure tetrafluoromethane from various sources were given previously in ref 2 and 3.

(6) S. D. Hamann, J. A. Lambert, and R. B. Thomas, *Australian J. Chem.*, **8**, 149 (1955).

(7) E. A. Guggenheim and M. L. McGlashan, *Proc. Roy. Soc. (London)*, **A206**, 448 (1951).

(8) M. D. G. Garner and J. C. McCoubrey, *Trans. Faraday Soc.*, **55**, 1524 (1959).

(9) J. A. Beattie, *Proc. Am. Acad. Arts Sci.*, **69**, 389 (1934).

(10) D. R. Douslin, R. T. Moore, J. P. Dawson, and G. Waddington, *J. Am. Chem. Soc.*, **80**, 2031 (1958).

(11) O. C. Bridgeman, *ibid.*, **49**, 1174 (1927).

(12) R. P. Greig and R. S. Dadson, *Br. J. Appl. Phys.*, **17**, 1633 (1966).

Gas density measurements were taken along isotherms at 25° intervals from 0 to 350° and at isometric points spaced at 0.5 mole l.⁻¹ intervals (except for the first interval) from 0.75 to 12.5 mole l.⁻¹. The pressure ranged from about 16 to 400 atm. Temperature of the compressibility cell was controlled and measured to 0.001° with platinum resistance thermometers that were calibrated at the National Bureau of Standards in terms of the international temperature scale [$T, ^\circ\text{K} = t, ^\circ\text{C} (\text{Int.}, 1948) + 273.16$]. Data previously reported for pure methane and pure tetrafluoromethane were also on this scale. To maintain a systematic basis for the entire system, this temperature definition was retained through the present study. For similar reasons the old definition of the liter (1 l. = 1000.028 cm³) was used in calculating gas densities. However, the cubic centimeter was the volume unit used to express the virial coefficients. Also, because of the need to refer the present data on the mixtures to previously published data on the pure components, methane and tetrafluoromethane, the recently defined value of the gas constant¹³ was not used. The following two values of the gas constant were used as appropriate: $R = 0.0820544$ l. atm deg⁻¹ mole⁻¹ and $R = 82.0567$ cm³ atm deg⁻¹ mole⁻¹.

Gas Densities

Unsmoothed values of the measured pressures of the mixtures are given in Table I as functions of density and temperature. Similar data for pure methane and tetrafluoromethane, also included in the tabulation, may be found in ref 2-4. The number of significant figures carried is consistent with the precision of the measurements. The accuracy, which is roughly a factor of 10 lower than the precision, was discussed in previous publications.^{2,3,10}

Virial Coefficients

A graphical method³ was used to evaluate the temperature-dependent coefficients, B_M , C_M , and D_M , in the virial expansion for mixtures in eq 1.

$$PV = RT[1 + (B_M/V) + (C_M/V^2) + (D_M/V^3) + \dots] \quad (1)$$

$$B_M = \lim_{1/V \rightarrow 0} [(PV/RT) - 1]V \quad (2)$$

$$C_M = \lim_{1/V \rightarrow 0} [(PV/RT) - 1]V - B_M]V \quad (3)$$

$$D_M = \lim_{1/V \rightarrow 0} \{ [(PV/RT) - 1]V - B_M]V - C_M \} V \quad (4)$$

At each temperature the terms in eq 2-4 were calcu-

lated from unsmoothed experimental values of P , V , and T (Table I), and the values were extrapolated to zero density to obtain B_M , C_M , and D_M (Table II) as coefficients of an infinite series in $1/V$.

At the lower temperatures the second virial coefficients are most negative for pure tetrafluoromethane (Figure 2), but they follow a trend toward more positive values as concentrations higher in mole fraction of methane are approached. At the upper temperatures a complete reversal in the order has occurred; however, the temperature-mole fraction surface of the plot is smooth and shows no inconsistencies. Also, second virial coefficients exhibit a maximum with respect to mole fraction over a well-defined temperature range extending from about 125 to 335°. The third virial coefficients (Figure 3), unlike the second virial coefficients, show regular variation from methane to tetrafluoromethane over the entire experimental temperature range. The fourth virial coefficients are also regular, although the precision and accuracy of the points are considerably lower. The characteristic increase of the fourth virial coefficients with respect to temperature, predicted theoretically by Boys and Shavitt¹⁴ and by Barker and Monaghan¹⁵ for substances that follow

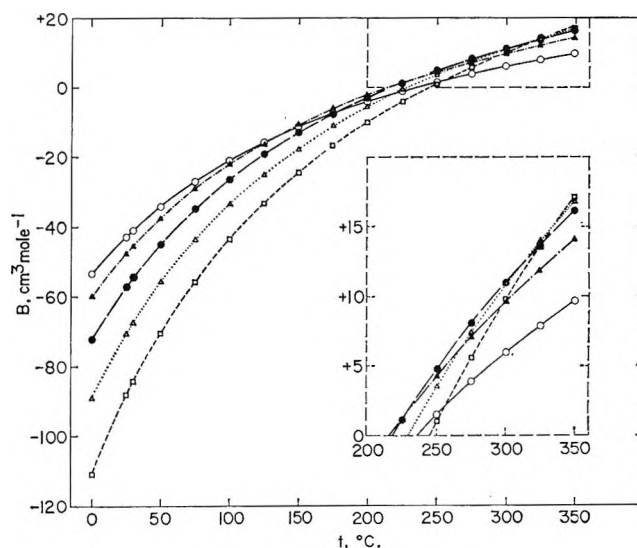


Figure 2. Second virial coefficients for the CH₄-CF₄ system. Insert shows expanded area above 200°: O, pure CH₄; ▲, 75% CH₄-25% CF₄; ●, 50% CH₄-50% CF₄; △, 25% CH₄-75% CF₄; □, pure CF₄.

(13) F. D. Rossini, *Pure Appl. Chem.*, **9**, 453 (1964).

(14) S. F. Boys and I. Shavitt, *Proc. Roy. Soc. (London)*, **A254**, 487 (1960).

(15) J. A. Barker and J. J. Monaghan, *J. Chem. Phys.*, **36**, 2564 (1962).

Table I: The Compressibility of the Methane-Tetrafluoromethane System

4, °C	Mole fraction of CH ₄ ^b	Density, moles l. ⁻¹ Pressure, normal atm													
		0.75 ^a	0.75 ^a	0.80	0.80 ^a	1.0	1.5	2.0	2.5	3.0	3.5	4.0	4.5	5.0	5.5
0.00	1.000000 ^c	16.1624	16.1614			21.2760	31.1261	40.5160	49.4837	58.0726	66.3433	74.3227	82.0686	89.6142	97.0294
	0.749787	16.0850	16.0854			21.1443	30.8479	40.0529	48.8067	57.1812	65.2283	72.9940	80.5681	87.9728	95.3005
	0.500050	15.9409	15.9419			20.8928	30.3098	39.1378	47.4506	55.3254	62.8369	70.0661	77.0647	83.9354	90.7306
	0.250066	15.7405	15.7392			20.5420	29.5485	37.8400	45.5149	52.6574	59.3760	65.7562	71.8879	77.8673	83.8063
	0.000000 ^d	15.480	15.478			20.086	28.559	36.149	42.974	49.150	54.804	60.039	64.967	69.704	74.369
25	1.000000 ^c	17.7840	17.7843			23.4749	34.5356	45.2050	55.5272	65.5470	75.3094	84.8673	94.2618	103.539	112.767
	0.749787	17.7242	17.7252			23.3749	34.3309	44.8681	55.0429	64.9361	74.5750	84.0430	93.4017	102.686	112.016
	0.500050	17.6033	17.6031			23.1624	33.8759	44.1056	53.9248	63.4107	72.6345	81.6687	90.6123	99.5272	108.490
	0.250066	17.4280	17.4257			22.8566	33.2152	42.9824	52.2481	61.1165	69.6744	78.0070	86.2225	94.4144	102.700
	0.000000 ^d	17.194	17.196			22.453	32.339	41.486	50.000	58.012	65.628	72.967	80.130	87.251	94.473
30	1.000000 ^c	18.1080	18.1069			23.9153	35.2180	46.1416	56.7336	67.0516	77.1242	86.9891	96.7208	106.336	115.913
	0.749787	18.0513	18.0516			23.8193	35.0236	45.8207	56.2885	66.4787	76.4408	86.2277	95.9309	105.616	115.319
	0.500050	17.9361	17.9349			23.6166	34.5850	45.0924	55.2064	65.0087	74.5732	83.9689	93.2864	102.601	112.014
	0.250066	17.7642	17.7613			23.3172	33.9441	43.9973	53.5801	62.7885	71.7069	80.4233	89.0556	97.7085	106.453
	0.000000 ^d	17.538	17.535			22.923	33.087	42.538	51.387	59.764	67.756	75.520	83.129	90.736	98.470
50	1.000000 ^c	19.3988	19.3986			25.6660	37.9248	49.8695	61.5277	72.9595	84.2087	95.3217	106.370	117.357	128.330
	0.749787	19.3587	19.3603			25.5974	37.7890	49.6507	61.2478	72.6281	83.8664	95.0259	106.156	117.333	128.625
	0.500050	19.2572	19.2572			25.4185	37.4100	49.0198	60.3231	71.3964	82.3108	93.1292	104.005	114.943	126.057
	0.250066	19.1036	19.1019			25.1528	36.8384	48.0538	58.8889	69.4477	79.8086	90.0802	100.365	110.809	121.447
	0.000000 ^d	18.898	18.899			24.792	36.057	46.720	56.893	66.701	76.251	85.656	95.045	104.587	114.393
75	1.000000 ^c	21.0150	21.0130			27.8521	41.3049	54.5003	67.4960	80.3269	93.0461	105.694	118.352	131.045	143.842
	0.749787	20.9891	20.9902			27.8103	41.2344	54.4041	67.3953	80.2608	93.0761	105.876	118.757	131.782	145.040
	0.500050	20.9050	20.9051			27.6625	40.9238	53.8987	66.6701	79.3034	91.8847	104.516	117.265	130.205	143.524
	0.250066	20.7703	20.7715			27.4342	40.4309	53.0780	65.4544	77.6670	89.8098	102.001	114.339	126.952	140.004
	0.000000 ^d	20.591	20.590			27.116	39.749	51.903	63.709	75.279	86.735	98.206	109.825	121.755	134.178
100	1.000000 ^c	22.6262	22.6252			30.0335	44.6749	59.1366	73.4508	87.6730	101.853	116.039	130.287	144.666	159.211
	0.749787	22.6169	22.6171			30.0192	44.6655	59.1480	73.5209	87.8617	102.208	116.677	131.312	146.193	161.429
	0.500050	22.5493	22.5495			29.9034	44.4260	58.7668	72.9899	87.1805	101.432	115.835	130.467	145.464	160.902
	0.250066	22.4368	22.4345			29.7059	44.0075	58.0684	71.9784	85.8461	99.7641	113.851	128.252	143.055	158.412
	0.000000 ^d	22.275	22.275			29.426	43.412	57.049	70.468	83.789	97.142	110.662	124.512	138.840	153.853
125	1.000000 ^c	24.2365	24.2360			32.2098	48.0390	63.7372	79.3594	94.9708	110.607	126.319	142.199	158.249	174.574
	0.749787	24.2404	24.2413			32.2281	48.0929	63.8531	79.6212	95.4207	111.329	127.440	143.798	160.505	177.663
	0.500050	24.1903	24.1909			32.1358	47.9076	63.5884	79.2523	94.9860	110.898	127.065	143.578	160.558	178.122
	0.250066	24.0941	24.0926			31.9692	47.5584	63.0211	78.4408	93.9363	109.625	125.594	142.005	158.998	176.772
	0.000000 ^d	23.952	23.953			31.725	47.047	62.155	77.175	92.224	107.462	123.034	139.086	155.832	173.413
150	1.000000 ^c	25.8440	25.8431	27.5564	27.5559	34.3849 ^e	51.3940 ^e	68.3426 ^e	85.2808 ^e	102.259 ^e	119.345 ^e	136.564 ^e	154.000 ^e	171.713 ^e	189.768 ^e
	0.749787	25.8634	25.8645			34.4229	51.5017	68.5730	85.6870	102.948	120.399	138.123	156.231	174.769	193.826
	0.500050	25.8279	25.8287			34.3645	51.3843	68.4052	85.5067	102.784	120.316	138.240	156.615	175.585	195.276
	0.250066	25.7453	25.7454			34.2253	51.1017	67.9572	84.8906	102.003	119.429	137.298	155.715	174.882	194.927
	0.000000 ^d	25.625	25.626			34.021	50.671	67.223	83.830	100.617	117.715	135.322	153.553	172.699	192.863

175	1.000000 ^e	27.4509	27.4497	29.2755	29.2756	36.5579 ^e	54.7434 ^e	72.9307 ^e	91.1701 ^e	109.520 ^e	128.040 ^e	146.795 ^e	165.823 ^e	185.146 ^e	205.005 ^e
	0.749787	27.4845	27.4849			36.6233	54.9141	73.2680	91.7621	110.485	129.469	148.840	168.663	189.055	210.063
	0.500050	27.4648	27.4651			36.5894	54.8587	73.2111	91.7413	110.548	129.722	149.400	169.663	190.639	212.449
	0.250066	27.3984	27.3988			36.4809	54.6451	72.8827	91.3094	110.045	129.219	148.979	169.421	190.778	213.213
	0.000000 ^d	27.296	27.296			36.304	54.274	72.282	90.460	108.963	127.937	147.553	168.020	189.528	212.277
200	1.000000 ^e			30.9920	30.9922	38.7272	58.0860	77.5132	97.0589	116.775	136.715	156.955	177.561	198.575	220.144
	0.749787	29.1041	29.1057			38.8182	58.3112	77.9516	97.8049	117.954	138.475	159.478	181.020	203.195	226.187
	0.500050	29.0987	29.0996			38.8089	58.3128	78.0042	97.9516	118.283	139.092	160.498	182.589	205.570	229.491
	0.250066	29.0481	29.0480			38.7279	58.1575	77.7772	97.7058	118.046	138.947	160.571	183.023	206.520	231.291
	0.000000 ^d	28.964	28.965			38.585	57.868	77.316	97.066	117.270	138.103	159.733	182.364	206.259	231.582
225	1.000000 ^e			32.7081	32.7084	40.8956	61.4245	82.0866	102.917	123.999	145.375	167.119	189.312	212.021	235.257
	0.749787	30.7235	30.7248			41.0100	61.7149	82.6324	103.842	125.431	147.480	170.089	193.373	217.399	242.200
	0.500050	30.7305	30.7321			41.0268	61.7723	82.7890	104.158	126.010	148.441	171.563	195.552	220.445	246.481
	0.250066	30.6954	30.6965			40.9726	61.6760	82.6830	104.073	126.027	148.662	172.111	196.586	222.238	249.332
	0.000000 ^d	30.627	30.629			40.860	61.455	82.331	103.639	125.550	148.221	171.872	196.686	222.912	250.816
250	1.000000 ^e			34.4223	34.4237	43.0621	64.7602	86.6533	108.773	131.203	154.010	177.253	201.004	225.361	250.332
	0.749787	32.3417	32.3398			43.2007	65.1037	87.3027	109.861	132.903	156.450	180.695	205.636	231.453	258.311
	0.500050	32.3622	32.3628			43.2489	65.2170	87.5516	110.332	133.713	157.736	182.585	208.380	235.310	263.483
	0.250066	32.3414	32.3423			43.2149	65.1827	87.5518	110.430	133.981	158.323	183.657	210.108	237.918	267.120
	0.000000 ^d	32.289	32.291			43.132	65.034	87.334	110.200	133.807	158.325	183.973	210.974	239.569	270.100
275	1.000000 ^e			36.1365	36.1367	45.2272	68.0907	91.2179	114.629	138.414	162.627	187.368	212.701	238.667	265.369
	0.749787	33.9573	33.9584			45.3917	68.4914	91.9612	115.871	140.326	165.422	191.228	217.887	245.555	274.259
	0.500050	33.9914	33.9931			45.4579	68.6645	92.3003	116.508	141.374	167.024	193.580	221.218	250.073	280.311
	0.250066	33.9858	33.9869			45.4534	68.6821	92.4235	116.778	141.920	167.976	195.150	223.608	253.517	285.192
	0.000000 ^d	33.949	33.951			45.398	68.596	92.326	116.738	142.032	168.391	196.014	225.145	256.087	289.161
300	1.000000 ^e			37.8460	37.8491	47.3886	71.4160	95.7579	120.452	145.577	171.224	197.433	224.288	251.930	280.323
	0.749787	35.5736	35.5746			47.5782	71.8736	96.6130	121.865	147.761	174.360	201.768	230.133	259.553	290.103
	0.500050	35.6222	35.6218			47.6689	72.0995	97.0721	122.663	149.026	176.290	204.570	234.034	264.863	297.150
	0.250066	35.6268	35.6260			47.6883	72.1745	97.2747	123.088	149.799	177.575	206.598	237.038	269.118	303.090
	0.000000 ^d	35.609	35.609			47.661	72.165	97.306	123.266	150.212	178.382	207.995	239.280	272.536	308.116
325	1.000000 ^e			39.5550	39.5583	49.5510	74.7400	100.309	126.284	152.779	179.812	207.506	235.918	265.158	295.283
	0.749787	37.1902	37.1890			49.7704	75.2559	101.264	127.860	155.153	183.255	212.267	242.360	273.530	305.936
	0.500050	37.2476	37.2492			49.8777	75.5355	101.815	128.827	156.665	185.557	215.589	246.900	279.631	314.030
	0.250066	37.2663	37.2662			49.9185	75.6690	102.124	129.402	157.725	187.155	217.978	250.416	284.564	320.779
	0.000000 ^d	37.266	37.264			49.924	75.723	102.278	129.773	158.415	188.385	219.957	253.412	288.853	327.091
350	1.000000 ^e			41.2690	41.2673	51.7135	78.0693	104.859	132.137	159.947	188.443	217.607	247.584	278.472	310.315
	0.749787	38.8045	38.8044			51.9617	78.6474	105.928	133.871	162.603	192.208	222.808	254.542	287.523	321.856
	0.500050	38.8774	38.8768			52.0861	78.9689	106.571	134.973	164.352	194.812	226.530	259.684	294.464	330.986
	0.250066	38.9080	38.9102			52.1480	79.1551	106.973	135.718	165.595	196.734	229.426	263.774	300.094	338.573
	0.000000 ^d	38.921	38.922			52.187	79.273	107.240	136.267	166.576	198.378	231.925	267.505	305.438	346.066

Table I (Continued)

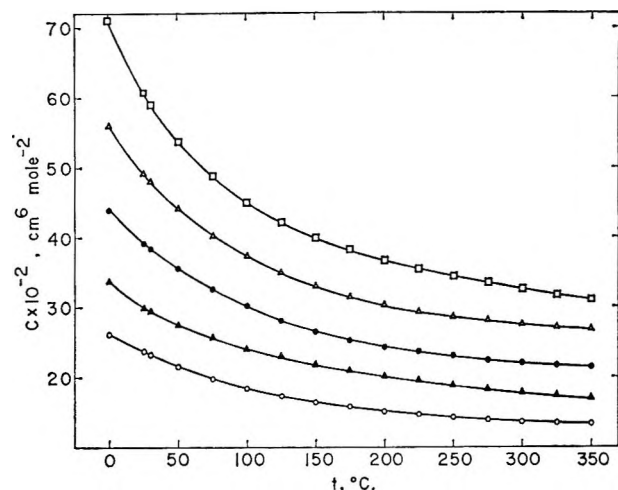
t , °C	Mole fraction of CH_4^b	Density, moles l. ⁻¹													
		6.0	6.5	7.0	7.5	8.0	8.5	9.0	9.5	10.0	10.5	11.0	11.5	12.0	12.5
0.00	1.000000 ^c	104.298	111.579	118.918	126.182	133.639	141.219	149.119	157.224	165.782	174.687	184.338	194.474	205.488	217.395
	0.749787	102.579	109.911	117.399	125.051	132.933	141.209	149.946	159.266	169.406	180.253	192.254	205.391	219.842	236.034
	0.500050	97.5682	104.479	111.628	119.073	126.908	135.315	144.360	154.266	165.277	177.555	191.499	207.078	224.994	245.439
	0.250066	89.7749	95.8982	102.269	109.042	116.418	124.499	133.537	143.728	155.383	168.940	184.833	203.331	225.318	251.051
	0.000000 ^d	79.050	83.903	89.061	94.676	100.960	108.149	116.575	126.561	138.458	152.884	170.481	192.000	218.629	251.029
	1.000000 ^c	121.969	131.203	140.549	150.052	159.756	169.730	180.054	190.894	202.147	214.101	226.684	240.267	254.577	270.208
25	0.749787	117.366	130.908	140.760	150.855	161.357	172.497	184.223	196.720	210.145	224.579	240.330	257.787	276.777	297.813
	0.500050	111.609	126.984	136.738	146.947	157.761	169.374	181.842	195.476	210.417	227.172	245.646	266.351	289.606	315.901
	0.250066	111.219	120.046	129.297	139.275	150.025	161.786	174.856	189.413	205.939	224.868	246.481	271.242	300.281	333.482
	0.000000 ^d	101.908	109.726	118.131	127.244	137.455	148.916	162.056	177.339	195.101	216.126	241.054	270.777	306.072	348.263
	1.000000 ^c	125.497	135.131	144.889	154.733	164.949	175.412	186.265	197.499	209.326	221.865	235.176	249.205	264.380	280.535
	0.749787	125.121	135.078	145.354	155.927	166.968	178.629	190.871	203.856	218.064	233.253	249.733	267.839	287.519	309.389
30	0.500050	121.601	131.441	141.697	152.483	163.902	176.075	189.276	203.621	219.383	236.918	256.284	277.946	302.345	329.837
	0.250066	115.480	124.856	134.741	145.314	156.762	169.238	183.107	198.606	216.067	235.990	258.697	284.865	314.838	350.309
	0.000000 ^d	106.456	114.879	123.929	133.791	144.774	157.077	171.140	187.469	206.428	228.708	254.939	286.356	323.269	367.430
	1.000000 ^c	139.414	150.695	162.061	173.665	185.682	198.049	210.984	224.393	238.376	253.217	268.975	285.756	303.533	322.698
	0.749787	140.134	151.900	164.037	176.634	189.844	203.672	218.376	234.052	250.855	269.025	288.677	310.143	333.346	359.171
	0.500050	137.513	149.353	161.694	174.650	188.531	203.317	219.283	236.629	255.780	276.704	299.790	325.484	353.948	386.367
50	0.250066	132.462	144.058	156.315	169.396	183.666	199.136	216.290	235.283	256.629	280.710	307.995	339.070	374.791	
	0.000000 ^d	124.621	135.463	147.186	159.922	174.093	189.908	207.791	228.320	251.970	279.425	311.330	348.658	392.619	
	1.000000 ^c	156.818	169.943	183.434	197.194	211.417	226.196	241.565	257.611	274.412	292.143	310.911	330.722	351.987	375.024
	0.749787	158.630	172.614	187.034	202.141	217.953	234.588	252.171	270.954	291.092	312.725	336.417	361.761	389.450	
	0.500050	157.236	171.505	186.443	202.243	219.077	236.989	256.347	277.379	300.515	325.590	353.297	384.077		
	0.250066	153.565	167.845	183.005	199.333	216.900	236.136	257.260	280.806	306.974	336.245	368.960			
75	0.000000 ^d	147.212	161.150	176.143	192.482	210.584	230.884	253.472	279.421	308.736	342.440	381.498			
	1.000000 ^c	174.002	189.050	204.636	220.518	236.939	254.061	271.832	290.627	310.141	330.719	352.625	375.886	400.624	
	0.749787	177.041	193.193	210.025	227.497	245.891	265.308	286.057	307.822	331.352	356.556	383.783			
	0.500050	176.920	193.636	211.216	229.796	249.588	270.859	293.706	318.464	345.412	374.920				
	0.250066	174.525	191.580	209.733	229.112	250.182	273.191	298.296	326.054	356.869	391.556				
	0.000000 ^d	169.728	186.712	205.075	225.134	247.200	271.743	299.330	330.350	365.751					
100	1.000000 ^c	191.168	208.256	225.715	243.822	262.544	282.021	302.205	323.578	345.911	369.406	394.299			
	0.749787	195.370	213.691	232.942	252.818	273.833	296.148	319.513	344.639	371.425	400.035				
	0.500050	196.396	215.559	235.843	257.117	279.939	304.376	330.720	359.136						
	0.250066	195.409	215.080	236.134	258.822	283.251	309.835	338.994	371.291						
	0.000000 ^d	192.127	212.147	233.889	257.529	283.630	312.493	344.771	381.244						
	1.000000 ^c	208.237 ^e	227.197 ^e	246.717 ^e	266.876 ^e	287.833 ^e	309.534 ^e	332.261 ^e	356.027 ^e	381.126 ^e					
150	0.749787	213.594	234.120	255.457	277.869	301.437	326.573	352.928	381.033						
	0.500050	215.844	237.408	260.100	284.375	310.095	337.635	367.331	399.435						
	0.250066	216.064	238.560	262.550	288.282	316.317	346.489	379.702							
	0.000000 ^d	214.330	237.418	262.452	289.777	319.795	353.276	390.238							

175	1.000000 ^c	225.308 ^e	246.196 ^e	267.698 ^e	289.992 ^e	313.206 ^e	337.297 ^e	362.459 ^e	388.973 ^e
	0.749787	231.861	254.627	278.289	303.166	329.325	357.062	386.363	
	0.500050	235.336	259.269	284.657	311.570	340.213	371.172		
	0.250066	236.894	262.035	288.985	318.070	349.431	383.359		
	0.000000 ^d	236.618	262.764	291.064	322.043	356.107	393.701		
200	1.000000 ^e	242.212	265.065	288.562	312.932	338.389	364.663	392.389	
	0.749787	249.947	274.807	300.821	328.104	356.898	387.257		
	0.500050	254.590	281.092	308.982	338.812	370.368			
	0.250066	257.424	285.308	315.089	347.267	381.846			
	0.000000 ^d	258.762	287.988	319.607	354.291	392.333			
225	1.000000 ^e	259.190	283.857	309.437	335.895	363.447	392.131		
	0.749787	268.101	295.134	323.389	353.200	384.316			
	0.500050	273.890	302.714	333.266	365.752	400.375			
	0.250066	278.008	308.579	341.385	376.463				
	0.000000 ^d	280.728	312.999	348.121	386.496				
250	1.000000 ^e	276.096	302.647	330.194	358.764	388.486			
	0.749787	286.180	315.287	345.869	377.956				
	0.500050	293.044	324.218	357.374	392.538				
	0.250066	298.427	331.778	367.390					
	0.000000 ^d	302.842	338.173	376.424					
275	1.000000 ^e	292.971	321.402	350.927	381.550				
	0.749787	304.100	335.481	368.226					
	0.500050	312.138	345.743	381.443					
	0.250066	318.950	354.810	393.381					
	0.000000 ^d	324.652	362.875						
300	1.000000 ^e	309.736	340.056	371.469					
	0.749787	322.028	355.365	390.307					
	0.500050	331.221	367.250						
	0.250066	339.124	377.798						
	0.000000 ^d	346.323	387.599						
325	1.000000 ^e	326.437	358.611	391.861					
	0.749787	339.895	375.236						
	0.500050	350.308	388.726						
	0.250066	359.485	400.513						
	0.000000 ^d	368.163							
350	1.000000 ^e	343.223	377.366						
	0.749787	357.782	395.180						
	0.500050	369.397							
	0.250066	379.585							
	0.000000 ^d	389.660							

^a Check measurement. ^b To retain maximum precision, more significant figures in the mole fraction values were carried than is justified by the accuracy. The estimated accuracy is discussed in the Experimental Section. ^c From ref. 2. ^d From ref. 3. ^e Average of two determinations.

Table II: Second, Third, and Fourth Virial Coefficients of the Methane-Tetrafluoromethane System

$t, ^\circ\text{C}$	Nominal composition, mole fraction of CH_4					Nominal composition, mole fraction of CF_4									
	0.00 ^a	0.25	0.50	0.75	1.00 ^b	0.00 ^a	0.25	0.50	0.75	1.00 ^b					
	$B_M, \text{cm}^3 \text{mole}^{-1}$					$D_M \times 10^{-4}, \text{cm}^3 \text{mole}^{-1}$									
0	-111.00	-89.13	-72.26	-60.04	-53.35	+71.0	+56.10	+43.92	+33.70	+26.20	+0.5	+0.2	+0.1	+0.6	+0.5
25	-88.30	-70.67	-57.15	-47.54	-42.82	60.7	49.25	39.17	29.90	23.70	2.1	1.6	0.2	1.3	0.5
30	-84.40	-67.42	-54.50	-45.37	-40.91	59.0	47.90	38.25	29.32	23.20	2.7	2.0	0.3	1.5	0.5
50	-70.40	-55.85	-44.99	-37.45	-34.23	53.8	44.00	35.50	27.50	21.50	3.8	3.4	1.0	2.0	1.3
75	-55.70	-43.77	-34.97	-29.10	-27.06	48.7	40.25	32.55	25.52	19.75	4.9	4.5	2.9	2.7	2.1
100	-43.50	-33.57	-26.44	-21.98	-21.00	44.9	37.10	30.00	23.80	18.34	6.4	6.2	4.7	3.4	2.7
125	-33.20	-25.08	-19.31	-16.03	-15.87	42.1	34.83	27.96	21.60	17.27	8.0	7.8	6.6	4.3	3.1
150	-24.40	-17.73	-13.10	-10.90	-11.40	39.8	32.88	26.35	22.08	16.40	9.7	9.6	7.7	4.8	3.5
175	-16.80	-11.28	-7.72	-6.33	-7.56	38.1	31.28	25.17	20.80	15.85	11.4	11.1	8.9	5.3	3.8
200	-10.10	-5.77	-3.07	-2.37	-4.16	36.6	30.16	24.30	20.00	15.14	12.8	12.4	9.7	5.7	4.3
225	-4.25	-0.80	+1.10	+1.14	-1.16	35.4	28.10	23.56	19.36	14.65	14.3	13.4	10.3	6.4	4.8
250	+1.00	+3.50	4.76	4.27	+1.49	34.4	26.50	22.96	18.70	14.20	15.8	14.3	10.8	7.0	5.2
275	5.60	7.40	8.03	7.10	3.89	33.5	27.90	22.42	18.10	13.85	17.5	15.1	11.4	7.6	5.5
300	9.80	10.85	10.98	9.60	5.98	32.5	27.40	22.00	17.75	13.60	19.5	15.6	11.8	7.9	5.7
325	13.60	13.96	13.67	11.87	7.88	31.8	27.05	21.70	17.25	13.45	21.0	16.0	12.2	8.4	5.8
350	17.05	16.78	16.12	14.07	9.66	31.0	26.80	21.40	16.75	13.30	22.3	16.3	12.5	8.8	5.9

^a Taken from ref 3. ^b Taken from ref 2.Figure 3. Third virial coefficients: O, pure CH_4 ; \blacktriangle , 75% CH_4 -25% CF_4 ; \bullet , 50% CH_4 -50% CF_4 ; \triangle , 25% CH_4 -75% CF_4 ; \square , pure CF_4 .

the Lennard-Jones potential in this temperature range, was obtained for the mixtures as well as for the pure materials.

Theoretical expressions for the virial coefficients of mixtures in terms of cross-term coefficients can be obtained from the configuration integral for multicomponent systems. The expression for the second virial coefficient of a binary mixture

$$B_M = X_1^2 B_{11} + 2X_1 X_2 B_{12} + X_2^2 B_{22} \quad (5)$$

in which X_1 is the mole fraction of methane, X_2 is the mole fraction of tetrafluoromethane, B_{11} is the second virial coefficient of methane, B_{12} is the second virial coefficient for the unlike molecule interaction, and B_{22} is the second virial coefficient of tetrafluoromethane, is usually referred to as the Lennard-Jones and Cook¹⁶ relationship. Values of B_{12} (Table III) were calculated from eq 5 for each of the three mixtures by direct substitution of the experimental values of B_M , X_1 , X_2 , B_{11} , and B_{22} .

The variation of B_{12} with mole fraction reflects the experimental inaccuracy of the data on the two pure substances as well as of the data on the mixtures because the evaluation of B_{12} by difference collects all of the error in this term. Therefore, the small variational trend of B_{12} with mole fraction is thought to be systematic in the experimental data rather than indicating that eq 5 is not completely representative of the nature of the system. A simple arithmetical average, \bar{B}_{12} , for the three mixtures is in very close agreement

(16) J. E. Lennard-Jones and W. R. Cook, *Proc. Roy. Soc. (London)*, **A115**, 334 (1927).

Table III: Cross-Term Second Virial Coefficients of Methane-Tetrafluoromethane as a Function of Composition and Temperature

t , °C	Nominal composition, mole fraction of CH ₄			\bar{B}_{12} , ^a cm ³ mole ⁻¹
	0.25	0.50	0.75	
	B_{12} , cm ³ mole ⁻¹			
0	-62.30	-62.35	-61.56	-62.07
25	-48.88	-48.75	-47.81	-48.48
30	-46.37	-46.35	-45.54	-46.09
50	-37.64	-37.67	-36.76	-37.36
75	-28.67	-28.56	-27.70	-28.31
100	-20.78	-20.63	-19.87	-20.43
125	-14.44	-14.09	-13.40	-13.98
150	-8.78	-8.30	-7.90	-8.33
175	-3.62	-3.26	-2.74	-3.21
200	+0.45	+0.99	+1.62	+1.02
225	4.43	4.90	5.48	4.94
250	7.59	8.27	8.98	8.28
275	10.69	11.31	12.16	11.39
300	13.24	14.07	14.98	14.10
325	15.51	16.60	17.55	16.55
350	17.56	18.89	20.18	18.88

^a Averaged arithmetically.**Table IV:** Mixed Third Virial Coefficients

$$C_M = X_1^3 C_{111} + 3X_1^2 X_2 C_{112} + 3X_1 X_2^2 C_{122} + X_2^3 C_{222}$$

t , °C	$C_{112} \times 10^{-2}$, cm ⁶ mole ⁻²		$C_{122} \times 10^{-2}$, cm ⁶ mole ⁻²	
	Exptl ^a	Calcd ^b	Exptl ^a	Calcd ^c
0	+34.76	+36.5	+49.74	+50.9
25	30.26	32.4	45.65	44.4
30	29.90	31.7	44.28	43.2
50	28.59	29.2	40.64	39.6
75	26.65	26.7	37.24	36.0
100	25.01	24.7	33.96	33.3
125	23.76	23.2	31.40	31.3
150	22.87	22.0	29.20	29.6
175	22.25	21.2	27.39	28.4
200	21.44	20.3	26.58	27.3
225	20.91	19.7	25.59	26.4
250	19.85	19.1	25.54	25.6
275	18.92	18.5	25.40	24.9
300	18.32	18.0	25.35	24.2
325	17.34	17.7	25.70	23.7
350	16.17	17.5	26.35	23.3

^a Averaged arithmetically. ^b $C_{112} = C_{111}(C_{222}/C_{111})^{1/2}$. ^c $C_{122} = C_{222}(C_{111}/C_{222})^{1/2}$.

with the results for the 0.50 mole fraction of CH₄ mixture.

Expansion of the configuration integral for the third and fourth virial coefficients of binary mixtures

$$C_M = X_1^3 C_{111} + 3X_1^2 X_2 C_{112} + 3X_1 X_2^2 C_{122} + X_2^3 C_{222} \quad (6)$$

and

$$D_M = X_1^4 D_{1111} + 4X_1^3 X_2 D_{1112} + 6X_1^2 X_2^2 D_{1122} + 4X_1 X_2^3 D_{1222} + X_2^4 D_{2222} \quad (7)$$

generates two cross-term third virial coefficients and three cross-term fourth virial coefficients. Since the three sets of values that could be derived for C_{112} and C_{122} from the experimental data were in fairly good agreement and showed no significant trends, they were simply averaged arithmetically (Table IV). However, if the averaged values for C_{112} and C_{122} were to be re-substituted into eq 6, a small but insignificant error in the calculated values of C_M would necessarily appear.

Calculated cross-term coefficients (columns 3 and 5, Table IV), obtained from the empirical combinatory rule $C_{ijk} = (C_{iii}C_{jjj}C_{kkk})^{1/3}$ proposed by Connolly,¹⁷ are believed to be as accurate as the experimental results.

Since there are three cross-term fourth virial coefficients, the data on three mixtures provided only a single numerical solution for each coefficient. The results of this solution are given (Table V) only to

Table V: Experimental Mixed Fourth Virial Coefficients

$$D_M = X_1^4 D_{1111} + 4X_1^3 X_2 D_{1112} + 6X_1^2 X_2^2 D_{1122} + 4X_1 X_2^3 D_{1222} + X_2^4 D_{2222}$$

t , °C	$D_{112} \times 10^{-4}$, cm ⁹ mole ⁻³	$D_{122} \times 10^{-4}$, cm ⁹ mole ⁻³	$D_{222} \times 10^{-4}$, cm ⁹ mole ⁻³
	0	+1.7	-1.5
25	5.6	-7.1	5.1
30	6.5	-8.1	6.0
50	7.2	-8.8	8.3
75	4.6	-1.2	7.1
100	3.2	+3.8	7.6
125	2.4	9.0	7.7
150	2.7	9.7	10.3
175	2.3	12.0	11.5
200	2.4	12.7	13.1
225	3.8	12.1	14.5
250	5.1	11.4	15.7
275	6.0	11.9	16.0
300	5.9	13.4	15.0
325	6.8	13.9	14.4
350	7.5	14.5	13.8

show order of magnitude and general trend with temperature. Because of the obvious limitations on their accuracies, they are probably of little value for testing combinatory rules, and no attempt was made to use them in this manner.

(17) J. F. Connolly, *Phys. Fluids*, **4**, 1494 (1961).

Table VI: Critical and Boyle Constants

Experimental data				
	$T_B, ^\circ\text{K}$	$V_B,$ $\text{cm}^3 \text{mole}^{-1}$ ^a	$T_c, ^\circ\text{K}$	$V_c,$ $\text{cm}^3 \text{mole}^{-1}$
CH ₄	509.3	54.34	191.06 ^b	99.0
CF ₄	518.14	104.13	227.65 ^c	...
CF ₄	194.1 (pseudo)	193.2 (pseudo)
(B ₁₂)	467.0	78.75
Argon	410.5 ^d	39.87 ^d
Krypton	584.4 ^e	46.92 ^e
Mixing Rules				
	$T_{12B}, ^\circ\text{K}$	$V_{12B},$ $\text{cm}^3 \text{mole}^{-1}$	$T_{12c}, ^\circ\text{K}$	$V_{12c},$ $\text{cm}^3 \text{mole}^{-1}$
CH ₄ -CF ₄	{ 513.7 (eq 8)	76.56 (eq 9)	192.6 (eq 11)	140.9 (eq 12)
	{ 496.0 (eq 10)	...	185.6 (eq 13)	...

^a By definition, $V_B = (TdB/dT)_{T=T_B}$. ^b K. A. Kobe and R. E. Lynn, Jr., *Chem. Rev.*, **52**, 117 (1953); American Petroleum Institute Research Project 44 on "Selected Values of Physical and Thermodynamic Properties of Hydrocarbons and Related Compounds." ^c D. L. Fiske, *Refriger. Eng.*, **57**, 336 (1949). ^d Evaluated from the second virial coefficient data of Michels, *et al.*,¹⁹ and Whalley and Schneider.²⁰ ^e Evaluated from the second virial coefficient data of Beattie, *et al.*²¹

Application of the Principle of Corresponding States

Before an attempt was made to apply the mixing rules to corresponding states parameters,⁷ the experimental second virial coefficients, B_{11} , B_{22} , and B_{12} , were examined for congruity with the principle of corresponding states in terms of the Boyle and critical points. The Boyle-point constants, T_B and $V_B = (TdB/dT)_{T=T_B}$,¹⁸ were found to be more tractable parameters than the critical constants T_c and V_c . The reason is that the reduced Boyle parameters for the unlike-molecule interactions can be evaluated experimentally and tested to determine if they agree with the corresponding states function defined by the pure components. A similar test with reduced critical parameters is not possible because the unlike-molecule critical temperature and volume are not experimentally determined quantities. Thus, the examination of a mixture in terms of the Boyle point has the advantage that it allows one to decide whether the experimental cross-term virial coefficients follow the principle of corresponding states and, if they do, allows the behavior of the mixing laws to be more clearly interpreted.

The Boyle-point corresponding states function (Figure 4) is remarkably accurate for the second virial coefficients of the cross-term as well as for the second virial coefficients of pure methane and pure tetrafluoromethane. Argon^{19,20} and krypton,²¹ which also agree accurately with the Boyle function, were included to show that the function does indeed represent true corresponding states behavior. The Boyle constants (Table VI) were derived from accurate empirical representa-

tions of the second virial data by the Lennard-Jones [n , 6] potentials and their first derivatives with respect to temperature. For CH₄ the L-J [28, 6] potential, $\theta = 248.3^\circ\text{K}$ and $b_0 = 54.39 \text{ cm}^3 \text{mole}^{-1}$, was fitted to the data of Table II; for CF₄ the L-J [500, 6] potential, $\theta = 416.6^\circ\text{K}$ and $b_0 = 89.50 \text{ cm}^3 \text{mole}^{-1}$, was fitted to the data of Table II; for the cross-term B_{12} the L-J [30, 6] potential, $\theta = 234.2^\circ\text{K}$ and $b_0 = 77.98 \text{ cm}^3 \text{mole}^{-1}$, was fitted to the data of Table II; for argon the L-J [17, 6] potential, $\theta = 155.0^\circ\text{K}$ and $b_0 = 44.14 \text{ cm}^3 \text{mole}^{-1}$, was fitted to the data of Michels, Wijker, and Wijker¹⁹ and Whalley and Schneider²⁰; for krypton the L-J [24, 6] potential, $\theta = 266.1^\circ\text{K}$ and $b_0 = 48.20 \text{ cm}^3 \text{mole}^{-1}$, was fitted to the data of Beattie, Brierley, and Barriault.²¹

Contrary to the general trend of results indicated by Guggenheim and McGlashan⁷ for a variety of systems following the corresponding states principle, the geometrical mean rule for Boyle temperature

$$T_{12B} = (T_{1B}T_{2B})^{1/2} \quad (8)$$

and the Lorentz rule for Boyle volume

$$V_{12B} = 1/8(V_{1B}^{1/3} + V_{2B}^{1/3})^3 \quad (9)$$

did not furnish values of T_{12B} and V_{12B} that corre-

(18) T. Kihara, *Rev. Mod. Phys.*, **25**, 831 (1953).

(19) A. Michels, Hub. Wijker, and Hk Wijker, *Physica*, **15**, 627 (1949).

(20) E. Whalley and W. G. Schneider, *J. Chem. Phys.*, **23**, 1644 (1955).

(21) J. A. Beattie, J. S. Brierley, and R. J. Barriault, *ibid.*, **20**, 1613 (1952).

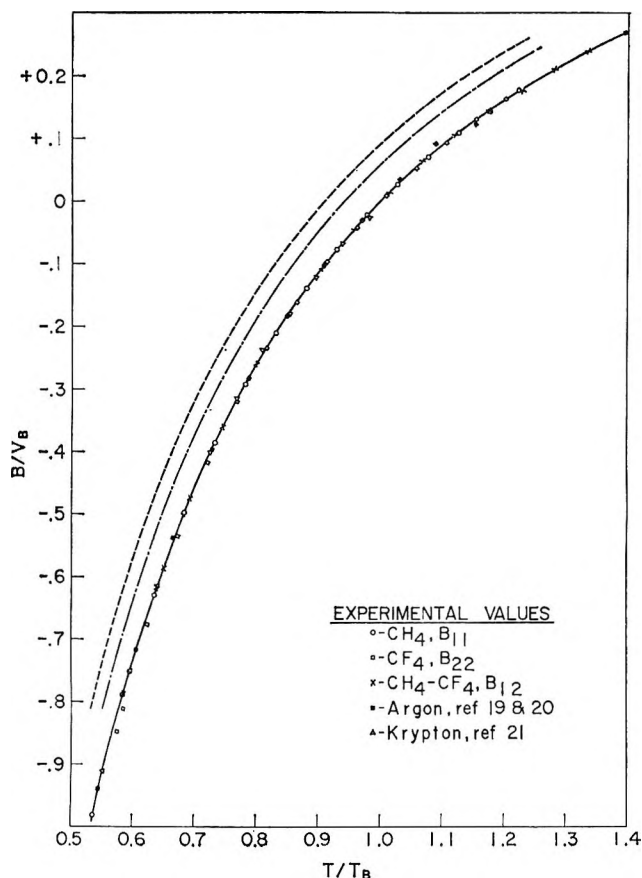


Figure 4. Corresponding states correlation in terms of Boyle-point parameters, —, eq 8 and 9 for B_{12} , ---, eq 9 and 10 for B_{12} , — · —.

sponded with the experimentally determined values in Table VI. Also, the reduced mixed second virial coefficient values, shown as the dashed line in Figure 4, no longer agreed with the corresponding states function. When the mixture rule for Boyle temperature contained a factor for the difference in volumes of the molecules, as suggested by Hudson and McCoubrey²²

$$T_{12c} = \left[\frac{V_{1B} V_{2B}}{(V_{1B}^{1/3} + V_{2B}^{1/3})^6} \right] 2^6 (T_{1B} T_{2B})^{1/2} \quad (10)$$

the calculated reduced second virial coefficients moved closer to the corresponding states line, but the agreement was still unsatisfactory. No correction was applied for the ionization potentials because they are not greatly different for methane and tetrafluoromethane. Values for methane vary between 13.1 and 14.5 ev,²³ and a recently estimated value²⁴ for tetrafluoromethane lies between 14.9 and 15.1 ev. Thus, a correction factor, $2(I_1 I_2)^{1/2} / (I_1 + I_2) = 0.998$, based on the greatest differences in the ionization potentials, makes no significant difference in the estimated mixed Boyle temperature.

Results of the examination of the above system in terms of the critical reference points are presented in Figure 5. The critical volume of tetrafluoromethane is not determined. Its experimental critical temperature, reported by Fiske,²⁵ does not appear to conform to a corresponding states relationship with methane. Therefore, the pseudo-critical temperature and volume (Table VI) were derived by fitting second virial coefficient data for tetrafluoromethane to the corresponding states second virial coefficient function defined by methane. Values for the mixed critical or pseudo-critical constants, calculated by equations similar to eq 8-10, as follows

$$T_{12c} = (T_{1c} T_{2c})^{1/2} \quad (11)$$

$$V_{12c} = 1/8 (V_{1c}^{1/3} + V_{2c}^{1/3})^3 \quad (12)$$

$$T_{12c} = \left[\frac{V_{1c} V_{2c}}{(V_{1c}^{1/3} + V_{2c}^{1/3})^6} \right] 2^6 (T_{1c} T_{2c})^{1/2} \quad (13)$$

failed to provide a satisfactory corresponding states correlation of the cross-term second virial coefficient. The deviations from the corresponding states function were in the same direction and about the same magnitude as found in the Boyle-point correlation.

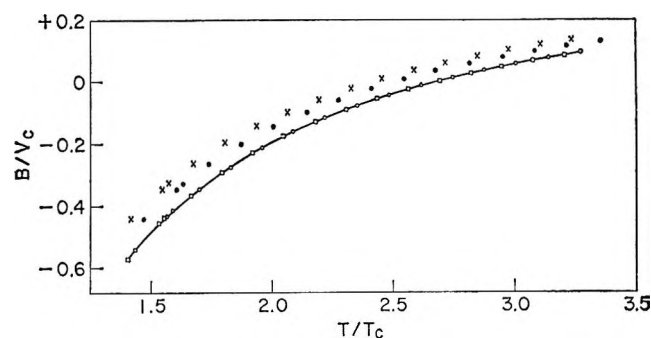


Figure 5. Corresponding states correlation in terms of critical point parameters: O, pure CH₄; □, pure CF₄; pseudo-critical constants, Table VI; ×, B_{12} , eq 11 and 12; ●, B_{12} , eq 12 and 13.

Conclusion

The geometrical-mean rule for reduced temperature is not an accurate basis for extending the principle of corresponding states to the cross-term second virial

(22) G. H. Hudson and J. C. McCoubrey, *Trans. Faraday Soc.*, **56**, 761 (1960).

(23) T. M. Reed, III, *J. Phys. Chem.*, **59**, 428 (1955); J. D. Morrison and A. J. C. Nicholson, *J. Chem. Phys.*, **20**, 1021 (1952); W. C. Price, *Chem. Rev.*, **41**, 257 (1947).

(24) R. W. Kiser and D. L. Hobrock, *J. Am. Chem. Soc.*, **87**, 922 (1965).

(25) D. L. Fiske, *Refriger. Eng.*, **57**, 336 (1949).

coefficients of the methane-tetrafluoromethane system. This conclusion was reached after examining the system in terms of both the Boyle reference points and the critical reference points. An advantage possessed by the Boyle-point correlation, not widely recognized apparently, is that the cross-term reduced variables can be determined experimentally, thus making a direct test of the corresponding states principle on mixtures possible without involving the mixing rules. Alternatively, the mixing rules can be tested on a corresponding states correlation without having to contend, possibly,

with an unknown factor associated with the exactness of the corresponding states principle itself.

It is evident from the values of Table VI that the geometrical-mean Boyle temperature lies between that of methane and tetrafluoromethane and, therefore, is nearly 50°K above the experimental value of the Boyle temperature of the mixture, T_{12B} . If Boyle temperatures are assumed proportional to interaction energy, the obvious conclusion is that the unlike molecule interaction represents a new situation not related to the like molecule interactions by any kind of average.

The Halide Ion Activity of Dyes and Organic Salts in Aqueous Solution

by J. F. Padday

Research Laboratories, Kodak Limited, Wealdstone, Harrow, Middlesex, England (Received March 27, 1967)

The ionic interaction hypothesis to explain metachromasy of some cationic dyes in aqueous solution has been tested experimentally. Electrometric measurements of the halide counterion activity of these dyes at concentrations where marked metachromasy took place showed no indication of ion-counterion association. Similar measurements of the counterion activity of alkyltrimethylammonium bromides in aqueous solution showed that above the critical micelle concentration, obtained from surface tension measurements, strong ion-counterion association took place. Explanations of metachromasy of the dyes, particularly that in terms of the formation of dimers, are discussed.

The metachromatic behavior of many types of dyes in aqueous solution has been the subject of investigations¹⁻⁴ which have been reviewed elsewhere.¹ The metachromatic behavior of some cyanine, carbocyanine, and thiocyanine dyes in aqueous solution has attracted particular attention because the spectral perturbations that are dependent on dye concentration follow a general pattern. This pattern involves the appearance of a broad shoulder, hypsochromic to the main peak, as the concentration of dye increases until at relatively high concentrations, the shoulder develops into the principal absorption peak. The hypsochromic band has been attributed to an aggregation state of the dye, the dimer, by Scheibe and many other investigators.⁴

McKay⁵ found no evidence of aggregation, using a polarographic technique, of one cyanine dye that exhibited metachromasy. Hillson and McKay¹ then attempted to explain metachromasy of cyanine dyes, rhodamine B, methylene blue, and some other dyes in

(1) R. B. McKay and P. J. Hillson, *Trans. Faraday Soc.*, **61**, 1800 (1965); P. J. Hillson and R. B. McKay, *Nature*, **210**, 297 (1966).

(2) M. J. Blandamer, M. C. R. Symons, and G. S. P. Verma, *Chem. Commun.*, 629 (1965).

(3) F. Feichtmayr and J. Schleg, *Ber. Bunsenges, Physik. Chem.*, **68**, 95 (1964).

(4) W. West and S. Pearce, *J. Phys. Chem.*, **69**, 1894 (1965); B. H. Carroll, *Phot. Sci. Eng.*, **5**, 65 (1961); S. E. Sheppard, *Rev. Mod. Phys.*, **14**, 303 (1942); G. Scheibe, *Kolloid Z.*, **82**, 1 (1938).

(5) R. B. McKay, *Trans. Faraday Soc.*, **61**, 1787 (1965).

terms of an hypothesis involving the association of the dye with its counterion, following the suggestion of Feichtmayr and Schlag³ for some triphenylmethane dyes. McKay and Hillson further maintained that their hypothesis was consistent with the same type of metachromasy that occurred when the dielectric constant of the solvent was lowered, as such lowering greatly enhanced the ion-counterion interaction. It thus appeared that their hypothesis was in direct conflict with that of Scheibe.

This study set out to test the ion-counterion interaction hypothesis by measuring the counterion activity of a number of these dyes, the metachromasy of which was typical.

Experimental Section

Materials. Quaternary Ammonium Compounds. Octadecyl-, tetradecyl-, and dodecyltrimethylammonium bromides were obtained in a pure form and will be referred to as OTAB, TTAB, and DTAB, respectively. These compounds were further purified by recrystallization from water. Elementary analyses of the compounds indicated that the OTAB and TTAB were better than 99% pure but that the DTAB was impure in that the amount of carbon found (56.1%) was appreciably lower than that required (58.4%).

The impurity present in the DTAB lowered the cmc below the accepted value of 0.015 mole/l. (see Table I). The cmc's of TTAB and OTAB were in reasonable agreement with literature values. However, the conclusions sought concerning ion association at the cmc were equally valid whether for pure or impure DTAB as the bromide ion activity followed that expected from the concentration below the measured cmc.

Dyes. The mean ionic activities of five cationic dye salts were measured. They were as follows: dye I, 1,1'-diethyl-2,2'-cyanine bromide; dye II, 1,1'-diethyl-2,2'-carbocyanine bromide; dye III, 3,3'-diethylthiacyanine bromide; dye IV, 3,3'-diethylthiadibromocyanine bromide; and dye V, the chloride salt of rhodamine B (C. I. Index No. 45170). Elementary analyses of these dyes showed that the halide ion concentrations of the dyes were within 1% of the expected value. Other halides were not found. The analyses of dyes III and IV agreed with values calculated from the formula weight, but dyes I, II, and V were explained on the basis of the retention of two molecules of water, as found by McKay⁵ for dye II. On dehydration under vacuum, they gained their anhydrous formula weight within 1.5%.

Changes in dye ion activity coefficient at high concentrations estimated from spectral changes indicated that 50% or more of the dye ions changed their form.

Table I: Critical Micelle Concentrations of TABs (mole per liter)

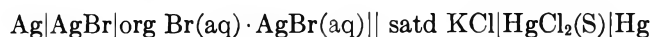
Source	Cmc, mole/l.		
	Dodecyl	Tetra-decyl	Octa-decyl
This study from surface tension	0.004	0.0032	0.00015
This study from emf	0.005	0.004	0.00010
Phillips ^a	0.0153	0.00302	
Bair and Kraus ^b	0.019		0.000117
Scott and Tartar ^c	0.0159	0.00316	
Debye ^d		0.00304	
Trap and Hermans ^e		0.0036	
Venables and Nauman ^f		0.0035	

^a J. N. Phillips, *Trans. Faraday Soc.*, **51**, 561 (1955). ^b E. J. Bair and C. A. Kraus, *J. Am. Chem. Soc.*, **73**, 1129 (1951). ^c A. B. Scott and H. V. Tartar, *ibid.*, **65**, 692 (1943). ^d P. Debye, *J. Phys. Chem.*, **53**, 1 (1949). ^e H. J. L. Trap and J. J. Hermans, *Koninkl. Akad. Wetenschap. Proc. Ser. B*, **58**, 97 (1955). ^f R. L. Venables and R. V. Nauman, *J. Phys. Chem.*, **68**, 3498 (1964).

Small amounts of retained solvent were unlikely to account for so big a change.

Method. Surface tensions of the solutions of the TABs were measured with a modified Wilhelmy plate balance⁶ and care was taken to ensure that the angle of contact was always zero. The temperature of the solution was kept within $\pm 0.5^\circ$ of 25.0° .

Measurements of emf were made on a cell composed of a saturated calomel electrode bridged to the solution of organic salt in which was immersed a silver-silver halide electrode forming the cell



The silver halide electrodes were prepared by slowly depositing crystalline silver electrolytically onto a platinum wire sealed into a glass tube. The silver halide was formed by electrodeposition in a 1 M solution of potassium halide with the silvered platinum as the anode.

Electrodes were made and used in pairs. Pairs deviating by more than 0.5 mv were discarded. Electrodes were prepared and used in the darkroom so that photolysis of the dye was reduced to a minimum. The saturated calomel electrode was of the porous pin type as supplied by V. A. Howe Ltd. These electrodes were found to be very stable, yet with a very low rate of flow of potassium chloride solution through the porous pin. Analysis showed that, after the calomel electrode was

(6) J. F. Padday, Proceedings of the Second International Congress of Surface Activity, London, 1957, Vol. I, p 1.

left in 30 ml of distilled water for 24 hr, the final concentration of chloride ions did not exceed 10^{-6} M. During measurement, the electrodes were never immersed in the solution to be measured for more than 0.5 hr; hence the "leak" of chloride ions into the system could not measurably affect the halide ion activity or the state of the dye cation. All emf measurements were carried out at $25.0 \pm 0.05^\circ$ and measured with a reproducibility of ± 0.2 mv with a "pH meter 4" supplied by V. A. Howe Ltd. Spectral data were obtained by measuring the transmission densities with a Hardy recording spectrophotometer and then replotted the curves to show molecular extinction coefficients.

Results

N-Alkyltrimethylammonium Bromides. The surface tensions of aqueous solutions of the TAB's are shown in Figure 1. The cmc's of these solutions were obtained by taking the intersection of the tangent with the maximum gradient with the flat portion (extrapolated

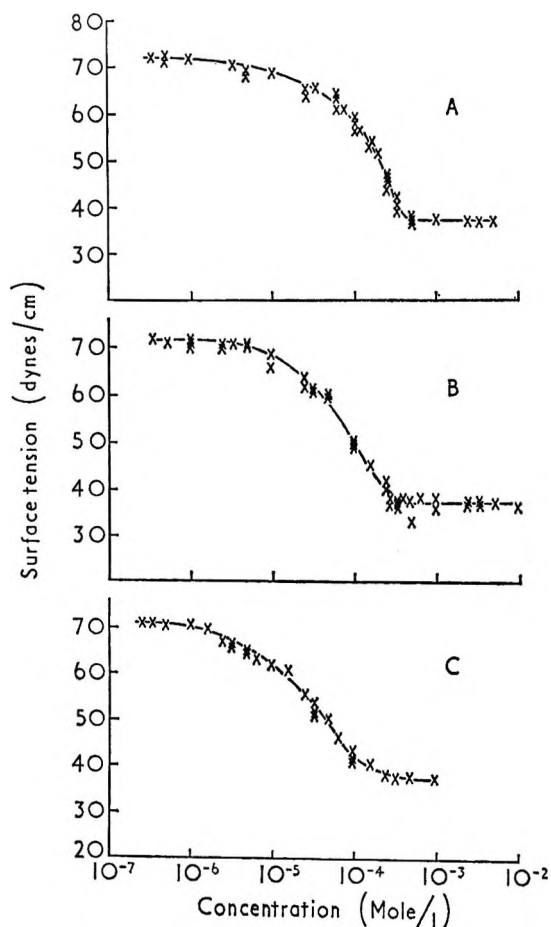


Figure 1. Surface tension of alkyltrimethylammonium bromides in aqueous solution as a function of concentration: A, dodecyl; B, tetradecyl; C, octadecyl.

backwards) of the curve at high concentration. The cmc's obtained in this way are given in Table I, together with cmc's obtained from emf measurements and values reported in the literature. The bromide activity of the solutions was obtained by comparing the emf's of a reversible cell containing first a solution of TAB as electrolyte and then a solution of KBr of equivalent concentration.

The emf of the KBr solutions gave a gradient of 59.0 mv per unit of log concentration in the range 10^{-4} to 10^{-6} M. Activities of KBr were measured up to concentrations of 10^{-1} M. Small variations in E_0 , the intercept of the ideal calibration curve on the emf axis, were found when changing silver bromide electrodes and were compensated for by recalibration with KBr solutions. Results are shown in Figure 2, where $(E - E_0)/59.0$ was plotted as a function of the concentration of the bromide in solution on a logarithmic scale, E and E_0 being expressed in millivolts. The ideal slope of this plot is a straight line of gradient unity and deviations from this line indicated interionic interactions. The experimental values of emf of KBr solutions followed the logarithm of the concentration corrected with a mean activity coefficient calculated according to the Debye-Hückel equation, with a value of 4.4 Å for distance of closest approach, following McInnes.⁷ The broken line of Figure 2 is the theoretical activity on this basis and fits the experimental points within 0.5 mv over the concentration range 10^{-6} to 10^{-1} M.

Measurements of the emf of cells with octadecyl-

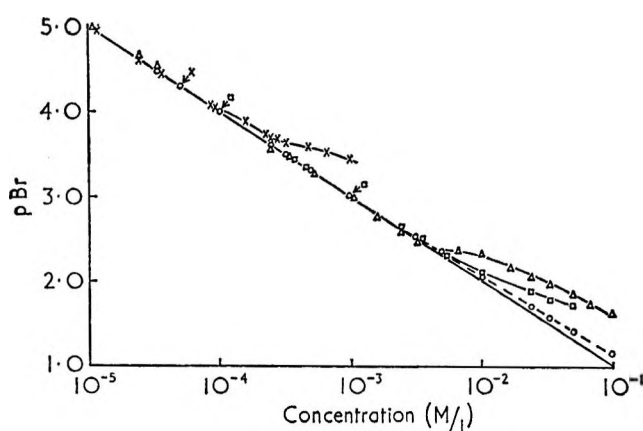


Figure 2. Activity of bromide ions in aqueous solution of alkyltrimethylammonium and potassium bromides as a function of log concentration: \square , dodecyl; Δ , tetradecyl; \times , octadecyl; \circ , potassium.

(7) D. A. McInnes, "The Principles of Electrochemistry," Dover Publications, New York, N. Y., 1961, p 165.

trimethylammonium bromide (OTAB) as electrolyte showed that their mean ionic activity coefficients were unity at concentrations below $1.2 \times 10^{-4} M$. As the concentration increased, the cmc activity coefficients fell below unity.

Solutions of tetradecyl- and dodecyltrimethylammonium bromides showed a similar behavior and their mean ionic activity coefficients again decreased from unity at concentrations higher than their respective cmc's.

With solutions of all three TAB's, the breakaway of the activity curve from that of the KBr solution was sufficiently marked to enable the concentration at which deviation first appeared to be estimated. The critical concentrations of the deviations are tabulated with the cmc's of the solutions in Table I and show internal agreement for impure DTAB and reasonable agreement with the results of other workers for TTAB and OTAB.

Dyes. The activities of the halide counterions of each dye in aqueous solution at 25° were measured as for the TAB's. The results for the dyes were treated in a similar way, the pBr of dyes I, II, III, and IV and pCl of dye V, as measured from the emf, being plotted as a function of the logarithm of the concentration (Figure 3).

It should be noted that the method of plotting tends to mask experimental error. However, the best straight line through the experimental points of the plots for dyes I, III, and IV produced gradients of 1.00 ± 0.01 and intercepts of 0.00 ± 0.01 when the gradient was expressed as pBr/pC , where C is the concentration of the dye in solution. The points for emf measurements of dye II were displaced to the right-hand side although with a correct gradient of 1.00, thus showing that the mean ionic activity coefficient did not change.

The mean ionic activity coefficient of dyes I, III, and IV indicated that the dyes were both fully dissociated at all concentrations between 10^{-4} and $10^{-6} M$ and dye V similarly up to $10^{-3} M$.

Dye V was much more soluble than the other four cyanine dyes and as the spectral changes for this dye occur at higher concentrations, emf measurements were performed in the concentration range 10^{-3} to $10^{-5} M$.

Whereas dye I obeyed Beer's law, the other dyes all showed metachromatic behavior within the concentrations of these activity measurements. As an example, the molecular extinction coefficient of dye II is plotted as a function of wavelength for solutions of different concentrations in Figure 4. The absorption at the principal peak drops to about one-third of its maximum value.

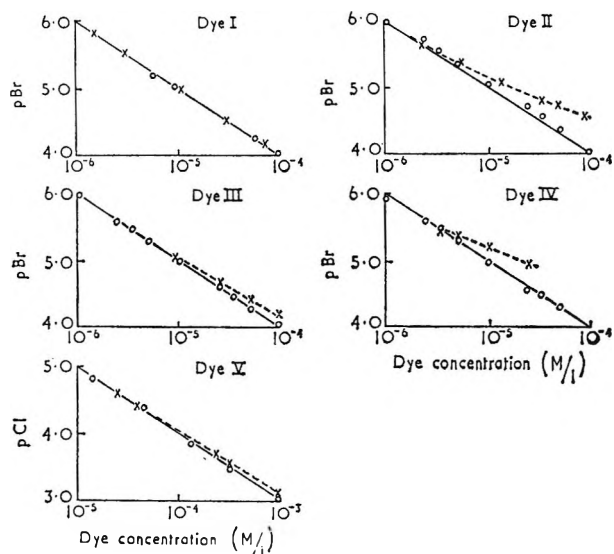


Figure 3. O, Activity of halide ions, expressed as pBr , and pCl in aqueous solutions of dyes as a function of log concentration of dyes I, II, III, and IV as bromide salts and dye V as chloride salt; X, activity of dyes on the same basis, derived from spectral data.

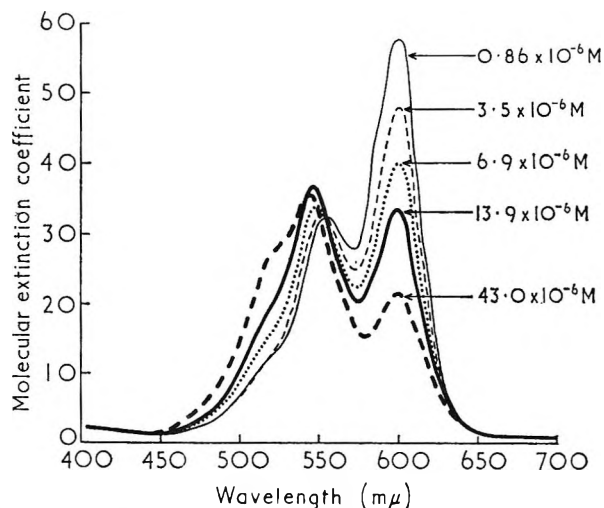


Figure 4. The molecular extinction coefficient of dye II as a function of wavelength at different concentrations in aqueous solution.

Analysis of the data of Figure 4 for dye II and of similar absorption spectra for the other dyes indicates that at least two species of dye are present. One species (here defined as the unperturbed dye ion) is that exhibiting a spectrum obeying Beer's law in alcoholic solution and at low concentrations ($10^{-6} M$) in aqueous solution, the spectra in both solutions being identical. At greater concentrations in aqueous solution, spectra of these dyes change in a way suggesting that the

amount of unperturbed dye diminishes and a new form of dye (perturbed) is produced. The proportion, α , of unperturbed dye to the total amount present is given by

$$\alpha = \frac{\epsilon}{\epsilon_{\max}}$$

where ϵ is the molecular extinction coefficient at the wavelength of the peak of the unperturbed form at a given concentration, approximated according to the method of West,⁴ and ϵ_{\max} is the molecular extinction coefficient, at the same wavelength, below 10^{-6} M or in alcoholic solution.

The proportion α is, in fact, the activity coefficient of the single dye ion and has been plotted as such in Figure 3. The values of $-\log(\text{dye}^+)$ are plotted on the same scale as $p\text{Br}$ and are indicated by (\times), where the effective concentration (dye^+) of dye ions is α , times the total concentration of dye. The data of Figure 3 indicate clearly that metachromasy of dye cations takes place without any measurable association of halide counterions.

Discussion

The method of measuring halide ion activities from emf measurements of concentration cells without transference is known to work well with silver halide electrodes, provided the electrodes remain reversible and undergo no chemical change. These conditions were obtained here. The emf of the concentration cells with KCl and KBr as electrolyte was a linear function of the logarithm of the concentration with a gradient of 59.0 mv in the range 10^{-6} to 10^{-4} M. That the responses of both electrodes were unaffected by dye solution was shown by their ability to give reproducible potentials with potassium halide solutions before and after use with dye.

Silver bromide electrodes are reversible to both silver ions and bromide ions and saturate the aqueous electrolyte with silver bromide. The bromide ion concentration of these experiments was always greater than the silver ion concentration; hence activity corrections arose from electrostatic attractions between the bromide and its salt cation (K^+ , dye^+ , or TAB^+).

The emf data gave the thermodynamic activity of the bromide ions in the electrolyte, and the activity coefficient obtained therefrom is the mean ionic activity coefficient of the bromide and its cation. The mean ionic coefficient of potassium bromide followed the Debye-Hückel equation,⁸ between 10^{-6} and 10^{-1} M according to

$$-\log f_{\pm} = \frac{Z^+Z^-A\sqrt{w}}{1 + \beta a\sqrt{w}} \quad (1)$$

where f_{\pm} is the mean ionic activity coefficient, Z^+ and Z^- are the respective charges on the cation and anion, A is a constant equal to 0.5056 to 25° for water, β is a constant equal to 0.3286 at 25° for water, a is the minimum interionic distance in angstroms between the center of the anion and the center of the cation, and w is the mean ionic strength of the electrolyte.

The Debye-Hückel equation shows that between the concentrations 10^{-4} and 10^{-6} M the activity and concentration of bromide ions should not differ by more than 1.2% (i.e., 0.3 mv) for all the cations K^+ , dye^+ , and TAB^+ , provided no aggregation of cations takes place and the solute behaves as a uni-univalent electrolyte. The varying size of the cations will make no difference because at the low concentrations the denominator of eq 1 is nearly unity and the limiting Debye-Hückel law applies.

TAB's form relatively large clusters or micelles of positive ions above the cmc, with 40-100 in each micelle. By changing Z^+ from 1 to 40 and correcting the ionic strength for the changes in concentration, it is clear that f_{\pm} will decrease rapidly from unity for solutions of TAB's above the cmc. As is well known,⁹ the very much greater cationic charge has the effect of binding a proportion of bromide ions so that the mean ionic activity coefficient of the TAB's falls above the cmc.

According to Debye,⁹ TTAB forms micelles of 75 molecular units in water and the fraction of these units fully ionized is 0.14. The counterion activity may thus be estimated at a concentration of 10^{-2} M from Debye's data, on the assumption that all micelles are of the same size. Thus if all cations in excess of 4×10^{-3} M (the cmc) were present as micelles, then the concentrations of bound counterions would be about 5.2×10^{-3} mole/l. and of unbound 0.8×10^{-3} mole/l. The counterion activity on this basis would be 4.8×10^{-3} M (or $p\text{Br}$ 2.32). The counterion activity of TTAB at a concentration of 10^{-2} M is found here to be 5.0×10^{-3} M (or $p\text{Br}$ 2.30). Thus these data tended to confirm that when micelles or aggregates formed, they did so with the considerable uptake of counterions (85% in the case of the TTAB). It is therefore reasonable to suppose that large aggregates or ionic associates of cationic dyes in solutions would be readily determined from changes in counterion activity. These experiments indicate that no significant counterion binding to these dyes takes place at these concentrations in aqueous solution.

As ion-counterion association was not found with these dyes, it was concluded that ion-pair formation,¹

(8) See ref 7, p 147.

(9) See Table I, footnote d.

whether induced by direct electrostatic attraction,³ by indirect cohesive forces of the solvent,² or by the formation of large aggregates of these dyes in aqueous solution, must be excluded from any hypothesis accounting for the formation of their perturbed forms.

West and Pearce⁴ proposed that a carbocyanine dye (dye II) and each of a group of thiocyanine dyes dimerized at concentrations between 10^{-5} and 10^{-4} *M* and calculated the association constants of two similarly charged ions. The ion association hypothesis of Hillson and McKay¹ allows a similar association constant but due to oppositely charged ions.

These data are consistent with West's association constants for dimerization of some cyanine dyes and are opposed to the ion association hypothesis as any ion pairing must affect the mean ionic activity coefficient. Dimerization or polymerization of dye cations will lead to an increase in Z^+ , the charge on the effective cation in the Debye-Hückel law. At these concentrations the limiting law may be applied and expressed in terms of the concentration *C* of dye salt added. In Table II the coefficients of the square root of *c* for the term $\log f_{\pm}$ are given for monomers, dimers, trimers, and tetramers, on the assumption that all dye cations are present as the respective polymer. The mean ionic activity coefficient is then calculated for a dye concentration of 10^{-4} *M*.

It is clear that if all dye at 10^{-4} *M* were present as dimers, then the deviation of the emf from that of a KBr solution would be only 0.7 mv. West has shown, and these data confirm, that only a proportion of dye is

Table II: Activity Coefficients on the Basis of the Debye-Hückel Limiting Law at 10^{-4} *M*

	Charge		Coeff of \sqrt{c}	f_{\pm}	$-(RT/ZF)$ $\ln f_{\pm}$, mv
	Cation	Anion			
Monomer	1	1	0.5056	0.9885	0.30
Dimer	2	1	1.242	0.9720	0.732
Trimer	3	1	2.150	0.9517	1.27
Tetramer	4	1	3.205	0.9289	1.89

present as dimers at 10^{-4} *M*; hence the activity coefficient will be nearly unity and the bromide ion activity as measured by emf will not be measurably different from its concentration even though dimers are present.

As the number of cations forming the aggregate increases, the activity corrections become greater. As activity corrections were all within the limits of experimental error, it is concluded that dimers are probably formed. Trimers could also be consistent with these data (though not with West's), but higher aggregates would bring the behavior of the dyes nearer to the behavior of the TAB's above the cmc's with consequent deviation in the emf.

The forces holding a dimer together against electrostatic forces are very likely dispersion forces. The density of dispersion electrons in these ions is great and it would appear energetically favorable for two ions to come together by a process of hydrophobic bonding.

The Adsorption and Oxidation of Hydrocarbons on Noble Metal Electrodes.

IV. *n*-Hexane on Smooth Platinum at 130°

by S. B. Brummer and M. J. Turner

Tyco Laboratories, Inc., Waltham, Massachusetts (Received March 28, 1967)

The oxidative adsorption of *n*-hexane on smooth Pt electrodes in 12 *M* H₃PO₄ solutions at 130° has been studied with electrochemical pulse techniques. Anodic stripping provides a quantitative measure of the adsorbate. Initial adsorption at low potentials is limited by diffusion in solution and occurs as virtually unchanged *n*-C₆H₁₄. Steady-state adsorption increases from 0.05 to 0.20 v (*vs.* rhe) and subsequently declines to zero at 0.80 v. It increases with *n*-C₆H₁₄ pressure but less than proportionally. The steady-state adsorbate comprises mostly partially reacted *n*-C₆H₁₄ rather than unchanged fuel. Part of the adsorbate, the CH- α material, is cathodically desorbed below 0.05 v. Its coverage shows the same potential and pressure dependence as the total adsorbate. The residue, not cathodically desorbable, comprises two parts, the CH- β and O type. The O type, the major constituent of the residue, releases 1.4 electrons per site on oxidation to CO₂ and is similar to O-type C₃H₈ and "reduced CO₂." Coverage with CH- β and O type is insensitive to fuel pressure. The chemical composition of these species and their probable roles in the over-all hydrocarbon-carbon dioxide reaction are discussed.

I. Introduction

This paper is part of a study of the basic mechanisms of the anodic oxidation of saturated hydrocarbons. Previously,¹⁻³ we reported results for the oxidative adsorption of C₃H₈ on smooth Pt from hot (80-130°), concentrated (78 wt %, 12 *M*) H₃PO₄ solutions. These conditions approximate those for a useful hydrocarbon anode.⁴

In the earlier work it was shown that the adsorption of C₃H₈ leads to the formation of three partially oxidized adsorbed residues.^{3,5} These residues are of three generic types: the CH- α , the CH- β , and the O type. The CH- α is cathodically desorbable, relatively unreactive toward oxidation, and probably comprises a mixture of (partly dehydrogenated) alkyl radicals. Its composition changes with potential. The composition of the CH- β species is also a function of potential. It is unreactive toward both reduction and oxidation and is probably a carbonaceous polymer. The O type, the major species in terms of coverage, has the same composition at all potentials. It releases \sim 1.3 electrons per covered site on oxidation to CO₂ and this indicates that it is oxygenated. It is similar to the reduced

CO₂ reported by Giner.^{6,7} O type is relatively easily oxidized at high potentials but its over-all properties suggest that its presence on the electrode is the major stumbling block to the efficient usage of the electrode's surface for the C₃H₈-CO₂ reaction.³

There are considerable variations in the reactivity of saturated hydrocarbons toward oxidation on Pt^{8,9} and it is of interest, therefore, to examine the adsorption of other hydrocarbons, particularly those which are

(1) S. B. Brummer, J. I. Ford, and M. J. Turner, *J. Phys. Chem.*, **69**, 3434 (1965).

(2) S. B. Brummer and M. J. Turner, "Hydrocarbon Fuel Cell Technology," B. S. Baker, Ed., Academic Press Inc., New York, N. Y., 1965, p 409.

(3) S. B. Brummer and M. J. Turner, *J. Phys. Chem.*, **71**, 2825 (1967).

(4) W. T. Grubb and L. W. Niedrach, *J. Electrochem. Soc.*, **110**, 1086 (1963).

(5) S. B. Brummer, *ibid.*, **113**, 1042 (1966).

(6) J. Giner, *Electrochim. Acta*, **8**, 857 (1963).

(7) S. B. Brummer and M. J. Turner, submitted for publication.

(8) Reports by General Electric Co. on Contracts DA 44-009-AMC-479(T) and DA 44-009-ENG-4309(T).

(9) H. Binder, A. Köhling, H. Krupp, K. Richter, and G. Sandstede, *J. Electrochem. Soc.*, **112**, 355 (1965).

less reactive. Accordingly, we have studied the oxidative adsorption of *n*-hexane on smooth Pt from 80% H₃PO₄ solutions at 130°.

II. Experimental Section

The principal method employed to analyze the adsorption of the hydrocarbon involves the use of potentiostat-applied potential steps to clean the electrode and to adsorb under well-defined diffusional conditions. The adsorbate is sampled with a rapid galvanostatic pulse. This method is essentially that of Gilman.¹⁰ The potential sequence used to clean the electrode was described earlier^{1,3} and the particular sequence used to analyze each adsorption experiment will be indicated in the Results section.

Most of the equipment, the methods of obtaining these pulses, and the procedures for purification and water-vapor control of the electrolyte were described earlier.³ Electrodes were usually thermocouple grade Pt wires but, where good semiinfinite linear diffusional conditions were required, smooth (99.98%) Pt foils were used. The electrodes were flame-annealed to minimize roughening.¹ Results are given in terms of "real area" (r cm²) which is defined as equivalent to 210 μcoulombs of H atoms (a monolayer) cathodically deposited in 1–2 msec.¹¹

n-Hexane was research grade (Phillips Petroleum 99.96 mole %) and was carried into the system with an N₂ carrier. To regulate the concentration of *n*-hexane in the carrier, the N₂ was passed through a thermostatically controlled flask of *n*-hexane before being saturated with H₂O as before.¹ The vapor pressure of *n*-hexane was obtained from Timmermans.¹² The water vapor pressure was controlled at 480 mm, which at 130° corresponds to 80 wt % H₃PO₄.¹³

The reference electrode was the dynamic hydrogen reference electrode described by Giner.¹⁴ Potentials are referred to the reversible hydrogen electrode in the test solution (rhe).

III. Results and Discussion

Anodic Stripping of Adsorbed n-C₆H₁₄. Anodic galvanostatic stripping curves for adsorbed *n*-C₆H₁₄ are similar to those found earlier for C₃H₈.¹ Adsorbed material is oxidized in the region where the surface of the Pt electrode is normally oxidized. Thus, in this region four processes can contribute to the charge passed: oxidation of previously adsorbed material ($Q_{\text{ads}}^{n\text{-hex}}$),¹⁵ oxidation of the electrode ($Q_{\text{electrode}}$), oxidation of *n*-C₆H₁₄ diffusing to the electrode during the stripping transient ($Q_{\text{diff}}^{n\text{-hex}}$), and double-layer charging (Q_{dl}). Thus

$$Q_{\text{total}}^{n\text{-hex}} = Q_{\text{ads}}^{n\text{-hex}} + Q_{\text{electrode}} + Q_{\text{diff}}^{n\text{-hex}} + Q_{\text{dl}} \quad (1)$$

To assess the correction to be made for the last three terms in eq 1, Q_{total} for a given time of adsorption was investigated as a function of stripping rate (anodic current density). Typical results are shown in Figure 1.¹⁶ The data taken after 49 sec at 0.20 v represent a situation where considerable adsorption has occurred. The data after 10 msec at 0.20 v are similar to those found with N₂ and represent a situation where insignificant adsorption can occur. In this case

$$Q_{\text{total}}^{\text{N}_2} = Q_{\text{electrode}}^{\text{N}_2} + Q_{\text{diff}}^{n\text{-hex}} + Q_{\text{dl}}^{\text{N}_2} \quad (2)$$

If the three quantities on the right-hand side of eq 2 were identical with those in eq 1, then

$$Q_{\text{total}}^{n\text{-hex}} - Q_{\text{total}}^{\text{N}_2} = Q_{\text{ads}}^{n\text{-hex}} \quad (3)$$

In general, one would not expect $Q_{\text{ads}}^{n\text{-hex}}$ to depend on the rate of charging and hence nondependence of this difference on anodic charging rate would indicate good allowance for the last three terms in eq 1 and accurate measure of $Q_{\text{ads}}^{n\text{-hex}}$.

The difference is independent of current density over more than two orders of magnitude (Figure 1). Similar results were found over a wide range of conditions (0.20–0.40 v, 10–200 sec of adsorption) and this suggests not only that correct allowance is being made for electrode oxidation but also that the stripping charge, $Q_{\text{ads}}^{n\text{-hex}}$, corresponds exactly to the charge to oxidize all the adsorbate to CO₂. This assumption is used in our further considerations of the data. Measurements were generally taken at 10–20 ma/r cm².

Adsorption Kinetics. Typical data for a foil electrode in stagnant solution are shown in Figure 2. We see that, initially, $Q_{\text{ads}}^{n\text{-hex}}$ increases linearly with $\tau_{\text{ads}}^{1/2}$ at 0.20 and 0.30 v. Eventually, divergence from linearity is found and this is more rapid at the higher potential. At 0.40 v the adsorption rate is always lower than at 0.20 and 0.30 v. Similar effects were found in the pressure range 17–250 mm of *n*-C₆H₁₄.

(10) S. Gilman, *J. Phys. Chem.*, **67**, 78 (1963).

(11) This assumption is discussed in detail by S. B. Brummer, *J. Phys. Chem.*, **69**, 562 (1965).

(12) J. Timmermans, "Physico-Chemical Constants of Pure Organic Compounds," Elsevier Publishing Co., New York, N. Y., 1950.

(13) Monsanto Technical Bulletin No. P-26, Monsanto Chemical Co., St. Louis, Mo.

(14) J. Giner, *J. Electrochem. Soc.*, **111**, 376 (1964).

(15) "Adsorbed *n*-hexane" is to be taken to mean material adsorbed from solutions containing *n*-hexane. It is not meant to imply that the adsorbate is *n*-hexane itself.

(16) The method used to derive the Q_{total} values was described in ref 3. This minimizes possible errors from Q_{dl} . Also, we may note that the possible contribution of $Q_{\text{diff}}^{n\text{-hex}}$ is very small so that the major correction to be made is $Q_{\text{electrode}}$.

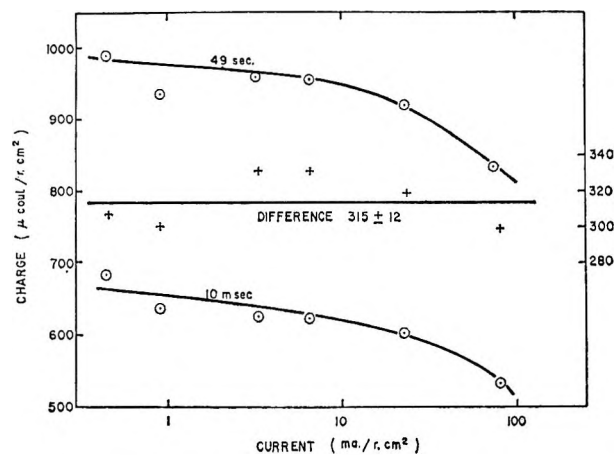


Figure 1. Stripping charge as a function of measuring current density for n -hexane adsorbed at 0.20 v for 49 sec under 115 mm partial pressure.

The initial Q vs. $\tau^{1/2}$ plots, similar over a range of potential, suggest that adsorption onto a clean electrode is limited by diffusion in the solution. This was found previously for the adsorption of C_3H_8 .^{1,2} The slopes of these linear Q vs. $\tau^{1/2}$ plots at low potentials are shown in Figure 3 as a function of n - C_6H_{14} pressure. The slope $dQ/d\tau^{1/2}$ is linear in p and the plot goes through the origin. This substantiates that the initial rate of adsorption of n - C_6H_{14} is limited by diffusion in the solution and suggests that the initial adsorbate is similar over a range of potentials. The latter indicates that the initial adsorbate is virtually unchanged (*i.e.*, perhaps slightly dehydrogenated) n - C_6H_{14} .

A diffusion coefficient for n - C_6H_{14} may be calculated from the line in Figure 3. Thus the slope of the line is $605 \mu\text{coulombs/g cm}^2 \text{ sec}^{1/2}$. This should equal $2nF \cdot (D/\pi)^{1/2} H$ ¹⁷ for accumulation of adsorbate at a rate limited by semiinfinite linear diffusion. Here, n is the number of electrons involved in oxidizing the adsorbate ($n = 38$ for n - C_6H_{14} to CO_2), F the faraday, D the diffusion coefficient, and H Henry's law coefficient for n - C_6H_{14} in 80% H_3PO_4 . If we take H as 3.9×10^{-8} mole/cc atm,¹⁸ we can calculate a value of 1.6×10^{-5} cm^2/sec for D . This is a minimum value for D ,¹⁸ but even so it is a little higher than expected. Thus, using Walden's rule it predicts somewhat too high a value for D in room-temperature water. Similarly, the value is higher than that calculated for C_3H_8 in 78% acid, 0.79×10^{-5} .¹⁹

Both of these values, and the complex fuel solubility-temperature- H_3PO_4 concentration relations,¹⁸ suggest that the hydrocarbons may be effective Frank-Evans²⁰ "structure breakers" of the highly associated concentrated H_3PO_4 solution. If this is so, the larger n - C_6H_{14} molecule is apparently the more effective. The

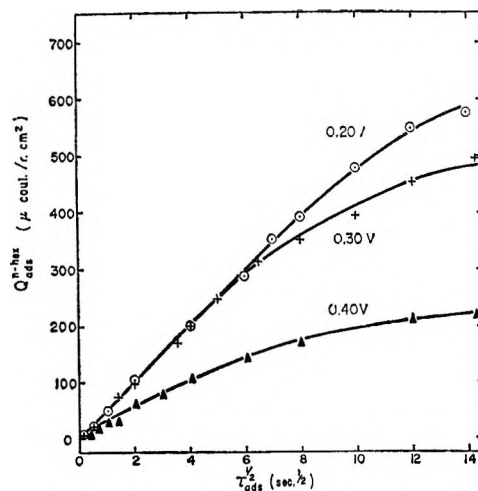


Figure 2. Adsorption of n -hexane as a function of time and potential under 127 mm partial pressure ($R \approx 2.25$).

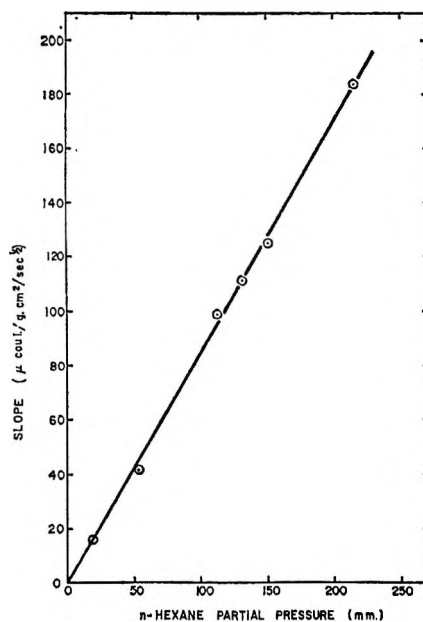


Figure 3. Slope of Q vs. $\tau^{1/2}$ plots at 0.20 v as a function of n -hexane partial pressure.

(17) H. A. Laitinen and I. M. Kolthoff, *J. Am. Chem. Soc.*, **61**, 3344 (1939).

(18) This value is taken from a report by K. E. Gubbins and R. D. Walker (University of Florida) on Contract DA 49-186-45(X), June 1965. The figure refers to 85% H_3PO_4 and examination of the concentration dependence of their data and of that reported by the General Electric Co. (on Contracts DA 44-009-AMC-479(T) and DA 44-009-ENG-4909, Dec 1964, June 1965, Dec 1965) suggests a lower value in 80% H_3PO_4 . This would raise the actual diffusion coefficient compared with that calculated here. Similarly, the value taken for $n(38)$ assumes that the adsorbate is unchanged n - C_6H_{14} . Since dissociative adsorption followed by H_{ads} ionization is very likely, this is a maximum value. Lowering n would also raise the value of D .

(19) Recalculated from the data of ref 2 based on the vapor pressure of 78% H_3PO_4 rather than the 80% acid reported in ref 2.

(20) H. S. Frank and M. W. Evans, *J. Chem. Phys.*, **13**, 507 (1945).

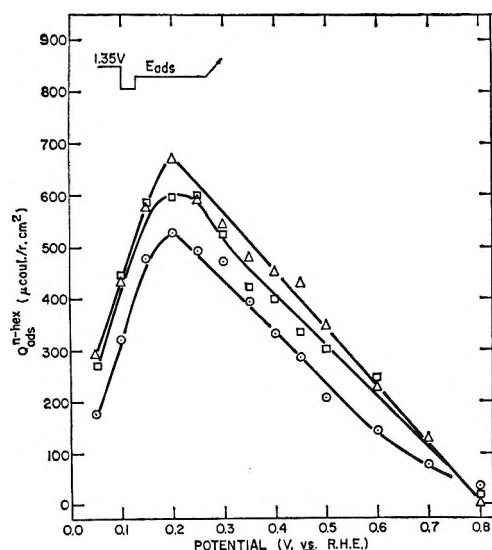


Figure 4. Steady-state adsorption of n -hexane as a function of potential at 130°: \circ , 17 mm; \square , 46.5 mm; Δ , 102 mm partial pressure.

values of D for n - C_6H_{14} are eminently reasonable and if anything a little high. There is then no conflict with the previous conclusion that initial adsorption is limited by fuel diffusion in the solution.

Steady-State Adsorption of n - C_6H_{14} . Eventually, at each potential, the amount of adsorbate reaches a steady state. This is shown as a function of potential and pressure in Figure 4. The procedure for obtaining $Q_{ads}^{C_6H_{14}}$ was as follows. After cleaning the electrode, the solution was left unstirred for 60 sec to begin formation of an adsorbed layer without appreciable competition from impurities.²¹ The solution was then gas stirred to allow adsorption and reaction of n - C_6H_{14} . This also equilibrates the solution in the vicinity of the electrode with the bulk. Finally, stirring was discontinued for 60 sec to allow quiescent conditions to be reestablished before applying the anodic stripping pulse. Variation of this time without stirring from 5 sec to 5 min gave no change in Q_{ads}^{n-hex} , indicating no mass-transport problems in the steady state.

We see (Figure 4) that adsorption is appreciable over the whole range from 0.05 to 0.80 v with a maximum of oxidizable material at ~ 0.20 v. The data are very similar to those for C_3H_8 ,¹⁻³ although the maximum charge to oxidize the adsorbate is a little higher here. Increasing n - C_6H_{14} pressure causes greater adsorption but the effect is small; *i.e.*, the increase in Q_{ads}^{n-hex} is less than linear with pressure. Indeed it increases more directly as $\log p$, as might perhaps be expected for a Temkin adsorption isotherm. The approximate linearity of the Q vs. E data of Figure 4 might also suggest a Temkin isotherm but, as has been pointed out,⁵ cau-

tion must be used in interpreting the data in any such way owing to the two observations that part of the adsorption is irreversible and that the adsorbate comprises more than one species. In addition, we should note that while Q_{ads}^{n-hex} is an accurate measure of the charge to oxidize the adsorbate, it is not necessarily a good guide to coverage since we shall show that the average oxidation state of the adsorbate changes with potential.

The structure and properties of the steady-state adsorbate are of prime interest in the analysis of the over-all n - C_6H_{14} - CO_2 reaction. Therefore we have emphasized this aspect in our further studies.

As with C_3H_8 , we have found that part of the adsorbate may be cathodically desorbed. This part we call the CH- α species without intending to imply that it is exactly the same as for C_3H_8 but rather that it is generically similar, *i.e.*, a collection of (partly dehydrogenated) alkyl radicals.²² The amount of this material is shown as a function of potential at two n - C_6H_{14} pressures in Figure 5. The experimental procedure for obtaining these curves was as follows. The steady-state adsorbate was obtained as above and the potential was lowered to 0.03 v for 10 sec. This was found to be sufficient to remove all the cathodically desorbable material. The potential was then brought back to the adsorption potential for 1 sec to oxidize any H_2 generated at 0.03 v. No appreciable re-adsorption occurs during this time. The remaining adsorbate, the residue, was then stripped anodically. We then define $Q^{CH-\alpha}$ as $Q_{ads}^{n-hex} - Q_{res}$; these are the data shown in Figure 5.

The variation of $Q^{CH-\alpha}$ with potential and pressure closely parallels the behavior of Q_{ads}^{n-hex} itself (Figure 4). Thus $Q^{CH-\alpha}$ is zero at ~ 0.05 v, increases to a maximum at ~ 0.20 v, and then slowly declines to zero at 0.80 v. This is similar to the behavior found for C_3H_8 ³ save that there is much more CH- α for n - C_6H_{14} . Thus, at the maximum, we find 400 μ coulombs/r cm^2 for n - C_6H_{14} but only 175 μ coulombs/r cm^2 for C_3H_8 despite the fact that the C_3H_8 pressure and Henry's law coefficient are higher; *i.e.*, its actual solution concentration is greater. We may conclude then that an important effect of increasing the size of the adsorbing hydrocarbon is to increase the amount of CH- α material. This was also found by Niedrach and Tochner²³ in the progression from C_3H_8 to n - C_4H_{10} .

(21) In unstirred solutions, we find no impurity adsorption (<10 μ coulombs/r cm^2) in 100 sec.

(22) The nomenclature for the adsorbed species was discussed in ref 3 and 5. Briefly, those species which we judge (perhaps partly by analogy with the data for C_3H_8) to have most of the C-H bonds of the hydrocarbon converted to C-O bonds we call O types. Those where most of the C-H bonds are intact are called CH types.

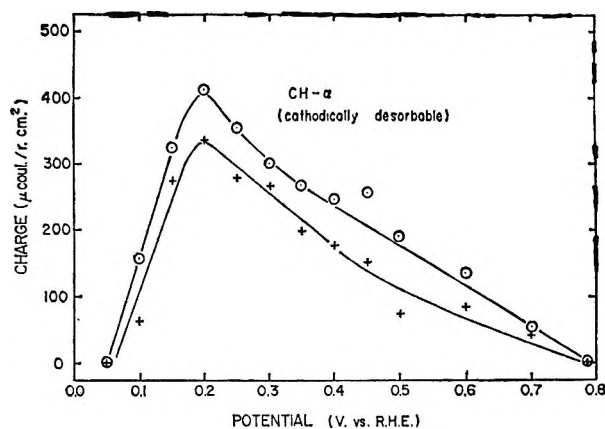


Figure 5. Charge lost on cathodic desorption for *n*-hexane (CH- α) as a function of potential at 130°: +, 17 mm; ○, 102 mm.

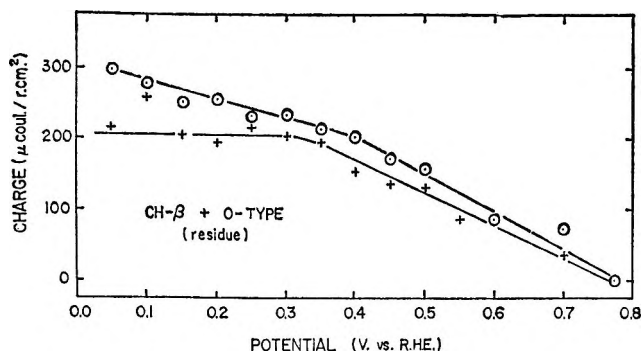


Figure 6. Charge to oxidize noncathodically desorbable residue for *n*-hexane as a function of potential at 130°: +, 17 mm; ○, 102 mm.

The effect of pressure on $Q^{\text{CH-}\alpha}$ is small but more significant at more anodic potentials, where oxidation of *n*-C₆H₁₄ becomes significant. A similar result was reported for C₃H₈, but there, $Q^{\text{CH-}\alpha}$ was sensitive to pressure at all potentials.

The charge remaining after removal of CH- α , Q_{res} , is shown as a function of potential and pressure in Figure 6. We see that Q_{res} is relatively insensitive to potential. Thus from 0.05 to 0.80 v, it decreases from ~300 $\mu\text{coulombs/r cm}^2$ to zero at 102 mm and from ~210 $\mu\text{coulombs/r cm}^2$ to zero at 17 mm. Apart from the point at 0.05 v, the effect of pressure is small and there is never more than a 20% change in Q_{res} over a sixfold pressure range. It is significant that the dependence of Q_{res} on p is least at anodic potentials where the overall *n*-C₆H₁₄-CO₂ reaction goes at an appreciable rate. This suggests that the residue is not involved directly in the over-all reaction. This is discussed later.

Fine Structure of the Residue. The fine structure of the residue can be studied with the anodic desorption

method developed earlier and used to characterize HCOOH_{ads},²⁴ CO_{ads},²⁵ and C₃H₈.^{2,3} The procedure is as follows. We adsorb the steady-state coverage with fuel at a given potential, desorb the CH- α , and return to E_{ads} to oxidize H₂. This isolates the residue on the electrode. Then we raise the potential such that normally little or no adsorption occurs (e.g., 0.80 v). The residue slowly oxidizes (or desorbs) and we follow the desorption of the adsorbed residue. Specifically we follow Q_{res} and θ_{org}^c as a function of time. θ_{org}^c is the fraction of the surface occupied by organic and is determined by cathodic H-atom deposition. The use of this method to estimate coverage has been discussed in detail in ref 3 and 24. The slope of the Q vs. θ plot gives us $[e]$, the number of electrons released per covered site on oxidation of the adsorbate (to CO₂). $[e]$ is obviously of prime importance in defining the oxidation state of the residues and in attempting to establish their relationship to the original fuel. Changes in $[e]$ during the analysis (desorption) of a given preformed residue are taken as evidence for the presence of different adsorbed species in the original adsorbate or at least as a sign of different modes of bonding within the original adsorbate.³

Results²⁶ for residues produced at various potentials under 17 mm partial pressure of *n*-C₆H₁₄ are shown in Figure 7. It is evident that the residue consists of two parts at each potential. The first part, which is most readily oxidized at 0.80 v, covers about 40% of the electrode and releases 1.4 electrons per site when it is oxidized. This is clearly to be equated to the O-type species found for C₃H₈ for which $[e]$ is 1.3.³ Such a low $[e]$ value strongly suggests the substantial oxygenation of this material. We note that as for C₃H₈ this, the most highly oxidized species, is the easiest to oxidize further, at least at high potentials.

The second part of the residue to oxidize at 0.80 v covers less than 10% of the electrode and has an $[e]$ value of 5.5 ± 1.5 electrons per site. This value obviously implies minor, if any, oxygenation of the residue. The species is generically similar to the CH- β , or polymeric, adsorbate found with C₃H₈, but it is evidently

(23) L. W. Niedrach and M. Tochner, Report by General Electric Co. on Contract DA 44-009-AMC-479(T), Dec 1965; *J. Electrochem. Soc.*, **114**, 17 (1967).

(24) See S. B. Brummer, ref 11.

(25) S. B. Brummer and J. I. Ford, **69**, 1355 (1965).

(26) After short times at 0.80 v, a small reduction wave (oxide?) is found during the measurement of θ_{H}^c ($= 1 - \theta_{\text{org}}^c$). This wave slightly interferes with the accurate determination of θ_{H}^c . To eliminate it, an extra potential step (2.5 msec at 0.60 v) was inserted before applying the cathodic current pulse. This extra potential step did not change the amount of adsorbed material being analyzed from the 0.80-v step.

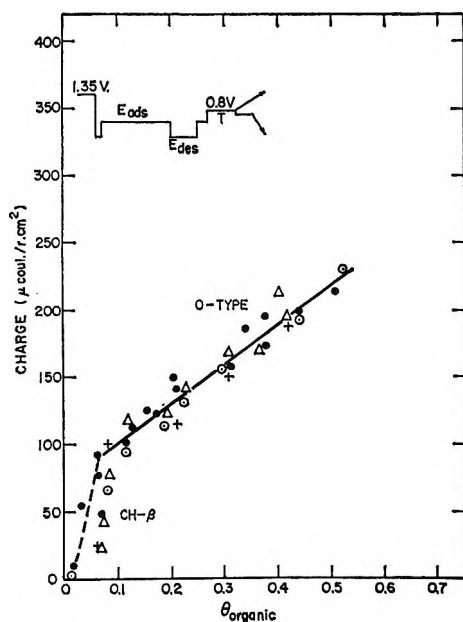


Figure 7. Desorption at 0.80 v of noncathodically desorbable material adsorbed at various potentials under 17 mm of *n*-hexane at 130°: +, 0.15 v; Δ, 0.20 v; ○, 0.25 v; ●, 0.35 v.

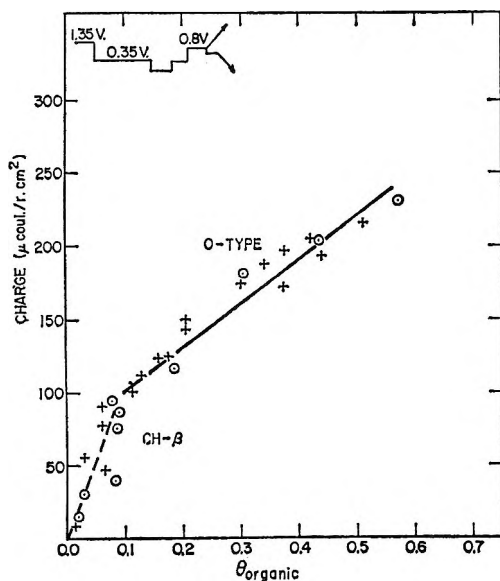


Figure 8. Desorption at 0.80 v of noncathodically desorbable material, adsorbed at 0.35 v under various pressures of *n*-hexane at 130°: +, 17 mm; ○, 102 mm.

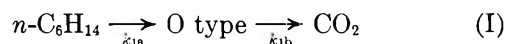
not the same material since $[e]_{\text{CH-}\beta}$ for C_3H_8 was lower, *e.g.*, 4.1 at 0.22 v and 2.5 at 0.30 v.

The structure of the adsorbed residue is, then, exactly analogous to that for the lower hydrocarbon, C_3H_8 . One of the species, O type, is in fact identical for the two hydrocarbons. The other, CH- β , is more reduced for $n\text{-C}_6\text{H}_{14}$ than for C_3H_8 . Also, the composition and the

amount of adsorbed CH- β are not evident functions of the potential of adsorption as they were with C_3H_8 .

The relative amounts of O type and CH- β are not sensitive to the pressure (Figure 8) and this shows, as found with C_3H_8 ,³ that the insensitivity of the residue to fuel pressure reflects the fact that both of its components are pressure insensitive. This has important implications for the involvement of the adsorbed species in the over-all $n\text{-C}_6\text{H}_{14}\text{-CO}_2$ reaction.

Role of Adsorbed Species in Over-All Reaction. The results of this investigation confirm those reported for C_3H_8 .³ Thus, while the oxidation of O type is the easiest of all the adsorbed species, its coverage is not sufficiently pressure sensitive to allow the conclusion that it is in fact involved in the over-all reaction. Thus, in the scheme



the over-all rate would have to equal the oxidation rate of O type. Since the current is pressure sensitive, coverage with O type would have to be pressure sensitive, particularly at more anodic potentials. Since $\theta_{\text{O type}}$ is not pressure sensitive, the reaction does not proceed *via* O type.²⁷ We have already discussed the implication of this conclusion,³ which is that since the formation of O type probably consumes very reactive intermediates to form a refractory residue, it may be the worst possible thing that can happen on the working anode.

One must then attempt to correlate the over-all reaction with the properties of one of the other adsorbed species since oxidation of $n\text{-C}_6\text{H}_{14}$ to CO_2 without adsorption seems unlikely. The CH- β material does not seem a likely candidate since it is very refractory toward oxidation and its coverage is not sensitive to pressure.

The sensitivity of $Q_{\text{CH-}\alpha}$ toward p at anodic potentials suggests its possible involvement in the over-all reaction, but there are two difficulties with postulating the reactivity of the CH- α species: its amount increases with increasing molecular weight while the over-all hydrocarbon reactivity decreases and the observation, both here and by others,^{23,28-30} that oxidation of CH- α at high potentials is more difficult than that of O type.

The possible solution of the second difficulty may be

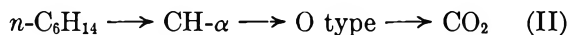
(27) This is not to say that reaction I cannot occur—it definitely can, *e.g.*, in the stripping of the adsorbed layer—but rather that at low potentials it does not represent the path that the hydrocarbon-carbon dioxide reaction actually does take.

(28) S. Gilman, *Trans. Faraday Soc.*, **61**, 2561 (1965).

(29) L. W. Niedrach, S. Gilman, and I. Weinstock, *J. Electrochem. Soc.*, **112**, 1161 (1965).

(30) L. W. Niedrach, *ibid.*, **113**, 645 (1966).

that CH- α oxidation has a lower potential dependence than O-type oxidation and is relatively faster at low potentials. Then the *parallel reactions* which form CH- α and O type could lead to the observations. Note that involvement of CH- α implies that a consecutive sequence

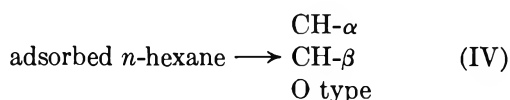
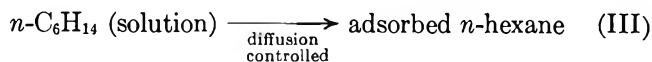


is impossible because of the insensitivity of θ_{Otype} on p .

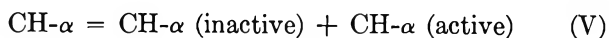
The possible solution to the molecular weight effect on CH- α is to postulate that this material comprises several distinct parts, some active and some inactive. Such a hypothesis is clearly reasonable in terms of what we know about hydrocarbon cracking³¹ and the products of hydrogenation of the CH- α material.³² Thus, we know that for C₃H₈, CH- α comprises C₁, C₂, and C₃ fragments. Niedrach³⁰ has suggested that the C₁ fragments may be the reactive species and we have indicated that the possible ready formation of O type from these C₁ fragments could be the major stumbling block to the efficient usage of the electrode for the over-all reaction.

If a certain part of the CH- α material is active in the over-all reaction, then growth of CH- α with molecular weight and the lesser activity of the higher hydrocarbons may suggest that at sufficiently high molecular weights the inefficiency of CH- α utilization to produce the active species (*e.g.*, C₁ fragments) becomes the major stumbling block in the over-all scheme. The low value for θ_{Otype} and the high values of $Q_{\text{CH-}\alpha}$ for $n\text{-C}_6\text{H}_{14}$ compared with C₃H₈ certainly support this contention.

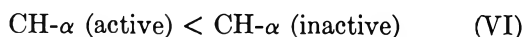
The following represents our present views on the mechanism of hydrocarbon oxidation. In the *transient* condition, we have



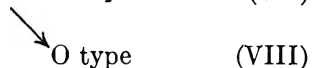
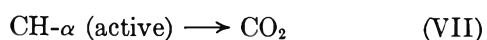
Further, we postulate that



Here



and



The major inefficiency in use of the surface results either from reaction V or from reaction VIII. With the lower hydrocarbons, reaction VIII, the formation of O type, is postulated. For higher hydrocarbons, reaction V is probably the culprit.

The mechanism above is tentative. If it were true, we would still have to decide whether in the *steady-state* rate limitation of the over-all reaction occurs from reaction VII or from the slowness of the initial adsorption, reaction III. We can see, however, that even without a complete knowledge of the mechanism of this over-all process, the most urgent priority for improving the efficiency of the reaction is to understand the modes of formation and oxidation of the reaction-blocking species, CH- α (inactive) and O type.

IV. Summary and Conclusions

(1) Anodic stripping is a quantitative method to estimate "adsorbed n -hexane" in 80% H₃PO₄ at 130°.

(2) Initial adsorption at low potentials is limited by diffusion in solution. The initial adsorbate is almost unchanged $n\text{-C}_6\text{H}_{14}$.

(3) Steady-state adsorption is low below 0.05 v, increases to a maximum at ~ 0.20 v, and decreases to zero by 0.80 v. The adsorption increases with $n\text{-C}_6\text{H}_{14}$ pressure but less than proportionally.

(4) The steady-state adsorbate is not entirely the originally adsorbed $n\text{-C}_6\text{H}_{14}$. Thus, part of the adsorbate, the CH- α material, can be cathodically desorbed. This material probably consists of (partially dehydrogenated) alkyl radicals. $Q_{\text{CH-}\alpha}$ shows the same potential dependence as $Q_{\text{ads}}^{n\text{-hex}}$, *i.e.*, it is zero at 0.05 v, increases to a maximum at ~ 0.20 v, and subsequently slowly declines to zero at 0.80 v. The amount of CH- α is much larger for $n\text{-C}_6\text{H}_{14}$ than C₃H₈.³ $Q_{\text{CH-}\alpha}$ is sensitive to $n\text{-C}_6\text{H}_{14}$ pressure, particularly at anodic potentials where the over-all oxidation process $n\text{-C}_6\text{H}_{14} \rightarrow \text{CO}_2$ is appreciable.

(5) The residue, that part of the steady-state adsorbate not cathodically desorbable, is insensitive to $n\text{-C}_6\text{H}_{14}$ pressure. It comprises two parts, the CH- β and O type. Oxidation of these two materials releases 5.5 and 1.4 electrons per site, respectively.

(6) The O type, which is probably oxygenated, is similar to the species found for C₃H₈³ and is identical⁷ with the "reduced CO₂" of Giner.^{6,33,34} Its oxidation at high potentials (0.70 and 0.80 v) is easier than that

(31) G. C. Bond. "Catalysis by Metals," Academic Press Inc., New York, N. Y., 1962.

(32) L. W. Niedrach, *J. Electrochem. Soc.*, **111**, 1309 (1964).

(33) J. Giner, *Electrochim. Acta*, **9**, 63 (1964).

(34) J. Giner, paper presented at C.I.T.C.E. Meeting in London, England, Sept 1964.

of CH- β or CH- α , but its insensitivity to n -C₆H₁₄ pressure rules out its direct involvement in the over-all reaction.

(7) Present evidence suggests that O type, CH- β , and most of the CH- α adsorbates are inactive for the over-all reaction. Indeed, they are deleterious both in blocking the surface and in "locking up" what would otherwise be a large concentration of an active intermediate. This active intermediate is postulated to be part of the CH- α material. It is suggested that formation of O type is the major inefficiency for use of the surface by low hydrocarbons, e.g., C₃H₈, and formation of inactive CH- α is the major problem for higher hydrocarbons.

Acknowledgments. We are pleased to acknowledge support of this work by the U. S. Army Engineer Research and Development Laboratories, Fort Belvoir, Va., on Contract DA 44-009-AMC-1408(T).

Appendix

Notation

CH- α , CH- β Types of adsorbate in which most of the C-H bonds in the original hydrocarbon have not been converted to C-O bonds

E	Potential (voltage <i>vs.</i> reversible hydrogen electrode)
E_{ads}	Potential of adsorption
E_{des}	Potential of desorption
$[e]_i$	Average number of electrons released in the complete oxidation to CO ₂ of adsorbed species i per surface atom which it covers
geom cm ² or g cm ²	Geometric area of the electrode
Q	Charge (μ coulombs/r cm ²)
Q_{ads}^{u-hex}	Charge to oxidize adsorbed n -hexane
$Q_{CH-\alpha}$	Charge lost on cathodic desorption
Q_{res}	Charge to oxidize noncathodically desorbable residue
O type	Type of adsorbate in which most of the C-H bonds in the original hydrocarbon have been converted to C-O bonds
rhe	Reversible hydrogen electrode
real cm ² or r cm ²	Real area, equivalent to 210 μ coulombs for the maximum cathodic H-atom charge on a clean electrode
θ_i	Fraction of surface covered by species i
θ_H^c	Ratio of the cathodic H-atom charge under a given circumstance to the maximum value (clean surface) at the same temperature
θ_{org}^o	Fraction of the surface covered by organic, operationally defined as $(1 - \theta_H^c)$
τ	Time, sec
τ_{ads}	Time of adsorption
τ_{des}	Time of desorption
τ_E	Time at potential E

Quantitative Studies of Ultrasonic Vibration Potentials in

Polyelectrolyte Solutions^{1a}

by R. Zana^{1b} and E. Yeager

Department of Chemistry and Condensed State Center, Case Western Reserve University, Cleveland, Ohio
(Received March 29, 1967)

The propagation of ultrasonic waves through polyelectrolyte solutions gives rise to alternating potential differences (polyelectrolyte vibration potentials) within the solution. A theory for the effect is developed on the basis of the polymer bead model and the earlier theoretical treatment for ionic vibration potentials. Measurements of the polyelectrolyte vibration potentials at 220 kHz have been carried out with polyacrylic acid and other polyelectrolytes as a function of concentration of polyelectrolyte, per cent neutralization, and the nature and concentration of added salts. The agreement between theory and experimental values is quantitative. Polyelectrolyte vibration potential measurements appear capable of providing information concerning counterion bonding and the volumes of the monomer units within the polymer beads.

I. Introduction

The interaction of sound waves with ions in solutions gives rise to alternating potential differences within the solution.²⁻⁴ While this electrical effect has been studied quantitatively in simple ionic solutions⁵ and colloidal suspensions,³ relatively little attention has heretofore been given to polyelectrolyte solutions.⁴ The purpose of the present paper is to present quantitative results for polyelectrolytes and to interpret them in terms of a proposed mechanism.

Ultrasonic vibration potentials were first predicted for simple ionic solutions by Debye⁶ in 1933, but experimental verification² of the existence of the effect was not realized until 1949. This delay reflects difficulties associated with the detection and measurement of the effect principally because of the small magnitude (less than $10 \mu\text{v cm}^{-1} \text{ sec}$). Recently, substantial improvements in apparatus have made possible quantitative measurements of ionic vibration potential (ivp) with an accuracy of $\pm 5\%$. Data obtained with this apparatus have been used for the direct evaluation of the partial molal volumes for individual ions.⁵

The generation of ac potentials in colloidal suspensions was first predicted by Rutgers⁷ in 1938 and has been treated theoretically by various workers.⁸⁻¹¹ The large magnitude of colloidal vibration potentials (cvp)

(up to $10^{-2} \text{ v cm}^{-1} \text{ sec}$) has facilitated the quantitative measurement of this effect.^{3,12,13}

The first detection and preliminary measurements of polyelectrolyte vibration potentials⁴ (pvp) were reported in 1962. Because of the limited accuracy of the data, however, these measurements were semiquantitative at the best and did not reveal any special promise for the effect as a tool for the study of polyelectrolytes.

(1) (a) Research supported by the U. S. Office of Naval Research; (b) on leave from CRM-CNRS, Strasbourg, France.

(2) E. Yeager, J. Bugosh, F. Hovorka, and J. McCarthy, *J. Chem. Phys.*, **17**, 411 (1949).

(3) E. Yeager, H. Dietrick, and F. Hovorka, *J. Acoust. Soc. Am.*, **25**, 456 (1953).

(4) J. Booker, E. Yeager, and F. Hovorka, Proceedings of the Fourth International Congress on Acoustics, Copenhagen, 1962, Paper J45.

(5) R. Zana and E. Yeager, *J. Phys. Chem.*, **70**, 954 (1966); **71**, 521 (1967).

(6) P. Debye, *J. Chem. Phys.*, **1**, 13 (1933).

(7) A. Rutgers, *Physica*, **5**, 46 (1938).

(8) J. Hermans, *Phil. Mag.*, **25**, 426 (1938); **26**, 679 (1938).

(9) J. Vidts, *Mededel. Koninkl. Vlaam. Acad. Wetenschap., Belg. Kl. Wetenschap.*, **3**, 5 (1945).

(10) J. Enderby, *Proc. Roy. Soc. (London)*, **A207**, 329 (1951).

(11) F. Booth and J. Enderby, *ibid.*, **A208**, 321 (1952).

(12) A. Rutgers and J. Vidts, *Nature*, **165**, 109 (1950).

(13) J. Causse, *Compt. Rend.*, **230**, 826 (1950).

With the development of more sophisticated apparatus, quantitative measurements with accuracies of $\pm 5\%$ have become possible. No comprehensive theoretical treatment of pvp, however, has been presented, at least in part because of the formidable complexity of the hydrodynamic and electrical problems involved in carrying out such a treatment for polyelectrolytes.

II. Possible Models for Polyelectrolyte Vibration Potentials

The mechanism of pvp can be appreciated by considering the behavior for two extremes of configuration for a polyion. If the polyion has a tightly coiled configuration, then it may be considered the equivalent of a charged sphere surrounded by an ionic atmosphere of predominantly opposite charge under some conditions, particularly at low ionic strength. Under these circumstances, pvp should be generated according to a mechanism analogous to that involved in cvp and illustrated in Figure 1. In the presence of the material waves, the normally symmetrical ionic atmosphere surrounding each colloidal particle is periodically distorted because of differences in the dynamic reactions of the central colloidal particle and the simple ions of the ionic atmosphere. The sine curve in Figure 1 represents a sound wave traveling through the suspension. The lengths of the arrows indicate the relative displacement of the colloidal particle and the ions. For purposes of illustrations, the colloidal particles have arbitrarily been assumed to have a negative charge and the ions in the surrounding atmosphere to be predominantly positive. The periodic distortion of the ionic atmosphere gives rise to an alternating dipole and consequently alternating potentials between positions separated by a phase distance other than an integral multiple of the wavelength. This mechanism henceforth in this paper will be referred to as the cvp mechanism.

The expression given by eq 1 and 1a has been developed for cvp by Enderby¹⁰

$$\frac{\Phi}{a} = 3.0 \times 10^5 \frac{n_c W_c R_c z_c}{\eta u} \frac{B}{(1+b)(b^4 + \gamma^2)^{1/2}} \quad (1)$$

where

$$\gamma = \omega R_c^2 / \eta k t \quad (1a)$$

Φ is the rms potential in volts, a is the rms velocity amplitude of the sound waves of angular frequency ω , η is the viscosity of the solution, n_c is the number of colloidal particles per unit volume, W_c is the apparent mass of the average colloidal particle (mass of the particle minus the mass of the free displaced solvent), R_c and z_c are the radius and number of unit charges for

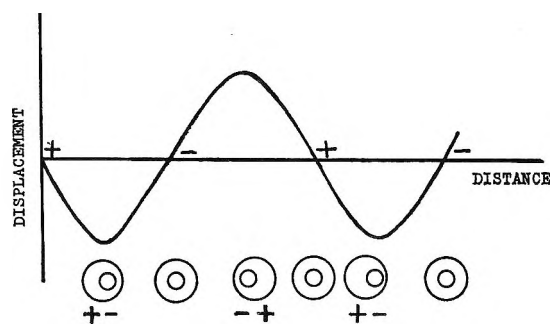


Figure 1. Mechanism for colloidal vibration potentials.

the average colloidal particle, u is the average mobility of the ions in the ionic atmosphere, and b is the ratio of the particle radius R_c to the Debye-Hückel thickness ($1/\kappa$) of the ionic atmosphere. The function B depends on b and ranges from 96 to 144. Equation 1 is applicable only for a uni-univalent supporting electrolyte and is further restricted by the assumption that the mobility of the anions and the cations of the ionic atmosphere are approximately equal. A more complete equation is available.¹¹ From eq 1, it is apparent that the observed ac potentials will tend to be largest for high colloid concentrations and low ionic concentrations. Such has been verified experimentally for colloidal suspensions of silica.³

When the polyion is in an extended configuration, various portions of the polymer molecule may be considered to behave somewhat independently of each other. Under such circumstances the mechanism for the generation of pvp might be expected to be closer to that for ivp. Differences in amplitude and phase of the displacements of the various ions including the polyions lead to periodic excesses of charge at any point in the sound field and consequently to alternating potential differences.¹⁴

The theoretical treatment of ivp¹⁵ yields eq 2 for the rms potential

$$\frac{\Phi}{a} = 0.155 \left[\frac{W_+ t_+}{z_+} - \frac{W_- t_-}{z_-} \right] \quad (2)$$

where Φ is in microvolts and a is in centimeters per second. The subscripts $+$, $-$ refer to cations and anions, respectively. The quantities W , t , and z are the apparent molar mass, the transport number, and the number of unit charges on the ionic species indicated by the subscripts. The apparent molar mass is defined

(14) Figure 1, ref 5, will help the reader to understand the mechanism for the generation of ivp.

(15) J. Bugosh, E. Yeager, and F. Hovorka, *J. Chem. Phys.*, **15**, 592 (1947).

as the molar mass of the solvated ion minus that of the free displaced solvent.

For actual solutions of polyelectrolytes, it is doubtful whether either the ivp or cvp model can be used vigorously to interpret the observed data; eq 1 and 2, however, can be used to identify critical parameters which must be considered. The ivp model seems more appropriate in terms of present concepts of polyelectrolyte even in the unneutralized state since the polyions can hardly be considered ordinarily as a tightly coiled polymer molecule.^{16,17}

III. Development of the Ivp Model for Polyelectrolytes

The bead model for describing the dynamic properties of polymers as developed by Debye¹⁸ is particularly appropriate for interpreting the dynamic behavior of polyions in sound fields. At ultrasonic frequencies, low compared to the mass relaxation frequency,¹⁹ the displacements of the polymer molecules relative to the solvent as well as one portion of the polymer relative to other portions of the same polymer molecule during the propagation of the sound waves through the system are very small. Consequently, the various segments or beads of the polymer can be viewed as moving independently in considering only first-order dynamic effects of the material waves.

If electrophoretic and relaxation terms associated with the ionic atmosphere and the diffusion term are neglected, the general expression for ionic vibration potential per unit velocity amplitude in water is¹⁵

$$\frac{\Phi}{a} = \phi = k \frac{\sum n_j z_j w_j}{\rho_j} \bigg/ \frac{\sum n_j z_j^2}{\rho_j} \quad (3)$$

where k is a constant, n_j is the number of ions of the j type per unit volume, ρ_j is the frictional coefficient, z_j is the charge, and w_j is the apparent mass.

For a solution containing a polyacid P partially neutralized with a base GOH, the species present in the solution and the corresponding values for n_j and z_j are given by eq 4-6 for polymer beads, hydrogen ions, and G cations, respectively

$$z_B = -\theta(1 - \beta)X; \quad n_B = NC_P/X \quad (4a,b)$$

$$z_H = +1; \quad n_H = N(\theta - \alpha)C_P \quad (5a,b)$$

$$z_G = +1; \quad n_G = N(\alpha - \theta\beta)C_P \quad (6a,b)$$

where α is the per cent neutralization, θ is the fraction of the acid groups on the polyion which are ionized, X is the number of monomer units per polymer bead, C_P is the polymer concentration, and N is Avogadro's number. The counterion binding is taken into account by the introduction of β which corresponds to the frac-

tion of the charge on the polymer bead compensated by associated univalent cations.

In eq 3 all values of w_j are known from the molecular weights and partial molal volumes⁵ except the apparent mass of the polymer bead w_B . It has been shown⁵ that

$$w_j = (M_j - s_0 \bar{V}_j)/N \quad (7)$$

where s_0 is the solvent density and M_j and \bar{V}_j are the molecular weight and the partial molal volume of the j species. The frictional coefficients ρ_j also are known from transport or diffusion coefficients for all species except the polymer bead. From eq 3 to 6, the pvp in microvolts per unit velocity amplitude (1 cm/sec) is

$$\phi_{\alpha,0} = 0.155 \frac{(\theta - \alpha)W_H u_H + (\alpha - \theta\beta)W_G u_G - W_M u_B}{(\theta - \alpha)u_H + (\alpha - \theta\beta)u_G + (1 - \beta)\theta u_B} \quad (8)$$

where W_j is the apparent molar mass of the species indicated by the subscript and

$$W_B = XW_M; \quad u_B = (1 - \beta)\theta X/\rho_B \quad (8a,b)$$

The quantities u_H , u_G , and u_B are the mobilities of the species indicated by the subscripts and W_M corresponds to the apparent molar mass per monomer unit in the bead. The apparent molar mass of the monomer is a function of α since the mass of the polymer bead increases principally because of counterion binding when α increases, as will be discussed later (see part VIB, eq 18).

Consider a polyelectrolyte solution containing a univalent salt C^+A^- at a concentration C_S . The counterion binding term β will now be made up of two components, β_G and β_C . These components of the counterion binding term are assumed to be proportional to the relative concentrations of each type of cation present in the solution. Consequently, the concentrations of the bound ions of type G^+ and C^+ are given by the expressions

$$\theta\beta C_P \frac{\alpha C_P}{\alpha C_P + C_S}$$

(16) W. Kuhn, O. Kunzle, and A. Katchalsky, *Helv. Chim. Acta*, **31**, 1994 (1948); A. Oth and P. Doty, *J. Phys. Chem.*, **56**, 43 (1952).

(17) C. Tanford, "Physical Chemistry of Macromolecules," John Wiley and Sons, Inc., New York, N. Y., 1965.

(18) P. Debye, *J. Chem. Phys.*, **14**, 636 (1946).

(19) The mass relaxation frequency corresponds to that frequency at which the product ωm equals ρ where ω is the angular frequency, m the mass of the particle, and ρ the drag coefficient. For simple ions, the mass relaxation frequency is in the range 10^{12} to 10^{13} Hz in aqueous solutions. For the polymer beads in typical linear polyelectrolytes, the mass relaxation frequencies could be expected to be at least 10^{11} Hz and hence still very high compared to the frequencies at which ultrasonic vibration potentials measurements can be made.

and

$$\theta\beta C_P \frac{C_S}{\alpha C_P + C_S}$$

respectively. Under these conditions, the pvp are given by

$$\phi_{\alpha, C_S} = \frac{\phi_P}{1 + K} + \frac{\phi_S}{1 + (1/K)} \quad (9)$$

where

$$\phi_P = 0.155 \frac{(\theta - \alpha)W_H u_H + (\overline{W}u)_{G,C}(\alpha - \theta\beta) - W_M u_B}{(\theta - \alpha)u_H + \bar{u}_{G,C}(\alpha - \theta\beta) + u_B\theta(1 - \beta)} \quad (9a)$$

$$\phi_S = 0.155 \frac{(\overline{W}u)_{G,C} - W_A u_A}{\bar{u}_{G,C} + u_A} \quad (9b)$$

$$K = \left[\frac{\bar{u}_{G,C} + u_A}{(\theta - \alpha)u_H + \bar{u}_{G,C}(\alpha - \theta\beta) + u_B\theta(1 - \beta)} \right] \frac{C_S}{C_P} \quad (9c)$$

with

$$\bar{u}_{G,C} = u_G \frac{\alpha C_P}{\alpha C_P + C_S} + u_C \frac{C_S}{\alpha C_P + C_S} \quad (9d)$$

$$(\overline{W}u)_{G,C} = W_{GUG} \frac{\alpha C_P}{\alpha C_P + C_S} + W_{CUC} \frac{C_S}{\alpha C_P + C_S} \quad (9e)$$

The value for W_M depends on C_S as well as C_{G^+} (see part VIC, eq 20).

If the cations G^+ and C^+ are the same, $(\overline{W}u)_{C,G} = W_{GUG}$, $\bar{u}_{G,S} = u_G$, $\phi_P = \phi_{\alpha,0}$ (see eq 8), and ϕ_S then becomes

$$\phi_{CA} = 0.155 \frac{W_{GUG} - W_{AU_A}}{u_A + u_G} \quad (10)$$

which corresponds to the ivp for a solution containing only the salt C^+A^- (or G^+A^-). Likewise

$$K = \left[\frac{u_G + u_A}{(\theta - \alpha)u_H + (\alpha - \theta\beta)u_G + \theta(1 - \beta)u_B} \right] \frac{C_S}{C_P} \quad (11)$$

The term K can be shown to be the ratio of the conductivity of a solution containing only the salt G^+A^- or C^+A^- at the concentration C_S to the conductance of the polyelectrolyte solution without the salt present, providing u_B is assumed independent of C_S and the ionic atmosphere effects on the conductivity are neglected.

IV. Apparatus and Experimental Procedures

The experiments have been carried out at 220 kHz and 22° with the double-probe technique according to the procedures described in an earlier paper on ivp.⁵ The apparatus was essentially the same except for the input section of the amplifier which afforded higher input impedance to the detection system and hence decreased the loading effects. Much care must be exercised not to cause substantial errors through loading effects particularly with polyelectrolyte solutions of low conductivity. The principal measure taken to increase the input impedance involved the use of a second differential cathode follower stage in advance of the switch assembly used in connecting the detection system to either the probe assembly or the calibrating ac voltage source (see Figure 4 in ref 5). The input impedance of the detection system in the present work was 3 to 4 pf shunted by 1.5 megohms to ground in each channel. The maximum error encountered with the most dilute polyelectrolyte solution involved in the present work as a result of loading effects is estimated not to have exceeded 5%.

Table I indicates the polyelectrolytes which have been examined and their sources. Four different samples of polyacrylic acid (A_1 , A_2 , A_3 , and A_5) were obtained in the form of 25% solutions of the unneutralized acid. The average molecular weights have been determined by viscometry in 2 N NaOH solution according to the equation²⁰ $[\eta] = 4.27 \times 10^{-3} \times P^{0.69}$ where $[\eta]$ is the intrinsic viscosity and P is the degree of polymerization. In preliminary measurements, samples A_3 and A_5 were purified by precipitation in a NaCl-saturated aqueous solution followed by dialysis for 1 week against HCl solutions and for 4 days against distilled water. Subsequent checks of the intrinsic viscosity indicated that the molecular weights of the purified products were slightly higher than those of the initial products because of the loss of low molecular weight components during the precipitation-purification step. For a given polyelectrolyte concentration, however, the pvp of the purified polyelectrolyte was the same as that for the nonpurified material. Consequently, the purification of the PAA samples was not continued for the remainder of the measurements.

The polyelectrolyte concentrations were determined by potentiometric titrations with an excess of NaOH solution in the presence of an excess of NaCl.

The poly-L-glutamic acid (PGA) was obtained in the form of the sodium salt monohydrate (NaPG). Partially neutralized samples were prepared by acidification with HCl of an NaPG solution and subsequent removal

(20) Y. Hittori, Dissertation, Nagoya University, 1954.

Table I: Polyelectrolytes Studied in the Present Work

Name	Formula	Mol wt	Source
Polyacrylic acid (PAA)	$\left[\begin{array}{c} \text{—CH—CH}_2\text{—} \\ \\ \text{CO}_2\text{H} \end{array} \right]_n$	A ₁ , 25,000 ^a A ₂ , 120,000 ^a A ₃ , 130,000 ^a A ₅ , 250,000 ^a	Rohm and Haas Co.
Poly-L-glutamic acid (PGA)	$\left[\begin{array}{c} \text{—CH—CO—NH—} \\ \\ (\text{CH}_2)_2\text{—CO}_2\text{H} \end{array} \right]_n$	74,000	Pilot Chemical Co.
Carboxymethylcellulose (CMC)	$\left[\begin{array}{c} \text{—O—CH—(CHR)}_2\text{—CH—} \\ \quad \quad \\ \text{RH}_2\text{C—CH—O} \end{array} \right]_n$ R = —OCH ₂ CO ₂ H	Unknown (<100,000)	Hercules Powder Co.

^a Determined from viscosity.

of the NaCl by continuous dialysis against distilled water for 4 days at which time no detectable Cl⁻ was revealed by the conventional AgCl test. The degree of neutralization was then calculated from the dry weight of the strongly dialyzed solution and potentiometric titration data. The molecular weight listed in Table I was determined from the average degree of polymerization specified by the manufacturer.

The carboxymethylcellulose (CMC) sample was of low but unknown molecular weight (certainly less than 100,000) and had a degree of substitution between 0.65 and 0.85 as compared with the maximum value of three to be expected if the three OH groups of the glucose monomer are replaced by OCH₂CO₂H. No difference was found in the pvp measurements in solution prepared from CMC powder and those prepared from dialyzed material, thus indicating no significant concentration of extraneous ions.

V. Experimental Results

The concentration dependence of the pvp in the PAA solutions is shown in Figure 2 for unneutralized PAA of various molecular weights and in Figure 3 for various per cent neutralization. In each instance the effect decreases with increasing concentration. This same trend was observed in the neutralized solutions of PGA and CMC (see Figure 4). In contrast, the observed ivp for propionic acid solutions increased with increasing concentrations (see Figure 2) and furthermore it is of opposite phase.²¹ The deviation from linearity in Figures 2-4 cannot be explained on the basis of loading effects but appears to be intrinsic to the mechanism.

Figure 2 indicates that at a given concentration for molecular weights in the range 120,000-250,000, the pvp are essentially the same within the experimental

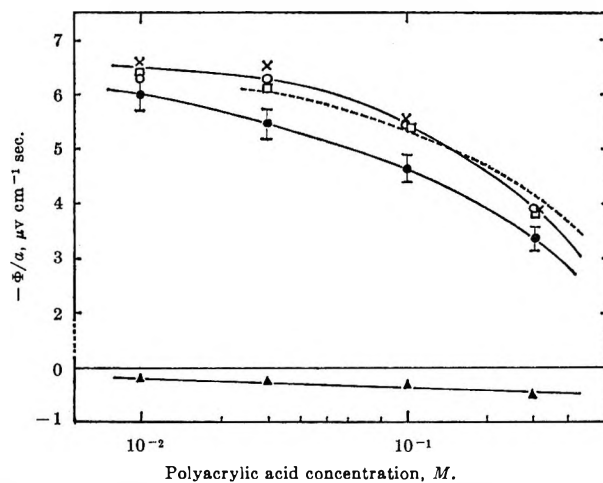


Figure 2. Effect of molecular weight on polyelectrolyte vibration potentials for PAA: ●, A₁ ($M_n = 25,000$); □, A₂ ($M_n = 120,000$); ×, A₃ ($M_n = 130,000$); ○, A₅ ($M_n = 250,000$); ▲, propionic acid; ----, theoretical curve for samples A₂, A₃, and A₅. (The estimated error limits are indicated on the curve for A₁; similar error limits apply also to the points for A₂, A₃, and A₅.)

accuracy and only a 6-15% increase (depending on the concentration) occurs in going from a molecular weight of 25,000 to 250,000—a tenfold increase. In fact, the difference between the curve for sample A₁ and the composite curve for the other samples is only slightly greater than the experimental precision although still quite discernible because it occurs over the complete concentration range.

The dependence of the pvp on the degree of neu-

(21) The phase is defined as positive for ionic solutions such as CsCl where $t_+W_+/z_+ > t_-W_-/z_-$ in eq 2. The negative values listed for the polyelectrolytes in, for example, Figure 2 indicate that the phase of the observed effect in these solutions was opposite to that for CsCl.

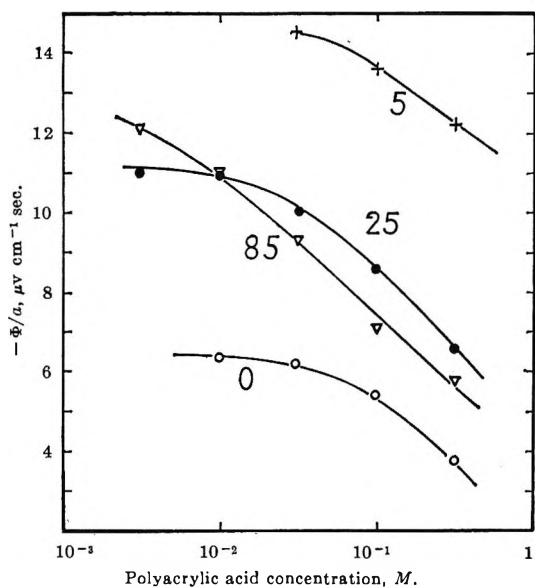


Figure 3. Effect of per cent neutralization (α) on polyelectrolyte vibration potentials for PAA (sample A_2). Per cent neutralization is indicated on each curve.

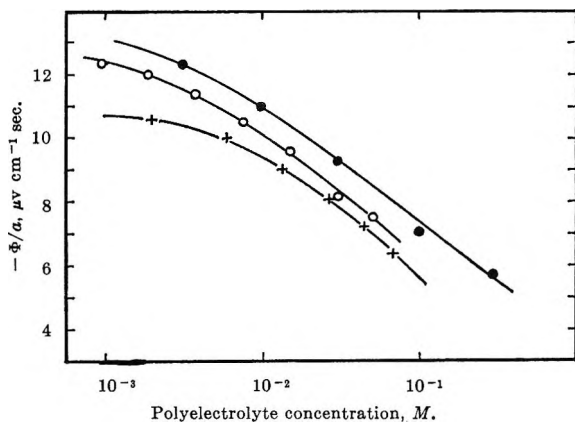


Figure 4. Concentration dependence of polyelectrolyte vibration potentials for various polyelectrolytes: +, sodium poly-L-glutamic acid (random coil configuration); O, sodium carboxymethylcellulose; ●, lithium polyacrylate (prepared from A_2).

neutralization is shown for PAA solutions for various concentrations and molecular weights in Figure 5 and for various gegenions in Figures 6 and 7. Again the effect appears to have a very small dependence on molecular weight. The curves for samples A_1 , A_2 , and A_5 in Figure 5 correspond to different molecular weights. The pvp for these three samples of different M_w may be the same for a given concentration within the experimental accuracy except for the region around the maximum. The minima in the various curves for PAA solutions in Figure 5 appear to be quite real. The dependence of the vibration potentials on α for propionic

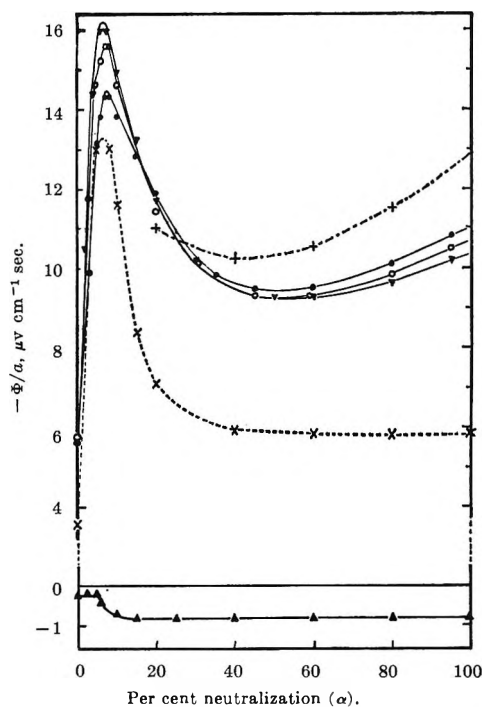


Figure 5. Dependence of polyelectrolyte vibration potentials on per cent neutralization for various PAA solutions: +, A_2 at 0.003 M; v, A_2 at 0.03 M; x, A_2 at 0.3 M; ●, A_1 at 0.03 M; O, A_5 at 0.03 M; ▲, propionic acid at 0.03 M.

acid solution (also shown in Figure 5) is distinctly different from that for a PAA solution. Reliable data are not available for the dependence of the effect on α in 0.003 M PAA solutions at low values of α because the internal impedance associated with the effect becomes high and leads to errors arising from loading effects.

The experimental data represented in Figures 6 and 7 (solid lines in each) show a surprisingly large dependence of the pvp on the type of gegenions involved in the neutralization. This behavior is in strong contrast to that encountered with other properties²² which are usually not very sensitive to the specific gegenion and will be explained on the basis of eq 8 and 19 in the Discussion.

A comparison of curves 1-3 in Figure 6 indicates a strong dependence of the observed effect on the molecular weight or more properly the apparent molar mass W_G of the gegenion for a given ionic mobility. With CsOH the maximum disappears and the minimum becomes sufficiently pronounced that the phase of the effect inverts for values of α between approximately 10 and 40%. In contrast, with the tetraalkylammonium ions the maximum is enhanced and the minimum is no longer evident.

(22) *E.g.*, H. Gregor, D. Gold, and M. Frederick, *J. Polymer Sci.*, **23**, 467 (1957).

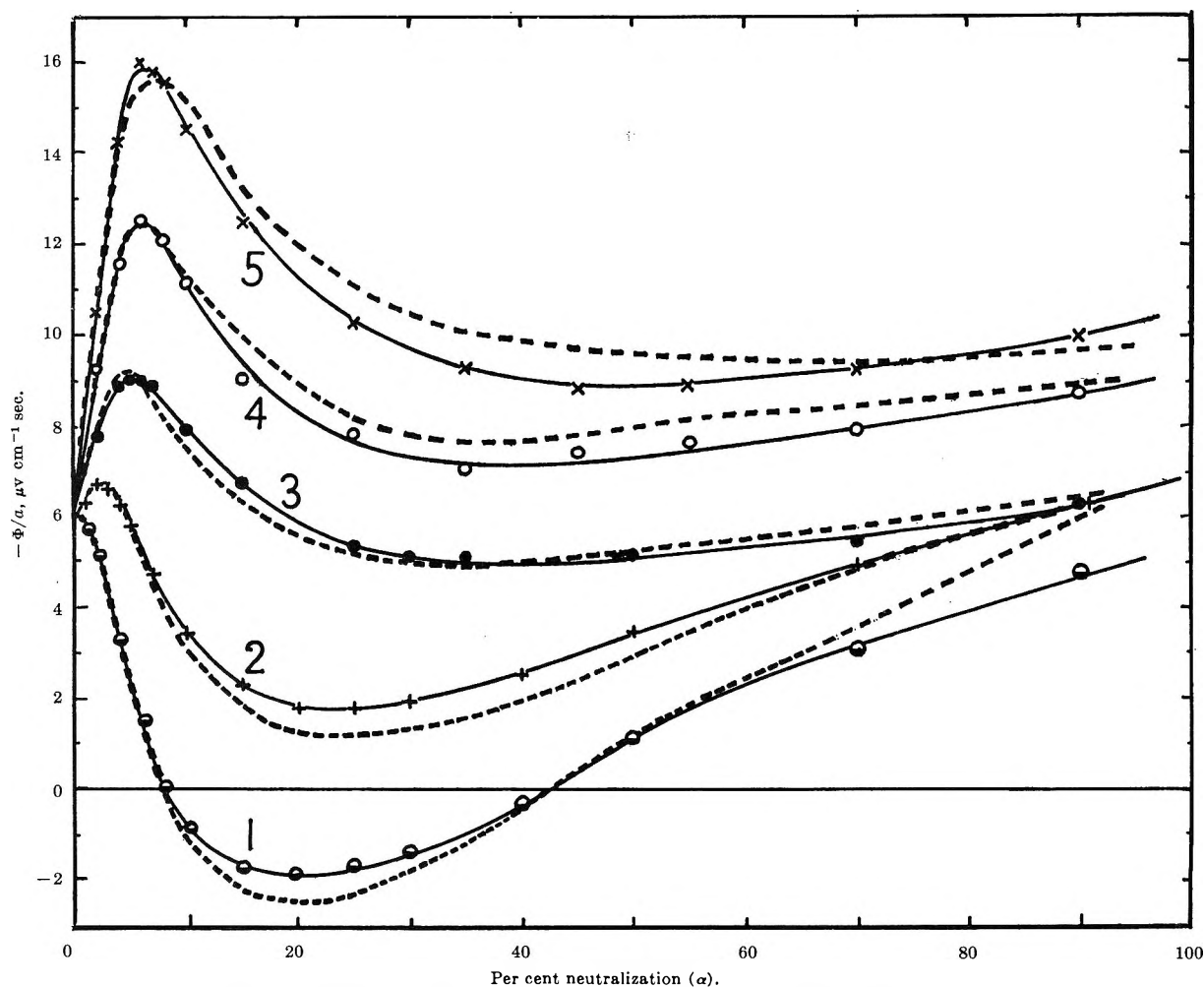


Figure 6. Effect of type of alkali metal hydroxide used to neutralize 0.03 *M* PAA (sample A₃, $M_n = 130,000$). Experimental curves (—) and theoretical curves (---) for: ●, CsOH; +, RbOH; ●, KOH; ○, NaOH; ×, LiOH.

From Figure 8 it is evident that the addition of a salt such as LiCl to the PAA solution depresses the maximum and even at only moderate concentration leads to the complete disappearance of the maximum. In considering this graph, one should note that the *ivp* in LiCl solutions have been found⁵ to be zero, thus indicating that $W_{Li^+}t_{Li^+} = W_{Cl^-}t_{Cl^-}$ for this salt (see eq 2).

The neutralization of the PAA with alkali earth hydroxides leads to a distinctly different dependence of *pvp* on the per cent neutralization (see Figure 9). The pronounced increase in the effect to extraordinarily large values for *pvp* arises because of the formation of colloidal aggregates.²³ The arrows on each curve indicate the per cent neutralization at which turbidity was perceptible.

Effects of adding different salts on the *pvp* in PAA are shown in Figures 10–13 for various degrees of neutralization, PAA concentrations, and various types of salts. LiCl, NH₄Cl, and NaHCO₃ all have *ivp*'s es-

entially equal to zero (within $0.2 \mu V cm^{-1} sec$) when by themselves in solutions. The ordinates in Figures 10–12 represent the ratio (*R*) of the *pvp* in the various solutions to the *pvp* in the corresponding polyelectrolyte solutions with no salt. In each instance these salts decrease the *pvp* and when present in sufficient quantity, suppress the observed effect to virtually zero. For the addition of salts with small intrinsic *ivp*, the shape of the normalized curves is generally the same for all of the polyelectrolytes (see Figures 10–12). This behavior as well as the shifts in the curves along the abscissas with different per cent neutralizations, polymer concentrations, and types of polymer will be shown to support the *ivp* model (see Discussion).

With salts for which the *ivp* are not zero when each is present as the only ionic species, their addition to the PAA solution may increase (NaI in Figure 13), de-

(23) T. Wall and W. Drenan, *J. Polymer Sci.*, **7**, 83 (1951).

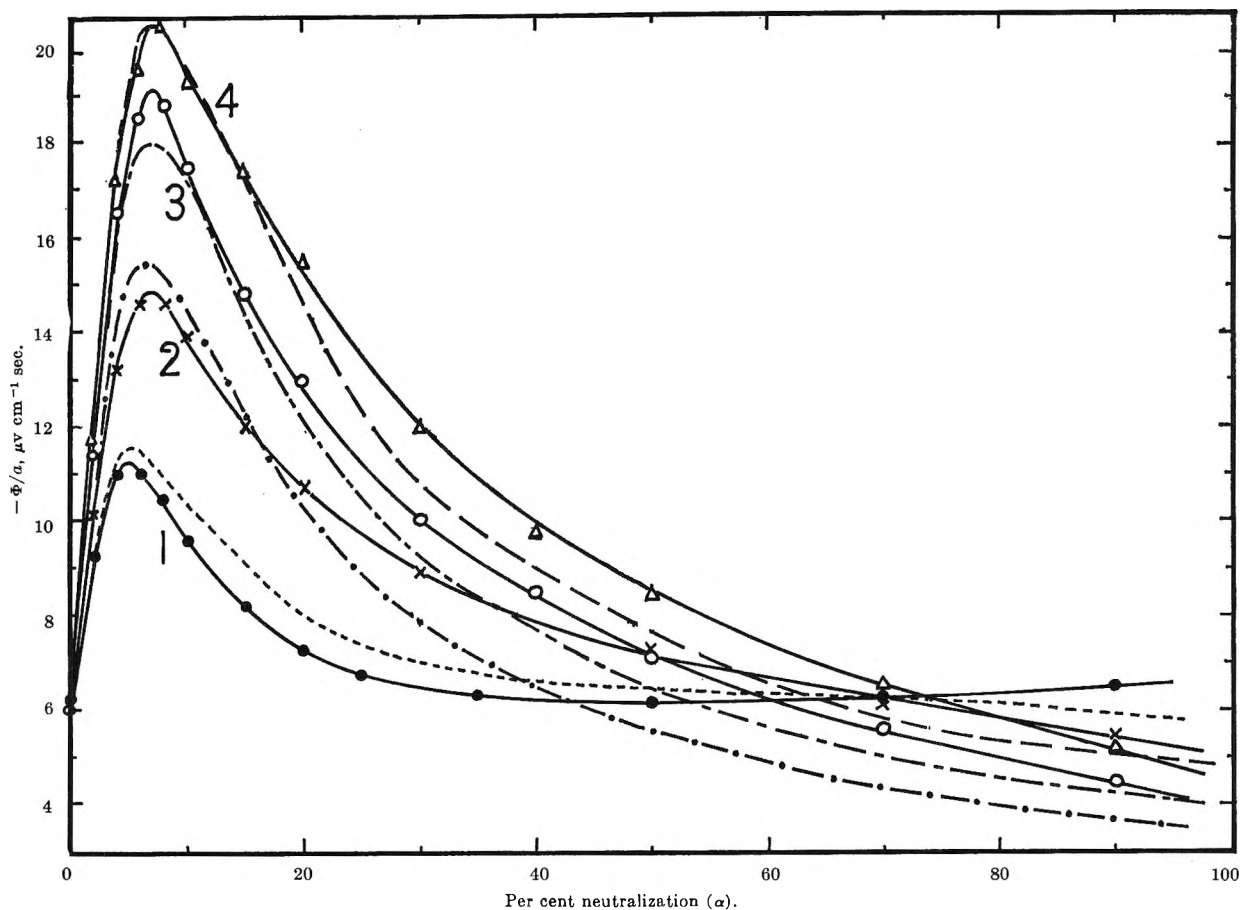


Figure 7. Effect of type of tetraalkylammonium hydroxide used to neutralize 0.03 *M* PAA (sample A₃, $M_n = 130,000$). Experimental curves (—) and theoretical curves (---) for: ●, NH₄OH; ×, (CH₃)₄NOH; O, (C₂H₅)₄NOH; Δ, (C₃H₇)₄NOH.

crease (*e.g.*, KI), or leave relatively unchanged (*e.g.*, LiIO₃) the observed pvp. With cations of large apparent molar mass (*e.g.*, CsCl), the phase of the pvp may be changed.

The effect of adding salt to solutions of Na-CMC and Na-PGA (Figure 14) is similar to that encountered with PAA. The quantity $\log [(1 - R)/R]$ rather than R has been plotted on the ordinates in Figure 14 for reasons that will be evident in the Discussion (see part VIC). The conversion of PGA from the rodlike configuration to the random-coil configuration²⁴ with increasing pH results in a significant change in the pvp. The pvp in the absence of added salt for PGA at pH 5.4 is $-13.7 \mu\text{V cm}^{-1} \text{sec}$ (corresponding to the rodlike configuration) while the effect at pH 7.2 is $-8.4 \mu\text{V cm}^{-1} \text{sec}$ (corresponding to the random-coil configuration).

VI. Discussion of Results

A. Dependence of Pvp on Polyelectrolyte Concentration. The decrease of pvp with increasing polyelectrolyte concentration (see Figures 2–4) is in accord with predictions based on the ivp model and known proper-

ties of polyelectrolyte solutions. In Figure 2 the dashed line corresponds to the dependence of the pvp on polyelectrolyte concentration calculated in the following manner. For $\alpha = 0$, eq 8 reduces to

$$\phi_{0,0} = 0.155(W_H - W_M t_B / \theta) \quad (12)$$

The quantity u_B in the denominator of eq 8 has been assumed negligible compared to u_H . The transference number for the polymer bead (t_B) is related to the mobilities of the polymer bead (u_B) and hydrogen ion (u_H) by the equation

$$t_B = \frac{u_B}{u_H + u_B} \approx \frac{u_B}{u_H} = \frac{\theta X}{\rho_B} \quad (13)$$

where $u_B \ll u_H$.

The quantity θ in eq 12 has been determined from pH measurements at various concentrations for PAA (sample A₂) with $M_n = 120,000$ corresponding to a degree of polymerization of 1650. The quantity t_B

(24) P. Doty, A. Wada, J. Yang, and E. Blout, *J. Polymer Sci.*, **23**, 851 (1957).

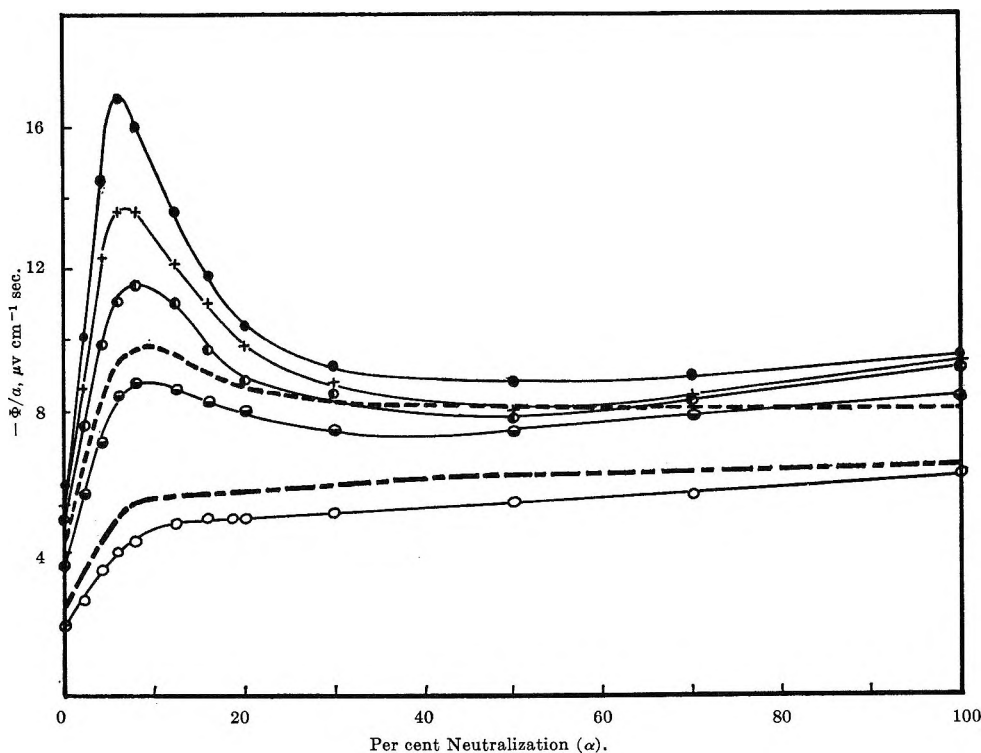


Figure 8. Effect of addition of LiCl on the neutralization of 0.03 *M* PAA (sample A₂, $M_n = 120,000$) with LiOH: ●, no LiCl; +, 0.0001 *M* LiCl; ●, 0.0003 *M* LiCl; ●, 0.001 *M* LiCl (—, experimental curve; ---, theoretical curve); ○, 0.003 *M* LiCl (—, experimental curve; ---, theoretical curve).

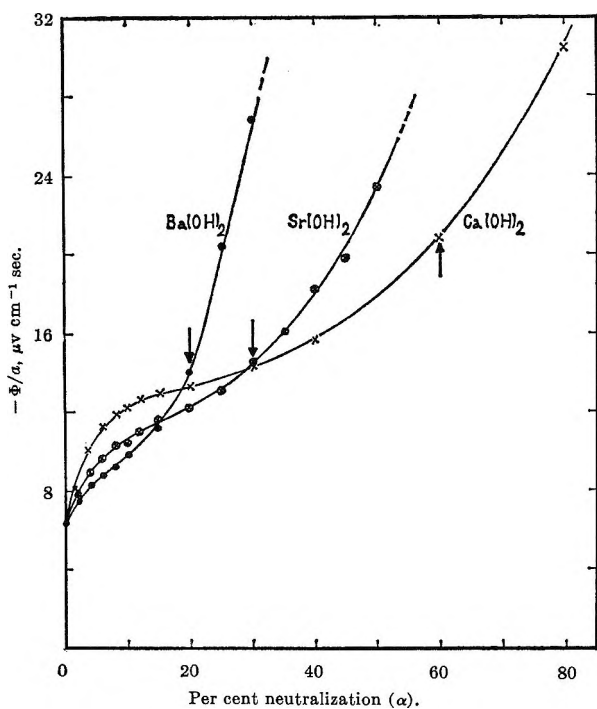


Figure 9. Effect of neutralization with alkali earth hydroxides for 0.01 *M* PAA (sample A₂, $M_n = 120,000$).

has been obtained from the data of Wall, *et al.*²⁵ The term W_H in eq 12 has been taken as 6.5 g/mole on the basis of ivp measurements in simple electrolytes.⁵ Only the quantity W_M in eq 12 is unknown. The value for this quantity has been obtained by plotting the three experimental points for 0.03, 0.1, and 0.3 *M* PAA against the parameter t_B/θ and has been found to be 25.6 g/mole. The various parameters used in the calculation are summarized in Table II. The experimental data for the 10^{-2} *M* solution were not used in this calculation since the data of Wall, *et al.*,²⁵ do not extend to sufficiently low concentrations.

Propionic acid and the propionate ion may be considered as the monomeric units for PAA in the unneutralized state and the totally dissociated state, respectively. Consequently, some justification for the assumption that W_M is independent of C_P for the unneutralized polymer may be obtained by considering the change in the apparent molar mass of propionic acid attending the ionization. Density data²⁶ indicate

(25) F. Wall, G. Stent, and J. Ondrejcin, *J. Phys. Chem.*, **59**, 979 (1950).

(26) "International Critical Tables," Vol. 3, McGraw-Hill Book Co., Inc., New York, N. Y., 1928, p 112.

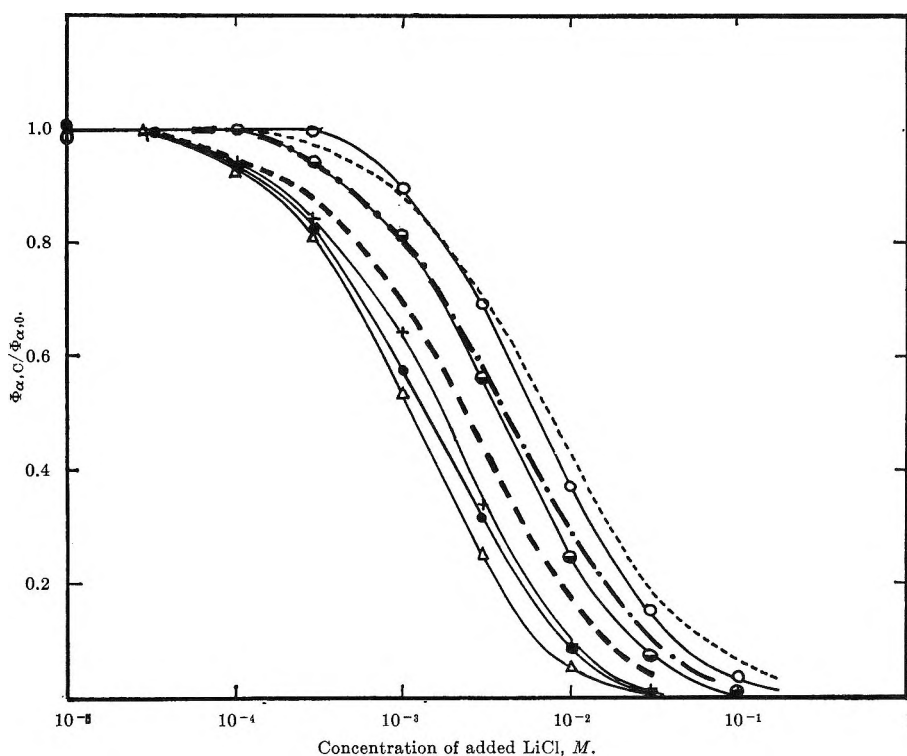


Figure 10. Relative change of polyelectrolyte vibration potential with concentration of added LiCl at various per cent neutralization (α) of 0.03 M PAA (sample A₂, $M_n = 130,000$, neutralization with LiOH): +, $\alpha = 0$, $\phi_{0,0} = -6.1$ (—, experimental curve; ---, theoretical curve); Δ , $\alpha = 3\%$, $\phi_{3,0} = -12.6$; \bullet , $\alpha = 10\%$, $\phi_{10,0} = -14.8$; \bullet , $\alpha = 30\%$, $\phi_{30,0} = -9.6$ (—, experimental curve; · — ·, theoretical curve); \circ , $\alpha = 100\%$, $\phi_{100,0} = -9.6$ (—, experimental curve; ----, theoretical curve). (All values for $\phi_{\alpha,0}$ are expressed in $\mu\text{v cm}^{-1} \text{ sec.}$)

Table II: Parameters Used in the Calculation of the Theoretical Curve in Figure 2

C_P^a (M)	pH ^b	θ^c	t_B^d	$\phi_{0,0}, \mu\text{v cm}^{-1} \text{ sec.}$	
				Calcd ^e	Exptl
0.03	3.15	2.36	4.15	6.0	6.2
0.05	2.98	2.10	3.58	5.7	...
0.1	2.79	1.63	2.60	5.3	5.5
0.2	2.60	1.26	1.82	4.8	...
0.3	2.51	1.03	1.35	4.2	3.85

^a Polymer concentration expressed in moles of monomer per liter. ^b Measured as part of present work. ^c Calculated from pH. ^d From the data for t_B vs. θ for sample 3 in the work of Wall, *et al.*²⁵ ^e Calculated on the basis of eq 12 using an average value $W_M = 25.6$ g/mole.

the apparent molar mass of un-ionized propionic acid to be 7 ± 0.5 g/mole, whereas unpublished ionic vibration potentials data²⁷ in alkali metal propionates yield a value of 14 ± 1 g/mole for the apparent molar mass of the propionate ion. Thus an approximate change of 7 g/mole of acid group dissociated would be anticipated for the polyelectrolyte. Since the change in the dissociation degree θ over the range of concentration

represented in Figure 2 is from 0.024 to 0.010, the corresponding change in W_M is estimated to be $0.016 \times 7 \simeq 0.1$ g/mole or quite negligible compared to the experimental value $W_M = 25.6$ g/mole of monomer.

The volume (\bar{V}_M) of the polymer per monomer unit can be calculated from the apparent molar mass of the polymer per monomer unit by means of eq 7 and the value 72.1 g/mole for the molecular weight of the monomer unit. From the experimental value for W_M of 25.6 g/mole, \bar{V}_M is found to be 46 cm^3/mole . This number is substantially smaller than the value 67 cm^3/mole calculated for propionic acid using eq 7 with the apparent molar mass taken as 7 g/mole as discussed earlier. A somewhat smaller value is to be expected for the volume of the polymer per monomer unit than for the corresponding free monomeric acid even if the polymer is uncoiled on the basis of steric considerations and the tendency of the water to form a cage-like structure around the hydrocarbon structure of the simple acid and the polymer molecule. The coiling of the polymer should produce a further decrease in the volume of the polymer per monomer unit.

(27) R. Zana and E. Yeager, submitted for publication.

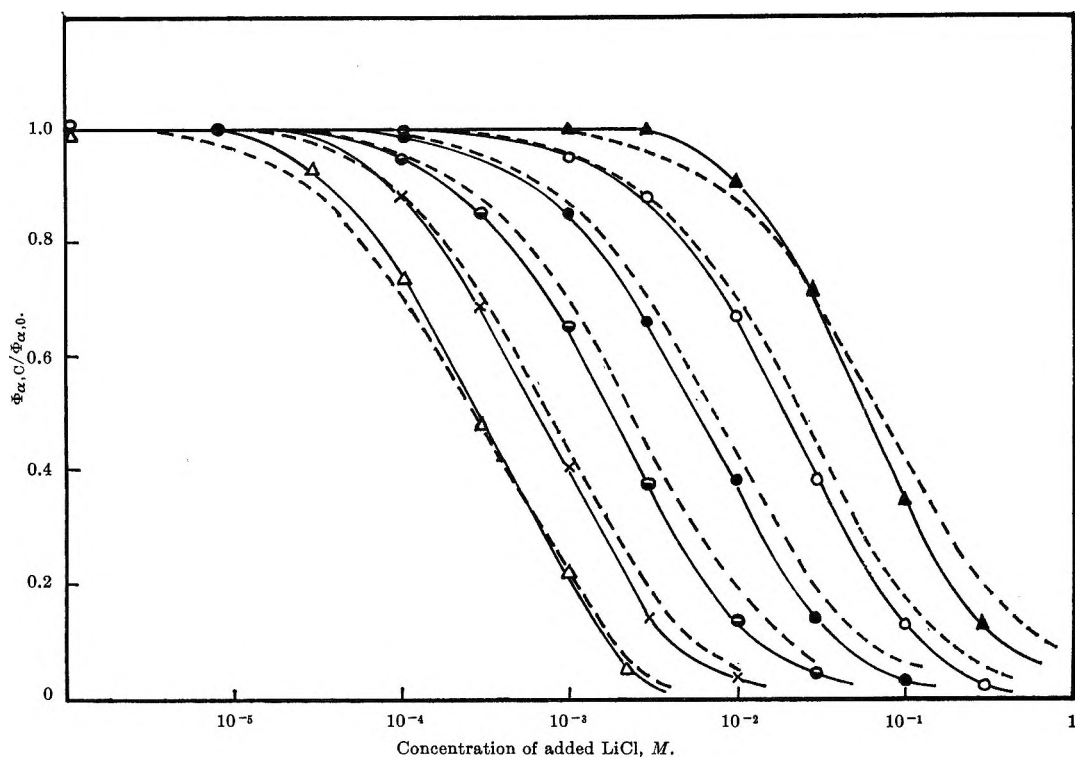


Figure 11. Relative change of polyelectrolyte vibration potentials with concentration of added LiCl for various concentrations of PAA, sample A₂, 100% neutralized with LiOH: Δ , $C_P = 0.001 M$, $\phi_{100,0} = -13.1$; \times , $C_P = 0.003 M$, $\phi_{100,0} = -12.5$; \odot , $C_P = 0.01 M$, $\phi_{100,0} = -11.6$; \bullet , $C_P = 0.03 M$, $\phi_{100,0} = -9.6$; \circ , $C_P = 0.1 M$, $\phi_{100,0} = -8.4$; \blacktriangle , $C_P = 0.3 M$, $\phi_{100,0} = -6.0$. (All values for $\phi_{100,0}$ are expressed in $\mu\text{V cm}^{-1} \text{sec}$; —, experimental curves; ---, theoretical curves.)

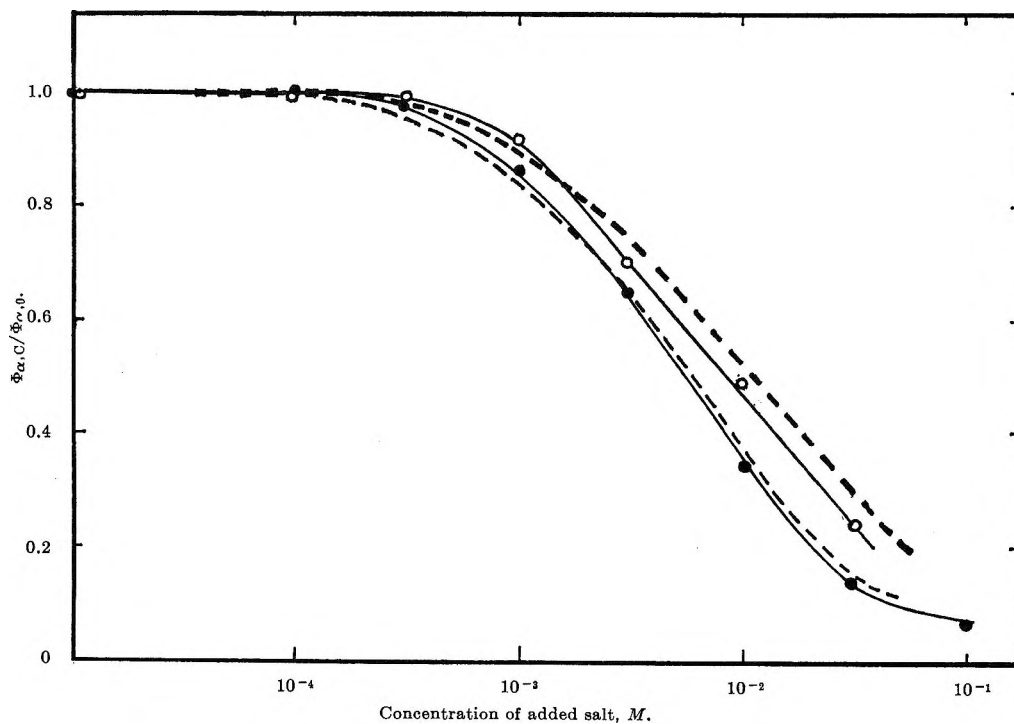


Figure 12. Effect of adding salts whose ivp's are zero to 0.03 M PAA, sample A₂, 100% neutralized with LiOH; $\phi_{100,0} = -9.6 \mu\text{V cm}^{-1} \text{sec}$: \bullet , NH_4Cl ; \circ , NaHCO_3 (—, experimental curves; ---, theoretical curves).

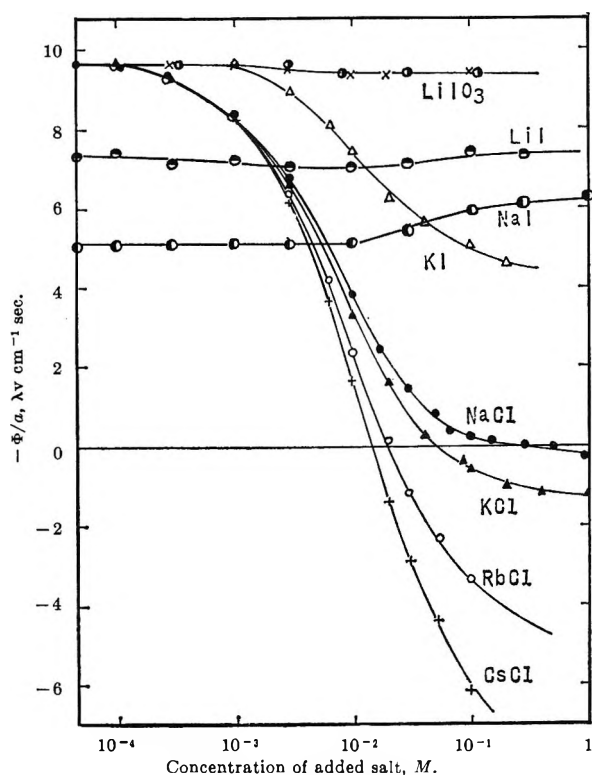


Figure 13. Effect of adding various salts to PAA. Sample A₂ ($M_\eta = 120,000$), 0.03 M, 100% neutralized with LiOH: \bullet , LiIO₃; Δ , KI; \circ , NaCl; \blacktriangle , KCl; \circ , RbCl; $+$, CsCl. Sample A₂, 0.03 M, 25% neutralized with LiOH: \times , LiIO₃. Sample A₃ ($M_\eta = 130,000$), 0.03 M, 0.5% neutralized with LiOH: \circ , LiI. Sample A₃, 0.1 M, unneutralized: \bullet , NaI.

B. Dependence of Pvp on Per Cent Neutralization in the Absence of Added Salt. The variation of pvp with per cent neutralization has been calculated from eq 8 for the neutralization of 0.03 N PAA (sample 3) with NaOH and KOH. For 0–10% neutralization, the calculation has been carried out in the following manner. The quantities $\theta - \alpha$, $\alpha - \theta\beta$, and $(1 - \beta)\theta$ are related to the specific conductivity κ' of the polyelectrolyte solution by eq 14–17, where κ_H , κ_G , and κ_B are the contri-

$$\kappa' = \kappa_H + \kappa_G + \kappa_B \quad (14)$$

$$\kappa_H = (\theta - \alpha)C_P F u_H / 1000 \quad (15)$$

$$\kappa_G = (\alpha - \theta\beta)C_P F u_G / 1000 \quad (16)$$

$$\kappa_B = (1 - \beta)\theta C_P F u_B / 1000 \quad (17)$$

butions to κ' from the H⁺, the gegenion (Na⁺ or K⁺), and the charged polyion, u_H , u_G , and u_B are the mobilities of the species indicated by the subscripts, and F is the Faraday constant. Wall and his co-workers^{25,28,29} have evaluated the parameters β and θ as a function of α for the neutralization of PAA with NaOH and KOH

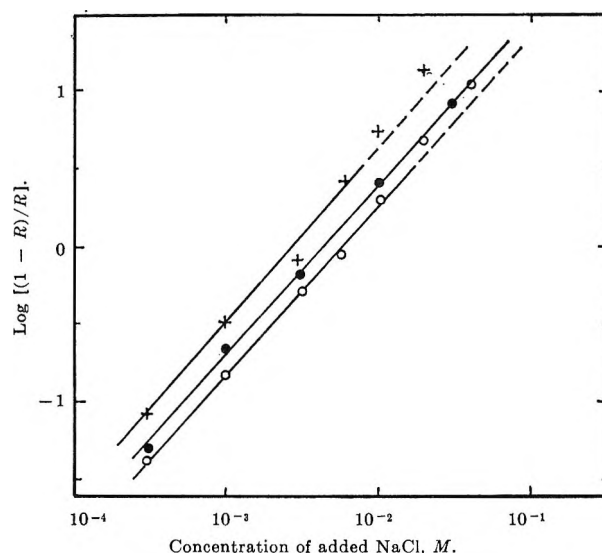


Figure 14. Effect of adding NaCl to various polyelectrolytes: $+$, 0.02 M poly-L-glutamic acid at pH 5.4 (rodlike configuration), $\phi_{\alpha,0} = -13.7 \mu\text{V cm}^{-1} \text{sec}$; \circ , 0.02 M poly-L-glutamic acid at pH 7.2 (random-coil configuration) $\phi_{\alpha,0} = -8.4 \mu\text{V cm}^{-1} \text{sec}$; \bullet , 0.012 M sodium carboxymethylcellulose, $\phi_{\alpha,0} = -9.6 \mu\text{V cm}^{-1} \text{sec}$.

for $\alpha \geq 10\%$. In order to obtain values for β at $\alpha < 10\%$, the data of these workers for β have been plotted vs. α , a smooth curve drawn through the points including the origin, and the values for β at $\alpha < 10\%$ estimated from the smooth curve. A similar procedure has been used to obtain u_B at $\alpha < 10\%$ except that the curve was extended through $u_B F = 14.5 \text{ ohm}^{-1} \text{cm}^2$ at $\alpha = 0$ on the basis of the literature data²⁵ for unneutralized PAA. With the values for β and u_B obtained in this way, the quantity θ has been determined from the experimental data for κ' (see Table III) by means of eq 14–17. For $\alpha > 10\%$, the data of Wall and his co-workers^{25,28,29} for θ and β as well as u_B have been used directly in eq 8 to obtain the theoretical curves in Figure 6 (dashed lines) for neutralization with NaOH and KOH.

The dependence of W_M on per cent neutralization must be taken into account because of the change in the apparent molar mass of the polymer bead resulting from dissociation (electrostriction effect) and counterion binding. This has been done by means of eq 18.

$$W_M = 26.5 + W_G \theta \beta + 7(\theta - 0.024) \quad (18)$$

The quantity 26.5 g/mole represents the value for W_M at $\alpha = 0$ and has been determined by means of eq

(28) J. Huizenga, P. Grieger, and F. Wall, *J. Am. Chem. Soc.*, **72**, 2636 (1950).

(29) F. Wall and R. Donrenaus, *ibid.*, **76**, 1557 (1954); **82**, 5599 (1960).

Table III: Parameters Used in the Calculation of the Theoretical Curves in Figures 6 and 7

$10^2\alpha$	$10^4\kappa',^a$ ohm ⁻¹ cm ⁻¹	$u_B F,^b$ ohm ⁻¹ cm ²	$10^2\beta^b$	$10^{2\theta} \times$ $(1 - \beta)^b$	$10^{2\theta^c}$
0	2.67	14.5	0	2.35	2.35
1	2.25	16	0	2.85	2.85
2	2.07	17.5	0	3.46	3.46
4	1.83	20.1	1	4.84	4.84
6	1.94	22.4	4	6.35	6.56
8	2.20	24.4	7.5	7.80	8.42
10	2.50	26.4	11.0	9.30	10.3
15	3.20	31.4	18	12.30	15.1
20	4.00	34.0	24	15.4	20
30	5.30	40.0	31.7	20.6	30
40	6.20	43.8	40.5	23.8	40
50	6.85	45	47.5	26.2	50
70	7.78	45	58.0	29.4	70
90	8.30	43.5	65	31.6	90
100	...	42.5	67.5	32.5	100

^a Measured as part of present work. ^b Based on experimental data of Wall, *et al.*,^{25,28,29} expressed as equivalent ionic conductance ($F = \text{Faraday}$). ^c Calculated according to procedure in text for $\alpha \leq 10\%$.

12 from the experimental pvp in 0.03 *M* PAA (unneutralized sample of A_3 ; $\phi_{0,0} = -6.2 \mu\text{V cm}^{-1} \text{sec}$) and the values for θ and t_B listed in Table II. The second term represents the increase of apparent mass per monomer due to the counterion binding. The bound gegenion should retain all of its water in the inner coordination sphere and most of the water in its outer coordination sphere. Consequently, the apparent molar mass rather than the intrinsic molar mass of the gegenion has been used in the counterion binding term. The values of W_G have been obtained from ionic vibration potentials and are reported in an earlier paper.⁵ The third term in eq 18 represents the increase of apparent mass per monomer arising because of the dissociation of the acid groups in the polyion and the resulting electrostriction of the surrounding water molecules. On the basis of the comparison of the apparent molar masses of the propionic acid and the propionate ion (as described earlier), the coefficient in this term has been set equal to 7 g/mole. This coefficient has been multiplied by $(\theta - 0.024)$ rather than just θ since $\theta = 0.024$ at $\alpha = 0$ when $W_M = 26.5 \text{ g/mole}$.

The parameters involved in the calculations of the theoretical curves for neutralization with NaOH and KOH in Figure 6 are listed in Table III. One can see that for $\alpha > 15\%$, $\theta = \alpha$ and eq 8 then reduces to

$$\phi_{\alpha,0} = 0.155 \frac{W_G u_G - W_M u_B [\theta(1 - \beta)]^{-1}}{u_G + u_B} \mu\text{V cm}^{-1} \text{sec} \quad (19)$$

Considering the accuracy of the pvp data as well as the apparent accuracy of the literature data for θ , β , and u_B , the theoretical and experimental curves for neutralization with NaOH and KOH compare quite favorably.

The same calculation has been carried out for the neutralization with LiOH, RbOH, and CsOH in Figure 6 and NH_4OH in Figure 7 with the assumption that θ , β , and u_B are the same as for KOH. Justification for this assumption is to be found in the fact that the data of Wall, *et al.*,^{28,29} revealed no difference in these quantities for NaOH and KOH and also the good agreement between the theoretical and experimental pvp curves in Figures 6 and 7.

For the calculation of the theoretical curves corresponding to neutralization with the tetraalkylammonium hydroxides, the counterion binding terms in eq 8 and 18 have been neglected (*i.e.*, $\beta = 0$) and u_B again assumed to be the same as for NaOH. Some justification for the dropping of the terms involving β may be found in the fact that several workers^{22,30} have concluded that the interaction of tetraalkylammonium ions with polyions is much smaller than that for alkali metal cations because of the much larger ionic radii of the tetraalkylammonium ions. In addition, the coefficients of β (u_G and W_G) in eq 8 and 18 are smaller for the tetraethyl and propylammonium ions than for the alkali metal cations. The agreement between the theoretical and experimental curves in Figure 7 is relatively good except for $(\text{CH}_3)_4\text{NOH}$ at higher α . The experimental curve for this base crosses those for the $(\text{C}_2\text{H}_5)_4\text{NOH}$ and $(\text{C}_3\text{H}_7)_4\text{NOH}$ rather than running parallel. Since the $(\text{CH}_3)_4\text{N}^+$ cation is considerably smaller than the high homologs, counterion binding is probably the explanation for this behavior. An alternate approach is to use the experimental data in Figure 7 in conjunction with eq 18 and 19 to estimate the extent of the counterion binding. For $(\text{C}_2\text{H}_5)_4\text{NOH}$ and $(\text{C}_3\text{H}_7)_4\text{NOH}$ and $0.3 \leq \alpha \leq 0.9$, β has been found to be relatively constant and equal approximately to 20%. For $(\text{CH}_3)_4\text{NOH}$, β has been found to be a function of α and equal to 50, 41, 31, 16, and 9% for $\alpha = 0.9, 0.7, 0.5, 0.3,$ and 0.2 , respectively. Even so, the counterion binding is substantially smaller for $(\text{CH}_3)_4\text{N}^+$ than the alkali metal cations (see Table III).

In introducing corrections for counterion binding in the calculation of pvp, no distinction has been made between strongly bound and loosely bound gegenions. Wall's values for β were obtained^{28,29} by a technique which should yield the total fraction of charges on the polyion compensated by bound gegenions. Gill,

(30) A. Packter, *J. Polymer Sci.*, A2, 2771 (1964).

et al.,^{31,32} have used a steady-state electrolysis technique to determine the value of β corresponding to more tightly bound gegenions. The value of β so determined is zero up to 40% neutralization for a 0.04 M PAA solution neutralized with NaOH and approaches the value of Wall, *et al.*,^{28,29} at 100% neutralization. If the values of Gill, *et al.*, for β are used in making the counterion binding correction, the calculated pvp at intermediate values of α deviate from the experimental pvp by a far greater amount than when the data of Wall, *et al.*, are used. For example, for Cs^+ , according to Gill, *et al.*,³² $\beta = 0$ for $0 < \alpha < 0.5$. The calculated pvp at $\alpha = 0.5$ would be approximately $+9 \mu\text{v cm}^{-1} \text{ sec}$ as compared with the experimental value of $-1 \mu\text{v cm}^{-1} \text{ sec}$. Theoretical justification for the use of β values reflecting loosely as well as tightly bound gegenions is to be found in the fact that the pvp are dependent theoretically only on the time-average values for the charges, apparent masses, and frictional coefficients of the various charged species. This is true to a close approximation even when the lifetimes of the aggregates become comparable to the period of the sound waves.

C. Salt Effect on Pvp. The variation of the pvp with per cent neutralization with LiOH in the presence of the salt LiCl has been calculated using eq 9 where $\phi_P (= \phi_{\alpha,0})$ has been obtained from eq 8 and K from eq 11. The assumption has been made that θ , β , and u_B are not affected by the LiCl which is present only at relatively low concentration³³ ($C_S \leq 0.003 M$). For LiCl, ivp measurements⁵ indicate that ϕ_{CA} is zero for practical purposes. The theoretical curves are given for two concentrations ($C_S = 0.001$ and $0.003 M$) in Figure 8. For the other LiCl concentrations, the agreement between theory and experiment is just as good. If experimental rather than theoretical values are used for $\phi_{\alpha,0}$ in eq 9, the theoretical curves are even closer to the experimental curves.

The theoretical curves in Figures 10 and 11 have been calculated in the same manner as the theoretical curves in Figure 8 with $\phi_S (= \phi_{CA})$ set equal to zero in eq 9 as before.

Equation 9 predicts no change of the pvp with the addition of a salt provided (1) the cations of the salt are the same as those of the base used for neutralization, (2) the ivp for the solutions containing just the salt is the same as the pvp of the polyelectrolyte solution before addition of the salt (*i.e.*, $\phi_{CA} = \phi_{\alpha,0}$), and (3) θ , β , and u_B remain unchanged. This prediction is confirmed by the constancy of the pvp observed during the addition of LiI and LiIO₃ in Figure 13. This constancy, however, should not be interpreted as evidence that θ , β , and u_B remain unchanged with the addition of salt

even in excess of 0.1 M. An examination of eq 8, 9, and 9c reveals loss of sensitivity to these parameters when $C_S > C_P$. Wall and Eitel,³³ however, have shown that θ , β , and u_B are relatively insensitive to C_S during the addition of NaCl to PAA solutions, 100% neutralized with NaOH, even for C_S as high as 0.15 M.

Figure 12 shows the effect of NH_4Cl and NaHCO_3 on the pvp of 0.03 M PAA, 100% neutralized with LiOH. For NH_4Cl and NaHCO_3 , ϕ_{CA} has been found experimentally to be zero, but ϕ_S is not zero since the added cations (NH_4^+ or Na^+) are not the same as the initial cation (Li^+). The general expressions for ϕ_P , ϕ_S , and K given by eq 9a-c have been used in the calculation of the theoretical curves (dashed lines) given in Figure 12. In these calculations the apparent molar mass of the polymer bead per monomer unit has been taken as

$$W_M = 26.5 + 7(\theta - 0.024) + \theta\beta \left[W_G \frac{\alpha C_P}{\alpha C_P + C_S} + W_C \frac{C_S}{\alpha C_P + C_S} \right] \quad (20)$$

As before, the assumption has been made that θ , β , and u_B remain unchanged with the addition of the salt but that the counterion binding of each type of cation is proportional to its relative concentration. In eq 20, W_C was taken as 6 and 30 g/mole for NH_4^+ and Na^+ , respectively, on the basis of earlier ivp measurements.⁵

The theoretical pvp values corresponding to the other curves in Figure 13 are listed in Table IV together with the experimental values. In all instances the agreement between the theoretical and experimental values is within the experimental accuracy. The importance of taking into account the interchange of initially bound cations and the cations from the added salt is to be appreciated from the following example. For the addition of CsCl with $C_S = 0.01 M$, the calculated pvp values are $+2.7$ and $-2.4 \mu\text{v cm}^{-1} \text{ sec}$ without exchange and with exchange, respectively, taken into account while the experimental value is $-1.6 \mu\text{v cm}^{-1} \text{ sec}$.

The data available for the Na-PGA and Na-CMC solutions are insufficient to pursue the calculation of theoretical values for the pvp in these solutions in a manner similar to that for PAA. With the addition of NaCl (for which ϕ_{CA} is quite small), the dependence of the parameter $R = \phi_{\alpha,CS}/\phi_{\alpha,0}$ on C_S , however, should be similar for each polyelectrolyte provided θ , β , and u_B remain unchanged during the addition of the salt and the cations of the salt and the base used

(31) G. Ferry and S. Gill, *J. Phys. Chem.*, **66**, 999 (1962).

(32) L. Noll and S. Gill, *ibid.*, **67**, 498 (1963).

(33) F. Wall and M. Eitel, *J. Am. Chem. Soc.*, **79**, 1556 (1957).

Table IV: Calculations of the Vibration Potential ($\mu\text{v cm}^{-1} \text{ sec}$) for 0.03 *M* PAA (100% Neutralized with LiOH) in Presence of Uni-univalent Salt

Salt concn, <i>M</i>	$\phi_{\alpha}, C_s, \mu\text{v cm}^{-1} \text{ sec}$									
	NaCl		KCl		RbCl		CsCl		KI	
	Theoret	Exptl	Theoret	Exptl	Theoret	Exptl	Theoret	Exptl	Theoret	Exptl
10^{-3}	-8.4	-8.4	-8.3	-8.5	-8.3	-8.2	-8.3	-8.2
3×10^{-3}	-6.9	-6.8	-6.4	-6.6	-6.5	-6.3	-6.4	-6.1	-8.6	-8.8
10^{-2}	-4.0	-3.8	-3.5	-3.3	-3.2	-2.3	-2.4	-1.6	-7.6	-7.4
3×10^{-2}	-1.7	-1.5	-1.0	-0.7	0.9	1.2	2.0	2.9	-6.3	-5.9
10^{-1}	-0.2	-0.1	0.8	0.6	3.2	3.4	5.6	6.2	-5.1	-5.1

for neutralization are the same. For these conditions, it can be shown from eq 9 and 9a-c that

$$\log \frac{1-R}{R} = \log K' + \log C_s \quad (21)$$

where K' is a constant that depends on the polyelectrolyte. This expression is confirmed experimentally by the linear behavior evident in Figure 14.

VII. Conclusions

From the present study the following conclusions can be reached.

1. Polyelectrolyte vibration potentials depend on the nature, concentration, and per cent neutralization of the polyelectrolyte as well as on the nature of the gegenion and on the nature and concentration of any added salt.
2. The experimental results are in quantitative agreement with theory based on the ionic vibration potential mechanism and the polymer bead model.

3. The pvp can be used to determine the partial molal volume of a monomer unit in the polymer bead model. (The value is $46 \text{ cm}^3/\text{mole}$ for unneutralized polyacrylic acid.)

In the present study the theoretical effort has been directed to calculating the pvp from other data including counterion binding data. If this procedure is reversed, pvp measurements may provide a means for obtaining information concerning counterion binding. It is doubtful whether pvp measurements will generally prove competitive with other approaches for obtaining such information. An important exception, however, may be the interchange of bound ions of very different apparent molar masses (*e.g.*, K^+ and Cs^+) to which the pvp data are quite sensitive even though the difference in mobilities may be small.

Acknowledgment. The authors are pleased to acknowledge the support of this research by the Office of Naval Research.

Electrochemical Reduction of Aromatic Nitro Compounds in the Presence of Proton Donors

by Steven H. Cadle, Paul R. Tice,¹ and James Q. Chambers²

Department of Chemistry, University of Colorado, Boulder, Colorado 80302 (Received April 10, 1967)

The effect of proton donors on the electrochemical reduction of aromatic nitro compounds in nonaqueous solvents has been studied. In the presence of certain proton donors, the nitro compound is reduced by two independent pathways: a reversible one-electron step and an irreversible process that yields a mixture of the corresponding phenylhydroxylamine and azoxybenzene. The irreversible process occurs at potentials more positive than the one-electron reduction for the proton donors *p*-toluenesulfonic, trichloroacetic, *o*-phthalic, salicylic, benzoic, and *p*-hydroxybenzoic acids and *N,N*-diethylanilinium perchlorate. It is suggested that the reduction proceeds *via* a hydrogen-bonded complex formed between the nitro compound and the acid in the double layer.

Introduction

The effect of proton donors on electrochemical processes in aprotic solvents has been investigated for the reduction of aromatic hydrocarbons³⁻⁵ and carbonyl compounds.⁴ For these processes the role of the acid is usually to protonate the radical species resulting from the addition of one electron, thus making the subsequent additions of electrons easier. Accordingly, two one-electron waves coalesce to one two-electron wave upon the addition of a proton source in the reduction of hydrocarbons.³ In this paper the effect of proton donors in nonaqueous solvents on the reduction of aromatic nitro compounds is investigated.

The one-electron reduction of nitro compounds has been well studied by electrochemical methods,^{6,7} by electron spin resonance (esr) spectroscopy in nonaqueous⁸ and aqueous⁹ media, and by visible absorption spectroscopy in nonaqueous¹⁰ and aqueous^{11,12} media. In these solvent systems the anion radical of the nitro compound is found to be the species formed by the primary electrode process. In recent years, some of the details of the many-electron reduction process in neutral and alkaline media have been elucidated by electrochemical^{11,13,14} and pulse radiolysis¹⁵ techniques. In these media the radical anion or its protonated form can either diffuse into the bulk solution and act as a reducing agent or can be further reduced in a series of heterogeneous reactions at the electrode surface.¹³

When aromatic nitro compounds are reduced in the presence of a proton donor in nonaqueous solvents, independent reduction waves for both a reversible one-electron and an irreversible many-electron process are observed. The irreversible reduction wave occurs at potentials more positive than the one-electron wave and resembles descriptions of "preprotonation"¹⁶ and "prior

(1) National Science Foundation Undergraduate Research Participation Fellow.

(2) To whom correspondence should be addressed.

(3) G. J. Hoijtink, J. van Schooten, E. de Boer, and W. I. Aalkersberg, *Rec. Trav. Chim.*, **73**, 355 (1954).

(4) P. H. Given and M. E. Peover, *J. Chem. Soc.*, 385 (1960).

(5) K. S. V. Santhanam and A. J. Bard, *J. Am. Chem. Soc.*, **88**, 2669 (1966).

(6) L. Holleck and H. J. Exner, *Z. Elektrochem.*, **56**, 46 (1952).

(7) L. Holleck and D. Becher, *J. Electroanal. Chem.*, **4**, 321 (1962).

(8) D. H. Geske and A. M. Maki, *J. Am. Chem. Soc.*, **82**, 2671 (1960).

(9) L. H. Piette, P. Ludwig, and R. N. Adams, *ibid.*, **84**, 4212 (1962).

(10) W. Kemula and R. Sioda, *Nature*, **197**, 588 (1963).

(11) B. Kastening, *Electrochim. Acta*, **9**, 241 (1964).

(12) J. Q. Chambers and R. N. Adams, *Mol. Phys.*, **9**, 413 (1965).

(13) R. Koopmann and H. Gerischer, *Ber. Bunsenges. Physik. Chem.*, **70**, 127 (1966).

(14) B. Kastening, *Z. Anal. Chem.*, **224**, 196 (1967).

(15) K. D. Asmus, A. Wigger, and A. Henglein, *Ber. Bunsenges. Physik. Chem.*, **70**, 862 (1966).

(16) S. G. Mairanovskii, *J. Electroanal. Chem.*, **4**, 166 (1962).

protonation¹⁴ processes described in the literature. In these mechanisms the substrate is viewed as being protonated in the electrical double layer prior to electron transfer. Given and Peover⁴ reported electrochemical waves of this kind for the reduction of benzophenone, benzaldehyde, and xanthone in dimethylformamide in the presence of benzoic acid, and Mairanovskii¹⁶ has suggested that this is a general mechanism for reductions in buffer solutions. Other workers have observed similar effects of proton donors on reduction waves of azobenzene¹⁷ and nitro compounds.^{18,19}

The many-electron pathway was found to depend markedly on the choice of proton donor. This paper reports on the effect of proton source, solvent, supporting electrolyte, and electrode material on the many-electron process.

Experimental Section

Practical grade acetonitrile which had been in contact with calcium hydride for several days was purified by rapid distillation (once or twice) over phosphorus pentoxide followed by a slow distillation from calcium hydride. The tetraethylammonium perchlorate (TEAP) was prepared from the bromide (TEABr) and lithium perchlorate and recrystallized from water several times until the washings gave a negative test for bromide. The *p*-chloronitrobenzene (*p*-CINB) and the TEABr were recrystallized from ethanol. The diethylanilinium perchlorate was prepared following directions in the literature.²⁰ All other chemicals were reagent grade and used without further purification.

The apparatus used to obtain the cyclic voltammograms has been described previously.^{21,22} The equipment for chronopotentiometry was conventional. The constant potential coulometer was based on a design given by Underkoffler and Shain²³ and employed a Heath Model EUW-19A operational amplifier module. The current-time curves were displayed on a Mosley Model 135A X-Y recorder using a sweep generator²¹ as a time base.

The hanging-drop electrode was prepared by hanging three drops of mercury collected from a dropping-mercury capillary on a mercury-plated platinum wire which had been force fitted through a bullet-shaped Teflon plug and sanded flush with the Teflon. The hanging-drop electrode had an area of 6.4×10^{-2} cm². The platinum working electrode was a commercial Beckman electrode. The reference electrode was a saturated calomel electrode which was separated from the working electrode compartment by a salt bridge containing the solution being studied and a fine-porosity sintered-glass frit. The potentials reported in this work were found to be reproducible to ± 0.02 v

over a period of several months. The counterelectrode was a large platinum coil or foil immersed directly in the test solution. The solutions were well deaerated with prepurified nitrogen which had been saturated with the solvent. Occasionally air was purposely introduced into the solution. In all cases oxygen could be eliminated as the cause of the many-electron waves anodic of the one-electron wave. The experiments were carried out at $24 \pm 2^\circ$.

The coulometric analyses were performed on 25.0-ml aliquots of acetonitrile solutions which were 2.0×10^{-3} M in *p*-CINB and 0.10 M in TEABr. The acid concentration of these solutions varied from 2.0×10^{-3} to 8.0×10^{-3} M. The electrolysis vessel was a 50-ml beaker fitted with a rubber stopper which had been bored to allow insertion of the electrodes and a nitrogen inlet tube. A mercury-pool electrode served as the cathode and an Ag-AgBr electrode was the counterelectrode. The reference electrode arrangement described above was used. Nitrogen was bubbled through the cell during the electrolysis. Cyclic voltammetry and dme polarography were used to select an electrolysis potential between the many- and the one-electron reduction waves. After every 1000 sec the electrolysis was stopped and a cyclic voltammogram or polarogram was recorded. The electrolysis was continued in this fashion until the current had diminished to a small fraction of its original value and the many-electron wave had all but disappeared. The reduction products of some of the constant-potential electrolyses were isolated by addition of deaerated ether to precipitate the TEABr and evaporation of the supernatant to dryness under nitrogen. The products were identified by their ultraviolet and mass spectra. The procedure for the *in situ* electrolysis in a cavity of an esr spectrometer has been described.²⁴

Results and Discussion

In the absence of a proton donor, the reduction of aromatic nitro compounds proceeds by a simple reversible one-electron step to produce the radical anion.

(17) J. H. Sharp, Ph.D. Thesis, University of New South Wales, Sidney, Australia, 1966.

(18) W. Kemula and R. Sioda, *Bull. Acad. Polon. Sci., Ser. Sci. Chim.*, **10**, 107 (1962).

(19) A. M. Hartley, private communication.

(20) S. Bruckenstein and I. M. Kolthoff, *J. Am. Chem. Soc.*, **78**, 2974 (1956).

(21) J. R. Alden, J. Q. Chambers, and R. N. Adams, *J. Electroanal. Chem.*, **5**, 152 (1963).

(22) C. A. Chambers and J. Q. Chambers, *J. Am. Chem. Soc.*, **88**, 2922 (1966).

(23) W. L. Underkoffler and I. Shain, *Anal. Chem.*, **35**, 1778 (1963).

(24) R. N. Adams, *J. Electroanal. Chem.*, **8**, 151 (1964).

A further reduction of the radical anion occurs at more negative potentials (-1.3 to -1.4 v *vs.* sce) in which protons are furnished by the solvent and which was not studied in this work. When a proton donor is added to nonaqueous solvents (*e.g.*, acetonitrile, dimethylformamide) containing a supporting electrolyte and the nitro compound, a wave appears at potentials more positive than the one-electron process. In the experiment illustrated in Figures 1 and 2, the nitro compound was *p*-chloronitrobenzene (*p*-ClNB), the proton donor was *o*-phthalic acid, the supporting electrolyte was 0.1 M TEAP, and the solvent was acetonitrile. The new wave can be seen at *ca.* -0.60 v *vs.* sce. (The phthalic acid was electroinactive in the potential region more positive than *ca.* -1.3 v *vs.* sce.) As the concentration of the *o*-phthalic acid was increased, the height of this wave increased linearly and the height of the one-electron nitro wave decreased. The height of this wave increased to that of a three- or four-electron wave and simultaneously the one-electron wave at -1.1 v disappeared from the cyclic voltammograms (Figures 1 and 2).

The most striking feature of the many-electron wave is that it is influenced markedly by the proton donor chosen. The half-peak potential ($E_{p/2}$) for a peak voltammogram or the quarter-wave potential ($E_{\tau/4}$) for a chronopotentiogram varied by *ca.* 0.5 v depending on the acid used. The most positive half-peak potentials were observed for trichloroacetic acid and *p*-toluenesulfonic acid. (The behavior of these acids is complicated by the fact that they are electroactive at potentials more positive than the one-electron process at -1.1 v. This is in accord with the work of Vlcek²⁵ and Kolthoff,²⁶ who found that the overpotential for the evolution of hydrogen on mercury in acetonitrile was much less than in water. The many-electron nitro reduction waves for these two acids occurred *ca.* 0.1–0.2 v more positive than the currents observed in the presence of the acids alone.) The most negative wave before the one-electron wave was observed in the presence of benzoic acid. In this case the many-electron wave was merged with the one-electron wave. No waves at potentials more positive than the one-electron wave were found for phenol, hydroquinones, or water (at low concentrations). The data are summarized in Table I.

A many-electron wave at potentials more positive than the one-electron wave was also observed for different nitro compounds, in the solvents dimethylformamide, dimethyl sulfoxide, and propylene carbonate, and in the presence of a TEABr-supporting electrolyte. The wave was obtained using both platinum and mercury working electrodes although it was 0.1–0.2 v more negative on platinum and more drawn-out.

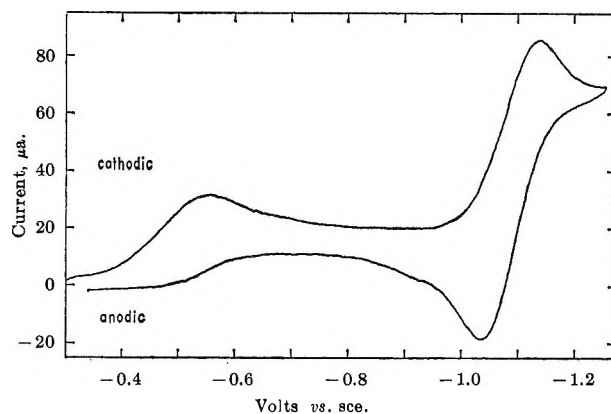


Figure 1. Effect of a proton donor on the *p*-ClNB reduction. Cyclic voltammogram of 4.18 mM *p*-ClNB, 1.76 mM *o*-phthalic acid, and 0.1 M TEAP in acetonitrile. Sweep rate, 60 mv/sec; electrode area, 6.4×10^{-2} cm².

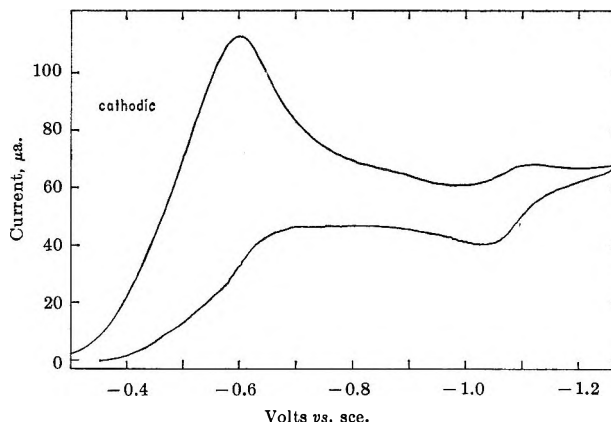


Figure 2. Effect of a proton donor on the *p*-ClNB reduction. Same as Figure 1 except 6.95 mM *o*-phthalic acid was used.

These data are given in Table II. It is clear that the process involved in these reduction waves is a general one.

The reduction of the *p*-chloronitrobenzene–phthalic acid–acetonitrile system using either TEAP or TEABr as a supporting electrolyte was chosen from those of Tables I and II for a more detailed study. This choice was made because the chemicals are easily obtained in a pure state and the use of *o*-phthalic acid as a donor gave a many-electron wave well separated from the one-electron wave.

The parameters which characterize typical single-sweep peak voltammograms of the many-electron wave are given in Table III. These data do not describe the process in a simple manner. At low ratios (*R*) of acid

(25) A. A. Vlcek, *Collection Czech. Chem. Commun.*, **20**, 636 (1955).

(26) J. F. Coetzee and I. M. Kolthoff, *J. Am. Chem. Soc.*, **79**, 6110 (1957).

Table I: Reduction of *p*-Chloronitrobenzene in the Presence of Different Proton Donors^a

Proton donor	Many-electron reduction			One-electron reduction E_p^b
	$E_{\tau/4}$	$E_{p/2}^b$	E_p^b	
<i>p</i> -Toluenesulfonic acid			-0.49 ^c	-1.11
Trichloroacetic acid	-0.54 ($i = 90.0 \mu\text{A}$) ^c			...
<i>N,N</i> -Diethylanilinium perchlorate		-0.56	-0.65	-1.14
<i>o</i> -Phthalic acid	-0.65 ($i = 95.7 \mu\text{A}$)			...
<i>o</i> -Phthalic acid ^d		-0.58	-0.68	-1.16
Salicylic acid			-0.84 ^e	-1.13
<i>p</i> -Hydroxybenzoic acid		-0.81	-0.87	<i>f</i>
Benzoic acid			ca. -1.05 ^g	-1.12

^a The solutions were 4 mM in *p*-CINB, 10 mM in proton donor, and 0.1 M in TEAP, and the solvent was acetonitrile unless noted otherwise. An HDE of area $6.4 \times 10^{-2} \text{ cm}^2$ was employed. Units: volts vs. sce. ^b The sweep rate was 60 mv/sec. ^c These waves occur near a poorly defined background process. ^d The concentration of acid was 8 mM. ^e Split wave. ^f The one-electron wave was distorted. ^g The wave was merged with the one-electron wave.

Table II: Reduction of Nitrobenzene Derivatives in the Presence of *o*-Phthalic Acid in Different Solvents^{a,b}

Electrode	Solvent-electrolyte	Nitro compound	Many-electron reduction ^c		One-electron reduction ^e E_p
			$E_{p/2}$	E_p	
Pt	AN-0.1 M TEAP	<i>p</i> -Nitrobenzaldehyde	-0.67	-0.77	-0.97
Pt	AN-0.1 M TEAP	<i>p</i> -Nitroaniline	-0.76	-0.85	-1.42
Pt	AN-0.1 M TEAP	Nitrobenzene	-0.75	-0.86	-1.19
Pt	AN-0.1 M TEAP	<i>p</i> -Nitroanisole	-0.82	-0.93	...
Hg	DMSO-0.1 M TEAP	<i>p</i> -CINB	-0.81	-0.88	-1.06
Hg	PC-0.1 M TEAP	<i>p</i> -CINB ^c	-0.515	-0.605	-1.05
Hg	DMF-0.1 M TEAP	<i>p</i> -CINB	($E_{\tau/4} = -0.88 \text{ v at } 106 \mu\text{A}$)		...
Pt	AN-0.1 M TEAP	<i>p</i> -CINB	-0.69	-0.88	-1.17
Hg	AN-0.1 M TEABr	<i>p</i> -CINB ^d	-0.76	-0.88	-1.07

^a Abbreviations: *p*-CINB, *p*-chloronitrobenzene; DMSO, dimethyl sulfoxide; DMF, dimethylformamide; AN, acetonitrile; TEAP, tetraethylammonium perchlorate; TEABr, tetraethylammonium bromide; PC, propylene carbonate. ^b The solutions were 4 mM in nitro compound, 10 mM in phthalic acid, and 0.1 M in supporting electrolyte unless noted otherwise. The sweep rate was 60 mv/sec. ^c The concentration of *o*-phthalic acid was 2.4 mM and the concentration of *p*-CINB was 2 mM. ^d The concentration of *o*-phthalic acid was 8 mM and the concentration of *p*-CINB was 2 mM. ^e Units: volts vs. sce.

(HA) to nitro compound the value of $E_{p/2}$ became more negative by ca. 45 mv per decade increase in the acid concentration. At large values of R ($[p\text{-CINB}] = 0.25 \text{ mM}$, $[\text{HA}] > 1 \text{ mM}$), the value of $E_{p/2}$ became constant or slightly more positive as the acid concentration was increased. The width of the wave was not constant, but became broader as the acid concentration increased and the αn_a values calculated from the equation²⁷

$$\alpha n_a = \frac{48}{E_p - E_{p/2}} \quad (1)$$

decreased from 0.57 to 0.37 in the experiment of Table III. The value of $i_p/V^{1/2}$ was constant within the limits expected for spherical diffusion for sweep rates

from 24 to 2000 mv/sec. The many-electron wave did not display any reversible character at sweep rates up to ca. 10 v/sec.

Analogous behavior was found from the chronopotentiometric studies. The value of the chronopotentiometric constant, $i\tau^{1/2}$, for the many-electron wave was directly proportional to the *p*-CINB concentration at high ratios (R) and directly proportional to the HA concentration at low R ($< \sim 4$). Figure 3 shows a graph of $i\tau^{1/2}$ vs. R in which the values of $i\tau^{1/2}$ have been adjusted to those of 4 mM *p*-CINB (i.e., a value of $i\tau^{1/2}$ obtained on an 8 mM HA-2 mM *p*-CINB solution was multiplied by 2 before plotting in Figure

(27) R. S. Nicholson and I. Shain, *Anal. Chem.*, **36**, 706 (1964).

Table III: Peak Voltammogram Parameters; Reduction of 4.18 mM *p*-ClNB in 0.1 M TEAP-CH₃CN^a

[<i>o</i> -Phthalic acid], mM	$E_{p/2}$, mv vs. sce	$E_{p/2} - E_p$, v vs. sce	$i_p/V^{1/2}[\text{HA}]$, $\mu\text{A (mv/sec)}^{-1/2}$ mM ⁻¹
0.445	-424	...	2.27
0.96	-445	0.084	2.14
1.76	-459	0.098	2.15
2.88	-459	0.105	2.11
3.90	-461	0.105	2.10
5.50	-468	0.121	2.03
6.95	-479	0.122	2.04
9.25	-495	0.130	2.01

^a The sweep rate was 60 mv/sec. The area of the HDE was 6.4×10^{-2} cm². ^b Broad peak.

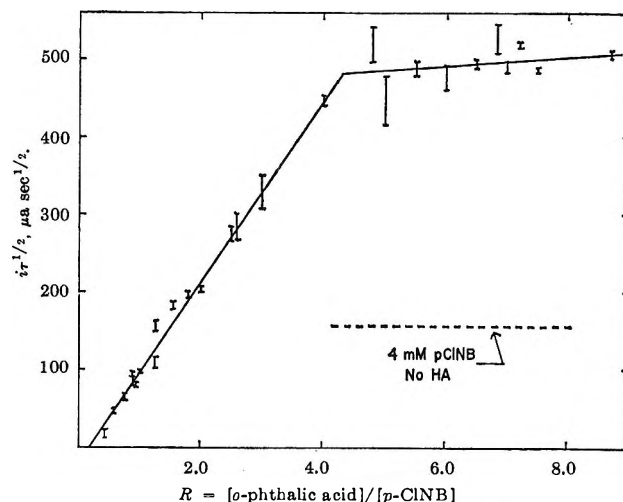


Figure 3. Variation of $i_{\tau}^{1/2}$ with R . The $i_{\tau}^{1/2}$ values have been multiplied by $(4 \times 10^{-3})/[p\text{-ClNB}]$. The solid horizontal lines indicate the average deviation of two to four measurements ($3 < \tau < 15$ sec).

3). At a ratio of *ca.* 4:1 the value of $i_{\tau}^{1/2}$ became constant which indicates that four protons are required for the many-electron reduction. This would correspond to the expected reduction to the *p*-chlorophenylhydroxylamine. However, the value of $i_{\tau}^{1/2}$ at $R > 4$ was only 3.3 times that of the simple one-electron reduction of *p*-ClNB in the absence of proton donor (the dashed line in Figure 3). The value of $i_{\tau}^{1/2}$ was constant within the expected limits for spherical diffusion except at the lowest ratios studied where some kinetic control was evident. This probably accounts for the nonzero intercept in Figure 3.

Table IV: Correlation of Peak Potentials with $-\text{Log } a_{\text{H}^+}$ and $\text{p}K_{\text{HA}}^{\text{b}}$

Acid	E_p , v vs. sce	$-\text{Log } a_{\text{H}^+}$	$\text{p}K_{\text{HA}}^{\text{b}}$
<i>p</i> -Toluenesulfonic acid	-0.49	3.46 ^c	6.2
Salicylic acid	-0.84	8.72	16.7
<i>p</i> -Hydroxybenzoic acid	-0.87	10.85	20.8
Benzoic acid	~ -1.1	10.57	20.7

^a The solutions were 10 mM in the acid, 4 mM in *p*-ClNB, and 0.1 M in TEAP. ^b I. M. Kolthoff and M. K. Chantooni, Jr., *J. Phys. Chem.*, **70**, 856 (1966). ^c The data of I. M. Kolthoff and M. K. Chantooni, Jr., *J. Am. Chem. Soc.*, **87**, 4428 (1965), for 2,5-dichlorobenzenesulfonic acid were used to calculate this value.

Acetonitrile solutions of *o*-phthalic acid and *p*-ClNB were analyzed also by controlled-potential coulometry at potentials past the many-electron wave. It was found that 1.1 ± 0.1 electrons (corrected for background) were required per mole of acid. The elec-

trolyses were followed by either cyclic voltammetry or dme polarography. It is interesting to note that the height of the one-electron wave does not decrease as the nitro compound is reduced by the many-electron process since every nitro molecule which is reduced uses four acid molecules and thus frees another nitro molecule for the one-electron wave. The ultraviolet and the mass spectra of the crude electrolysis products were consistent with the presence of *p*-chlorophenylhydroxylamine, and the chlorine isotopic cluster in the mass spectrum at *m/e* values of 266, 268, and 270 clearly indicated the presence of 4,4'-dichloroazoxybenzene. The spectral correlations were made by comparison with authentic samples of the suspected products. Electrolysis at controlled potentials corresponding to the many-electron wave in the cavity of an esr spectrometer did not produce radical signals. However, an increase of the potential of the mercury pool to that of the one-electron wave immediately resulted in the appearance of the 27-line spectrum of the radical anion of *p*-ClNB.

The significant result of this study is the wide range of potentials observed with different proton donors for the many-electron wave which indicates a correlation with the strengths of the various weak acids used. Table IV gives the hydrogen ion activities of the solutions in Table I for which data are available. The data are not conclusive, but within an order of magnitude, the potential of the many-electron wave is seen to become more negative by 0.06 v/pH unit. The hydrogen ion activities of the 10 mM solutions in Table IV were calculated from eq 2 and 3. The activity

coefficients were estimated from the Debye-Hückel limiting law

$$a_{H^+} = f(K'_{2(HA)}[HA]^2 + K'_{HA}[HA])^{1/2} \quad (2a)$$

where

$$K'_{2(HA)} = \frac{K_{2(HA)}}{f^2} = \frac{[H^+][HA_2^-]}{[HA]^2} \quad (2b)$$

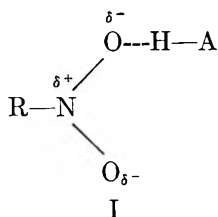
and

$$K'_{HA} = \frac{K_{HA}}{f^2} = \frac{[H^+][A^-]}{[HA]} \quad (2c)$$

$$10^{-2} = [A^-] + [HA] + 2[HA_2^-] \quad (3)$$

for 1:1 electrolytes, $-\log f = 1.64\sqrt{\mu}$ at 25°. The values of the dissociation constants, K_{HA} and $K_{2(HA)}$, in acetonitrile were taken from the work of Kolthoff and Chantooni.²⁸ These calculations assume that perchloric acid behaves as a strong acid and that the tetraalkylammonium salts are completely dissociated in acetonitrile.^{29,30} The data for 2,5-dichlorobenzenesulfonic acid²⁹ were used to estimate the a_{H^+} of the *p*-toluenesulfonic acid solution.

To accommodate these facts, the rate-controlling step is suggested to involve the reduction of a hydrogen-bonded complex (I) formed at the electrode surface



between the nitro compound and the acid. Complete proton transfer is not assumed since reduction of *p*-CINB in the presence of two acids (*e.g.*, *o*-phthalic and benzoic) gave distinct many-electron waves for both acids corresponding to the potentials in Table I. A similar mechanism has been proposed by Given and Peover.⁴ The potential dependence of these "prior protonation" waves (Table III) is not completely consistent with this hypothesis. The wave becomes *more negative* as the acid concentration is increased at low ratios of acid to *p*-CINB. This is the opposite effect expected for a rapid chemical equilibrium preceding the rate-controlling step. It has been shown¹⁶

that potential changes of "preprotonation" waves can be correlated with the change in the potential drop across the diffuse double layer, and at low ratios, *R*, the addition of *N,N*-diethylanilinium perchlorate to a 0.1 *M* TEAP-acetonitrile solution resulted in a real decrease in the drop time of a dme capillary. (In our hands, the drop time measurements in acetonitrile were difficult to reproduce.) Part of the unexplained E_p vs. $[HA]$ behavior is probably due to changes in the potential drop across the diffuse double layer which were not taken into account in this work.

The complex (I) must be formed near the electrode surface or become a much stronger complex in the double layer than in the bulk of the solution. Nitro compounds do form weak hydrogen bonds in solution³¹ but these are not strong enough to account for the large changes in observed rate. Furthermore, the solution chemistry does not indicate complex formation. The ultraviolet spectrum of a mixture of *o*-phthalic and *p*-CINB was equal to the sum of the separate spectra and conductometric titration curves of the acid with *N,N*-diethylaniline showed little change upon addition of *p*-CINB to the titration vessel. The pK_a^0 of nitrobenzene on the Hammett acidity scale is -11.38 ,³² and on this basis protonation of the nitro compounds would not be expected under the conditions of this study.

These "prior protonation" waves could easily be used to determine acid concentrations in nonaqueous solvents as is indicated in Figure 3 and Table III. However, the most significant aspect of this work is the correlation of E_p for the many-electron wave with the pK_{HA} values (Table IV). This result implies that the rate-controlling step involves the dissociation of the complex (I) at the electrode surface.

Acknowledgment. This research was supported in part by a Frederick Gardner Cottrell grant from the Research Corp.

(28) I. M. Kolthoff and M. K. Chantooni, Jr., *J. Phys. Chem.*, **70**, 856 (1966).

(29) I. M. Kolthoff and M. K. Chantooni, Jr., *J. Am. Chem. Soc.*, **87**, 4428 (1965).

(30) I. M. Kolthoff, S. Bruckenstein, and M. K. Chantooni, Jr., *ibid.*, **83**, 3927 (1961).

(31) W. F. Baitinger, P. von R. Schleyer, T. S. S. R. Murtry, and L. Robinson, *Tetrahedron*, **20**, 1635 (1964).

(32) M. A. Paul and F. A. Long, *Chem. Rev.*, **57**, 1 (1957).

An Examination of the Zwanzig Theory of Dielectric Friction

by Gordon Atkinson and Yoshihiro Mori

Department of Chemistry, University of Maryland, College Park, Maryland 20740 (Received April 11, 1967)

The Zwanzig theory of dielectric friction has been applied to alkali metal ions in a variety of solvents and to a number of ions in dioxane-water and glycerol-water mixtures. In all cases the theory gives a good qualitative description of the effect of dielectric relaxation on ion mobility.

It is generally conceded that one of the greatest limitations of present electrolyte solution theory is the naive model assumed for the solvent. The Debye-Fuoss-Onsager solvent is a classical continuum completely characterizable by macroscopic parameters such as dielectric constant, viscosity, and density. Furthermore, in the most rigorous developments of the theory, it is assumed that the bulk solvent parameters are those of the pure solvent unmodified by the presence of ions.

Careful examination of both equilibrium and non-equilibrium properties of electrolytes shows a number of characteristic breakdowns in the theoretical predictions: (1) theories limited to very low concentrations, (2) thermodynamic constants found to be dependent on experimental method, (3) specific solvent effects noted in many properties, and (4) inability of theories to deal with infinite dilution values of properties.

Coincident with the development of theories based on the continuum solvent have been attempts to consider the solvent in more detail. Only a few years after the fundamental paper with Debye, Hückel¹ considered the effect of ions on the dielectric constant of the solvent. Other important contributions have been made by Scatchard,² Eigen,³ Glueckauf,⁴ and Stokes and Robinson.⁵ Unfortunately, most of these approaches involve a somewhat arbitrary and artificial division of the solvent into solvate solvent and bulk solvent. No serious effective attempt was made to consider the dynamic character of the solvent⁶ or the solvent structure.⁷

In 1959, Fuoss⁸ reexamined the effect of dielectric constant on ionic mobility and proposed that dielectric relaxation in the solvent caused by ion motion leads to excess frictional resistance. In a heuristic argument he

suggested that Stokes' law (all symbols are defined in the Appendix)

$$\lambda_i^0 = \mathfrak{F}^2 / (N6\pi\eta r_i) \quad (1)$$

be replaced by

$$\lambda_i^0 = \mathfrak{F}^2 / [N6\pi\eta(r_i + (S/\epsilon_0))] \quad (2)$$

where S is an empirical constant. Then in 1961, Boyd⁹ derived an analogous equation and showed that it gave effects of the correct magnitude in some nonhydrogen-

$$\lambda_i^0 = \frac{\mathfrak{F}^2}{N[6\pi\eta r_i + 4/9(e^2\tau/r_i^3\epsilon_0)]} \quad (3)$$

bonding solvent mixtures. Finally, Zwanzig¹⁰ did the same derivation with fewer approximations and obtained the equation

$$\lambda_i^0 = \frac{\mathfrak{F}^2}{N\left[6\pi\eta r_i + \frac{2e^2\tau}{3r_i^3}\left(\frac{\epsilon_0 - \epsilon_\infty}{\epsilon_0^2}\right)\right]} \quad (4)$$

(1) E. Hückel, *Physik. Z.*, **26**, 93 (1925).

(2) G. Scatchard, *Chem. Rev.*, **19**, 309 (1936).

(3) E. Wicke and M. Eigen, *Z. Elektrochem.*, **57**, 319 (1953).

(4) E. Glueckauf in "The Structure of Electrolytic Solutions," W. J. Hamer, Ed., John Wiley and Sons, Inc., New York, N. Y., 1959, Chapter 7.

(5) R. A. Robinson and R. H. Stokes, *Ann. N. Y. Acad. Sci.*, **51**, 593 (1949).

(6) *E.g.*, T. A. Litovitz and C. M. Davis in "Physical Acoustics," Vol. II, Part A, W. M. Mason, Ed., Academic Press Inc., New York, N. Y., 1965, Chapter 5.

(7) H. S. Frank and W. Y. Wen, *Discussions Faraday Soc.*, **24**, 133 (1957).

(8) R. M. Fuoss, *Proc. Natl. Acad. Sci. U. S.*, **45**, 807 (1959).

(9) R. H. Boyd, *J. Chem. Phys.*, **35**, 1281 (1961).

(10) R. Zwanzig, *ibid.*, **38**, 1603 (1963).

However, neither Zwanzig nor others have checked the applicability of eq 4.

We feel that this is an important oversight. The Fuoss-Boyd-Zwanzig equation (FBZ) introduces the concept of a dynamic solvent whose properties are affected by the presence of ions. This is a real advance in our thinking about the solvent. Now, this is not a panacea for all our problems. The Zwanzig solvent is still a continuum solvent. As has been pointed out so effectively by Kay and his co-workers,¹¹ the structural effects of the ions on the solvent must be considered in any quantitative explanation of ion mobility. However, the FBZ equation relates the deviation from the Walden rule to the independently measurable solvent parameters ϵ_0 , ϵ_∞ , and τ . The only parameter not available independently is r_i , the Stokes radius. Although Zwanzig seems to assume that this is identical with the ion radius, it would be very startling if this turned out to be true.

Calculations

Table I summarizes the ionic conductances of the alkali metals in some pure solvents while Table II gives the solvent parameters needed for the FBZ calculation. Equation 4 can be rearranged to give

$$\frac{\mathcal{F}^2}{N\eta\lambda_i^0} = 6\pi r_i + \frac{2e^2}{3r_i^2} \left[\frac{\tau(\epsilon_0 - \epsilon_\infty)}{\epsilon_0^2} \right] \quad (5)$$

so that a plot of $\mathcal{F}^2/N\eta\lambda_i^0$ vs. the solvent function

$$\left[\frac{\tau(\epsilon_0 - \epsilon_\infty)}{\epsilon_0^2} \right]$$

should be a straight line with an intercept $6\pi r_i$ and a slope of $(2e^2/3r_i^2)$. Figure 1 shows this FBZ plot [$L^* = 6\pi r_i + (2e^2/3r_i^2)R^*$] for the above data. The over-all pattern is clearly a straight line. However, the D₂O points are below the H₂O points and some of the other solvent points are quite a distance off the line.

It was then considered of interest to examine the applicability of the FBZ equation to a mixed-solvent sys-

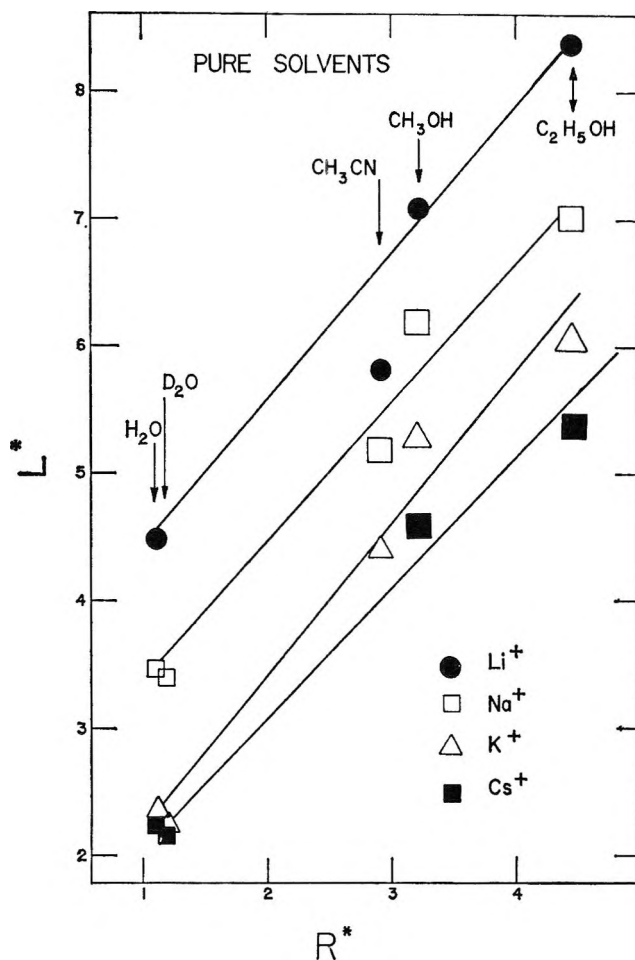


Figure 1.

Table II: Pure Solvent Parameters (25°)

Solvent	ϵ_0	ϵ_∞	$10^{11}r$	$10^2\eta$
H ₂ O	78.54	5.5 ^b	0.83 ^a	0.8903 ^d
D ₂ O	78.06 ^f	5.4 ^e	1.09 ^d	1.094 ^f
CH ₃ OH	32.66 ^h	5.3 ^b	6.9 ^g	0.552 ^h
C ₂ H ₅ OH	24.30 ^j	4.5 ⁱ	14.4 ^g	1.084 ^j
CH ₃ CN	36.01 ^l	1.81 ^k	3.8 ^k	0.344 ^l

^a J. B. Hasted, G. H. Haggis, and P. Hutton, *Trans. Faraday Soc.*, **47**, 577 (1951). ^b J. P. Poley, *Appl. Sci. Res., Sect. B*, **4**, 337 (1955). ^c J. F. Swindells, J. R. Coe, and T. B. Godfrey, *J. Res. Natl. Bur. Std.*, **48**, 1 (1952). ^d D. E. Woessner, *J. Chem. Phys.*, **40**, 2341 (1964). ^e Average value of H₂O and CH₃OH. ^f R. L. Kay and D. F. Evans, *J. Phys. Chem.*, **69**, 4216 (1965). ^g G. F. Böttcher, "Theory of Electric Polarisation," Elsevier Publishing Co., New York, N. Y., 1952, Chapter X. ^h F. Accascina, A. D'Aprano, and R. M. Fuoss, *J. Am. Chem. Soc.*, **81**, 1301 (1959). ⁱ M. W. Sagal, *J. Chem. Phys.*, **36**, 2437 (1962). ^j J. R. Graham, G. S. Kell, and A. R. Gordon, *J. Am. Chem. Soc.*, **79**, 2352 (1957). ^k R. Krishmaji and A. Mansingh, *J. Chem. Phys.*, **41**, 827 (1964). ^l D. S. Berns and R. M. Fuoss, *J. Am. Chem. Soc.*, **82**, 5585 (1960).

Table I: Ionic Conductances^{a,b}

Solvent	Li ⁺	Na ⁺	K ⁺	Cs ⁺
H ₂ O	38.70	50.10	73.50	77.30
D ₂ O	...	41.62	61.40	64.44
CH ₃ OH	39.55	45.17	52.44	60.83
C ₂ H ₅ OH	17.07	20.30	23.55	26.46
CH ₃ CN	77.25	86.40	102.92	101.63

^a Reference 11. ^b Rb⁺ is not included since conductances are only available in two of the solvents.

(11) R. L. Kay and D. F. Evans, *J. Phys. Chem.*, **70**, 2325 (1966).

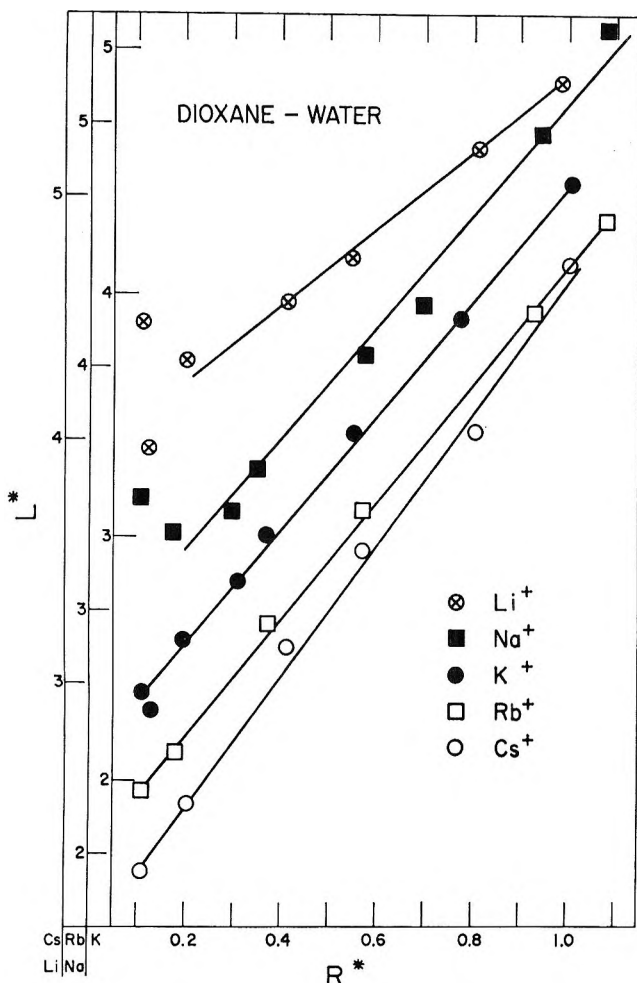


Figure 2.

tem. By means of an extensive set of data due to R. M. Fuoss and his students¹² on the conductance of alkali metal halides in dioxane-water mixtures and transference number data of HCl in the same solvent,¹³ it is possible to estimate λ_i^0 for Li^+ , Na^+ , K^+ , Rb^+ , Cs^+ , Cl^- , Br^- , and I^- in a variety of solvent compositions. The necessary solvent parameters are summarized in Table III. Figure 2 shows the FBZ plot for the cations and Figure 3 the plot for the anions. Both plots are good straight lines.

We then decided to examine the glycerol-water system. In marked contrast with the results in most water-organic mixtures, the Walden product in glycerol mixtures increases with increasing organic content.¹⁴ Unfortunately, no transference number data are available for these mixtures. Therefore, we have assumed that $T_+^0 = 0.50$ in the case of both salts. This is probably a reasonable assumption for KCl but not as good for the Et_4NPic . For the evaluation of τ_D , ϵ_0 , and

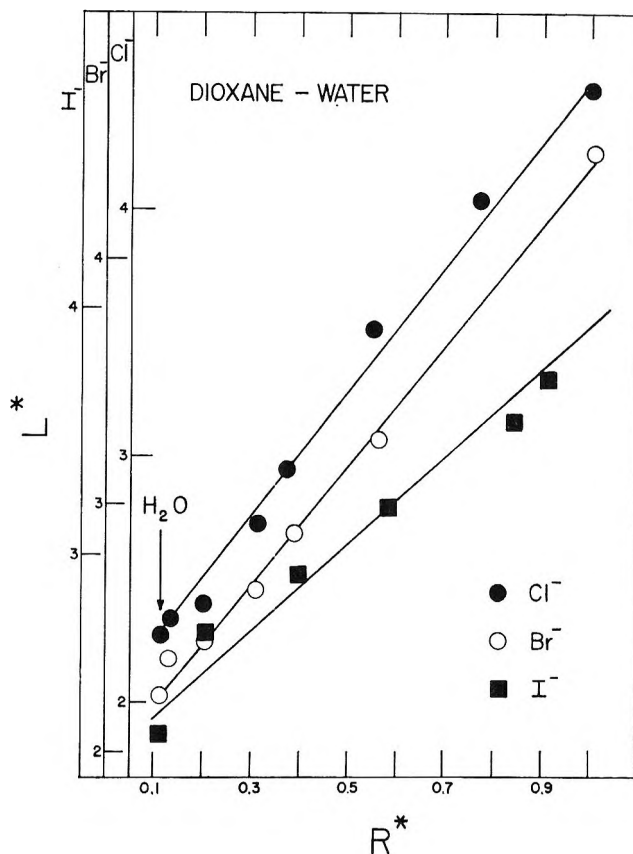


Figure 3.

ϵ_∞ we have used the extensive low-temperature work on such solvent mixtures¹⁵⁻¹⁷ and the following extrapolation techniques to obtain 25° data: (1) ϵ_0 vs. $1/T$ is a straight line for the mixtures studied; (2) ϵ_∞ is essentially independent of T in the range studied and varies linearly with mole fraction from pure glycerol (4.0) to pure water (5.5); (3) a plot of $\ln \tau_D$ vs. $1/(T - T_\infty)$ yields the 25° value; (4) a plot of $\ln \tau_D$ vs. X_{glycerol} gives the correct concentration values. The results of the preceding extrapolations were used to prepare a master plot of $(\tau/\eta)[(\epsilon_0 - \epsilon_\infty)/\epsilon_0^2]$ vs.

(12) Rb(II) : T. L. Fabry and R. M. Fuoss, *J. Phys. Chem.*, **68**, 974 (1964); CsCl : J. C. Justice and R. M. Fuoss, *ibid.*, **67**, 1707 (1963); RbBr : J. E. Lind, Jr., and R. M. Fuoss, *ibid.*, **66**, 1727 (1962); KCl : R. M. Fuoss and J. E. Lind, Jr., *ibid.*, **65**, 999 (1961); RbCl : R. W. Kunze and R. M. Fuoss, *ibid.*, **67**, 914 (1963); LiCl : T. L. Fabry and R. M. Fuoss, *ibid.*, **58**, 971 (1954); NaCl : R. W. Kunze and R. M. Fuoss, *ibid.*, **67**, 911 (1963).

(13) B. B. Owens and G. W. Waters, *J. Am. Chem. Soc.*, **60**, 2371 (1938).

(14) KCl : F. Accascina and S. Petrucci, *Ric. Sci.*, **29**, 1640 (1959); Et_4NPic : F. Accascina and S. Petrucci, *ibid.*, **30**, 3 (1960).

(15) D. J. Denney and R. H. Cole, *J. Chem. Phys.*, **23**, 1767 (1955).

(16) G. E. McDuffie, Jr., R. G. Quinn, and T. A. Litovitz, *ibid.*, **37**, 239 (1962).

(17) G. E. McDuffie, Jr., and T. A. Litovitz, *ibid.*, **37**, 1699 (1962).

Table III: Dioxane-Water Solvent Parameters (25°)

Ref	% dioxane (w/w)	ϵ_0	ϵ_∞	$10^{12}\tau_D$	$10^7\eta^d$
a	95.15	3.84	2.34	15.6	1.054
a	91.94	5.22	2.57	18.5	1.142
a	88.00	7.12	2.68	20.7	1.249
a	83.02	10.06	2.81	23.6	1.365
a	76.53	14.20	2.95	23.5	1.508
a	67.96	21.44	3.18	24.0	1.950
a	55.69	31.19	3.58	21.0	1.972
b	45.2	39.1	c	14.3	1.833
b	33.2	47.9	c	12.7	1.577
b	24.9	58.0	c	11.1	1.400
b	14.2	68.7	c	9.5	1.176
b	0.0	78.54	5.50	8.3	0.8903

^a S. K. Garg and C. P. Smyth, *J. Chem. Phys.*, **43**, 2959 (1965). ^b J. B. Hasted, G. H. Haggis, and P. Hutton, *Trans. Faraday Soc.*, **47**, 577 (1951). ^c Interpolated values. ^d Interpolated from data of T. L. Fabry and R. M. Fuoss, *J. Phys. Chem.*, **68**, 971, 974 (1964). These data were used to prepare a master plot of $\tau(\epsilon_0 - \epsilon_\infty)/\eta\epsilon_0^2$. The values necessary for Figures 2 and 3 were picked off the master plot.

X_{glycerol} from which needed values could be obtained.

Figure 4 shows the FBZ plots for the glycerol-water system. Although a slight curvature can be discerned, the plots are quite close to linear over the whole solvent range. It should be noted that the viscosity increases by over three orders of magnitude as we go from pure water to pure glycerol.

Equation 5 indicates that some hydrodynamic radius can be calculated from both the intercept and the slope of the FBZ plots. Table IV gives these for the four alkali metal ions examined. The slope and intercept radii agree poorly for a given ion. The intercept r_i values show in a crude way the decrease in size with increasing ion size usually attributed to decreased solvation. In the case of K^+ in glycerol-water mixtures r_i (intercept) is 0.58 Å and r_i (slope) is 3.0 Å. The dioxane-water calculations show similar trends.

Conclusions

The Zwanzig equation has been shown to give cor-

Table IV: Radii Comparison (Å)

Ion	r_i (intercept)	r_i (slope)	r (Pauling)
Li ⁺	1.69	5.1	0.60
Na ⁺	1.22	5.3	0.95
K ⁺	0.60	5.2	1.33
Cs ⁺	0.64	5.4	1.69

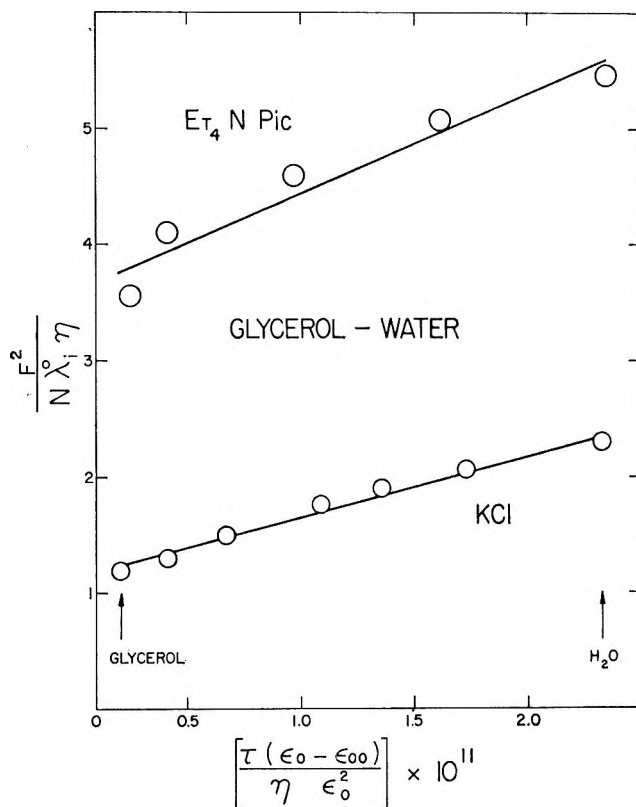


Figure 4.

rect over-all trends in the effect of solvent dielectric relaxation on ion mobility. This is true both in pure solvents and also in solvent mixtures of very different character. The very different behavior of the Walden product of KCl in glycerol-water and dioxane-water mixtures is qualitatively explained by the Zwanzig equation. The difference between r_i (slope) and r_i (intercept) is not too disturbing. The intercept value still reflects factors closely related to the ion-solvent interaction for a particular ion. The slope value—the real concern of the Zwanzig theory—is identical for the four alkali metal ions. This could be interpreted as a distance beyond which the solvent is no longer affected by the ion field. In short, the Zwanzig theory may be reminding us that the concept of an ion radius in a structured solvent is not an easily defined parameter. Furthermore, it has been pointed out¹⁸ that the “wetted” sphere of the Stokes law is to some extent inconsistent with the Zwanzig treatment which ignores the existence of stream lines in the medium. A more consistent approach is being formulated at present. It

(18) H. S. Frank in “Chemical Physics of Ionic Solutions,” B. E. Conway and R. G. Barradas, Ed., John Wiley and Sons, Inc., New York, N. Y., 1966, Chapter 4.

should be noted that Zwanzig examined only the special case where the rate of dielectric relaxation is slower than the rate of solvent exchange. The relative constancy of solvent-exchange rates on simple monovalent ions¹⁹ probably helps us obtain the relatively good qualitative agreement. However, a more general treatment must probably consider the relationship between solvent-exchange rates and ion mobility in a more detailed way.

Acknowledgments. The authors wish to acknowledge the invaluable aid of Professor G. E. McDuffie, Jr., of the Department of Electrical Engineering, Catholic University, in the interpretation of the dielectric data. The work was supported by the U. S. Atomic Energy Commission under Contract AT-(40-1)-2983.

Appendix

Symbols

λ_i^0	Equivalent conductance of the i th ion at infinite dilution
\mathcal{F}	Faraday
N	Avogadro's number
η	Bulk viscosity of the solvent
r_i	"Stokes" radius of the i th ion
S	Empirical constant of the Fuoss equation
ϵ_0	Static (low-frequency) dielectric constant of the solvent
e	Electronic charge
τ	Dielectric relaxation time of the solvent
ϵ_∞	Optical (infinite frequency) dielectric constant of the solvent

(19) M. Eigen in "Coordination Chemistry: Seventh International Conference," Butterworth and Co. Ltd., London, 1963, p 97.

Temperature Effects on Nature and Reactions of Metastable Species in

γ -Irradiated 3-Methylpentane-Carbon Tetrachloride Glasses at 20 and 77°K¹

by R. F. C. Claridge, R. M. Iyer, and J. E. Willard

Department of Chemistry, University of Wisconsin, Madison, Wisconsin 53706 (Received April 17, 1967)

γ Irradiation at 20°K of 3-methylpentane (3MP) glass containing 1 mole % CCl₄ produces a new trapped reaction intermediate (absorbing at 3660 Å), which is not observed at 77°K, but does not produce the "CCl₄⁺" (4800-Å peak) species^{2,3} found following 77°K irradiations. The new species decays at a measurable rate at 50°K and very rapidly at 77°K. It is bleached at 20°K by radiation in its own absorption band. Possible assignments of the new peak are discussed because caging effects are greater. It is suggested that the absence of the 4800-Å peak following irradiations made below 77°K is due to temperature sensitivity of the specialized charge-migration process necessary to produce "CCl₄⁺."

Introduction

CCl₄ present in 3-methylpentane glass during γ irradiation at 77°K is an effective electron scavenger, producing radicals with G of about 1 by the CCl₄ + e⁻ → CCl₃ + Cl⁻ reaction, as deduced from esr measurements.⁴ The effect of charge scavengers on its optical spectra indicates that it is also a positive charge scavenger.^{2,3} It has been proposed that a peak

at 4800 Å is attributable to CCl₄⁺, formed by migration of an excited positive state of 3MP until it encounters

(1) This work was supported in part by U. S. Atomic Energy Commission Contract AT(11-1)-32 and by the W. F. Vilas Trust of the University of Wisconsin.

(2) J. P. Guarino and W. H. Hamill, *J. Am. Chem. Soc.*, **86**, 777 (1964).

(3) D. W. Skelly and W. H. Hamill, *J. Phys. Chem.*, **70**, 1630 (1966).

(4) M. Shirom and J. E. Willard, unpublished work.

and ionizes a CCl_4 solute molecule.^{2,3} The excited state is invoked because the gas-phase ionization potential of 3MP is less than that of CCl_4 . We report here experiments which show that the 4800-Å peak does not appear following γ irradiations at 20°K and that a peak is seen at 3660 Å which is not formed at 77°. These results suggest that there may be large effects of temperature on both the probability of transfer of positive charge and of dissociative electron capture.

Experimental Section

Phillips Pure grade 3MP was purified by passage through 8 ft of freshly activated silica gel. Mallinckrodt Low Sulfur CCl_4 was used as received, since samples purified by gas chromatography gave identical results. Samples of the desired concentration of CCl_4 in 3MP were degassed by the freeze-pump-thaw method and distilled on the vacuum line through P_2O_5 into a reaction cell designed to be held in a Cryotip⁵ refrigeration unit during γ irradiation and scanning of the spectrum with a Cary recording spectrophotometer. The cell was made by machining a 15 mm \times 5 mm hole in a $\frac{1}{8}$ in. thick strip of brass or copper. Its optical faces were Suprasil plates cemented onto either side of the opening with silicone cement. A 22-gauge syringe needle, soldered into a hole through one end of the cell frame, furnished an opening for evacuation and for addition of reactants. A glass capillary tube surrounding the needle, and sealed to the cell at its base with silicone cement, was used for attaching the cell to the vacuum line and sealing it off under vacuum. Soldered to the opposite end of the cell was a 0.25-in. length of 0.25-in. diameter threaded rod for joining the cell to the cooling finger of the Cryotip.

The empty cell held a vacuum well. Reactants were condensed into it from the vacuum line as liquids by cooling the threaded rod at the base. Since the silicone cement is somewhat permeable to 3MP, some loss of liquid to the vacuum in the Cryotip housing occasionally occurs before the solidification temperature is reached. Copper-constantan thermocouples, placed under an indium gasket at the junction to the cooling finger and in a hole filled with Crycon grease at the far end of the cell frame, indicated that the temperature difference between the top and bottom of the cell was less than 1.0°K throughout the range studied.

A sample of CCl_4 in 3MP sealed in a 5-mm i.d. Suprasil tube, mounted in a copper holder shaped like a tuning fork, packed with Cry-con grease to ensure good thermal contact, gave the same optical spectra as samples in cells with cemented windows, showing that the spectra of the latter were not influenced by contamination from the cement. The flat cells were

used in most experiments because they have better optical properties and afford better thermal contact between the cooling finger and the sample.

The relatively slow rates of cooling with the Cryotip, compared to immersion in liquid nitrogen, make it more difficult to obtain glasses with substances which crystallize easily. However, 3MP and its dilute solutions formed clear glasses readily. These remained uncracked to temperatures somewhat below 77°K, but invariably cracked on lowering the temperature to 20°K. The reflectance losses caused by the cracks were compensated by a neutral density filter in the reference beam during spectrophotometric readings.

The vacuum jacket of the Cryotip head was provided with a tubular well into which a Co^{60} source could be lowered to give a dose rate on the sample of 3.3×10^{17} ev g^{-1} min^{-1} . Following irradiation, the Cryotip unit was transferred to a Cary 14 spectrophotometer where the spectrum of the sample could be determined while the analyzing beam passed through Suprasil windows on the sides of the vacuum jacket.

Temperatures in the 20–77°K region were measured with a precision of about 1°K by means of copper-constantan thermocouples, with the reference junction at 77°K, using a microvoltmeter to provide full-scale deflection on a chart recorder for ranges as low as 0.05 mv. The millivolt difference between 77 and 20°K was always within 0.05 mv of the literature value of 0.73 mv.⁶

Results

Figure 1 shows the spectra of a sample of 3MP containing 2 mole % CCl_4 following each of several successive γ irradiations at 20°K.

Similar 3MP- CCl_4 glasses irradiated at 77°K give no peak in the 3660-Å region but only the broad peak at 4800 Å which has been attributed to CCl_4^+ .³ The latter is not produced at 20°K and is not changed in intensity or wavelength by lowering the temperature to 20°K after formation at 77°K. The 3660-Å peak is stable in the dark at 20°K, but decay occurs at 55°K with a half-life of about 30 min and is complete in less than 2 min at 77°K. No new peak grows as the 3660-Å absorption decays, except for a slight increase in the 4500-Å region. (A broad absorption in the region of 4000–5000 Å with optical density of 0.1–0.2 remains after decay of a 3660-Å peak with initial OD =

(5) The Cryotip unit, manufactured by the Air Products Co., utilizes the expansion of nitrogen and hydrogen gases to maintain temperatures down to 20°K with a cooling capacity of 4 w.

(6) C. M. Herzfeld, Ed., "Temperature: Its Measurement and Control for Science and Industry," Reinhold Publishing Corp., New York, N. Y., 1962, Part II.

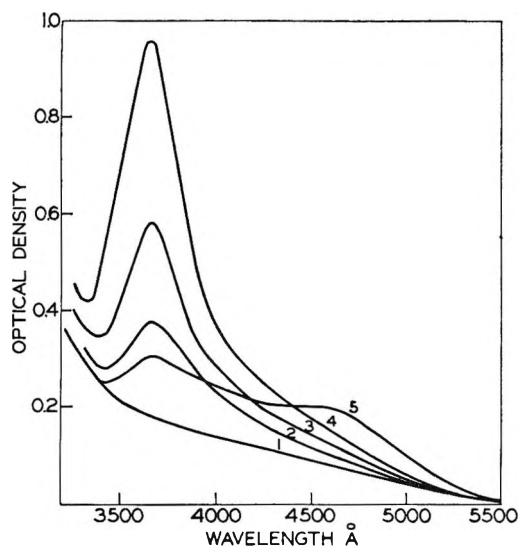


Figure 1. Spectra of 3MP glass containing 2 mole % CCl_4 , following γ irradiations and measurements at 20°K : curve 1, before irradiation; curves 2-4, following each of successive irradiations; curve 5, spectrum after photobleaching with 3700-Å radiation following recording of curve 4.

1.5.) These facts suggest that the 4800-Å species and 3660-Å species are not genetically related and that the production of each is critically dependent on temperature.

The following additional characteristics of the 3660-Å peak have been observed.

(1) The intensity from 1 mole % CCl_4 in 3MP at 20°K is unaffected by the presence of 2 mole % 2-methylpentene-1 (2MP-1) or 2 mole % C_6H_6 . The 2MP-1 did not give the 6800-Å peak³ attributable to 2MP-1^+ .

(2) $n\text{-C}_3\text{H}_7\text{Cl}$ or CH_2Cl_2 in 3MP during γ irradiation at 20°K does not produce a 3660-Å peak. The only spectral change is a small increase in absorption at 2700 Å, superimposed on the rising absorption of the unirradiated system in this region.

(3) If γ irradiation of 1 mole % CCl_4 in 3MP is carried out at neither 77 nor 20°K but at an intermediate temperature of 70°K , two peaks are produced: a broad absorption with a maximum at 4500 Å and a sharp peak at 3660 Å which is about 15% as intense as that produced at 20°K by the same dose.

(4) The initial rate of increase in optical density with dose at 20°K is the same for 1 and 2 mole % CCl_4 in 3MP. One experiment at 10 mole % suggests that it is significantly lower at this concentration.

(5) The rate of increase in optical density with dose decreases with increasing dose. In one experiment five successive doses of 1.6×10^{18} ev g^{-1} each increased the

optical density by 0.21 ± 0.01 unit, but subsequent doses gave 0.18, 0.16, and 0.14 unit.

(6) The 3660-Å peak is readily bleached by light in the 3700-Å range from a monochromator, without generating any new peak.

(7) The 3660-Å peak produced at 20°K in 3MP containing 2 mole % CCl_4 is not altered by the presence of 2 mole % $\text{C}_2\text{H}_5\text{I}$, nor is the 4500-Å peak from the $\text{C}_2\text{H}_5\text{I}$ enhanced by the CCl_4 , as it is at 77°K .⁷

(8) γ Irradiation of pure polycrystalline CCl_4 at 20°K produces a peak at 3450 Å with a small shoulder at 4000 Å similar to those at 77°K , reported earlier⁸ and observed in the current work. Scattering by the cracked sample at low wavelengths precluded observation of the 2700-Å peak in the 20°K experiments. On warming from 20 to 100°K , the 3450-Å peak decays by about 40%, an effect similar to the decay in samples irradiated at 77°K .⁸

Discussion

The 4800-Å peak produced by the irradiation of 3MP containing CCl_4 at 77°K has been tentatively ascribed² to CCl_4^+ formed by charge transfer *via* excited 3MP^+ ions. The evidence that the species must be cationic is convincing.² The evidence from the present work that the yield of the cation at 70°K is much less than at 77°K and unobservable at 20°K indicates that either the mechanism of positive charge migration or of charge transfer from the solvent to the CCl_4 is not effective at the lower temperatures. The transfer of positive charge from a 3MP matrix at 77°K to CCl_4 requires a different type of "positive hole" than transfer to toluene.³ If a specific electronic or vibrational excitation is required, to allow resonant transfer, it is, perhaps, not surprising that changes in the density and/or the internal strains in the matrix should increase the probability of the energy being degraded by other paths.

Further evidence of specificity of the processes by which positive charge is transferred is given by the fact that the 6800-Å peak,² attributed to 2MP-1^+ in γ -irradiated $3\text{MP-CCl}_4\text{-2MP-1}$ glass at 77°K , is not produced at 20°K , whereas the 4500-Å peak produced in $3\text{MP-CCl}_4\text{-C}_2\text{H}_5\text{I}$ glass at 77°K and attributed to $\text{C}_2\text{H}_5\text{I}^+$ is produced at 20°K .

The 3660-Å peak produced in 3MP-CCl_4 at 20°K must represent either ϵ species not produced at 77°K or one which is consumed nearly as rapidly as it is formed. Among the species to be considered are Cl ,

(7) R. F. C. Claridge and J. E. Willard, *J. Am. Chem. Soc.*, **89**, 510 (1967).

(8) T. Shida and W. H. Hamill, *J. Chem. Phys.*, **44**, 2369 (1966).

CCl_3 , Cl_2 , CCl_4^+ , CCl_4^- , Cl^- , Cl_2^- , and complexes of these with CCl_4 . Assuming that the 4800-A peak at 77°K is correctly assigned to CCl_4^+ , this ion is eliminated. CCl_3 and Cl^- are eliminated by the fact that γ -irradiated 3MP- CCl_4 glass at 77°K which shows esr evidence for dissociative electron capture does not show absorption at 3660 Å. Cl^- is further eliminated by the absence of a 3660-Å peak following γ irradiation of CH_2Cl_2 and $n\text{-C}_3\text{H}_7\text{Cl}$ in 3MP at 20°K. The absorption spectrum of Cl_2 is in the 3660-Å range, but this species would not be expected to diffuse sufficiently rapidly at 55°K (or 77°K) to encounter other reactive reaction products (radicals and olefins) at a rate which could account for the observed 3660-Å decay. Reaction of Cl_2 with the solvent could not occur at 77°K in these solutions, which were maintained in the dark except as exposed to the weak analyzing beam. Unless there is clumping of CCl_4 in the matrix, formation of Cl_2^- , as of Cl_2 , appears very improbable. We, therefore, arrive at the hypothesis that the species responsible for the 3660-Å peak is CCl_4^- and that its formation at 20 and 70°K, but not at 77°K, is attributable to increased occurrence of nondissociative capture ($\text{CCl}_4 + e^- \rightarrow \text{CCl}_4^-$) as a result of increased caging effectiveness

of the medium. In terms of the CCl_4^- hypothesis, the onset of decay of the 3660-Å peak at about 50°K may be attributed to increased mobility of positive charge, with consequent neutralization of the anion.⁹

At the present state of knowledge of the mechanisms of positive charge transfer in organic matrices, all plausible possibilities should be considered for further investigation. These include sequences of proton transfer of the type $3\text{MPH}^+ + 3\text{MP} \rightarrow 3\text{MP} + 3\text{MPH}^+$, with eventual formation of CCl_4H^+ or HCl^+ . Such a process, producing a species absorbing at 4800 Å, would avoid the necessity for postulating migration of excitation energy coupled with positive charge, as proposed^{2,3} for the formation of CCl_4^+ . It would not be implausible for such a process to have an activation energy which would lead to the temperature dependence reported in the present work.

(9) NOTE ADDED IN PROOF. Recent work in our laboratory by A. Ekstrom indicates that the $G(\text{CCl}_3)$ produced by γ irradiation of 1% CCl_4 in 3MP at 20°K, and observable by esr, is equivalent to that at 77°K. This indicates that lowering the temperature to 20°K does not reduce the probability of dissociative capture, and that assignment of the 3660-Å peak to CCl_4^- may therefore not be correct.

The Crystal Structures of Bismuth Halide Complex Salts. I. 2-Picolinium

Tetrabromobismuthate(III) and Tetraiodobismuthate(III)¹by B. Ken Robertson,² W. Gant McPherson, and Edward A. Meyers*Department of Chemistry, Texas A & M University, College Station, Texas (Received April 25, 1967)*

2-Picolinium tetrabromobismuthate(III) and tetraiodobismuthate(III) are isomorphous. The anions in both structures show distorted octahedral packing of halogen atoms around bismuth, with two pairs of halogen bridges linking neighboring bismuth atoms. The two unshared bromine atoms are located at 2.63 ± 0.02 and 2.65 ± 0.02 Å from Bi, and the Br–Bi–Br angle is $93.2 \pm 0.6^\circ$. The corresponding values for the iodine structure are 2.87 ± 0.02 and 2.90 ± 0.02 Å, and the I–Bi–I angle is $93.7 \pm 0.5^\circ$. There is little evidence for the influence of the Bi "lone pair" upon the coordination around Bi in either structure. The various bond angles and distances in the halogen bridges are irregular, but the total Pauling bond order for the bismuth–halogen bonds is close to 3 for both structures.

Introduction

Many amine salts of group V halogen complexes have been prepared by Whealy and his co-workers.^{3,4} Since relatively little X-ray structural work has been done on bismuth compounds, the ready availability of a number of amine salts of bismuth–halogen complexes made a study of some of these materials seem attractive. Moreover, the structural work done on a number of salts of antimony(III) halogen complexes^{5–8} had indicated that interesting structural effects were apparent, presumably due to the presence of the "lone pair" of electrons on the antimony atom. The 2-picolinium salts of BiBr_4^{1-} (III) and BiI_4^{1-} (III) were selected for study because good single crystals were easily produced and because the presence of a bulky organic cation was expected to make the resolution of the heavy atoms relatively easy and the absorption effects relatively small.

Experimental Section

The preparations of 2-picolinium BiBr_4 (III) and BiI_4 (III) have been described previously.^{3,4} Needle-shaped single crystals of the salts were grown from water–acetone or water–isopropyl alcohol mixtures that contained the appropriate halogen acid. Examination of the crystals with filtered Mo X radiation revealed that the crystals of the two compounds were iso-

morphous, and that they were monoclinic with systematic absences for (*h*0*l*) with *l* odd and for (0*k*0) with *k* odd, characteristic of $\text{P}2_1/\text{c}-\text{C}_{2h}$.⁵ For convenience, the reflections were indexed on the basis of B-centered cells which made β close to 90° . The equivalent positions in these cells of the (nonconventional) space group $\text{B}2_1/\text{c}$ are: $\pm(x, y, z)$; $\pm(x, 1/2 - y, 1/2 + z)$; $\pm(1/2 + x, y, 1/2 + z)$; $\pm(1/2 + x, 1/2 - y, z)$. The cell dimensions and densities are as follows. BiBr_4 : $a = 24.66 \pm 0.04$; $b = 13.40 \pm 0.03$, $c = 7.63 \pm 0.02$ Å; $\beta = 90.0 \pm 0.5^\circ$; d_{obsd} (floatation) = 3.25 ± 0.08 g/cc; $d_{\text{calcd}} = 3.28$ g/cc for $Z = 8$. For BiI_4 : $a = 26.14 \pm 0.04$; $b = 14.06 \pm 0.03$; $c = 8.03 \pm 0.02$ Å; $\beta =$

(1) This paper was presented at the Joint Southeast-Southwest Regional Meeting of the American Chemical Society, Memphis, Tenn., Dec 2, 1965.

(2) Submitted to the Graduate College of Texas A & M University in partial fulfillment of the requirements for the degree of Doctor of Philosophy, Aug 1965.

(3) J. F. Osborn, Master's Thesis, Texas A & M University, 1960.

(4) J. C. Scott, Master's Thesis, Texas A & M University, 1960.

(5) A. Bystrom and K. A. Wilhelmi, *Arkiv Kemi*, **3**, 461 (1951).

(6) A. Bystrom, S. Backlund, and K. A. Wilhelmi, *ibid.*, **4**, 175 (1952).

(7) A. Bystrom, S. Backlund, and K. A. Wilhelmi, *ibid.*, **6**, 77 (1953).

(8) M. Edstrand, M. Inge, and N. Ingri, *Acta Chem. Scand.*, **9**, 122 (1955).

$90.4 \pm 0.5^\circ$; d_{obsd} (pycnometer) = 3.63 ± 0.05 g/cc; d_{calcd} = 3.60 g/cc for $Z = 8$.

For each compound, a slender needle-shaped crystal enclosed in a thin-walled glass capillary was mounted on the Buerger precession camera and timed exposures were made of a number of zones with the use of Zr filtered Mo X radiation, ($\lambda = 0.7107$ Å). For BiI₄, Weissenberg data for the ($hk0$) zone were also collected by means of Ni-filtered Cu radiation ($\lambda = 1.5418$ Å) and a multiple film pack. The intensities were read with a Welch Densichron, Model I. Lorentz and polarization corrections were applied to the intensity and approximate corrections were made for absorption by the nearly cylindrical crystals. For BiBr₄, $(\mu R)_{\text{Mo}} = 4.0$; for BiI₄, $(\mu R)_{\text{Mo}} = 1.2$ and $(\mu R)_{\text{Cu}} = 5.4$. Approximately 280 reflections were available for each structure. These data were obtained from the ($h0l$), ($0kl$), ($h\bar{h}l$), (hkh) and ($h\bar{k}h$) zones for BiBr₄ and from the ($h0l$), ($0kl$) and ($hk0$) zones for BiI₄.

Patterson syntheses were calculated⁹ for the [010] and [100] projections and their interpretation was straightforward. The trial coordinates for the bismuth and halogen atoms were refined by least-squares techniques,¹⁰ and appropriate Fourier and difference Fourier syntheses⁹ were examined. With the use of individual atom isotropic temperature factors and the inclusion of only bismuth and halogen atom parameters, $R_2 = \{\sum(|F_o| - |F_c|)^2 / \sum |F_o|^2\}^{1/2} = 0.155$ for the BiBr₄ structure, and $R_2 = 0.138$ for the BiI₄ structure. The atomic scattering factors used were taken from the International Tables for X-Ray Diffraction, Volume III, Kynoch Press, 1962, pp 206-207 for Br, p 211 for I, and p 212 for Bi.

The placement of the 2-picolinium group was accomplished primarily by packing considerations in the BiBr₄ structure. The results were supported by the appearance of several difference Fourier syntheses and by improvement in R_2 when light atom contributions were included in F_c . The coordinates for the light atoms were transferred from the BiBr₄ to the BiI₄ structure, and a number of attempts were made to refine the positions of the light atoms in both structures by means of least-squares techniques. In the attempted refinements, large oscillations in the light atom parameters occurred, and it was at first decided to use the coordinates obtained from packing considerations and to abandon the effort to refine them further. The final values of R_2 , with the light atoms included, were 0.112 and 0.126 for BiBr₄ and BiI₄, respectively. In the final refinements of the heavy atoms, the light-atom scattering factors were all taken to be that of carbon, and their temperature factors were all assigned a value of $B = 7.5$ Å².

At the suggestion of a referee, a number of other analyses were performed upon the data.

(1) The least-squares program¹⁰ was modified to permit the introduction of a convergence factor¹¹ in order to damp the oscillations in the refinement of the light-atom coordinates. A weighting scheme was also adopted, in which $\omega = 1$, $|F_o| < 600$; $\omega = 0.25$, $600 < |F_o| < 900$; $\omega = 0$, $|F_o| > 900$ for the BiI₄ structure, and in which $\omega = 1$, $|F_o| < 450$; $\omega = 0.25$, $450 < |F_o| < 650$; $\omega = 0$, $|F_o| > 650$ for the BiBr₄ structure. After more than 24 cycles of refinement, for each structure, all parameter shifts were less than 10% of their estimated standard errors. There were no significant changes in any of the bond distances or angles that involved the Bi and halogen atoms, when compared to the values obtained with unit weights, and with the light atoms fixed by packing considerations.

(2) The least-squares program¹⁰ was also modified to permit the calculation of structure factors in which the effect of anomalous dispersion was included (both real and imaginary parts). Again with unit weights and light atoms fixed by packing, no significant changes were found.

In addition to the above, calculations were made (a) in which the light atoms were fixed by packing and (b) in which the light atoms were excluded completely from the calculations. In order to make a fair comparison, the weighting scheme described above in (1) was used. The only result was, again, to alter slightly the uncertainties in the bond distances and angles among the heavy atoms, but to leave their calculated values essentially unchanged.

The net result of the various calculations is probably the generation of more confidence in the values given in Tables I and II for the heavy atom parameters and related properties which are the topics of interest in this study. The values given in Tables I and II are based upon unit weights, no correction for anomalous dispersion, and with the light-atom coordinates fixed by packing. The uncertainties in bond angles and distances that involve light atoms refined by procedure 1 above are so large as to make their values unreliable (estimated error in bond distances approximately 0.4 Å, estimated error in bond angles approximately 25°).

(9) W. G. Sly, D. P. Shoemaker, and J. H. Van den Hende, "Two and Three-Dimensional Crystallographic Fourier Summation Program for the IBM 7090 Computer," CBRL-22M-62, Massachusetts Institute of Technology, Esso Research and Engineering Co., 1962.

(10) W. R. Busing, K. O. Martin, and H. A. Levy, "OR FLS, A Fortran Crystallographic Least-Squares Program," ORNL-TM-305, Oak Ridge National Laboratory, Oak Ridge, Tenn., 1962.

(11) J. S. Rollett, Ed., "Computing Methods in Crystallography," Pergamon Press, London, 1962, p 8C.

Table I: Atomic Coordinates from Least-Squares Refinement (Uncertainties Are in Parentheses and Apply to the Last Digits of a Number.)

Atom	x/a	y/b	z/c	$B, \text{Å}^2$
2-Picolinium Tetrabromobismuthate(III)				
Bi	0.1194 (2)	0.1658 (4)	0.4630 (6)	3.06 (11)
Br (1)	0.0637 (8)	0.0078 (13)	0.3664 (14)	4.36 (31)
Br (2)	0.0457 (9)	0.3029 (11)	0.2425 (16)	4.10 (31)
Br (3)	0.1851 (12)	0.3527 (10)	0.6388 (16)	4.01 (34)
Br (4)	0.1885 (12)	0.0592 (10)	0.6529 (16)	4.10 (34)
C (1)	0.442	0.405	0.134	7.5
C (2)	0.390	0.358	0.055	7.5
C (3)	0.351	0.422	-0.025	7.5
C (4)	0.306	0.383	-0.105	7.5
C (5)	0.299	0.281	-0.105	7.5
C (6)	0.335	0.220	-0.025	7.5
C (7)	0.381	0.254	0.055	7.5
2-Picolinium Tetraiodobismuthate(III)				
Bi	0.1209 (2)	0.1613 (5)	0.4490 (8)	2.19 (10)
I (1)	0.0618 (4)	0.0007 (10)	0.3431 (15)	3.36 (21)
I (2)	0.0463 (4)	0.3127 (9)	0.2510 (16)	3.39 (21)
I (3)	0.1859 (4)	0.3487 (8)	0.6248 (19)	2.75 (21)
I (4)	0.1938 (4)	0.0452 (10)	0.6276 (22)	3.82 (27)
C (1)	0.436	0.397	0.122	7.5
C (2)	0.387	0.353	0.051	7.5
C (3)	0.351	0.414	-0.025	7.5
C (4)	0.308	0.377	-0.101	7.5
C (5)	0.301	0.280	-0.101	7.5
C (6)	0.335	0.221	-0.025	7.5
C (7)	0.379	0.254	0.051	7.5

Discussion

In both the BiBr_4 and the BiI_4 structures it was found that each Bi atom was surrounded by an irregular octahedron of halogen neighbors and that four halogen bridges connected adjacent Bi atoms. The configuration of the octahedral unit in BiBr_4 is shown in Figure 1, and the relevant bond angles and distances¹² are listed in Table II for BiBr_4 and BiI_4 .

An electron diffraction study of $\text{BiBr}_3(\text{g})$ ¹³ has given $\overline{\text{BiBr}} = 2.63 \pm 0.02 \text{ Å}$, $\text{Br-Bi-Br} = 100 \pm 4^\circ$. This distance compares well with $\overline{\text{BiBr}}(1) = 2.63 \pm 0.02 \text{ Å}$ and $\overline{\text{BiBr}}(4) = 2.65 \pm 0.02 \text{ Å}$, but the angle is considerably different, since $\text{Br}(1)\text{-Bi-Br}(4) = 93.2 \pm 0.6^\circ$. The structure of $\text{BiI}_3(\text{s})$ has been determined most recently by electron diffraction,¹⁴ and the results indicate that each Bi atom is surrounded by an octahedron of I atoms, with $\overline{\text{BiI}} = 3.07 \text{ Å}$, $\overline{\text{BiBi}}' = 4.33 \text{ Å}$. Each Bi atom is linked to three other Bi atoms through three pairs of halogen bridges. The earlier X-ray diffraction studies^{15,16} give similar coordination of I around Bi, and nearly the same interatomic distances. By means of Pauling's equation for bond order¹⁷

$$d_n = d_1 - 0.6 \log n$$

it is possible to estimate the value of d_1 for $\overline{\text{BiI}}$, if it is assumed that the bond order n in $\text{BiI}_3(\text{s})$ is $1/2$. The value of the single bond bismuth-iodine length is calculated to be 2.89 Å, which is very close to the values of $\overline{\text{BiI}}(1) = 2.87 \pm 0.02 \text{ Å}$ and $\overline{\text{BiI}}(4) = 2.90 \pm 0.02 \text{ Å}$.

The longer bonds in both structures involve halogen atoms that are linked to two Bi atoms. In one rectangle in BiBr_4 , the bonds $\overline{\text{BiBr}}(3') = 2.97 \pm 0.2 \text{ Å}$ and $\overline{\text{BiBr}}(2) = 3.08 \text{ Å}$ form the bridge to an adjacent Bi atom at $4.43 \pm 0.01 \text{ Å}$. In the other rectangle, $\overline{\text{BiBr}}(2') = 2.83 \pm 0.02 \text{ Å}$ and $\overline{\text{BiBr}}(3) = 3.27 \pm 0.02 \text{ Å}$.

The longest bonds are directly opposite the shortest bonds in the structures. This is similar to the situation in $(\text{NH}_4)_2\text{SbCl}_5$,⁸ where the $\overline{\text{SbCl}}$ bond opposite the

(12) W. R. Busing, K. O. Martin, and H. A. Levy, "OR FFE, A Fortran Crystallographic Function and Error Program," ORNL-TM-306, Oak Ridge National Laboratory, Oak Ridge, Tenn., 1964.

(13) H. A. Skinner and L. E. Sutton, *Trans. Faraday Soc.*, **36**, 681 (1941).

(14) Z. G. Pinsker, *Tr. Inst. Kristallogr. Akad. Nauk SSSR*, **7**, 35 (1952); *Struct. Rept.*, **17**, 356 (1953).

(15) H. Braekken, *Z. Krist.*, **74**, 67 (1930).

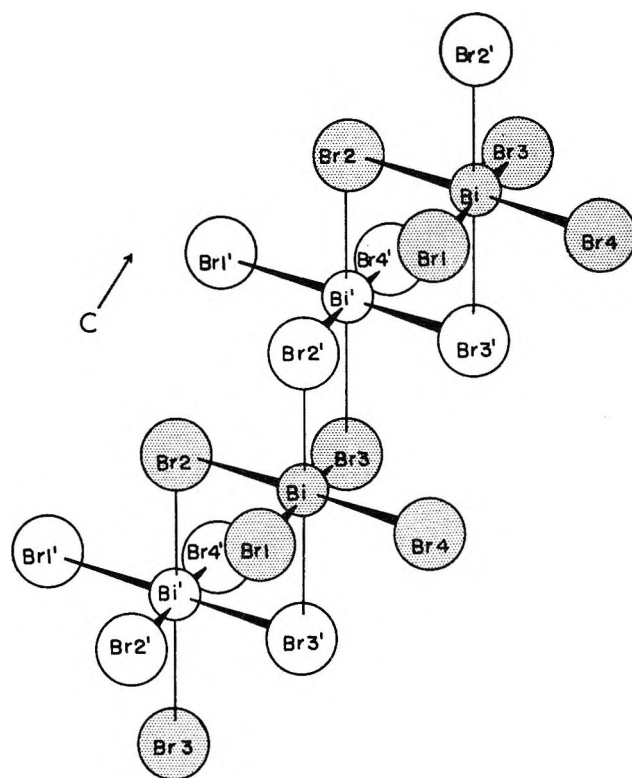
(16) J. Backer in L. Vegard, *Skrifter Norske Videnskaps-Akad. Oslo. I. Mat. Naturv. Kl.*, **2**, 73 (1947).

(17) L. Pauling, *J. Am. Chem. Soc.*, **69**, 542 (1947).

Table II

Bond	Bond distances, Å	
	BiBr ₄ ⁻	BiI ₄ ⁻
BiX(1)	2.63 ± 0.02	2.87 ± 0.01
BiX(2)	3.08 ± 0.02	3.31 ± 0.02
BiX(3)	3.27 ± 0.02	3.45 ± 0.01
BiX(4)	2.65 ± 0.03	2.90 ± 0.02
BiX(2)'	2.83 ± 0.02	3.11 ± 0.02
BiX(3)'	2.97 ± 0.02	3.09 ± 0.02
BiBi'	4.43 ± 0.01	4.73 ± 0.01

Angle	Bond angles, deg	
	BiBr ₄ ⁻	BiI ₄ ⁻
X(1)-Bi-X(2)	91.1 ± 0.6	92.3 ± 0.4
X(1)-Bi-X(4)	93.2 ± 0.6	93.7 ± 0.5
X(1)-Bi-X(2)'	89.7 ± 0.6	89.4 ± 0.4
X(1)-Bi-X(3)'	89.1 ± 0.6	90.4 ± 0.4
X(2)-Bi-X(3)	93.4 ± 0.6	90.1 ± 0.4
X(2)-Bi-X(2)'	86.8 ± 0.6	86.1 ± 0.3
X(2)-Bi-X(3)'	85.2 ± 0.6	86.9 ± 0.4
X(3)-Bi-X(4)	82.5 ± 0.5	84.1 ± 0.4
X(3)-Bi-X(2)'	84.0 ± 0.5	84.1 ± 0.4
X(3)-Bi-X(3)'	97.8 ± 0.8	96.4 ± 0.4
X(4)-Bi-X(2)'	94.6 ± 0.6	95.1 ± 0.5
X(4)-Bi-X(3)'	93.5 ± 0.6	91.9 ± 0.5
Bi-X(2)-Bi'	97.0 ± 0.7	94.8 ± 0.4
Bi-X(3)-Bi'	90.4 ± 0.7	92.4 ± 0.4

Figure 1. Schematic representation of BiBr₄⁻ showing infinite chain structure.

“lone pair” of electrons is 2.36 Å compared to 2.62 Å for the other four SbCl bonds and compared to the value found for SbCl, in SiCl₃(g), of 2.325 ± 0.005 Å.¹⁸ However, even the longest distance in BiBr₄ corresponds to an appreciable bond, certainly greater than that observed on the “lone pair” side in SbF₄,^{5,6} SbF₅,⁷ or SbCl₅.⁸ Indeed, the outstanding characteristic of the structures of BiBr₄ and BiI₄, as well as BiI₃, appears to be the lack of influence that the “lone pair” of Bi appears to have in the determination of the coordination number around Bi. A very similar result has been found in the preliminary results that we have obtained for 2-picolinium SbI₄, crystals of which are isomorphous with the BiBr₄ and BiI₄ crystals examined in this study.

The position of the 2-picolinium group was obtained by packing considerations and the placement of this group is shown in Figure 2, a projection along the *c* axis of BiBr₄. The ring-to-ring contact distances are 3.3 Å or greater. With the exception of C(3), all distances from ring atoms to heavy atoms in BiBr₄ are 3.55 Å or greater. C(3), which should correspond to *N*, has been placed 3.27 Å from the closest Br(3) and 3.53 Å from the closest Br(4). The ring distances are 1.39 ± 0.02 Å, the C(1)-C(2) distance is 1.56 Å, and the ring angles are 120 ± 2°.

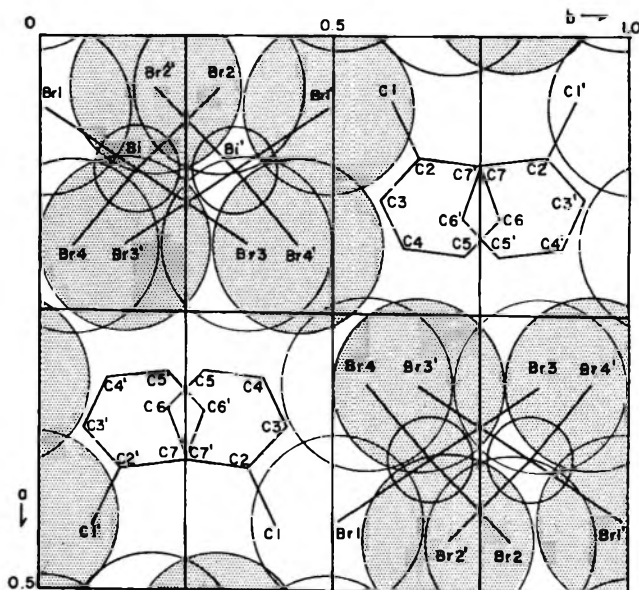


Figure 2. Schematic projection of structure on (001). Picolinium ring placed by packing considerations.

Acknowledgments. The financial support of The Robert A. Welch Foundation is gratefully acknowledged. The facilities of the Data Processing Center

(18) P. Kisliuk, *J. Chem. Phys.*, 22, 86 (1954).

of the Texas A & M University System have been used extensively in the course of this research. Dr. Roger

D. Whealy has kindly supplied us with samples of the compounds studied.

Liquid-Liquid Phase Separation in Alkali Metal-Ammonia Solutions. III.

Sodium with Added Sodium Bromide and Azide

by Patricia White Doumaux¹ and Andrew Patterson, Jr.

Sterling Chemistry Laboratory, Yale University, New Haven, Connecticut 06520

Accepted and Transmitted by The Faraday Society (February 20, 1967)

Experimental data are given for the effect on phase separation in sodium-liquid ammonia solutions of adding varying amounts of sodium salts. Measurements were made at -32.90° with sodium azide and at -32.90 and -56.39° with added sodium bromide. The data are compared with previously reported measurements on sodium iodide. The additions all raise the consolute temperature, broaden the temperature-composition curve, and alter the distribution of components: at a given temperature as the total salt is increased, the salt migrates to the dilute phase and the sodium metal to the concentrated phase. The magnitude of these effects varies, approximately linearly, with the amount of salt added, but depends also on the salt used in the order $\text{NaI} > \text{NaN}_3 > \text{NaBr}$, the most effective listed first.

Introduction

In a previous paper,² the effect of adding sodium iodide on liquid-liquid phase separation in sodium-ammonia solutions was examined. It was not found possible to explain the results in terms of a simple common ion effect. On extending these measurements to include salts with other anionic constituents as reported in this paper, one finds that although the concentration of the salt is a significant factor, it is principally the anion of the salt which influences the results. This finding is further supported by data on phase separation in the sodium-potassium-ammonia system which are reported separately.³

Experimental Section

In preliminary measurements, sodium thiocyanate, sodium sulfide, sodium chloride, sodium cyanide, and sodium tetraphenylborate additions were tested. The

first two reacted with the metal-ammonia solution, and the remainder were too insoluble to bring about phase separation at temperatures of -33° and below for which data on sodium iodide were available for comparison. Sodium bromide and azide suffered none of these failings; they were studied in detail by a procedure which was essentially that of Schettler and Patterson,² with minor modifications. Samples were taken of the separated phases, the ammonia was quantitatively removed, and aqueous solutions of the residues were analyzed for base and salt by successive titrations

(1) This paper contains material taken from a dissertation submitted by P. W. Doumaux to the Graduate School, Yale University, in partial fulfillment of the requirements of the degree of Doctor of Philosophy, Sept 1966.

(2) P. D. Schettler and A. Patterson, *J. Phys. Chem.*, **68**, 2870 (1964).

(3) P. W. Doumaux and A. Patterson, *ibid.*, **71**, 3540 (1967).

with nitric acid and silver nitrate. Because of the dissimilar properties of the silver precipitates, different equivalent point determinations had to be used for each. The precision of the analyses has been tested not only by examining the reproducibility of each of the silver determinations, but also by studying the over-all precision possible as a consequence of all the sample and solution manipulations. A series of samples containing metal, sodium chloride, and ammonia were analyzed. The chloride-containing solutions do not separate into two phases, so the partitioned samples obtained with the Schettler apparatus were necessarily identical. The deviations in the analyses from all manipulative steps were found to lie within 1-2%, usually 1%. As a further check on the azide analyses, a series of titrations were compared with gravimetric determinations of silver azide, the results falling well within these limits. Details of the handling of the different salts were as follows.

Sodium bromide was dried for 5 hr in an Aberhalden pistol using toluene, stored over Drierite, and weighed in air. Both phenolphthalein and differential platinum electrode end-point determinations were made. Bromide was determined with silver nitrate using the same electrodes. In only one determination, that listed last at -56.39° in Table I, 0.01 *m* silver nitrate was used instead of the 0.1 *m* solutions otherwise employed. Reagent grade sodium azide was dried

at 50° for 21 hr and weighed in air. The glassware baking-out procedure normally used was modified to limit the temperature to 50° , but this was followed by prolonged evacuation under "stick-vacuum" conditions before the solution was prepared. It was found that azide samples invariably exploded on being warmed to room temperature for weighing, but that an equally satisfactory analysis for ammonia could be made by absorbing it in standard 1 *m* nitric acid in a gas washing bottle and titrating the excess with 1 *m* sodium hydroxide. A silver wire differential electrode had to be used for the azide analyses, both an adsorption indicator and the platinum electrodes being unsatisfactory. The chloride analyses were made with dichlorofluorescein indicator.

The other manipulations were made in the same way as described earlier;² the temperatures were the same. It should be noted that the temperature -32.90° is in fact the same and should be substituted for that reported by Schettler and Patterson² as -33.35° . The -32.90° figure is correct, the lower figure having been in error owing to the use of a reversed sign in correcting Mueller bridge resistance readings.

Results

The bromide and azide determinations are listed in Table I. Figures 1 and 2 display mole fraction in the dilute phase *vs.* mole fraction in the concentrated phase for sodium (Figure 1) and salt (Figure 2) as a function of temperature and salt used; the data for iodide of ref 2 are included. Figure 3 is a plot of mole fraction salt *vs.* mole fraction sodium for both phases, the type of plot used in ref 2, where the plot was split into two parts of different scale. The data are crowded together on a plot made to the scale used here, but on a suitably expanded scale the tie lines joining corresponding points can be extrapolated to a consolute point for metal and salt. The results, at -32.90° , are $N_{\text{Na}} = 0.0369$, $N_{\text{NaI}} = 0.00255$; $N_{\text{Na}} = 0.0358$, $N_{\text{NaN}_3} = 0.00340$; $N_{\text{Na}} = 0.0361$, $N_{\text{NaBr}} = 0.00408$ (arranged in order of increasing mole fraction of added salt).

Discussion

At -32.90° , the results for iodide, azide, and bromide are similar. As the total concentration of salt is increased, the dilute phase has increased salt and decreased sodium concentration; the concentrated phase exhibits the reverse behavior. In general, at a given temperature, adding salt permits lower and higher concentrations of sodium to remain in equilibrium with each other than would have been allowed in the absence of salt, thus broadening the phase separation curve. If the sodium metal data are plotted as in Figure 2 of

Table I: Liquid-Liquid Phase Separation Data on Sodium-Ammonia Solutions with Added Sodium Salts

Dilute phase		Coned phase	
N_{Na}^a	N_{NaX}	N_{Na}	N_{NaX}
Temperature, -32.90° ; Salt, Sodium Bromide			
0.0128	0.0197	0.0660	0.00215
0.0131	0.0208	0.0656	0.00224
0.0134	0.0209	0.0635	0.00227
0.0176	0.0151	0.0612	0.00239
0.0196	0.0120	0.0588	0.00241
0.0253	0.00747	0.0507	0.00295
0.0286	0.00515	0.0472	0.00292
0.0309	0.00544	0.0399	0.00404
0.0355	0.00392	0.0350	0.00333
Temperature, -56.39° ; Salt, Sodium Bromide			
0.0154	0.00311	0.0763	0.000285
0.0163	0.00156	0.0764	0.0000807
Temperature, -32.90° ; Salt, Sodium Azide			
0.00737	0.0340	0.0734	0.00148
0.0114	0.0244	0.0686	0.000986
0.0211	0.00856	0.0538	0.00195
0.0228	0.00752	0.0524	0.00230

^a All concentrations are mole fractions.

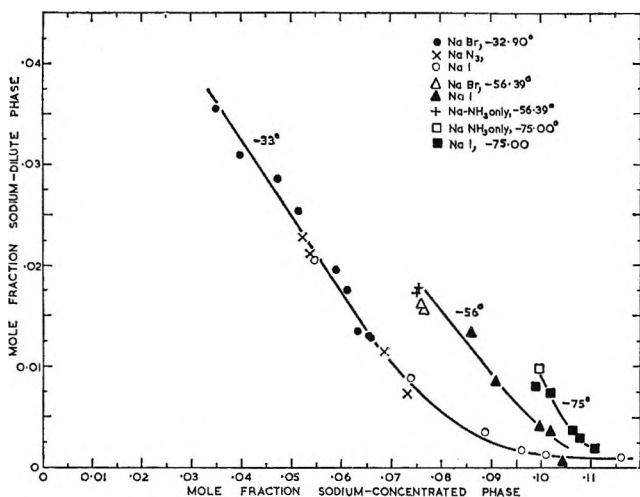


Figure 1. Plot of mole fraction sodium in dilute phase *vs.* concentrated phase. Data are given for three salts and three temperatures as specified in the legend. At temperatures below the consolute point for sodium alone, points have been included for the consolute concentrations of sodium without added salt.

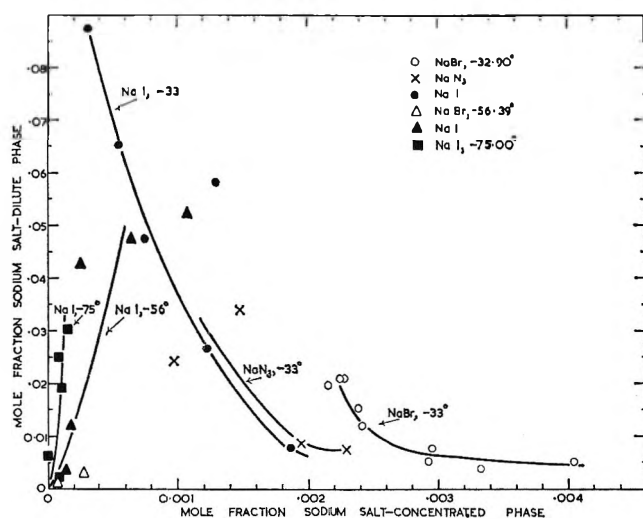


Figure 2. Plot of mole fraction of sodium salt in dilute phase *vs.* concentrated phase. Data are given for three salts and three temperatures as specified in the legend. As is discussed in the text, the trend of data below the consolute temperature for sodium alone is entirely different from that above, *i.e.*, at -33° .

Schettler and Patterson,⁴ all data will fall outside or above the temperature-composition curve, depending on the temperature. A concomitant effect of adding salt is to raise the consolute temperature above that permitted for metal alone. In the results reported earlier on sodium iodide,² it was not clear why the behavior of the salt in the concentrated phase at -56 and -75° was the reverse of what has just been described. Even though the bromide results at -56° are frag-

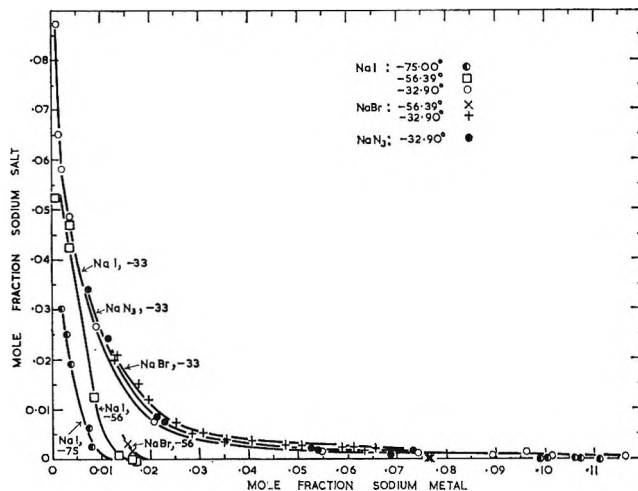


Figure 3. Plot of mole fraction sodium salt *vs.* mole fraction sodium metal for additions of sodium iodide, bromide, and azide as noted in the legend. Corresponding concentrated- and dilute-phase points should properly be connected by tie lines, but these are omitted for greater clarity. Refer to the text for a discussion of the appearance of these data on a suitably large-scale graph.

mentary because of the low solubility of the salt, it is now apparent that the iodide behavior was not an artifact. Below the consolute temperature for sodium alone, the concentrated phase curves (as in Figure 3) proceed to intersect the sodium axis at a point corresponding to zero sodium salt, at the permitted sodium concentrations for the temperature in question, with the necessary consequence that all other points have larger concentrations of salt than zero, a concentration increasing with total salt concentration. Above the consolute temperature for sodium alone, the concentrated phase curve proceeds to a consolute point having concentrations of sodium and salt larger than any other value on the concentrated phase curve, which does not intersect the sodium axis, and which thus has a reverse slope to the concentrated phase curves at the two lower temperatures. At -32.90° , the mole fractions of salt required to effect phase separation stand in the order $\text{NaI} < \text{NaN}_3 < \text{NaBr}$. The mole fractions of sodium at the extrapolated consolute points are the same, within $\pm 1.6\%$, approximately the precision of plotting and reading the graphs.

In Figure 1, the data for all three salts fall on the same curve at a given temperature, while in Figure 2 three separate curves result depending on the salt in question, thus demonstrating that while the effect depends upon the concentration of salt added, it depends

(4) P. D. Schettler and A. Patterson, *J. Phys. Chem.*, **68**, 2865 (1964).

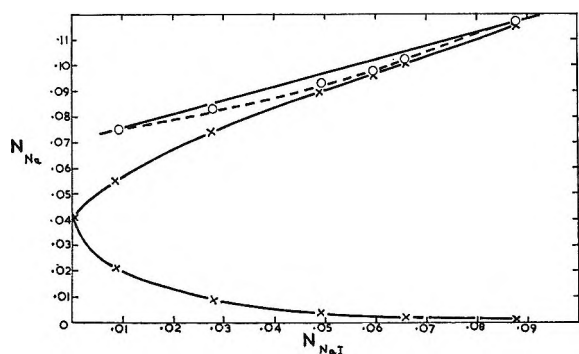


Figure 4. Plot of mole fraction sodium *vs.* mole fraction sodium iodide (total). The three curves, reading from the top down, are sodium, total, with the actual data shown as the dotted curve, and a straight line drawn for comparison; middle curve, sodium, concentrated phase; bottom curve, sodium, dilute phase.

also on the salt used. Since each salt has the same cation, the distinctive effect must depend on the anion. Figure 4 is a plot of N_{Na} *vs.* $N_{\text{NaI}}(\text{total})$. The three curves result from combining the data in ref 2 so as to yield $N_{\text{Na}}(\text{total})$, top curve; $N_{\text{Na}}(\text{concentrated})$, middle curve; and $N_{\text{Na}}(\text{dilute})$, bottom curve, plotted against $N_{\text{NaI}}(\text{total})$ in each case. This plot shows that total mole fraction of sodium is approximately linear in total mole fraction of added salt. The dilute and concentrated curves have been extrapolated to the sodium-only point, on which they converge in a smoothly parabolic manner. Very similar curves result for azide and bromide though the range of salt concentration covered is smaller.

The dependence of the effect on the salt used could arise in at least two different ways, a stoichiometric common-ion effect, or a specific ionic interaction. It can be shown, with data on two additional salts, that the first explanation is entirely unsatisfactory, the second more attractive.

In the solutions studied here, the concentration of sodium lies (at temperatures above -78°) from about 0.4 to 2.6 *m*, dilute phase, and from 2.6 to 6 *m*, concentrated phase. Arnold and Patterson⁵ have proposed a model for these solutions which gives the species present in this range, in order of decreasing concentration, as Na^+ , Na_2 , M' (for example, Nae^- or e_2^{2-}), e^- , and Na^0 . The actual concentrations cannot safely be calculated, but the concentration of Na^+ is some 10^2 -fold greater than that of Na^0 , with the other species lying between. In assessing the possible interactions of these several species, the two neutral ones should play no important part, while the negative diamagnetic species would be less important in interactions with electrons since it is stabilized by spin pairing, though the negative charge

might be important in electrostatic interactions. The solvation behavior of all the species might affect the metal-salt interactions.

Ionization constants have been determined for sodium iodide and bromide in liquid ammonia, though not for azide. The values are NaI , 2.80×10^{-3} and NaBr , 2.898×10^{-3} , from the work of Kraus and his associates.^{6,7} Gunn and Green⁸ have obtained a rather different value for sodium iodide through consideration of heats of solution of sodium in the presence of sodium iodide. The concentrations are nearer those in this work and iodide was present, but as there are no comparable data for bromide, we must accept the data of Kraus^{6,7} and assume the azide behaves in a similar way. The small difference between the bromide and iodide ionization constants and the probability that the ionization of the salts is effectively suppressed by the large concentration of Na^+ present in the mixtures make these assumptions reasonable. It would be desirable to have data on sodium azide ionization; we propose to undertake a study to remedy this lack. In any case, the presence of an unionized species, NaX , is insufficient to account for the results through a common-ion effect.

Catterall and Symons⁹ have studied esr *g* shifts in alkali metal-ammonia solutions in the presence of added salts. Sodium iodide gave a large negative Δg , bromide a small negative Δg , and chloride and amide a negligible shift. Azide was not studied. In the esr measurements, the effect of varying the alkali metal cation in the salt of a particular anion was noticeable only with iodide, but in any case the effect was much subsidiary to that of the anion. These authors considered that quantum mechanical interactions between solvated electrons and solvated anions or salt ion pairs were the important source of the effects they observed. The salt-metal ratios used were up to 200-fold larger than those employed in our study. The similarity of the results—the large effect of iodide and the smaller effect of bromide—suggests that a specific interaction between the solvated electron and an ion-paired salt is a much more likely source of the phase separation observations than a common-ion effect in which the original Kraus equilibrium, $\text{Na}^0 \rightleftharpoons \text{Na}^+ + \text{e}^-$, is shifted toward the left by added sodium salt. Indeed, the shift, owing to electron-salt interactions, is presumably to the right. As Figure 1 clearly shows, cation or metal behavior is not distinctively affected by the salt used,

(5) E. Arnold and A. Patterson, *J. Chem. Phys.*, **41**, 3089 (1964).

(6) C. A. Kraus and W. C. Bray, *J. Am. Chem. Soc.*, **35**, 1315 (1913).

(7) V. F. Hnizda and C. A. Kraus, *ibid.*, **71**, 1565 (1949).

(8) S. R. Gunn and L. G. Green, *J. Chem. Phys.*, **36**, 368 (1962).

(9) R. Catterall and M. C. R. Symons, *J. Chem. Soc.*, 4342 (1964).

as is also found in ref 3, which shows the relatively minor effect of cation or metal interactions.

It should be noted that, while the migration of the metal from the dilute to the concentrated phase with increasing added salt is a consequence of the effect of the salt in raising and broadening the temperature-concentration curve, the migration of the salt to the dilute phase is contrary to what would be expected from any of the commonly observed examples of phase separation. The recent work of Eisen and Jaffe¹⁰ is typical of the usual behavior: the concentration of the salt should increase in both phases. In the present experiments, whether or not the temperature of observation is above or below the consolute point of sodium, the majority of the salt appears in the dilute phase. Just what role it plays there is a matter of interest and speculation.

We have proposed in a separate paper¹¹ a model for two-component phase separation emphasizing the calculation of the chemical potential of the solute. Although the model is inadequate to cope with the three-component problem, in terms of the chemical potential, the effect of the salt is to raise it in the dilute phase and lower it in the concentrated phase, in spite of the lesser

and greater concentrations of metal present. Taken together, the salt studies examined in this paper strongly suggest that electron-anion interactions make this possible, and that the order of the salts found depends on quantum electronic interactions with the anion, a possibility which should be checked by esr measurements on metal-azide solutions. The migration of the salt to the dilute phase is less easily understood. Since the metal is principally in the form of Na^+ , it may be that electrostatic effects are important. Alternatively, considerable quantities of solvent ammonia are bound to metal in the concentrated phase, so it may be that the dilute phase is a better solvent for the salt.

Acknowledgment. This work was supported by the National Science Foundation. The hospitality of the Physical Chemistry Laboratory, Oxford University, extended to A. P. and the assistance and continuing interest of Dr. Paul Schettler during this work are gratefully noted.

(10) E. O. Eisen and J. Jaffe, *J. Chem. Eng. Data*, **11**, 480 (1966).

(11) P. D. Schettler, P. W. Doumaux, and A. Patterson, paper V in this series, submitted for publication.

Liquid-Liquid Phase Separation in Alkali Metal-Ammonia

Solutions. IV. Sodium and Potassium

by Patricia White Doumaux and Andrew Patterson, Jr.

Sterling Chemistry Laboratory, Yale University, New Haven, Connecticut 06520

Accepted and Transmitted by The Faraday Society (February 20, 1967)

The phenomenon of liquid-liquid phase separation in ammonia solutions containing both sodium and potassium has been examined over a range of concentrations of both metals at two temperatures, -56.39 and -75.00° . Separate analyses were made for both metals with a precision of about 1%. Perceptible, but not large, metal₁-metal₂ interactions occur which cannot, from these experiments alone, be assigned with certainty solely to the metal atoms or to the positive ions.

In earlier papers^{1,2} we have examined the effect on phase separation in sodium-ammonia solutions when metal salts are added. The results indicated that the effect of the salt depended upon its anionic constituent, and it seemed most likely (from other experimental measurements) that interactions between the electrons in the solution and the anion of a solvated ion-paired salt molecule were responsible for the observed broadening of the miscibility gap and raising of the consolute temperature. In spite of this at least self-consistent interpretation of our data, the kinds of models for behavior of alkali metal-ammonia solutions which one invokes are not all in agreement and are often dependent upon the kind of experiment employed and the system studied. Thus, conductivity measurements on alkali metal salt-liquid ammonia systems by Hnizda and Kraus³ indicated a much smaller interaction of the halide ion with the solvent than is the case with the cation. On the other hand, Catterall and Symons⁴ have found the effect of the cation on esr g shifts in solutions containing both metal and salt to be greatly subsidiary to that of the anion of the salt used, as was also our finding in our phase separation measurements.^{1,2} While these results are not necessarily in conflict—in one case salt only is present, while in the other both salt and metal are involved—and while it is likely that ion solvation was the important factor in Kraus' work but a quite different interaction responsible for the results in that of Catterall and Symons, we felt it desirable to investigate the importance of possible

metal₁-metal₂ or metal ion₁-metal ion₂ interactions on phase separation. We have done this through a study of phase separation in solutions containing both sodium and potassium. It is of interest that Professor Kraus, in his prefatory note to the "Colloque Weyl" presentations,⁵ suggested just such an investigation. We plan to extend these measurements to other alkali metal systems.

Experimental Section

The procedures used were essentially those earlier described.^{1,2} Total alkalinity was determined on the mixed metal hydroxide residues by titration with nitric acid. Potassium was determined in this solution remaining from the titration by a gravimetric procedure developed by Kohler,⁶ employing sodium tetraphenylborate. Measurements were made at -56.39 and -75.00° . One determination was made at -32.90° to afford a check on the precision of the analyses; as might have been expected, phase separation was not observed.

(1) P. D. Schettler and A. Patterson, *J. Phys. Chem.*, **68**, 2870 (1964).

(2) Part III: P. W. Doumaux and A. Patterson, *ibid.*, **71**, 3535 (1967).

(3) V. F. Hnizda and C. A. Kraus, *J. Am. Chem. Soc.*, **71**, 1565 (1949).

(4) R. Catterall and M. C. R. Symons, *J. Chem. Soc.*, 4342 (1964).

(5) C. A. Kraus, Foreword, "Solutions Métal-Ammoniac—Propriétés Physicochimiques, Colloque Weyl," G. Lepoutre and M. J. Sienko, Ed., W. A. Benjamin, Inc., New York, N. Y., 1964.

(6) M. Kohler, *Z. Anal. Chem.*, **138**, 9 (1953).

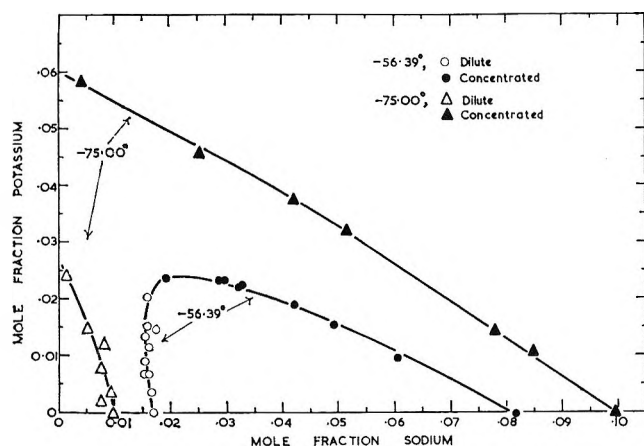


Figure 1. Plot of mole fraction of potassium vs. mole fraction of sodium for data on phase separation of solutions containing sodium, potassium, and liquid ammonia. Measurements were made at the two temperatures indicated in the legend.

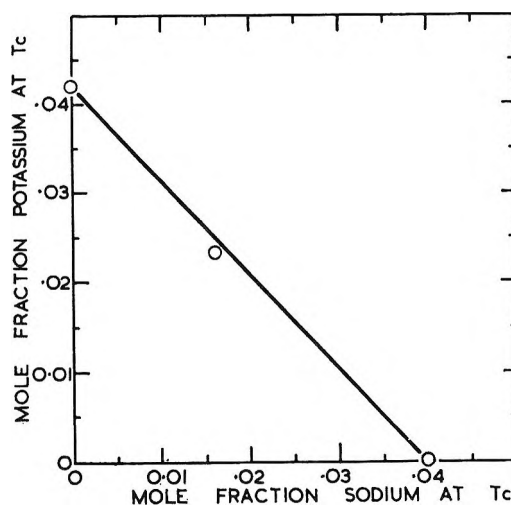


Figure 2. Plot of mole fraction of potassium vs. mole fraction of sodium at the consolute temperature, with the extrapolated value for a solution containing both sodium and potassium, obtained from the data of Figure 1 at -56.39° at center. This is a one-dimensional projection of the mole fraction of potassium-mole fraction of sodium-consolute temperature surface.

Table I: Liquid-Liquid Phase Separation Data on Sodium-Potassium-Ammonia Solutions

Dilute phase		Concd phase	
N_{Na}^a	N_K	N_{Na}	N_K
Temperature, -56.39°			
0.0153	0.00677
0.0155	0.00919	0.0421	0.0188
0.0162	0.0118	0.039 ^b	0.025 ^b
0.0156	0.0135	0.0328	0.0224
0.0162	0.00694	0.0493	0.0154
0.0175	0.0147	0.0322	0.0223
0.0166	0.00392	0.0603	0.00985
...	...	0.0299	0.0233
0.0159	0.0151	0.0289	0.0234
0.0159	0.0202	0.0194	0.0236
Temperature, -75.00°			
0.00812	0.0120	0.0420	0.0376
0.00768	0.00824	0.0515	0.0319
0.0077 ^b	0.0020 ^b	0.0849	0.0109
0.00507	0.0148	0.0252	0.0459
0.00954	0.00342	0.0777	0.0144
0.00128	0.0242	0.00394	0.0584
0.00986	None ^c	0.0997	None ^c

^a All concentrations are in mole fractions. ^b Data given in two significant figures were estimated due to small loss of ammonia before analysis. ^c The notation "none" indicates a determination on sodium alone.

Results

The data are shown in Table I and in Figure 1 in the form of plots of mole fraction sodium in dilute and concentrated phases at the two temperatures studied. Because the sodium phase separation data available⁷

did not extend as low as -75.00° , a determination was made on sodium alone at that temperature. Earlier, Schettler⁷ had extrapolated data on solutions containing sodium iodide to zero concentration sodium iodide; his extrapolated values and the present results check closely, the preferred experimental values being $N_{Na}(\text{dilute}) = 0.00986$, $N_{Na}(\text{concd}) = 0.0997$. In Figure 2 of ref 7 the data are plotted as mole ratios, while mole fractions are used here. Data for potassium alone were read from a large-scale plot of data of ref 7 since a number of points had been determined near -75.00° . In the determination at -32.90° on separated samples of the same solution, the results were: "dilute phase" sample, $N_K = 0.00631$, $N_{Na} = 0.0474$; "concentrated phase" sample, $N_K = 0.00625$, $N_{Na} = 0.0470$.

Discussion

The reproducibility of the data is of the same order as that in the study of bromide and azide where multiple determinations are made on the same sample,² about 1%; the data of Schettler on sodium-sodium iodide are appreciably better, but this is a much more favorable system, from the point of view of analysis, on which to work.

In Figure 1, the -75° data pass smoothly and with but little curvature from the potassium to the sodium axis; the curvature of the data at -56.39° is more pro-

(7) P. D. Schettler and A. Patterson, *J. Phys. Chem.*, **68**, 2865 (1964).

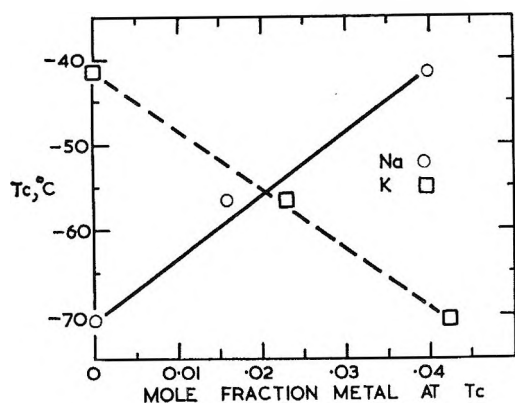


Figure 3. Plot of consolute temperature *vs.* mole fraction of metal at the consolute temperature for sodium and potassium in mixed solutions as indicated in the legend. As in Figure 2, this is a one-dimensional projection of the three-variable surface.

nounced, but this in part is presumably due to the fact that this temperature is above the consolute temperature for potassium, in which connection the data on sodium-sodium iodide² below and above the consolute temperature of sodium should be recalled. At -56.39° , by extrapolating the midpoints of the tie lines, we obtain a consolute point for this temperature of $N_K =$

0.0232 and $N_{Na} = 0.0159$. Using these values and those for sodium and potassium two-component systems, -41.55° , $N_{Na} = 0.0398$, -70.05° , $N_K = 0.0421$, one can construct a two-dimensional projection of the temperature, N_{Na} , N_K surface in two graphs, Figures 2 and 3. These show small but significant deviations from a straight line connecting the extreme two-component points: about 1.4° in the temperature *vs.* mole fraction metal, and 8% in the mole fraction metal at consolute temperature plots. Such deviations from linearity could be due to differences between interactions of the two metals with the solvent, to specific interactions between the two ions themselves, or to a combination of both. The present data are not sufficient to decide this point. The deviations, though small, are significant, for they exceed by some tenfold the precision of the measurements. Kraus' suggestion⁵ that mixed-metal studies be extended to include the alkaline earth metals is then of much interest since the charge on the metal ion becomes one of the variables available for examination. We propose to pursue this point.

Acknowledgment. This work was supported by the National Science Foundation.

The "Sieve Effect" in Chlorella Suspensions^{1a}

by M. Das, E. Rabinowitch, L. Szalay,^{1b} and G. Papageorgiou^{1c}

Department of Botany, University of Illinois, Urbana, Illinois (Received August 12, 1966)

The absorption band of a suspension of strongly absorbing particles is flatter than that of a true solution containing the same number of absorbing molecules. This diminishing effectiveness of absorption is due to mutual screening of molecules in the particles; this effect is stronger at the wavelengths where the optical density of this particle is higher, causing reduction in height as well as broadening of the absorption band ("sieve effect"). To eliminate the sieve effect, *Chlorella pyrenoidosa* was disintegrated by sonication. If sonication was carried out aerobically in the (slightly acid) growth medium, chemical bleaching of chlorophyll overcompensated, after a few minutes of sonication, the increase in absorption caused by removal of the sieve effect; but when it was carried out in argon-saturated, slightly alkaline solution, the height of the band kept increasing, reaching a steady level after about 60 min of sonication. The spectrum of such fully disintegrated suspensions is tentatively considered as that of intact pigments in associations with the same molecules as in the living cell. Experimental "flattening coefficients" were determined from this spectrum and compared with theoretical values, calculated for suspensions of particles of a certain size and shape.

Introduction

Duysens^{2a} first discussed the influence on the apparent absorption spectrum of cell suspensions of the nonuniform distribution of pigments. Rabinowitch^{2b} gave a somewhat different analysis of the same problem (based on twice repeated application of Beer's law, first to the pigment molecules within a particle and then to the suspension, treating particles as giant molecules). Both treatments led to the same equation. The problem has also been discussed by investigators³ interested in the absorption properties of colloidal dye suspensions—a somewhat simpler case than that of live cells, because within the dye particles, the concentration of the pigment is constant; also, the size and shape of particles can be made more uniform than those of cells (*e.g.*, in a suspension of unicellular algae).

The phenomenon was called by Rabinowitch "sieve effect"—a graphic if not quite adequate name, which we will continue using because of its convenience. The sieve effect reduces the absorption of a suspension, compared to that of the same amount of pigment in true solution, at all wavelengths; however, the extent of this reduction depends on the strength of absorption within a single particle and is therefore strongest in the peaks of

the absorption bands (where a single algal cell may absorb over 50% of incident light) and weakest in the valleys between them. The stronger the band, the more strongly it is reduced in height by the sieve effect. Consequently, the sieve effect causes an apparent flattening of the absorption spectrum.

Such a flattening is in fact shown by all published absorption spectra of cell suspensions (or leaves) when compared with the spectra of cell extracts. It should be (but often has not been) taken into account in attempts to reconstruct the spectra of cells or leaves from those of the several pigments contained in them.

One may ask which of the several observed differences between the absorption spectra of cells and extracts can be attributed to the sieve effect. Interactions of pigment molecules, among themselves and with other cell

(1) (a) This work was supported by National Science Foundation Grant GB 3305 and Atomic Energy Commission Grant AT(11-1)-1502; (b) supported by the Inter-University Committee on Travel Grants, on leave from the University of Szeged, Hungary; (c) supported by National Institutes of Health, Grant PH-GM-13913.

(2) (a) L. N. M. Duysens, Thesis, Utrecht, The Netherlands, 1952, p 21; L. N. M. Duysens, *Biochim. Biophys. Acta*, **19**, 1 (1956);

(b) E. Rabinowitch, "Photosynthesis and Related Processes," Vol. II.2, Interscience Publishers, Inc., New York, N. Y., 1956, p 1863.

(3) R. J. Gledhill and D. B. Julian, *J. Opt. Soc. Am.*, **53**, 239 (1963).

materials, are another cause of spectral changes. (We presume that scattering, that can completely distort the apparent absorption spectrum when measurements are made in transmitted light, has been eliminated by the use of an integrating sphere and that we can neglect the distortion of the spectrum caused, in an integrating sphere, by repeated passages through the absorption cuvet; cf. Butler.⁴) The well-known *shift* in the band positions *in vivo* toward the longer waves, for example, cannot be due to the sieve effect and must be attributed to molecular interactions (in analogy to the well-known band shifts from solvent to solvent); the same must be true of the *splitting* of the absorption bands *in vivo* into two (or more) components.^{5,6} The *flattening* of the absorption bands seems, on the other hand, to be due largely to the sieve effect and the same seems to be true, in the case of chlorophyll *in vivo* and *in vitro*, of the change in the relative intensities of the two main absorption bands. In solution, the blue (Soret) band of chlorophyll is stronger than the red band; it is therefore also more strongly affected by the sieve effect. This causes a decline, *in vivo*, of the intensity ratio, *R*, of the blue compared to the red band. The splitting of the red absorption band of chlorophyll *in vivo* into two components also must contribute to its flattening, but this influence is secondary compared to that of the sieve effect, as shown by the fact that in cell sonicates, the value of *R* can be substantially increased by removal of the sieve effect, while the doublet structure of the red band remains unchanged.

Specific effects of solvents on the absorption bands of chlorophyll in solutions are well known (Kundt's original work in 1878,⁷ leading to the so-called Kundt's rule, according to which absorption bands shift toward longer wavelengths with increasing refractivity of the solvent, was carried out on chlorophyll). Since then, many other studies have been made, the most recent one being that of Seely and Jensen.⁸ The solvents affect not only the position of a band, but also its shape and thus also its height. This makes it impossible to evaluate the sieve effect by comparison of the absorption spectra of *cell-suspensions* with those of pigment *extracts*. Table I shows, as an example, the changes in the height and width of the red absorption band of *Chlorella* cells upon extraction into three different solvents. The flattening of the red band *in vivo*, compared to its height *in vitro*, varies between 0.66 (if comparison is made with a pyridine extract) and 0.84 (if comparison is made with an ethanol extract).

Sonication with an ultrasonic generator breaks the cells into fragments. One may hope that in this mechanical disintegration the pigment molecules are not changed chemically and remain associated with their

Table I: Comparison of Absorption Spectra of Cell Suspensions and Cell Extracts in Three Solvents

Material	λ_{\max} , nm	Half-band width ΔF , ^a nm	Optical density $\alpha(\lambda_{\max})$	$[\alpha_{\text{sus}}(\lambda_{\max}) - \alpha_{\text{res}} \times (\lambda_{\max})] / \alpha_{\text{ext}}(\lambda_{\max})$
Suspension	675	35.0	0.500	
Methanol extract	666.5	23.0	0.635	0.76
Residue of methanol extract	672.5	~25.0	~0.017	
Ethanol extract	666.5	20.5	0.353	
Residue of ethanol extract	672.5	33.4	0.205	0.84
Suspension	675	35.0	0.290	
Pyridine extract	671	20.0	0.310	0.66
Residue of pyridine extract	672	35.0	0.085	

^a Full width at half the maximum intensity, determined on the long wave side of the band to eliminate the effects of chlorophyll b.

original partners so that the intrinsic *in vivo* pigment spectra are unchanged and only the distortion due to the sieve effect is eliminated. The following experiments suggest that this is in fact largely the case, provided sonication is carried out with proper precautions. Ultrasonic irradiation produces cavitation and thus high local pressure and local heating. These can lead to chemical changes, particularly in the sensitive chlorophyll molecules (as well as in associated protein molecules). Such changes are illustrated by Figure 1, which shows the effects of prolonged sonication of *Chlorella* cells in an aerobic, unbuffered (slightly acid) growth medium. At first, after brief sonication (4 min), the red absorption band increases in intensity (as one would expect from reduction of the sieve effect); but upon longer sonication, this effect is overcompensated by a general bleaching, accompanied by a shift of the red band toward shorter wave. After 1 hr of sonication under these conditions, the red band is reduced to about 70% of its original height and its peak shifted from 675 to 670 nm. Bleaching suggests chemical damage, while band shift indicates a change in the state of association of the pigment molecules. The fluorescence

(4) W. L. Butler, *Ann. Rev. Plant Physiol.*, **15**, 451 (1964); *J. Opt. Soc. Am.*, **52**, 292 (1962).

(5) C. N. Cederstrand, E. Rabinowitch, and Govindjee, *Biochim. Biophys. Acta*, **126**, 1 (1966).

(6) C. S. French in "Light and Life," W. D. McElroy and B. Glass, Ed., The Johns Hopkins Press, Baltimore, Md., 1961, p 447.

(7) A. Kundt, *Ann. Phys.*, **4**, 34 (1878).

(8) G. R. Seely and R. G. Jensen, *Spectrochim. Acta*, **21**, 1835 (1965); E. Szalay, L. Szalay, and N. R. Murty, unpublished results.

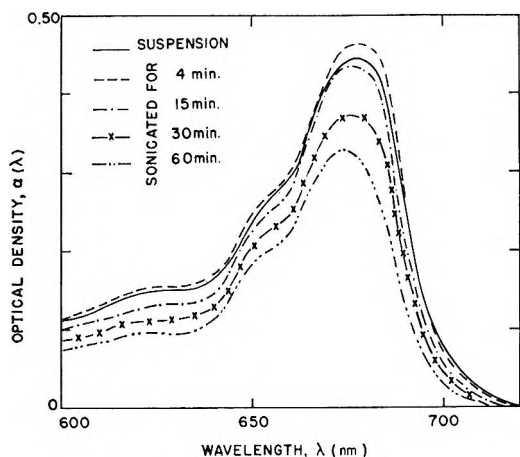


Figure 1. Effect on the red absorption band in *Chlorella pyrenoidosa* suspension of sonication in culture medium, pH 5.7, under aerobic conditions.

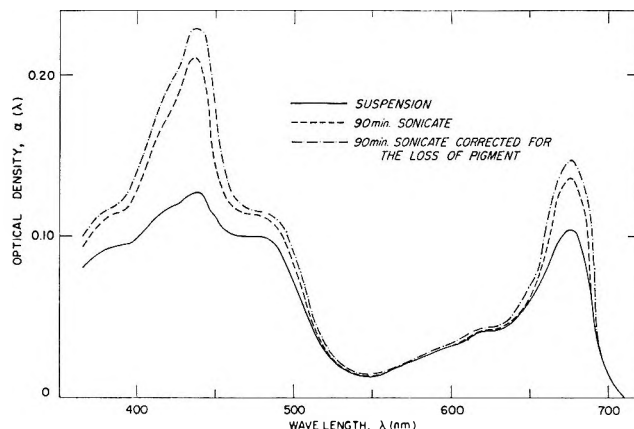


Figure 2. Effect on the absorption spectrum in *Chlorella pyrenoidosa* suspension of sonication in alkaline medium (pH 7.8) under anaerobic conditions.

properties are changed too; Das and Govindjee⁹ noted that after 30 min aerobic sonication in the (slightly acid) growth medium, the decline of the action spectrum curve ("red drop") of fluorescence is observed (at room temperature) only beyond 705 nm, as compared to 680 nm in the original suspension. Furthermore, the additional fluorescence band at 723 nm, observed in chlorella suspensions at -196° , is absent in this sonicate. Apparently, sonication in an acid, aerobic medium causes preferential destruction of a long wave form of chlorophyll *a*, which is only weakly fluorescent at room temperature and which becomes fluorescent at -196° with an emission maximum at 723 nm (perhaps, Kok's pigment "C700").¹⁰

It is known that chlorophyll is particularly sensitive to two kinds of chemical change—oxidations (particularly in light) and pheophytinization (replacement of magnesium by hydrogen). Carrying sonication out under *anaerobic* conditions (*e.g.*, in pure argon), eliminating oxidative processes, was found to reduce markedly the spectral effects of sonication; carrying it out in an alkaline buffer (*e.g.*, at pH 7.8) improved the results even more significantly. Figure 2 shows the results of combining both precautions. Even after 90 min of sonication under these conditions, no substantial bleaching or band shift is noticeable. If one extracts the pigment completely from an aliquot of cells before and after such sonication and measures the absorption spectra of the extracts, the difference in the height of the red peak indicates that only 6–9% of the pigment (more exactly, 6–9% of absorption in the peak of the red band) had been lost. Apart from this loss, the spectrum of the extract prepared from the 90-min sonicate is practically identical with that of the extract prepared directly from

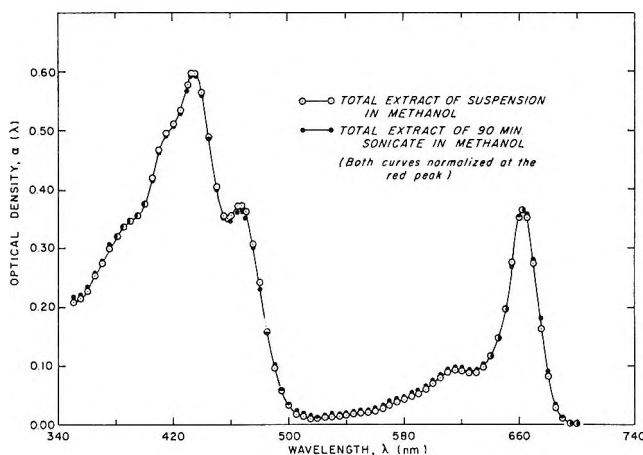


Figure 3. Absorption spectra of methanolic pigment extracted directly from *Chlorella pyrenoidosa* suspension and from a 90-min anaerobic sonicate prepared at pH 7.8. (The latter corrected for a 9% loss of pigment by equalizing the heights of the red band.)

the cells (Figure 3). The fluorescence yield of the sonicate (about 3–4%) also is not significantly different from that of the original suspension. Its excitation spectrum still shows a "red drop" (shifted slightly to the longer waves, from 680 to about 690 nm) and an additional fluorescence band is observed, at -196° , at 723 nm.⁹

Experiments by Williams¹¹ suggested that if sonication in a nonbuffered, aerobic medium is stopped after 1–2 min, after which the nonfragmented cells (about

(9) M. Das and Govindjee, *Biochim. Biophys. Acta*, in press.

(10) B. Kok in "Plant Biochemistry," J. Bonner and J. Barner, Ed., Academic Press Inc., New York, N. Y., 1965, pp 916, 917.

(11) P. Williams, unpublished results.

80–90% of the total) are removed by centrifugation, the absorption spectrum of the supernatant suspension is similar to that of the above-described product of prolonged, anaerobic sonication in alkaline solution. It seems that during such a short sonication, when only a small proportion of cells are broken up, no significant chemical change has time to occur, even in an acid, aerobic medium.

Experimental Section

Culturing. *Chlorella pyrenoidosa* cultures were grown in an inorganic medium. Air containing 5% CO₂ was bubbled through the cultures. The vessel was continuously illuminated by "medium intensity" white light and the cells were harvested after a 20–80-fold increase in population.¹² Absorption spectra of the suspension and of the sonicate were measured in the integrating sphere attachment of a Bausch and Lomb 505 spectrophotometer. Fluorescence (which is added to transmission in the integrating sphere) was neglected because the yield of fluorescence, in both suspension and sonicate, is only of the order of 3%.

Sonication. Before sonication, the chlorella suspension (age, 4 days) was centrifuged for 30 sec at 3450 rpm to get rid of abnormally heavy cells or cell aggregates. The supernatant was decanted and recentrifuged for 5 min at the same speed, precipitating all cells. The second supernatant was rejected and the residue re-suspended in phosphate buffer (0.06 M Na₂HPO₄, 0.007 M KH₂PO₄, and 0.1 M KCl, pH 7.8). The suspension (50 ml) was placed in the chamber of the sonicating machine (Raytheon ultrasonic generator, Model D.F. 101, operating at 10 kc and 250 w) and argon was bubbled through it. The argon was purified by passing through a train consisting of alkaline pyrogallol, concentrated H₂SO₄, and water, and then dried by passing through two tubes with calcium chloride. After 1 hr, the inlet and the outlet of the chamber were closed and the suspension was sonicated for 10, 20, 30, 45, 60, or 90 min. With cooling by ice water, the "macroscopic" internal temperature in the sonication vessel stayed at about 14–15°.

Extraction Tests. Aliquots of 10 ml of the suspension used for sonication and of the different sonicates were placed in stainless steel tubes and centrifuged for 2 hr in an ultracentrifuge at 26,000 rpm. The supernatants were decanted and rejected. Anhydrous methanol (10 ml) was then added to the residue and covered tubes were left for 1 hr in the dark. They were then recentrifuged for 2 hr under similar conditions (26,000 rpm); the supernatant, containing the extracted pigments, was decanted and kept in the dark in the cold room. The small practically colorless residue was resuspended in

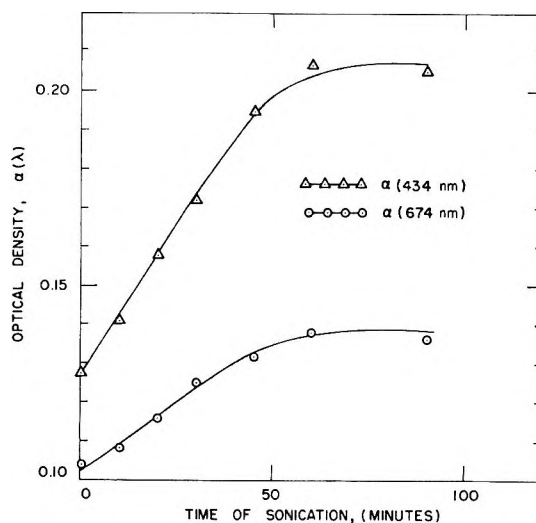


Figure 4. Dependence of the height of the blue and the red absorption band on time of sonication in *Chlorella pyrenoidosa* suspension (under anaerobic conditions and in alkaline medium).

the same volume (10 ml) of the phosphate buffer and checked for incompleteness of extraction (*i.e.*, for presence of pigment bands in the absorption spectrum). The spectra of the methanol extracts were measured in transmitted light, and those of the resuspended residue were measured in the integrating sphere.

Results

Figure 2 shows the results of anaerobic sonication at pH 7.8 of 4-day-old chlorella cells. The lower curve is the absorption spectrum of the suspension and the middle curve is that of the 90-min sonicate. The absorption curves of suspensions obtained by 10-, 20-, 30-, 45-, and 60-min sonication lie between these two curves. The positions of the blue and the red peak are unchanged (*cf.* also Figure 3). The changes in the ratios of the heights of the blue and red peaks and in the half-width of the red band and the losses of the pigment caused by sonication (as determined by extraction) are listed in Table II; the "flattening coefficient" $Q_A = \alpha/\alpha_{\max}$ (where α_{\max} refers to the maximum intensity reached after prolonged sonication) is given in columns 7 and 8. The upper curve in Figure 2 represents the spectrum of the 90-min sonicate corrected for the loss of pigment, as determined by extraction (9% in this particular experiment). Table II and Figure 4 show the gradual increase in the height of the absorption peaks with sonication time. After 1 hr, it approaches a maximum, which remains unchanged after an additional 30 min of sonication. The results suggest that after 60-min sonication

(12) Govindjee and E. Rabinowitch, *Biophys. J.*, 1, 73 (1960).

Table II: Absorption Characteristics of Cell Sonicates^a

Time sonicated, min 1	$\alpha(434)$ 2	$\alpha(674)$ 3	$\alpha(434)/\alpha(674)$ 4	Loss of pigment, % 5	Half-width of red band, nm 6	Q_A (corrected for pigment loss)		$Q_A(434)/Q_A(674)$ 9
						434 nm 7	674 nm 8	
0	0.127	0.104	1.22	...	35.0	0.55	0.70	1.27
10	0.141	0.108	1.30	4	34.0	0.64	0.75	1.17
20	0.163	0.116	1.40	5	32.0	0.74	0.82	1.11
30	0.172	0.125	1.38	8	32.0	0.81	0.91	1.12
45	0.195	0.132	1.47	8	31.0	0.92	0.96	1.04
60	0.212	0.138	1.54	9	28.5	1.00	1.00	1.00
90	0.210	0.136 ^b	1.54	9	28.5	1.00	1.00	(1.00)

^a Sonicated at pH 7.8 under anaerobic conditions. ^b These limiting values α_{max} are supposed to be proportional to the intrinsic absorption coefficients at the two wavelengths.

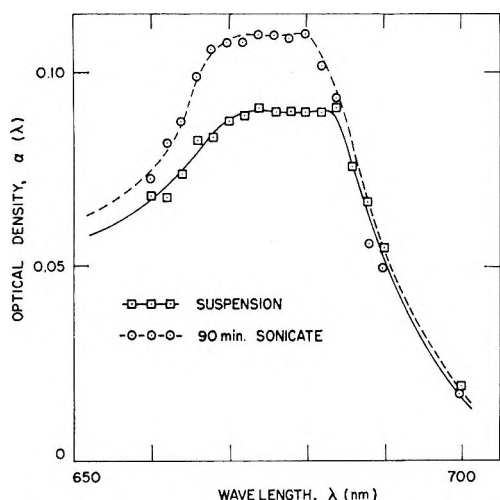


Figure 5. The shape of the red absorption band of *Chlorella pyrenoidosa* in suspension and in sonicate (prepared under anaerobic conditions, at pH 7.8). Measured with monochromatic light beams of 1-nm half-band width.

in our machine, the sieve effect of chlorella cells is removed practically completely, with only a slight loss of the pigment and without apparent change either in the state of the remaining pigment (*i.e.*, without a shift in the peak position) or in its composition (*i.e.*, without change in the band shape).

Similar results were obtained in another experiment, with a different culture of the same age (4 days). Before sonication, the optical density, α , was 0.128 at 434 nm and 0.104 at 674 nm; after 90-min sonication, it rose to $\alpha(434) = 0.209$ and $\alpha(674) = 0.134$. The apparent loss of pigment was, in this case, about 7%. In an older culture (12 days), a slightly lesser effect of sonication was observed: before sonication, $\alpha(434) = 0.189$, $\alpha(674) = 0.164$; after 60-min sonication, $\alpha(434)$

$= 0.306$, $\alpha(674) = 0.208$; the apparent loss of pigment was, in this case, about 6%. The ratios $\alpha(434)/\alpha(674)$ in the sonicate were, in these three examples, $R = 1.54, 1.55, \text{ and } 1.47$.

In an earlier paper from this laboratory,⁵ the red absorption band of chlorella was shown to have a flat top and was analyzed, with the help of a computer, into three gaussian curves with peaks at 650.5 (chlorophyll b), 668, and 683 nm (two chlorophyll a components). The half-widths of these components bands are 18.5, 17, and 18 nm, respectively. Since the over-all band is widened by the sieve effect (*cf.* Table II) which is reduced by sonication, we repeated the analysis on the sonicate using the same instrument used by Cederstrand, *et al.*⁵ Figure 5 compares the shapes of the red band peak in chlorella suspension (solid line) with that in a 90-min sonicate. The doublet structure, suggesting two chlorophyll a band components of approximately equal intensity, is clearly retained in the sonicate; however, because of the smaller half-width of the band in the sonicate (28.5 nm instead of 35 nm according to Table II), the two calculated band components are, in the sonicate, somewhat closer together than in the suspension—at about 670 and 680 nm (instead of 668 and 683 nm).

Discussion

One can compare the "experimental" flattening coefficients Q_A , listed in Table II, with "theoretical" values calculated for suspensions of identical simple particles. The latter depend on the shape and size of the postulated particles and the concentration (and distribution) of pigments in them.

The simplest model that can be used as a first approximation is a sphere, uniformly filled with a solution of pigments. For an average radius of r (centimeters)

and an average pigment concentration of c moles per liter, the maximum optical density, α_p (that opposing the passage of a beam traversing the sphere along its diameter), is

$$\alpha_p = 2\alpha cr \quad (1)$$

where α is the intrinsic molecular absorption coefficient. The *average* particle transmission (for a suspension so thin that no mutual shading of particles has to be taken into account) is, according to Duysens^{2a}

$$\bar{T} = 2[1 - (1 + \alpha_p)e^{-\alpha_p}]\alpha_p^{-2} \quad (2)$$

and the flattening coefficient, Q_A , is

$$Q_A = \frac{3(1 - \bar{T})}{2\alpha_p} \quad (3)$$

(As the suspension becomes thicker and the average number of particles encountered by a beam becomes significantly >1 , the flattening decreases; ultimately the flattening coefficient approaches unity, as can be easily seen by envisaging a volume closely packed with particles.)

Equations 2 and 3 show that for spherical particles, the flattening coefficient Q_A is a function of α_p alone; *i.e.*, for a given value of the product cr in eq 1, it is a function of the molecular extinction coefficient α alone. If the α values are known for two λ 's (*e.g.*, from observations on sonicates, *cf.* the last row in Table II), one can calculate, using eq 2 and 3, the flattening coefficient at one λ (*e.g.*, at 434 nm) from that at another λ (*e.g.*, at 674 nm). (This amounts in essence to using one Q_A value and the corresponding α value to calculate cr and using the so-calculated cr value to calculate Q_A for a different α .)

Carrying this calculation out one finds that eq 2 and 3 (*i.e.*, the simple spherical model) do not adequately explain the results shown in Table II. This is shown, *e.g.*, by comparison of the observed with the calculated ratios of the intensities of the blue and the red band in the cell suspension. *Qualitatively*, the increase in this ratio in passing from cell suspension to sonicate (down column 4) is an expected consequence of gradually decreasing sieve effect, but *quantitatively*, this change is not quite as strong as one calculates from eq 3 and 2. More precisely, the sphere model makes one expect, for $Q_A(674) = 0.70$ and $Q_A(434) = 0.55$ (*cf.* columns 8 and 7 in Table II), $\alpha(434)/\alpha(674) = 1.38$, while the experimental value is 1.22.

(If reliable values of cr —the product of pigment concentration and diameter of the cells—were available, one could check the experimental values of $Q_A(434)$ and

$Q_A(674)$ separately, but since these are known only very roughly, we are left with the possibility of checking the compatibility of the experimental $Q_A(434)/Q_A(674)$ and $\alpha(434)/\alpha(674)$ ratios with those calculated for the spherical model.) We find from this test that the sieve effect in a chlorella solution is somewhat weaker than calculated for a suspension of uniformly colored spheres.

One factor accounting for this discrepancy could be that the chlorella cell is not a uniformly colored sphere; rather, the color resides in a bell-shaped chloroplast surrounding the colorless central plasma. Calculation of the sieve effect for a *hollow sphere* proves to be rather complicated; we do not give here the results because they suggest that (unless the sphere is very thin) the sieve effect of a hollow sphere is not significantly different from that of a solid sphere (of the same cross section and containing the same amount of pigment). This analytical conclusion agrees with what one would expect from simple physical considerations.

A second difference between chlorella cells and uniformly colored spheres is that the former are elongated—ellipsoids of revolution rather than spheres. Duysens^{2a} suggested that the expression for Q_A of a (thin) suspension of nonspherical particles should differ from eq 3 by a "form factor," which is essentially the volume-surface ratio for the particle, relative to the same ratio for a sphere. Deviation from spherical shape should thus lead (for constant volume and identical pigment concentration) to a decrease in the sieve effect. (Obviously, the average transmission of an arbitrarily oriented nonspherical particle is equal to that of a nonuniformly colored sphere of a diameter larger than that of a spherical particle of the same volume; thus the average mutual shading of particles must be smaller in the nonspherical compared to the spherical particle.)

A third factor, which also could affect the sieve effect of chlorella cells, is that the index of refraction of the colored particles is higher than that of the medium. This affects the average path of a beam traversing the particle. Calculations of the sieve effect in relation to all these factors are being continued and may be reported in a subsequent paper.

It may be worth mentioning here that the sieve effect is much smaller or practically nil for the blue-green alga *Anacystis nidulans*. This must be due to the fact these cells are much smaller and contain less pigment, so that the value of cr in eq 1 is considerably smaller than in chlorella.

Undoubtedly, changes in particle size (and consequent reduction of the sieve effect) are not all that happens to pigment upon sonication. The mechanical breaking up of the chloroplasts is bound to disrupt mutual association between some pigment molecules, as well as that

between these and other molecules in the pigment complex *in vivo*. However, our results—in particular, the absence of a noticeable band shift even after 90 min of sonication—suggest that the effect of such “chemical” changes upon the spectrum are minor compared to that of the “geometrical” change (the “sieve effect”). More precise evaluations of the sonication effect will

have to take into account also the other changes caused by sonication.

Acknowledgments. We are thankful to Dr. Govindjee for his helpful discussions during this investigation. Thanks are due to Dr. L. M. Black for permission to use his ultracentrifuge and to Mrs. Ruth St. John for her aid in centrifugations.

Coordination Disproportionation Equilibria in Solution. I.

Aluminum Chloride in Acetonitrile

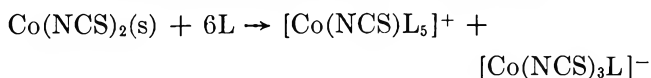
by W. Libuś and D. Puchalska

Department of Physical Chemistry of the Technical University of Gdańsk, Gdańsk, Poland

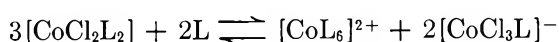
Accepted and Transmitted by The Faraday Society (January 6, 1967)

Coordination disproportionation equilibria of the type $(k + l)MA_z \rightleftharpoons lMA_{z-k}^{k+} + kMA_{z+l}^{l-}$ are proposed as a general explanation of the electrolytic properties of some metal halogenides in nonaqueous solvents. The magnitude of the coordination disproportionation constant is shown to depend critically upon the relative stabilities of tetrahedral and octahedral complexes formed in the system. Solutions of $AlCl_3$ in acetonitrile were examined conductometrically. A complete coordination disproportionation of the solute, according to the reaction $2AlCl_3(s) + 4L \rightarrow [AlCl_2L_4]^+ + [AlCl_4]^-$, was inferred from the limiting slope of the equivalent conductance curve.

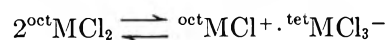
The dissolution of anhydrous $Co(NCS)_2$ in acetonitrile had previously been shown¹ to be accompanied by the coordination disproportionation reaction



L being the solvent molecule. The complex electrolyte thus formed consists of a six-coordinate octahedral cation and a four-coordinate tetrahedral anion. Further experiments² showed that coordination disproportionation, though not complete, also occurs when $CoCl_2$ is dissolved in the same solvent. The equilibrium taking place in the resulting solution is



The formation of tetrahedral anionic species $[MCl_3L]^-$ in dimethylformamide solutions of $MnCl_2$, $FeCl_2$, $CoCl_2$, $NiCl_2$, and $CuCl_2$ was also shown by Katzin³ and, using his original notation, ascribed to the coordination disproportionation reaction



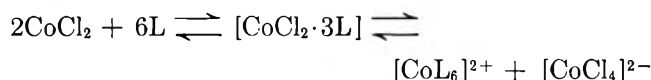
Katzin also predicted that solvents of a low base strength but a high dielectric constant should, in general, favor coordination disproportionation of metal halides.

(1) W. Libuś, *Roczniki Chem.*, **35**, 411 (1961).

(2) W. Libuś, *ibid.*, **36**, 999 (1962).

(3) L. I. Katzin, *J. Chem. Phys.*, **36**, 3034 (1962).

Essentially different equilibria were frequently suggested by a number of authors⁴⁻⁶ in their interpretation of similar systems. Janz, Marcinkowski, and Venkatesetty, for instance, ascribed the spectroscopic and conductometric properties of the system $\text{CoCl}_2\text{-CH}_3\text{CN}$, in contrast to our findings, to the system of equilibria⁶



Considering these divergent interpretations, we recently extended our earlier experiments to other systems and higher concentration ranges. Several other instances of coordination disproportionation equilibria were additionally found and will be reported in the present series of papers. It seems evident now that coordination disproportionation, as suggested by Katzin, is a reaction frequently occurring in solutions of metal halogenides in polar solvents. In our opinion the properties of many solutions of these compounds may be rationalized in terms of that type of equilibria. In the present paper a general discussion of factors affecting coordination disproportionation will be given. A presentation of experimental results regarding AlCl_3 solutions in acetonitrile will follow.

Definitions and Basic Relations

Octahedral and tetrahedral complexes of the metal ion were found to be involved in coordination disproportionation equilibria occurring in solutions of cobalt(II) salts. It is conceivable, however, that other configurations might also be responsible for the occurrence of that phenomenon. Coordination disproportionation involving tetrahedral and octahedral complexes must, obviously, in some way depend upon the relative stability of these complexes. It is necessary, therefore, prior to discussing that problem, to introduce some definitions and relations regarding configurational equilibria.

If we assume that mononuclear tetrahedral and octahedral complexes may be formed in a solution of a metal salt MA_z , then two series of complexes, namely, $[\text{MA}_n\text{L}_{6-n}]$ (octahedral) and $[\text{MA}_n\text{L}_{4-n}]$ (tetrahedral), must be taken into account, L denoting the solvent molecule. While some of them may exist in the form of only one structural modification, others may be equilibrium mixtures of two or more isomers, e.g., *cis* and *trans* modifications of $[\text{MA}_2\text{L}_4]$. The present discussion will disregard the configurational equilibria that may occur between the various possible structural modifications of an octahedral or a tetrahedral complex of a given composition, as they, most probably, play an insignificant role in the coordination disproportiona-

tion. We shall, using the shorter notations ${}^o\text{MA}_n$ and ${}^t\text{MA}_n$ in place of $\text{MA}_n\text{L}_{6-n}$ and $\text{MA}_n\text{L}_{4-n}$, define the stability constants ${}^o\beta_n$ and ${}^t\beta_n$ of the octahedral and tetrahedral complexes, respectively, as

$${}^o\beta_n = \frac{\{ {}^o\text{MA}_n \}}{\{ {}^o\text{M} \} \{ \text{A} \}^n}; \quad {}^t\beta_n = \frac{\{ {}^t\text{MA}_n \}}{\{ {}^o\text{M} \} \{ \text{A} \}^n} \quad (1)$$

braces denoting activities. In these definitions, the solvent activity is assumed to be constant. The configurational equilibrium constant, κ_n , will, under the assumed conditions, be defined as

$$\kappa_n = \frac{\{ {}^t\text{MA}_n \}}{\{ {}^o\text{MA}_n \}} \quad (2)$$

That quantity is related to the equilibrium



and may be used as a measure of the relative stability of tetrahedral and octahedral modifications of the empirical complex MA_z . It can thus be seen that

$${}^o\beta_n \kappa_n = {}^t\beta_n \quad (4)$$

It is obvious that the stability constant, β_n , of a complex in solution, as determined by standard methods, relates to the sum of complexes, all of which have the same empirical formula MA_z . In order to derive the relation between the conventional stability constant, β_n , and the stability constants of individual modifications of the complex MA_z for a system in which octahedral and tetrahedral complexes are formed, the condition of constant solvent activity must be assumed. An unequivocal definition of β_n would otherwise not be possible. Thus

$$\beta_n = \frac{\{ \text{MA}_z \}}{\{ \text{M} \} \{ \text{A} \}^n} \quad (5)$$

Let us assume that infinitely dilute solutions of the species MA_z , M, and A are the corresponding reference states for the activities. For a solution sufficiently dilute to be treated as ideally dilute, we shall have

$$\beta_n = \frac{[\text{MA}_z]^*}{[\text{M}]^* ([\text{A}])^n} \quad (6)$$

asterisks denoting concentrations relating to the assumed conditions. For a system where both octahedral and tetrahedral complexes are formed, we shall have

(4) P. A. D. de Maine and E. Koubek, *J. Inorg. Nucl. Chem.*, **11**, 329 (1959).

(5) D. W. Meek and R. S. Drago, *J. Am. Chem. Soc.*, **83**, 4322 (1961).

(6) G. J. Janz, A. E. Marcinkowski, and H. V. Venkatesetty, *Electrochim. Acta*, **8**, 867 (1963).

$$[\text{MA}_n]^* = [{}^{\circ}\text{MA}_n]^* + [{}^t\text{MA}_n]^* \quad (7)$$

and

$$[\text{M}]^* = [{}^{\circ}\text{M}]^* + [{}^t\text{M}]^*$$

where ${}^{\circ}\text{M}$ and ${}^t\text{M}$ denote the ML_6 and ML_4 solvo complexes, respectively. Combining eq 6 and 7 the relation

$$\beta_n \left(\frac{[{}^t\text{M}]}{[{}^{\circ}\text{M}]} + 1 \right) = \frac{[{}^{\circ}\text{MA}_n]^*}{[{}^{\circ}\text{M}]^*([\text{A}]^*)^n} + \frac{[{}^t\text{MA}_n]^*}{[{}^t\text{M}]^*([\text{A}]^*)^n} \quad (8)$$

is obtained which, if definitions 1 and 3 are applied, can be given the form of

$$\beta_n(\alpha_0 + 1) = {}^{\circ}\beta_n + {}^t\beta_n \quad (9)$$

or, if eq 4 is taken into account, that of

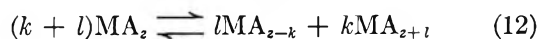
$$\beta_n(\alpha_0 + 1) = {}^{\circ}\beta_n(\alpha_n + 1) \quad (10)$$

The quantity α_0 relates to the equilibrium



and its value is likely to be very small for the majority of real systems.

A reversible coordination disproportionation reaction may be formulated in the general way



The disproportionation equilibrium constant will then be given by

$$D_{k,l} = \frac{\{\text{MA}_{z-k}\}^l \{\text{MA}_{z+l}\}^k}{\{\text{MA}_z\}^{k+l}} \quad (13)$$

and, as it is seen

$$D_{k,l} = \frac{\beta_{z-k}^l \beta_{z+l}^k}{\beta_z^{k+l}} \quad (14)$$

If the corresponding expressions resulting from eq 10 are inserted in place of the conventional stability constants β_{z-k} , β_z , and β_{z+l} , we obtain

$$\log D_{k,l} = \log {}^{\circ}D_{k,l} + \log Q_{k,l} \quad (15)$$

where

$${}^{\circ}D_{k,l} = \frac{{}^{\circ}\beta_{z-k}^l {}^{\circ}\beta_{z+l}^k}{{}^{\circ}\beta_z^{k+l}} \quad (16)$$

and

$$Q_{k,l} = \frac{(1 + \alpha_{z-k})^l (1 + \alpha_{z+l})^k}{(1 + \alpha_z)^{k+l}} \quad (17)$$

The contributions of $\log {}^{\circ}D_{k,l}$ and $\log Q_{k,l}$ to $\log D_{k,l}$ are now going to be discussed separately.

It is known^{7,8} that the stepwise formation constants,

K_n , often decrease regularly as n increases, as described by the empirical equation

$$\log K_n = \log K_1 - \delta(n - 1) \quad (18)$$

where δ is a constant for a given system. That relation applies very closely to such a system as Ni(II)-NH_3 , Co(II)-NH_3 ,⁹ or Al(III)-F^- in aqueous solution⁸ where, most probably, only octahedral complexes are formed. The dependence of $\log K_n$ upon n , on the contrary, becomes irregular for systems where, in the process of stepwise complex formation, there occur changes in the configuration of the complex or in the electronic ground state of the metal.⁸ It seems justified to assume, on the basis of these findings, that eq 18 applies to the stepwise complex formation involving equivalent coordination positions of the metal ion. Taking into account that ${}^{\circ}\beta_n = \prod_{r=1}^n {}^{\circ}K_r$, where ${}^{\circ}K_n$ is the formation constant of the octahedral complex ${}^{\circ}\text{MA}_n$ defined by

$${}^{\circ}K_n = \frac{\{{}^{\circ}\text{MA}_n\}}{\{{}^{\circ}\text{MA}_{n-1}\} \{\text{A}\}} \quad (19)$$

we obtain

$${}^{\circ}D_{k,l} = \frac{(K_{z+1} \dots K_{z+l})^k}{(K_{z-k+1} \dots K_z)^l} \quad (20)$$

Then, applying eq 18 to the formation constants of octahedral complexes

$$\log {}^{\circ}D_{k,l} = -\delta \left(k \sum_1^{l-1} n + l \sum_1^k n \right) \quad (21)$$

It follows that $\log {}^{\circ}D_{1,1} = -\delta$, $\log {}^{\circ}D_{2,1} = -3\delta$, and $\log {}^{\circ}D_{2,2} = -8\delta$. At present no data are available allowing the evaluation of δ for systems in which coordination disproportionation has been found or may be suspected. Nevertheless, inspection of experimental data regarding aqueous systems,⁸ as well as simple argumentation, leads to the conclusion that δ should exceed unity for halogenide complexes of di- and trivalent metals, especially in solvents of dielectric constants lower than that of water. It follows therefrom that $\log {}^{\circ}D_{k,l}$ should, for such systems, always have considerable negative values. High values of the over-all disproportionation constant, $D_{k,l}$, may thus result only from the contribution of $\log Q_{k,l}$ which, in turn, is determined by the magnitudes of the configurational

(7) C. L. van P. van Eck, *Rec. Trav. Chim.*, **72**, 529 (1953).

(8) F. J. C. Rossotti in "Modern Coordination Chemistry," by J. Lewis and R. G. Wilkins, Ed., Interscience Publishers, Inc., New York, N. Y., 1960, p 34.

(9) Data from J. Bjerrum, Thesis, 1941.

equilibrium constants. When there is no formation of tetrahedral complexes in a system and, consequently, $\kappa_n = 0$ for all possible values of n , then $\log D_{k,l} = \log {}^{\circ}D_{k,l}$ and will be negative. Let us consider the effect of a gradual increase of the stability of tetrahedral complexes on the magnitude of the over-all coordination disproportionation constant. In doing so, the generalization may be taken into account that, for a given system, the magnitudes of the configurational equilibrium constants always follow the order $\kappa_1 \ll \kappa_2 \ll \kappa_3 \ll \kappa_4$.¹⁰ Thus, on passing from systems of low stability of tetrahedral complexes to those in which it becomes increasingly higher, the situation met with will be that $\kappa_{z+l} \gg 1$, while $\kappa_z \ll 1$ and $\kappa_{z-k} \ll 1$. Under these conditions $\log Q_{k,l} = k \log \kappa_{z+l}$, and its positive value may exceed the negative value of $\log {}^{\circ}D_{k,l}$. It is then that coordination disproportionation will take place. On passing to systems of a still higher stability of the tetrahedral configuration, for which $\kappa_z \gg 1$, while $\kappa_{z-k} \ll 1$, the magnitude of Q_k might be expected to decrease. This should be so because of the difference in power exponents of expressions involving κ_z and κ_{z+l} , respectively, in eq 17.

A more detailed discussion of the above problem would be possible if an equation relating κ_n to n were known. Our conclusions can, at present, be summarized in the following two points. (i) It is highly unlikely that coordination disproportionation should, to any measurable extent, occur in systems in which complexes of only one configuration, either octahedral or tetrahedral, are formed. (ii) The magnitude of the coordination disproportionation constant should depend critically on the relative stability of the tetrahedral and octahedral complexes in the system. Results regarding several cases of coordination disproportionation, obtained in this laboratory, will be reported in the series of papers to follow. A short investigation of AlCl_3 solutions in acetonitrile will be presented below.

Experimental Section

Materials. Anhydrous aluminum chloride was prepared by heating chemically pure grade aluminum chips in a dry HCl gas atmosphere. The product was sublimed twice under vacuum. The white crystalline material obtained was kept in sealed ampoules.

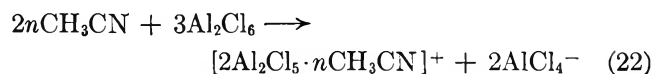
Acetonitrile. The starting material, a technical grade acetonitrile, was purified by repeated drying over phosphorus pentoxide and fractionally distilled through a ~ 30 -plate column. The product was kept in a dry-air atmosphere. The physical constants of the final material were bp 81.6° (760 mm) and specific conductance $(1-6) \times 10^{-7} \text{ ohm}^{-1} \text{ cm}^{-1}$ at 25° . The water

content in the solvent, as determined by the Fischer method, was lower than 0.01%.

Procedures. The Jones and Josephs conductance bridge, as modified by Luder,¹¹ was used. The measurements were performed at a constant temperature of $25 \pm 0.01^\circ$. Three conductance cells of cell constants 0.04705, 0.4072, and $2.9315 \pm 0.0005 \text{ cm}^{-1}$ were used as required. Preparation of solutions and further manipulations were performed in a drybox. Concentrations of stock solutions were determined gravimetrically by means of 8-hydroxyquinoline.

Results and Discussion

The aluminum chloride-acetonitrile system has recently been investigated by Schmulbach.¹² The molecular weight of the solute (201 ± 5 , determined ebulliometrically), observation of Raman lines which were ascribed to the anion AlCl_4^- , and the fact that the solutions were electrically conducting led Schmulbach to formulate the underlying reaction



We thought it more likely, however, that it is coordination disproportionation that might be responsible for the formation of the $[\text{AlCl}_4]^-$ complex anion and for the other properties of AlCl_3 solutions in acetonitrile. It seemed possible that in these solutions there might occur coordination disproportionation of the simplest type, namely, such as results in the formation of a binary complex electrolyte. Were this the case, the simplest and most direct way of obtaining evidence would be to perform conductometric measurements.

The dependence of the molar conductance, Λ_c , of AlCl_3 on the square root of its molar concentration, as determined in the present work, is shown in Figure 1. It is seen that, with increasing concentration, Λ_c at first increases rapidly and then, after reaching the maximum, decreases less steeply. The position of the maximum and the first part of the curve were found to depend critically on the water content in the solution. This effect is illustrated by curves 1, 2, and 3 in Figure 1. It can be seen that the decrease in Λ_c is brought about by increase in water concentration only at a sufficiently low aluminum chloride concentration. Water concentration, when kept low, was at the same time of only negligible influence on the part of the curve corresponding to higher concentrations. Curve 1 in Figure 1 was obtained by using a most carefully dried

(10) W. Libuš, Proceedings of the Symposium on the Theory and Structure of Complex Compounds, Wrocław, Poland, 1964, p 537.

(11) W. F. Luder, *J. Am. Chem. Soc.*, **62**, 89 (1940).

(12) C. D. Schmulbach, *J. Inorg. Nucl. Chem.*, **26**, 745 (1964).

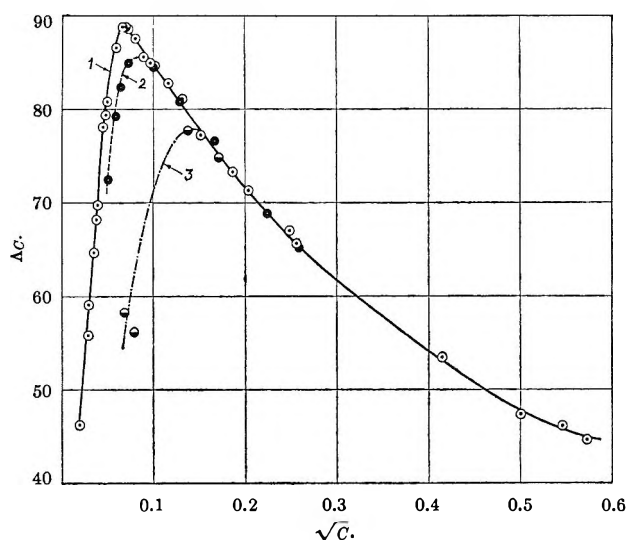


Figure 1. The concentration dependence of the molar conductance of AlCl_3 in acetonitrile solution at 25° . Water content in the solvent: curve 1, below 0.01%; curve 2, 0.02%; curve 3, 0.03%.

solvent of less than 0.01% water content, as controlled by Karl Fischer titration. The position of the maximum in the $\Lambda_c(\sqrt{C})$ curve here observed corresponded to the concentration of 0.0046 M in aluminum chloride. The above observations indicate that the effect produced by water on Λ_c at AlCl_3 concentrations higher than ca. 0.005 M could, in this series of experiments, be assumed negligible and disregarded. A possible explanation of the influence of water on Λ_c will be given further in this section, while now the water-independent part of the curve will be discussed. In this point we shall follow the course previously applied to the $\text{Co}(\text{NCS})_2\text{-CH}_3\text{CN}$ system.¹

Figure 1 shows a linear section in the Λ_c vs. $C^{1/2}$ plot which corresponds to concentrations within the range 0.03 M and may suggest the presence of a completely dissociated, binary electrolyte. The value of $97.9 \text{ ohm}^{-1} \text{ cm}^2 \text{ mole}^{-1}$ for the limiting molar conductance of AlCl_3 in acetonitrile at 25° was obtained on extrapolating this part of the curve to zero concentration (Figure 2, curve $\Lambda_c(\sqrt{C})$). The limiting Onsager slope calculated therefrom for a binary electrolyte produced according to the reaction $\text{AlCl}_3 \rightarrow \text{AlCl}_2^+ + \text{Cl}^-$ would be given by the straight line $\Lambda_{C(\text{theor})}$ (assumed value of the dielectric constant of the solvent, 36.7). The fact that the experimental and the calculated curves lie with the first above the second definitely eliminates simple dissociation as a possible basis for explaining the experimental results. If, on the other hand, the simplest possible disproportionation is assumed, *viz.*

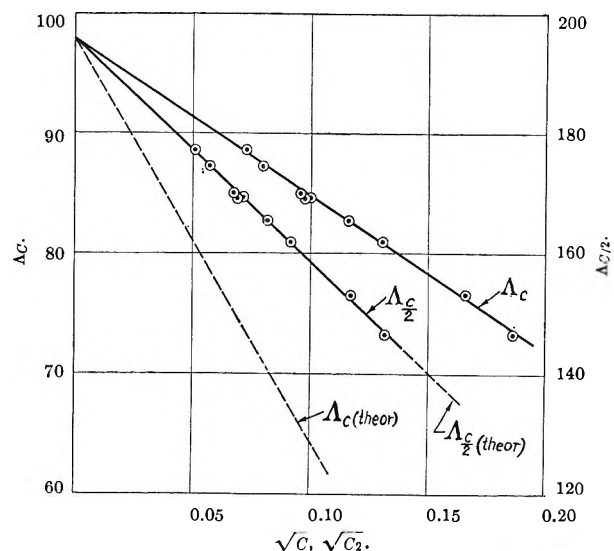
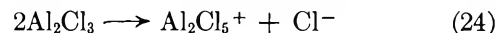


Figure 2. The plots of Λ_c and $\Lambda_{C/2}$ (see text) against $C^{1/2}$ and $(C/2)^{1/2}$, respectively, as compared with the limiting Onsager lines calculated in both cases.

then the equivalent conductance curve of the resulting electrolyte, its concentration being $C_{\text{AlCl}_3}/2$, would be represented by the curve $\Lambda_{C/2}(\sqrt{C}/2)$ in Figure 2. The limiting molar conductance, $\Lambda_{C/2}^0$, found by extrapolation would then be $195.8 \text{ ohm}^{-1} \text{ cm}^2 \text{ mole}^{-1}$. The Onsager slope calculated therefrom is represented by the line $\Lambda_{C/2(\text{theor})}$. The theoretical line is seen here to coincide very closely with the experimental curve. This coincidence may provide evidence for the presence of aluminum chloride in dilute acetonitrile solutions in the form of a completely dissociated univalent electrolyte whose equivalent concentration equals half the molar concentration of AlCl_3 . It seems reasonable to account for that fact by assuming the occurrence of the disproportionation reaction (23), although the reaction



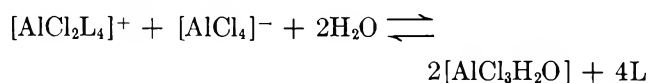
might also result in the formation of a binary electrolyte of the same concentration. The latter alternative can, however, not be accepted, as it does not account for the formation of AlCl_4^- anions and is, moreover, not likely to occur in a polar donor solvent. On the other hand, the other scheme involving polynuclear species, as proposed by Schulbach, also cannot be accepted, as it offers no explanation for the inferred interrelation between the concentration of the electrolyte formed and the total concentration of aluminum chloride in solution. In conclusion, it seems that only in coordination disproportionation eq 23 may lie the explanation for the conductometric observations illustrated in Figure 2, on the one hand, and for the formation of AlCl_4^- anions, on the other. If, in addition, the final

inferences of the theoretical section as well as the known stereochemical properties of aluminum(III) are taken into account, it must be concluded that the most likely formulation of the complex electrolyte formed in solutions of AlCl_3 in acetonitrile should be: $[\text{AlCl}_2\text{L}_4]^+[\text{AlCl}_4]^-$. It is noteworthy that, as was reported in ref 1, both conductometric and spectrophotometric experiments showed complete disproportionation of $\text{Co}(\text{NCS})_2$ in acetonitrile producing the $[\text{Co}(\text{NCS})\text{L}_5]^+[\text{Co}(\text{NCS})_3\text{L}]^-$ complex electrolyte. The limiting molar conductance of this electrolyte was found to be $114.5 \text{ ohm}^{-1} \text{ cm}^2 \text{ mole}^{-1}$ at 25° . This value compares very reasonably with that found for $[\text{AlCl}_2\text{L}_4]^+[\text{AlCl}_4]^-$ in this work ($195.8 \text{ ohm}^{-1} \text{ cm}^2 \text{ mole}^{-1}$) if the expected differences in the diameter of the complex ions involved in the two cases are taken into account. This is another argument supporting our interpretation.

A short comment must be given on the procedure used here for evaluation of the conductometric data. It is obvious that only complete coordination disproportionation producing a binary electrolyte can be demonstrated by the method used in this work. Furthermore, any appreciable association of ions in Bjerrum's sense would interfere with this kind of evaluation of conductometric data. Fortunately, Bjerrum's critical distance, r_{min} , for univalent ions in acetonitrile at 25° equals 7.6 Å. This is somewhat less than what the distance of closest approach may amount to in the case of a complex electrolyte such as $[\text{AlCl}_2\text{L}_4]^+[\text{AlCl}_4]^-$ or $[\text{Co}(\text{NCS})\text{L}_5]^+[\text{Co}(\text{NCS})_3\text{L}]^-$, where L is the acetonitrile molecule. On the other hand, if the solution of AlCl_3 in aceto-

nitrile contained the ions $[\text{Al}_2\text{Cl}_5\text{L}]^+$ and Cl^- , the expected distance of closest approach would be by far smaller than 7.6 Å, and an electrostatic association of these ions would be very likely. Consequently, theoretical Onsager slopes could not be expected for an electrolyte of this type.

An interesting property of the aluminum chloride-acetonitrile system, when studied conductometrically, consists in the occurrence of a sharp maximum in the molar conductance curve. It has already been shown that the presence of minute amounts of water, which lowers the molar conductance of AlCl_3 , is responsible for this effect. Definite statements concerning the underlying reaction are not possible now, but it seems very probable that the reaction



may play an essential role. Since the total concentration of water should be approximately constant in a series of experiments (performed using the same fraction of solvent), its influence on the molar conductance of AlCl_3 should be greatest at lowest concentrations of the latter, decreasing gradually with increasing concentration. In this way the occurrence of the above-mentioned maximum in the $\Delta_c(\sqrt{C})$ curve becomes understandable, but a detailed study of this effect will require the elaboration of a new technique for controlling and determining very small concentrations of water in acetonitrile solution.

Pressure Effects on Glass Transition in Polymers. II.¹ A Study of the Factors Affecting dT_g/dP Values

by Umberto Bianchi, Antonio Turturro, and Giampiero Basile

*Institute of Industrial Chemistry,
Section V of the National Center on Macromolecules, University of Genoa, Genoa, Italy*

Accepted and Transmitted by The Faraday Society (January 16, 1967)

New dilatometric measurements under different pressures, for polyvinyl acetate and polyvinyl chloride, are presented to show the importance of the procedure used in determining dT_g/dP values. These results provide an experimental confirmation of the necessity to introduce a third variable, like the Davies and Jones Z parameter, to describe the state of vitreous polymers. It follows that the glass transition temperature T_g is dependent not only on P but also on Z and that only $(\partial T_g/\partial P)_Z$ should be coincident with $\Delta\beta/\Delta\alpha$.

Introduction

The suggestion that the understanding of glass properties in vitreous polymers requires a three-variable treatment was advanced many years ago.²

The main point is that a glass property, like the specific volume, is not dependent only on the temperature T and pressure P , but also on a third variable, Z , which can vary according to the kind of process used to generate that glass.^{3,4}

A particular process can be classified, for instance, according to the time scale used in it, but we will show that other processes can be devised which have identical time scales but can nevertheless generate glasses with different Z values.

Assuming the necessity of introduction of the Z parameter, it follows that for any given polymer the glass transition temperature T_g is a function of two variables, such as P and Z , and we can write

$$\frac{dT_g}{dP} = \left(\frac{\partial T_g}{\partial P}\right)_Z + \left(\frac{\partial T_g}{\partial Z}\right)_P \times \frac{dZ}{dP} \quad (1)$$

Remembering that to measure a dT_g/dP value we need *at least two distinct experiments*, eq 1 shows what is the effect of an eventual difference dZ in the Z values of the two glasses which are compared, with two important consequences; the first is that, as can be easily shown,⁴ only $(\partial T_g/\partial P)_Z$ and *not* dT_g/dP , should be coincident with $\Delta\beta/\Delta\alpha$. The second is that one can expect dT_g/dP values reported for the same polymer by

different authors to differ according to the particular experimental procedure used.

Considering the first point, the inequality

$$\frac{dT_g}{dP} \neq \frac{\Delta\beta}{\Delta\alpha}$$

has been amply confirmed by a now compelling experimental evidence.¹ From this fact we must deduce that the procedures normally used to measure dT_g/dP fail to compare glasses with the same Z value.

Considering the second point, it is a common opinion that dT_g/dP values derived for the same polymer by different authors and methods are essentially in good agreement. We consider this opinion to be questionable, not only on the basis of known dT_g/dP values,^{5,6} but also because we have recently⁷ been able to show, in the case of polyvinyl chloride (PVC) the strong influence on dT_g/dP played by the experimental method used.

In ref 7 we have shown that the cooling of a liquid sample of PVC along an isochore gives $dT_g/dP =$

- (1) Part I of this series: U. Bianchi, *J. Phys. Chem.*, **69**, 1497 (1965).
- (2) R. O. Davies and G. O. Jones, *Advan. Phys.*, **2**, 370 (1953).
- (3) A. J. Kovacs, *Fortschr. Hochpolymer. Forsch.*, **3**, 394 (1964).
- (4) G. Gee, *Polymer*, **7**, 177 (1966).
- (5) J. M. O'Reilly, *J. Polymer Sci.*, **57**, 429 (1962).
- (6) K. H. Hellwege, W. Knappe, and P. Lehmann, *Kolloid Z.*, **183**, 110 (1962).
- (7) A. Turturro and U. Bianchi, *Chim. Ind. (Milan)*, in press.

0.028°/atm, to be compared with the Hellwege⁶ value $dT_g/dP = 0.013^\circ/\text{atm}$, obtained by a compression study along an isotherm. In addition, we have previously studied¹ a sample of polyvinyl acetate (PVAc) and derived again from the cooling of a liquid along an isochore, a dT_g/dP equal to $0.022^\circ/\text{atm}$ which has been considered in agreement with the $dT_g/dP = 0.020^\circ/\text{atm}$ reported by McKinney, *et al.*,⁸ obtained by specific volume measurements along isobars (*with pressure applied to the liquid*). We now consider this agreement as fortuitous and essentially due to the low accuracy of the values reported in ref 8. We will present in the following a new set of specific volume measurements, from which we derive $dT_g/dP = 0.015^\circ/\text{atm}$, which is in the expected disagreement with the result of the isochore experiments.

It is thus apparent that the method has great importance in determining dT_g/dP values and that the most commonly used way to measure dT_g/dP , *i.e.*, isobaric or isothermal experiments with pressure applied in the liquid region, is less suited to produce glasses under different pressures with identical or at least similar Z values.

As a procedure to measure a dT_g/dP value as near as possible to $(\partial T_g/\partial P)_Z$, we propose the cycle shown in Figure 1. Line ABC is the isobar at 1 atm, GFD or HED are isobars at a higher pressure; T_B is the glass transition temperature observable using a given cooling rate from C to A. This cooling rate represents the "recipe" to produce at any time the glass A, with a given (and reproducible) Z value.

The line CDEH is the normal cycle used to measure $\Delta T_g/\Delta P$; the pressure ΔP is applied in C and the sample is subsequently cooled along DEH. T_E is the new glass transition temperature, and glass H, originated from a precompressed liquid, has a different Z value as compared with glass A.

The line AGFD is the cycle we propose: after having prepared the starting glass A, the same pressure ΔP is applied on the glassy polymer until a state G is reached. The heating of G along GFD, with the same heating rate as used before, will produce a transition at T_F with the creation of liquid D.

We expect the Z value in glass G to be much nearer to the Z value in A and to differ from the Z in glass H; this means that the line GF should be appreciably distinct from HE and therefore $T_E \neq T_F$. The cycle of Figure 1 has been performed experimentally on two samples of PVAc and PVC, whose main characterization is given in Table I.

Experimental Section

The special dilatometer used in this work is capable of

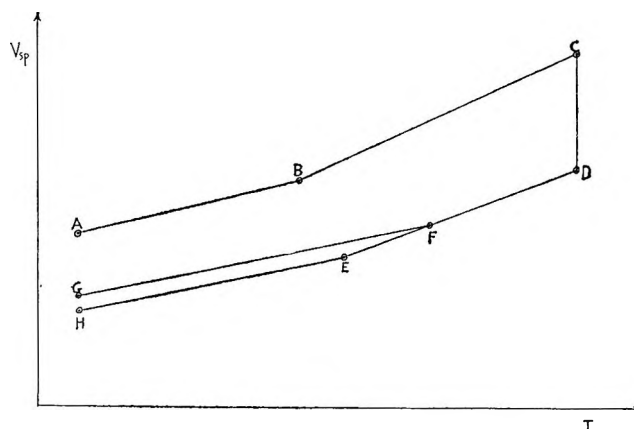


Figure 1. Cycle proposed to measure a dT_g/dP value as near as possible to $(\partial T_g/\partial P)_Z$: line ABC, isobar at a given pressure, P ; line HED, isobar at pressure $P + \Delta P$, with application of ΔP on C; line GFD, isobar at pressure $P + \Delta P$, with application of ΔP on A.

Table I: The Main Characteristics of PVAc and PVC

Polymer	ρ , g/cc at 25°	$\alpha_g \times 10^4$ deg ⁻¹ at 1 atm	$\alpha_l \times 10^4$ deg ⁻¹ at 1 atm	T_g , °C at 1 atm
PVAc	1.194	2.49	6.87	22.0
PVC	1.390	2.57	5.73	72.2

withstanding a maximum pressure of about 500 atm, and is equipped with two tempered glass windows which allow the direct cathetometer reading of the mercury column in the cell.

To check the effect played by window deformation under pressure on the readings, the apparatus has been used to measure the compressibility of carbon tetrachloride; compressibility values have been measured in several pressure ranges (50–100, 100–150, 150–200 atm, and so on) and, once extrapolated to zero pressure and 25°, gave a value of $108.8 \times 10^{-6} \text{ atm}^{-1}$, to be compared with the literature⁹ value of $108.7 \times 10^{-6} \text{ atm}^{-1}$.

Figures 2 and 3 show the results obtained for PVAc and PVC, respectively. As discussed in the Introduction, in both Figures 2 and 3 the points on the line DEH have been obtained by applying 300 atm on the liquid C and then by decreasing the temperature isobarically. Points on the line GF have been obtained by applying 300 atm on glass A and allowing the system to equilibrate until a 20-hr waiting did not reveal any

(8) J. E. McKinney and H. V. Belcher, *J. Res. Natl. Bur. Std.*, **67A**, 43 (1963).

(9) G. A. Holder and E. Whalley, *Trans. Faraday Soc.*, **58**, 2095 (1962).

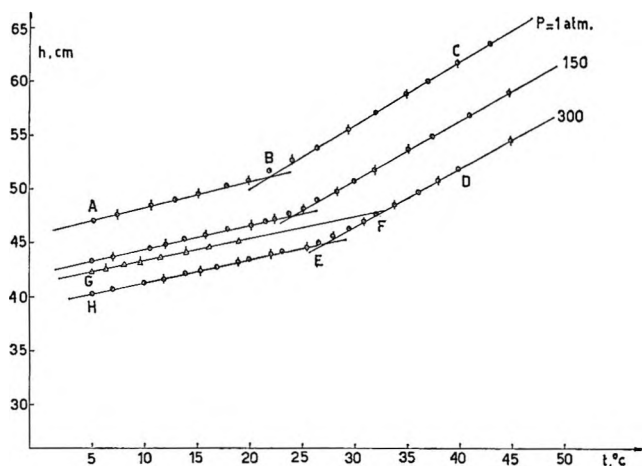


Figure 2. Cathetometer readings of PVAc plotted against temperature at several pressures. Different symbols denote different runs, performed both by increasing (\odot , \triangle) and decreasing (\ominus , Δ) the temperature.

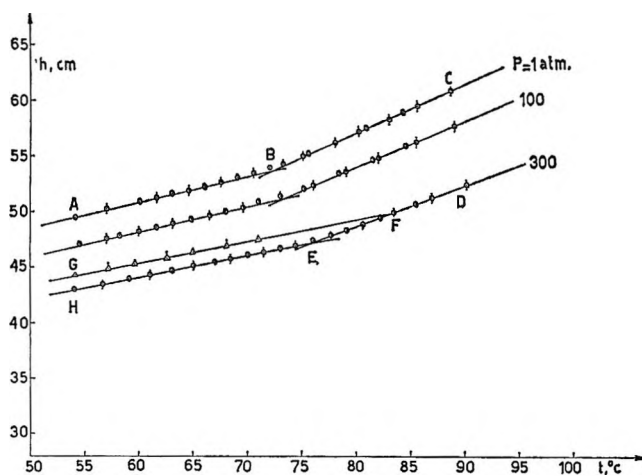


Figure 3. Cathetometer readings of PVC plotted against temperature at several pressures. Different symbols denote different runs as in Figure 2.

further volume change; the total equilibration time was around 50 hr. The sample therefore has been heated isobarically; we avoided reaching the glass transition region, where time effects make their appearance, and the V - T behavior was no longer reversible. In any case, heating and cooling rates were always equal to $5^\circ/\text{day}$.

Discussion

Table II contains the values of the quantities of present interest, derivable from Figures 2 and 3. Several comments are now possible. First of all, Figures 2 and 3 show beyond any doubt the importance of the experimental procedure used to measure T_g and therefore dT_g/dP . The application of 300 atm on the glass,

instead of on the liquid, resulted in a shift of T_g of 6° for PVAc and 7° for PVC; this shift is of course entirely due to the different nature of glasses G and H (see Figure 1, 2, or 3) and has nothing to do with usual time effects due to heating and cooling rates, these being identical in all the experiments performed.

The effect played by the Z parameter or in general by the third variable necessary to describe a given glass form is self-evident by looking at the two points in Figure 2 or 3: there we have two glasses at the same temperature and pressure which show reversible PVT behavior but that have two distinct specific volume values. A first indication of a similar effect has been given by Shishkin.¹⁰

Having shown how T_g depends on the way in which experiments are carried out, we turn now to dT_g/dP values. Table II shows how the effect here is dramatic. The cooling of a compressed liquid gives $dT_g/dP = 0.015$ and $0.013^\circ/\text{atm}$ for PVAc and PVC, respectively; the first value should be compared with the average value $0.02^\circ/\text{atm}$ given in ref 8, which we consider far less accurate, however. Our value for PVC is in very good agreement with that given by Hellwege, *et al.*,⁶ $dT_g/dP = 0.0135^\circ/\text{atm}$.

The application of pressure on the glassy polymers gives entirely different results: $dT_g/dP = 0.036$ and $0.038^\circ/\text{atm}$ for PVAc and PVC, respectively, this is more than double the originally reported values! $\Delta\beta/\Delta\alpha$, as well as dT_g/dP , are of course influenced by the change in procedure. Whereas β values are calculated from the change in volume at the two extreme pressures (1 and 300 atm) and are therefore to be considered average values in this pressure range, thermal expansion coefficients α can be derived at each pressure.

In the calculation of the $\Delta\beta/\Delta\alpha$ given in Table II, we have used an average $\overline{\Delta\alpha}$ given by the arithmetic mean of the two $\Delta\alpha$ values measured at 1 and 300 atm. This procedure has a small effect in the case of PVAc, where $\Delta\alpha$ values at 1 and 300 atm are different by only 3%, and a somewhat larger effect for PVC, for which $\Delta\alpha$ at 1 atm is $3.16 \times 10^{-4} \text{ deg}^{-1}$ and decreases to $2.35 \times 10^{-4} \text{ deg}^{-1}$ at 300 atm.

With regard to the comparison between dT_g/dP and $\Delta\beta/\Delta\alpha$ values, it is interesting to observe that the ratio $\Delta\beta/\Delta\alpha(dT_g/dP)^{-1}$ for PVC is equal to 2.7 in a usual experiment, but it decreases to 1.3 using the cycle we have proposed; the two analog values for PVAc are 1.8 and 1.4.

This result is in line with Gee's⁴ and our expectation and confirms that dT_g/dP values measured along the

(10) N. Shishkin, *Soviet Phys. Solid State*, 2, 322 (1960).

Table II: Relevant Data for Samples Obtained from Figures 2 and 3

P , atm	T_g , °C	$\alpha_g \times 10^4$, deg ⁻¹	$\alpha_l \times 10^4$, deg ⁻¹	$\Delta\alpha \times 10^4$, deg ⁻¹	$\beta_g \times 10^6$, atm ⁻¹	$\beta_l \times 10^6$, atm ⁻¹	$\Delta\beta \times 10^6$, atm ⁻¹	$\Delta\beta/\overline{\Delta\alpha}$, deg atm ⁻¹	$(dT_g/dP)_{\text{expt}}$ deg atm ⁻¹
Polyvinyl Acetate									
1	22.0	2.49	6.87	4.38					
150	24.2	2.30	6.49	4.19	3.55	4.71	1.16	0.028	0.015
300	26.6	2.10	6.23	4.13	3.44	4.51	1.07	0.026	0.015
300 ^a	33.0	2.10	6.23	4.13	2.34	4.51	2.17	0.051	0.037
Polyvinyl Chloride									
1	72.2	2.57	5.73	3.16					
100	73.4	2.42	5.18	2.76	3.63	4.52	0.89	0.032	0.012
300	76.3	2.15	4.50	2.35	3.27	4.14	0.87	0.037	0.014
300 ^a	83.5	2.15	4.50	2.35	2.82	4.14	1.32	0.048	0.038

^a Pressure has been applied on glass A. For the calculation of $\Delta\beta/\Delta\alpha$, we have used an average $\overline{\Delta\alpha}$ as indicated in the text.

cycle AGF of Figure 1 are among the known values the nearest to $(\partial T_g/\partial P)_Z$.

As a last point, we can compare our present results with dT_g/dP values obtained in ref 1 and 7 by internal pressure measurements, using a cycle which was essentially a cooling along an isochor, with a cooling rate of 4–5°/day.

Table III compares dT_g/dP values for PVAc and PVC obtained through three different experiments: experiment A, cooling of a liquid under constant pres-

sure; experiment B, heating of a glass under pressure; and experiment C, cooling of a liquid at constant volume (under decreasing pressure). The table shows quite convincingly how dT_g/dP , at a given heating or cooling rate, is a property not only of the polymer but also of the experiment.

We conclude by saying that the importance of the Z parameter cannot be dismissed in the study of glass properties; any information which, like the pressure effect on T_g , is based on the comparison between two or more glasses should be carefully analyzed in terms of a possible contribution originating from a ΔZ existing among the glasses investigated. Any further improvement of our knowledge in this field must obviously rest on a quantitative correlation between the Z parameter and the glass morphology.

Acknowledgments. We wish to thank Professor C. Rossi for several helpful discussions and Mr. V. Morando for the help given during the experimental work.

Table III: Values of dT_g/dP for Our Two Polymers Obtained through Three Different Experiments

Polymer	dT_g/dP , deg/atm		
	A	B	C
PVAc	0.015	0.037	0.022
PVC	0.013	0.038	0.028

An Electron Paramagnetic Resonance Study of Aliphatic Ether Free Radicals

by Takeshi Shiga,¹ Alain Boukhors, and Pierre Douzou

Institut de Biologie Physico-Chimique, Paris, France

Accepted and Transmitted by The Faraday Society (January 23, 1967)

Free radicals of aliphatic ethers were studied at room temperature in aqueous solutions using epr with a continuous-flow apparatus. All of the possible species of the free radicals could be produced from ethyl ether, 1,2-dimethoxyethane, 2-methoxyethanol, and diethylene glycol, employing two kinds of reagents—Fe(II)·EDTA + H₂O₂ and Ti(III) + H₂O₂. Hückel molecular orbital calculations were performed for these free radicals. In most cases, the experimental and theoretical values for the α - and β -proton hyperfine coupling constants agreed closely. A decrease in the α -proton coupling constant due to hydroxy, methoxy, and ethoxy substitution on the α -carbon atom could be explained as a result of an inductive or mesomeric effect of an oxygen atom. The low experimental values for the β -proton coupling constants of RO \dot{C} HCH₂OR type of free radicals were explained on the basis of an anisotropic rotational averaging. The theoretical values of the γ -proton coupling constants were always larger than the experimental values.

Introduction

The free radicals of the aliphatic hydrocarbon derivatives have been studied in the frozen solution^{2a} or in the crystalline state^{2b} using an irradiation technique. However, the development of a rapid-mixing and -flow technique combined with electron paramagnetic resonance (epr) spectroscopy has made it possible to observe short-lived free radicals in solution.³⁻⁵ The advantage of this technique was not only to determine the spin density distribution of free radicals in a solution state, but to study the phenomena such as a dissociation-association of a proton,^{6,7} an anisotropic molecular rotation,^{8,9} a chair-chair interconversion,¹⁰ etc. Also, this technique permits the production of free radicals which could not be obtained by conventional irradiation techniques. It has been reported, for instance, that an active reagent involved in the Ti(III) + H₂O₂ system is electrophilic.⁵ Consequently, one can obtain CH₃ \dot{C} HOH from ethanol. On the other hand, Fenton's reagent produces \dot{C} H₂CH₂OH, which could barely be produced by the OH radical.^{11,12} Therefore, by utilizing the Ti(III) + H₂O₂ system and Fenton's reagent, we have the possibility of observing at least two kinds of free radicals starting from the same substrate.

The study of the aliphatic free radicals is of interest

for the following reasons: (1) a comparison between the effects of hydroxy, methoxy, and ethoxy substituents on the α - and β -proton hyperfine coupling constants of the aliphatic hydrocarbons, which reflects an anisotropic rotation along the C-C axis and an inductive or mesomeric effect of the substituents; (2) a determination of the relationship between the spin density of the oxygen atom and the g value or the γ -proton coupling constants; (3) a comparison between the experimental and theoretical values of the hyperfine coupling constants and an estimation of a reasonable set

(1) On leave from the Faculty of Medicine, Osaka University, Osaka, Japan.

(2) (a) M. C. R. Symons and M. G. Townsend, *J. Chem. Soc.*, 263 (1959); (b) J. R. Morton, *Chem. Rev.*, **64**, 453 (1964).

(3) I. Yamazaki, H. S. Mason, and L. H. Piette, *Biochem. Biophys. Res. Commun.*, **1**, 336 (1959).

(4) D. C. Borg, *Nature*, **201**, 1087 (1964).

(5) W. T. Dixon and R. O. C. Norman, *J. Chem. Soc.*, 3119 (1963).

(6) I. Yamazaki and L. H. Piette, *J. Am. Chem. Soc.*, **87**, 986 (1965).

(7) H. Fischer, *Mol. Phys.*, **9**, 149 (1965).

(8) C. Corvaja, H. Fischer, and G. Giacometti, *Z. Physik. Chem.*, **45**, 1 (1965).

(9) W. T. Dixon, R. O. C. Norman, and A. Buley, *J. Chem. Soc.*, 3625 (1964).

(10) W. T. Dixon and R. O. C. Norman, *ibid.*, 4850 (1964).

(11) T. Shiga, *J. Phys. Chem.*, **69**, 3805 (1965).

(12) R. Livingston and H. Zeldes, *J. Chem. Phys.*, **44**, 1245 (1966).

for these parameters; (4) a confirmation of the character of the two reagents employed. The present discussion is more quantitative and unified than that found in the literature.^{9,11,13} In addition, we have succeeded, by employing these two reagents, in observing all of the different types of free radicals from etheric compounds. In some cases, we could also obtain free radicals which have not been found, because of the high flow rate of our flow apparatus.

On the above aspects, we will systematically discuss the proton hyperfine coupling constants of the oxygen-containing aliphatic free radicals.

Experimental Section

Apparatus. A Varian V-4502 epr spectrometer with a 100-kc field modulation unit and a 9-in. low-impedance magnet equipped with a Fieldial control unit were used. The microwave frequency measured by a Hewlett-Packard Model X-532B frequency meter ranged from 9505 to 9503 Mc. The rapid-mixing and -flow apparatus which we used was the same as the one reported previously¹¹ and permitted the observation of short-lived free radicals 5 msec after the mixing of the reagent and the substrate. The first derivatives of the epr absorption spectrum were recorded by a Moseley Model 7030AM X-Y recorder or by a Varian G-14A-2 strip chart recorder. An ethanol radical ($\text{CH}_3\dot{\text{C}}\text{HOH}$), which was produced by a similar manner as the other free radicals, was adopted as a standard for the measurement of the proton hyperfine coupling constants. The β -proton coupling constant of $\text{CH}_3\dot{\text{C}}\text{HOH}$ was reported to be 22.2¹¹ or 22.19¹² gauss at room temperature. A standard error of 0.016 gauss for this value was obtained with our equipment.

Theoretical calculations were carried out using the IBM 1130 computer.

Materials. $\text{FeSO}_4 \cdot 7\text{H}_2\text{O}$, TiCl_3 (15%), and H_2O_2 (30%) were obtained from Merck; ethylenediaminetetraacetic acid (Na_2 salt) (EDTA) from Prolabo; ethyl alcohol and ethyl ether from Prolabo; ethylene glycol, diethylene glycol, 2-methoxyethanol, and 1,2-dimethoxyethane from Fluka; phosphate salts and H_2SO_4 from Merck.

These materials were reagent grade and were used without further purification. N_2 gas was obtained from Air Liquide Co. (oxygen content <10 ppm).

Method. Two kinds of reagents were used in order to obtain the free radicals: (1) a 5 mM solution of Fe(II)-EDTA (molar ratio of 1:1) and a solution of H_2O_2 (2 ml of 30% $\text{H}_2\text{O}_2/1.$) each buffered at pH 7.0 with 0.067 M phosphate buffer; (2) a solution of Ti(III) (8 ml of 15% $\text{TiCl}_3/1.$) and a solution of H_2O_2 (2 ml of 30% $\text{H}_2\text{O}_2/1.$), each in 0.1 N H_2SO_4 ; the various sub-

strates were added to the solution of H_2O_2 , their concentrations being 5–10 vol. %. The two solutions were bubbled with N_2 gas in order to remove the dissolved O_2 and then injected and mixed in the special quartz cell.

The epr spectra were recorded during the flow, *i.e.*, 10–25 msec after the mixing of the two solutions. The experiments were carried out at 25°.

Results

Analysis of the Epr Spectra. Ethyl Ether. A free radical of ethyl ether, produced by the Ti(III) + H_2O_2 system has been reported^{9,13} which was identified as $\text{CH}_3\dot{\text{C}}\text{HOCH}_2\text{CH}_3$. However, with Fenton's reagent, ethyl ether gave a more complicated spectrum (Figure 1).

The spectrum could be analyzed as follows: (1) a doublet (1:1) of a quartet (1:3:3:1) of a narrow triplet (1:2:1), which was the same as the free radical produced by the Ti(III) + H_2O_2 system, $\text{CH}_3\dot{\text{C}}\text{HOCH}_2\text{CH}_3$; (2) a triplet (1:2:1) of a triplet (1:2:1), which could be identified as $\dot{\text{C}}\text{H}_2\text{CH}_2\text{OCH}_2\text{CH}_3$.

Diethylene Glycol. A free radical was produced by Fenton's reagent, whose spectrum consisted of a doublet (1:1) of a triplet (1:2:1) of a narrow triplet (1:2:1), but two sets of a narrow triplet were overlapped in the center (Figure 2). The signal could be identified as coming from $\text{HOCH}_2\dot{\text{C}}\text{HOCH}_2\text{CH}_2\text{OH}$.

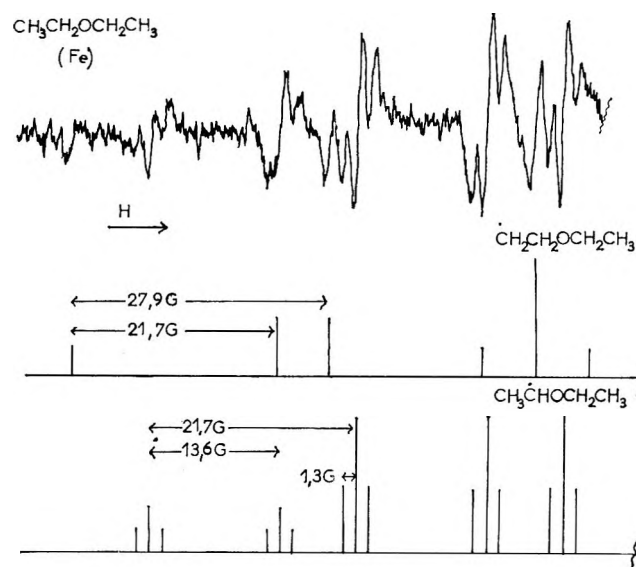


Figure 1. Epr spectrum of ethyl ether free radicals, produced by Fenton's reagent. Microwave power 6 db; modulation 100 kc, 0.4 gauss; time constant 0.3 sec; magnetic field scanning 100 gauss/2.5 min; at 25°.

(13) P. L. Kolker, *J. Chem. Soc.*, 5929 (1964).

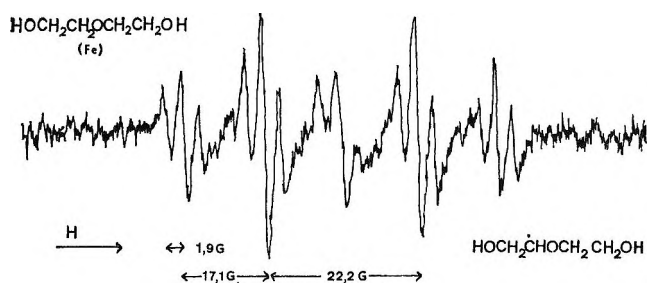


Figure 2. Epr spectrum of diethylene glycol free radicals, produced by Fenton's reagent. Microwave power 6 db; modulation 100 kc, 0.4 gauss; time constant 0.3 sec; magnetic field scanning 100 gauss/2.5 min; at 25°.

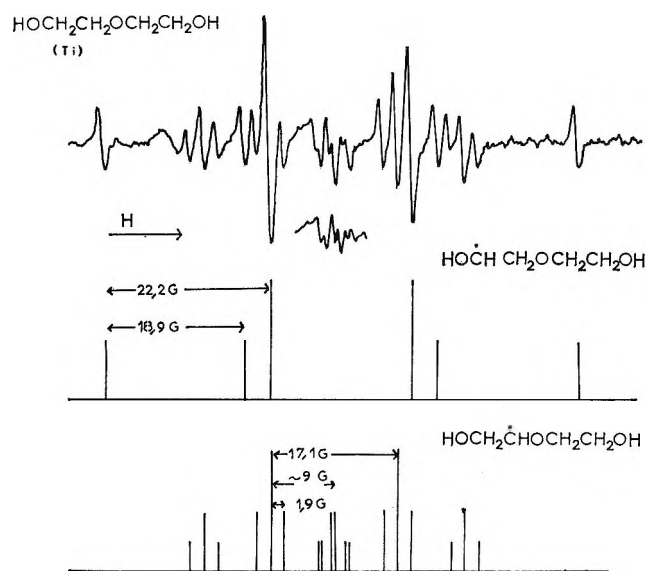


Figure 3. Epr spectrum of diethylene glycol free radicals, produced by the Ti(III) + H₂O₂ system. Microwave power 6 db; modulation 100 kc, 0.4 gauss (or 0.2 gauss shown below); time constant 0.3 sec; magnetic field scanning 100 gauss/2.5 min; at 25°.

The spectrum of the free radicals produced by the Ti(III) + H₂O₂ system exhibited a complicated structure (Figure 3), which could be analyzed as consisting of two different kinds of free radicals: (1) HOCH₂- \dot{C} HOCH₂CH₂OH, which was the same as the one produced by Fenton's reagent; (2) a doublet (1:1) of a triplet (1:2:1) attributed to HO \dot{C} HCH₂OCH₂CH₂OH.

2-Methoxyethanol. The spectrum of the free radicals, obtained by the Ti(III) + H₂O₂ system (Figure 4), consisted of: (1) a triplet (1:2:1) of a narrow triplet (1:2:1), identified as \dot{C} H₂OCH₂CH₂OH;¹³ (2) a doublet (1:1) of a triplet (1:2:1) of a narrow multiplet (probably 1:3:3:1), arising from CH₃OCH₂ \dot{C} HOH.

The free radicals produced by Fenton's reagent gave a spectrum shown in Figure 5. Again, two signals were superimposed: (1) a triplet (1:2:1) of a narrow triplet

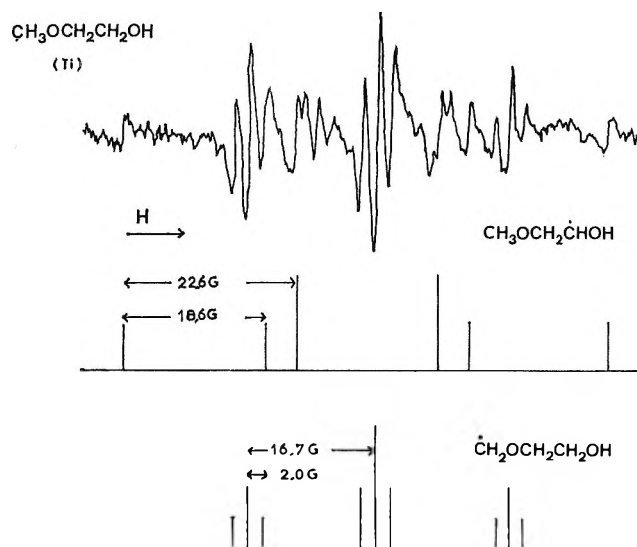


Figure 4. Epr spectrum of 2-methoxyethanol free radicals, produced by the Ti(III) + H₂O₂ system. Microwave power 6 db; modulation 100 kc, 0.4 gauss; time constant 0.3 sec; magnetic field scanning 100 gauss/2.5 min; at 25°.

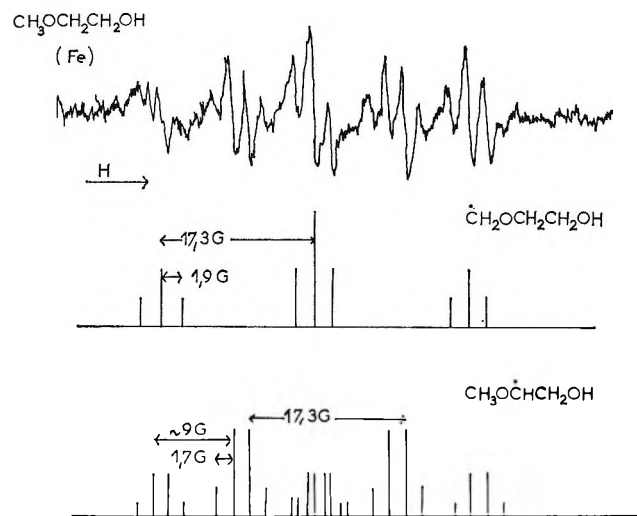


Figure 5. Epr spectrum of 2-methoxyethanol free radicals, produced by Fenton's reagent. Microwave power 6 db; modulation 100 kc, 0.4 gauss; time constant 0.3 sec; magnetic field scanning 100 gauss/2.5 min; at 25°.

(1:2:1) was the same as one of the signals obtained by the Ti(III) + H₂O₂ system, \dot{C} H₂OCH₂CH₂OH; (2) a doublet (1:1) of a narrow quartet (1:3:3:1) could be seen clearly. Furthermore, a narrow multiplet at the low-field end which was attributed to one of the triplets arising from \dot{C} H₂OCH₂CH₂OH could not be a simple triplet but a multiplet of a superimposing triplet and quartet. Therefore, the spectrum was interpreted to be composed of six sets of a narrow quartet, arising from CH₃O \dot{C} HCH₂OH, but a set overlapped with an-

other narrow triplet at both ends of the spectrum and two sets of weak and narrow quartets superimposed with an intense and narrow triplet.

1,2-Dimethoxyethane. The coupling constants reported for the free radical $\dot{\text{C}}\text{H}_2\text{OCH}_2\text{CH}_2\text{OCH}_3$ ^{9, 13} produced by the Ti(III) + H₂O₂ system were not the same. We obtained a spectrum similar to that of Kolker which consisted of a triplet (1:2:1) of a narrow triplet (1:2:1). Furthermore, since our flow apparatus has a higher flow rate than the others, we could also obtain a spectrum of $\text{CH}_3\text{O}\dot{\text{C}}\text{HCH}_2\text{OCH}_3$, which was similar to that of Figure 5.

The spectrum obtained from the same compound by Fenton's reagent was similar to that shown in Figure 5 and also to that obtained with the Ti(III) + H₂O₂ system. Therefore, we concluded that two types of free radicals were produced: (1) $\text{CH}_3\text{O}\dot{\text{C}}\text{HCH}_2\text{OCH}_3$ and (2) $\dot{\text{C}}\text{H}_2\text{OCH}_2\text{CH}_2\text{OCH}_3$.

Theoretical Calculations. Hückel molecular orbital calculations were performed assuming the planarity of the molecules. The parameters used are listed in Table I. In order to test the validity of these parameters, calculations were performed on several alcohol radicals.

Table I: Hückel Parameters

Parameter	Value	Parameter	Value
h_{O}	+1.70	$k_{\text{C}-\text{CH}_2}$	+0.70
$h_{\text{O}-(\text{CH}_2-)}$	+1.60	$k_{\text{O}-\text{C}}$	+0.90
$h_{=\text{H}_1,=\text{H}_2}$	-0.20	$k_{\text{C}=\text{H}_1,\text{C}=\text{H}_2}$	+2.00
$h_{\text{C}-(\text{CH}_2-)}$	-0.10	$k_{\text{O}-\text{CH}_2}$	+0.60

The α -proton coupling constants were calculated from the electron density on the α -carbon atoms, using the formula $A = \rho Q$. ρ was obtained from the square of the coefficient of α -carbon atoms in the highest (semi)occupied molecular orbital, and a Q value of 22.5 gauss was adopted.¹⁴

The β - and γ -proton coupling constants were calculated from the coefficients of the corresponding hydrogen atoms in a similar manner, using a Q value of 210 gauss.¹⁵

The calculated values for coupling constants are summarized in Table II. It is seen that the agreement between the theoretical and experimental values is good, with the exception of a series of $\text{RO}\dot{\text{C}}\text{HCH}_2\text{OR}$ type of free radicals.

Discussion

Hyperfine Coupling Constants. (1) α -Proton Coupling Constants. The α -proton coupling constants are

between 21 and 23 gauss,^{8,9,11,16} in the case of $\text{CH}_2\text{-CH}_2\text{OR}$ type of free radicals where the α -carbon atoms and the oxygen atoms are separated. These values are similar to that of the alkyl free radicals.¹⁷ However, when a hydroxy, methoxy, or ethoxy group is attached to the α -carbon atoms, the α -proton coupling constants decrease to 17–19 gauss.^{5,11} This phenomenon was explained by Dixon and Norman as arising from a mesomeric effect of an oxygen atom⁵ and is interpreted on the basis of our calculations as arising from a significant delocalization of the odd electron on the oxygen atom. This kind of effect (inductive or mesomeric) is well accounted for by the present Hückel calculation.

On the other hand, Fischer has introduced a number of semiempirical parameters in order to calculate the spin densities on the α -carbon atom of the substituted methyl free radicals.^{18,19} The spin density on the α -carbon atom can be approximated by the equation: $\rho = \pi(1 - \Delta(X_i))$. The values of $\Delta(X_i)$ which depend on the substituents were estimated empirically. Using Fischer's $\Delta(X_i)$ values, good agreement is obtained between the calculated and experimental α -proton coupling constants. Therefore, the delocalization effect of the oxygen atoms is also well accounted for by Fischer's parameters.

In addition, a further decrease in the α -proton coupling constants was observed in the series of $\text{R}\dot{\text{C}}\text{HOH}$ type of free radicals. This fact has been noted previously by Dixon and Norman⁵ and confirmed by Shiga.¹¹ The α -proton coupling constants are between 13 and 15 gauss for $\text{R}\dot{\text{C}}\text{HOH}$, while between 17 and 19 gauss for $\dot{\text{C}}\text{H}_2\text{OR}$. The spin densities calculated by the Hückel method and the spin densities estimated by Fischer's formula both predict a small decrease in the α -proton coupling constants. It should be noted, however, that these values are somewhat overestimated. Therefore, in order to explain this small discrepancy, it may be necessary to propose some additional mechanism which leads to a decrease in the $Q_{\alpha\text{-CH}^{\text{H}}}$ values. Thus Fischer has postulated a modification of the $Q_{\alpha\text{-CH}^{\text{H}}}$ values depending on the degree of the inductive effect of the substituents. On the other hand, Fessenden has suggested "a slightly nonplanar configuration around the α -carbon of these free radicals."²⁰

(14) H. M. McConnell and D. B. Chesnut, *J. Chem. Phys.*, **28**, 107 (1958).

(15) D. B. Chesnut, *ibid.*, **29**, 43 (1958).

(16) P. Smith, J. T. Pearson, P. B. Wood, and T. C. Smith, *ibid.*, **43**, 1535 (1965).

(17) R. W. Fessenden and R. H. Schuler, *ibid.*, **39**, 2147 (1963).

(18) H. Fischer, *Z. Naturforsch.*, **19a**, 866 (1964).

(19) H. Fischer, *ibid.*, **20a**, 428 (1965).

(20) R. W. Fessenden, *J. Phys. Chem.*, **71**, 74 (1967).

Table II: Proton Hyperfine Coupling Constants (in gauss)

Compounds	Free radicals	Coupling constants			Spin density on oxygen	Reagent ^a	Ref
		α	β	γ			
Ethyl ether	$\dot{\text{C}}\text{H}_2\text{CH}_2\text{OCH}_2\text{CH}_3$	Exptl	21.7	27.9		Fe	
		Theoret	20.0	23.3			
	$\text{CH}_3\dot{\text{C}}\text{HOCH}_2\text{CH}_3$	Exptl	13.6	21.5	1.4	Ti	9
		Theoret	13.8	21.9	1.4	Ti	13
1,2-Dimethoxyethane	$\dot{\text{C}}\text{H}_2\text{OCH}_2\text{CH}_2\text{OCH}_3$	Exptl	16.9	20.4	2.8	0.140	
		Theoret	17.3		1.9		Fe
	$\text{CH}_3\text{O}\dot{\text{C}}\text{HCH}_2\text{OCH}_3$	Exptl	16.6		2.0		Ti
		Theoret	18.7		3.0	0.152	
	$\text{CH}_3\text{O}\dot{\text{C}}\text{HCH}_2\text{OCH}_3$	Exptl	18.1	$\sim 9^b$	1.9		Fe
		Theoret	18.3	~ 9	1.9		Ti
$\text{CH}_3\text{O}\dot{\text{C}}\text{HCH}_2\text{OCH}_3$	Exptl	16.9	20.0	2.8	0.150		
	Theoret	16.7		2.0		Fe	
2-Methoxyethanol	$\dot{\text{C}}\text{H}_2\text{OCH}_2\text{CH}_2\text{OH}$	Exptl	16.6		2.0		Ti
		Theoret	18.5		3.5	0.163	
	$\text{CH}_3\text{O}\dot{\text{C}}\text{HCH}_2\text{OH}$	Exptl	18.3	$\sim 9^b$	1.9		Fe
		Theoret	16.9	20.0	2.8	0.140	
	$\text{CH}_3\text{OCH}_2\dot{\text{C}}\text{HOH}$	Exptl	18.6	22.6			Ti
		Theoret	17.7	20.4		0.135	
Diethylene glycol	$\text{HO}\dot{\text{C}}\text{HCH}_2\text{OCH}_2\text{CH}_2\text{OH}$	Exptl	18.9	22.2			Ti
		Theoret	17.7	19.7		0.135	
	$\text{HOCH}_2\dot{\text{C}}\text{HOCH}_2\text{CH}_2\text{OH}$	Exptl	16.9	8.8	1.9		Fe
		Theoret	17.1	8.7	1.9		Ti
Methanol	$\dot{\text{C}}\text{H}_2\text{OH}$	Exptl	16.9	20.0	2.8	0.140	
		Theoret	17.2				Ti, Fe
	$\text{CH}_3\dot{\text{C}}\text{HOH}$	Exptl	17.38				OH
		Theoret	18.9			0.156	
Ethanol	$\text{CH}_3\dot{\text{C}}\text{HOH}$	Exptl	15.0	22.2			Ti
		Theoret	15.37	22.19			OH
	$\dot{\text{C}}\text{H}_2\text{CH}_2\text{OH}$	Exptl	17.2	20.8		0.139	
		Theoret	22.2	27.6			Fe
Isopropyl alcohol	$(\text{CH}_3)_2\dot{\text{C}}\text{OH}$	Exptl	20.1	23.0			
		Theoret		19.5			Ti
	$(\text{CH}_3)_2\dot{\text{C}}\text{OH}$	Exptl		19.66			OH
		Theoret		18.8		0.124	
Ethylene glycol	$\text{HOCH}_2\dot{\text{C}}\text{HOH}$	Exptl	17.6	9.4			Fe
		Theoret	17.54	9.94			OH
	$\text{HOCH}_2\dot{\text{C}}\text{HOH}$	Exptl	17.2	20.3		0.135	
		Theoret		10.1			Fe
Glycerol	$(\text{HOCH}_2)_2\dot{\text{C}}\text{OH}$	Exptl		18.5		0.125	
		Theoret					

^a The following abbreviations were used: Ti(III) + H₂O₂ system⁹ (Ti); Fe(II)-EDTA + H₂O₂¹¹ (= Fenton's reagent) (Fe); H₂O₂ + h ν ¹² (OH). ^b Approximate values.

It is not possible, however, to conclude from the present data which (if either) mechanism is dominant in explaining the discrepancy.

(2) *β -Proton Coupling Constants.* The substitution of OH or OR (R = CH₃, C₂H₅, C₂H₄OH, etc.) on the β -carbon atoms does not affect the β -proton coupling constants of $\dot{\text{C}}\text{H}_2\text{CH}_2\text{OR}$ type of free radicals. The values for the β -proton coupling constants are between 25 and 28 gauss and obey closely the $\langle \cos^2 \theta \rangle$ law.²¹

The β -proton coupling constants decrease, however, to 20–23 gauss for HO $\dot{\text{C}}\text{HCH}_2\text{OR}$ (R = CH₃, C₂H₅,

C₂H₄OH, etc.), in which the α -carbon atoms have less spin density initially owing to OH substitution; therefore this decrease in the β -proton coupling constant seems to follow closely the $\langle \cos^2 \theta \rangle$ law.²¹ The present calculation agrees well with the experimental values for the above two types of free radicals.

A considerable decrease in the β -proton coupling constants was observed for RO $\dot{\text{C}}\text{HCH}_2\text{OH}$ type of free

(21) C. Heller and H. M. McConnell, *J. Chem. Phys.*, **32**, 1535 (1960).

radicals, and for $\text{HO}\dot{\text{C}}\text{HCH}_2\text{OH}$ and $\text{HO}\dot{\text{C}}\text{HCH}(\text{OH})\text{-CH}_2\text{OH}$.¹¹ The observed values of β -proton coupling constants are about half of the calculated values. This systematic discrepancy does not arise from an inductive or a mesomeric effect of the substituents, because such an effect is accounted for in the Hückel calculations. In order to explain the discrepancy, we may consider a steric effect induced by substituents. Such an effect can give rise to a preference of the relative orientation of the p_z orbital on the α -carbon atom and the C-H bonds of the β -carbons and can cause an anisotropic rotational averaging of the β -proton coupling constants.^{9,12,16} The steric effect can arise from an intermolecular (with the same molecular species or with the reagent) or intramolecular complexing.

The first mechanism, *i.e.*, a steric hindrance of the rotation due to intermolecular complexing between the free radical and the ethylene glycols, has been suggested from the infrared^{22,23} and nmr^{24,25} data. This effect can be neglected, because the concentration of the ethylene glycols is sufficiently low in our case and because the similar kinds of free radicals such as $\dot{\text{C}}\text{H}_2\text{-CH}_2\text{OH}$, $\text{CH}_3\dot{\text{C}}\text{HCH}_2\text{OH}$, or $\dot{\text{C}}\text{H}_2\text{CH}(\text{OH})\text{CH}_2\text{OH}$ possess a normal β -proton coupling constant.¹¹

The second mechanism could arise from a steric hindrance of the rotation due to an intermolecular complexing between the free radical and the reagent used (Ti ion or Fe-EDTA, whose valency and structure are unknown). However, this mechanism seems doubtful, since the experimental facts do not favor the existence of such a complex for many alcohol radicals.¹¹ Although the charge and the size of the two reagents would be quite different, the decrease in the β -proton coupling constant was independent of the reagents used. Furthermore, the same order of magnitude for the decrease of the β -proton coupling constants has been observed for $\text{HO}\dot{\text{C}}\text{HCH}_2\text{Cl}$,¹¹ $\text{HO}\dot{\text{C}}\text{HCH}_2\text{NH}_2$,⁹ etc., but not for $\text{HO}\dot{\text{C}}\text{HCH}_2\text{OR}$. Therefore, we believe this decrease in β -proton coupling constants to be connected with an intramolecular steric effect.

The third mechanism, in which an intramolecular hydrogen bonding is assumed, seems possible on the basis of the infrared and nmr data. This explanation is not, however, favored by Livingston and Zeldes.¹² They have pointed out that the formation of an intramolecular hydrogen bond with a minimum approach of the hydrogen atom to the oxygen atom is not the steric configuration that minimizes $\langle \cos^2 \theta \rangle$, in connection with $\text{HO}\dot{\text{C}}\text{HCH}_2\text{OH}$ (see Figure 6(a) or 6(b)). Furthermore, an intramolecular hydrogen-bond mechanism cannot explain the abnormal β -proton coupling constant for $\text{CH}_3\text{O}\dot{\text{C}}\text{HCH}_2\text{OCH}_3$, nor the normal value for $\text{HO}\dot{\text{C}}\text{HCH}_2\text{OCH}_3$.

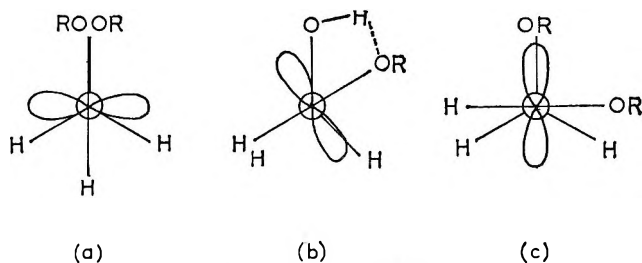


Figure 6. Bond orientation of the $\text{RO}\dot{\text{C}}\text{HCH}_2\text{OH}$ type of free radicals (see text).

Finally, we propose a fourth mechanism, that is shown in Figure 6(c). It is seen that the p_z orbital of the α -carbon atom possessing an odd electron (perpendicular to the C-C axis) has a preference to be parallel to the C-OH (or C-OR) bond on the β -carbon atom. This orientation of the orbitals, however, is valid only for $\text{RO}\dot{\text{C}}\text{HCH}_2\text{OH}$ (or OR) type of free radicals and for $\text{HO}\dot{\text{C}}\text{HCH}_2\text{OH}$.

(3) γ -Proton Coupling Constants. Agreement between the calculated spin density of oxygen and the experimental γ -proton coupling constants was expected. In this connection it should be noted that the experimental values do not vary with the compounds and that the calculated values for γ -proton coupling constants overestimate the spin densities. As discussed above, most of these free radicals seem to possess a special steric configuration (anisotropic rotation). It is therefore impossible at this point to consider the γ -proton coupling constants without further experimental knowledge.

g Values. Livingston and Zeldes¹² have noted that the spin density on the oxygen atom is intimately related to the g value. On the other hand, Stone²⁶ has proposed a theory which relates the g value to the calculated energy of the molecular orbital occupied by the odd electron. In Stone's theory the contribution of the nonbonding oxygen orbital is also discussed.

Unfortunately, very accurate g -value measurement (order of 0.0001 in Δg) was not possible (using our equipment). However, a small relative variation in g value could be made accurately, when two spectra were superimposed.

It is clearly seen from Figure 3 that $\text{HOCH}_2\dot{\text{C}}\text{HOC}_2\text{H}_4\text{OH}$ has a higher g value ($\Delta g = 0.0005$) than $\text{HO}\dot{\text{C}}\text{HCH}_2\text{OC}_2\text{H}_4\text{OH}$. The energy of the (semi)occupied

(22) L. P. Kuhn, *J. Am. Chem. Soc.*, **74**, 2492 (1952).

(23) L. P. Kuhn, *ibid.*, **80**, 5950 (1958).

(24) H. Saito, T. Yonezawa, S. Matsuoka, and K. Fukui, *Bull. Chem. Soc. Japan*, **39**, 989 (1966).

(25) J. Wieman, G. Dana, S. L. T. Thuan, and M. Brajmi, *Compt. Rend.*, **258**, 3724 (1964).

(26) A. J. Stone, *Mol. Phys.*, **6**, 509 (1963).

highest molecular orbital (0.457β for the former free radical, and 0.447β for the latter) and the spin density on the oxygen atom (0.140 for the former, and 0.135 for the latter) fit their view.

Other examples of the 2-methoxyethanol free radicals are given in Table III. It is seen that for these free radicals the agreement is not satisfactory.

Table III: Variation in g Values, Orbital Energies, and Spin Densities on the Oxygen Atom of 2-Methoxyethanol Free Radicals

	g value	Orbital energy (β)	Spin density on the oxygen atom
$\dot{\text{C}}\text{H}_2\text{OCH}_2\text{CH}_2\text{OH}$	Intermediate	-0.401	0.163
$\text{CH}_3\text{O}\dot{\text{C}}\text{HCH}_2\text{OH}$	Lowest	-0.457	0.140
$\text{CH}_3\text{OCH}_2\dot{\text{C}}\text{HOH}$	Highest	-0.447	0.135

Since the theoretical treatment of the g values for these free radicals involves many complex factors, it is difficult to explain the discrepancy at the present time.

Reactivity of the Two Reagents. The nature of the active reagents of the Ti(III) + H_2O_2 system and Fe(II) + H_2O_2 (Fenton's reagent), which are responsible for the hydrogen-abstraction reaction, are not well known. The free OH radical was proposed as the active reagent of the Ti(III) + H_2O_2 system by Dixon and Norman.⁵ The experimental facts suggest, how-

ever, a type of reactive complex between Ti ion and H_2O_2 (or OH).^{27,28} The existence of a reactive complex has also been considered in Fenton's reagent.¹¹ Livingston and Zeldes¹² have succeeded in producing pure OH radical by strong ultraviolet irradiation of H_2O_2 in solution. The OH is more electrophilic than the reagent involved in the Ti(III) + H_2O_2 system.

As discussed in the preceding paper,¹¹ it is impossible to measure the initial concentrations of different types of free radicals produced simultaneously. This experimental limitation arises from the fact that the "dead time" of our flow apparatus is 5 msec. Thus, the decay reaction of the free radicals starts before a measurement can be made. It can be said, however, that the active species of Fenton's reagent abstracts a hydrogen from both carbons of ethyl ether while the Ti(III) + H_2O_2 system does not attack the carbon farthest from the etheric oxygen.

Therefore, we suggest that Fenton's reagent is not electrophilic but rather nucleophilic in character.

Acknowledgment. This work was supported by the Direction des Recherches et Moyens d'Essais (Division de Chimie) and by the Public Health Service (Contract GM 12.289.01, National Institute of General Medical Science). The authors wish to thank Dr. J. P. Malrieu for his helpful advice concerning the theoretical calculations.

(27) L. H. Piette and G. Bulow, *Chem. Abstr.*, **64**, 1396a (1966).

(28) Y. S. Chiang, J. Craddock, D. Mickewich, and T. Turkevich, *J. Phys. Chem.*, **70**, 3509 (1966).

The Solubility of Silver Chloride and the Concentrations of Silver-Containing Species in Ethanol-Water Mixtures

by K. P. Anderson, E. A. Butler, D. R. Anderson, and E. M. Woolley

Department of Chemistry, Brigham Young University, Provo, Utah (Received February 28, 1967)

Values of the solubility of silver chloride at chloride ion concentrations between 10^{-5} and 10^{-1} M were determined in 0, 10, 20, 40, and 50% by weight ethanol-water mixtures using a radio tracer technique with ^{110}Ag . Values of the solubility product constant (K_{sp}), the associated silver chloride formation constant (K_0), and the dichloroargentate ion formation constant (K_1) for each solvent mixture were calculated by use of a modified least-squares analysis of the solubility data. It was found that the concentration of silver ion decreased, the concentration of associated silver chloride remained almost constant, and the concentration of dichloroargentate ion increased at a given chloride ion concentration as the per cent ethanol was increased. In other words, K_{sp} decreased from 1.76×10^{-10} to 7.77×10^{-12} , K_0 increased from 2.11×10^3 to 4.34×10^4 , and K_1 increased from 1.81×10^5 to 2.28×10^7 as the per cent ethanol was changed from 0 to 50.

Introduction

Although the solubility of silver chloride in water at various chloride ion concentrations has been extensively studied,¹⁻⁵ few investigations have been made of its solubility as a function of chloride ion concentration in aqueous-nonaqueous solvent mixtures. Several investigators⁶⁻⁸ have reported the total solubility of silver chloride in mixed solvents with no excess chloride ion present. Kratochvil and Težak^{3,9,10} reported values of the solubility of silver chloride at various chloride ion concentrations in mixed solvents. They calculated a value of the solubility product constant from the Ricci and Davis relationship¹¹ and obtained values of the equilibrium constants for all other silver-containing species in solution by drawing tangents to various parts of the solubility curves. In making those evaluations, Kratochvil and Težak assumed that the thermodynamic activity of each species was equal to its molar concentration and that only one silver-containing species was present in significant concentration at the point where the tangent was drawn.

This paper reports our investigation of the solubility of silver chloride in 0, 10, 20, 40, and 50% by weight ethanol-water mixtures at chloride ion concentrations between 10^{-5} and 10^{-1} M using a radio tracer technique with ^{110}Ag . Our purpose was to determine quantita-

tively the effect of the composition of the solvent on the concentrations and equilibrium constants of the silver-containing species in solution.

Experimental Section

Materials. All chemicals used were reagent grade. Solutions were prepared from doubly distilled water, which had a specific conductance of 1.3×10^{-6} $\text{ohm}^{-1} \text{cm}^{-1}$ at 25° . Gas chromatographic analysis of the absolute ethanol used in solution preparation indicated less than 0.1% water and showed no volatile organic impurities.

- (1) G. S. Forbes and H. I. Cole, *J. Am. Chem. Soc.*, **43**, 2492 (1921).
- (2) J. H. Jonte and D. S. Martin, *ibid.*, **74**, 2052 (1952).
- (3) J. Kratochvil, B. Težak, and V. B. Vouk, *Archiv. Chem.*, **26**, 191 (1954).
- (4) K. H. Lieser, *Z. Anorg. Allgem. Chem.*, **292**, 97 (1957).
- (5) G. L. Tingey, Masters Thesis, Brigham Young University, May 1959.
- (6) N. A. Izmailov and U. S. Chernyi, *Russ. J. Phys. Chem.*, **34**, 58 (1960).
- (7) F. K. Koch, *J. Chem. Soc.*, 1551 (1930).
- (8) D. C. Luehrs, R. T. Iwamoto, and J. Kleinberg, *Inorg. Chem.*, **5**, 201 (1966).
- (9) J. Kratochvil and B. Težak, *Archiv. Chem.*, **26**, 243 (1954).
- (10) J. Kratochvil and B. Težak, *Rec. Trav. Chim.*, **75**, 774 (1956).
- (11) J. E. Ricci and T. W. Davis, *J. Am. Chem. Soc.*, **62**, 407 (1940).

$^{110}\text{AgNO}_3$ solution (4 mcuries) was obtained from Oak Ridge National Laboratories and was used to prepare stock solutions of AgClO_4 . The $^{110}\text{AgNO}_3$ was mixed with 0.3 g of nonradioactive AgNO_3 in a cyanide solution and the silver was electroplated onto platinum. The silver was then dissolved in nitric acid and fumed three times to near dryness with perchloric acid. The residue, of initial specific activity *ca.* 5×10^7 cpm/mg of Ag, was diluted to about 1.7×10^{-4} *F* AgClO_4 and was stored in a light-protected container.

Procedure and Equipment. The experimental procedure was similar to that of Jonte and Martin² and Tingey.⁵ Equilibration samples were 25-ml solutions prepared in 30-ml screw-cap vials. Each cap was equipped with a cone-shaped polyethylene insert to prevent leakage. The AgClO_4 solution was pipetted into the vials last to minimize exposure of personnel and to prevent premature formation of insoluble species. The sealed vials were mounted on a rotating drum immersed in a water bath maintained at $25.00 \pm 0.01^\circ$. After equilibration for 1 week, the samples were centrifuged 6 min at 12,300 rpm in a Sorvall SS-1 Superspeed angle centrifuge mounted in an air bath maintained at $25.0 \pm 0.2^\circ$. Portions (2-ml) of each centrifuged solution were carefully withdrawn, evaporated to dryness, and analyzed for total silver content by using a thallium-activated NaI scintillation detector coupled to Tracerlab automatic counting apparatus. Twenty to thirty solubility determinations, each at a different chloride ion concentration, were made in each ethanol-water solvent mixture.

Calculations. The solubility product constant, K_{sp} , associated silver chloride formation constant, K_0 , and the dichloroargentate ion formation constant, K_1 , are defined by eq 1, 2, and 3, respectively^{2,5} in terms of the thermodynamic activities of the indicated species.

$$K_{\text{sp}} = a_{\text{Ag}^+} a_{\text{Cl}^-} \quad (1)$$

$$K_0 = \frac{a_{\text{AgCl}_{\text{assoc}}}}{a_{\text{Ag}^+} a_{\text{Cl}^-}} \quad (2)$$

$$\tilde{K}_1 = \frac{a_{\text{AgCl}_2^-}}{a_{\text{Ag}^+} a_{\text{Cl}^-}^2} \quad (3)$$

Combination of these three equations with the mass balance equation for total silver in solution gives eq 4, an expression for total molar silver concentration as a function of the equilibrium constants, thermodynamic activity coefficients, and the molar concentration of chloride ion. The activity coefficient of $\text{AgCl}_{\text{assoc}}$, γ^*_0 ,

$$[\text{Ag}_{\text{total}}] = \frac{K_{\text{sp}}}{[\text{Cl}^-] \gamma^*_1} + \frac{K_0 K_{\text{sp}}}{\gamma^*_0} + K_1 K_{\text{sp}} [\text{Cl}^-] \quad (4)$$

was assumed to be unity.^{2,5} The activity coefficients of all singly charged species, γ^*_1 , were assumed to be equal and were calculated from the extended Debye-Hückel expression¹²

$$\log \gamma^*_1 = -\frac{A(I)^{1/2}}{1 + Bd(I)^{1/2}} \quad (5)$$

where

$$A = 354.5(\rho/D^3)^{1/2} \quad (6)$$

$$B = 2.913 \times 10^8(\rho/D)^{1/2} \quad (7)$$

and

$$I = \frac{1}{2\rho} \sum C_i Z_i^2 \quad (8)$$

In eq 5-8, I is the ionic strength of the solution, ρ is the density of the solution in grams per milliliter,¹³ D is the dielectric constant¹⁴ of the mixed solvent, and d is the effective ionic diameter of the ions in solution expressed in centimeters. The value of d used in this work was 3.047×10^{-8} cm, so that $Bd = 1.000$ for water as the solvent.¹² The asterisk superscripts on the activity coefficients indicate that the standard states chosen were based upon infinite dilution in that solvent or solvent mixture in which the solubility was determined. Values of K_{sp} , K_0 , and K_1 were calculated simultaneously by means of a modified least-squares treatment¹⁵ of total silver concentration *vs.* chloride ion concentration data. The application of a relative-deviation least-squares method of data treatment permitted very small absolute deviations in the concentrations of species present in a low-concentration region to be as important in the determination of the shape of a solubility curve as much greater absolute deviations in a high-concentration region.

Results and Discussions

The solubility data and accompanying least-squares solubility curves for the solvent systems studied are shown in Figures 1 and 2. Figure 1 also shows values of $[\text{AgCl}_2^-]$, $[\text{AgCl}_{\text{assoc}}]$, and $[\text{Ag}^+]$ as a function of $[\text{Cl}^-]$ for the 9.88% ethanol system. These values were calculated from the values of K_{sp} , K_0 , and K_1 given in

(12) H. S. Harned and B. B. Owen, "The Physical Chemistry of Electrolytic Solutions," 3rd ed, Reinhold Publishing Corp., New York, N. Y., 1958, pp 42-92, 508-515.

(13) Values used in this work are interpolations of data from "International Critical Tables of Numerical Data," Vol. 3, 1st ed, E. W. Washburn, Ed., McGraw-Hill Book Co., Inc., New York, N. Y., 1928, p 116.

(14) Values used in this work were interpolations of data from G. Akerlöf, *J. Am. Chem. Soc.*, **54**, 4132 (1932).

(15) K. P. Anderson and R. L. Snow, *J. Chem. Educ.*, in press.

Table I: Equilibrium Constants for 0–50 wt % Ethanol–Water Mixtures

Wt % ethanol	Dielectric constant ^a	$K_{sp} \times 10^{12}$	SD, ^b %	$K_0 \times 10^{-3}$	SD, ^b %	$K_1 \times 10^{-6}$	SD, ^b %
0	78.54	176	11.0	2.11	10.0	1.81	8.3
9.88	72.87	90.4	6.4	4.61	6.1	3.76	6.3
19.99	67.00	59.9	5.3	6.16	4.5	6.57	3.4
40.12	54.93	17.0	3.5	18.6	5.9	66.4	4.6
50.02	48.99	7.77	9.2	43.4	8.6	228.0	9.9

^a See ref 14. ^b Percentage standard deviations calculated from the weighted relative deviations of the experimental solubility data points from the least-squares solubility curves in Figures 1 and 2.

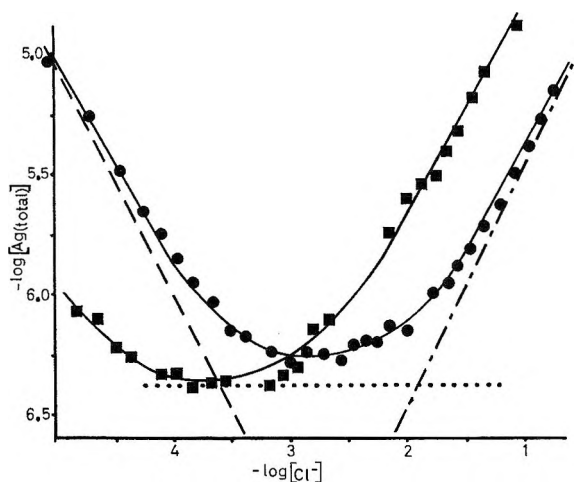


Figure 1. Solubility curves: ●—, 9.88% ethanol; ■—, 50.02% ethanol; ----, $\log [Ag^+]$ for 9.88% ethanol; , $\log [AgCl_{assoc}]$ for 9.88% ethanol; - · - , $\log [AgCl_2^-]$ for 9.88% ethanol.

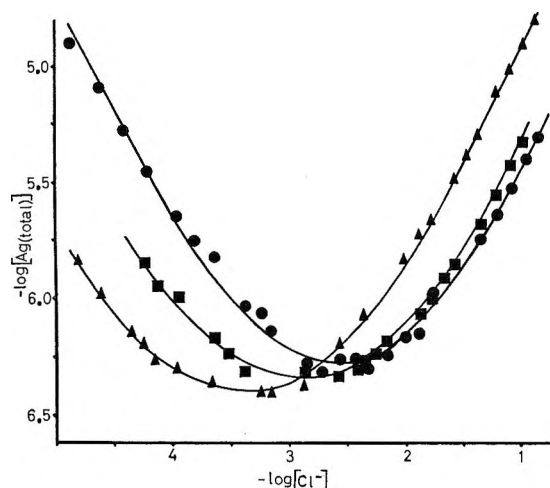


Figure 2. Solubility curves: ●—, water; ■—, 19.99% ethanol; —▲—, 40.12% ethanol.

Table I. The values of K_{sp} , K_0 , and K_1 for each solvent system in Table I were calculated from the modified

least-squares solubility curves in Figures 1 and 2. Since only small random deviations of the solubility data from solubility curve represented by eq 4 were observed, it was assumed that there were no appreciable concentrations of complexes of the form $AgCl_n^{1-n}$ where $n > 2$, even in 0.13 M chloride ion solutions.

Figures 1 and 2 show that the entire solubility curves were shifted toward the lower chloride ion concentrations as the per cent ethanol was increased. That is, $[Ag^+]$ decreased, $[AgCl_{assoc}]$ remained almost constant, and $[AgCl_2^-]$ increased at any given value of $[Cl^-]$. These trends are shown quantitatively in Figure 3, where values of $-\log K_{sp}$, $\log K_0$, and $\log K_1$ are plotted vs. the reciprocal of the dielectric constant of the solvent. Values given by Kratochvil and Težak⁹ are also shown.

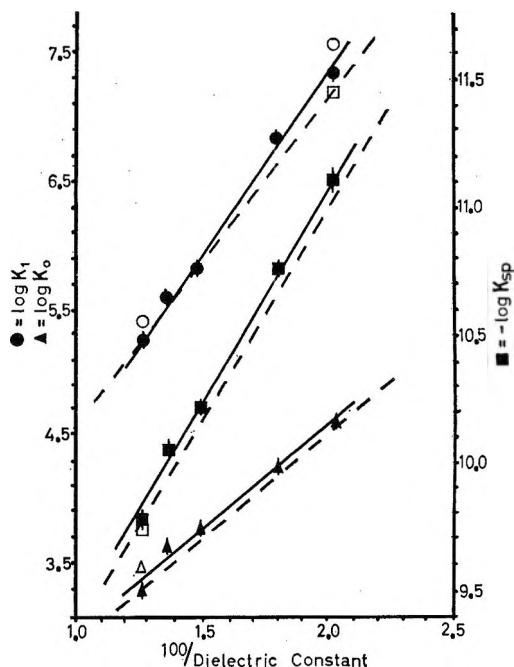


Figure 3. $\log K$ vs. $100/D$: ■, ▲, and ●, experimental values; □, Δ, and O, values reported by Kratochvil and Težak;¹⁰ ----, values predicted by Born's equation;¹⁸ —, least-squares fits of experimental points according to eq 9.

An equation derived by Born¹⁶ which considers electrostatic interactions has the general form

$$\log K' = M \left(\frac{1}{D'} - \frac{1}{D''} \right) + \log K'' \quad (9)$$

When applied to equilibria involving ions, K' and K'' are the equilibrium constants in media of dielectric constant D' and D'' , respectively, and M involves values for the radii of the ions. The solid lines in Figure 3 were obtained from least-squares analyses of the data in Table I. The broken lines were obtained from the Born equation by using values of 1.26, 1.81, and 4.88 Å

(the crystallographic radii) for the radii of silver ion, chloride ion, and dichloroargentate ion, respectively. Table II gives values of M for eq 9 for the lines in Figure 3. The linear relationship predicted by Born is apparent from Figure 3 and Table II.

As illustrated in Figure 1, about two-thirds of the total silver present at the solubility minimum is in the form of $\text{AgCl}_{\text{assoc}}$, whereas the remaining one-third is about equally distributed between the species Ag^+ and AgCl_2^- . As shown in Figure 3, Kratochvil and Težak⁹ reported higher values for the concentrations of $\text{AgCl}_{\text{assoc}}$, Ag^+ , and AgCl_2^- in water than determined in this study. Their method involved the determination of equilibrium constants by the construction of tangents to the solubility curve, a tacit assumption that at the minimum in the curve only $\text{AgCl}_{\text{assoc}}$ is present while at each extremity of the curve only one charged species is present. These investigators also assumed that all activity coefficients were unity.

Further investigation of various other solvent and slightly soluble salt systems should prove helpful in providing quantitative explanations of the effects of the dielectric constant of the solvent and the nature of the nonaqueous component on the concentrations of the various species present in solution and on the values of the constants for the equilibria among these species.

Table II: Values of M in Equation 9

Equilibrium constant	Measured M values ^a	AD, ^b %	Calcd M values ^c	% difference
K_{sp}	-171.4	5.36	-162.9	-5.22
K_0	161.9	5.85	162.9	-0.61
K_1	275.8	8.76	254.5	+8.37

^a From least-squares fit of the data in Table I according to eq 9. ^b Percentage average deviations calculated from the relative deviations of the experimental values of the constants from the least-squares line. ^c Calculated from Born's equation¹⁶ using values of 1.26, 1.81, and 4.88 Å for the radii of silver ion, chloride ion, and dichloroargentate ion, respectively.

(16) M. Born, *Z. Physik*, 1, 45 (1920).

Electrolytic Conductance in Plasticized Polystyrene^{1a,b}

by James R. Price^{1c} and Walter Dannhauser

Department of Chemistry, State University of New York at Buffalo, Buffalo, New York 14214
(Received March 6, 1967)

The dc conductance of tetra-*n*-butylammonium thiocyanate in a 20% (weight) diphenylmethane-80% polystyrene solvent has been determined over the range of salt concentration 3×10^{-4} to 0.1 *m* in the temperature range 70–100° for a range of applied field strengths from 0 to 12 kv/cm. The activation energy for conductance is 33 kcal/mole, independent of salt concentration and field strength. The equivalent conductance decreases with increasing salt concentration over the entire concentration range. These results are discussed in terms of the thermodynamics of ion association and the hydrodynamics of ion migration in such media. The assumption that triple ions make no contribution to the conductance because of their small mobility is developed and an experimental test of this conjecture is proposed.

Introduction

The basic equation for electrical conduction is

$$\kappa = \sum_j n_j e_j u_j \quad (1)$$

where κ is the specific conductance (mhos/cm), n_j is the number of charge carriers in unit volume (cm^3) of the *j*th type, each having charge e_j (coulombs) and mobility u_j ($\text{cm}^2/\text{volt sec}$). Despite many experimental studies of conduction in polymeric systems which, in turn, have generated much speculation about the conduction mechanism(s),² very little is actually known about these basic parameters in polymeric systems. Indeed, in the overwhelming majority of cases the nature of the charge carriers is not even known, to say nothing about their concentration and mobility. In polymeric systems it is especially difficult to distinguish experimentally between electronic semiconduction and electrolytic transport of charge. As in conductance studies of ordinary low molecular weight systems, one can evade the difficulty of determining the nature and concentration of naturally occurring charge carriers by suitably doping the polymer, either with radiation (or otherwise) generated electrons³ or by the addition of known amounts of an electrolyte.⁴ We chose the latter method. The experiments were beset with many difficulties, some of which have also been noted by others.⁴⁻⁶

Experimental Section

Thermally polymerized polystyrene,⁷ containing only traces of metallic impurities as shown by spectrographic analyses, was further purified by extracting benzene solutions of the polymer with conductivity water. An aliquot of tetra-*n*-butylammonium thiocyanate⁸ in benzene was added to a known weight of the purified polymer, also dissolved in benzene. The resulting dilute solution was freeze-dried and then vacuum dried at 65° for at least 3 days to ensure complete removal of

(1) (a) Supported by the National Science Foundation through Grant NSF-G18832; (b) taken in part from a thesis presented by J. R. P. to The Graduate School, State University of New York at Buffalo, in partial fulfillment of the requirements for the Doctor of Philosophy degree; (c) The Carborundum Co., Niagara Falls, N. Y.

(2) For recent reviews, see D. A. Seanor, *Advan. Polymer Sci.*, **4**, 317 (1965); W. O. Baker, *J. Polymer Sci.*, **C4**, 1633 (1963); N. Riehl, *Ann. Physik*, **6**, 93 (1957); A. T. McPherson, *Rubber Chem. Technol.*, **36**, 1230 (1963).

(3) K. Yahagi and A. Danno, *J. Appl. Phys.*, **34**, 804 (1963); P. K. Watson and T. M. Clancy, *Rev. Sci. Instr.*, **36**, 217 (1965). For a review see F. A. Bovey, "The Effects of Ionizing Radiation on Natural and Synthetic High Polymers," Interscience Publishers, Inc., New York, N. Y., 1958, Section III-6.

(4) (a) D. J. Mead and R. M. Fuoss, *J. Am. Chem. Soc.*, **67**, 1566 (1945); (b) L. H. Wartman, *SPE J.*, **20**, 254 (1964).

(5) A. Weinreib, *et al.*, *J. Chem. Phys.*, **43**, 701 (1965).

(6) A. H. Scott, *Natl. Acad. Sci. Natl. Res. Council Pub.* **1356**, 98 (1966).

(7) $\overline{DP} = 1200$ from intrinsic viscosity in benzene. We wish to thank the Dow Chemical Co. for their generous gift of this fine sample.

(8) L. E. Strong and C. A. Kraus, *J. Am. Chem. Soc.*, **72**, 166 (1950).

the benzene.⁹ This procedure yielded a homogeneous, porous, self-supporting shell of polymer which contained the salt. A known weight of diphenylmethane (DPM), enough to make the final sample 20% by weight DPM, was then distilled isopiesticly into the freeze-dried polymer. This technique ensured uniform mixing of the polymer, salt, and plasticizer even though the resulting solution is much too viscous to stir. The spongy samples were pressed between warm ferrotype plates into homogeneous, clear films which were stored in sealed containers. Despite its high boiling point (265°), DPM is quite volatile at room temperature and inadvertent changes of plasticizer concentration have been a source of experimental difficulty.

The use of ac methods is usually precluded in conductance studies of good insulators such as polymers and hydrocarbon liquids because the capacitive reactance of the sample is several orders of magnitude less than the resistance. Thus for samples used in our studies, it would have been necessary to resolve the loss tangent to 1×10^{-7} in order to measure a conductance of 10^{-15} mhos to 10% at a frequency of 16 Hz. Dc methods usually utilize the direct application of Ohm's law with an electrometer amplifier used as the ammeter, although specially designed bridges are now available for the tetraohm range. The essential features of our conductivity apparatus have already been described.¹⁰ The effective electrometer impedance was always maintained less than 0.1% of the sample resistance. The voltage range was 5–250 v, so that for samples whose nominal thickness was 0.02 cm the field strength was about 0.2–12 kv/cm. A new parallel plate conductivity cell, in which the electrode separation was fixed and essentially independent of temperature, was built. Samples flowed between the electrodes under their own weight at the test temperatures and stuck to the electrodes tenaciously so no electroding of the sample surfaces was necessary. During a run the cell was filled with dry nitrogen. Temperature control was to $\pm 0.1^\circ$.

A "run" consisted of measurements of the bulk leakage current through a given sample at various voltages at a fixed temperature, these measurements then being repeated at four temperatures in the range 70–100°. The current flowing through the sample after application of the constant voltage changed with time and gradually approached a steady-state, limiting, value. This was especially true of preliminary experiments with unplasticized samples and was always aggravated at low temperatures. The current was monitored until it had reached a steady state; this value was taken as the basis of all calculations of conductance. For the experimental conditions of the experiments

whose results are discussed below, the current always reached its steady-state value in less than 30 sec and usually had attained the steady state in the time (less than 5 sec) required to adjust the electrometer after the initial current surge. In order to define the steady-state current and to correct for possible electrometer drift, the charge current was usually monitored for about 200 sec. In some cases, however, we extended the time to several hours but found no significant change in the steady-state current. (A current of 10^{-10} amp flowing for 3 hr amounts to about 10^{-11} equiv, so that we do not expect to find changes in conductivity because of depletion of electrolyte or changes in the electrode surface due to electrolysis reactions.) After the sample had reached steady state, it was short circuited through the electrometer. The discharge current was also monitored until it had decayed to the level of the "background current" (see below) or to less than 1% of the steady-state charging current. The polarity of the applied voltage was reversed after each measurement so that in a sense we were performing ac measurements, albeit at a very low frequency. As an order-of-magnitude comparison we note that in 0.001 *M* aqueous KCl at 1000 Hz about 10^{-7} coulomb will be transported during each half-cycle under ordinary experimental conditions; this is the same as a current of 10^{-9} amp, a large current in our experiments, flowing for 100 sec, a typical charging time.

Results of duplicate runs at a given concentration (duplication included preparation of entirely different samples from the bulk polymer, salt, and plasticizer) varied by as much as $\pm 25\%$, but there were also some inexplicable fluctuations of more than $\pm 50\%$ among different specimens made from the *same* sample. Fortunately, because most of our analysis concerns the logarithm of the conductivity, the situation is tolerable if not entirely satisfactory.

The necessity of using dc methods has raised questions about the significance of the steady-state current as a measure of the true transport of charge through the bulk of the sample. The fact that time-dependent currents are found, portions of which are reversible on shorting the cell, shows that there are polarization phenomena involved in addition to the irreversible "true conductance." If the polarization is an electrode polarization which results in a space charge near each electrode with an attendant nonuniform potential gradient in the bulk of the sample, the measured (ap-

(9) F. M. Lewis and F. R. Mayo, *Ind. Eng. Chem. Anal. Ed.*, **17**, 134 (1945).

(10) R. A. Foss and W. Dannhauser, *J. Appl. Polymer Sci.*, **7**, 1015 (1963).

parent) steady-state conductance will depend on both conductive and diffusive transport in a complicated manner which is not readily amenable to analysis in the framework of electrolytic conductance theory.

Space-charge polarization has been studied recently by probe methods in hydrocarbons¹¹ and silicate glasses¹² and by conductance measurements of hydrocarbons.¹³ Of particular relevance to our work is the study of Fuoss and Elliott¹⁴ on polarization in solutions of tributylammonium picrate in tricresyl phosphate. The general conclusions of these investigations are that space-charge polarization may seriously distort interpretations of conductance studies based on steady-state currents and Ohm's law and that the magnitude of the error at a given time after the application of the polarizing field decreases as the current density decreases, presumably because it takes longer to build up the space charge. Fuoss and Elliott¹⁴ showed that the apparent conductance approached the steady state according to eq 2, and they suggested that the ex-

$$\kappa(t) = \kappa_{\infty} + (\kappa_0 - \kappa_{\infty}) \exp(-\alpha' \sqrt{t}) \quad (2)$$

ponential might be of the form $\exp(-\alpha \epsilon D t)^{1/2}$, a result which is in general accord with theories of diffusion limited electrode processes.¹⁵ In view of the low dielectric constant (ϵ) of our system, the short times (t) during which the electrodes were polarized, and the small diffusion coefficients (D) expected in such a viscous system (see below), we doubt if diffusion overpotentials could be a major source of experimental error.

It seems appropriate to mention here that the commonly suggested practice of extrapolating the time-dependent charging current back to zero time, and then using this value of the current for conductance calculations, will be completely erroneous unless it can be shown that the polarization is an electrode polarization of the type discussed above. Analyses of the transient charging current in various polymers, including plasticized polyvinyl chloride,¹⁶ polyoxymethylene,¹⁷ polyethylene terephthalate,¹⁸ and polyvinyl acetate and polymethyl methacrylate,¹⁹ showed that the reversible portion of the charge-discharge currents for the experimental conditions of those specific experiments was undoubtedly due to reorientation of the dipolar main-chain segments of the polymer. This polarization is independent of the irreversible transport of charge or of any electrode processes. In some preliminary experiments that we tried on unplasticized polystyrene, the time-dependent current completely dominated the steady-state component at all temperatures low enough so that polymer and/or electrolyte degradation did not interfere. Analysis of these transient currents accord-

ing to Hamon's method²⁰ yields a critical frequency of 0.08 Hz at 100° for polarization decay which lies exactly on the extrapolated curve of Baker, Auty, and Ritenour's dielectric loss data.²¹ This dielectric polarization is undoubtedly due to reorientation of the phenyl dipoles of the main chain. Baker, *et al.*, also studied dielectric loss of a polystyrene plasticized with 20% by weight diphenyl and showed that the isothermal critical frequency for dielectric loss increases greatly relative to the unplasticized polymer. At 70°, where our dc measurements on a sample plasticized with 20% by weight DPM indicate a polarization relaxation time substantially less than 1 sec, they report a critical frequency of about 50 Hz. We believe that the transient currents that we notice are due to dipolar reorientation of the polymer.²²

Finally, we wish to refer to several recent papers by Gavis²³ on the subject of electrical transport in low dielectric constant fluids. Gavis has solved the partial differential equation for electrical transport, subject to linearization conditions which seem physically reasonable for this type of system. Quite apart from experimental difficulties, he concludes that it will be necessary to use dc methods for meaningful conductance measurements in good dielectrics because of the considerable time required to form the equilibrium double layer at each electrode. Gavis provides criteria to decide the suitability of ac or dc methods and also shows that under

(11) E. O. Forster, *J. Chem. Phys.*, **37**, 1021 (1962).

(12) T. M. Proctor and P. M. Sutton, *J. Am. Ceram. Soc.*, **43**, 173 (1960).

(13) H. Bassler, P. Mayer, and N. Riehl, *Z. Naturforsch.*, **20a**, 394 (1965).

(14) R. M. Fuoss and M. A. Elliott, *J. Am. Chem. Soc.*, **67**, 1330 (1945).

(15) G. Kortum, "Treatise on Electrochemistry," 2nd ed, Elsevier Publishing Co., Amsterdam, 1965.

(16) W. Reddish, *Soc. Chem. Ind. (London) Monograph*, **5**, 138 (1959).

(17) G. Williams, *Polymer*, **4**, 27 (1963).

(18) W. Dannhauser, *Natl. Acad. Sci. Natl. Res. Council Pub.*, **396**, 49 (1956).

(19) H. U. Herwig and E. Jenekel, *Z. Elektrochem.*, **63**, 360 (1959).

(20) B. V. Hamon, *Proc. Inst. Elec. Engrs. (London)*, **99**, IV, 151 (1952).

(21) E. B. Baker, R. P. Auty, and G. J. Ritenour, *J. Chem. Phys.*, **21**, 159 (1953).

(22) An additional source of polarization in our samples is that due to dipolar reorientation of ion pair and higher aggregate dipoles. In benzene and similar mobile solvents the relaxation times of quaternary ammonium salt ion-pair dipoles is characteristically about 10^{-10} sec. The rotatory diffusion constant will surely increase on changing the viscosity from a few centipoise to the 10^9 centipoise characteristic of our samples, but it is certain that the increase is much less than predicted by a Stokes' law calculation using the macroscopic sample viscosity. Thus, we confidently expect that this polarization will be very fast compared to the time scale of our experiments.

(23) J. Gavis, *Chem. Eng. Sci.*, **19**, 237 (1964); *J. Chem. Phys.*, **41**, 3787 (1964); **43**, 3580 (1965).

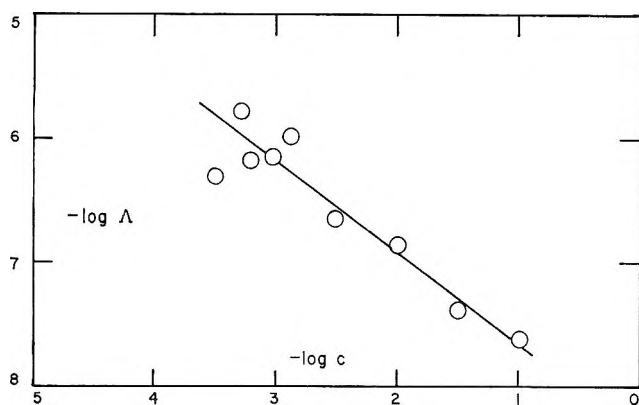


Figure 1. Equivalent conductance as a function of stoichiometric concentration of $(n\text{-C}_4\text{H}_9)_4\text{NSCN}$ in 20:80 DPM-PS at 89° .

certain conditions the steady-state current may be larger than predicted by Ohm's law as a result of diffusion-enhanced transport. According to Gavis' criteria, our steady-state currents are reliable indicators of the electrical transport of charge through the bulk of the sample.

Results

The equivalent conductance, Λ (the concentration is expressed as equivalents of salt per kilogram of solvent and the specific conductance is the zero-field value corrected for solvent conductance), of $(n\text{-Bu})_4\text{NSCN}$ in the 20:80 DPM-PS solvent has been determined from 3×10^{-4} to about $0.1 m$. The lower limit of the measurements was determined by the "background current" of the samples (see below); the upper limit was set by the apparent insolubility of the salt. A typical log-log plot of equivalent conductance as a function of stoichiometric salt concentration is shown in Figure 1.

The temperature dependence of the specific conductance, shown for one concentration in Figure 2, was found to be independent of electrolyte concentration—including $m = 0$, *i.e.*, undoped solvent—and also of field strength in our experimental range of 0–12 kv/cm. Expressed as a molar activation energy, the temperature coefficient of conduction is 33 kcal.

Electrical conduction in many polymeric systems has often been found to be nonohmic and our samples provide no exception. Plots of the conductance ratio $\kappa(E)/\kappa(E = 0)$ as a function of field strength E are reasonably linear with slopes in approximate agreement with Onsager's²⁴ field dissociation theory for a 1-1 electrolyte in a medium of dielectric constant of 2.6. However, as in previous work,¹⁰ the temperature variation of the field dependence is greater than the T^{-2} dependence predicted by Onsager.

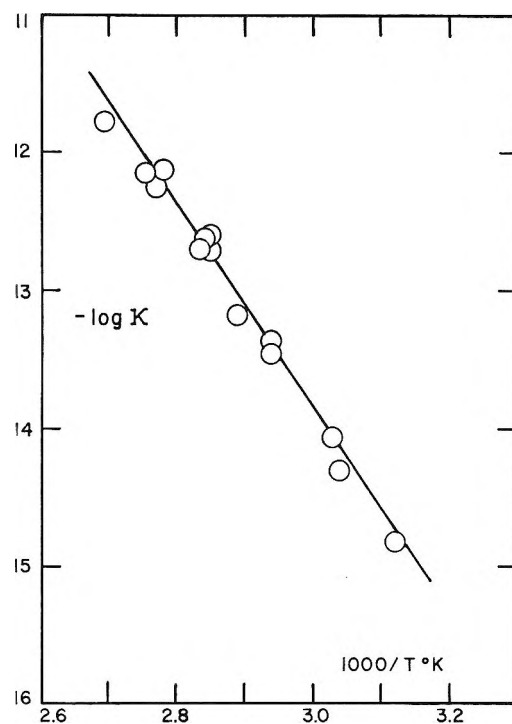


Figure 2. Specific conductance (mhos cm^{-1}) of $9.74 \times 10^{-4} m$ $(n\text{-C}_4\text{H}_9)_4\text{NSCN}$ in 20:80 DPM-PS as a function of reciprocal absolute temperature.

There are a number of interesting and provocative observations that we can describe only qualitatively thus far. Among these is that of spontaneous, persistent polarization of virgin samples; *i.e.*, samples to which a field had never been applied acted like batteries, generating small (*ca.* 10^{-12} amp at 70°) currents for at least several weeks when short-circuited across the electrometer input. This so-called "background current" was seemingly independent of sample preparation and treatment and was strictly superimposable on externally generated conduction currents. Thus, at low temperatures or salt concentrations, we often found the measured apparent conduction current to be opposed in polarity to the applied field. Subtraction of the background current from the observed current yielded consistent conduction currents, irrespective of the polarity of the applied field. The temperature dependence of the background current was unusual. In the plasticized systems the background current decreased rapidly with decreasing temperature, became too small to measure ($<10^{-14}$ amp) at about 60° , but reappeared at about 40° with reversed polarity and then increased in magnitude with further decrease in temperature. A few observations with unplasticized poly-

(24) L. Onsager, *J. Chem. Phys.*, **2**, 599 (1934).

Table I: Equivalent Conductance, Viscosity, Temperature, Dielectric Constant, and Conductance-Viscosity Product of Three Solvent-Solute Systems at an Electrolyte Concentration of $3.6 \times 10^{-4} N$

Solvent	Solute	Temp, °C	Dielectric constant	Solvent viscosity, mpoises	Λ	$\Lambda\eta$	Ref
<i>p</i> -Xylene	(<i>n</i> -C ₆ H ₁₁) ₄ NCNS	52	2.22	4.52	3.9×10^{-4}	1.8×10^{-3}	26a
<i>p</i> -Xylene	(<i>n</i> -C ₅ H ₁₁) ₄ NCNS	90	2.16	3.31	1.0×10^{-3}	3.3×10^{-3}	26b
Benzene	(<i>n</i> -C ₄ H ₉) ₄ NCNS	25	2.27	6.11	2.3×10^{-4}	1.4×10^{-3}	8
Plasticized polystyrene	(<i>n</i> -C ₄ H ₉) ₄ NCNS	90	2.67	10 ¹⁰	1.6×10^{-6}	1.6×10^4	This work

mer showed similar behavior, but the temperature of polarity reversal was about 130°. The origin of this polarization is not known.

Discussion

We consider the data in terms of the sphere-in-continuum model of electrolyte solution theory.²⁵ For ions whose distance of closest approach is a and which are in a medium of (low) dielectric constant ϵ , a critical parameter in the theory is e^2/akT . This parameter is just the ratio of the coulombic to the thermal energy and (as the exponent in a Boltzmann factor) it essentially governs the concentration of free ions.

While the dielectric constant enters exponentially, the viscosity of the medium enters into the conductance equations as a multiplicative factor if we assume the validity of Stokes' law as a first approximation. If Stokes' law did hold in polymeric systems we would expect the conductance of (*n*-Bu)₄NSCN in doped polystyrene to be related to the conductance of this (or a closely similar) salt in benzene, or other monomeric solvents of similar dielectric constant, by a factor approximately equal to the ratio of their fluidities. A comparison of our data with some obtained by Kraus and his colleagues for benzene or toluene solutions^{8,26} is given in Table I and shows this is not the case at all. The conductance-viscosity product, predicted to be a constant according to Walden's rule, is much too big for the PS-DPM system if the macroscopic viscosity²⁷ of the polymeric solvent is used. In the naivest sense it appears that the ions "feel" an effective viscosity of about 1 poise, approximately one ten-millionth that of the macroscopic viscosity. Intuitively, this is not unreasonable since one envisions that only a few neighboring polymer segments need to move to form a "hole" large enough for the ion to slip through²⁸ while, in the case of viscous flow, entire molecules, consisting of several hundred segments each, will have to move relative to one another.

Supporting evidence from a variety of experiments shows that the friction coefficient of small particles

moving in a polymeric matrix is considerably less than that deduced from the macroscopic viscosity. For example, Bovey and Tiers²⁹ noted that the nmr line width of the solvent in polymer solutions is narrow and independent of the macroscopic viscosity for many orders of magnitude change of the latter. Morton and Ferry³⁰ studied the sedimentation of microscopic particles (800–1900 Å in diameter) through viscous solutions and found sedimentation constants much greater than predicted by Stokes' law, the discrepancy increasing as the particle size decreased. Grün and Jeanneret³¹ have measured the tracer diffusion of several species of widely different molecular weight in a series of media, also of different molecular weight. When the medium was a lightly vulcanized rubber, of apparent viscosity of about 10⁶ poises, they found no agreement at all with the Stokes-Einstein equation. In fact, the effective viscosity was found to be about 1 poise.

From our experiments thus far we can draw no quantitative conclusions about the size of the polymer segments that are involved in the conduction process. This will require more extensive studies of conduction as a function of ion size and shape, polymer-plasticizer ratio, temperature, and pressure.

By considering the equilibria between single ions, ion pairs, and triple ions, Fuoss and Accascina²⁵ derived eq 3 for equivalent conductance at low electrolyte concentrations. Here K_A is the association constant for

$$\Lambda = \Lambda_0(K_{AC})^{-1/2} + (\lambda_0/kK_A^{1/2})c^{1/2} \quad (3)$$

ion-pair formation, k is the dissociation constant of

(25) R. M. Fuoss and P. Accascina, "Electrolytic Conductance," Interscience Publishers, Inc., New York, N. Y., 1959.

(26) (a) L. C. Kenaussis, E. C. Evers, and C. A. Kraus, *Proc. Natl. Acad. Sci. U. S.*, **48**, 121 (1962); (b) *ibid.*, **49**, 141 (1963).

(27) D. J. Plazek, private communication.

(28) A. T. DiBenedetto and D. R. Paul, *J. Polymer Sci.*, **A2**, 1001 (1964).

(29) F. A. Bovey and G. V. D. Tiers, *Fortschr. Hochpolymer. Forsch.*, **3**, 139 (1963).

(30) S. D. Morton and J. D. Ferry, *J. Phys. Chem.*, **63**, 1335 (1959).

(31) F. Grün and R. Jeanneret, *Helv. Chim. Acta*, **42**, 1798 (1959).

either type of triple ion, Λ_0 and λ_0 are the limiting equivalent conductances of the single and triple ions, respectively, and c is the stoichiometric concentration of salt. This equation predicts that, on a log-log plot like Figure 1, the curve should be linear with slope $-1/2$ at low concentrations, that it should go through a minimum at $c_{\min} = k\Lambda_0/\lambda_0$, and that it should again become linear with slope $+1/2$ at high concentrations. However, the assumptions implicit in the derivation of eq 3 are valid only at low concentrations, so predictions beyond the minimum are of questionable significance. The studies of Kraus and Fuoss³² and their colleagues on salts in fluid media of low dielectric constant convincingly verify the general nature of the equation.

Studies of $(n\text{-Bu})_4\text{NSCN}$ in benzene⁸ have not been carried to low enough concentrations to define the minimum, which must be at $c < 10^{-5}$ at 25°. If ion pairs and triple ions are formed only as a consequence of electrostatic interactions, we anticipate that c_{\min} should be about 10^{-5} for $(n\text{-Bu})_4\text{NSCN}$ in all solvents of $\epsilon \approx 2.5$ at 25°.

In the temperature range 70–100°, our conductance-concentration data are all similar in form to those at 89°, shown in Figure 1. Because of the large experimental errors, the value of the slope of the curve may be debatable (the straight line in Figure 1 is merely an estimate of a linear plot), but we can think of no reason to doubt that it is, in fact, negative. Accordingly, we are still effectively on the "low concentration" side of the conduction minimum even though, as indicated above, we anticipated this to be at about $10^{-5} m$.

We suggest that this seeming anomaly has a hydrodynamic rather than a thermodynamic basis. The position of the minimum corresponds to that concentration where single and triple ions make equal contributions to the conductivity; this is generally *not* the same as where single and triplet ions are present in equal concentrations. Thus for a given solvent, salt, and temperature, k is a constant and c_{\min} depends only on Λ_0/λ_0 . When working with low viscosity solutions of low dielectric constant, such as benzene, Λ_0 is usually estimated from single-ion equivalent conductances obtained in high dielectric constant liquids, with the subsequent application of Walden's rule. λ_0 cannot be obtained directly from experimental data. Fuoss²⁵ assumes $\lambda_0 \approx \Lambda_0/3$, which again makes implicit use of Stokes' law and the estimate that the triple ions are three times the size of the single ion. In this way k may be evaluated from the conductance data.

However, in the PS-DPM solvent we have shown that

Stokes' law is entirely inapplicable and the foregoing analysis cannot be used. We suggest that in this system, and presumably in any other highly viscous solvent, λ_0 is vastly smaller than $\Lambda_0/3$ and that triple ions (and even more so higher aggregates of nonzero charge) make no sensible contribution to the conductance *because their mobility is vanishingly small*. We have no conductance data yet to test this conjecture, but the diffusion data of Grün³¹ and Gromov³³ show that in polymeric systems the diffusion constant varies as an inverse power of the molecular weight of the diffusing species. For example, in lightly vulcanized rubber, Grün reports a more than 1000-fold difference in D for diffusing species of molecular weight 100 and 1000.

A particularly attractive test of our conjecture will be a determination of the conductance-concentration profile in the PS-DPM system as a function of the PS-DPM ratio.³⁴ In pure DPM we expect behavior like that in toluene or benzene, *i.e.*, a conductance minimum at $c \approx 10^{-5}$ and a positive slope at higher concentrations. With increasing PS content, as the viscosity of the solvent increases and the ratio Λ_0/λ_0 diverges increasingly from three to a very large value, we expect the conductance minimum to shift to progressively higher concentrations. In the definitive study of $(i\text{-C}_5\text{H}_{11})_4\text{NNC}_3$ in dioxane-water mixtures by Kraus and Fuoss,³² the conductance minimum shifted because changing the solvent composition changed k while Λ_0/λ_0 remained approximately constant; in the isodielectric, variable-viscosity solvent, k is expected to remain virtually constant but Λ_0/λ_0 will change. These experiments will be the basis for a future communication.

Acknowledgment. We wish to thank Dr. Donald J. Plazek of the Mellon Institute for measuring the viscosity of the 20:80 DPM-PS solvent for us. We also appreciate the National Science Foundation's generous financial support.

(32) C. A. Kraus and R. M. Fuoss, *J. Am. Chem. Soc.*, **55**, 21, 2387 (1933).

(33) V. K. Gromov, *et al.*, *Dokl. Akad. Nauk SSSR*, **165**, 347 (1965); *Chem. Abstr.*, **64**, 3700 (1966).

(34) It has often been proposed to use conductance data as a measure of plasticizer efficacy. In all reported experiments of this type, either the concentration of charge carriers was unknown and surely variable as the polymer-plasticizer ratio was changed, and/or the dielectric constant of the mixture was neither known nor kept constant. Under such circumstances one cannot expect conductance experiments to be of any significance as a measure of "internal viscosity."

Szilard-Chalmers Chemistry of $C_6H_{14}-RI^{127}-I^{129}_2$ Solutions^{1a}

by H. M. Chang^{1b} and J. E. Willard

Department of Chemistry, University of Wisconsin, Madison, Wisconsin (Received March 20, 1967)

When hexane containing $I_2(I^{127})$ and $I_2(I^{129})$ is irradiated with neutrons, nearly equal percentages of the I^{128} and the I^{130} formed appear in organic combination, indicating that the $I^{127}(n,\gamma)I^{128}$ process, the $I^{129}(n,\gamma)I^{130}$ process, and the isomeric transition process of I^{130m} endow the daughter atoms with equal or nearly equal chemical reactivity. When hexane containing $I_2(I^{129})$ and $i-C_3H_7I^{127}$ (or $C_2H_5I^{127}$) is irradiated with neutrons, the organic yields of I^{128} and I^{130} are again equal and the yields of $i-C_3H_7I^{128}$ and $i-C_3H_7I^{130}$ (or $C_2H_5I^{128}$ and $C_2H_5I^{130}$) are also equal, indicating little recombination of the recoil atoms with sibling partners. The mechanistic implications of these facts and the effects of concentration on the organic yields are considered.

Introduction

I^{128} atoms produced by the $I^{127}(n,\gamma)I^{128}$ process in solutions of alkyl iodides in hydrocarbons are preferentially stabilized in the form of the added RI molecules.² The distribution of other organic iodides formed is similar to that of I^{131} compounds formed when a similar solution, containing I^{131}_2 , is radiolyzed with γ rays.³ This and related evidence have led to the hypothesis that a significant fraction of atoms activated by radiative neutron capture became stabilized by combining with radiolytic fragments produced by conversion and Auger electrons emitted following the nuclear event.² To further evaluate the evidence, we have determined the organic yields, and the distribution of alkyl iodide products, for the two isotopes I^{128} (25 min) and I^{130} (12.5 hr), formed by the $I^{127}(n,\gamma)I^{128}$, $I^{129}(n,\gamma)I^{130}$, and $I^{130m}(IT)I^{130}$ processes, in hydrocarbon solutions containing $I_2(I^{129})$ and $i-C_3H_7I^{127}$ (or $C_2H_5I^{127}$). Isopropyl iodide was chosen for study because the yield of isopropyl radicals from the radiolysis of the hydrocarbon solvents is very low ($G = 0.04$)³ and the yield of isopropyl iodide from attack of recoil iodine atoms on the solvents is also low.²

Experimental Section

Reagents. The reagents were purified by methods similar to those described earlier.^{2,3} I^{129}_2 from the Oak Ridge National Laboratory was used as received. $I_2(I^{131})$ was prepared by heating $NaI(I^{131})$ with an excess of solid $Na_2Cr_2O_7$ on the vacuum line.³

Preparation and Analysis of Samples. Solutions of 0.1–0.5 ml of hydrocarbon containing known concentrations of RI and I_2 were degassed under vacuum and sealed in quartz or Pyrex for neutron irradiation. For organic yield determinations, irradiated ampoules were broken beneath layers of CCl_4 and aqueous $NaI-Na_2SO_3$ in a separatory funnel. After shaking, equal aliquots of the aqueous and organic layers were counted in screw-capped vials in the well of a scintillation counter. Yields of duplicate runs agreed within 1%.

For gas chromatographic analysis the irradiated samples were frozen in the bottom of the sample tubes, the tops of the tubes were broken off, 50 μ l of a mixture of organic iodide carriers (CH_3I , C_2H_5I , $i-C_3H_7I$, $n-C_3H_7I$, $n-C_4H_9I$, $n-C_5H_{11}I$, and $n-C_6H_{13}I$) and 0.5 ml of aqueous $NaI-Na_2SO_3$ solution were added, and the layers were mixed with the aid of a pipet and syringe. An aliquot of the extracted organic layer was injected onto the gas chromatographic column through a septum. Helium carrier gas was used with 12 ft \times 5 mm i.d. glass columns of firebrick coated with silicone oil. The effluent passed through a finger in the well of a scintillation counter, which operated a chart recorder,

(1) (a) This work was supported in part by U. S. Atomic Energy Commission, Contract AT(11-1)-32, by the W. F. Vilas Trust of the University of Wisconsin and by the World University Service; (b) on leave from Chung Chi College, Chinese University of Hong Kong, Hong Kong.

(2) P. R. Geissler and J. E. Willard, *J. Phys. Chem.*, **67**, 1675 (1963).

(3) P. R. Geissler and J. E. Willard, *J. Am. Chem. Soc.*, **84**, 4627 (1962).

and then through a Gow Mac thermal conductivity detector for determining times of emergence, or through traps used to catch individual products for accurate counting. The connecting tubing, including the finger, was heated with resistance wire to prevent condensation. To minimize thermal damage to the crystal, the finger was surrounded with a Teflon cup cooled by a stream of air from a hollow needle between the crystal and the Teflon. When compounds were to be trapped, the column was maintained at $85 \pm 0.1^\circ$ by an oil bath to ensure reproducible times of emergence. After the i - C_3H_7I was collected, the temperature was raised to 180° . The traps were U tubes of 3 mm i.d. tubing with two ground joints, filled to a height of 1.5 cm with firebrick coated with silicone oil, and cooled with Dry Ice. Preparatory to counting in the scintillation counter the sample was condensed to the bottom of the trap by vacuum line procedures. Tests with two traps in series indicated that a single trap is adequate. The activity recovered in the traps was regularly within 10% of that injected. Duplicate injections always gave good agreement. Samples trapped after passing through the Gow Mac thermal conductivity cell were not satisfactory for counting, because pyrolysis products formed in the cell exchanged radioiodine with subsequent samples of carrier iodide.

Irradiations. Neutron irradiations were made by placing the sealed sample tubes adjacent to the core of the University of Wisconsin swimming pool-type nuclear reactor, at a thermal neutron flux of about 5×10^{10} n cm^{-2} sec^{-1} and a γ -radiation flux of about 8×10^{17} ev g^{-1} min^{-1} . The usual irradiation time was 10 min.

Tests of Exchange Induced by Sample Preparation Procedures and Pile γ Radiation. Unirradiated samples of 0.4 mole % $I_2(I^{131})$ and 1 mole % i - C_3H_7I in C_6H_{14} showed less than 0.1% organic I^{131} on standing for 48 hr unsealed. When sealed in Pyrex, the organic uptake was about 0.1% but when sealed in quartz it was variable in the range of 1-3%. The higher uptake in quartz is attributed to illumination of the sample by the white hot quartz while sealing the sample tube. When samples sealed in Pyrex were irradiated in the nuclear reactor for 10 min at the standard position, the organic uptake of I^{131} was only 0.5%. Samples of 0.2 mole % I_2 and 10 mole % i - C_3H_7I gave similar results. Samples for gas chromatographic analysis were sealed in Pyrex. Quartz ampoules, sealed in a manner to minimize photochemical effects, were used for organic yield determinations, to avoid Na^{24} contamination in the inorganic phase.

The absence of appreciable thermal exchange in the above tests is consistent with results on the RI - I_2

exchange reported in the literature,⁴ which show rapid percentage exchange only at very low I_2 concentrations.

Results and Discussion

Comparison with Previous Work. *Yields of Low and High Boiling Fractions.* Previous investigations² of the yields of RI^{128} species resulting from the $I^{127}(n,\gamma)I^{128}$ process in solutions of 0.25 mole % I_2 and 6.7 mole % C_2H_5I in n - C_5H_{12} have shown that 15% of the organic activity is in $CH_3I + C_2H_5I$, 65% in C_2H_5I , and 20% in the gas chromatographic fractions from i - C_3H_7I through n - C_5H_{11I} . The yield for C_2H_5I is much higher and that for the third fraction much lower than found in expt 11 of Table I and in the analogous experiments (9 and 10) using C_6H_{14} solvent (including products through C_6H_{13I}). Tests to determine the cause of the discrepancy indicate that it is a result of loss of pentyl iodides on the Amberlite packing used at the entrance of the chromatography column in the earlier work to remove HI and I_2 . This removal was necessary because the whole sample was volatilized into the carrier gas by breaking the sample bulb on the column. In the present work, need for the Amberlite was avoided by washing the organic sample with aqueous sulfite prior to injection into the column. The error in the relative yield values of the previous work does not affect the mechanistic conclusions.

The present work was designed primarily for determination of the interaction of RI^{127} solute with I^{130} born from $I_2(I^{129})$. The recovery and gas chromatographic analyses of the i - C_3H_7I (Table I, expt 1-8) and C_2H_5I (Table I, expt 9, 10, and 11) are believed to be quite accurate. The high volatility of CH_3I and the low volatility of the C_6 and higher iodides apparently impaired the reproducibility of these fractions but not sufficiently to alter seriously the relative yields in the form of the i - C_3H_7I and C_2H_5I additives.

Similarity of I^{128} and I^{130} Yields from Neutron Irradiation of $I_2(I^{127} + I^{129})$ in n - C_6H_{14} . The average organic yields of I^{128} and of I^{130} from the neutron irradiation of $I_2(I^{127} + I^{129})$ in n - C_6H_{14} were nearly equal, indicating that the different nuclear processes producing the two species endow the daughter atoms with equal chemical reactivity. Their average yields were 34.0 and 35.5% at 0.6 mole % I_2 and 37.2 and 40.0% at 0.1 mole % I_2 . The data do not preclude a small isotope effect favoring higher organic yield of I^{130} , but the differences observed are not statistically significant.

Absence of Geminate Retention. To determine the extent of geminate retention following (n,γ) activation

(4) (a) H. Behrens and A. G. Maddock, *J. Chem. Phys.*, **22**, 1139 (1954); (b) N. V. Klassen and A. P. Baerg, *Can. J. Chem.*, **42**, 2684 (1964).

Table I: Organic Yields and Product Distributions from Irradiation of $I_2(I^{129})$ -RI Solutions in n - C_6H_{14}

Expt	[I_2], mole %	[i - C_3H_7I], mole %	Isotope counted	Total organic yield, % ^a	Organic activity, ^b %			
					CH ₃ I thru C ₂ H ₅ I	i -C ₃ H ₇ I	n -C ₃ H ₇ I thru n -C ₆ H ₁₃ I	Higher fractions
1	0.25	0	I^{130}	(37.2)	9.2	0.5	81	9.3
2	0.25	0.1	I^{130}	(36.8)	10.0	0.9	79.9	9.2
3	0.25	1	I^{130}	36.2	19.5	4.4	72.3	3.8
4	0.25	10	I^{130}	(35.5)	15.1	16.8	68.1	n.c.
5	0.25	10	I^{128}	34.2	8.8	17.2	74	n.c.
6	0.1	1	I^{128}	36.9	15.0	4.5	80.1	n.c.
7	0.1	1	I^{130}		19.3	4.5	76.2	n.c.
8	0.5	1	I^{130}	33.5 (31.9)	23.6	3.7	67.1	5.6
		[C ₂ H ₅ I]			CH ₃ I thru C ₂ H ₅ I	C ₂ H ₅ I	i -C ₃ H ₇ I thru n -C ₆ H ₁₃ I	
9	0.25	10	I^{128}		10.7	33.2	45.5	10.6
10	0.25	10	I^{130}		10.3	32.7	45.9	11.1
11 ^c	0.25	10	I^{130}		7.3	30.5	55.1	7.1

^a Organic yields in parentheses are for I^{128} determined on the same solutions used for gas chromatographic measurements of I^{130} .

^b The values are the per cent found in each fraction relative to the sum of the organic activity found in all the fractions collected. The notation n.c. in the last column indicates that no attempt was made to collect the activity emerging after $C_6H_{13}I$. ^c In C_5H_{12} solvent.

of iodine, the yields of i - $C_3H_7I^{128}$ and i - $C_3H_7I^{130}$ were determined after neutron irradiation of n - C_6H_{14} solutions containing both i - $C_3H_7I^{127}$ and $I_2(I^{129})$ (Table I). For this purpose it was assumed that chemical activation by the two nuclear processes is equivalent, as is indicated by the data of the preceding paragraph. i - C_3H_7I was chosen as the iodide solute for these tests, because its yield from attack of recoil iodine atoms on the solvent is negligible (Table I, expt 1).

In those solutions containing 10 mole % i - $C_3H_7I^{127}$ and 0.25 mole % $I_2(I^{127} + I^{129})$, over 95% of the I^{128} originates from i - $C_3H_7I^{127}$, while 100% of the I^{130} originates from $I_2(I^{129})$. Within the accuracy of the experiments (Table I, expt 4 and 5), the per cent of each of the activities found as i - C_3H_7I is identical. If there were appreciable failure of the C- I^{128} bond in i - C_3H_7I to rupture following the (n,γ) activation, the per cent of I^{128} found as i - C_3H_7I would be higher than the per cent of I^{130} . The results indicate that in these solutions geminate retention cannot be more than a few per cent at most, and may be zero.

The results are similar for solutions containing 0.1 mole % $I_2(I^{127} + I^{129})$ plus 1 mole % i - C_3H_7I . Here the i - $C_3H_7I^{128}$ and i - $C_3H_7I^{130}$ are 4.5% of the organic activity collected (Table I, expt 6 and 7). Since the fraction of the total activity found in organic combination is about 37%, failure of the C- I^{128} bond to rupture in only 1% of the (n,γ) events would contribute about

3% to the i - C_3H_7I percentage of the organic products. The i - C_3H_7I contribution by atoms which escape the geminate partner is 4.5% as shown by the i - $C_3H_7I^{130}$ yield. Therefore, if there were 1% failure of escape, i - $C_3H_7I^{128}$ would constitute *ca.* 7.5% (4.5 + 3) of the organic products. This difference is substantially greater than the experimental error of the measurements. Similar equality of RI^{128} and RI^{130} yields is obtained when $C_2H_5I^{127}$, rather than i - $C_3H_7I^{127}$, is used in solutions containing I^{129} (Table I, expt 9 and 10).

Low geminate retention such as reported above has also been observed for (n,γ) activation of all halogens in the gas phase.⁵

Role of I^{130m} . The work reported here was done prior to the discovery⁶ that 66% of radiative neutron capture by I^{129} produces I^{130m} (9.2 min), of which 77% decays by isomeric transition to the I^{130} ground state, while the remaining 23% decays directly to Xe^{130} . Since the irradiations of Table I were 10 min long and since our extraction procedures were normally started 20 min or more after irradiation, most of the I^{130m} decayed before the sample tubes were opened. Therefore, approximately 60% of the I^{130} atoms we measured

(5) See, for examples and references: J. E. Willard, "Chemical Effects of Nuclear Transformations," Vol. I, International Atomic Energy Agency, Vienna, 1961, p 215.

(6) D. D. Wilkey and J. E. Willard, *J. Chem. Phys.*, **44**, 970 (1966).

had achieved their final chemical state as a consequence of activation by isomeric transition, while the remainder had been activated only by the (n, γ) process. The similarity between the organic yields of I^{130} and I^{128} for samples of equal composition (Table I) is consistent with other evidence^{6,7} that the processes leading to chemical stabilization following isomeric transition and radiative neutron capture are similar. If, as the data suggest, the organic yields for I^{130} are somewhat higher than of I^{128} , this may reflect a lower percentage internal conversion following the (n, γ) events. There is evidence that the organic yields from the Br^{80m} and Br^{82m} isomeric transitions are higher than from the Br^{79} - $(n, \gamma)Br^{80}$ reaction in some cases but not in others,⁷ while the distribution of products is the same.

Autoradiation Hypothesis. Concentration Effects. The "autoradiation" hypothesis suggests that some atoms which have broken their chemical bonds as a result of activation by nuclear processes form new stable compounds by reaction with nearby radiolytic fragments of the solution, formed by their own conversion and Auger electrons (and by the charge-transfer and neutralization processes consequent to development of a high charge on the central atom). This hypothesis was suggested by the similarity of the distribution of RI^{131} products produced in γ -irradiated solutions of $I_2(I^{131})$ in C_3H_{12} and of RI^{128} products produced in neutron-irradiated solutions of I^{127}_2 in C_5H_{12} .² This similarity includes preferentially high yields in the form of any added RI, these being ascribed to reaction with R radicals formed by dissociative electron capture and I abstraction by H atoms. In the present work, solutions of 10, 1, and 0.1 mole % i - C_3H_7I in C_6H_{14} gave yields of i - C_3H_7I of 17, 4.4, and 0.9%, respectively (Table I, expt 2, 3, and 4). The fact that the yield is in all cases higher than the mole fraction shows the preferential incorporation in the form of solute noted earlier. The decrease in yield with decreasing concentration of i - C_3H_7I and the relative insensitivity (Table I, expt 3, 7, and 8) to the concentration of I_2 are qualitatively consistent with the results which

would be expected in terms of the autoradiation hypotheses. The present work confirms the fact that the yields in the form of RI are not the result of failure of bond rupture or geminate recombination.

Evidence for Geminate Retention in Other Solvents. Iyer and Martin⁸ have concluded that geminate retention of I^{130} produced in liquid mixtures of CH_3I and i - C_3H_7I containing RI^{129} occurs following 4% of the nuclear events (accounting for 10% of the organically bound I^{130}). This suggests that a greater caging effect may occur in an alkyl iodide solvent than in the hydrocarbon solvent used in the present work, consistent with evidence on the photochemical dissociation of I_2 in a series of solvents.⁹ Geminate retention following the isomeric transition of RBr^{80m} in dilute solutions of CH_3Br , C_6H_5Br , and CCl_3Br in liquid bromine is high (6, 13, and 13%, respectively).¹⁰ Such retention is also implied for polycrystalline n - C_4H_9Br at 77°K by the fact that the organic yields are much higher when the Br^{80m} is present as n - $C_4H_9Br^{80m}$ than when it is present as $Br_2(Br^{80m})$.¹¹

It should be noted that increases in the yield of an organic parent with increased molecular weight of solvent or decreased temperature do not necessarily imply geminate retention. Solutions of $Br_2(Br^{80m})$ undergoing isomeric transition in dilute solution in hydrocarbons¹² show increasing organic yield with increasing molecular weight of solvent and decreasing temperature, as discussed earlier.

(7) See, for examples and references: (a) J. F. Hornig and J. E. Willard, *J. Am. Chem. Soc.*, **79**, 4609 (1957); (b) R. M. Iyer and J. E. Willard, *ibid.*, **87**, 2494 (1965); (c) J. A. Merrigan, J. B. Nicholas, and E. P. Rack, *Radiochim. Acta*, in press.

(8) R. M. Iyer and G. Martin, "Chemical Effects of Nuclear Transformations," Vol. I, International Atomic Energy Agency, Vienna, 1961, p 281.

(9) F. W. Lampe and R. W. Noyes, *J. Am. Chem. Soc.*, **76**, 2140 (1954).

(10) R. S. H. Chiang and J. E. Willard, *ibid.*, **74**, 6213 (1952).

(11) R. M. A. Hahne and J. E. Willard, *J. Phys. Chem.*, **68**, 2582 (1964).

(12) S. Aditya and J. E. Willard, *J. Am. Chem. Soc.*, **79**, 3367 (1957).

Reaction of Dilute Aqueous CH₃I with Iodine Activated by Nuclear Processes¹

by D. D. Wilkey, J. F. Brensike, and J. E. Willard

Department of Chemistry, University of Wisconsin, Madison, Wisconsin (Received March 20, 1967)

Dilute aqueous solutions of CH₃I¹²⁷ and I₂(I¹²⁹) [or I⁻(I¹²⁹)] have been irradiated with neutrons and analyzed to determine the fractions of the I¹²⁷(n,γ)I¹²⁸ and I¹²⁹(n,γ)I¹³⁰ events which lead to I¹²⁸ and to I¹³⁰ in organic combination. The organic yield of each isotope is significant, confirming an earlier report² that organic combination of (n,γ)-activated iodine atoms can be achieved in aqueous CH₃I-I₂ systems, but showing that such combination does not require the geminate retention previously postulated.² The yields are independent of the I⁻ concentration from 10⁻⁵ to at least 10⁻³ mole % and increase with CH₃I concentration in the range from 1.8 × 10⁻³ mole % to the saturated solution concentration of 0.18 mole %. Like the (n,γ) processes, the I^{130m} → I¹³⁰ isomeric transition in aqueous solutions of 0.08 mole % CH₃I and 10⁻³ mole % I₂(I^{130m}) or I⁻(I^{130m}) leads to organically bound I¹³⁰, the organic yields being about 7%. The entry into organic combination of I atoms originating from I₂ or I⁻, and activated by the (n,γ) or IT process, seems to be explained most plausibly in terms of the autoradiation hypothesis. Techniques have been developed for correcting for thermal exchange in the systems used and it has been shown that photochemically produced I atoms do not exchange readily with CH₃I in aqueous solution.

Introduction

Sturm and Davis² have reported that when dilute solutions of CH₃I in H₂O containing I₃⁻ scavenger are irradiated with neutrons, 12% of the I¹²⁸ atoms formed by the I¹²⁷(n,γ)I¹²⁸ process are found in organic combination and they have attributed this to failure of rupture of the C-I bond following neutron capture by the iodine atoms. Evidence from other systems³ suggests, however, that geminate retention cannot be more than a few per cent. To determine whether geminate retention is required to explain the labeled organic product in this system, we have determined the organic yields of I¹³⁰ from the I¹²⁹(n,γ)I¹³⁰ process in aqueous solutions of CH₃I¹²⁷ containing I₂(I¹²⁹) and in solutions containing, I⁻(I¹²⁹). We have also determined the organic yields of the I^{130m} \xrightarrow{IT} I¹³⁰ process in H₂O-CH₃I-I₂(I^{130m}) and H₂O-CH₃I-I⁻(I^{130m}) solutions.

Experimental Section

Aqueous methyl iodide samples (10–15 cc) were irradiated in quartz bulbs, sealed with serum bottle caps protected by Teflon inserts to prevent CH₃I vapor from coming in contact with the rubber. The vapor

volumes over the solutions were kept very small to minimize the fraction of the methyl iodide in the vapor phase.

The CH₃I used was shown by gas chromatography to be >99% pure. I¹²⁹₂ was used as received from the Oak Ridge National Laboratories. Known concentrations of CH₃I and I₂ were obtained by dilution of saturated solutions. Tests with CH₃I¹³¹ of known specific activity (prepared by illuminating a solution of I₂(I¹³¹) in CH₃I with 2537-A radiation) showed that saturation could be achieved by vigorously shaking H₂O and CH₃I together for 30–60 min and confirmed the value of 0.18 mole % for the solubility at 22° reported in the literature.⁴ Aqueous I⁻(I¹²⁹) was prepared by reduc-

(1) This work was supported in part by U. S. Atomic Energy Commission, Contract AT(11-1)-32, and by the W. F. Vilas Trust of the University of Wisconsin.

(2) J. E. Sturm and D. G. Davis, Paper No. 106 presented before the Division of Physical Chemistry at the 140th National Meeting of the American Chemical Society, Chicago, Ill., Sept 1961.

(3) See, for example and references: (a) J. E. Willard, "Chemical Effects of Nuclear Transformations," International Atomic Energy Agency, Vienna, 1961; (b) H. M. Chang and J. E. Willard, *J. Phys. Chem.*, **71**, 3576 (1967).

(4) A. Rex, *Z. Physik. Chem. (Leipzig)*, **55**, 355 (1906).

ing I₂(I¹²⁹) solutions with SO₂ gas, following which the excess SO₂ was removed by bubbling nitrogen through the solution. To minimize thermal exchange, the total time for mixing of the CH₃I and I₂ or I⁻ solutions, irradiation, and extraction was made as short as possible (about 6 min between mixing and extraction of the first aliquot).

For analysis, aliquots were withdrawn from the irradiated samples through the serum cap, using a hypodermic syringe, and discharged into a CCl₄-aqueous SO₃²⁻ extracting mixture. After shaking, a known portion of each layer was placed in a screw-capped vial for counting in a well-type scintillation counter. Aliquots taken from each irradiated sample at known times following irradiation allowed correction for thermal exchange from a plot of organic incorporation of radioiodine *vs.* time of extraction. Similar extrapolation of the organic incorporation of the I¹³¹ tracer activity gave the thermal exchange rate as the slope and the radiation-induced exchange as the intercept. In determining the radiation-induced exchange for I¹²⁸ and I¹³⁰ from that of I¹³¹, correction was made for the fact that the I¹²⁸ and I¹³⁰ are not present at the start of the irradiation, making the average time for exchange less than for the I¹³¹.

Thermal exchange rates were about 0.1%/min at 25°. No exchange was detectable in 60 min at 0°. Radiation-induced exchange increased with increasing CH₃I concentration; at 0.1 mole % it was typically 2-5%, depending somewhat on the form and concentration of the inorganic iodine.

Resolution of the activities due to I¹²⁸ (25 min), I¹³⁰ (12.5 hr), and I¹³¹ (8 days) was possible by making several counting rate determinations on each sample at appropriate time intervals. Irradiations were for 1 min in the pneumatic tube of the University of Wisconsin reactor, at a thermal neutron flux of about 1 × 10¹² n cm⁻² sec⁻¹ and a γ-radiation flux of about 8 × 10¹⁸ ev g⁻¹ min⁻¹.

Results

Dependence of Organic Yield on Chemical Form of the Iodine Which Captures Neutrons. The corrected organic yields of a series of samples containing 0.09 mole % CH₃I and 10⁻³ mole % I₂, or 2 × 10⁻³ mole % I⁻, are given in Table I. The yields for I¹²⁸ and I¹³⁰ given on each horizontal line are for samples taken from the same CH₃I-I₂ or CN₃I-I⁻ solution. The yields given on line 1 of the I⁻ section of the table are for samples made from the same aqueous CH₃I preparation as those on line 1 of the I₂ section, and similarly for the other corresponding lines. In these solutions more than 95% of the I¹²⁸ activity is formed from CH₃I¹²⁷ while more

than 97% of the I¹³⁰ is formed from I₂(I¹²⁹) or I⁻(I¹²⁹). The monitoring of exchange by I¹³¹ indicates that less than 3% of the inorganic iodine ever entered organic combination by thermal or radiation-induced exchange prior to the midpoint of the 1-min irradiations.

Table I: Organic Yields from (n,γ) Activation of Aqueous Solutions of CH₃I¹²⁷ and I₂(I¹³⁰) or I⁻(I¹³⁰)^a

Scavenger	Organic yields, %	
	I ¹²⁸	I ¹³⁰
I ₂	8.9, 9.0	5.7, 5.8
	8.2, 8.1	5.7, 5.4
	13.2, 12.6, 12.1	7.7, 6.3, 6.3
Av	10.1	6.1
I ⁻	6.2, 6.4	3.6, 3.3
	7.0, 7.0	4.0, 4.0
	6.7, 6.5, 6.5	2.7, 2.6, 3.0
Av	6.6	3.3

^a Using 1 × 10⁻³ mole % I₂, 2 × 10⁻³ mole % I⁻, and approximately 9 × 10⁻² mole % CH₃I.

Activation by Isomeric Transition. Neutron irradiation of aqueous solutions of I₂(I¹²⁹ + I¹³¹) and I⁻(I¹²⁹ + I¹³¹) before mixing them with aqueous CH₃I solutions made possible the study of the organic yield of the I^{130m} \xrightarrow{IT} I¹³⁰ isomeric transition, in the absence of the effects of radiation-induced exchange and of the I¹²⁹(n,γ)I¹³⁰ process. Concentrations in the mixtures were 0.085 mole % CH₃I and 1 × 10⁻³ mole % I₂ or 2 × 10⁻³ mole % I⁻. The organic I¹³⁰ activity was determined as a function of time between mixing and extraction and the I¹³¹ uptake used to correct the I¹³⁰ yield for thermal exchange. The corrected organic I¹³⁰ activity increased with time between mixing and extraction at a rate consistent with the 9.2-min half-life⁵ of the I^{130m} \xrightarrow{IT} I¹³⁰ isomeric transition. After correction for the decay of I^{130m} between irradiation and mixing and for the fraction of the I¹³⁰ born in the ground state, the organic yield for the isomeric transition was estimated to be about 7%. The results were not sufficiently precise to determine whether or not there is a difference in yields from solutions of I₂(I¹²⁹) and of I⁻(I¹²⁹), as is indicated in Table I for n,γ activation.

Concentration Effects. The organic yield of I¹²⁸ from neutron irradiations of aqueous 0.10 mole % CH₃I containing I⁻(I¹²⁷ + I¹³¹) was independent of the I⁻ concentration from 10⁻³ to 10⁻⁵ mole %. Experiments in

(5) D. D. Wilkey and J. E. Willard, *J. Chem. Phys.*, **44**, 970 (1966).

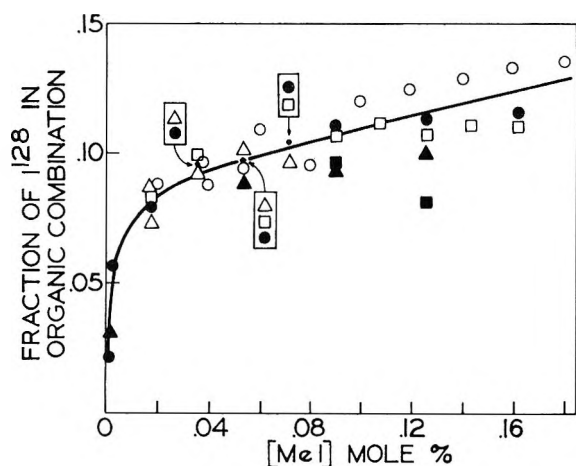


Figure 1. Effect of CH_3I concentration on the organic yield of I^{128} produced by the $\text{I}^{127}(n,\gamma)\text{I}^{128}$ reaction. Each type of point on the graph indicates a series of experiments made with different dilutions of the same saturated CH_3I solution. Dilution was accomplished by injecting aliquots of the CH_3I solutions below the surface of the scavenger solutions, through a syringe needle, except for the \circ series where normal pipetting was used. $1 \times 10^{-3} N$ scavenger was used in each case: \circ , Δ , \blacksquare , 0° irradiation, I_2 scavenger; \square , room temperature, I_2 ; \bullet , 0° , I^- ; \blacktriangle room temperature, I^- .

which I_2 or I^- was $1 \times 10^{-3} N$ (1.8×10^{-3} mole % I^- , 0.9×10^{-3} mole % I_2) were done at CH_3I concentrations over a 100-fold range from 2×10^{-3} to 1.8×10^{-1} mole %. Different techniques of analysis and different temperatures were investigated in an endeavor to minimize the loss of CH_3I vapor from the sample during preparation and analysis. The results, given in Figure 1, indicate a rapid increase in organic yield with increasing CH_3I concentration at the lowest concentrations followed by a relatively slow increase at the higher concentrations. The scatter of the points is believed to reflect the difficulty of preparing and maintaining accurately known concentrations of CH_3I in water. The data of Table I for I^{128} in the I_2 system would fall close to the curve of Figure 1 and those for the I^- solutions somewhat below.

Test for Thermal I Atom Exchange. It was important to learn whether I^{128} and I^{130} atoms which are neutralized and thermalized following production by the (n,γ) process can exchange readily with CH_3I in aqueous solution. We have illuminated aqueous solutions of 10^{-3} mole % $\text{I}_2(\text{I}^{131})$ and 0.1 mole % CH_3I with light of 4200–4400 Å absorbed by the I_2 (using a Bausch and Lomb monochromator). The length of the illumination was such that each I_2 molecule absorbed, on the average, five photons. Correction for thermal exchange was determined using an identical sample which was stored in the dark for the same length of time as the irradiated

sample. No observable photochemical exchange occurred. These results, together with evidence suggesting that cage escape of I atoms following absorption of a photon by I_2 in H_2O is probably high,⁶ indicate that the $\text{I}^* + \text{CH}_3\text{I} \rightarrow \text{CH}_3\text{I}^* + \text{I}$ exchange in water has a low probability per collision, if it occurs at all. Similar experiments in the gas phase indicate that the exchange probability is $\leq 10^{-3}$ per collision.⁷

Discussion

The results given above are in agreement with the report² that there is a significant organic yield of I^{128} from the $\text{I}^{127}(n,\gamma)\text{I}^{128}$ reaction in dilute aqueous solutions of $\text{CH}_3\text{I}^{127}$ scavenged with I_2 . They show, in addition, that iodine atoms from inorganic iodine (I_2 or I^-) activated by either the (n,γ) or isomeric transition process can enter organic combination in these systems. This indicates that failure of rupture of C–I bonds in CH_3I does not account for all of the organic yield of I^{128} from $\text{CH}_3\text{I}^{127}$, and possibly not for any of it. If the $\text{I}^{127}(n,\gamma)\text{I}^{128}$, $\text{I}^{129}(n,\gamma)\text{I}^{130}$, and $\text{I}^{130m} \xrightarrow{\text{IT}} \text{I}^{130}$ processes are about equally effective in chemical activation, as seems to be the case in $n\text{-C}_6\text{H}_{14}$ solution,^{3b} then it appears that some geminate retention or recombination contributes to the result that the organic yields of I^{128} (from $\text{CH}_3\text{I}^{127}$) are invariably higher than those of I^{130} (from I_2 or I^-) (Table I).

The organic yields of both I^{128} and I^{130} are lower when I^- scavenger is used than when I_2 is used (Table I). This is illustrated more clearly by the data of Table I than by those of Figure 1, because the former makes comparisons of I_2 and I^- using the same batch of CH_3I solution for both, thus assuring closer identity of the difficultly controlled CH_3I concentration than in the experiments of Figure 1. The lower yields in the I^- solutions cannot be due to differences in complexing with CH_3I , since the latter is present in such excess that most of the I^{128} must be born from uncomplexed $\text{CH}_3\text{I}^{127}$.

The organic yields from the $\text{I}^{130m} \xrightarrow{\text{IT}} \text{I}^{130}$ process indicate that a mechanism must exist by which an I^{130} atom which has undergone internal conversion and the Auger process in the presence of 0.1 mole % CH_3I has a probability of some 7% of encountering and reacting with an organic fragment formed from CH_3I (unless the inorganic iodine is complexed with CH_3I , or unless I^{130+} is sufficiently stable in water to persist until it encounters and reacts with CH_3I , or unless the $\text{I}^{130(x^+)}$ reacts with H_2O to form a species which can react with CH_3I). The most plausible means of producing such

(6) (a) F. W. Lampe and R. M. Noyes, *J. Am. Chem. Soc.*, **76**, 2140 (1954); (b) R. L. Strong and J. E. Willard, *ibid.*, **79**, 2089 (1957).

(7) S. Aditya and J. E. Willard, *J. Chem. Phys.*, **44**, 418 (1966).

fragments is radiolytic decomposition of the solvent envelope around the I atom by radiations the atom emits in reaching nuclear stability or by the subsequent charge neutralization processes, as postulated by the autoradiation hypothesis.⁸

Because the concentration of radicals formed in the volume immediately around the activated I atom must depend on the CH₃I concentration and because the atom may enter inorganic combination by reactions which compete with its reaction with organic radicals, the organic yield may be expected to increase with increasing concentration of CH₃I, as the data of Figure 1 indicate that it does. The shape of this curve is not pre-

dictable from available information. The factors determining it must include the fraction of the I¹²⁷(n,γ)I¹²⁸ events which are followed by internal conversion, the relative probability of emitting different numbers of Auger electrons following internal conversion, the probability of prompt formation of HI, HOI, or other inorganic species by I¹³⁰ atoms or ions before they encounter organic fragments, and the probability of formation, if any, of (CH₃I)_n, CH₃·I₂, CH₃I·I⁻, and (I₂)_n aggregates or complexes in solution.

(8) P. R. Geissler and J. E. Willard, *J. Phys. Chem.*, **67**, 1675 (1963).

Aqueous Systems at High Temperature. XX. The Dissociation Constant and Thermodynamic Functions for Magnesium Sulfate to 200^o^{1,2}

by William L. Marshall

Reactor Chemistry Division, Oak Ridge National Laboratory, Oak Ridge, Tennessee 37830
(Received April 3, 1967)

Values for the dissociation quotients of magnesium sulfate were obtained from the differences in the solubility of calcium sulfate and its hydrates in sodium chloride and in sea salt solutions at temperatures from 30 to 200° and at ionic strengths from very low to 6 *m*. These quotients were extrapolated to zero ionic strength by means of an extended Debye-Hückel expression to obtain the dissociation constants. The pK_d^0 values obtained varied from 2.5 at 30° to 4.0 at 200° and compared favorably (within 0.1 pK_d^0 unit) with the best literature values to 40°, the highest temperature of previous work. The constants show that magnesium and sulfate ions associate strongly with rising temperature like the previously observed but weaker association behavior of 1-1 electrolytes at very high temperatures (400-800°). By the use of the van't Hoff isochore, values of the thermodynamic quantities, ΔG° , ΔH° , ΔS° , and ΔC_p° were obtained. These values varied from 2.66 to 8.66 kcal mole⁻¹ for ΔG° , -4.08 to -11.0 kcal mole⁻¹ for ΔH° , and -24.7 to -41.5 cal mole⁻¹ deg⁻¹ for ΔS° from 0 to 200°, respectively, with an average value for ΔC_p° of -25 cal mole⁻¹ deg⁻¹.

Introduction

Experimental data on the dissociation behavior of 2-2 electrolytes at temperatures above ~50° are virtually nonexistent. This lack of information arises from the comparative difficulty of experimental measurements in aqueous solutions at high temperatures, especially above 100°, and the fact that in a virgin field the simpler (1-1 salts) systems usually are investigated first.³ Nevertheless, the dissociation behavior of 2-2 salts at high temperatures, and the attainment of activity coefficients, is of much interest in understanding the basic behavior of aqueous electrolytes.

At this laboratory, extensive measurements of the solubility of calcium sulfate (and its hydrates) have been made in solutions of mixed electrolytes containing molal ratios of salt components in sea water (herein called sea salt solutions) and in sodium chloride-water solutions^{4,5} at temperatures to 200° and at ionic strengths from ~0.05 to 6 *m*.

In sea water, the predominantly dissolved constituents are chloride (0.554 *m*), sodium (0.476 *m*), magnesium (0.0542 *m*), sulfate (0.0286 *m*), potassium

(0.0127 *m*), and calcium (0.0103 *m*); all other components combined contribute less than 0.004 *m*. Therefore, the effect of the remaining components on the solubility behavior of calcium sulfate should be very small. The chief differences in solubility behavior in sea salt solutions over those in sodium chloride solutions can then be attributed to the presence of magnesium, to a molal ratio SO₄/Ca equal to 2.66 instead of unity, and to the substitution of a small amount of potassium

(1) Work sponsored jointly by the U. S. Atomic Energy Commission and the Office of Saline Water, U. S. Department of the Interior, and performed at the Oak Ridge National Laboratory, which is operated by the Union Carbide Corp. Presented before the Division of Water, Air and Waste Chemistry at the 151st National Meeting of the American Chemical Society, Miami Beach, Fla., April 9-14, 1967.

(2) Previous paper in series: W. L. Marshall and R. Slusher, *J. Chem. Eng. Data*, in press.

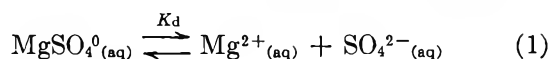
(3) E. U. Franck, *Z. Physik. Chem.* (Frankfurt), **8**, 92, 107, 192 (1956); *Angew. Chem.*, **73**, 309 (1961); J. K. Fogo, S. W. Benson, and C. S. Copeland, *J. Chem. Phys.*, **22**, 209, 212 (1954); A. S. Quist and W. L. Marshall, *J. Phys. Chem.*, **70**, 3714 (1966).

(4) W. L. Marshall and R. Slusher, *ibid.*, **70**, 4015 (1966).

(5) W. L. Marshall, R. Slusher, and E. V. Jones, *J. Chem. Eng. Data*, **9**, 187 (1964).

for sodium. An investigation at this laboratory on the solubility of CaSO_4 in Na_2SO_4 - NaCl - H_2O solutions⁶ has shown that solution molal ratios of 2.66 at constant ionic strengths have little effect ($\sim +2.5\%$) on the solubility product ($m_{\text{Ca}})(m_{\text{SO}_4}$). A substitution of KCl for NaCl to the extent of that in sea water, estimated from work performed also at this laboratory,⁶ showed little change ($\sim +1.5\%$ at an ionic strength of $3m$) in the solubility product for $\text{CaSO}_4 \cdot 2\text{H}_2\text{O}$ at 25° .

Therefore, with the assumption that the increase in solubility in a sea salt solution over that in a NaCl - H_2O solution of the same (formal) ionic strength is due predominantly to the formation of a neutral MgSO_4^0 species, an estimate of a dissociation quotient, K_d , for magnesium sulfate can be obtained. By means of



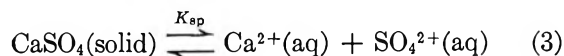
Debye-Hückel treatment, the dissociation quotients can be extrapolated to zero ionic strength to obtain the dissociation constant, K_d^0 , at each temperature, from which the thermodynamic functions can be calculated.

Mathematical Procedure

An expression for the dissociation quotient (K_d), assumed herein to be a constant at constant ionic strength, for magnesium sulfate according to the equilibrium of eq 1 can be written as

$$K_d = \frac{[\text{Mg}^{2+}][\text{SO}_4^{2-}]}{[\text{MgSO}_4^0]} \quad (2)$$

Let s = solubility of calcium sulfate, m = sulfate in excess of stoichiometric CaSO_4 , n = total magnesium, and x = $[\text{MgSO}_4^0]$ (all values in molalities). Then the solubility product for the equilibrium at ionic strength I



in the solution containing magnesium salts can be written

$$K_{sp} = (s)(s + m - x) \quad (4)$$

The expression for K_d becomes

$$K_d = \frac{(n - x)(s + m - x)}{(x)} \quad (5)$$

and upon substitution for x from eq 4

$$K_d = \frac{[n - m - s + (K_{sp}/s)](K_{sp}/s)}{[m + s - (K_{sp}/s)]} \quad (6)$$

The solubility product constant for calcium sulfate (or one of its hydrates) is equal to

$$K_{sp}^0 = K_{sp} \gamma_{\text{Ca}^{2+}} \gamma_{\text{SO}_4^{2-}} \quad (7)$$

where $(\gamma_{\text{Ca}^{2+}} \gamma_{\text{SO}_4^{2-}})^{1/2}$ is the mean activity coefficient of CaSO_4 . The equations are given elsewhere,⁴ together with all needed constants, to express the values of K_{sp} for $\text{CaSO}_4 \cdot 2\text{H}_2\text{O}$, $\text{CaSC}_4 \cdot 1/2\text{H}_2\text{O}$, or CaSO_4 in NaCl - H_2O solutions as a function of ionic strength and temperature

$$\log K_{sp} = \log K_{sp}^0 + 8S \frac{\sqrt{I}}{(1 + A_{sp}\sqrt{I})} + BI - CI^2 \quad (8)$$

where A_{sp} , B , and C are constants at each temperature and $8S$ is the Debye-Hückel limiting slope for a 2-2 electrolyte. The formal ionic strength, $I' = 1/2 \Sigma(mz^2)$, is corrected for the presence of MgSO_4^0 to give the true ionic strength, I .

$$I = I' - 4x \quad (9)$$

With an initial estimate of I equal to I' , eq 8 was used to obtain an initial value of K_{sp} . This value was used with eq 4 and 6 to obtain initial values of x and K_d . The value of x was substituted into eq 9 to obtain a better value for I and the procedure repeated until successive values of K_d differed by less than 0.1% .

The above procedure was repeated for all experimental solubilities given elsewhere,² which include our own results in sea salt solutions and those of Hara, *et al.*,⁷ Langelier, *et al.*,⁸ Posnjak,⁹ and Shaffer.¹⁰ Since the iteration method would be successful only if solubilities were greater in sea salt than in the analogous sodium chloride solutions, the method sometimes failed or gave highly uncertain results at 30 - 60° at low ionic strengths where the solubility differences approached or were within the experimental precision of the measurements; these values were not included in Figure 1 discussed in the next section.

Results

General. The dissociation constant for magnesium sulfate can be expressed by

$$K_d^0 = K_d \frac{\gamma_{\text{Mg}^{2+}} \gamma_{\text{SO}_4^{2-}}}{\gamma_{\text{MgSO}_4^0}} \quad (10)$$

where $\gamma_{\text{Mg}^{2+}}$, $\gamma_{\text{SO}_4^{2-}}$, and $\gamma_{\text{MgSO}_4^0}$ are the activity coefficients of the respective species. If we assume that

(6) L. B. Yeatts and W. L. Marshall, unpublished results.

(7) R. Hara, Y. Tanaka, and K. Nakamura, *Tech. Rept. Tohoku Imp. Univ.*, 11, 199 (1934).

(8) W. F. Langelier, D. H. Caldwell, W. B. Lawrence, and C. H. Spaulding, *Ind. Eng. Chem.*, 42, 126 (1950).

(9) E. Posnjak, *Am. J. Sci.*, 238, 559 (1940).

(10) L. H. Shaffer, *J. Chem. Eng. Data*, 12, 183 (1967).

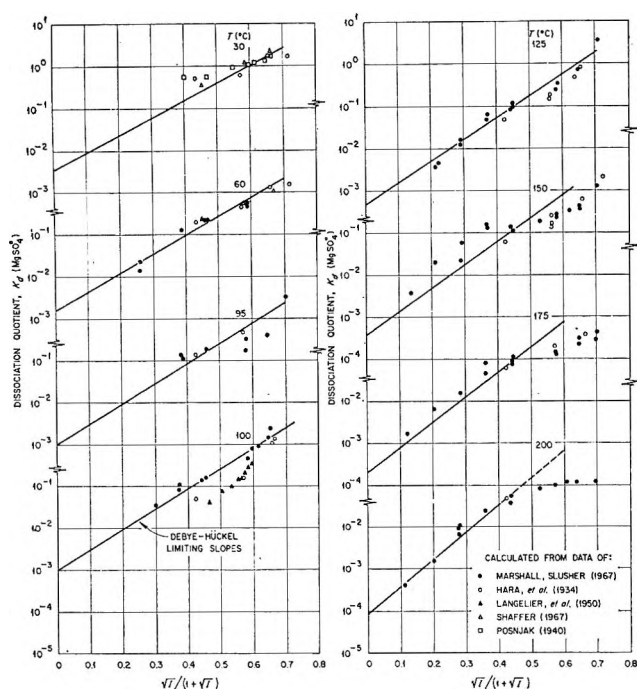


Figure 1. Variation of the dissociation quotient of magnesium sulfate with ionic strength (I) and temperature.

γ_{MgSO_4} is unity and independent of ionic strength, the other two activity coefficients can be expressed by an extended Debye-Hückel expression for the mean activity coefficient, $(\gamma_{\text{Mg}^{2+}}\gamma_{\text{SO}_4^{2-}})^{1/2} = \gamma_{\pm(\text{MgSO}_4)}$; thus

$$\log \gamma_{\pm(\text{MgSO}_4)} = -4S \frac{\sqrt{I}}{1 + A\sqrt{I}} \quad (11)$$

where A contains the ion-size parameter and S and I are already defined.

By substituting eq 11 for $\log \gamma_{\pm(\text{MgSO}_4)}$ into eq 10, the following relationship is obtained

$$\log K_d = \log K_d^0 + 8S\sqrt{I}/(1 + A\sqrt{I}) \quad (12)$$

which is similar to that for the solubility product of CaSO_4 (eq 8) but without the BI and CI^2 terms. This equation was used to describe the behavior of K_d at the several temperatures from 30 to 200° (with the exception of the few at 30 and 60° mentioned in the previous section). This description is shown in Figure 1 where the slopes drawn are the limiting Debye-Hückel slopes. In contrast to the behavior of the mean activity coefficient of CaSO_4 (from the solubility product behavior), a value of A equal to unity instead of 1.5–1.6 gave essentially the best fits. A least-square treatment was used but with elimination of some points, including those of Langelier at 100° and the divergent values at 175 and 200° at very high ionic strengths. The standard error in K_d^0 (the intercept at zero ionic

strength) for the several temperatures varied from about ± 0.05 to $\pm 0.12 \text{ p}K_d^0$ units (base 10). Although the scatter of calculated points appears great, each value of K_d was obtained from a relatively small difference between the solubility product in sea salt and that in sodium chloride solution shown in Figure 1 of ref 2. Agreement of the calculations from the several sets of data is good. A comment on the slight deviation of calculated values from those of Langelier, *et al.*,⁸ is given elsewhere.² The deviations at high ionic strengths at 175 and 200° could be eliminated mathematically by the addition of BI and CI^2 terms to eq 12, although this was not done.

Comparison with Low-Temperature Results. The values of $\log K_d^0$, obtained from the intercepts (at $I = 0$) on Figure 1, are plotted against $1/T$ (°K) in Figure 2. Included in this figure are all published values of $\log K_d^0$ that could be found over the temperature range 0–200°;^{11–22} the highest temperature of previously published values was 40°. The presently calculated value of K_d^0 at 30°, although having a large uncertainty, agrees well with the relatively recent values of Nancollas¹³ and also with those of Jones and Monk,¹⁶ the only previous studies made as a function of temperature (0–40° and 20–35°, respectively). A very recent result of Atkinson and Petrucci¹¹ at 25° falls slightly below the other values but appears to be in good agreement for the ultrasonics method used, which is applied chiefly to obtain rate constants. With the comparisons shown in Figure 2, it is felt that the dissociation constants presented herein are reasonably reliable to 200°. Their change with temperature shows that magnesium and sulfate ions associate strongly with rising temperature. The 1–1 electrolytes previously studied associate similarly with rising temperature but to a much less extent at comparable solution densities.³ This difference in degree of association

(11) G. Atkinson and S. Petrucci, *J. Phys. Chem.*, **70**, 3122 (1966).

(12) M. Eigen and K. Tamm, *Z. Elektrochem.*, **66**, 93, 107 (1962).

(13) G. H. Nancollas, *Discussions Faraday Soc.*, **24**, 108 (1957).

(14) J. Kenttämäa, *Suomen Kemistilehti*, **B29**, 59 (1956).

(15) P. G. M. Brown and J. E. Prue, *Proc. Roy. Soc. (London)*, **A232**, 320 (1955).

(16) H. W. Jones and C. B. Monk, *Trans. Faraday Soc.*, **48**, 929 (1952).

(17) H. S. Dunsmore and J. C. James, *J. Chem. Soc.*, 2925 (1951).

(18) A. Deubner and R. Heise, *Ann. Physik*, **9**, 213 (1951).

(19) W. A. Mason and W. J. Shutt, *Proc. Roy. Soc. (London)*, **A175**, 234 (1940).

(20) C. W. Davies, *J. Chem. Soc.*, 2093 (1938).

(21) R. W. Money and C. W. Davies, *Trans. Faraday Soc.*, **28**, 609 (1932).

(22) C. W. Davies, *ibid.*, **23**, 351 (1927).

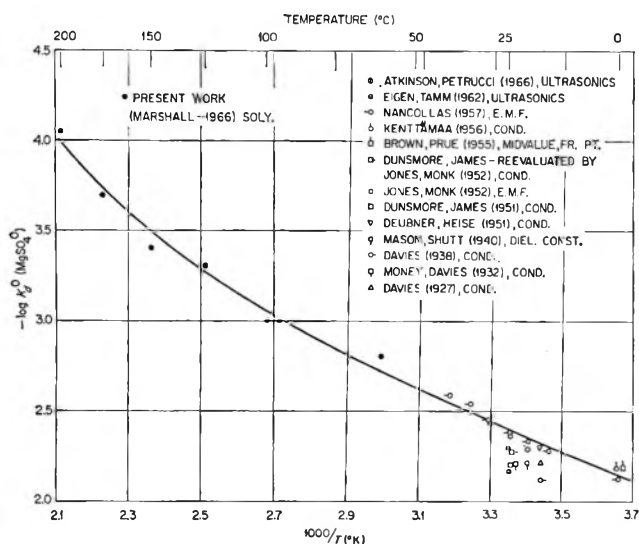


Figure 2. The dissociation constant of magnesium sulfate from 0 to 200°.

can be related directly to the differences in charge of divalent and monovalent ions.

Thermodynamic Functions

By using the van't Hoff isochore and an assumed linear dependency of ΔC_p° on temperature over the 0–200° range, the present values of $\log K_d^\circ$ and those of Nancollas,¹³ Jones and Monk,¹⁶ Brown and Prue,¹⁵ and Kenttämäa¹⁴ were fitted by a method of least squares as described previously⁴ to yield the following equation for $\log K_d^\circ$ as a function of temperature (°K).

$$\log K_d^\circ = -158.540 + 62.160 \log T + (4180.6/T) - 0.046298T \quad (13)$$

From the treatment of eq 13 by the usual methods,⁴ thermodynamic functions for the standard changes in free energy (ΔG°), enthalpy (ΔH°), entropy (ΔS°), and heat capacity (ΔC_p°) were obtained from 0 to 200°. The values are given in Table I. At 25° the values of ΔG° , ΔH° , and ΔS° in this table compare reasonably well with those of Nancollas¹³ of 3.22, -4.55, and -26.1 and of Jones and Monk¹⁶ of 3.2, -5.7, and -31, respectively.

When a constant value for ΔC_p° was assumed, eq 14 was obtained

$$\log K_d^\circ = 30.953 - 12.4547 \log T - (750.2/T) \quad (14)$$

which yielded an average value of ΔC_p° of -25 cal mole⁻¹ deg⁻¹ from 0 to 200°. Calculated values for ΔG° , ΔH° , and ΔS° from this equation were very little different from those given in Table I. Equation 13, however, gave a somewhat better fit to the data and

Table I: Standard Thermodynamic Quantities for the Equilibrium $\text{MgSO}_4^\circ(\text{aq}) \rightleftharpoons \text{Mg}^{2+}(\text{aq}) + \text{SO}_4^{2-}(\text{aq})$ (at $I = 0$)

T , °C	$-\log K_d^\circ$ ^a	ΔG° , kcal/mole	ΔH° , kcal/mole	ΔS° , cal/mole deg	ΔC_p° , cal/mole deg
0	2.129	2.661	-4.08	-24.7	+7.8
25	2.399	3.273	-4.01	-24.4	-2.8
50	2.631	3.890	-4.22	-25.1	-13.4
75	2.846	4.53	-4.68	-26.5	-24
100	3.057	5.22	-5.41	-28.5	-35
125	3.274	5.96	-6.41	-31.1	-45
150	3.501	6.78	-7.67	-34.1	-56
175	3.743	7.67	-9.20	-37.6	-66
200	4.002	8.66	-11.0	-41.5	-77
250 ^b	4.58	10.9	-15.4	-50.3	-98
300 ^b	5.23	13.7	-20.8	-60.2	-119
350 ^b	5.96	17.0	-27.3	-71.0	-140
370 ^b	6.27	18.5	-30.2	-75.6	-149

^a Use of eq 13 for all values. ^b Use of eq 13 for extrapolation; no experimentally attained values beyond 200°.

provided estimates for ΔC_p° as a function of temperature.

Another equation for $\log K_d^\circ$ was obtained by assuming that ΔC_p° varied as a quadratic function of temperature. This equation

$$\log K_d^\circ = 4091.991 - 1762.800 \log T - (87514.4/T) + 2.191689T - 0.001038956T^2 \quad (15)$$

indeed provided a maximum value of ΔC_p° at approximately 80° in accordance with maxima for ΔC_p° observed for other ionization reactions.²³ Nevertheless, both calculated thermodynamic quantities, ΔH° and ΔS° , although close to the values given in Table I, showed both maxima and minima between 0 and 200°. When all thermodynamic quantities were calculated to 350° by using eq 15, they approached unreasonably very low or very high values. Therefore, the four-constant eq 13 is believed to provide the best description to 200°, with estimates to 350°, of this equilibrium within the precision of the available values for K_d° .

Assigned Entropy and Heat Capacities for MgSO_4° at 0–200°. Criss and Cobble have assigned values for the entropy²⁴ and average heat capacity²⁵ of ions at temperatures from 25 to 200° by means of a correspondence principle and the use of experimentally derived assignments at low temperatures (based on a specific assign-

(23) Th. Ackermann and F. Schreiner, *Z. Elektrochem.*, **62**, 1143 (1958).

(24) C. M. Criss and J. W. Cobble, *J. Am. Chem. Soc.*, **86**, 5385 (1964).

(25) C. M. Criss and J. W. Cobble, *ibid.*, **86**, 5390 (1964).

ment of -5.0 eu at 25° for the hydrogen ion).²⁴ From Table I, average values for $\Delta\bar{C}_p]_{25}^t$ and also values for ΔS_t° can be obtained at $25, 60, 100, 150,$ and 200° for use with Criss and Cobble's estimates of ionic quantities at these temperatures. From eq 1 for the dissociation equilibrium, the (assigned) entropy of the neutral species, MgSO_4° , is equal to $[\bar{S}_t^\circ(\text{Mg}^{2+}) + \bar{S}_t^\circ(\text{SO}_4^{2-})]$ (from Criss and Cobble) minus ΔS_t° (from Table I) where t refers to the temperature. The average heat capacities for MgSO_4° are obtained by a similar relationship. The calculated values for the two quantities are given in Table II. They show that the entropy of MgSO_4° is relatively small and, surprisingly, changes very little with temperature. The average heat capacity, $\bar{C}_p]_{25}^t$, of MgSO_4° rises with increasing temperature.

Table II: The Entropy and Average Heat Capacity of $[\text{MgSO}_4^\circ]$

$T,$ $^\circ\text{C}$	$S_t^\circ,$ cal/mole deg	$\bar{C}_p]_{25}^t,$ cal/mole deg
25	-1.6	-50
60	-5.1	-39 ^a
100	-6.1	-25
150	-5.3	-10
200	-4.5 ^b	-2

^a From smoothed Criss and Cobble values²⁵ at 60° for $\bar{C}_p]_{25}^{60}$ for Mg^{2+} and SO_4^{2-} . ^b Calculated using smoothed value for SO_4^{2-} and extrapolated value for Mg^{2+} from Criss and Cobble²⁴ to 150° .

Application of Irreversible Thermodynamics to Electrolyte Solutions. III.

Equations for Isothermal Vector Transport Processes

in n -Component Systems¹

by Donald G. Miller

Lawrence Radiation Laboratory, University of California, Livermore, California 94550 (Received April 3, 1967)

Irreversible thermodynamics is applied to isothermal vector transport processes of an n -component system consisting of $n - 1$ electrolytes with a common anion dissolved in a neutral solvent. Rigorous expressions for the conductance Λ , transference numbers t_i , and solvent-fixed thermodynamic diffusion coefficients $(L_{ij})_0$ are given in terms of ionic transport coefficients, l_{ij} , and conversely. Rigorous expressions are also given for ion flows J_i in terms of t_i , Λ , and either $(L_{ij})_0$ or diffusion coefficients $(D_{ij})_0$. Limiting expressions at infinite dilution are given for L_{ij} and D_{ij} in terms of limiting ionic conductances.

I. Introduction

In previous papers, parts I² and II,³ isothermal vector transport processes in binary and ternary systems were treated in some detail, and comparisons with experiment were presented. In view of increasing interest in higher order systems, particularly the accurate

measurement of diffusion coefficients in quaternary systems,⁴ it seems worth presenting briefly the results

(1) This work was performed under the auspices of the U. S. Atomic Energy Commission.

(2) D. G. Miller, *J. Phys. Chem.*, **70**, 2639 (1966).

(3) D. G. Miller, *ibid.*, **71**, 616 (1967).

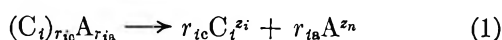
for the general case of an n -component system consisting of a neutral solvent and $n - 1$ binary electrolytes with a common anion. The common-cation case is obtained merely by relettering.

Limiting expressions at infinite dilution are also given for ordinary and thermodynamic diffusion coefficients. These may be of some practical use since, as far as is known, there are no complete experimental diffusion data on any quaternary or higher order system.

II. General Equations and Notation

Equations from papers I² and II³ will be distinguished by the prefixes I and II, respectively.

We introduce the following notation for our n -component system. Let the neutral solvent be denoted by subscript 0, the cations of the $n - 1$ binary electrolytes by subscripts running from 1 to $n - 1$, and the common anion by subscript n . Each individual electrolyte as a whole can also be denoted by the subscript of its cation. Each of these binary electrolytes ionizes as



where C_i denotes the cation, A the common anion, z_i the signed valence of the ions, and r_{ic} and r_{ia} the stoichiometric coefficients for the ionization.

If μ_i , μ_n , and μ_{in} are the chemical potentials in joules per mole for the cation i , anion, and electrolyte as a whole, respectively, then

$$\mu_{in} = r_{ic}\mu_i + r_{ia}\mu_n \quad i = 1, \dots, n - 1 \quad (2)$$

Moreover, by charge conservation

$$r_{ic}z_i + r_{ia}z_n = 0 \quad i = 1, \dots, n - 1 \quad (3)$$

If c_i ($i = 1, \dots, n - 1$) are the concentrations in moles per liter of the electrolytes as a whole, then the number of equivalents per liter of a cation is given by

$$N_i = r_{ic}z_i c_i \quad i = 1, \dots, n - 1 \quad (4)$$

The total number of equivalents per liter, N , is the same as the number of equivalents per liter of the anion and is

$$N = \sum_{i=1}^{n-1} r_{ic}z_i c_i = -z_n \sum_{i=1}^{n-1} r_{ia} c_i = N_n \quad (5)$$

The *equivalent fraction* is defined as

$$x_i = N_i/N \quad (6)$$

and $x_n = 1$.

The expression for μ_{in} is given in terms of the activity a_i of the electrolyte as a whole by

$$\mu_{in} = \mu_{in}^0 + \hat{R}T \ln a_i \quad i = 1, \dots, n - 1 \quad (7)$$

where T is the absolute temperature in degrees Kelvin,

\hat{R} is the gas constant in joules per mole degree, and μ_{in}^0 is a function of T only. This can be written in terms of the moles per liter mean activity coefficient y_i of the binary electrolyte i as⁵

$$a_i = c_{ic}^{r_{ic}} c_{ia}^{r_{ia}} y_i^{r_i} \quad (8)$$

where r_i , the total number of ions of electrolyte i on ionization, is

$$r_i = r_{ic} + r_{ia} \quad (9)$$

For a common anion system

$$c_{ic} = r_{ic} c_i; \quad c_{ia} = \sum_{l=1}^{n-1} r_{la} c_l \quad (10)$$

so that

$$a_i = (r_{ic} c_i)^{r_{ic}} \left(\sum_{l=1}^{n-1} r_{la} c_l \right)^{r_{ia}} y_i^{r_i} \quad (11)$$

Chemical potential derivatives will be useful. Therefore, substituting eq 11 into 7, differentiating, and making use of eq 5 and 6, we obtain upon relettering

$$\mu_{kj} = \frac{\partial \mu_{kn}}{\partial c_j} = \frac{\hat{R}T}{c_j} \left[r_{kc} \delta_{kj} + r_{ka} x_j + r_{kc} c_j \frac{\partial \ln y_k}{\partial c_j} \right]$$

common anion system, $k, j = 1, \dots, n - 1$ (12)

where the notation μ_{kj} is defined by eq 12, and δ_{kj} is the Kronecker δ .

We now turn to the irreversible thermodynamic description of this system. There are $n + 1$ diffusion constituents, *i.e.*, n ions and the solvent. However only n of them are independent, because of a choice of reference frame and because of the Gibbs-Duhem equation.² As before,^{2,5} it is convenient to choose the solvent-fixed reference frame and choose the n ion flows as the independent set. In this situation we may write

$$J_i = \sum_{j=1}^n l_{ij} X_j \quad i = 1, \dots, n \quad (13)$$

where J_i are the solvent-fixed ion flows in moles/cm² sec, l_{ij} the solvent-fixed ionic transport coefficients in mole²/joule cm sec, and X_j the thermodynamic forces (in one dimension) given by

$$X_j = - \left[\frac{\partial \mu_j}{\partial x} + z_j \mathfrak{F} \frac{\partial \phi}{\partial x} \right] \quad j = 1, \dots, n \quad (14)$$

where \mathfrak{F} is the Faraday in coulombs per equivalent, ϕ the electrical potential in volts, and x the distance in

(4) H. Kim and L. J. Gosting, private communication.

(5) D. G. Miller, *J. Phys. Chem.*, **63**, 570 (1959); corrections, *ibid.*, **63**, 2089 (1959).

centimeters. The solvent flow J_0 is zero on this reference frame.

Because the J_i and X_i have been properly chosen,^{2,6} the Onsager reciprocal relations (ORR)

$$l_{ij} = l_{ji} \quad i, j = 1, \dots, n \quad (15)$$

are valid. Consequently, only $n(n + 1)/2$ of the n^2 l_{ij} are independent.

We now turn to the general equations for pure diffusion, where the flows are those of electrolytes as a whole. The generalized Fick law expressions in terms of solvent-fixed flows and solvent-fixed diffusion coefficients $(D_{ij})_0$ are

$$J_{in} = -\sum_{j=1}^{n-1} (\hat{D}_{ij})_0 \frac{\partial c_j}{\partial x} \quad i = 1, \dots, n-1 \quad (16)$$

and in terms of solvent-fixed thermodynamic diffusion coefficients $(L_{ij})_0$ in mole²/joule cm sec are

$$J_{in} = -\sum_{j=1}^{n-1} (L_{ij})_0 \frac{\partial \mu_{jn}}{\partial x} \quad i = 1, \dots, n-1 \quad (17)$$

where the flows of electrolyte as a whole J_{in} in moles/cm² sec are

$$J_{in} = \frac{J_i}{r_{ic}} \quad i = 1, \dots, n-1 \quad (18)$$

and where $(\hat{D}_{ij})_0$ (in liters/cm sec) are given in terms of the usual diffusion coefficients (in cm²/sec) by

$$(\hat{D}_{ij})_0 = (D_{ij})_0 / 1000.027 \quad (19)$$

The $(\hat{D}_{ij})_0$ are related to the $(L_{ij})_0$ and conversely by the equations⁷

$$(\hat{D}_{ij})_0 = \sum_{k=1}^{n-1} (L_{ik})_0 \mu_{kj} \quad i, j = 1, \dots, n-1 \quad (20)$$

III. Relations among the Transport Quantities

The analysis of conductance leading to eq I-15 and II-12 is straightforwardly generalized for the n -component system, yielding

$$\alpha = \frac{\lambda}{\mathcal{F}^2} = \frac{\Lambda N}{10^3 \mathcal{F}^2} = \sum_{k=1}^n \sum_{l=1}^n z_k l_k z_l \quad (21)$$

where λ is the specific conductance in (ohm cm)⁻¹, Λ is the equivalent conductance in cm²/ohm equiv, and α is defined by eq 21. Similarly, the analyses leading to eqs I-22 and II-14 for the Hittorf transference number yield directly the general result

$$t_i = \frac{z_i}{\alpha} \sum_{l=1}^n z_l l_{il} \quad i = 1, \dots, n \quad (22)$$

The pure diffusion case is more complex. The argument is everywhere analogous to that leading from eq

II-23 to II-25, except that sums run from 1 to n . The bracketed term of eq II-25 can be written in general in terms of electrolytes as a whole as

$$z_i \frac{\partial \mu_j}{\partial x} - z_j \frac{\partial \mu_i}{\partial x} = (1 - \delta_{jn}) \frac{z_i}{r_{jc}} \frac{\partial \mu_{jn}}{\partial x} - (1 - \delta_{in}) \frac{z_j}{r_{ic}} \frac{\partial \mu_{in}}{\partial x} \quad (23)$$

When $j = n$, the first term on the right side vanishes; when $l = n$, the second term vanishes; and when $j = l$, the whole thing vanishes. When eq 23 is substituted into the generalized eq II-25, with the above conditions applied and a dummy index appropriately relettered, one obtains the generalization of eq II-27 with $i, j = 1, \dots, n-1$ and $k, l = 1, \dots, n$. Identification of terms yields the result analogous to eq II-28

$$(L_{ij})_0 = \frac{1}{\alpha r_{ic} r_{jc}} \sum_{k=1}^n \sum_{l=1}^n z_k z_l (l_{ij} l_{kl} - l_{il} l_{kj}) \quad i, j = 1, \dots, n-1 \quad (24)$$

Because the ORR apply to the l_{ij} , eq 24 has the consequence that there are $(n-1)(n-2)/2$ ORR among the $(L_{ij})_0$. Therefore, only $n(n-1)/2$ of the $(L_{ij})_0$ are independent. Consequently, eq 20 implies that only $n(n-1)/2$ of the $(D_{ij})_0$ are independent as well. The independent quantities are the conductance, $n-1$ transference numbers, and $n(n-1)/2$ diffusion coefficients. These add up to $n(n+1)/2$ independent experimental quantities, which is precisely the number of independent l_{ij} . Consequently, eq 21, 22, and 24 can be solved simultaneously for the l_{ij} .

The technique is as follows. For $i, j = 1, \dots, n-1$, form the sum of $(\alpha^2 t_i l_j / z_i z_j) + \alpha r_{ic} r_{jc} (L_{ij})_0$. After appropriate cancellation, one obtains

$$l_{ij} = \frac{\alpha t_i t_j}{z_i z_j} + r_{ic} r_{jc} (L_{ij})_0 \quad i, j = 1, \dots, n-1 \quad (25)$$

To obtain l_{in} , eq 25 is substituted into eq 22, which after rearrangement yields

$$l_{in} = \frac{\alpha t_i t_n}{z_i z_n} + r_{ic} \sum_{l=1}^{n-1} r_{lc} (L_{il})_0 \quad i = 1, \dots, n-1 \quad (26)$$

Finally, l_{nn} is obtained by substituting eq 25 and 26 into eq 22 for t_n , yielding eq 27.

(6) S. R. DeGroot and P. Mazur, "Non-Equilibrium Thermodynamics," Interscience Publishers, Inc., New York, N. Y., 1962, pp 64-69.

(7) J. G. Kirkwood, R. L. Baldwin, P. J. Dunlop, L. J. Gosting, and G. Kegeles, *J. Chem. Phys.*, **33**, 1505 (1960).

$$l_{nn} = \frac{\alpha t_n^2}{z_n^2} + \sum_{k=1}^{n-1} \sum_{l=1}^{n-1} r_{ka} r_{la} (L_{kl})_0 \quad (27)$$

With eq 3, eq 25-27 can be combined into the single equation

$$l_{ij} = \frac{\alpha t_j}{z_i z_j} + \frac{z_n^2}{z_i z_j} \sum_{k=1}^{n-1} \sum_{l=1}^{n-1} (\delta_{ik} - \delta_{in}) \times (\delta_{jl} - \delta_{jn}) r_{ka} r_{la} (L_{kl})_0 \quad i, j = 1, \dots, n-1 \quad (28)$$

Equations 21, 22, 24, and 28 are the desired relations between the l_{ij} and the ordinarily measured transport quantities when $\Lambda N/10^3 \mathcal{F}^2$ is substituted for α .

IV. Flaws in Terms of Experimental Quantities

We now turn our attention to expressing ion flows J_i in terms of the usual experimental quantities t_i , Λ , and $(D_{ij})_0$. If we substitute eq 28 into eq 13, we obtain

$$J_i = -\frac{\alpha t_i}{z_i} \left[\mathcal{F} \frac{\partial \phi}{\partial x} + \sum_{j=1}^n \frac{t_j}{z_j} \frac{\partial \mu_j}{\partial x} \right] + \{ \} \quad i = 1, \dots, n \quad (29)$$

where $\{ \}$ is a triple summation term involving X_j and the $(L_{kl})_0$ term of eq 28. If the Kronecker δ terms of the $\{ \}$ are multiplied out and the four δ products are applied separately, the triple sums become double sums. By appropriately relettering a dummy index, adding up the four double sums, factoring, and canceling, we find that the $\partial \phi / \partial x$ terms cancel and the $\partial \mu_j / \partial x$ terms combine to form gradients of electrolytes as a whole. When the result is substituted into eq 29, we obtain

$$J_i = -\frac{\alpha t_i}{z_i} \left[\mathcal{F} \frac{\partial \phi}{\partial x} + \sum_{j=1}^n \frac{t_j}{z_j} \frac{\partial \mu_j}{\partial x} \right] + \frac{z_n}{z_i} \sum_{j=1}^{n-1} \sum_{k=1}^{n-1} (\delta_{ik} - \delta_{in}) r_{ka} (L_{kj})_0 \frac{\partial \mu_{jn}}{\partial x} \quad (30)$$

where the last term on the right side is the $\{ \}$.

The first term of the right side of eq 30 can be written in terms of the current density I as

$$I = \sum_{i=1}^n z_i J_i \mathcal{F} = -\sum_{i=1}^n \alpha t_i \mathcal{F} \left[\frac{\partial \phi}{\partial x} + \sum_{j=1}^n \frac{t_j}{z_j} \frac{\partial \mu_j}{\partial x} \right] + \sum_{i=1}^n z_i \{ \} \quad (31)$$

where $\{ \}$ is again the last term of the right side of eq 29 or 30.

The sum over the $z_i \{ \}$ is found to be identically zero and $\sum t_i = 1$. Hence

$$-\frac{I}{\mathcal{F} \alpha} = \mathcal{F} \frac{\partial \phi}{\partial x} + \sum_{j=1}^n \frac{t_j}{z_j} \frac{\partial \mu_j}{\partial x} \quad (32)$$

If eq 32 is substituted into 29, we obtain

$$J_i = \frac{t_i}{z_i} \frac{I}{\mathcal{F}} + \frac{z_n}{z_i} \sum_{j=1}^{n-1} \sum_{k=1}^{n-1} (\delta_{ik} - \delta_{in}) r_{ka} (L_{kj})_0 \frac{\partial \mu_{jn}}{\partial x} \quad (33)$$

Moreover, because the right sides of eq 16 and 17 are equal, eq 30 and 33 can be written in terms of diffusion coefficients as

$$J_i = -\frac{\alpha t_i}{z_i} \left[\mathcal{F} \frac{\partial \phi}{\partial x} + \sum_{j=1}^n \frac{t_j}{z_j} \frac{\partial \mu_j}{\partial x} \right] + \frac{z_n}{z_i} \sum_{j=1}^{n-1} \sum_{k=1}^{n-1} (\delta_{ik} - \delta_{in}) r_{ka} (\hat{D}_{kj})_0 \frac{\partial c_j}{\partial x} \quad (34)$$

$$J_i = \frac{t_i}{z_i} \frac{I}{\mathcal{F}} + \frac{z_n}{z_i} \sum_{j=1}^{n-1} \sum_{k=1}^{n-1} (\delta_{ik} - \delta_{in}) r_{ka} (\hat{D}_{kj})_0 \frac{\partial c_j}{\partial x} \quad (35)$$

Equations 30, 33, 34, and 35 are the desired general expressions for J_i ($i = 1, \dots, n$) in terms of experimental quantities⁸ and represent the general statement of superposition of diffusion and electrical flows.

V. Limiting Equations at Infinite Dilution

In paper II,³ we considered a number of approximations for ternary l_{ij} in strong electrolyte solutions, which in turn led to estimates of Λ , t_i , $(L_{ij})_0$, and $(D_{ij})_0$. The success of these estimates depended on how many binary data were available. However, fair estimates of $(L_{ij})_0$ and $(D_{ij})_0$ could be obtained from the infinite dilution approximation, although Λ and t_i were unsatisfactory at finite concentrations. Therefore it seems reasonable that infinite dilution equations should yield a fair estimate of $(L_{ij})_0$ and $(D_{ij})_0$ for higher order systems, and this approximation has the advantage that only the limiting ionic conductances are required.

The infinite dilution approximation analogous to eq II-68 is

$$\frac{l_{ij}^0}{N} = \frac{\delta_{ij} x_i \alpha_i^0}{N z_i^2} = \frac{\delta_{ij} x_i \Lambda_i^0}{10^3 z_i^2 \mathcal{F}^2} \quad i, j = 1, \dots, n \quad (36)$$

where the superscript zero refers to infinite dilution, Λ_i^0 is the limiting ionic conductance, and all ionic cross terms l_{ij}^0/N are zero.

Substitution of eq 36 into eq 21 and 22 yields the trivial results

$$\Lambda^0 = \sum_{i=1}^n x_i \Lambda_i^0 \quad (37)$$

$$t_i = x_i \Lambda_i^0 / \Lambda^0 \quad i = 1, \dots, n \quad (38)$$

If we substitute eq 36 into eq 24, factor out the unsummed i quantities, apply the various Kronecker δ 's,

(8) The μ_j of eq 30 and 34 are of course not really "experimental." However, in the analysis of any experiment either the $[]$ vanishes or the J_i 's are coupled with external electrodes such that the μ_j 's combine to form expressions involving only electrolytes as a whole and the ϕ term is absorbed in a measurable emf.

use eq 37, and use the fact that $\delta_{ij}/z_i = \delta_{ij}/z_j$, we obtain the nontrivial result

$$\frac{L_{ij}^0}{N} = \frac{x_i \Lambda_i^0 [\delta_{ij} \Lambda^0 - x_j \Lambda_j^0]}{10^3 r_{ic} r_{jc} z_i z_j \mathcal{F}^2 \Lambda^0} \quad i, j = 1, \dots, n-1 \quad (39)$$

which is analogous to eq II-72, II-73, and II-74.

To get a diffusion coefficient expression, we need the limiting expression for μ_{kj} , namely

$$\mu_{kj} = \frac{\hat{R}T}{c_j} [r_{kc} \delta_{kj} + r_{ka} x_j] \quad (40)$$

This is obtained from eq 12 by noting that $c_j \partial \ln y_k / \partial c_j$ goes to zero as $S^{1/2}$ as a result of the Debye-Hückel theory, where S is the ionic strength.

If we substitute eq 39 and 40 into eq 20, multiply

out and apply the various Kronecker δ terms, cancel and rearrange, and use $\delta_{ij}/z_j = \delta_{ij}/z_i$ and eq 19, we obtain

$$D_{ij}^0 = \frac{r_{ja} \Lambda_i^0 \hat{R}T}{r_{ia} \Lambda^0 \mathcal{F}^2} \left[\frac{\delta_{ij} \Lambda^0}{z_i} - x_i \left(\frac{\Lambda_j^0}{z_j} + \frac{\Lambda_n^0}{z_n} \right) \right] \quad i, j = 1, \dots, n-1 \quad (41)$$

which is analogous to eq II-76 to II-79. Equations 41 are the n -ary analogs of the Nernst-Hartley equation.

VI. Remarks

The quaternary system equations are easily obtained by specializing the general eq 21, 22, 24, 28, 30, 33, 34, 35, 39, or 41.

Better estimates for diffusion coefficients can be obtained by means of better approximations to l_{ij} and by data or better approximations for μ_{kj} .

Carbon-13 Nuclear Magnetic Resonance Studies of 4-Substituted Pyridines

by H. L. Retcofsky and R. A. Friedel

U. S. Department of the Interior, Bureau of Mines, Pittsburgh Coal Research Center, Pittsburgh, Pennsylvania 15213 (Received April 3, 1967)

Carbon-13 magnetic resonance spectra of nine 4-substituted pyridines have been obtained and analyzed. Both electron-releasing and -withdrawing substituents were investigated. Substituent effects were generally within ± 3 ppm of those found in the corresponding monosubstituted benzenes and suggest similar shielding mechanisms for the two classes of compounds. The β -vinyl carbon shielding in 4-vinylpyridine supports the common proposal that the nitrogen atom in pyridine resembles electronically the CNO_2 group in nitrobenzene.

Introduction

During the course of an extensive investigation of the structure of coal using spectroscopic techniques, the need for a collection of carbon-13 magnetic resonance spectra of nitrogen-containing heterocyclic molecules became evident since these materials are used extensively as extracting agents for coal and have been shown to form molecular complexes with coal. Heterocyclic

nitrogen is generally assumed to be present in coal although its existence has never been confirmed.

C^{13} nuclear magnetic resonance parameters obtained for nine 4-substituted pyridines are reported here as the first phase of an investigation of carbon shieldings and spin-spin couplings in monosubstituted pyridines. Data for the parent compound and 4-picoline have been previously published.¹ The 4-substituted compounds

were examined first since their spectra are relatively simple and peak assignments are practically unambiguous. A study of the effects of substituents on the shieldings of the ring carbons in these compounds proved invaluable in making assignments in the spectra of the 2- and 3-substituted pyridines which give more complicated spectra; data for the latter compounds will be reported in later papers in this series.

Experimental Section

Nuclear Magnetic Resonance Spectra. All spectra were obtained under rapid-passage, dispersion mode operating conditions at a spectrometer frequency of 15.085 MHz. Experimental conditions were essentially those reported previously² except that slower sweep rates and a sample cell similar to that designed by Spiesecke and Schneider³ were employed. The cell consisted of two concentric spherical compartments, the inner one of which contained the reference compound CH₃C¹³OOH. No provision for sample spinning was provided. The conventional side-band technique⁴ was used for spectral calibration. All chemical shifts were subsequently referred to carbon disulfide and are designated δ_c . To ensure accurate chemical shift determinations, the distance between the nmr signal of the secondary standard and that of carbon disulfide was measured at frequent intervals and found not to exceed ± 0.2 ppm. Carbon shieldings for the series of pyridines could be reproduced to better than 0.5 ppm.

Materials. The compounds contained only naturally occurring carbon-13 and were examined as neat liquids except for 4-cyanopyridine and 4-aminopyridine which were studied as saturated solutions in dioxane and ethanol, respectively. 4-Vinylpyridine and 4-*t*-butylpyridine were products of Reilly Chemical and Tar Corp. Samples of the acetyl, vinyl, and alkyl compounds were generously donated by the Laramie Petroleum Research Center, U. S. Bureau of Mines. 4-Bromopyridine was obtained from Pfaltz & Bauer, Inc. The acetyl, aldehyde, amino, and cyano derivatives were Aldrich Chemical Co. products.

Results

Spectral Assignments. The C¹³ nmr spectra of 4-substituted pyridines should each consist of a singlet for C-4 and doublets for CH-2 and -6 and CH-3 and -5 since only one-bond carbon-hydrogen spin-spin couplings are generally resolvable under the experimental conditions employed. Assignment of spectral peaks to specific doublets was made on the basis of spin-coupling constants ($J_{C^{13}-H} \sim 175 \pm 25$ cps) but was confirmed in all cases by double-resonance experiments. Double resonance was also used to locate singlets partially ob-

scured by doublet components. The technique is illustrated in Figure 1.

All C-4 assignments were straightforward with the exception of that for the 4-cyano compound, the spectrum of which exhibited two singlets separated by only 3.4 ppm. Thus the resonance frequencies of both C-4 and the nitrile carbon fall in the aromatic spectral region. To alleviate any ambiguity, spectra of benzonitrile and the 2- and 3-cyanopyridines were run. A singlet near δ_c 75 ppm was found in the spectrum of each of these compounds; thus the peak closest to this position in the spectrum of 4-cyanopyridine (δ_c 76.2 ppm) is assigned to the nitrile carbon. The remaining singlet (δ_c 72.8 ppm) must then be assigned to C-4. Assignments of the spectral doublets to specific carbons were made on the basis of the known shifts for pyridine¹ and the substituent effects reported for monosubstituted benzenes.⁵ All other peaks such as those due to carbonyl and alkyl groups fall into distinct regions of the C¹³ nmr spectrum and can easily be assigned on the basis of position and spin-spin coupling patterns. It is

Table I: C¹³ Magnetic Shieldings in 4-Substituted Pyridines (ppm from CS₂)

Substituent	Aromatic carbons			Other
	CH-2	CH-3	C-4	
H ^a	43.1	69.2	57.3	
NH ₂	44.1	83.9	37.4	
Br	41.9	55.9	60.3	
CH ₃ ^a	43.6	67.9	46.0	172.2 (CH ₃)
CH ₂ CH ₃	43.9	70.6	41.4	165.4 (CH ₂) 179.8 (CH ₃)
CH(CH ₃) ₂	42.7	71.0	35.9	159.7 (CH) 170.1 (CH ₃)
C(CH ₃) ₃	43.0	72.6	33.9	158.6 (<i>t</i> -C) 162.7 (CH ₃)
CH=CH ₂	42.8	72.3	48.7	58.2 (vinyl CH) 74.8 (vinyl CH ₂)
CN	42.2	67.0	72.8	76.2 (CN)
COCH ₃	42.3	71.8	50.6	-4.1 (C=O) 166.8 (CH ₃)
CHO	42.2	70.9	51.8	1.0 (C=O)

^a Data from ref 1.

- (1) P. C. Lauterbur, *J. Chem. Phys.*, **43**, 360 (1965).
- (2) R. A. Friedel and H. L. Retcofsky, *J. Am. Chem. Soc.*, **85**, 1300 (1963).
- (3) H. Spiesecke and W. G. Schneider, *J. Chem. Phys.*, **35**, 722 (1961).
- (4) J. A. Pople, W. G. Schneider, and H. J. Bernstein, "High-Resolution Nuclear Magnetic Resonance," McGraw-Hill Book Co., Inc., New York, N. Y., 1959, p 74.
- (5) H. Spiesecke and W. G. Schneider, *J. Chem. Phys.*, **35**, 731 (1961).

Table II: Substituent Effects on Ring Carbon Shieldings in 4-Substituted Pyridines and Monosubstituted Benzenes^a

Substituent (X)	$\Delta\delta$, ppm								
	Pyridines, CH-2	Benzenes, <i>meta</i>	Diff	Pyridines, CH-3	Benzenes, <i>ortho</i>	Diff	Pyridines, C-4	Benzenes, C-X	Diff
NH ₂	1.0	-1.3	2.3	14.7	12.4	2.3	-19.9	-19.6	-0.3
Br	-1.2	-2.2	1.0	-3.3	-3.3	0	3.0	5.4	-2.4
CH ₃ ^b	0.5	-0.3	0.8	-1.3	-0.3	-1.0	-11.3	-9.1	-2.2
CH ₂ CH ₃	0.8	-1.6	2.4	1.4	2.7	-1.3	-15.9	-16.1	0.2
CH(CH ₃) ₂	-0.4	0.7	-1.1	1.8	2.6	-0.8	-21.4	-19.8	-1.6
C(CH ₃) ₃	-0.1	0.3	-0.4	3.4	3.3	0.1	-23.4	-22.2	-1.2
CH=CH ₂	-0.3	0.8	-1.1	3.1	0.8	2.3	-8.6	-8.6	0
CN	-0.9	-1.3	0.4	-2.2	-4.3	2.1	15.5	15.6	-0.1
COCH ₃	-0.8	-0.2	-0.6	2.6	-0.2	2.8	-6.7	-9.3	2.6
CHO	-0.9	-1.2	0.3	1.7	-1.2	2.9	-5.5	-9.0	3.5

^a Data for monosubstituted benzenes taken from ref 5-7 except those for benzonitrile which were obtained in this laboratory. ^b Carbon shieldings for 4-methylpyridine taken from ref 1.

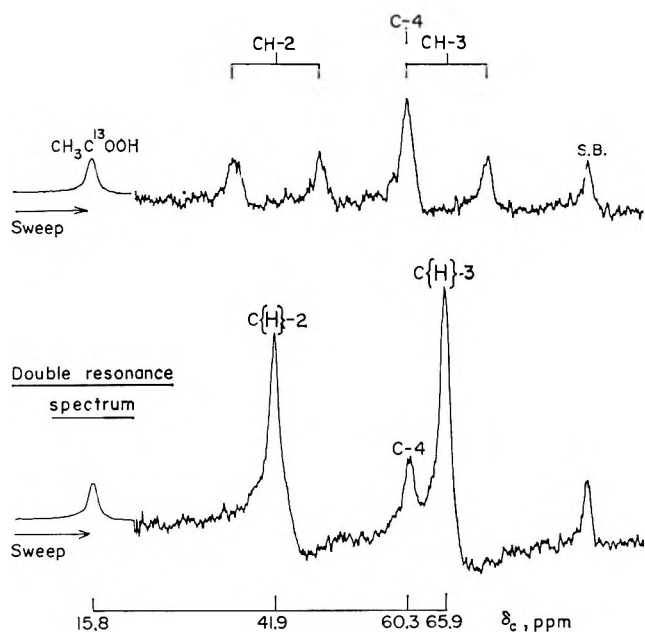


Figure 1. ¹³C magnetic resonance spectrum (15.085 MHz) and double-resonance spectrum of 4-bromopyridine.

doubtful that any other assignments than those made here can be substantiated.

Shieldings and Couplings. Magnetic shieldings of all carbon-13 nuclei in the nine compounds studied are given in Table I. Lauterbur's data for pyridine and 4-picoline are also included.¹ Average values of one-bond carbon-hydrogen spin-coupling constants are presented later in this paper.

Substituent Effects on Ring Carbon Shieldings. The effects on the ring carbon shieldings, when the hydrogen atom in the 4-position of pyridine is replaced by a substituent, are approximately the same as those found for the corresponding carbon atoms in mono-

substituted benzenes (Table II). Values for the latter compounds⁵⁻⁷ and differences between the two sets of substituent effects are also included. These differences which represent deviations from the additivity relations originally proposed by Lauterbur^{8,9} for aromatic carbon shieldings are in many cases larger than the accumulative experimental error ($\sim \pm 1.3$ ppm⁶). Values for 4-aminopyridine, the only case involving a strong electron-releasing substituent, may be misleading since the hydrogen-bonding solvent ethanol was used. Ethanol was needed in order to obtain spectra having a sufficiently high signal-to-noise ratio to allow accurate chemical shift determinations.

Ring Carbon Shieldings. Lauterbur has shown that the ring carbon shieldings in pyridine and other unsubstituted azines reflect local π -electron densities.¹ Replacement of the hydrogen in the 4 position of pyridine with substituents possessing various degrees of electron-withdrawing and electron-releasing capabilities alters the charge distributions in the ring and hopefully this would be reflected in the nuclear magnetic shieldings. Spiesscke and Schneider⁵ have adequately shown that for monosubstituted benzenes it is only at the *para* position that the trend in carbon shieldings is consistent with that expected from variations in charge densities arising from resonance effects of the substituents; the observed shieldings are nearly linearly related to Hammett's σ_p constants. Substituent effects on the shieldings of the *meta* carbons, *ortho* carbons, and carbons directly bonded to substituents, which correspond to the CH-2, CH-3, and C-4 carbons

(6) K. S. Dhami and J. B. Stothers, *Can. J. Chem.*, **43**, 479 (1965).

(7) K. S. Dhami and J. B. Stothers, *ibid.*, **43**, 510 (1965).

(8) P. C. Lauterbur, *J. Am. Chem. Soc.*, **83**, 1838 (1961).

(9) P. C. Lauterbur, *ibid.*, **83**, 1846 (1961).

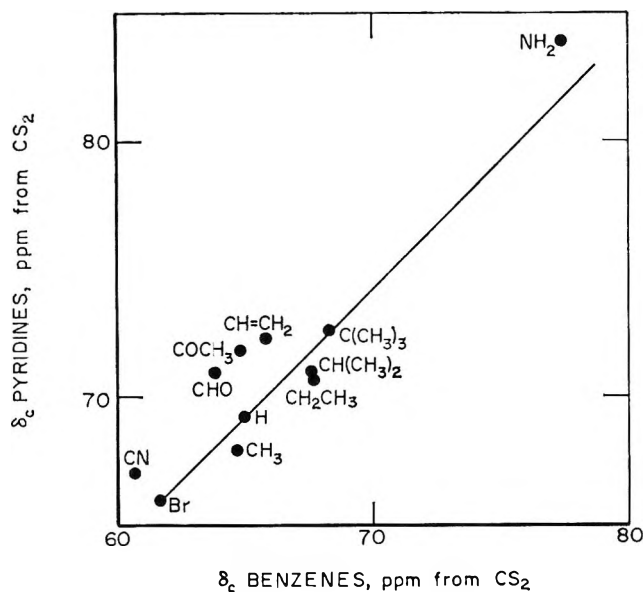


Figure 2. Magnetic shieldings of the substituted carbon atoms in 4-substituted pyridines and monosubstituted benzenes.

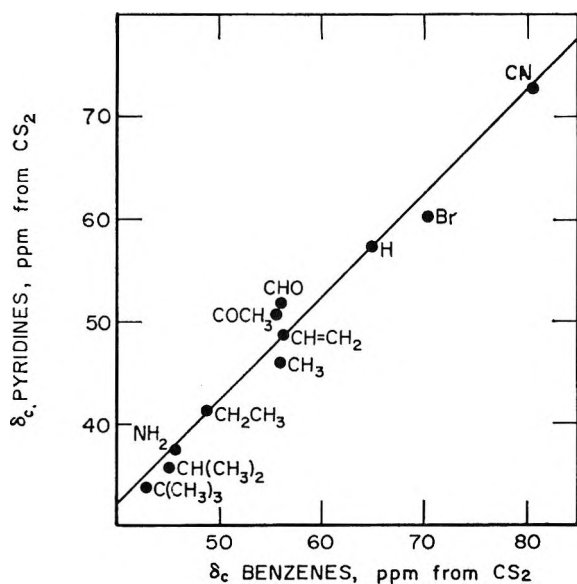


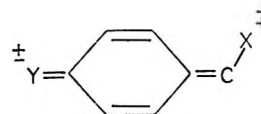
Figure 3. Magnetic shieldings of the carbon atoms *ortho* to substituents in 4-substituted pyridines and monosubstituted benzenes.

in 4-substituted pyridines, were not found to correlate with any single unique property of the substituents.

The pyridine shieldings are plotted against the corresponding benzene shieldings in Figures 2 and 3; only those for C-4 and CH-3 are considered since the total spread of CH-2 shieldings is only ± 1.1 ppm for the substituents investigated. The solid lines in the plot represent pyridine shieldings calculated using the substituent effects for monosubstituted benzenes and

assuming perfect additivity of these effects. The scatter of individual data, though in many cases larger than that expected from cumulative experimental errors, is not great (-2.4 ppm to $+3.5$ ppm), considering the total range of chemical shifts (35.4 ppm for C-4 and 18.0 ppm for CH-3). For *para*-disubstituted benzenes^{6,7,10} it was found that carbon shieldings are generally additive to $\sim \pm 2$ ppm even in cases in which a strongly electron-releasing group was pitted against a strongly attracting one. As was found for the *para*-disubstituted benzenes, except for the styrenes which represent a somewhat special case,⁷ deviations from additivity for the 4-substituted pyridines do not appear to be simply related to the electronic properties of the substituent. Nevertheless, the over-all pyridine data suggest, to a first approximation, that the shielding mechanisms in the pyridines are virtually the same as those in the benzenes. A similar conclusion regarding the proton shieldings has been reported by Wu and Dailey¹¹ from their study of nine 4-substituted pyridines. These authors also calculated HMO π -electron densities for the CH-2 and CH-3 carbons in these pyridines. In the present work it was found that the calculated charge densities are not simply related to the carbon shieldings. In this respect, it should be pointed out that recent theoretical interpretations of carbon shieldings suggest that the neglect of σ -electron densities is not warranted.^{12,13}

Other Carbon Shieldings. Carbonyl and Vinyl Carbons. It has been reported that substituent effects are not detectable in the shieldings of carbonyl and vinyl carbon atoms that are directly bonded to aromatic rings in *meta*- and *para*-substituted acetophenones,⁶ benzaldehydes,¹⁴ and styrenes.⁷ In contrast, a well-defined linear correlation was found to exist between Hammett's chemical reactivity parameters and the β -vinyl carbon shieldings in the styrene series.⁷ This has been explained on the basis of resonance hybrids such as



(as well as others) being important contributors to the electronic structures of these molecules in the ground

(10) G. B. Savitsky, *J. Phys. Chem.*, **67**, 2723 (1963).

(11) T. K. Wu and B. P. Dailey, *J. Chem. Phys.*, **41**, 3307 (1964).

(12) J. A. Pople, private communication.

(13) T. D. Alger, D. M. Grant, and E. G. Paul, *J. Am. Chem. Soc.*, **88**, 5397 (1966).

(14) J. B. Stothers and P. C. Lauterbur, *Can. J. Chem.*, **42**, 1563 (1964).

state since these indicate that the most pronounced changes in electron density of the substituent group C-X would occur at the nuclei located at the terminus of the resonance system. Evidence for a similar situation in the case of the 4-substituted pyridines is shown in Table III, which lists the shieldings of the carbons directly bonded to the unsaturated rings in 4-acetylpyridine, 4-pyridinecarboxaldehyde, and 4-vinylpyridine as well as those of the corresponding *para*-disubstituted benzenes. Good agreement is found in all three cases, suggesting that analogous resonance hybrids are important in the 4-substituted pyridines. Further evidence for this was obtained by using the Stothers correlation⁷ between the β -carbon shieldings in *para*-substituted styrenes and σ_p constants to evaluate a σ_p constant for the 4-pyridyl group. The resulting value 0.8 compares favorably with the kinetically obtained 0.93¹⁵ and with the 1.07¹⁵ calculated theoretically by Jaffé, although it must be pointed out that the nmr datum necessarily assumes that any transmission coefficient involved in the attenuation of electron release to the β -vinyl carbon by an intervening benzene ring is negligible. Nevertheless, the β -vinyl carbon shielding in 4-vinylpyridine (δ_c 74.8 ppm) is identical within

Table III: Carbonyl and α -Vinyl Carbon Shieldings in 4-Substituted Pyridines and *para*-Disubstituted Benzenes

X	δ_c , ppm	
	4-X-pyridine	1-Y,1-X-benzene ^a
COCH ₃	-4.1	-3.2 \pm 0.6 ^b
CHO	1.0	2.7 \pm 1.3 ^c
CH=CH ₂	58.3	58.7 \pm 2.5 ^d

^a Several Y groups of varying electronic properties were investigated. ^b Reference 6. ^c Reference 14. ^d Reference 7.

experimental error with that in 4-nitrostyrene⁷ indicating that the nitrogen atom in pyridine resembles electronically the CNO₂ group in nitrobenzene. This is often proposed.

Acetyl Methyl Carbon. The methyl carbon shielding in 4-acetylpyridine, δ_c 166.8 ppm, falls within the range δ_c 167 \pm 1.0 ppm reported for the corresponding carbons in a series of 15 *meta*- and *para*-substituted acetophenones.⁶

Nitrile Carbons. No extensive studies of carbon shieldings in organic nitrile groups have been reported and only one value appears in the literature.¹⁶ Table IV lists nitrile carbon shieldings for five compounds, four of which were measured in this laboratory. Little difference between the shieldings in benzonitrile and acetonitrile is evident, although the shielding in the

4-pyridyl compound is slightly higher than either of these. All three nitrile shieldings are considerably higher than those for the two ionic substances investigated.

Table IV: Representative Nitrile Carbon Shieldings

	δ_c
4-Cyanopyridine	76.2
Benzonitrile	74.1
Acetonitrile	73 ^a
(C≡N) ⁻ aqueous	27.0
K ₄ Mo(CN) ₆	40.3

^a Reference 16.

Alkyl Carbons. The alkyl carbon shieldings for the series 4-methyl, 4-ethyl, 4-isopropyl, and 4-*t*-butyl pyridines are all within experimental error of the average literature values^{6,8,17,18} for the corresponding shieldings in the alkyl benzenes. Increasing methyl substitution results in deshielding of both the α and β aliphatic carbons which parallels the normally accepted order of inductive effects of the alkyl groups. The α -carbon shieldings are not linearly related to the number of methyl substituents in either case, an effect which has tentatively been attributed by Savitsky¹⁷ to hyperconjugative interactions for the alkyl benzenes.

Spin-Spin Coupling Constants. The accuracy with which spin-spin coupling constants can be determined from rapid-passage dispersion mode spectra is of the order of \pm 3 cps; thus only pronounced variations can be detected. For the ring carbons the one-bond carbon-hydrogen couplings are 180 \pm 6 and 164 \pm 8 cps for CH-2 and -6 and CH-3 and -5, respectively. The corresponding values for pyridine, measured in the proton spectrum, are 179 and 163 cps.² The aldehydic coupling in 4-pyridinecarboxaldehyde is 130 cps, aliphatic couplings in the alkylpyridines fall in the range 125-129 cps, and the two vinyl couplings in 4-vinylpyridine are 165 and 167 cps for the internal and terminal positions, respectively.

Acknowledgment. The authors wish to thank F. R. McDonald for supplying many of the samples, G. P. Thompson for valuable technical assistance, and C. E. Griffin for helpful discussions.

(15) H. H. Jaffé, *J. Chem. Phys.*, **20**, 1554 (1952).

(16) P. C. Lauterbur, *ibid.*, **26**, 217 (1957).

(17) G. B. Savitsky and K. Namikawa, *J. Phys. Chem.*, **67**, 2430 (1963).

(18) W. R. Woolfenden and D. M. Grant, *J. Am. Chem. Soc.*, **88**, 1496 (1966).

Molecular Complexes of Aromatic Nitrile N-Oxides with Iodine, β -Naphthol, and Phenol

by Tanekazu Kubota, Masumi Yamakawa, Mamoru Takasuka,
Kouji Iwatani, Hideko Akazawa, and Itaru Tanaka

Shionogi Research Laboratory, Shionogi and Co., Ltd., Fukushima-ku, Osaka, Japan (Received April 10, 1967)

The 1:1 iodine complex of 2,4,6-trimethylbenzotrile N-oxide (TMBNO) was studied spectrophotometrically in CCl_4 solvent. Thermodynamic constants obtained were $K = 2.25$ l./mole (14.6°), $\Delta H = -3.87$ kcal/mole, and $\Delta S = -11.84$ eu. The visible iodine band shifted to $451 \text{ m}\mu$ upon complex formation. To compare the iodine complexing ability with the hydrogen bonding power, the following three-component systems were also studied by ultraviolet and infrared spectroscopic methods, and these thermodynamic constants were obtained: $K = 15.4$ l./mole (26.3°), $\Delta H = -4.90$ kcal/mole, and $\Delta S = -10.95$ eu for the system TMBNO + β -naphthol + CCl_4 (solvent); $K = 3.8$ l./mole (22.2°) for the phenol complex of TMBNO in CCl_4 ; and $K = \text{ca. } 2\text{--}5$ l./mole (21.2°) for the system 9-anthronitrile N-oxide + phenol + *n*-heptane. The above results are discussed on the basis of CT theory and on the basis of the analyses of the electronic and infrared spectra of nitrile N-oxides and their related compounds. The complexing ability of the nitrile N-oxides used in this study is considerably lower than that of the amine N-oxides such as pyridine N-oxide and trimethylamine N-oxide. This is attributed mainly to the π -type resonance interaction shown in Figure 1 and it is discussed in the text.

The charge transfer (CT) type complexes of aliphatic and aromatic tertiary amine N-oxides with iodine, phenol, naphthols, etc., were hitherto studied quantitatively by spectroscopic methods.¹ It was concluded that (i) the complexes are $n\text{-}\sigma$ type with the site of n -donor action at the oxygen atom, (ii) molecular complexing ability of aliphatic tertiary amine N-oxides such as trimethylamine N-oxide is greater than that of aromatic tertiary amine N-oxides such as pyridine N-oxide, and (iii) iodine complexing ability parallels hydrogen bonding power for a series of oxo compounds including tertiary amine N-oxides. The same fact has been pointed out experimentally and theoretically for other systems.²

The above results, especially (ii), were mainly ascribed to the fact that in the case of aliphatic tertiary amine N-oxides there is no π -conjugated system involving the $\text{N} \rightarrow \text{O}$ dative bond, so that the oxygen atom in the dative bond is surely more negative than that for the aromatic tertiary amine N-oxides, where the oxygen $2p\pi$ electrons can interact with the rest of the

π -electron system. Thus, n -donor action at the oxygen atom in the aliphatic type amine oxides is larger than that at the oxygen atom in the aromatic amine oxides, because a greater electron accumulation on the oxygen atom will increase the CT force.

From the above point of view, it would seem to be very interesting and valuable to study the molecular interaction of benzonitrile N-oxides with iodine and some proton donors in comparison with the usual tertiary amine N-oxides studied hitherto,¹ since aromatic nitrile N-oxides, which are a type of aromatic tertiary amine N-oxide, would seem to have a nature different from other common aliphatic and aromatic amine N-oxides such as trimethylamine oxide and

(1) (a) T. Kubota, *J. Am. Chem. Soc.*, **87**, 458 (1965); (b) T. Kubota, *ibid.*, **88**, 211 (1966), and other papers given therein.

(2) R. S. Mulliken, *J. Chim. Phys.*, **61**, 20 (1964); R. S. Mulliken and W. B. Person, *Ann. Rev. Phys. Chem.*, **13**, 107 (1962), and other papers given therein; H. Tsubomura, *J. Am. Chem. Soc.*, **82**, 40 (1960); V. G. Krishna and M. Chowdhury, *J. Phys. Chem.*, **67**, 1067 (1963).

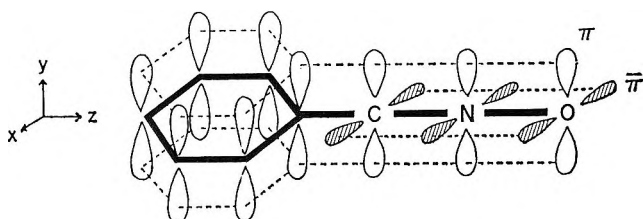
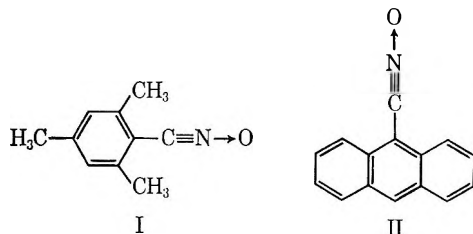


Figure 1. Schematic π -resonance systems of benzonitrile N-oxides.

pyridine oxide. This is because the π -conjugated system of these nitrile N-oxides can be pictured as in Figure 1, assuming that the oxygen atom is in the same plane as the rest of the π -system³ of benzonitrile, and that the $\text{>C}\equiv\text{N}\rightarrow\text{O}$ group has a linear configuration, which has been reasonably predicted.³ That is, of the three oxygen lone pair orbitals P_x , P_y , and σ_n , both P_x and P_y can enter into π -conjugation, so that a considerable decrease in net electronic charge on the oxygen atom is expected. Thus, the predicted intermolecular interaction ability of the nitrile oxides seems to be less than for other kinds of N-oxides reported hitherto.¹ In this paper, iodine and hydrogen bonding complexing abilities of 2,4,6-trimethylbenzonitrile N-oxide (TMBNO)⁴ (I) and 9-anthronitrile N-oxide (ANO) (II) are investigated quantitatively and the results are discussed and compared with other spectral and thermodynamic data so far reported.



Experimental Section

Materials. 2,4,6-Trimethylbenzonitrile N-oxide was prepared by the reaction of 2,4,6-trimethylbenzaloxime with NaOBr at low temperature ($\sim -10^\circ$), as was reported by Grundmann,⁵ then recrystallized several times with methanol or diethyl ether: nonhygroscopic colorless needles, mp $111\text{--}112^\circ$, were obtained. The elementary analyses of C, N, and H agreed well with the calculated values. (*Anal.* Calcd: C, 74.51; H, 6.88; N, 8.69. Found: C, 74.37; H, 6.92; N, 8.66.) This compound was always kept in a desiccator protected from light, stored in the refrigerator, and was recrystallized just before use. The infrared spectrum in CCl_4 gave characteristic bands of strong intensity at 2289 and 1355 cm^{-1} , and the chemical properties of this nitrile oxide agreed with Grundmann's descrip-

tion,⁶ for example, deoxygenation with $(\text{CH}_3\text{O})_3\text{P}$ easily led to the 2,4,6-trimethylbenzonitrile with good yield. The starting material, 2,4,6-trimethylbenzaloxime (mp $124\text{--}126^\circ$: mixture of the *syn* and *anti* forms) was synthesized by the well-known method: the reaction of hydroxylamine with the corresponding aldehyde, which was prepared according to the method reported by Fuson, *et al.*⁷

9-Anthronitrile N-oxide was also prepared by the reaction of 9-anthroaloxime with NaOBr,⁵ then recrystallized several times from methanol until elementary analyses of C, N, and H were in good agreement with the calculated values. (*Anal.* Calcd: C, 82.18; H, 4.14; N, 6.39. Found: C, 81.99; H, 4.24; N, 6.37.) The product was nonhygroscopic, crystalline, with mp $128.5\text{--}129.5^\circ$. Deoxygenation with $(\text{CH}_3\text{O})_3\text{P}$ also gave 9-anthronitrile with quite a good yield.⁶ Infrared spectra showed obviously strong bands at 2286 , 1382 , and 1299 cm^{-1} . This nitrile oxide was always kept in a desiccator protected from light, stored in a refrigerator, and recrystallized just before use. Starting material, 9-anthroaloxime (mp $163\text{--}164^\circ$: recrystallized from ethanol) was prepared by the common reaction of hydroxylamine with the corresponding aldehyde (mp $103\text{--}104^\circ$: recrystallized from glacial acetic acid), which was synthesized by the method recommended by Fieser.⁸

Phenol of special pure grade obtained from Wako Junyaku Co. was distilled twice under reduced pressure ($\sim 24\text{ mm Hg}$), and the middle portion (bp $94.5\text{--}95.5^\circ$) of the last distillate was used for the experiment and was kept in a desiccator.

β -Naphthol of special pure grade obtained from Wako Junyaku Co. was recrystallized from aqueous ethanol, then recrystallized twice from ligroin: mp $122.0\text{--}122.8^\circ$.

Iodine of special pure grade obtained from Wako Junyaku Co. was sublimed twice under reduced pres-

(3) Quite recently, these predictions were confirmed by the X-ray analyses of 2,4,6-trimethylbenzonitrile N-oxide, etc. M. Shiro, *et al.*, paper presented at the 20th annual meeting of the Chemical Society of Japan, Tokyo, April 1967.

(4) Although benzonitrile N-oxide seems to be better for the present purpose, this compound is not so stable at room temperature and undergoes transformation into furoxan, so that we could not employ this one.

(5) G. Grundmann and J. M. Dean, *Angew. Chem. Intern. Ed.*, **3**, 585 (1964).

(6) C. Grundmann and H. D. Frommelt, *J. Org. Chem.*, **30**, 2077 (1965).

(7) R. C. Fuson, E. C. Horning, S. P. Rowland, and M. L. Ward, "Organic Syntheses," Coll. Vol. 3, John Wiley and Sons, Inc., New York, N. Y., 1962, p 549.

(8) L. F. Fieser, J. L. Hartwell, and J. E. Jones, "Organic Syntheses," Coll. Vol. 3, John Wiley and Sons, Inc., New York, N. Y., 1962, p 98.

sure and was kept in a desiccator protected from the light.

Solvents used were carbon tetrachloride and *n*-heptane. Spectrograde carbon tetrachloride purchased from Merck Co. was dried sufficiently with CaCl_2 , then subjected to a rectifying distillation using a good efficient column. Phillips pure grade (99 mole % minimum) *n*-heptane was shaken with concentrated H_2SO_4 and fuming H_2SO_4 , then with water, dilute NaOH , and again with water. After distillation, it was dried over sodium wire and distilled using a good efficient column through a chromatographic tube packed with active alumina.

Method. A Beckman Model DK-2A spectrophotometer equipped with a temperature-regulated cell holder was used for recording the visible and ultraviolet absorption spectra. A temperature constant to within $\pm 0.5^\circ$ was maintained by circulating water from a thermostat through the cell holder. Dry nitrogen gas was flushed through the spectrophotometer during the recording of the spectra below room temperature to prevent the condensation of atmospheric moisture inside the spectrophotometer sample compartment. The cells used were 1-cm matched quartz cells equipped with stoppers and 0.1-cm quartz cells. Two kinds of 0.1-cm cell were used: one was a sandwich-type cell available from Beckman and the other was made by inserting a quartz spacer in the matched 1.00-cm cell.⁹ Infrared spectra were measured using two Nihon Bunko spectrometers: one was a high-resolution Model DS-402-G which was employed for the hydrogen bonding study of phenol with TMBNO using a 0.5-cm NaCl cell,¹⁰ and the other was a Model DS-201-B, with which the spectral region $600\text{--}4000\text{ cm}^{-1}$ was recorded.

All of the sampling and measurements were made in a well air-conditioned room. Also, to minimize hydration effects on the experimental results, the flasks, pipets, absorption cell, etc., were flushed with a jet of N_2 gas before use.

Stability of the Complexes. Under the experimental conditions employed here, the iodine and the hydrogen bonding complexes with TMBNO are stable. The absorption spectra of the mixed solutions were reproduced within 1% several hours after the preparation of sample solutions. The same stability as was mentioned above was also observed on the hydrogen bonding complex of 9-anthronitrile N-oxide with phenol. All measurements of the spectra were made within 1 hr at most after preparation of the mixed solutions.

Results

Spectral and Thermodynamic Constants of the Iodine and Hydrogen Bonding Complexes with 2,4,6-Trimethylbenzonitrile N-Oxide. As is shown in Figure 2, the

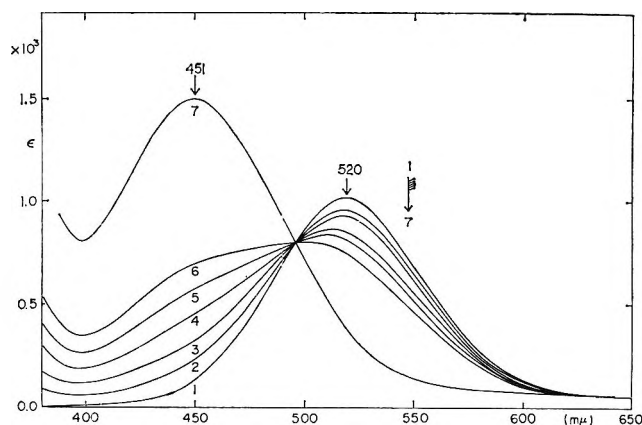


Figure 2. The visible absorption spectra of iodine-2,4,6-trimethylbenzonitrile N-oxide in CCl_4 (1-cm cell, 14.6°). Curve 1 is for iodine, 9.413×10^{-4} mole/l. The concentrations of the nitrile N-oxide are 3.51×10^{-2} , 7.03×10^{-2} , 14.1×10^{-2} , 21.1×10^{-2} , and 31.6×10^{-2} mole/l. for curves 2, 3, 4, 5, and 6, respectively. Curve 7 is for the absorption due solely to the complexed iodine molecule.

iodine visible band with an absorption maximum at $520\text{ m}\mu$ in CCl_4 showed a blue shift upon addition of a considerable amount of TMBNO, and there is obviously a fine isosbestic point. These results indicate that there are two absorbing species which could be complex and uncomplexed iodine, and that the complex is in equilibrium with the uncomplexed iodine. The same behavior is also clearly visible in Figure 3, where the ${}^1\text{L}_b$ band¹ of β -naphthol in *n*-heptane was shifted to a longer wavelength by adding a considerable amount of TMBNO. Since the experimental conditions yielding Figures 2 and 3 completely satisfy the necessary relationship (the concentration (C_D^0) of the electron donor (TMBNO) is much larger than that (C_A^0) of electron acceptors (I_2 or β -naphthol)), we can safely apply the well-known eq 1^{1,11} to calculate the equilibrium constant K defined by eq 2.

$$\epsilon = \frac{1}{K} \left(\frac{\epsilon_A - \epsilon}{C_D^0} \right) + \epsilon_{DA} \quad (1)$$

$$K = C_{DA} / (C_D^0 - C_{DA})(C_A^0 - C_{DA}) \quad (2)$$

Here ϵ_A and ϵ_{DA} are the molecular extinction coefficients of the electron acceptor and of the complex, respectively, while ϵ is an apparent extinction coefficient of the electron acceptor calculated using the C_A^0 at a

(9) In this case, special care described in previous papers¹ was also taken.

(10) Since this nitrile oxide exhibits a weak overtone band at 3623 cm^{-1} , we could not use much longer cells.

(11) T. Kubota, M. Yamakawa, and Y. Mori, *Bull. Chem. Soc. Japan*, **36**, 1552 (1963).

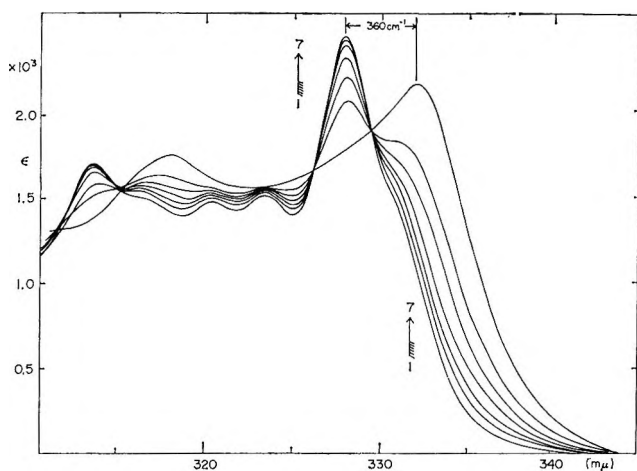


Figure 3. The near-ultraviolet absorption spectra of β -naphthol-2,4,6-trimethylbenzonitrile N-oxide in *n*-heptane (1-cm cell, 16.0°). Curve 1 is for β -naphthol, 3.09×10^{-4} mole/l. The concentrations of the nitrile N-oxide are 4.56×10^{-3} , 9.12×10^{-3} , 1.82×10^{-2} , 3.65×10^{-2} , and 7.29×10^{-2} mole/l. for curves 2, 3, 4, 5, and 6, respectively. Curve 7 is for the absorption due solely to the hydrogen-bonded β -naphthol.

suitable wavelength. The linear relation of ϵ vs. $(\epsilon_A - \epsilon)/C_D^0$ was well satisfied for the experiments shown in Figures 2 and 3. The evaluated K values are included in Table I, and in Table II are shown the heats of formation (ΔH) of the complexes, which were obtained from the temperature dependence of K values shown in Table I by applying the familiar formula; $R \ln K = -\Delta H(1/T) + \Delta S$; here the plot of $R \ln K$ vs. $(1/T)$ closely approached a straight line. In Figures 2 and 3, the spectrum due solely to the complex itself was also given. These were calculated at various wavelengths using eq 1, the known values of ϵ_A and ϵ , and the average value of K reported in Table I. The values of the oscillator strength f^{12} and transition moment $M^{1,13}$ were also calculated from the spectrum of the complex itself for the I_2 -TMBNO complex (see Figure 2 and Table II). For the system shown in Figure 3, the above spectroscopic constants could not be obtained because a considerable overlap of the spectrum of each component (β -naphthol and TMBNO) occurs in the wavelength region less than 310 $m\mu$, so that only the band shift caused by the hydrogen bonding was accurately obtained, as is seen in Figure 3. The results are collected in Table II.

Identification of the CT band pertinent to the iodine complex of TMBNO was next tried in CCl_4 solvent. As will be reported in other papers,¹⁴ TMBNO absorbs strongly from $\sim 300 m\mu$ to shorter wavelengths, so we have tried the measurement under the following condition: the ultraviolet spectra of mixed solutions con-

Table I: Equilibrium Constants Obtained at Different Wavelengths^a and Temperatures

A. Iodine Complex with 2,4,6-Trimethylbenzonitrile N-Oxide in CCl_4 ^b

Temp, °C	K , l./mole (ϵ , l./mole cm)			Δv
	450 $m\mu$	460 $m\mu$	470 $m\mu$	
4.5	2.73 (1630)	2.84 (1510)	3.14 (1250)	2.90
6.6	2.55 (1650)	2.62 (1530)	2.88 (1300)	2.68
14.6	2.24 (1490)	2.27 (1430)	2.23 (1310)	2.25
23.6	1.73 (1620)	1.78 (1390)	2.00 (1160)	1.84
30.9	1.59 (1330)	1.40 (1440)	1.89 (1160)	1.62
42.4	1.31 (1200)	1.12 (1320)	1.21 (1200)	1.21

B. Hydrogen Bonding Complex of 2,4,6-Trimethylbenzonitrile N-Oxide with β -Naphthol in *n*-Heptane

	332.5 $m\mu$	334 $m\mu$	335 $m\mu$	Δv
5.0	29.9 (2360)	27.8 (2070)	...	28.9
11.6	21.5 (2570)	22.8 (2220)	22.2 (1750)	22.2
16.0	23.4 (2230)	19.3 (2050)	...	21.3
26.3	16.6 (2430)	14.3 (2170)	...	15.4
31.2	13.5 (2120)	12.9 (1870)	12.9 (1410)	13.1

C. Hydrogen Bonding Complex of 9-Anthronitrile N-Oxide with Phenol in *n*-Heptane

	413 $m\mu$	407 $m\mu$	382 $m\mu$	Δv
21.2	5.2	2.9	2.3	3.5

D. Hydrogen Bonding Complex of 2,4,6-Trimethylbenzonitrile N-Oxide with Phenol in CCl_4

	3462 cm^{-1}	3429 cm^{-1}	3401 cm^{-1}	Δv
22.2	4.21	3.93	3.24	3.81

^a The large change in intensity was observed at these wavelengths. Data shown above were derived by treating the observed values with the least-squares method except for the case of the system C, where the K values were not so well reproduced (see also footnote 19 in text). However, K values were always within 2-5. ^b Spectral changes for systems A, B, C, and D are, respectively, for the iodine visible band, the 1L_b band of β -naphthol, the 1L_a band of 9-anthronitrile N-oxide, and the OH stretching band of phenol.

posed of a constant concentration of TMBNO and variable iodine concentrations are recorded using thin cells. Unfortunately, however, the K values for the present system (see Table I) are very small, requiring a quite high iodine concentration (>0.1 mole/l.) for the present purpose. That is, the small value of K , ab-

(12) The calculation was approximately carried out by means of the equation, $\int \epsilon \cdot d\bar{\nu} \approx \epsilon_{\max} \cdot \Delta\bar{\nu}^{1/2}$, where $\Delta\bar{\nu}^{1/2}$ is the half-width of the band in cm^{-1} .

(13) H. Tsubomura and R. P. Larg, *J. Am. Chem. Soc.*, **83**, 2085 (1961).

(14) M. Yamakawa, T. Kubota, and H. Akazawa, *Bull. Chem. Soc. Japan*, **40**, 1600 (1967).

Table II: Thermodynamic and Spectral Data of CT Type Molecular Complexes with Tertiary Amine N-Oxides

Iodine Complexes								
Compound	Solvent	K, l./mole (temp, °C)	-ΔH, kcal/mole	Shifted I ₂ band				Ref
				λ _{max}	ε _{DA,max} (temp, °C)	f ^a	M ^a	
Trimethylamine N-oxide	CH ₂ Cl ₂	5660 (22)	10.0	391-392	2810 (22)	0.058	2.19	c
Tribenzylamine N-oxide	CH ₂ Cl ₂	3470 (20)	10.5	393-394	2580 (20)	0.054	2.12	c
Pyridine N-oxide	CCl ₄	77.9 (23)	5.85	441	1860 (23)	0.033	1.75	c
N-Methylbenzaloxime	CCl ₄	35.8 (15)	5.25	446	2180 (15)	0.039	1.93	c
2,4,6-Trimethylbenzoxime N-oxide	CCl ₄	2.25 (14.6)	3.87 ± 0.3	451	1490 (14.6)	0.029 ^b	1.67	d
			(ΔS = -11.84 eu)					
Hydrogen Bonding Complexes								
Compound	Proton donor	Solvent	K, l./mole (temp, °C)	-ΔH, kcal/mole	Δν, cm ⁻¹			
						Ref		
Trimethylamine N-oxide	{ Phenol β-Naphthol	CH ₂ Cl ₂	3680 (20.5)	7.9	~648 ^f	e		
		CH ₂ Cl ₂	6560 (20.7)	...	657 ^f	e		
Quinoline N-oxide	Phenol	CCl ₄	146 (26.7)	5.1	...	h		
			158 (26.7)	5.7	...			
Acridine N-oxide	Phenol	n-Heptane	140 (26.0)	i		
2,4,6-Trimethylbenzoxime N-oxide	{ Phenol β-Naphthol	CCl ₄	3.81 (22.2)	...	183 ^g	d		
		n-Heptane	15.4 (26.3)	4.9 ± 0.3	360 ^f	d		
			(ΔS = -10.95 eu)					
9-Anthronitrile N-oxide	Phenol	n-Heptane	2 ~ 5 (21.2)	d		

^a See text and footnote 12. ^b The value 4560 cm⁻¹ of Δν_{1/2} for the calculation of f^a was obtained assuming that on a scale linear in energy (cm⁻¹), the short wavelength side of the absorption peak is symmetrical to that of the long wavelength side of the absorption, an assumption made in a previous paper. ^c Footnote 1a in text. ^d Present work. ^e Footnote 1b in text. ^f Shift of the longest wavelength peak of ¹L_b band. ^g Shift of OH stretching vibration band of phenol. ^h T. Kubota, *J. Pharm. Sci. Japan*, **74**, 831 (1954); **75**, 1540 (1955). ⁱ T. Kubota and H. Miyazaki, *J. Chem. Soc. Japan, Pure Chem. Sect.*, **79**, 916 (1958).

sorption due to I₄, and the limited solubility of iodine are limiting factors in determining the position of the CT peak. However, after various experiments, it can be stated that the wavelength of the peak is below 310 mμ.

The hydrogen bonding complex of TMBNO with phenol was also studied by recording the OH stretching frequency (ν_{OH}) for the system TMBNO + phenol + CCl₄. The result is shown in Figure 4. However, the change of the electronic spectra of phenol due to the hydrogen bonding with TMBNO could not be measured because of the strong overlap of both the absorption bands. Under the experimental conditions indicated in Figure 4, unfortunately, the relation C_D⁰ ≫ C_A⁰ or C_D⁰ ≪ C_A⁰ is not satisfied, so we cannot apply eq 1 to get the equilibrium constant K. However, it was easily predicted that the K value for the present system is quite small (K ≲ 5), and some order estimations led to the conclusion that the term (C_{AD})² is negligible in value compared with the other quantities. Moreover, the hydrogen-bonded ν_{OH} band is almost completely separated from that of free ν_{OH}, so the above conditions did allow us to employ the Andrews and Keefer equa-

tion,¹⁵ eq 3, to evaluate the K value. Here the relation C_{AD} = D_{AD}/ε_{AD}l was used, where D_{AD} is the optical density owing to the complex DA and l is the cell length.

$$\frac{C_D^0 C_A^0}{D_{AD}(C_D^0 + C_A^0)} = \frac{1}{K \epsilon_{AD} l} \frac{1}{(C_D^0 + C_A^0)} + \frac{1}{\epsilon_{AD} l} \quad (3)$$

The plot of C_D⁰C_A⁰/D_{AD}(C_D⁰ + C_A⁰) against 1/(C_D⁰ + C_A⁰) gave a straight line at 3462, 3429, and 3401 cm⁻¹. The K values thus obtained are listed in Table I.

Spectral Behavior of 9-Anthronitrile N-Oxide Caused by the Hydrogen Bonding with Phenol, and the K Value.

The hydrogen bonding interaction was also studied for the system ANO + phenol + n-heptane (solvent), where attention was directed to the spectral change of ANO upon addition of phenol. In Figure 5 is shown the experimental result. We can see there that the band, the character of which is clearly ¹L_a¹⁶ with probably a

(15) L. J. Andrews and R. M. Keefer, *J. Am. Chem. Soc.*, **75**, 3776 (1953).

(16) Platt's notation was used: J. R. Platt, *J. Chem. Phys.*, **17**, 484 (1949).

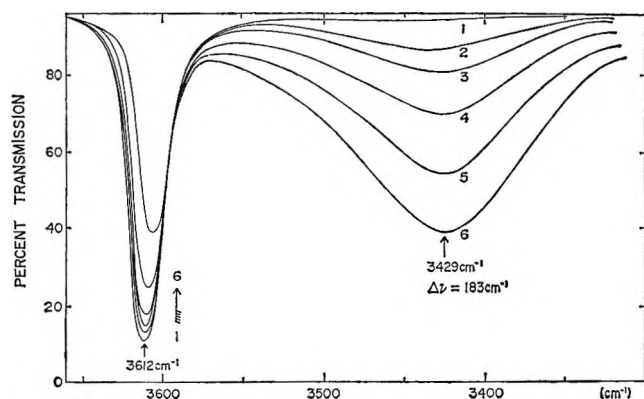


Figure 4. The lower frequency shift of the OH stretching band of phenol caused by hydrogen bond formation with 2,4,6-trimethylbenzotrile N-oxide in CCl_4 (5-mm cell, 22.2°). Curve 1 is for phenol, 1.081×10^{-2} mole/l. The concentrations of 2,4,6-trimethylbenzotrile N-oxide are 1.03×10^{-2} , 2.07×10^{-2} , 4.14×10^{-2} , 8.28×10^{-2} , and 16.55×10^{-2} mole/l. for curves 2, 3, 4, 5, and 6, respectively.

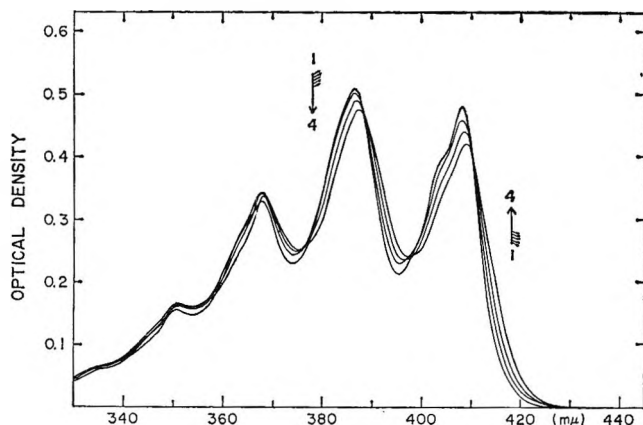


Figure 5. The near-ultraviolet absorption spectra of anthronitrile N-oxide-phenol in *n*-heptane (1-cm cell, 21.2°). Curve 1 is for anthronitrile N-oxide, 4.015×10^{-5} mole/l. The concentrations of phenol are 4.30×10^{-2} , 8.59×10^{-2} , and 17.18×10^{-2} mole/l. for curves 2, 3, and 4, respectively.

hidden weak 1L_b component, shows a slight red shift with the addition of phenol.^{17,18} Since the spectral change of ANO occurs only at relatively high concentrations of phenol as is seen in Figure 5, the condition for eq 1 is now satisfied, and the apparent K values¹⁹ were calculated. However, the scatter of each point from the linear plot expected from eq 1 was larger¹⁹ than in other systems described in the preceding chapter, so that the accuracy of the apparent K values was less than in other systems. The apparent K values obtained at different wavelengths were within about 2-5; the values are shown in Table I. These K values

would be of the same order of magnitude as those obtained by the infrared spectral method for the hydrogen bonding of phenol with TMBNO as was mentioned before, where hydrogen bond formation was verified by the shift of the OH stretching frequency. Now it may be said that the hydrogen bonding effect of phenol on ANO would be a main factor to bring about the spectral change of ANO shown in Figure 5.

Discussion

CT Type Complex Formation Ability of Nitrileoxides. As is clearly seen from Tables I and II, both the values K and ΔH pertinent to the iodine and hydrogen bonding complex formations of nitrile N-oxides used here are smaller than those for the other kinds of tertiary amine N-oxides such as pyridine N-oxide and trimethylamine N-oxide.¹ In connection with these results, it should be noted that the CH_3 groups which occupy two positions *ortho* to the $\text{C}\equiv\text{N}\rightarrow\text{O}$ group in TMBNO do not exercise steric hindrance on the whole conjugated system.^{3,20} Here the oxygen atom in the $\text{C}\equiv\text{N}\rightarrow\text{O}$ group acts as the active site for complex formation.²¹ This

(17) This behavior seems to be a little different from that expected, because the $\pi\text{-}\pi^*$ type strong bands, especially the longest wavelength band, of many heterocyclic N-oxides, aromatic nitrones, TMBNO and its homologs, and also $n\text{-}\sigma^*$ band of trimethylamine N-oxide, etc., shift more or less to shorter wavelength with hydrogen bonding interaction or in solvents such as alcohols, water, etc., as has already been discussed from the viewpoint of the electronic structures.^{14,18} Nevertheless, it is not unusual that this solvent effect (hydrogen bonding) on the electronic spectra of nitrile oxides is weaker than in other type N-oxides mentioned above.¹⁸ In fact, the ANO 1L_b band lies at 408.3, 386.5, 367.3 $m\mu$, 407.8, 386.7, 366.9 $m\mu$, and 408.6, 386.2, 366.0 $m\mu$ in *n*-heptane, alcohol, and water, respectively. The discussion will be presented in a forthcoming paper.¹⁴

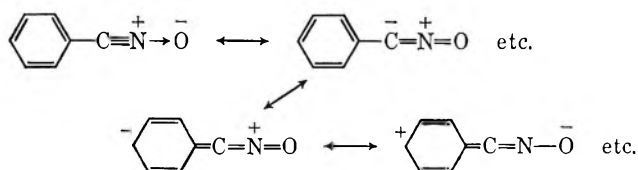
(18) (a) T. Kubota and H. Miyazaki, *Chem. Pharm. Bull.* (Tokyo), **9**, 948 (1961); (b) T. Kubota and M. Yamakawa, *Bull. Chem. Soc. Japan*, **35**, 555 (1962); **36**, 1564 (1963); (c) T. Kubota, M. Yamakawa, and I. Tanaka, *J. Mol. Spectry.*, **20**, 226 (1966).

(19) It is remembered that Person (W. B. Person, *J. Am. Chem. Soc.*, **87**, 167 (1965)) examined the experimental conditions to get the reliable K values of weak 1:1 CT complexes. Various concentrations of phenol adopted here satisfied the above conditions. Under the present conditions, however, it seems that the phenol engages in some self-association. This factor was disregarded in obtaining the apparent K values. In addition, the spectral change brought about by adding the phenol is small. These factors probably cause the scatter of each point from the linear relation expected from eq 1.

(20) This same conclusion was also derived from the interpretation of the electronic spectrum of mesitoyl cation: S. Nagakura, K. Fukui, and Z. Yoshida, Ed., "Organic Quantum Chemistry," Kagakudojin, Kyoto, 1966, p 151 (in Japanese). See also H. Hosoya and S. Nagakura, *Spectrochim. Acta*, **17**, 324 (1961).

(21) This was also verified from the infrared spectroscopic study. The N-oxide stretching band ($\bar{\nu}_{\text{NO}}$) of pyridine N-oxide and other N-oxides is sensitive to the formation of iodine and hydrogen bonding complexes with the oxygen atom of the $\text{N}\rightarrow\text{O}$ bond, and shifts strongly to lower frequency ($\sim 40\text{ cm}^{-1}$). The same phenomena were observed for the present systems with the results that, for instance, $\Delta\bar{\nu}_{\text{NO}}$ is, respectively, 15 and 16 cm^{-1} for 1:1 complex formation of iodine with TMBNO and 2,6-dimethylbenzotrile N-oxide in CS_2 solvent, where the other bands show only a slight intensity change with complex formation: T. Kubota, K. Ezumi, M. Yamakawa, and Y. Matsui, *J. Mol. Spectry.*, in press.

weak complex formation ability of nitrile N-oxides is now attributed to the fact mentioned in the Introduction. That is, since there are two π -conjugated systems, π and $\bar{\pi}$ systems, in nitrile N-oxides as is shown in Figure 1, a considerable decrease of the net charge on the oxygen atom in question is expected, so that the n-type electron donor ability is decreased compared with that of the other kinds of N-oxides. Concerning this problem, it is valuable to point out that the electronic spectra of, for example, substituted benzonitrile N-oxides were quite different from those of the corresponding nitriles. In other words, the above nitrile N-oxides show a red shift of the 1L_b band of the corresponding nitriles and also have a strong π - π^* band in the near-ultraviolet region, where the corresponding nitriles do not show any strong bands.^{14,22} Moreover, infrared spectroscopic studies of nitrile N-oxides were recently carried out by us and other authors.^{23,24} Beck and Feldl²⁵ quite recently reported the molecular structure of fulminic acid, the simplest nitrile N-oxide $H-C\equiv N\rightarrow O$, based on the analyses of its infrared spectrum in the gas phase. This report shows that the molecule $H-C\equiv N\rightarrow O$ may be considered as pseudo-dinitrogen oxide ($N\equiv N\rightarrow O$) from the considerable volume of analogous spectral data of these two molecules. Thus, fulminic acid could well be described by the resonance formulas $H-C\equiv N\rightarrow O \leftrightarrow H-C=N=O$, etc.²⁵ When infrared spectra of substituted benzonitrile N-oxides, ANO, etc., were recorded, we always observed two strong bands in the regions 2280–2300 and 1330–1390 cm^{-1} . The former is doubtlessly due to the $C\equiv N$ stretching band $\bar{\nu}_{C\equiv N}$ and the latter would be assigned to the N–O stretching band $\bar{\nu}_{N-O}$. There is no obvious band in the corresponding nitriles,²³ although the above two bands seem to be coupled to each other. This conclusion was also given by Califano, *et al.*,²³ and is consistent with that for the $H-C\equiv N\rightarrow O$ molecule mentioned above.²⁵ This $\bar{\nu}_{N-O}$ is significantly higher than ν_{N-O} ($\approx 940\text{ cm}^{-1}$) of the aliphatic tertiary amine N-oxides²⁶ and also is higher than $\bar{\nu}_{N-O}$ (1264 cm^{-1} in CCl_4) of pyridine N-oxide.²⁷ It now seems to be confirmed that the resonance forms shown below are reasonable.



From the viewpoint of molecular orbital (MO) theory,²² the aforementioned resonance forms will be formally expressed as in Figure 1.²⁸ They are prob-

ably responsible for the weak complexing ability of the oxygen atom in nitrile oxides as was discussed earlier.

In addition to the main conclusion for the weak complexing ability of the $-C\equiv N\rightarrow O$ group mentioned above, we derive the same conclusion by focusing attention on the $N\rightarrow O$ σ bond itself, although the following seems not to be an important factor. It is reasonable that the N atom donor σ orbital in the $N\rightarrow O$ dative bond is sp , sp^2 , and sp^3 hybridized ones for $\equiv N\rightarrow O$ (nitrile oxide), $\gtrsim N\rightarrow O$ (pyridine oxide), and $\gtrsim N\rightarrow O$ (trimethylamineoxide) bonds, respectively. As is well known, the electronegativity of the atom, whose σ -hybridized orbital participates in a σ -bond formation, increases with the increasing s character of the hybridized orbital in question.²⁹ Then, σ -bonding electrons in $\equiv N\rightarrow O$ bond will be more attracted toward the nitrogen atom, resulting in the decrease of n-type donor ability of the oxygen atom. For this same reason, the H atom in the $\equiv C-H$ bond has a larger acidic nature compared with the H atoms in $\gtrsim C-H$ and $\gtrsim C-H$ bonds.^{29,30} Moreover, it has been verified that the overlap charge between ϕ_{2s}^N and $\phi_{2p_z}^O$ atomic orbitals is displaced toward the atom that presents the 2s orbital,³¹ because the 2s orbital is smaller than the

(22) To be published later in detail from the experimental and theoretical points of view. As an example, TMBNO and 2,4,6-trimethylbenzonitrile exhibit the following absorption bands in *n*-heptane: 294.2 $m\mu$ (ϵ 667), 269.8 (12,800), 262.7 (15,000), 219.9 (26,900), 214.7 (26,100), and 198.4 (37,300) for the former, and 288.3 (1270), 284.0 (922), 278.3 (999), 236.3 (12,300), 208.5 (56,100), and 204.0 (53,100) for the latter. Data similar to the above were also obtained for the other substituted benzonitrile N-oxides.

(23) S. Califano, R. Moccia, R. Scarpati, and G. Speroni, *J. Chem. Phys.*, **26**, 1777 (1957).

(24) R. H. Wily and B. J. Wakefield, *J. Org. Chem.*, **25**, 546 (1960).

(25) W. Beck and K. Feldl, *Angew. Chem. Intern. Ed.*, **5**, 722 (1966).

(26) Y. Matsui and T. Kubota, *J. Chem. Soc. Japan, Pure Chem. Sec.*, **83**, 985 (1962); P. A. Giguere and D. Chin, *Can. J. Chem.*, **39**, 1214 (1961); D. Cook, *ibid.*, **41**, 1127 (1963); Y. Kuroda and M. Kimura, *Spectrochim. Acta*, **22**, 47 (1966).

(27) H. Shindo, *Chem. Pharm. Bull. (Tokyo)*, **7**, 791 (1959); A. R. Katritzky, "Physical Methods in Heterocyclic Chemistry," Vol. II, Academic Press, Inc., New York, N. Y., 1963, p 283.

(28) It was recently shown that the isocyanate group would also have the character of a triple bond based on the calculation by extended Hückel method; H. Kato and T. Yonezawa, private communication.

(29) C. A. Coulson, "Valence," Oxford University Press, London, 1953, p 207.

(30) S. Walker and H. Straw, "Spectroscopy II (Ultraviolet, Visible, Infrared, and Raman Spectroscopy)," Chapman and Hall, Ltd., London, 1962, p 141.

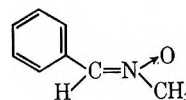
(31) Defining that ϕ_{2s}^N and $\phi_{2p_z}^O$ are the σ -atomic orbitals of N and O atoms having the effective nuclear charge parameter $\bar{h} = 1/2(h_N + h_O)$.^{18c} This approximation is reasonable for the $N\rightarrow O$ dative bond.^{18c} The calculation of the two center integral $\langle \phi_{2s}^N | Z | \phi_{2p_z}^O \rangle$ at an $N\rightarrow O$ bond distance of 1.388 Å shows that the center of gravity of the electrons is at ~ 0.1 Å toward the nitrogen atom from the center of the $N\rightarrow O$ bond. See also C. A. Coulson and M. T. Rogers, *J. Chem. Phys.*, **35**, 593 (1961), and the tables (ADI 6817) deposited by them into the Library of Congress, Photoduplication Service, Washington, D. C. 20540.

2p orbital. From this viewpoint, and since the s character of the nitrogen σ -donor orbital in the $\equiv\text{N}\rightarrow\text{O}$ bond is larger than that of the other kinds of $\text{N}\rightarrow\text{O}$ bonds, it would follow that the oxygen atom in the $\text{C}\equiv\text{N}\rightarrow\text{O}$ bond has lower basicity than in other kinds of N -oxides.³¹

Spectroscopic Behavior of the CT Type Complexes with Nitrile N-Oxides and the Comparison of Thermodynamic Constants of Hydrogen Bonding and Iodine Complexes. First let us consider the iodine complexes with TMBNO. As is seen from Table II the values of the spectral constants pertinent to the shifted I_2 band (*i.e.*, band position, oscillator strength, f , and transition moment, M) are parallel to the corresponding thermodynamic values among the three kinds of tertiary amine N -oxides. This result follows reasonably from CT theory. It should be especially noted that K and ΔH values obtained for the TMBNO- I_2 complex are quite small and are of the same order as the values for the I_2 complexes with ethyl ether ($K = 1.16$ l./mole (20°), $\Delta H = -4.2$ kcal/mole in *n*-heptane)³² and benzonitrile ($K = 0.8$ l./mole (20°) in CCl_4).³³ The fact that the CT band peak of the benzonitrile- I_2 complex has been estimated to be in the wavelength region less than $300 \text{ m}\mu$ ³³ is consistent with the present result that the CT peak due to the TMBNO- I_2 complex will appear at a wavelength less than $310 \text{ m}\mu$.

Next, attention should be paid to the hydrogen bonding complexes of nitrile oxides employed here. It is now clear from Tables I and II that the TMBNO and ANO have weaker hydrogen bonding ability than other kinds of tertiary amine N -oxides. At the same time, the red shift (360 cm^{-1}) of the β -naphthol $^1\text{L}_b$ band brought about by the hydrogen bonding with TMBNO is also small and is compatible with values for acetonitrile (200 cm^{-1})³⁴ and ethyl ether (410 cm^{-1}),³⁵ but is much smaller than that of trimethylamine N -oxide (657 cm^{-1})^{1b} and triethylamine (590 cm^{-1}).³⁵ The same conclusion was also derived from the following observation: the smaller frequency shift $\Delta\bar{\nu}_{\text{OH}}$ of the OH stretching bands of methanol caused by the hy-

drogen bonding with TMBNO, CH_3CN ,³⁶ and benzonitrile³⁶ were, respectively, 58, 78, and 73 cm^{-1} in CCl_4 . These values should be compared with $\Delta\bar{\nu}_{\text{OH}} = 238 \text{ cm}^{-1}$, which was obtained for the system¹¹ $\text{CH}_3\text{-OH} + \text{N-methylbenzaldoxime}^{37} + \text{CCl}_4$. Moreover,



the shift $\Delta\bar{\nu}_{\text{OH}}$ for the system phenol + TMBNO + CCl_4 is only 183 cm^{-1} (see Figure 4).³⁸ Keeping in mind the experimental results on the intermolecular interaction ability of TMBNO and ANO, we can safely say that (i) the electron donating power of $-\text{C}\equiv\text{N}\rightarrow\text{O}$ group is weak and of the same order as in a nitrile group or ethers, and that (ii) hydrogen bonding and iodine complexing abilities of $-\text{C}\equiv\text{N}\rightarrow\text{O}$ group run parallel to each other. Thus conclusion (i) would be explained by considering the conjugated system shown in Figure 1 and also by examining the nature of the $\text{N}\rightarrow\text{O}$ σ bond itself as was already described. Conclusion (ii) is now reasonable from CT theory.²

Acknowledgments. The authors wish to express their thanks to Professor R. S. Mulliken of the University of Chicago and to Professor S. Nagakura of the University of Tokyo for discussions. Thanks are also due to Professor Emeritus E. Ochiai of the University of Tokyo for valuable advice.

(32) M. Brandon, M. Tamres, and S. Searles, *J. Am. Chem. Soc.*, **82**, 2129 (1960); M. Tamres and M. Brandon, *ibid.*, **82**, 2134 (1960).

(33) P. Klabeo, *ibid.*, **84**, 3458 (1962).

(34) N. Mataga and Y. Kaifu, *Mol. Phys.*, **7**, 137 (1963).

(35) S. Nagakura and M. Gouterman, *J. Chem. Phys.*, **26**, 881 (1957).

(36) A. Allerhand and P. von R. Schleyer, *J. Am. Chem. Soc.*, **85**, 866 (1963).

(37) The structure is a typical nitron.

(38) For the nitrile compounds, the values shown below were reported in CCl_4 : $\Delta\bar{\nu}_{\text{OH}} = 151$ and $K = 4.89$ for acetonitrile, and $\Delta\bar{\nu}_{\text{OH}} = 147$ and $K = 3.45$ for benzonitrile. S. C. White and H. W. Thompson, *Proc. Roy. Soc. (London)*, **A291**, 460 (1965).

The Transient Potentials Produced by the Creation or Annihilation of the Diffuse Double Layer in Dilute Solutions

by Fred C. Anson

Contribution No. 3516 from the Gates and Crellin Laboratories of Chemistry, California Institute of Technology, Pasadena, California 91109 (Received April 19, 1967)

Changes in the electronic charge density on electrode surfaces are accompanied by changes in the ionic concentrations next to the electrode even in the absence of faradaic electrode reactions. In dilute solutions of electrolyte these concentration changes produce appreciable transient potentials arising from both the ionic strength dependence of the diffuse double-layer capacity and the concentration cell created by the concentration changes. A derivation of the equations describing this behavior is given and the magnitudes of the transient potentials resulting from galvanostatic and coulometric charge injection are calculated.

The properties and behavior of the diffuse double layer at charged electrode-electrolyte interfaces under nonequilibrium conditions have received considerable recent attention.^{1,2} The problem was also considered much earlier by Ferry³ and by Grahame,⁴ who concluded that for most accessible experimental situations "the effects of concentration polarization on the (double-layer) capacity are inappreciable."

Recent experiments in these laboratories⁵ involving the rapid injection of charge into a mercury electrode contained in dilute solutions (0.5–1 mM) of electrolytes led to a calculation of the magnitude of the transient effects to be expected when the charge on the electrode is suddenly altered and the electrolyte concentration just outside the diffuse double layer differs from that in the bulk of the solution. The results of these calculations for the two cases of galvanostatic (current-step) and coulometric (charge-step) perturbation are quite similar to the equation given by Barker² for the case of alternating current perturbation. However, since the derivation given here is more detailed and conventional, it seemed worth presenting it to facilitate understanding of the physical situation giving rise to the calculated effects.

The problem is the following. When the charge density (or potential) of an electrode is abruptly altered, the ions that are attracted toward (or repelled from) the electrode surface in order to create the diffuse double

layer corresponding to the new charge density must come from (or be expelled into) the initially homogeneous solution just outside the diffuse layer. In solutions containing a high concentration of electrolyte (0.1–1 M) the resulting concentration perturbations are extremely minute and the diffuse layer can be safely assumed to remain in equilibrium with a solution having the composition of the bulk (at least in the absence of ionic specific adsorption). However, in more dilute solutions the concentration changes produced just outside the diffuse layer can be far from negligible. In such cases the diffuse layer resulting initially after the perturbation will be in equilibrium with a concentration of electrolyte different from that in the bulk, and its properties (*e.g.*, capacity) will vary in time as the concentration just outside the diffuse layer equilibrates with the bulk concentration.

To calculate the magnitude of this transient effect, we may consider an experiment in which we change the charge density of an ideally polarized mercury electrode in a solution of a single, uni-univalent salt and calculate

(1) P. Delahay, *J. Phys. Chem.*, **70**, 2067, 2373, 3150 (1966); **71**, 779 (1967).

(2) G. C. Barker, *J. Electroanal. Chem.*, **12**, 495 (1966).

(3) J. D. Ferry, *J. Chem. Phys.*, **16**, 737 (1948).

(4) D. C. Grahame, *J. Am. Chem. Soc.*, **68**, 301 (1946).

(5) F. C. Anson, *Anal. Chem.*, **38**, 1924 (1966).

the resulting change in the potential of the electrode measured with respect to a nonpolarizable reference electrode (in a cell with liquid junction)

$$dE = \left(\frac{\partial E}{\partial q^m}\right) dq^m + \left(\frac{\partial E}{\partial \mu}\right)_{q^m} d\mu \quad (1)$$

where E is the measured potential of the mercury electrode, q^m is the electronic charge density on the mercury surface, and μ is the chemical potential of the salt composing the electrolyte.

The first term on the right-hand side of eq 1 is the reciprocal of the differential double-layer capacity, C . Making this substitution, eq 1 can be rewritten

$$dE = \frac{1}{C} \left[dq^m + \left(\frac{\partial q^m}{\partial \mu}\right)_E d\mu \right] \quad (2)$$

The coefficient $(\partial q^m / \partial \mu)_E$ can be obtained from the electrocapillary equation⁶ and the relation

$$\left(\frac{\partial E^-}{\partial \mu}\right)_E = -\frac{1}{2F} \quad (3)$$

where E^- is the potential of the mercury electrode with respect to a reference electrode reversible to the anion of the electrolyte in a cell without liquid junction, and F is the Faraday.

The result is

$$\left(\frac{\partial q^m}{\partial \mu}\right)_E = \frac{C}{F} \left[\left(\frac{\partial q_+}{\partial q^m}\right)_\mu - \frac{1}{2} \right] \quad (4)$$

where q_+ is the charge in the diffuse double layer due to cations. For cases where there is no specific adsorption of either ion of the electrolyte the coefficient $(\partial q_+ / \partial q^m)_\mu$ can be calculated directly from the Gouy-Chapman theory of the diffuse double layer as described in detail by Parsons.⁶ Grahame⁷ termed this coefficient "the transference number of the cation in the double layer" while Barker² calls it "the effective transference number for the cation at the boundary" between the diffuse layer and the solution. It measures the fraction of the total charge moving into or out of the diffuse layer that is carried by cations; it will be abbreviated here as T_{d1}^+ .

For electrolytes in which neither ion is specifically adsorbed at the concentrations employed, an assumption that will be made throughout the following discussion, the value of T_{d1}^+ (and T_{d1}^-) can be readily calculated from diffuse layer theory.⁶ Thus, T_{d1}^+ will be 0.5 at the point of zero charge (pzc) and will approach unity as the potential is made more negative, or zero as the potential is made more positive.⁸

Substitution of eq 4 into eq 2 yields

$$dE = \left(\frac{1}{C}\right) dq^m + \frac{1}{F} [T_{d1}^+ - 1/2] d\mu \quad (5)$$

Equation 5 gives the changes in potential that would result from the effect of a charge perturbation on the double layer. There is an additional source of potential change arising from the fact that the concentration perturbation which gives rise to the second term on the right-hand side of eq 5 also constitutes a concentration cell which will contribute to the measured potential change by an amount

$$dE_c = \frac{(T_b^+ - T_b^-)}{2F} d\mu \quad (6)$$

where T_b^+ and T_b^- are the *bulk* transference numbers of the cation and anion, respectively, and μ is the chemical potential of the salt.

The total measured potential change is the sum of eq 5 and 6

$$dE_{tot} = \left(\frac{1}{C}\right) dq^m + \frac{1}{F} [(T_{d1}^+ - 1/2) - 1/2(T_b^+ - T_b^-)] d\mu \quad (7)$$

Equation 7 can be simplified by noting that $T_b^+ + T_b^- = 1$ for a single electrolyte

$$dE_{tot} = \left(\frac{1}{C}\right) dq^m + \frac{\Delta T^+}{F} d\mu \quad (8)$$

where ΔT^+ is the difference between the cation transference numbers at the outer boundary of the diffuse double layer and in the bulk of the solution, *i.e.*, $\Delta T^+ = T_{d1}^+ - T_b^+$. Inasmuch as this whole treatment will only be of importance in rather dilute solutions, it seems justifiable to approximate the salt activity by its concentration and write (for univalent electrolytes)

$$d\mu = 2RT d \ln C_{salt} \quad (9)$$

Substitution in eq 8 then gives

$$dE_{tot} = \left(\frac{1}{C}\right) dq^m + 2\Delta T^+ \frac{RT}{F} d \ln C_{salt, x=0} \quad (10)$$

The first term on the right-hand side of eq 10 corre-

(6) R. Parsons, *Proc. Intern. Congr. Surface Activity*, 2nd, London, 1957, 3, 38 (1957).

(7) D. G. Grahame, *J. Chem. Phys.*, 16, 1117 (1948).

(8) In the presence of specific adsorption T_{d1}^+ and T_{d1}^- may exceed unity or become negative and the qualitative conclusions that are about to be presented with the assumption of no specific adsorption will not hold. The equations given will still apply, however, and the behavior to be expected can be predicted if appropriate values for T_{d1}^+ and T_{d1}^- are available.

sponds to the usual equilibrium potential change resulting from charging of the double layer. The second term represents the (usually neglected) transient potential change arising from the concentration changes produced by the movement of ions into and out of the diffuse double layer. To evaluate the magnitude of this term the mass transfer problem must be solved for the particular experimental technique employed to perturb the double layer. It is apparent already, however, that the contribution from the second term will not vanish even at the point of zero charge for salts with bulk cation (or anion) transference numbers much different from 0.5 (e.g., strong acids or bases).

The Mass-Transfer Problem. In the case of a pure binary electrolyte having equal cation and anion concentrations C_+ and C_- it is well known⁹⁻¹¹ that the Fick diffusion equation in the presence of migration becomes

$$\frac{\partial C_+}{\partial t} = D_s \frac{\partial^2 C_+}{\partial x^2} \quad (11)$$

where

$$D_s = \frac{2D_+D_-}{D_+ + D_-} \quad (12)$$

and D_+ and D_- are the individual ionic diffusion coefficients of the cation and anion, respectively.

We are interested in the case where no faradaic reaction occurs at the electrode but the fluxes of both cations and anions at the outer boundary of the diffuse layer are nevertheless nonzero because they cross this boundary in the formation of the diffuse double layer.¹² These fluxes in the presence of migration are⁹

$$f_+ = D_+ \left(\frac{\partial C_+}{\partial x} + C_+ \frac{F}{RT} \frac{\partial \varphi}{\partial x} \right) \quad (13)$$

$$f_- = D_- \left(\frac{\partial C_-}{\partial x} - C_- \frac{F}{RT} \frac{\partial \varphi}{\partial x} \right) \quad (14)$$

where $\partial \varphi / \partial x$ is the potential gradient to which the ions are subjected. If we consider first the case of charging the electrode by means of a constant current, i , the boundary conditions are

$$D_+ \left(\frac{\partial C_+}{\partial x} + C_+ \frac{F}{RT} \frac{\partial \varphi}{\partial x} \right)_{x=0} = \frac{i}{F} T_{dl}^+ \quad (15)$$

and

$$D_- \left(\frac{\partial C_-}{\partial x} - C_- \frac{F}{RT} \frac{\partial \varphi}{\partial x} \right)_{x=0} = - \frac{i}{F} T_{dl}^- \quad (16)$$

where T_{dl}^+ and T_{dl}^- are the effective cation and anion transference numbers at the boundary of the diffuse

layer. Applying the condition of electroneutrality outside the diffuse layer (i.e., $C_+ = C_-$), multiplying (15) by D_- and (16) by D_+ and summing, the terms in $\partial \varphi / \partial x$ can be eliminated to obtain

$$2D_+D_- \left(\frac{\partial C_+}{\partial x} \right)_{x=0} = \frac{i}{F} (T_{dl}^+ D_- - T_{dl}^- D_+) \quad (17)$$

Equation 17 is the chief boundary condition to be applied to solve eq 11. The other boundary conditions are the usual $C_+ = C_- = C^0$ for all x when $t = 0$ and $C_+ = C_- = C^0$ for all t when $x \rightarrow \infty$.

The solution to eq 11 for these conditions is

$$C_{+x=0} = C^0 - \frac{2iD_s^{1/2}t^{1/2}}{\sqrt{\pi}AF \left(\frac{2D_-D_+}{T_{dl}^+D_- - T_{dl}^-D_+} \right)} \quad (18)$$

where $C_{+x=0}$ is the concentration of cation at the outer boundary of the diffuse layer, C^0 is the bulk salt concentration, A is the electrode area, and the other terms have been previously defined. Equation 18 can be rearranged and simplified with the use of eq 12 and by noting that

$$\frac{D_+}{D_+ + D_-} = T_b^+ \text{ and } \frac{D_-}{D_+ + D_-} = T_b^- \quad (19)$$

The result is

$$C_{+x=0} = C^0 - \left(\frac{2it^{1/2}}{\sqrt{\pi}FAD_s^{1/2}} \right) \Delta T^+ \quad (20)$$

where ΔT^+ is once again the difference in cation transference number between the boundary of the diffuse double layer and the bulk of the solution.

Equation 20 leads to several interesting observations. Inasmuch as $C_+ = C_- = C_{\text{salt}}$, eq 20 gives the time dependence of the salt concentration at the surface of the electrode. It may be useful to trace the way this concentration changes during the course of a typical experiment. Suppose the electrode potential is initially quite positive of the pzc, e.g., 0 v vs. sce, in a solution of salt having equal anion and cation bulk transference numbers $T_b^+ = T_b^- = 0.5$, and a cathodic current step is applied (i.e., $i > 0$). $T_{dl}^+ = (\partial q_+ / \partial q^m)_\mu$ will be essentially zero at this potential (assuming

(9) M. D. Morris and J. J. Lingane, *J. Electroanal. Chem.*, **6**, 300 (1963).

(10) H. L. Kies, *ibid.*, **4**, 156 (1962).

(11) V. G. Levich, "Physicochemical Hydrodynamics," Prentice-Hall, Inc., Englewood Cliffs, N. J., 1962, p 280 ff.

(12) For the purposes of the mass-transfer calculations the reasonable initial assumption can be made that the diffuse-layer thickness is vanishingly small compared with the distances moved by the diffusing and migrating ions. The $x = 0$ plane can then be considered to coincide with the outer boundary of the diffuse layer rather than with the true surface of the electrode.

no specific adsorption), the concentration of salt at the electrode surface (*i.e.*, just outside the diffuse layer) will increase continuously as the current flows, and the electrode potential moves toward the pzc. When the potential reaches the vicinity of the pzc T_{d1}^+ will have increased to 0.5 and the salt concentration at the electrode surface will reach a maximum and momentarily stop changing even though the current continues to flow. As the potential moves cathodic of the pzc T_{d1}^+ becomes larger than 0.5 and the salt concentration thus begins to be decreased by the current flow. By the time the potential becomes much more negative than the pzc, T_{d1}^+ will have reached unity and the current will be decreasing the salt concentration at the maximum rate.

For certain combinations of ΔT^+ and i , eq 20 implies that a transition time, τ , would ultimately be reached at which the salt concentration at the electrode surface would be decreased to zero

$$\tau^{1/2} = \frac{\sqrt{\pi A F D_s^{1/2} C^0}}{2i \Delta T^+} \quad (21)$$

The assumptions involved in the derivation of eq 20 are not valid for the extreme conditions implied by eq 21 (*i.e.*, pure, salt-free solvent at the electrode) and no clear significance can be attached to this transition time. It may be important, however, to calculate τ so that at the currents and salt concentrations employed in experiments this time is not too closely approached and certainly not exceeded.

So long as $T_b^+ = T_b^-$ it is a general consequence of eq 20 that, regardless of the initial electrode potential, whenever the current is of such a sign that the potential moves away from the pzc the surface salt concentration decreases and *vice versa*. This conclusion is also valid for nonconstant current techniques.

The Transient Potential Change. Equation 20 provides the surface concentration needed for the evaluation of the second term in eq 10

$$dE_{\text{trans}} = 2\Delta T^+ \frac{RT}{F} \left(\frac{dC_{\text{salt}}}{C_{\text{salt}}} \right)_{x=0} = -2(\Delta T^+)^2 \frac{RT}{F^2} \frac{it^{-1/2} dt}{\sqrt{\pi A D_s^{1/2} C_{\text{salt}} x=0}} \quad (22)$$

This equation closely resembles the equation given by Barker² for the case of a small ac perturbation. The fact that ΔT^+ enters the equation squared means that the transient potential observed will be of the same sign on either side of the pzc even though ($T_{d1}^+ - T_b^+$) will change sign near the pzc for salts having T_b^+ values near 0.5. The physical reason for this is that

the sign of ΔT^+ and the sign of the change in salt concentration at the surface are not independent.

With the aid of eqs 20 and 21, eq 22 may be rewritten as

$$dE_{\text{trans}} = \frac{RT}{F} \Delta T^+ \frac{dt}{t \left[1 \pm \left(\frac{\tau}{t} \right)^{1/2} \right]} \quad (23)$$

Integration of eq 23 is not straightforward because ΔT^+ is a complex function of potential and therefore of time. However, at potentials far from the pzc ΔT^+ becomes essentially constant and equal to $-T_b^+$ for positive potentials or T_b^- for negative potentials. In the latter case, for example, integration of eq 23 gives

$$\Delta E_{\text{trans}} = 2 \frac{RT}{F} T_b^- \ln \left[1 \pm \left(\frac{t}{\tau} \right)^{1/2} \right] \quad (24)$$

As an example, for a 1 mM solution of salt having $T_b^+ = 0.5$ and $D_s = 10^{-5}$ cm²/sec, injection of 10 μ coulombs/cm² of positive charge with currents of 10^{-3} , 10^{-2} , or 10^{-1} amp/cm² leads to values of ΔE_{trans} of 0.9, 7.7, or 38.2 mv, respectively. These are the values that would be observed at the instant that the current was turned off. They would, of course, decay toward zero as diffusion eliminates the concentration gradient of salt produced at the electrode by the charge injection.¹³ The magnitude of ΔE_{trans} is quite small even for rather dilute solutions. The considerable experimental problems associated with rapid injection of significant amounts of charge through dilute solutions having high resistances make the observation of ΔE_{trans} very difficult. With the advent of high-power pulse generators,¹⁴ however, it may be possible to do so.

Coulostatic Charge Injection. If, instead of injecting the charge with a constant current, the discharge of a small capacitor into the cell is employed, the resulting concentration perturbations are slightly different. For dilute solutions the resistance of the solution remains essentially constant throughout the charge injection so that the current will be given by

$$i = \frac{E_{\text{cap}}}{R_s} e^{-t/R_s C_i} \quad (25)$$

where E_{cap} is the voltage to which the injecting capacitor is charged, R_s is the solution resistance, and C_i is the capacitance of the injecting capacitor, assumed to

(13) If the current is turned off at time t_{off} , ΔE_{trans} will decay according to

$$\Delta E_{\text{trans}} = 2 \frac{RT}{F} T_b^- \ln \left[1 \pm \frac{t^{1/2} - (t - t_{\text{off}})^{1/2}}{\tau^{1/2}} \right]$$

(14) For example, Model 350 high-power pulse generator, Velonex Division of Pulse Engineering, Inc., Santa Clara, Calif.

be negligibly small compared with the capacity of the electrode. The experiment can be considered as chronopotentiometry with an exponentially decreasing current. The problem is then to solve eq 11 again for the boundary conditions given by eq 17 and 25. The result is

$$C_+ = C^0 - \frac{2E_{\text{cap}}\Delta T^+}{FAR_s D_s^{1/2}} \left(\frac{R_s C_i}{\pi} \right)^{1/2} \text{DI} \left(\frac{t}{R_s C_i} \right)^{1/2} \quad (26)$$

where $\text{DI}(\lambda)$ is Dawson's integral defined by¹⁵

$$\text{DI}(\lambda) = e^{-\lambda^2} \int_0^\lambda e^{V^2} dV \quad (27)$$

and the other terms have all been previously defined. Figure 1 shows how Dawson's integral depends on its argument. The perturbation in the salt concentration at the electrode surface will follow this curve reaching its maximum value at a time given by $(t/R_s C_i)^{1/2} = 0.92$.

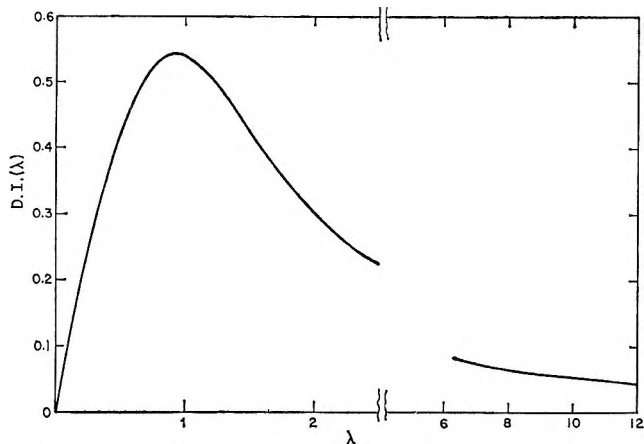


Figure 1. Dawson's integral as a function of its argument. The maximum value of the integral is 0.541 which occurs for an argument of 0.92.

As was true with constant current charge injection, eq 26 predicts that for certain combinations of E_{cap} and ΔT^+ the surface concentration of salt will be reduced to zero. However, it suffices to make certain that C_+ remains nonzero when $(t/R_s C_i)^{1/2} = 0.92$ and Dawson's integral attains its maximum value of 0.541 to assure that the salt concentration at the electrode remains nonzero at all times in the experiment.

The transient potential change produced by the charge injection is given as before by integration of the second term in eq 10. If we again consider experiments far from the pzc so that ΔT^+ can be considered approximately constant and equal to $-T_b^+$ or T_b^- , this integration leads to

$$\Delta E_{\text{trans}} = \mp 2 \frac{RT}{F} T_b^\pm \ln \frac{C_{\text{salt}, t=0}}{C^0} \quad (28)$$

where $C_{\text{salt}, t=0}$ is given by eq 26.

Barker² presented an equation for the transient potential in the case of coulostatic charging which does not correspond to the combination of eq 26 and 28. The reason for the difference is that Barker considered the hypothetical case in which the electrode can be considered to be charged instantaneously. The resistance in dilute electrolyte solutions prevents the realization of this idealized experiment in practice so that eq 26 and 28 should represent a better approximation.

As an example, for a 1 mM solution of salt with $T_b^- = 0.5$ and $D_s = 10^{-5}$ cm²/sec and a 0.03-cm² hanging mercury drop electrode, the effective solution resistance is about 25×10^3 ohms. Suppose that 10 $\mu\text{coulombs/cm}^2$ of charge is injected so that the electrode potential moves toward the pzc and the salt concentration at the electrode surface increases. The 10 $\mu\text{coulombs/cm}^2$ of charge can be supplied with various combinations of E_{cap} and C_i . Typical combinations might be $C_i = 0.03 \mu\text{f}$, $E_{\text{cap}} = 10$ v; $C_i = 0.003 \mu\text{f}$, $E_{\text{cap}} = 100$ v; $C_i = 0.0003 \mu\text{f}$, $E_{\text{cap}} = 1000$ v. In each case the maximum value of ΔE_{trans} will occur at a time given by $(t/R_s C)^{1/2} = 0.92$ because of the properties of Dawson's integral. However, at times this early in the experiment the current flowing is still quite significant and the ohmic potential drop masks ΔE_{trans} . It is more realistic to calculate the value of ΔE_{trans} at a time when the current has decayed to the point that the ohmic potential drop is, say, 10 mv. For the E_{cap} values of 10, 100, and 1000 v the times at which the ohmic drop falls to 10 mv can be calculated from eq 25 to be 5.2 msec, 0.69 msec, and 86 μsec , respectively. At these times the values of ΔE_{trans} calculated from eq 26 and 28 and the tabulated values for Dawson's integral¹⁵ are 3.6, 8.3, and 18.4 mv, respectively. Thus even at these late times in the experiment the remaining ohmic potential drop exceeds or is comparable to the transient potential perturbation for all reasonable experimental conditions. Calculations for both lower and higher salt concentrations lead to the same conclusion and it appears that, for a given high voltage source, coulostatic charge injection is less suitable than injection by a current step for experimental measurements of ΔE_{trans} . By the same token, these calculations show that in coulostatic experiments with dilute solutions of reactants capable of undergoing charge transfer at the electrode, complications arising from

(15) "Handbook of Mathematical Functions," Applied Mathematics Series 55, National Bureau of Standards, Washington, D. C., 1964, p 319.

the concentration perturbations produced during the injection generally will be small and will die away quickly, so that the standard mass transfer analysis¹⁶ of the resulting data should be possible if appropriate time scales are chosen for the experiments.

Finally, it is of interest to apply eq 26 and 28 to the recent coulometric experiments of Delahay, de Levie, and Guiliani¹⁷ in which double-layer capacitances were evaluated in extremely dilute solutions of salts. Because very small charges were injected in each experiment and relatively long times were allowed to elapse before the resulting potential changes were measured, the calculations show that the magnitudes of ΔE_{trans} were completely negligible at the times the potentials were measured. However, at shorter times the values of ΔE_{trans} should have been significant compared to the size of the potential changes being measured and it is possible that this effect may have contributed to some of the drifting potentials observed by Delahay, *et al.*¹⁷ As an example, at a potential 0.2 v negative of the pzc for the $10^{-5} M$ solution of NaF employed by Delahay, *et al.*,¹⁷ one calculates that the measured equilibrium

change in potential for the experimental conditions employed was *ca.* 1.4 mv. The value of ΔE_{trans} calculated from eq 26 and 28 under the same conditions is 1.2 mv after 1 msec, 0.3 mv after 10 msec, and 0.09 mv after 100 msec. These values for ΔE_{trans} were obtained by using the following parameters (taken from the paper of Delahay, *et al.*¹⁷) in eq 26: $C^0 = 10^{-8}$ mole/cm³. $E_{\text{cap}} = 1.0$ v, $R_s = 10^6$ ohm (estimated), $C_i = 500$ pf, $A = 0.041$ cm². D_s was assumed to be 10^{-5} cm²/sec. ΔT^+ and T_b^+ were both taken to be 0.5.

Acknowledgment. Very helpful discussions with Dr. Roger Parsons, Dr. Janet Jones, and Mr. Joseph Christie are gratefully acknowledged. This work was supported in part by the U. S. Army Research Office (Durham). The author is an Alfred P. Sloan Foundation Research Fellow.

(16) P. Delahay, *J. Phys. Chem.*, **66**, 2204 (1962).

(17) P. Delahay, R. de Levie, and A.-M. Guiliani, *Electrochim. Acta*, **11**, 1141 (1966).

Solubilization of a Water-Insoluble Dye. II¹

by Hans Schott²

Research Center, Lever Brothers Company, Edgewater, New Jersey (Received May 8, 1967)

A method for determining number-average micellar molecular weights (mmw) by dye solubilization previously described³ was based on the fact that the solubilization limit was one molecule of Orange OT per micelle. This had been established with sodium decane-sulfonate (SDSO₃), dodecyl sulfate (SDS), and two C₁₂ ethylene oxide (EO) condensates. This method was extended to micelles of nonionic detergents with larger hydrocarbon cores and to cationic detergents. Light scattering gave the same mmw as dye solubilization for nonylphenol(EO)₃₀ and dodecyltrimethylammonium bromide (DTAB), but tripled the mmw for C₁₈(EO)₁₈ and cetylpyridinium chloride (CPyC), indicating that the latter two detergents solubilized three dye molecules/micelle at saturation. Dye solubilization is therefore not an absolute method for determining mmw. It can be used to show relative changes of mmw as a function of solubilized, flexible-chain impurities or concentration of added electrolytes and provides the lowest possible mmw. Mmw of ionic detergents determined by light scattering were 1.00 or 3.00 times the mmw determined by dye solubilization in the presence of swamping electrolyte. The mmw of the ionic detergents determined by light scattering apparently decreased with decreasing amounts of added electrolyte, becoming smaller, in the case of DTAB, than the mmw determined by dye solubilization. Since decreasing amounts of added electrolyte either had no effect on the mmw of ionic detergents determined by dye solubilization or caused a small increase, a reexamination of the interpretation of light scattering theory for highly charged micelles seems in order. The number of carbon atoms in the micellar hydrocarbon core associated with one solubilized dye molecule was found to decrease in the order: SDSO₃, SDS, DTAB, CPyC, C₁₂(EO)₁₆, C₁₂(EO)₂₈, C₁₈(EO)₁₈, nonylphenol(EO)₃₀. This is also the order of increasing size of the polar head groups, indicating that the larger the latter, the more loosely packed are the micelles and the greater their solubilizing power.

Introduction

The preceding paper³ described a method for determining number-average micellar molecular weights (mmw), based on work with one C₁₀ and three C₁₂ detergents. It resulted from the finding that, at saturation, one molecule of the water-insoluble, oil-soluble dye Orange OT was solubilized by each micelle. Critical micelle concentration (cmc) and mmw were calculated from the amount of solubilized dye, which was determined spectroscopically. The mmw which can be obtained by this method for other detergents might be smaller than those obtained by light scattering or ultracentrifugation for two reasons. (a) In case of a rather wide distribution of mmw, the weight-average values are always larger than the number-average

values. (b) If each micelle could accommodate two, three, etc. dye molecules, the apparent mmw determined by dye solubilization would be one-half, one-third, etc. of the correct value.

The dye solubilization method gave good agreement with light scattering and ultracentrifugation data in the case of two nonionic detergents³ and with data for sodium dodecyl sulfate (SDS) obtained in the presence of swamping electrolyte.⁴ This agreement between

(1) Presented at the 154th National Meeting of the American Chemical Society, Chicago, Ill., Sept 10-15, 1967.

(2) U. S. Forest Products Laboratory, Madison, Wis. 53705.

(3) H. Schott, *J. Phys. Chem.*, **70**, 2966 (1966).

(4) E. W. Anacker, R. M. Rush, and J. S. Johnson, *ibid.*, **68**, 81 (1964).

the weight-average and number-average values, as well as the single, sharp peaks in the equilibrium sedimentation schlieren patterns, indicates that the micelles were monodisperse.

For the anionic detergent, the mmw values determined by light scattering were found to decrease as the concentration of added electrolyte decreased,⁴ whereas the mmw values determined by dye solubilization were constant at NaCl molarities of 0.1, 0.03, and 0. Since it is highly unlikely that, at saturation, there is less than one dye molecule solubilized by each micelle, the mmw values obtained by solubilization are the lowest possible values. Moreover, there are important unresolved questions in the interpretation of light-scattering data for mmw determination in multi-component systems in general⁵ and for highly charged particles in media of low ionic strength in particular.^{6,7} Thus, the results of dye solubilization supported Hutchinson's conclusion⁸ that reexamination of the light-scattering data indicated independence of the mmw of ionic micelles from concentration of added electrolyte.

It had been found that small amounts of impurities such as hydrocarbons and long-chain alcohols did not affect the solubilization of Orange OT.³

The purpose of the present work was (a) to extend the dye solubilization method to cationic detergents, choosing those studied extensively by Tartar⁹⁻¹¹ and by Anacker^{4,12,13} and (b) to examine the applicability of the method to micelles with hydrophobic portions considerably greater than those studied previously.³ Assuming the micelles to be spherical, with a core consisting of a hydrocarbon droplet of the same density as the bulk density of the hydrocarbon moiety of the detergent, the following radii are calculated for the hydrocarbon cores of the detergents of the preceding paper: 17.4 Å for 1-dodecanol-28 ethylene oxide, C₁₂(EO)₂₈; 18.5 Å for C₁₂(EO)₁₆; 28.1 Å for sodium decanesulfonate (SDSO₃); and 22.6 Å for SDS. Since it seemed questionable whether a single dye molecule could preempt a hydrocarbon core much larger than the above, it was of interest to ascertain how large a hydrocarbon core could be filled up by a single dye molecule and how many dye molecules could be contained in the larger cores at saturation. The latter number would then represent the factor by which the mmw determined by dye solubilization would be too small.

Experimental Section

Materials. Purification of Orange OT (1-*o*-tolylazo-2-naphthol) has been described.¹⁴ Both nonionic detergents used were made by General Aniline & Film

Corp. One was the commercial product Igepal CO 880, a branched nonylphenol with 30 EO units, NPh-(EO)₃₀, which was purified by ultrafiltration.¹⁴ The other was stearyl alcohol with 14 EO units. It gave cloudy solutions in water at room temperature, presumably owing to unreacted stearyl alcohol, which cleared up reversibly on warming. The product was soluble in hot ligroin (bp 97-103°) except for a small residue identified as sodium phosphate. On cooling, 28% of the detergent remained in solution while 72% precipitated. The former fraction contained 6.8 EO by nmr analysis of the hydroxyl proton. The major fraction, which contained 18.5 EO and gave clear solutions in cold water, C₁₈(EO)₁₈, was used for the present work. Removal of residual ligroin by heating under reduced pressure of nitrogen introduced no carbonyl groups that could be detected in the infrared spectrum of an 8% solution in tetrachloroethylene.

Hexadecyltrimethylammonium bromide (CETAB), technical grade of Matheson Coleman and Bell, was twice recrystallized from acetone containing about 5% water and once treated with ethyl acetate. Cetylpyridinium chloride (CPyC) and dodecyltrimethylammonium bromide (DTAB) were made by Fine Organics, Inc. (Lodi, N. J.). Both were recrystallized twice from acetone containing some ethanol and once from benzene. Purified CPyC contained 10.27% Cl and 4.08% N (theory 10.43 and 4.12%, respectively), while DTAB analyzed 25.67% Br and 4.39% N (theory 25.92 and 4.54%, respectively).

Methods. The procedures were the same as before³ with the following two exceptions. Solutions used for light scattering and for absorbancy measurements were filtered through Millipore filters GS (mean pore size 0.22 μ) instead of ultrafine sintered-glass filters and plugs of cotton. Comparison of the filter media showed that the Millipore filters were equivalent to the other two. Moreover, they eliminated the need for cleaning glass filters and afforded much speedier filtration than cotton plugs. The filters sorbed some Orange OT, so that the initial portions of the filtrates were colorless

- (5) R. K. Bullough, *Proc. Roy. Soc. (London)*, **A275**, 271 (1963).
- (6) E. F. Casassa and H. Eisenberg, *Advan. Protein Chem.*, **19**, 287 (1964).
- (7) J. P. Kratochvil, L. E. Oppenheimer, and M. Kerker, *J. Phys. Chem.*, **70**, 2834 (1966).
- (8) E. Hutchinson, *J. Colloid Sci.*, **9**, 191 (1954).
- (9) H. V. Tartar, *J. Phys. Chem.*, **59**, 1195 (1955).
- (10) H. V. Tartar and A. L. M. Lelong, *ibid.*, **59**, 1185 (1955).
- (11) H. V. Tartar, *J. Colloid Sci.*, **14**, 115 (1959).
- (12) E. W. Anacker, *J. Phys. Chem.*, **62**, 41 (1958).
- (13) E. W. Anacker and H. M. Ghose, *ibid.*, **67**, 1713 (1963).
- (14) H. Schott, *ibid.*, **68**, 3612 (1964).

but became readily saturated with the dye. The practice of discarding the first 80 ml of the filtered solutions prevented further loss of solubilized dye.

The light-scattering photometer was recalibrated with sucrose solutions¹⁵ using the technique of Princen.¹⁶ The Rayleigh ratio for benzene was found to be $48.2 \times 10^{-6} \text{ cm}^{-1}$ at $436 \text{ m}\mu$, in good agreement with published values.¹⁷ Since the light scattering apparatus had no temperature control, the temperature of the solutions varied between 26 and 30° during turbidity measurements.

Results

Molar Extinction Coefficient. The molar extinction coefficient ϵ of Orange OT was determined by adding small, measured volumes of acetone solutions of the dye to 2.0% detergent solutions and measuring the absorbancy $A = \log(I_0/I) = \epsilon Lc$, where I_0 is the reference intensity, measured on the plateau at $650 \text{ m}\mu$, I is the intensity at the absorption maximum around $500 \text{ m}\mu$, L is the path length in centimeters, and c the molar concentration. The absorption spectrum in the visible range of Orange OT solubilized by cationic detergents resembles that of the dye solubilized by anionic detergents. The strongest absorption is at $499 \text{ m}\mu$, with a weaker maximum appearing as a shoulder centered apparently at $522 \text{ m}\mu$. Figure 1 is a Beer's law plot showing that dye solubilized by three cationic detergents had the same extinction coefficient. The mean value of ϵ , calculated by the method of least squares as the slope of the straight line going through the origin, is $1.872 \times 10^4 \text{ l./mole cm}$, the standard deviation of the mean is 0.012×10^4 , and the range of values is $\pm 0.034 \times 10^4$. Dye solubilized by the two nonionic detergents had the same ϵ as reported for the other

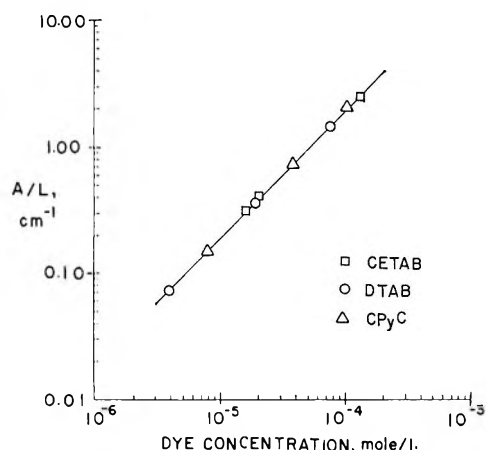


Figure 1. Beer's law plot for Orange OT solubilized by cationic detergents, on a double logarithmic scale.

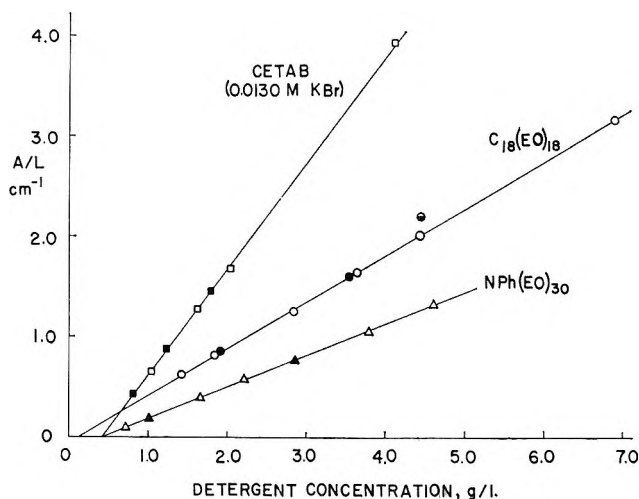


Figure 2. Absorbancy of nonionic and cationic detergent solutions saturated with Orange OT. Solid symbols represent mixtures prepared by diluting more concentrated solutions saturated with dye.

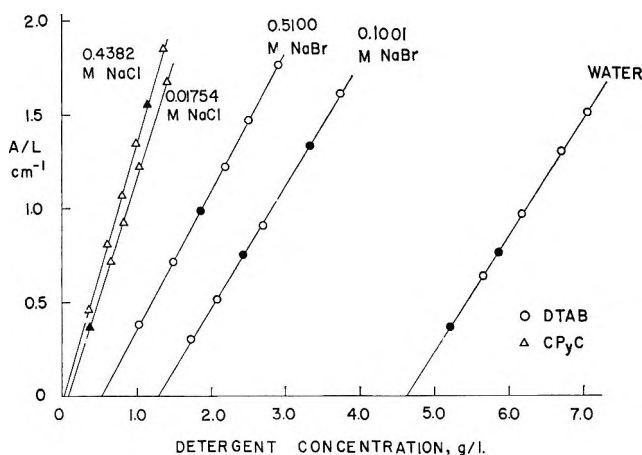


Figure 3. Absorbancy of cationic detergent solutions saturated with Orange OT. Solid symbols represent mixtures prepared by diluting more concentrated solutions saturated with dye.

nonionic detergents,^{3,14} namely, $1.740 \times 10^4 \text{ l./mole cm}$.

Critical Micelle Concentrations. The cmc values listed in Table I were determined by dye solubilization. The absorbancy vs. detergent concentration plots of solutions saturated with dye (Figures 2 and 3) were linear, and their extrapolated intercepts with the abscissa mark the cmc. The constants in the equation of these linear plots (eq 1)

(15) S. H. Maron and R. L. H. Lou, *J. Phys. Chem.*, **59**, 231 (1955).

(16) L. H. Princen, Thesis, University of Utrecht, 1959.

(17) B. A. Brice, M. Halwer, and R. Speiser, *J. Opt. Soc. Am.*, **40**, 768 (1950).

Table I: Critical Micelle Concentrations and Micellar Molecular Weights

	Cmc, g/l.	Micellar molecular weights, standard deviation, ^a and range, ^b determined by	
		Dye solubilization ^c	Light scattering
Nonionic detergents at 25°			
C ₁₈ (EO) ₁₈ (water)	0.134	36,975 ± 205 (±743)	110,660 ± 1820
NPh(EO) ₃₀ (water)	0.4259	55,697 ± 106 (±397)	56,930 ± 1770
CETAB at 34°			
0.0130 M KBr	0.4347	17,628 ± 104 (±437)	See text for lit. values
DTAB at 28°			
Water	4.627	30,442 ± 71 (±202)	
0.1001 M NaBr	1.2886	28,821 ± 208 (±618)	
0.510 M NaBr	0.5152	25,578 ± 106 (±288)	
CPyC at 30°			
0.01754 M NaCl	0.0797	14,874 ± 85 (±272)	
0.4382 M NaCl	0.0171	13,762 ± 17 (±50)	

^a Of the mean. ^b In parentheses. ^c Mmw calculated as $bL\epsilon$.

$$c = \text{cmc} + b(A/L) \quad (1)$$

were calculated by the method of least squares. The solubility of Orange OT in water was found to be less than 2×10^{-9} mole/l. It was somewhat larger in some detergent solutions below the cmc but still negligible compared to the solubility above the cmc.

The cmc values listed in Table I agree within 10% with those reported for NPh(EO)₃₀,¹⁸ for DTAB in water,^{4,10,19-22} in 0.10 M NaBr,⁴ and in 0.51 M NaBr,^{4,13} and for CPyC in 0.44 M NaCl.¹² The only significant discrepancy between published cmc values and those of Table I is in the case of CPyC in 0.0175 M NaCl, where the present value, 0.0797 g/l., is considerably larger than the reported 0.0408 g/l. figure of Anacker.¹² Since the cmc value of CPyC in 0.44 M NaCl of Anacker¹² and that of Table I agree within 5%, it is interesting to ascertain which of the two values in 0.0175 M NaCl is consistent with Hartley's cmc value for CPyC in water, namely, 0.306 g/l.²³ Linear interpolation of log cmc vs. the logarithm of the total gegenion concentration²⁴ gives a cmc value of 0.0748 g/l. in 0.0175 M NaCl, which agrees with the value of Table I within 6%.

Micellar Molecular Weights from Amount of Solubilized Dye. The following two assumptions are made to calculate mmw from absorbancy of detergent solutions saturated with dye: (a) one dye molecule is solubilized per micelle; (b) the concentration of detergent not associated into micelles is constant and equal to the cmc. Then, mmw equals $b\epsilon$, with b defined by eq 1. The second assumption is not strictly correct,^{14,25} but this causes only very small errors in mmw. As discussed above, errors in the first assumption lead to

decreases in the apparent mmw by integral factors equal to the number of dye molecules solubilized per micelle.

As is seen in Table I, the mmw of C₁₈(EO)₁₈ determined by light scattering is greater than that determined by dye solubilization by a factor of 2.99, indicating that there are three dye molecules solubilized per micelle.

The following alternate possibilities to explain this discrepancy were considered and discarded.

(a) The dye solubilization experiments were made at $25.0 \pm 0.2^\circ$ whereas turbidities were measured between 26 and 30° , and it is known that increasing temperatures cause the turbidity of nonionic detergent solutions to rise, especially near the cloud point. However, the turbidity of a 4.432-g/l. solution of C₁₈(EO)₁₈ was the same at 22.5 and 29° . The absorbancy of this solution saturated with dye increased by only 7% in going from 25 to 30° . The half-filled circle in Figure 2 represents the absorbancy of the solution saturated at 30° .

(18) L. Hsiao, H. N. Dunning, and P. B. Lorenz, *J. Phys. Chem.*, **60**, 657 (1956).

(19) A. B. Scott and H. V. Tartar, *J. Am. Chem. Soc.*, **65**, 692 (1943).

(20) H. B. Klevens, *J. Phys. Colloid Chem.*, **52**, 130 (1948).

(21) P. Debye, *Ann. N. Y. Acad. Sci.*, **51**, 575 (1949).

(22) H. J. L. Trap and J. J. Hermans, *Koninkl. Ned. Akad. Wetenschap., Proc., Ser. B*, **58**, 97 (1955).

(23) G. S. Hartley, *J. Chem. Soc.*, 1968 (1938).

(24) K. Shinoda, T. Nakagawa, B. Tamamushi, and T. Isemura, "Colloidal Surfactants," Academic Press Inc., New York, N. Y., 1963.

(25) P. Elworthy and K. J. Mysels, *J. Colloid Interface Sci.*, **21**, 331 (1966).

(b) Most of the detergent solutions used to measure turbidity were more concentrated than those used for dye solubilization measurements, and higher concentrations often lead to larger micelles, culminating in gel formation. However, the range of concentrations overlapped (1.435–6.94 g/l. for dye solubilization and 2.000–16.61 g/l. for light scattering.) Moreover, the absorbancy *vs.* detergent concentration plot (Figure 1) and the Debye plot were linear, indicating that the mmw was constant and independent of detergent concentration in the range studied.

(c) The difference between the cmc values determined by solubilization (0.134 g/l. at 25°) and by light scattering (0.20 ± 0.07 g/l. at 26–29°) is much too small to account for the discrepancy in mmw.

(d) Filtration of the solutions through Millipore filters did not reduce the detergent concentration through micelle retention, since the solids content of the filtered solutions were routinely compared to the initial concentrations as weighed out, and the largest difference ever found was 1% of the concentration.

The mmw of NPh(EO)₃₀ determined by light scattering and by dye solubilization are identical within the accuracy of the measurements, since the difference is smaller than its standard deviation. As noted previously,³ the precision of the mmw determination by dye solubilization is an order of magnitude better than that of the light-scattering method.

The following aggregation numbers have been reported for CETAB by light scattering: Tartar,¹¹ 79.6 (water, 30°); Debye,²¹ 169.3 (0.0130 *M* KBr, 30°); Trap and Hermans,²² 207.4 (0.0125 *M* KBr, 30°) and 270.0 (0.025 *M* KBr, 30°). These values are all larger than the apparent aggregation number found by dye solubilization, 48.4 (0.0130 *M* KBr, 34°), indicating that each CETAB micelle holds more than one dye molecule at saturation, probably four or five. However, at higher salt concentrations, dissymmetry measurements²⁶ gave aggregation numbers of 2181 (0.178 *M* KBr, 34°) and 5103 (0.233 *M* KBr, 34°) while ultracentrifugation²⁷ gave 3375 (0.2 *M* KBr, 30°) and 6119 (0.4 *M* KBr, 30°), both on the assumption of rod-shaped micelles. This may be considered incipient precipitation by salting out.

The aggregation numbers found for DTAB by dye solubilization at 28° were (Table I): 98.7 (water), 93.5 (0.100 *M* NaBr), and 83.0 (0.510 *M* NaBr). Published values, obtained by light scattering, include: Tartar and Lelong,¹⁰ 50.0 (water, 23°); Debye,²¹ 50.3 (water, 30°) and 56.4 (0.0130 *M* KBr, 30°); Trap and Hermans,²² 62.3 (water, 30°), 68.4 (0.0125 *M* KBr, 30°), 77.2 (0.025 *M* KBr, 30°), and 108.3 (0.050 *M* KBr, 30°); Anacker and Ghose,¹³ 84 (0.500 *M* NaBr, 31°).

Anacker, Rush, and Johnson⁴ found: 61 and 52 (water, 25°); 74 and 71 (0.100 *M* NaBr, 25°); 90 and 86 (0.502 *M* NaBr, 25°); 86–89 and 79–81 (0.510 *M* NaBr, 25°), where the first aggregation numbers of each pair of values were calculated for the best value of *z* (micellar charge) and the second numbers were calculated for *z* = 0.

The agreement between mmw from dye solubilization and from light-scattering measurements is good at higher concentrations of added salt, where the interpretation of the turbidity measurements is best understood.^{7,8} This indicates that each DTAB micelle solubilizes one dye molecule at saturation.

The aggregation numbers of CPyC found by dye solubilization at 30° were 43.7 in 0.01754 *M* NaCl and 40.5 in 0.4382 *M* NaCl (Table I). Anacker obtained 95 and 92.5 (0.01754 *M* NaCl, 31°); 117 and 114 (0.05843 *M* NaCl, 31°); 135 and 130 (0.4382 *M* NaCl, 31°); 137 and 131 (0.7304 *M* NaCl, 31°) by light scattering.¹² The diffusion measurements of Hartley and Runnicles,²⁸ made in CPyC solutions containing between 0.1 and 1.0 *M* NaCl, showed independence of micellar size from NaCl concentration within ±5%; observed radii were in the 26–28-Å range. Using the mean radius of 27.2 Å gives an association number of 134; water of hydration was neglected on the assumption that steric hindrance of the nitrogen prevents extensive hydration. The mmw determined by diffusion agrees with that determined by light scattering in solutions containing the highest salt concentrations and is three times larger than the mmw determined by dye solubilization. This indicates that the CPyC micelles solubilize three dye molecules at saturation.

As in the case of DTAB, light-scattering measurements indicate a sizable increase in mmw with increasing concentration of added electrolyte, while dye solubilization indicates a small decrease. The diffusion measurements show no trend, which is not necessarily in conflict with the dye solubilization measurements since the precision of the diffusion measurements is probably too small to detect a 7–8% decrease: an uncertainty of ±5% in the radius corresponds to an uncertainty of ±12% in the mmw.

Discussion

Solubilizing Power of Detergents toward Orange OT. The extremely low solubility of Orange OT in water, considered together with its moderate solubility in sol-

(26) P. Debye and E. W. Anacker, *J. Phys. Colloid Chem.*, **55**, 644 (1951).

(27) K. Granath, *Acta Chem. Scand.*, **7**, 297 (1953).

(28) G. S. Hartley and D. F. Runnicles, *Proc. Roy. Soc. (London)*, **A168**, 420 (1938).

vents of medium and low polarity, indicates that the hydroxyl group of the naphthol ring is internally hydrogen bonded to the azo group. This is favored by the proximity of the two groups. The most likely location for the solubilized dye is in the hydrocarbon interior of the micelles.^{23,29}

Table II summarizes the observation that a small, discrete, integral number of dye molecules is solubilized by each micelle, the number being characteristic of the detergent. This is in contrast to most other solubilizates, many molecules of which can be solubilized by each micelle and which swell the micelles in the process. The explanation for the difference in behavior lies probably in structural dissimilarities. Most of the

Table II: Limits of Solubilization and Solubility of Orange OT

Detergent	Radius of micellar hydrocarbon core, A	Dye molecules solubilized per micelle	Carbon atoms ^a per solubilized dye molecule
SDSO ₃	28.1	1	2860
SDS	22.6	1	1536
C ₁₂ (EO) ₁₅	18.5	1	836
C ₁₂ (EO) ₂₅	17.4	1	701
NPh(EO) ₃₀	14.9	1	542
C ₁₈ (EO) ₁₆	23.8	3	626
DTAB	19.6-20.8	1	996-1188
CETAB	28.2	(5)	(960)
CPyC	26.7	3	910

Solvent	Solubility at 27°, moles of Orange OT/l.	Carbon atoms per dissolved dye molecule
<i>n</i> -Dodecane	0.0238	2208
<i>n</i> -Hexadecane	0.0279	1947

^a In the main hydrocarbon chain only, except for CPyC, where all carbon atoms were counted, and for NPh(EO)₃₀, where the branches of the alkyl chain were included.

other solubilizates studied are small molecules or consist largely of flexible chains which are capable of assuming rather symmetrical configurations and which blend into the hydrocarbon environment of the micellar core. The micellar core has probably a liquid-like structure, and these solubilized molecules mix and entangle readily with the hydrocarbon chains of the detergent molecules, becoming practically indistinguishable from them. The Orange OT molecule on the other hand is highly asymmetrical and rigid: for maximum resonance and color, the benzene and naphthalene rings should be coplanar. The solubilized dye molecule preserves its distinct character.

The dye molecule is an elongated trapezium; its greatest length is 15 Å, and its smallest width is 7 Å. It is of interest to compare this 15-Å dimension with the radius of the hydrocarbon core of the micelles of the different detergents shown in Table II. Whereas one dye molecule preempts a hydrocarbon core with a 28-Å radius in the case of SDSO₃, smaller cores contain at saturation three or more dye molecules in the case of two cationic and one nonionic detergent.

This is also shown in the last column of Table II, which lists the number of carbon atoms in the micellar hydrocarbon core per solubilized dye molecule. This number is seen to be the greatest for detergents with the smallest head group. For SDSO₃, it exceeds the number of carbon atoms of solvent per dissolved dye molecule found for saturated solutions of dye in bulk paraffins (although this number might be smaller for decane). The area per head group increases in going from anionic to cationic detergents and is largest for nonionic detergents. This is illustrated by the following representative limiting areas per molecule at the air-water interface: 31 Å² for sodium alkanesulfonates and alkyl sulfates or 37 Å² for SDS^{30,31} and 59-60 Å² for alkylpyridinium bromides, 61 Å² for tetradecyltrimethylammonium bromide.³² Approximate values for nonionic detergents are 80 Å² for C₁₂(EO)₁₄, 90 Å² for C₁₈(EO)₁₄, and 110 Å² for C₁₂(EO)₃₀.³³ The larger area per head group probably results in looser micelles, with less dense hydrocarbon cores, thereby increasing the solubilizing power.³² It is interesting to note that Orange OT solubilized by the cationic and nonionic detergents requires fewer carbon atoms per dye molecule than Orange OT dissolved in bulk paraffins, probably owing to the greater free volume in the core of the more loosely packed nonionic and cationic micelles.

Limitations in Determining Mmw by Dye Solubilization. Mmw determination by dye solubilization is not an absolute method, since a solubilization limit of *n* dye molecules per micelle will result in an mmw which is *n* times too low, *n* being a small integer different from zero. However, dye solubilization can serve as an adjunct method for mmw determination: It provides the lowest possible mmw value, because it is improbable that micelles solubilize less than one dye molecule at saturation. If other methods give lower values, they

(29) P. A. Winsor, "Solvent Properties of Amphiphilic Compounds," Butterworth and Co. Ltd., London, 1954.

(30) A. P. Brady, *J. Colloid Sci.*, **4**, 417 (1949).

(31) B. A. Pethica, *Trans. Faraday Soc.*, **50**, 413 (1954).

(32) R. L. Venable and R. V. Nauman, *J. Phys. Chem.*, **68**, 3498 (1964).

(33) M. J. Schick, *J. Colloid Sci.*, **17**, 801 (1962).

should be seriously questioned. Provided that the micelles are predominantly monodisperse, light scattering, diffusion, and other weight-averaging techniques can only give mmw's which are 1.00, 2.00, 3.00, etc. times greater than that determined by dye solubilization. Polydispersity is indicated when the weight-average mmw exceeds that determined by dye solubilization by a nonintegral factor.

Dye solubilization can be used as a fast, precise, and theoretically uncomplicated method for determining relative changes in mmw; it requires no supporting electrolyte nor assumptions regarding particle shape or charge. Solubilized flexible-chain impurities were shown not to affect the 1:1 ratio of dye molecules to micelles of $C_{12}(EO)_{16}$, $C_{12}(EO)_{28}$, and $SDSO_3$.^{3,14} Therefore, the method can be used to study the effect of such additives on mmw. It might also be suitable to study the effect of temperature, different counterions, etc.

The fact that light scattering showed considerable increase in the mmw of cationic detergents with increasing salt concentration may well be due to shortcomings in the interpretation of turbidity measurements.^{6,7} The best values are probably those obtained at the higher salt concentrations, where the mmw was found to be independent of further salt addition. It is

in this situation that the effective charge of the micelles is suppressed, *i.e.*, swamped by added salt,⁸ so that the micelles become effectively "nonionic," and here the agreement among light-scattering and diffusion measurements and dye solubilization was found to be best. In the case of nonionic detergents, light scattering, ultracentrifugation, and dye solubilization mmw agreed well, provided the latter were corrected, where necessary, for solubilization limits of more than one dye molecule per micelle.

As was found for SDS, dye solubilization showed a small but unmistakable drop in the mmw of cationic detergents at higher concentrations of added electrolyte. In the case of SDS and DTAB, Anacker, Rush, and Johnson⁴ have found indications of polydispersity at about the same electrolyte concentrations. Therefore, departure from monodispersity, particularly the appearance of larger micelles brought about by added electrolyte prior to salting out, may have caused a decrease in the number-average mmw.

Acknowledgments. The author is indebted to Professor D. G. Dervichian and Dr. E. D. Goddard for helpful discussions, to Fine Organics, Inc., for the CPyC and purified DTAB, and to the Lever Brothers Co. for permission to publish this paper.

Clathrates of Tetra(4-methylpyridine)nickel(II) Thiocyanate. II.

Competition for Sites in the Host Lattice¹

by Sr. M. Juana Minton and Norman O. Smith

Department of Chemistry, Fordham University, New York, New York 10458 (Received June 1, 1967)

The study of the competition for occupancy in the host lattice, $\text{Ni}(4\text{-mepy})_4(\text{SCN})_2$, between the members of the following pairs of guests was studied at 25° by analyzing the equilibrium solid phases given by known mixtures of the host with the pairs: *p*-xylene-ethylbenzene, *p*-xylene-toluene, ethylbenzene-toluene, *p*-xylene-*p*-dichlorobenzene. In all four systems the solid phase is a solid solution of one clathrate in the other, both clathrates having a guest/host ratio of unity. In the first three systems there is a complete series of solid solutions; in the last the composition can be varied from 0 to about 50% of the *p*-dichlorobenzene clathrate. In each system the ratio of the guests in the clathrate phase is different from that in the coexisting liquid. The order of preference in clathration is *p*-xylene > ethylbenzene > toluene and *p*-xylene > *p*-dichlorobenzene. In all four systems there is an approximately linear relation between $\log R_s$ and $\log R_l$, where R_s is the mole ratio of the two guests in the solid and R_l that in the coexisting liquid phase. Activity coefficients of the clathrated guests as a function of composition are estimated. Calorimetric measurements of the enthalpy of clathration of ethylbenzene and toluene are reported. An attempt to correlate these and earlier values for *p*-xylene and *p*-dichlorobenzene with the results of the distribution study is discussed. A brief study of the kinetics of uptake of ethylbenzene and *p*-xylene by the host is reported.

Clathrates are a type of inclusion compound and are defined by Powell² as intermolecular compounds which involve the complete enclosure of a molecule of one component by one or more molecules of another. One category of clathrate is that in which coordination compounds comprise the host lattice. Numerous examples of such materials have been reported^{3,4} but the application of the term clathrate to most of these is based on indirect evidence. Jeffrey and co-workers⁵ have reported single crystal studies on $\text{Ni}(4\text{-mepy})_4(\text{SCN})_2$ (I) and shown that the powder patterns of Hart and Smith, described in the first paper of this series,⁶ are consistent with a host framework structure of eight molecules per unit cell.

The work of Schaeffer, *et al.*,³ with I included studies of its preference for *p*-disubstituted benzenes over other C₈ aromatic guests. However, polycomponent mixtures were used for the most part, dissolved in a solvent, thus not making it possible to reach clear-cut conclusions concerning the behavior of only two competing

guests. Furthermore, the temperatures were not defined, a given system was not studied over a range of guest-to-guest ratio, and there was no assurance that equilibrium had been attained. Hanotier and de Radzitzky and co-workers,⁷ in their studies of competitive clathration by α -aryllalkylamine complexes of

(1) Taken in part from the Ph.D. Thesis of M. J. M., Fordham University, 1966. Portions of this paper were presented before the Physical Chemistry Division of the American Chemical Society in Detroit, Mich., April 1965.

(2) H. M. Powell, *J. Chem. Soc.*, 61 (1948).

(3) W. D. Schaeffer, W. S. Dorsey, D. A. Skinner, and C. G. Christian, *J. Am. Chem. Soc.*, 79, 5870 (1957).

(4) P. de Radzitzky and J. Hanotier, *Ind. Eng. Chem. Process Design Develop.*, 1, 10 (1962).

(5) D. Belitskus, G. A. Jeffrey, R. K. McMullan, and N. C. Stephenson, *Inorg. Chem.*, 2, 873 (1963).

(6) M. I. Hart, Jr., and N. O. Smith, *J. Am. Chem. Soc.*, 84, 1816 (1962).

(7) J. Hanotier, M. Hanotier-Bridoux, and P. de Radzitzky, *Bull. Soc. Chim. Belges*, 74, 381 (1965); J. Hanotier, J. Brändli, and P. de Radzitzky, *ibid.*, 75, 265 (1966).

Ni(II), also used a solvent and their phase studies for any one guest pair were fragmentary. Gawalek and Konnecke⁸ have discussed the selectivities shown by several coordination compounds and attributed the phenomenon to differences in solubility of the host in the various guests and to the different polarizabilities of the guests themselves. A detailed study of the competition between two guests for sites in the host lattice was undertaken by us to give more information concerning a possible dependence of the preference on the initial guest ratio taken, to indicate whether a clathrate with two guests is a mixture or solid solution, and to suggest whether both guests occupy the same type of lattice site. It was hoped also that the distribution behavior could be correlated with enthalpies of clathration, some data for which were already available.⁶

Experimental Section

Materials. Compound I was prepared from reagent grade chemicals by the method of Logan and Carle.⁹ The product was washed repeatedly with water to remove excess thiocyanate and the nearly dry material washed with heptane and stored over KOH. A typical batch, analyzed gravimetrically for nickel with dimethylglyoxime, gave 10.71% (calcd 10.73) and, analyzed volumetrically for thiocyanate using standard potassium iodate,¹⁰ gave 21.19% (calcd 21.21).

The guest materials were "highest purity," further purified by distillation or, with *p*-dichlorobenzene, distillation followed by recrystallization from ethanol. Clathrates were prepared from I by suspending the latter in the pure liquid guest or, with *p*-dichlorobenzene, in a solution of the guest in heptane, for several hours. The extent of clathration was varied by varying the amount of washing of the clathrate and the time of drying. The products were analyzed for thiocyanate and the guest content was computed by difference. When washing and air drying are minimal the highest clathrate content is obtained. With ethylbenzene, preparations analyzing 0.990 ± 0.005 mole of guest per mole of host were obtained; with toluene, this ratio was 0.956 ± 0.008 . To demonstrate that the 4-methylpyridine-nickel ratio still corresponded to four, the base was determined by solution in standard sulfuric acid solution and back-titration with standard potassium hydroxide, using methyl orange as indicator. Coordination numbers between 4.0 and 4.3 were found for the complex and several clathrates.

Distribution Studies. Known mixtures containing 2.000 g of complex and a total of 10 ml of the two guests, in ratios varying from 1/10 to 10/1, were made up in duplicate and stirred at $25.00 \pm 0.05^\circ$ for 4–17 days.

The duplicates differed only as follows: in the one, the first guest was mixed with complex and allowed to stand for at least 0.5 hr before the other guest was added; in the other, the order was reversed. When one of the guests was *p*-dichlorobenzene (a solid), one of the members of each duplicate pair was made up by adding the requisite quantity of *p*-dichlorobenzene in the form of its clathrate to a solution of *p*-dichlorobenzene in the other guest. After equilibration, the solid phases were removed by filtration, dissolved in 1:1 hydrochloric acid, extracted with solvent, and analyzed. For the *p*-xylene-ethylbenzene and *p*-xylene-toluene pairs, the solvent was heptane and the solutions were analyzed by ultraviolet spectrophotometry using a Cary 15 recording instrument. For the other two systems hexane was used as solvent and analysis was done by gas chromatography using an F & M 500 instrument with a column of Apiezon L on Chromasorb. The results were accurate to $\pm 1.5\%$, as judged by comparison with known mixtures. The solubility of *p*-dichlorobenzene in *p*-xylene was measured by approach both from under- and oversaturation.

Calorimetry. Enthalpies of clathration were determined for ethylbenzene and toluene at 25° as described in an earlier paper.⁶ The guest content was varied from about 0.7 to 1.0 mole/mole of host. Such a range of composition could be prepared by removal of guest from the fully clathrated material as described above, without collapse of the clathrate-type structure of the host.

Kinetic Studies. The uptake of *p*-xylene and ethylbenzene (separately) by the complex from heptane solution at 25° was followed with time, stirring meanwhile. Initial concentration of guest varied from 0.16 to 0.94 mole/l. and there was always more than sufficient guest present to form a 1:1 clathrate with the complex. Aliquots of the liquid phase were taken at known times, diluted, and analyzed by ultraviolet spectrophotometry.

Results and Discussion

Distribution Studies. The analysis of the solid phases gave satisfactory agreement between the members of each duplicate. The results are therefore those for equilibrium. From the solid-phase compositions and the known initial total compositions it is possible to extrapolate with little error to the liquid-phase compositions. The resulting mole ratios of the two guests in the coexisting liquid and solid phases, denoted respec-

(8) G. Gawalek and H. G. Konnecke, *Chem. Tech.*, **15**, 609 (1963).

(9) A. V. Logan and D. W. Carle, *J. Am. Chem. Soc.*, **74**, 5224 (1952).

(10) R. Lang, *Z. Anorg. Allgem. Chem.*, **142**, 290 (1925).

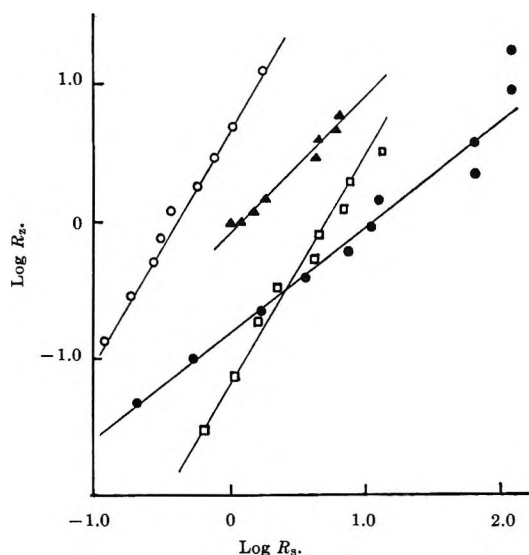


Figure 1. Distribution of guests between liquid and clathrate phases: ●, *p*-xylene-ethylbenzene; □, *p*-xylene-toluene; ○, toluene-ethylbenzene; ▲, *p*-xylene-*p*-dichlorobenzene.

where $R_1 = (X_A)_1/(X_B)_1$ and $R_s = (X_A)_s/(X_B)_s$. $(X_A)_s$ and $(X_B)_s$ are taken as the number of moles of A or B per mole of total guest. It follows that

$$\log R_1 = \log R_s + \log (\gamma_A/\gamma_B)_s - \log (\gamma_A/\gamma_B)_1 \quad (4)$$

For all the systems studied it seems reasonable to regard the liquid phase as nearly ideal. The binary system *p*-xylene-ethylbenzene was found ideal at 135° by Redlich and Kister¹³ and so was the system ethylbenzene-toluene at 25° by Arm, Hügli, and Signer.¹⁴ Heats of mixing for the system *p*-xylene-toluene by Cheesman and Ladner¹⁵ at 24.4° were found to be small. Both *p*-xylene and *p*-dichlorobenzene are nonpolar and have similar estimated liquid molar volumes (124 and 115 cc mole⁻¹) and solubility parameters (8.75 and 9.4) at 25°, so would also be expected to comprise a nearly ideal system. A measurement of the solubility of *p*-dichlorobenzene in *p*-xylene at 25° yielded $X_{C_6H_4Cl_2} = 0.529$, in agreement with the calculated ideal value of 0.532 from its heat of fusion. For these reasons we may replace $\log (\gamma_A/\gamma_B)_1$ by zero in eq 4 to give

$$\log R_1 = \log R_s + \log (\gamma_A/\gamma_B)_s \quad (5)$$

Comparison of eq 1 and 5 suggests that deviations of $(\gamma_A)_s$ and $(\gamma_B)_s$ from unity give rise to the factor m through the relation $(\gamma_A)_s/(\gamma_B)_s = C(R_s)^{m-1}$ for reasons as yet unknown.

Regardless of any assumption of linearity in Figure 1, eq 2 can be written as

$$(X_A)_1/(X_A)_s(\gamma_A)_s = 1; \quad (X_B)_1/(X_B)_s(\gamma_B)_s = 1 \quad (6)$$

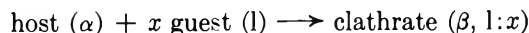
by putting $(\gamma_A)_1 = (\gamma_B)_1 = k_A = k_B = 1$. With these relations, $(\gamma_A)_s$ and $(\gamma_B)_s$ were calculated for the clathrated guests from the experimental mole fractions. They are presented in Table III. Small deviations from ideality in the liquid would not alter the values seriously or the implication that the one-sidedness of the distributions is caused by considerable deviations from ideality in the solid state in each system, the deviations being least for the *p*-xylene-*p*-dichlorobenzene pair where both guests are *para*-substituted compounds.

Table III: Activity Coefficients of Clathrated Guests (Assuming Ideal Liquid Solutions)

$(X_A)_s$ <i>p</i> -Xylene(A)-ethylbenzene(B)	$(\gamma_A)_s$	$(\gamma_B)_s$	$(X_A)_s$ <i>p</i> -Xylene(A)-toluene(B)	$(\gamma_A)_s$	$(\gamma_B)_s$
0.992	0.95	6.75	0.386	0.07	1.58
0.992	0.91	12.50	0.522	0.13	1.98
0.985	0.80	14.00	0.622	0.25	2.22
0.985	0.72	20.8	0.693	0.36	2.44
0.928	0.63	5.95	0.810	0.43	3.44
0.919	0.52	6.46	0.822	0.55	3.10
0.885	0.43	5.41	0.874	0.63	3.57
0.784	0.35	3.20	0.885	0.74	2.97
0.632	0.28	2.28	0.931	0.82	3.40
0.355	0.25	1.42	Ethylbenzene(A)-toluene(B)		
0.189	0.24	1.17	0.893	0.99	1.09
			0.839	0.92	1.41
			0.784	0.85	1.56
			0.755	0.75	1.76
			0.860	0.96	1.27
			0.821	0.97	1.13
			0.814	0.92	1.36
			0.711	0.84	1.39
			0.640	0.85	1.27
			0.551	0.91	1.11
			0.507	0.95	1.06
			<i>p</i> -Xylene(A)- <i>p</i> -dichlorobenzene(B)		
			0.868	0.98	1.11
			0.860	0.96	1.27
			0.821	0.97	1.13
			0.814	0.92	1.36
			0.711	0.84	1.39
			0.640	0.85	1.27
			0.551	0.91	1.11
			0.507	0.95	1.06

X-Ray powder diffraction patterns of the three hydrocarbon clathrates and of some of their solid solutions, taken with Cu K α radiation, were nearly identical. This supports the conclusion reached above that one clathrate forms solid solutions with the other.

Calorimetry. The enthalpy changes measured directly were those for



(13) O. Redlich and A. T. Kister, *J. Am. Chem. Soc.*, **71**, 505 (1949).

(14) H. Arm, G. Hügli, and R. Signer, *Helv. Chim. Acta*, **40**, 1200 (1957).

(15) G. R. Cheesman and W. R. Ladner, *Proc. Roy. Soc. (London)*, **A229**, 387 (1955).

where the guests were ethylbenzene and toluene. As discussed in the previous paper,⁶ the α and β designations allow for the possibility of a change in the host lattice in accommodating the guest. Table IV gives the heat effects found. The data are plotted in Figure 2. The variation for both systems appears to be linear. With this assumption the best straight line, found by least squares, was extrapolated to $x = 0$ to give $\Delta H_{298} = 0.00$ and -0.80 kcal/mole of host for the change from the α (or stable) form of the host to the unoccupied β form present in the ethylbenzene and toluene clathrates, respectively. There is, of course, considerable uncertainty involved in the extrapolation. (These figures may be compared with the quantities -0.51 and $+1.80$ kcal/mole found⁶ for the corresponding unoccupied *p*-xylene and *p*-dichlorobenzene lattices, respectively.) Extrapolation in the other direction gives $\Delta H_{298} = -7.74$ and -7.11 kcal/mole for the formation of the 1:1 clathrates of ethylbenzene and toluene, respectively, from the α form of the host and the liquid guest.

Table IV: Enthalpy of Clathration

Ethylbenzene		Toluene	
x	$-\Delta H_{298}$, kcal/mole of host	x	$-\Delta H_{298}$, kcal/mole of host
0.994	7.66	0.959	6.84
0.950	7.40	0.940	6.72
0.882	6.69	0.907	6.58
0.808	6.46	0.747	5.45
0.682	5.19	0.666	5.03
0.664	5.14		

The slopes of these lines at the 1:1 composition give the enthalpy change for the transfer of 1 mole of liquid guest to the 1:1 clathrate, except for *p*-dichlorobenzene where the slope must be corrected by the heat of fusion of the guest (4.4 kcal/mole¹⁶). The values of this quantity are $\Delta H_{298} = -7.7$, -7.7 , -6.3 , and -10.2 kcal/mole of guest for *p*-xylene, ethylbenzene, toluene, and *p*-dichlorobenzene(1), respectively.

It was thought that there might be some correlation between these data and those of Figure 1, but such is not apparent. The change in enthalpy on clathration of *p*-xylene and ethylbenzene are indistinguishable and yet the former is strongly clathrated in preference to the latter when both are present. The enthalpy change for *p*-dichlorobenzene is noticeably larger than that for *p*-xylene and yet the former is less strongly clathrated

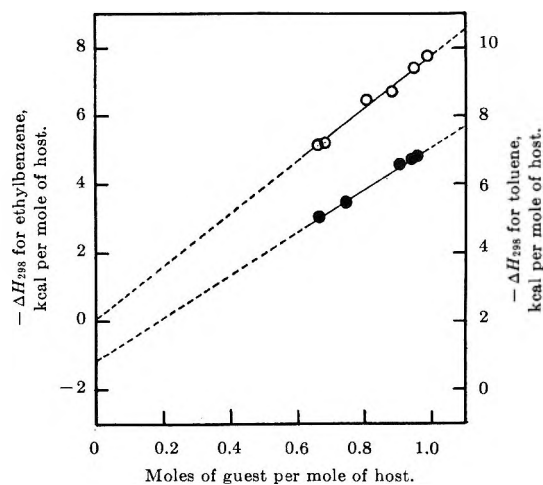


Figure 2. Heat of clathration: —○—, ethylbenzene; —●—, toluene.

when both are present. It appears that the mixed clathrate is too nonideal for any such simple correlation to exist, so that the enthalpy of clathration of each guest in the mixed clathrate is appreciably different from what it is when the other guest is absent.

Kinetic Studies. The concentration of *p*-xylene (or ethylbenzene) in the heptane showed an unexpected small, but definite, initial rise followed, after about 0.5 hr, by a gradual decrease as clathration removed the guest. The time necessary for the completion of the clathration was found to vary from 8 hr for the most concentrated solution to 48 hr for the most dilute. The unexpected initial rise appears to be the result of a relatively rapid initial absorption of heptane by the host.

Clathration of the heptane does not seem to be a factor here, for when the latter is stirred by itself with I, analysis shows that the filtered, dried solid contains no heptane. When I was stirred with *p*-xylene in cyclohexane, the initial rise in *p*-xylene concentration was not observed. It is conceivable that the phenomenon involves temporary inclusion of the heptane but not of the cyclohexane by I in suspension, the heptane being readily dissipated when the filtered solid is dried. The marked difference is flexibility and size of the two molecules could account for their different behavior.

Acknowledgment. Acknowledgment is made to the donors of the Petroleum Research Fund, administered by the American Chemical Society, for the support of this research.

(16) "International Critical Tables," Vol. 5, McGraw-Hill Book Co., New York, N. Y., 1928, p 133.

Thermodynamics of Aqueous Mixtures of Electrolytes and Nonelectrolytes.

III.¹ Transfer of Acetic Acid from Water to Nine 1 *m* Alkali

Halides and Nitrates at 25°

by J. H. Stern, J. P. Sandstrom, and A. Hermann

Department of Chemistry, California State College at Long Beach, Long Beach, California 90804
(Received June 5, 1967)

Partial molal enthalpies of transfer of undissociated acetic acid from water to aqueous 1 *m* solutions of the chlorides, bromides, and nitrates of lithium, sodium, and potassium were determined calorimetrically at 25°. The enthalpies range from -225 to 106 cal/mole and were combined with free energies of transfer calculated from distribution equilibrium data to yield partial molal entropies of transfer. All thermodynamic properties decrease generally in the order Li⁺, Na⁺, K⁺, and Cl⁻, Br⁻, and NO₃⁻ and appear to be composed of additive ionic contributions. A partial explanation of the observed trends of the free energy of transfer in terms of changes in solution structure is proposed and the limiting relationship between the thermodynamic properties of transfer of nonelectrolytes and electrolytes is discussed.

I. Introduction

This is the third and most extensive in a series of investigations¹ on the thermodynamics of interaction between solutes in the ternary electrolyte–nonelectrolyte–water systems. It is hoped that such studies will help toward establishing a model for interactions of this type and toward the eventual development of a theoretical formulation of limiting behavior in these systems.

The interaction between electrolytes and nonelectrolytes in aqueous solution can be characterized in terms of the activity coefficient of the nonelectrolyte γ_3 , relative to the hypothetical 1 *m* solute standard state in pure water. The activity coefficient γ_3 may be expressed as a function of the concentrations of the electrolyte m_2 and nonelectrolyte m_3 in a power series²

$$\log \gamma_3 = \sum_{n,m} k_{nm} m_3^n m_2^m \quad (1)$$

In expanded form this equation may be written as

$$\log \gamma_3 = k_{32} m_2 + k_{33} m_3 + k_{32}' m_2^2 + \dots \quad (2)$$

The coefficients k_{32} and k_{32}' are electrolyte–nonelectrolyte interaction parameters, while k_{33} is a self-interaction

parameter of the nonelectrolyte representing deviations from Henry's law.³ If the linear terms of eq 2 are sufficient, the limiting electrolyte–nonelectrolyte parameter may be expressed as

$$\lim_{\substack{m_2 \rightarrow 0 \\ m_3 \rightarrow 0}} \left(\frac{\partial \log \gamma_3}{\partial m_2} \right) = k_{32} \quad (3)$$

The coefficients of the linear concentration terms are usually of the same order of magnitude.³

At sufficiently low solute concentrations the slope of a plot of $\log \gamma_3$ vs. m_2 should be constant and equal to k_{32} . Such behavior has been observed for various nonelectrolytes at low m_3 over wide ranges of electrolyte concentrations.^{2,4} Under these conditions k_{32} may be expressed

(1) Previous papers in this series: (a) J. H. Stern and A. Hermann, *J. Phys. Chem.*, **71**, 306 (1967); (b) J. H. Stern and A. Hermann, *ibid.*, **71**, 309 (1967).

(2) F. A. Long and W. F. McDevitt, *Chem. Rev.*, **51**, 119 (1952).

(3) (a) L. Brewer, T. R. Simonson, and L. K. J. Tong, *J. Phys. Chem.*, **65**, 420 (1961); (b) G. N. Lewis and M. Randall, "Thermodynamics," K. S. Pitzer and L. Brewer, Ed., McGraw-Hill Book Co., Inc., New York, N. Y., 1961, pp 587, 589.

(4) H. S. Harned and B. B. Owen, "The Physical Chemistry of Electrolytic Solutions," 3rd ed, Reinhold Publishing Corp., New York, N. Y., 1958, p 531.

as the sum of the interactions between the nonelectrolyte and the cation and anion, respectively. Thus for a salt MX

$$k_{32} = k_{32}^{M^+} + k_{32}^{X^-} \quad (4)$$

where $k_{32}^{M^+}$ and $k_{32}^{X^-}$ are the ion–nonelectrolyte coefficients.

The electrolyte–nonelectrolyte coefficient k_{32} may be determined by a variety of methods, including measurements of the distribution of the nonelectrolyte between aqueous solutions and an immiscible reference phase.² This method yields an expression for the activity coefficient ratio γ_3/γ_3^0 , where γ_3^0 is the activity coefficient of the nonelectrolyte in the electrolyte-free aqueous solution at molality m_3^0 . If the linear terms of eq 2 are sufficient and since $\log \gamma_3^0 = k_{33}m_3^0$,³ then

$$\log \gamma_3/\gamma_3^0 = k_{32}m_2 + k_{33}(m_3 - m_3^0) \quad (5)$$

In the distribution method m_3 and m_3^0 can be made sufficiently low so that the contribution of the self-interaction term to $\log \gamma_3/\gamma_3^0$ is negligible and thus

$$\log \gamma_3/\gamma_3^0 = k_{32}m_2 \quad (6)$$

Values of $\log \gamma_3/\gamma_3^0$ were calculated from Sugden's studies at 25° of acetic acid distributed between amyl alcohol and water or aqueous salt solutions, respectively.⁵

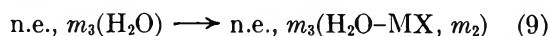
The variation of k_{32} with temperature is of importance since it provides an alternate criterion of additivity. If eq 4 and 6 are obeyed, then

$$\frac{d \log \gamma_3/\gamma_3^0}{dT} = m_2 \frac{dk_{32}}{dT} = \left(\frac{dk_{32}^{M^+}}{dT} + \frac{dk_{32}^{X^-}}{dT} \right) m_2 \quad (7)$$

This temperature derivative may be determined from

$$2.303 \frac{d \log \gamma_3/\gamma_3^0}{dT} = \frac{-\overline{\Delta H}_3}{RT^2} \quad (8)$$

where $\overline{\Delta H}_3$ is the partial molal enthalpy of transfer of the nonelectrolyte (n.e.) from water to aqueous electrolyte solutions



Under limiting conditions $\overline{\Delta H}_3$ depends on independent contributions from M^+ and X^- and thus the difference in $\overline{\Delta H}_3$ for various pairs of electrolytes having a common ion at the same value of m_2 should be constant. It is not possible at this time to deduce the absolute contributions of the individual ions.

The partial molal enthalpy of transfer ($\overline{\Delta H}_3$) of HOAc was determined by the difference between the enthalpy of solution of glacial acetic acid in aqueous salt solution, ΔH_3 , and in water, respectively, ΔH_3^0 .

$$\overline{\Delta H}_3 = \Delta H_3 - \Delta H_3^0 \quad (10)$$

The enthalpies of transfer in combination with free energies of transfer, $\overline{\Delta F}_3$, where

$$\overline{\Delta F}_3 = 2.303RT \log \gamma_3/\gamma_3^0 \quad (11)$$

yield the partial molal entropies of transfer, $\overline{\Delta S}_3$

$$\overline{\Delta S}_3 = \frac{\overline{\Delta H}_3 - \overline{\Delta F}_3}{T} \quad (12)$$

Some attempts have been made to relate $\overline{\Delta S}_3$ to the microstructure of such systems.^{1a,6} However, partly due to the lack of such data and the complex nature of the interactions no satisfactory correlations have been obtained.

It may be noted that since $\overline{\Delta H}_3$ fixes the temperature coefficient of γ_3 , prediction of high-temperature properties of such solutions is possible.^{1b}

II. Experimental Section

Calorimeter and Measurements. The calorimeter has been described previously⁷ and was located in a laboratory which was temperature regulated at 25°. All measurements were carried out at $25.00 \pm 0.05^\circ$. Sealed glass ampoules with weighed quantities of pure acetic acid were submerged in 450 g of liquid contained in the dewar. Both water and salt solutions contained a sufficient quantity of hydrochloric acid (ca. 2 mmoles) to limit the dissociation of acetic acid to less than 1%.⁸ An increase in the amount of hydrochloric acid to reduce the dissociation to less than 0.5% had no measurable effect on ΔH_3 . After crushing the ampoule against the bottom of the dewar, mixing proceeded very rapidly and thermal equilibrium was attained in less than 5 sec. Electrical calibrations before and after each run were made to obtain the average energy equivalent of the calorimeter.

Materials. All materials were AR grade. Pure acetic acid (label analysis 100.0%) was titrated in aqueous solution against standard sodium hydroxide (HOAc found 99.95%). All salts were dried at 120° overnight and dissolved to 1 *m* concentrations with weighed quantities of distilled CO₂-free water.

III. Results and Discussion

The enthalpies of solution of acetic acid in water (ΔH_3^0) and in 1 *m* salt solutions (ΔH_3) are shown in Table I. Variations in quantity of acetic acid in the ampoule and consequently in its final concentration

(5) J. N. Sugden, *J. Chem. Soc.*, 128, 174 (1926); see also ref 4, p 535.

(6) H. S. Frank and M. W. Evans, *J. Chem. Phys.*, 13, 507 (1945).

(7) J. H. Stern and C. W. Anderson, *J. Phys. Chem.*, 68, 2528 (1964).

(8) See ref 4, p 675.

Table I: Enthalpies of Solution of Acetic Acid in Water (ΔH_3°) and in 1 *m*. Electrolyte Solutions (ΔH_3)

Solution	$-\Delta H_3^\circ$ ^a and $-\Delta H_3$	HOAc, mmoles
Water	286	11.14
	277	9.903
	282	7.620
	276	14.77
	Mean 280 ± 5	
LiCl	176	10.50
	169	6.432
	177	11.86
	174	12.20
	Mean 174 ± 4	
NaCl	311	8.818
	308	6.674
	317	7.742
	320	15.10
	Mean 314 ± 6	
KCl	430	9.469
	437	9.774
	428	8.859
	432	7.808
	Mean 432 ± 5	
LiBr	214	9.863
	221	7.175
	222	10.27
	221	11.42
	Mean 220 ± 4	
NaBr	351	8.005
	347	7.241
	354	17.88
	353	6.651
	Mean 351 ± 4	
KBr	466	10.39
	474	7.221
	491	11.30
	479	9.107
	Mean 478 ± 12	
LiNO ₃	276	8.201
	279	10.99
	275	12.71
	Mean 277 ± 4	
NaNO ₃	382	10.13
	375	10.65
	375	8.575
	Mean 377 ± 6	
KNO ₃	509	10.51
	505	11.94
	501	11.29
	Mean 505 ± 7	

^a All enthalpies in calories per mole.

(over-all range 0.015–0.044 *m*) resulted in essentially constant enthalpies. All uncertainty intervals associated with mean values are their standard deviations multiplied by factors necessary to give 90% confidence levels.

Table II shows calculated values of free energies, enthalpies, and entropies of transfer.

Table II: Summary of $\overline{\Delta F}_3$, $\overline{\Delta H}_3$, and $\overline{\Delta S}_3$

Electrolyte	$\overline{\Delta F}_3$, cal/mole	$\overline{\Delta H}_3$, cal/mole	$\overline{\Delta S}_3$, cal/mole deg
LiCl	102 ± 10 ^a	106 ± 6 ^b	0.00 ^c
NaCl	85 ± 9	-34 ± 8	-0.40
KCl	38 ± 5	-152 ± 7	-0.65
LiBr	87 ± 9	60 ± 6	-0.10
NaBr	68 ± 7	-71 ± 6	-0.45
KBr	18 ± 5	-188 ± 13	-0.70
LiNO ₃	28 ± 5	3 ± 6	-0.10
NaNO ₃	14 ± 10	-97 ± 8	-0.35
KNO ₃	-28 ± 5	-225 ± 9	-0.65

^a Estimated uncertainty. ^b Over-all uncertainty is $[(e_{\text{H}_2\text{O}})^2 + (e_{\text{MX}})^2]^{1/2}$ where $e_{\text{H}_2\text{O}}$ and e_{MX} are tabulated uncertainties of ΔH_3° and ΔH_3 , respectively. ^c Uncertainty in $\overline{\Delta S}_3$ is ±0.05 cal/mole deg or less.

Since the differences in the values of Table II between salts with a common ion remain essentially constant, the properties for each electrolyte are composed of additive contributions from the component ions. These differences have been calculated for all possible combinations in Table II⁹ and their average values are shown in Table III with an estimated uncertainty of *ca.* ±12 cal/mole or ±0.05 cal/mole deg. Differences between values of k_{32} and dk_{32}/dT may be obtained from eq 11, 6, and 7.

The $\Delta(\overline{\Delta F}_3)$ values for cation and anion interchange follow the same general trend observed with other acidic

Table III: Ion Contribution Differences

Ion pair	$\Delta(\overline{\Delta F}_3)$, cal/mole	$\Delta(\overline{\Delta H}_3)$, cal/mole	$\Delta(\overline{\Delta S}_3)$, cal/mole deg
Li ⁺ -Na ⁺	17	124	0.35
Na ⁺ -K ⁺	46	121	0.25
Cl ⁻ -Br ⁻	17	40	0.05
Br ⁻ -NO ₃ ⁻	53	40	-0.05

(9) For example values of Li⁺-Na⁺ were obtained from the average of the differences of the thermodynamic properties of transfer between LiCl-NaCl, LiBr-NaBr, and LiNO₃-NaNO₃.

nonelectrolytes. According to McDevit and Long,² the observed trends may be partially accounted for by considering the most likely orientation and polarization of water molecules in the solvation spheres of the ions. For cations, the water molecules should be oriented with the protons facing outward with maximum polarization expected for the cation with the highest charge density. Therefore repulsion between an acidic nonelectrolyte and hydration spheres of cations may occur, with the magnitude of repulsion decreasing from Li^+ to K^+ .

The orientation of water molecules in the hydration sphere of the larger anions is reversed and the polarization is reduced. Thus one would expect $\Delta(\overline{\Delta F}_3)$ to increase from Cl^- to NO_3^- with smaller changes than those for the cations. The observed trend appears to be opposite to that expected on the basis of orientation and polarization considerations alone and may be explained by postulating an exchange of water and nonelectrolyte molecules in the solvation sphere of the anion.

It may be observed that the contribution of $\overline{\Delta S}_3$ to $\overline{\Delta F}_3$ is primarily cation sensitive, while that of $\overline{\Delta H}_3$ depends on both ions, with the cation supplying the major share. The free-energy difference (Table III) between tabulated pairs of ions of like charge is thus mainly an entropy effect.

The thermodynamic properties of transfer are related to the analogous effect of electrolyte transfer in the presence of a nonelectrolyte in aqueous solution. It can be shown¹⁰ that

$$k_{32} = k_{23} \quad (13)$$

where k_{23} is the nonelectrolyte–electrolyte parameter. Thus, if the temperature derivatives of k_{32} and k_{23} are equal, it follows that in the limiting region

$$\frac{\overline{\Delta H}_2}{\overline{\Delta H}_3} = \frac{m_3}{m_2} \quad (14)$$

where $\overline{\Delta H}_2$ is the enthalpy of transfer of the electrolyte at very low m_2 from water to aqueous nonelectrolyte solutions at m_3 . Equations 13 and 14 can be used for prediction of electrolyte activity coefficients and their temperature derivatives in the presence of nonelectrolytes. The equality of k_{32} and k_{23} was demonstrated¹¹ for nitromethane and a variety of salts. Measurements at this laboratory of $\overline{\Delta H}_2$ and $\overline{\Delta H}_3$ for the system nitromethane–potassium chloride indicate the validity of eq 14 when small quantities of solute are present in 1 *m* aqueous salt or nitromethane solutions, respectively. Under these conditions $\overline{\Delta H}_2$ and $\overline{\Delta H}_3$ are equal within experimental error.¹² Further such studies on acetic acid systems are in progress.

Acknowledgment. The authors wish to thank the U. S. Army Research Office (Durham) and the Long Beach California State College Foundation for financial assistance.

(10) See ref 3b, p 586.

(11) G. R. Haugen and H. L. Friedman, *J. Phys. Chem.*, **60**, 1363 (1956).

(12) J. H. Stern and D. Fost, unpublished data.

Equilibrium Pressures of Hydrogen Dissolved in α -Zirconium

by Franco Ricca

Institute of Analytical Chemistry, University of Turin, Turin, Italy

and Tiziano A. Giorgi

SAES-Getters Research Laboratory, Milan, Italy

Accepted and Transmitted by The Faraday Society (February 7, 1967)

The pressures of gaseous hydrogen at equilibrium with hydrogen solutions in α -zirconium have been measured in an ultrahigh-vacuum (UHV) system, by using an omegatron mass spectrometer, over the temperature interval from 450 to 750° and for hydrogen-to-metal atom ratios in the region of 10^{-4} . The solutions were found to follow Sievert's law; a constant relative partial molal enthalpy of -12.41 kcal/g-atom was determined, and the relative partial molal entropy was proved to be essentially independent of temperature. The partial molal entropy of dissolved hydrogen and the relative partial molal free energy were evaluated at 500° for different atom ratios from 10^{-4} to 10^{-3} .

Introduction

In studies of hydrogen solution in transition metal exothermic occluders considerable attention is often paid to zirconium, although only sparse data are actually available about the very low concentrations of hydrogen in the α phase of the metal. Therefore, it seemed useful to investigate the equilibrium between H_2 and α -Zr at sufficiently low concentrations to ensure both the stability of the α phase and the applicability of the thermodynamics of ideal dilute solutions to the system under study.

The experimental difficulties involved in the treatment of the samples and in the measurement of very low hydrogen pressures were faced by degassing the sample at high temperature in an UHV system by means of induced eddy currents, by measuring the hydrogen pressure with a micro mass spectrometer, and by employing lanthanum hexaboride coated filaments in all the gauges. Under these conditions, consistent data were gathered for a thermodynamic treatment of hydrogen dissolved in α -Zr.

Experimental Section

The pumping system was of the usual UHV type, with two fractionating oil diffusion pumps in series and liquid nitrogen cooled metal traps. The measuring device, shown in detail in Figure 1, was all in borosili-

cate glass except for valve V2 (a bakeable, 1.5-in., all-metal UHV bellows-type tap). It was contained in a baking oven and could be heated to 450°. This part of the system was comprised of: two ground-glass spherical joint isolation valves V1 and V3, of which V1 carried a capillary of known conductance; three Bayard-Alpert ionization gauges BAG-1, BAG-2, and BAG-3, all with lanthanum hexaboride covered tungsten filaments;¹ an omegatron type of mass spectrometer,² with a rhenium filament also covered with lanthanum hexaboride; and two sorption cells C and C'.

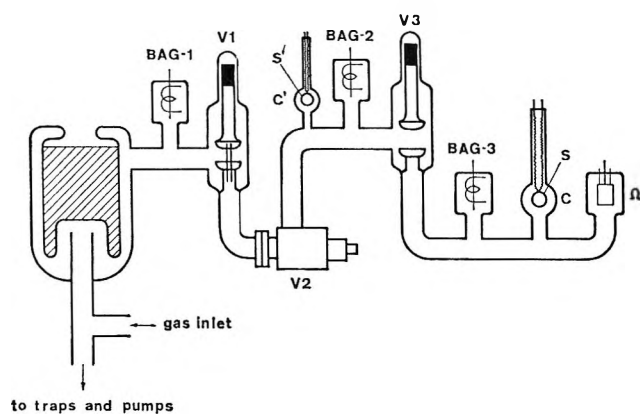
The sample chamber C consisted of a glass tube through which two tungsten rods (2-mm diameter) were sealed, welded to a Pt—Pt-13% Rh thermocouple of 0.35-mm diameter and of 300-mm length. Each thermocouple wire element was independently wound into a spiral^{3,4} and the other extremities of the spirals were welded to a ring of about 5-mm diameter, made up of the same platinum wire, which formed the core of

(1) J. M. Lafferty, *J. Appl. Phys.*, **22**, 299 (1951).

(2) W. Steckelmacher and J. D. Buckingham, *Nuovo Cimento Suppl.*, **1**, 418 (1963).

(3) No insulating materials have been used, as it was reported that they may cause instability of the thermocouple elements at high temperatures.⁴

(4) B. E. Walker, C. T. Ewing, and R. R. Miller, *Rev. Sci. Instr.*, **36**, 601, 816 (1965).



to traps and pumps
Figure 1. Measuring apparatus.

the suspended sample S. The sample was made of zirconium powder (459 mg), pressed to the core at 100 kg/mm² so as to form a "doughnut" of rectangular cross section which enabled uniform heating by externally induced eddy currents, thus avoiding the use of heaters and supports, normally acting as sources of heavy contamination within the cell. A similar sample S', consisting of titanium, was introduced in C' and employed to sorb the gas initially, in order to obtain a better metering of the inflow, to further purify the hydrogen, and to enable a faster transfer of the gas to the zirconium sample.

The low hydrogen concentrations employed prevent appreciable errors in the thermocouple response caused by the diffusion of hydrogen in the thermocouple metals,⁵ while no detectable alloying of zirconium with the thermocouple materials was found after the various thermal treatments on the sample. The temperature error was estimated to be $\pm 0.5\%$.

A pressure of the order of 10^{-9} torr could be attained in the isolated system when both the Bayard-Alpert gauges and the omegatron were switched on,⁶ but the pressure monitored by the omegatron fell well below 10^{-10} torr when the Bayard-Alpert gauges were switched off.⁷ This revealed an outgassing from the gauges, due to the fact that the high electron currents which are necessary for a proper degassing could not be produced without causing damage to the lanthanum hexaboride coating of the filaments. However, such a limited outgassing was in no way troublesome, since BAG-2, in contact with the subsidiary sample S' which was able to retain the emitted impurities, was operated only when V3 was closed and so could not transfer its degassing products to the sample S, while, on the other hand, BAG-3 was never functioning during equilibrium measurements but was only used for controlling the calibration of the omegatron at the end of any measuring run.

Both sorbing samples S and S' were subjected to a preliminary thermal processing, which consisted of gradually bringing them to 1050° and of maintaining them at such a temperature for 30 min under dynamic vacuum conditions, in order to remove dissolved gases and evaporable impurities and to sinter the compressed powder to such an extent that no appreciable changes could occur during subsequent heat treatments. Since this produced the evaporation of part of their metal impurities,⁸ after cooling and back filling of the system with argon, the samples were removed and transferred to an argon-filled container, and the metallized parts of the system were substituted with new clean parts. The system was then flushed with argon and the sorbing samples were remounted. A new heating of the samples to 1050° produced no further metal evaporation.

If no particular precautions were taken in the subsequent cooling of the zirconium sample, reliable hydrogen pressures could not be obtained; this was interpreted as due to the partial presence of β -Zr in nonequilibrium conditions in the cold sample. Hence, to facilitate the complete transition from the β to the α phase (temperature of transition for pure zirconium 863–865°^{9,10}), the sample was then maintained at 800° for 15 hr under a pressure less than 10^{-9} torr.

After the sample was prepared, V3 was closed and through V1 a known conductance was introduced between the manifold and C' (the zirconium sample S being isolated from the system). The temperature of S' was raised to about 600° and a suitable hydrogen pressure was established on BAG-1.¹¹ The pumping action of S' and the inflow of hydrogen could be measured by applying the usual Knudsen formulas. If the pressure on BAG-2 increased to 10^{-5} torr, the temperature of S' was lowered by some 50 or 100°. When the right quantity of hydrogen had been sorbed by S', V2 was closed, BAG-2 switched off, and V3 opened; S was heated to 600° and S' to 1000°; then S was gradually brought to approximately 100°. In this way, even for the largest quantities of hydrogen em-

(5) R. J. Galagali, *Brit. J. Appl. Phys.*, **15**, 208 (1964).

(6) The Bayard-Alpert gauges were operated at 10 μ a and the omegatron at 2.5 μ a ionizing current.

(7) L. A. Pétermann, *Vakuum-Tech.*, **11**, 200 (1962).

(8) The analysis supplied with the zirconium indicated the following impurity contents (in ppm): Al, 24.0; B, <0.2; Cd, <0.5; Co, <5.0; Cr, 40.0; Cu, <20.0; Fe, 310.0; Hf, 46.0; Mg, 40.0; Mn, 25.0; Mo, <10.0; N, 15.0; Ni, 10.0; Pb, 20.0; Si, 50.0; Sn, 5.0; Ti, <20.0; V, <20.0; W, <40.0; Zn, <50.0; Cl, <10.0.

(9) T. B. Douglas, *J. Res. Natl. Bur. Std.*, **A67**, 403 (1963).

(10) J. D. Fast, "Interactions of Metals and Gases," Philips Technical Library, Eindhoven, The Netherlands, 1965, p 176.

(11) Spectroscopically pure hydrogen from the British Oxygen Co. Ltd. was used.

ployed in these experiments, 2 hr was sufficient for completely transferring the hydrogen from S' to S. A maximum residual pressure of 10^{-8} torr was observed with S' kept at 1000° and the analysis of this residual gas ambient gave 98% hydrogen, the balance being essentially noble gases. At this point V3 was closed and experimenting initiated.

By varying the temperature of the sample, equilibrium pressures were measured over the temperature range from 450 to 750° and the pressure range from 10^{-6} to 10^{-4} torr.¹² Stabilizing times of about 20 min proved to be sufficient to attain equilibrium in the explored range of temperatures and concentrations. When measurements with a given concentration were terminated, the omegatron calibration for hydrogen was checked against BAG-3, over the pressure range of interest. To carry out another series of measurements, with a different concentration, all of the hydrogen had to be removed from the samples S and S', by maintaining them at 800° for 15 hr under a dynamic vacuum (pressure $<10^{-9}$ torr); then the same procedure already described could be followed for a new quantity of hydrogen to be introduced.

Finally, a number of checks were carried out to control the attainment of true equilibrium conditions (by comparison of pressures obtained with increasing and decreasing temperatures), the stability of the sample (by comparison of data at the beginning and at the end of a complete series of measurements), and the equivalence of different zirconium samples.

Results and Discussion

In Figure 2, the logarithm of the equilibrium pres-

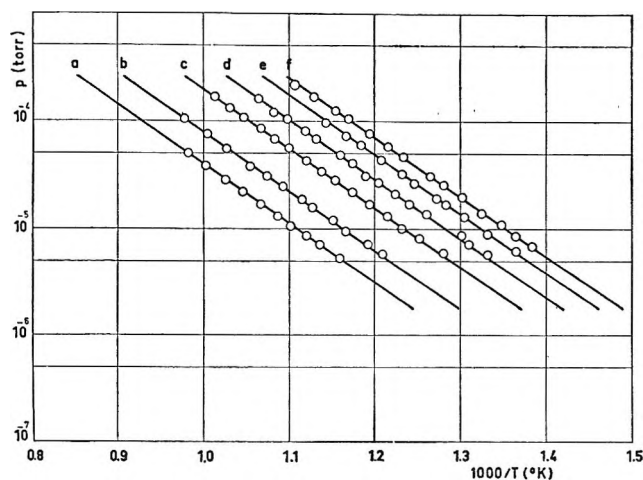


Figure 2. Equilibrium pressure as a function of temperature in the H_2 - α -Zr system. Weight of the sample, 459 mg. Sorbed quantities (in cm^3 torr at 25°): a, 12.4; b, 18.4; c, 27.9; d, 38.7; e, 48.9; f, 60.0.

sure is plotted as a function of the reciprocal temperature; the different points for a given hydrogen concentration fall on a straight line. The continuous lines in this figure have been drawn from the linear equations calculated by the least-squares method, whose intercepts and slopes are given in Table I, together with the relative standard deviations. From this table it may be observed that all of the lines are actually parallel to each other; the mean value of the slope is $\bar{b} = -5426$ and the standard deviation from the average is $s = 30$ (less than 0.6%), which is within the limits of the standard deviation of the slope for a single straight line.

Table I: Dependence of the Equilibrium Pressure on Temperature, at Different Concentrations^a

q_{H_2}	$\log p = a + b(1/T)$			
	a	s_a	b	s_b
12.4	1.035	0.038	-5446	35
18.4	1.270	0.038	-5379	34
27.9	1.734	0.035	-5446	30
38.7	1.943	0.057	-5379	48
48.9	2.197	0.037	-5429	29
60.0	2.396	0.045	-5457	36

^a p in torr; T in $^\circ K$; q_{H_2} in cm^3 torr at 25° ; weight of Zr 459 mg.

For each of the hydrogen concentrations examined, hydrogen pressures at 50° intervals, in the range 450 – 750° , were interpolated from the experimentally determined relationships reported in Table I; at each temperature the logarithm of the hydrogen pressure was found to be a linear function of the logarithm of the square of the hydrogen concentration in α -Zr. The corresponding equations have been calculated by the least-squares method and the obtained slopes presented a mean value of 0.995 with standard deviations of the slope for single straight lines all below 0.015, so that it could be concluded that, in the explored concentration range, hydrogen solutions in α -Zr follow Sievert's law. This is better seen from plots in Figure 3, where the straight lines have been drawn with the fixed slope of 45° through the "center of gravity" of the coordinates for each set of data at a given temperature.

As a consequence of the results previously illustrated, the relationship between concentration, temperature, and equilibrium pressure may be expressed by

$$\log p = A + \log [(q_{H_2}/q_{Zr})^2] + \bar{b}(1/T) \quad (1)$$

(12) Usual corrections were introduced for the thermomolecular flow at different temperatures.

where A may be easily calculated from the intercepts α of the straight lines in Figure 3 through the equation

$$A = \alpha - \bar{b}(1/T) \quad (2)$$

From the values calculated in this way for each temperature, the mean value $\bar{A} = 4.133 \pm 0.001$ was obtained. The extremely good agreement between the A values calculated at different temperatures possibly arises from error compensation between α and \bar{b}/T . An estimated error of about 2% may, however, be assumed by considering experimental errors in T and standard deviations in \bar{b} and α .

Equation 1 may be written as

$$\log p = 4.133 + \log [(q_{\text{H}_2}/q_{\text{Zr}})^2] - 5426(1/T) \quad (3)$$

(where p is in torr, q_{H_2} is in cm^3 torr at 25° , q_{Zr} is in mg, and T is in $^\circ\text{K}$), or also as

$$\ln p = 12.134 + \ln [(N_{\text{H}}/N_{\text{Zr}})^2] - 12,494(1/T) \quad (4)$$

(where p is in atmospheres and N_{Zr} and N_{H} are, respectively, the number of metal atoms in the zirconium sample and the number of hydrogen atoms dissolved in it).

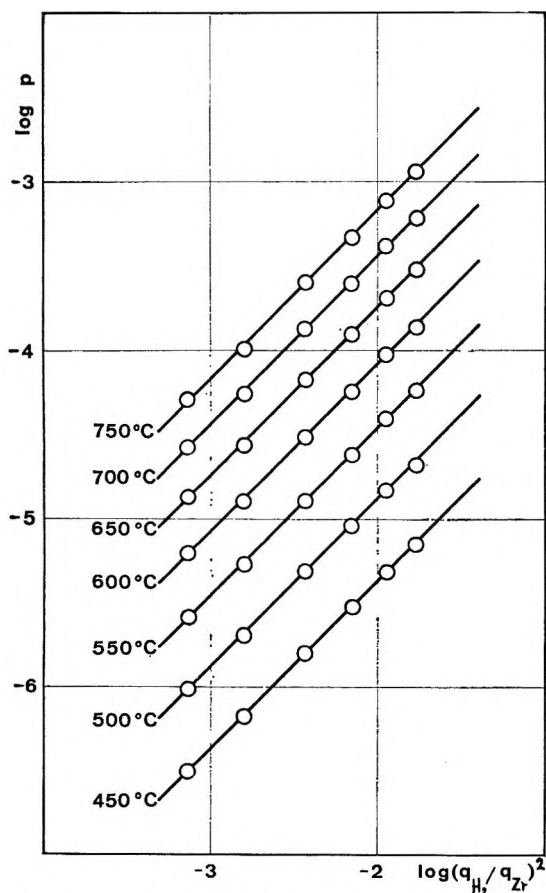


Figure 3. Sievert's plots for H_2 in α -Zr.

The fact that Sievert's law is obeyed by the present data confirms that the sorption of hydrogen by zirconium is a dissociative process. The equilibrium conditions between the hydrogen in solution and that in the gaseous phase may therefore be written as

$$\bar{G}_{\text{H}(\alpha)} = 1/2 G_{\text{H}_2(\text{g})} \quad (5)$$

(where $\bar{G}_{\text{H}(\alpha)}$ is the partial free energy per g-atom of hydrogen dissolved in α -Zr and $G_{\text{H}_2(\text{g})}$ is the free energy per mole of hydrogen in the gaseous phase), or also

$$\bar{G}_{\text{H}(\alpha)} = 1/2 G^\circ_{\text{H}_2(\text{g})} + 1/2 RT \ln p \quad (6)$$

(where $G^\circ_{\text{H}_2(\text{g})}$ is the standard molal free energy of gaseous hydrogen and p is the hydrogen pressure in atmospheres). Equation 6 may be written in the form

$$1/2 R \ln p = -(\bar{S}_{\text{H}(\alpha)} - 1/2 S^\circ_{\text{H}_2(\text{g})}) + (\bar{H}_{\text{H}(\alpha)} - 1/2 H^\circ_{\text{H}_2(\text{g})}) \frac{1}{T} \quad (7)$$

where $\bar{S}_{\text{H}(\alpha)}$, $S^\circ_{\text{H}_2(\text{g})}$, $\bar{H}_{\text{H}(\alpha)}$, and $H^\circ_{\text{H}_2(\text{g})}$ are referred to the same conditions already defined for $\bar{G}_{\text{H}(\alpha)}$ and $G^\circ_{\text{H}_2(\text{g})}$. Comparison of eq 7 with eq 4 gives for the relative partial molal entropy (partial molal entropy of solution)

$$\Delta S = \bar{S}_{\text{H}(\alpha)} - 1/2 S^\circ_{\text{H}_2(\text{g})} = -\{12.057 + 1/2 R \ln [(N_{\text{H}}/N_{\text{Zr}})^2]\} (\pm 0.250) \text{ eu/g-atom} \quad (8)$$

and for the relative partial molal enthalpy (partial molal enthalpy of solution)

$$\Delta H = \bar{H}_{\text{H}(\alpha)} - 1/2 H^\circ_{\text{H}_2(\text{g})} = -12,410 (\pm 75) \text{ cal/g-atom} \quad (9)$$

Therefore, in the range of temperatures and concentrations experimentally investigated and within the approximations explicitly furnished above, two points must be put in evidence.

(1) The relative partial molal enthalpy for hydrogen is independent of both temperature and concentration. Independence from concentration reflects the behavior of an ideal dilute solution, while independence from temperature requires that, throughout a temperature interval of a few hundred degrees, there should be parallel trends in both the partial molal enthalpy of dissolved hydrogen and the standard enthalpy per g-atom of gaseous hydrogen.

(2) The relative partial molal entropy for hydrogen is essentially independent of temperature.

This means that, throughout a temperature interval of a few hundred degrees, the partial molal entropy of

dissolved hydrogen and the standard entropy per g-atom of gaseous hydrogen have a temperature dependence which does not differ by more than $\pm 1\%$.

The value of the relative partial molal enthalpy may be compared with the data available in the literature for hydrogen in solution in α -Zr. A few of the Zr-H₂ phase equilibria studies have been reviewed and summarized by Libowitz¹³ and more recently an almost complete collection of enthalpy data has been presented by Westlake.¹⁴ The relative partial molal enthalpies for the solution of hydrogen in α -Zr are reported in Table II. It is evident that appreciable discrepancies exist between the different authors, even if all of the determinations are quite recent. In particular it must be noted that the only value referring to a region of concentrations below the hydrogen-to-metal ratio of 0.06 (and in this sense better comparable with our measurements) is the exceptionally low one of Mallett and Albrecht.¹⁵

Values of ΔS , as calculated for different concentrations in the range experimentally investigated in the

Table II: Relative Partial Molal Enthalpies for the Solution of H₂ in α -Zr

Ref	ΔH , kcal/g-atom	Experimental data
a	-13.80	Heat content measurements
b	-14.25	Pressure-composition-temperature curves
c	-12.30 ^d	Pressure-composition-temperature curves
e	-7.85	Pressure-composition-temperature curves
f	-14.45 ^g	Pressure-composition-temperature curves
h	-12.41	Pressure-composition-temperature curves

^a T. B. Douglas, *J. Am. Chem. Soc.*, **80**, 5040 (1948). ^b E. A. Gulbransen and K. F. Andrew, *J. Metals*, **7**, 136 (1955). ^c C. E. Ells and A. D. McQuillan, *J. Inst. Metals*, **85**, 89 (1956). ^d Estimated by Westlake¹⁴ from published curves. ^e M. W. Mallett and W. M. Albrecht, *J. Electrochem. Soc.*, **104**, 142 (1957). ^f J. R. Morton and D. S. Stark, *Trans. Faraday Soc.*, **56**, 351 (1960). ^g Determined for D₂ solution in α -Zr. ^h Present work.

Table III: Entropy and Free Energy Dependence on Concentration for H₂ Solutions in α -Zr

$N_{\text{H}}/N_{\text{Zr}}$	ΔS , eu/g-atom	$\bar{S}_{\text{H}(\alpha)}^{500^\circ}$, eu/g-atom	ΔG_{500° , kcal/g-atom
1×10^{-4}	6.24	25.18	-17.24
2×10^{-4}	4.87	23.80	-16.17
3×10^{-4}	4.06	22.99	-15.55
4×10^{-4}	3.49	22.42	-15.11
5×10^{-4}	3.05	21.98	-14.77
6×10^{-4}	2.69	21.61	-14.49
7×10^{-4}	2.38	21.31	-14.25
8×10^{-4}	2.11	21.04	-14.04
9×10^{-4}	1.88	20.81	-13.86
1×10^{-3}	1.67	20.60	-13.70

present work, are given in Table III, together with the corresponding data for the partial molal entropy of dissolved hydrogen $\bar{S}_{\text{H}(\alpha)}$ and for the relative partial molal free energy $\Delta G = \bar{G}_{\text{H}(\alpha)} - (1/2)G_{\text{H}_2(\text{g})}^\circ$, both evaluated at 500°.

As far as the dependence of the relative partial molal entropy on concentration is concerned, it was shown by Gulbransen and Andrew¹⁶ that a relationship of the form encountered in present measurements may be explained by assuming the hydrogen atoms to be localized in the tetrahedral interstices of the hexagonal compact lattice of α -Zr and to be characterized by purely vibrational motion. It has now to be seen if the above relationship necessarily requires the assumed model and if the model itself is really consistent with the whole of the experimental data which may be obtained for this system. In fact, some doubts on this point are arising from the established constancy of the relative partial molal entropy with temperature, as well as from the values found for the partial molal entropy of dissolved hydrogen, which appear to be somewhat higher than expected in a purely vibrational state.

(13) G. G. Libowitz, *J. Nucl. Mater.*, **2**, 1 (1960).

(14) D. G. Westlake, *ibid.*, **7**, 346 (1962).

(15) See Table II, footnote e.

(16) See Table II, footnote b.

Thermodynamic Properties of Hydrogen and Deuterium in α -Zirconium

by Franco Ricca

Institute of Analytical Chemistry, University of Turin, Turin, Italy

Accepted and Transmitted by The Faraday Society (February 28, 1967)

Solutions of deuterium in α -zirconium, in the atom ratio range of 10^{-4} , have been studied over the temperature interval from 450 to 800°. Only minor differences were found to distinguish the deuterium from the hydrogen solutions. The data gathered for both gases have been discussed in terms of the model of Gulbransen and Andrew, which assumes the dissolved atoms to occupy the tetrahedral interstices in the metal lattice and their motion to be a purely vibrational one. Such a model was not found applicable to the experimental data, which seem to indicate a larger mobility of dissolved species.

Introduction

In a previous article,¹ the equilibrium between hydrogen in the gaseous phase and hydrogen dissolved in α -Zr, at hydrogen-to-metal atom ratios from 10^{-4} to 10^{-3} , was considered. The low hydrogen concentrations and the experimental technique used allowed the study of this equilibrium over quite an extended range of pressures and temperatures. The data obtained from these measurements should therefore provide an effective test of the widely employed model of Gulbransen and Andrew² for hydrogen solutions in α -Zr, which is based on the well-known statistical treatment of Martin and Rees^{3,4} and which has been recently proposed as a widely applicable model for the occluded gases in transition metals.^{5,6}

This model assumes that hydrogen occupies as atoms the tetrahedral interstices in the zirconium lattice and that hydrogen atoms are characterized by only vibrational motion. In fact, the hydrogen sorption was confirmed to be dissociative in our case (Sievert's law was observed) and the system was shown to behave as an ideal dilute solution (partial molal enthalpy of solution was invariant with concentration). However, some doubts concerning the applicability of a purely vibrational model may arise when considering the invariance of the relative partial molal enthalpy and entropy with temperature, as well as the rather high values of the partial molal entropy of the dissolved hydrogen.

In order to ensure a more extended experimental basis for a discussion on this point, the system D_2 - α -Zr was

studied with methods and techniques strictly similar to those previously employed for hydrogen. The results of these measurements are reported and a discussion is presented of the data relative to both hydrogen and deuterium in solution in α -Zr, in terms of the model of Gulbransen and Andrew.

Experimental Section

Vacuum system, equipment, zirconium, thermal treatment of the sample, and experimental procedure were the same as previously illustrated.¹ A zirconium sample of 450 mg was used and 99.5% deuterium from 20th Century Electronics Ltd. was employed.

The deuterium pressure was measured by the height of the mass 4 peak from the omegatron spectra. The instrument was calibrated on this peak. A check of the height of peaks 3, 2, and 1 showed that, throughout the course of the experiments, the HD partial pressure, resulting from equilibration, was always below 2%. Since the hydrogen concentrations were very low and the partial pressure of deuterium could be directly monitored by the omegatron and since previous measurements had shown that the solution in α -Zr could be

-
- (1) F. Ricca and T. A. Giorgi, *J. Phys. Chem.*, **71**, 3627 (1967).
 - (2) E. A. Gulbransen and K. F. Andrew, *J. Metals*, **7**, 136 (1955).
 - (3) A. L. G. Rees, *Trans. Faraday Soc.*, **50**, 335 (1954).
 - (4) S. L. H. Martin and A. L. G. Rees, *ibid.*, **50**, 343 (1954).
 - (5) O. M. Katz and E. A. Gulbransen in "Non-stoichiometric Compounds," Academic Press Inc., New York, N. Y., 1964, p 210.
 - (6) J. D. Fast, "Interaction of Metals and Gases," Philips Technical Library, Eindhoven, The Netherlands, 1965, p 175.

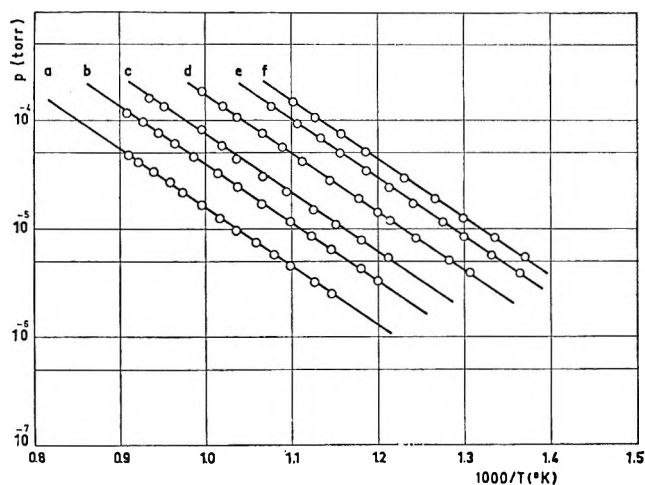


Figure 1. Equilibrium pressure as a function of temperature in the D_2 - α -Zr system. Weight of the sample, 450 mg. Sorbed quantities (in cm^3 torr at 25°): a, 7.9; b, 12.9; c, 17.4; d, 27.5; e, 37.4; f, 47.2.

considered an ideal dilute solution, no allowance has been made for the fact that actually the system was a ternary one.

Results

Experimental data concerning the equilibrium pressure of deuterium on the zirconium sample at different temperatures are plotted in Figure 1. The continuous straight lines, corresponding to different deuterium concentrations, were drawn according to the linear equations obtained from the experimental points by the least-squares method. Intercepts, slopes, and related standard deviations are reported in Table I.

Table I: Dependence of the Equilibrium Pressure on Temperature at Different Concentrations^a

$\log p = a + b(1/T)$				
q_{D_2}	a	s_a	b	s_b
7.9	0.629	0.022	-5442	22
12.9	0.940	0.010	-5357	10
17.4	1.204	0.042	-5351	40
27.5	1.620	0.021	-5392	18
37.4	1.920	0.036	-5382	29
47.2	2.065	0.041	-5356	33

^a p in torr; T in $^\circ\text{K}$; q_{D_2} in cm^3 torr at 25° ; weight of Zr, 450 mg.

Also in the present case, as previously found for hydrogen, the straight lines are all parallel to each other, with an average slope $\bar{b} = -5380$ and with a standard deviation from the average $s = 34$ (less than 0.7%).

From the different equations of Table I, which refer to the different quantities of deuterium in solution, it has been possible to calculate, at regular intervals of 50° , in the temperature region from 450 to 800° (experimental temperature range 456 - 828°), the necessary data for the Sievert's plots in Figure 2. It may be observed that also in the case of deuterium Sievert's law is closely followed: the continuous lines in Figure 2 have been drawn with a slope of 45° through the "center of gravity" of the coordinates for each set of points. From their intercepts α and using the equation $A = \alpha - \bar{b}(1/T)$, the mean value $\bar{A} = 4.058 \pm 0.001$ was obtained, so that the relationship between concentration, temperature, and equilibrium pressure could be expressed as

$$\log p = 4.058 + \log [(q_{D_2}/q_{Zr})^2] - 5380(1/T) \quad (1)$$

(p is torr; q_{D_2} is in cm^3 torr at 25° ; q_{Zr} is in mg; T is in $^\circ\text{K}$) or also as

$$\ln p = 11.961 + \ln [(N_D/N_{Zr})^2] - 12,388(1/T) \quad (2)$$

(p is in atm; N_D and N_{Zr} are in atoms).

By considering the thermodynamical equilibrium between the deuterium in the gaseous phase and the deuterium in solution within the zirconium, the follow-

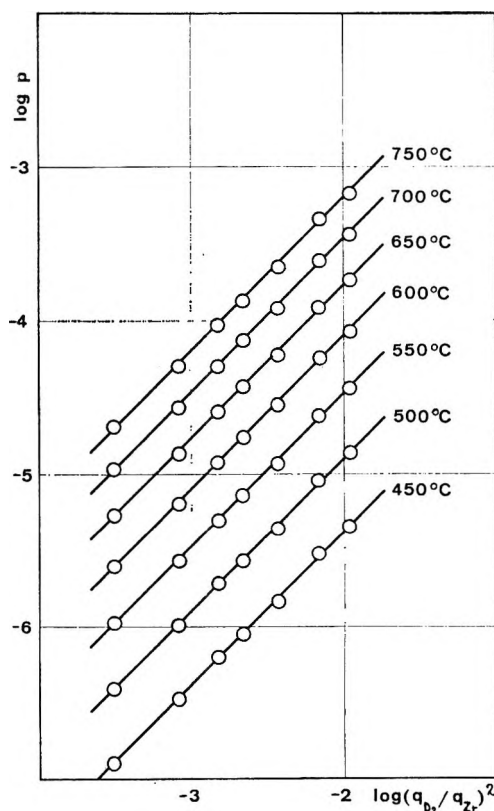


Figure 2. Sievert's plots for D_2 in α -Zr.

ing expressions were obtained for the relative partial molal entropy and for the relative partial molal enthalpy

$$\Delta S = -11.885 + \frac{1}{2}R \ln [(N_D/N_{Zr})^2] (\pm 0.250) \text{ eu/g-atom} \quad (3)$$

$$\Delta H = -12,310 (\pm 85) \text{ cal/g-atom} \quad (4)$$

The relative partial molal entropies, calculated from eq 3 for the same concentrations already considered for hydrogen, are shown in Table II. In this same table, the corresponding values of both the partial molal entropy of dissolved deuterium and the relative partial molal free energy at 500° are also given.

Table II: Entropy and Free Energy Dependence on Concentration for D₂ Solutions in α -Zr

N_D/N_{Zr}	ΔS , eu/g- atom	$\bar{S}_D(\alpha)_{500^\circ}$, eu/g- atom	ΔG_{500° , kcal/g- atom
1×10^{-4}	6.42	27.09	-17.27
2×10^{-4}	5.04	25.71	-16.21
3×10^{-4}	4.24	24.91	-15.58
4×10^{-4}	3.66	24.34	-15.14
5×10^{-4}	3.22	23.89	-14.80
6×10^{-4}	2.86	25.53	-14.52
7×10^{-4}	2.55	23.23	-14.28
8×10^{-4}	2.29	22.96	-14.08
9×10^{-4}	2.05	22.73	-13.90
1×10^{-3}	1.84	22.52	-13.73

The results obtained with deuterium confirm that, within the limits of the approximations furnished above, Sievert's law is obeyed, the relative partial molal enthalpy is constant with respect to both concentration and temperature, and the relative partial molal entropy is constant with temperature. Only minor quantitative differences characterize the two dissolved species, amounting to about 1% between their relative partial molal enthalpies and between their relative partial molal free energies at 500°, which is near the limits of the estimated experimental error. Also the difference between the constant terms in the ΔS expressions for hydrogen and deuterium is within the error limits; however, the partial molal entropies of dissolved species, as evaluated at 500° in the concentration range of Table II, are greater for deuterium than for hydrogen by an amount (7–10%) which largely overcomes these limits.

The Model of Gulbransen and Andrew

The close-packed hexagonal α phase of zirconium has four tetrahedrally coordinated interstitial sites (in fact

trigonal pyramidal) per unit cell, located at $(\frac{2}{3}, \frac{1}{3}, \frac{1}{6})$, $(\frac{2}{3}, \frac{1}{3}, \frac{5}{6})$, $(0, 0, \frac{1}{2})$, and $(0, 0, \frac{2}{3})$. Since a unit cell contains two zirconium atoms, there are two such sites per metal atom. Besides the tetrahedral interstices, there are also octahedrally coordinated interstitial sites, one per zirconium atom. This situation is essentially unaltered for zirconium hydrides and deuterides in both face-centered cubic and tetragonal phase. X-Ray and neutron diffraction studies have shown that in the stoichiometric compounds ZrH₂ and ZrD₂, as well as in the hydrides and deuterides of the other metals in this subgroup, the hydrogen or deuterium atoms are situated in the tetrahedral sites while the octahedral sites are empty.⁷⁻⁹

It is known from neutron-scattering experiments that zirconium hydrides have, in addition to the usual band of acoustical frequencies, also a sharp "optical" frequency, corresponding to vibrations of the individual hydrogen atoms. In the face-centered cubic δ -hydride, because of the higher symmetry at each hydrogen site, the three modes of vibration of a single hydrogen atom must have all nearly the same frequency. In the tetragonal ϵ -hydride, there should be a doubly degenerate frequency. However, an adequate fit of experimental data is obtainable by assuming that the environment of the hydrogen atoms is nearly isotropic, in spite of the compression along one axis. Finally also for the body-centered cubic β -hydride, unstable at room temperature, the not strictly valid hypothesis of a triply degenerate vibration mode was proved useful in constructing a model in accordance with thermodynamic data. Since in all of these cases the hydrogen atoms are vibrating nearly independently, with the metal atoms practically stationary, the vibrating frequencies for the deuterium atoms in corresponding deuterides can be obtained by using a factor $(1/\sqrt{2})$.

The frequencies and the Einstein characteristic temperatures for the "optical" vibrations of hydrogen atoms in the different zirconium hydrides have been calculated from the data available in the literature and are given in Table III. In the same table, the vibrational entropies at 500° calculated by the equation

$$S_v = R[(h\nu/kT)(e^{h\nu/kT} - 1)^{-1} - \ln(1 - e^{-h\nu/kT})] \quad (5)$$

are also given, as obtained by assuming the vibrations

(7) S. S. Sidhu, L. Heaton, and D. D. Zaubers, *Acta Cryst.*, **9**, 607 (1956).

(8) S. S. Sidhu, L. Heaton, and M. H. Mueller, *J. Appl. Phys.*, **30**, 1323 (1959).

(9) S. S. Sidhu, N. S. S. Murthy, F. P. Campos, and D. D. Zaubers, *Advances in Chemistry Series*, No. 39, American Chemical Society, Washington, D. C., 1963, p 87.

Table III: Frequencies, Characteristic Temperatures, and Entropies of Hydrogen Atoms in Different Zirconium Hydrides

Phase	Ref	Experimental data	ν , sec ⁻¹	θ_E , °K	$S_{H,vib}$, eu/g-atom	$S_{D,vib}$, eu/g-atom
ϵ (tetr)	a	Neutron diffraction	3.38×10^{13}	1622	2.53	4.13
		Heat capacity	3.57×10^{13}	1713	2.30	3.85
δ (fcc)	c	Neutron diffraction	3.14×10^{13}	1506	2.84	4.50
		Neutron diffraction				
β (bcc)	e	Neutron diffraction	3.31×10^{13}	1588	2.62	4.23
		f	Thermodynamic data	4.32×10^{13}	2073	1.60

^a A. D. B. Woods, B. N. Brockhouse, M. Sakamoto, and R. N. Sinclair, At. Energy Can. Ltd., Chalk River, Ont., AECL-1088 (1960).
^b H. E. Flotow and D. W. Osborne, *J. Chem. Phys.*, **34**, 1418 (1961). ^c I. Pelah, C. M. Eisenhauer, D. J. Hughes, and H. Palevsky, *Phys. Rev.*, **108**, 1091 (1957). ^d A. Andresen, A. W. McReynolds, M. Nelkin, M. Rosenbluth, and W. L. Whittemore, *ibid.*, **108**, 1092 (1957). ^e W. L. Whittemore and A. W. McReynolds, *ibid.*, **113**, 806 (1959). ^f T. B. Douglas, *J. Chem. Phys.*, 2248 (1964).

to be isotropic. The corresponding vibrational entropies for deuterium at the same temperature are given as well.

The model put forward by Gulbransen and Andrew² for the solution of hydrogen in α -Zr assumes that the hydrogen is dissolved in the α phase of the metal as atoms localized within the same tetrahedral sites which they would occupy in the stoichiometric hydride. Such atoms would be characterized by vibrational motion within these interstices and the partial molal entropy of hydrogen in the α phase would then be the sum of the vibrational entropy and of the entropy of number and position of the atoms distributed over the sites available

$$\bar{S}_{H(\alpha)} = \bar{S}_{H,vib} + \bar{S}_p \quad (6)$$

Gulbransen and Andrew assume that changes in the partial molal entropy with changes in concentration of the dissolved hydrogen are purely due to the entropy of number and position \bar{S}_p , while the partial molal entropy of vibration $\bar{S}_{H,vib}$ remains constant.

When a random distribution is considered, the entropy of number and position of N_H atoms arranged in N_s sites is

$$S_p = R \ln \frac{N_H!}{N_H!(N_s - N_H)!} \quad (7)$$

and the corresponding partial molal entropy for dissolved hydrogen, taking into account the assumed model, can be written as

$$\bar{S}_p = \frac{\partial S_p}{\partial N_H} = -R \ln \frac{N_H}{N_s - N_H} = -R \ln \frac{N_H}{2N_{Zr} - N_H} \quad (8)$$

where N_{Zr} is the number of zirconium atoms.

Hence, following Gulbransen and Andrew, a convenient reference standard for the partial molal en-

trophy of hydrogen in solution is the concentration $N_H = N_{Zr}$,¹⁰ referring to this standard concentration, from eq 8 one obtains $\bar{S}_p = 0$, and the partial molal entropy of dissolved hydrogen reduces to its vibrational entropy. The same must obviously be true for deuterium, so that the following results are obtained

$$\begin{cases} \bar{S}_{H(\alpha)}^\circ = \bar{S}_{H,vib} \\ \bar{S}_{D(\alpha)}^\circ = \bar{S}_{D,vib} \end{cases} \quad (9)$$

It follows that in the assumed model the partial molal entropy of vibration is given by the standard partial molal entropy of dissolved species.

On the other hand, it was previously found

$$\begin{cases} \Delta S_H = \bar{S}_{H(\alpha)} - 1/2 \bar{S}_{H_2(g)}^\circ = \\ \quad 12.057 + 1/2 R \ln [(N_H/N_{Zr})^2] \\ \Delta S_D = \bar{S}_{D(\alpha)} - 1/2 \bar{S}_{D_2(g)}^\circ = \\ \quad 11.885 + 1/2 R \ln [(N_D/N_{Zr})^2] \end{cases} \quad (10)$$

so that, with reference to the standard concentration $N_H = N_{Zr}$ (or $N_D = N_{Zr}$), one obtains

$$\begin{cases} \bar{S}_{H(\alpha)}^\circ = 12.057 + 1/2 \bar{S}_{H_2(g)}^\circ \\ \bar{S}_{D(\alpha)}^\circ = 11.885 + 1/2 \bar{S}_{D_2(g)}^\circ \end{cases} \quad (11)$$

From expressions 9 and 11, the vibrational entropies for dissolved hydrogen and deuterium atoms are immediately obtained at any temperature, and the related frequencies and characteristic temperatures may easily be calculated.

Gulbransen and Andrew found experimentally, at 500°, two different values of the standard partial molal entropy of hydrogen: 3.9 eu/g-atom in the α phase and 1.9 eu/g-atom in the zirconium hydride δ phase.

(10) It must however be pointed out that the concentration which has been chosen as a standard is much in excess of the maximum solubility in the α phase.

Since the tetrahedral interstices in α -Zr occur in pairs, with spacing of 1.29 Å in the c direction, they assumed that such a difference arose from the fact that one "exceptional" mode of vibration had to be considered, in which the hydrogen atom essentially oscillated between the two adjacent sites, while two other nearly normal modes of vibration were maintained, similar to those found for the hydride.¹¹ As a consequence they put for the hydride $\bar{S}_{\delta,\text{vib}} = 3S_{\nu,\text{norm}} = 1.9$ eu/g-atom, from which $\nu_{\text{norm}} = 3.98 \times 10^{13}$ sec⁻¹ and $\theta_E = 1910^\circ\text{K}$ can be calculated,¹² while, for the hydrogen dissolved in α -Zr, they put $\bar{S}_{\alpha,\text{vib}} = 2S_{\nu,\text{norm}} + S_{\nu,\text{exc}} = 3.9$ eu/g-atom, from which $\nu_{\text{exc}} = 1.21 \times 10^{13}$ sec⁻¹ and $\theta_E = 581^\circ\text{K}$ can be calculated.

In order to test the applicability of the model of Gulbransen and Andrew to the results obtained in this work for D₂ and in the preceding one for H₂, both at very low concentrations in α -Zr, the "exceptional" frequency has been calculated for the two gases at different temperatures t , by assuming the "normal" frequency to be that found by Flotow and Osborne (footnote *b* of Table III) for the ϵ -hydride, which is the nearest to the average of all the frequencies quoted in Table III. The "exceptional frequencies," ν_{exc} , and the relative Einstein characteristic temperatures $\theta_{E,\text{exc}}$ are given in Table IV for hydrogen and in Table V for deuterium, together with the "isotropic frequencies" ν_{isot} and the relative characteristic temperatures $\theta_{E,\text{isot}}$ which were obtained by partially abandoning the above model and by assuming isotropic vibrations also in the α phase. In the second column of both tables, the standard partial molal entropies of the dissolved species $\bar{S}_{H,\text{vib}}$ and $\bar{S}_{D,\text{vib}}$ are reproduced, as they were calculated using tabulated standard entropies of normal hydrogen and deuterium.^{13,14}

Table IV: Vibrational Modes of Hydrogen Atoms in α -Zr (Model of Gulbransen and Andrew)

t , °C	$\bar{S}_{H,\text{vib}}$, eu/g- atom	ν_{exc} , sec ⁻¹	$\theta_{E,\text{exc}}$, °K	ν_{isot} , sec ⁻¹	$\theta_{E,\text{isot}}$, °K
450	6.65	2.88×10^{12}	138	1.39×10^{13}	667
500	6.87	2.96×10^{12}	142	1.43×10^{13}	685
550	7.10	3.10×10^{12}	149	1.46×10^{13}	700
600	7.30	3.22×10^{12}	155	1.49×10^{13}	718
650	7.51	3.35×10^{12}	161	1.52×10^{13}	730
700	7.70	3.47×10^{12}	166	1.55×10^{13}	744
750	7.88	3.62×10^{12}	174	1.58×10^{13}	759

From Tables IV and V the following points emerge.

(a) The calculated frequencies and characteristic temperatures are by far too low to be associated with

a vibrational motion of hydrogen or deuterium atoms contained in the small tetrahedral interstices of the α -Zr lattice.

Table V: Vibration Modes of Deuterium Atoms in α -Zr (Model of Gulbransen and Andrew)

t , °C	$\bar{S}_{D,\text{vib}}$, eu/g- atom	ν_{exc} , sec ⁻¹	$\theta_{E,\text{exc}}$, °K	ν_{isot} , sec ⁻¹	$\theta_{E,\text{isot}}$, °K
450	8.53	1.83×10^{12}	88	9.97×10^{12}	479
500	8.79	1.92×10^{12}	92	1.02×10^{13}	489
550	9.02	2.02×10^{12}	97	1.04×10^{13}	500
600	9.23	2.12×10^{12}	102	1.06×10^{13}	511
650	9.44	2.22×10^{12}	107	1.09×10^{13}	522
700	9.64	2.33×10^{12}	112	1.11×10^{13}	531
750	9.82	2.44×10^{12}	117	1.13×10^{13}	542
800	10.00	2.55×10^{12}	122	1.15×10^{13}	552

(b) Both the "isotropic" and the "exceptional" θ_E show a net increase with temperature, which means that a single optical term cannot be employed to describe the behavior of hydrogen or deuterium atoms in α -Zr, nor can this be done by simply introducing a second optical term. This seems to exclude the possibility that it may simply be a matter of considering octahedral rather than tetrahedral sites. So it appears that the model of Gulbransen and Andrew cannot be applied to the systems here examined, in particular with regard to the localization of dissolved atoms in defined sites within the metal lattice. Obviously this is contrary to the procedure which was used in distinguishing the configurational from the vibrational term in the partial molal entropies, so that further speculations on this basis, if possible, have to be considered with caution.

Nevertheless, it appears quite clear that deviations are in the sense of a larger mobility of dissolved hydrogen and deuterium, so that these results may probably be accounted for by considering, with Coogan and

(11) This assumption however puts some doubts on the choice of the standard concentration, since it implies the distribution of the hydrogen atoms between "dual" sites, made up of pairs of twin interstitial tetrahedral sites.

(12) It may be noticed that the frequency calculated by Gulbransen and Andrew for the hydrogen in the δ phase is somewhat higher than experimentally determined by neutron diffraction studies.

(13) Landolt-Börnstein, "Zahlenwerte und Funktionen aus Physik-Chemie-Astronomie-Geophysik und Technik," Vol. 4, Springer-Verlag, Berlin, 1961, p. 430.

(14) J. Hilsenrath, C. W. Beckett, W. S. Benedict, L. Fano, H. J. Hoge, J. F. Masi, R. L. Nuttal, Y. S. Touloukian, and H. W. Woolley, "Tables of Thermal Properties of Gases," National Bureau of Standards Circular 564, U. S. Government Printing Office, Washington, D. C., 1955.

Gutowsky,¹⁵ the unique property of the hydrogen atom that removal of one electron results in the complete exposure of the nucleus, of negligible size. Furthermore, such results are in line with studies on heat capacities of transition metal hydrides^{16,17} which showed the necessity of assuming a diffusional (or translational) hydrogen contribution.

However, further data have to be gathered on other

comparable systems, and similar measurements have been undertaken on very dilute solutions of H₂ and D₂ in the α phase of Hf and Ti.

(15) C. K. Coogan and H. S. Gutowsky, *J. Chem. Phys.*, **36**, 110 (1962).

(16) Z. Bieganski and B. Stalinski, *Bull. Acad. Polon. Sci., Ser. Sci. Chim.*, **9**, 367 (1961).

(17) Z. Bieganski and B. Stalinski, *ibid.*, **11**, 579 (1963).

Controlled Potential Studies on the Kolbe Reaction and the Role of Coadsorbed Surface Oxides. I. Platinum in Trifluoroacetate Solutions

by B. E. Conway and A. K. Vijh

Department of Chemistry, University of Ottawa, Ottawa, Canada (Received January 26, 1967)

The electrochemical kinetics of the Kolbe reaction on platinum have been examined in solutions of potassium trifluoroacetate in trifluoroacetic acid by potentiostatic, galvanostatic, and potentiodynamic techniques. The trifluoro acid has been used to minimize side reactions involving H abstraction. The effect of the presence of water in relation to the development of surface oxide films and associated inhibition effects is investigated. A general scheme of mechanisms is outlined and examined in the light of the experimental results. It is suggested that the high Tafel slopes associated with the reaction arise because of dipole layer films having barrierlike properties. The principles involved in the interpretation of experimental results are examined in relation to the possible reaction mechanisms. At high anodic potentials, the reaction is shown to proceed on an oxide film at Pt with possible coadsorption of species derived by discharge from the carboxylate anion.

General Introduction

The following introduction is intended to cover material presented in this paper and in part II.

The formation of a hydrocarbon on electrolysis of acetate solutions was first reported by Faraday¹ and studied in more detail by Kolbe.² Previous work which has established the phenomenology of this reaction from the point of view of synthetic organic chemistry has been the subject of several reviews,³⁻⁵ but only in the case of simple carboxylates where the reaction path is uncomplicated by extensive side reactions is this ap-

proach of interest in the work reported here. The electrochemical aspects of this reaction have, however, not been explored adequately and only recently have

(1) M. Faraday, *Pogg. Ann.*, **33**, 438 (1834).

(2) H. Kolbe, *Ann.*, **69**, 257 (1849).

(3) C. J. Brockman, "Electro-Organic Chemistry," John Wiley and Sons, Inc., New York, N. Y., 1926.

(4) B. C. L. Weedon, *Quart. Rev.* (London), **6**, 380 (1952); A. K. Vijh and B. E. Conway, *Chem. Rev.*, in press.

(5) M. J. Allen, "Organic Electrode Processes," Reinhold Publishing Corp., New York, N. Y., 1958.

papers appeared⁶⁻⁸ in which an attempt has been made to understand the kinetics of well-defined examples of the reaction from an electrochemical point of view, *e.g.*, through current (*i*)-potential (*V*)^{7,9-11} relations. Early theories on the mechanism, of historical interest only, have been examined previously.⁴⁻⁷ A heterogeneous free-radical type of mechanism involving a number of consecutive elementary steps in the over-all Kolbe reaction, as discussed previously,⁷ and first proposed by Shukla and Walker (*e.g.*, see ref 4 and 5) will form the basis of the discussion here.

In the present papers (parts I and II), the mechanism of the Kolbe reaction is examined in terms of heterogeneous reactions initiated by a potential dependent charge transfer from the carboxylate anion RCOO^- . As in our previous work,⁷ the trifluoro ($\text{R} = \text{CF}_3$) salt and acid were chosen since yields of C_2F_6 are good⁷ and any side reactions (not constituting the "Kolbe coupling" process) involving H abstraction when $\text{R} = \text{CH}_3$ or C_2H_5 are minimized.

The heterogeneous nature of the reaction when R is small, *e.g.*, CH_3 , has not always been appreciated and this has resulted, for example, in seemingly questionable calculations^{10,12} and arguments¹³ being presented in some earlier studies. The electrochemical study of the reaction has been further pursued in the present work by examining the following matters.

(i) In our previous work,⁷ the kinetics were studied galvanostatically; potentiostatic and potentiodynamic techniques which are preferable for the study of organic reactions¹⁴ have now been employed. In practice, the steady-state potentiostatic method is able to distinguish any structure in the transition region⁷ of the *i*-*V* curve as one process changes to another and inflections or current maxima arise; also hysteresis between ascending and descending *i*-*V* curves becomes well characterized and product yields are more meaningful.

(ii) Information on the coverage by, and identity of, adsorbed intermediates has been obtained by use of galvanostatic and potentiodynamic transients.

(iii) The products of electrolysis, previously reported,⁷ have been qualitatively checked and confirmed under various conditions.

Three types of solutions were studied: completely anhydrous solutions of potassium trifluoroacetate (KTFA) in trifluoroacetic acid (TFA), nominally anhydrous solutions of KTFA in TFA (*i.e.*, with traces of water present), and KTFA in TFA containing 30% water. The assessment of the role of surface oxide films originating from water in the solvent will be a principal aspect of the present studies.

Experimental Section

The experimental details described here also apply to part II. General techniques for electrochemical kinetic measurements under high-purity conditions were used as previously described;^{15,16} a thermostated cell, as employed earlier,^{7,16} was used. Reagent grade trifluoroacetic acid (bp 70-72) was kept over boric anhydride with stirring for 48 hr and then refluxed over a quantity of fresh boric anhydride for 2-3 hr and distilled. After a repeated distillation, the fraction distilling at 71.0-71.2 (760 mm) was collected and used in the experiments. Potassium trifluoroacetate was prepared by neutralizing previously purified TFA with potassium hydroxide (analytical grade) and recrystallizing the product twice from conductivity water containing freshly redistilled spectroscopically pure dioxane as a precipitant. The dried salt was then redried under vacuum at about 100° for 24 hr before use in each experiment. The purest commercially available trifluoroacetic anhydride (see below) was purified by a double distillation and a middle fraction boiling at 45° was finally collected.

Solutions of KTFA were prepared by dissolving the vacuum-dried salt in the purified TFA which had been transferred by pressure of nitrogen (without contact with the atmosphere) to a known weight of the salt to give the concentration desired. This solution was regarded as "pure," but microscopic traces of water may have been present initially (*e.g.*, from adsorption on the cell walls) or might have entered the cell by diffusion from the atmosphere (despite the precautions described below). In order to obtain "very" anhydrous conditions¹⁷ in certain runs, purified trifluoroacetic anhydride

(6) T. Dickenson and W. F. K. Wynne-Jones, *Trans. Faraday Soc.*, **58**, 382, 388, 400 (1962).

(7) B. E. Conway and M. Dzieciuch, *Can. J. Chem.*, **41**, 21, 38, 55 (1963); see also M. Dzieciuch, Ph.D. Thesis, Ottawa, 1962.

(8) M. Fleischmann, J. R. Mansfield, and W. F. K. Wynne-Jones, *J. Electroanal. Chem.*, **10**, 511 and 522 (1965); C. Wilson and W. T. Lippencott, *J. Am. Chem. Soc.*, **78**, 4290 (1956).

(9) G. S. Pande and S. N. Shukla, *Electrochim. Acta*, **4**, 215 (1961).

(10) K. Sugino, T. Sekine, and N. Sato, *J. Electrochem. Tech.*, **1**, 112 (1963); see also Abstract No. 167, Extended Abstracts of a Symposium of the Electro-Organic Division of the Electrochemical Society, San Francisco, Calif., May 9-13, 1965.

(11) M. Leung, J. Herz, and H. W. Salzberg, *J. Org. Chem.*, **30**, 310 (1965).

(12) L. Ebersson, *Acta Chim. Scand.*, **17**, 2004 (1963); *cf.* B. E. Conway and A. K. Vijh, *Electrochim. Acta*, **12**, 102 (1967).

(13) G. Thiessen, *Record Chem. Progr.*, **21**, 243 (1960).

(14) B. E. Conway, "Theory and Principles of Electrode Processes," Ronald Press, New York, N. Y., 1965; see also *Progr. Reaction Kinetics*, **4**, 399 (1967).

(15) A. M. Azzam, J. O'M. Bockris, B. E. Conway, and H. Rosenberg, *Trans. Faraday Soc.*, **46**, 918 (1950).

(16) B. E. Conway, E. M. Beatty, and P. A. D. de Maine, *Electrochim. Acta*, **7**, 39 (1962); *Proc. Roy. Soc. (London)*, **A256**, 128 (1960).

was added as described above. The solutions were maintained in a dry condition by use of drying tubes on all the gas outlets and diffusion of atmospheric moisture into the test electrode compartment of the cell was minimized by placing the cell in a drybox containing dewar flasks of evaporating liquid nitrogen. The three types of solutions used were prepared as follows and were chosen in order to examine the role of coadsorbed oxides derived from water.

(a) "Very" anhydrous solutions (1 M KTFA-TFA) were prepared by dissolving the dried KTFA in the dry TFA; 1% of trifluoroacetic anhydride was then added and the solution was agitated for 0.5 hr by bubbling dry purified CO₂ (medical grade). This treatment was devised to remove the last traces of water from the solution by the reaction $\text{CF}_3\text{COOCOFCF}_3 + \text{H}_2\text{O} \rightarrow 2\text{CF}_3\text{COOH}$.

(b) "Nominally" anhydrous solutions (1 M KTFA-TFA) were prepared as in (a) above, except that no anhydride was added.

(c) Aqueous solutions (1 M KTFA-TFA) were prepared as in (b) but contained 30% by volume of redistilled water.

All gases (CO₂, N₂, and H₂) used in the experiments were purified as previously described.^{7,16}

Electrodes of spectroscopically pure Pt (and Au, part II) were prepared by a standardized method to maximize reproducibility of measurements. The wire was first cleaned for 24 hr in benzene under reflux and then heated for 2-5 min in a stream of pure dry hydrogen at 450°; the wire was finally sealed under hydrogen in glass bulbs.¹⁸ Hydrogen reference electrodes were used.⁷

Characterization of the Products of Electrolysis. The anode gases, collected in a special cell,⁷ were condensed into an evacuated trap at liquid air temperatures for gas characterization studies. The temperature of the trap was then raised to -50° so that all the "Kolbe" products were in gaseous form but any traces of the acid (condensed from the electrolyte) in the trap were still solid. The gases in the trap were then analyzed by vapor phase chromatography using a silica gel adsorbent and employing known gas mixtures for calibration.

Exploration of Suitable Conditions for Coulombic Yield Studies. In the coulombic efficiency studies the question of the solubility of the Kolbe products is a problem. By means of a simple solubility apparatus,¹⁹ the solubility of C₂F₆ in pure TFA was determined as ca. 33 ml/100 ml of solution. Such a solubility precludes the possibility of quantitative coulombic efficiency studies except at high current densities in presaturated solutions.⁷ Presaturation of the solutions was, however, considered undesirable since it would be difficult to

distinguish whether the products being measured originated electrolytically or arose by degassing of the solution. In aqueous solutions, the solubility is much less of a problem.

Electrochemical Measurements and Electrical Circuits. The potentiostatic polarization circuit consisted of a Wenking potentiostat for controlled potential polarizations, an ammeter (Sensitive Research micromilliammeter, Model 5), and a potentiometer (Radiometer Model PHM-4b, input impedance = 10¹³ ohms). The potentiodynamic circuit was based on that described by Will and Knorr²⁰ and has been described elsewhere.²¹ The circuit for potential decay measurement and differentiation was adapted from the ones described previously.^{7,22}

Experimental Procedure in Runs. (a) *Polarization Measurements.* The solution was cooled thermostatically to 5° by circulation of coolant through glass coils sealed in the cell⁷ with carbon dioxide bubbling through the solution. The encapsulated electrodes were lowered successively under the solution and the glass bulbs surrounding the electrodes were shattered by means of a glass probe.¹⁸ After adjustment of each electrode against the Luggin capillary, current and potential measurements were carried out over a potential range of about 0.0 to 3.0 v (*vs.* the reversible hydrogen electrode). Current measurements were made after the electrode had been held for 60 sec at each controlled potential. This yielded a somewhat arbitrary, though standardized and reproducible, procedure in which the currents obtained were practically steady, yet the electrodes were not subjected to the possibility of any long-time poisoning effects as sometimes occurs, *e.g.*, in the hydrogen evolution reaction. Very reproducible results are obtained providing the timing is standardized, as we have also found with other anodic reactions.

(b) *Potentiodynamic measurements*²⁰ were made with a calibrated single ramp and repetitive triangular wave forms; currents were recorded on an oscilloscope.

(c) *Potential Decay Measurements.* The procedure was similar to that described previously;^{7,16} full details have been given elsewhere.²¹

(17) The degree of dryness attained in these experiments was probably substantially better than that in our earlier controlled current studies.⁷

(18) J. O'M. Bockris, B. E. Conway, and W. Mehl, *J. Sci. Instr.*, **33**, 400 (1956); **25**, 283 (1948); *Rev. Sci. Instr.*, **28**, 209 (1957).

(19) B. E. Conway, J. E. Desnoyers, and A. C. Smith, *Phil. Trans. Roy. Soc. London*, **A256**, 389 (1964); G. Åkerlof, *J. Am. Chem. Soc.*, **57**, 1198 (1935).

(20) F. Will and C. A. Knorr, *Z. Elektrochem.*, **64**, 258 (1960).

(21) A. K. Vijh, Ph.D. Thesis, Ottawa, 1966.

(22) H. A. Kozłowska and B. E. Conway, *J. Electroanal. Chem.*, **7**, 109 (1964).

Principles to be Used in the Discussion of Experimental Results

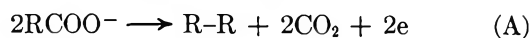
The results obtained by the various approaches employed are rather complex and their discussion requires some initial examination of the mechanisms that may be involved, the principles to be used, and the types of arguments to be developed. Since these principles and arguments are not always conventional, they require first some description as below.

(a) *Kinetic Analysis of the Steady-State Current-Potential Relations.* Tafel slopes, b , have been used in favorable cases as diagnostic criteria for mechanisms of electrode reactions for many years. In some earlier studies on the Kolbe reaction²³⁻³² and even more recently,^{9-11,33} the importance of current and potential has, however, not always been adequately recognized. Dickenson and Wynne-Jones⁶ were the first authors to discuss current-potential relations for the Kolbe reaction in terms of kinetic parameters (*e.g.*, b) and surface coverage effects. The limiting b values for various steps in several pathways were first evaluated by Conway and Dzieciuch.⁷

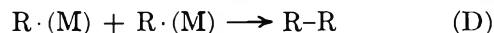
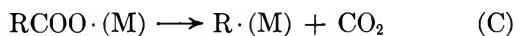
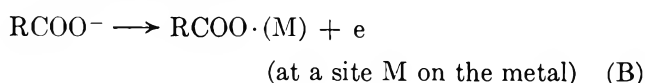
A steep rise (*i.e.*, a transition region) in a potentiostatic i - V relation can correspond, in the absence of diffusion limitation, to either a range of potentials over which the electrode is becoming covered by some adsorbed species^{34,35} or to transition to a region of potential where alternative and more facile reactions are proceeding, or to both effects. If a Tafel line is observed in the post-transition region (*i.e.*, at more anodic potentials), it can sometimes be assumed^{34,35} that an over-all Faradaic process to which this Tafel line corresponds is proceeding on an electrode covered by some adsorbed species produced at lower potentials;^{36,37} this seems, in fact, to be the case at Pt in aqueous solutions. Hysteresis between the ascending and descending curves of a steady-state (potentiostatic) current-potential relation suggests further the presence of an irreversibly adsorbed electroactive species, *e.g.*, in the presence of water, surface oxide.

In general, most electrochemical reactions, except perhaps one-electron ionic redox processes, must proceed by at least two consecutive steps^{38,39} and it is unlikely that the Kolbe reaction is an exception.

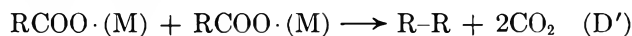
In the over-all reaction ($R = CF_3$)



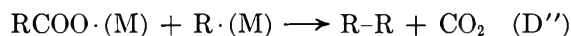
the following sequence of consecutive elementary steps⁴⁰ involving adsorbed intermediates⁴¹ may be envisaged⁷ and will be referred to in the ensuing discussion.



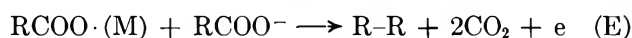
or, following step B



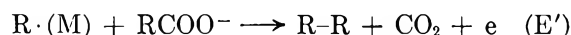
or



and alternatively, following step B



or



Steps D, D', and D'' are kinetically (but not chemically) equivalent since each one is a "recombination step." Steps E and E' are again kinetically equivalent,

(23) S. Glasstone and A. Hickling, *J. Chem. Soc.*, 1878 (1934); *Chem. Rev.*, 25, 407 (1939).

(24) D. A. Fairweather and O. J. Walker, *J. Chem. Soc.*, 3111 (1926).

(25) S. N. Shukla and O. J. Walker, *Trans. Faraday Soc.*, 27, 722 (1931).

(26) G. Preuner and E. B. Ludlam, *Z. Physik. Chem. (Frankfurt)*, 59, 682 (1907).

(27) K. Hopfgartner, *Monatsh. Soc.*, 32, 523 (1911).

(28) J. Salausé, *Bull. Soc. Chim. France*, 37, 522 (1925); *Compt. Rend.*, 180, 662 (1925).

(29) C. Schall, *Z. Elektrochem.*, 3, 83 (1896).

(30) F. Fichter, *Trans. Electrochem. Soc.*, 75, 309 (1939).

(31) S. Glasstone and A. Hickling, *ibid.*, 75, 333 (1939).

(32) B. C. L. Weedon, *Quart. Rev. (London)*, 6, 380 (1952); *Advan. Org. Chem.*, 1, 1 (1960).

(33) K. Sugino, T. Sekine, and N. Sato, *J. Electrochem. Tech.*, 1, 112 (1963).

(34) D. Gilroy and B. E. Conway, *J. Phys. Chem.*, 69, 1259 (1965).

(35) V. S. Bazotzky and Yu. B. Vasilev, *Electrochim. Acta*, 9, 869 (1964).

(36) J. O'M. Bockris and A. M. Azzam, *Trans. Faraday Soc.*, 48, 145 (1952).

(37) B. I. Podlovchenko, O. A. Petry, A. N. Frumkin, and H. Lal, *J. Electroanal. Chem.*, 11, 12 (1966).

(38) In a recent general comment by Anson,³⁸ this seems to be doubted. However, for reactions producing molecular products differing in stoichiometry from the reactant ions, the necessity for two or more steps would seem an obvious requirement.

(39) F. Anson, *J. Chem. Educ.*, 43, A470 (1966); for a fuller discussion of this matter in relation to adsorption of radical intermediates, see A. K. Vijh and B. E. Conway, *Chem. Rev.*, in press, and ref 14.

(40) A number of other side reactions such as formation of RH by H abstraction or formation of esters by reaction of R· with RCOO· may also occur.⁴ However, in most of the present work, conditions have been chosen to minimize such processes,⁷ *e.g.*, by choosing $R = CF_3$.

(41) Adsorption of intermediate species has not always been appreciated by organic chemists who have studied the Kolbe reaction. Thus, the reactivity of such species when adsorbed must not be confused with the supposed high reactivity of such species in homogeneous phases.^{12,39}

radical-ion reactions. Tafel slopes for the above reaction sequences have been derived previously⁷ taking into account the nature of possible isotherms for the adsorption of intermediates.

For simplicity of discussion, the kinetically indistinguishable steps will be ignored for the present so that the above scheme is reduced to one of the type $B \rightarrow C \rightarrow D$ or E . Important consequences of the above reaction scheme in terms of coverage effects are as follows.

If the discharge step B were rate determining, coverage θ of the electrode by $\text{RCOO}\cdot$ would tend to be small. However, this does not imply that the electrode may not be covered by some electroinactive species chemisorbed from the solution. If any step other than B were rate determining, partial or complete coverage would tend to be observed in transient studies, if the adsorbed species were electroactive, *i.e.*, cathodically reducible. We have mentioned these points since the relations between coverage effects and kinetics have not always been considered in previous discussions.^{10,33,42}

(b) "Identification" of Adsorbed Species. Kinetic arguments, as in (a) above, must be supported, if possible, by procedures which help to identify the type of intermediates or coadsorbed species formed from the solvent. However, electrochemical measurements usually only lead to such conclusions indirectly. When information is obtained from several different directions, as in the study of the present reaction, such methods can be of greater value. Further elucidation of the identity of adsorbed species may be obtained in favorable cases by use of C^{14} -labeled reactants.^{43,44} The following matters have been considered in the present work.

(i) *Potential of Commencement of a Tafel Region.* In a steady-state i - V curve, the potential at which the Tafel region commences in relation to the behavior of the Tafel line for a known process may enable some preliminary conclusions to be made. The Tafel line for the Kolbe reaction at Pt in aqueous solution of $\text{KTFA} + \text{TFA}$ commences above 2.1 v, suggesting that in the part of the transition region (Figure 1) from 1.7 (which is approximately the potential at which the Tafel region for oxygen evolution in inorganic acid solutions normally arises at current densities $< 10^{-6}$ amp cm^{-2}) to 2.1 v, formation of some adsorbed intermediates (possibly $\text{CF}_3\text{-COO}\cdot$ or $\text{CF}_3\cdot$ or in aqueous media surface oxide, see below) has perhaps taken place. However, the possibility of oxidation of trace impurities or the occurrence of alternative (side) reactions in this potential range must be recognized; the current densities involved are, however, too small to allow coulombic analysis to be made.

(ii) *Rest potential* is a qualitative guide³⁷ to the identity of adsorbed species; *e.g.*, if a "stable" surface

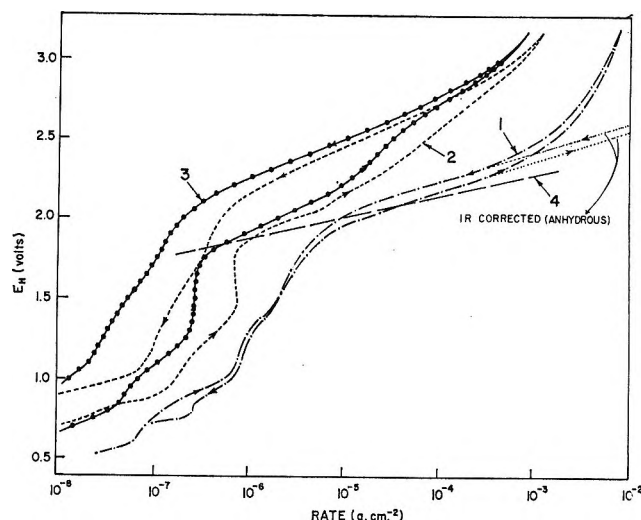


Figure 1. Platinum-1 M CF_3COOK in CF_3COOH , steady-state current-potential relation: 1, with anhydride, $b = 0.215$ v; 2, without anhydride, $b = 0.27$ v; 3, with added water, $b = 0.25$ v; and 4, Pt-1 M H_2SO_4 , $b = 0.14$ v. Note: a typical population of experimental points has been shown on one of the graphs; a typical resistance potential drop (iR) at higher current densities has also been shown.

oxide is involved, the rest potential is usually near the reversible potential for the oxygen evolution reaction, *i.e.*, 1.23 v.

(iii) *Inhibition Inflection.* In certain organic oxidations, a characteristic inflection (passivation) is observed in the current-potential relation followed by a normal linear Tafel region indicating that either (a) discharge can occur onto the layer of inhibiting species after appreciable coverage has been reached or (b) a new mechanism can arise as the potential is made more anodic.³⁴

(iv) *Magnitudes of Charge Q and Adsorption Pseudocapacity⁴⁵ C in Galvanostatic Transients.* Q and C can, in some cases, be a useful guide to the identity of the adsorbed species in relation to theoretically estimated values for various species at $\theta = 1$ for the appropriate real area.⁴⁶ The corresponding capacity maxima C_{max} and the potentials $V_{C_{\text{max}}}$ at which they occur are also of interest⁴⁵ (see below).

(42) M. Fleischmann, J. R. Mansfield, and W. F. K. Wynne-Jones, *J. Electroanal. Chem.*, **10**, 511, 522 (1965).

(43) H. Dahms and M. Green, *J. Electrochem. Soc.*, **110**, 1075 (1963).

(44) E. Gileadi, B. T. Rubin, and J. O'M. Bockris, *J. Phys. Chem.*, **69**, 3335 (1965); B. E. Conway and L. Marincic, in course of publication (the adsorption of C^{14} -labeled acetate has been studied in this latter work).

(45) B. E. Conway, E. Gileadi, and H. Kozłowska, *J. Electrochem. Soc.*, **112**, 341 (1964).

(46) S. B. Brummer, J. I. Ford, and M. J. Turner, *J. Phys. Chem.*, **69**, 3424 (1965).

(v) *Relations between Solution Composition and Magnitudes of C and Q.* The comparison of Q and C for anhydrous and water-containing solutions may lead to some estimate of Q and C contributions attributable to surface oxide only.

(vi) *Potentials of Arrests in Cathodic Discharge Profiles.* $V_{C_{\max}}$ values (see iv above) for the C-V profiles can be helpful in the identification of the adsorbed species, e.g., in relation to the presence of a surface oxide. Similar arguments apply to charging peaks in potentiodynamic profiles.

(vii) *Effect of i_{cath} on the C-V Profiles.* The effect of i_{cath} on C_{\max} and $V_{C_{\max}}$ may also be of value in the identification of an adsorbed species. Thus increase in i_{cath} should shift C_{\max} to higher values and $V_{C_{\max}}$ to more cathodic potentials.⁴⁵ In the present investigation, shifts in the values of C_{\max} and $V_{C_{\max}}$ agree with the theoretically predicted trend⁴⁵ only when the presence of one adsorbed species seems to be indicated (see part II).

(viii) *Q vs. Rate Relations.* Here, if increased Q values correspond to decreased rates, Q is probably associated with an inhibiting, coadsorbed species; if this is observed only when some water is present and Q increases with increasing water content, inhibiting surface oxide is indicated.

Results

The principal qualitative features of the results are summarized in Table I and described below.

(i) *Potentiostatic Steady-State Log [i]-Potential Relationships.* These relations at platinum in very anhydrous, nominally anhydrous, and in aqueous solutions are shown in Figure 1; the Tafel line for the oxygen evolution reaction on platinum in aqueous 1 M H₂SO₄ is also shown. The galvanostatic Tafel relations have been given previously.⁷

Hysteresis between the ascending and descending log [i]-V curves is negligible when the solutions are completely anhydrous (Figure 1) but is increased in the nominally anhydrous solutions. Similar results are found for anhydrous acetate-acetic acid solutions.⁴⁷ Also the rates, at a given potential, are lower in comparison with those for the "very" anhydrous solutions. The hysteresis is further enhanced and the rates are correspondingly diminished in excess water. In all cases, linear Tafel relations are observed⁷ in the post-transition region with Tafel slopes (b) on the descending curves equal to 0.25 ("very" anhydrous solutions), 0.220 (nominally anhydrous solutions), and 0.215 v (aqueous solutions). For comparison, the Tafel line for oxygen evolution on Pt in H₂SO₄ (Figure 1) exhibits a slope of 0.14 v.

The rest potentials (i.e., the potential on a slow descending log [i]-V curve at which the current would just tend to become cathodic) are as follows: for completely anhydrous solutions, 0.50 v; solutions containing traces of water, 0.90 v; and solutions containing excess of water, ca. 0.95 v.

(ii) *Self-Discharge and Galvanostatic Reduction Behavior from Potentiostatically Maintained Anode Potentials.* (a) *Self-Discharge Behavior.* In completely anhydrous solutions, no arrests are observed in the open-circuit potential-time relations and the capacity values are of the order of the double-layer capacity (<100 $\mu\text{f cm}^{-2}$). The rest potential attained a few minutes after cessation of polarization is 0.6 v; in the nominally anhydrous solutions it is ca. 0.9 v.

The open-circuit decay profiles for aqueous solutions show no arrests, but the calculated⁴⁸ capacities (400-500 $\mu\text{f cm}^{-2}$) are substantially higher than C_{dl} ; also, the rest potential has a high value of 1.175 v. However, only on galvanostatic reduction from this rest potential are arrests in the resulting potential-time curve observed, indicating a stable film. The value of the capacity maximum, C_{\max} , associated with the main arrest is 2680 $\mu\text{f cm}^{-2}$ and the potential at which it occurs, $V_{C_{\max}}$, is 0.58 v. (The value of charge Q_1 for this arrest is 0.53 mcoulomb cm^{-2} . Another arrest is observed around 0.15 v associated with a charge $Q_2 = 0.39$ mcoulomb cm^{-2} .)

(b) *Direct Galvanostatic Reduction Behavior.* In cathodic discharge transients, no arrests are observed in completely anhydrous solutions, so that Q values could not be calculated. Values of C_{\max} are of the order of C_{dl} .

Reduction transients from potentials up to 2.7 v in nominally anhydrous solutions are also not associated with any arrests. Slight arrests appearing after ca. 72 hr have elapsed from the commencement of the run are presumably due to diffusion of moisture into the solution. C_{\max} is then between 250 and 450 $\mu\text{f cm}^{-2}$ depending on i_{cath} (the cathodic current density used in the discharge) and the moisture content. The plot of i_{cath} vs. $1/\tau$ is linear (Figure 2); the slope gives a charge $Q_{\text{total}} = 0.11$ mcoulomb cm^{-2} . Here τ is the transition time for cathodic reduction of the adspecies, viz., $i_{\text{cath}}\tau = Q$. On the differentiated transient (Figure 3), it is the time between two capacity minima.²² A pure discharge process for removal of an adspecies is therefore indicated. Although these C and Q values have

(47) A. K. Vijh and B. E. Conway, *Z. Anal. Chem.*, **224**, 149, 160 (1967); **230**, 81 (1967).

(48) B. E. Conway and P. L. Bourgalet, *Trans. Faraday Soc.*, **58**, 593 (1962).

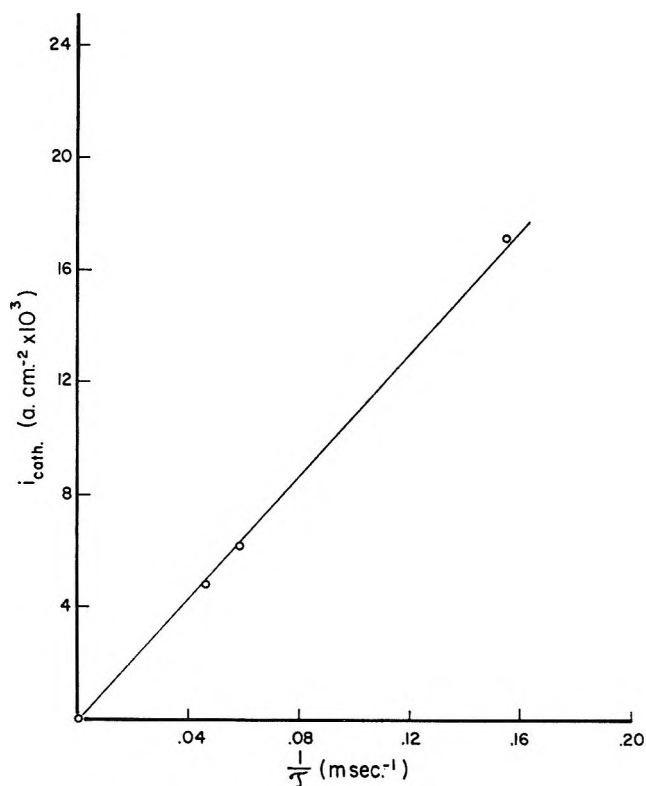


Figure 2. Platinum-1 M CF_3COOK in CF_3COOH (nominally anhydrous solution), a plot of i_{cath} vs. $1/\tau$.

only a semiquantitative significance because of indeterminacy in the trace water content, they have an important bearing on the role of water content in the solution.

Q increases with increasing initial polarization potential V_i as shown by the transients in Figure 3. No peak (*i.e.*, capacity maximum) is observed in completely anhydrous solution while only a slight arrest is observed in nominally anhydrous solutions. Only in aqueous solutions are appreciable cathodic reduction arrests observed, corresponding to significant electrode surface coverage; C_{max} is $1650 \mu\text{f cm}^{-2}$ and $V_{C_{\text{max}}}$ ranges between 0.6 and 0.2 v, depending on i_{cath} . Increasing i_{cath} tends to shift $V_{C_{\text{max}}}$ to more cathodic potentials though the trend in the shift of C_{max} is not regular (Figure 4); the C - V profiles are shown in Figure 5. The i_{cath} vs. $1/\tau$ plots for a given V_i indicate again a pure (dis)charging process with $Q = 1.05 \text{ mcoulomb cm}^{-2}$, *i.e.*, ten times larger than the value for nominally anhydrous solutions.

The charge Q measured with respect to the potentials of either of the capacity minima is independent of V_i (Figure 6). This figure also demonstrates the satisfactory resolution in differentiated charging curves and the consequent facilitation of evaluation of Q .

(iii) Potentiodynamic Current-Potential Relations

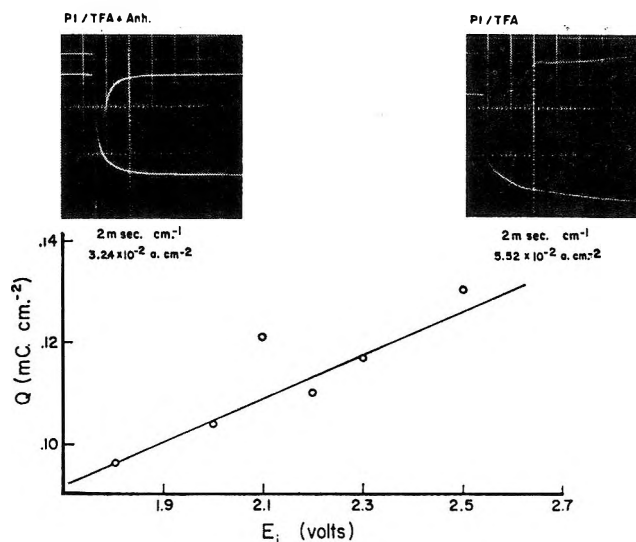


Figure 3. Platinum-1 M CF_3COOK in CF_3COOH (nominally anhydrous solution), a plot of Q vs. E_i (or V_i).

(Repetitive "Triangular" Wave Form). In completely anhydrous solutions, no current peaks are observed. Normal separation between the cathodic and anodic curves arises with $C \neq C_{\text{dl}}$. In nominally anhydrous solutions, significant peak currents are observed but are not linear in $(dV/dt)^{1/2}$ and are hence not diffusion controlled. However, the charge Q for the main cathodic peak depends significantly on dV/dt as does that for oxide reduction found⁴⁹ in pure aqueous H_2SO_4 .

In the aqueous solutions, the main purpose of the potentiodynamic experiments was to observe the surface oxide reduction region.⁴⁷ The cathodic oxide reduction peak and the cathodic and anodic H peaks (Figures 7-9) are similar^{20,47} to those for a TFA- or KTFA-free aqueous solution containing H_2SO_4 or K_2SO_4 alone, provided that $V \gg 1.6 \text{ v}$ (E_{H}). The presence of KTFA up to 1.3 M in aqueous medium (Figure 7), or of TFA itself (Figures 8, 9) in 0.1 M H_2SO_4 up to 2.6 M, also does not radically modify the hydrogen peaks, so that strong, irreversible specific adsorption of the carboxylate anion or the molecule does not seem to be involved (see below). In the TFA-containing solutions in 0.1 M aqueous H_2SO_4 , increasing TFA concentration produces a small but significant progressive change in the anodic oxide formation region (see Figure 8) and the oxide reduction peak is somewhat reduced. The hydrogen peaks are slightly shifted but the cathodic and anodic charges about the median line are little changed. (However, a general upward shift of the

(49) B. E. Conway and D. Gilroy, Report to U. S. Army Engineer Research Labs, Ft. Belvoir, on Contract No. CP70A1-63-4 (1966); *Can. J. Chem.*, in press.

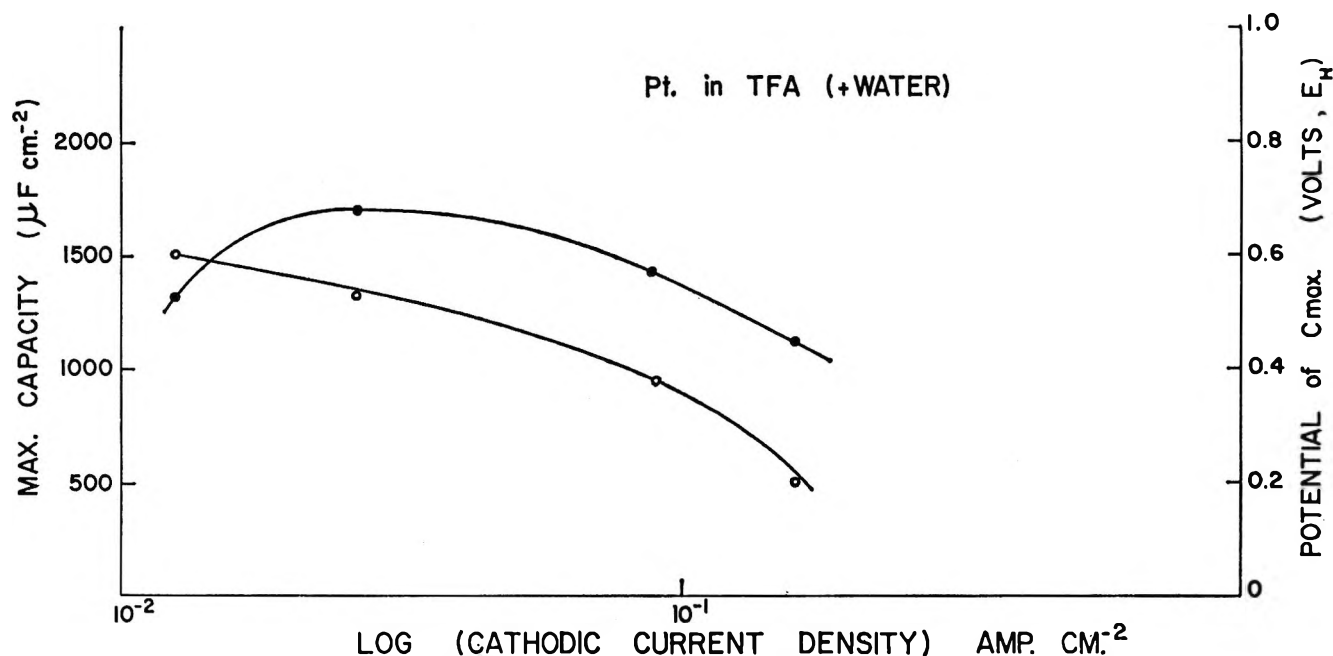


Figure 4. Platinum-1 M CF_3COOK in ($\text{CF}_3\text{COOH} + \text{water}$): ●, plot of C_{max} vs. i_{cath} ; ○, plot of $V_{C_{\text{max}}}$ vs. i_{cath} .

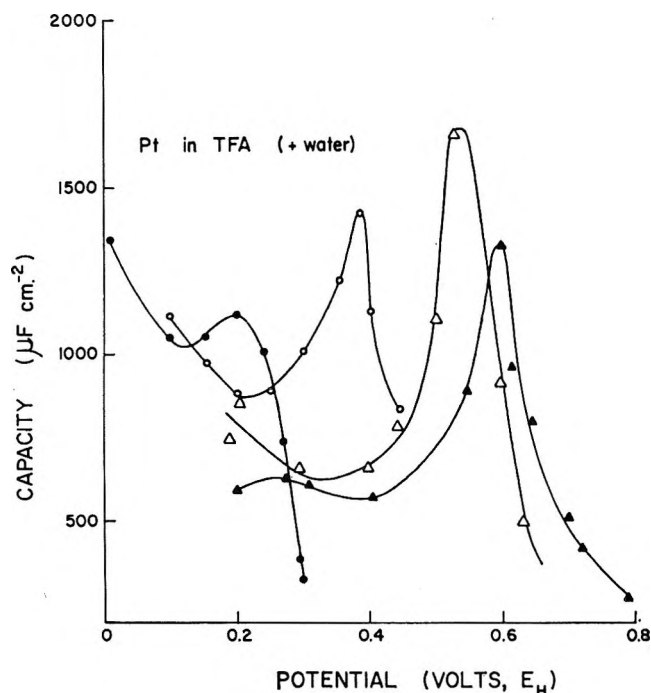


Figure 5. Platinum-1 M CF_3COOK in ($\text{CF}_3\text{COOH} + \text{water}$); C - V profiles as a function of charging cathodic current density, i_{cath} (amp cm^{-2}), for the adsorbed species in the Kolbe electrooxidation: ▲, 1.25×10^{-2} ; △, 2.65×10^{-2} ; ○, 8.82×10^{-2} ; ●, $1.62 \times 10^{-1} \text{ A cm}^{-2}$.

whole region occurs with increasing TFA concentration even when N_2 is bubbled at a rapid rate; this effect seems to be due to a superimposed cathodic O_2 reduction cur-

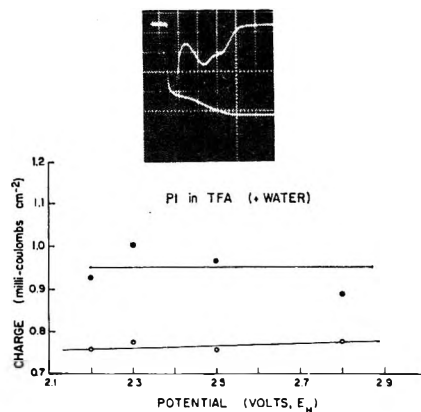


Figure 6. Platinum-1 M CF_3COOK in ($\text{CF}_3\text{COOH} + \text{water}$); plots of Q for each of the two peaks (see photograph) vs. E_i (or V_i).

rent since (a) it decreases with increasing rate of N_2 bubbling and (b) it is only significant when the potential scan increasingly goes into the region where some O_2 is also evolved with C_2F_6 .)

When the potential scan is extended to ca. 3.0 v E_H in the 0.1 M H_2SO_4 -2.6 M TFA solutions, an inflection in the anodic-going curve is seen at ca. 2.3 v (Figure 9) followed by a current maximum in the i - V curve at ca. 2.7 v E_H (Figure 9). A normal direction of the i - V curve is regained at ca. 3.0 v after a typical^{34,35} kinetic inhibition reversal of the Tafel line. The large current maximum is apparently determined by a kinetically controlled passivation effect (and not by an

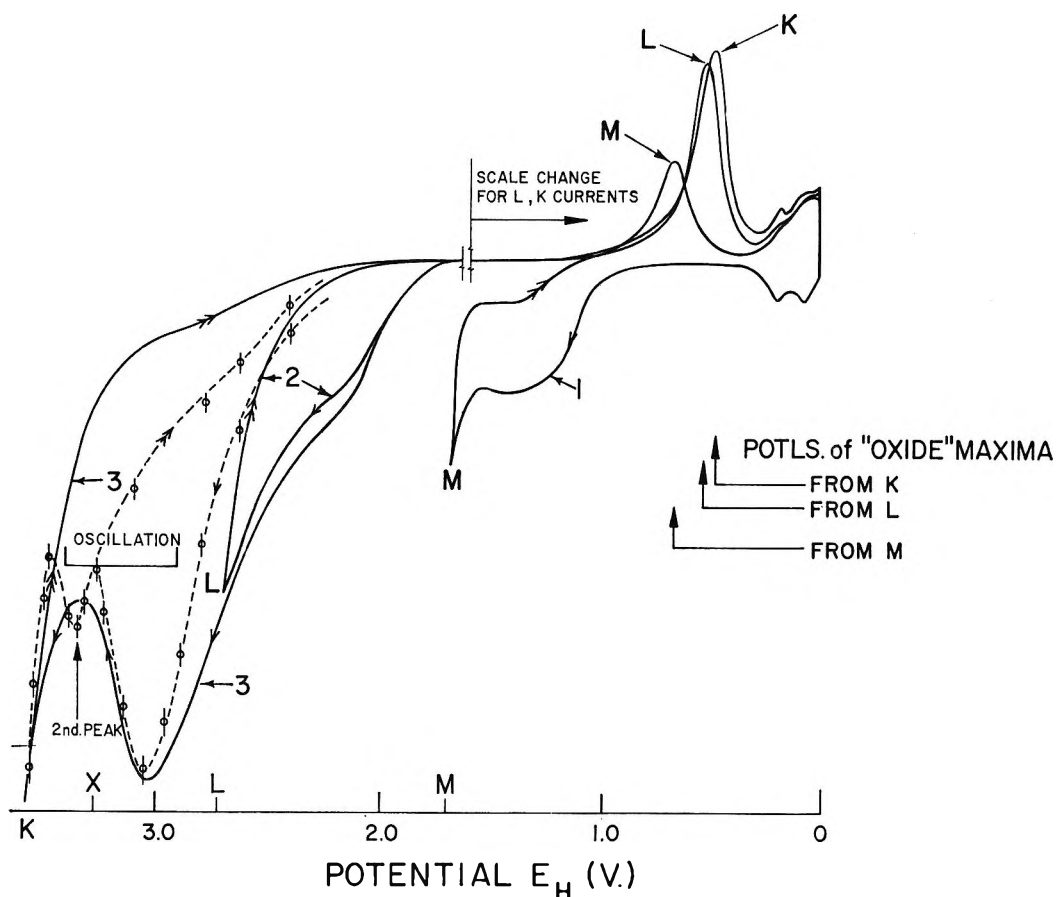


Figure 7. Potentiodynamic profiles for 1.3 *M* aqueous KTFA in 0.01 *M* CF_3COOH + excess water showing oxide reduction region from three anodic potentials at 0.17 v sec^{-1} : limit $K = 3.7 \text{ v } E_H$; limit $L = 2.75 \text{ v } E_H$, and limit $M = 1.7 \text{ v } E_H$; current sensitivity 0–1.7 v, $25 \mu\text{a cm}^{-2}$; over range 1.7–3.7 v, 80 times less. Individual points are steady-state values, 30 sec at each point. (Two peaks are observed at 3.0 and 3.3 v.)

anodic charging process—the currents are in any case too large) since the maximum current depends little on sweep rate (*cf.* the steady-state points in Figure 7) from $dV/dt = 0.38$ to $dV/dt = 0.038 \text{ v sec}^{-1}$ (Figure 9) and also arises in steady-state conditions. In the KTFA solution, the limiting current occurs at *ca.* $2.9 \text{ v } E_H$ (Figure 7) so that it does not seem that the inhibition effect is due to specific adsorption of *anions* since the effect might then have been expected to be more developed in the KTFA than in the H_2SO_4 –TFA system and to have occurred at lower rather than higher anodic potentials, respectively, in these two types of solution. The inhibition effect is irreversible, since the profile of changing anodic current in the cathodic direction of sweep is very different from that in the anodic direction, a type of effect which usually indicates that the change of surface condition of the electrode which led to the inhibition is maintained in the descending potential sweep over the potential range where the inhibition effect was originally initiated.

After the anodic scan has been extended to *ca.* $2.9 \text{ v } E_H$, the cathodic surface oxide reduction peak becomes significantly shifted by *ca.* 0.14 v to more cathodic potentials (Figures 7–9). This effect is “reversible” in the sense that if the anodic scan range is reduced back to *ca.* $1.6 \text{ v } E_H$, the oxide reduction peak returns to its usual position, while if higher anodic potentials are again scanned, the initial shift is manifested once more. Qualitatively, the effect is largely independent of scan rate from 0.38 to 0.01 v sec^{-1} .

The charge for surface oxide reduction between 0.8 and 0.5 v is evidently increased substantially once the potential has been taken into the region 2.9 – 3.9 v and the apparent shift of the pseudo-capacitance maximum⁴⁵ associated with the oxide reduction may be connected with this effect since it is generally found,⁴⁹ *e.g.*, in pure aqueous H_2SO_4 , that the higher is the scan taken into the oxide formation and O_2 evolution region, the more is the corresponding oxide reduction peak (in the cathodic trace) shifted to less anodic potentials.⁵⁰ Normally,

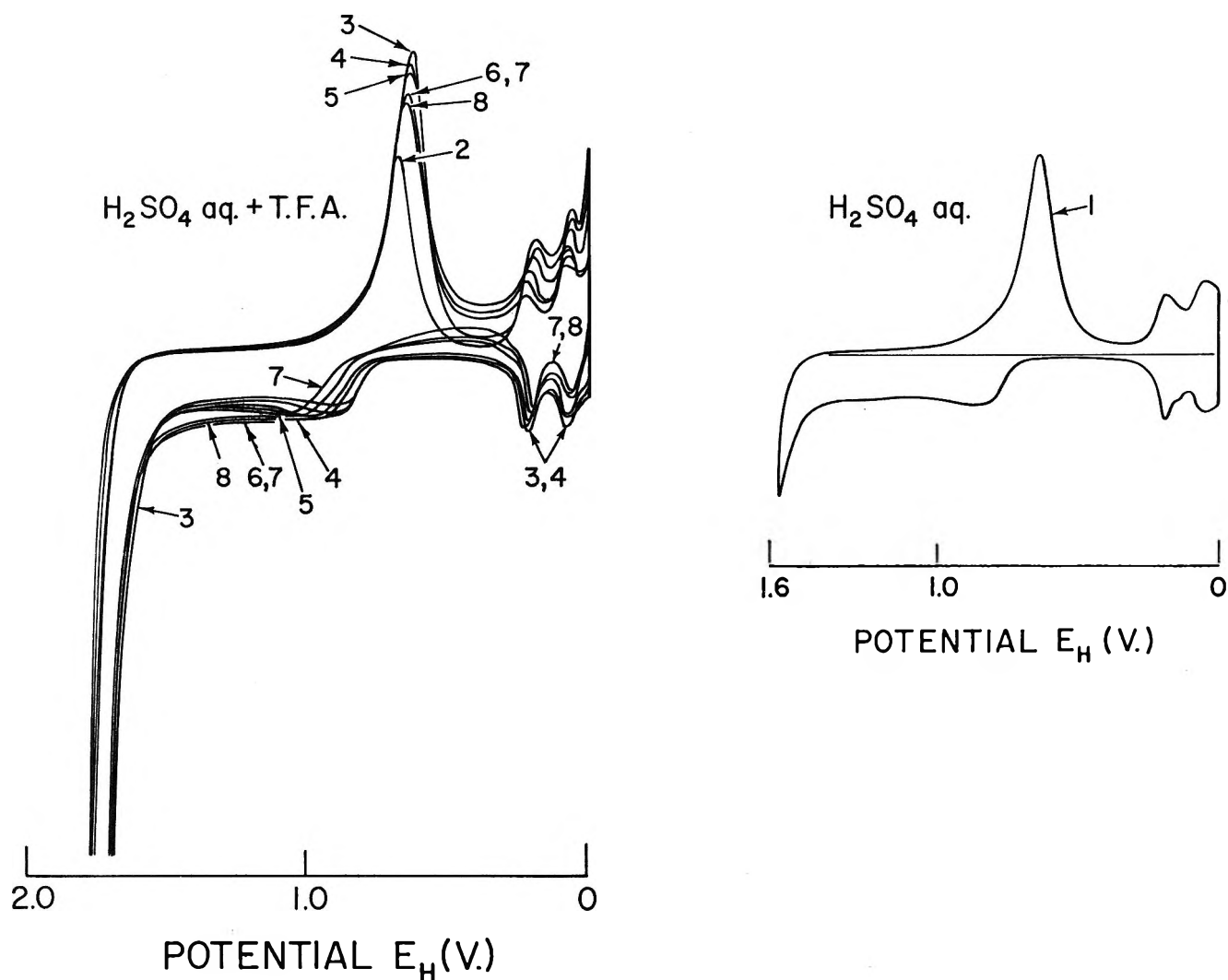


Figure 8. Potentiodynamic profiles for 0.1 M aqueous H_2SO_4 (curves 1 and 2) and for 0.1 M H_2SO_4 + successive additions of TFA up to 2.0 M . Region scanned is only just into that for solution decomposition: curve 3, 0.1 M TFA; 4, 0.2 M TFA; 5, 0.5 M TFA; 6, 0.5 M TFA; 7, 1.3 M TFA; 8, 1.6 M TFA. Current sensitivity $25\ \mu\text{A cm}^{-2}$; $0.17\ \text{V sec}^{-1}$.

however, in the absence of a carboxylate or carboxylic acid at moderate concentration, such high anodic potentials cannot practically be reached.

(iv) *Products of Electrolysis.* Anodic products of electrolysis were characterized and it was found that CO_2 and C_2F_6 were produced in all the three types of solutions, in agreement with results of previous studies.⁷

Discussion of Results and Mechanisms

(i) *Kolbe Reaction on Platinum in Anhydrous KTFA-TFA Solutions.* The following experimental facts (see Table I) indicate the absence of significant quantities of electroactive (*i.e.*, cathodically reducible) adsorbed species on the electrode in this case: (a) low values of the rest potential ($<0.5\ \text{V}$), (b) absence of hysteresis in the i - V relations (Figure 1), (c) absence of

arrests in open-circuit and cathodic transients (see photograph in Figure 3), (d) low values of quasi-steady potential obtained on open-circuit decay, (e) small values ($<100\ \mu\text{f cm}^{-2}$) of C_{max} , and (f) absence of peaks in potentiodynamic sweep runs. Additionally, a high Tafel slope of $0.215\ \text{V}$ is observed in the post-transition region (Figure 1). High Tafel slopes [$>(2.3)(2RT/F)$, $\beta = 0.5$] are characteristic of the reaction and are also found for aqueous as well as for the nonaqueous solutions.

Since all the mechanisms B to E' considered above lead⁷ to Tafel slopes less than or equal to $(2.3)(2RT/F)$,

(50) B. E. Conway and M. A. Sattar, Proceedings of the Conference of the Advisory Group for Aerospace Research and Development, NATO, Liège, 1967.

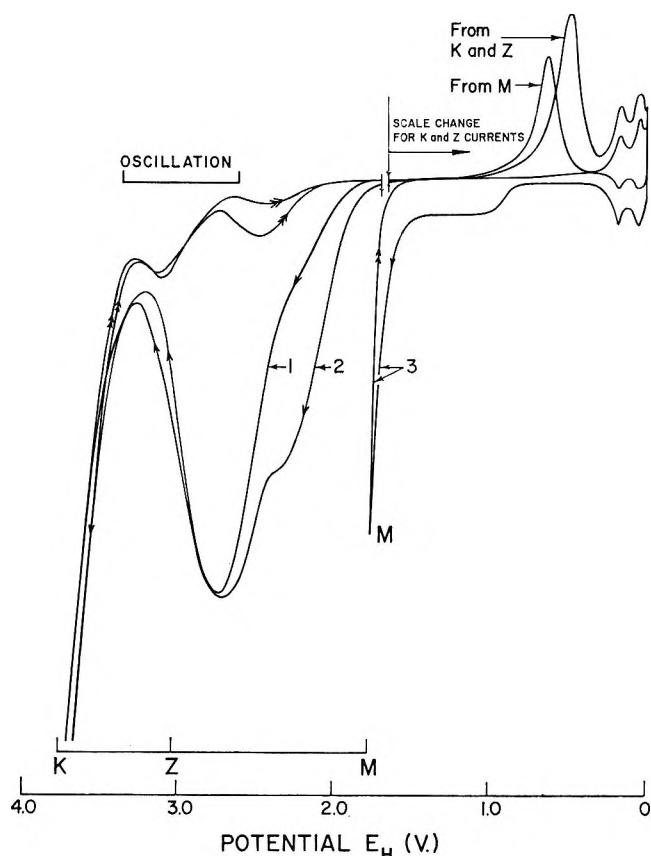


Figure 9. Potentiodynamic profiles for 0.1 *M* aqueous $\text{H}_2\text{SO}_4 + 2.6 \text{ M TFA}$. Scan extends into Kolbe region and shows inhibition effects above 2.9 v and shift of oxide reduction region in the range 0.9–0.5 v E_H : curve 3, to limit *M* 1.8 v E_H , 0.17 v sec^{-1} ; curves 1, 2, to limit *K*, 3.8 v E_H , at scan rates 0.038 and 0.38 v sec^{-1} , respectively. Current sensitivity is in the range *M*–*K*, 5 $\mu\text{a cm}^{-2}$; in range 0–1.8 v E_H , 25 $\mu\text{a cm}^{-2}$, 0.17 v sec^{-1} .

the observation of anomalously high Tafel slopes requires some special consideration. Low values of β would, of course, account for the high values of b in the discharge step B or in the radical-ion desorption steps E or E' with coverage θ by $\text{RCOO}\cdot$ or $\text{R}\cdot$ independent of potential (*i.e.*, when $\theta \rightarrow 1$); a value of $\beta = 0.27$ would, in fact, be required. However, it is an important aspect of the present argument and treatment of the results that the intrinsic symmetry factor β (in the absence of dipole- or barrier-layer effects,⁷ see below) would have a value near to 0.5 ($\pm 10\%$). The justification for this may be sought from the fact that for many qualitatively quite different ion discharge reactions, β is close to 0.5 when other evidence indicates that a barrier layer is not present or could not under any circumstances be involved. Also, theoretically, a value of β close to 0.5 is expected for most reactions⁵¹ as may be deduced by consideration of potential energy barriers for discharge

processes.^{52–54} In this connection, it is of interest to note that for different types of acids and bases, Brønsted's coefficient, α , which has a significance closely analogous¹⁴ to that of β , is often also near to 0.5. Finally, it cannot be argued that low values of β , and hence high values of Tafel slopes, arise for some intrinsic geometrical or other special reason (*e.g.*, anion adsorption, see below) in the case of discharge of carboxylate ions since a more normal value of β corresponds to the observed Tafel line in the case of the acetate Kolbe reaction ($\text{R} = \text{CH}_3$) in strictly anhydrous solutions⁴⁷ but not in water. In the latter case,⁴⁷ b is 0.26 up to 2.6 v E_H and falls *suddenly* to 0.165 beyond 2.5 v. This could hardly be explained either in terms of anion adsorption or in terms of variation of slopes of potential energy diagrams.⁵³ A sudden change in the properties of a dipole-oxide barrier layer seems more probable, *e.g.*, through changes of orientation or film conductivity.

Fioshin and co-workers⁵⁵ have invoked specific adsorption of acetate ions (a) as a possible factor leading to increased Tafel slopes and (b) as the reason for inhibition of O_2 evolution by competition with water adsorption. However, the mechanism of this effect was not examined and it is evident from their experimental data that reactions other than the supposed O_2 evolution (in the potential range 1.1–1.45 v $E_{\text{satd cal}}$) were proceeding, since the observed current densities seem to be too large by a factor of *ca.* 10^5 for O_2 evolution alone on smooth Pt. Some other side oxidation processes involving discharge and further oxidation of the acetate ion (to CH_3OH , CO_2 , etc.) must be presumed to have been occurring. While some effect of acetate ions may be involved in determining the b values in the above work,⁵⁵ it seems unlikely that such large effects as are observed can originate in this way. From another point of view, it may be noted that the inhibition effects which occur with the trifluoroacetate system arise both in KTFA solutions and in aqueous H_2SO_4 containing TFA itself where the carboxylate anion concentration must, relatively, be very small. At such low concentrations as would be involved, the extent of adsorption of even highly specifically adsorbed anions such as I^- would probably be insufficient to account for such marked kinetic effects in b . Furthermore, in the pres-

(51) N. S. Hush, *J. Chem. Phys.*, **28**, 962 (1958).

(52) J. A. V. Butler, *Proc. Roy. Soc. (London)*, **A157**, 423 (1936).

(53) J. O'M. Bockris and R. Parsons, *Trans. Faraday Soc.*, **47**, 914 (1951); J. O'M. Bockris and A. Despic, *J. Chem. Phys.*, **32**, 339 (1960).

(54) J. O'M. Bockris and D. B. Matthews, *Proc. Roy. Soc. (London)*, **A292**, 479 (1966).

(55) M. Y. Fioshin, G. P. Girina, and V. E. Kazarinov, *Elektrokhymia*, **1**, 478 (1965); *cf.* M. Y. Fioshin and Y. B. Vasilev, *Dokl. Akad. Nauk SSSR*, **134**, 879 (1960).

Table I: Behavior at Platinum

EXPERIMENTAL EVIDENCE	SOLUTION: 1M CF ₃ COOH IN CF ₃ COOH + 1M CF ₃ COOH + 1% CF ₃ CO ₂ O ₂ COOP ₃	SOLUTION: 1M CF ₃ COOH IN CF ₃ COOH IN H ₂ O	REMARKS (GENERAL)
1. <u>CURRENT-POTENTIAL RELATIONS</u>			
(1) TAFEL SLOPES.	(1) 0.215 V	(1) 0.22 V	(1) 0.25 V
(11) HYSTERESIS?	(11) NO HYSTERESIS	(11) HYSTERESIS	(11) LARGE HYSTERESIS.
(111) REST POTENTIAL.	(111) 0.5 V	(111) 0.9 V	(111) 0.950 V
(1V) ADDITIONAL FEATURES OR COMMENTS			WITH INCREASING AMOUNTS OF H ₂ O IN THE SOLUTION, HYSTERESIS BECOMES LARGER, RATE BECOMES LOWER, AND THE REST POTENTIAL BECOMES HIGHER.
2. <u>OPEN-CIRCUIT DECAYS</u>			
(1) ARREST?	(1) NO ARRESTS.	(1) NO ARRESTS.	(1) NO ARREST.
(11) MAGNITUDE OF C	(11) d.l. CAPACITY (< 100 μF cm ⁻²).	(11) d.l. CAPACITY (< 100 μF cm ⁻²).	(11) C _{max.} = 468 μF cm ⁻² AT 1.405 V.
(111) RESIDUAL POTENTIAL.	(111) 0.6 V	(111) 0.9 V	(111) 1.175 V.
(1V) FORCED DECAY FROM RESIDUAL POTENTIAL?			(1V) FORCED DECAY OF RESIDUAL POTENTIAL GIVES ARRESTS.
(a) VALUES OF C _{max.} AND V _{Cmax.}			(a) C _{max.} = 2684 μF cm ⁻² ; V _{Cmax.} = 0.58 V.
(b) VALUES OF Q AND POTENTIALS OF ARRESTS CORRESPONDING TO Q.			(b) Q ₁ = 0.537 mCcm ⁻² (0.58 V). Q ₂ = 0.292 mCcm ⁻² (0.15 V).
(1V) ADDITIONAL FEATURES OR COMMENTS.			PSEUDO-CAPACITY ON OPEN-CIRCUIT DECAY OBSERVED ONLY IN THE AQUEOUS CASE. RESIDUAL POTENTIAL INCREASES WITH THE INCREASE IN THE AMOUNT OF H ₂ O PRESENT IN THE SOLUTION.

3. FORCED DECATS				
(1) ARREST?	(1) NO ARRESTS OBSERVED IN VERY FRESH SOLUTIONS; AFTER 72 HOURS SOME ARRESTS OBSERVED.	(1) NO ARRESTS OBSERVED IN VERY FRESH SOLUTIONS; AFTER 72 HOURS SOME ARRESTS OBSERVED.	(1) STRAIGHT LINE FOR CATHODIC PEAK; HENCE CATHODIC PEAK IS DIFFUSION-CONTROLLED.	ARRESTS AND APPRECIABLE PSEUDO-CAPACITY AND CHARGE ASSOCIATED WITH ARRESTS INCREASE WITH INCREASING AMOUNTS OF H ₂ O PRESENT.
(11) C _{max} AND V _{Cmax} VALUES.	(11) C _{max} ≈ 2.10/4F cm ⁻² ; V _{Cmax} = 75 mV.	(11) C _{max} ≈ 2.10/4F cm ⁻² ; V _{Cmax} = 75 mV.	(11) FOR ANODIC PEAK, WHEN dV/dt IS INCREASED TEN TIMES, q DECREASES APPROX. TO 30% OF ITS ORIGINAL VALUE.	IN EVERY CASE WHERE A PEAK WAS OBSERVED, CURRENTS ASSOCIATED WITH THE PEAK WERE FOUND TO BE COMPOSITE CURRENTS, e.g., CHARGING CURRENTS, FARADIC CURRENTS, AND DIFFUSION CURRENTS.
(111) EFFECT OF i _{cath} ON C _{max} AND V _{Cmax} .	(111) NOT STUDIED SINCE C VALUES C _d ≈ 1.	(111) DETAILED C vs. V PROFILE (AT VARIOUS i _{cath} VALUES) NOT STUDIED SINCE IT HAS NO QUANTITATIVE SIGNIFICANCE DUE TO INDETERMINATE FRACES OF H ₂ O PRESENT.	(111) PEAKS ARE NOT CHARGING PEAKS SINCE CATHODIC PEAK IS DIFFUSION CONTROLLED AND ANODIC PEAK SHOWS COMPOSITE CURRENTS SINCE q DEPENDS APPRECIABLY ON dV/dt.	
(1V) PLOT OF i _{cath} vs. 1/q _{1/2} AT A GIVEN V ₁ ; q FROM THIS PLOT.	(1V) THIS PLOT COULD NOT BE MADE SINCE THERE WERE NO ARRESTS.	(1V) STRAIGHT LINE; 0.108 μCcm ⁻² .	(1V) q IS INDEPENDENT OF V ₁ IN THE RANGE 2.2 V TO 2.9 V.	
(V) PLOT OF q vs. V ₁ .	(V) NO q CALCULATED SINCE THERE WERE NO ARRESTS.	(V) q INCREASES WITH V ₁ .	(V) q IS INDEPENDENT OF V ₁ IN THE RANGE 2.2 V TO 2.9 V.	
(VI) ADDITIONAL FEATURES OR COMMENTS.	(VI) ABOVE FEATURES INDICATE EITHER ABSENCE OF ADSORBED INTERMEDIATES OR PRESENCE OF INVERTIBLY ADSORBED (i.e., IRREVERSIBLE OR "ELECTRO-INACTIVE") INTERMEDIATES.	(VI) ARRESTS AND q AND PSEUDO-CAPACITANCE ASSOCIATED WITH THESE ARRESTS, APPEAR ONLY AFTER 72 HOURS OF SOLUTION PREPARATION - PRESUMABLY SOME MOISTURE ENTERS THE SOLUTION FROM THE ATMOSPHERE BY DIFFUSION DURING THIS TIME AND IS RESPONSIBLE FOR THE ORIGIN OF SPECIES ADSORBED ON THE ELECTRODE AS INDICATED BY FORCED DISCHARGE BEHAVIOUR.	(VI) IN THIS AQUEOUS CASE, APPRECIABLE PSEUDO-CAPACITANCE IS OBSERVED AND q IS TEN TIMES MORE THAN THE CASE WHEN TRACES OF WATER ARE PRESENT. THIS INDICATES THAT IN THIS CASE, THERE IS APPRECIABLE COVERAGE OF THE ELECTRODE BY SPECIES WHICH ORIGINATE FROM H ₂ O.	
4. SHEAR RULE	(1) NO DATA OBSERVED; JUST ESTIMATIONS.	(1) NO STRAIGHT LINE OBTAINED; HENCE PEAK CURRENT NOT DIFFUSION-CONTROLLED.	(1) STRAIGHT LINE FOR CATHODIC PEAK; HENCE CATHODIC PEAK IS DIFFUSION-CONTROLLED.	
(11) DEPENDENCE OF q ON (dV/dt)	(11) CAPACITY ASSOCIATED WITH THE HYDROLYSIS IS d.l. CAPACITY (≈ 20/4F cm ⁻²).	(11) WHEN (dV/dt) IS INCREASED TEN TIMES, q DECREASES APPROX. TO 25% OF ITS ORIGINAL VALUE.	(11) FOR ANODIC PEAK, WHEN dV/dt IS INCREASED TEN TIMES, q DECREASES APPROX. TO 30% OF ITS ORIGINAL VALUE.	
(111) IF CHARGING PEAKS, q VALUES FOR THE PEAKS	(111) CAPACITY ASSOCIATED WITH THE HYDROLYSIS IS d.l. CAPACITY (≈ 20/4F cm ⁻²).	(111) PEAKS ARE NOT CHARGING PEAKS SINCE CATHODIC PEAK IS DIFFUSION CONTROLLED AND ANODIC PEAK SHOWS COMPOSITE CURRENTS SINCE q DEPENDS ON dV/dt.	(111) PEAKS ARE NOT CHARGING PEAKS SINCE CATHODIC PEAK IS DIFFUSION CONTROLLED AND ANODIC PEAK SHOWS COMPOSITE CURRENTS SINCE q DEPENDS APPRECIABLY ON dV/dt.	
(1V) C _{max} AND V _{Cmax}	(1V) C, q AND V _{Cmax} ETC. NOT CALCULATED SINCE PEAK CURRENTS ARE COMPOSITE CURRENTS.	(1V) C, q AND V _{Cmax} ETC. NOT CALCULATED SINCE PEAK CURRENTS ARE COMPOSITE CURRENTS.	(1V) C, q AND V _{Cmax} ETC. NOT CALCULATED SINCE PEAK CURRENTS ARE COMPOSITE CURRENTS.	
(V) EFFECT OF dV/dt ON C _{max} AND V _{Cmax} .	(V) ADDITIONAL FEATURES OR COMMENTS.	(V) C, q AND V _{Cmax} ETC. NOT CALCULATED SINCE PEAK CURRENTS ARE COMPOSITE CURRENTS.	(V) C, q AND V _{Cmax} ETC. NOT CALCULATED SINCE PEAK CURRENTS ARE COMPOSITE CURRENTS.	
5. PRODUCTS OF ELECTROLYSIS REACTIONS	C ₂ F ₆ , CO ₂ AND A SMALL AMOUNT OF C ₄ F ₈ OBSERVED AT c.d.'s > 2x10 ⁻³ a.cm. ≈ 2 APPROX. (1.e., E ₁ > 2.3 V)	C ₂ F ₆ , CO ₂ AND A SMALL AMOUNT OF C ₄ F ₈ OBSERVED AT c.d.'s > 2x10 ⁻³ a.cm. ≈ 2 APPROX. (1.e., E ₁ > 2.3 V)	C ₂ F ₆ , CO ₂ AND A SMALL AMOUNT OF C ₄ F ₈ OBSERVED AT c.d.'s > 2x10 ⁻³ a.cm. ≈ 2 APPROX. (1.e., E ₁ > 2.3 V)	KOLBE ELECTROLYSIS PRODUCTS AT HIGHER POTENTIALS (E ₁ > 2.5 V) IN ALL THE ABOVE CASES.

ent work itself, no appreciable effect on the H chemisorption peaks in potentiodynamic scanning is observed in the KTFA solutions whereas Br^- and I^- are known to cause quite substantial effects at Pt.⁵⁶ It is difficult therefore to attribute the kinetic effects in the Tafel relations to specifically adsorbed trifluoroacetate anions. Lack of specific adsorption might also be inferred by analogy with the acetate case where 1- C^{14} -labeled acetate ion is not found to be specifically adsorbed at Pt.⁴⁴ In another case, the anodic evolution of Cl_2 at Pt, anomalous Tafel slopes are not observed⁵⁷ yet the Cl^- anion is specifically adsorbed.

The results have therefore forced us to consider⁵⁸ the presence of a dipole adlayer of adsorbed $\text{CF}_3\cdot$ or $\text{CF}_3\text{COO}\cdot$ species as the origin of the high b values through a dipole "barrier-layer" type of effect such as had been postulated previously.⁷ Similar effects occur in the oxygen evolution reaction at Au and Au-Pd alloys.⁵⁹ If such a dipole layer or a thin and moderately conducting barrier-layer film is present at the interface, part of the total metal-solution potential drop can fall across this film (*cf.* the extreme case of the barrier layers at metals such as Ta, Zr^{60-62}) and part across the ionic double layer, through which the ion discharge takes place. This latter process then occurs with an effective symmetry factor (referred to the total metal-solution potential difference) which can be less than 0.5 and may be as low as 0.25-0.2 depending on the properties of the electrode metal and the dipole or barrier film.^{47,59} Specifically adsorbed anions could, of course, set up an unusually high potential difference across the inner Helmholtz plane, but there is no reason to suppose that the discharge of the anions which are *already* in such a layer should be associated with a low β value (*cf.* the case of Cl_2 evolution⁵⁷). In the case of the dipole-layer model, the transition state in discharge-type reactions would be forced further away from the metal surface with a resulting low value of the effective β referred to the total metal-solution potential difference between the metal and the inner limit of the diffuse layer. The situation is shown in Figure 10.

Returning now to the experimental results, we have to reconcile the apparently contradictory experimental evidence from the high Tafel slopes and that indicated from the transient measurements in a-e above (since the former, we have proposed, can indicate some dipole layer of adspecies and the latter indicates absence of electroactive species). A possible resolution of this difficulty is to suppose that (a) the electrode is appreciably covered by an electroinactive⁶³ dipolar species, corresponding to the fact that the Kolbe reaction is proceeding in the post-transition region and hence probably on a surface covered by some intermediate(s) and (b) that

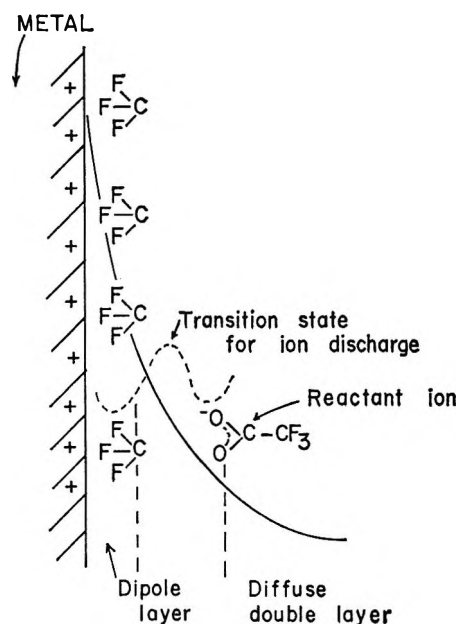


Figure 10.

this species sets up a dipole layer potential difference influencing the discharge kinetics (see below).

In terms of these suggestions, the following mechanism may be proposed for the CF_3COO^- Kolbe reaction at Pt in "very" anhydrous solutions: the discharge step B is followed by the decarboxylation C and desorption of $\text{CF}_3\cdot$ by E'. The Tafel slopes for steps C or D will, to a first approximation, be independent of the value of β involved in the discharge step and will have values⁷ of

$$\frac{b}{2.3} = \frac{RT}{F} \text{ or } \infty (\theta_{\text{CF}_3\text{COO}^-} \rightarrow 1) \text{ for C}$$

$$\frac{RT}{2F} \text{ or } \infty (\theta_{\text{CF}_3\cdot} \rightarrow 1) \text{ for D}$$

Hence, steps C or D cannot on any reasonable basis account for the experimental situation. Similarly, steps

(56) M. Breiter, *Electrochim. Acta*, **8**, 925 (1963); *cf.* A. Slygin and A. N. Frumkin, *Acta Physicochim.*, **3**, 791 (1935); **5**, 819 (1936).

(57) F. T. Chang and H. Wick, *Z. Physik. Chem.*, **A172**, 448 (1935).

(58) An alternative theoretical explanation of anomalously high Tafel slopes has been examined elsewhere and has been found to be inapplicable to the present reaction.⁴⁴

(59) J. J. MacDonald and B. E. Conway, *Proc. Roy. Soc. (London)*, **A269**, 419 (1962).

(60) H. Gohr and E. Lange, *Z. Elektrochem.*, **63**, 673 (1958).

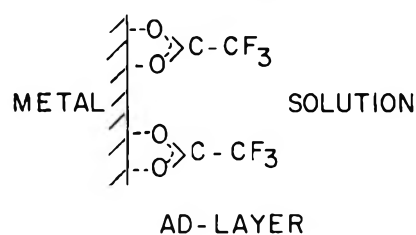
(61) R. E. Meyer, *J. Electrochem. Soc.*, **107**, 847 (1960).

(62) L. Young, "Anodic Films," Academic Press Inc., New York, N. Y., 1961.

(63) An electroinactive radical may be defined as one which is adsorbed in a highly irreversible manner on the electrode surface and is not susceptible to facile reduction in a cathodic transient.

of the type D' or D'' are eliminated.⁷ Steps E or E' could proceed with a dipole layer of $\text{CF}_3\text{COO}\cdot$ or $\text{CF}_3\cdot$, respectively, by means of a radical-ion discharge process.

It is now necessary to speculate on the nature of the supposed adsorbed electroinactive species. The dipole layer must presumably consist of either $\text{CF}_3\cdot$ or $\text{CF}_3\text{COO}\cdot$ dipoles or both. If $\text{CF}_3\text{COO}\cdot$ were present on the electrode, it might be expected to have its oxygen atoms, which have a partial negative charge due to resonance and induction effects, oriented toward the positively charged electrode with binding to the Pt metal through "Pt-O" bonds as shown below.



In cathodic transients, $\text{CF}_3\text{COO}\cdot$ thus adsorbed might be expected to behave like a "substituted" oxide and thus be reducible in the reverse of B (and hence be "electroactive") like other oxygenated species adsorbed through "Pt-O" bonds, *e.g.*, $\text{OH}\cdot$ or $\text{O}\cdot$ and Pt. Hence it is believed that the electroinactive species is more likely to be $\text{CF}_3\cdot$ than $\text{CF}_3\text{COO}\cdot$. If this deduction is accepted, steps D', D'', and E need not be considered further. On the basis of the arguments given above that the high Tafel slopes indicate the presence of a dipole type of barrier layer, it may be concluded that $\theta_{\text{CF}_3\cdot}$ is appreciable. Step B could not then be rate determining since such a condition would imply $\theta_{\text{CF}_3\cdot} \rightarrow 0$. Similarly, step C could not be rate determining since it would involve appreciable coverage by the supposed electroactive species $\text{CF}_3\text{COO}\cdot$ as the adsorbed intermediate against which we have argued above. However, if it were argued that the adsorbed intermediate is $\text{CF}_3\text{COO}\cdot$, it would be expected that a limiting current would then be observed at high coverage⁷ following a lower slope, $< (2.3)(2RT/F)$, at lower potentials; neither of these possibilities is in agreement with the experimental slope of *ca.* $(2.3)(7RT/2F)$. The only likely step is therefore E'; low-coverage conditions when E' is the r.d.s. must be rejected because neither low coverage is indicated by the experimental $\log [i]-V$ relation nor are the experimental Tafel slopes $(2.3) \cdot (7RT/2F)$ at all close to the one $[(2.3)(2RT/3F)]$ (in general, this slope is $2.3RT/(1 + \beta)F$ so that even if β were unusually small, $b < (2.3)(RT/F)$, and not a high value) for low-coverage conditions with E' as the r.d.s. We are thus reduced to the possibility that E' is the

r.d.s. in the above scheme with $\theta_{\text{CF}_3\cdot} \rightarrow 1$. For a normal value of $\beta = 0.5$, b is $(2.3)(2RT/F)$ in this case, but if at appreciable coverage by $\text{CF}_3\cdot$ a dipole layer of irreversibly adsorbed $\text{CF}_3\cdot$ is set up, the effective value β' of β can then become⁶⁻⁷ less than 0.5 with a corresponding increase in the value of the Tafel slope deduced, $(2.3)(RT/\beta'F)$. Obviously, if rather less than half of the total metal-solution potential drop operated across the $\text{CF}_3\cdot$ dipole layer, the experimental Tafel slope would be accounted for.

While the validity of some of the arguments and conclusions given above depends on the correctness or otherwise of the suggested dipole layer effect, it is to be stressed that mechanisms C, D, D', D'', and the low-coverage cases for E and E' are eliminated on other, less ambiguous grounds, since such cases lead⁷ relatively unequivocally to Tafel slopes $\ll (2.3)(2RT/F)$, independently of the assumed value of β or the nature of the isotherm for adsorption of the intermediates.

In order to have an effective dipole barrier layer largely of the electroinactive $\text{CF}_3\cdot$ radicals, as is required by the high b values and absence of arrests in the cathodic transients, it is necessary to assume that in step C the equilibrium lies mostly to the right (indicated by the double arrow). Some $\text{CF}_3\text{COO}\cdot$ species could, however, also be present at low coverage in step C without changing the conclusions made above.

(ii) *Kolbe Reaction in Nominally Anhydrous Solutions.* As indicated in Table I, high Tafel slopes $[(2.3)(9RT/2F)]$ are again observed in the post-transition region (Figure 1), possibly indicating a "barrier" layer. The rest potential of *ca.* 0.9 v (*cf.* the value of 0.5 v for the anhydride-treated solution) suggests partial coverage by oxide; this is supported by the appearance of hysteresis between the ascending and descending $\log [i]-V$ relations (Figure 1), an effect which indicates (since this behavior occurs in virtually all anodic oxidations where oxide is present) that the surface is covered by some species which is irreversibly formed but in this case is electroactive.⁶⁴ Since the only additional constituent in this solution is water (present in traces), this/these species must arise from the traces of water. In nominally anhydrous solution, the rate at a given potential⁶⁵ is lower than the corresponding rate in

(64) If the species were irreversibly adsorbed and electroinactive, as apparently in the case of the completely anhydrous solutions, the barrier layer-solution interface would behave (in regard to absence of hysteresis) like a metal-solution interface in the $\log [i]-V$ relations with a consequent absence of hysteresis in the ascending and the descending $\log [i]-V$ curves (Figure 1). Hysteresis appears because of irreversibility in the formation and reduction of the species produced in the ascending curve. The presence of some electroinactive species on the electrode, it must be emphasized, does not imply, of course, that the electrode surface is inactive for the over-all Faradaic process.

completely anhydrous solutions (Figure 1). Traces of water thus tend to inhibit the Kolbe reaction, presumably due to cocoverage by oxide.

For the reduction transients, Q_{total} is 0.11 mCoulomb cm^{-2} and $C_{\text{max}} = 250\text{--}450 \mu\text{f cm}^{-2}$ (Table I) under the nominally anhydrous conditions. Since Q_{total} is much less than that attained in excess water (see below) yet significant charge can arise in cathodic transients when traces of water are present, it seems most reasonable to suppose that the reaction proceeds essentially by the same mechanism as in the case of completely anhydrous solutions, but on a somewhat diminished free-metal area. The high Tafel slope, similar to that in the completely anhydrous solution, suggests that the same species $\text{CF}_3\cdot$ is involved but that the electroactive species is co-adsorbed oxide^{66,67} extending, possibly in domains, only over part of the surface.⁶⁸

The significance of the measured Q_{total} in terms of inhibition effects is indicated in the following arguments.

In Figure 11, for a given type of solution, a curve is shown passing through a family of points each representing, for a particular potential, the value of Q and the corresponding steady-state rate at that potential; the rate increases with increasing Q . However, the increase in rate and in Q may arise independently of each other; part of the increase in rate will obviously be due to the increasing potential implicitly represented by the ascending direction of points on the Q axis.

Increase in Q with increasing rate may correspond to either a relative inhibition or a relative enhancement in rate depending on whether Q refers to a species derived from the water present or to a species involved in the reaction itself. We may argue as follows that the Q measured involves principally a species (surface oxide) not involved directly as an intermediate. If Q represented the charge associated with an inhibiting oxide species and the coverage by this species increased with V , either a change of sign of the Tafel slope or a relative increase of Tafel slope (compared with that in completely anhydrous solutions) should be observed.³⁴ Figure 1 shows that this is the case; the reaction is not only substantially inhibited at a given potential $> ca. 1.9 \text{ v } E_{\text{H}}$ but more hysteresis, characteristic of oxide involvement, is apparent. The species electroactive in the transients must presumably be surface oxide (possibly with some coadsorbed $\text{CF}_3\text{COO}\cdot$; see Figure 12), since $\text{CF}_3\cdot$ is believed to be electroinactive and hence incapable of being observed in the discharge profiles. The following facts support the view that a fraction of Q_{total} corresponds to coadsorbed oxide associated with a charge Q_{oxide} : when excess water is added to the solution, Q_{total} increases but the rate decreases (Table I, Figure 1). It seems reasonable to regard this increase

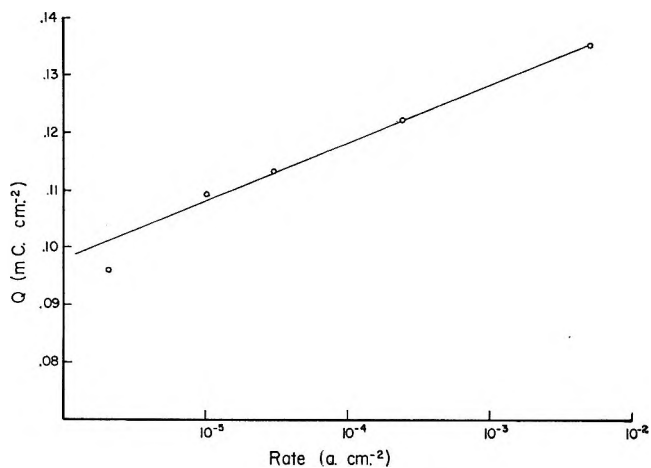


Figure 11. Platinum-1 M CF_3COOK in CF_3COOH (nominally anhydrous solution), a plot of Q vs. rate.

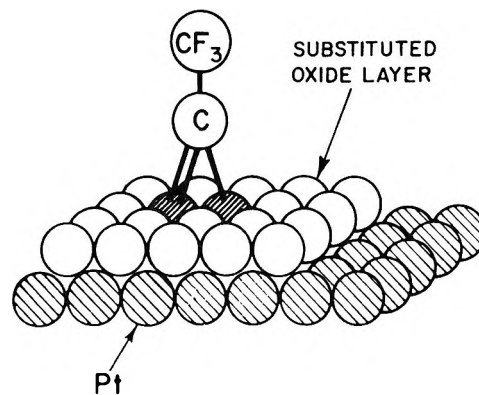


Figure 12. A schematic representation of the "substituted oxide" layer adsorbed on the substrate platinum metal.

in Q_{total} as arising from an increased contribution by Q_{oxide} when water is present in increasing amounts up to excess, an effect which decreases the rate, as observed. Increased inhibition of the Kolbe reaction with increased amounts of water added to a nonaqueous solution was also observed by Fairweather and Walker⁶⁹ in terms of product yields.

(65) Elsewhere,⁴⁷ we have shown that the rates in aqueous and nonaqueous solutions can be legitimately compared at the same nominal potential on the H_2 scale since the reversible potentials for the Kolbe reaction in the given solutions are the same on this scale. The standard reversible potentials, of course, differ.

(66) That the surface oxide itself, at Pt, does not give rise to barrier layer effects is indicated by the observation of normal Tafel slopes (*ca.* $(2.3)(2RT/F)$) in oxygen evolution at Pt.⁶⁷

(67) J. O'M. Bockris and A. K. M. S. Huq, *Proc. Roy. Soc. (London)*, **A237**, 227 (1956).

(68) B. E. Conway, N. Marincic, D. Gilroy, and E. Rudd, *J. Electrochem. Soc.*, **113**, 1144 (1965); B. E. Conway and A. J. Vijn, *J. Org. Chem.*, **31**, 4283 (1966).

(69) D. A. Fairweather and O. J. Walker, *J. Chem. Soc.*, 3111 (1926).

The sequence of consecutive steps in the reaction mechanism would be essentially the same as indicated in (1) but with participation of oxide as the inhibiting and electroactive species. Here the value of β/β' required to account for the b values is ≈ 2.25 .

(iii) *Kolbe Reaction in Aqueous Solutions (1 M KTFA in TFA + 30% H₂O)*. The experimental observations (Table I) indicate, within the limitations discussed above, that the mechanism is essentially the same as that in nominally anhydrous solutions. However, there is an increased contribution of Q_{oxide} and C_{oxide} to the total Q and C values, with consequently increased inhibition effects. All the experimental evidence (Table I) points to the fact that there is an increased coverage by oxide on the electrode in aqueous solutions. Hysteresis in the $\log [i]-V$ relations is enhanced (compared with the behavior in the nonaqueous solutions) and the rates are correspondingly diminished (Figure 1). In the reduction transients, large arrests are observed (see photograph in Figure 6) with Q_{total} and C_{max} now 1.05 mcoulombs cm^{-2} and 1650 $\mu\text{F cm}^{-2}$, respectively (Table I), indicating that the electrode is covered by electroactive species; that the electrode tends to be "completely" covered is also shown by the fact that Q now becomes almost independent of V_i at high potentials (Figure 6), as also indicated from the potentiodynamic results (Figures 7-9). In Figure 5, $V_{C_{\text{max}}}$ lies between 0.6 v and 0.2 v depending on $i_{\text{cath.}}$.⁴⁵ This is roughly the potential range where $V_{C_{\text{max}}}$ for the oxide reduction peak would be expected (~ 0.6 v). On open-circuit decay, a substantial pseudo-capacity (Table I) and a rest potential of 1.175 v suggest the presence of surface oxide. Discharge from this potential gives two arrests which correspond to the C_{max} values in the $C-V$ profiles (Figure 13; cf. Figures 7-9). The values of $V_{C_{\text{max}}}$ are 0.58 and 0.15 v (Figure 13) and the corresponding charges are $Q_1 = 0.537$ mcoulomb cm^{-2} and $Q_2 = 0.392$ mcoulomb cm^{-2} , respectively, indicating that the two arrests are due to reduction of oxide (0.58 v) and deposition of hydrogen (0.15 v, cf. Figures 7-9).

High Tafel slopes $[(2.3)(4RT/F)]$ indicate again a barrier-layer type of film on the electrode. That this Tafel slope refers to a process in which the Kolbe reaction participates and not to O₂ evolution alone follows from (a) the potential at which the Tafel region is observed to commence, *viz.* > 2.1 v, and (b) the coulombic efficiency at high current density where yields of C₂F₆ are substantial.⁷ The Tafel region for the oxygen evolution reaction (o.e.r.) would normally commence at substantially lower potentials as indicated by the current-potential relation for the o.e.r.⁶⁸ at Pt in 1 M H₂SO₄ shown for comparison in Figure 1;

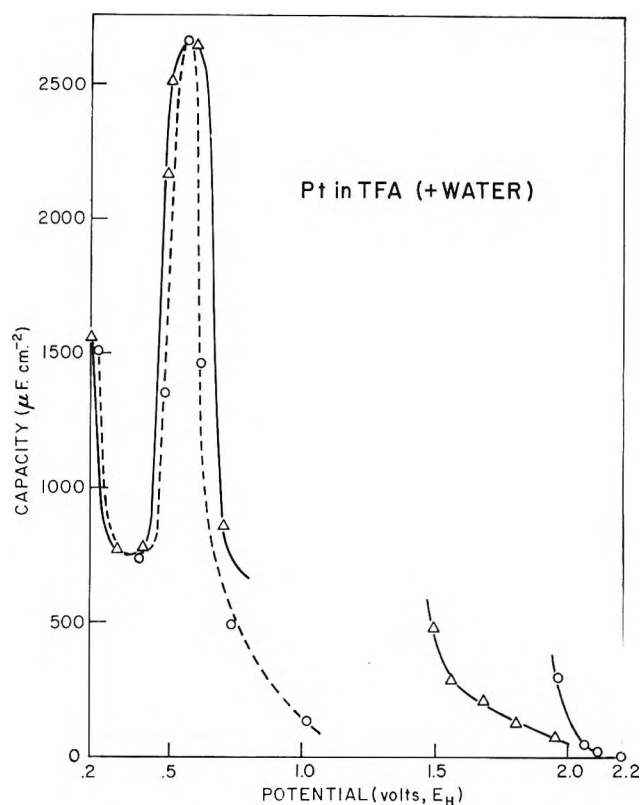


Figure 13. Platinum-1 M CF₃COOK in (CF₃COOK + water); $C-V$ profiles calculated from open-circuit emf decay curves and from curves obtained on forced decay from the residual potential.

in neutral solutions, the o.e.r. would commence at even lower anodic potentials. It must be noted, however, that in the range of potentials studied in the steady-state work, oxygen evolution is appreciable (up to 50% at the lower anodic potentials) and only at the highest potential (2.8 v) in Figure 1 does the Tafel relation approach the second inhibition region (cf. ref 70 for the acetate case) demonstrated in Figures 7 and 9. Also, in the further region beyond this reversal of the direction of the $i-V$ curve, the potentials are too high, the attainable current density range is too short, and the occurrence of oscillations (Figures 7, 9) makes it difficult to characterize a Tafel line for that region. It is unlikely that the kinetic inhibition effect exhibited at high potentials in Figures 7 and 9 originates from oxide coverage effects since the oxide has already been laid down extensively⁷¹ by *ca.* 1.5 v E_H and the "recoverable charge" in the cathodic sweep between 0.5 and 0.9 v is almost independent of whether the anode

(70) M. Ya. Fioshin and Yu. B. Vasilev, *Dokl. Akad. Nauk SSSR*, **134**, 879 (1960); see also ref 55.

(71) S. Gilman, *Electrochim. Acta*, **9**, 1025 (1964).

potential has been taken to *L* or *K* in Figure 7 or to corresponding potentials in Figure 9. The effect may therefore arise from coadsorption of species formed in the Kolbe reaction or to some equivalent modification of the electrocatalytic properties of the oxide surface by the species ($\text{CF}_3\cdot$, $\text{CF}_3\text{COO}\cdot$) involved in steps in that reaction, as discussed above.

In summary, the results indicate within the limitations of assumptions about the dipole layer that the mechanism for the Kolbe reaction of Pt in aqueous solutions of KTFA + TFA up to 2.8 v E_H is similar to that in the nominally anhydrous solutions, *i.e.*, an initial discharge step^{71a} (B) is followed by a r.d.s. of the type E' proceeding at a surface oxide layer with coadsorption of $\text{CF}_3\cdot$ and possibly some $\text{CF}_3\text{COO}\cdot$. The later possibility arises since if the peak at 0.58 v were entirely due to surface oxide, the ratio Q_1/Q_2 would be expected⁷¹ to be >4 at the high value of V_i (2.5 v) reached in the present case. The experimental value of Q_1/Q_2 is, however, only 1.37, indicating that at least part of the coverage (with $V_{C_{\text{max}}} = 0.58$ v) appears to be associated with a species bulkier than oxide. Any blocking of H adsorption would give larger rather than smaller Q_1/Q_2 values. Again this peak could not be associated with $\text{CF}_3\text{COO}\cdot$ only (or $\text{CF}_3\cdot$ only for that matter) since the expected Q_1/Q_2 ratio in that case would be less than unity.

(iv) *Role of Oxide.* The conclusion that oxide ad-species tend to inhibit the Kolbe reaction on Pt is supported by Figure 14 where curves are drawn for given potentials over three points, each of which represents a Q -log [rate] relation at the indicated potential for the three solutions studied. At potentials lower than that (*viz.*, *ca.* 2.1 v) beyond which the Kolbe reaction proceeds at appreciable rates with a linear Tafel relation, Q values are increased on going from nominally anhydrous to the aqueous solution and the rates are correspondingly increased. This suggests that with increasing water content, Q_{oxide} and the rate for the o.e.r. increases. However, on going from aqueous to the non-aqueous solutions at this potential, Q decreases but the rate increases; this indicates that with decreased amounts of water, Q_{total} decreases probably because of

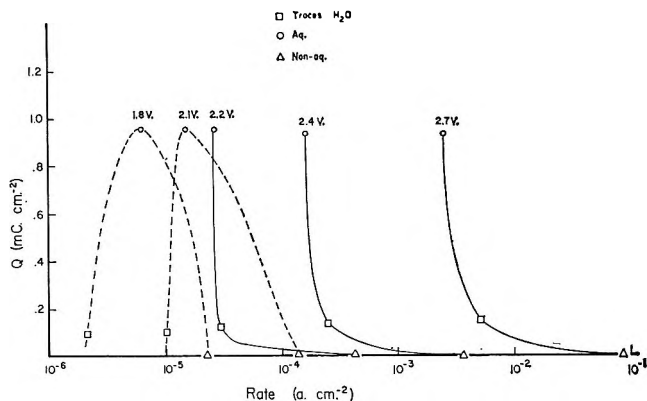


Figure 14. Platinum-1 M CF_3COOK in CF_3COOH , plots of Q vs. rate at various anodic potentials for completely anhydrous (Δ), nominally anhydrous (\square), and aqueous solutions (\circ).

a decrease in Q_{oxide} but the rate continues increasing due, perhaps, to the process being now a composite one, *i.e.*, with contributions from the Kolbe reaction and O_2 evolution⁷² reactions. Only at potentials (>2.1 v) at which yield studies indicate that the Kolbe reaction is the major electrode process does the relation between the rate, the Q , and the water content become more rational in terms of oxide inhibition effects alone.

Acknowledgments. A. K. V. acknowledges the award of a research fellowship by the Sprague Electric Co. Support for this work from the National Research Council, Canada, is gratefully acknowledged.

(71a) NOTE ADDED IN PROOF. Since this paper was submitted, Fleischmann, *et al.* [M. Fleischmann, J. R. Mansfield, H. R. Thirsk, T. Wilson, and W. F. K. Wynne-Jones, *Electrochim. Acta*, 12, 967 (1967)] have given a detailed analysis of the kinetics of the acetate Kolbe reaction under pulsed electrolysis conditions and find that the discharge step is rate controlling, in agreement with our earlier conclusions for this case,⁴⁷ based on other types of evidence.

(72) This is the case of aqueous medium⁷ as confirmed here. At the potentials involved here, the rate of evolution of products is too small to conduct a quantitative coulombic analysis and at higher potentials the problem of solubility of C_2F_6 complicates quantitative measurements in nonaqueous medium. However, the previous work⁷ indicates substantial yields of the Kolbe product at higher anodic potentials, as is also confirmed in the present work.

Controlled Potential Studies on the Kolbe Reaction and the Role of Coadsorbed Surface Oxides. II. The Reaction at Gold

by A. K. Vijh and B. E. Conway

Department of Chemistry, University of Ottawa, Ottawa, Canada (Received January 26, 1967)

The kinetic behavior of the Kolbe reaction at gold in completely anhydrous, nominally anhydrous, and aqueous trifluoroacetic acid solutions has been examined by applying experimental methods used in part I. Results obtained from steady-state and nonsteady-state measurements are presented. The role of surface oxide at the electrode is considered in relation to the possible involvement of other electroactive intermediates in the reaction sequence. In the presence of traces or excess of water in the solutions, coadsorption of oxide derived electrochemically from the water occurs and the oxide is shown to be an inhibiting species. Oxygen is then the main reaction product in excess water.

A general introduction and the experimental approaches used have been given in part I. In this paper, results of various steady-state and nonsteady-state measurements are given for the Kolbe reaction at gold in very anhydrous, nominally anhydrous, and aqueous 1 M KTFA-TFA solutions. Tentative mechanistic conclusions have been drawn in relation to the presence of coadsorbed surface oxide, using the approaches described in part I. The case of gold is one of some special interest since the Kolbe reaction with acetate proceeds efficiently only in nonaqueous solution, methanol being a major product in aqueous medium.¹

Results

The results for the case of gold in TFA solutions are summarized in Table I and examined in more detail below.

(i) *Steady-State Potentiostatic Log [i]-V Relations.* For the case of gold, the types of solutions studied and the sequence in which they were examined were as discussed in part I for platinum. Results are shown in Figure 1. Again, under completely anhydrous conditions, little hysteresis is observed in the transition region in the log [i]-V curves. The transition region is followed by linear Tafel behavior (slope $b = 0.16$ v). In the presence of traces of water (0.1%), the transition region does not extend directly into a normal Tafel line as in the anhydrous solution case but a reversal of direction is observed over the range 1.6-1.8 v. This behavior is

characteristic of inhibition effects discussed recently by Bagotsky and Vasilev² and by Gilroy and Conway.² The inversion is followed by a linear Tafel region with a slope $b = 0.175$ v. In solutions containing excess water, not only is the rate diminished and the hysteresis between the ascending and descending log [i]-V plots enhanced, but the characteristic inhibition behavior observed with traces of water is apparently largely obscured. This arises probably because the hysteresis is now large enough to encompass the whole potential range over which the original inhibition inversion was observed. Linear Tafel behavior still arises, however, in the post-transition region with a slope of the descending curve of $b = 0.170$ v. The rest potential (see part I) is also characteristically different in the three cases. In anhydrous solutions, it is 0.25 v, in solutions containing traces of water, 0.90 v, and in solutions containing excess of water, 1.25 v.

(ii) *Open-Circuit and Cathodic Reduction Behavior from Potentiostatically Maintained Anode Potentials.* Potential-time relationships, observed on open circuit and cathodic reduction from various anodic potentials, were investigated in the three types of solutions referred

(1) B. C. L. Weedon, *Quart. Rev. (London)*, **6**, 389 (1952); A. K. Vijh and B. E. Conway, *Z. Anal. Chem.*, **230**, 81 (1967).

(2) V. S. Bagotsky and Y. B. Vasilev, *Electrochim. Acta*, **9**, 869 (1964); see also D. Gilroy and B. E. Conway, *J. Phys. Chem.*, **69**, 1259 (1965), and B. E. Conway, "Theory and Principles of Electrode Processes," Ronald Press, New York, N. Y., 1965.

Table I: Behavior at Gold

EXPERIMENTAL EVIDENCE	SOLUTION: 1M CF_3COOH IN CF_3COOH + 1% $\text{CF}_3\text{CO}_2\text{OCCF}_3$	SOLUTION: 1M CF_3COOK IN CF_3COOH	SOLUTION: 1M CF_3COOK IN CF_3COOH + 1M CF_3COOK IN H_2O	REMARKS (GENERAL)
1. CURRENT-POTENTIAL RELATIONS				
(1) TAPEL SLOPES	(1) 0.160 V	(1) 0.175 V	(1) 0.170 V	
(11) HYSTERESIS?	(11) NO HYSTERESIS	(11) HYSTERESIS: "INHIBITION REND" OBSERVED.	(11) LARGE HYSTERESIS	WITH INCREASING AMOUNTS OF H_2O IN THE SOLUTION, HYSTERESIS BECOMES LARGER, RATE BECOMES LOWER, AND THE REST POTENTIAL BECOMES HIGHER
(111) REST POTENTIAL.	(111) 0.25 V	(111) 0.9 V	(111) 1.25 V	
(1V) ADDITIONAL FEATURES OR COMMENTS.				
2. OPEN-CIRCUIT DECAYS				
(1) ARREST?	(1) VERY SLIGHT ARREST.	(1) ARREST OBSERVED; $V_1 = 2.5$ V.		
(11) MAGNITUDE OF C	(11) $C_{\text{max.}} = 90\text{-}140 \mu\text{F cm}^{-2}$ DEPENDENT ON V_1 .	(11) $C_{\text{max.}} = 60 \mu\text{F cm}^{-2}$ ($V_{\text{Cmax.}} = 1.62$ V; $V_1 = 2.5$ V) $C_{\text{max.}} = 225 \mu\text{F cm}^{-2}$ ($V_{\text{Cmax.}} = 1.37$ V; $V_1 = 1.8$ V)	(11) $2500 \mu\text{F cm}^{-2}$	
(111) RESIDUAL POTENTIAL.	(111) 0.4 V.	(111) 0.9 V.	(111) 1.3 V	POT. PSEUDO-CAPACITY AND RESIDUAL POTENTIAL TEND TOWARDS HIGHER VALUES WITH INCREASING AMOUNTS OF H_2O PRESENT IN THE SOLUTION.
(1V) FORCED DECAY FROM RESIDUAL POTENTIAL? (a) VALUES OF $C_{\text{max.}}$ AND $V_{\text{Cmax.}}$ (b) VALUES OF Q AND POTENTIALS OF ARRESTS CORRESPONDING TO Q.				
(1V) ADDITIONAL FEATURES OR COMMENTS.				

<p>3. <u>FORCED DECAYS</u></p> <p>(1) ARREST?</p> <p>(11) C_{max} AND V_{Cmax} VALUES.</p> <p>(111) EFFECT OF i_{cath} ON C_{max} AND V_{Cmax}.</p> <p>(1V) PLOT OF i_{cath} vs. $1/q_1$ AT A GIVEN V_1; q FROM THIS PLOT.</p> <p>(V) PLOT OF q vs. V_1.</p> <p>(V1) ADDITIONAL FEATURES OR COMMENTS.</p>	<p>(1) ARREST OBSERVED.</p> <p>(11) $C_{max} = 100 \mu\text{F cm}^{-2}$; $V_{Cmax} = 0.15$ TO 0.68 V DEPENDING ON i_{cath}.</p> <p>(111) INCREASING i_{cath} SHIFTS C_{max} TO HIGHER VALUES AND V_{Cmax} TO LESS ANODIC VALUES.</p> <p>(1V) STRAIGHT LINE; $q = 0.084 \text{ mCcm}^{-2}$.</p> <p>(V) q INCREASES WITH V_1.</p>	<p>(1) LONG ARREST.</p> <p>(11) $C_{max} \approx 500$ TO $1500 \mu\text{F cm}^{-2}$ DEPENDING ON i_{cath}; $V_{Cmax} \approx -0.35$ V TO 0.85 V DEPENDING ON i_{cath}.</p> <p>(111) WITH INCREASING i_{cath}, V_{Cmax} SHIFTS TO LESS ANODIC VALUES BUT TREND IN THE SHIFT OF C_{max} IS DIFFICULT TO ESTABLISH.</p> <p>(1V) STRAIGHT LINE; $q = 0.175 \text{ mCcm}^{-2}$.</p> <p>(V) q INCREASES WITH INCREASING V_1.</p>	<p>(*) AN ARREST IS OBSERVED.</p> <p>(11) $C_{max} = 2250$ TO $7500 \mu\text{F cm}^{-2}$ DEPENDING ON i_{cath}; $V_{Cmax} \approx 0.89$ V TO 1.05 V DEPENDING ON i_{cath}.</p> <p>(111) WITH INCREASING i_{cath}, V_{Cmax} GETS SHIPPED TO LESS ANODIC VALUES BUT THE TREND IN THE SHIFT OF C_{max} IS DIFFICULT TO ESTABLISH.</p> <p>(1V) STRAIGHT LINE; $q = 1.09 \text{ mCcm}^{-2}$.</p> <p>(V) q INCREASES WITH INCREASING V_1.</p>	<p>BOTH C AND q VALUES INCREASE WITH INCREASING AMOUNTS OF H_2O PRESENT IN THE SOLUTION. ALSO, WITH INCREASING V_1, q SHOWS A MORE RAPID INCREASE WITH INCREASING AMOUNTS OF H_2O PRESENT IN THE SOLUTION.</p>
<p>4. <u>SWEEP RUNS</u></p> <p>(1) PLOT OF PEAK CURRENT vs. $(dV/dt)^{1/2}$.</p> <p>(11) DEPENDENCE OF q ON (dV/dt)</p> <p>(111) IF CHARGING PEAKS, q VALUES FOR THE PEAKS.</p> <p>(1V) C_{max} AND V_{Cmax}.</p> <p>(V) EFFECT OF (dV/dt) ON C_{max} AND V_{Cmax}.</p> <p>(V1) ADDITIONAL FEATURES OR COMMENTS.</p> <p>5. <u>PRODUCTS OF ELECTROLYSIS</u></p> <p>REMARKS</p>	<p>(1) STRAIGHT LINE BOTH FOR ANODIC AND CATHODIC PEAKS.</p> <p>(11) STRAIGHT LINE BOTH FOR ANODIC AND CATHODIC PEAKS.</p> <p>C_2F_6, CO_2 AND A SMALL AMOUNT OF CF_4 OBSERVED AT c.d.'s $> 5 \times 10^{-3} \text{ a.cm}^{-2}$ APPROX. (i.e., $E_H > 2.2$ V).</p>	<p>(1) STRAIGHT LINE FOR ANODIC PEAK; CATHODIC PEAK NOT WELL-DEFINED.</p> <p>C_2F_6 AND CO_2 OBSERVED AT c.d.'s $> 5 \times 10^{-3} \text{ a.cm}^{-2}$ APPROX. (i.e., $E_H > 2.2$ V).</p>	<p>(1) STRAIGHT LINE BOTH FOR ANODIC AND CATHODIC PEAKS.</p> <p>C_2F_6 AND CO_2 OBSERVED AT c.d.'s $> 5 \times 10^{-3} \text{ a.cm}^{-2}$ APPROX. (i.e., $E_H > 2.2$ V).</p>	<p>DIFFUSION-CONTROLLED PEAKS OBSERVED IN ALL THE THREE CASES DUE, PRESUMABLY, TO ANODIC DISSOLUTION OF GOLD.</p> <p>KOLBE REACTION PROCEEDS AT HIGHER POTENTIALS ($E_H > 2.2$ V) IN ALL THE THREE CASES.</p>

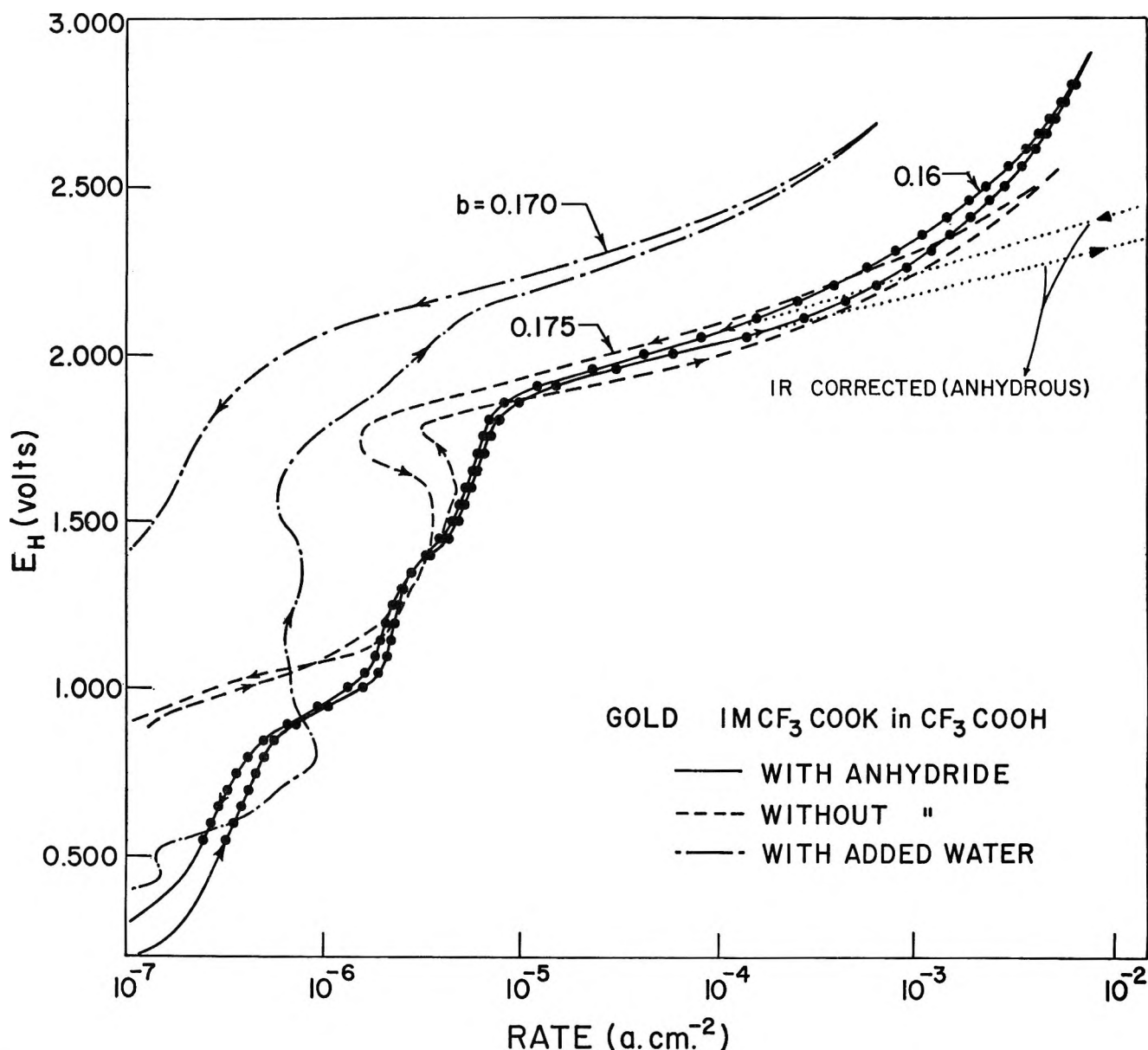


Figure 1. Gold-1 M CF_3COOK in CF_3COOH , steady-state current-potential relations: —, with anhydride; ---, without anhydride; - · - ·, with added water. Note: (i) a typical population of experimental points has been shown on one of the graphs; (ii) a typical resistance potential drop (iR) at higher current densities has been shown; (iii) an inhibition inflection may be noted in the nominally anhydrous solution around 1.7 v, *i.e.*, just below the commencement of the linear Tafel region. The complete lack of hysteresis in the most anhydrous solutions (solid lines with points) is to be noted.

to previously (part I); the results are summarized in Table I, sections 2 and 3.

(a) *Open-Circuit Decay Behavior.* In completely anhydrous solutions, a slight arrest was observed on open-circuit decay; C_{max} is of the order of 90–140 μf cm^{-2} , depending on V_i , the initial polarization potential. The rest potential is 0.4 v. In solutions containing traces of water, a longer arrest is observed on open-circuit decay. The values of C_{max} and $V_{C_{max}}$ depend

on V_i and are as follows: $C_{max} = 60 \mu f$ cm^{-2} , $V_{C_{max}} = 1.62$ v, $V_i = 2.5$ v; $C_{max} = 225 \mu f$ cm^{-2} , $V_{C_{max}} = 1.37$ v, $V_i = 1.8$ v. The rest potential in this case is 0.9 v, which is higher than that observed under completely anhydrous conditions.

In solutions containing excess of water, no arrests are observed in the open-circuit decay though the values of C calculated³ from the self-discharge profiles are very high ($>2500 \mu f$ cm^{-2}) and are indicative of the presence

of some adsorbed electroactive species. The rest potential observed is quite high (1.3 v), indicating a stable adsorbed species; the latter can be reduced by a cathodic pulse (see below) and appears to be surface oxide.

(b) *Cathodic Reduction Behavior.* Cathodic charging transients in completely anhydrous solutions show arrests with $C_{\max} \doteq 100 \mu\text{f cm}^{-2}$ and $V_{C_{\max}}$ between 0.15 and 0.68 v. Both C_{\max} and $V_{C_{\max}}$ depend on i_{cath} . Increasing i_{cath} shifts C_{\max} to higher values and $V_{C_{\max}}$ to more cathodic potentials (Figure 2); C - V profiles for four values of i_{cath} , computed from the differentiated potential-time relations,⁴ are shown in Figure 3.

A plot of i_{cath} vs. $1/\tau$ gives a straight line (Figure 4) and the associated charge, Q_{total} , is 0.084 mcoulomb cm^{-2} . In Figure 4, a plot of i_{cath} vs. $1/\tau^{1/2}$ is also shown in order to emphasize the absence of any diffusion-controlled process. The plot of Q vs. V_i (Figure 5) indicates that Q increases with V_i .

Cathodic reduction transients (Figure 5) in the nominally anhydrous solutions show quite long arrests. Values of C_{\max} range from ca. 500 to 1580 $\mu\text{f cm}^{-2}$ and those of $V_{C_{\max}}$ range from 0.35 to 0.85 v, both values being dependent on i_{cath} ; $V_{C_{\max}}$ shifts to more cathodic values.

The plot of i_{cath} vs. $1/\tau$ is linear and the charge Q is 0.175 mcoulomb cm^{-2} . This Q is about twice as large as that observed in very anhydrous solutions. Q also increases with V_i (Figure 5).

For solutions containing excess water, the longest arrests in the cathodic transients are observed. In this case, C attains much higher values than those found for electrodes in anhydrous solutions or in solutions with traces of water. The C_{\max} ranges from 2500 to 7500 $\mu\text{f cm}^{-2}$ and $V_{C_{\max}}$ from 0.89 to 1.05 v. Both C_{\max} and $V_{C_{\max}}$ values depend on i_{cath} , but the shifts in $V_{C_{\max}}$ and C_{\max} do not show any regular trends with increasing i_{cath} .

The i_{cath} vs. $1/\tau$ plot is again linear with $Q = 1.09$ mcoulombs cm^{-2} , *i.e.*, Q is several times greater than the values obtained in either of the other two types of solutions; Q also increases, as usual, with V_i (Figure 5).

(iii) *Potentiodynamic Current-Potential Relations.* In completely anhydrous solutions, both anodic and cathodic peaks are found to be diffusion controlled as shown by the linear relations between peak current densities and $(dV/dt)^{1/2}$ for each of the two peaks (Figure 6).

In the nominally anhydrous solutions, only the anodic peak is well defined; again diffusion control is indicated from $(dV/dt)^{1/2}$ plots. In solutions containing excess water, both anodic and cathodic peaks are found to be diffusion controlled. All of these effects are believed

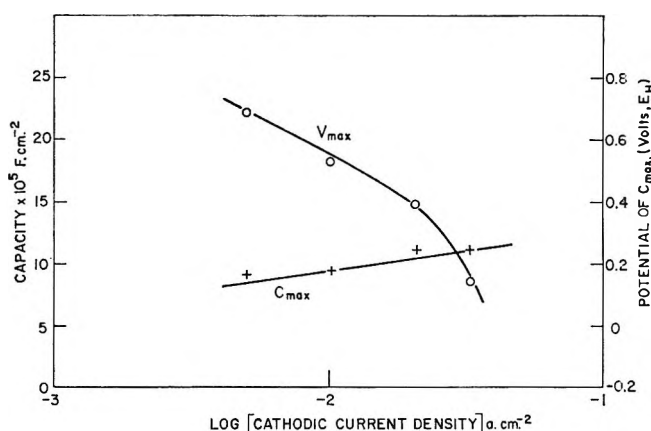


Figure 2. Gold-1 M CF_3COOK in $(\text{CF}_3\text{COOH} + 1\% (\text{CF}_3\text{CO})_2\text{O})$: \times , plot of C_{\max} vs. i_{cath} ; O , plot of $V_{C_{\max}}$ vs. i_{cath} .

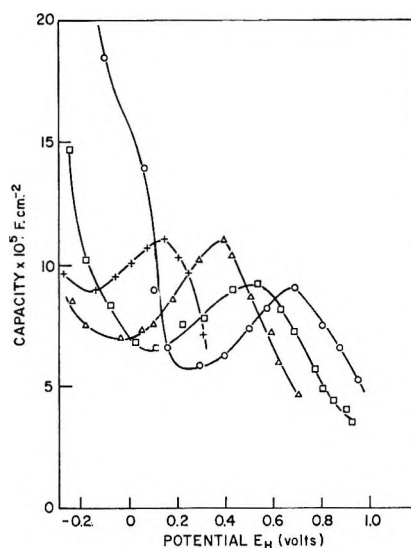


Figure 3. Gold-1 M CF_3COOK in $(\text{CF}_3\text{COOH} + 1\% (\text{CF}_3\text{CO})_2\text{O})$; C - V profiles as a function of cathodic charging current density, i_{cath} (amp cm^{-2}) for the adsorbed species in the Kolbe electrooxidation: O , 5.02×10^{-3} ; \square , 1.0×10^{-2} ; Δ , 2.1×10^{-2} ; $+$, 3.28×10^{-2} .

to be due to dissolution and redeposition of gold under the cycling conditions where a protective oxide film does not have an opportunity to be formed. This illustrates an important point, namely, that conclusions on the electrochemical behavior of a reaction should not be based entirely on one method, *e.g.*, the single potentiodynamic transients from prior steady controlled potentials do not show this behavior.

(3) B. E. Conway and P. L. Bourgalet, *Trans. Faraday Soc.*, **58**, 593 (1962); see also V. I. Past and I. A. Jofa, *Zh. Fiz. Khim.*, **33**, 913, 1230 (1959); *Dokl. Akad. Nauk SSSR*, **106**, 1050 (1956).

(4) H. A. Kozłowska and B. E. Conway, *J. Electroanal. Chem.*, **7**, 109 (1964).

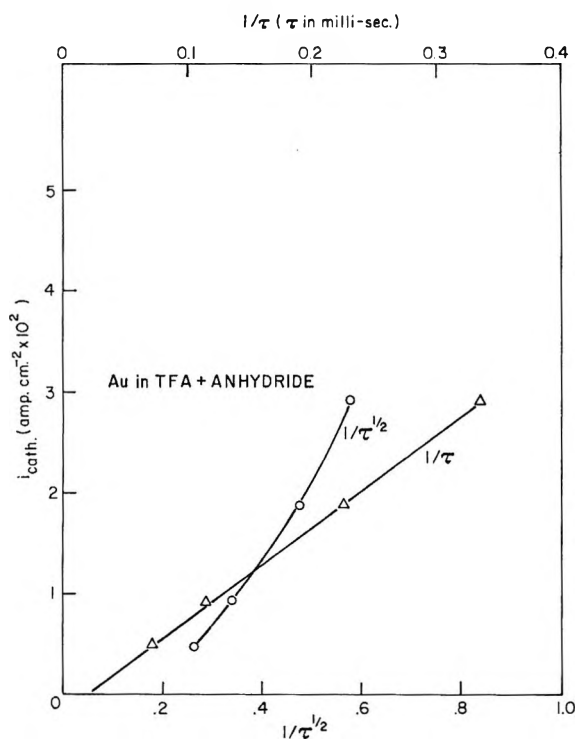


Figure 4. Gold-1 M CF_3COOK in ($\text{CF}_3\text{COOH} + 1\%$ (CF_3CO) $_2$); plots of i_{cath} vs. $1/\tau$ (Δ) and i_{cath} vs. $1/\tau^{1/2}$ (\circ).

(iv) *Products of Electrolysis.* The Kolbe products were characterised by vpc and it was found that CO_2 and C_2F_6 were produced in all the three types of solutions, in agreement with previous observations.⁵ In aqueous solutions, however, the yield of C_2F_6 was smaller than in the nonaqueous medium and oxygen is the main secondary product.

Discussion

In this section, conclusions on the role of surface oxides in mechanisms for the Kolbe reaction on gold in 1 M KTFA-TFA solutions are proposed and are based on the principles discussed in part I.

(i) *Reaction in Completely Anhydrous Solution (with Trifluoroacetic Anhydride Present).* Several features of the experimental results for the Kolbe reaction on gold are similar to those for Pt in this solution (compare Tables I in part I and here); less abnormal Tafel slopes⁶ ($b = 0.160$ v) than those found at Pt are, however, observed in the post-transition region and the absence of hysteresis in the $\log [i] - V$ curves and low rest potentials in both cases are to be noted (compare Figures 1 in part I and here). However, the evidence from the non-steady-state measurements indicates a qualitatively different behavior on the two metal anodes. Thus, an appreciable arrest is observed on open-circuit decay on gold with C values lying between 90 and 140 $\mu\text{f cm}^{-2}$

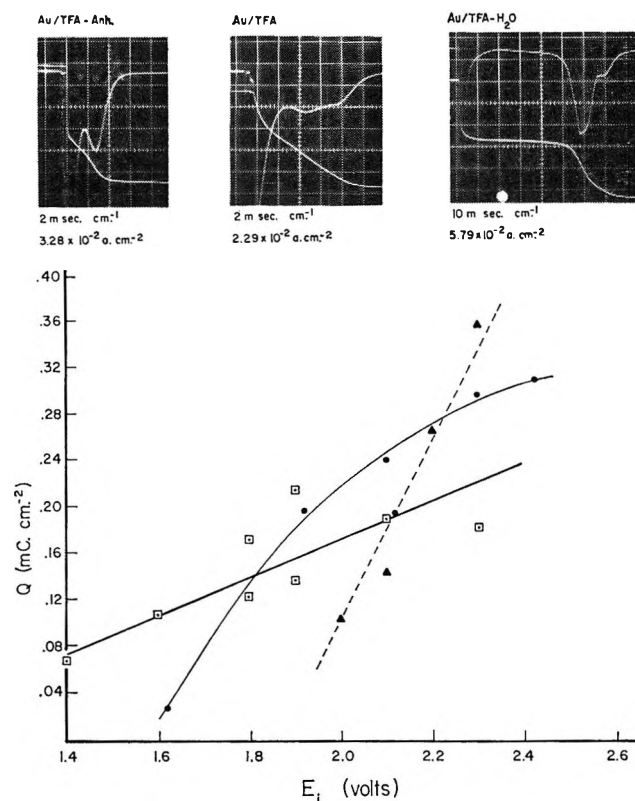


Figure 5. Gold-1 M CF_3COOK in CF_3COOH solutions; plots of Q vs. E_i (or V_i): \square , very anhydrous solutions; \bullet , nominally anhydrous solutions; \blacktriangle , aqueous solutions. (Direct and differential charging curves shown above in photos.)

depending on V_i and $Q = 0.084$ mcoulomb cm^{-2} . These C and Q values could suggest the presence of some adsorbed intermediates, but this inference is not unambiguous since the C values are only marginally larger than C_{dl} . However, under identical conditions at Pt (part I), Q is negligible. A low value of the rest potential (0.4 v; cf. the similar results for Pt) indicates the absence of an oxide and this result confirms indirectly that the added trifluoroacetic anhydride was effective in removing the last traces of water from the solution (cf. the case of Pt). An arrest is observed, however, in the cathodic transients (see photograph in Figure 5) which might indicate the presence of an electroactive intermediate, but the maximum capacity associated with this arrest is again only marginally larger than C_{dl} and

(5) B. E. Conway and M. Dzieciuch, *Can. J. Chem.*, **41**, 21, 38, 55 (1963).

(6) The indication here of a dipole layer type of film on the basis of anomalous b values is by no means as clear as in the Pt case since the slopes are not so anomalously large. However, the general characteristics of the reaction are similar and the presence of some electroactive species is in this case indicated in the nonaqueous solution case by the value of Q .

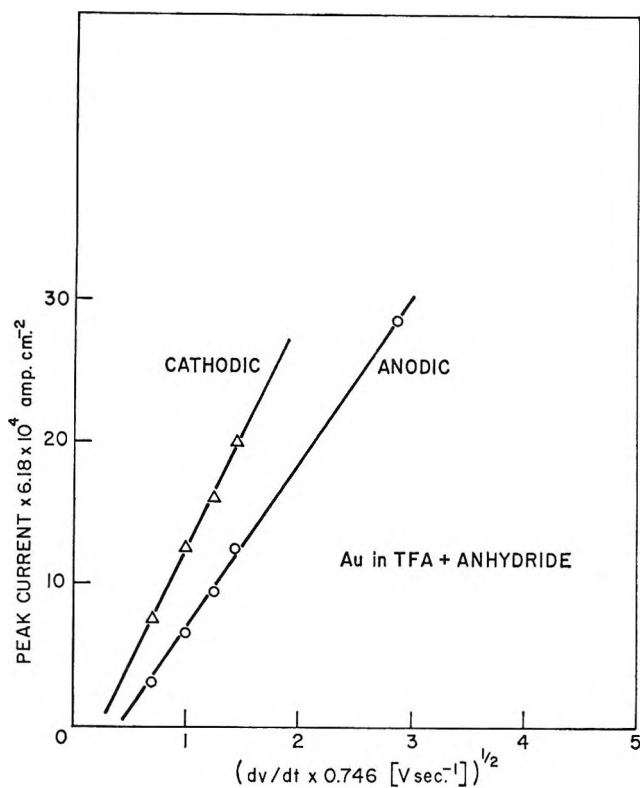


Figure 6. Gold-1 *M* CF_3COOK in $(\text{CF}_3\text{COOH} + 1\% (\text{CF}_3\text{CO})_2\text{O})$; plots of peak current vs. $(dV/dt)^{1/2}$, both for anodic (O) and cathodic (Δ) peaks.

hence is not an unambiguous indication of the presence of an adsorbed intermediate. Nevertheless, the value of Q (0.084 mCoulomb cm^{-2}) calculated from these arrests, although small, is by no means negligible (Table I) and seems rather too large for a change of ionic charge in the double layer. This Q value could thus correspond to partial coverage of the electrode by a rather small-sized adspecies (oxide?) or to more substantial coverage by a more bulky species (CF_3COO^- or $\text{CF}_3\cdot$?). While the evidence from the values of Q and C is too indefinite to pursue any quantitative discussion of coverage effects, it is worth recording that the presence on the electrode of an adsorbed species produced by discharge from the solution is suggested by the fact that the shifts in C_{max} and $V_{C_{\text{max}}}$ with increasing i_{cath} used in the discharge transients are in the theoretically expected direction,⁷ i.e., increasing i_{cath} shifts C_{max} to higher values and $V_{C_{\text{max}}}$ to more cathodic potentials (Figures 2 and 3).

Figure 5 shows that Q increases with increasing V_i . The Q value (taken in the Kolbe region, $V_i > 2.25$ v) for completely anhydrous solutions is smaller than that for the solutions containing traces or excess of water. The three transients in Figure 5 show that the arrests ex-

pressed as $i_{\text{cath}}\tau$ become larger with increasing amounts of water present.

(ii) *Reaction in Nominally Anhydrous Solutions.* The experimental results for this case have been summarized in Table I. C_2F_6 is again a principal product of the reaction. In these solutions, the features of the steady-state $\log [i]-V$ relation are characteristically different from those associated with the current-potential relations for completely anhydrous solutions (Figure 1). The presence of traces of water gives rise to hysteresis in the current-potential relations and a characteristic reversal of the direction of the current-potential relation appears around 1.8 v; also, the value of the rest potential increases to 0.9 v. All these features suggest the presence of a coadsorbed surface oxide. The value of the Tafel slope (0.175 v) suggests, now, the onset of some dipole or barrier layer effects in the kinetics (cf. ref 7, 59, and 61 in part I).

On open-circuit decay, an arrest is observed and C depends on V_i . The double-layer capacity (ca. $60 \mu\text{f cm}^{-2}$) is observed⁸ when $V_i = 2.5$ but when $V_i = 1.8$ v, the value of C_{max} is $225 \mu\text{f cm}^{-2}$, suggesting the presence of an oxide (or other species) on the electrode, which is also supported by the observed rest potential of ca. 0.9 v. This receives some confirmation from the appreciable arrest which is observed in the cathodic transient (see photograph in Figure 5), giving high values of capacity (ca. $500-1500 \mu\text{f cm}^{-2}$). The shifts in $V_{C_{\text{max}}}$ with increasing i_{cath} are in the predicted direction⁷ (Table I) for faradaic reduction of an electroactive adsorbed species.

Evidence suggesting significant coadsorption of an oxide is as follows: in the presence of traces of water, the over-all rate at a given potential is lower than that in the completely anhydrous solutions (Figure 1), but the value of Q (0.175 mCoulomb cm^{-2}) is twice as large, suggesting that part or all of this charge is associated with reduction of a species (surface oxide) which originates from water and inhibits the Kolbe reaction.

(iii) *Reaction in Aqueous Solutions.* The experimental observations for this case have been summarized in Table I; C_2F_6 is again the product but the yield is not so large as in the nonaqueous solutions. The Tafel slope is 0.17 v. In general, in aqueous solutions, coadsorption by an oxide is substantially greater than in the nominally anhydrous medium with a consequently

(7) B. E. Conway, E. Gileadi, and H. Kozłowska, *J. Electrochem. Soc.*, 112, 341 (1965).

(8) The observation of a low C at high potentials and larger values at lower potentials is quite consistent with potential-dependent coverage by an adspecies involved (cf. ref 3). At high potentials, the oxide layer may have reached constant coverage or thickness, so that only the double-layer capacity (characteristic of the oxide surface) is observed.

increased inhibition of the Kolbe reaction. This is supported by the following evidence.

(a) In the steady-state current potential relations (Figure 1), enhanced hysteresis between the ascending and descending curves is observed; a higher rest potential (1.25 v) and a lower rate at a given potential as compared with the rate in completely and nominally anhydrous solutions under corresponding conditions are found.

(b) The values of both the pseudo-capacity (*ca.* 2500 $\mu\text{f cm}^{-2}$, Table I) obtained from open-circuit emf decay profiles and the rest potential (1.3 v) are higher than those in the nonaqueous case.

(c) High values of Q are obtained from the cathodic transients (1.09 mcoulombs cm^{-2}) and very high values (*ca.* 2250–7500 $\mu\text{f cm}^{-2}$) of C_{max} are found.

(d) Any systematic trend of shifts in C_{max} with increasing i_{cath} such as would occur if oxide alone were present is difficult to establish; hence, the possibility of the presence of more than one species should be recognized, *e.g.*, $\text{CF}_3\text{COO}\cdot$ or $\text{CF}_3\cdot$ coadsorbed with oxide (*cf.* part I).

(e) In the plot of Q vs. V_i (Figure 5), high Q values at higher potentials suggest the presence of appreciable amounts of surface oxide.

(iv) *Role of Oxide.* It has been suggested in the foregoing discussion that in the kinetics of the Kolbe reaction at gold, the role of oxide, which originates from traces or excess of water present in the solutions, is a purely inhibitory one. This is supported further by the following evidence.

(a) In Figure 7 a family of curves of Q vs. rate is shown (*cf.* part I) for the three types of solution studied. Each curve is plotted for a given value of potential in the potential range over which a Tafel line for the Kolbe reaction is obtained; *i.e.*, $> ca. 2.1$ v. Each curve is drawn through three points, each representing a value of Q (obtained from the cathodic transients) plotted with respect to the corresponding rate at the given potential^{9,10} (obtained from the steady-state current potential relations) for the three solutions studied. It is to be noted that at a given potential, proceeding in the sequence "completely anhydrous" \rightarrow "nominally anhydrous" \rightarrow "aqueous solution," an *increase* in Q and a *decrease* in rate arises. This shows rather directly that with increased Q associated with increased amounts of H_2O in the solution, the rate is correspondingly decreased; *i.e.*, the surface oxide plays an inhibitory role. The effects are larger at higher anodic potentials where oxide film growth is usually more extensive.

(b) In Figure 8, a family of curves is shown which illustrate the same point in a related way. Each of the three solid lines represents the Q vs. rate relation cover-

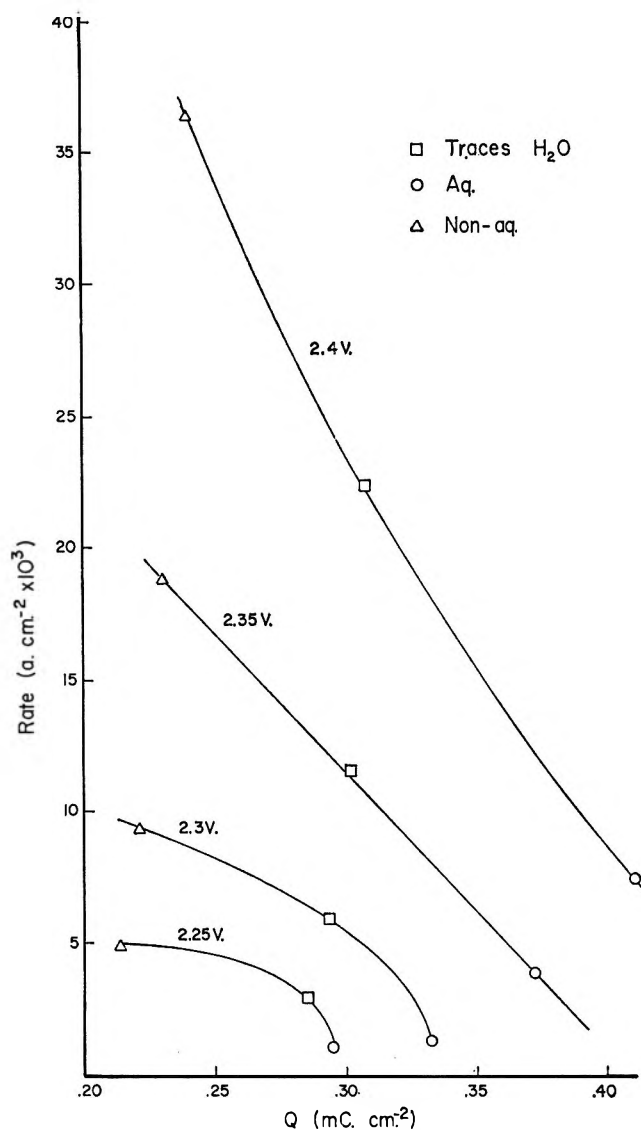


Figure 7. Gold-1 M CF_3COOK in CF_3COOH solutions: plots of Q vs. rate at various anodic potentials for very anhydrous (Δ), nominally anhydrous (\square), and aqueous (\circ) solutions.

ing the whole Tafel region (and a small upper part of the transition region) for completely anhydrous, nominally anhydrous, and aqueous solutions, respectively. It is seen that $\Delta[\text{rate}]/\Delta Q$ decreases with increasing amounts of water present in the solution. Thus, with increasing water an increasing proportion of the total Q arises from a species (*e.g.*, surface oxide) which does not apparently contribute to an increase in rate of the Kolbe reaction

(9) This is legitimate, as we have pointed out in part I, in relation to the actual reversible potentials which on the H_2 scale can be shown¹⁰ to be independent of solvent acid.

(10) B. E. Conway and A. K. Vijh, *Z. Anal. Chem.*, **224**, 149 (1967).

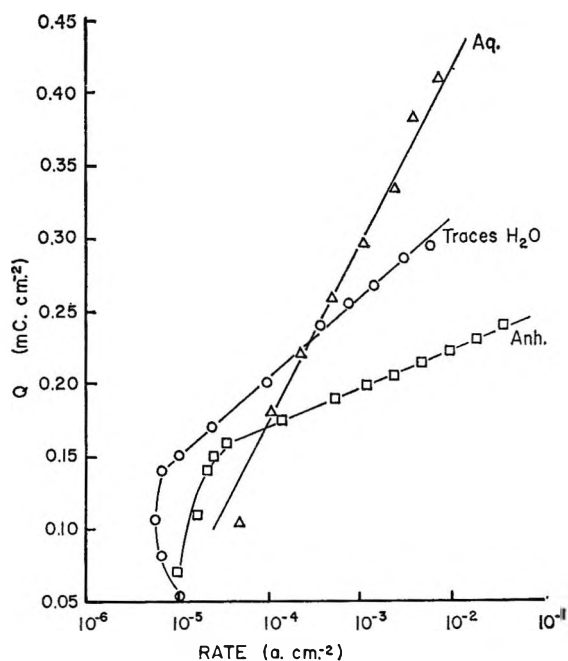


Figure 8. Gold-1 M CF_3COOK in CF_3COOH solutions: plots of Q vs. rate for completely anhydrous ($\square-\square$), nominally anhydrous ($\circ-\circ$), and aqueous ($\triangle-\triangle$) solutions.

and even inhibits it by rendering unavailable the sites required for the reaction to occur.

(v) *Inhibition Reversal Effect.* In the potentiostatic steady-state $\log [i]-V$ relations for gold in the nominally anhydrous solutions (Figure 1), an inhibition effect is observed in the potential region 1.6 to ca. 1.8 v indicative of a coadsorbed inhibiting species;² however, complete reversal of the direction of the $\log [i]-V$ relation (negative b values) is not always observed when the presence of a coadsorbed inhibiting species is suggested by other evidence. The reversal effect would tend to be observed only when both i (*i.e.*, the rate) and θ (*i.e.*, the coverage) are dependent on potential over the same range of potentials. In such a case, the rate i could be expressed in a general way as

$$i = ke^{\alpha VF/RT} e^{-k'VF/RT} = e^{(\alpha-k')VF/RT}$$

where k' is a coefficient expressing² the potential dependence of θ and α is a transfer coefficient determining the potential dependence of the rate in the usual way. When $k' > \alpha$, a reversal in the direction of the $\log [i]-V$ relation would be observed (Figure 1) as treated previously.² However, if k is finite but smaller than α , only a change of slope in the $\log [i]-V$ line would be observed; a reversal effect is actually a special case of this change of slope, *i.e.*, when the slope changes in sign and kinetics hence exhibit an inversion in their dependence on potential (see also Figures 7-9 in part I,

where such effects are exhibited at high anodic potentials).

(vi) *Anion Adsorption and Anomalous Tafel Slopes.* The Tafel slopes observed in the present case are only marginally greater than 0.12 v. Such effects would possibly arise from specific anion adsorption in the double layer.¹¹ In that case the initial discharge process could be rate determining instead of the electrochemical desorption step, suggested as a possible mechanism in the foregoing discussion. However, this is believed to be unlikely for the following reasons.

(a) If anion adsorption leads to these high Tafel slopes, only a nominal apparent coverage if any (and not one corresponding to 0.084 mcoulomb cm^{-2}) would be observed in the cathodic transient in very anhydrous TFA solutions. Also anion adsorption in other reactions, *e.g.*, Cl_2 evolution, does not necessarily lead to anomalous Tafel slopes as we have pointed out in part I.

(b) Similar behavior would be expected in the case of the Kolbe reaction at platinum (see part I) where the much more anomalous Tafel slopes, it was suggested (part I), arise from the presence of a dipole barrier layer since the anomalies observed seem to be beyond the range of double-layer effects.

(c) If specific anion adsorption were involved, the ratio $Q_{\text{oxide}}/Q_{\text{hydrogen}}$, to a first approximation, would not be affected; *i.e.*, at high anodic potentials reached in the Kolbe reaction $Q_{\text{oxide}}/Q_{\text{hydrogen}}$ in trifluoroacetate solutions (or acetate solutions for that matter) would be expected to be comparable with the value of this ratio obtained for sulfuric acid solutions. However, it is found that on cathodic reduction from the rest potential

$$\frac{Q_1(V_{C_{\text{max}}} = 0.58 \text{ v})}{Q_2(V_{C_{\text{max}}} = 0.15 \text{ v})}$$

i.e.

$$\frac{Q_{\text{oxide}}}{Q_{\text{hydrogen}}} = 1.37$$

for platinum in trifluoroacetate solutions (see part I, Table I) as compared with a value greater than 4 (at a polarization potential greater than 2.5 v) found for the ratio $Q_{\text{oxide}}/Q_{\text{hydrogen}}$ in the case of platinum in sulfuric acid.¹² Similar results¹³ with respect to the ratio $Q_{\text{oxide}}/Q_{\text{hydrogen}}$ have also been obtained for the case of the Kolbe reaction proceeding on platinum in aqueous acetate solutions, where again, participation of double-layer (*i.e.*, specific anion adsorption) effects seem to be

(11) M. J. Fioshin and Y. B. Vasilev, *Dokl. Akad. Nauk SSSR*, **134**, 879 (1960).

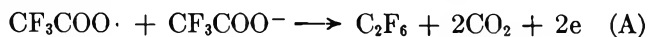
(12) S. Gilman, *Electrochim. Acta*, **9**, 1025 (1964).

(13) A. K. Vijh and B. E. Conway, *Z. Anal. Chem.*, **224**, 160 (1967).

excluded as the probable origin of anomalously high Tafel slopes. The value of the above ratio seems to suggest that only a *part* of the electrode (in the Kolbe reaction in aqueous medium) is covered by oxide and the rest is occupied by a layer involving coadsorbed Kolbe species, *e.g.*, $\text{RCOO}\cdot$ (see Figure 12, part I).

(d) If specific adsorption effects were responsible for the anomalously high Tafel slopes, such effects would be enhanced with increasing acetate ion concentration. However, the observation of almost *parallel* Tafel lines by Fioshin and Vasilev¹¹ for various acetate concentrations over the range 0.1–4 *N* seems to indicate that specific anion adsorption effects are not the origin of the high Tafel slopes.

(vii) *Mechanisms.* Owing to the complexity of the present results, it is not possible to propose at all unambiguously a mechanism for the Kolbe reaction on gold with trifluoroacetate. If the significant charge measurable¹⁴ in the cathodic transients for the completely anhydrous solutions were attributable to an electroactive species in the Kolbe reaction itself, an electrochemical desorption step of the type



would be suggested⁵ with coverage by $\text{CF}_3\text{COO}\cdot$ significant. However, a low, potential-dependent coverage would lead⁵ relatively unambiguously (*cf.* part I) to $b < (2.3)(2RT/F)$ [in fact $(2.3)(2RT/3F)$ probably]

($\beta \doteq 0.5$), which is not observed. For eq A to proceed with a Tafel slope of *ca.* 0.12, the charge for $\text{CF}_3\text{COO}\cdot$ adsorption would have to be close to that for a monolayer and much larger than that observed. The second possibility of $\text{CF}_3\cdot$ being the electroactive species, and hence reducible at Au, we believe, is unlikely. However, if that were the case, the mechanism following ion discharge and decarboxylation would be



at appreciable coverage by $\text{CF}_3\cdot$ in order to account for a Tafel slope of 0.12. If step B were involved under such conditions, it is difficult to see why the kinetic behavior should not be more similar to that on Pt with higher Tafel slope associated with a dipole layer of $\text{CF}_3\cdot$.

In the aqueous medium, the kinetic behavior is dominated by the effects associated with the presence of the oxide film, leading to inhibition effects and hysteresis between the current-potential relations for anodic-going and cathodic-going changes of potential.

Acknowledgment. A. K. V. is indebted to the Sprague Electric Co. for the award of a Fellowship. Further financial support for this work from the National Research Council, Canada, is gratefully acknowledged.

(14) The significant cathodic *Q* value would not seem to be due to the presence of water, since the rest potential is 0.4 v and the solutions were as anhydrous as in the work with Pt (part I).

Standard Potentials of the Silver-Silver Chloride Electrode in Ethylene Glycol and Its Aqueous Mixtures at Different Temperatures and Related Thermodynamic Quantities

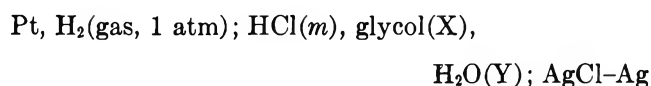
by Utpal Sen, Kiron Kumar Kundu, and Mihir Nath Das

Physical Chemistry Laboratories, Jadavpur University, Calcutta 32, India (Received December 8, 1966)

The standard potential of the silver-silver chloride electrode in ethylene glycol and in several glycol-water mixtures (containing 10, 30, 50, 70, and 90% glycol by weight) have been determined at 5, 15, 25, 35, and 45°, using a cell of the type: Pt, H₂(gas, 1 atm); HCl(*m*); AgCl-Ag. The values of E_m° in each solvent have been represented as a function of temperature. The activity coefficients of hydrochloric acid (0.005–0.1 *m*) in these media at 5, 25, and 45° have been evaluated. The standard free energy change and the standard entropy change for the process of transfer of HCl from water to each of the other media were calculated from the E_N° values and their temperature coefficients for the respective solvents. The electrostatic contribution toward the total free energy and entropy of transfer was computed on the basis of the Born equation and hence the nonelectrostatic part of the thermodynamic quantities has been evaluated. The results have been interpreted in terms of the breakdown of the water structure on the addition of glycol.

Introduction

In some previous investigations^{1–3} the standard potentials of the Ag-AgCl electrode were determined in ethylene glycol-water mixtures (containing up to 60% glycol by weight) at 25°. Kundu and Das⁴ determined the standard potential of the Ag-AgCl electrode in pure ethylene glycol at 30°. In the present work, the authors have determined the standard potentials of the Ag-AgCl electrode in several glycol-water mixtures (10–90%) as well as in pure ethylene glycol at five temperatures ranging from 5 to 45°. A cell of the following type has been used for the purpose



Experimental Section

Ethylene glycol (analytical reagent, Merck) was purified by the method described earlier.⁴ The distilled glycol was preserved in a desiccator. Water distilled in an all-glass apparatus, having a specific conductance of the order of $0.8 \times 10^{-6} \text{ ohm}^{-1} \text{ cm}^{-1}$, was used. The

solvent mixtures of various percentages were made by weight.

The experimental procedures for preparing the cell solutions, the silver-silver chloride electrode, the hydrogen electrode, and hydrogen gas were the same as described earlier.⁴ Measurements were made at 5, 15, 25, 35, and 45° with a Leeds and Northrup K-type potentiometer and a moving coil galvanometer. The thermostat maintained a temperature within $\pm 0.1^\circ$.

All measurements were taken by two Ag-AgCl electrodes for each solution. The equilibrium was reached in 3–4 hr after the passage of hydrogen started. After equilibrium had been attained, the emf remained constant for about 2 hr with a maximum variation of ± 0.2 mv. The readings for 25° were taken at first, followed by higher temperatures. The readings for 25° were

(1) S. B. Knight, J. F. Masi, and D. Rossel, *J. Am. Chem. Soc.*, **68**, 661 (1946).

(2) H. D. Crockford, S. B. Knight, and H. A. Staton, *ibid.*, **72**, 2164 (1950).

(3) B. H. Claussen and C. M. French, *Trans. Faraday Soc.*, **51**, 1124 (1955).

(4) K. K. Kundu and M. N. Das, *J. Chem. Eng. Data*, **9**, 87 (1964).

Table I: Electromotive Force of the Cell (from 5 to 45°) in Volts (Uncertainty, ± 0.0002 v)

m_{HCl}	Temp, °C					m_{HCl}	Temp, °C				
	5	15	25	35	45		5	15	25	35	45
	(a) 10% Glycol						(d) 70% Glycol				
0.00525	0.4820	0.4857	0.4891	0.4915	0.4927	0.00720	0.4302	0.4304	0.4300	0.4294	0.4277
0.00577	0.4778	0.4812	0.4841	0.4865	0.4878	0.00789	0.4257	0.4260	0.4254	0.4244	0.4230
0.00661	0.4714	0.4748	0.4776	0.4798	0.4808	0.00865	0.4216	0.4213	0.4210	0.4199	0.4182
0.00763	0.4648	0.4679	0.4707	0.4722	0.4732	0.00984	0.4158	0.4154	0.4148	0.4136	0.4114
0.00889	0.4576	0.4604	0.4628	0.4644	0.4650	0.0130	0.4030	0.4025	0.4014	0.3997	0.3970
0.00964	0.4542	0.4570	0.4592	0.4607	0.4612	0.0200	0.3840	0.3827	0.3812	0.3788	0.3753
0.0122	0.4431	0.4456	0.4475	0.4474	0.4485	0.0237	0.3762	0.3747	0.3727	0.3700	0.3669
0.0178	0.4263	0.4270	0.4292	0.4301	0.4294	0.0318	0.3630	0.3614	0.3585	0.3558	0.3523
0.0204	0.4201	0.4218	0.4228	0.4226	0.4224	0.0412	0.3516	0.3490	0.3467	0.3433	0.3394
0.0254	0.4103	0.4115	0.4118	0.4110	0.4105	0.0448	0.3477	0.3449	0.3422	0.3390	0.3345
0.0309	0.4014	0.4015	0.4027	0.4022	0.4009	0.0491	0.3432	0.3403	0.3376	0.3341	0.3298
0.0432	0.3859	0.3865	0.3863	0.3856	0.3837	0.0586	0.3360	0.3326	0.3299	0.3260	0.3220
0.0562	0.3740	0.3742	0.3734	0.3724	0.3700	0.0726	0.3268	0.3237	0.3205	0.3165	0.3118
0.0648	0.3688	0.3678	0.3670	0.3658	0.3636	0.0909	0.3166	0.3134	0.3100	0.3054	0.3005
0.0876	0.3535	0.3531	0.3522	0.3504	0.3477						
0.1076	0.3445	0.3439	0.3426	0.3404	0.3373						
	(b) 30% Glycol						(e) 90% Glycol				
0.00490	0.4743	0.4778	0.4808	0.4830	0.4843	0.00513	0.4021	0.4007	0.3983	0.3960	0.3932
0.00708	0.4574	0.4604	0.4625	0.4641	0.4648	0.00617	0.3946	0.3921	0.3898	0.3874	0.3838
0.00737	0.4554	0.4585	0.4608	0.4620	0.4628	0.00626	0.3934	0.3911	0.3893	0.3861	0.3830
0.00852	0.4491	0.4508	0.4538	0.4549	0.4557	0.00680	0.3900	0.3870	0.3855	0.3817	0.3785
0.00984	0.4422	0.4445	0.4463	0.4472	0.4474	0.00778	0.3840	0.3810	0.3787	0.3755	0.3721
0.0119	0.4336	0.4358	0.4371	0.4380	0.4379	0.00908	0.3766	0.3740	0.3713	0.3679	0.3642
0.0145	0.4243	0.4256	0.4279	0.4271	0.4272	0.0109	0.3693	0.3670	0.3632	0.3595	0.3557
0.0178	0.4155	0.4167	0.4177	0.4177	0.4171	0.0156	0.3534	0.3497	0.3461	0.3422	0.3377
0.0203	0.4092	0.4105	0.4111	0.4109	0.4099	0.0241	0.3353	0.3308	0.3261	0.3215	0.3165
0.0265	0.3969	0.3979	0.3983	0.3980	0.3969	0.0300	0.3256	0.3200	0.3160	0.3110	0.3058
0.0294	0.3925	0.3934	0.3934	0.3925	0.3913	0.0339	0.3200	0.3145	0.3105	0.3053	0.3000
0.0350	0.3847	0.3851	0.3850	0.3842	0.3822	0.0416	0.3108	0.3055	0.3000	0.2956	0.2902
0.0402	0.3787	0.3787	0.3781	0.3775	0.3752	0.0482	0.3044	0.2987	0.2942	0.2887	0.2829
0.0508	0.3688	0.3687	0.3676	0.3659	0.3637	0.0586	0.2964	0.2894	0.2850	0.2783	0.2733
0.0525	0.3666	0.3664	0.3655	0.3639	0.3618	0.0613	0.2949	0.2882	0.2832	0.2770	0.2710
0.0618	0.3593	0.3588	0.3576	0.3563	0.3534	0.0651	0.2908	0.2848	0.2800	0.2743	0.2682
0.0824	0.3469	0.3457	0.3444	0.3421	0.3392	0.0777	0.2835	0.2773	0.2719	0.2655	0.2598
						0.0785	0.2830	0.2765	0.2716	0.2652	0.2592
						0.1084	0.2693	0.2610	0.2565	0.2496	0.2430
	(c) 50% Glycol						(f) 100% Glycol				
0.00407	0.4707	0.4744	0.4772	0.4787	0.4795	0.00570	0.3045	0.3029	0.3011	0.2995	0.2963
0.00517	0.4600	0.4630	0.4654	0.4661	0.4668	0.00636	0.2996	0.2982	0.2954	0.2933	0.2905
0.00602	0.4530	0.4560	0.4580	0.4587	0.4590	0.00662	0.2975	0.2953	0.2934	0.2915	0.2880
0.00689	0.4471	0.4492	0.4514	0.4520	0.4520	0.00743	0.2932	0.2905	0.2883	0.2860	0.2826
0.00798	0.4402	0.4424	0.4443	0.4448	0.4442	0.00798	0.2899	0.2876	0.2853	0.2828	0.2794
0.00878	0.4358	0.4380	0.4399	0.4398	0.4393	0.00801	0.2897	0.2872	0.2850	0.2823	0.2789
0.00998	0.4300	0.4320	0.4333	0.4329	0.4327	0.0110	0.2762	0.2735	0.2708	0.2682	0.2643
0.0139	0.4191	0.4162	0.4171	0.4166	0.4156	0.0116	0.2736	0.2705	0.2683	0.2652	0.2610
0.0183	0.4023	0.4035	0.4040	0.4030	0.4016	0.0144	0.2647	0.2620	0.2591	0.2560	0.2510
0.0218	0.3948	0.3952	0.3958	0.3943	0.3926	0.0232	0.2355	0.2411	0.2380	0.2338	0.2290
0.0282	0.3831	0.3834	0.3833	0.3817	0.3794	0.0254	0.2414	0.2377	0.2341	0.2297	0.2247
0.0358	0.3727	0.3729	0.3722	0.3705	0.3676	0.0288	0.2356	0.2318	0.2278	0.2234	0.2186
0.0435	0.3637	0.3635	0.3626	0.3604	0.3575	0.0368	0.2286	0.2225	0.2168	0.2130	0.2070
0.0510	0.3568	0.3560	0.3549	0.3528	0.3492	0.0429	0.2181	0.2136	0.2096	0.2054	0.1989
0.0637	0.3467	0.3463	0.3444	0.3420	0.3381	0.0567	0.2063	0.2016	0.1971	0.1926	0.1868
0.0785	0.3375	0.3366	0.3347	0.3320	0.3277	0.0669	0.2000	0.1962	0.1908	0.1864	0.1800
						0.0692	0.1981	0.1937	0.1877	0.1842	0.1771
						0.0823	0.1913	0.1859	0.1809	0.1762	0.1700
0.00426	0.4540	0.4552	0.4555	0.4559	0.4545	0.0873	0.1881	0.1834	0.1785	0.1733	0.1669
0.00495	0.4469	0.4474	0.4479	0.4477	0.4466	0.0951	0.1861	0.1806	0.1753	0.1698	0.1635
0.00545	0.4429	0.4432	0.4436	0.4431	0.4422	0.0977	0.1846	0.1794	0.1742	0.1687	0.1623
0.00627	0.4360	0.4358	0.4363	0.4358	0.4349	0.1075	0.1815	0.1752	0.1690	0.1645	0.1581

taken again after the measurements for the other temperatures, the two readings agreeing within ± 0.2 mv.

Densities of the various glycol-water mixtures at the different temperatures used in this work were determined by Banerjee.^{5,6} Vapor pressures of the solvents at the respective temperatures were obtained by the method of interpolation and extrapolation from the results of Trimble and Potts⁷ and of Curme and Johnston.⁸ The dielectric constants (D) of the solvents were taken from Åkerlof's data.⁹ The collected values are shown in ref 6.

Results and Discussion

Standard Potentials. The standard potentials E_m° of the cell were obtained by using a function $E^{\circ'}$ defined as¹⁰

$$E^{\circ'} = E + 2k \log m - \frac{2kS_f c^{1/2}}{1 + \delta Bc^{1/2}} - 2k \log (1 + 0.002 m M_{XY})$$

$$= E_m^\circ + f(m) \quad (1)$$

where E is the observed electromotive force of the cell at a molal concentration m , E_m° the standard potential of the cell on the molal scale, S_f and B the Debye-Hückel constants for a particular solvent and temperature, c the molarity of HCl, δ the ion size parameter, $k = 2.3026 RT/F$, and M_{XY} the average molecular weight of the solvent.

Table I gives the observed values of the electromotive force of the cell at different temperatures from 5 to 45°. All the emf values are corrected to 1 atm hydrogen pressure. The values of $E^{\circ'}$ were plotted against the molalities of HCl and the curve was extrapolated to $m = 0$ to obtain the value of E_m° of the Ag-AgCl electrode, the results being given in Table II. For illustration, the extrapolations for 50% glycol at different temperatures are shown in Figure 1. The value of 5 has been taken as the ion size parameter (δ) for all the solvent media at different temperatures. Reasonable alterations in the value of δ do not have any detectable influence on the value of E_m° as obtained by extrapolation.

The values of E_m° in Table II can be represented as a function of temperature by equations, obtained by the method of least squares, which are given below together with the equation for water as the solvent.¹⁰

0% Glycol

$$E_m^\circ = 0.2224 - 6.396 \times 10^{-4}(t - 25) - 3.18 \times 10^{-6}(t - 25)^2 \quad (2)$$

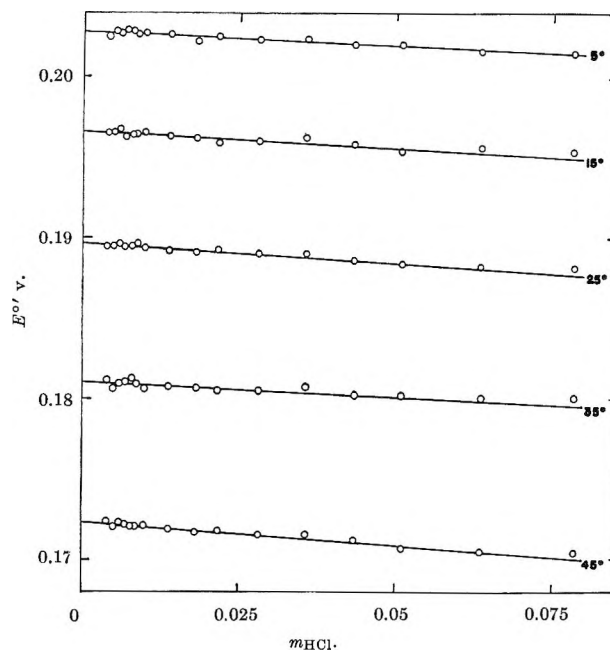


Figure 1. Extrapolation of emf data to give E_m° for Ag-AgCl electrode in 50% glycol-water mixtures at different temperatures.

Table II: Standard Potentials of Ag-AgCl Electrode in Glycol-Water Mixtures at 25° (Uncertainty, ± 0.0003 v)

Wt % glycol	E_m° , v	E_c° , v	E_N° , v
0 ^a	0.22246	0.22158	0.01602
10	0.2151	0.2156	0.0126
30	0.2030	0.2048	0.0089
50	0.1896	0.1927	0.0057
70	0.1689	0.1730	-0.0022
90	0.1183	0.1233	-0.0357
100	0.0235	0.0288	-0.1194

^a H. S. Harned and B. B. Owen, "The Physical Chemistry of Electrolytic Solutions," 3rd ed, Reinhold Publishing Corp., New York, N. Y., 1958, p 462.

10% Glycol

$$E_m^\circ = 0.2151 - 6.56 \times 10^{-4}(t - 25) - 3.71 \times 10^{-6}(t - 25)^2 \quad (3)$$

(5) S. K. Banerjee, Doctoral Thesis, Jadavpur University, 1965.

(6) S. K. Banerjee, K. K. Kundu, and M. N. Das, *J. Chem. Soc. (A)*, 161 (1967).

(7) H. M. Trimble and W. Potts, *Ind. Eng. Chem.*, **27**, 66 (1935).

(8) G. O. Curme and F. Johnston, "Glycols," Reinhold Publishing Corp., New York, N. Y., 1952.

(9) G. Åkerlof, *J. Am. Chem. Soc.*, **54**, 4125 (1932).

(10) H. S. Harned and B. B. Owen, "The Physical Chemistry of Electrolytic Solutions," 3rd ed, Reinhold Publishing Corp., New York, N. Y., 1958.

30% Glycol

$$E_m^\circ = 0.2030 - 6.95 \times 10^{-4}(t - 25) - 3.93 \times 10^{-6}(t - 25)^2 \quad (4)$$

50% Glycol

$$E_m^\circ = 0.1894 - 7.65 \times 10^{-4}(t - 25) - 4.64 \times 10^{-6}(t - 25)^2 \quad (5)$$

70% Glycol

$$E_m^\circ = 0.1692 - 9.61 \times 10^{-4}(t - 25) - 3.57 \times 10^{-6}(t - 25)^2 \quad (6)$$

90% Glycol

$$E_m^\circ = 0.1183 - 1.20 \times 10^{-3}(t - 25) - 1.71 \times 10^{-6}(t - 25)^2 \quad (7)$$

100% Glycol

$$E_m^\circ = 0.0235 - 1.16 \times 10^{-3}(t - 25) - 1.79 \times 10^{-6}(t - 25)^2 \quad (8)$$

The values of the standard potentials on the molar and mole fraction scales, E_c° and E_N° , respectively, have been computed with the help of the equations

$$E_c^\circ = E_m^\circ + 2k \log d_0 \quad (9)$$

and

$$E_N^\circ = E_m^\circ - 2k \log \frac{1000}{M_{XY}} \quad (10)$$

where d_0 is the density of the solvent at the particular temperature. The values at 25° are given in Table III.

Table III: E_m° of Ag-AgCl Electrode in Glycol-Water Mixtures at Different Temperatures (Uncertainty, ± 0.0003 v)

Wt % glycol	Temp. °C				
	5	15	25	35	45
0 ^a	0.2340	0.2286	0.2225	0.2157	0.2083
10	0.2267	0.2212	0.2151	0.2082	0.2005
30	0.2152	0.2095	0.2030	0.1954	0.1875
50	0.2028	0.1965	0.1896	0.1810	0.1723
70	0.1867	0.1786	0.1689	0.1590	0.1485
90	0.1415	0.1298	0.1183	0.1064	0.0937
100	0.0460	0.0349	0.0235	0.0118	-0.0004

^a See ref a in Table II, p 456.

Activity Coefficients of HCl in Ethylene Glycol and Its Aqueous Mixtures. Activity coefficients of HCl in ethylene glycol and its aqueous mixtures at temperatures 5, 25, and 45° were computed from the equation

$$\log {}_s^s\gamma = \frac{E_m^\circ - E}{2k} - \log m \quad (11)$$

using the respective values of E_m° evaluated above. The activity coefficients (${}_s^s\gamma$) are referred to a value of unity for the infinitely dilute solutions in the respective solvents. The values of ${}_s^s\gamma$ were plotted against molality on a large scale and from the plots the activity coefficients at round values of molalities were read off and assembled in Table IV. An error of ± 0.2 mv in the emf value corresponds to an error of the order of ± 0.006 unit in $\log {}_s^s\gamma$ at 25°. As expected from Debye-Hückel theory, the value of ${}_s^s\gamma$ at a particular molality progressively decreases with increasing proportions of glycol, because of a lowering in the dielectric constant of the medium.

The activity coefficients of an electrolyte in different solvents become amenable to comparison only when referred to the same standard state, *e.g.*, the hypothetical ideal unimolal aqueous solution. The activity coefficient of an electrolyte at any concentration, designated as ${}_w^s\gamma$ in any solvent, referred to the aqueous standard, can be expressed as a product,¹¹ shown as

$${}_w^s\gamma = m\gamma {}_s^s\gamma \quad (12)$$

where $m\gamma$ is the medium effect, which was calculated from the E_m° values for water and the respective media. The values of ${}_s^s\gamma$ were then utilized to calculate ${}_w^s\gamma$ at different concentrations of HCl in all the media, and the values are tabulated in Table V. The values of $m\gamma$ slowly increases with increasing proportions of glycol, reaching a value of nearly 8 in 90% glycol (from unity in water), but abruptly rises to about 48 in pure glycol.

Standard Free Energy and Entropy of Transfer of HCl from Water. The standard free energy change accompanying the transfer of 1 mole of HCl from water to another medium is directly given by

$$\Delta G^\circ = -F({}_s^sE_N^\circ - {}_w^sE_N^\circ) \quad (13)$$

The standard potential on the mole fraction scale is used because that will eliminate energy changes due to concentration changes. The values of ΔG° (in calories) calculated from the standard potentials at 25° are shown in Table VI. The values are probably accurate within ± 8 cal.

It may be seen from Table VI that ΔG° becomes more and more positive with increasing proportions of glycol in the medium. Thus the transfer of HCl from water to the glycol-water solvents is not a spontaneous

(11) R. G. Bates, "Determination of pH," John Wiley and Sons, Inc., New York, N. Y., 1964, p 190.

Table IV: Activity Coefficients (γ) of HCl at 5, 25, and 45° in Glycol-Water Mixtures

m_{HCl}	Wt % glycol								
	10%			30%			50%		
	5°	25°	45°	5°	25°	45°	5°	25°	45°
0.005	0.928	0.926	0.922	0.918	0.915	0.910	0.907	0.902	0.895
0.01	0.902	0.899	0.894	0.893	0.887	0.881	0.877	0.870	0.862
0.02	0.872	0.868	0.861	0.860	0.853	0.854	0.843	0.835	0.825
0.03	0.852	0.847	0.839	0.839	0.831	0.822	0.821	0.812	0.801
0.05	0.827	0.820	0.810	0.813	0.805	0.793	0.795	0.786	0.773
0.07	0.810	0.802	0.791	0.798	0.787	0.775	0.780	0.768	0.755
0.1	0.795	0.785	0.774	0.778	0.768	0.755	0.758	0.745	0.731

m_{HCl}	Wt % glycol								
	70%			90%			100%		
	5°	25°	45°	5°	25°	45°	5°	25°	45°
0.005	0.880	0.872	0.864	0.842	0.832	0.823	0.815	0.807	0.795
0.01	0.855	0.845	0.835	0.803	0.793	0.782	0.756	0.748	0.735
0.02	0.818	0.806	0.794	0.750	0.741	0.725	0.696	0.682	0.665
0.03	0.795	0.782	0.765	0.725	0.710	0.692	0.660	0.645	0.627
0.05	0.765	0.747	0.730	0.692	0.675	0.655	0.624	0.605	0.583
0.07	0.743	0.725	0.705	0.672	0.654	0.629	0.596	0.578	0.555
0.1	0.722	0.702	0.680	0.650	0.627	0.600	0.568	0.550	0.520

Table V: γ of HCl in Glycol-Water Mixtures at 25°

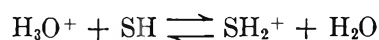
m_{HCl}	Wt % glycol					
	10	30	50	70	90	100
0	1.153	1.456	1.893	2.833	7.586	47.97
0.005	1.068	1.335	1.708	2.468	6.311	38.81
0.01	1.036	1.294	1.647	2.394	6.016	35.88
0.02	1.000	1.245	1.581	2.283	5.620	32.72
0.03	0.976	1.213	1.538	2.216	5.388	30.94
0.05	0.945	1.174	1.488	2.116	5.121	28.97
0.07	0.925	1.148	1.454	2.054	4.962	27.73
0.1	0.905	1.120	1.411	1.989	4.756	26.38

Table VI: Standard Free Energy and Entropy of Transfer of HCl from Water to Glycol-Water Media at 25°

Wt % glycol	ΔG° , cal mole ⁻¹	$\Delta G^\circ_{\text{el}}$, cal mole ⁻¹	$\Delta G^\circ_{\text{c}}$, cal mole ⁻¹	ΔS° , cal mole ⁻¹ deg ⁻¹	$\Delta S^\circ_{\text{el}}$, cal mole ⁻¹ deg ⁻¹	$\Delta S^\circ_{\text{c}}$, cal mole ⁻¹ deg ⁻¹
10	80	74	6	-0.1	-0.3	0.2
30	163	242	-79	-0.3	-2.4	2.1
50	238	467	-229	-1.1	-4.5	3.4
70	420	835	-415	-4.7	-7.2	2.5
90	1425	1535	-110	-8.9	-9.8	0.9
100	3119	2087	1032	-7.1	-12.4	4.7

process with the solute in the standard state in either medium. Obviously, the dielectric constant of the medium plays a dominant role in the process of transfer. An additional factor is also involved, *i.e.*, the chemical

interaction which includes the breakdown of one type of solvation shell and the creation of another. In the case of an acidic solute like HCl, we must also take into account the fact that a protolytic process is involved in the transfer from aqueous to another amphiprotic solvent (SH).



So long as the water content in the medium is high enough, H_3O^+ (solvated) may be the dominant species, rather than SH_2^+ (solvated), unless SH happens to possess strongly basic properties. In any case, however, there will be a competition between H_2O and SH for the proton, and a proton partition equilibrium will be set up. In the present case, as the glycol content increases, more and more protons will tend to combine with glycol molecules. The transfer process should thus include a definite chemical reaction in addition to a change in the state of mere solvation. The total free energy (ΔG°) of transfer may thus be considered to consist of two parts: electrostatic ($\Delta G^\circ_{\text{el}}$) and non-electrostatic or chemical ($\Delta G^\circ_{\text{c}}$). The electrostatic part of the free energy change may be computed from the Born equation

$$\Delta G^\circ_{\text{el}} = \frac{Ne^2}{2} \left(\frac{1}{r_+} + \frac{1}{r_-} \right) \left(\frac{1}{D_s} - \frac{1}{D_w} \right) \quad (14)$$

The value of $\Delta G^\circ_{\text{c}}$ may then be obtained by the difference between ΔG° and $\Delta G^\circ_{\text{el}}$. $\Delta G^\circ_{\text{el}}$ has been calculated from Born equation, by taking the radius of the

"hydrogen ion" as 2.76 Å (the diameter of a water molecule),¹² and that of the chloride ion as 1.81 Å (the crystallographic radius). For all the media including anhydrous glycol, the radius of the hydrogen ion has been arbitrarily taken as 2.76 Å, though this is unwarranted at least for the anhydrous solvent. The values of ΔG°_{el} (in calories) so calculated for 25° are presented in Table VI (third column). The fourth column in Table VI gives the values of ΔG°_c as obtained by subtracting ΔG°_{el} from ΔG° .

The standard entropy change of the transfer process (ΔS°) has been evaluated from the temperature coefficient of the standard electrode potentials, using the equation

$$\Delta S^{\circ} = - \left[\frac{\partial(\Delta G^{\circ})}{\partial T} \right]_P = F \left[\frac{\partial({}^s E_N^{\circ})}{\partial T} - \frac{\partial({}^w E_N^{\circ})}{\partial T} \right]_P \quad (15)$$

The values of ΔS° at 25° are shown in Table VI. For the purpose of this calculation, eq 2 to 8 for E_m° were used in combination with eq 10 for E_N° .

As in the case of the free energy of transfer, the entropy change also consists of two parts: (i) electrostatic (ΔS°_{el}) and (ii) nonelectrostatic (ΔS°_c). The electrostatic part of the entropy change may be obtained by differentiating eq 14 whereby we have

$$\Delta S^{\circ}_{el} = - \left[\frac{\partial(\Delta G^{\circ}_{el})}{\partial T} \right]_P = - \frac{Ne^2}{2} \left(\frac{1}{r_+} + \frac{1}{r_-} \right) \left[\left(\frac{1}{D_w} \frac{d \ln D_w}{dT} \right) - \left(\frac{1}{D_s} \frac{d \ln D_s}{dT} \right) \right] \quad (16)$$

To use this equation, the values of $d \ln D/dT$ for the various media must be known. These values have been calculated from the empirical equation

$$D = D_0 e^{-T/\theta} \quad (17)$$

where D is the dielectric constant at temperature T and D_0 and θ constants characteristic of the medium.¹³ By differentiating with respect to T , we have

$$\frac{d \ln D}{dT} = -\frac{1}{\theta} \quad (18)$$

Hence, eq 16 reduces to

$$\Delta S^{\circ}_{el} = - \frac{Ne^2}{2} \left(\frac{1}{r_+} + \frac{1}{r_-} \right) \left(\frac{1}{D_s \theta_s} - \frac{1}{D_w \theta_w} \right) \quad (19)$$

The values of θ (shown below) for the respective media were calculated from the slopes of the straight lines obtained by plotting $\log D$ against T .

Wt % glycol	0	10	30	50	70	90	100
θ	219	217	194	180	174	185	194

The nonelectrostatic or chemical part of the entropy of transfer (ΔS°_c) of HCl from water to any other medium was obtained by subtracting ΔS°_{el} from the total entropy change (ΔS°) evaluated by eq 15. The values so computed for 25° are shown in Table VI.

It will be seen from Table V, though the total free energy change involved in the transfer process for each of the glycol-water media is positive, the chemical part for the free energy change is negative, ignoring the small value of 6 cal for 10% glycol. Thus, so far as the chemical interaction is concerned, it is favorable for the transfer process from water to the aqueous glycol media, but electrostatic factors predominating over the chemical interaction lead to an over-all unfavorable effect on the transfer process.

Assuming tentatively that very little free energy change (due to chemical interaction or solvation) is involved in the transfer of the accompanying chloride ion, ΔG°_c may be approximately equated to the standard free energy change for the transfer of the proton from water to the other medium. Thus, it may be concluded that in the standard state the proton tends to be preferentially solvated in the glycol-water medium rather than in the pure aqueous medium. For the pure glycol medium, however, it will be seen from Table VI that ΔG°_c has a large positive value. The numerical value may not have exact significance, since this value was computed by taking the radius of the hydrogen ion the same as for water and the aqueous organic media (*viz.*, the diameter of a water molecule), but in any case, the positive sign of ΔG°_c does have real significance. It shows that water has a greater chemical affinity for the proton than ethylene glycol, or in other words, glycol is a weaker base than water. This is just what is to be expected on the basis of chemical properties, and acid-base studies by Kundu and Das¹⁴ also led to the same conclusion.

It is rather surprising, however, why the addition of glycol to water should make the mixed media more basic than pure water as indicated by the negative values of ΔG°_c . The results indicate that the addition of glycol to water increases the over-all basicity of the medium which rises to a maximum (around 70% glycol), further addition of glycol leading to decreased basicity. Dissociation constants of several cation acids in methanol-

(12) M. Paabo, R. G. Bates, and R. A. Robinson, *J. Phys. Chem.*, **70**, 247 (1966).

(13) R. W. Gurney, "Ionic Processes in Solution," McGraw-Hill Book Co., Inc., New York, N. Y., 1953, p 16.

(14) K. K. Kundu and M. N. Das, *J. Chem. Eng. Data*, **9**, 82 (1964).

water mixtures^{12,15-17} also indicate that as methanol is added to water, the basicity increases passing through a maximum. Factors involving liquid structure may have something to do with this apparent anomaly. It has been suggested¹⁸ that the addition of alcohol to water promotes a breakdown of the water structure. The basic oxygen centers of the water molecules thus become free for the attachment of the incoming protons. A similar situation is very likely in glycol-water systems as well. Though ethylene glycol is intrinsically more acidic and less basic than water,¹⁴ the addition of glycol to water makes free water molecules, disengaged from the iceberg structure, increasingly available to the protons. The process of breakdown of the water structure continues and presumably becomes complete at a certain concentration of glycol, after which the basicity decreases as the solvent becomes still richer in the more acidic constituent, the glycol.

Some insight into the structural factors involved in the transfer process might be obtained from the values of the entropy change accompanying the transfer. It will be seen from Table VI that the total entropy change is always negative. When allowance is made for the electrostatic part of the entropy change, the contribution from the chemical interaction (ΔS°_c) comes out as positive. No simple trend is, however, discernible in

the magnitude of the values of ΔS°_c . Moreover, in view of the uncertainty in the radius terms used in Born equation, quantitative significance can hardly be attached to the values obtained. Another factor involves the uncertainty in the dielectric constant of the medium. By using Hepler's equation¹⁹ which takes into account the dielectric saturation, probably more reliable values for ΔG°_{el} might be obtained for the process of transfer, but even then the uncertainty in the radii of the ions would remain. The values of ΔG°_c calculated with the simple Born equation may, however, be regarded as sufficiently significant for the purpose of drawing certain general conclusions as presented above.

Acknowledgment. The work was done under a project financed by the National Bureau of Standards, Washington, D. C.

(15) E. E. Sager, R. A. Robinson, and R. G. Bates, *J. Res. Natl. Bur. Std.*, **68A**, 305 (1964).

(16) M. Woodhead, M. Paabo, R. A. Robinson, and R. G. Bates, *ibid.*, **69A**, 263 (1965).

(17) A. L. Bacarella, E. Grunwald, H. P. Marshall, and E. L. Purlee, *J. Org. Chem.*, **20**, 747 (1965).

(18) E. A. Braude and E. S. Stern, *J. Chem. Soc.*, 1976 (1948).

(19) L. C. Hepler, *Australian J. Chem.*, **17**, 587 (1964).

Relationship between Chemical Reactivity and the Hyperfine

Structure of Polycyclic Hydrocarbons¹

by Charles P. Poole, Jr., and O. F. Griffith, III

Department of Physics, University of South Carolina, Columbia, South Carolina (Received February 27, 1967)

The hyperfine coupling constants a_i of a polycyclic hydrocarbon are found to be closely related to the observed reactivity rates at various sites in the molecule. These coupling constants provide an experimental determination of the spin density at the various molecular sites, and this is numerically equal to one-half the frontier electron density. A detailed comparison is made of the phenanthrene nitration reaction, and the coupling constants a_i are found to be closely proportional to the logarithm of the reaction rate k_i . The frontier electron densities scatter somewhat from a straight line and the other reactivity constants π_{ii} , F_i , L_i , S_i , and N_i exhibit a very poor correlation with these reactivity data. A general agreement is found between the experimental electron spin resonance hyperfine coupling constants and the observed order of reactivities at various sites in naphthalene, anthracene, phenanthrene, pyrene, chrysene, 1,2-benzanthracene, 3,4-benzpyrene, and perylene.

Introduction

Several authors²⁻⁵ have reviewed the use of molecular orbital theory to calculate chemical reaction rates. A number of indices of reactivity have been suggested and used to explain the relative reactivities of the individual sites within a given molecule (intramolecular relative reactivity) and the reactivities derived from a comparison between different molecules (intermolecular relative reactivity). Salem⁴ has given an extensive discussion of phenanthrene, and Table I presents the data collected by him, using the molecule numbering convention shown in Figure 1. The computational procedure often begins with the simple mathematical model of the molecule called the Hückel molecular orbital (HMO) approximation, and it provides values of the various indices of reactivity. Most of the indices are functions of the Hückel coefficients C_{ki} , but ordinarily no independent experimental checks are made of the values for these coefficients. Other indices depend upon postulated intermediate states with energies which are not accessible to measurement.

Over the past few years a number of investigators have employed the technique of electron spin resonance (esr) to measure the hyperfine coupling constants of many radical ions. Of particular interest to us here are the measurements that have been carried out with

polycyclic hydrocarbons. The measured hyperfine splittings correlate well in most cases with spin densities calculated by the Hückel method. We shall show the very close relationship between these measured hyperfine constants and the frontier electron densities suggested by Fukui, *et al.*,⁶⁻⁸ as indices of chemical reactivity.

Hyperfine Structure and Reactivity

The electron spin resonance (esr) spectra arising from radical ions formed from polycyclic hydrocarbons have been widely studied. The subject has been reviewed

(1) This work is supported by the National Institutes of Health, Grant No. CA06401-05.

(2) (a) B. Pullman and A. Pullman, *Progr. Org. Chem.*, **4**, 31 (1958); (b) H. H. Greenwood and R. McWeeny, *Advan. Phys. Org. Chem.*, **4**, 73 (1966).

(3) B. Pullman and A. Pullman, "Quantum Biochemistry," Interscience Publishers, Inc., New York, N. Y., 1963, pp 155-181.

(4) L. Salem, "The Molecular Orbital Theory of Conjugated Systems," W. A. Benjamin, Inc., New York, N. Y., 1966.

(5) S. Glasstone, "Textbook of Organic Chemistry," 2nd ed, The Macmillan Co., New York, N. Y., 1960.

(6) K. Fukui, T. Yonezawa, and H. Shingu, *J. Chem. Phys.*, **20**, 722 (1952).

(7) K. Fukui, T. Yonezawa, and H. Shingu, *ibid.*, **22**, 1433 (1954).

(8) K. Fukui, T. Yonezawa, and C. Nagata, *Bull. Chem. Soc. Japan*, **27**, 423 (1954); *J. Chem. Phys.*, **26**, 831 (1957).

Table I: Comparison of Phenanthrene Nitration Reactivities k_i , with Several Theoretical Indices (f_i , π_{ii} , F_i , L_i , S_i , N_i), Theoretical Spin Densities, ρ_i , and Experimental Hyperfine Coupling Constants, a_i

Position	Log (k_i/k_n)	Exptl HFS constant ^b a_i	HMO spin density ^c ρ_i	Frontier electron density ^a f_i	Self-polarizabilities ^a π_{ii}	Free valence index ^a F_i	Localization energy ^a L_i	Superdelocalizabilities ^a S_i	Reactivity no. ^a N_i
9	0.02	4.43	0.172	0.344	0.442	0.451	2.298	0.997	1.80
1	-0.11	3.71	0.116	0.232	0.439	0.450	2.317	0.977	1.86
3	-0.19	2.88	0.099	0.198	0.409	0.408	2.453	0.893	2.04
2	-0.71	0.43	0.002	0.004	0.403	0.402	2.497	0.860	2.18
4	-0.77	0.63	0.054	0.108	0.429	0.441	2.365	0.939	1.96

^a Data from tabulations in ref 4; k_n is the reactivity of the α position of naphthalene. ^b F. Möbius, *Z. Naturforsch.*, **20**, 1102 (1965). From Hückel molecular orbital calculations. H. M. McConnell, *J. Chem. Phys.*, **28**, 1188 (1958); H. M. McConnell and D. B. Chestnut, *ibid.*, **27**, 984 (1957); **28**, 107 (1958). See also T. C. Sayetta and J. D. Memory, *J. Chem. Phys.*, **40**, 2748 (1964).

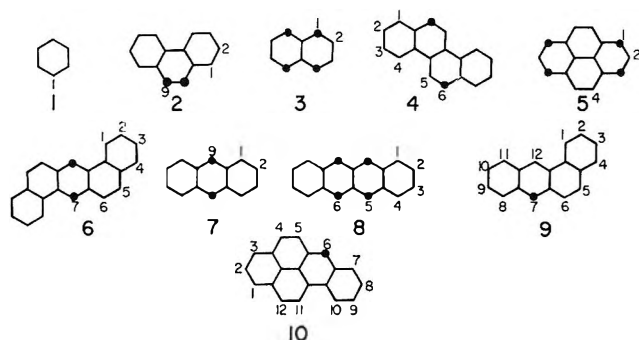


Figure 1. Polycyclic hydrocarbon molecules with sites of maximum frontier electron density (Hückel spin density) indicated: 1, benzene; 2, phenanthrene; 3, naphthalene; 4, chrysene; 5, pyrene; 6, 1,2:5,6-dibenzanthracene; 7, anthracene; 8, naphthacene; 9, 1,2-benzanthracene; 10, 3,4-benzpyrene.

through 1963 by Carrington⁹ and recently by Bowers.¹⁰ Negative radical ions form readily by polarographic techniques¹¹⁻¹⁵ and in alkali metal solutions.^{16,17} Positive radical ions have been prepared in sulfuric acid^{17,18} and by other methods such as oxidation with SbCl_5 .¹⁹ The hyperfine splittings of the esr spectra are often sufficiently well resolved to provide experimental hyperfine coupling constants, and many such constants have been tabulated in the literature. McConnell^{20,21} related the hyperfine coupling constant a_i to the unpaired Hückel spin density ρ_i residing at an atom by eq 1. The spin density may be calculated by the simple

$$a_i = Q\rho_i \quad (1)$$

Hückel approximation^{22,23} and Q is a semiempirical constant with the values $Q_- = 28.6$ gauss for negative ions and $Q_+ = 35.7$ gauss for positive ions. The measured hyperfine coupling constants are usually compared to calculated spin densities, through either the McConnell^{20,21} or Colpa-Bolton²⁴ theories, and

empirical electron distributions may be postulated. Both theories provide about the same agreement with the available data on hydrocarbon radical ions.^{15,19} An individual radical ion ordinarily has a Q value close to the appropriate average value.

The experimental hyperfine coupling constants and theoretical HMO spin densities for phenanthrene¹⁵ are shown in columns three and four, respectively, of Table I. The Hückel order was used in assigning the experimental coupling constants. Although errors in the assignment of spin densities to individual sites will be more likely if there are two values very close together, comparisons such as that shown in Figure 2a will not be significantly affected, precisely because of the closeness of the values.

- (9) A. Carrington, *Quart. Rev. (London)*, **17**, 66 (1963).
 (10) K. W. Bowers, "Advances in Magnetic Resonance," Vol. 1, Academic Press Inc., New York, N. Y., 1966, p 31.
 (11) A. H. Maki and D. H. Geske, *J. Chem. Phys.*, **30**, 1356 (1959).
 (12) D. H. Geske and A. H. Maki, *J. Am. Chem. Soc.*, **82**, 2671 (1960).
 (13) P. H. Rieger, I. Bernal, W. H. Reinmuth, and G. K. Fraenkel, *ibid.*, **85**, 683 (1963).
 (14) R. Dehl and G. K. Fraenkel, *J. Chem. Phys.*, **39**, 1793 (1963).
 (15) See Table I, footnote b.
 (16) G. J. Hoijsink, J. Townsend, and S. I. Weissman, *J. Chem. Phys.*, **34**, 507 (1961).
 (17) E. de Boer and S. I. Weissman, *J. Am. Chem. Soc.*, **80**, 4549 (1958).
 (18) J. S. Hyde and H. W. Brown, *J. Chem. Phys.*, **37**, 368 (1962).
 (19) I. C. Lewis and L. S. Singer, *ibid.*, **43**, 2712 (1965).
 (20) H. M. McConnell, *ibid.*, **24**, 764 (1956).
 (21) See Table I, footnote c.
 (22) A. Streitwieser, J. I. Brauman, and C. A. Coulson, Supplemental Tables of Molecular Orbital Calculations with Dictionary of Electron Calculations, Pergamon Press Inc., New York, N. Y., 1965.
 (23) E. Heilbronner and P. A. Straub, "Hückel Molecular Orbitals," Springer-Verlag, N. Y., Inc., New York, N. Y., 1966.
 (24) J. P. Colpa and J. R. Bolton, *Mol. Phys.*, **6**, 273 (1963).

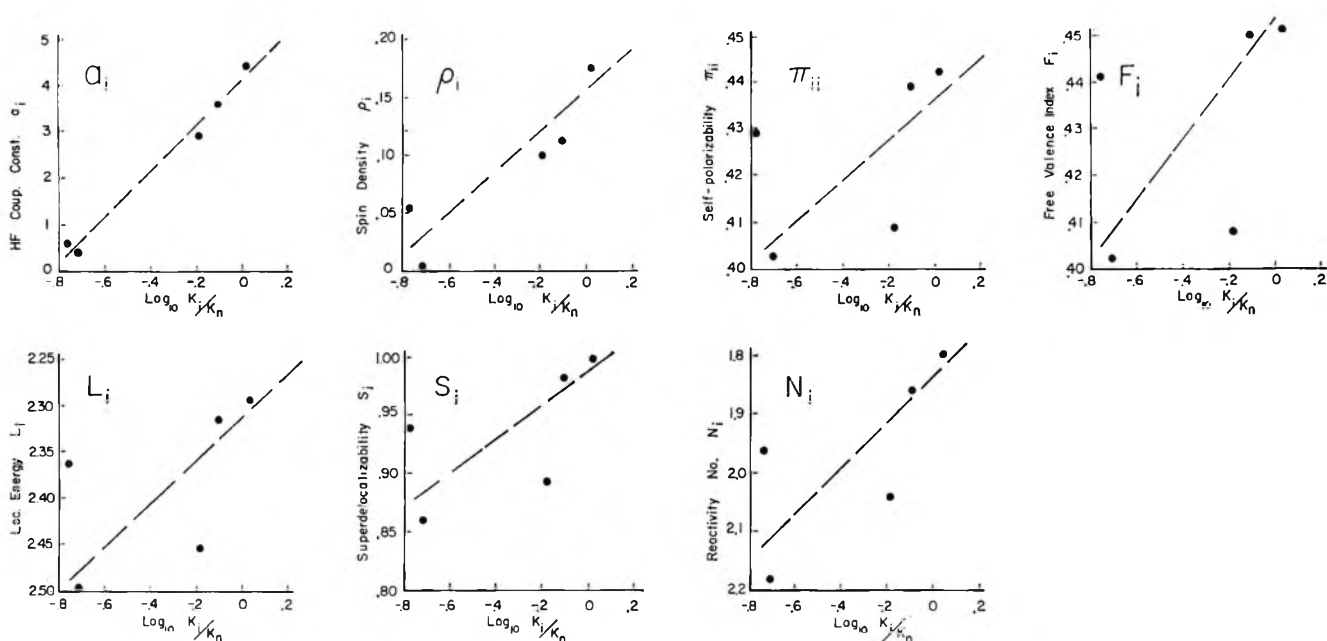


Figure 2. Graphs showing the data in columns 3–10 of Table I plotted against the logarithm of the relative reactivities k_i/k_n . Note that some ordinate scales are inverted to allow graphic comparison.

Table II: Comparison of Various Reactivities with Hückel Spin Densities ρ_i at the Molecular Sites Indicated

Compound	Reaction	Order of reactivity ^a	Order of Hückel spin densities
Naphthalene	Acylation	1 > 2	1 > 2
Anthracene	Ketone formation	9 > 1 > 2	9 > 1 > 2
Phenanthrene	Nitration	3 > 1 > 2	
Phenanthrene	Acetylation, CS ₂ solvent	3 > 9 > 2 > 1 > 4	9 > 1 > 3 > 4 > 2
Phenanthrene	Acetylation, C ₂ H ₄ Cl ₂ solvent	9 > 3 > 2 > 1 > 4	
Pyrene	Acylation	1 > others	1 > 4 > 2
Chrysene	Acylation	6 > 3 ≈ 2 > others	6 > 1 > 4 ≈ 3 ≈ 5 > 2
1,2-Benzanthracene	Acylation	7 > 10 > 9 > 3 ≈ 2	8 > 7 > 9 > 12 > 5 > 2 > 11 > 6 > 10 > 4 > 3 > 1
3,4-Benzpyrene	Normal substitution	6 > others	1 > others > 6
3,4-Benzpyrene	Acylation	1 > others	
Perylene	Acylation	3 > others	3 > 1 > 2

^a These data were compiled from "Freidel-Crafts and Related Reactions," G. A. Olah, Ed., Vol. 3, John Wiley and Sons, Inc., New York, N. Y., 1964.

It is interesting to compare quantitatively the various indices in columns 6–10 in Table I with the logarithm of the relative reaction rate,^{4,25} and this is done in Figure 2. A glance at this figure reveals four things: (1) the five indices calculated by molecular orbital methods do not correlate well with the reactivity; (2) the spin densities ρ_i , calculated by the molecular orbital theory do correlate well; (3) the frontier electron densities f_i equal twice the respective spin densities ρ_i and hence give the same correlation; and (4) the experimentally determined hyperfine coupling constants a_i provide an

excellent linear fit to the reactivity data. Note that it is no longer necessary to invoke steric hindrance²⁶ to explain the very low reactivity of position 4 when one uses the hyperfine coupling constants determined by esr data.

Detailed reactivity data of the type discussed for

(25) E. C. Kooyman and E. Farenhorst, *Trans. Faraday Soc.*, **49**, 58 (1953).

(26) M. J. Dewar, T. Mole, and E. W. T. Warford, *J. Chem. Soc.*, 3581 (1956).

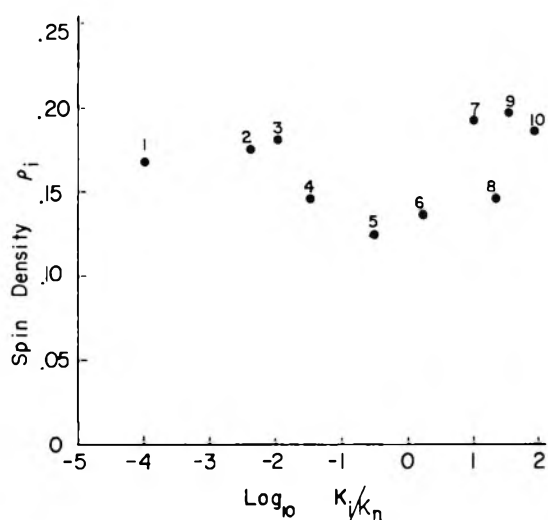


Figure 3. Calculated Hückel molecular orbital spin density (ρ_i) as a function of the logarithm of the reaction rate for the radical reaction ($\text{CCl}_3 \cdot + \text{hydrocarbon}$). Numbers indicate compounds shown in Figure 1.

phenanthrene are not available for a large number of polycyclic hydrocarbons, but the orders of reactivity have been measured for many of them. Table II compares some of these data with the order of the HMO spin densities, and a good over-all correlation is evident. In the case of 1,2-benzanthracene the order of reactivity $7 > 10 > 9 > 3 \approx 2$ tends to follow the order $7 > 9 > 2 > 10 > 3$ of these Hückel coefficients except for position 10, but many high-spin density positions do not appear in the former list due to the lack of detectable reactivities.

The preceding discussion shows that the spin densities and hyperfine coupling constants provide self-consistent internal reactivity coefficients for determining the relative reactivities at different positions in a molecule. The value of these indices for comparing different molecules is shown in Figures 3 and 4 where ρ_i and a_i , respectively, are plotted against $\log k_i$ for the most reactive sites of several polycyclic molecules. When a least-squares fit is attempted, the large scatter in these data prevents us from drawing definite conclusions regarding the correlation of the reactivity with the charge density ρ_i and the coupling constant a_i for different molecules. There does appear, however, to be a slight correlation between the hyperfine coupling constant and the reactivity, as indicated in Figure 4.

Thus we see that the hyperfine coupling constants a_i and spin densities ρ_i exhibit a very good intramolecular correlation and a possible intermolecular correlation with reaction rates. In each case the experimentally determined hyperfine coupling constants correlate

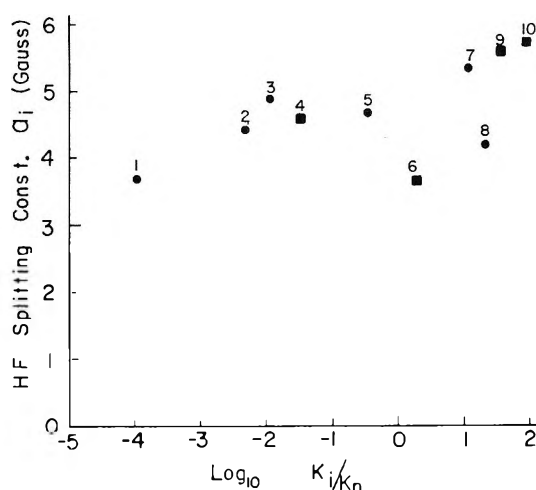


Figure 4. Experimentally determined hyperfine coupling constants a_i for the most reactive site plotted against the logarithm of the reactivity for the compounds listed in Figures 1 and 3: ●, obtained from the experimental hyperfine coupling constants; ■, computed from experimentally determined Q values and Hückel spin densities (cf. Salem,⁴ p 295, and Kooyman and Farenhorst²⁵).

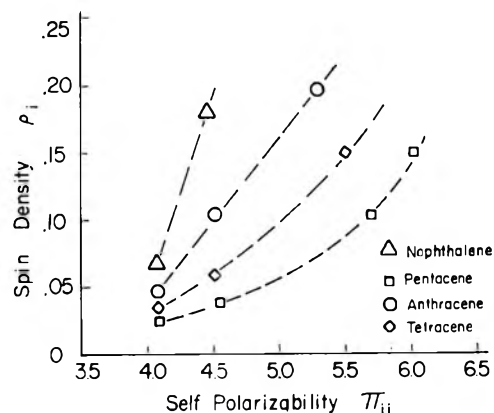


Figure 5. Relationship between spin densities ρ_i calculated by the Hückel method and the atom-atom self-polarizabilities π_{ii} for the series of linear polycyclic hydrocarbons.

better than the calculated spin densities. This correlation means that we may expect a_i and ρ_i to be closely related to the various molecular indices for a series of atomic sites. The spin density is half of the corresponding frontier electron density, as observed above. Another example of such a correlation is shown in Figure 5 where we plot ρ_i against the atom-atom self-polarizability π_{ii} . The figure shows the regular trend of each individual molecule (intramolecular effect) and the differences between molecules (intermolecular effect) noted above. For even alternate hydrocarbons, the four

indices π_{ii} , F_i , L_i , and S_i all predict the same order of activity, so they should all exhibit correlations with spin density of the type shown in Figure 5. Some molecules such as phenanthrene do not show a regular intramolecular correlation, but in this case it is the hyperfine coupling constants which follow the reactivities.

Conclusions

In this paper we have shown that the hyperfine coupling constants are good quantitative indices of relative chemical reactivity rates at various sites in a polycyclic hydrocarbon molecule. Various conventional molecular orbital reactivity indices are found to be unsatisfactory in this respect.

NOTES

Exact Geometrical Parameters for Pendular Ring Fluid

by James C. Melrose and George C. Wallick

Mobil Oil Corporation, Dallas, Texas 75221
(Received April 5, 1967)

That a fluid can be confined in the region of the contact point between two spherical solid particles by means of "capillary action" is well known. Such fluid is often said to be in a pendular ring configuration, and the problem of specifying the volume, meniscus area, and pressure deficiency is a classical problem in the theory of capillarity. The shape of the meniscus separating the pendular ring fluid from the surrounding fluid (vapor or liquid) is described by an equation due to Laplace,^{1,2} which relates the pressure deficiency to the fluid-fluid interfacial tension. From this equation it follows that, if gravitational distortion can be ignored, the meniscus must assume the form of a surface of constant mean curvature.³

For many cases of interest it can be supposed that the two spheres are identical in size and that the properties of both solid-fluid interfaces are uniform at all points in the region in which the meniscus meets the solid surface. It follows from the latter specification, together with Young's equation,⁴ that the three-phase line of contact is characterized by a uniform contact angle. When this is so, the boundary conditions for Laplace's equation have cylindrical symmetry. This establishes the fact that the meniscus will also take the form of a surface of revolution. Among surfaces of revolution, only the sphere, cylinder, unduloid, catenoid, and

nodoid are also surfaces of constant mean curvature.^{5,6} In the case of pendular ring fluid, the appropriate configuration of the meniscus is that of the nodoid. Since the two spheres are identical in size, the section of the nodoid involved is symmetrical with respect to the contact plane.

The availability of these classical results^{7,8} makes it possible to assess both the mathematical nature and the importance of various approximations which have been used in obtaining numerical solutions to the nodoid problem. Recently, Mayer and Stowe⁹ have treated the problem by assuming the meniscus profile to be a circular arc. They then relate the curvature to differential changes in the volume, meniscus area, and area of contact between the solid and the confined fluid. The toroidal meniscus configuration was also assumed by Rose¹⁰ and by earlier authors. In this previous work, it was recognized that the torus surface is not

(1) J. C. Maxwell, "Capillary Action," in *Encyclopedia Britannica*, 9th ed, 1875; "Scientific Papers," Vol. II, Cambridge University Press, London, 1890, p 541.

(2) The classical hydrostatic and thermodynamic theories have been reconciled and extended by F. P. Buff, "The Theory of Capillarity," in "Handbuch der Physik," Vol. 10, Springer-Verlag, Berlin, 1960.

(3) J. A. F. Plateau, "Statique expérimentale et théorique des liquides," Vol. 1, Gauthier-Villars, Paris, 1873, p 6.

(4) T. Young, *Phil. Trans. Roy. Soc. London*, **95**, 65 (1805).

(5) J. A. F. Plateau, ref 3, p 131.

(6) A lucid review is given by D. W. Thompson, "On Growth and Form," J. T. Bonner, Ed., Cambridge University Press, London, 1961, pp 53-61.

(7) H. Bojasse, "Capillarité, phénomènes superficiels," Delagrave, Paris, 1924, pp 49-66.

(8) G. Bakker, "Kapillarität und Oberflächenspannung," in "Handbuch der Experimentalphysik," Vol. VI, Akademische Verlagsgesellschaft, Leipzig, 1928, pp 120-124.

(9) R. P. Mayer and R. A. Stowe, *J. Phys. Chem.*, **70**, 3867 (1966).

(10) W. Rose, *J. Appl. Phys.*, **29**, 687 (1958).

of these parameters. Denoting the area by Ω , this expression is

$$\Omega = 2\pi R^2 (\sin^2 \psi) \{ [\cos(\theta + \psi)] + [\sin(\theta + \psi)](\sin \psi)(1 + \cos \psi)^{-1} \} - J \{ (3V/2) + \pi R^2(1 - \cos \psi)^2 \} \quad (1)$$

This simple and useful result has not been explicitly pointed out in previous treatments of the nodoid problem. In Table II, numerical values for the reduced area, Ω/R^2 , are given. These values were obtained by means of eq 1, using the corresponding reduced values of J and V from Table I.

Table II: Nodoid Solutions for Meniscus Area

ψ , deg	$10\Omega/R^2$		
	$\theta = 0^\circ$	$\theta = 20^\circ$	$\theta = 40^\circ$
5	0.0608	0.0513	0.0458
10	0.4515	0.3887	0.3527
15	1.4175	1.2442	1.1486
20	3.1309	2.8013	2.6306
25	5.7087	5.2050	4.9710
30	9.2252	8.5693	8.3220
32.68	10.579
35	13.723	12.984	
40	19.221	18.519	
44.77	...	24.895	
45	25.721		
50	33.209		
55.64	42.819		

In the limit of vanishing curvature and for the special case of zero contact angle, the meniscus area obeys an elementary relationship involving that portion of the total area of the two spheres which is in contact with the pendular ring fluid. It follows from eq 1 that the area of the meniscus, which is now a catenoid tangent to the spheres, is simply the *harmonic mean* of the contacted and noncontacted areas of the two spheres. Since this theorem holds for the catenoid (a minimal surface in mathematical terminology), it will necessarily fail for the surface of a torus.

In summary, it is concluded that the approximation which Mayer and Stowe adopt gives results having an accuracy which is entirely adequate for many purposes. However, it should be emphasized that the method they employ is not exact and may yield errors of unacceptable magnitude for certain problems involving capillary-held fluids.

Acknowledgment. We are indebted to Dr. S.-T. Hwang for assistance in obtaining the results given in Table II. Appreciation is also expressed to the Mobil Oil Corp. for permitting publication of this work.

Proton Magnetic Resonance Studies on Some Metal Complexes of Methyliminodiacetic Acid and Hydroxyethyliminodiacetic Acid^{1a}

by G. H. Nancollas and A. C. Park^{1b}

Chemistry Department, State University of New York at Buffalo, Buffalo, New York 14214 (Received May 25, 1967)

In recent years, the metal complexing ability of ethylenediaminetetraacetic acid (EDTA) and its derivatives has been the subject of a large number of studies. The strong complexes formed with the normally weakly associating alkaline earth metal ions are of particular interest insofar as their structure in solution is concerned. Hoard and his co-workers²⁻⁴ have established the crystal structures of a number of heavy metal ion complexes of EDTA, but the validity of the assumption that the aqueous species have geometries which are not essentially different from those in the crystalline state has not yet been established. It is therefore desirable to use as many physical methods as possible in order to determine the structures of the species in solution and the nature and strengths of the bonds formed. Thermodynamic data, while providing valuable information about the overall energy changes taking place in a reaction, can give no insight into the specific interactions involved within a single species. On the other hand, spectral changes, brought about by variations in electron distributions within a ligand due to interaction with different metal ions, can afford information of this nature. So far, infrared and nuclear magnetic resonance (nmr) spectroscopy have proved to be the techniques most useful in the study of complexes, and many workers^{5,6} have been involved in the interpretation of data obtained from these sources.

In the present work, proton magnetic resonance studies have been carried out on the alkaline earth metal ion complexes of N-methyliminodiacetic acid (MIDA) and hydroxyethyliminodiacetic acid (HEIDA) which represent simple analogs of the analytically im-

(1) (a) Supported in part by N.S.F. Grant No. GP-6042; (b) Postdoctoral Fellow, Chemistry Department, Cornell University, Ithaca, N. Y.

(2) H. A. Weakliem and J. L. Hoard, *J. Am. Chem. Soc.*, **81**, 549 (1959).

(3) G. S. Smith and J. L. Hoard, *ibid.*, **81**, 556 (1959).

(4) J. L. Hoard, M. Lind, and J. V. Silverton, *ibid.*, **83**, 2770 (1961).

(5) D. T. Sawyer and J. E. Tackett, *ibid.*, **85**, 2390 (1963).

(6) R. J. Day and C. N. Reilly, *Anal. Chem.*, **36**, 1073 (1964).

portant complexing agents EDTA and EGTA, respectively.

Experimental Section

Proton magnetic resonance (pmr) measurements were made with a Varian A60 spectrometer. Chemical shifts were measured in parts per million (ppm) relative to an external benzene reference. Measurements of pH were made using a Beckman Research pH meter, the electrodes being standardized with National Bureau of Standards standard buffer solutions, prepared according to Bates.⁷

MIDA was prepared by the method of Schwarzenbach, *et al.*⁸ *Anal.* Calcd: C, 40.82, H, 6.17, N, 9.52. Found, C, 40.62; H, 5.91, N, 9.63. HEIDA obtained from the Dow Chemical Co. was used without further purification. Magnesium and calcium solutions were analyzed by EDTA titrations and strontium and barium by gravimetric methods. Variations in the pH of metal aminocarboxylate solutions were brought about by small addition of 5 *N* solutions of potassium hydroxide or hydrochloric acid. It was necessary to use fairly concentrated solutions, 0.2 *M* in K_2Z or K_2MZ (M^{2+} = metal ion; Z^{2-} = MIDA or HEIDA anion), in order to obtain suitable nmr signals.

Results and Discussion

Protonation schemes, as described by Kula, *et al.*,⁹ for EDTA, were established for the free anions (Z^{2-}) and the alkaline earth metal ion complexes (MZ) of MIDA and HEIDA. Typical plots of changes of chemical shifts (ppm relative to benzene) with pH for the nonlabile protons, c and d on $MIDA^{2-}$ and b, c, and d on $HEIDA^{2-}$ are shown in Figures 1 and 2. In solutions containing metal ions, chemical shifts of nonlabile protons on both ligands remained constant down to the pH values at which inflexion I in the figures occurred. This first inflexion appeared at lower pH values for more stable complexes. Table I gives chemical shifts produced in the Z^{2-} ions by interaction with either a proton or a metal ion at high pH values; EDTA⁹ and EGTA¹⁰ values are included for comparison. The barium complex of HEIDA could not be studied because of precipitation at high pH values.

The pmr spectrum of the free MIDA anion showed two sharp singlet bands corresponding to the c and d protons. The four d hydrogens on the HEIDA anion also gave rise to a sharp singlet, and in addition, two triplets were observed due to the nonequivalence of the protons b and c. The absence of broadening or splitting of any of these bands in the spectra of the complexes indicated rapid exchange of ligands between metal ions at all pH values.⁹

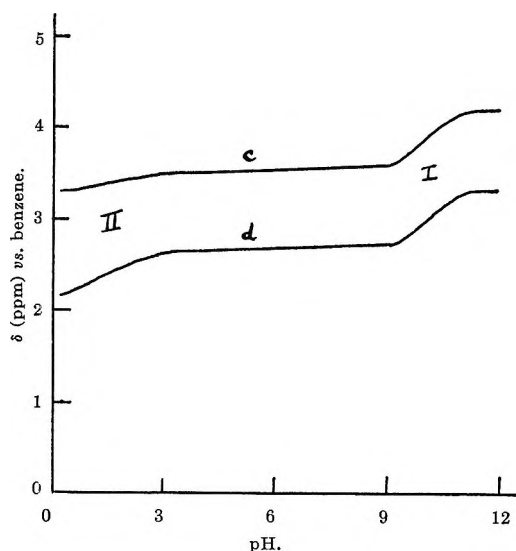


Figure 1. Chemical shift of MIDA at various pH values.

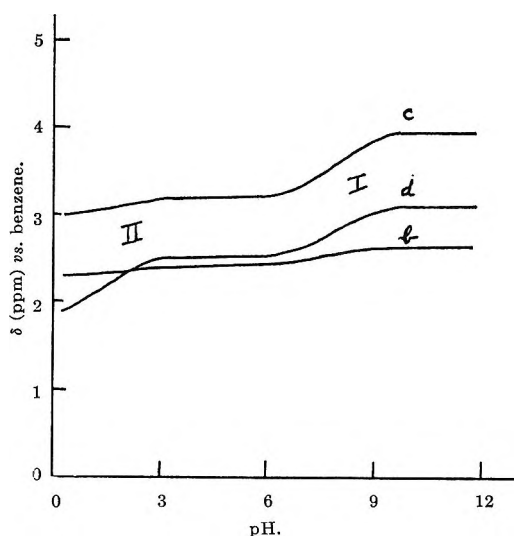
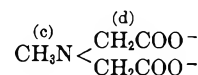
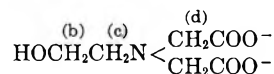


Figure 2. Chemical shift of HEIDA at various pH values.



Equivalent downfield shifts of both c and d protons for both ligands on monoprotection of the Z^{2-} ions

(7) R. G. Bates, "Electrometric pH Determinations," Chapman and Hall, Ltd., London, 1954.

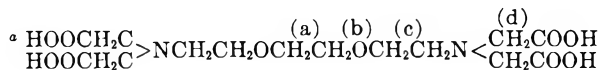
(8) G. Schwarzenbach, E. Kampitsch, and R. Steiner, *Helv. Chim. Acta*, **28**, 1133 (1945).

(9) R. J. Kula, D. T. Sawyer, S. I. Chan, and C. M. Finley, *J. Am. Chem. Soc.*, **85**, 2930 (1963).

(10) A. Bryson and G. H. Nancollas, *Chem. Ind. (London)*, 654 (1965).

Table I: Chemical Shift Differences

	HZ - (δ_{Z^2} - δ_{HZ^-})	MgZ	CaZ	SrZ	BaZ
$\Delta = -(\delta_{Z^2} - \delta_{MZ^-})$					
MIDA					
c Singlet	-0.64	-0.19	-0.06	0.10	0.08
d Singlet	-0.64	-0.15	-0.12	0.10	0.10
HEIDA					
b Triplet	-0.35	-0.11	-0.08	-0.08	...
c Triplet	-0.66	-0.12	0.11	0.13	...
d Singlet	-0.61	-0.16	0.04	0.03	...
	H ₂ Z ²⁻ - (δ_{Z^2} - $\delta_{H_2Z^{2-}}$)	MgZ ²⁻	CaZ ²⁻	SrZ ²⁻	BaZ ²⁻
$\Delta = -(\delta_{Z^2} - \delta_{MZ^{2-}})$					
EDTA ⁹					
c Singlet	-0.91	0.01	0.08	0.16	0.20
d Singlet	-0.65	-0.03	-0.01	0.04	0.06
EGTA ^{9,10}					
a Singlet	-0.07	-0.11	-0.15	-0.09	-0.05
b Triplet	-0.27	-0.00	-0.07	-0.02	0.01
c Triplet	-0.69	-0.10	-0.03	0.10	0.16
d Singlet	-0.62	-0.13	-0.05	0.06	0.08



(inflexion I in Figures 1 and 2 and Table I) indicates that this first proton is associated with the nitrogen atoms. Any further protonation must involve the carboxylate groups since only d protons are significantly deshielded at inflexion II. The appreciable downfield chemical shifts of the b protons of HEIDA in the presence of metal ions at high pH values indicates that the hydroxyl oxygen atom is involved in coordination. This additional binding is undoubtedly the reason for the enhanced stability of the 1:1 complexes of HEIDA¹¹ with Ca²⁺ (log *K* = 4.63), Sr²⁺ (log *K* = 3.77), and Ba²⁺ (log *K* = 3.42) as compared to those with MIDA,¹¹ which have log *K* values of 3.75, 2.85, and 2.59, respectively. The strain involved in forming another chelate ring around the small Mg²⁺ ion, in the HEIDA complex, apparently compensates for any increase in stability expected from formation of an extra bond, leading to log *K* values of 3.44 for both of these ligands with the magnesium ion. Chelate complexes between aminocarboxylate ligands and Mg²⁺ ions almost always have endothermic heats of formation due, at least in part, to the strain involved in the chelate rings.¹²

The inductive effect of positively charged metal ions would be expected to deshield protons on the ligands, but in many cases an increase in shielding is seen, as

shown in Table I. This has been termed "long range" shielding by Day and Reilly.¹³ It is clear that complex formation gives rise to more profound redistributions of electron densities within the ligands than could have been anticipated purely on the basis of the electron attracting capabilities of the positively charged metal ions. In complexes involving large ions with low charge densities, such as Sr²⁺ and Ba²⁺, inductive deshielding effects would be expected to be small. In such cases the structural requirements imposed upon the ligands by the metal ions must give rise to electronic distributions in which the negative charge density in the environments of the nonlabile protons is enhanced over that in the free anions. In complexes with all four metal ions, the c protons are shielded to the greatest extent. Since rotation about single bonds can bring carboxylate oxygen atoms into close proximity with the c hydrogens, a significant contribution to shielding must be assigned to the carboxylate groups.

In cases where a downfield shift is observed, binding of a ligand site adjacent to the shifted protons is indicated; hence, it can be concluded from shifts in the c proton resonances, shown in Table I, that magnesium-nitrogen bonds are formed with MIDA, HEIDA, and EGTA, and calcium-nitrogen bonds are formed with MIDA and EGTA. Since inductive deshielding must outweigh long-range shielding effects for a net downfield shift to be observed, the absence of such a shift does not preclude binding. For all four ligands in Table I, the greatest deshielding of the nonlabile protons is observed for the magnesium complexes. This suggests that stronger bonds are formed between the Mg²⁺ ion and the ligands than with the Ca²⁺ ion and is the order anticipated on the basis of electrostatic potentials of the cations. The conclusion is not inconsistent with the fact that the thermodynamic stabilities of the calcium complexes are greater than those of the magnesium complexes¹⁴ since thermodynamic functions measure energy differences between the free (hydrated) and complexed species, while spectral changes are related to specific interactions within the complexes themselves. In further support of stronger bonding in the magnesium complexes, it has been suggested by Grigor'ev, *et al.*,¹⁵ on the basis of shifts ob-

(11) G. Schwarzenbach, G. Anderegg, W. Schneider, and H. Senn, *Helv. Chim. Acta*, **38**, 1147 (1955).

(12) G. H. Nancollas, "Interactions in Electrolyte Solutions," Elsevier Publishing Co., Amsterdam, 1966.

(13) R. J. Day and C. N. Reilly, *Anal. Chem.*, **37**, 1326 (1965).

(14) "Stability Constants of Metal-ion Complexes," Special Publication No. 17, The Chemical Society, London, 1964.

(15) A. I. Grigorev, N. M. Prutkova, N. D. Metrofanova, L. L. Martynenko, and V. I. Spitsyn, *Dokl. Akad. Nauk SSSR*, **161**, 328 (1965).

served in the infrared spectra of the alkaline earth ion complexes of iminodiacetic acid and nitrilotriacetic acid, that the covalent character of the bonds in these complexes increases along the series Ba < Sr < Ca < Mg.

Liquid-Phase Radiolysis of 2,3,4- and 2,2,4-Trimethylpentanes. Interpretation of Carbon-Carbon Bond Rupture Reactions from the Effects of Additives

by T. Kudo¹

Laboratory of Physical Chemistry, Tokyo Institute of Technology, Ookayama, Meguro-ku, Tokyo, Japan (Received January 17, 1967)

Some recently reported results indicate that iodine does not act as a scavenging reagent only for reactive intermediates, *i.e.*, hydrogen atoms, free radicals, and electron and carbonium ions. In the radiolysis of pure cyclohexane, postirradiative addition of iodine resulted in liberating hydrogen iodide of $G(\text{HI}) = 0.4^2$ and gave rise to a new product with $\lambda_{\text{max}} \cong 270 \text{ m}\mu$, a region in which conjugated olefins are known to absorb.³ In the >5000-Å wavelength photolysis, gas-phase reactions of iodine atoms with *n*-butenes occurred effectively at 65° to yield butadiene and hydrogen iodide in addition to isomerization products.⁴

In the present work, the author has studied the effect of postirradiative addition of iodine on the products from γ -irradiated 2,2,4- and 2,3,4-trimethylpentanes, and has obtained remarkably reduced yields of olefin products. This implied that the radical yields of the products cannot be obtained by using iodine as a radical scavenging reagent. Based on this result, a revised interpretation is given of the previously reported G values of C-C bond rupture reactions of 2,2,4-trimethylpentane (2,2,4-TMP).⁵

Experimental Section

Materials. 2,2,4-TMP, Eastman, and 2,3,4-TMP, Phillips 99.5% grade, were passed through silica gel before use to remove possible olefins and were then used without further purification. In those experimental runs which were carried out with more than 10 mmoles/l. of added iodine, both of the hydrocarbons were used as received because the scavenging that occurred depended substantially upon the iodine used rather than on any impurities contained in unpurified samples. Iodine was of guaranteed grade and was used without

purification. Methyl methacrylate monomer (MMA), labeled extra pure, was used without further purification. The stabilizer, hydroquinone, was not removed. Authentic hydrocarbon samples for identification of radiolysis products were of adequate purity. All materials were commercially supplied by Soekawa Chemicals Co., Ltd.

γ -Ray Irradiations. A ⁶⁰Co γ irradiator, where a sample could be kept completely in the dark during irradiation, was employed. The absorbed dose rate was $1.76 \times 10^{17} \text{ ev g}^{-1} \text{ min}^{-1}$ as determined by the FeSO₄ dosimeter, taking $G(\text{Fe}^{3+})$ as 15.5. A glass cylinder, 3.5 cm in i.d. and 2.5 cm high, was used as an irradiation cell, in which 5 ml of the material for radiolysis was sealed after several degassing cycles in a conventional manner. Irradiations were carried out at room temperature to a total dose of $2.53 \times 10^{20} \text{ ev g}^{-1}$. Sample solutions of known concentration of iodine and MMA were prepared, respectively, from weighed amounts of 8.2 to 42 mg of iodine and volumetrical addition of 7.5 to 48 μl of MMA. In experiments with postirradiatively added iodine, pure 2,2,4- or 2,3,4-TMP samples were irradiated, hydrogen and methane were evacuated from the sample frozen at 77°K, and the sample was distilled into other cells with break-off seals in which a known weight of iodine had been sublimed. The samples prepared in this way were held at room temperature for more than 1 day before analysis in order to promote unknown but apparently existing reactions in the cell.

Analysis of Products. The methods were the same as those described in the previous note.⁵ Hydrogen and methane were analyzed by *P-V-T* measurements conventional in this laboratory. Other products were analyzed by gas chromatography.

Results and Discussion

2,3,4-Trimethylpentane. G values (molecules/100 ev) of hydrogen, methane, and the C₃ and C₅ products formed by carbon-carbon bond rupture are shown in Table I. It should be noted from the results of runs 1 and 2 that material balance between C₃ and C₅ products is very good, on which basis parenthesized values of C₅ are recalculated and used thereafter. Results of experiments with added iodine are shown in runs 3 to 8. For the yields of propane, isopentane, and iso-

(1) The Government Chemical Industrial Research Institute, Tokyo, Hon-machi 1, Shibuya-ku, Tokyo, Japan.

(2) J. Roberts and W. H. Hamill, *J. Phys. Chem.*, **67**, 2446 (1963).

(3) S. Z. Toma and W. H. Hamill, *J. Am. Chem. Soc.*, **86**, 1478 (1964).

(4) M. H. Back and R. J. Cvetanović, *Can. J. Chem.*, **41**, 1406 (1963).

(5) T. Kudo and S. Shida, *J. Phys. Chem.*, **67**, 2871 (1963).

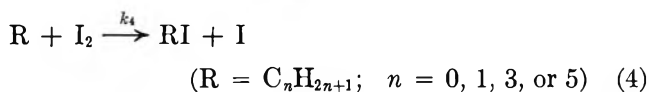
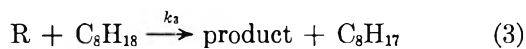
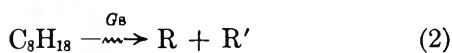
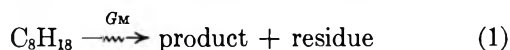
Table I: G Values^a for Products from γ -Irradiated 2,3,4-Trimethylpentane at a Total Dose of 2.5×10^{20} ev g⁻¹

Run	Additive, mM	Product					
		H ₂	CH ₄	C ₃ H ₈	C ₅ H ₈	<i>i</i> -C ₆ H ₁₂	<i>i</i> -C ₈ H ₁₆
1, 2 ^b	...	3.32	0.49	1.44	1.68	2.93 (2.70)	0.46 (0.42)
3	I ₂ (6.8)	2.29	0.30	0.85	1.12	1.3 (1.2)	0.25 (0.23)
4	I ₂ (11.7)	2.24	0.25	0.74	0.84	1.4 (1.3)	0.18 (0.17)
5	I ₂ (14.2)	2.15	0.25	0.83	0.67	1.3 (1.2)	0.10 (0.09)
6	I ₂ (16.5)	2.13	0.23	0.72	0.57	1.2 (1.1)	0.06 (0.06)
7	I ₂ (23)	2.11	0.23	0.74	0.44	1.3 (1.2)	0.03 (0.03)
8	I ₃ (30)	2.06	0.23	0.67	0.34 ^d	1.23 (1.13)	0 (0)
9	MMA (14)	3.08	0.41	0.98	1.39	2.1 (2.0)	0.43 (0.40)
10	MMA (55)	2.52	0.28	0.75	1.00	1.3 (1.2)	0.31 (0.29)
11	I ₂ ^c (17)	1.54	0.53	2.8 (2.5)	0.50 (0.46)
12	I ₂ ^c (23.6)	1.69	0.52	3.15 (2.9)	0.46 (0.42)
13	I ₂ ^c (29)	1.75	0.38	3.2 (2.9)	0.36 (0.33)

^a G values (molecules/100 ev) given in this table were obtained from yields in μ moles multiplied by 0.0688 and values in parentheses were calculated based on the normalized $G_0(\text{C}_3)$ taken to be equal to $G_0(\text{C}_5) = 1.44 + 1.68 = 3.12$, which assumes complete material balance between C₃ and C₅ products. Dropped numbers indicate relative errors between analytical data. Absolute experimental values may contain about 3% errors maximum. ^b Mean G_0 values obtained from two runs are presented on this line. ^c Iodine was postirradiatively added *in vacuo* after hydrogen and methane were removed. ^d This value may become zero beyond the saturated concentration of iodine.

pentenes, limiting values are attained. Also, for propylene, a limiting value of zero is to be expected, based on an equation applied to hydrogen by Forrestal and Hamill⁶ and Hardwick.⁷

The following reaction scheme, mainly occurring in the system with added iodine, is considered.



where R is, as a first approximation, necessarily fated to form RH and not to recombine or disproportionate with other radicals. From the steady-state kinetics, expression 5 is obtained.

$$\frac{1}{G_{I_2}} = \frac{1}{G_S} \left[1 + \frac{k_3 (\text{C}_8\text{H}_{18})}{k_4 (\text{I}_2)} \right] \quad (5)$$

where G_{I_2} is a reduced yield of a product at a known concentration of I₂, and G_S is a scavenged yield of the product at infinite concentration, and therefore is a constant. (I₂)₀, the concentration of iodine initially added in 2,3,4-TMP, was assumed to be invariable within a rough approximation. Experimentally, there is no apparent fading of color of iodine as shown similarly in the case of 2,2,4-TMP.⁸ This type of equation has successfully been applied to the case of R = H.^{6,7}

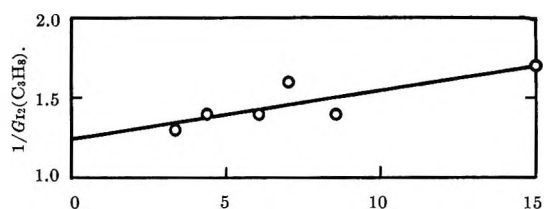


Figure 1. Kinetic plot for the reaction of propyl radicals with iodine in 2,3,4-trimethylpentane.

Figure 1 shows an example of least-square plotting for propane. Very curiously, the plots for the olefinic products showed good linearity. Calculated G_M values for all the products but the olefins were reasonably in accord with the limiting values estimated from Table I: 1.99, 0.18, 0.63, and 1.17 for H₂, CH₄, C₃H₈, and *i*-C₆H₁₂, respectively. k_3/k_4 for H₂, CH₄, and C₃H₈ were found in the same order of magnitude: 2.5, 6.3 and 4.2×10^{-4} , respectively, and 5.6×10^{-5} for *i*-C₆H₁₂ is smaller by a factor of 10. A value 3.8×10^{-4} has been reported for H₂ from cyclohexane using iodine as a scavenger.⁶ Hardwick obtained for H₂ $k_3/k_4 \sim 10^{-3}$ for several alkanes using MMA as a scavenger.⁹ This may indicate that k_4 is larger for I₂ than for MMA.

Molecular yields are calculated from the results for C₃ and C₅ shown in runs 8 to 13 in Table I. It is as-

(6) L. J. Forrestal and W. H. Hamill, *J. Am. Chem. Soc.*, **83**, 1535 (1961).

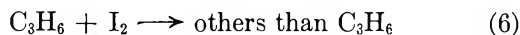
(7) T. J. Hardwick, *J. Phys. Chem.*, **66**, 1611 (1962).

(8) Reference 3, cited in ref 2 of this paper.

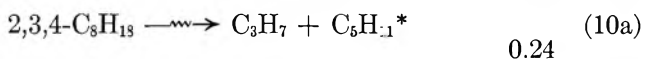
(9) T. J. Hardwick, *J. Phys. Chem.*, **65**, 101 (1961).

sumed that I₂ scavenger (run 8) gives true molecular yields for alkanes, and that MMA scavenger gives true molecular yields for olefins. The molecular olefinic yields (run 10) are normalized to the alkane yields in run 8 to give the following set of yields: 0.67 for propane, parenthesized 1.13 for isopentane, $1.0 \times 0.67/0.75 = 0.89$ for propylene, and parenthesized $0.29 \times 1.2/1.3 = 0.27$ for isopentene. Scavenged yields for the C₃ and C₅ products may be obtained by subtracting these "molecular" yields from the *G* values measured without additives (*G*₀, runs 1 and 2). The molecular and scavenged yields for the products from γ -irradiated 2,3,4-TMP are given in Table II.

The values for the two olefins of run 8 in Table I seem not to represent real, unscavenged yields since the olefins are reduced in quantity with postirradiatively added I₂ (runs 11–13) while saturated hydrocarbon products C₃H₈ and *i*-C₅H₁₂ are not reduced. The increased alkane yields in runs 11–13 may be within experimental error and will not be discussed further. It seems to be quite reasonable that, in the radiolysis with added iodine, measured yields of olefins should generally result both from (a) radical or precursor scavenging reaction by iodine and (b) postirradiative reaction of iodine with olefins, *e.g.*, propylene as



Providing that the additives used to make up Table II tolerably scavenged radical species without suffering interference with ionic processes and that C–C bond ruptures for the formation of C₃ and C₅ occurred in the set of reactions 7–11, *G* values of the reactions are calculated as



where asterisks are used to indicate those excited neutral species which are not scavengeable. In the calculation, *G* values in Table II were used as follows: *e.g.*, $G_S(\text{C}_3\text{H}_7) = 0.77 + 0.79 = 1.56 = G(7) + G(10)$, $G_M(\text{C}_3\text{H}_8) = 0.67 = G(8) + G(11)$. The *G* value given for reaction 7 may be a lower limit because of the possibility that the products react further.

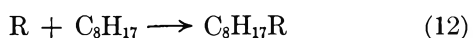


Table II: Molecular and Scavenged Yields for Products from γ -Irradiated 2,3,4-Trimethylpentane at a Total Dose of 2.5×10^{20} ev g⁻¹

	Product					
	H ₂	CH ₄	C ₃ H ₈	C ₃ H ₆	<i>i</i> -C ₅ H ₁₂ ^a	<i>i</i> -C ₅ H ₁₀ ^a
<i>G</i> ₀	3.32	0.49	1.44	1.68	2.70	0.42
<i>G</i> _M	2.06	0.23	0.67	0.89	1.13	0.27
<i>G</i> _S	1.26	0.26	0.77	0.79	1.57	0.15

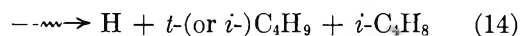
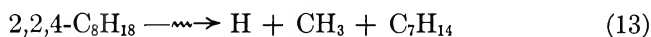
^a Obtained from the parenthesized value in Table I.

where R = C₃H₇ or C₅H₁₁, but by assuming rough equivalence of the reactivities of these radicals to C₃H₁₇ and other radicals produced, one can consider the C₃–C₅ bond rupture reactions¹⁰ to be based only on complete material balance (Table I), as shown for (7)–(11). If reactions 10 and 11 occur exclusively *via* the processes of type b, *G* values of both reactions correspond quantitatively to relative intensities (R.I.) from 50-v mass spectral data,¹¹ as shown below.

$$\text{R.I.}(\text{C}_3\text{H}_7^+)/\text{R.I.}(\text{C}_5\text{H}_{11}^+) = 100/61.9 = 1.62$$

$$G(\text{C}_3\text{H}_7^+)/G(\text{C}_5\text{H}_{11}^+) = 0.40/0.24 = 1.67$$

2,2,4-Trimethylpentane. The same remarkable postirradiative effect of iodine on isobutene was also found in the case of propylene with 2,3,4-TMP. Tables II and III were obtained from Table I. Because of a lack of other necessary experimental values, we cannot calculate decisively the *G* values of C₁–C₇ and C₄–C₄ bond rupture reactions. One of the problems in the calculation is to decide whether the following type of reaction should be taken into account



This reaction appeared to have a foundation because of data obtained spuriously with pure 2,2,4-TMP and 2,2,4-TMP-I₂ solutions.⁵ Williams¹² has energetically presented the possibility of its existence for neo-type alkanes. Falconer¹³ has suggested that 2-methylallyl radicals are produced by the reaction of hydrogen atoms with isobutene. These facts seem to verify its existence in general.

Importance of the Interaction of Olefinic Products and

(10) The definition of "structure of reaction" is given in T. Kudo and S. Shida, *J. Phys. Chem.*, **71**, 1971 (1967).

(11) American Petroleum Institute Research Project 44, "Catalog of Mass Spectral Data," National Bureau of Standards, Washington, D. C.

(12) T. F. Williams, *Trans. Faraday Soc.*, **57**, 755 (1961).

(13) J. W. Falconer, *Nature*, **198**, 985 (1963).

Table III: Molecular and Scavenged Yields for Products from γ -Irradiated 2,2,4-Trimethylpentane at a Total Dose of 2.5×10^{20} ev g^{-1}

	Product						
	H ₂	CH ₄	C ₃ H ₆	<i>i</i> -C ₄ H ₁₀	<i>i</i> -C ₄ H ₈	C ₇ H ₁₆ ^c	C ₇ H ₁₄ ^c
G ₀	2.19	1.27	0.27	2.75	2.1	0.44	0.83
G _M	1.25 ^a	0.57 ^a	0.19 ^b	1.1 ^a	1.0 ^b	0.15 ^a	0.58 ^b
G _S	0.94	0.70	0.08	1.65	1.1	0.29	0.25

^a Value obtained with iodine. ^b Value obtained with MMA. ^c Corrected value based on material balance between CH₄ and C₇ products and taking $G(\text{CH}_4) = 1.27$ for pure 2,2,4-TMP.

Iodine in the Radiolytic Environment. The evidence of the existence of reactions between olefinic products and iodine, shown, for example, by reaction 6, should make one cautious of using iodine as an additive in radiolysis or photolysis. Since, in the cases of reaction 6 and of isobutene in the radiolysis of 2,2,4-TMP, conjugated olefins cannot be formed without addition of a carbon-carbon bond or rearrangement of the skeleton of carbon atoms, a more general reaction mechanism concerning the conjugated olefin formation suggested by Hamill, *et al.*,^{2,3} is implied. In the gas phase, interaction also occurs.¹⁴

Acknowledgment. The author wishes to thank Professor S. Shida for his kind advice, and Mr. H. Tomita of the Government Chemical Industrial Research Institute, Tokyo, for his very helpful criticisms with respect to purities of the materials used in this work.

(14) T. Miyazki, unpublished results.

A Nuclear Quadrupole Resonance Study of Several Tribromide Ions

by Gary L. Breneman and Roger D. Willett

Department of Chemistry, Washington State University, Pullman, Washington 99163 (Received February 21, 1967)

Structure studies of several compounds containing the tribromide ion have shown that the configuration of the tribromide ion can vary considerably depending on the cation present in the crystal. In $[(\text{CH}_3)_3\text{NH}^+]_2\text{Br}^-\text{Br}_3^-$, the tribromide ion is very nearly symmetrical with bond lengths of 2.53 and 2.54 Å.¹ In CsBr₃, the tribromide ion is definitely not symmetrical with bond lengths of 2.44 and 2.70 Å.² In PBr₇, the tribromide ion is distorted even further with bond lengths of 2.39 and

2.91 Å.³ In all three cases the ions are nearly linear with the angles between the bonds being 171, 177.5, and 177.3°, respectively. A nuclear quadrupole resonance (nqr) study of these compounds was undertaken to determine the differences in charge distribution on the different tribromide ions. NH₄Br₃ was also included in this study since its lattice constants and space group⁴ indicate it has the same structure as CsBr₃.

Samples of PBr₇, CsBr₃, and NH₄Br₃ were prepared as described earlier.²⁻⁴

The $[(\text{CH}_3)_3\text{NH}^+]_2\text{Br}^-\text{Br}_3^-$ was prepared by adding Br₂ to (CH₃)₃NHBr in CCl₄. The solvent evaporated leaving a red, viscous liquid. After about 3 weeks this liquid crystallized into orange crystals. X-Ray analysis showed that the crystals had the same unit cell as $[(\text{CH}_3)_3\text{NH}^+]_2\text{Br}^-\text{Br}_3^-$. All of the samples were placed in glass vials, each holding about 3 cm³ of the sample.

The apparatus used to observe the nuclear quadrupole transitions was a superregenerative radiofrequency spectrometer quenched at about 300 kc/sec.^{5,6} The samples were enclosed in a brass shield that was immersed in an ice bath. Heating by the radiofrequency coil around the sample caused temperature variations of several degrees, so that the sample temperatures are only approximate. The resonances of both isotopes of bromine (Br⁷⁹ and Br⁸¹) were observed in all cases. The ratio of frequencies was measured to assign resonances to the proper isotopes. While frequencies could be measured to about 0.01%, errors in frequency of about 0.1% may exist because the shape of the lines made it difficult to identify the center of the resonance and the center of the oscillator frequency spectrum.

Since the tribromide ions whose structures have been determined are linear and the nqr results for NH₄I₃⁷ show that the asymmetry parameter is negligible in that case, it was decided that the assumption that the asymmetry parameter was essentially zero would be reasonable. This made possible a calculation of the coupling constants which are also shown in Table I. No resonances were found for $[(\text{CH}_3)_3\text{NH}^+]_2\text{Br}^-\text{Br}_3^-$. The range of frequencies searched was 420-350 Mc/sec in this case.

If some assumptions are made about the bonding in the tribromide ion, the formal charge for a given bro-

(1) C. Romers and E. W. M. Keulemans, *Proc. Koninkl. Ned. Akad. Wetenschap.*, **B61**, 345 (1958).

(2) G. L. Breneman and R. D. Willett, submitted for publication.

(3) G. L. Breneman and R. D. Willett, *Acta Cryst.*, in press.

(4) G. L. Breneman and R. D. Willett, in preparation.

(5) J. L. Ragle, Ph.D. Thesis, Washington State University, 1957.

(6) H. G. Dehmelt, *Z. Physik*, **130**, 356 (1951).

(7) S. Kojima, K. Tsukada, S. Ogawa, and A. Shimauchi, *J. Chem. Phys.*, **23**, 1963 (1955).

Table I: Nuclear Quadrupole Resonance Results

Compound	Bromine isotope	Temp, °C	Frequency, Mc/sec	Coupling constant	Atomic charge
PBr ₇	79	10	403.0	-806.0	0.047
	81	10	336.9	-673.8	
	79	0	286.6	-573.2	-0.256
	81	0	239.5	-479.0	
CsBr ₃	79	10	407.0	-814.0	0.057
	81	10	340.4	-680.8	
	79	0	251.7	-503.4	-0.347
	81	0	210.4	-420.8	
NH ₄ Br ₃	79	10	408.2	-816.4	0.60
	81	10	341.2	-682.4	

mine atom can be calculated from the coupling constant using the Townes and Dailey method.^{8,9} The effect of s and d hybridization and ionic character should be small in this case where the electronegativities are about the same, and π bonding should also be unimportant. The atomic coupling constant used for Br⁷⁹ was 769.76.⁹ The calculated charges are shown in Table I.

Since the qualitative MO approach of Havinga and Wiebenga¹⁰ was successful for I₃⁻, it should also be successful for Br₃⁻ in light of the similarity of the two ions shown in the comparison of configuration of the ions with total ion lengths.² Calculations were carried out for Br₃⁻ similar to those for I₃⁻. The zero approximation was identical with that for I₃⁻. In the first approximation, 0.2β was added to the Coulomb integral, α , to account for bromine being more electronegative than iodine, 0.1β was added for the two end atoms to account for the formal charge found in the zero approximation, and 0.1β and 0.3β were added for the end atom on the longer bond to account for the asymmetrical environments in CsBr₃ and PBr₇. The calculations were also carried out for a more extreme distortion by adding 1.7β to the atom on the long bond end.

The results of these calculations are compared to the actual configurations of the ions in Figure 1. If the results for the symmetrical ion and for the slightly distorted ion in CsBr₃ are compared with the results for I₃⁻,¹⁰ it is apparent that the charges are different. The only difference in the calculations for Br₃⁻ and I₃⁻ was the 0.2β added in the Br₃⁻ case to account for the greater electronegativity of bromine. This results in the charge being shifted slightly outward to the end atoms, as would be expected for an increase in electronegativity.

Since a qualitative picture of the charge distribution is now known, it is possible to assign the nqr frequencies to particular atoms in the tribromide ion by comparing

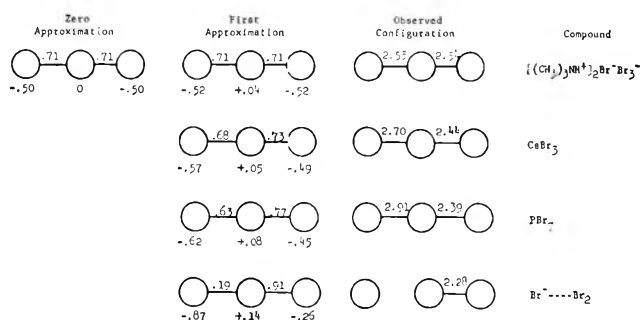


Figure 1. Comparison of MO calculations with configuration of tribromide ions.

the charge calculated from the observed frequency with the charges found in the MO calculations. The three frequencies that gave coupling constants larger than the atomic coupling constant and thus resulted in a very slightly positive charge can immediately be identified with the center atom in the tribromide ion. The two frequencies that gave coupling constants smaller than the atomic coupling constant and thus resulted in a slightly negative charge can be identified with the end atom on the short bond.

It can be seen that the nqr results are extremely sensitive to the configuration of the tribromide ion, especially for the end atom where the frequency changed from 251.7 to 286.6 Mc/sec in going from CsBr₃ to PBr₇ while the short bond length changed by only 0.21 Å. It may be possible to predict fairly accurate bond lengths just from the nqr frequency of the end atom. The charges on the center atom show behavior not predicted by the MO calculations. Assuming that Br₃⁻ is more distorted in NH₄Br₃ than in CsBr₃ as for I₃⁻ in NH₄I₃¹¹ and CsI₃,¹² the slightly higher charge for the center atom in NH₄Br₃ (0.060) than in CsBr₃ (0.057) is explained by the MO calculations: as distortion increases, the charge on the center atom also increases. It would be expected from this that the center atom in PBr₇ would have an even larger charge, but this is not observed. It can be seen in the calculations that even in the case where Br₃⁻ is almost dissociated into Br⁻ and Br₂, the charge on the center atom is still increasing. This is unrealistic as the charge on the atoms in Br₂ will be zero when dissociation is complete. Therefore, somewhere along in the distortion the charge

(8) C. H. Townes and B. P. Dailey, *J. Chem. Phys.*, **17**, 782 (1949).

(9) T. P. Das and E. L. Hahn, "Nuclear Quadrupole Resonance Spectroscopy," Academic Press, Inc., New York, N. Y., 1958.

(10) E. E. Havinga and E. F. Wiebenga, *Rec. Trav. Chim.*, **78**, 724 (1951).

(11) R. C. L. Mooney, *Z. Krist.*, **90**, 143 (1935).

(12) H. A. Tasman and K. F. Boswijk, *Acta Cryst.*, **8**, 59 (1955).

on the center atom will stop increasing and start decreasing. It may be that the Br_3^- ion in PBr_7 is past this point. This explains the low value for the charge of the center atom (0.047).

Mass Spectrometric-Knudsen Cell Study of the Gaseous Oxides of Platinum¹

by J. H. Norman, H. Gene Staley,
and Wayne E. Bell

General Dynamics, General Atomic Division,
John Jay Hopkins Laboratory for Pure and Applied Science,
San Diego, California (Received February 27, 1967)

The existence of $\text{Pt}_x\text{O}_2(\text{g})$ as a major vaporizing species of platinum in oxygen at $\sim 1500^\circ$ has been demonstrated by Schäfer and Heitland^{2a} using data obtained by Holborn, *et al.*,^{2b} who employed a hot-wire method, and by Schneider and Esch,³ Elliott,⁴ Schäfer and Tebben,⁵ and Alcock and Hooper,⁶ who used transpiration methods. Alcock and Hooper varied the platinum activity by dissolving the metal in gold and showed that $x = 1$. Also, the kinetics of the oxidation of platinum has been studied.^{7,8} Several of the previous investigations^{3,4,6} yielded thermodynamic data for the formation of $\text{PtO}_2(\text{g})$.

The present investigation, which used a Knudsen cell-mass spectrometer technique: (1) confirmed the species $\text{PtO}_2(\text{g})$; (2) established the existence of $\text{PtO}(\text{g})$; (3) yielded thermodynamic data for the formation of the two oxide species; and (4) yielded enthalpy data for the vaporization of platinum metal.

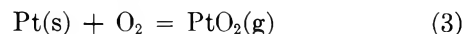
Experimental Section

The apparatus and methods used in this study quite closely parallel those previously employed.⁹ An alumina Knudsen cell was used that was loaded with platinum powder (Johnson Matthey, 99.99% purity), placed inside a molybdenum outer crucible, and heated by electron bombardment. The cell was provided with an oxygen-feed tube. The ratio of metal evaporating area to orifice area (orifice diameter, 0.16 cm; length, 0.12 cm) was greater than 100; this seems sufficient for the attainment of equilibrium, on the basis of the results of Fryburg and Petrus,⁸ which indicate that the formation of $\text{PtO}_2(\text{g})$ is quite rapid under our experimental conditions. Cell temperatures were determined optically by sighting onto the alumina crucible through two 0.16-cm holes in the outer molybdenum cell wall which was 0.08 cm thick. Furnace conditions

were adjusted to equate the optical temperatures for the top and bottom portions of the Knudsen cell.

Appearance Potentials. The ions PtO_2^+ , PtO^+ , and Pt^+ were observed and their appearance potentials were measured to be 11.2, 10.1, and 9.0 v, respectively, using the appearance potential of mercury (10.4 v) as a standard. A secondary appearance potential for PtO^+ (from PtO_2) occurred at 14.8 v. The accuracy of these potentials is believed to be ± 0.3 v. The measured appearance potential of Pt^+ is in good agreement with the first ionization potential for platinum (9.0 ± 0.1), according to Kiser's compilation.¹⁰

Identification of Vapor Species. To identify the vapor species, the oxygen pressure dependence of the intensities of the primary ions was determined at a potential of 14 v (which is below any determined secondary appearance potentials). Within experimental error, the PtO_2^+ signal was proportional to the oxygen pressure, P_{O_2} , the PtO^+ signal was proportional to $P_{\text{O}_2}^{1/2}$, and the Pt^+ signal was independent of P_{O_2} , indicating that all three ions were parent ions. These results show that the important vaporization reactions were



under the conditions of our experiments.

Vaporization of Platinum. In measuring the partial pressures of $\text{PtO}(\text{g})$ and $\text{PtO}_2(\text{g})$, it was desirable to use the vapor pressure of platinum as a reference; therefore, a cursory study of the evaporation of platinum was performed. The intensity of the Pt^+ signal, I_{Pt} , was measured as a function of temperature in the range 1750–2050°K in three separate determinations (about seven points per determination were obtained) without oxygen flowing into the cell. A few points were taken

(1) This research was supported in part by the U. S. Atomic Energy Commission under Contract AT(04-3)-164.

(2) (a) H. Schäfer and H. J. Heitland, *Z. Anorg. Allgem. Chem.*, **304**, 249 (1960); (b) L. Holborn, F. Henning, and L. Austin, *Abhandl. Deut. Akad. Wiss. Berlin, Kl. Math. Physik Tech.*, **4**, 85 (1904).

(3) V. A. Schneider and U. Esch, *Z. Elektrochem.*, **49**, 55 (1943).

(4) G. R. B. Elliott, UCRL-1831, 1952.

(5) H. Schäfer and A. Tebben, *Z. Anorg. Allgem. Chem.*, **304**, 317 (1960).

(6) C. B. Alcock and G. W. Hooper, *Proc. Roy. Soc. (London)*, **A254**, 551 (1960).

(7) E. K. Rideal and O. H. Wansbrough-Jones, *ibid.*, **A123**, 202 (1929).

(8) G. C. Fryburg and H. M. Petrus, *J. Electrochem. Soc.*, **108**, 496 (1961).

(9) J. H. Norman, H. G. Staley, and W. E. Bell, *J. Phys. Chem.*, **69**, 1373 (1965).

(10) R. W. Kiser, TID-6142, 1960.

Table I: Pressure Calibration Data

Species	Mass	Alumina cell, 2018°K			Platinum cell, 1933°K		
		$E - A^a$	I , mv	P , atm	$E - A^a$	I , mv	P_{PtO_2}/P_{O_2}
O	16	8.0	630	1.78×10^{-5}	8.4	165	
O ₂	34	9.1	123	5.5×10^{-4}	9.5	25	
Pt	195	5.6	2.80	(1.25×10^{-7})			8.6×10^{-8}
PtO	211	4.5	0.105	5.5×10^{-9}			
PtO ₂	227	3.4	0.073	4.7×10^{-9}	10.8	0.045	

^a E , ionizing potential; A , appearance potential.

Table II: Experimental PtO₂⁺ vs. T Data

A. Platinum Heat of Vaporization Study

T , °K	I_{Pt^+} , mv	T , °K	I_{Pt^+} , mv	T , °K	I_{Pt^+} , mv
2003	9.45	1943	3.95	1943	2.45
1938	3.10	2043	21.0	2023	8.40
2038	18.3	1851	0.885	1983	4.75
1913	2.22	1750	0.115	2058	15.2 ^a
1878	1.10	2003	11.7	1867	0.705
1983	8.05	1908	2.25	1908	1.40
1791	0.25	1802	0.395		
1834	0.60				
1760	0.105				

B. Platinum Monoxide Heat of Vaporization Study

T , °K	I_{PtO^+} , mv	T , °K	I_{PtO^+} , mv	T , °K	I_{PtO^+} , mv	T , °K	I_{PtO^+} , mv
1963	0.085	2003	0.095	2018	0.152	1973	0.125
2003	0.140	2048	0.157 ^a	1958	0.072	2008	0.178
2028	0.192	1978	0.070	1998	0.113	1928	0.073
1988	0.115	2028	0.120	2033	0.170	1993	0.157
1903	0.037	1933	0.047	1908	0.035	2038	0.255
1938	0.063	1918	0.025	1933	0.050	1913	0.065
1878	0.030	1958	0.050	1833	0.025	1958	0.100
						1898	0.050
						1873	0.033

C. Platinum Dioxide Heat of Vaporization Study

T , °K	$I_{PtO_2^+}$, mv	T , °K	$I_{PtO_2^+}$, mv	T , °K	$I_{PtO_2^+}$, mv	T , °K	$I_{PtO_2^+}$, mv
1968	0.194	1893	0.140	1978	0.245	1958	0.170
1998	0.202	1993	0.230	1835	0.125	1824	0.080
2033	0.235	2033	0.265	2013	0.265	1689	0.035
1933	0.155	1840	0.120	1683	0.050	1883	0.108
1862	0.120	1933	0.170	1883	0.140	1739	0.050
1893	0.130	1802	0.095	1745	0.070	1978	0.180
1829	0.090	1760	0.080				

^a Above Pt melting point.

at temperatures just above the melting point of platinum. Neither a vapor pressure nor a heat of vaporization discontinuity was noted; however, the anticipated

heat of vaporization or discontinuity was not expected to be resolvable by the data.

The resulting temperature dependence data, plotted

as $I_{\text{Pt}}T$ vs. $1/T$, yielded second-law $\Delta H_{1900} = 129.5 \pm 2.5$ kcal/mole for reaction 1, where 1900°K is the mean temperature of the measurements. The uncertainties are standard deviations of a single measurement. Combining the ΔH_{1900} value with $(H_T - H_{298})$ data from Stull and Sinke¹¹ gives $\Delta H_{298} = 131.9 \pm 2.5$ kcal/mole. This value agrees within experimental error with the second-law ΔH_{298} value of 135 ± 2 kcal/mole reported by Dreger and Margrave¹² and with the third-law ΔH_{298} values of 135 ± 0.85 kcal/mole reported by Dreger and Margrave,¹² 135 ± 1.0 kcal/mole reported by Hampson and Walker¹³ and 134.6 kcal/mole calculated by Hampson and Walker¹³ from the data of Jones, *et al.*¹⁴ The agreement among the various values is adequate justification for using reported vapor pressures of platinum to calibrate the Knudsen cell-mass spectrometer system for determination of the partial pressure of PtO(g) and PtO₂(g).

Gaseous Oxide Studies. To determine partial pressure values for the gaseous oxides, P_x , intensities, I_x^+ , of PtO₂⁺, PtO⁺, Pt⁺, O₂⁺, and O⁺ were measured simultaneously at 2018°K . In obtaining partial pressure values from these data, a vapor pressure value of 1.25×10^{-7} atm for platinum at 2018°K , as calculated from the equation given by Hampson and Walker,¹³ was accepted as correct. The ratio of cross sections, σ_x , of O and Pt was estimated to be 0.107, from information given by Otvos and Stevenson.¹⁵ Additivity of atomic cross sections was assumed. Multiplier gains inversely proportional to the square root of the molecular weight, $\sqrt{M_x}$, were used in the pressure calibration method described by Inghram and Drowart¹⁶ and by eq

$$P_x = \frac{KI_x^+T\sqrt{M_x}}{\sigma_x(E_x - A_x)} \quad (4)$$

4 where E_x is the ionizing voltage, A_x is the appearance potential, T is the temperature in $^\circ\text{K}$, and K is the general proportionality constant. This procedure gave partial pressure values described in Table I.

The $P_{\text{O}}/P_{\text{O}_2}^{1/2}$ ratio (7.6×10^{-4}) agrees with the value of 7.7×10^{-4} derived from data of Stull and Sinke.¹¹ This agreement suggests that the method of pressure calibration was satisfactory.

The temperature dependence of the intensity of PtO⁺ was measured in the range 1890 – 2040°K and that of PtO₂⁺ was measured in the range 1700 – 2040°K . The oxygen feed to the cell was held at a constant high level during the measurements. Four signal temperature dependence determinations were made for each ion and the data are presented in Table II. Plots of $\log(I_{\text{PtO}}T^{3/4})$ vs. $1/T$ and $\log(I_{\text{PtO}_2}T^{1/2})$ vs. $1/T$ yielded $\Delta H_{2000} = 100.5 \pm 4.6$ kcal/mole for reaction 2 and $\Delta H_{1900} = 36.6 \pm 2.3$ kcal/mole for reaction 3. The

fractional exponents associated with T arise because under constant O₂ flux according to the Knudsen equation the oxygen pressure varied with $T^{1/2}$. Using these values and the measured partial pressures, one calculates $\Delta S_{2000}^\circ = 19.5 \pm 2.3$ eu for reaction 2 and $\Delta S_{2000}^\circ = -5.0 \pm 1.1$ eu for reaction 3, assuming no errors in the pressure measurements (note that the calculation of the entropy for reaction 3 is independent of the pressure calibration and depends only on cross section ratios, gain ratios, etc.).

On the basis of the average of heat capacity data for MO(g)-type molecules given by Kelley,¹⁷ C_P for PtO(g) is estimated to be $8.45 + 0.03 \times 10^{-3}T - 0.83 \times 10^5T^{-2}$ cal/ $^\circ\text{K}$ mole. Combining this result with heat capacity data for Pt(s) and O₂, one obtains $\Delta C_P = -0.94 - 1.46 \times 10^{-3}T - 0.69 \times 10^5T^{-2}$ cal/ $^\circ\text{K}$ -mole for reaction 2.

Combining this value of ΔC_P with the ΔH_{2000} values given above, one obtains $\Delta H_{298}^\circ = 105 \pm 5$ kcal/mole and $\Delta S_{298}^\circ = 24.2 \pm 3$ eu for reaction 2. The uncertainties were estimated. Within the uncertainty, the ΔS_{298}° value is in accord with the typical entropy of formation (20.6 eu) for MO(g)-type molecules cited by Searcy.¹⁸ Also, using Brewer's¹⁹ $(F^\circ - H^\circ_0)/T$ value for PtO(g) and other values from Stull and Sinke,¹¹ a ΔH°_0 third-law value of 106 ± 6 kcal/mole was obtained for comparison.

No C_P data for PtO₂(g) or similar gaseous molecules were found; however, the ΔC_P for reaction 3 is probably near zero. Therefore, the ΔH and ΔS values cited above for this reaction are applicable at other temperatures but with a little greater uncertainty.

The enthalpy value for reaction 3 is in good agreement with $\Delta H^\circ_{1430} = 40.7$ kcal/mole reported by Schäfer and Tebben⁵ and $\Delta H^\circ_{1300} = 39.3$ kcal/mole reported by Alcock and Hooper.⁶ However, our entropy value for

(11) D. R. Stull and G. C. Sinke in *Advances in Chemistry Series*, No. 18, American Chemical Society, Washington, D. C., 1956, p 153.

(12) L. H. Dreger and J. L. Margrave, *J. Phys. Chem.*, **64**, 1323 (1960).

(13) R. F. Hampson and R. F. Walker, *J. Res. Natl. Bur. Std.*, **65A**, 289 (1961).

(14) H. A. Jones, I. Langmuir, and G. M. Mackay, *Phys. Rev.*, **30**, 201 (1927).

(15) J. W. Otvos and D. P. Stevenson, *J. Am. Chem. Soc.*, **78**, 546 (1956).

(16) M. G. Inghram and J. Drowart in "Proceedings of the International Symposium on High Temperature Technology," McGraw-Hill Book Co., Inc., New York, N. Y., 1959, pp 219–240.

(17) K. K. Kelley, U. S. Bureau of Mines Bulletin 584, U. S. Government Printing Office, Washington, D. C., 1960.

(18) A. W. Searcy in "Survey of Progress in Chemistry," Vol. I, A. F. Scott, Ed., Academic Press, Inc., New York, N. Y., 1963, pp 35–79.

(19) L. Brewer and M. S. Chandrasekharajah, "Free Energy Functions for Gaseous Monoxides," UCRL-8713 (1959).

reaction 3 is appreciably less than the $\Delta S_{1400}^{\circ} = 1.74$ eu and $\Delta S_{1300}^{\circ} = 0.93$ eu reported by these respective investigators. This difference means that our K_P values for reaction 3 are about a factor of 10 lower than values found by previous investigators using the transpiration method.

Because of the discord in the vapor pressure data for reaction 3, an experiment was performed to determine whether equilibrium pressures were being obtained under our conditions. An all-platinum Knudsen cell with added platinum wire was employed. The effective orifice area of this cell was about that of the alumina cell used in the previous measurements. The ratio of platinum (evaporation) surface area to orifice area using this system was at least a factor of 40 higher than using the alumina cell. Use of the platinum cell at 1933°K yielded a pressure ratio P_{PtO_2}/P_{O_2} that was essentially identical with the ratio found using the alumina cell at this temperature (see Table I), indicating that equilibrium was attained in both measuring systems.

The partial pressure data for PtO_2 determined mass spectrometrically are not in agreement with data obtained by previous investigators using the transpiration method. There appears to be little reason to question strongly the transpiration data. It is possible that the ionization efficiency for PtO_2 used in our studies is too high; *i.e.*, either electrons are not as effective as suggested by the model of Otvos and Stevenson¹⁵ or formation of undetectable fragments such as $Pt^+ + K.E.$, $PtO^+ + K.E.$, O^+ or O_2^+ is pronounced. Lack of agreement with vapor pressures measured by other methods for certain noble metal oxides has been suspected in other cases²⁰ and calls for a study of ionization cross sections, if at all feasible.

(20) J. H. Norman, H. G. Staley, and W. E. Bell, "Mass Spectrometric Study of the Noble Metal Oxides: Ruthenium-Oxygen System," General Atomic Report GA-7468 (1966).

Ethane Diffusion in Ion-Exchanged Synthetic Zeolites of Type A Containing Water

by W. Rudloff^{1a} and W. W. Brandt^{1b}

Department of Chemistry, Illinois Institute of Technology, Chicago, Illinois 60616 (Received March 7, 1967)

The diffusion of gas molecules in zeolites and the self-diffusion of mobile cations in these materials are undoubtedly and strongly dependent on the crystal

structure *per se*, and on the number and types of structural defects present.² If one wishes to study the diffusion mechanism, it is at times very advisable to use zeolite samples of identical origin and geometry, modified by ion exchange or by the introduction of "guest" molecules other than the diffusate. In this way, the structural characteristics mentioned above become relatively unimportant and the attractive or repulsive interactions of diffusate, guest molecules, mobile cations, and the crystal lattice, as well as the possible cooperation between these species, can be seen more clearly.

This approach has been used by several other authors^{3,4} and in the present study. It seems to be sound as long as the zeolite structure is not appreciably altered owing to the ion exchange or uptake of guest molecules.⁵

The various alkali ion exchanged forms of a zeolite sorbent are of particular interest because model calculations on the ion-molecule and ion-lattice interactions to be expected in some such systems have been reported in the literature.^{3,4,6} Similarly, the idea of cooperation between diffusing and (relatively) stationary species is not new³ but calls for careful testing by experiment.

Experimental Section

The samples used in the present study have been described earlier.⁴ The mobile cations were exchanged using the percolation method of Freeman and Stamires.⁷ The mole ratios of [alkali ions introduced]/[residual calcium (plus sodium) present in the original material] were 1.3, 2.4, and 2.0, for the Li^+ , Na^+ , and K^+ forms, respectively. The degassed zeolite contained less than 0.05% H_2O prior to the experiments.

The experimental method and the data treatment were described previously.^{2a,8}

(1) (a) Abstracted, in part, from the work done by W. Rudloff in partial fulfillment of the research requirement for the Ph.D. degree in the Department of Chemistry at Illinois Institute of Technology; (b) Department of Chemistry, University of Wisconsin-Milwaukee, Milwaukee, Wis. 53201.

(2) (a) W. W. Brandt and W. Rudloff, *Z. Physik. Chem.* (Frankfurt), **42**, 201 (1964); (b) L. L. Ames, *Am. Mineralogist*, **50**, 465 (1965).

(3) R. M. Barrer, R. F. Bartholomew, and L. V. C. Rees, *J. Phys. Chem. Solids*, **24**, 51 (1963).

(4) W. W. Brandt and W. Rudloff, *ibid.*, **26**, 741 (1965).

(5) R. M. Barrer and D. L. Peterson, *J. Phys. Chem.*, **68**, 3427 (1964).

(6) R. M. Barrer and W. I. Stuart, *Proc. Roy. Soc. (London)*, **A249**, 464 (1959).

(7) D. C. Freeman and D. N. Stamires, *J. Chem. Phys.*, **35**, 799 (1961).

(8) W. W. Brandt and W. Rudloff, *J. Phys. Chem. Solids*, **25**, 167 (1964).

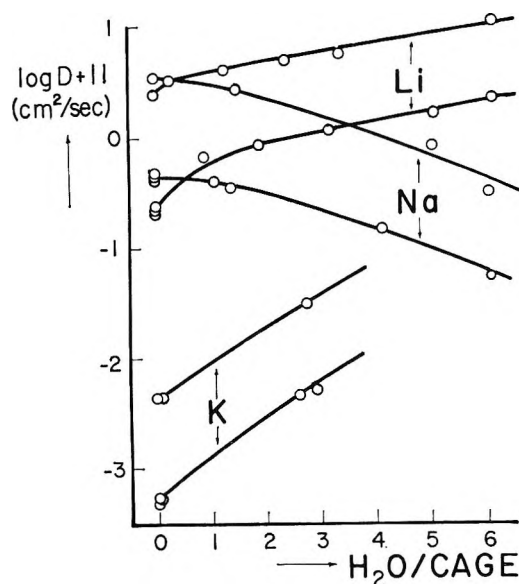


Figure 1. Logarithm of the ethane diffusion coefficients, D (cm^2/sec), against the average number of H_2O molecules present per cage of the synthetic zeolite of Type A, containing largely Li^+ , Na^+ , and K^+ exchangeable cations. The upper curve of each pair was obtained at an experimental temperature of approximately 78° , the lower at 24° .

Results and Discussion

The ethane diffusion coefficients obtained at several temperatures for the various cation-exchanged forms of the Type A zeolite are plotted in Figure 1 as a function of the amount of sorbed water present. One notes that both the actual values of the diffusion coefficients of ethane and their change with increasing H_2O concentration do not vary monotonically in the series Li^+ , Na^+ , and K^+ zeolite.

From electrical conductivity measurements it appears that Li^+ ions in a dehydrated zeolite interact very strongly with the sorption sites present on the internal surfaces of this sorbent.⁷ Also, Li^+ ions tend to be solvated more strongly than Na^+ or Li^+ in electrolytic solutions^{9,10} and presumably also in the zeolite. Finally, Barrer and Gibbons¹¹ noted that CO_2 sorbed on various ion-exchanged faujasites encountered the energetically most heterogeneous set of sorption sites in the Li^+ -exchanged form of that zeolite. In view of these results, it appears that the water molecules sorbed on the present samples before the ethane-diffusion experiments occupy some of the strongest sorption sites, presumably close to the Li^+ cations. As a consequence, ethane molecules are not immobilized from time to time, and thus there is no depression of the apparent diffusion coefficients, in contrast to the situation in dehydrated zeolite.¹² In accordance, the measured diffusion co-

efficients increase with the amount of water present in the sorbent.

In the K^+ -exchanged zeolite, it seems likely that the cation has to move somewhat to permit an ethane molecule to pass the "window" connecting two zeolite cavities.⁴ The sorption of water molecules probably causes a shift of the cation equilibrium position toward the interior of the cavity, similar to what has been found for the Na^+ -exchanged Type A zeolite.¹³ As a result, the degree to which a K^+ ion must cooperate in an ethane-diffusion step is lessened, and the corresponding diffusion coefficient increases with the H_2O concentration. In both Li^+ - and K^+ -exchanged zeolites, one would expect a decrease of the diffusion coefficients with increasing H_2O concentrations near saturation. This region is not investigated here because the pressure-volume method used in the present measurement⁸ does not allow one to keep large H_2O sorbate contents constant during a given ethane diffusion experiment.

In any case, the data obtained on the Na^+ -exchanged zeolite show (1) that in some respect H_2O molecules present can hinder the ethane diffusion, perhaps, but not necessarily, by steric interaction and (2) that results obtained on the Li^+ and K^+ zeolites, though superficially similar, are reasonably interpreted by making reference to two different molecular variables. This finding is analogous and perhaps related to the various changes in the electrical conductivity with the concentration of various guest molecules present.¹⁴

Acknowledgment. This work was supported by the U. S. Atomic Energy Commission under Contract AT-(11-1)-920.

(9) J. Kielland, *J. Am. Chem. Soc.*, **59**, 1675 (1937).

(10) A. Knappwost, W. Gunsser, and H. Lechert, *Z. Naturforsch.*, **21a**, 1200 (1966).

(11) R. M. Barrer and R. M. Gibbons, *Trans. Faraday Soc.*, **61**, 948 (1965).

(12) S. Crank, "The Mathematics of Diffusion," Oxford University Press, London, 1956, p 121, eq 8-3.

(13) P. A. Howell, *J. Phys. Chem.*, **64**, 364 (1960).

(14) D. N. Stamires, *J. Chem. Phys.*, **36**, 3174 (1962).

The Electron Spin Resonance Spectrum of Chloranilic Acid Trianion Radical

by M. Broze and Z. Luz

Isotope Department, The Weizmann Institute of Science, Rehovoth, Israel (Received March 23, 1967)

In the present work we wish to describe the esr spectrum of chloranilic acid trianion radical and discuss the

magnitude of the chlorine hyperfine splittings in relation to similar splittings in other π radicals. The radical (in the following referred to as DDBSQ) was prepared by reduction of 2,5-dihydroxy-3,6-dichloro-1,4-benzoquinone with sodium dithionite ($\text{Na}_2\text{S}_2\text{O}_4$) in alkaline aqueous solution (6 *N* NaOH) by a similar procedure to that described for the analogous radical 2,5-dioxo-1,4-benzosemiquinone (DBSQ).^{1,2} The radical is stable for many hours thus permitting an easy study of its esr spectrum. At low resolution the spectrum consists of a strong line with two pairs of satellites (see Figure 1) attributed to the two inequivalent kinds of ^{13}C atoms. The two pairs are slightly asymmetric and the inner one is not completely resolved from the main line. By comparison with the results for DBSQ^{1,2} and by arguments similar to those put forth by Das and Fraenkel,² it follows that the smaller and bigger splittings correspond, respectively, to carbon atoms 1 and 3 (numbering as in ref 2) with ^{13}C hyperfine splitting constants (hfs) of $a^1\text{C} = +2.71$ gauss and $a^3\text{C} = -8.17$ gauss. For comparison, the corresponding hfs in DBSQ are $+2.63$ and -6.66 gauss, respectively.

The next and more interesting feature of the esr spectrum of DDBSQ is the hfs due to the chlorine nuclei. This splitting can only be observed when the spectrum is recorded under conditions suitable for high resolution, *i.e.*, low-sweep field modulation amplitude and low microwave power. Optimal spectra were obtained

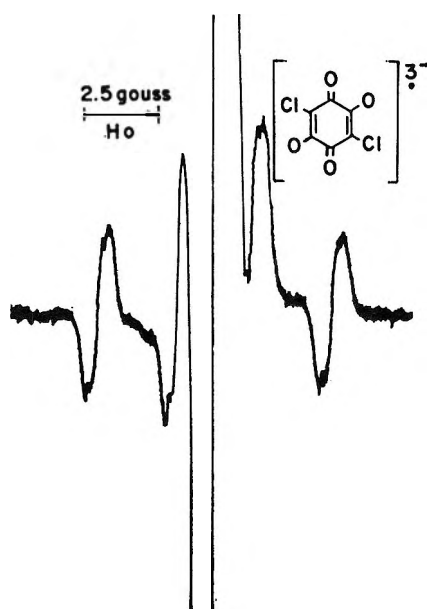


Figure 1. ^{13}C satellites in the esr spectrum of DDBSQ. The radical was prepared by reduction of chloranilic acid with $\text{Na}_2\text{S}_2\text{O}_4$ in alkaline aqueous solution. The structure observed in each of the satellites is due to unresolved splitting of the chlorine nuclei (*cf.* Figure 2).

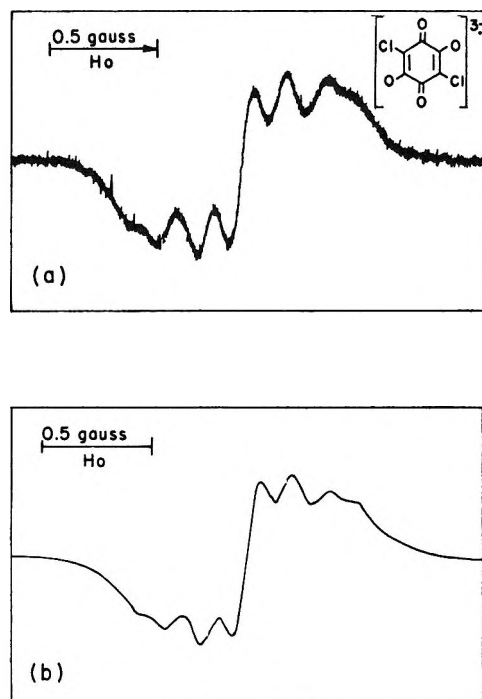


Figure 2. (a) The esr spectrum of the main line of DDBSQ. The modulation amplitude was 0.01 gauss and the radiofrequency power at the cavity about 3–4 mw. The structure is due to hyperfine splitting by the chlorine nuclei. (b) Computed spectrum of the derivative of the absorption line of DDBSQ with $a_{\text{Cl}} = 0.18$ gauss and $\Delta = 0.155$ gauss (see text).

by experimenting with different values of these parameters. In Figure 2(a) we present a typical spectrum of the main line of DDBSQ in which the structure, which we attribute to chlorine hfs, is clearly observed. To check this interpretation and to obtain values for the chlorine hfs constants, a_{Cl} , and the line width, we compared this spectrum with theoretically computed spectra of DDBSQ using various a_{Cl} and line-width values. The best fit was obtained with $|a_{\text{Cl}}| = 0.180 \pm 0.010$ gauss and $\Delta = 0.155 \pm 0.010$ gauss, where a_{Cl} refers to ^{35}Cl and Δ is half the width of half-maximum intensity of the absorption mode for all of the hyperfine components. The theoretically computed spectrum for these parameters is shown in Figure 2(b). This spectrum was calculated as a superposition of the spectra due to the various isotopic species of ^{35}Cl and ^{37}Cl , taking into account their natural abundance and their different magnetic moments. (Both isotopes have a magnetic spin quantum number of $3/2$.) It is interesting to note that a theoretical spectrum calculated by

(1) D. C. Reitz, F. Dravnieks, and J. E. Wertz, *J. Chem. Phys.* **33**, 1880 (1960).

(2) M. R. Das and G. K. Fraenkel, *ibid.*, **42**, 1350 (1965).

Table I: Chlorine Hfs and Calculated p- π Spin Densities for Some π Radicals

	$ a_{Cl} $, gauss	ρ_C^e	ρ_{Cl}^e	$ Q_{CCl}^{Cl} $, gauss
DDBSQ	0.18	-0.053	-0.001	3.4
2-Oxo-3-chloro-1,4-naphthoquinone	0.12 ^a	-0.036	-0.001	3.3
2,3-Dichloronaphthazarine	0.19 ^b	0.027	0.002	7.0
p-Chloronitrobenzene	0.24 ^c	0.167	0.003	1.4
o-Chloronitrobenzene	0.17 ^c	0.135	0.002	1.3
Perchlorodiphenylchloromethyl	2.5 ^d	0.544-1.03 ^f	0.010-0.040 ^f	4.6-2.5 ^f

^a Taken from ref 4. ^b Taken from ref 5. ^c Taken from ref 6. ^d Chlorine splitting due to the methyl chlorine atom.⁷ ^e ρ_{Cl} and ρ_C are the p- π spin densities on the chlorine and the neighboring carbon atoms, respectively, calculated by McLachlan's method.⁸ The molecular orbital parameters for chlorine were⁹ $\alpha_{Cl} = \alpha + 2.0\beta$ and $\beta_{CCl} = 0.4\beta$; the parameters for the nitro group were¹⁰ $\alpha_N = \alpha + 2.2\beta$, $\alpha_0 = \alpha + 1.4\beta$, $\beta_{NO} = 1.67\beta$, and $\beta_{CN} = 1.2\beta$. The average oxygen parameters in DDBSQ and in 2-oxo-3-chloro-1,4-naphthoquinone were¹¹ $\alpha_0 = \alpha + 1.42\beta$ and $\beta_{CO} = 1.46\beta$; and in 2,3-dichloro-1,4-naphthazarine were¹² $\alpha_0 = \alpha + 1.8\beta$ and $\beta_{CO} = 1.4\beta$. ^f The left and right figures correspond, respectively, to the C-Cl bond being coplanar and perpendicular to the two benzene rings.

considering ³⁵Cl nuclei only shows quite a different structure; in particular, the resolution of the outer lines of the septuplet is much more pronounced than in Figure 2.

Chlorine hfs values have been determined for only a small number of other π radicals.³ These are summarized in Table I.⁴⁻¹²

Venkataraman, Segal, and Fraenkel¹³ have carefully studied a number of chloro-substituted semiquinones but did not observe any chlorine hfs. For these compounds a_{Cl} is thus smaller than the corresponding line widths, *i.e.*, smaller than ~ 0.1 gauss.

The sign of a_{Cl} can, in principle, be determined from the variation in the line width of the various hyperfine components.² Unfortunately, it seems that in none of the compounds listed in Table I were these variations significant enough to make such a determination possible, and therefore only the absolute values of a_{Cl} are given.

It is common practice to compare hfs in π radicals with the p- π spin density distribution, and on physical grounds the following general expression for a_{Cl} is expected¹⁴

$$a_{Cl} = Q_{CCl}^{Cl} \rho_C + Q_{ClC}^{Cl} \rho_{Cl} \quad (1)$$

In this equation ρ_{Cl} and ρ_C are the p- π spin densities on the chlorine and neighboring carbon atoms, respectively, and the Q 's are the so-called σ - π interaction constants. Values for ρ are given in Table I. They were calculated by McLachlan's⁸ method, because this method gives a good fit with the proton hfs in the chloronitrobenzene radicals and avoids zero ρ_C values in DDBSQ and in 2-oxo-3-chloro-1,4-naphthoquinone. It may be seen that roughly a linear relationship exists between $|a_{Cl}|$ and both $|\rho_{Cl}|$ and $|\rho_C|$. However, because of the smallness of ρ_{Cl} , the second term in eq 1

is not expected to contribute significantly to a_{Cl} unless Q_{ClC}^{Cl} is of the order of 100 gauss. If we neglect this term, eq 1 reduces to

$$a_{Cl} = Q_{CCl}^{Cl} \rho_C \quad (2)$$

which is of the same form suggested for proton¹⁵ and fluorine¹⁶ hfs. In the last column of Table I we give values calculated for $|Q_{CCl}^{Cl}|$ using eq 2. Part of the scatter in these values is no doubt due to the unavoidable approximate nature of estimating spin densities, in particular small ones. In view of this limitation $|Q_{CCl}^{Cl}|$ may be considered quite constant and its values set in the range 1.5-3.5 gauss, though the absence of

(3) Very recently, R. O. C. Norman and B. C. Gilbert, *J. Phys. Chem.*, **71**, 17 (1967), have reported large hfs due to halogen nuclei in a number of iminoxy radicals. In these compounds, which are considered σ radicals, the dominant contribution to the hfs comes apparently from the direct overlap between oxygen and halogen orbitals in the molecular plane—a different mechanism from that described below for the π radicals.

(4) T. C. Hollocher, N. M. Tooney, and R. Adman, *Nature*, **197**, 74 (1963).

(5) L. H. Piette, M. Okamura, G. P. Rabold, R. T. Ogata, R. E. Moore, and P. J. Scheuer, *J. Phys. Chem.*, **71**, 29 (1967).

(6) P. B. Ayscough, F. P. Sargent, and R. Wilson, *J. Chem. Soc.*, 5418 (1963).

(7) M. Ballester and J. Riera, *J. Am. Chem. Soc.*, **86**, 4505 (1964).

(8) L. D. McLachlan, *Mol. Phys.*, **3**, 233 (1960).

(9) A. Streitwieser, Jr., "Molecular Orbital Theory for Organic Chemists," John Wiley and Sons Inc., New York, N. Y., 1961, pp 125, 126.

(10) P. H. Rieger and G. K. Fraenkel, *J. Chem. Phys.*, **39**, 609 (1965).

(11) M. Broze, Z. Luz, and B. L. Silver, *ibid.*, **46**, 4891 (1967).

(12) W. R. Miller, Jr., Ph.D. Thesis, Columbia University, 1965.

(13) B. Venkataraman, B. G. Segal, and G. K. Fraenkel, *J. Chem. Phys.*, **30**, 1006 (1959).

(14) M. Karplus and G. K. Fraenkel, *ibid.*, **35**, 1312 (1961).

(15) H. M. McConnell, *ibid.*, **24**, 633, 764 (1956).

(16) D. A. Anderson, P. J. Frank, and H. S. Gutowsky, *ibid.*, **32**, 196 (1960); see, however, M. Kaplan, J. R. Bolton, and G. K. Fraenkel, *ibid.*, **42**, 955 (1965).

chlorine hfs in the chloro-substituted semiquinones studied by Venkataraman, *et al.*,¹³ suggests a somewhat lower value for these compounds.

Following the theory for proton and ¹³C hfs, an expression for Q_{CCl}^{Cl} (neglecting overlap and bond polarity) may be derived^{14,15}

$$Q_{CCl}^{Cl} = -\frac{2}{\sqrt{3}} \xi(3s)_{Cl}^2 \eta \frac{\lambda^2}{1 + \lambda^2} \quad (3)$$

where $\xi = (8\pi/3)(\mu_{Cl}/I_{Cl})$, λ is the degree of hybridization of the chlorine bonding orbital, σ_{Cl}

$$\sigma_{Cl} = \frac{1}{\sqrt{1 + \lambda^2}} [\lambda(3s) + (3p)] \quad (4)$$

and η is the mixing coefficient of the excited state in the σ - π configuration interaction¹⁴ and is of the order of 5×10^{-2} . The value of $\xi(3s)_{Cl}^2$ was estimated from SCF wave functions to be 1.7×10^3 gauss,¹⁷ and, thus, using for Q_{CCl}^{Cl} the value -2.5 gauss where the sign is that expected from eq 3, we get about 2-3% 3s character in the bonding orbital σ_{Cl} (eq 4). Though small, a certain amount of hybridization is crucial to the understanding of chlorine hfs in π radicals. Hybridization of the same order of magnitude is also necessary to explain the magnitude and direction of the dipole moment in chloro-substituted organic compounds.¹⁸ However, the above picture is perhaps too simple-minded and other mechanisms may also contribute to chlorine hfs; in particular the neglect of the second term in eq 1 may be unjustified. It is also interesting to point out that in most of the examples listed in Table I the chlorine atom responsible for the splitting is geometrically close to some heteroatom, mostly oxygen. It is possible that nonbonding orbitals of, *e.g.*, oxygen may also play a role in chlorine hfs.

The spectrometer used was a Varian ESR X-band spectrometer, Model V 4502-12, with 100-kc/sec modulation frequency.

(17) M. C. R. Symons, *Advan. Phys. Org. Chem.*, **1**, 332 (1961).

(18) C. A. Coulson, "Valence," 2nd ed, Oxford University Press, London, 1961, pp 220, 221, 265.

Self-Consistent Field Correlations of Polarographic Oxidation Potentials

by Gerald Jay Gleicher and Mary Kay Gleicher

Department of Chemistry, Oregon State University,
Corvallis, Oregon 97331 (Received April 24, 1967)

One of the most successful applications of the Hückel molecular orbital (HMO) theory has been in the correla-

tion of polarographic oxidation and reduction potentials.¹ Hoijtink² has carried out such a correlation utilizing data obtained by Lund for the oxidation potentials of 11 aromatic hydrocarbons in acetonitrile at a silver-silver ion electrode.³ Pysh and Yang have treated a larger set of compounds in an examination of the oxidation potentials of 49 aromatic and alkylaromatic molecules in the same solvent at a rotating platinum electrode.⁴

As the Hückel theory makes no provision for electronic interactions, the experimentally obtained potential was plotted against the energy of the highest occupied molecular orbital from which the electron would be removed.

The purpose of this investigation was twofold in nature. First, it was felt that, even within the framework of the above simple method, a possible improvement of the correlation might be obtained if the energies of the highest occupied orbital were calculated *via* a self-consistent field (SCF) approach. The second aspect is even more fundamental in its nature. If electron interaction is explicitly included, as in an SCF approach, removal of a single electron from the highest occupied orbital will no longer yield the true electron configuration of the resulting radical cation. The reason for this lies in the fact that the unpaired electron will experience a different set of interactions with electrons of similar spin than with those of opposed spin.⁵ The energy of the resulting radical cation should, therefore, be independently calculated for some system in which electrons of α and β spin are not paired in the lower lying orbitals. Rather, the electrons should be considered as occupying different one-electron orbitals.⁶ If this model is utilized, it is possible to solve, *via* a single determinant, for the energy of the system.

The energies of the π -electron systems were calculated utilizing the appropriate closed-shell or open-shell modification of the SCF approach.⁷ In our calculations the two-center electron-repulsion integrals (ii , jj) were determined from the standard Pariser-Parr-Pople approach and the resonance integral, β , was derived from ground-state physical properties.⁸ Evaluation of the

(1) A. Streitwieser, Jr., "Molecular Orbital Theory for Organic Chemists," John Wiley and Sons, Inc., New York, N. Y., 1961, p 173 ff.

(2) G. J. Hoijtink, *Rec. Trav. Chim.*, **77**, 555 (1958).

(3) H. Lund, *Acta Chem. Scand.*, **11**, 1323 (1957).

(4) E. S. Pysh and N. C. Yang, *J. Am. Chem. Soc.*, **85**, 2123 (1963).

(5) L. Salem, "The Molecular Orbital Theory of Conjugated Systems," W. A. Benjamin, Inc., New York, N. Y., 1966, p 264 ff.

(6) J. A. Pople and R. K. Nesbit, *J. Chem. Phys.*, **22**, 571 (1954).

(7) A. L. H. Chung and M. J. S. Dewar, *ibid.*, **42**, 756 (1965).

(8) M. J. S. Dewar and G. J. Gleicher, *ibid.*, **44**, 759 (1966).

Table I: Correlation^a of Polarographic Oxidation Potentials

Molecule	$E_{112,ox}^{b,c}$	Energy of highest occupied orbital ^e		$\Delta E^{d,e}$
		Fixed bond	Variable bond	
Azulene	0.71	1.548	1.413	1.832
Naphthacene	0.77	1.948	1.740	2.236
Perylene	0.85	1.841	1.605	2.236
3-Methylcholanthrene	0.87	1.966	1.794	2.295
9,10-Dimethylanthracene	0.87	2.100	1.895	2.200
1,2-Benzpyrene	0.94	1.822	1.585	2.237
9-Methylanthracene	0.96	1.811	1.616	2.064
7,12-Dimethyltetraphene	0.96	1.964	1.779	2.247
3,4-Benztetraphene	1.01	1.651	1.450	1.960
1,12-Benzperylene	1.01	1.648	1.477	1.935
1,2,4,5-Dibenzpyrene	1.01	1.740	1.546	2.061
12-Methyltetraphene	1.07	1.691	1.512	2.003
7-Methyltetraphene	1.08	1.716	1.532	2.021
Anthracene	1.09	1.562	1.361	1.781
8-Methyltetraphene	1.13	1.620	1.425	1.899
1-Methyltetraphene	1.14	1.459	1.270	1.729
2-Methyltetraphene	1.14	1.612	1.423	1.885
3-Methyltetraphene	1.14	1.540	1.374	1.820
10-Methyltetraphene	1.14	1.602	1.424	1.882
11-Methyltetraphene	1.14	1.605	1.414	1.899
4-Methyltetraphene	1.15	1.555	1.350	1.834
5-Methyltetraphene	1.15	1.651	1.458	1.986
6-Methyltetraphene	1.15	1.583	1.403	1.886
9-Methyltetraphene	1.15	1.572	1.401	1.867
2,3,4,5-Dibenzpyrene	1.15	1.689	1.483	2.081
Pyrene	1.16	1.584	1.374	1.808
Tetraphene	1.18	1.481	1.292	1.758
1,2,5,6-Dibenzanthracene	1.19	1.450	1.256	1.830
Acenaphthalene	1.21	0.906	0.661	1.474
Coronene	1.23	1.433	1.253	1.685
1,2,3,4-Dibenzanthracene	1.25	1.371	1.230	1.705
1,2,7,8-Dibenzanthracene	1.26	1.398	1.230	1.664
4,5-Benzpyrene	1.27	1.451	1.296	1.719
Picene	1.33	1.389	1.174	1.680
Chrysene	1.35	1.327	1.138	1.587
2,3-Dimethylnaphthalene	1.35	1.276	1.025	1.414
2,6-Dimethylnaphthalene	1.36	1.289	1.186	1.420
1-Methylnaphthalene	1.43	1.203	1.046	1.337
2-Methylnaphthalene	1.45	1.104	0.967	1.243
Fluoranthene	1.45	1.146	1.001	1.347
Phenanthrene	1.50	1.061	0.903	1.281
Naphthalene	1.54	0.966	0.806	1.078
Triphenylene	1.55	0.955	0.884	1.198
Biphenyl	1.74	0.775	0.711	0.980
<i>p</i> -Xylene	1.77	0.750	0.768	0.586
Mesitylene	1.80	0.506	0.522	0.541
<i>o</i> -Xylene	1.89	0.612	0.623	0.614
<i>m</i> -Xylene	1.91	0.523	0.552	0.578
Toluene	1.98	0.363	0.383	0.345
Benzene	2.30	0.000	0.000	0.000

^a Taken relative to benzene equal to zero. ^b Reference 4. ^c In volts. ^d Based on energies calculated for structures with all bonds equal to 1.40 Å. ^e In electron volts.

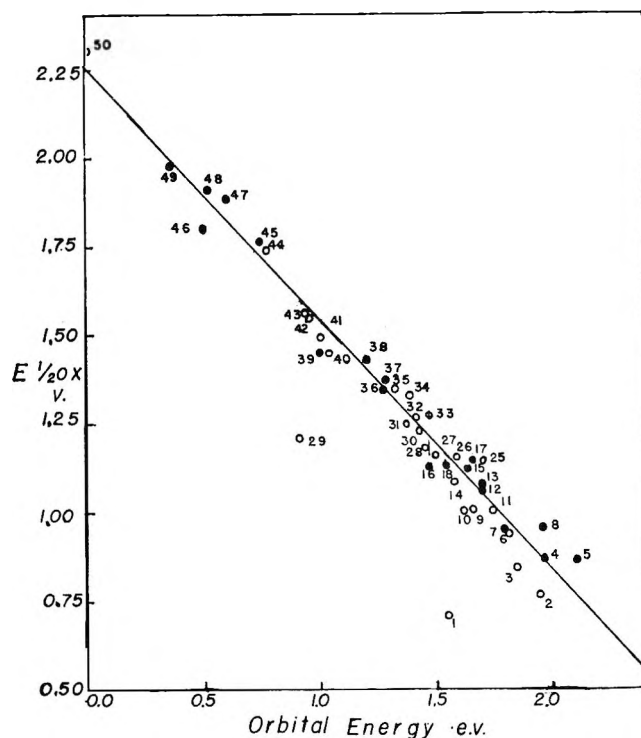


Figure 1. Plot of polarographic oxidation potentials against the energy of the highest occupied molecular orbital of the neutral molecule as calculated by an SCF approach with constant bond lengths. Points 19–24 have been omitted to preserve clarity: O, aromatic molecules; ●, alkylaromatic molecules. Numbering follows the order of Table I.

energy of the neutral molecules was carried out *via* two related methods. In the first, the molecule was treated with all bonds assigned an average length of 1.40 Å. In the second approach, an extra degree of self-consistency was introduced. At the end of each iteration new values for the internuclear separation between pairs of bonded atoms were determined *via* the relationship with the bond order shown in eq 1.

$$r_{ij} = 1.515 - 0.176p_{ij} \quad (1)$$

These in turn were used to reevaluate the corresponding electron repulsion integrals and resonance integrals.^{8,9} Calculations on the open-shell systems were performed utilizing the condition of a fixed geometry. The variable-bond-length approach was not utilized here because of possible errors associated with it for charged systems.¹⁰

As can be seen in Table I, nearly half the molecules considered are alkyl derivatives of aromatics. To take

(9) M. J. S. Dewar and G. J. Gleicher, *J. Am. Chem. Soc.*, **87**, 685 (1965).

(10) M. J. S. Dewar and C. C. Thompson, Jr., *ibid.*, **87**, 4414 (1965).

Table II: Constants for Linear Correlation

System	Ref	Slope	Intercept	Av dev	Correln coeff
Pysh and Yang	<i>c</i>	0.08	0.922
	<i>d</i>	0.05	0.982
Highest occupied orbital (fixed bond)	<i>a</i>	-0.700	2.226	0.06	0.955
	<i>b</i>	-0.711	2.259	0.04	-0.988
	<i>c</i>	-0.706	2.224	0.07	-0.931
	<i>d</i>	-0.757	2.308	0.03	-0.989
Highest occupied orbital (variable bond)	<i>a</i>	-0.792	2.233	0.06	-0.946
	<i>b</i>	-0.819	2.282	0.05	-0.984
	<i>c</i>	-0.807	2.209	0.07	-0.926
	<i>d</i>	-0.861	2.308	0.03	-0.990
Energy difference	<i>a</i>	-0.587	2.213	0.06	-0.963
	<i>b</i>	-0.582	2.217	0.05	-0.984
	<i>c</i>	-0.640	2.299	0.07	-0.940
	<i>d</i>	-0.631	2.308	0.04	-0.988

^a All points (50) treated. ^b All points but azulene and acenaphthalene (48) treated. ^c All unalkylated hydrocarbons (25) treated. ^d All unalkylated hydrocarbons but azulene and acenaphthalene (23) treated.

the effect of alkyl substitution into account, a simple inductive model was used in which the substituent was treated as lowering the valence state ionization potential of the carbon atom to which it was attached by 1.26 ev. This value has been empirically obtained by Streitwieser and utilized in discussions of ionization potentials and polarographic reduction potentials.¹¹

Table I presents the 50 systems which were considered. The oxidation potentials of 49 of these were taken from the study by Pysh and Yang.⁴ The 50th system, biphenyl, is the only compound examined by Lund³ which was not redone in the later work. Because of the difference in reference electrodes, Lund's values theoretically should be increased by 0.30 v.¹² Of the ten hydrocarbons common to both systems, however, Pysh and Yang's values average only 0.27 v higher than those of Lund. This latter factor was used in assigning a value to biphenyl. The values for the energies of the highest occupied orbitals and the energy differences between the radical cation and the closed-shell parent hydrocarbon are all given relative to that of benzene taken as zero. Thus, a number larger than zero indicates a hydrocarbon which is oxidized at a lower potential.

Linear correlation could be obtained when either the energy of the highest occupied orbital in the parent hydrocarbon or the energy difference between the radical cation and the parent system was plotted against the oxidation potential. The resulting equations are given by

$$E_{1/2ox} = aX + b \quad (2)$$

where *X* represents either of these calculated quantities. Table II lists the constants for this equation and related terms as calculated from a least-squares determination.

Comparison of the results obtained in this study with those of Pysh and Yang⁴ are of interest. In the earlier study, correlation of only the unalkylated hydrocarbons was attempted. The few alkyl derivatives examined deviated from the line calculated from the other points. The deviation of all of the alkyl points was negative. Inclusion of these points within an SCF calculation leads to no appreciable added uncertainty. Moreover, the points for these alkyl aromatics are randomly displaced about the least-squares line. As an example, a plot of the oxidation potential against the energy of the highest occupied orbitals as calculated in the fixed bond lengths approach is shown in Figure 1. The points for azulene and acenaphthalene are the only ones omitted in determining the correlation. These two points deviate significantly from the correlation just as in the earlier studies. The SCF approach utilized has had success in correlating the properties of nonalternant hydrocarbons. We conclude that the explanation of Pysh and Yang concerning specific interactions of these systems with solvent is probably correct. The only other nonalternant molecule considered was fluoranthene. The average deviation of the calculated oxidation potential from the experimental value based

(11) A. Streitwieser, Jr., *J. Phys. Chem.*, **66**, 368 (1962); A. Streitwieser, Jr., and I. Schwager, *ibid.*, **66**, 2316 (1962).

(12) R. C. Larson, R. T. Iwamoto, and R. N. Adams, *Anal. Chim. Acta*, **25**, 371 (1961).

on the 12 correlations shown in Table II is only ± 0.016 v for this system.

It appears that these SCF approaches give a small, but real, improvement over the HMO method used to date. The latter method, however, is definitely less complex and the question of whether the small improvement is worth the extra effort is a moot one. We feel that the real advantage of the calculations described here will be in treating nonalternant and alternant systems within the same correlation. Mention must also be made to the fact that the theoretically more sound idea of correlation with an energy difference rather than a ground-state property does not particularly improve results. It appears that in all of the systems treated here, a fortuitous correlation exists between this quantity and the energy of the highest occupied orbital. If this is truly general, future investigations should be greatly simplified.

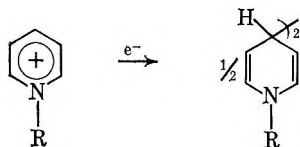
Acknowledgment. We wish to extend our thanks to the Computer Center of Oregon State University for generously supplying the facilities necessary for carrying out these calculations.

Anomalous Reductive Dimerizations of Alkylpyridinium Ions

by William T. Bowie¹ and Martin Feldman

Department of Chemistry, Howard University, Washington, D. C. (Received May 5, 1967)

The reductive dimerization of N-alkylpyridinium ions in aqueous solution, which yields 1,1'-dialkyl-1,1',4,4'-tetrahydropyridyls, may be brought about by sodium amalgam,² electrolysis,³ or chromous or vanadous ion.⁴



We have begun a study of the mechanism of reduction of stable organic cations with metal ions in order to compare the rates of electron transfer with the relative electron affinities of the cations.⁵ We have noted an apparent anomaly in the reduction of N-alkylpyridinium ions: according to their one-electron reversible polarographic reduction potentials in aqueous solution,

N-alkylpyridinium ions *should not be reduced* by chromous or vanadous ion.

Table I⁶⁻¹¹ summarizes the results of experiments in which salts of several organic cations were allowed to react with chromous perchlorate. The cations are listed in the order of their half-wave reduction potentials, the pyridinium ions being the most difficult to reduce. The chromous-chromic potential, relative to sce, is included, and those ions listed above this potential should not accept an electron from chromous ion.

Table I: Reduction of Organic Cations with Chromous Perchlorate

Cation	$-E_{1/2}$, v vs. sce	—Cr(ClO ₄) ₂ reduction—	
		Anion	Yield, %
1,2,4,6-Tetramethylpyridinium	(1.8) ^a	ClO ₄	32 (5 hr)
		Cl	47 (5 hr)
N-Methylpyridinium	1.47 ⁷	I	(b)
		NO ₃	0
N-Benzylpyridinium		Cl	34 (24 hr)
		NO ₃	0 (24 hr)
1-Benzyl-3-carbamidopyridinium	1.06 ⁷	ClO ₄	53 ⁸
2,4,6-Trimethylpyrylium	0.85 ^{5, 9}	ClO ₄	0 (12 hr)
		Cl	0 (12 hr)
Cr(II)	0.66 (E°)		
2,4,6-Triphenylpyrylium	0.30 ⁹	Cl	(c)
Tropylium	0.27 ¹⁰	ClO ₄	100 (rapid)
		Cl	100 (rapid)

^a Estimate based on charge-transfer spectra of iodide salt. See ref 6. ^b The dimer has not been isolated from this reaction or from the sodium amalgam reduction, but its characteristic behavior, including its unusual color changes, serves to establish its formation.¹¹ ^c As described in ref 4; actual yield not reported. Reduced by VCl₂ as well as CrCl₂.

As shown in Table I, we have found no evidence for the reduction of 2,4,6-trimethylpyrylium ion by chromous

- (1) NASA Predoctoral Trainee, 1966-1967.
- (2) A. W. Hofmann, *Ber.*, **14**, 1503 (1881).
- (3) B. Emmert, *ibid.*, **42**, 1997 (1909).
- (4) J. B. Conant and A. W. Sloan, *J. Am. Chem. Soc.*, **45**, 2466 (1923).
- (5) M. Feldman and S. Winstein, *Tetrahedron Letters*, 853 (1962).
- (6) M. Feldman, Ph.D. Thesis, University of California at Los Angeles, 1963.
- (7) P. C. Tompkins and C. L. A. Schmidt, *Univ. California Publ. Physiol.*, **8**, 237 (1944).
- (8) K. Wallenfels and M. Gellrich, *Chem. Ber.*, **92**, 1406 (1959). Coupling occurs at the 6 position for this ion.
- (9) E. Gird and A. T. Balaban, *J. Electroanal. Chem.*, **4**, 48 (1962).
- (10) P. Zuman and J. Chodkowsky, *Collection Czech. Chem. Commun.*, **27**, 759 (1962).
- (11) B. Emmert and R. Buchert, *Ber.*, **54**, 204 (1921).

perchlorate or chloride, which is in agreement with their relative reduction potentials. After 12 hr, zinc dust was added to the reaction mixture and the unreacted pyrylium ion was reductively dimerized to the known bipyran^{6,12} (90% yield). Bipyran which was added to the chromous solutions and allowed to stand for 24 hr could be recovered, and we conclude that chromous ion does not reduce the trimethylpyrylium ion. Similar experiments indicate that vanadous ion (E° 0.45 v vs. sce) is likewise ineffective in the reduction of the trimethylpyrylium ion.

In contrast to the expected behavior of the trimethylpyrylium ion, the pyridinium ions *are* reduced by chromous ion. The presence of halide ion seems to be required for the reduction of N-methyl and N-benzylpyridinium ions, but not for 1,2,4,6-tetramethylpyridinium ion.¹³ The apparent anomaly is not limited to chromous ion; zinc¹⁴ (E° 1.0 v vs. sce) reductively dimerizes N-benzylpyridinium chloride (99% yield), N-benzylpyridinium nitrate (38%), and N-methylpyridinium iodide¹⁵ in neutral aqueous solutions.

The reduction potentials of N-alkylpyridinium ions which have no ring substituents have been reported by several workers and are in the range of 1.3–1.5 v.^{7,16–18} These values appear reasonable, since the high reduction potentials of the pyridinium ions parallel the large charge-transfer transition energies of pyridinium iodides, relative to pyrylium or tropylium iodides.⁵ Thus, we cannot attribute the surprising behavior of the alkylpyridinium ions to inaccurate measurement of the reduction potentials, but we decline to offer an alternative explanation for these facile reductions.¹⁹

Experimental Section

All salts and dimeric products have been previously prepared, and their physical properties and chemical behavior agree with those reported in the literature. In a typical reduction with $\text{Cr}(\text{ClO}_4)_2$, 10 mequiv of the organic salt was dissolved in 30 ml of water, which was acidified with HClO_4 to prevent hydrolysis of the tropylium and pyrylium salts. The solution was purged with oxygen-free nitrogen for 1 hr, after which 20 ml of 1 N $\text{Cr}(\text{ClO}_4)_2$ was added. The solution was allowed to stand for at least 5 hr under nitrogen and, for salts of low solubility, gently warmed. At the end of the reaction period, the aqueous solution was extracted with five 40-ml portions of ether (for the pyridinium salts, the solutions were made basic before extraction).

Evaporation of the dried ether extract yielded the dimer. In some reactions KCl was added to the reaction solution, and the pyridinium halides were con-

verted to nitrates with AgNO_3 . Zinc reductions were carried out as described by Balaban.¹²

(12) A. R. Balaban, C. Bratu, and C. N. Rentea, *Tetrahedron*, **20**, 265 (1964).

(13) E. M. Kosower and E. J. Poziomek (*J. Am. Chem. Soc.*, **86**, 5515 (1964)) note the need for iodide ion in the reduction of 1-ethyl-4-carbomethoxy-pyridinium ion to the stable pyridinyl radical, using magnesium in acetonitrile.

(14) E. Weitz, *et al.* (*Ber.*, **57**, 153 (1924)), have claimed that zinc does not reduce N-alkylpyridinium ions, although zinc will reduce N-phenylpyridinium ion. In view of the virtually quantitative yield obtained in our reduction of N-benzylpyridinium chloride, we are puzzled by Weitz's unsuccessful reactions.

(15) See footnote b, Table I.

(16) F. Sorm and Z. Sormova, *Chem. Listy*, **42**, 82 (1948).

(17) E. L. Colichman and P. A. O'Donovan, *J. Am. Chem. Soc.*, **76**, 3588 (1954).

(18) H. Yasuda and S. Kitagawa, *Yakugaku Kenkyu*, **27**, 779 (1955); *Chem. Abstr.*, **51**, 13246f (1957).

(19) Complex formation between the pyridinium ion and the reducing agent, followed either by dissociation of the complex subsequent to or simultaneous with electron transfer, or by a bimolecular reaction of the complex to form the dimer, might be suggested as alternatives which could resolve the anomaly. Such explanations, however, must take into account the variety of active reducing agents (zinc metal, chromous, and vanadous ions), as well as the "normal" behavior of the trimethylpyrylium ion. If the complex involved bonding between the metal and a particular carbon atom, the pyrylium ion should be much more reactive than the pyridinium ions, by analogy to their reaction with nucleophiles. It is difficult to assess the relative stabilities of π -bonded metal complexes of pyridinium and pyrylium ions, but if the frequencies of charge-transfer bands of their iodide salts are relevant here, again the pyrylium ion would be predicted to form the more stable complex.

Chlorine Nuclear Quadrupole Resonance in the Symmetrical Hydrogen Dichloride Ion

by J. C. Evans and G. Y-S. Lo

Chemical Physics Research Laboratory, The Dow Chemical Company, Midland, Michigan 48640 (Received May 16, 1967)

Previous attempts¹ to record the Cl^{35} nuclear quadrupole resonance (nqr) of several hydrogen dichloride salts yielded only one resonance, that of tetramethylammonium hydrogen dichloride near 20 MHz. This frequency indicated an unsymmetrical structure for the ClHCl ion in this salt, which agreed with the conclusion reached earlier² from vibrational data. Repeated attempts with different preparations have now yielded another Cl^{35} resonance, near 12 MHz, for tetraethylammonium hydrogen dichloride. The large frequency shift shows that markedly different electric field gradi-

(1) J. C. Evans and G. Y-S. Lo, *J. Phys. Chem.*, **70**, 2702 (1966).

(2) J. C. Evans and G. Y-S. Lo, *ibid.*, **70**, 11 (1966).

ents can exist at the Cl nuclei in ClHCl^- ions located in different molecular environments. Estimates of the corresponding chlorine electron densities may be derived, and further insights into the nature of the hydrogen bond may thus be achieved.

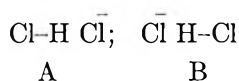
Experimental Section

Tetraethylammonium hydrogen dichloride (Eastman), dried by azeotropic distillation with benzene followed by prolonged exposure to vacuum, was dissolved in dried methylene chloride. Anhydrous HCl (Matheson) was passed into the solution; cyclohexane was added to induce crystallization of the desired hydrogen dichloride salt. Titration of a known amount with standard NaOH solution, and its infrared spectrum, served to characterize the product.

The 10–26-MHz range was scanned using a super-regenerative instrument based on a published design.³ With the sample held at 26°, one resonance (S/N approximately 3) was observed at 11.89 ± 0.03 MHz. This was assigned to Cl^{35} ; the Cl^{37} resonance was below the noise level. At 77°K, under poorer filling-factor conditions, the Cl^{35} resonance could not be detected; its position was estimated, assuming a temperature shift comparable to that previously observed¹ to be approximately 12.3 MHz.

Discussion

The earlier discussion¹ showed that if the two equivalently contributing resonance hybrids A and B

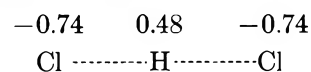


where the Cl–H bond is the same as that in the HCl molecule in crystalline HCl, provide an adequate description of the symmetric $[\text{ClHCl}]^-$ ion, then the two Cl nuclei should yield a single Cl^{35} resonance near 13 MHz. The value near 20 MHz observed for tetramethylammonium hydrogen dichloride was interpreted in terms of an unsymmetrical structure to which A and B did not contribute equally. The present case of a resonance near 12 MHz indicates the presence of a symmetrical anion; the lack of splitting shows crystallographic as well as chemical equivalence. The vibrational data also indicated high symmetry for the anion in this crystal.² We shall accept the symmetrical structure and investigate the electron distribution implied by the observed Cl^{35} resonance. The interpretation follows Townes and Dailey's methods.⁴

In terms of resonance among several idealized covalent and ionic structures, the symmetrical ClHCl^- ion may be described by three main contributing structures

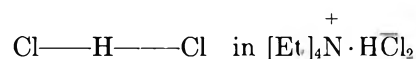
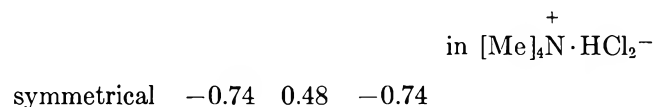
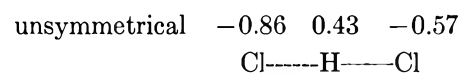
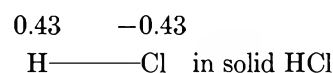


where the Cl–H in the two equivalent structures (I) and (II) is the purely covalent structure, not the hydrogen chloride molecule. The relative contributions of these structures may be determined from the observed Cl^{35} resonance (the estimated value of 12.3 MHz at 77°K was used) and the value of 109.7 MHz for the coupling constant of covalently bonded Cl in structure I and the value zero for Cl^- . With the usual assumption of 15% s character for the Cl bonding orbital, the approximate charge distribution is calculated to be



The LCAO–MO description of the symmetrical ion yields the same charge distribution; the relation between chlorine coupling constant and the bonding parameters for this model is given in ref 1.

We now have approximate charge distributions, derived from nqr data, for hydrogen dichloride ions of two different structures. Also available is the charge distribution for solid HCl, which consists of molecular HCl units bonded through relatively weak hydrogen bonds, derived in the same manner from the published Cl^{35} resonance value.⁵



This series shows that the electronic-charge redistribution which occurs as a chloride ion approaches a hydrogen chloride molecule along its symmetry axis to form a hydrogen bond is largely a transfer of charge from the chloride ion to the vicinity of the other chlorine atom. The charge density near the hydrogen atom remains almost unchanged.

(3) G. E. Peterson and P. M. Bridenbaugh, *Rev. Sci. Instr.*, **35**, 698 (1964).

(4) C. H. Townes and B. P. Dailey, *J. Chem. Phys.*, **17**, 782 (1949); **23**, 118 (1955).

(5) H. C. Allen, *J. Phys. Chem.*, **57**, 501 (1953).

"Virtual" Coupling in the Nuclear Magnetic Resonance Spectra of Substituted Cycloheptatrienes

by K. W. Egger and W. R. Moser

Monsanto Research SA, Zürich, Switzerland

Accepted and Transmitted by the Faraday Society
(February 27, 1967)

The nmr spectra of 1-, 2-, 3-, and 7-methylcyclohepta-1,3,5-triene, subsequently denoted as 1-, 2-, 3-, and 7-MCHT, respectively, have been investigated in connection with kinetic and thermochemical studies on these isomers.¹ The high resolution nmr spectra of the MCHT isomers, including double-irradiation experiments, served to assign unequivocally the proper structure to the individual isomers.

Fragmented data on nmr spectra of substituted cycloheptatrienes are available in the literature,² but no consistent interpretation of these spectra has been given. The calculated spectrum of cycloheptatriene itself, using AA'BB' mathematics, has been shown to reproduce accurately the observed spectrum.³

The spectra of the MCHT isomers reported here would be likewise correctly defined by similar calculation, but they also offer a consistent and unique observation of the effect of "virtual coupling" as outlined by Musher and Corey.⁴ The unusual splitting appearing in these spectra can be adequately accounted for by utilizing a simple restricted first-order analysis. The preparation and isolation of the individual MCHT isomers has been reported previously.¹

The nmr spectra (Varian HA 100) for 1-, 2-, 3-, and 7-MCHT are shown along with the decoupled spectra in Figure 1. The coupling constants, based on the assignment discussed below, are given in Table I. Both the 7 and 1 isomers are readily identified by the characteristic doublet structures for the absorption of the methyl and the methylene group, respectively. The double resonance experiments on the two remaining isomers (Figure 1c and e) show that only the spectra presented in Figure 1d satisfies the coupling pattern, which has to be expected from the structure of 2-methylcycloheptatriene (two nonidentical hydrogens coupled to the methylene, only one of which is further coupled to another hydrogen).

The assignment of the various absorption bands to the individual hydrogens is incorporated into Figure 1. The assignment of the methyl and methylene groups are evident and need no comment. The hydrogens in

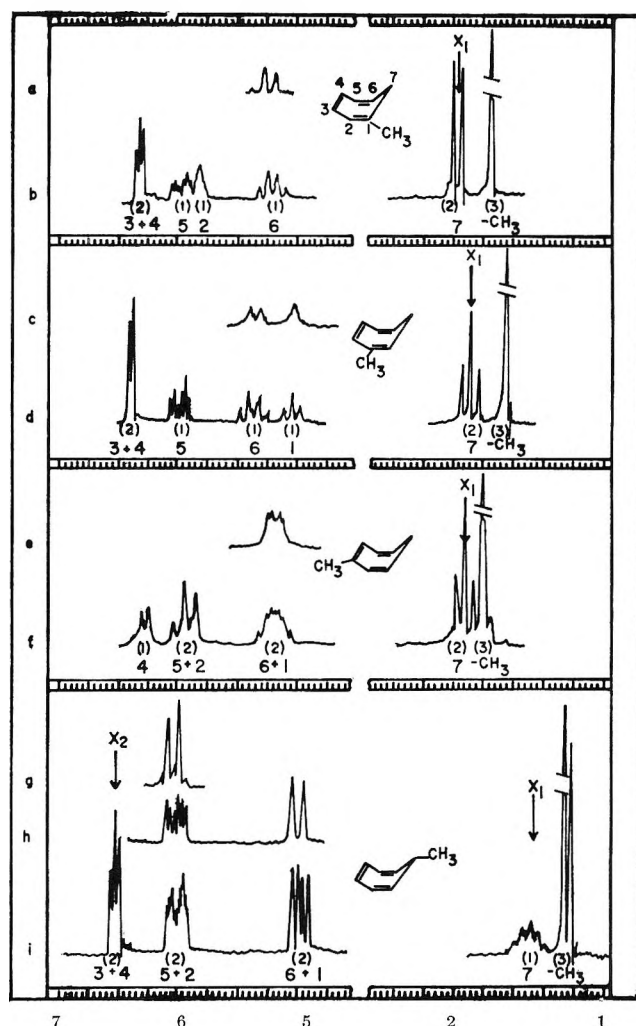


Figure 1.

positions 1 and 6 (see Figure 1) are clearly identified looking at the spectra obtained after irradiation at the position of the methylene frequency. The H_6 absorption becomes apparent from the collapse of the quartet in the irradiated spectra of 1-MCHT. The other band affected by this irradiation in the 2 and 7 isomers is assigned to H_1 . The absorption at the lowest field strength is shown by double irradiation in 7-MCHT to arise from the chemically equivalent hydrogens H_3 and

(1) K. W. Egger, *J. Am. Chem. Soc.*, **89**, 3688 (1967).

(2) (a) A. P. TerBorg, H. Kloosterziel, *et al.*, *Rec. Trav. Chim.*, **82**, 717, 741, and 1189 (1963); (b) R. W. Murray and M. L. Kaplan, *J. Am. Chem. Soc.*, **88**, 3527 (1966); (c) E. Müller, H. Kessler, H. Fricke, and W. Kiedaisch, *Ann.*, **675**, 63 (1964); (d) M. A. Bennett, L. Pratt, and G. Wilkinsor, *J. Chem. Soc.*, 2037 (1961); (e) R. Burton, L. Pratt, and G. Wilkinson, *ibid.*, 595 (1961).

(3) (a) J. B. Lambert, L. J. Durham, P. Lepoutere, and J. D. Roberts, *J. Am. Chem. Soc.*, **87**, 3896 (1965); (b) H. Günther and H. H. Hinrichs, *Tetrahedron Letters*, 787 (1966).

(4) J. I. Musher and E. J. Corey, *Tetrahedron*, **18**, 791 (1962).

Table I: Coupling Constants (cps) for the Protons in the MCHT Isomers^b

	7-MCHT	3-MCHT	2-MCHT	1-MCHT
J_{1-2}	8.7	9.5
J_{5-6}	8.7	6.0	9.5	9.5
J_{1-7}	5.3	6.8	6.8	...
J_{6-7}	5.3	6.8	6.8	6.8
J_{4-5}	...	6.5
$J_{2-3,1}^a$	3.2
$J_{5-3,4}^a$	3.2	...	3.2	3.2

^a Apparent coupling constants. ^b MCHT stands for methylcycloheptatriene.

H₄. This assignment is substantiated with the relative intensities of this absorption band in the various isomers. The remaining two hydrogens H₂ and H₅ can be distinctively assigned, looking at the spectra of the 2-MCHT (H₂ missing) as compared to all the other isomers. In addition, the assignment of the band at τ 4.00 to H₅ is verified by the measured coupling constant $J_{5,6}$ (9.5 cps) which is also seen as $J_{6,5}$ in the decoupled spectra of 1-MCHT. With confidence in the above assignment of the absorption bands, one can now look at the interesting aspects of the "abnormal" features evident in these spectra, *i.e.*, the unusual splitting found in the H₂, H₃, H₄, and H₅ bands. The doublet of triplets for H₅ found in the spectra of 7-, 2-, and 1-methylcyclohepta-1,3,5-triene⁵ has the same line separation in each of the triplets (3.2 cps) as the one measured for the H₃ and H₄ absorption band. The large doublet splitting (9.5 cps) in H₅ is of course due to the coupling with H₆. The equal line separation in each of the triplets gives the appearance that H₅ is effectively equally coupled to both H₃ and H₄.

Based on reported coupling constants, one would predict $J_{4,5}$ to be of the order of 4–10 cps and $J_{3,5}$ in the range of 0–0.3 cps. The unusual multiplicity as well as the apparently equal line separation measured for the proton systems H₃–H₄–H₅ and H₂–H₃–H₄ are best rationalized with restricted first-order analysis.^{4,6,7} These MCHT systems satisfy the conditions for "virtual" coupling,⁴ *i.e.*, a chemical shift of ~ 0 between H₃ and H₄ and strong coupling between H₃–H₄ and H₄–H₅. Musher and Corey⁴ calculated a similar example of the AA'B system, where $(\nu_A - \nu_{A'}) = 0$, $J_{A'B} = 6.5$ cps, and $J_{AA'} = 10.5$ cps, which also afforded a skewed triplet B absorption and equal line separation with a splitting of $1/2 J_{A'B}$.

In 3-MCHT, with no possibility for this type of long-range coupling, one observes the normal nonperturbed splitting ($J_{4,5} = 6.5$ cps) which is, as expected, twice as large as the corresponding coupling (3.2 cps) in the

case of the other isomers, involving apparent "virtual" coupling.

It remains to be explained why the spectra of the 1 and 7 isomers show a triplet structure instead of a doublet for the H₃–H₄ band. This type of pattern can be interpreted to demonstrate the independent participation of the H₃ and H₄ hydrogens in a virtually coupled system with H₂ and H₅ simultaneously. The total line separation in this triplet is 6.4 cps, meaning that the magnitude of the apparent coupling of H₂ with the system is 3.2 cps. It is then not surprising that the band for H₂ appears as a broad multiplet due to its virtual coupling and further perturbation by long-range coupling with the methyl group.

The same type of simplified interpretation of otherwise complex spectra can be applied to the spectra of cycloheptatriene^{2c,3a} and 1,6-cycloheptatriene dicarboxylic acid.⁸ Both these compounds meet the requirements of virtual coupling and the reported coupling constants and chemical shifts for the cycloheptatriene are in perfect agreement with the interpretation given in this note to the methylcycloheptatriene isomers.

The information available in the literature for other substituted cycloheptatrienes² further substantiates the assignment and interpretation given for the methylcycloheptatriene isomers.

(5) In the 7-MCHT isomer, the triplet is readily apparent, looking at the H₂, H₅ absorption after decoupling the interaction with the hydrogen in the 7 position.

(6) J. D. Roberts, "An Introduction to the Analysis of Spin-Spin Splitting in High Resolution Nuclear Magnetic Resonance Spectra," W. A. Benjamin, New York, N. Y., 1961, p 76.

(7) K. B. Wiberg and B. J. Nist, "Interpretation of NMR-Spectra," W. A. Benjamin, Inc., New York, N. Y., 1961, p 21.

(8) R. Darms, T. Threlfall, M. Pesaro, and A. Eschenmoser, *Helv. Chim. Acta*, **46**, 2893 (1963).

The Activation Energy of Hydrated Electron Reactions¹

by M. Anbar² and Edwin J. Hart

Chemistry Division, Argonne National Laboratory,
Argonne, Illinois (Received May 17, 1967)

An activation energy, E_A , of 3.5 ± 0.4 kcal/mole has recently been reported for several hydrated electron reactions that range in rate from 6×10^{10} down to

(1) Based on work performed under the auspices of the U. S. Atomic Energy Commission.

(2) The Weizmann Institute of Science, Rehovoth, Israel.

Table I: Activation Energies, E_A , of a Number of Reactions of Hydrated Electrons

Compound	Matrix	pH	Obsd 1st-order decay $\times 10^{-6} \text{ sec}^{-1}$		$k_{\text{solute}},$ $M^{-1} \text{ sec}^{-1}$ $\times 10^{-8},^b$	$E_A, \text{ kcal/mole}^c$		$k_{\text{diff}}^d \times$ $10^{-10} M^{-1}$ sec^{-1}
			$k'_{\text{matrix}},^a$ 25°	$k'_{\text{solute}},^a$ 25°		Matrix	Solute	
$\text{ClCH}_2\text{COO}^-$	H_2O	11.0	0.115	1.2	8.9	2.9 ± 0.5	2.8 ± 0.4	1.05
$\text{ClCH}_2\text{COO}^-$	D_2O	11.2	0.12	1.96	9.2	4.0 ± 0.5	3.2 ± 0.4	1.05
$\text{ClCH}_2\text{CH}_2\text{OH}$	H_2O	11.0	0.115	2.1	3.3	2.9 ± 0.5	3.1 ± 0.6	1.3
$\text{ClCH}_2\text{CH}_2\text{COO}^-$	H_2O	11.0	0.22	2.4	4.4	3.6 ± 0.4	3.6 ± 0.4	1.0
MnEDTA^{2-}	0.05 M EDTA	11.3	0.39	0.83	0.015	4.0 ± 0.6	4.0 ± 0.6	0.85

^a $k'_{\text{matrix}} = d \ln [e_{\text{aq}}^-]/dt$; $k'_{\text{solute}} = d \ln [e_{\text{aq}}^-]/dt$. ^b $k_{\text{solute}} = (k_{\text{solute}} - k'_{\text{matrix}})/(\text{concn of solute}, M)$. ^c $E_A = R[d \ln k_s/d(1/T)]$.
^d From Debye equation assuming $r(e_{\text{aq}}^-) = 2.5 \text{ \AA}$; $D(e_{\text{aq}}^-) = 4.5 \times 10^{-5} \text{ cm}^2 \text{ sec}^{-1}$.

$3 \times 10^5 M^{-1} \text{ sec}^{-1}$.³ These results, derived from the difference in temperature dependence of two processes, are open to criticism because the method is indirect. In the present study, we use the direct method of pulse radiolysis and obtain the rate constants, k , of the reactions at each temperature by following the decay of the optical absorption band of e_{aq}^- . Both light and heavy water were used in the chloroacetic acid studies.

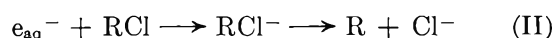
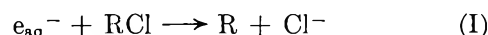
The rate constants were measured by the usual electron pulse technique.⁴ The main departure was the use of a thermostated multiple reflection cell utilizing a 6328-A laser as the spectrophotometric analyzing light beam.⁵ With this system, 6 to 8 passes providing optical path lengths of 24 to 32 cm were readily available. With temperatures constant within $\pm 0.1^\circ$, the rates were measured at 2, 10, 19, 28, 48, and 62° . The slopes, $d \ln k/d(1/T)$, were linear within the temperature range studied, and within our experimental error of $\pm 15\%$ no deviation from linearity was observed. In each case, the rate of disappearance of e_{aq}^- in the matrix was subtracted from the over-all rate of disappearance of e_{aq}^- in the presence of the solute. From the slope, $d \ln k/d(1/T)$, for the matrices we were able to obtain E_A for the matrix, as well as for the solute reactions with e_{aq}^- . The results are presented in Table I.

The reaction, $e_{\text{aq}}^- + \text{ClCH}_2\text{COO}^-$, has an E_A of $2.8 \pm 0.4 \text{ kcal/mole}$. By comparing columns 8 and 9 of Table I, one sees that the rate constant, k_s , for this reaction is more than an order of magnitude slower than the expected diffusion controlled rate (k_{diff}) of $1.05 \times 10^{10} M^{-1} \text{ sec}^{-1}$. If the difference between k_s and $k_{\text{diff}(s)}$ for this reaction is due to a difference in activation energy, this would require ΔE_A of about 1.5 kcal/mole. Since the apparent E_A for diffusion-controlled reactions in aqueous solution is about 3.0 kcal/mole,⁶ the expected activation energy $E_A(\text{calcd})$ would be about 4.5 kcal, *i.e.*, significantly higher than the experimental value of $2.8 \pm 0.4 \text{ kcal/mole}$.

In heavy water, the activation energy for the chloroacetate ion reaction is $3.2 \pm 0.4 \text{ kcal/mole}$, not significantly higher than in light water. This result is not surprising, since E_A of diffusion in D_2O inferred from viscosity⁶ is only 7% higher in D_2O than in H_2O .⁷

Nearly identical rate constants are found for $\text{ClCH}_2\text{CH}_2\text{OH}$ and $\text{ClCH}_2\text{CH}_2\text{COO}^-$. They are lower than that of the $\text{ClCH}_2\text{COO}^-$ reaction by a factor of about 2.5, and still they all have activation energies which are equal within experimental error.

Two alternative mechanisms have been suggested for haloaliphatic-hydrated electron reactions.⁸



According to mechanism I, the R-Cl bond is broken during the rate-determining step, whereas in mechanism II, RCl^- forms as a short-lived intermediate. Comparing the difference in enthalpies for reactions of e_{aq}^- with $\text{ClCH}_2\text{COO}^-$ and with $\text{ClCH}_2\text{CH}_2\text{COO}^-$ gives a higher ΔH of about 10 kcal/mole for mechanism I.⁹ If the e_{aq}^- reaction proceeded by mechanism I, this difference in ΔH would be reflected by a corresponding increase in E_A .¹⁰ Thus the equivalence in E , for both of these $e_{\text{aq}}^- + \text{RCl}$ reactions supports the idea that

(3) M. Anbar, Z. Alfassi, and H. Reissler, *J. Am. Chem. Soc.*, **89**, 1263 (1967).

(4) J. K. Thomas, S. Gordon, and E. J. Hart, *J. Phys. Chem.*, **68**, 1524 (1964).

(5) E. J. Hart, E. M. Fielden, and M. Anbar, *ibid.*, in press.

(6) M. Eigen, W. Krase, G. Maass, and L. deMaeyer, *Progr. Chem. Kinetics*, **2**, 287 (1963).

(7) I. Kirshenbaum, "Physical Properties and Analysis of Heavy Water," McGraw-Hill Book Co., Inc., New York, N. Y., 1951, p 33.

(8) M. Anbar, *Advances in Chemistry Series*, No. 50, American Chemical Society, Washington, D. C., 1965, p 55.

(9) T. C. Cottrell, "The Strengths of Chemical Bonds," Butterworth and Co. Ltd., London, 1958.

(10) T. O. Edwards, "Inorganic Reaction Mechanisms," W. A. Benjamin, Inc., New York, N. Y., 1964, Chapter 3.

the rate-determining step of e_{aq}^- reactions generally involves the addition of the electron to the substrate molecule *via* mechanism II.⁸ Subsequently, the cleavage of the R-Cl bond takes place.

The ethylenediaminetetraacetate complex of manganese ($MnEDTA^{2-}$) cannot be readily reduced by e_{aq}^- . Its rate constant is $1.5 \times 10^6 M^{-1} sec^{-1}$ at 25° . Consequently, we selected it in order to see if inert solutes possessed higher activation energies than those controlled by diffusion. We find an activation energy of 4.0 ± 0.6 kcal/mole for this reaction and consider it to be equal, within experimental error, to the activation energies of the faster reactions cited above, and even to the diffusion-controlled ones. The slowness of the $MnEDTA^{2-}$ reduction cannot under any circumstances be due to an increase in E_A as has been suggested for the $e_{aq}^- + Mn^{2+}(aq)$ reaction.¹¹ Even if there is a slight increase in E_A for this slow reaction, it is very far from the expected increase of over 5 kcal/mole.

All e_{aq}^- reactions, including those of the matrix as well as those of the solutes, possess E_A in the range from 2.8 ± 0.4 to 4.0 ± 0.6 kcal/mole. In view of the relatively large experimental error, we assume that the same average E_A of 3.4 ± 0.4 prevails for all of these reactions. This value also agrees with that of 3.5 ± 0.4 kcal/mole obtained by competition kinetics.³

It should be noted that owing to the fact that $k_{obsd} = (k_{diff} \times k)/(k_{diff} + k)$,⁶ the observed E_A will remain practically constant and equal to the E_A of the diffusion-controlled reactions, $E_A(diff)$, for any actual value of E_A , ranging from zero to $E_A(diff)$ for reactions which have a "normal" preexponential factor, of the order of $10^{12} M^{-1} sec^{-1}$. In the case $E_A = E_A(diff) = 3.0$ kcal/mole, an experimental value of E_A of 3.4 kcal/mole would be observed for reactions with a "normal" preexponential factor. For reactions which have a significantly smaller preexponential factor, the measured activation energy is the actual activation energy of the reaction. This E_A seems still to be the same for a great number of e_{aq}^- reactions; thus it seems to be *independent* of the nature of the substrate and of the free energy of activation involved. This energy of activation could be the energy required to *reorganize* the hydration sphere around the electron. It is substantially lower than the energy of hydration of e_{aq}^- and it should be equal to the energy required to create a hole in the solvent, *i.e.*, the E_A of diffusion.

The electron distribution in the solute ion or molecule is the principal factor determining e_{aq}^- reactivity in the primary step.⁸ We associated high reactivity with a ready access of e_{aq}^- to a favorable vacant orbital. This distribution of electrons in the molecule, which

might be changed by electron excitation, will be unaffected by temperatures up to 100° , and the parameter which determines the rate constant will thus be the probability of finding an electron vacancy on the substrate molecule. This probability, represented by the entropy of activation, is temperature independent in our range of temperatures. Our findings that E_A for all $e_{aq}^- + S \rightarrow S^-$ reactions is equal supports these conclusions.

One may regard e_{aq}^- reactions as electron transfer processes that involve an extra-molecular electron. These processes still obey the Franck-Condon principle, and the slow reactions of e_{aq}^- may be treated as forbidden electronic transitions having a probability much smaller than unity. Speculative as this concept may seem, it serves as a practical working hypothesis for continuing research on the reactions of e_{aq}^- .

(11) J. H. Baxendale, E. M. Fielden, and J. P. Keene, *Proc. Roy. Soc. (London)*, **A286**, 320 (1965).

An Analysis of the Excess Charge Effect in Alternant Conjugated Hydrocarbon Radical-Ions

by James R. Bolton¹

Department of Chemistry, University of Minnesota, Minneapolis, Minnesota (Received May 26, 1967)

It is well known that in conjugated hydrocarbon radical-ions, proton hyperfine splittings are usually larger in positive ions than for corresponding positions in the negative ions. This has been called the "excess charge effect." Colpa and Bolton² were the first to interpret this effect and ascribed it to a second-order correction in the derivation of the McConnell relation.³ They proposed the relation

$$a_i^H = [Q_{CH}^H(0) + K_{CH}^H \epsilon_i^\pi] \rho_i^\pi \quad (1)$$

where ρ_i^π is the π -electron spin density at the carbon atom i , ϵ_i^π is the excess charge ($\epsilon_i^\pi = 1 - q_i^\pi$ where q_i^π is the total π -electron density at the carbon atom i), a_i^H is the hyperfine splitting constant for the proton attached to the carbon atom i , and $Q_{CH}^H(0)$ and K_{CH}^H are constants.

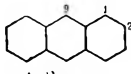
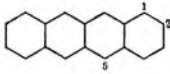
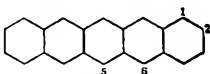
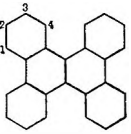
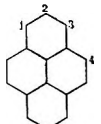
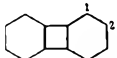
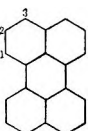
Although the original derivation of eq 1 was later shown to predict a positive sign for K_{CH}^H (experiment

(1) Alfred P. Sloan Research Fellow.

(2) J. P. Colpa and J. R. Bolton, *Mol. Phys.*, **6**, 273 (1963).

(3) H. M. McConnell, *J. Chem. Phys.*, **24**, 633, 764 (1956); *Proc. Natl. Acad. Sci. U. S.*, **53**, 721 (1957).

Table I: Experimental Hyperfine Splittings for a Group of Alternant Aromatic Hydrocarbon Positive and Negative Ions

Hydrocarbon	Ring position	Number in Figure 1	Hyperfine splittings, gauss					Residuals
			a_+^H	a_-^H	\bar{a}^H	Δa^H		
 Anthracene	9	1	6.533 ^a	5.337 ^a	5.935	0.598	0.023	
	1	2	3.061	2.740	2.901	0.16	-0.013	
	2		1.379	1.509	1.444	-0.065		
 Tetracene	5	3	5.061 ^{b,c}	4.226 ^c	4.644	0.418	0.038	
	1	4	1.694	1.541	1.618	-0.077	0.031	
	2		1.030	1.162	1.096	-0.066		
 Pentacene	6	5	5.083 ^d	4.263 ^d	4.673	0.410	0.025	
	5	6	3.554	3.032	3.293	0.261	-0.070	
	1		(0.975) ^e	(0.915) ^e	0.945	0.030		
	2		(0.757) ^e	(0.870) ^e	0.814	-0.057		
 Dibenzofluorene	1		0.60 ^f	0.62 ^f	0.610	-0.010		
	2	7	1.99	1.71	1.850	0.140	0.080	
	3		<0.03	<0.03		
	4	8	2.28	2.06	2.170	0.110	0.027	
 Pyrene	1	9	2.12 ^f	2.08 ^f	2.100	0.020	-0.057	
	2		-1.18	-1.09	-1.135	-0.045		
	4	8	5.38	4.75	5.065	0.315	-0.137	
 Biphenylene	1		0.18 ^g	0.18 ^c	0.18	0.000		
	2	11	3.58	2.74	3.16	0.420	0.231	
 Perylene	1	12	3.054 ^c	3.043 ^c	3.049	0.006	-0.158	
	2		-0.446	-0.450	-0.448	0.002		
	3	13	4.053	3.493	3.773	0.280	0.029	
Benzene	1	14	4.44 ^g	3.75 ^h	4.095	0.345	0.048	
Coronene	1	15	1.53 ^f	1.47 ^f	1.50	0.060	0.020	

^a Reference 8. ^b Reference 9. ^c Reference 10. ^d Reference 11. ^e Assignment uncertain. ^f Reference 5. ^g G. Vincow, private communication. ^h Reference 12.

indicates a negative sign), subsequent calculations indicate that $Q_{CH}^H(0)$ and K_{CH}^H should both be negative.⁴

Some attempts have been made to confirm eq 1 from experimental data;^{1,5} however, these all suffer from having to use theoretically calculated values of ρ_i^π . In this note it will be shown that the form of eq 1 can be checked by using only experimental hyperfine splittings and two very plausible assumptions.

The first assumption is that the pairing theorem^{6,7} holds exactly. This has been demonstrated for the anthracene positive and negative ions.⁸ In order to test the validity of eq 1, the results of all known pairs of alternant aromatic hydrocarbon positive and negative

ions are employed. Secondly, the assumption is made that $|\epsilon_i^\pi| = \rho_i^\pi$. This holds exactly for Hückel molecular orbitals and is a good approximation for more advanced calculations, especially at high spin density positions where the discrepancies are largest. Thus eq 1 can be written as

- (4) J. R. Bolton, *J. Chem. Phys.*, **43**, 309 (1965).
 (5) (a) T. C. Sayetta and J. D. Memory, *ibid.*, **40**, 2748 (1964);
 (b) I. C. Lewis and L. S. Singer, *ibid.*, **43**, 2712 (1965).
 (6) A. D. McLachlan, *Mol. Phys.*, **2**, 271 (1959).
 (7) J. Koultecky, *J. Chem. Phys.*, **44**, 3702 (1966).
 (8) J. R. Bolton and G. K. Fraenkel, *ibid.*, **40**, 3307 (1964).

$$a_i^H = Q_{CH}^H(0)\rho_i^\pi \pm K_{CH}^H\rho_i^{\pi 2} \quad (2)$$

where the + sign applies for positive ions and the - sign for negative ions.

From the pairing theorem, ρ_i^π must be the same for corresponding positions in the positive and negative ions. The following definitions are made

$$\Delta a = \frac{a_+ - a_-}{2} \quad (3)$$

$$\bar{a} = \frac{a_+ + a_-}{2} \quad (4)$$

where a_+ and a_- are the hyperfine splittings in the positive and negative ions, respectively. On making the appropriate substitutions, the following relation can be derived

$$\Delta a = \frac{K_{CH}^H}{[Q_{CH}^H(0)]^2} \bar{a}^2 \quad (5)$$

(Note that Δa and \bar{a} are both experimental observables.)

The data for the available aromatic hydrocarbon radical-ions are presented in Table I⁹⁻¹² and are plotted in Figure 1. The agreement with eq 5 is more than satisfactory. Using $Q_{CH}^H(0) = -27.0$ gauss,⁸ K_{CH}^H is computed to be -12.9 ± 1.1 gauss from the slope of the regression line in Figure 1. The slope was computed from the weighted mean of $\Delta a_i/\bar{a}_i^2$, using a weighting factor was of \bar{a}^4 . This procedure assumes that

the errors in Δa are constant. The error in the slope is one standard deviation. In Figure 1 only those positions having a hyperfine splitting greater than 1.5 gauss have been plotted, as it is only for the larger hyperfine splittings that a significant excess charge effect is expected. It is to be noted that for some of the positions, Δa is negative. However, all of these positions have small hyperfine splittings and some other effect may be causing these small differences.

In conclusion, it is apparent that *either* eq 1 *and* the pairing theorem must hold *or* a breakdown in the pairing theorem must occur. The latter is rather unlikely in view of the evidence in favor of the pairing theorem.

Acknowledgment. The author wishes to thank the National Science Foundation for financial support under Grant No. NSF GP5847.

(9) J. S. Hyde and H. W. Brown, *J. Chem. Phys.*, **37**, 368 (1962).

(10) J. R. Bolton, unpublished work.

(11) J. R. Bolton, *J. Chem. Phys.*, **46**, 408 (1967).

(12) J. R. Bolton, *J. Mol. Phys.*, **6**, 219 (1963).

The Calculation of Photostationary States in Systems $A \rightleftharpoons B$ When Only A Is Known

by Ernst Fischer

Photochemical Laboratory, The Weizmann Institute of Science, Rehovoth, Israel (Received December 21, 1966)

In studying photoisomerizations it often happens that the product of the phototransformation $A \rightarrow B$ is not known in the pure state and cannot be isolated for technical reasons, such as lack of thermal stability or lack of stability toward oxidation by oxygen.

It will be shown that the extent of the above phototransformation, and thus the absorption spectrum of B, can be estimated by measuring the absorption spectra obtained after a photostationary state has been reached by irradiation "to completion" with light at two different wavelengths. The essential experimental requirement for the application of the suggested method is thus that the system $A \rightleftharpoons B$ is sufficiently stable both thermally and photochemically (= absence of side reactions) to make possible the establishment of true photostationary states.

Method

In a solution of the photoreversible system $A \xrightleftharpoons{h\nu} B$ in a nonabsorbing solvent, a photostationary state will be

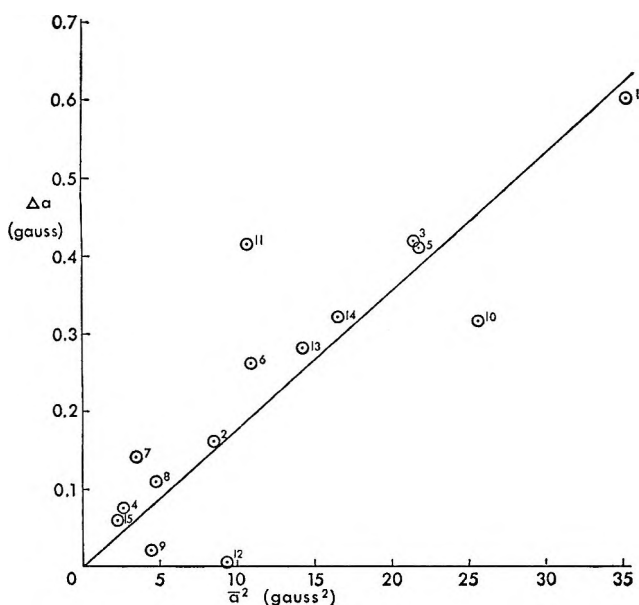


Figure 1. A plot of Δa vs. \bar{a}^2 for the data presented in Table I. Points are keyed by number to column 3 of Table I. The solid line was computed using a weighted least-squares procedure (see text) with all 15 points included.

established by irradiation at any wavelength absorbed by both A and B. Henceforth we shall deal only with such states and all concentrations will be those in the photostationary state attained with light at the wavelength indicated by the subscript.

Denoting concentrations by A and B, quantum yields $A \xrightarrow{h\nu} B$ by ϕ_A and $B \xrightarrow{h\nu} A$ by ϕ_B , and extinction coefficients by ϵ , we have¹ for the photostationary state at any wavelength λ

$$\left(\frac{A}{B}\right)_\lambda = \left(\frac{\phi_B}{\phi_A}\right)_\lambda \left(\frac{\epsilon_B}{\epsilon_A}\right)_\lambda = \left(\frac{\phi_B}{\phi_A}\right)_\lambda \left(\frac{D_B}{D_A}\right)_\lambda \quad (1)$$

where D_A and D_B denote the optical densities, at this wavelength, of similar solutions containing only A or only B, respectively, (*i.e.*, the equilibrium $A \rightleftharpoons B$ is shifted completely toward either A or B).

When comparing the results of irradiation at any two wavelengths, we have two equations of type (1), one of each wavelength. If we assume that the ratio ϕ_A/ϕ_B does not differ at the two wavelengths,² then by taking the ratio between these two equations, ϕ_A/ϕ_B will cancel out and we end up with eq 2.

$$\left(\frac{A}{B}\right)_1 / \left(\frac{A}{B}\right)_2 = \left(\frac{D_B}{D_A}\right)_1 / \left(\frac{D_B}{D_A}\right)_2 \quad (2)$$

If we denote the extent of conversion $A \rightarrow B$ at any particular λ of irradiation by α , we get

$$\left(\frac{A}{B}\right)_\lambda = \left(\frac{1 - \alpha}{\alpha}\right)_\lambda$$

Insertion in the left side of (2) leads to

$$\frac{1 - \alpha_1 / 1 - \alpha_2}{\alpha_1} = \left(\frac{D_B}{D_A}\right)_1 / \left(\frac{D_B}{D_A}\right)_2 \quad (3)$$

It remains to express D_B , which is unknown, in terms of experimental data and the α 's. The optical density at any particular wavelength λ of a mixture of A and B, where the over-all concentration $[A] + [B]$ is constant, will be given by

$$D = D_A(1 - \alpha) + D_B\alpha$$

If we denote by Δ the observed change in optical density when starting from A only, $\Delta = D_{\text{obsd}} - D_A$, we get after rearrangement

$$D_B = D_A + \Delta/\alpha \quad (4)$$

at wavelength λ . Introducing (4) into (3) we have

$$\frac{1 - \alpha_1 / 1 - \alpha_2}{\alpha_1} = \left(\frac{D_B}{D_A}\right)_1 / \left(\frac{D_B}{D_A}\right)_2 = \left(\frac{D_{A_1} + \Delta_1/\alpha_1}{D_{A_1}}\right) / \left(\frac{D_{A_2} + \Delta_2/\alpha_2}{D_{A_2}}\right) = \left(1 + \frac{\Delta_1/D_1}{\alpha_1}\right) / \left(1 + \frac{\Delta_2/D_2}{\alpha_2}\right) \quad (5)$$

For the sake of simplicity D_A has been replaced by D in the final equation, where Δ/D denotes the relative change of absorbance observed at a wavelength λ when a solution of A is photoequilibrated with light at this wavelength.

Furthermore, the ratio of the α 's for two different photostationary states, resulting from irradiation by two different wavelengths, is equal to the corresponding ratio of Δ 's measured at a wavelength chosen so as to maximize the Δ 's. Denoting this ratio by n , $\alpha_1 = n\alpha_2$, and inserting it into (5) we get

$$\frac{1 - n\alpha_2}{n(1 - \alpha_2)} = \left(1 + \frac{\Delta_1/D_1}{n\alpha_2}\right) / \left(1 + \frac{\Delta_2/D_2}{\alpha_2}\right)$$

where (Δ/D) is the relative change in absorbance at that particular wavelength, λ_1 or λ_2 , when passing from pure A to the photostationary state attained by irradiation at the same wavelength.

Multiplying the right-hand side of the expression by α_2 we get

$$\frac{1 - n\alpha_2}{n(1 - \alpha_2)} = [\alpha_2 + (\Delta_1/nD_1)] / [\alpha_2 + (\Delta_2/D_2)] \quad (6)$$

Developing this expression, we finally arrive at

$$\alpha_2 = \left(\frac{\Delta_1}{D_1} - \frac{\Delta_2}{D_2}\right) / \left(1 + \frac{\Delta_1}{D_1} - n\left(1 + \frac{\Delta_2}{D_2}\right)\right) \quad (7)$$

The numerical value of α_2 determined by this equation may then be used to calculate the spectrum of pure B by means of eq 4. For the special case where λ_2 is the wavelength of an isobestic point, $\Delta_2 = 0$ and

$$\alpha_2 = \alpha_1 = \left(\frac{\Delta_1}{D_1}\right) / \left(1 + \frac{\Delta_1}{D_1} - n\right)$$

or

$$\frac{1}{\alpha_1} = 1 + \frac{D_1}{\Delta_1}(1 - n) \quad (8)$$

Here α_1 and α_i denote the extents of photoconversion with light of wavelength λ_1 and of the wavelength λ_i of the isobestic point or region, respectively, and n is defined by $\alpha_1 = n\alpha_i$.

In applying eq 7 and 8, care should be taken to use the correct sign for Δ (+ for an increase, - for a decrease, as a result of irradiation). For an estimate of n , it is not necessary to use a wavelength region where only

(1) (a) G. Zimmerman, L. Chow, and U. Paik, *J. Am. Chem. Soc.*, **80**, 3528 (1958); (b) S. Malkin and E. Fischer, *J. Phys. Chem.*, **66**, 2482 (1962).

(2) The approximate validity of this assumption has been shown, *e.g.*, in ref 1. However, in view of the uncertainty involved, the method is to be used only when more direct methods are not applicable.

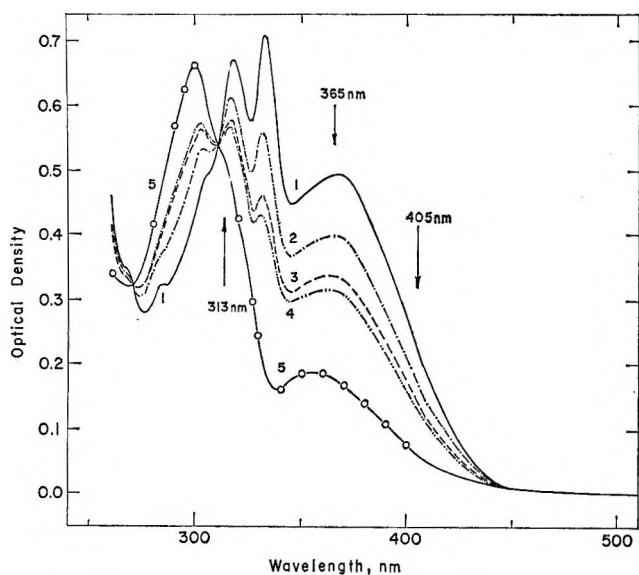


Figure 1. Absorption spectra of compound I, $7 \times 10^{-6} M$ in methylcyclohexane, 10-mm cell, at -100° : 1, before irradiation (assumed to be 100% *trans*); 2, photostationary state attained by irradiation at 313 nm; 3, the same as 2 but at 365 nm; 4, the same as 2 but at 405 nm; 5, extrapolated absorption spectrum of pure *cis*-I, assuming that in the photostationary state attained at 365 nm approximately one-half of *trans*-I is converted into *cis*-I. (Application of eq 7 to curves 3 and 4 yields $\alpha_{365} = 0.52$. Application of eq 8 to curves 2 and 3 yields $\alpha_{365} = 0.53$. The isosbestic point is at 312 nm.)

one of the two isomers absorbs, since according to eq 4 the observed change in absorbance Δ at a suitable wavelength is proportional to the extent of transformation α . For the special case $n = 1$, *i.e.*, when the extent of conversion is observed to be independent of the wavelength of the light used for irradiation, eq 7 reduces to

$$\alpha_2 = \left(\frac{\Delta_1}{D_1} - \frac{\Delta_2}{D_2} \right) / \left(\frac{\Delta_1}{D_1} - \frac{\Delta_2}{D_2} \right)$$

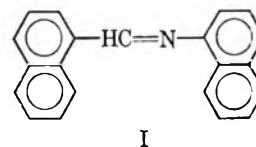
i.e., $\alpha_2 = 1$ and $\alpha_1 = 1$, *except* for $\Delta_1/D_1 = \Delta_2/D_2$, which is the trivial case of two wavelengths at which the ratio ϵ_A/ϵ_B is identical. In this case α is obviously undetermined. This means that whenever it is observed that the change resulting from irradiation is independent of the wavelength of the photoactive light, while the relative changes in absorbance do change with wavelength, the conclusion is that the photoconversion $A \rightarrow B$ is complete. This can only result from $\phi_B \ll \phi_A$, or $\phi_B = 0$.

Examples

The method will first be applied to the case of *cis-trans* azobenzene, for which Zimmerman and collaborators¹ have accurately determined the absorption spectra of both isomers. A $1.5 \times 10^{-3} M$ solution of *trans*-

azobenzene in methylcyclohexane was photoequilibrated with light at 436 and at 510 nm. The observed values needed for eq 7 were $n = \alpha_{436}/\alpha_{510} = 0.60$, $(\Delta/D)_{436} = +0.325$, $(\Delta/D)_{510} = +0.19 \pm 0.02$, leading to $\alpha_{510} = 0.22 \pm 0.02$ and $\alpha_{436} = 0.13 \pm 0.02$. The ratio between the peak optical densities of the *cis* form (at 440 nm) and the *trans* form (at 450 nm) is calculated from these values as 3.16 ± 0.2 , which compares well with Zimmerman's value of 2.95 for this ratio.

Figure 1 shows the application of the method to a case where the isomers cannot be isolated, namely, the photoisomerization of anil I described earlier.³ Here thermal reversion takes place above about -80° , and



therefore the irradiation and measurements were carried out at -100° .

Conclusion

The experimental data necessary in the above method are the absorption spectra of pure A before irradiation and after photoequilibration at two different wavelengths for which it may be assumed that the ratio of quantum yields ϕ_A/ϕ_B does not differ markedly (such as within one absorption band). Such behavior is quite common. When one of the two wavelengths happens to be that of the isosbestic point or region, the calculation is simplified.

(3) E. Fischer and Y. Frei, *J. Chem. Phys.*, **27**, 808 (1957).

Breakthrough of Poisoning Multivalent Ions across a Permselective Membrane during Electrodialysis

by F. de Kőrös and E. Zeigerson

The Negev Institute for Arid Zone Research, Beersheva, Israel

Accepted and Transmitted by the Faraday Society
(March 20, 1967)

Counterions of higher valency may become attached to the fixed ionic sites of a permselective membrane so strongly that they partially overneutralize the fixed charges and thus change the sign of permselectivity of the membrane.¹⁻³ This implies that a bipolar mem-

brane must be formed during the period that the multivalent ions are being introduced into the membrane from one side by a direct current. When the poisoning multivalent ions reach the opposite side of the membrane and begin to break through into the adjoining solution, the membrane's sign of permselectivity becomes inverted across its whole cross section and it ceases to be bipolar.

We tested this assumption by inserting an anion-exchange membrane (American Machine and Foundry Co.) into a four-cell electrolysytic apparatus with a 0.1 N $K_4Fe(CN)_6$ solution in the cell on the cathode side of the membrane and a 0.1 N $NaNO_3$ solution on its other side. The electrode compartments were filled with 0.1 N KCl solutions and were separated by an anion-exchange membrane on the anode side and a cation-exchange membrane on the cathode side from the two compartments adjoining the central membrane. Current electrodes were of Ag|AgCl plates. Two Ag|AgCl wire electrodes were fixed at 4 mm from both sides of the test membrane. The current was stabilized by a resistance at a predetermined value and was read on an avometer. The potential measuring Ag|AgCl electrodes were connected to an E.S.I. Model 300 compensator. Before the current was turned on, the potential difference between the measuring electrodes was determined: it was the sum of the biionic potential across the membrane and the asymmetry potential due to one electrode being immersed in a $K_4Fe(CN)_6$ solution and the other in $NaNO_3$. The potential drop in the solutions at the current used in the experiment was determined separately. Both the asymmetry and biionic potentials and the potential drop in the solutions were eventually subtracted from the potential values read during the experiment, so that only the potential drop across the membrane remained.

The experiment began by turning on the current at its predetermined value and from then on the potential across the membrane was determined as a function of the time. Figure 1 shows how this potential changed in the course of the experiment. Starting from the low value corresponding to 2 ohms/cm² of the unpoisoned membrane, the voltage drop immediately began to rise as the current introduced the poisoning ferrocyanide ion into the membrane.⁴ From this moment on, the cathode side of the membrane was poisoned by the strongly bound and therefore slow-moving ferrocyanide ion, thus being transformed to a cation selective layer because of the free negative valencies of these ions. A plane front of this poisoned layer was now progressing slowly toward the anode side of the membrane. The steadily decreasing free anionic layer on the opposite

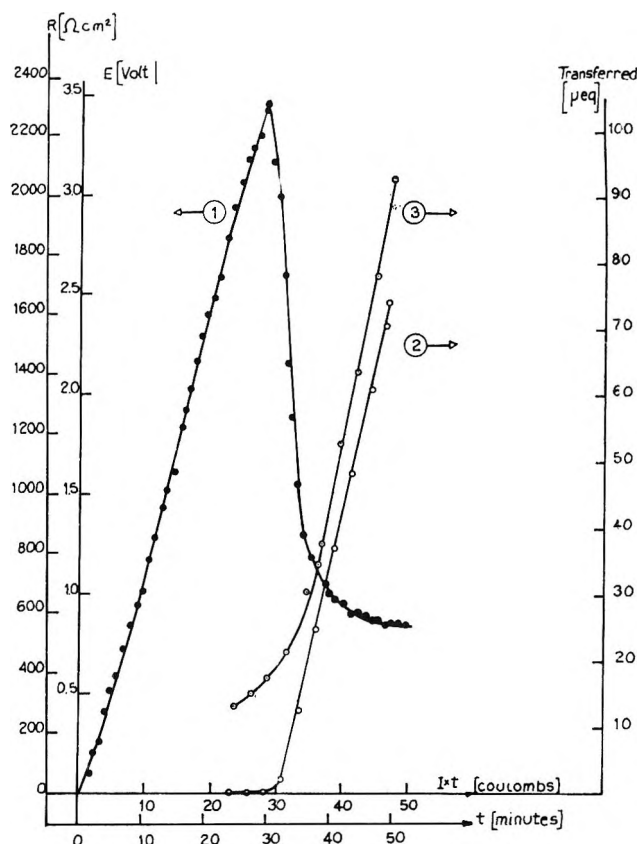


Figure 1. Breakthrough of poisoning ferrocyanide ions after being introduced into an AMF anionic membrane from one side by an electric current. The peak occurs at the moment when ferrocyanide reaches the opposite side of the membrane: curve 1, variation of resistance (potential) with time; curve 2, variation of $[Fe(CN)_6]^{4-}$ ion concentration (in the $NaNO_3$ solution) with time; curve 3, variation of Na^+ ion concentration (in the ferrocyanide solution) with time.

side of the membrane ought to have closed the way of any Na^+ ions trying to enter it from the anode side toward the cathode.

This situation corresponds to the closing direction of a biionic (sandwich) membrane.⁵⁻⁹ If the ferrocyanide ions would be held so strongly that they could not move at all, it would mean that cations were extracted from the

(1) N. W. Rosenberg, J. B. H. George, and W. D. Potter, *J. Electrochem. Soc.*, **104**, 111 (1957).

(2) G. Schultz, *Z. Anorg. Allgem. Chem.*, **301**, 97 (1959).

(3) F. Kőrösy, *Nature*, **191**, 1363 (1961).

(4) J. M. Tobias, D. P. Agin, and R. Pavlowski, *J. Gen. Physiol.*, **45** (2), 989 (1962).

(5) V. J. Frilette, *J. Phys. Chem.*, **60**, 435 (1956).

(6) B. Lovreček, A. Despic, and J. O. M. Bockris, *ibid.*, **63**, 750 (1959).

(7) A. Mauro, *Biophys. J.*, **2**, 179 (1962).

(8) P. Läger, *Ber. Bunsenges. Physik. Chem.*, **68** (6), 534 (1964).

(9) F. Kőrösy, *Israel J. Chem.*, **3**, 22 (1966).

cation-exchange layer toward the cathode, while anions were being extracted toward the anode from the anion-exchange layer. Eventually no counter ions would be left in the membrane except those which were driven "illegally" into the forbidden domains by an increased potential. In normal bipolar membranes the ions of water take over a large part of current conduction under such conditions and generate alkali and acid, respectively, on the two sides of the membrane. In our experiment no pH changes were observed. The transient bipolar membrane which came into being during the progress of the poisoned, sign-inverted layer does not behave exactly like a stationary bipolar membrane. The reason is that the poison ions are not held strongly enough in the membrane to be utterly immobilized; they continue to proceed toward the anode but they do so with difficulty. This is why the voltage drop necessary to drive them across the membrane increases linearly with time, that is, with the thickness of the layer progressing across the membrane. Curve 1 in the figure shows that it increases linearly until after 31.5 min (corresponding to 28.3 coulombs having passed). At this moment it has reached 3.46 v which corresponds to 2300 ohms/cm² resistance at the current density 1.5 ma/cm² of the experiment. This is the high resistance of the ferrocyanide poisoned membrane just before the poison breaks through its anodic surface. At this moment the voltage drop, that is, the resistance, of the membrane begins to fall dramatically.

The explanation is clear. As soon as the sign-inverted, poisoned layer reaches the solution facing the anodic side of the membrane, the membrane has become a cation-exchange membrane throughout its thickness, and now Na⁺ ions are able to enter more freely toward the cathode. They do this as secondary, positive counterions of the poisoned membrane, neutralizing a few of the ferrocyanide valencies which up to then have been bound to membrane sites. An amount of ferrocyanide equivalent to the intruding Na⁺ is being pressed into the membrane from its cathode side, thus ensuring electroneutrality.

The voltage drop (or the resistance) now begins to level out at the steady-state value of 0.85 v (570 ohms cm²). At this stage two contrary streams of ions are traversing the membrane, the slowly moving ferrocyanide ions toward the anode and the relatively few but much more mobile Na⁺ ions toward the cathode.

Samples were taken during the experiment from the cells on both sides of the membrane. Ferrocyanide was determined (by the dipyriddy method) as its concentration increased in the NaNO₃ solution, and sodium (by flame photometry) increased in the ferrocyanide. Curves 2 and 3 in Figure 1 show the results of these de-

terminations. The breakthrough of the ferrocyanide ion shows a sharp knee on curve 2 exactly at the moment when the resistance curve 1 has reached its peak value. This confirms our explanation—resistance rises exactly up to the moment that the membrane has become poisoned throughout its thickness.

Sodium appears in the cell on the cathode side of the membrane before the resistance peak, unlike the ferrocyanide on the opposite side. This is due to the fact that the membrane is only about 95% permselective so that Na⁺ is being transferred all the time although at a low rate. As it is, the Na⁺ curve (curve 3) shows that 17 μ equiv of Na⁺ was transferred up to the moment of ferrocyanide breakthrough. This is equal to 1.65 coulombs transported, while the total number of coulombs having traversed the membrane up to breakthrough was 28.5. Hence 28.5 - 1.6 = 26.9 coulombs must have been necessary to fill the membrane with ferrocyanide ions until the latter began to break through it on the other side. This is equivalent to 0.28 mequiv of ferrocyanide in a 10-cm² membrane which weighed 0.29 g in the dry state. For 1 g dry membrane we thus arrive at 0.96 mequiv of ferrocyanide content at breakthrough. The actual capacity of the membrane is 1.2 mequiv/g. Perhaps the progressing front is not a complete plane and reaches the anodic face of the membrane sooner on some places than on others.

It is difficult to tell exactly when the Na⁺ curve shows a break. It seems that it begins to rise at the time that the ferrocyanide breaks through. The Na⁺ curve reaches its new steady-state value about 9 min later (= 8.5 coulombs). The interval between is evidently necessary to redistribute the ferrocyanide and its "secondary" Na⁺ counterions, until the stationary state has been reached. However, 19 coulombs pass the membrane from the time of breakthrough until the resistance becomes constant, so that the final steady state is probably attained only at that time. The final linear parts of the two ion transference curves correspond to a continuous transport of 0.45 coulomb by ferrocyanide and 0.55 coulomb by Na⁺ ions for each coulomb transported.

Another experiment at a current density of 4.5 ma/cm² resulted in a ferrocyanide breakthrough after the passage of 27 coulombs, as compared with 28.5 coulombs in the 1.5-ma/cm² experiment. In view of the differences between separate pieces of the same membrane, the agreement between the values is satisfactory.

It is possible to calculate approximately the mobility of ferrocyanide ion in the membrane during the first part of the experiment until it breaks through. The linear rise of the voltage-time curve shows that the field strength across the poisoned part of the membrane

remains constant. The membrane was 0.3 mm thick. The breakthrough occurred after 1900 sec at a voltage drop of 3.4 v across the membrane, that is, at a field strength of 113 v/cm. This yields $1.4 \times 10^{-7}/\text{cm}^2/\text{v sec}$ as mobility. Two other experiments under other current densities again yielded 2×10^{-7} . More exact determinations will have to follow, but the order of magnitude seems to be established.

It is much more difficult to calculate the mobility of the Na^+ ions in the period from breakthrough of ferrocyanide to the breakthrough of secondary sodium counterions into the cathode side because the moment of this final breakthrough is less well determined. How-

ever, the order of magnitude of this mobility can be estimated. Calculating with the final steady-state voltage and 700 sec for Na^+ breakthrough, one arrives at about $2 \times 10^{-6}/\text{cm}^2/\text{v sec}$. The experiments are continuing and counterions and co-ions will be determined analytically at different points of the breakthrough curve.

Acknowledgment. This work has been performed under Grant No. 14-01-0001-766 of the Office of Saline Water, Washington, D. C. We are indebted to Dr. Y. Michaeli of the Weizmann Institute, Rehovoth, for fruitful discussion and to Miss M. Zevulun for most valuable assistance during the experiments.

COMMUNICATIONS TO THE EDITOR

Reply to the Comments of the Paper "Gibbs Equation for the Adsorption of Organic Ions in Presence and Absence of Neutral Salts"

Sir: The kT coefficient m' of the Gibbs equation for the adsorption of the uni-univalent organic electrolyte has been given by our equation¹

$$m' = 1 + \frac{1}{1 - n_{\text{Cl}^-}/n_{\text{Na}^+}} \frac{C_{\text{R}'}}{C_{\text{R}'} + C} \quad (1)$$

with the assumption that the Gouy model of the electrical double layer exists at the charged liquid interface. Ratio $n_{\text{Cl}^-}/n_{\text{Na}^+}$ in eq 1 has been assumed by us to be equal to $C_{\text{Cl}^-}^{\text{S}}/C_{\text{Na}^+}^{\text{S}}$ and this in turn has been evaluated using the simpler forms of Boltzmann equations, so that eq 1 will assume the form

$$m' = 1 + \frac{1}{1 + x(1 - e^{-2e\psi/kT})} \quad (2)$$

where x is equal to $C/C_{\text{R}'}$ and ψ is the absolute magnitude of the potential of the double layer without negative sign included.

However, Bijsterbosch and van den Hul,² in a recent comment, have pointed out that Grahame³ has already used integrated forms of the Boltzmann equations in order to evaluate $n_{\text{Cl}^-}/n_{\text{Na}^+}$. Using this treatment in eq 1, they have shown

$$m'' = 1 + \frac{1}{1 + x \left[1 - \frac{1 - e^{-e\psi/2kT}}{e^{e\psi/2kT} - 1} \right]} \quad (3)$$

where m'' is the kT coefficient. However, eq 3 on simplification will reduce to the form

$$m'' = 1 + \frac{1}{1 + x(1 - e^{-e\psi/2kT})} \quad (4)$$

A close examination of eq 2 and 4 confirms the similarity in their forms. The only difference lies in the exponential power which for eq 4 is $-e\psi/2kT$, whereas that for eq 2 is four times greater in magnitude. In view of this similarity, the graphical comparison of the values of m' and m'' as made by these workers² was not necessary. The m' vs. x curves given in our paper¹ for ψ equal to 5, 10, 30, and 40 mv, respectively, will in fact correspond to 20, 40, 120, and 160 mv of surface potentials if eq 4 is assumed to be valid in place of eq 2. The conclusion made by Bijsterbosch and van den Hul that above 30 mv potential, kT coefficients calculated with the help of eq 2 and 3 are identical is therefore incorrect for obvious reasons.

It seems to me that eq 4 is more logical than eq 2 in

(1) D. K. Chattoraj, *J. Phys. Chem.*, **70**, 2687 (1966).

(2) B. H. Bijsterbosch and H. J. van den Hul, *ibid.*, **71**, 1169 (1967).

(3) D. C. Grahame, *Chem. Rev.*, **41**, 481 (1947).

view of the nonuniform distribution of the inorganic ions in the surface phase. The use of the integrated forms of the Boltzmann equations is therefore also recommended for our subsequent treatment of the Gibbs equations for polyelectrolyte⁴ and micelle⁵ adsorption. The term $(1 - e^{-2e\psi/kT})$ occurring in all these cases for the equations of kT coefficient m' is to be replaced by $(1 - e^{-e\psi/2kT})$ due to this modification. It should be noticed that as a result of this modification, the kT coefficient in the intermediate range of x will be significantly dependent on the value of ψ . Only when ψ is equal to or above 120 mv, $e^{-e\psi/2kT}$ will be much less than unity and the value of the kT coefficient will be independent of the potential of the double layer.

(4) D. K. Chattoraj, *J. Phys. Chem.*, **70**, 3743 (1966).

(5) D. K. Chattoraj, *ibid.*, **71**, 455 (1967).

CHEMISTRY DEPARTMENT
JADAVPUR UNIVERSITY
CALCUTTA-32, INDIA

D. K. CHATTORAJ

RECEIVED JULY 17, 1967

Self-Diffusion in Simple Liquids. The Linear Trajectory Approximation¹

Sir: Palyvos and Davis² (PD) have calculated the friction coefficient (defined by $\zeta = kTD^{-1}$ where D is the self-diffusion coefficient) using the linear trajectory approximation (LTA) in the Rice-Allnatt theory.^{3,4} PD concluded that this approximation is fairly reliable, yielding values of D within 10–40% of actual over the entire liquid range. The basis for this conclusion is a comparison of the calculated values with experimental data from Naghizadeh and Rice.⁵ We will show this comparison is unreliable, requiring gross extrapolation of the experimental data.

Naghizadeh and Rice fitted the temperature and pressure dependence of their experimental results essentially assuming, but not establishing, a relationship of the form

$$D = A \exp(-BT^{-1} - CP) \quad (1)$$

Their data and fitting are shown in Figure 1. We have analyzed the data by multivariate regression, obtaining objective values of the coefficients in eq 1 and establishing confidence limits. These curves are also included in Figure 1; the fits for the isobars of krypton and the 57.5-atm isobar of argon differ significantly, other isobars only slightly.

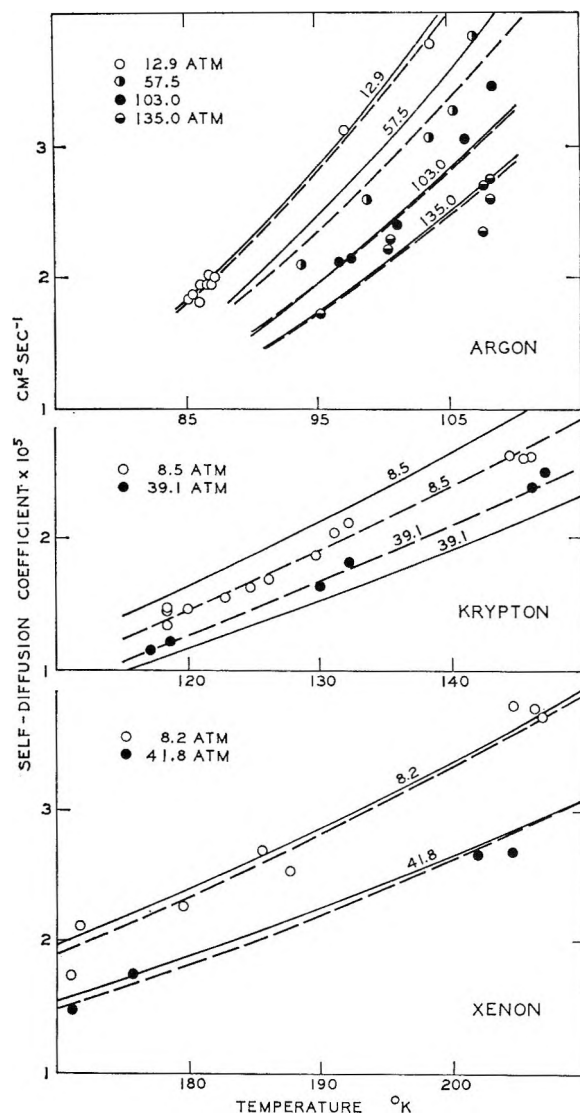


Figure 1. Experimental data for the self-diffusion coefficient and isobars fitted: —, fit by Naghizadeh and Rice;⁵ - - -, regression of eq 1.

In Figure 2, LTA-predicted values of D along the coexistence curve for argon, krypton, and xenon are compared with the PD extrapolation of the experimental data and with our estimate and wide 95% confidence intervals obtained from eq 1. At lower temperatures, where a direct comparison with experiment is feasible, the following deviations between theory and experiment (expressed as a percentage of the experimental

(1) Work supported by the Directorate of Chemical Sciences of the U. S. Air Force Office of Scientific Research under Contract No. AF 49(638)-1273.

(2) J. A. Palyvos and H. T. Davis, *J. Phys. Chem.*, **71**, 439 (1967).

(3) S. A. Rice and A. R. Allnatt, *J. Chem. Phys.*, **34**, 2144 (1961).

(4) A. R. Allnatt and S. A. Rice, *ibid.*, **34**, 2156 (1961).

(5) J. Naghizadeh and S. A. Rice, *ibid.*, **36**, 2710 (1962).

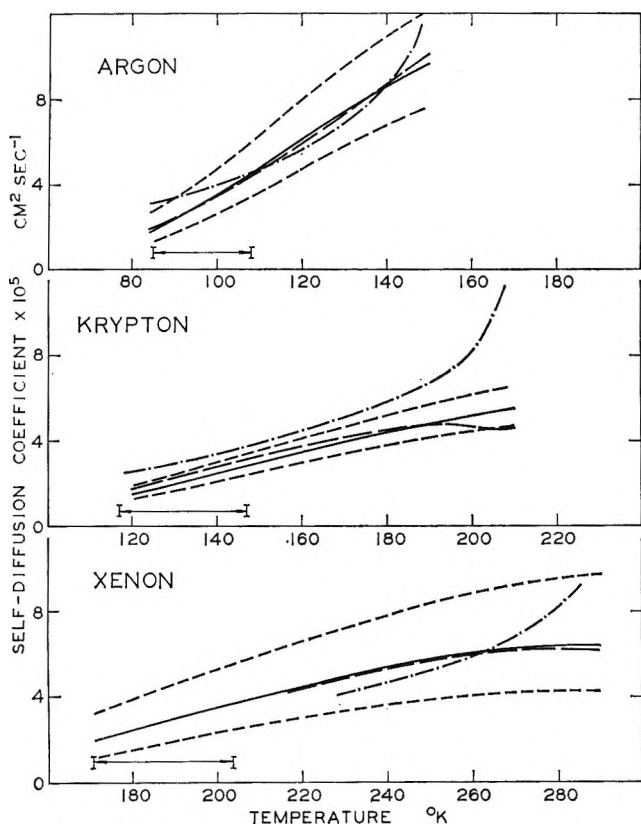


Figure 2. The self-diffusion coefficient along the coexistence curve: $|\longleftrightarrow|$, experimental temperature range; —, regression eq 1; - - -, 95% confidence limits on eq 1; - - - - , PD extrapolation of experimental data;² · · · · , linear trajectory approximation.²

value) are obtained: argon (85°K) 167%; krypton (120°K) 167%; and xenon (200°K) 82%.

The PD analysis does not seem a convincing verification of the LTA-RA theory.

DIVISION OF CHEMISTRY AND
CHEMICAL ENGINEERING
CALIFORNIA INSTITUTE OF TECHNOLOGY
PASADENA, CALIFORNIA 91109

A. F. COLLINGS
C. J. PINGS

RECEIVED MAY 19, 1967

Living Anionic Polymerization under an Electric Field

Sir: For a better understanding of the growing species in polymerization reactions, the influence of an electric field on the rate of polymerization has been investigated. Our results show that the rates of cationic polymerizations are generally increased by the field, whereas free radical polymerizations are not affected.¹

It has been tentatively proposed that the field-facilitated dissociation of ion pairs at growing chain ends may be responsible for the accelerating effect, on the assumption that the propagation rate constant of free ions (k_p'') is much larger than that of ion pairs (k_p'). Though this interpretation appeared reasonable, it lacked clear support because of the intricate mechanism of the cationic polymerizations. In the present paper, we give some experimental data for a living anionic polymerization of styrene initiated by *n*-butyllithium (*n*-BuLi) in a series of mixtures of benzene and tetrahydrofuran (THF), where the propagation process only needs to be considered.

The possible influence of even small impurities was taken into account; our experiments were carried out using a high-vacuum line and CaH₂, Na-K alloy, or Na mirror as drying agents. The *n*-BuLi was prepared from butylbromide and lithium metal.² Polystyryllithium, used as seed polymer, (degree of polymerization, about 15) was prepared with *n*-BuLi. The polymerizations were conducted at 25° in a glass vessel specially designed and equipped with an optical cell. A pair of parallel platinum electrodes, on which the dc voltage was applied, was sealed into the cell. The polymerization rate was determined spectrophotometrically.

Table I gives the main results. It is worth mentioning first that the observed propagation rate constant without field (k_{p0}) agrees well with the value reported previously.³ Second, the rate constant in a

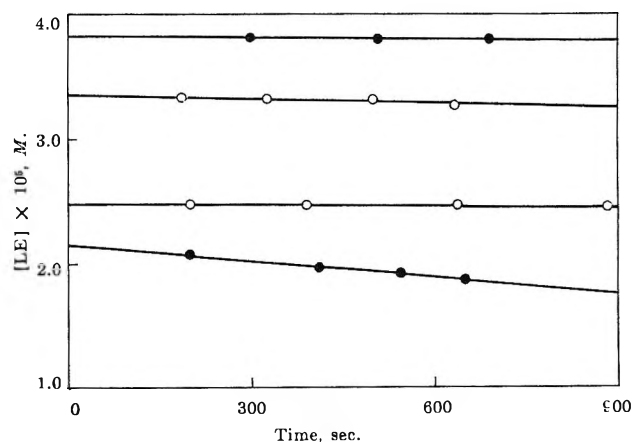


Figure 1. Time dependence of the concentration of living ends for THF, 40 vol. %, 25°: ●, 5 kv/cm; ○, 0 kv/cm.

(1) See, for example, I. Sakurada, N. Ise, and T. Ashida, *Makromol. Chem.*, **95**, 1 (1966); I. Sakurada, N. Ise, Y. Tanaka, and Y. Hayashi, *J. Polymer Sci.*, *A-1*, **4**, 2801 (1966).

(2) T. Fujimoto, N. Ozaki, and M. Nagasawa, *ibid.*, *A-3*, 2259 (1965).

(3) S. Bywater and D. J. Worsfold, *J. Phys. Chem.*, **70**, 162 (1966).

field of 5 kv/cm (k_{pE}) is larger than k_{p0} except for 10% THF mixture. It seems that the accelerating effect increases with the increasing dielectric constant (D) in agreement with our previous findings for cationic systems.² Finally, as shown in Figure 1, the concentration of living ends [LE] is practically time independent, with and without field. This result seems to indicate that no living ends are produced or consumed in the field and that the accelerating effects cannot be explained in terms of the so-called electroinitiation mechanism.⁴

Table I: Kinetic Data of Living Anionic Polymerization of Styrene at 25°

Volume fraction of THF, %	D	[LE] × 10 ⁶ , M	Field strength, kv/cm	$k_p, M^{-1} \text{sec}^{-1}$	
				Obsd	Lit. ^a
10	2.69	7.6	0	2.07	2.1
			5	2.07	
30	3.58	1.9	0	14.1	15
			5	20.4	
40	4.05	3.9	0	2.0	28
			5	38	
44.5	4.27	1.0	0	...	34
			5	110	

^a Estimated using k_p values and activation energy data given by Bywater and Worsfold³ at 20°.

The second and third findings support the important role of free ions and ion pairs proposed previously,⁵ and simultaneously our own interpretation of field effects on cationic polymerization.¹ Furthermore, by using benzene-THF mixtures we were able to exclude the specific role of 1,2-dichloroethane and nitrobenzene where the large field effects had been observed.

Because of the large difference between k_p'' and k_p' reported earlier,⁵ it is worth mentioning finally that we were able to observe the accelerating effect even for very weak electric fields, where the increase of conductivity of weak electrolyte solutions is, due to the second Wien effect, hardly detectable.

(4) For electrolytically initiated polymerizations, see, for example, B. L. Funt and F. D. Williams, *J. Polymer Sci.*, A-2, 865 (1964).

(5) D. N. Bhattacharyya, C. L. Lee, J. Smid, and M. Szwarc, *Polymer*, 5, 54 (1964); H. Hostalka, R. V. Figini, and G. V. Schulz, *Makromol. Chem.*, 71, 198 (1964).

DEPARTMENT OF POLYMER CHEMISTRY
KYOTO UNIVERSITY
KYOTO, JAPAN

ICHIRO SAKURADA
NORIO ISE
HIDEO HIROHARA
TETSUO MAKINO

RECEIVED JUNE 30, 1967

Radiation Chemical Studies with Heavy Ion Radiations¹

Sir: To date, except for a few experiments with fission fragments, liquid-phase radiation chemical studies with heavy ions have been confined to particles of low mass and charge (*i.e.*, protons, deuterons, and helium ions) where the linear energy transfer (LET) of the radiation is in the range of 0.5–25 ev/A.² While reliable measurements of the dependence of differential radiation yields on LET can be made up to a few ev/A with these radiations, measurements at higher LET's are more difficult because of the short range at the necessarily low particle energies. In any event, for protons the maximum LET available in water is of the order of 7 ev/A and for helium ions of the order of 25 ev/A, and it becomes necessary to use more massive highly charged particles to obtain information at higher LET's.³ The experiments briefly reported here indicate that practical radiation chemical experiments at high LET's can be carried out with the heavy ion beams made available by the Yale University Heavy Ion Linear Accelerator (HILAC).

Preliminary experiments on the ferrous sulfate system (0.01 M Fe²⁺ in aerated 0.8 N H₂SO₄, no chloride) have been carried out with 120-Mev C⁶⁺ ions from the HILAC. The range of these ions is 65 mg/cm², so that window problems are of relatively minor importance. The irradiation arrangement was very similar to that used in earlier studies with cyclotron radiations.^{2a} Absolute radiation chemical yields were determined from a knowledge of the amount of chemical reaction, the particle energy, and the integrated beam current. The ferric ion concentration was measured spectrophotometrically at 305 mμ and the energy of the undegraded beam determined from magnetic measurements in the beam analyzing system. Measurement of the integrated current presents the most serious of the problems associated with this type of experiment since difficulties due to secondary electron emission, charge exchange in the ion beam itself, and current displacement effects in the window system analogous to those previously observed with protons and helium ions⁴ are all present. Secondary electron

(1) Supported in part by the U. S. Atomic Energy Commission.

(2) For typical experiments with cyclotron and Van de Graaff radiations, see: (a) R. H. Schuler and A. O. Allen, *J. Am. Chem. Soc.*, 79, 1565 (1957); (b) E. J. Hart, W. J. Ramler, and S. R. Rocklin, *Radiation Res.*, 4, 378 (1956); (c) W. G. Burns, R. A. Holroyd, and G. W. Klein, *J. Phys. Chem.*, 70, 910 (1966).

(3) For a discussion of the energy loss by heavy ions, see H. A. Bethe and J. Ashkin in "Experimental Nuclear Physics," Vol. I, E. Segre, Ed., John Wiley and Sons, Inc., New York, N. Y., 1953, Chapter II; L. C. Northcliffe, *Ann. Rev. Nucl. Sci.*, 13, 67 (1963).

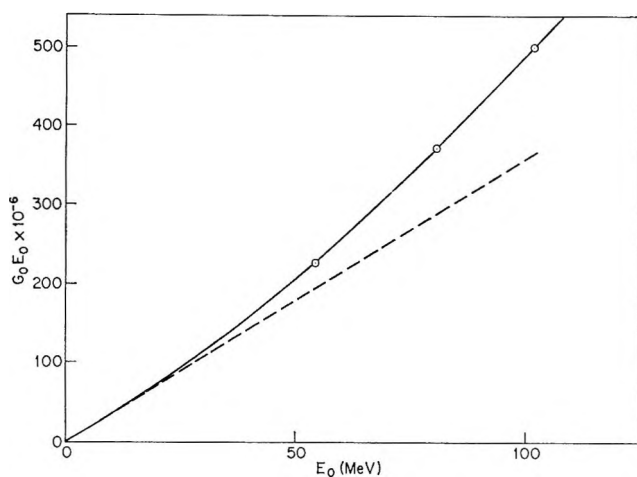


Figure 1. Dependence on particle energy of the integrated yield ($G_0 E_0$) for oxidation of ferrous ion (0.01 M in aerated 0.8 N H_2SO_4) by C^{6+} ions. Dashed line corresponds to a limiting G of 3.6 as expected for radiations of infinite LET (cf. ref 2a). The differential yield over the interval 50–100 Mev is seen to be considerably ($\sim 60\%$) higher.

currents in the beam-defining system were eliminated by the application of a transverse magnetic field. The sum of the effects due to charge exchange and current displacement was measured as described previously⁴ by stopping the beam in the irradiation cell and measuring the relative window and cell currents. For the full energy beam it was shown that 3.57 units of charge were collected in the cell for each irradiating C^{6+} ion. Yields at reduced energies were determined by degrading the beam with aluminum foils of known thickness.

At the maximum energy transmitted by the window system (102 Mev) the yield is found to be linearly dependent on dose from an average dose⁵ of 10^{18} to 6×10^{18} ev/g. The yield for eight experiments was 4.94 molecules/100 ev and had a high degree of reproducibility as indicated by a standard deviation within the measurements of only 0.05. Measurements were also made at reduced energies of 80 and 54 Mev where the residual ranges are 32 and 20 mg/cm². The integrated yields are plotted in Figure 1 as a function of particle energy. The average values of $G_i (= d(G_0 E_0)/dE_0)$ over the two energy intervals are, respectively, 6.1 and 5.6 (mean dE/dx of 20 and 25 ev/A), and are believed to be known on the absolute scale to the order of 5%. These differential yields are substantially higher than the value of 4.2 observed for E^{10} (n, α) Li^7 radiations⁶ where the LET is in the same range as for the present radiations. This difference presumably reflects the greater importance of high energy δ -rays for the heavier ions which effectively increases the diameter of the

track of the ionizing particle. A similar effect was previously noted in an intercomparison of the results from helium ion and proton irradiations at the same LET.^{2a}

The results obtained with ferrous sulfate demonstrate that detailed quantitative studies can be readily carried out with radiations having LET's in the range of 25 ev/A. The HILAC proves to be a particularly good instrument for this type of study because of the highly defined nature of the radiation available from it. It seems likely that it will be possible to use even heavier ions from this instrument to extend the range of practical radiation chemical experiments to LET's of the order of 100 ev/A. Further exploratory studies are in progress.

(4) R. H. Schuler and A. O. Allen, *Rev. Sci. Instr.*, **26**, 1128 (1955).

(5) The beam is stopped in an irradiation volume ~ 0.02 cm³ and distributed over the sample volume 20 cm³ by rapid stirring. Beam densities of $\sim 10^{10}$ (particles/cm²/sec) were used. Because of the lesser importance of radical reactions, solute depletion causes less complication than in the case of electron irradiations.

(6) R. H. Schuler and N. F. Barr, *J. Am. Chem. Soc.*, **78**, 5766 (1956).

RADIATION RESEARCH LABORATORIES ROBERT H. SCHULER
MELLON INSTITUTE
PITTSBURGH, PENNSYLVANIA 15213
HEAVY ION ACCELERATOR LABORATORY
YALE UNIVERSITY
NEW HAVEN, CONNECTICUT

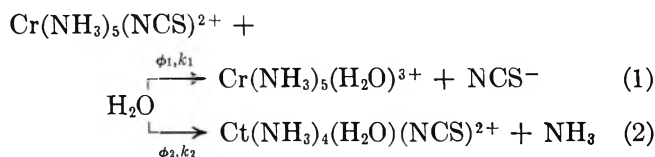
RECEIVED JULY 17, 1967

Specificity of the Photochemical and Thermal Aquation of Thiocyanatopentaamminechromium(III) Ion

Sir: In a recent paper,¹ empirically developed rules were presented which appeared able to predict the photochemical behavior of Cr(III) complexes. These could be understood on the basis that it was the spatial distribution of the σ antibonding electron of the lowest excited quartet state that determined which ligand would be photolabilized. The direct implication was that where more than one mode of ligand substitution was possible, the course of the photochemical reaction could not necessarily be inferred from that of the thermal behavior.

An especially simple potential illustration of this dichotomy is that of the photochemistry *vs.* the thermal reaction chemistry of $Cr(NH_3)_5X^{2+}$ complexes. With $X = NCS^-$, the two reaction modes are

(1) A. W. Adamson, *J. Phys. Chem.*, **71**, 798 (1967).



Only reaction 1 has previously been noted to occur thermally;² ammonia aquation was not looked for. The above-mentioned empirical rules predict $\phi_2 \gg \phi_1$; experimentally, ϕ_1 has been reported to be 0.015 at 500 m μ ,² while there is only a qualitative indication that ϕ_2 is not negligible.³ In the case of X = Cl⁻, k_1 has been reported,² but no estimate of k_2 appears to exist; ϕ_2 has been measured, and ϕ_1 has been estimated to be small.^{4,5} The literature thus suggests without definitely establishing a difference in the reaction chemistry of the excited *vs.* the ground state of such complexes, and the present study was undertaken to clarify the situation.

The complex was prepared from [Cr(NH₃)₅(H₂O)](NO₃)₃ by reaction with concentrated aqueous sodium thiocyanate, and its composition (as the perchlorate salt) was confirmed by analysis for chromium, ammonia, and thiocyanate. The visible absorption spectrum comprises one broad peak at 487 m μ and a small one at 363 m μ , with respective extinction coefficients of 84.0 and 53.0.⁶ The reactions reported here are for 0.01 M complex in 0.1 N sulfuric acid (ionic strength, $\mu = 0.17$). The general photolysis procedure was as previously described,⁷ as was that for analysis of released thiocyanate ion. Released ammonia was determined⁸ after its separation from the reaction mixture by an ion-exchange procedure.

We find that for the thermal reaction, values of k_1 are 1.75×10^{-7} and 2.37×10^{-6} (in sec⁻¹) at 25 and 45°. The corresponding activation energy of 24.6 kcal/mole agrees well with the previous value;² the earlier reported value of k_1 at 25° is lower than ours (9.4×10^{-8} sec⁻¹), but is for pH 2.5 and $\mu = 0.05$. Thermal release of ammonia also occurred, but with an apparent first-order rate constant which increased steadily with degree of reaction, evidently due to stepwise aquation of Cr(NH₃)₅(H₂O)³⁺. The rate constants extrapolated to zero time were 9×10^{-8} and 8×10^{-7} (in sec⁻¹) for the two temperatures. However, the reported rate constant for the aquation of Cr(NH₃)₅(H₂O)³⁺ is *ca.* 2×10^{-5} sec⁻¹ (40°, 0.4 M HNO₃),⁹ or comparable to k_1 . It is thus possible that even at short times the observed ammonia release is due to this reaction, following reaction 1; the actual values of k_2 may thus be much smaller than the above extrapolated rate constants. We conclude that the ratio k_2/k_1 has an upper limit of *ca.* 0.5, but may actually be much less.

The photochemical results are summarized in Table I. The ratio ϕ_2/ϕ_1 is about 20, only moderately dependent on temperature and on which quartet band is irradiated. Unlike the situation with the thermal studies, the principal product in this case, Cr(NH₃)₄(H₂O)(NCS)²⁺, is relatively stable. No thermal release of ammonia or of thiocyanate occurred over 24 hr at 25° other than that expected from the aquation of the unphotolyzed parent complex.

Table I: Photoaquation of Cr(NH₃)₅(NCS)²⁺

Temp, °C	370 m μ		490 m μ	
	ϕ_1	ϕ_2	ϕ_1	ϕ_2
5.0	0.024	0.39	0.019	0.42
25.0	0.030	0.46	0.021	0.48
45.0	0.040	0.53	0.024	0.53
E^{*a}	2.2	1.4	1.0	0.83

^a Apparent activation energy in kcal/mole.

We find, then, that the ratio ϕ_2/ϕ_1 is at least 40 times greater than the ratio k_2/k_1 . The indicated conclusion is that the excited state of Cr(III) complexes (presumably the lowest excited quartet state) has a discoverable and characteristic chemistry distinct from that of the ground state, contrary to the suggestion that photoreactions of Cr(III) species consist merely of a photocatalysis of a thermal reaction.¹⁰ Current further work is directed toward the isomeric characterization of the photolysis product, the determination of ϕ_1 and ϕ_2 for wavelengths in the doublet absorption region, and the setting of a still lower limit to k_2 .

Acknowledgment. Support of these investigations by the U. S. Atomic Energy Commission (RDL and

(2) A. W. Adamson and R. G. Wilkins, *J. Am. Chem. Soc.*, **76**, 3379 (1954).

(3) W. C. Waggener, J. A. Mattern, and G. H. Cartledge, *ibid.*, **81**, 2958 (1959).

(4) L. Moggi, F. Bolletta, and V. Balzani, *Ric. Sci.*, **36**, 1228 (1966).

(5) H. F. Wasgestian and H. L. Schäfer, private communication.

(6) M. Linhard, H. Siebert, and M. Weigel, *Z. Anorg. Allgem. Chem.*, **278**, 287 (1955).

(7) E. Wegner and A. W. Adamson, *J. Am. Chem. Soc.*, **88**, 394 (1966).

(8) A. Crowther and R. Large, *Analyst*, **81**, 64 (1956).

(9) J. Bjerrum and E. Jörgensen, *J. Inorg. Nucl. Chem.*, **8**, 313 (1958).

(10) E. L. Wehry, *Quart. Rev. (London)*, **21**, 213 (1967).

AWA) and by the National Science Foundation (EZ) is gratefully acknowledged.

DEPARTMENT OF CHEMISTRY
UNIVERSITY OF SOUTHERN CALIFORNIA
LOS ANGELES, CALIFORNIA 90007

ROBERT D. LINDHOLM
EDOARDO ZINATO
ARTHUR W. ADAMSON

RECEIVED JULY 24, 1967

Energy Transfer in Thermal Methyl Isocyanide Isomerization. Collision Cross Sections of *n*-Alkanes¹

Sir: Very extensive data will probably be required in order to characterize the structural and molecular parameters that govern collisional vibrational energy exchange in thermal unimolecular reaction systems and, in general, between complex molecules at high levels of internal excitation.² An important desideratum is a knowledge of relevant collision cross sections. Present practice is to transfer values derived from other phenomena, but no immediate justification of this custom and of these values is available. This communication describes the determination of a self-consistent set of relative collision cross sections appropriate to the energy-transfer phenomenon. Results are given for the activation of methyl isocyanide by *n*-alkanes in the second-order region of the isomerization reaction.

The relative efficiencies²⁻⁴ of inert activators M, compared with the parent substrate A, generally tend to increase with molecular size (boiling point).^{2,3,5} For the closely related species of a homologous series, the relative efficiency β_{μ} , corrected for reduced mass effects on collision rates, is expected to increase with chain length. Beyond some critical size, further increase in β_{μ} is here assumed to depend primarily on the increase in effective collisional diameter, s_{AM} , and not on an increase in intrinsic efficiency. On this basis

$$\beta_{\mu(n+i)}/\beta_{\mu n} = (s_{AMn} + i\Delta s_{AM})^2/s_{AMn}^2 \quad (1)$$

where i is an increment to n , the number of carbons in the chain, and Δs_{AM} is the average increment in diameter per CH_2 increment. Then, for some possibly limited range

$$R = [\beta_{\mu(n+i)}/\beta_{\mu n}]^{1/2} - 1 = i\Delta s_{AM}/s_{AMn} \quad (2)$$

and a linear relation between R and i , of slope $\Delta s_{AM}/s_{AMn}$, is predicted.

The efficiency of *n*-alkanes in promoting isomerization has been measured up to C_{10} at 280.5° . The

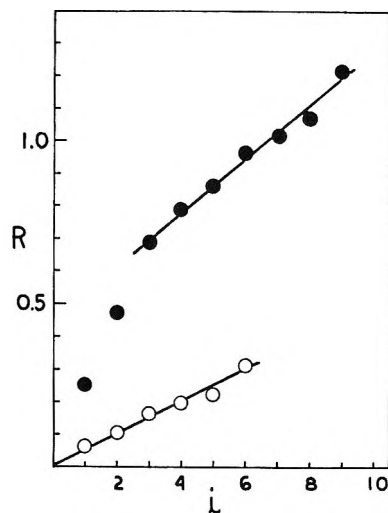


Figure 1. Plot of R vs. i for *n*-alkane-activated isomerization of CH_3NC at 280.5° : Filled circles, $n = 1$; open circles, $n = 4$.

technique described earlier² was followed with only minor modification. The mixture compositions corresponded to infinite dilution⁶ of substrate by alkane.

Results are summarized in Figure 1. Each point is based on 5-15 runs. Above propane, the behavior corresponds to the assumption of eq 1. $\beta_0(\infty)$, the efficiency β_{μ} corrected for cross-section change, is thus constant for higher alkanes (and equals 0.66) and the linear prediction of eq 2 is verified. The slope is $\Delta s_{AM}/s_{AM4} = 0.0482$, and Δs_{AM} is 0.27 Å based on the viscosity-related values $\sigma_{\text{butane}} = 5.20$ Å (ref 7) and $\sigma_{\text{CH}_3\text{NC}} = 4.47$ Å (ref 2), combined as $\sigma_{AM4} = (\sigma_{\text{CH}_3\text{NC}} + \sigma_{\text{butane}})/2$; σ is the Lennard-Jones potential constant and is related to s through the collision integral.^{2,7} Δs involves the combining rule and represents only half of the change in the alkane diameter.

The average increment $\Delta\sigma(\text{CH}_2) = 0.47$ Å was found from Δs_{AM} together with the relative values of σ_{Mn} for alkanes. The latter are compared (first two rows of

(1) This work was supported by the National Science Foundation.

(2) F. J. Fletcher, B. S. Rabinovitch, K. W. Watkins, and D. J. Locker, *J. Phys. Chem.*, **70**, 2823 (1966).

(3) (a) D. J. Wilson and H. S. Johnston, *J. Am. Chem. Soc.*, **75**, 5763 (1953); (b) M. Volpe and H. S. Johnston, *ibid.*, **78**, 3903 (1956).

(4) (a) D. C. Tardy and B. S. Rabinovitch, *J. Chem. Phys.*, **45**, 3720 (1966); (b) D. C. Tardy and B. S. Rabinovitch, *J. Chem. Phys.*, in press.

(5) T. L. Cottrell and J. C. McCoubrey, "Molecular Energy Transfer in Gases," Butterworth and Co. Ltd., London, 1961, Chapter 7.

(6) B. S. Rabinovitch, D. C. Tardy, and Y. N. Lin, *J. Phys. Chem.*, **71**, 1549 (1967).

(7) J. O. Hirschfelder, C. F. Curtiss, and R. B. Bird, "Molecular Theory of Gases and Liquids," John Wiley and Sons, Inc., New York, N. Y., 1954.

Table I

		n							
		4	5	6	7	8	9	10	
$\sigma_{M_n}, \text{ \AA}$	{	$\beta_0(\infty) = 0.66$	(5.20) ^a	5.67	6.14	6.61	7.08	7.55	8.02
		viscosity	5.20	5.70	6.20	6.80	7.50	8.40	
		$\beta_0(\infty) = 1$	(5.20) ^a	5.79	6.38	6.97	7.56	8.15	8.74

^a The value $\epsilon/k = 325^\circ\text{K}$ was used for all alkanes $n = 4-10$; see ref 7 for ϵ/k estimates for alkanes.

Table I) with values derived with use of the Lennard-Jones potential from viscosity measurements (ref 7) and smoothed. The relative increments $\Delta\sigma$ are approximately the same from C_4 to C_7 for both phenomena but diverge beyond that.

The hypothesis may now be adopted that $\beta_0(\infty)$ is unity for all higher alkanes whose efficiency per collision was found constant. This supposition is actually more plausible⁴ than its antithesis. It leads to a reevaluation of the relative cross sections of alkanes and isocyanide. If σ_{butane} is retained, $\sigma_{\text{CH}_2\text{NC}}$ increases from 4.47 to 6.76 \AA . The average incremental values become $\Delta\sigma_{\text{SAM}} = 0.33$ and $\Delta\sigma(\text{CH}_2) = 0.59$ \AA . Correspondence with the viscosity-related σ_{M_n} values is now good at all n (last two rows of table), perhaps coincidentally.

Although molecular diameters determined from

viscosity or virial coefficient measurements are not necessarily proper values for use in high internal energy systems, any disparity may well average less than 50% in general. Isocyanides are, of course, exceptional molecules if only in the magnitudes of their dipole moments. The method of this investigation may be extended in principle to a variety of substrates and homologous series and to the determination of $\Delta\sigma$ for other structural units. Work is continuing.

(8) Department of Chemistry, Colorado State University, Fort Collins, Colo.

DEPARTMENT OF CHEMISTRY
UNIVERSITY OF WASHINGTON
SEATTLE, WASHINGTON 98105

B. S. RABINOVITCH
Y. N. LIN
SIU C. CHAN
K. W. WATKINS⁸

RECEIVED AUGUST 5, 1967